Short Papers in the Geologic and Hydrologic Sciences, Articles 147-292

GEOLOGICAL SURVEY RESEARCH 1961

GEOLOGICAL SURVEY PROFESSIONAL PAPER 424-C

Scientific notes and summaries of investigations prepared by members of the Geologic and Water Resources Divisions in the fields of geology, hydrology, and allied sciences

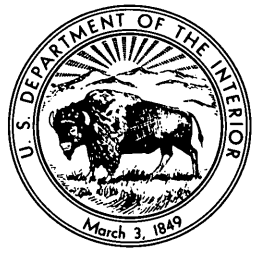

UNITED STATES GOVERNMENT PRINTING OFFICE, WASHINGTON : 1961

UNITED STATES DEPARTMENT OF THE INTERIOR

STEWART L. UDALL, *Secretary*

GEOLOGICAL SURVEY

Thomas B. Nolan, *Director*

For sale by the Superintendent of Documents, U.S. Government Printing Office
Washington 25, D.C.

FOREWORD

The scientific and economic results of work by the United States Geological Survey during the fiscal year 1961, the 12 months ending June 30, 1961, is being summarized in four volumes. This volume includes 146 short papers on subjects in the fields of geology, hydrology, and related sciences, prepared by members of the Geologic and Water Resources Divisions of the Survey. Some of these papers announce new discoveries or present observations on problems of limited scope; the others draw conclusions from more extensive or continuing investigations that in large part will be described in greater detail in reports to be published at a later date.

Other volumes in the series are Professional Paper 424–A, which gives a synopsis of the more important new findings resulting from work during the fiscal year, and Professional Papers 424–B and 424–D, which contain additional short papers like those in the present volume.

Thomas B. Nolan,
Director.

CONTENTS

GEOLOGICAL SURVEY RESEARCH 1961

SHORT PAPERS IN THE GEOLOGIC AND HYDROLOGIC SCIENCES, ARTICLES 147–292

GEOLOGY OF METALLIFEROUS DEPOSITS

147. GOLD DEPOSITS IN THE FRENCH GULCH-DEADWOOD DISTRICT, SHASTA AND TRINITY COUNTIES, CALIFORNIA

By JOHN P. ALBERS, Menlo Park, Calif.

Work done in cooperation with the State of California, Department of Natural Resources, Division of Mines

The French Gulch-Deadwood gold mining district forms an east-west belt about 9 miles long and 1 mile wide in the northern part of the French Gulch quadrangle, California. Production, mostly prior to 1933, amounts to about 29.2 million dollars if price is reckoned at $35 per ounce. Each of five mines has yielded gold valued at more than one million dollars. Those mines having the largest yield have been the Brown Bear (about 15.2 million dollars) and the Gladstone (about 6.9 million dollars). From 1942 to 1961 the district was inactive except for small lessee operations.

Figure 147.1 shows the French Gulch-Deadwood district proper and some additional area to give the reader a broader picture of the geologic setting. Rock units, from oldest to youngest, are: Copley greenstone, Balaklala rhyolite, Kennett formation, Bragdon formation, Shasta Bally batholith, and dikes and sills of silicic porphyries. The Copley (Devonian) and Balaklala (Devonian) formations are mafic volcanic rocks and silicic volcanic rocks, respectively. The Kennett and Bragdon formations, which overlie the volcanic units, consist chiefly of shale, siltstone, and conglomerate. Actually, the map includes only a very small body of siliceous shale thought to be Kennett formation, near the southeastern corner. The Bragdon formation is informally subdivided into a lower unit of shale and siltstone, and an upper unit in which sandstone and conglomerate are about as abundant as shale. Because the Bragdon formation is markedly discordant on the underlying rocks in most places it is inferred to overlie a thrust fault, here called the Spring Creek thrust. The thrusting predates the intrusive rocks of the area.

The Paleozoic rocks are intruded by the Shasta Bally batholith of leucocratic granitoid quartz diorite and granodiorite, and by dikes and sills of "birdseye" porphyry. Under the locally used term of "birdseye" porphyry several compositional varieties, ranging from nonquartzose diorite porphyry to highly silicic quartz porphyry, are included. Nearly all have euhedral to subhedral phenocrysts of plagioclase in a sugary or aphanitic groundmass; and in some varieties quartz, biotite, and hornblende also form phenocrysts. One dike that has a granitoid texture is nearly identical with the quartz diorite of the batholith, and all the dikes are regarded as apophyses of the batholith.

Pertinent structural features are the low irregular eastward-trending arch shown by the outcrop pattern of the Copley-Balaklala unit in the northern part of figure 147.1, and a mile-wide zone of fractured Bragdon formation lying just south of the arch, marked in its western part by numerous dikes and sills of "birdseye" porphyry (figs. 147.1 and 147.2). The more productive gold deposits are in this zone. The geometry of the arch is highly irregular and difficult to describe, partly because it is greatly complicated by faults and

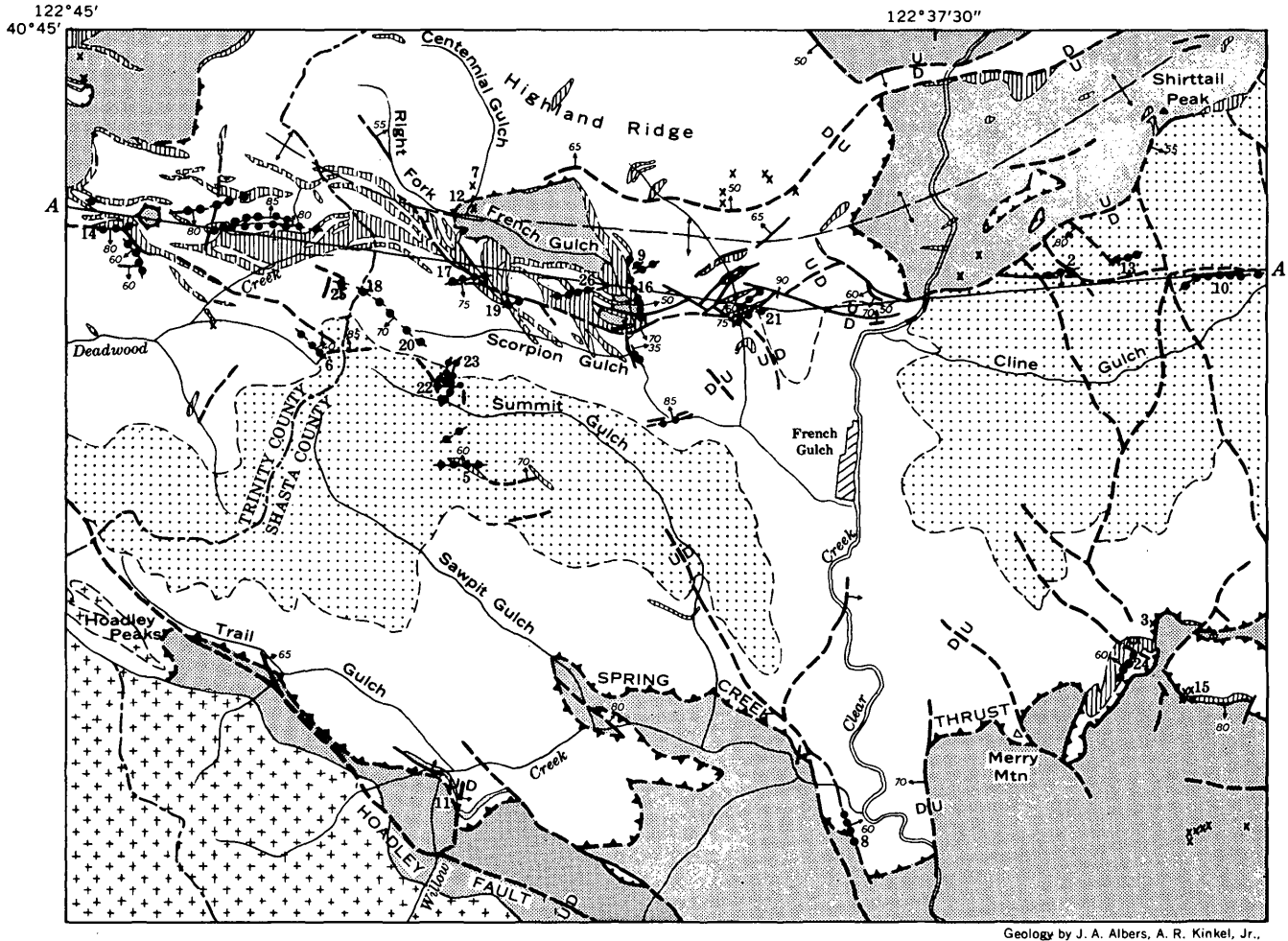

EXPLANATION

Diorite porphyry and quartz porphyry dikes and sills *Locally designated "birdseye" porphyry*

Shasta Bally batholith (quartz diorite)

Kennett(?) and Bragdon formations, undifferentiated *Upper conglomerate unit of Bragdon shown by stipple pattern*

Copley and Balaklala formations, undifferentiated

JURASSIC OR CRETACEOUS

DEVONIAN AND MISSISSIPPIAN

DEVONIAN(?)

Contact *Dashed where approximately located*

Approximate axis of arch

Fault, showing dip *Dashed where approximately located. U, upthrown side; D, downthrown side*

Quartz vein, showing dip

Spring Creek thrust beneath Bragdon formation *Dashed where approximately located*

Pit, trench, or adit

LIST OF MINES

1. Accident mine
2. American mine
3. Bright Star mine
4. Brown Bear mine
5. Brunswick mine
6. Calmich mine
7. Centenial mine
8. Eldorado mine
9. Franklin mine
10. Gladstone mine
11. Greenhorn mine (sulfide)
12. Honeycomb mine
13. JIC mine
14. Larry mine
15. Mad Mule mine
16. Milkmaid mine
17. Niagara mine
18. Niagara Summit mine
19. Philadelphia mine
20. Scorpion mine
21. Three Sisters mine
22. Summit mine
23. Tom Green mine
24. Truscott mine
25. Vermont and Montezuma mines
26. Washington mine

FIGURE 147.1.—Generalized geology of the French Gulch-Deadwood district and distribution of mines and prospects.

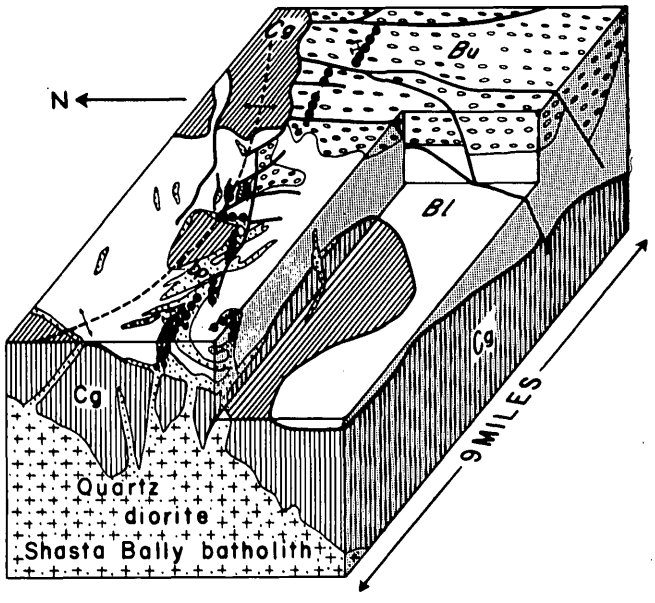

FIGURE 147.2.—Diagram showing relation of "birdseye" porphyry dikes and gold lodes to eastward-trending arch (dashed line) and to inferred subjacent salient of Shasta Bally batholith. Cg, Copley greenstone and Balaklala rhyolite; Bl, lower unit, Bragdon formation; Bu, upper unit, Bragdon formation; bp, "birdseye" porphyry. Brown Bear mine is at near end of diagram and Gladstone mine is at far end.

partly because the Bragdon formation was folded before the arch was formed. The arch seems to plunge at a low angle from the west edge of the area shown on the map (fig. 147.1) eastward to Clear Creek where it turns northeastward and rises again in Shirttail Peak. This rise is at least partly due to faulting. The arch is inferred to be underlain by a salient of the Shasta Bally batholith, which crops out 2 miles west of the map area. The marked mineralogical similarity between the dikes and the bathholith, the textural and mineralogical similarity of one dike to the batholith, and the arangement of the dikes parallel to the crest of the arch support this inference. Tension fractures that are roughly parallel in strike to the axis of the salient would be formed by the upward push of the magma, and become occupied by dikes and quartz veins as shown diagrammatically on figure 147.2.

The gold deposits are of two main types: (a) moderate to gently dipping quartz and quartz-calcite veins along the thrust contact below the Bragdon formation, and (b) steeply dipping quartz and quartz-calcite fissure veins in the Bragdon formation. "Birdseye" porphyry intrusives are commonly associated with both types, and, as the veins clearly cut the porphyry, they are younger. From veins of the first type has come most of the gold of the Washington mine and numerous small pocket deposits. Veins of the second type were mined at the Brown Bear, Niagara, American, Gladstone, and Summit mines. Ore shoots in the Brown Bear mine, from which over half the gold in the district has come, are mainly at intersections of veins with opposing dips or at the intersection of veins with contacts between shale and porphyry. The ore shoots are nearly horizontal, owing to the general parallelism in strike of the main structures. In the Niagara, American, and Summit mines ore shoots are also commonly at the intersection of veins with each other or with contacts between different rocks. In the Gladstone mine, for which we have only meager data, it seems likely that ore controls are similar. Where steeps veins cut the Copley greenstone, as in the Washington mine, they are commonly narrow and of poor grade, and only at the contact with the Bragdon and above have they been very productive.

The mineral composition of the veins shows little variation. Quartz is the chief gangue mineral; calcite and mica are present in minor amounts, and locally manganese oxide occurs near the surface. Pyrite, galena, sphalerite, arsenopyrite, and rarely chalcopyrite are sulfide minerals commonly present. Gold is in the sulfide minerals, but occurs mainly as free gold—much of it coarse enough to be seen with the unaided eye.

Much of the gold, reportedly, was along contacts between the veins and black slickensided graphitic shale, or associated with inclusions of graphitic shale in the vein. Hershey (1910, p. 741–742), Ferguson (1914, p. 40–43), and Emmons (1937, p. 35–36) have noted the importance of carbon or graphite as a precipitating agent for gold, and Hershey thought that the common localization of gold deposits along the contact between the Copley and Bragdon formations resulted from precipitation of gold being carried in ascending solutions when they passed from the Copley greenstone into the carbonaceous material at the Bragdon contact. Certainly the presence of the Washington mine and numerous small deposits at this contract suggest that the change in rock type was partly responsible for the localization of the gold. Inasmuch as the gold in the rich veins in the Bragdon came from ascending solutions, it represents a residue that must have come past the favorable contact, and the possibility of finding additional ore at depth in mines that have not penetrated to this contact appears promising. The depths to which mines have penetrated in relation to the inferred depth of the Copley contact are shown on the geologic section (fig. 147.3).

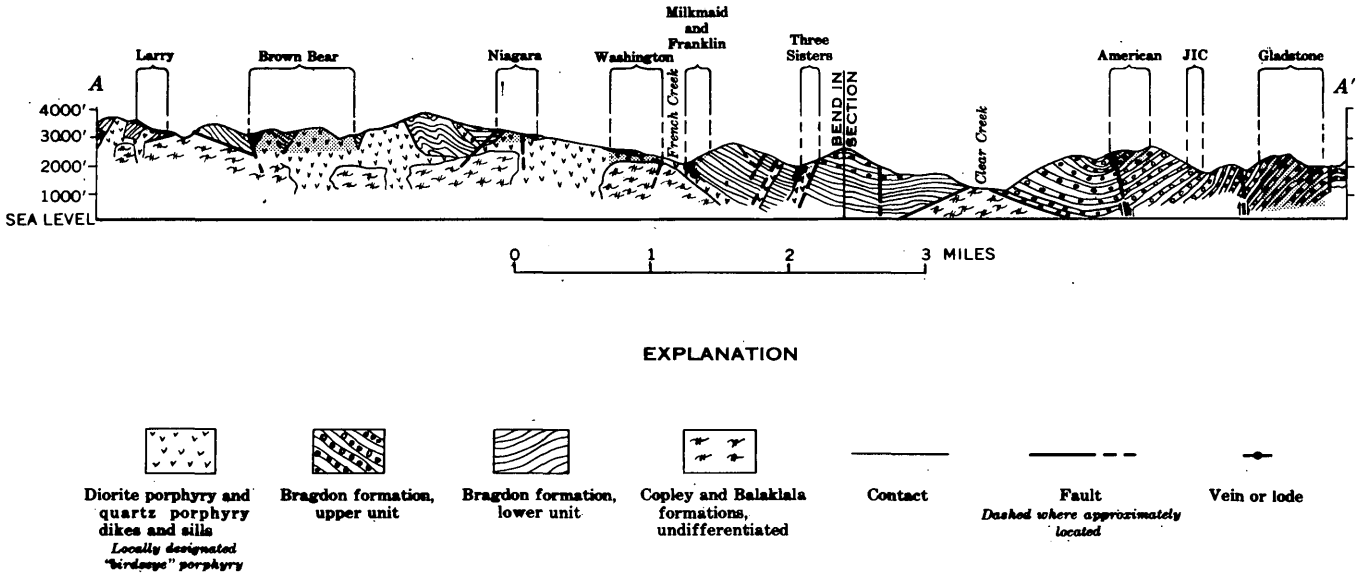

FIGURE 147.3.—Geologic section along French Gulch-Deadwood district. Approximate depth and lateral extent of workings (projected to plane of section) are shown by shaded areas.

As most of the mines were inaccessible during our field studies, for this report I have relied heavily on maps and private reports prepared during periods when the mines were in operation. I am most grateful to the property owners who have kindly made the information available to me.

REFERENCES

Emmons, W. H., 1937, Gold deposits of the world: New York, McGraw-Hill Book Co., Inc., 562 p.

Ferguson, H. G., 1914, Gold lodes of the Weaverville quadrangle, California: U.S. Geol. Survey Bull. 540, p. 22–79.

Hershey, O. H., 1910, Origin of gold pockets in northern California: Mining and Sci. Press, v. 101, p. 741–742.

148. PALEOTOPOGRAPHIC CONTROL OF A URANIUM MINERAL BELT, SHIRLEY BASIN, WYOMING

By E. N. HARSHMAN, Denver, Colo.

The Shirley Basin, about 35 miles south of Casper, Wyo., contains one of the major uranium ore reserves in the United States. Geologic studies of the basin have established a relation between the pre-Wind River topography and a mineral belt containing the major uranium deposits.

At least 5,000 holes have been drilled in the Shirley Basin; most of them penetrated Cretaceous rocks that underlie the ore-bearing Wind River formation. Drill cuttings from about 800 of these holes have been logged by Geological Survey personnel; and lithologic, gamma ray, and resistivity logs of additional holes have been made available to the Geological Survey by mine operators in the basin. These data are the basis for a paleotopographic map of the eastern part of the Shirley Basin and for conclusions about factors that may have controlled deposition of the major ore bodies.

The Wind River formation of Eocene age, host for the Shirley Basin uranium deposits, consists of intertonguing and interbedded compacted but uncemented or poorly cemented gravel, sand, silt, and clay of continental origin. It is overlain unconformably by tuffaceous claystone, siltstone, and sandstone of the White River formation of Oligocene age; but along the north rim of the basin, conglomerate, sandstone,

and tuff of the Arikaree formation, Miocene in age, overlie the White River rocks. The Tertiary strata have been tilted about 1° north.

Most of the Wind River sediments were derived from granitic rocks west and (or) southwest of the Shirley Basin. They were deposited in a low area that was eroded in Cretaceous and older rocks and that lay between the Laramie Mountains to the northeast and the Shirley Mountains to the southwest.

Individual uranium deposits in the Shirley Basin contain from a few thousand to several hundred thousand tons of ore. Material now being mined contains about 0.60 percent U_3O_8, and selected samples contain as much as 10 percent U_3O_8. The ore is unoxidized. It is from 100 to 500 feet below the ground surface and from a few to 400 feet below the present water table. The ore-bearing zones are predominantly coarse- to medium-grained sandstone; however, silt and clay are present in appreciable amounts. Crossbeds, sand-filled channels, cut banks, carbonized plant debris, and other features common to most uranium deposits in sandstone characterize the ore zones in the Shirley Basin.

Mineralogic studies of a few high-grade ore samples show the uranium mineral to be fine-grained uraninite associated with fine-grained pyrite, marcasite, and organic material. Uraninite coats sand grains, fills interstices between grains, and occasionally fills fractures in sand grains.

Figure 148.1 (p. C–6), a generalized paleotopographic map of the eastern part of the Shirley Basin, shows a prominent ridge on the pre-Wind River erosion surface. This ridge is held up by the indurated Wall Creek sandstone member at the top of the Frontier formation of Late Cretaceous age. In the mapped area, the ridge is buried 125 to 350 feet deep by Wind River and (or) White River strata. One mile southeast of the mapped area the Tertiary formations are eroded away, and the ridge is a conspicuous feature of the present landscape. Where exposed, the Wall Creek sandstone member strikes about N. 35° W. and dips 6° SW.; drill-hole data indicate a smiliar strike but slightly flatter dip for the rocks in the buried extension of the ridge. In the northern part of the basin the buried ridge has a relief of about 400 feet; southward the relief gradually decreases to about 100 feet. The buried part of the ridge has been breached by ancient drainage channels in at least two areas.

The largest and highest grade uranium deposits now developed in the Shirley Basin are in a belt that lies along the west slope of the buried ridge (fig. 148.1). Although simple in plan view the belt is composite, consisting of an upper and lower ore zone separated by silty clay 50 to 75 feet thick. In the northern part of the belt the larger deposits are in the upper zone; in the southern part they are restricted to the lower zone. Most of the ore deposits in the mineral belt lie below the elevation of the crest of the ridge.

The buried ridge is believed to have controlled the position of the belt of favorable Wind River strata. Streams originating west of the ridge and flowing easterly were diverted parallel to the ridge and deposited sediment against it. Early in the cycle of basin filling, swampy flood-plain conditions developed near the west toe of the ridge; these conditions persisted until the ridge was buried by Wind River sediments. Burial was accomplished in relatively early Wind River times in the southern part of the area where the ridge was low and in late Wind River times in the northern part where the ridge was high. As a result of the depositional environment, strata just west of the ridge consisted of permeable sand interbedded with silt, clay, and organic material, an ideal environment for subsequent deposition of uranium.

In addition to its influence on Wind River lithology, the ridge diverted eastward-flowing uranium-bearing ground water through the chemically and physically favorable belt of Wind River strata. The combination of favorable ground and the migration of uranium-bearing ground water through it is believed to have resulted in the present mineral belt and its large high-grade uranium deposits.

Other deposits have been discovered in the Shirley Basin both east and west of the belt where physical and geochemical conditions locally were favorable for uranium deposition.

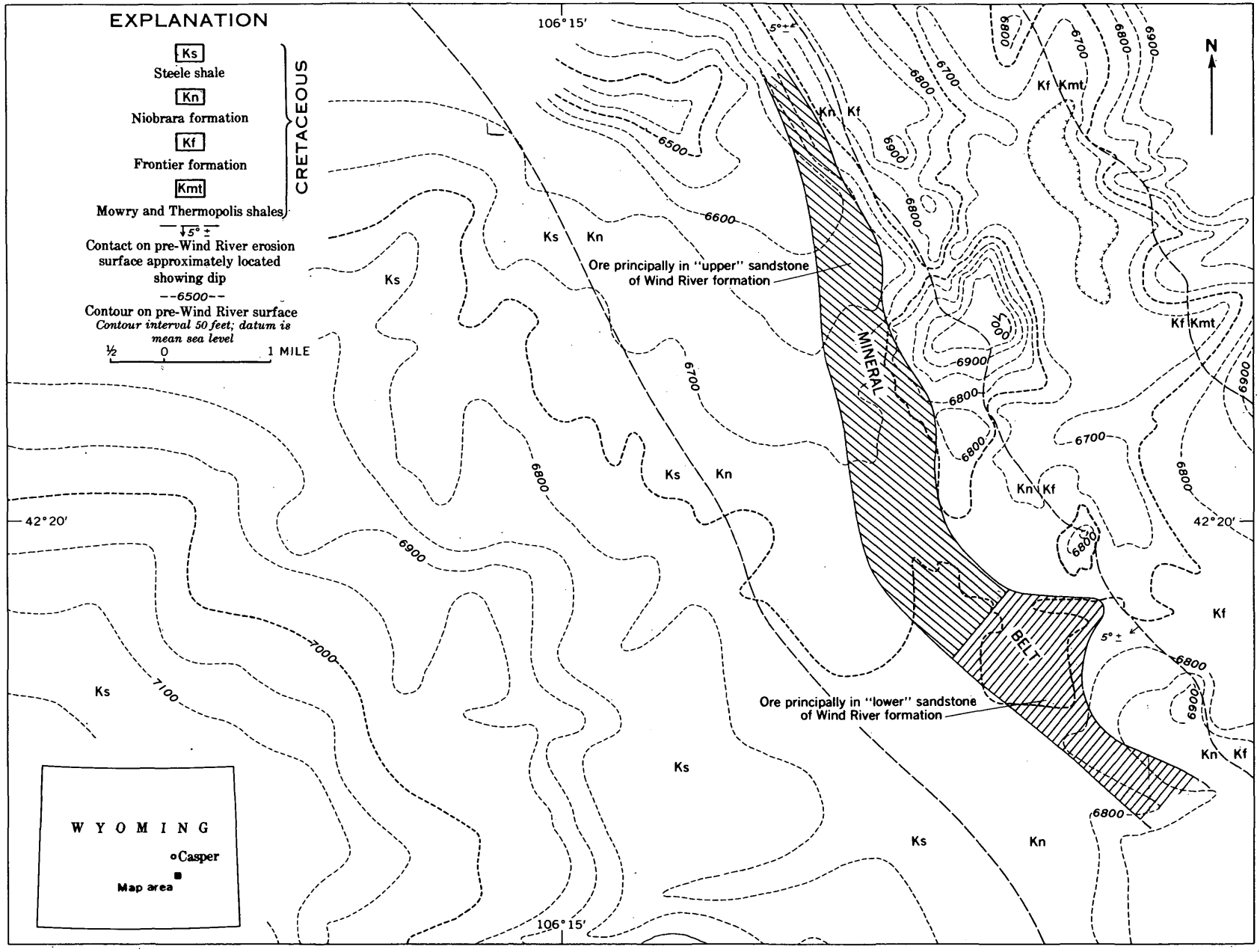

FIGURE 148.1.—Generalized paleotopographic map of the eastern part of the Shirley Basin, Wyoming, showing relation of a mineral belt to the pre-Wind River erosion surface, and paleogeology.

149. ORIGIN AND EVOLUTION OF ORE AND GANGUE-FORMING SOLUTIONS, SILVERTON CALDERA, SAN JUAN MOUNTAINS, COLORADO

By WILBUR S. BURBANK and ROBERT G. LUEDKE, Exeter, N.H., and Washington, D.C.

Work done in cooperation with the Colorado State Metal Mining Fund Board

Comparative evolutions of vein, chimney, and hot-spring deposits about the Silverton caldera indicate considerable mixing of primitive ore-forming solutions with solutions containing end-products of rock alteration and with meteoric waters. Gangue-rich vein deposits and sulfide-rich and gangue-poor chimney deposits were formed.

This outline omits supporting evidence for some assertions and includes speculations not susceptible of proof, but it affords a working hypothesis that has proved of value in a continuing study of the ore deposits.

The setting of the ore deposits (fig. 149.1) comprises a volcanic pile of Tertiary age, a mile or more thick and aggregating more than a thousand cubic miles in volume, centering about the Silverton caldera. Following a late volcanic caldron subsidence within the caldera bounds, the central complex and its surroundings were subjected to igneous intrusion of deep origin, arching of the formations, radial fissuring, and a final collapse that resulted in radial and peripheral graben structures. Radial fissures were invaded in turn by igneous dikes, by injections of clastic debris, and by numerous stages of vein-forming solutions that yielded the compound type of veins illustrated in figure 149.2.

In certain belts where tensional stresses were evidently minimized, both intrusive bodies and later ore deposits tended to assume pipelike or chimney forms (fig. 149.1).

Gangue minerals commonly were deposited first upon each reopening of fissures and were followed by sulfides mixed with gangue or devoid of gangue. The first-stage gangues are commonly quartz (rarely carbonate, fig. 149.2*B*), followed by the bulk of the base-metal sulfides. In some veins of outer zones, barite is an early mineral, but not uncommonly it is partly or largely replaced by quartz. Rhodochrosite (or manganocalcite) is here later than barite. Where inner and outer zones overlap, early quartz and sulfides have preceded barite and sulfides. Rhodonite gangue follows early quartz and the bulk of the base-metal sulfides (fig. 149.2*A*). Additional quartz and sulfides, locally with adularia, fluorite, and carbonate, follow. In more complex manganese silicate gangues, friedelite and tephroite are early, but later reaction with SiO_2 forms rhodonite, or reaction with CO_2 forms rhodochrosite (Burbank, 1933). Free gold and silver-rich sulfosalts generally accompany later gangue assemblages, and barren quartz-calcite or quartz may terminate vein formation. Traces of fluorite are common with quartz intergrown with sulfides, but the fluorite may be partly leached or replaced by quartz. Sparse hubnerite is associated locally with late quartz-pyrite gangue. Sericite is a common alteration product of early vein stages and clay minerals of later ones, but zonal alteration also developed in vein walls.

In chimney deposits the massive sulfides with some intergrown barite, sericite, and clayey products of rock decomposition fill leached cavernous openings in silicified rocks (fig. 149.3). A little late fluorite, rhodochrosite, and free gold occur in some deposits, and fluorite is locally capped with gypsum. Enargite is a common copper mineral of chimneys but not of veins.

Certain events of vein evolution may be correlated with the then-existing environment by reference to figure 149.3. Accompanying late intrusions of gabbroic and granodioritic magmas, the caldera core and its surroundings were invaded by gases and solutions causing widespread pre-ore propylitization of the rocks (Burbank, 1960). Initial openings of fissures resulted in explosive injections of clastic dikes, indicating that a considerable pressure of fluids had been built up in the root zones. With succeeding reopenings, at diminished pressures, the fluids in fractured rocks were forced by expanding gases into newly formed spaces, carrying with them fractionated end-products of rock decomposition. These solutions in considerable part yielded the early gangues that followed fissure openings. Solutions from deeper magmatic sources, which had little (if any) role in propylitic alteration, then entered the partly gangue-choked fissures, mixing to some extent with solutions from altered rock, and deposited sulfide and sulfide-gangue ores. As these mixed solutions reached the levels of meteoric circulation in fissures, partial oxidation and further dilution took place. Certain geochemical

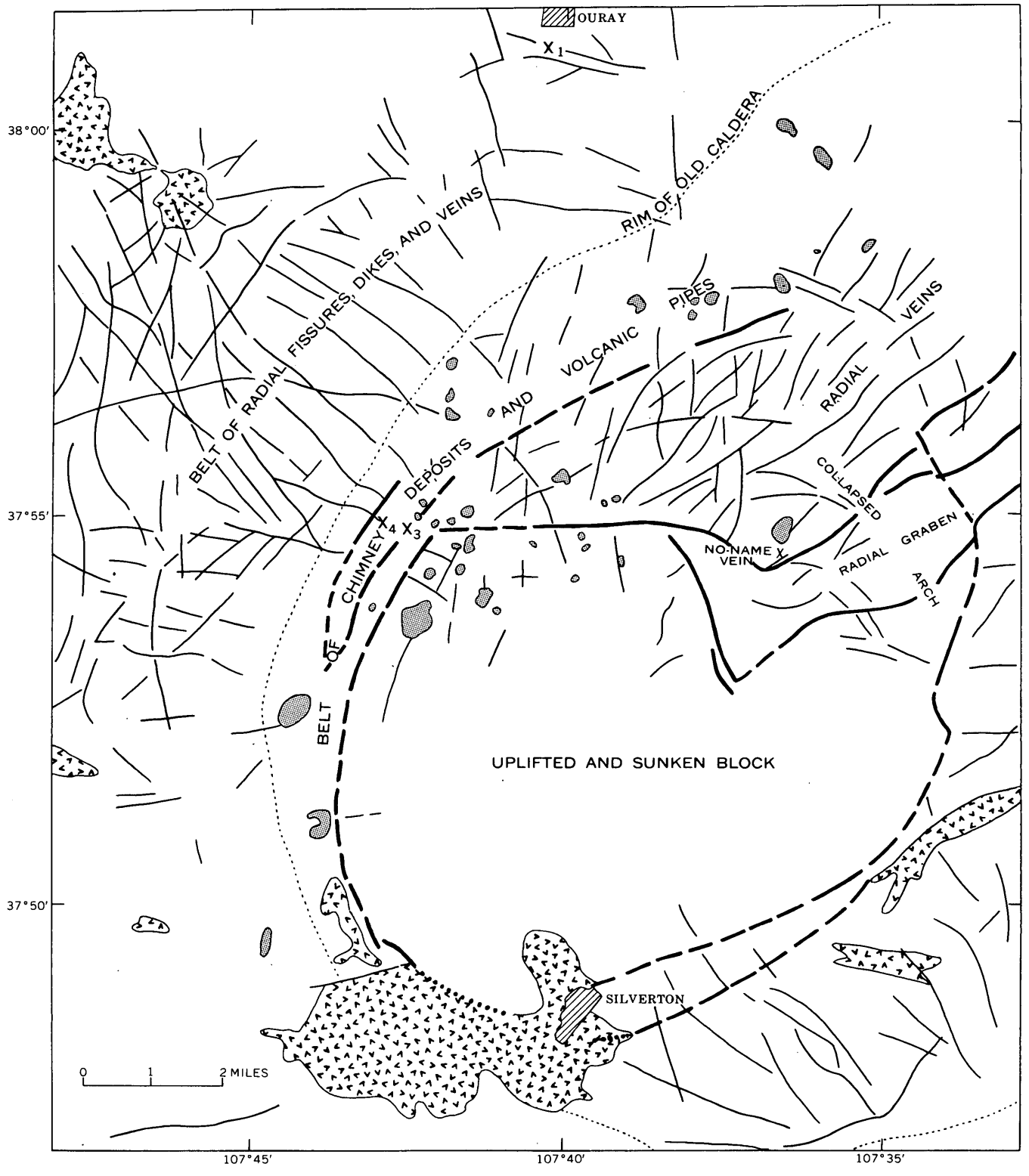

FIGURE 149.1.—Structural map of Silverton caldera and vicinity. Larger intrusive bodies, V-pattern; volcanic pipes, stippled pattern; faults, heavy lines; dikes and veins, light lines; locations of hot spring and meteoric water samples, X. Uplift of caldera core and northeast arch and their subsequent collapse caused compression along rim belt. Magmas and ore solutions worked upward along narrow vertical channels as contrasted with outer belts of tensional stresses.

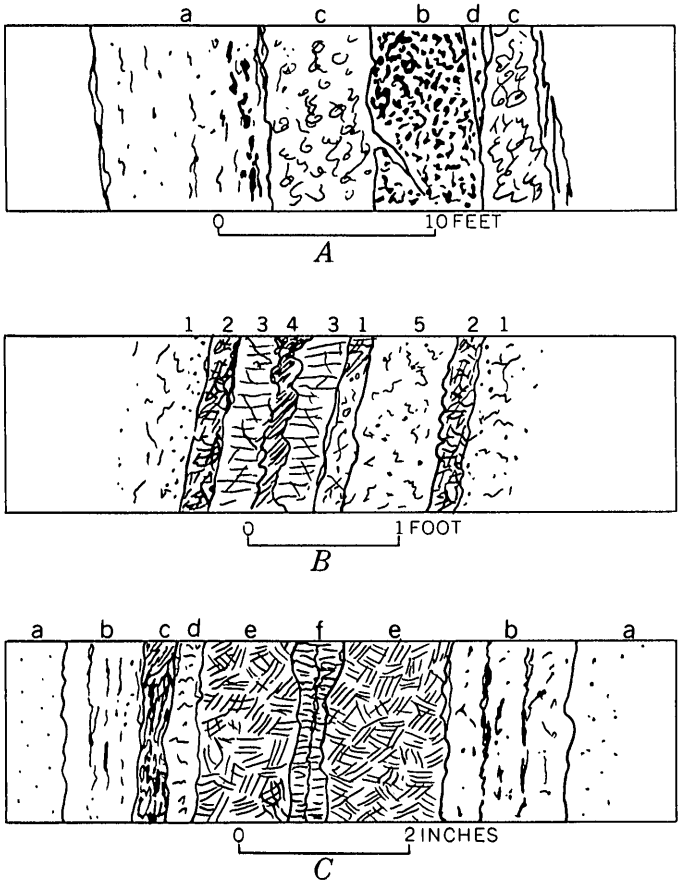

FIGURE 149.2.—Macro-structures of compound veins, Silverton caldera. *A*, No-Name vein, Eureka Gulch, northeast graben area; a, coarse quartz with pyrite and a little sphalerite; b, mainly sphalerite, chalcopyrite, and galena intergrown with quartz (50 to 70 percent sulfides by weight); c, rhodonite ribs with patches of tephroite, friedelite, and carbonate; d, quartz. *B*, Mendota vein, Telluride district, outer northwest radial vein systems (after Purington, 1898); 1, country rock, pyritized and sericitized near walls; 2 (left) sphalerite with calcite; 2 (right) sphalerite and galena; 3, white quartz; 4, rhodochrosite; 5, bluish quartz with finely disseminated sulfides and sulfosalts. *C*, London vein, Mineral Point, northeast radial vein system (after Ransome, 1901); a, country rock; b, quartz and chalcopyrite; c, tetrahedrite; d, quartz; e, galena; f, quartz.

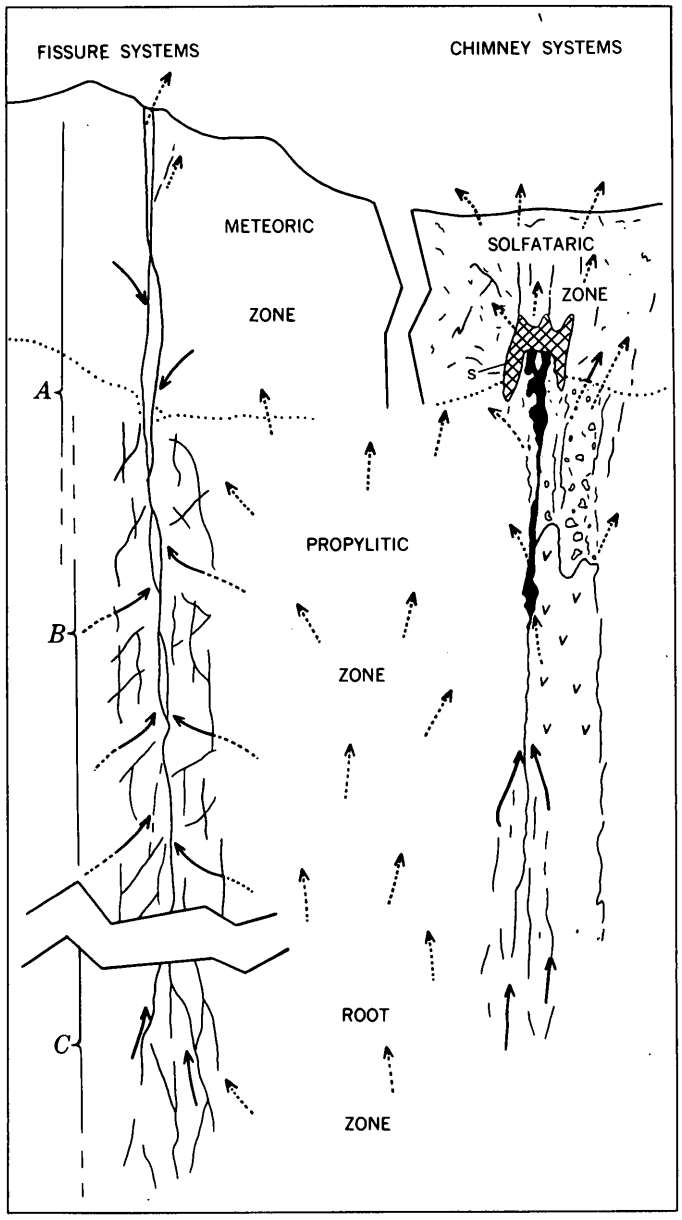

FIGURE 149.3.—Depth zones in fissure and chimney systems of Silverton caldera mineralized belts. *A*, Zone of mixing of mineralizing solutions with partly oxygenated meteoric waters (locally 3,000 to 4,000 feet deep); *B*, zone of influx of fractionated end-products of rock alteration and of mixing with meteoric waters from above and sulfide solutions from below; *C*, zone of influx of primitive ore solutions and products of deep rock alteration. Chimney deposits are in rocks locally preheated by volcanic pipes, with only minor influx of solutions from zone *B*. Chimney feeders are not reopened as frequently as feeders of fissure systems. S, siliceous envelope of altered and mineralized ground; black areas indicate sulfide deposits. Propylitic zone represents rocks charged with carbon dioxide and other gases under pressure, coming from deep-seated sources of caldera core. Dotted arrows indicate general movements of gases, solid arrows movement of solutions.

depth zones were thus established in the vein channels (fig. 149.3).

Igneous emanations causing propylitization consisted largely of CO_2, H_2O, minor H_2S, and presumably halogens, but much of the sulfur evidently remained behind in complexes of the sulfide solutions at their sources. Processes in the root zones and walls of fissures involving these early fluids would have certain predictable effects on the evolutions of gangue-forming solutions. (a) Release of gases from altering solutions would tend to fractionate solutions as

601530 O—61——2

they moved towards the fissures, leaving behind less soluble substances. (b) Solid solution and decomposition (as in carbonates) and reaction relations in other mineral series would tend to enrich escaping solutions in certain constituents. For example, Ca–Mn mixed carbonates subjected to isothermal loss of CO_2 pressure tend to become depleted in the Mn molecule, which is enriched in any fluid remainder (Goldsmith and Graff, 1957). The formation of pyrite and chlorite would tend to fix Fe and Mg. Thus, remaining solutions, highly fractionated and subjected to mixing or reaction with siliceous solutions or minerals, could form the manganese silicate gangues or the manganese oxides of hot-spring deposits (analysis 1, table 149.1; analyses 1 to 3, 5, table 149.2).

The early quartz of the base-metal stage (fig. 149.2) could result from attack of CO_2 solutions on ferromagnesian minerals with formation of mixed carbonates and release of silica (Knopf, 1929, p. 44–45). Source rocks at depth accordingly might have been partly desilicated prior to secretion of manganese. Early tephroite and friedelite of the manganese silicate suite indicate that initial solutions were locally deficient in silica. Fluorides seem unaccountably late in many vein sequences and in their continuing deposition from Recent hot-spring waters (analysis 2, table 149.1; analysis 4, table 149.2). The association of early barite with fluorite, creedite, and gearksutite in the vein at Wagonwheel Gap (Emmons and Larsen, 1913, Larsen and Wells, 1916), and the presence of some H_2S in associated hot-spring waters (analysis 2, table 149.1) are permissive evidence that partial oxidation of H_2S could have taken place. Thus, some fluorine may have been leached by action of nascent SO_4—on wall rocks or on earlier sericite and fluorite gangue of deeper vein zones. But part of sulfate in spring waters is probably of connate or meteoric origin (analyses 3 and 4, table 149.1) and some possibly of magmatic origin. Leaching of fluorite and its replacement by quartz, noted in late Tertiary veins, also indicates that fluorine in its various mineral associations advanced surfacewards by repeated deposition and resolution. The same is true in some degree for barium.

Comparison of bulk composition of oxide deposits of Ouray hot springs with manganese silicates of the No-Name vein (analyses 1–3, 5, table 149.2) indicates that the spring waters could be similar to those of the gangue solutions of the veins, except in degree of dilu-

TABLE 149.1—*Chemical analyses of some hot-spring and meteoric waters of the Silverton caldera, San Juan Mountains, Colo.*

[In parts per million; ----, not looked for]

	Ouray hot spring	Wagonwheel Gap hot spring	Treasury Tunnel meteoric waters	
	Sample 1	Sample 2	Sample 3	Sample 4
SiO_2	49	92	96	47
Fe	.42	.02	.36	.36
Mn	.92	.31	.2	----
Ca	376	67	310	44.7
Mg	6.1	0	13.5	5.6
Na	111	477	126.5	169.2
K	8.0	40	21.5	54
Li	1.0	2.3	----	----
HCO_3	128	1,020	48	98.2
SO_4	1,030	169	990	477
Cl	45	206	1.4	1.0
F	3.0	6.8	----	----
PO_4	.06	.11	----	----
B	.23	6.8	----	----
H_2S	.0	.7	----	----
Solids	1,760	1,560	1,630	990
pH	6.8	6.7	----	----
Temperature	143°F	144°F	cold	cold
Discharge	15 gpm	20 gpm	----	----

Sample 1; lab. no. 850; H. C. Whitehead, analyst; collected by D. E. White and R. W. Lakin.
Sample 2; lab. no. 849; H. C. Whitehead, analyst; collected by D. E. White and R. W. Lakin.
Sample 3; lab. no. 6456: E. T. Erickson, analyst; collected by W. S. Burbank: from fissure 1,390 feet from portal Treasury Tunnel (about 650 feet vertically underground).
Sample 4: lab. no. 6458; E. T. Erickson, analyst; collected by W. S. Burbank; from fissure vein 2,864 feet from portal Treasury Tunnel (about 800 feet vertically underground).

TABLE 149.2.—*Semiquantitative spectrographic analyses of hot-spring deposits and of manganese silicate gangue of late Tertiary veins, San Juan Mountains, Colo.*

[In percent: M, greater than 10 percent; ----, not looked for; (a) not detectable, wet chemical tests]

	Ouray hot springs			Wagonwheel Gap	No-Name vein
	Sample 1	Sample 2	Sample 3	Sample 4	Sample 5
Si	----	X	----	----	M
Al	----	.X	----	----	.3
Fe	7.0	X	0.7	----	.15
Mg	.15	----	.07	----	.3
Ca	----	X	----	----	.7
Na	----	.X	----	----	.0
K	----	----	----	----	.0
Mn	15.0	XX	30	----	M
Ag	----	----	----	----	.003
Ba	.7	X	.7	0.045	.0
B	----	----	----	----	.007
Be	.015	.0X	.001	----	.0003
Cu	.0015	.0X	.03	(a)	.015
Pb	.07	.00X	.7	(a)	.3
Sb	.02	.0X	.3	----	.0
Zn	.02	.0X	.2	.007	.15
W	.2	X	1.0	----	.0
F	----	----	----	.22	----

Sample 1; lab. no. 58–1145; U. Oda, E. F. Cooley, analysts; collected by D. E. White and R. W. Lakin; from material being deposited at time of sampling, Pavillion spring.
Sample 2; lab. no. 52–1637; R. C. Havens, analyst; collected by W. S. Burbank and C. T. Pierson; from old travertine, Pavillion spring.
Sample 3; lab. no. 58–1139; U. Oda, E. F. Cooley, analysts; collected by D. E. White and R. W. Lakin; from oxide vein in fissure occupied by hot waters.
Sample 4; Wagonwheel Gap; George Steiger, analyst; Emmons and Larsen, 1913; travertine.
Sample 5; lab. no. 287139; N. M. Conklin, analyst; collected by W. S. Burbank and R. G. Luedke· manganese silicate gangue from 5-foot rib of vein (fig. 149.2*A*), Sunnyside mine, northeast graben area (fig. 149). Chemical analysis of a separate sample from a dump, representing considerable early friedelite and tephroite with rhodonite and selected for volatile determinations gave (in percent): Mn, 40.4; As, 0.043; CO_2, 0.30; total S, 0.18; sulfide S, 0.04; H_2O+, 3.94; H_2O-, 0.05; P_2O_5, 0.01; Cl, 0.64; F, 0.21; E. J. Fennelly, I. C. Frost, D. L. Skinner, E. L. Munson, analysts.

tion and oxidation. An exception is tungsten in the oxides but not in the silicates, perhaps indicative that leaching of previously formed gangue assemblages could be a factor in origin of the hot-spring waters.

The overall low base-metal content of some vein gangues and spring deposits is consistent with a low sulfide content of corresponding gangue-forming solutions; hence a different source for these solutions is suggested from those forming the bulk of the sulfides. It is noteworthy that in chimney channels, where reopening and pressure release were minimized, the ore deposits are characteristically low in gangue content. These ore solutions, coming directly from depth with less dilution from wall-rock sources, deposited chiefly sulfides with abrupt loss of pressure in shallow ground and with partial mixing with oxygenated waters of the solfataric zone. These more primitive sulfide solutions contained considerable H_2S as shown by widespread pyritic and solfataric alteration of the enclosing rocks.

REFERENCES

Burbank, W. S., 1933, The manganese minerals of the Sunnyside veins, Eureka Gulch, Colorado: Am. Mineralogist, v. 18, p. 513–527.

——— 1960, Pre-ore propylitization, Silverton caldera, Colorado, *in* Short papers in the geological sciences: U.S. Geol. Survey Prof. Paper 400–B, p. B12–B13.

Emmons, W. H., and Larsen, E. S., 1913, The hot springs and mineral deposits of Wagonwheel Gap, Colo.: Econ. Geology, v. 8, p. 233–236.

Goldsmith, J. R., and Graff, D. L., 1957, The system CaO–MnO–CO_2; solid solution and decomposition relations: Geochim. et Cosmochim. Acta, v. 11, p. 310–334.

Knopf, Adolph, 1929, The Mother Lode system of California: U.S. Geol. Survey Prof. Paper 157, 88 p.

Larsen, E. S., and Wells, R. C., 1916, Some minerals from the fluorite-barite vein near Wagonwheel Gap, Colo.: Natl. Acad. Sci. Proc., v. 2, p. 360.

Purington, C. W., 1898, Preliminary report on the mining industries of the Telluride quadrangle, Colorado: U.S. Geol. Survey Ann. Rept. 18, pt. 3, p. 745–748.

Ransome, F. L., 1901, A report on economic geology of the Silverton quadrangle, Colorado: U.S. Geol. Survey Bull. 182, 265 p.

150. GEOLOGIC EVENTS CULMINATING IN PRIMARY METALLIZATION IN THE CENTRAL MINING DISTRICT, GRANT COUNTY, NEW MEXICO

By W. R. Jones, R. M. Hernon, and W. P. Pratt, Denver, Colo.

In the Central mining district of New Mexico, where recorded production of minerals now exceeds one billion dollars, a sequence of geologic events in the interval between Late Cretaceous and Miocene time culminated in the formation of ores of iron, copper, zinc, lead, molybdenum, and silver.

Although the age of primary metallization is not known in terms of years or even in terms of the early Tertiary epochs, there being no strata of these epochs present, it is known relative to a sequence of rocks intruded within the Late Cretaceous to Miocene time interval. Some 30 or more distinct varieties of intrusive rocks, assignable to four age groups, have been recognized in the district. From oldest to youngest, these groups are:

1. Generally concordant plutons—thin and thick sills, laccoliths, and bysmaliths.
2. Mafic plugs and dike swarms spatially and temporally related to mafic flows and breccia.
3. Discordant plutons—stocks and apophyses and upward-flaring masses.
4. Dike swarms and plugs.

Few age relations are known between units of groups 1, 2, or 3 owing to the lack of cross-cutting relations. However, relative ages of units of group 4 are well established; the units are assignable to five subgroups, which are, from oldest to youngest:

1. Granodiorite porphyry dikes (2 or 3 varieties).
2. Quartz monzonite porphyry dikes (1 variety).
3. Quartz latite porphyry of the Republic and Turnerville dike complexes (1 or 2 varieties).
4. Quartz latite porphyry plugs and dikes (3 or 4 varieties).
5. Rhyodacite porphyry plug and dikes (3 or 4 varieties).

The ranges in modal and normative composition of several rocks of the four groups are shown on figure 150.1. The distribution of the four main age groups

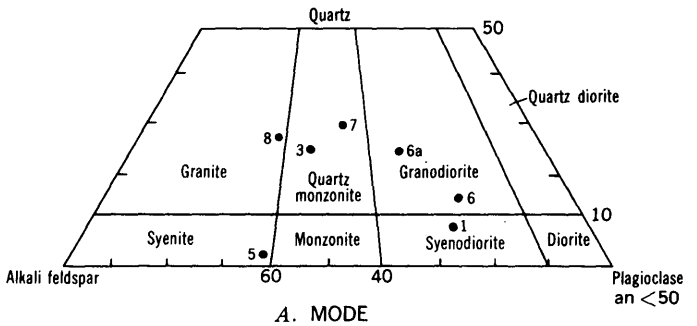

A. MODE

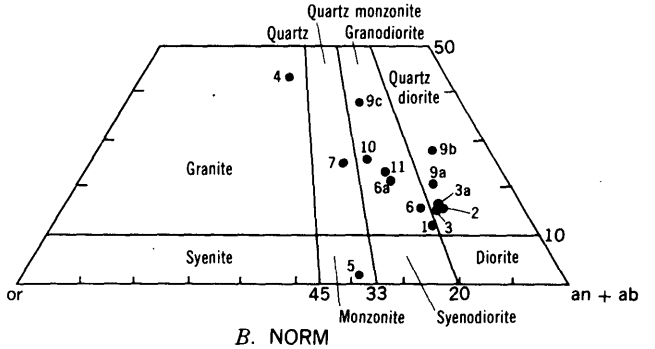

B. NORM

Concordant plutons Age group 1
- 1. Syenodiorite porphyry
- 2. Quartz diorite porphyry
- 3., 3a. Hornblende quartz diorite porphyry
- 4. Rhyolite porphyry

Mafic plutons Age group 2
- 5. Calcitrachyte porphyry

Discordant plutons Age group 3
- 6., 6a. Granodiorite of Hanover-Fierro pluton 6. South lobe; 6a. main mass.
- 7. Quartz monzonite of Santa Rita stock
- 8. Quartz latite of Copper Flat pluton

Dike swarms and plugs Age group 4
- 9a., 9b., 9c. Granodiorite porphyry dikes
- 10. Quartz monzonite porphyry dike
- 11. Rhyodacite porphyry dike (post ore)

FIGURE 150.1.—Modes and norms of some intrusive rocks in the Central mining district, Grant County, N. Mex. Limiting proportions in modal plot, *A*, are those used by Nockolds (1954); limiting proportions in normative plot, *B*, are derived empirically from plot of Nockolds' average norms.

at the present level of truncation is shown on figures 150.2 and 150.3.

The groups and units of the intrusive sequence serve as time-markers within the Late Cretaceous-Miocene interval and reveal stages of folding, faulting, and mineralization that otherwise might appear to have occurred during a single episode. Use of the intrusive sequence for chronological purposes is beset, of course, by several inherent difficulties and must be supplemented by geological reasoning.

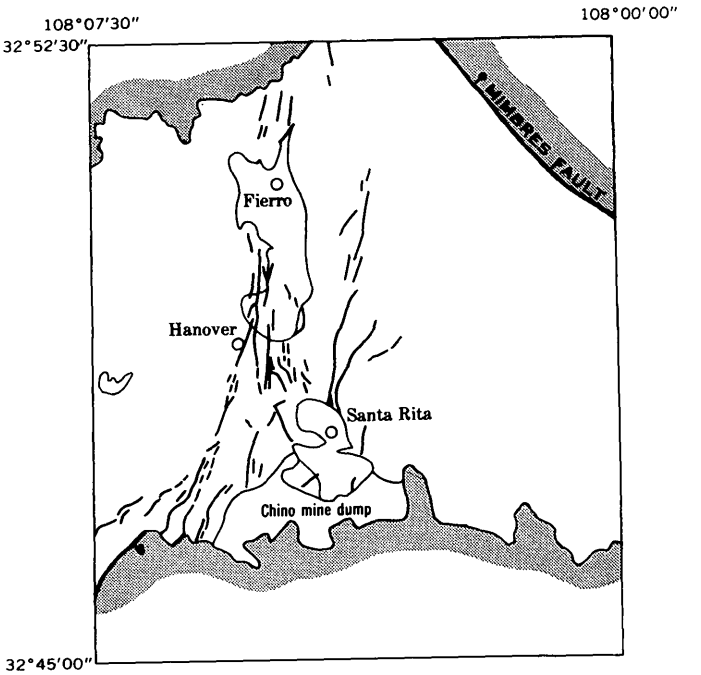

A. Granodiorite porphyry dikes

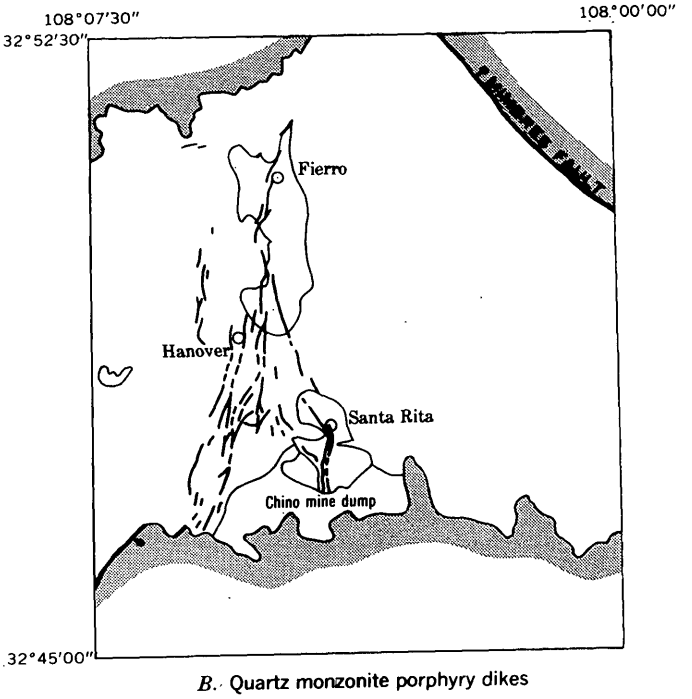

B. Quartz monzonite porphyry dikes

EXPLANATION

Edge of Miocene and younger rocks

0 1 2 MILES

FIGURE 150.2.—Granodiorite porphyry and quartz monzonite porphyry dike swarms within Santa Rita quadrangle, New Mexico.

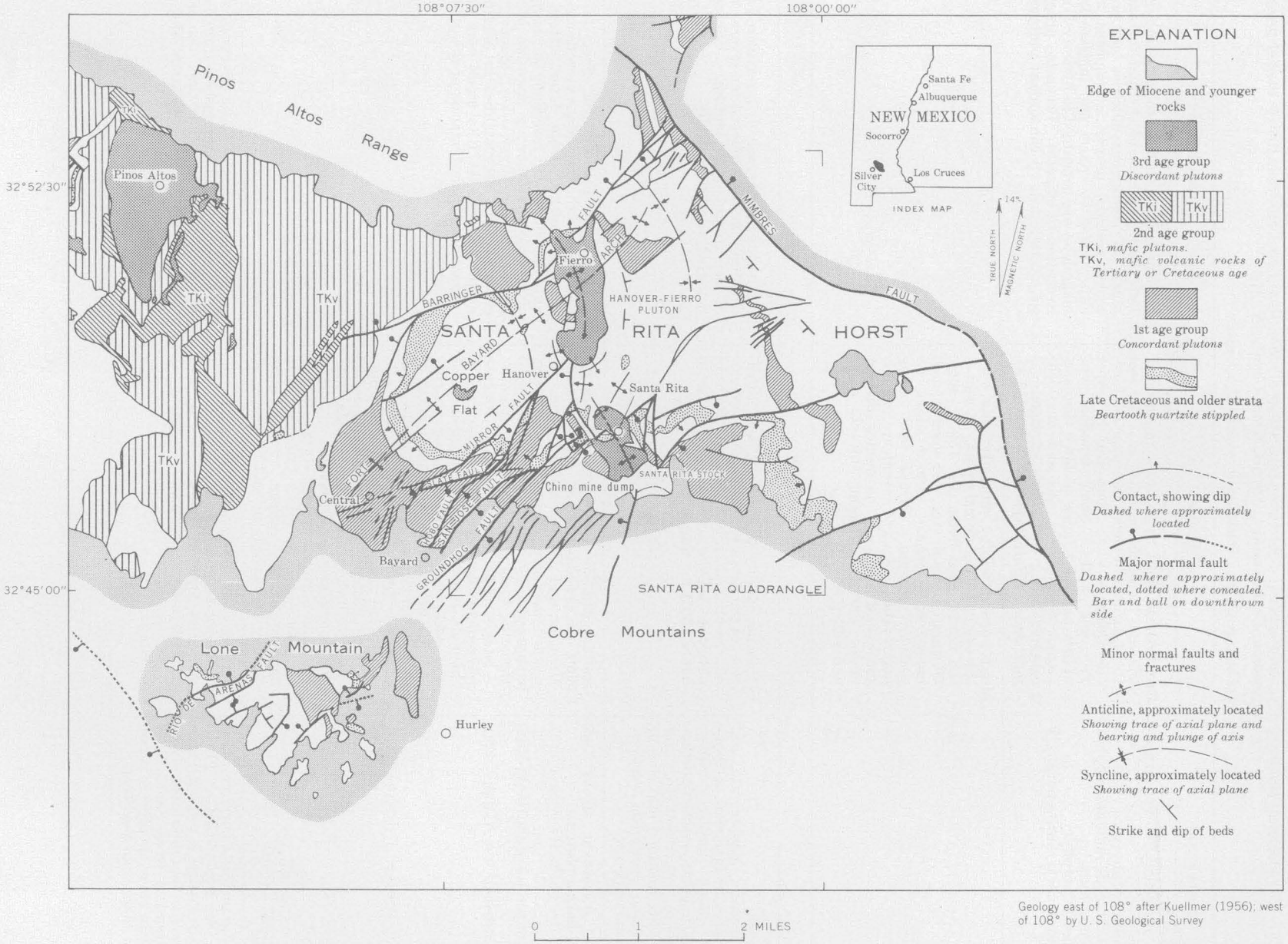

FIGURE 150.3.—Structural setting of the Central mining district, Grant County, N. Mex.

TABLE 150.1.—*Chronological summary of igneous activity, deformation, and mineralization from Late Cretaceous time to time of primary ore deposition, Central mining district, Grant County, N. Mex.*

[Earliest events at top of table; most recent events at bottom]

Igneous activity	Deformation	Mineralization
Intrusion of generally concordant plutons: Syenodiorite porphyry Augite-hornblende andesite porphyry Rhyolite porphyry Quartz diorite porphyry Hornblende-quartz diorite porphyry	Great domal uplift by multiple injection of sills and laccoliths as much as 1,100 feet thick, largely in shales of Upper Cretaceous Colorado shale, but also in upper Paleozoic strata. Some trapdoor-type uplifts produced faults of large displacement. Overlapping sills and laccoliths centered along line south of Barringer fault underlie Fort Bayard arch (fig. 150.3).	Alteration largely confined to the porphyries. Very little evidence of thermal metamorphism of contiguous siliceous carbonate rocks; residual interstitial aqueous fluid either failed to collect and migrate from magma or was consumed in hydrolysis and hydration of silicates. Pervasive propylitic alteration in all concordant plutons.
	Major normal faulting, and differential subsidence in area of domal uplift. Result is the Santa Rita horst (fig. 150.3), some 40 square miles in area, and several small horsts and grabens formed along its southern margin. Strata bent along major faults. Area of subsidence extends south and north of the mining district under younger Miocene volcanic rocks and valley-fill.	
Erosional epoch		
Volcanic epoch: Andesite breccia, agglomerate, and mafic flows, and intrusion of thousands of mafic porphyry dikes. Plugs and irregular plutons of orthoclase gabbro, calcitrachyte, and augite syenite intruded into core of great volcano centered west of Central mining district.	Fracturing largely to the west and northwest of the Santa Rita horst, development of radial and broad arcuate fracture patterns. (Dike swarms omitted from figure 150.3 for simplicity.)	Andesite breccia pervasively propylitized and thermally metamorphosed for several tens of feet around mafic plutons; zeolite and hematite alteration locally.
Intrusion of discordant stocks and upward-flaring plutons: Granodiorites of the Hanover-Fierro pluton. Quartz monzonites of the Santa Rita stock. Quartz latites of the Copper Flat pluton.	Great deformation caused by forcible intrusion of granodiorite in area between Hanover and Fierro; earliest surge expanded just below level of present surface, compressing strata in peripheral folds and thrusting them outward a short distance. A later, stronger surge created an elongate piercement dome normal to the axis of the Fort Bayard arch; strata along west and east margins were turned sharply upward and thinned. Emplacement of quartz monzonite stock at Santa Rita created a northwest-trending dome and obliterated several major faults, but, unlike the Hanover pluton, barely reached the level of the present surface; pulsations during emplacement brecciated large area west and northwest of the stock. Surges of magma at Copper Flat expanded near level of present surface, causing some doming and folding in wall rocks.	Any thermal or metasomatic effects in the wall rocks of the discordant plutons cannot be distinguished from later effects of hypogene fluids that rose along the margins of the plutons following intrusion of the granodiorite porphyry dikes. Some chalcopyrite blebs disseminated in unaltered parts of the Santa Rita stock may have formed during consolidation of the quartz-orthoclase matrix.
Intrusion of grandiorite porphyry dike swarm. (See fig. 150.2*A*.) These dikes invade fissures in walls of major faults as well as the faults themselves. Dikes extending from Santa Rita stock may be stock apophyses, hence somewhat older than the others.	Steep fractures of dominantly north and northeast trend and a few of northwest trend developed as shown by the pattern of dikes in figure 150.2*A*.	Any thermal or metasomatic effects in wall rocks cannot be distinguished from later effects of hypogene fluids that rose along these dikes after consolidation and reopening.

TABLE 150.1.—*Chronological summary of igneous activity, deformation, and mineralization from Late Cretaceous time to time of primary ore deposition, Central mining district, Grant County, N. Mex.*—Continued

[Earliest events at top of table; most recent events at bottom]

Igneous activity	Deformation	Mineralization
	Erosional Epoch—Continued	
	Existing faults reactivated, breaking the stocks and granodiorite dikes loose from their wall rocks, thus providing deep conduits for the hypogene fluids accumulated below. Breccia pipes within the Santa Rita stock and in the area to the west and northwest may have developed at this time, if not earlier. Santa Rita stock crackled and the part of Hanover-Fierro pluton near Fierro sheared at this time.	Main epoch of primary metallization. Large surge of hypogene fluid rose along margins of stocks and obliquely up faults intersecting those margins, causing pyrometasomatic alteration in wall rocks for considerable distance from conduits. Carbonate rocks silicated and recrystallized; shales baked, epidotized, or converted to hornfels; granodiorite dikes, many of which were major channelways, and older porphyries epidotized and chloritized. Porphyries in Bayard area altered to calcite-sericite-clay-quartz rock close to veins and to chlorite-sericite-epidote for several tens of feet away from veins, grading into mildly propylitized rock. Magnetite-chalcopyrite ores formed in carbonate rocks close to parts of the Santa Rita and Hanover-Fierro plutons. Chalcopyrite, molybdenite, adularia, quartz, and chlorite filled fissures in propylitized parts of Santa Rita stock, apparently somewhat before the argillic phase of alteration and the metallization that accompanied it. Sphalerite with only minor galena and chalcopyrite formed replacement bodies in carbonate rocks between Hanover and Santa Rita, and around the south lobe of the Hanover-Fierro pluton. Sphalerite-galena, and sphalerite-galena-chalcopyrite veins and replacement bodies formed along major faults (Groundhog, Hobo, Mirror, Barringer), along most granodiorite dikes, and around pluton at Copper Flat. During a late phase of the metallization, great volumes of porphyry at Santa Rita, both sills and stock, were altered to montmorillonite and biotite, and also to kaolin-alunite-illite-quartz rock in which pyrite and chalcopyrite formed disseminations and veins. Small volumes of porphyry were completely silicified. Similar but less widespread alteration took place in the Hanover-Fierro pluton near Fierro. Supergene processes subsequently intensified this primary argillic alteration.
Intrusion of quartz monzonite porphyry dike swarm. (See fig. 150.2*B*).	Renewed fracturing along earlier faults into which granodiorite dikes were intruded. (Compare fig. 150.2*A* and *B*.) Composite dikes common. Minor reopening and fracturing along quartz monzonite dikes.	Thermal and metasomatic effects insignificant. Dikes are mildly to moderately propylitized and sericitized although locally intensely argillized by supergene waters. Dikes in Santa Rita stock contain some chalcopyrite and, locally, much pyrite. West of the stock, dikes are cut by a few veinlets containing galena and sphalerite. Dikes were intruded during waning of metallization, or were followed by a second, much weaker, period of metallization.

The chronology of the area from Late Cretaceous time to the time of primary ore deposition is summarized in table 150.1. The geologic history prior to Late Cretaceous time has been described elsewhere (Hernon, Jones, and Moore, 1953); in brief, at the onset of Laramide igneous activity, flat-lying and undeformed sedimentary rocks of Paleozoic and Late Cretaceous age, aggregating about 6,000 feet in thickness, blanketed the Precambrian crystalline basement complex.

Clearly, the porphyries, the folds and faults, the altered rock, and the ore deposits in the Paleozoic and Cretaceous strata are all genetically related to a large body of magma emplaced in the basement rocks, and to its cooling and consolidation during early Tertiary time.

REFERENCES

Hernon, R. M., Jones, W. R., and Moore, S. L., 1953, Some geologic features of the Santa Rita quadrangle, New Mexico, *in* New Mexico Geol. Soc. Guidebook 4th Ann. Field Conf., 1953: p. 117–130.

Kuellmer, F. J., compiler, 1956, Geologic map of Hillsboro Peak thirty-minute quadrangle: New Mexico Bur. Mines and Mineral Resources, 30-minute Quad. Ser., no. 1 [Geol. Map 1].

Nockolds, S. R., 1954, Average chemical compositions of some igneous rocks: Geol. Soc. America Bull., v. 65, p. 1007–1032.

GEOLOGY OF LIGHT METALS AND INDUSTRIAL METALS

151. BERYLLIUM IN STREAM SEDIMENTS FROM THE TIN-TUNGSTEN PROVINCES OF THE SEWARD PENINSULA, ALASKA

By C. L. Sainsbury, Armin W. Helz, Charles S. Annell, and Harold Westley, Menlo Park, Calif., and Washington, D.C.

Previous work summarized by McKelvey (1960, p. A5) has shown that the tin districts of the Seward Peninsula, Alaska, contain promising amounts of beryllium. Geochemical reconnaissance[1] of the principal areas of tin-tungsten lode deposits of the Seward Peninsula, has shown that beryllium is concentrated in the stream sediments of Cassiterite Creek near the Lost River mine in the Teller B–5 quadrangle (fig. 151.1). Total sediments downstream or downslope from the Lost River mine contain as much as 160 ppm (parts per million) beryllium. The east extension of a dike that contains the main tin ore shoot of the Lost River mine is within the drainage basin of nearby Camp Creek, and sediments from Camp Creek consistently contain more than 110 ppm (fig. 151.1). Upstream from the Lost River mine the beryllium content of stream sediments decreases abruptly to less than 3 ppm, which is the regional background value of sediments from streams that drain the limestone bedrock.

[1] Field work by C. L. Sainsbury; laboratory determinations of beryllium by Armin Helz, Charles Annell, and Harold Westley by use of the direct-reading spectrograph.

Other sediment samples in the vicinity of Lost River that are rich in beryllium (fig. 151.1) include samples from below the Bessie and Mabel prospect, which contains tin and tungstein in an altered dike similar to the ore deposits at the Lost River mine; samples from an altered area along the north contact of a granite stock on Tin Creek; and samples of stream sediments and slope wash from granite at the head-waters of Lost River. Samples from the last-named locality contain up to 47 ppm beryllium, the richer samples being slope wash from disintegrating contact rock rich in idocrase. Idocrase from the Lost River area is known to be consistently high in beryllium (McKelvey, 1960, p. A5).

Some randomly selected samples of banded fluorite-tactite rock at the Lost River mine contain up to 0.15 percent beryllium, and all the specimens of fluorite-tactite rock contained more than 3 ppm beryllium. The beryllium content is highest in samples of fluorite-tactite rock from the walls of the tin-bearing dike where banded fluorite-tactite rock constitutes continuous bodies of minable size but of unknown average

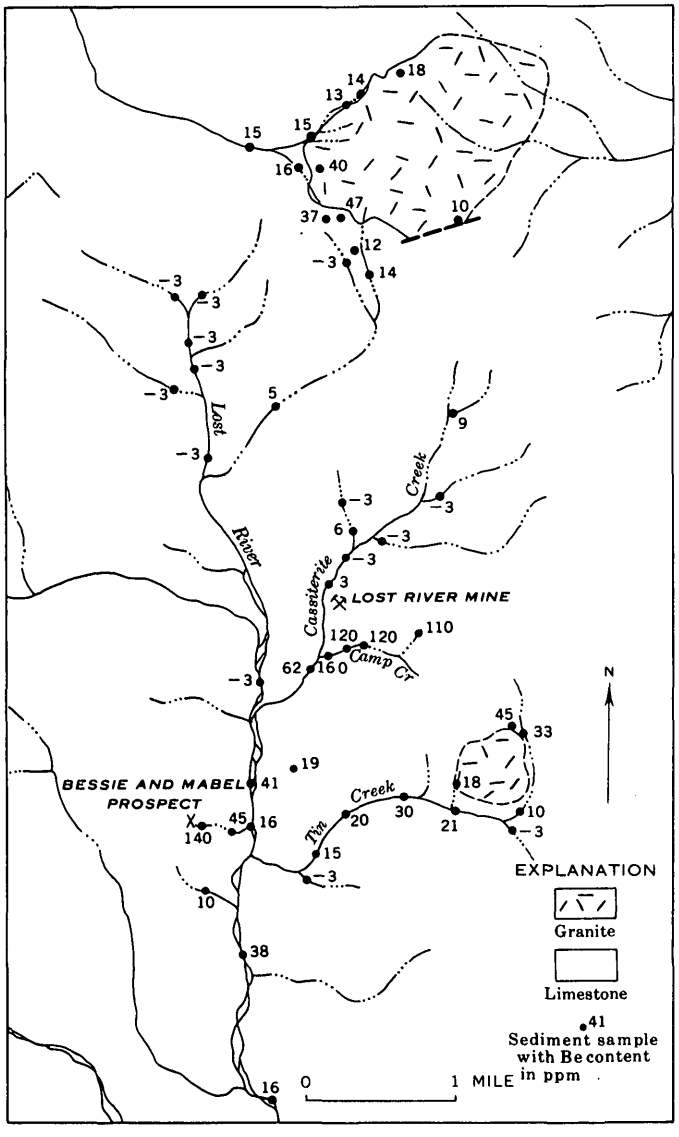

FIGURE 151.1.—Map showing location and beryllium content of sediment samples, Lost River area, Seward Peninsula, Alaska.

grade of beryllium. Beryl, phenacite, and chrysoberyl occur at the Lost River mine; secondary beryllium minerals perhaps will be found.

Stream sediments from the Ear Mountain area 50 miles northeast of Lost River contain less than 20 ppm beryllium, although a broad zone surrounding the granite stock which intrudes limestone and limy schists at this locality contains more than the background, which appears to be less than 3 ppm beryllium. Rock samples from a tin-tungsten prospect at the Winfield shaft on the north contact of the granite at Ear Mountain contain up to 380 ppm beryllium, the higher values being in fluorite-tactite rock rich in idocrase.

A granite stock intrudes limestone at the Cape Mountain area, 30 miles northwest of the Lost River mine. Sediment samples in this area generally contained less beryllium than those from the Ear Mountain and Lost River areas. Only one sample contained as much as 20 ppm. This sample was slope wash from an old dump at a tin prospect on a tourmalinized dike.

The analyses reported above and other work in the Seward Peninsula (McKelvey, 1960, p. A5) suggest that the bedrock source of beryllium in the stream sediments is both the granite and the tin lodes. Beryllium is particularly concentrated in or near tin-bearing greisen and fluoritized tactite, and in local areas of argillic alteration of hypothermal origin, particularly in the Lost River area.

REFERENCES

McKelvey, V. E., compiler, 1960, Geological Survey research 1960, synopsis of geologic results: U.S. Geol. Survey Prof. Paper 400–A, 136 p.

Sainsbury, C. L., 1960, Metallization and post-mineral hypogene argillization, Lost River tin mine, Alaska: Econ. Geology, v. 55, p. 1478–1506.

Sharp, W. N., and Hawley, C. C., 1960, Bertrandite-bearing greisen, a new beryllium ore, in the Lake George district, Colorado, *in* Short papers in the geological sciences: U.S. Geol. Survey Prof. Paper 400–B, p. B73–B74.

152. SLATE FROM THE GREENVILLE QUADRANGLE, MAINE, AS POTENTIAL LIGHTWEIGHT AGGREGATE MATERIAL

By Gilbert H. Espenshade and Howard P. Hamlin, Washington, D.C., and Bureau of Mines, Norris, Tenn.

In the course of mapping the geology of the Greenville quadrangle in the western part of the "slate belt" of central Maine, a large sample of slate was collected from a roadside exposure by G. H. Espenshade, and was tested for suitability as source material for bloated lightweight aggregate by H. P. Hamlin. The test results indicate that slate of the type sampled, which underlies many square miles of the region, expands when fired in a rotary kiln under controlled conditions to produce lightweight aggregate of good quality.

Two stratigraphic units have been recognized in mapping the Greenville quadrangle; their age relation has been worked out by determination of the upper boundary from graded bedding at numerous localities. The older unit consists mainly of dark reddish-brown fine-grained limy sandstone and thin beds of slate, and the younger unit is predominantly dark-gray slate and some beds of dark-gray siltstone and fine-grained sandstone. The dark-gray slate is composed mainly of white mica, chlorite, and very fine grained quartz; some biotite and very fine pyrite and graphitic material are characteristically present. The age of the younger unit cannot be conclusively determined from the few known fossils, but an Early Devonian age is indicated by the lithologic similarity to the Seboomook formation about 30 miles farther north (Boucot and others, 1960); the older unit may be Silurian or Devonian.

The rocks are folded in northeast-trending isoclinal folds with the younger unit exposed in the southeast quarter of the Greenville quadrangle in synclines underlying Doe Hill, Buck Hill, and Doughty Hill, and in the northern half of the quadrangle in a folded belt nearly 10 miles wide. A large body of gabbro and two smaller bodies of granitic rock have intruded these rocks, and have formed contact aureoles of hornfels and andalusite schist that are very similar to the contact metamorphic rocks around the Onawa pluton, a few miles east in the Sebec Lake quadrangle (Philbrick, 1936). The major geologic features that have been mapped in the Greenville quadrangle by Espenshade are shown on the map by Boucot and others (1960).

Slate has been quarried for material for the manufacture of milled slate for electrical switchboards and for other uses from 3 linear belts near Monson and Blanchard, apparently from two distinct stratigraphic horizons. A group of quarries near the Shirley-Blanchard townline and a group of quarries near Parrot and Monson seem to be in slate beds that are at the base of the younger unit. Quarries extending in a line southwest from the Farm quarries and the Hillside quarry of the Portland-Monson Slate Co. (U.S. Geol. Survey topographic map of Sebec Lake quadrangle, 1950) are in slate beds higher in the younger unit. At both stratigraphic positions, the slate is in beds that are commonly 1 to 10 feet thick and are interbedded with sandstone beds of similar thickness. Slaty cleavage seems to be developed best where slate and sandstone are interbedded; several intersecting sets of poor slaty cleavage generally occur where sandstone beds are absent.

Previous tests of the dark-gray slate from the Monson area, reported by Conley (1942), Trefethen (1955), and Caldwell (1959), showed that the slate had bloating characteristics. Because these samples were presumably taken from quarries or dumps at places where slate is closely interbedded with sandstone that probably is nonbloating, it seemed advisable to test a large sample from a stratigraphic position where sandstone was scarce or absent. Accordingly, a chip sample of slate weighing about 230 pounds and representing about 280 feet across strike was taken from the prominent roadside exposure on the hilltop about 0.6 mile southeast of Lower Shirley Corner, on State Highway 15 between Greenville and Monson. The beds of slate at this exposure appear to be more than 1,000 feet stratigraphically above the base of the younger unit.

Preliminary tests were made on small portions of the slate sample to determine bloating temperature, general firing characteristics, and some other properties as shown on figure 152.1 and table 152.1. Data from these preliminary tests showed that the slate had a short firing range, but probably would be amenable to the rotary kiln method of processing.

The slate sample was tested by the procedures described by Klinefelter and Hamlin (1957) for evaluating raw materials for manufacture of lightweight aggregate by the rotary kiln process. These tests yielded data shown on tables 152.2 to 152.4.

Crushing tests of three slate samples yielded the size fractions given in table 152.2. Samples crushed through roll and jaw crushers gave elongate, thin, platy particles; some improvement resulted when the samples were processed by a gyratory crusher (sample 2), but further study of crushing techniques and equipment is recommended.

A preliminary rotary kiln test of a 25-pound sample (ranging from <1-inch to dust size) was made to determine the general processing characteristics and to adjust the kiln variables (rotation speed, slope, feed rate, and so forth). Excessive sticking and logging prevented completion of the test; examination of the fired material showed that the <1-inch–>¾-inch particles were not expanded, whereas the <8-mesh material was overfired and partially melted. Consequently, all <8-mesh material was removed from subsequent samples.

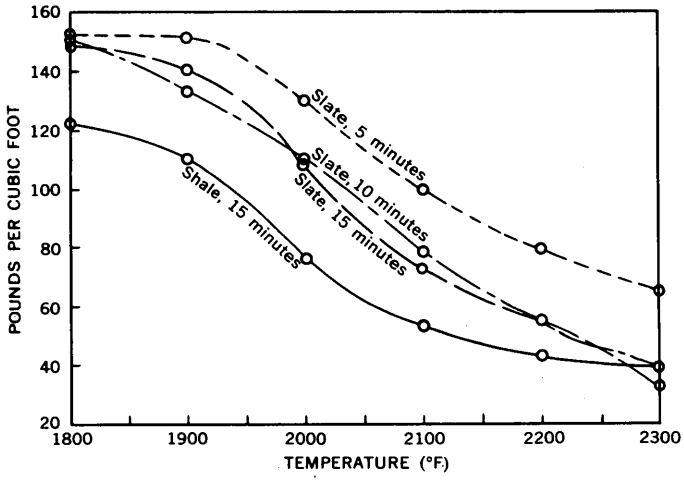

FIGURE 152.1.—Results of preliminary bloating tests of sample of slate from Maine compared with test of sample of shale that is used commercially as raw material for lightweight aggregate. Time interval indicates retention time of sample in kiln.

TABLE 152.1.—*Preliminary bloating tests of slate sample from Maine heated in electric kiln for different time periods*

Temperature, degrees F	Retention time								
	5 minutes			10 minutes			15 minutes		
	Pounds per cubic foot	Absorption (percent)	Remarks	Pounds per cubic foot	Absorption (percent)	Remarks	Pounds per cubic foot	Absorption (percent)	Remarks
1800	152. 0	3. 2	No bloating	150. 8	3. 2	No bloating	148. 8	3. 0	No bloating.
1900	151. 4	3. 2	No bloating	132. 7	4. 9	No bloating	140. 5	5. 3	No bloating.
2000	129. 6	5. 6	Slight bloating	110. 3	7. 3	Fair bloating	108. 4	3. 6	Fair bloating.
2100	99. 1	8. 3	Fair bloating	77. 9	9. 4	Good bloating	72. 2	9. 0	Good bloating, slightly sticky.
2200	78. 5	8. 9	Good bloating, slightly sticky.	55. 4	10. 5	Good bloating, slightly sticky.	55. 4	7. 8	Good bloating, sticky.
2300	65. 4	11. 6	Good bloating, very sticky.	39. 2	10. 4	Overbloated, very sticky.	33. 0	9. 7	Overbloated, very sticky.

TABLE 152.2.—*Screen analyses of crushed slate samples (unfired)*

[In percent]

U.S. Standard screen sizes	Sample		
	1	2	3
1- to 1½-inch	13. 4		
¾- to 1-inch	10. 0	10. 2	
½- to ¾-inch	30. 5	30. 8	25. 2
4-mesh to ½-inch	12. 2	22. 5	40. 8
8-mesh to 4-mesh	14. 6	20. 0	13. 6
<8-mesh	19. 3	16. 5	20. 4
Totals	100. 0	100. 0	100. 0

The results of rotary kiln tests on samples of three different feed sizes are given by table 152.3. During tests 1 and 2, when the expanding temperature of the larger particles was reached, the >8-mesh material was overfired and very sticky. Considerable logging occurred, and the kiln temperature had to be reduced before the material would flow evenly through the kiln. The aggregate from test 3, using kiln feed of <¾-inch–>8-mesh size range, proved to be superior to the aggregate produced in tests 1 and 2, showing that a very good aggregate can be made from the slate if the kiln feed size range is closely controlled. Screen analyses of aggregate from these three tests crushed to <⅜-inch (the usual crushing size for concrete building units) are given by table 152.4.

Standard 2-inch concrete cubes were made from the aggregate of rotary kiln test 3; the characteristics of this concrete compare favorably with the properties of concrete made from two commercial aggregates as shown by table 152.5.

It is concluded that slate from Maine of the type tested, which underlies many square miles of the region, will make a good-quality lightweight aggregate.

TABLE 152.3.—*Rotary kiln tests*

	Sample		
	1	2	3
Feed size	1½-inch to 8-mesh.	1-inch to 8-mesh.	¾-inch to 8-mesh.
Weight of raw material (pounds per cubic foot).	89.6	88.5	86.0.
Temperature, degrees F:			
Maximum	2075	2075	2085.
Optimum	2060	2050	2040.
Minimum	2030	2020	2010.
Weight of aggregate (pounds per cubic foot):			
A.S.T.M. container method.	62.5	47.5	48.0.
Laboratory suspended weight method.	87.9	75.3	73.0.
Absorption (percent)	6.8	6.7	9.5.
Effect of quenching	Deleterious.	Deleterious.	Deleterious.
Processing characteristics	Poor	Fair	Good.

TABLE 152.4.—*Screen analyses of fired aggregate crushed to less than ⅜-inch*

[In percent]

U.S. Standard screen sizes	Sample		
	1	2	3
4-mesh to ⅜-inch	35. 6	32. 2	29. 6
8-mesh to 4-mesh	32. 5	39. 6	40. 5
20-mesh to 8-mesh	18. 6	20. 0	17. 1
65-mesh to 20-mesh	5. 2	6. 0	6. 6
<65-mesh	8. 1	2. 2	6. 2
Total	100. 0	100. 0	100. 0

TABLE 152.5.—*Concrete performance tests*

	Lightweight aggregate from the Maine slate	Commercial lightweight aggregate	
		1	2
Batch composition, percent of sizes:			
⅜-inch to 4-mesh	50	50	50.
<4-mesh	50	50	50.
Mixing characteristics [1]	Fairly smooth working.	Harsh and short working.	Very harsh working.
Two-inch cubes: [2]			
Bulk density	1.59	1.39	1.63.
Pounds per cubic foot [3]	99.1	86.6	101.5.
Absorption (percent)	12.0	21.8	12.5.
Compression (pounds per square inch).	7500	2500	5800.

[1] Mix: 1 volume cement to 5 volumes aggregate.
[2] Concrete made of aggregate sized to A.S.T.M. specifications.
[3] Laboratory suspended weight method.

REFERENCES

Boucot, A. J., Griscom, Andrew, Allingham, J. W., and Dempsey, W. J., 1960, Geologic and aeromagnetic map of northern Maine, scale 1:250,000: U.S. Geol. Survey open-file report.

Caldwell, D. W., 1959, Glacial lake and glacial marine clays of the Farmington area, Maine. Origin and possible use as lightweight aggregate: Maine Geol. Survey Spec. Geol. Studies Series no. 3.

Conley, J. E., 1942, Waste slate as a raw-material source of lightweight aggregates: Am. Inst. Mining Metall. Petroleum Engineers Trans., v. 148, p. 161–166.

Klinefelter, T. A., and Hamlin, H. P., 1957, Syllabus of clay testing: U.S. Bur. Mines Bull. 565.

Philbrick, S. S., 1936, The contact metamorphism of the Onawa pluton, Piscataquis County, Maine: Am. Jour. Sci., 5th ser., v. 31, p. 1–40.

Trefethen, J. M., 1955, Lightweight aggregate in Maine, *in* Report of the State Geologist, 1953–1954: Maine Devel. Comm., p. 83–85.

GEOLOGY OF FUELS

153. SPHEROIDAL COAL IN THE TRINIDAD COAL FIELD, SOUTH-CENTRAL COLORADO

By Ross B. JOHNSON, Denver, Colo.

Coal in the Trinidad coal field, Huerfano and Las Animas Counties, Colo., locally exhibits two distinct types of spheroidal structures that are here called type A and type B. Spheroids of type A are mainly non-banded and are composed of many closely spaced layers separated by subconcentric fracture planes. Spheroids of type B are usually banded, and are not composed of closely spaced layers. The spheroids occur in beds in the Vermejo formation of Late Cretaceous age and in the Raton formation of Late Cretaceous and Paleocene age (Wood and others, 1951; Wood, Johnson, and Dixon, 1956). The coal-bearing formations underlie the trough of the structural Raton basin (Johnson and Wood, 1956, p. 707).

The spheroid-bearing coal is of high volatile *A*, *B*, and *C* bituminous rank. The two types of spheroids

range from less than 1 inch to about 5 inches in the greatest dimension. The size is determined laterally by nearly vertical joints and vertically by siltstone and shale partings in the coal. Most of the spheroids occur with the long axis normal to bedding planes. The sides of the spheroids are flattened along joint planes against adjoining spheroids. Curved surfaces of the spheroids apparently cut across banding (if present) and cleat and cleavage without displacement of these features.

Most of the spheroidal structures in the coal field are of type A, and they are most common in the Raton formation. Type A spheroidal coal is not usually near any known igneous rocks or faults and folds, and is not associated with any particular sedimentary structure. It is confined mainly to an area near the axis of the basin west of Trinidad, Colo. In this area most of the coal is normally banded, nonspheroidal, and commonly has coking properties. Spheroidal coal occurs at isolated localities where one or more of the coal beds are made up all or in part of the spheroidal structures. Spheroids of type A are composed mainly of nonbanded, finely cleated, evenly textured, glossy coal. They exhibit many closely spaced layers separated by subconcentric fracture planes. The curved surfaces formed by the fracture planes are bright, smooth, and polished. Locally, only the upper half of the spheroids are clearly developed.

Bright, smooth, and polished curved surfaces that characterize type A spheroids are possibly due to tectonic movements. Lateral movement of siltstone and shale partings along the upper and lower surfaces of the coal layers, as a result of the subsidence of the basin, may have produced stresses responsible for the curved fractures. As an alternative mode of origin, type A spheroids may have been produced by shrinkage during lithification of uniformly nonbanded coal in local areas in which the coal had an original high content of water; however, shrinkage does not account for the polishing of the fracture surfaces.

The second type of spheroidal coal, type B, is found locally near mafic dikes and sills (Moore, 1947, p. 247–250), and may extend outward from these intrusive rocks as much as several hundred feet. Spheroids of type B are most abundant in the eastern and northeastern parts of the coal field near Walsenburg, Colo., where igneous rocks are common. They differ from type A in that they are usually banded, and contain no subconcentric fracture planes. Spheroids of type B occur in coals without coking properties, but may also be found in coals with coking properties. These spheroids are uniformly microbanded internally with incipient cleat and cleavage, and there is neither megascopic nor microscopic evidence of original or healed subconcentric fractures within the spheroids. The banding extends from spheroid to spheroid without apparent displacement. Where spheroidal coal is near a sill, there is little or no alteration of sandstone, siltstone, or shale beds that lie between the igneous rocks and the spheroidal coal, and the coal itself does not appear to be changed significantly in rank. No spheroidal structures have been observed in coal next to a sill or dike. These spheroids are not fragmentary coal-pebbles (Stutzer and Noé, 1940, p. 253–255), concretionary coal-balls (Moore, 1947, p. 242–243; p. 246–247), or natural briquettes (Schopf, 1949, p. 82). Analyses of type B spheroidal coal (Moore, 1947, p. 248) show that these structures locally contain no moisture, and, at some places, nearly 15 percent less volatile matter than ordinary nonspheroidal coal from the same beds (Johnson, 1958, p. 579). Spheroidal coal of type B seems to be due to shrinkage caused by some of the moisture and volatile matter in the coal being driven off by the heat of the intrusive rock.

REFERENCES

Johnson, R. B., 1958, Geology and coal resources of the Walsenburg area, Huerfano County, Colo.: U.S. Geol. Survey Bull. 1042–0, p. 557–583.

Johnson, R. B., and Wood, G. H., 1956, Stratigraphy of Upper Cretaceous and Tertiary rocks of Raton basin, Colorado and New Mexico: Am. Assoc. Petroleum Geologists Bull., v. 40, no. 4, p. 707–721.

Moore, E. S., 1947, Coal: New York, John Wiley and Sons, 473 p.

Schopf, J. M., 1949, Naturally briquetted coal from a bed in western Pennsylvania: Jour. Geology, v. 57, no. 1, p. 79–82.

Stutzer, Otto, and Noé, A. C., 1940, Geology of coal: Chicago, Ill., Univ. Chicago Press, 461 p.

Wood, G. H., Johnson, R. B., and Dixon, G. H., 1956, Geology and coal resources of the Gulnare, Cuchara Pass, and Stonewall area, Huerfano and Las Animas Counties, Colo.: U.S. Geol. Survey Coal Inv. Map C–26.

Wood, G. H., Johnson, R. B., Eargle, D. H., Duffner, R. T., and Major, Harald, 1951, Geology and coal resources of the Stonewall-Tercio area, Las Animas County, Colo.: U.S. Geol. Survey Coal Inv. Map C–4.

154. POTENTIAL OIL-SHALE RESERVES OF THE GREEN RIVER FORMATION IN THE SOUTHEASTERN UINTA BASIN, UTAH AND COLORADO

By W. B. Cashion, Denver, Colo.

The Green River formation, composed of lacustrine sediments deposited during Eocene time, underlies large areas in Colorado, Wyoming, and Utah and contains many oil-shale beds which have potential economic importance. In Utah the Green River formation is largely confined to the Uinta Basin, a depositional and structural basin that includes a large area in northeastern Utah and a small adjoining part of western Colorado. The potential oil yield of the Green River formation in part of the eastern Uinta Basin was estimated earlier (Cashion, 1957, p. 135) to be 100 billion barrels; this estimate was for an oil-shale sequence 15 or more feet thick in an area of 1,000 square miles, which has an average oil yield of 15 gallons per ton of rock. The new and more reliable estimate presented here is for the same sequence in an area of 690 square miles lying within the 1,000 square miles considered in the earlier estimate. The new estimate of the potential shale-oil reserves of this 690-square-mile area is about 53 billion barrels, whereas the estimate for the same area based on data available in 1957 was about 42 billion barrels. The new estimate of shale-oil reserves is based on assays of samples from 39 core holes, 15 exploratory wells, and 20 outcrops. These data represent additional oil-yield determinations on samples from 26 more core holes and exploratory wells than were available in 1957.

Oil-shale beds.—The oil shales of the Green River formation are more or less magnesian marlstones containing organic matter derived chiefly from aquatic organisms or waxy spores and pollen grains (Bradley, 1931, p. 7, 8, and 52). The organic matter is only slightly soluble in ordinary petroleum solvents, but a large proportion is distillable into artificial petroleum. The Mahogany oil-shale bed, which crops out in a large area in the southeastern part of the Uinta Basin (fig. 154.1), is the thickest oil-rich shale bed in the Green River formation. The Mahogany bed has its maximum thickness along a depositional axis which trends approximately east-west (fig. 154.1) and lies near the confluence of White River and Evacuation Creek. The thickness of the Mahogany bed ranges from about 2 feet in T. 18 S., R. 19 E. to about 8 feet in T. 10 S., R. 25 E. A stratigraphic sequence that is rich in organic matter extends as much as 300 feet above the Mahogany bed and as much as 400 feet below it. Only part of this sequence, however, has an average oil yield of 15 gallons per ton. The oil yields of samples from the area of the map range from a fraction of a gallon per ton to 95 gallons per ton. Each of these 2 extreme assays are of samples representing units 1 foot thick.

Classification of reserves.—Because oil-shale deposits in the United States are not being commercially exploited at present, but perhaps will be developed at some future time, they may be classified as potential reserves. The potential reserves described in this report are divided into two categories, indicated and inferred, which are intended to show the relative reliability of the data used in making estimates of potential oil yield. This breakdown is patterned after the one used by Donnell (1957, p. 260) in estimating oil-shale reserves of the Piceance Creek basin. The estimates of indicated potential reserves are based on assays of samples from core holes and drill cuttings from exploratory wells because weathered oil-shale beds may have lost much of their original oil content. Assays of core samples are more reliable than assays of drill cuttings because drill-cutting samples may be contaminated by rock fragments from units higher in the drill hole, and also because they represent thick sample units, generally 10 feet. Assays of drill cuttings are adequate, however, for estimating indicated potential reserves of oil shale. The estimates of inferred potential reserves are based on assays of outcrop samples or interpolation between widely spaced exploratory wells and core holes. The oil yield of samples from outcrop is somewhat dependent on the degree of weathering of the beds sampled and are less reliable, therefore, for making estimates of oil-shale reserves. For example, a sample of weathered shale from the Mahogany bed of the Green River formation assayed at 12.8 gallons of oil per ton, whereas a sample of unweathered shale taken 2 feet beneath the surface assayed at 45.5 gallons per ton (Guthrie, 1938, p. 99). Although assay oil yields of weathered samples are

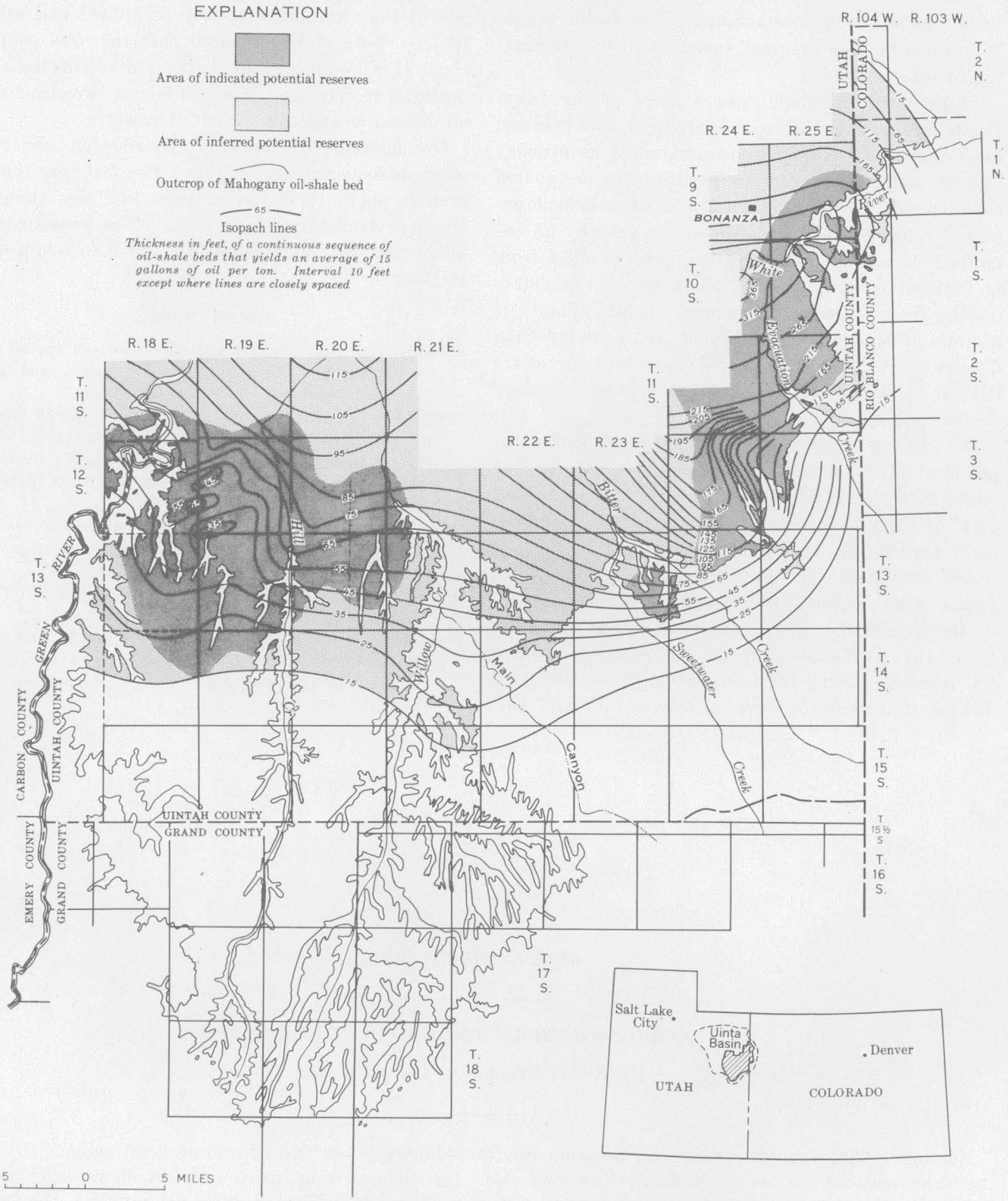

FIGURE 154.1.—Map showing outcrop of the Mahogany oil-shale bed and thickness of oil-shale sequence in the Green River formation (Eocene) that yields an average of 15 gallons of oil per ton.

known to be low, a constant upgrading factor cannot be applied because of great variation in the weathering of oil-shale beds.

In preparing oil-shale reserve maps of the Uinta Basin, such as that shown on figure 154.1, core-hole and exploratory well localities are designated as primary control points, and outcrop localities are designated as secondary control points. Areas of indicated potential reserves are delineated on the map by an encircling boundary drawn approximately 2 miles from an isolated primary control point, or approximately 2 miles from the outermost primary control points of a group in which any two adjacent points are less than 6 miles apart. Areas of inferred potential reserves are defined by boundaries based on data from secondary control points.

Oil yield of the deposits—All figures given here of potential oil-shale reserves pertain to a sequence of rocks 15 or more feet thick that has an average oil yield of 15 gallons per ton. No allowances have been made for losses in mining and retorting.

The area shown in figure 154.1 includes about 315 square miles underlain by oil-shale beds classed as indicated potential reserves, and about 375 square miles underlain by oil-shale beds classed as inferred potential reserves. Using the information shown on figure 154.1 and assuming a potential oil yield of 1,157 barrels of shale oil per acre-foot (Stanfield and others, 1957, p. 2–5), it is estimated that the area contains about 27 billion barrels of shale oil classed as indicated potential reserves and about 26 billion barrels of shale oil classed as inferred potential reserves.

Overburden.—Thickness of overburden above the oil-shale sequence ranges from a few feet near the outcrop to about 1,300 feet at some localities along the northern boundary of the area. The overburden is about 400 feet thick where the oil-shale sequence is thickest.

REFERENCES

Bradley, W. H., 1931, Origin and microfossils of the oil shale of the Green River formation of Colorado and Utah: U.S. Geol. Survey Prof. Paper 168, 58 p.

Cashion, W. B., 1957, Stratigraphic relations and oil shale of the Green River formation in the eastern Uinta Basin, *in* Intermountain Assoc. Petroleum Geologists Guidebook, 8th Ann. Field Conf., Geology of the Uinta Basin: p. 131–135.

Donnell, J. R., 1957, Preliminary report on oil-shale resources of Piceance Creek Basin northwestern Colorado: U.S. Geol. Survey Bull. 1042–H, p. 255–271.

Guthrie, Boyd, 1938, Studies of certain properties of oil shale and shale oil: U.S. Bur. Mines Bull. 415, 159 p.

Stanfield, K. E., Rose, C. K., McAuley, W. S., and Tesch, W. J., Jr., 1957, Oil yields of sections of Green River oil shale in Colorado, 1952–54: U.S. Bur. Mines Rept. Inv. 5321, 132 p.

HYDROLOGIC STUDIES

155. BOULTON'S INTEGRAL FOR PUMPING-TEST ANALYSIS

By R. W. Stallman, Denver, Colo.

Boulton (1954) derived an integral equation relating drawdown at the water table to time and the radius from a pumping well, which is founded partly on a consideration of vertical flow components not included in Theis' equation (1935). Flow conditions assumed by Boulton are shown schematically on figure 155.1, and may be stated as follows: (a) The aquifer is homogeneous and of infinite areal extent; (b) storage changes take place only by dewatering as the water table is lowered during pumping. The specific yield is constant with time and radius; (c) the pumped well fully penetrates the aquifer; (d) the velocity of flow at the well face is uniform throughout the aquifer thickness; (e) the rate of discharge of the

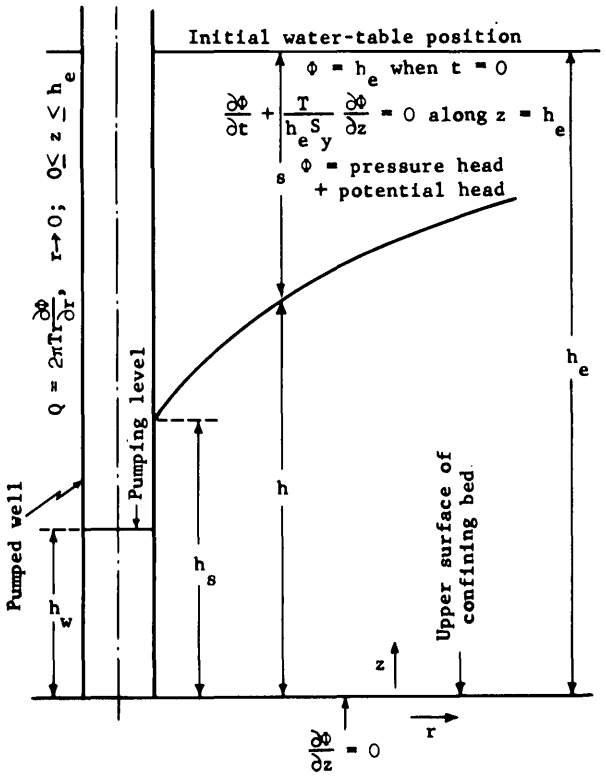

FIGURE 155.1.—Boundary conditions satisfied by Boulton's solution.

pumped well is constant with time; (f) all flow lines originate at the water table and terminate at the well face; (g) changes in potential due to dewatering are defined along the static water-table position, where radial flow components are always negligible, or zero; and (h) changes in saturated thickness of the aquifer, due to dewatering, are negligible.

Boulton's integral (1954, p. 569, eq. 9) satisfying these assumptions may be written in algebraic form as

$$s=\frac{114.6\ Q}{T}\ 2[V\ (\rho,\ \tau)] \tag{1}$$

in which s is the change in water-table position, in feet; Q is the rate of discharge of the pumped well in gpm; T is the aquifer transmissibility, in gallons per day per foot before dewatering takes place. The terms ρ and τ are nondimensional and are defined as

$$\rho=r/h_e \tag{2}$$

and

$$\tau=0.134\frac{Tt}{S_y h_e^2} \tag{3}$$

in which r is the distance from the center of the discharging well to the point at which s is observed, in feet; h_e is the initial saturated thickness of the aquifer, in feet; S_y is the specific yield; and, t is the elapsed time between commencement of pumping and the instant of observing s, in days. It may be noted that ρ and τ are the two fundamental nondimensional factors of the familiar "u" in the Theis (1935) analysis, to which they are related by

$$u=\frac{\rho^2}{4\tau}=\frac{1.87\ r^2 S}{Tt}. \tag{4}$$

Direct comparison between the Theis and Boulton equations is made possible by means of equation 4.

Boulton's integral, represented here by the term $2[V\ (\rho,\ \tau)]$ in equation 1, is not easy to evaluate numerically. In his original work, Boulton published a short table of $V(\rho,\ \tau)$ covering 4 values of τ and 6 values of ρ. Although informative, this table is insufficient for field use and for making detailed comparisons with the Theis equation. In 1958 the U.S. Geological Survey's Branch of Computation calculated additional numerical values of Boulton's integral expanding the range of the table of values to $1\times10^{-4}\leq\tau\leq 17.78$ and $1\times10^{-3}\leq\rho\leq 10.00$. This set of computations was made to determine the general shape of the curves resulting from the integral and to serve as a guide for future detailed tabulation. The writer is indebted to James R. Marsheck and Edward Monasterski, mathematicians, U.S. Geological Survey, for all the mathematical investigation, computer programming, and computer operation incident to calculating values of $2[V\ (\rho,\ \tau)]$ presented here. Thanks are due to Prof. Boulton for his advice on the numerical formulas used for evaluating the integral.

Results of the computations and corresponding values of $1/u$ are given in table 155.1. Values of Boulton's integral may be found in this table from the example that follows: For $\rho=3.162\times10^{-2}$ and $\tau=1.000\times10^{-1}$; the diagonal drawn upward and toward the right from $\tau=1.000\times10^{-1}$ is followed to the column $\rho=3.162\times10^{-2}$. There the value of the integral is found to be 3.6065, and the value of $1/u$ is found on the same line at the right side of the table to be 4.000×10^{2}. Curves of $2[V\ (\rho,\ \tau)]$ versus $1/u$ are shown on figure 155.2 for individual values of ρ. Logarithmic plots of s versus t or s versus t/r^2 from an individual observation well may be matched with the appropriate ρ-curve of figure 155.2 to solve for T and S_y in the same way as in the standard graphical solution of the Theis equation (see Brown, 1953, for example). However, it is to be noted that, for small values of ρ, large segments of the type curves have no characteristic curvature suitable for obtaining a graphical solution. Where the curves form essentially straight lines in figure 155.2, corresponding match points

601530 O—61——3

TABLE 155.1.—*Values of Boulton's (1954) integral for analysis of water-table drawdowns observed near a pumping well in an unconfined aquifer*

$\tau = 0.134\frac{Tt}{S_y h_e^2}$	$\rho = \frac{r}{h_e}$																	$1/u = \frac{Tt}{1.87r^2S_y}$
	1×10^{-3}	1.78×10^{-3}	3.16×10^{-3}	5.62×10^{-3}	1.000×10^{-2}	1.778×10^{-2}	3.162×10^{-2}	5.623×10^{-2}	1.000×10^{-1}	1.778×10^{-1}	3.162×10^{-1}	5.623×10^{-1}	1.000	1.778	3.162	5.623	10.000	
												.0002306	.0002560	.0001774				1.265×10^{-3}
												.0004042	.0004474	.0003172				2.249
											.0004986	.0007212	.0008010	.0005636	.0001578			4.000
											.0008954	.0012574	.0014272	.0009876	.0002838			7.112
										.0009898	.0015898	.0022388	.0025362	.0017900	.0005186			1.265×10^{-2}
										.0017858	.0027858	.0039848	.0045176	.0032224	.0009694			2.249
									.0018632	.0031610	.0049864	.0070766	.0080494	.0058168	.0018770	.0002098		4.000
									.0033604	.0055298	.0088342	.012593	.014379	.010397	.0038410	.0006358		7.112
								.0034358	.0059588	.0098854	.015704	.022437	.025762	.019593	.0084142	.0022624	.0007910	1.265×10^{-1}
								.0061902	.010428	.017579	.027919	.040081	.046375	.037417	.020048	.0089866	.0044668	2.249
							.0062040	.010940	.018633	.031207	.049682	.071279	.084017	.073740	.051156	.033930	.026908	4.000
							.011173	.019153	.033231	.055502	.088574	.12739	.15372	.14723	.13184	.096570	.091474	7.112
						.011127	.019803	.034355	.058884	.098977	.15738	.22763	.28296	.30172	.30952	.31328		1.265×10^{0}
						.020010	.034654	.060932	.10469	.17562	.27931	.40516	.51455	.58068	.61361	.62657		2.249
					.019867	.035554	.062029	.10803	.18605	.31113	.49241	.70715	.88680	.98613	1.0252			4.000
					.035761	.062322	.11016	.19191	.33045	.54718	.84916	1.1700	1.3851	1.4765	1.5065			7.112
				.035454	.063568	.11121	.19523	.34175	.58208	.94365	1.3897	1.7625	1.9464	2.0096				1.265×10^{1}
				.063809	.11121	.19752	.34597	.59900	.99700	1.5390	2.0751	2.4019	2.5246	2.5629				2.249
			.063149	.11340	.19834	.34928	.61033	1.0310	1.6334	2.3039	2.8059	3.0319	3.1046					4.000
			.11363	.19822	.35181	.61438	1.0491	1.6896	2.4551	3.1288	3.5072	3.6421	3.6833					7.112
		.11217	.20177	.35271	.61778	1.0606	1.7212	2.5503	3.3601	3.9202	4.1618	4.2378						1.265×10^{2}
		.20167	.35186	.62097	1.0646	1.7394	2.6049	3.5124	4.2459	4.6509	4.7826	4.8248						2.249
1.0×10^{-4}	.19954	.35722	.62148	1.0683	1.7495	2.6382	3.6065	4.4787	5.0730	5.3064	5.3834							4.000
1.8	.35785	.61853	1.0718	1.7554	2.6559	3.6624	4.6547	5.4032	5.7972	5.9306	5.9729							7.112
3.2	.62913	1.0703	1.7586	2.6675	3.6942	4.7388	5.6257	6.2206	6.4552	6.5330								1.265×10^{3}
5.6	1.0677	1.7604	2.6725	3.7145	4.7805	5.7778	6.5510	6.9472	7.0805	7.1234								2.249
1.00×10^{-3}	1.7614	2.6726	3.7252	4.8140	5.8702	6.7737	7.3623	7.6059	7.6834									4.000
1.78	2.6790	3.7267	4.8334	5.9252	6.9254	7.6915	8.0980	8.2315	8.2740									7.112
3.16	3.7316	4.8408	5.9567	7.0193	7.9236	8.5133	8.7570	8.8346										1.265×10^{4}
5.62	4.8472	5.9710	7.0734	8.0768	8.8422	9.2454	9.3828	9.4253										2.249
1.000×10^{-2}	5.9833	7.1012	8.1697	9.0757	9.6642	9.9098	9.9857											4.000
1.778	7.1208	8.2202	9.2268	9.9946	10.396	10.535	10.577											7.112
3.162	8.2533	9.3173	10.228	10.817	11.060	11.133												1.265×10^{5}
5.623	9.3731	10.375	11.140	11.549	11.685	11.710												2.249
1.000×10^{-1}	10.470	11.376	11.971	12.212	12.284													4.000
1.778	11.528	12.888	12.700	12.842	12.868													7.112
3.162	12.529	13.119	13.364	13.436														1.265×10^{6}
5.623	13.441	13.855	13.999															2.249
1.000	14.272	14.511	14.586															4.000
1.778	15.008	15.130																7.112
3.162	15.651	15.716																1.265×10^{7}
5.623	16.382																	2.249
10.00	16.697																	4.000
17.78																		

on the data plot and type curve may be selected such that the ratio $s/2$ $[V(\rho, \tau)]$ can take on a wide range of values. Thus, the solution for T by equation 1 is indeterminate for small values of ρ. Similarly the solution for T/S_y is indeterminate where the curves of figure 155.2 are essentially straight.

Figure 155.3 (p. C–28) shows the nature of drawdown profiles, and changes in them, as the time of pumping increases. Curves for small values of τ (less than about 1×10^{-2}) exhibit little or no characteristic curvature, and therefore the solution for T and S_y from field observations is indeterminate in that region. For the purpose of making comparisons, similar curves were calculated by means of the Theis equation and plotted in figure 155.3 for the same τ-values as used in the construction of profiles determined from the Boulton equation.

The general limits of usefulness of the Boulton solution for analyzing pumping-test data may be ascertained by comparing it with the Theis equation, and inspecting the type curves shown on figures 155.2 and 155.3. With limits defined only approximately, it can be concluded that: (a) The Boulton solution is practically identical with the Theis equation for $\tau>5$ and (or) $\rho>10$; (b) T and S_y may be calculated by graphical

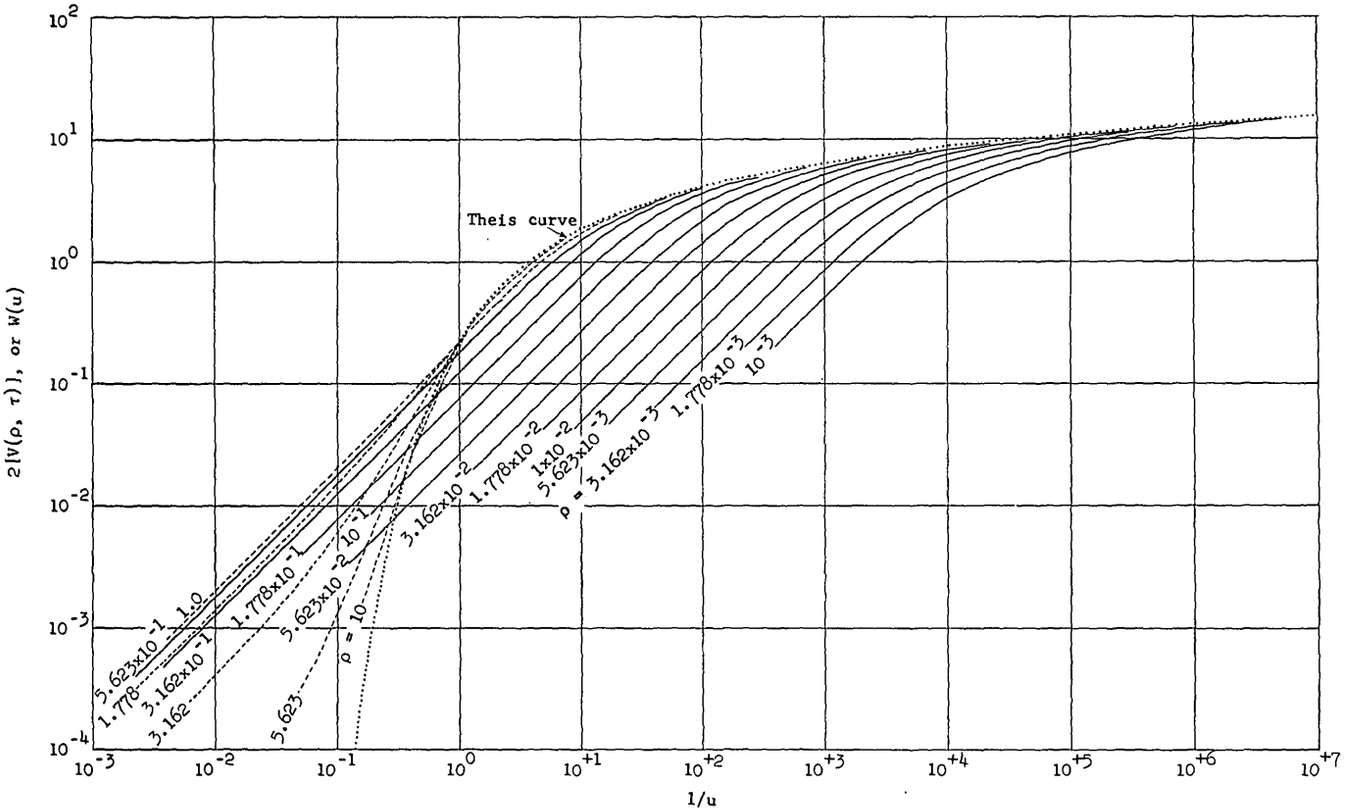

FIGURE 155.2.—Boulton's integral versus $1/u$ for selected values of ρ. ($u=1.87\ r^2S_y/Tt$; and, $\rho=r/h_e$.)

solution of Boulton's equation from logarithmic plots of observed drawdown versus radius over the interval $5\times10^{-2}<\tau<5$; (c) T and S_y may be calculated by graphical solution of Boulton's equation from logarithmic plots of observed drawdown versus time over the interval $3<\rho<10$; and, (d) solutions for T and S_y by the Boulton equation are indeterminate for $\tau<5\times10^{-2}$ and $\rho<3$.

Three sets of pumping-test data reported by Wenzel (1942, p. 127 and following) are shown on figure 155.4 (p. C–29). The solid curves are plots of drawdown versus t/r^2 for individual wells; the dotted curves were calculated by substituting in equation 3 Wenzel's values of T, S_y, and the initial and final times of observation. Each test was made, using fully penetrating pumped wells, in shallow unconfined sands and gravels. Because all the computed values of τ in figure 155.4 are nearly equal to or greater than 5, it follows that the plotted data from each test should define a single curve congruent with the Theis curve. Obviously this result is not realized. Thus, it appears highly probable that the flow conditions in the vicinity of the pumped well are not described adequately by either the Theis or Boulton expression. Previously it has been assumed that analyses of pumping tests in unconfined aquifers, using the Theis equation, were inaccurate because the effects of vertical flow components were not considered. Evidently if we are to achieve a significant improvement in test analyses, other factors must also be taken into account in the derivation of analytical equations which state the relationships among known variables of flow.

REFERENCES

Boulton, N. S., 1954, The drawdown of the water-table under nonsteady conditions near a pumped well in an unconfined formation: Inst. Civil Engineers Proc., Part III, 564–579.

Brown, R. H., 1953, Selected procedures for analyzing aquifer test data: Am. Water Works Assoc. Jour., p. 844–866

Theis, C. V., 1935, The relation between the lowering of the piezometric surface and the rate and duration of discharge of a well using groundwater storage: Am. Geophys. Union Trans., p. 519–524.

Wenzel, L. K., 1942, Methods for determining permeability of water-bearing materials: U.S. Geol. Survey Water-Supply Paper 887, 192 p.

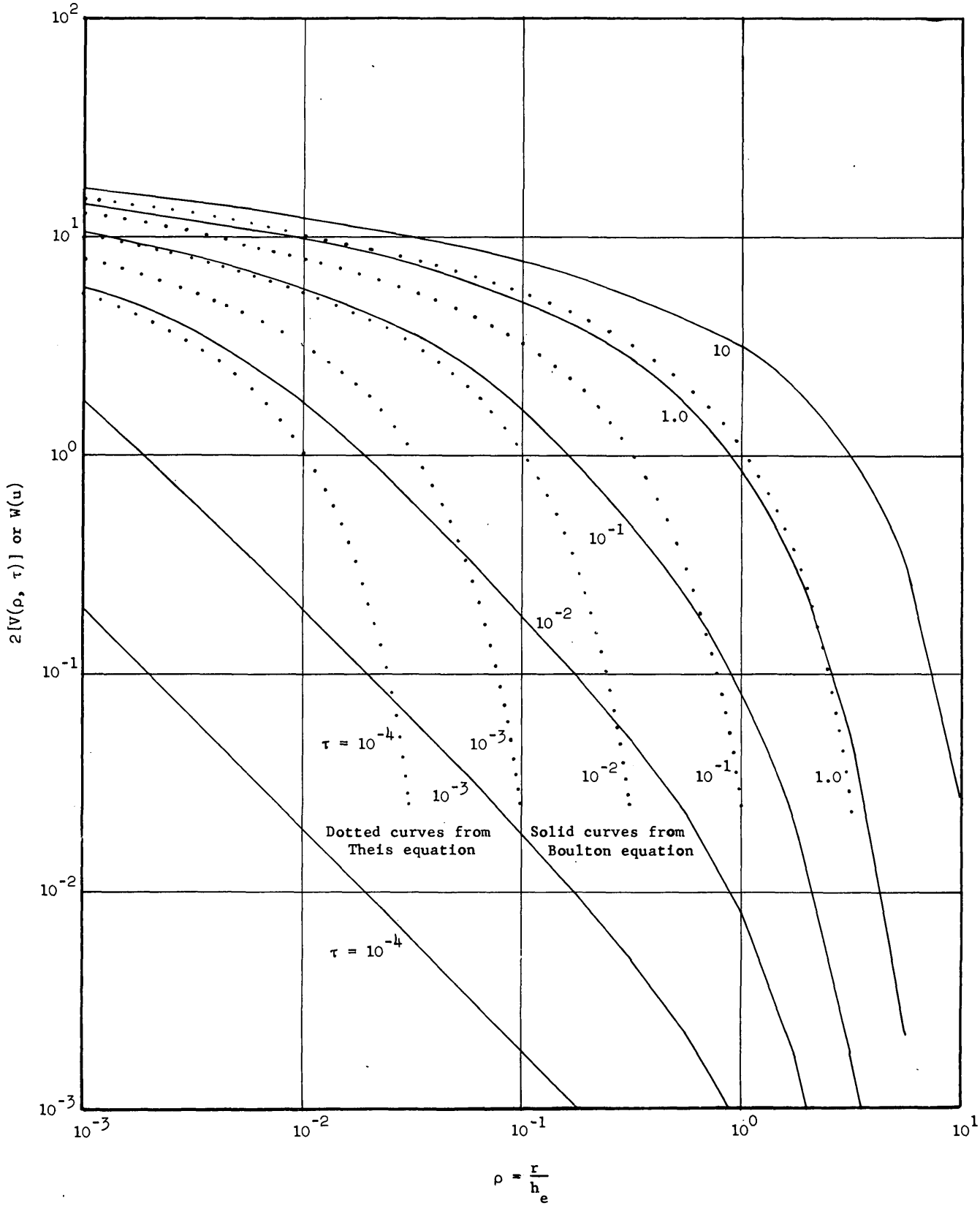

FIGURE 155.3.—Boulton's integral and $W(u)$ versus ρ for selected values of τ. ($W(u)$ defined by Wenzel, 1942, p. 88, eq. (88); $\rho = r/h_e$; and $\tau = 0.34\ Tt/S_y h_e^2$.)

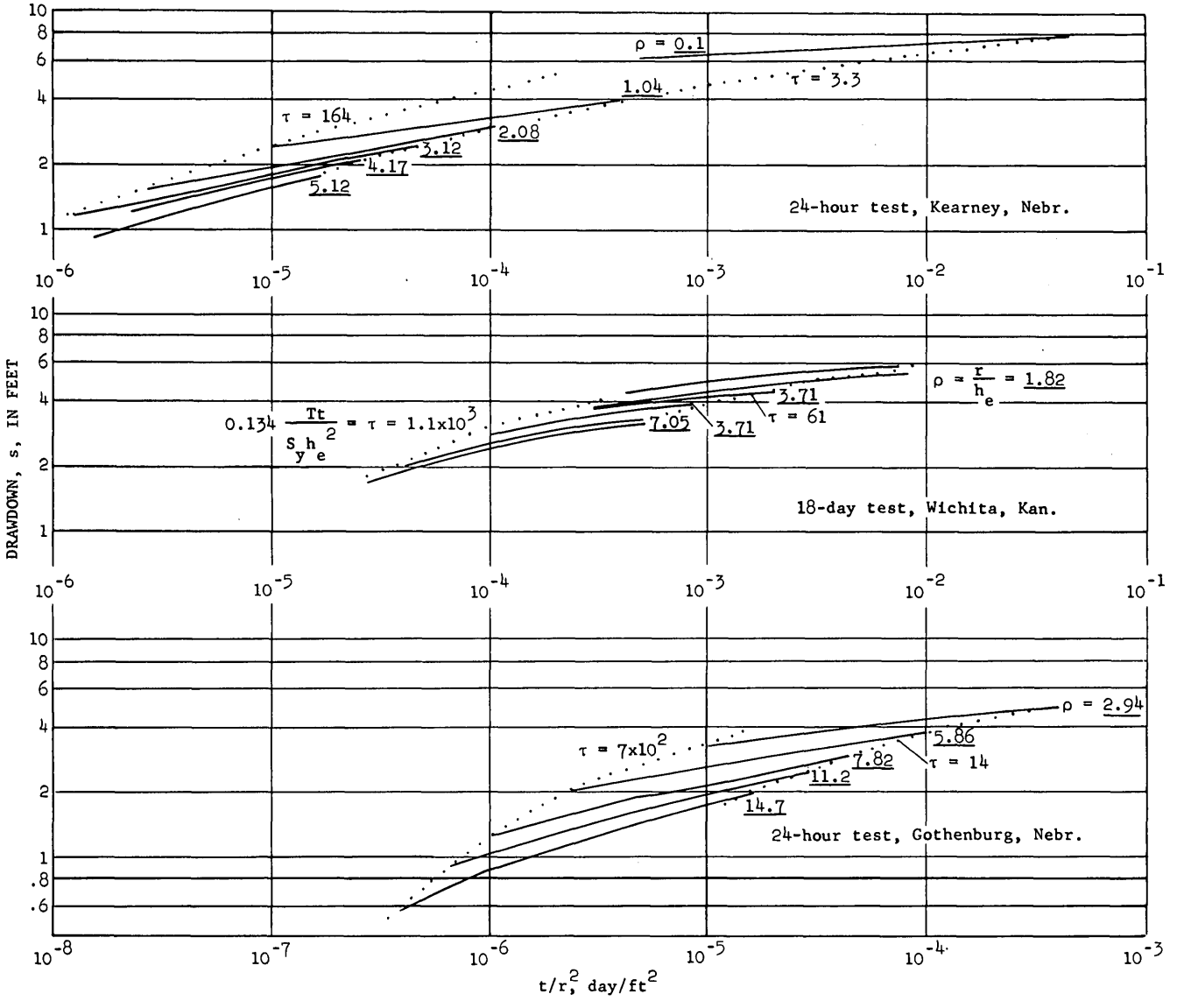

FIGURE 155.4.—Pumping-test data from unconfined aquifers in Kansas and Nebraska (after Wenzel, 1942, p. 127 and following).

156. INFLUENCE OF RIPARIAN VEGETATION ON CHANNEL SHAPE, NORTHEASTERN ARIZONA

By Richard F. Hadley, Denver, Colo.

About 80 percent of the vegetation is saltcedar (*Tamarix pentandra*) within the arroyo walls of Oraibi Wash, which empties into the Little Colorado River in northeastern Arizona. Saltcedar is an aggressive, naturalizing, and spreading shrub that is native in the area extending from western Europe to the Himalaya Mountains (Robinson, 1958, p. 74), and that probably was introduced to northern Arizona late in the 19th century. The seeds from saltcedar shrubs are easily spread over large areas by water and wind, and they germinate rapidly where there is plentiful moisture, which in semiarid areas is primarily along channels and on flood plains of streams. A photograph taken in 1909 by H. E. Gregory near the mouth of Oraibi Wash shows no saltcedar in an area that was overgrown with it in 1960.

Seedlings of saltcedar are shown in figure 156.1 growing along the bank of Oraibi Wash. The high-water line of a recent flow runs through the center of the photograph from top to bottom. Any seedlings that might have been growing on the channel (left) side of the high-water line have been washed away by the current. Dietz (1952, p. 250) has noted the establishment of seedlings along the high-water lines in stream channels, and he commented on the importance of this process in forming channel bars. Clearly, any flooding while the plants are small will inundate them, and their influence on channel shape and roughness will be negligible. If relatively small amounts of water flow down the channel for a few years after germination of the seeds, however, the shrubs may become large enough to promote sedimentation along the channel banks and on the flood plain by increasing roughness and thus reducing velocity of flow.

Planetable maps were made of a reach of the channel of Oraibi Wash where the growth of riparian vegetation and channel shape could be measured. The reach is 250 feet long and the bed and banks of the channel are composed of fine to medium sand and silt. A survey was made in October 1958, and another in August 1960.

The larger saltcedar shrubs in the reach at the time of the first survey ranged in height from 1.5 to 3.5 feet; many seedlings were less than 2 inches high. Growth-ring counts showed that some of these shrubs had reached heights of 1.5 to 2 feet in 1 year. In 1960, the same shrubs ranged in height from 4 to 6 feet; many of the seedlings had been washed away or buried by floods.

Changes in the channel geometry during the 2 years between observations are quite apparent. The average width of the channel was 20.9 feet in 1958 and 17.8 feet in 1960. The mean channel depth was 1.1 feet in 1958 and 1.3 feet in 1960. The channel slope increased from .0037 ft/ft to .0042 ft/ft between 1958 and 1960.

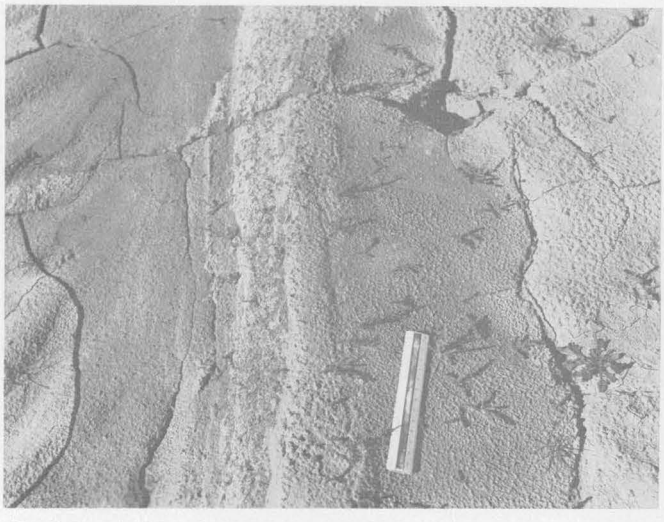

Figure 156.1.—Saltcedar seedlings less than 2 inches high along the channel bank of Oraibi Wash, Ariz.

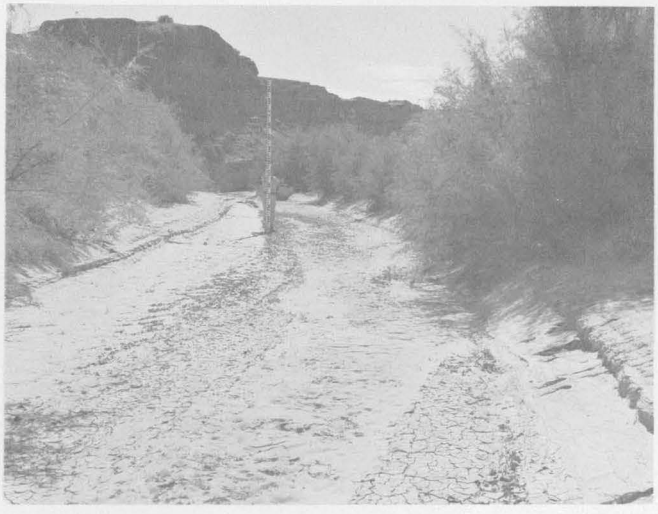

Figure 156.2.—Oraibi Wash channel in lower reach showing dense growth of saltcedar and fresh sediment deposits along banks.

The channel in this reach, therefore, is being restricted and degraded under the influence of the encroaching vegetation. Deposition is occurring on the banks and flood plain among the rows of saltcedar shrubs. Fresh sediment as much as 0.5 foot thick was measured on the flood plain in 1960. The rapid growth of the shrubs doubtless will continue to increase roughness and induce deposition on the banks and flood plain and gradually reduce the channel width until all flood waters will be forced over the banks and onto the flood plain. Observations in the lower reaches of Oraibi Wash (see fig. 156.2) where saltcedar shrubs are more firmly established indicate that this is the probable sequence of events in this drainage basin.

REFERENCES

Dietz, R. A., 1952, The evolution of a gravel bar: Missouri Bot. Garden Annals, v. 39, p. 250.

Robinson, T. W., 1958, Phreatophytes: U.S. Geol. Survey Water-Supply Paper 1423, 84 p.

157. RELATION BETWEEN MEDIAN GRAIN SIZE AND PERMEABILITY IN THE ARKANSAS RIVER VALLEY, ARKANSAS

By M. S. Bedinger, Little Rock, Ark.

Work done in cooperation with the U.S. Army, Corps of Engineers

Hydrogeologic studies in the Arkansas River valley required that the transmissibility (permeability times thickness) of the alluvial materials be determined at many places in a large area. Logs of many test holes were available, but only at a few places was it feasible to determine permeabilities of the aquifer by laboratory determinations and pumping tests.

The laboratory determinations of permeability were made on disturbed samples from drill holes. Recomposition of a sample to its original state is not possible; however, laboratory determinations give the approximate order of magnitude of permeability and are useful in indicating relative values of permeability.

To determine the relation between grain size and permeability, laboratory determinations of median grain size and permeability were plotted on a graph as shown by figure 157.1. A scattering of points is to be expected because of differences in sorting, sphericity, and arrangement of the grains. However, in spite of the scatter, a relation between median grain size and permeability is apparent. The relation shown by the graph can be expressed as

$$k=Cd^2$$

where the permeability, k, is proportional to the square of the median grain size, d; and C is a constant.

This is the same relation found by Slichter (1899) for porous media of spheres of uniform size and ar-

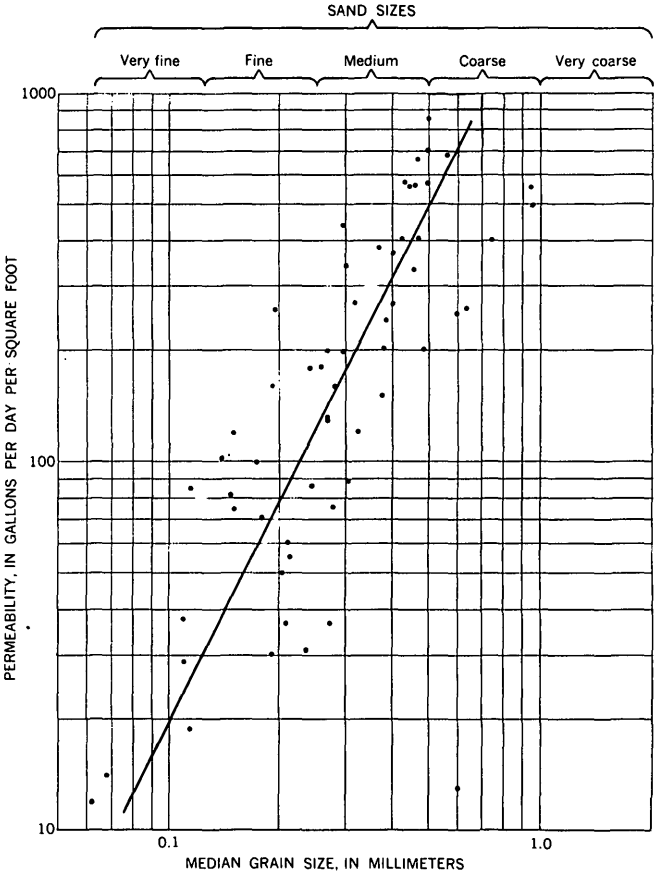

FIGURE 157.1.—Relation between median grain size and permeability in the Arkansas River valley, Arkansas.

rangement, and a similar relation has been expressed by other investigators in dealing with natural materials. This relation is approximately true for unconsolidated earth materials, within the range of "sand" and "finer gravel" sizes that are rounded and well sorted.

Using permeabilities read from the diagram (fig. 157.1), the transmissibility was estimated from test-hole logs at places where pumping tests had been made. In estimating the transmissibility a permeability was assigned to each lithologic unit in the log based on the approximate average grain size of the unit and degree of sorting as indicated by the description of the unit in the log.

The estimated transmissibilities were slightly lower than the transmissibilities from pumping tests. Consequently, the average permeabilities were arbitrarily assigned larger values so that the estimated transmissibilities agreed with the results of the pumping tests. The resulting permeabilities are given below.

Choice of values within the indicated ranges is a matter of care and judgement in examination of the drill cuttings, but after a little experience this generally can be done with fair to good accuracy.

Permeabilities of alluvial materials of the Arkansas River valley

[Gallons per day per square foot]

Type of material	Range in field coefficient of permeability
Sand, very coarse, and very fine gravel	6,000–15,000
Sand, very coarse	3,000– 9,000
Sand, coarse and very coarse	1,500– 4,000
Sand, coarse	800– 2,000
Sand, medium and coarse	400– 1,000
Sand, medium	200– 500
Sand, fine and medium	100– 250
Sand, fine	50– 140
Sand, very fine and fine	20– 60
Sand, very fine	10– 30

This method should be usable in many areas underlain by alluvial materials, but the values given above are not necessarily applicable to other areas. Comparisons between field and laboratory determinations should be made and adjusted as needed before attempting to apply the method elsewhere.

REFERENCES

Slichter, C. S., 1899, Theoretical investigation of the motion of ground waters: U.S. Geol. Survey 19th Ann. Rept., 1897–98, pt. 2, p. 295–384.

158. INFLUENCE OF PIEZOMETER HOLE DIAMETER ON DEPTH DETERMINATIONS IN A SMOOTH OPEN CHANNEL

By W. W. Emmett, Atlanta, Ga.

The accuracy of flowing-liquid analyses, whether the flow be in open channels or enclosed conduits, is limited by the degree of accuracy with which flow measurements are possible. In open-channel flow, the depth is often measured by means of a piezometer; the piezometric head is recorded on a manometer. An alternative method of measuring the depth is by a point gage. Commonly, simultaneous readings from a manometer and a point gage yield different values for the depth. These differences in values may be a significant percentage of the depth. A laboratory investigation [1] provides sufficient data to define the influence of piezometer hole diameter on piezometric-head measurements.

All tests for the investigation were conducted in the hydraulics laboratory of the Georgia Institute of Technology. A piezometer test section was located at the downstream end of a permanent laboratory flume, 10 inches wide, 18 inches deep, and 22 feet long. An electrically operated jack permitted adjustment in slope of the flume. An adjustable sluice gate and a sliding tailgate provided controls for uniform flow. Discharges were measured by either weight-time measurements or by a calibrated bend meter in the supply line.

A plan view of the piezometer test section is shown in figure 158.1. Twenty-four piezometer openings were carefully drilled into the stainless steel floor of the test section. An exception was the smallest opening which was drilled into a ¼-inch brass plug. The

[1] Emmett, 1961, Piezometric measurement of depth in open channels: Unpublished thesis, Georgia Inst. Tech.

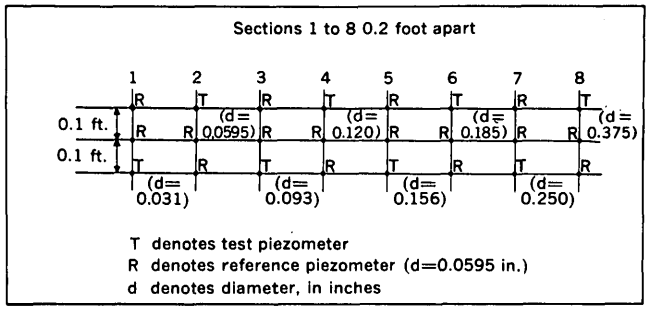

FIGURE 158.1.—Plan view of piezometer test section.

brass plug was threaded into and finished flush with the stainless steel floor plate. The piezometers were arranged at eight transverse sections, each section consisting of one test piezometer and two reference piezometers. From center to center, the piezometers at each section were located 0.1 foot apart. The test piezometer was one of the outer piezometers and its position was alternated from section to section. The piezometer sections were 0.2 foot apart. The last piezometer section was located 1.85 feet from the tailgate. Since only shallow depths were investigated, this distance was considered to be upstream of any influence of curvilinear flow due to tailgate or brink conditions. The test-piezometer diameters ranged from 0.031 to 0.375 inch and increased in the downstream direction. All reference piezometers were of constant diameter (0.0595 inch).

For all piezometers the length-diameter ratio was kept constant at a value of three by drilling the proper piezometer length into brass blocks attached to the underside of the piezometer test section. Copper tubing connected each of the piezometer taps to a manifold from which any one piezometer could be connected to any of several recording devices. All leads were of equal length to avoid the possibility of a relative influence of tubing length.

After establishment of uniform flow, piezometric heads were recorded for each of the 24 piezometer openings on two constant-displacement manometers (0.175 and 1.725 inches in diameter) and a differential-type pressure transducer. An advantage of the small manometer was its rapid response to fluctuations in the piezometric level. The large manometer gave a time-average piezometric reading. Gage zeroes for the instruments corresponded to the channel-floor elevation. Depths were then recorded as the piezometric head above the channel floor.

The range of conditions covered by the tests included channel slopes from 0.00291 to 0.0349, Froude numbers from 0.70 to 3.50, and depths from 0.084 to 0.173 feet.

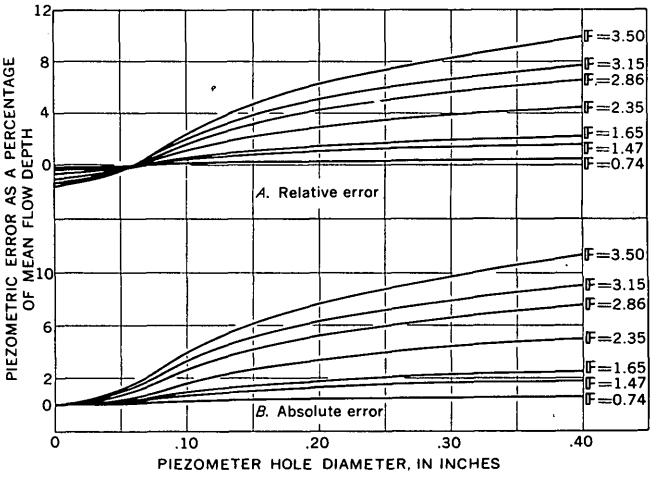

FIGURE 158.2.—Piezometric error, in percent of mean flow depth, as a function of the piezometer hole diameter and Froude number (F).

To indicate the relative influence of piezometer size, the depth obtained from the centerline reference piezometer, D_r, was subtracted from the depth obtained from the adjacent test piezometer, D_t. The resulting difference, plotted as a function of the respective test diameter, expressed the relative error due to piezometer diameter. In this manner, effects of slight nonuniform flow conditions were eliminated inasmuch as each reference piezometer was at the same channel section as the test piezometer.

The relative-error curves obtained from the described procedure revealed that the error was not only a function of the piezometer hole diameter, but was also dependent on the depth and the velocity of flow.

The effect of depth was eliminated by dividing the relative error of each test by the mean flow depth, D_m. The results were expressed as a percentage of the mean depth. This dimensionless relative-error parameter, $(D_t-D_r)/D_m$, is shown as a function of the piezometer hole diameter on figure 158.2 *A*.

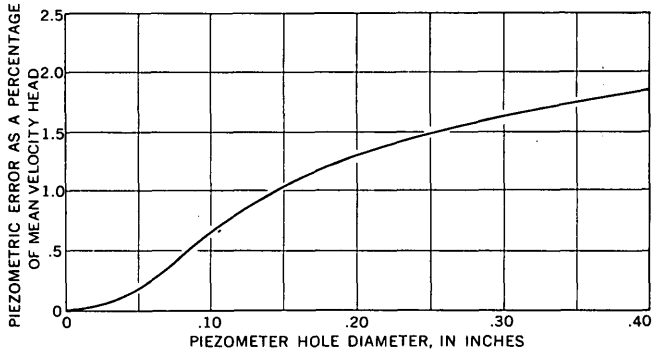

FIGURE 158.3.—Piezometer error in percent of mean velocity head as a function of the piezometer hole diameter.

To express the error in absolute rather than relative values, figure 158.2*B* was obtained from figure 158.2*A* by extrapolation to a zero diameter hole. The trend established by the curves in figure 158.2*A* indicated that there was no absolute error at a zero diameter hole. Thus, the curves were redrawn allowing the relative error to correspond with the absolute value.

Many experiments have confirmed that the static-pressure error is proportional to the dynamic head. For each test, the absolute error was divided by the mean velocity head, $V^2/2g$. When plotted as a function of the piezometer hole diameter, this dimensionless-error parameter defined the single curve shown in figure 158.3. This curve shows the piezometric error as a function of the piezometer hole diameter.

159. VARIATION OF MANNING'S *n* IN A SMOOTH RECTANGULAR OPEN CHANNEL

By Carl M. Lester, Atlanta, Ga.

A study of uniform flow in a rigid open channel has resulted in an analysis of the variation of Manning's n with the Froude number and the slope of the test channel.

The study was made in the hydraulics laboratory of the Georgia Institute of Technology. The experimental channel used is 3½ feet wide, 18 inches deep, and 81 feet long. The sides and bottom are constructed of steel plates; the inner surfaces are finished with synthetic enamel paint. Discharge is measured by venturi and orifice meters in the supply piping. Water surface levels are measured by point gages and floor piezometers. For a fixed discharge and slope, the depth of flow was regulated either by an adjustable head gate or tail gate, depending upon whether the flow was supercritical or subcritical. The normal flow depth was determined by a measurement of the surface profile at a depth just greater than the normal (M1 or S2 curve), and at a depth just smaller than the normal (M2 or S3 curve). The normal depth was then interpolated between the two backwater curves.

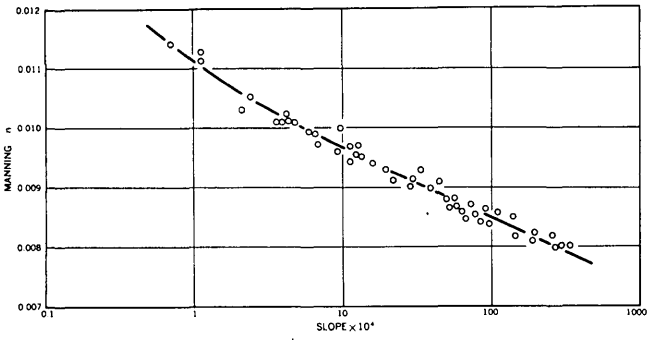

FIGURE 159.1.—Variation of Manning's n with slope for test data.

Twenty-four test runs were made in the subcritical flow range, and 25 in the supercritical flow range. The depth of flow, y, was varied from 0.10 to 0.50 foot, the discharge from 0.30 to 7.30 cubic foot per second, and the slope of the channel from 0.00007 to 0.0330.

The computed value of Manning's n varied between 0.0080 and 0.0114, a difference of about 42 percent. Analysis of the data disclosed an excellent correlation of the value of n both with flume slope, S_o, and Froude number, $\mathbf{F}=V/\sqrt{gy}$ where V is mean velocity (figs. 159.1 and 159.2).

For fully developed turbulent flow in smooth pipes, the generally accepted relation between the friction factor, f, and Reynolds number, $\mathbf{R}$, is the Karman-Prandtl resistance equation:

$$\frac{1}{\sqrt{f}}=2\log \mathbf{R}\sqrt{f}-0.8. \qquad (1)$$

The test results demonstrate that the same general form of resistance equation is applicable to the smooth open channel described above, provided that the hydraulic radius, r, is incorporated in the Reynolds number and the friction factor. The relation between the friction factor, $f=8rS_og/V^2$, and Reynolds number, $\mathbf{R}=4rV/\nu$, (ν is kinematic viscosity) for the laboratory channel is:

$$\frac{1}{\sqrt{f}}=2.03\log \mathbf{R}\sqrt{f}-1.30. \qquad (2)$$

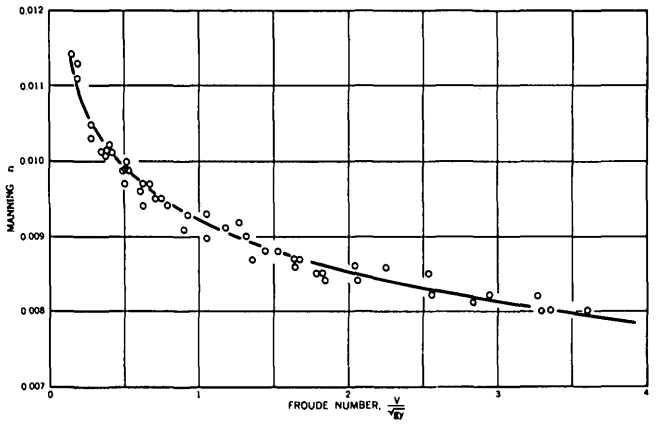

FIGURE 159.2.—Variation of Manning's n with Froude number for test data.

Manning's n and the friction factor f are related by the equation:

$$\frac{1}{\sqrt{f}}=\frac{1.486\ r^{1/6}}{\sqrt{8g}\quad n}. \tag{3}$$

In order to clarify the relation shown in figures 159.1 and 159.2, it is of interest to compute n directly from equations 2 and 3 for the range of flow conditions tested.

In figure 159.3, the value of n is shown as a function of channel slope. This relation was obtained from the simultaneous solution of equations 2 and 3 for a channel having the dimensions of the test channel. Slope was computed for arbitrarily assumed values of velocity and depth. The kinematic viscosity was assumed constant and equal to 1×10^{-5}. The curve drawn

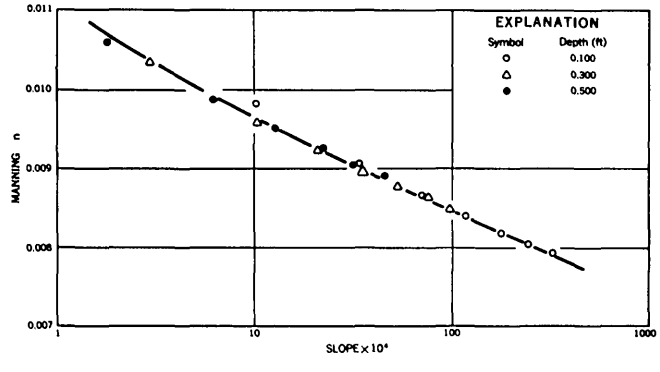

FIGURE 159.3.—Variation of Manning's n with slope by solution of equations 2 and 3.

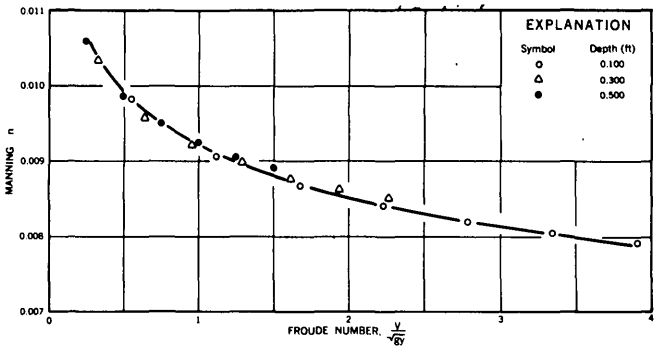

FIGURE 159.4.—Variation of Manning's n with Froude number by solution of equations 2 and 3.

through the points is the same as the one shown on figure 159.1. There is a small residual correlation of n values with depth; however, a single curve is a satisfactory average of the three depths considered.

In figure 159.4, equations 2 and 3 are solved to show n as a function of Froude number. The curve shown is the same as the one on figure 159.2. Again, a small variation of n with depth is apparent.

From equations 2 and 3 it is apparent that

$$f=\varphi(\mathbf{R}),$$

and

$$\frac{r^{1/6}}{n}=\phi(f)=\phi(\mathbf{R}). \tag{4}$$

From equation 4,

$$n=\phi(\mathbf{R}, r). \tag{5}$$

For a given channel the hydraulic radius, r, is a function of the depth of flow, y

$$\mathrm{r}=\phi(\mathrm{y}). \tag{6}$$

If kinematic viscosity is assumed constant, the basic variables of flow are reduced to three, only two of which are independent. Therefore, if the velocity and depth are known, the Reynolds number is fixed. It follows that,

$$\mathbf{R}=\phi(\mathbf{F}, y). \tag{7}$$

Combination of equations 5, and 6, and 7 leads to

$$n=\phi'(\mathbf{F}, y). \tag{8}$$

Figure 159.4 indicates that the influence of the depth of flow is small for the range of depths considered.

160. VARIATION OF FLOOD RATIOS WITH SIZE OF DRAINAGE AREA

By D. R. Dawdy, Phoenix, Ariz.

The index-flood method for expressing regional flood-frequency relations consists of two parts. The first is a correlation of the mean annual flood with various parameters of the drainage basin, of which size of drainage area has been the most important and sometimes the only parameter used. The second part is the construction of a flood-frequency curve, that shows floods of any given recurrence interval as having a constant ratio to the mean annual flood. An assumption that the same ratio can be used for different basins is not in accord with the general observation that smaller drainage areas have steeper frequency curves. Some data have been examined that show the variation of the flood ratio with size of drainage area, and the results are described in this paper.

In a study of flood-frequency relations in New England, peak discharge Q_T, for various recurrence intervals, T, was related to drainage area size, A, by the regression equation

$$Q_T = aA^b$$

where a and b are constants. It was found that the effect of size of drainage area, as measured by the exponent, b, varied with recurrence interval as follows:

T, in years	b	$b_T - b_{2.33}$
2.33	0.845	0
5	.822	−0.023
10	.794	−.051
25	.759	−.086
50	.680	−.165

The figures in the last column approximately determine the slope of the average curve relating the flood ratio $Q_T/Q_{2.33}$ to size of drainage area.

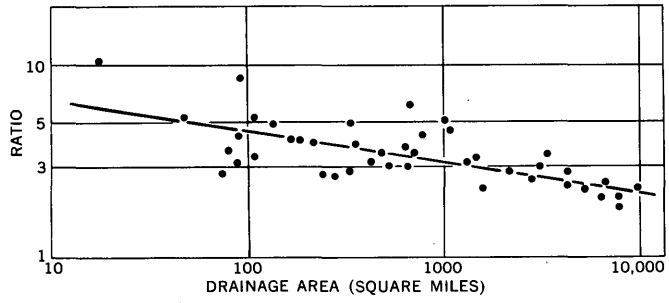

FIGURE 160.1.—Relation of drainage area to the ratio of historical flood (estimated recurrence interval between 100 and 199 years) to median flood for some New England streams.

Additional data for historical flood peaks in New England were examined as a check on the findings. All historical floods were divided into three groups on the basis of estimated recurrence interval, and graphs were made relating the ratios of historical flood to median flood with drainage area. The regression slope of the resulting curve for each group is given below, and the curve for group 2 given on figure 160.1.

Group	Recurrence interval, in years	Regression slope
1	50–99	−0.178
2	100–199	−.160
3	200 or more	−.141

Kuiper (1957) presents ratios of the 1 percent (100-year) flood to the mean annual flood for 100 North American rivers. When these data were grouped by river basins, it was found that for all basins except the Arkansas, the flood ratios are inversely proportional to drainage area, and the average regression slope is about −0.10. Figure 160.2 shows the relation for the Missouri-Mississippi River basin, which has the largest range in sizes of drainage basins.

Finally, using data from several statewide flood-frequency reports, ratios of 50-year flood to median flood were computed and plotted against drainage area. The resulting curve for each state showed a negative slope that averaged about −0.07 for all the curves. Figure 160.3 shows curves for 30 stations in Illinois for which the 50-year floods were satisfactorily defined by Mitchell (1954). Thirteen of the stations are in central Illinois, and 17 in northern or southern Illinois. Shown on figure 160.3 are the curves for the central division of Illinois and for the combined north-

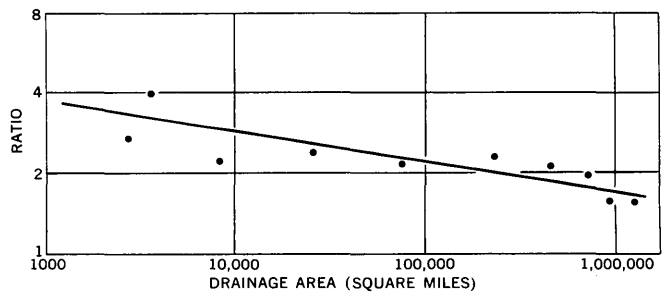

FIGURE 160.2.—Relation of drainage area to the ratio of the 100-year flood to mean flood for streams in the Missouri-Mississippi River basins.

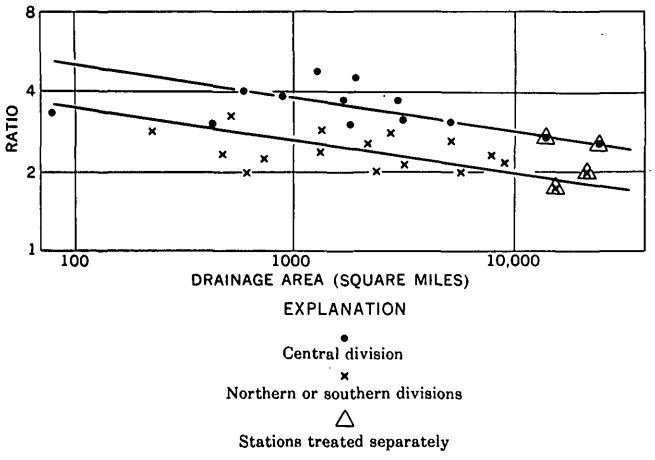

FIGURE 160.3.—Relation of drainage area to the ratio of the 50-year flood to the median flood for streams in Illinois. Data from Mitchell (1954).

ern and southern divisions. Each curve slopes −0.10. Incidentally, the Wabash River stations, which drain mainly the central division, and the Illinois River stations, which drain mainly the northern division, have flood ratios that are consistent with others in their respective divisions. Mitchell (1954), who did not consider the relation of flood ratio to drainage area, provided a separate dimensionless frequency curve for the Illinois River, and included the Wabash in his northern-southern division.

REFERENCES

Kuiper, E., 1957, 100 frequency curves of North American Rivers: Am. Soc. Civil Engineers Proc., v. 83, no. HY 5, Paper 1395, 31 p.

Mitchell, William D., 1954, Floods in Illinois, magnitude and frequency: Illinois Div. Waterways, 386 p.

161. ERRORS IN STREAMFLOW MEASUREMENT

By I. E. ANDERSON, Washington, D.C.

The accuracy of measurement of a constant discharge by the current-meter method depends on the number of observations of depth and velocity which are obtained and the reliability of the revolution-velocity rating of the current meter. This relation has been defined by a study of the individual components of the total error.

The usual method of making a discharge measurement is explained by reference to figure 161.1. The depth of flow in the cross section is measured with a sounding line at locations 1, 2, 3, and so forth. As the depth is measured, observations of velocity are obtained with the current meter at two points which are 0.2 of the depth and 0.8 of the depth from the water surface. Each observation of velocity represents the average velocity at the point during the period of observation which is about 45 seconds. The discharge is computed by:

$$Q=d_1\left(\frac{V_{.2}+V_{.8}}{2}\right)_1\left(\frac{b_1}{2}+\frac{b_2}{2}\right)+d_2\left(\frac{V_{.2}+V_{.8}}{2}\right)_2\left(\frac{b_2}{2}+\frac{b_3}{2}\right)+\cdots$$

where Q is discharge in cubic feet per second, d is depth in feet, b is the distance between locations in feet, and V is velocity in feet per second.

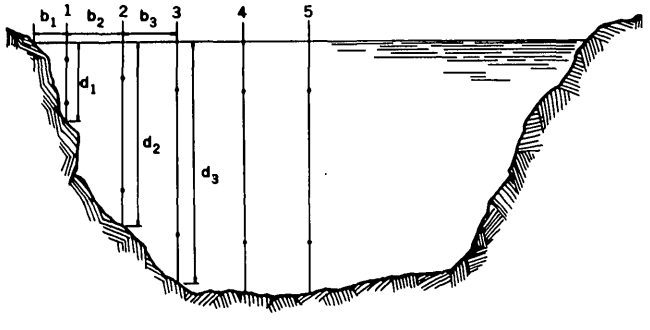

FIGURE 161.1.—Definition of method of discharge measurement. Dot shows place of velocity observation; d, depth; b, width.

Assuming no error in measurement of depth at a point or in measurement of the width of the cross section, the component errors in the discharge measurement and the related assumptions are:

1. The error, X_m, due to the assumption that the revolution-velocity rating of the current meter, which is based on towing the meter in still water, is unaffected by stream turbulence and the condition of the meter.
2. The error, X_v, due to the assumption that the mean of the velocity observations at 0.2 depth and 0.8 depth equals the mean in the vertical at locations 1, 2, 3, and so forth, during the time period of observation.

3. The error, X_p, due to the assumption that the mean of the velocity observations at 0.2 and 0.8 depth at one location does not vary with time.
4. The error, X_h, due to the assumption that the velocity and depth vary uniformly from locations 1 to 2 to 3, and so forth.

Assuming that these errors are independent, the total error, X_Q, is equal to the square root of the sum of the squares of the component errors. The errors X_m, X_v, X_p, X_h, and X_Q are given in terms of the standard error of discharge in percent of mean.

Meter error, X_m.—The Price current meters used by the Geological Survey are individually rated at the National Bureau of Standards by towing the meter through still water. To check the accuracy of these ratings, a group of meters was also rated at the David Taylor Model Basin and at Colorado State University. The deviation of ratings for any one meter was less than 1 percent.

The instrument error due to rating the meter in still water and operating it in turbulent flow is more difficult to evaluate. However, 10 duplicate measurements made on the Mississippi River at Vicksburg, Miss., first using the Ott current meter and then the Price current meter, agree within 1 percent. Similar comparative tests on the outflow rivers of the Great Lakes in 1959 led the Corps of Engineers to conclude that there is no significant difference in the result of velocity observations with the Ott and Price meters. Because the Ott meter tends to under-register and the Price to over-register in turbulent flows, these comparisons indicate that the effect of turbulence in measurement of stream flow is very small.

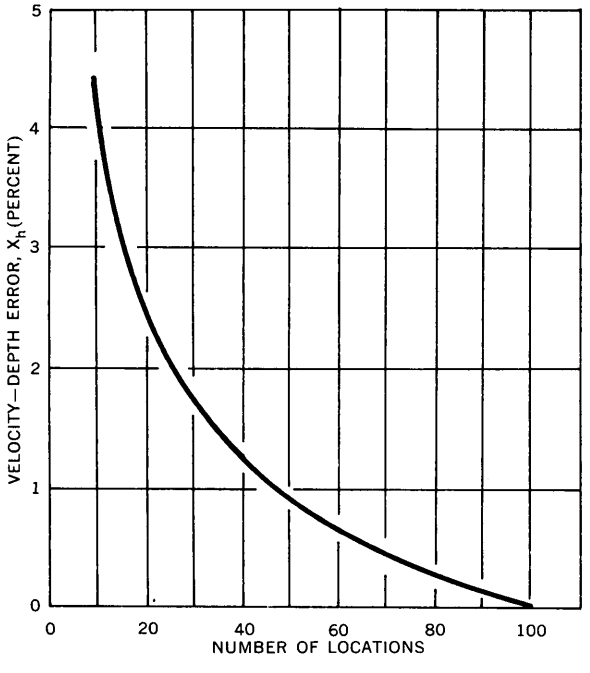

FIGURE 161.2.—Relation of the velocity-depth error, X_h, to the number of locations in a cross section at which observations of depth and velocity are obtained.

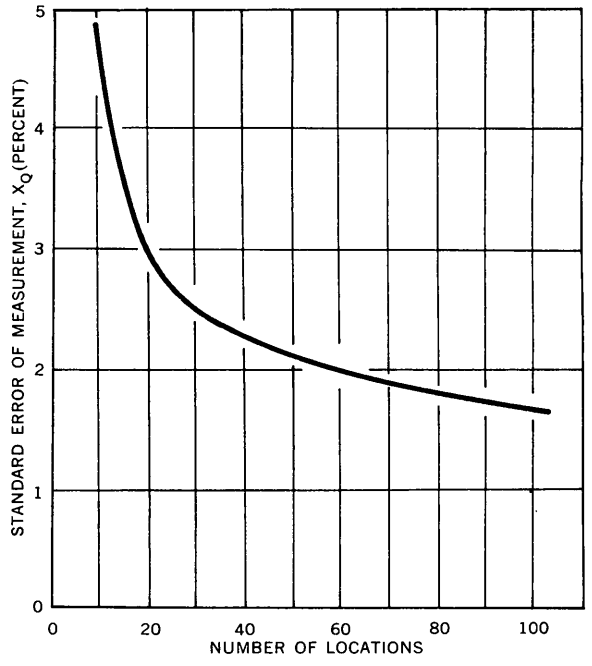

FIGURE 161.3.—Standard error of discharge measurements made by the 0.2 and 0.8 method using a 45-second time period for observation of velocity.

On the basis of these and other comparative tests the meter error, X_m, is assigned a value of 1 percent.

Velocity error, X_v.—The velocity error, X_v, due to the assumption that the average of the velocity observations at 0.2 depth and 0.8 depth is equal to the mean of the velocities in the vertical profile from the stream bed to the water surface, has been evaluated empirically. Comparisons were made of the discharge at 100 different stream sites computed from velocity observations at 11 points in each vertical at each location shown as 1, 2, 3, and so forth on figure 161.1, and the discharge computed from the velocity observed at 0.2 depth and 0.8 depth at these same locations. The error, X_v, determined by the comparison was 1.5 percent.

Velocity pulsation error, X_p.—Because the velocity of flow at any point in a section of flow varies randomly with time, even with a constant discharge, an error, X_p, is introduced. This error in discharge is related to the time period of observation of the velocity at a point. The error was evaluated for a sample of 23 streams by comparing the mean velocity at a point for short time periods with the mean for a 2-hour period.

The error, X_v, when individual velocities are observed for a 45-second time period, and the 0.2 depth and 0.8 depth method of velocity observation is used at n locations, is equal to $4.3/\sqrt{n}$.

Velocity-depth error, X_h.—The error due to nonuniform variation of depth and velocity from locations 1 to 2 to 3 and so forth (fig. 161.1) is a function of the number of locations at which observations are taken. The error was evaluated at 130 stream sites by comparing the discharge computed from observations at 100 locations per site with the discharge computed from observations at fewer locations. The relation between X_h and number of locations is shown on figure 161.2.

Total error.—The discharge measurement error, X_Q, based on the combination of the component errors, is given on figure 161.3 for a 45-second period of observation and the 0.2 depth and 0.8 depth method of velocity observation. According to this relation, if the velocity and depth are observed at 20 or more locations in the cross section, the error in the total discharge is expected to be less than 3 percent for 67 percent of the discharge measurements.

162. COMPUTATION OF HOMOGENEOUS FLOWS IN TIDAL REACHES BY FINITE-DIFFERENCE METHOD

By R. A. Baltzer and John Shen, Lansing, Mich., and Washington, D.C.

Unsteady flows in tidal reaches result from the intrusion of sequences of translatory waves through the coastal outlets. In its broad sense, river flow in tidal reaches is the composite flow resulting from the superposition of translatory-wave motion upon otherwise undisturbed open-channel streamflow.

Astronomical tides, although known to be the primary cause of tidal flows, are seldom the only causative factor. Storm surges and seismic disturbances are also significant. Waves of the latter origins are neither periodic nor continuously sustained. Consequently, tidal flow can only be classified as a semiperiodic phenomenon.

Fundamentally, tidal flow in an open channel can be described by two differential equations: one expressing the conservation of mass, or the equation of continuity; and the other expressing conservation of momentum, or the equation of motion.

Under conditions of moderately unsteady, open-channel flow, the components of velocity and acceleration across the channel, and particularly the component of acceleration in the vertical direction, are all relatively insignificant and hence may be neglected. This simplification is valid provided that no abrupt wave such as a tidal bore occurs. Thus, for an idealized tidal reach the flow is treated as one dimensional. Moreover, the density of the fluid is assumed to be homogeneous. On the basis of these assumptions, the following system of equations may be derived:

$$\frac{\partial Q}{\partial x}+b\frac{\partial z}{\partial t}=0; \tag{1}$$

and,

$$\frac{\partial z}{\partial x}+\frac{u}{g}\frac{\partial u}{\partial x}+\frac{1}{g}\frac{\partial u}{\partial t}+u|u|\frac{A^2}{K^2}=0, \tag{2}$$

in which, x is the distance measured in the downstream direction along the channel; t is the time; Q is the discharge; A is the cross-sectional area of the channel; b is the width of the water surface, z is the water-surface elevation; g is the acceleration of gravity; u is the mean velocity of flow; and K is the conveyance of the channel.

A schematic tidal reach is shown on figure 162.1. An annex section, m, is also provided to simulate the overflow section. In general, the velocity of flow in the overflow portion is negligible and may thus be excluded from the dynamical equation.

The term, $\frac{u}{g}\frac{\partial u}{\partial x}$, in equation 2 is generally of small magnitude and hence may be disregarded with practically no sacrifice in accuracy, provided the mathematical representation is limited to tidal flow in increments of channel of reasonably uniform cross section.

With the foregoing assumptions, and by using the relations, $Q=Au$, and $b'=b+m$, equations 1 and 2 may be written as:

$$\frac{\partial Q}{\partial x}+b'\frac{\partial z}{\partial t}+q=0; \tag{3}$$

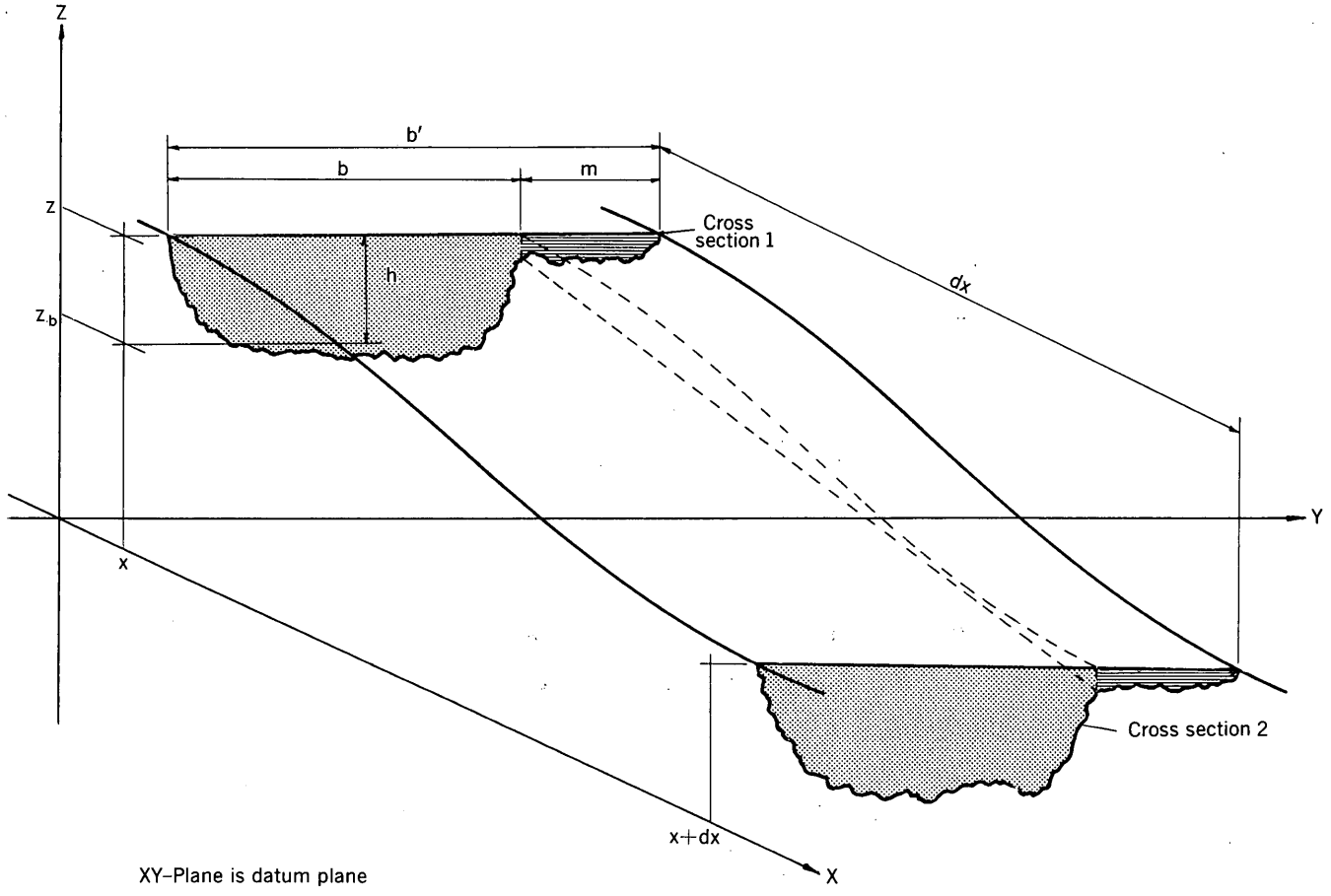

FIGURE 162.1.—A schematic tidal reach.

and,

$$\frac{\partial z}{\partial x}+\frac{1}{gA}\frac{\partial Q}{\partial t}+\lambda\frac{Q^2}{K^2}=0, \quad (4)$$

in which q represents any lateral diversion from the reach, and λ is a sign operator to be used to maintain the proper directional sense of the nonlinear resistance term. By definition, $\lambda=|Q|/Q$.

The above two equations are in the form of a set of first-order nonlinear hyperbolic partial differential equations in two independent variables. An explicit analytical solution of such a set of equations is not possible. Thus, one is forced to adopt numerical, finite-difference methods of solution. In addition, the initial conditions and the boundary conditions must also be satisfied to obtain a uniquely defined solution.

Fourier series offer one possible means for evaluating the boundary-value problem (Dronkers and Schönfeld, 1955, p. 11–24). However, this technique is precluded because the superposed fluctuations are not strictly periodic.

Power series offers another means for evaluating the tidal-flow equations (Dronkers, 1949, p. 330–337, 479–487). In fact, Taylor series is the basis for the particular evaluation technique developed as a result of this study.

By expanding equations 3 and 4 in Taylor series about an arbitrarily selected point in a tidal reach at a particular moment of time, and using successive iterations, one gets

$$z_x=z_o-\lambda\frac{Q^2}{K^2}x-\frac{x}{gA}\frac{\partial Q}{\partial t}+\lambda\frac{Qb'x^2}{K^2}\frac{\partial z}{\partial t}+\frac{b'x^2}{2gA}\frac{\partial^2 z}{\partial t^2}$$
$$-\frac{2}{3}\frac{Q^2b'x^3}{K^4}\frac{\partial Q}{\partial t}-\frac{2}{3}\lambda\frac{Qb'x^3}{gAK^2}\frac{\partial^2 Q}{\partial t^2}-\lambda\frac{(b')^2x^3}{3K^2}\left(\frac{\partial z}{\partial t}\right)^2$$
$$-\frac{\lambda}{3}\frac{b'x^3}{gAK^2}\left(\frac{\partial Q}{\partial t}\right)^2-\frac{b'x^3}{6(gA)^2}\frac{\partial^3 Q}{\partial t^3}+\lambda\frac{Qx^2}{K^2}q$$
$$-\frac{2}{3}\lambda\frac{qb'x^3}{K^2}\frac{\partial z}{\partial t}-\frac{\lambda}{3}\frac{q^2}{K^2}x^3. \quad (5)$$

The above expression represents only the first three terms of the Taylor-series expansion. Fortunately, this was found to be more than sufficient to accurately

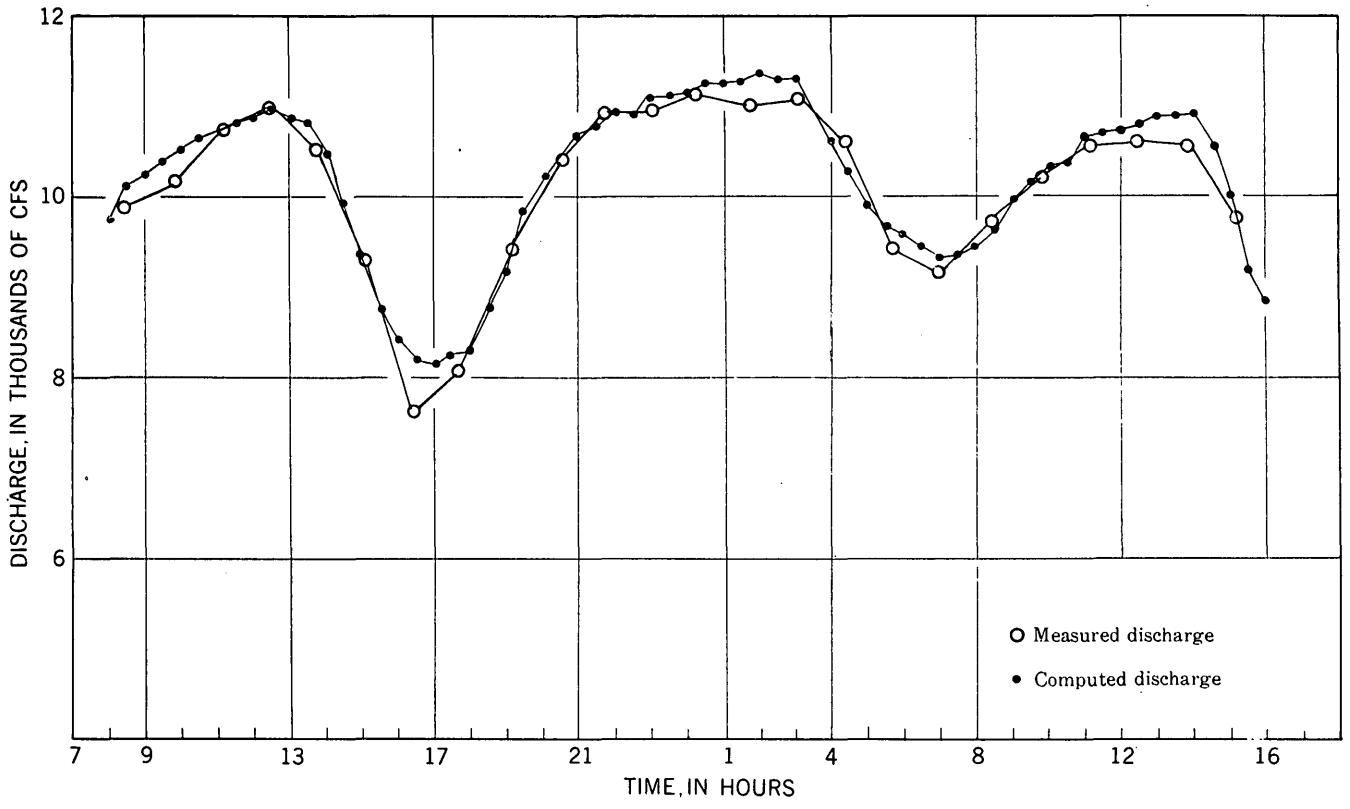

FIGURE 162.2.—Comparison of computed and measured discharge for Sacramento River at Sacramento, Calif., during January 30–31, 1957.

represent the tidal-flow solution. Rewriting this expression in the form of increments and eliminating secondary quantities, one obtains the expression

$$\Delta Q=\left[gA\frac{\Delta z}{\Delta x}-\lambda\frac{gAQ^2}{K^2}+\lambda\frac{gAQb'\Delta x}{K^2}\frac{\Delta z}{\Delta t}+\lambda\frac{gAQq}{K^2}\Delta x+\frac{b'\Delta x}{2}\frac{\Delta^2 z}{\Delta t^2}-\lambda\frac{gA(b')^2(\Delta x)^2}{3K^2}\left(\frac{\Delta z}{\Delta t}\right)^2\right]\Delta t, \quad (6)$$

in which ΔQ is the change in discharge during an increment of time, Δt; and $\Delta z=z_o-z_x$. This expression is valid provided the selected increment of reach length, Δx, and the time increment, Δt, are within the limits of convergence of the power series.

Thus, once the boundary values for a tidal reach, A, b, K, Δx and Δz are known, the value of ΔQ becomes uniquely defined. Then, by computing the change in discharge during each time increment and adding this value to the total discharge occurring at the beginning of the increment, the discharge at the beginning of the next increment is known. This process is simply repeated to obtain a sequence of values of discharge at the selected point in a tidal reach.

The method has been tested by computing the flow in the Sacramento River, Calif. Actual computations were carried out by a high speed digital computer. The computed results for the period of January 30–31, 1957 are compared with the measured discharge in figure 162.2 and close agreement is shown.

A similar test has also been made for Three-mile Slough in California with satisfactory results. An important characteristic of this technique is that even though an erroneous initial value of discharge may be assumed, the evaluation process converges to the correct values after only four or five cycles of computation provided that the power series is convergent.

REFERENCES

Dronkers, J. J., 1949, An iterative process for the solution of a boundary-value problem of a linear partial differential equation of the second order [Dutch text]: Koninkl Nederlandse Akad. Wetensch. Proc., v. 52.

Dronkers, J. J. and Schönfeld, J. C., 1955, Tidal computation in shallow water: Am. Soc. Civil Engineers Proc., v. 81, Separate no. 714.

601530 O—61——4

163. OBSERVATION OF UNSTEADY PHENOMENA IN AN OPEN CHANNEL

By Richard G. Godfrey, Washington, D.C.

Work done in cooperation with the U.S. Atomic Energy Commission

Observations of hydraulic events are commonly made at a fixed point as the phenomena pass. An example is the recording of the stage of a flood wave as it passes a gaging station. If the flood wave is changing shape as it progresses, the shape recorded at the gage will be different from the shape which would be defined by many simultaneous observations at points distributed throughout the length of the wave. This paper is concerned with measuring the longitudinal dispersion of a miscible tracer in water flowing in an open channel. The wave of tracer concentration is analyzed to demonstrate the differences between the time-concentration curve obtained from observations at one point over time and the distance-concentration curve obtained from simultaneous observations at many points. An example of the difference in the two curves is shown on figure 163.1. For the fixed observer the time from injection to peak concentration is shortened and the magnitude of the peak is increased.

Taylor (1954) has shown that for uniform flow the dispersion pattern has the following mathematical form in the one dimensional case:

$$C=Bt^{-\frac{1}{2}}\exp\frac{-(X-Vt)^2}{4Kt} \tag{1}$$

where C is the concentration; t is time after injection; X is distance from point of injection; V is mean velocity; K is the coefficient of dispersion; and B is a constant.

If the injection of the tracer is instantaneous in a line source across the stream, the constant may be evaluated as follows:

$$C=\frac{M}{A\sqrt{2\pi}\sqrt{2Kt}}\exp\frac{-(X-Vt)^2}{4Kt} \tag{2}$$

where M is the amount of tracer injected and A is the cross sectional area of the channel. Equation 2 can now be compared to the normal or Gaussian distribution

$$y=\frac{N}{\sqrt{2\pi}\sigma}\exp\frac{-(X-\overline{X})^2}{2\sigma^2} \tag{3}$$

where N is the number of observations, $\overline{X}$ is the mean of distribution, and σ is the standard deviation of the distribution. The comparison shows that:

$$\overline{X}=Vt$$
$$\sigma=\sqrt{2Kt}$$

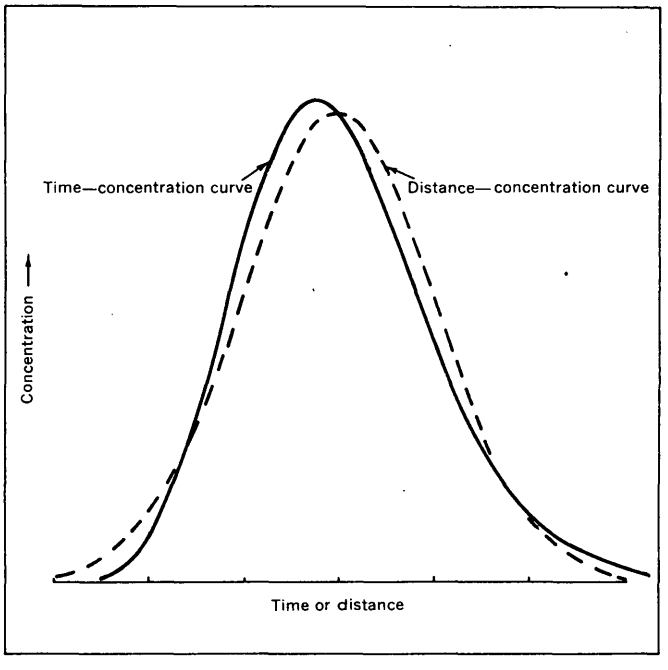

FIGURE 163.1.—Relation between time-concentration and distance-concentration curves for same event.

It can be seen that equation 2 is normal at any particular time, t. The peak value of concentration occurs when $x=Vt$ and is:

$$C_{max}=\frac{M}{A\sqrt{2\pi}\sqrt{2Kt}} \tag{4}$$

Thus the maximum concentration varies inversely with the square root of t.

In dispersion experiments it is far more feasible to measure concentrations of a tracer over time at one point rather than to measure the concentrations simultaneously at many points along a reach of channel. In conducting tests in a manner where x is held constant rather than t, something other than a normal distribution will be observed, as $\sigma=\sqrt{2Kt}$ is not constant.

By differentiating equation 2 with respect to t and setting the result equal to zero, the time of the maximum concentration t_{max}, is found to be:

$$t_{max}\ (x \text{ is constant})=\frac{(K^2+X^2V^2)^{\frac{1}{2}}-K}{V^2} \tag{5}$$

Differentiating equation 2 with respect to x yields

$$t_{max}\ (t \text{ is constant})=\frac{X}{V} \tag{6}$$

The first case represents the stationary observer watching the event pass. The second represents a set of simultaneous observations.

The ratio of equation 5 to equation 6, which is designated by R_T, reduces to:

$$R_T = -J + (J^2+1)^{\frac{1}{2}} \quad (7)$$

where J is a dimensionless constant:

$$J = \frac{K}{VX}$$

Substituting equation 5 in equation 2 and dividing this result by equation 4 yields the ratio, R_P, of the peak value of the time-concentration curve to that of the distance-concentration curve.

$$R_P = \left[\frac{1}{-J+(J^2+1)^{\frac{1}{2}}}\right]^{-\frac{1}{2}} \exp\left[\frac{1}{J}[1-(J^2+1)^{\frac{1}{2}}]\right]^{\frac{1}{2}} \quad (8)$$

Equations 7 and 8 are shown on figure 163.2. Note that the observed magnitude of R_P changes almost linearly with J. R_P can be closely approximated by:

$$R_P \approx 1 + \frac{K}{4VX}$$

The relation between R_T and J is more curvilinear, yet over the normally observed values of J (0 to 0.1) it can be approximated by:

$$R_T \approx 1 - \frac{K}{VX}$$

Dispersion tests have been conducted in 5 reaches of natural streams and 1 canal. The values of J have not exceeded 0.05 and were usually less than 0.01. From the above analysis it can be seen that under these conditions the observations over time will yield the same results as simultaneous observations.

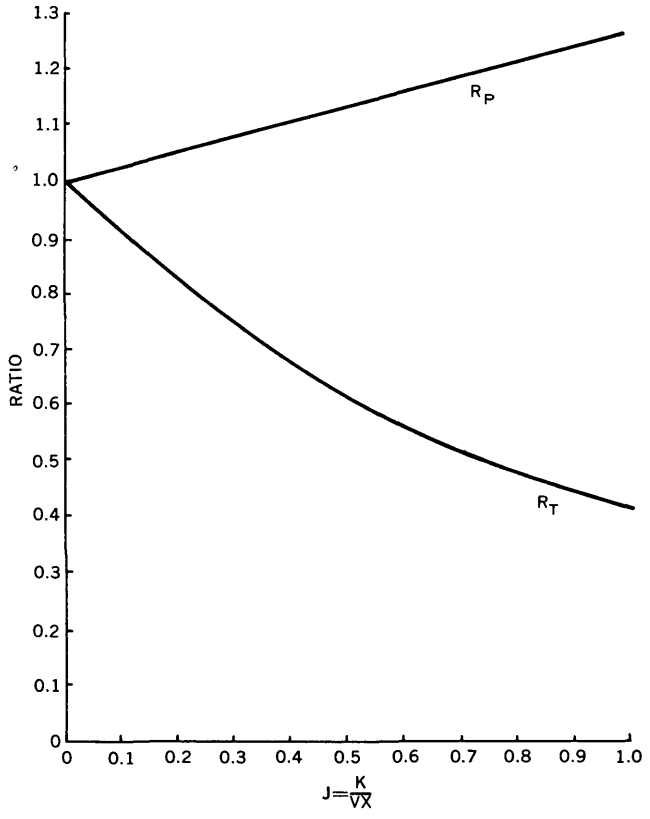

FIGURE 163.2.—Comparison of characteristics of time-concentration and distance-concentration curves. R_P is ratio of peak concentrations; R_T is ratio of elapsed times from injection of the tracer to the observed peak.

REFERENCES

Taylor, G. I., 1954, The dispersion of matter in turbulent flow through a pipe: Royal Soc. London Proc., A–223, p. 446–468.

164. SPECIAL YIELD OF SEDIMENTS OF THE HUMBOLDT RIVER VALLEY, HUMBOLDT COUNTY, NEVADA

By PHILIP COHEN, Carson City, Nev.

Work done in cooperation with the Nevada Department of Conservation and Natural Resources

Two hundred and nine sediment samples were collected in the fall of 1959 from the Humboldt River Valley near the city of Winnemucca in north-central Nevada, and were analyzed for specific yield and particle-size distribution in the Hydrologic Laboratory of the Geological Survey, Denver, Colo. The specific yields are needed to compute changes in ground-water storage within the area.

The specific yield of a rock or sediment was defined by Meinzer (1923, p. 28) as "* * * the ratio of (1) the volume of water which, after being saturated, it will yield by gravity to (2) its own volume." This ratio

multiplied by 100 expresses specific yield as a percentage. The definition does not state how long the sample should be allowed to drain; however, it is generally assumed that sufficient time is required to allow for complete gravity drainage.

Specific yields were determined in the laboratory by the indirect centrifuge-moisture-equivalent method. First, the porosities of the samples, expressed in percentages of the volume of the samples, were determined. Then the centrifuge-moisture equivalents, or the amounts of water retained by the samples after they were subjected to a force equal to 1,000 times the force of gravity for 1 hour, were determined, and were expressed, also, in percentages of the volume of the samples. Using a method described by Piper and others (1939, p. 118–119), the centrifuge-moisture equivalents were converted to specific retentions. The specific yields of the samples then were determined by the formula—

$$\text{Specific yield} = \text{porosity} - \text{specific retention}$$

The results of the laboratory analyses are summarized in table 164.1.

TABLE 164.1—*Specific yield of sediment samples from the Humboldt River Valley, Humboldt County, Nev.*

	Range of median diameters (millimeters)								All samples
	0.004–0.0625	0.0625–0.125	0.125–0.25	0.25–0.5	0.5–1	1–2	2–4	4–8	
Number of samples	121	15	17	23	6	19	7	1	209
Mean specific yield percent	19.1	21.4	25.9	25.9	22.2	20.8	17.4	17.4	20.7
Range of specific yield percent	1.0–34.1	2.5–36.5	7.0–35.4	7.2–39.5	10.7–35.3	4.6–36.2	4.9–27.4	------	1.0–39.5

From these data it can be seen that there is a large range in specific yield within each median particle-size class. All other factors being equal, specific yields should tend to approach a constant value within each particle-size class and should increase as the median particle sizes increase. The large range in specific yields within each particle-size class for the sediments sampled probably is due to the presence of sedimentary structures (especially in some of the finegrained sediments), differences in the degree of compaction of the sediments, and complex interrelationships among specific retention, median particle size, porosity, and sorting coefficient. The observed relations among these parameters for the sediments of the Humboldt River Valley are: (a) specific retention tends to increase as median particle size decreases; (b) porosity tends to increase as median particle size decreases; (c) porosity tends to be independent of the sorting coefficient; and (d) sorting coefficient tends to increase as median particle size decreases.

Table 164.1 shows that the mean specific yields for samples whose median particle sizes fall within the silt-size range is exceptionally high—about 19 percent. Piper and others (1939, p. 121) determined that the average specific yield of samples of very fine sand, silt, and clay is 4.2 percent. Kues and Twogood (1954, p. 33) found that the average specific yield of clay, clayey silt, and silt ranges from about 2 to 14 percent. The relatively high specific yields associated with the fine-grained sediments of the Humboldt River Valley probably is due to the fact that most of the sediment samples whose median particle sizes fall within the silt-size range were collected from recently deposited soil of the flood plain of the river. These sediments commonly are characterized by a moderately high secondary porosity caused by plant roots and burrowing invertebrate animals. In addition, because of the relatively shallow depth of burial, most of the fine-grained sediments have not been subjected to significant compaction by the weight of overlying sediments.

The mean specific yield of the 209 sediment samples is about 21 percent. While it is true that for some of the size classes the mean specific yields are somewhat lower or higher than 21 percent, it is significant that, for most size classes, these values do not differ substantially from 21 percent. The tendency for the mean specific yield to approach 21 percent probably is a consequence of relations (a) and (b) described above. As the median particle size changes, the porosity and specific retention tend to change in the same direction, and because porosity and specific retention tend to change at the same rate, the difference between the two (specific yield) tends to approach a constant value.

Terzaghi (1949, p. 352–353) indicated that specific yields determined by the centrifuge-moisture-equivalent method are related to time by the equation

$$t = (N^2)(\bar{t})$$

According to this equation, the degree of drainage of a saturated sample of thickness H, subjected to a centrifugal force equal to N times the force of gravity for a time $\bar{t}$ is equal to the degree of drainage due to gravity from a bed of the same material of NH thickness in time t. The method used to obtain the laboratory data presented in this paper involves subjecting samples approximately ½-inch thick to a centrifugal force equal to 1,000 times the force of gravity for 1 hour. Thus, the laboratory specific yields are indicative of the degree of drainage that would occur in a layer of sediments approximately 40 feet thick during a period of about 100 years.

Within the limitations imposed by the variability of the data and the complexity of the geology, the labora-

tory data can be used to arrive at an approximation of the total amount of ground water in storage. The laboratory method must be modified to evaluate changes in ground-water storage that occur during relatively short periods of time at shallow depths. The problems involved are especially critical for fine-grained sediments but also are serious for coarser sediments.

REFERENCES

Kues, H. A., and Twogood, D. A., 1954, San Luis unit, West San Joaquin Division, Central Valley Project (ultimate plan) including reconnaissance of Avenal Gap unit, App., Local water resources: U.S. Bur. Reclamation open-file report, 81 p.

Meinzer, O. E., 1923, Outline of ground-water hydrology, with definitions: U.S. Geol. Survey Water-Supply Paper 494, 71 p.

Piper, A. M., Gale, H. S., Thomas, H. E., and Robinson, T. W., 1939, Geology and ground-water hydrology of the Mokelumne area, California: U.S. Geol. Survey Water-Supply Paper 780, 230 p.

Terzaghi, K. V., 1949, Soil moisture, *in* Meinzer, O. E., Hydrology: New York, McGraw-Hill, p. 331–363.

165. VARIABLE DEPTH-DISCHARGE RELATIONS IN ALLUVIAL CHANNELS

By D. B. Simons, E. V. Richardson, and W. L. Haushild, Fort Collins, Colo.

The large changes in resistance to flow that occur in an alluvial channel significantly effect the stage-discharge and depth-discharge relations. The changes in resistance to flow are related to the two regimes of flow and forms of bed roughness. These regimes and the possible corresponding forms of bed roughness are as follows:

Regime	*Bed roughness*
Lower flow	Ripples; dunes with ripples superimposed; dunes.
	Transition zone connecting the two regimes of flow in which dunes are eliminated as boundary shear is increased.
Upper flow	Plane bed; standing waves; antidunes; violent antidunes.

The magnitude of the resistance to flow can change three-fold with changes in bed form. For example, the Manning n can be as small as 0.012 for a plane bed form and as large as 0.036 for a dune bed form.

The form of bed roughness depends on the magnitude of the shear stress exerted by the water on the bed, the fall velocity of the bed material, the shape of the reach and cross section, and the rate of change of discharge. In addition, depth-discharge relations are affected to a minor extent by scour and fill, by wind action, vegetation, and seepage forces.

Depth-discharge relations were studied in a recirculation-type laboratory flume 150 feet long, 8 feet wide, and 1.5 feet deep by using two different bed materials. Three general types of depth-discharge relations were found which are illustrated by the four curves shown on figure 165.1.

With lower regime bed forms, the depths and discharges for each flood event are related as shown by figure 165.1*A*, *B*, in which the curves form a loop or even cross to form two loops. The shape of the curves for a given reach of channel are infinite in number, because each new runoff event yields a different set of curves unless the flows and channel conditions are identical. In general, the shape of the curves depends on the bed roughness, the time it takes for the bed roughness to form, and the rate of change of discharge. The above three factors are determined primarily by the energy grade line, the fall velocity of the bed material, the magnitude of the discharge, and the rate of change of discharge with time.

The main reason for the loop curve illustrated by figure 165.1*A* is that the formation and alteration of roughness elements and hence resistance to flow lags behind the change in discharge. For instance, when discharge increases, the dune size does not increase at a rate corresponding to the rate at which the discharge and shear stress increase. Conversely, when discharge decreases, the rate of decrease in size of the dunes formed at a greater depth lags behind the rate of decrease of discharge, and resistance to flow is relatively large. Thus, the curve for increasing discharge and depth is lower than the curve for decreasing discharge and depth. The curve shown by figure 165.1*B* results

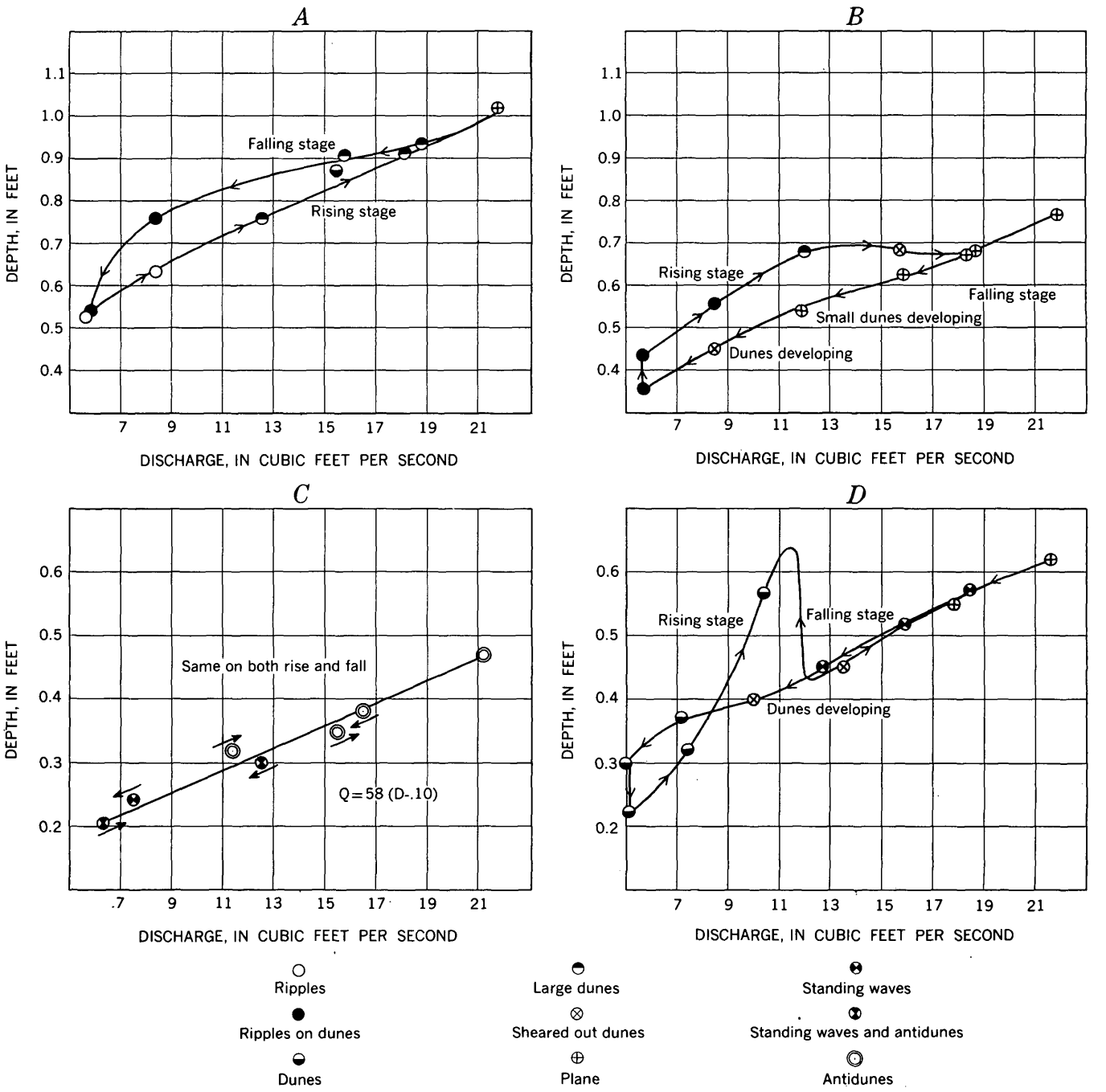

FIGURE 165.1.—Depth, discharge, and form of bed roughness in alluvial channels.

when the resistance of flow becomes larger with increasing depth and smaller with decreasing depth.

A second type of depth-discharge relation occurs when the bed form is always in the upper flow regime regardless of the discharge (fig. 165.1*C*). The depth-discharge curve is the same for both increasing and decreasing discharge inasmuch as only small changes in resistance to flow occur as the discharge and depth changes.

The third general relation of depth to discharge results when the shear stress varies over such a wide range that ripples and (or) dunes form at small discharges, and a plane bed, standing waves, or antidunes form at large discharges (fig. 165.1*D*). With shallow depths and low discharges, the depth-discharge relation will be similar to the first type of curve, but there will be a change at some intermediate discharge and depth to the relation illustrated by the second type of

curve. This change from the first type of curve to the second will result in a shift or break in the depth-discharge relation. The shift or break in the relation when the discharge is increasing will be to a shallower depth for the same discharge or a larger discharge for the same depth. When the discharge is decreasing, the shift or break will be to a deeper depth for the same discharge or the same depth for a smaller discharge. A break or shift in the depth-discharge relation results from an increase or decrease in resistance to flow as the flow regime changes. The change from one depth-discharge relation to the other will not occur at the same depth and discharge for the rising and falling stages, nor will it occur at the same depth and discharge from one runoff event to another.

Stage-discharge relations are affected by all the factors that determine the depth-discharge relations, but they are affected more by local scour and fill. Thus, stage-discharge curves may be similar to, or quite different from, corresponding depth-discharge curves—depending on the amount of scour or fill and the change in porosity of the bed with change in the form of bed roughness.

Colby (1960), Culbertson and Nordin (1960), and Dawdy (1961) find that the relations depicted on figure 165.1 apply in natural streams.

REFERENCES

Colby, D. R., 1960, Discontinuous rating curve for Pigeon Roost and Cuffawa Creeks in northern Mississippi: U.S. Dept. Agriculture, ARS 41–35.

Culbertson, J. K., and Nordin, C. F., 1960, Discussion of discharge formula for straight alluvial channels: Am. Soc. Civil Eng. Jour., v. 86, no. HY6.

Dawdy, D. R., 1961, Depth-discharge relation of alluvial streams: U.S. Geol. Survey Water-Supply Paper 1498–C.

166. LOWEST MULTI-YEAR MOVING AVERAGE COMPARED WITH MINIMUM INDEPENDENT MULTI-YEAR MEANS

By Clayton H. Hardison, Washington, D.C.

In areas where the lowest streamflow is insufficient to meet the demand, storage reservoirs are designed to carry over water from years of surplus to years of deficiency. Thus, the number and severity of consecutive years of low flow are factors in the designs of such reservoirs, as is also the probable frequency with which such years can be expected to recur. Strict statistical analysis of a record of given length requires that the frequency of occurrence of multi-year averages be computed by dividing the record into equal-length consecutive periods, and taking the minimum of these independent averages. In practice however, this arbitrary subdivision may obscure the lower discharge of a period of years that fell partly in one period and partly in an adjoining period. In the rest of this paper, the minimum independent averages are called minimum independent means to avoid confusion with other averages. The study of random numbers reported in this paper was undertaken to determine the difference between the lowest moving average and the minimum independent mean to determine how to obtain the lowest moving average for a 50-year recurrence interval from a distribution of independent multi-year means, such as given by the Corps of Engineers (1958).

By the use of random numbers from table 23 in Dixon and Massey, (1957) an estimate was obtained of the amount by which the lowest 10-year mean in 59 years of record is smaller than the 10-year minimum taken from 5 independent 10-year means. To make this estimate, the random numbers in table 23 were assumed to represent annual runoff, and 10-year means were computed for 5 successive groups of 10 years starting with year number 1; the lowest 10-year mean thus computed is 1.73. Then, starting with the second random number in table 23 and continuing through the the 51st random number, another set of five 10-year means was obtained of which the lowest is 1.87. This process was continued 8 more times, the last time starting with the 10th random number and ending with the 59th random number. The average of the 10 lowest means thus obtained is 1.83, and the lowest of the 50 means is 1.71—a difference of 0.12. As the figure of 1.71 is also the lowest moving 10-year average for

random numbers 1–59, this difference is an estimate of the probable difference between a minimum independent 10-year mean in a sample of 50 years and the lowest moving average to be plotted at the 50-year recurrence interval, because

$$\text{Recurrence interval}=\frac{n-t+1}{m}$$

where n is the number of years in the sample, m is the order number, and t is the number of years in the multi-year average. The results are listed on the first line of table 166.1.

TABLE 166.1.—*Computation of estimated difference between a minimum independent 10-year mean in 50 years of record and the lowest moving 10-year average at the 50-year recurrence interval*

Starting numbers	Average of 10 lowest or of 10 highest independent means		Difference between figures shown in second or third columns and the lowest or highest moving averages	
	Lowest	Highest	Lowest	Highest
1–10	1. 83	2. 55	0. 12	0. 15
51–60	1. 73	2. 50	. 09	. 32
101–110	1. 58	2. 04	. 11	. 30
151–160	1. 88	2. 58	. 05	. 16
201–210	1. 64	2. 33	. 15	. 27
251–260	1. 56	2. 36	. 23	. 23
301–310	1. 73	2. 38	. 13	. 10
351–360	1. 72	2. 64	. 43	. 09
401–410	1. 53	2. 22	. 20	. 13
451–460	1. 63	2. 12	. 19	. 09
Average	1. 68	[1] 2. 37	0. 170	0. 184
Overall average	1. 66		0. 18	

[1] Used as 1.63, because if scales were reversed, 0.37 above the mean of 2.00 would correspond with 0.37 below the same mean.

A second test was obtained by starting with the 51st random number, and 8 other estimates were obtained by starting with random numbers 50 items apart. The results are summarized in lines 2–10 of table 166.1. The average of the 10 averages is 1.68 and the average of the 10 differences is 0.170. The highest 10-year means in each 5 groups of 10 random numbers give another set of data which, when averaged with the results shown in columns 2 and 4 of table 166.1, give a mean of 1.66 and a difference of 0.18.

The difference given by this experiment, which is applicable only when the original data have a mean of 2.00 and a standard deviation of 1.00, can be applied to other normally distributed data by converting the difference in means to difference in their deficiency probability—the probability of occurrence of a mean equal to or less than a given amount. The first step in making this conversion is to decide at what probability to plot the lowest of five independent 10-year means, and the second step is to use the computed difference to obtain the probability for the lowest 10 year moving average with a 50-year recurrence interval.

On a cumulative probability distribution with a standard deviation of 0.316 (the theoretical standard deviation of 10-item means when the items have a standard deviation of 1.00), the 1.66 obtained from this experiment plots at a deficiency probability of about 15 percent as compared to 16.7 percent computed by the formula $\frac{100m}{n+1}$ and 13 percent by the formula $100(1-.5^{\frac{1}{n}})$. If the percent computed by the first formula, which is generally used in the Geological Survey, is accepted as giving the most probable plotting position for the lowest independent 10-item mean, the corresponding y value is 1.69, and when the average difference of 0.18 is subtracted from this, y is 1.51 and the corresponding percent becomes 6.3. (See fig. 166.1.) Thus, the lowest 10-year moving average with a recurrence interval of 50 years is enough smaller than the most probable minimum independent 10-year mean in 50 years to change the deficiency probability from 16.7 percent to 6.3 percent.

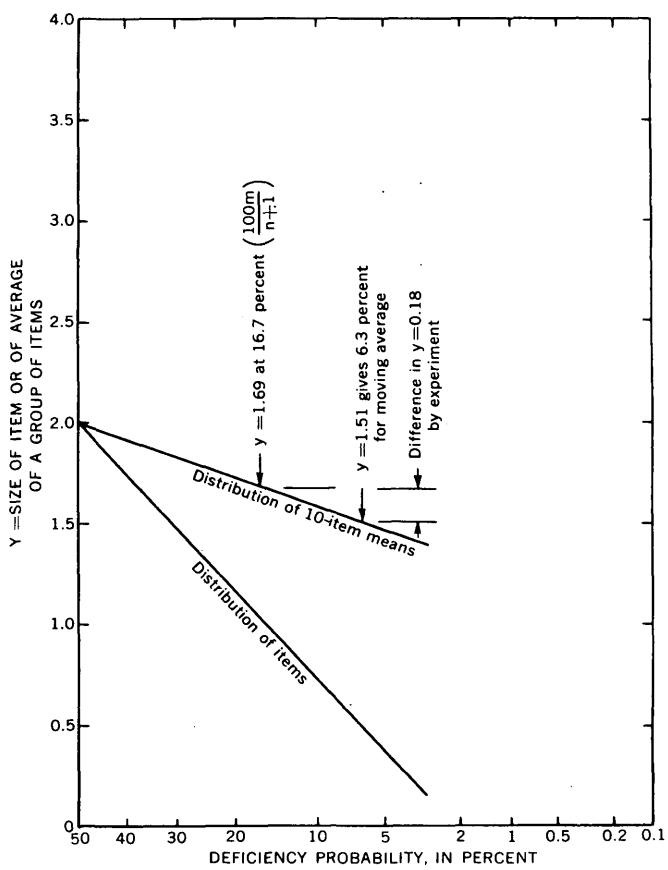

FIGURE 166.1.—Plotting position of lowest moving 10-year average in a 59-event sample.

Results from similar experiments with moving averages of 2, 4, and 20 events in a series of 50 events, together with those for the 10-event groups are summarized in the following table:

Number of events in the average	2	4	10	20
Number of groups (n) in 50 years	25	12½	5	2½
$\frac{100m}{n+1}$ (deficiency probability for minimum independent mean, in percent)	3. 8	7. 4	16. 7	28. 6
Corresponding y for independent events	. 75	1. 28	1. 69	1. 87
Average difference between independent and moving averages, from experiment	. 13	. 21	. 18	. 14
Average y for moving averages	. 62	1. 07	1. 51	1. 73
Deficiency probability for moving averages with recurrence intervals of 50 years, in percent	2. 4	2. 9	6. 3	11

Based on this experiment, the percentages shown in the last line should be used if the lowest moving average with a recurrence interval of 50 years is to be obtained from a distribution of independent means. If the percentages are to be used to help define a cumulative frequency distribution of independent multi-year means, the number of years in the sample should be increased by one less than the number of years in the multi-year average. For example, the figure to plot at 6.3 percent is the lowest 10-year average in 59 years. Although these percentages are but estimates based on a small experiment with normally distributed random numbers, they give an indication of the size of the difference between the lowest moving average of natural events and minimum independent means.

REFERENCES

Dixon, W. J., and Massey, F. J., Jr., 1957, Introduction to statistical analysis: 2d ed., New York, McGraw-Hill Book Co., p. 452–456.

U.S. Corps of Engineers, 1958, Long-duration runoff volumes, Flood volume studies, Tech. Bull. 5: Sacramento, Calif., U.S. Army Engr. Dist.

167. BANKFULL DEPTH AND DEPTH OF FLOW FOR MEAN ANNUAL FLOOD, PIEDMONT PROVINCE

By F. A. Kilpatrick, Atlanta, Ga.

The relation between bankfull depth and the depth of flow of the mean annual flood has been analyzed at 41 places in the Piedmont Province of the southeastern United States. The channel size and shape were determined along a reach of channel at each of 26 sites where the frequency of flood discharge was known from gaging station records. Less detailed surveys were made at an additional 15 sites at which the frequency of flood discharge was interpolated from regional analysis of station records. An average of 12 cross sections spaced about 2 channel widths apart were measured at the 26 regular sites, and 2 or 3 cross sections spaced about 7 channel widths apart were measured at the 15 supplementary sites. High-water marks for one or more floods per reach were noted.

Bankfull depth, D_B, is the difference in height between the top of the stream channel and the corresponding average elevation of the stream bed. The top of the stream channel may be taken as the average elevation of the flood plain, or a bench along the channel at a lower elevation.

If bankfull elevations are plotted against distance along the channel, abrupt discontinuities are found at points where there is a major change in channel slope. Within a single reach of channel, bankfull stage does not always correspond to the same discharge. This may be due in part to the fact that bankfull stage is at the level of the flood plain in one subreach and at the level of a predominant bench at a lower elevation in another subreach.

Several investigators (W. B. Langbein, written communication, 1953; Wolman, 1955; Wolman and Leopold, 1957) have reported that the discharge at bankfull stage is roughly equal to the mean annual flood, and that it has an average recurrence interval of 2.33 years. Information from the present work shows (fig. 167.1) that the recurrence interval of bankfull discharge at the 40 sites in the Piedmont ranges

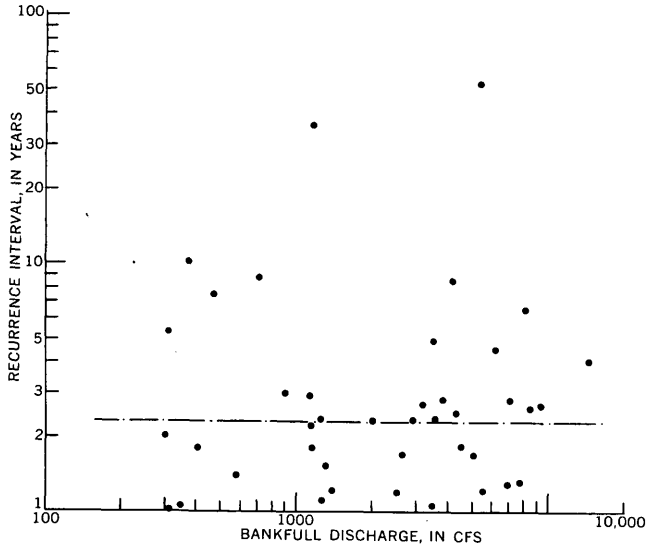

FIGURE 167.1.—Recurrence interval of bankfull discharge, in cubic feet per second, at 41 sites in the Piedmont. Line shows average recurrence interval according to some previous investigators.

from 1 to 55 years, but that on the average the bankfull discharge does represent the mean annual flood.

The depth of water, D_F, during the mean annual flood can be related to bankfull depth and to the corresponding longitudinal slope of the bench or flood plain. The slope of the benches is approximately equal to the slope of the water surface at bankfull stage. The stage during the mean annual flood is derived from discharge measurements. Where the stage of the mean annual flood is greater than bankfull stage, the average bed elevation of the main channel is used to compute D_F. The regression equation which expresses the relation among the depth of mean annual flood, bankfull depth, and slope of the bench or flood plain for 41 sites is

$$D_F = 0.33\ D_B^{1/2}\ S^{-1/3} \qquad (1)$$

The standard error is 12 percent and both regression coefficients are significant at the 0.001 level. The relation is shown graphically on figure 167.2.

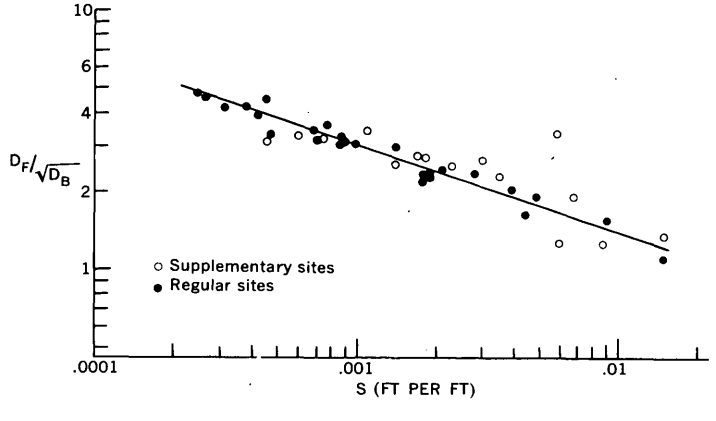

FIGURE 167.2.—Relation of depth of water during the mean annual flood, bankfull depth, and slope in feet per foot, of the top of the channel for 41 sites in the Piedmont.

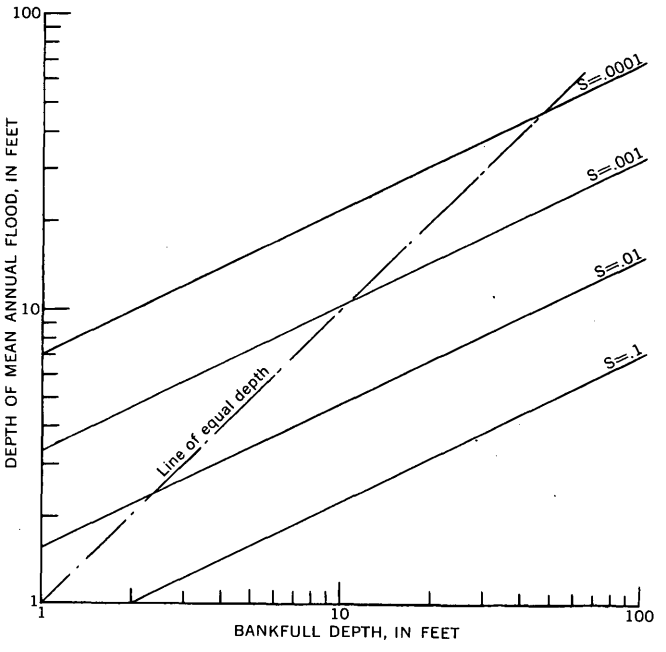

FIGURE 167.3.—Relation of bankfull depth to depth of mean annual flood for different slope (s) of the top of the channel.

In figure 167.3, equation (1) is shown for different slopes, and a line of equal depth is superposed. In general, where slopes are gentle, the mean annual flood will overflow the stream banks; where slopes are steep, the channel capacity is greater than that required. To the left of the equal-depth line bankfull stage is defined by flood plains and to the right by lower benches.

REFERENCES

Wolman, M. G., 1955, The natural channel of Brandywine Creek, Pennsylvania: U.S. Geol. Survey Prof. Paper 271, 56 p.

Wolman, M. G., and Leopold, L. B., 1957, River flood plains; some observations on their formation: U.S. Geol. Survey Prof. Paper 282–C, p. 87–109.

GEOLOGY AND HYDROLOGY OF EASTERN UNITED STATES

168. BOUNDARY MOUNTAIN ANTICLINORIUM, WEST-CENTRAL MAINE AND NORTHERN NEW HAMPSHIRE

By ARDEN L. ALBEE, Pasadena, Calif.

Recent geologic mapping in west-central Maine, northern New Hampshire, and adjacent Quebec has resulted in a new stratigraphic and structural interpretation. This summary and the accompanying map (fig. 168.1) is based upon the work of many other geologists as well as upon mapping by the author from 1956 to 1959. Direct use has been made of A. J. Boucot's work in the Moose River synclinorium (Boucot, 1953 [1]; 1961; written and oral communications, 1960), of R. A. Marleau's work in Quebec (Marleau, 1957; 1958; thesis, 1958 [2], written and oral communications, 1960), of Albee and E. L. Boudette's work in the Attean quadrangle (fig. 168.1, B–5) and of a compilation edited by Boucot and A. Griscom (Boucot and others, 1960). Recent work by John Green (oral communication, 1960) in northern New Hampshire was important in crystallizing the author's interpretations.

A major anticlinorium, the Boundary Mountain anticlinorium, extends from northern New Hampshire northeast into Maine; it is outlined on the map by a regional unconformity between rocks of probable Cambrian and Ordovician age in its core, and units of Silurian and Early Devonian on its margins. In Maine a major unnamed anticline splits off to the east and extends about 65 miles to the northeast. The Moose River synclinorium lies between the two anticlinoriums and contains a great thickness of well-dated rock of Early Devonian age. Northwest of and parallel to the Boundary Mountain anticlinorium a sandy facies of the Devonian outlines the core of the Frontenac synclinorium. The existence of the Frontenac synclinorium is best demonstrated by pillow-bearing volcanic rocks on either limb, which indicate the upper surfaces of the beds. (See footnote 2.) Cambrian and Ordovician rocks crop out northwest of the Frontenac synclinorium in the core of the Green Mountain-Sutton Mountain anticlinorium.

PRE-UPPER SILURIAN ROCKS

Reconnaissance mapping suggests that at least three major units can be distinguished in the pre-Upper Silurian rocks, but the relative age of these units is not known. The two slate and phyllite units east of the Moose River synclinorium include a felsic volcanic unit having Middle Ordovician fossils. The eastern unit seems to be continuous with rocks mapped as the Albee formation of Ordovician age by John Green (written communication, 1960) in northern New Hampshire. The northern part of the Boundary Mountain anticlinorium is underlain by a quartzo-feldspathic granulite or gneiss containing abundant lithic fragments. Although the granulite is assigned to the Precambrian by Boucot (1961) it is unlike the known Precambrian rocks of central Vermont and of the Canadian Shield north of the St. Lawrence River and is believed to be of Cambrian and (or) Ordovician age. The rock is not too dissimilar to rocks in northern New Hampshire, which are assigned to the Ordovician, and seems to intertongue along the Maine-New Hampshire border with the extension of these rocks. More detailed mapping by John Green (oral communication, 1960) in the Second Lake quadrangle (D–2) also seems to support this interpretation. The pre-Silurian rocks are intruded by hornblende diorite or gabbro, which in turn is intruded in the Attean quadrangle (B–5) by coarse-grained porphyritic quartz monzonite. Similarity of lithologic characteristics and of stratigraphic relationships suggest that the quartz monzonite is equivalent to the Highlandcroft plutonic series of New Hampshire (Billings, 1956, p. 46–48, 106).

SILURIAN ROCKS

The Silurian rocks occur in discontinuous lenticular units and include limestone, calcareous sandstone and mudstone, conglomerate, arkose, limestone conglomerate, and felsic volcanic rocks. Many units are dated by paleontologic evidence as Late Silurian and one as Early Silurian, (northern edge of Stratton quadrangle, D–5), but several can be accurately dated only as pre-Early Devonian. In the areas mapped by Boucot in the Spencer Lake quadrangle (C–5) and by Albee and Boudette in the Attean quadrangle (B–5), several lines of evidence suggest that the Silurian rocks were deposited near a shore with strong local relief.

[1] Boucot, A. J., 1953, The Lower Devonian rocks of west-central Maine: Unpub. Ph.D. thesis, Harvard Univ.

[2] Marleau, R. A., 1958, Geology of the Woburn, East Megantic and Armstrong areas, Frontenac and Beauce counties, Quebec: Unpub. Ph.D. thesis, Univ. Laval.

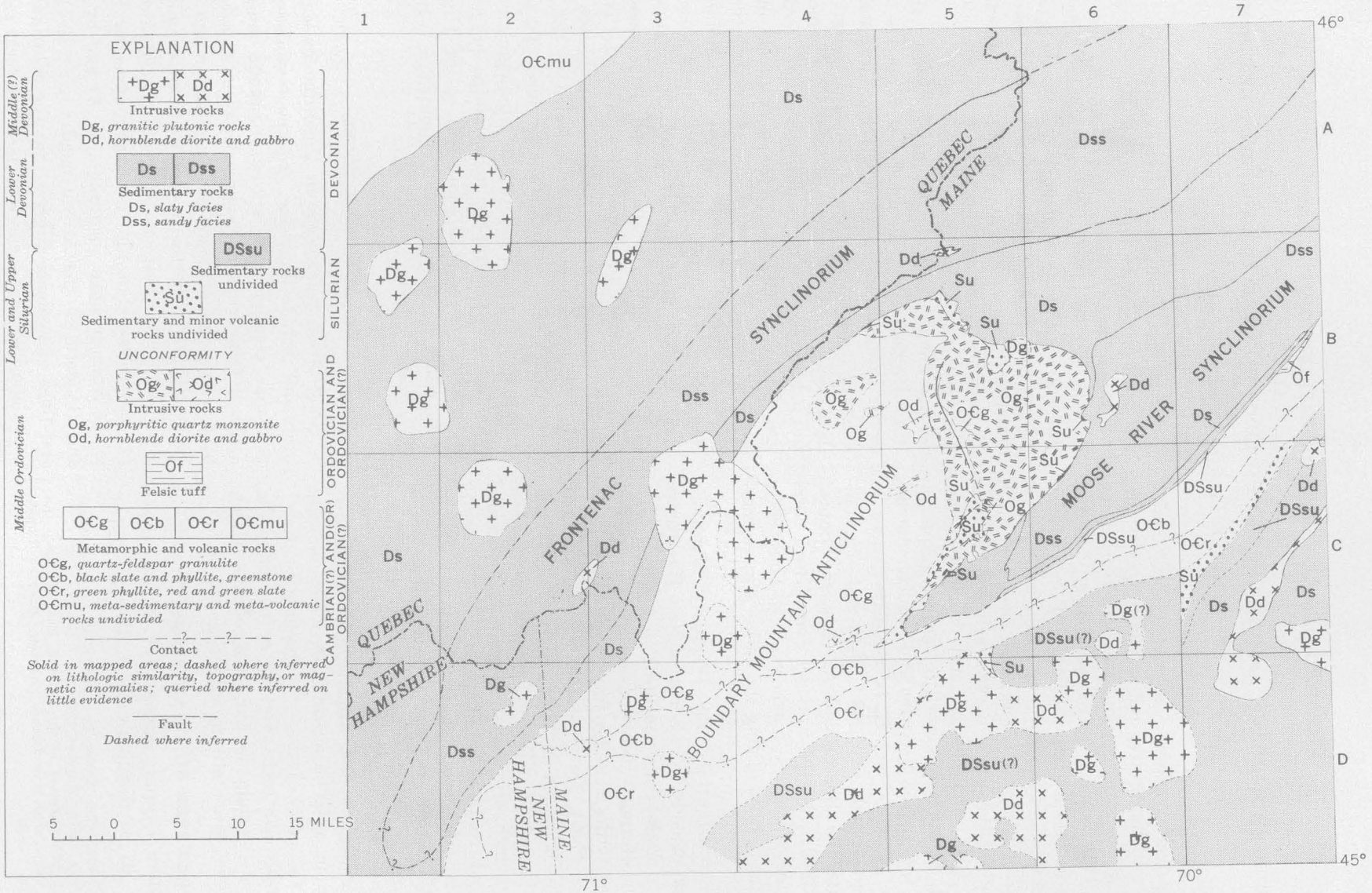

FIGURE 168.1.—Simplified geologic map of west-central Maine, northern New Hampshire, and adjacent Quebec.

DEVONIAN ROCKS

Several lithologic facies have been distinguished within the Devonian rocks. Dark-colored argillaceous sandstone interbedded with minor gray slate and felsic volcanic rocks within the Moose River synclinorium contains abundant Early Devonian fossils. Slate in and adjacent to the Moose River synclinorium also contains Early Devonian fossils, but no fossils have been found in the sandy unit within the Frontenac synclinorium, which consists predominantly of massive argillaceous sandstone and minor slate and volcanic rock. The western unit is characterized by argillaceous and arenaceous limestone, slate, and sandstone, and contains Early Devonian fossils at its base in rocks similar to the Silurian rocks described above. The slate unit in the northeastern part of figure 168.1 is overlain by the sandy facies of both the Frontenac and Moose River synclinoriums, but the slate and sand facies are also in part laterally equivalent. In the Attean quadrangle (B–5) fossiliferous Upper Silurian rocks intertongue with the lowermost portion of the gray slate. Thus, although the dark-colored slate, sandstone, and limestone is probably predominantly Early Devonian in age, they may locally be Middle Devonian or Late Silurian.

POST-LOWER DEVONIAN INTRUSIVE ROCKS AND METAMORPHISM

The pre-Upper Silurian, the Silurian, and the Devonian rocks all have undergone regional metamorphism of chlorite grade in the northern and western part of the area and higher grade to the southeast. Hornblende diorite and gabbro masses intrude the Lower Devonian rocks and seem to have been somewhat affected by the regional metamorphism. Plutons, predominantly of medium-grained biotite quartz monzonite, but including some more mafic rocks, intrude all the metasedimentary units and are surrounded by contact-metamorphic aureoles. Isotopic ages for metamorphic or igneous minerals from several units (Hurley and others, 1959) suggest that the regional metamorphism and the intrusion of the Devonian quartz monzonite occurred nearly simultaneously in Middle Devonian time.

MAGNITUDE OF THE TACONIC OROGENY IN THE AREA

In the Spencer Lake (C–5) and Attean (B–5) quadrangles several lines of evidence indicate that the pre-Upper Silurian rocks were emergent during much of Late Silurian and Early Devonian time. The evidence includes observed relief on the surface of the pre-Upper Silurian rocks, including the presence of possible fossil seacliffs and seastacks, and intertonguing of rock composed of large angular blocks of pre-Upper Silurian rock debris in Upper Silurian or Lower Devonian reefal material with slate of the same age. Along the west side of the Boundary Mountain anticlinorium none of the conglomeratic or calcareous Upper Silurian units has yet been found and slate of probably Early Devonian age rests directly upon the pre-Upper Silurian rock. The absence of the Upper Silurian rocks could be the result of a major fault or of removal by erosion in Early Devonian time. It seems more likely, however, that the presence of Upper Silurian units with near-shore characteristics on the east side of the Boundary Mountain anticlinorium represents a coincidence between the locations of the folded Upper Silurian shore-line and the present erosion surface, and that the absence of these near-shore deposits on the west side results from the onlap of the slate facies onto the pre-Upper Silurian surface. The Upper Silurian near-shore deposits, if originally present, are now below the present erosion surface.

The distribution of pre-Upper Silurian units is not yet known in detail, but likely trends of a number of pre-Upper Silurian units are shown on figure 168.1. There appears to be a continuous sequence of these units from northwest to southeast across the Boundary Mountain anticlinorium without major repetition, and the trends do not seem to be directly related to the Middle Devonian deformation which formed the Moose River synclinorium. The relation of these apparently steeply dipping contacts to the Silurian and Devonian contacts at the south end of the Moose River synclinorium suggests that the Taconic orogeny in this area involved major deformation rather than just a tilting of the older rocks.

Other evidence suggests that the Taconic orogeny involved metamorphism of fairly high grade. Relict sillimanite, partly altered to white mica, and garnet occur at several places in the quartzo-feldspathic granulite of the Attean (B–5) and Spencer Lake (C–5) quadrangles. These occurrences are apparently well away from any intrusive mass and the Middle Devonian metamorphism in the Attean quadrangle (B–5) is only of chlorite grade. Further work may indicate that the Taconic orogeny was a major event in this area, involving metamorphism of the sillimanite grade. It should be recognized, however, that the validity of this suggestion depends on the correct-

ness of assigning an Ordovician and (or) Cambrian age, rather than a Precambrian age, to the pre-Upper Silurian granulite.

REFERENCES

Billings, M. P., 1956, The Geology of New Hampshire, Part II, Bedrock geology: New Hampshire State Planning and Development Commission, Concord, N.H., 203 p.

Boucot, A. J., 1961, Stratigraphy of the Moose River synclinorium, Maine: U.S. Geol. Survey Bull. 1111–E, p. 153–188.

Boucot, A. J., Griscom, Andrew, Allingham, J. W., and Dempsey, W. J., 1960, Geologic and aeromagnetic map of northern Maine: U.S. Geol. Survey Open File Maps, 5 sheets.

Hurley, P. M., Boucot, A. J., Albee, A. L., Faul, Henry, Pinson, W. H., and Fairbairn, H. W., 1959, Minimum age of the Lower Devonian slate near Jackman, Maine: Geol. Soc. America Bull., v. 70, p. 947–950.

Marleau, R. A., 1957, Woburn area, electoral district of Frontenac: Quebec Dept. Mines Prog. Rept. 336.

——— 1958, East Megantic and Armstrong areas, electoral districts of Frontenac and Beauce: Quebec Dept. Mines Prog. Rept. 362.

169. AXIAL-PLANE FOLDING IN SOUTHEASTERN CONNECTICUT

By Richard Goldsmith, Denver, Colo.

Work done in cooperation with the Connecticut Geological and Natural History Survey

The bedrock of southeastern Connecticut is a crystalline complex of granitic to granodioritic gneisses and of sedimentary and probably volcanic rocks of high (sillimanite) metamorphic grade. Granitic and quartz-monzonitic gneisses and granodioritic gneiss comprise from 30 to 50 percent of the complex. Biotite-quartz-feldspar gneiss and hornblende-biotite-feldspar gneiss, probably in part metavolcanic rocks, comprise about 30 percent. The remainder is quartzite, calc-silicate rock, and pelitic and semi-pelitic schist and gneiss. Most of the granitic rocks are concordantly to semiconcordantly intercalated among the other rocks. No unconformities have been recognized. The units are distributed in a complex fold pattern resulting from continuous deformation or more than one episode of deformation.

Certain key units are helpful in tracing the fold pattern of the bedrock sequence. One is an aegirine-augite granitic gneiss, which is in phacolithic bodies along a particular horizon of interlayered amphibolite and light-colored feldspathic gneiss and granodioritic gneiss. Mapping of this distinctive assemblage and the adjacent rocks has revealed the fold pattern indicated on figure 169.1. Note that the trace of the axial plane of the syncline in the garnet-mica schist and gneiss has been involved in later folding along easterly-trending axial planes. In figure 169.2 the aegirine-augite granitic gneiss and the horizon in which it appears are used to illustrate in three dimensions the type of folding characteristic of the area.

The overturned folded syncline shown in figures 169.1 and 169.2 lies in its northwestern part along Hunts Brook in the Montville quadrangle and is here called the Hunts Brook syncline. It appears to be continuous with a syncline of regional significance in quadrangles to the west, called by L. Lundgren (written communication, 1959) the Chester syncline. The fold is interpreted as a syncline rather than an anticline on the basis of stratigraphic and structural relations in quadrangles to the west and northwest mapped by Lundgren and to the north and northwest mapped by G. L. Snyder.

Symmetry on opposite sides of the axis of the Hunts Brook syncline is not perfect as the aegirine-augite granitic gneiss appears only on one limb. In figure 169.1, the granodioritic gneiss complex on the west limb is too thin to show at the scale of the map. The biotite-quartz-feldspar gneiss unit also is much thinner in the west limb than in the east limb.

The plunge of the overturned Hunts Brook syncline is eastward or southeastward in the northwest corner of the Montville quadrangle. In the adjacent quadrangles to the west, the plunge of Lundgren's Chester syncline is westward and the garnet mica schist and

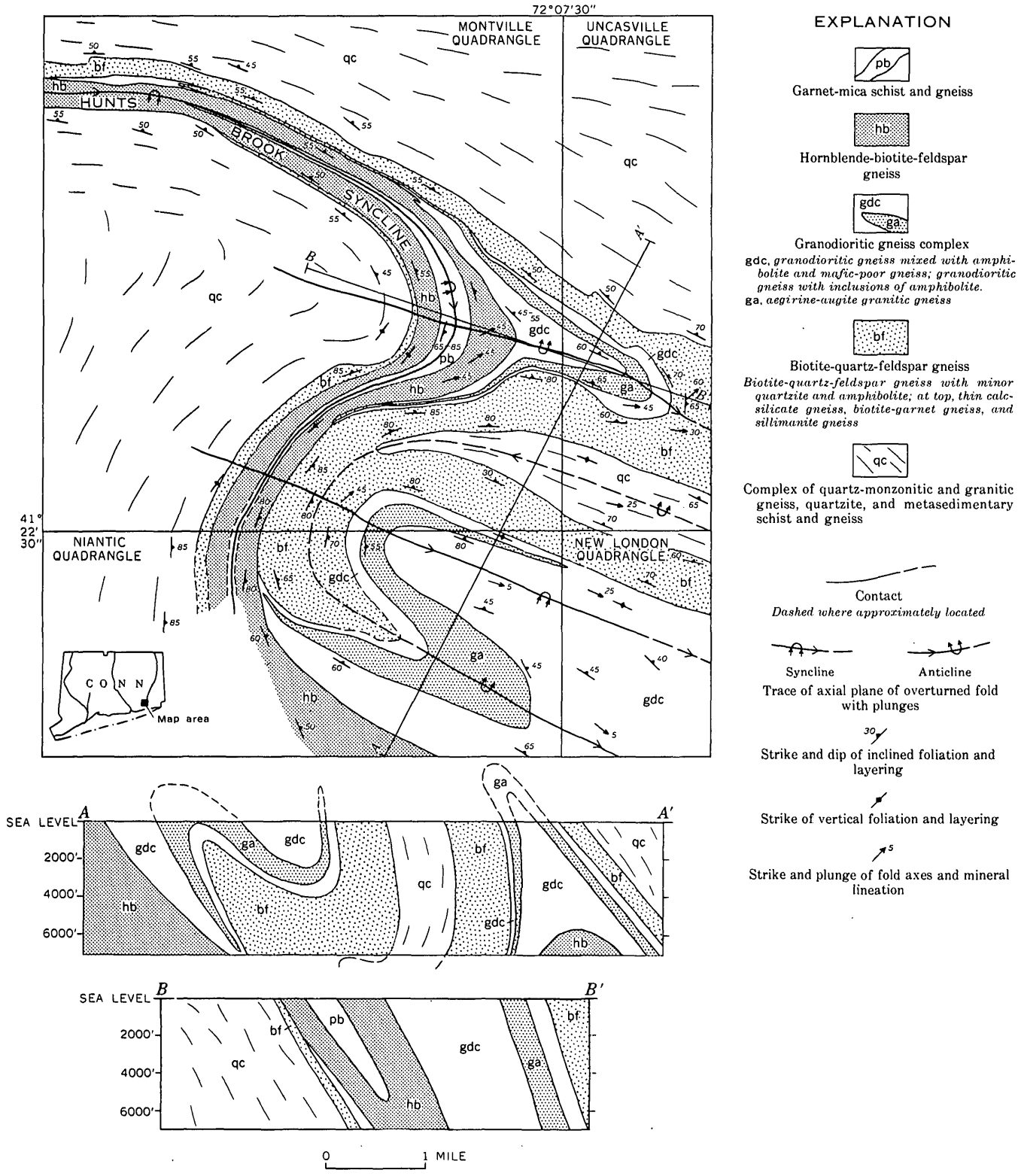

FIGURE 169.1.—Geologic map and sections of parts of the Uncasville, Montville, Niantic, and New London quadrangles, Connecticut.

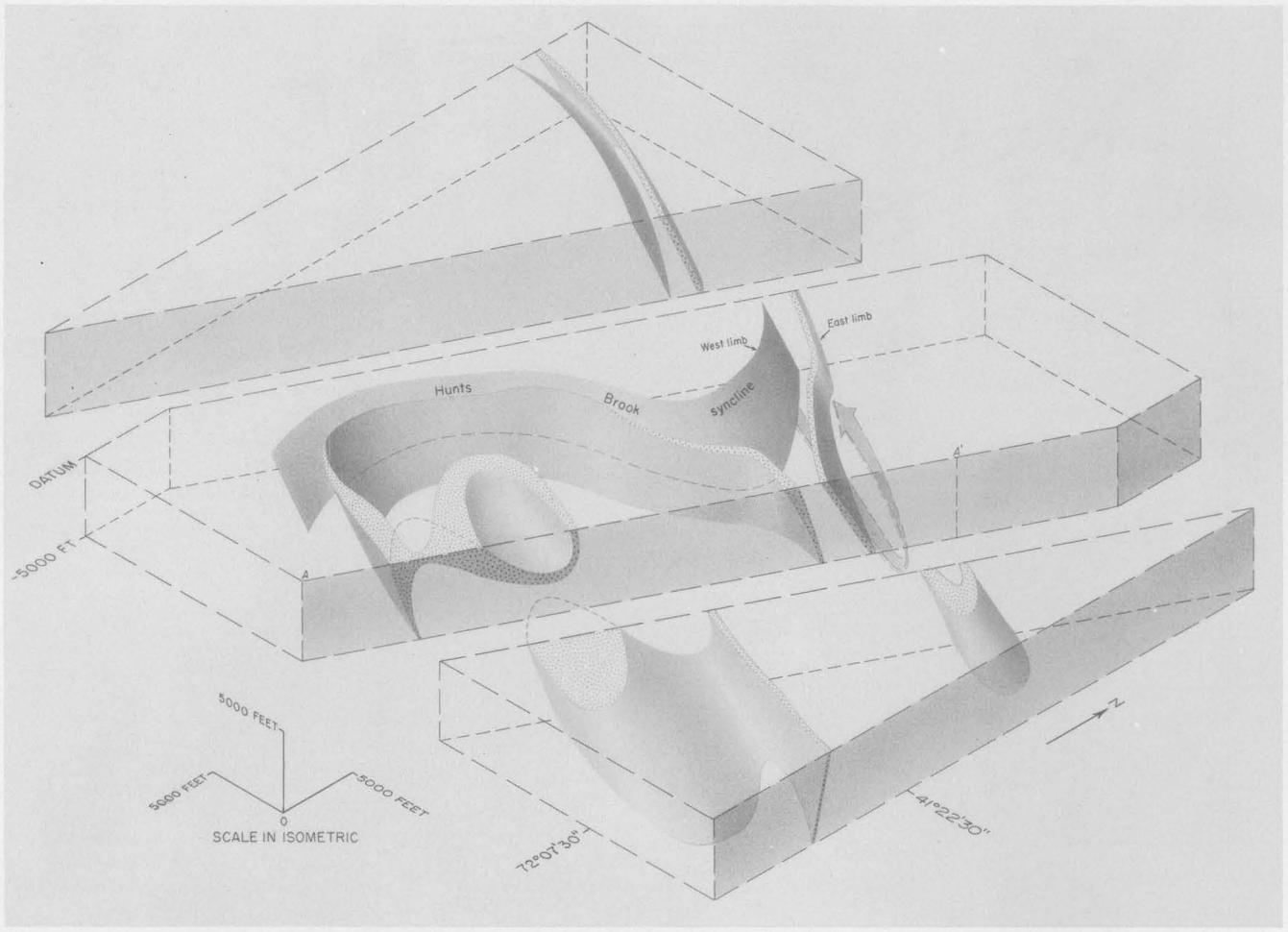

FIGURE 169.2.—Isometric diagram showing folding of the Hunts Brook syncline as marked by the aegirine-augite granitic gneiss (stippled) and its corresponding horizon on east and west limbs.

gneiss, as well as younger rocks, appear again in the core of the syncline (Lundgren, written communication, 1959).

The anticline to the east of, and corresponding to, the Hunts Brook syncline is involved with it in the later folding, and the plunge of its arcuate axis swings from northwestward to southeastward. The trough of the Hunts Brook syncline rises in the northern later-formed anticline along line of section *B–B*1 (north side of section *A–A*1). Representation of units at depth is schematic. The nose of the old anticline lies to the southwest of this younger anticline and is partly downfolded in the younger syncline.

The original trend of the rock units at the time of the formation of the Hunts Brook syncline is problematical. It may have been westerly or more northerly according to whether a northwest-trending shear couple or purely northeast-southwest compression was involved in the later folding. Traces of axial planes of the later folds trend west-northwest. Axes of minor folds near the Hunts Creek syncline plunge relatively steeply to the northeast. The steep attitudes of foliation and layering in the larger flexures also indicate fairly steeply plunging axes. This pattern suggests north-south compression, perhaps with an appreciable right-lateral component during the later folding. Mineral lineation and fold axes plunge gently to moderately southeastward near the secondary fold in the Niantic and New London quadrangles, probably largely under the influence of the later folding on foliation and layering oriented differently from that along the main Hunts Brook syncline.

The trend of the axial planes of the secondary folds is fairly consistent throughout the area of the four quadrangles. Plunges of minor fold axes are consistent locally but not regionally. The pattern probably reflects local adaptation to later deformation of differently oriented parts of previously formed folds, but it may reflect a more complex history of deformation throughout the area.

One should not conclude from the map that rocks in the Hunts Creek syncline were folded between relatively massive blocks of the complex of quartz-monzonitic and granitic gneiss and metasedimentary rocks to the northeast and southwest. Equally complicated folding in this complex is revealed by mapping the many diverse rock types within it; this folding conforms to the same general pattern as in the rocks along the overturned Hunts Brook syncline.

The thinning and thickening of the rock units indicate considerable rock flowage. The minor drag folds on both limbs near the crest of the secondary fold involving the aegirine-augite granitic gneiss in the Uncasville quadrangle indicate flowage of material into it. No evidence of cataclasis exists in this part of the area and the pattern, texture, and mineralogy of the rocks indicate deformation at a fairly high temperature, perhaps during or penecontemporaneous with mobilization and intrusion of rocks of the granodioritic gneiss complex. Older igneous rocks in the complex of quartz-monzonitic and granitic gneiss and metasedimentary rocks may have been recrystallized and even remobilized during this time.

The axial-plane folding may be an expression of the behavior of the rocks at depth, perhaps during an early phase of deformation that at higher levels, and perhaps at a later time, resulted in the generally westward-trending Honey Hill thrust fault (Lundgren, Goldsmith, and Snyder, 1958) about 5 miles to the north of the area shown on figure 169.1. The direction of movement of the secondary folding of the Hunts Brook syncline appears to be consistent with the right-lateral movement inferred on the Honey Hill fault.

REFERENCE

Lundgren, L., Jr., Goldsmith, R., and Snyder, G. L., 1958: Major thrust fault in southeastern Connecticut [abs.]: Geol. Soc. America Bull., v. 69, no. 12, pt. 2, p. 1606.

170. A FROST-WEDGED BEDROCK LOCALITY IN SOUTHEASTERN MASSACHUSETTS

By Carl Koteff, Boston, Mass.

Work done in cooperation with the Massachusetts Department of Public Works

A bedrock exposure in southeastern Massachusetts exhibits unusually wide joint openings that apparently are unique in the area. This exposure is on the western border of the town of Rochester, approximately 10 miles north of New Bedford and about 1,000 feet southwest of Little Quittacas Pond in the Assawompset Pond quadrangle. It is an isolated knob elongated in a northwest direction and is about 200 feet long and 125 feet wide. The highest part of the knob is about 25 feet above the surrounding ground.

The bedrock in this area was mapped as the Dedham granodiorite, of Devonian(?) age, by Emerson (1917, p. 175–176), who extended the name from the intrusive body at the type locality southeastward to the granites of the Narragansett structural basin. The rock is mainly coarse-grained quartz, feldspar, and amphibole, and has a weak to strong foliation.

The main joint set is parallel to the foliation, strikes N. 35° E., and dips vertically or steeply southeast. A secondary joint set is approximately normal to the main set and dips 65° to 70° NE. A third joint set, dipping gently northeast, is exposed on the sides of the knob. The openings (fig. 170.1) are as much as 3 feet wide along joints of the main set, and as much as 1 foot wide along joints of the secondary set. The observed depth of the openings is as much as 10 feet, but the total depth is obscured by soil. The openings along joints of the main set are spaced from 1 to 5 feet apart, and most of them extend the entire width of the exposure. The openings along the secondary set of joints are much more widely spaced and terminate at their intersection with the main set. A joint of the third set is exposed at only one place about 7 feet below the surface. Here the movement of an overlying block along the joint has slightly widened the opening of the secondary joint above this point, but has not affected the width of the opening along the main

601530 O—61——5

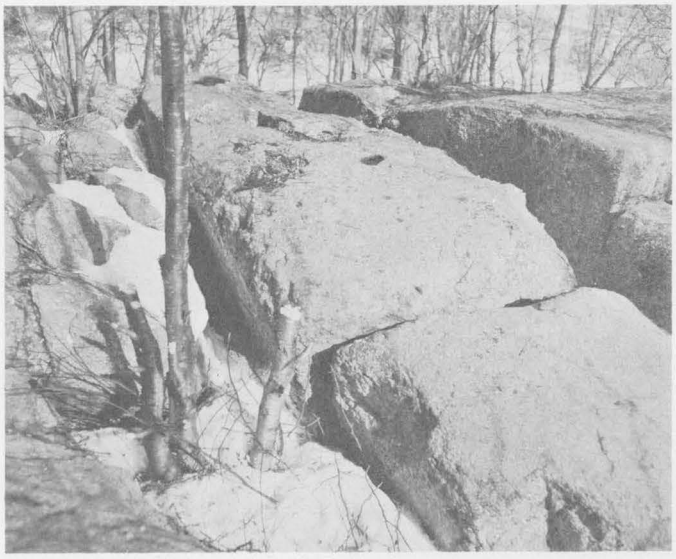

FIGURE 170.1.—Openings along the main set of joints. Width of the block in the center is about 5 feet; secondary joint opening in right foreground.

joint. The openings along the two nearly vertical joint sets extend below this third joint.

It seems clear that all the openings are a result of the movement of the blocks along the nearly horizontal joints of the third set, and that the movement has been caused by frost wedging. Water or water vapor entering these joints would act, upon freezing, as a lubricant and facilitate the lateral movement of the blocks forced apart by the pressure of ice forming in the nearly vertical joints. H. T. U. Smith (1953) has described similar frost-wedging phenomena at the "rock cities" near Olean and Salamanca, N. Y., and he believes (oral communication, 1961) that large blocks of conglomerate there slid over an underlying shale, although the contact was not exposed. The nearly horizontal joints described here probably served a similar function. Yardley (1951) has described frost thrusting in the Northwest Territories, Canada, where ice in virtually horizontal joints has thrust individual blocks upward. At the Little Quittacas Pond locality the direction of easiest relief of stress was lateral rather than vertical.

Root wedging does not appear to be a probable cause for the joint separations because this process would tend to wedge out individual blocks. The extent of the openings from one side of the knob to the other, their relative number, and their unusual width seem to preclude root wedging as a process for their formation. Also, weathering apparently has not contributed appreciably to the widening of the openings. Any rounding of the individual blocks by chemical or mechanical processes seems to have taken place before, and not after, the advance and retreat of the last ice sheet. What rounding there is has affected only isolated edges of the blocks, and is not very extensive as shown by the angularity of the joint faces (fig. 170.1).

The frost wedging at Little Quittacas Pond probably did not take place until the withdrawal of the last ice sheet, because any advance of ice over the bedrock knob in its present form, and in its exposed and isolated position, would have moved the individual blocks from their present alinement, even if they were not picked up by the ice. It appears more likely that the frost wedging occurred during a time of perennially frozen ground. Thus, the age of the frost wedging is placed as late glacial during the time when periglacial conditions existed near the margin of the receding ice.

REFERENCES

Emerson, B. K., 1917, Geology of Massachusetts and Rhode Island: U.S. Geol. Survey Bull. 597, 289 p.

Smith, H. T. U., 1953, Periglacial frost wedging in the "rock cities" of southwestern New York [abs.]: Geol. Soc. America Bull., v. 64, p. 1474.

Yardley, D. H., 1951, Frost-thrusting in the Northwest Territories: Jour. Geology, v. 59, p. 65–69.

171. LATE-GLACIAL MARINE DEPOSITS IN THE SALEM QUADRANGLE, MASSACHUSETTS

By Robert N. Oldale, Boston, Mass.

Work done in cooperation with the Massachusetts Department of Public Works

Late-glacial marine deposits occur along the northeast coast of Massachusetts. In the Salem quadrangle, Massachusetts, these deposits have been mapped along the coast and inland along the valleys from sea level to altitudes as high as 50 feet. Deposits of till, ice-contact stratified drift, and outwash are associated with marine clay, silt, fine- to medium-grained sand, and gravel. The lower part of the marine unit is clay interbedded with layers of fine- to medium-grained sand in beds that range from a few inches to 5 feet in thickness. The upper part is predominantly sand with minor amounts of gravel. Adjacent to the coast marine sediments 60 feet or more thick fill the valleys; they become thinner up the valleys and grade into glaciofluvial outwash. The marine deposits are oxidized from blue gray to brown to a depth of 5 feet. The marine unit overlies till and ice-contact stratified drift; the contact is sharp and there is no mixing of the deposits.

Several outwash deposits in the quadrangle are interbedded with and in part overlie the marine unit. The upper ends of these outwash deposits terminate at ice-contact slopes that mark the position of glacial ice during their formation (fig. 171.1). Near the ice contact the outwash is coarse-grained sand and gravel, but these beds grade down-stream into finer grained

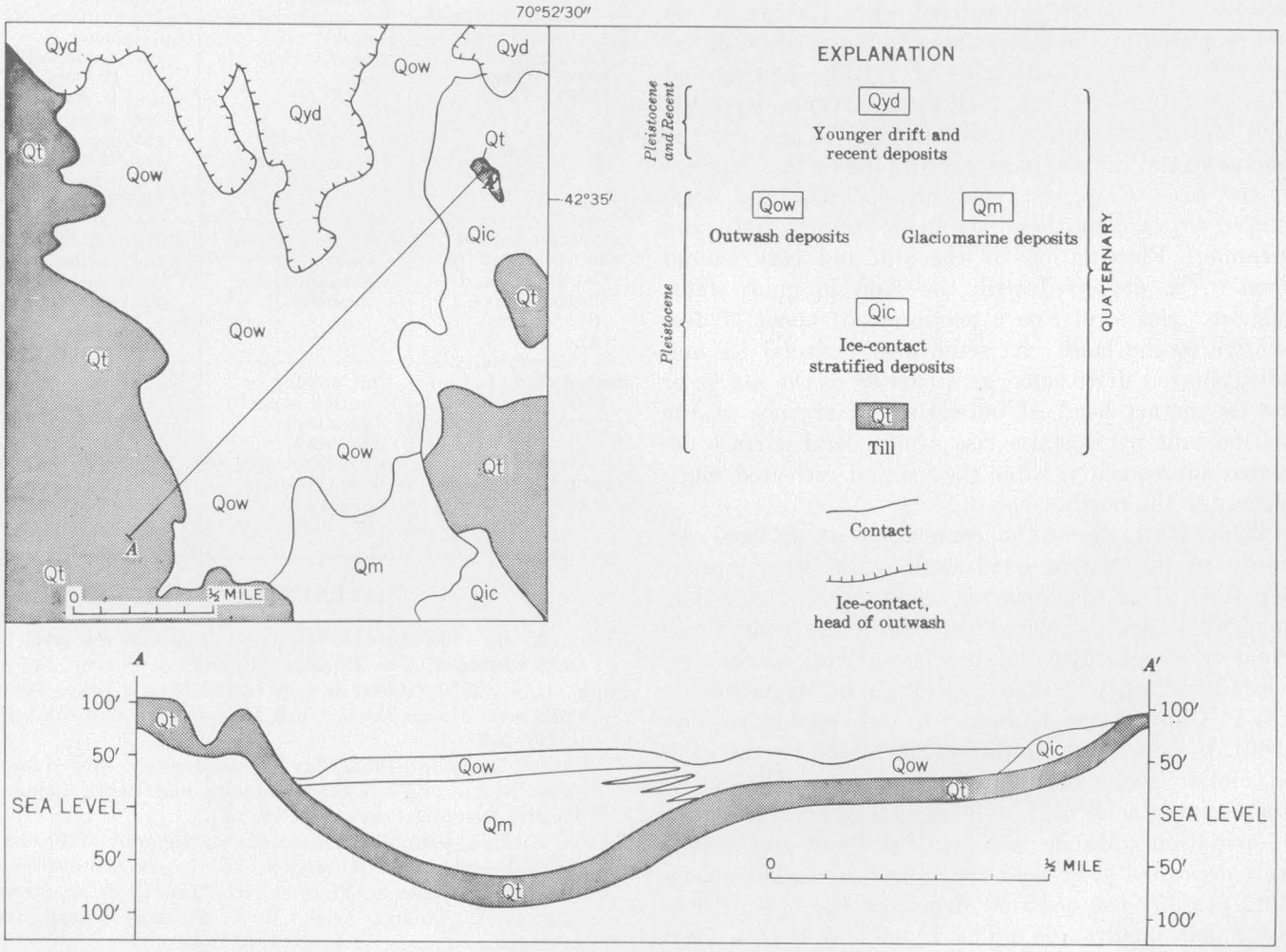

Figure 171.1.—Generalized map and section showing the contact relations between glaciofluvial and glaciomarine deposits in the east-central part of the Salem quadrangle.

deposits. Where in contact with the marine deposits the outwash is composed of fine- to coarse-grained sand and fine-grained gravel. The contact between the glaciofluvial outwash and the marine unit is gradational both laterally and vertically. The contact shown on the map, figure 171.1, is arbitrary and represents a zone several hundred feet wide. Silty clay more than 50 feet thick was found beneath the outwash about 1,800 feet northeast of Hunt Memorial Hospital in Danvers. About 400 feet north of the intersection of Maple and Burley Streets, Wenham, silty clay of possible marine origin is interbedded with sand and gravel within 1,000 feet of the ice-contact head of outwash.

The coastline was farther east than at present before the formation of the outwash and the marine unit, as shown by ice-contact deposits along the coast that have graded upper surfaces at altitudes of 50 feet, and that partly extend below the marine unit. Subaerial conditions persisted long enough for ice blocks to melt and for collapse topography to develop in the ice-contact deposits. Submergence occurred when the glacial ice had retreated up the valleys near to the position of the ice-contact heads of outwash (fig. 171.1). During and after retreat of the ice, meltwater streams deposited sand and gravel as outwash between the ice and the marine strandline and in gently dipping deltaic deposits in the sea. Clay, silt, and fine-grained sand were carried seaward by these meltwater streams and shore currents. Flocculation of the silt and clay caused them to be deposited with the sand in quiet water offshore. Sea-level rose a maximum of about 50 feet relative to the land. At some places glacial ice and ice-supported drift acted as a barrier to the sea as at the ice-contact head of outwash. Emergence of the marine unit by isostatic rise of the land surface occurred subsequently, after the ice had retreated much farther to the north.

Table 171.1 shows the correlation of surficial deposits in the Salem quadrangle with other nearby deposits. The glaciomarine deposits in the Salem quadrangle are correlated with the clays near Fresh Pond in Cambridge and the late-glacial marine deposits north of the Salem quadrangle in Massachusetts (N. P. Cuppels and E. Sammel, oral communications, 1960), in New Hampshire, and in Maine on the basis of similar geographic and stratigraphic relations to nonmarine glacial drift and because of similar depths of oxidation. Marine sediments at Lynn and Boston were deposited at or near the end of an earlier glaciation, possibly the one that deposited the older till in the Salem quadrangle. The Lynn and Boston clays described by Judson (1949) are generally oxidized as much as five feet deeper than the Salem clays and are unconformably overlain by stratified drift that is probably equivalent to the younger till and stratified drift of the Salem quadrangle.

Kaye (Art. 34, Prof. Paper 424–B) has recognized multiple glaciomarine clays in the Boston basin and has described their relations to other drift units in the basin. The youngest glaciomarine clay described by Kaye is equivalent to the Boston clay. Clays of this age have not been found in the Salem quadrangle, but they may be completely buried by younger deposits.

TABLE 171.1.—*Stratigraphic relations of surficial deposits in the Salem quadrangle with deposits in nearby areas*

Boston, Lynn, and Cambridge, Mass.	Salem quadrangle, Massachusetts	Massachusetts north of the Salem quadrangle, New Hampshire, and Maine
Recent alluvium and marine deposits.	Recent alluvium and marine deposits.	Recent alluvium and marine deposits.
——Unconformity——	——Unconformity——	——Unconformity——
Clays near Fresh Pond at Cambridge (Chute, 1959).	Late-glacial marine deposits.	Late-glacial marine deposits (N. P. Cuppels and E. Sammel, oral communications, 1960; Goldthwait, 1953; Bloom, 1960).
Lexington drift of Judson (1949) at Cambridge and Boston (Kaye, Art. 34, prof. paper 424–B.	Younger till and associated glaciofluvial deposits.	Drift underlying the marine deposits along the coast.
——Unconformity——		
Boston clay (Judson, 1949).	Unit missing or buried beneath younger deposits.	No deposits described.
	——Unconformity——	
Boston till of Judson (1949).	Older till found mostly in drumlins.	

REFERENCES

Bloom, A. L., 1960, Late Pleistocene changes of sea level in southwestern Maine: Augusta, Maine Geol. Survey, 143 p.

Chute, N. E., 1959, Glacial geology of the Mystic Lakes-Fresh Pond area, Massachusetts: U.S. Geol. Survey Bull. 1061–F, p. 187–212.

Goldthwait, Lawrence, 1953, Clays of southeastern New Hampshire: New Hampshire State Planning and Devel. Comm., Mineral Resource Survey, pt. 15, 15 p.

Judson, Sheldon, 1949, The Pleistocene stratigraphy of Boston, Massachusetts and its relation to the Boylston Street Fishweir, *in* Johnson, Fredrick, ed., The Boylston Street Fishweir II: Phillips Acad., R. S. Peabody Found. for Archaeology Papers, v. 4, no. 1, p. 7–48.

172. END MORAINES ON KITTATINNY MOUNTAIN, SUSSEX COUNTY, NEW JERSEY

By James P. Minard, Washington, D.C.

Several end moraines and eskers were discovered in a thickly wooded region in an area of about 40 square miles on Kittatinny Mountain, in northern New Jersey, by the author in 1952 during mapping of Sussex County as part of a Statewide engineering soil survey (Minard and others, 1954). These deposits first were located and mapped on vertical aerial photographs, on which they appear as conspicuous ridges. Field study since 1952 confirms the presence and extent of the deposits. The moraines extend as two belts entirely across the mountain; similar deposits lie in the valleys on either side of the mountain. Salisbury (1902, p. 276 and 354) in his classic study made several references to the heavily wooded nature of Kittatinny Mountain, but except for noting a slight suggestion of morainal topography southeast of Mashipacong Pond he indicated an absence of recessional moraines everywhere on the mountain.

The end or recessional moraines now can be traced almost continuously across Sussex County from west to east (fig. 172.1). The "crevasse filling" of Salisbury at Ogdensburg (Salisbury, 1902, p. 124, 272, and 414–415) is probably another segment of the previously mapped recessional moraines that extend from Culvers Lake nearly to Ogdensburg, and it fills part of the gap between these moraines and the one mapped by Salisbury (Spencer and others, 1908) one mile northeast of Ogdensburg (fig. 172.1). Study of aerial photographs of the region east and northeast of Ogdensburg shows several small end moraines in Morris and Passaic Counties, between those in Sussex County and those in Bergen County to the east. These deposits are smaller and less conspicuous than those in Sussex County and are not discussed here.

Belts of end or recessional moraines are now known to extend nearly continuously across northern New Jersey; it seems possible that similar moraines may extend westward across the Delaware River into Pennsylvania. The presence of such a continuous prominent recessional moraine, 12 to 30 miles north of the main Wisconsin terminal moraine at and south of Stanhope, would suggest a static ice front for a considerable length of time, and possibly a major substage of the Wisconsin.

BEDROCK GEOLOGY

Kittatinny Mountain is underlain by sedimentary rocks of Silurian age. The Shawangunk conglomerate, a resistant gray quartzitic sandstone and conglomerate, forms the high prominent main ridge of Kittatinny Mountain which rises abruptly as much as 800 feet above Kittatinny Valley to the southeast. The main crest of the mountain is largely glacier-scoured bedrock. The formation is about 1,600 feet thick, strikes nearly northeast, and dips 20° to 50° NW. Lying conformably on it is the High Falls formation, about 1,800 feet thick, composed of basal gray resistant quartzite interbedded with and overlain by red and green sandstone, siltstone, and shale. Sets of glacial striae, clearly evident on surfaces of exposed beds of red sandstone, indicate two directions of ice movement —one nearly parallel to the northeast strike of the formation and the other considerably more westerly. Deep, narrow Wallpack-Mill Brook Valley, along the northwest side of the mountain, is underlain by sandstone, shale, and limestone of Late Silurian and Early Devonian age. Broad Kittatinny Valley to the southeast is underlain by Martinsburg shale and slate of Ordovician age and by Kittatinny limestone of Cambrian and Ordovician age. Intruded between the Shawangunk and the Martinsburg is a mass of nepheline syenite approximately 2 miles long and 800 to 900 feet wide on the ground surface. This rock forms a very rough surfaced bench above the valley just north of Beemerville. About half a mile east of the north end of the syenite is an oval, steep-sided hill, composed of volcanic breccia, surrounded by Martinsburg shale.

DESCRIPTIONS OF THE MORAINES AND ESKERS

Two belts of end moraines cross the mountain. The southern belt extends from a point on the crest of the mountain 1.1 miles northeast of Culvers Lake, westward and northward to a point 1.2 miles southeasterly from Abertown. The northern belt extends from a point on the main crest of the mountain 1.4 miles northwest of Beemerville, northward and westward nearly to Four Corners. Each belt consists of several segments that range from 0.05 mile to 0.75 mile in width, from 0.35 mile to nearly 8 miles in length, and from 20 feet to 90 feet in height. The two largest lie mostly in a high intermontane valley, occupied by the east fork of Flat Brook (Big Flat Brook), between the primary and secondary ridges of the mountain. Lateral moraines form narrow ridges on and near the main crest of the mountain and almost parallel to it. Others form curved ridges on the west slope of the main ridge and at its west base. Ground moraine

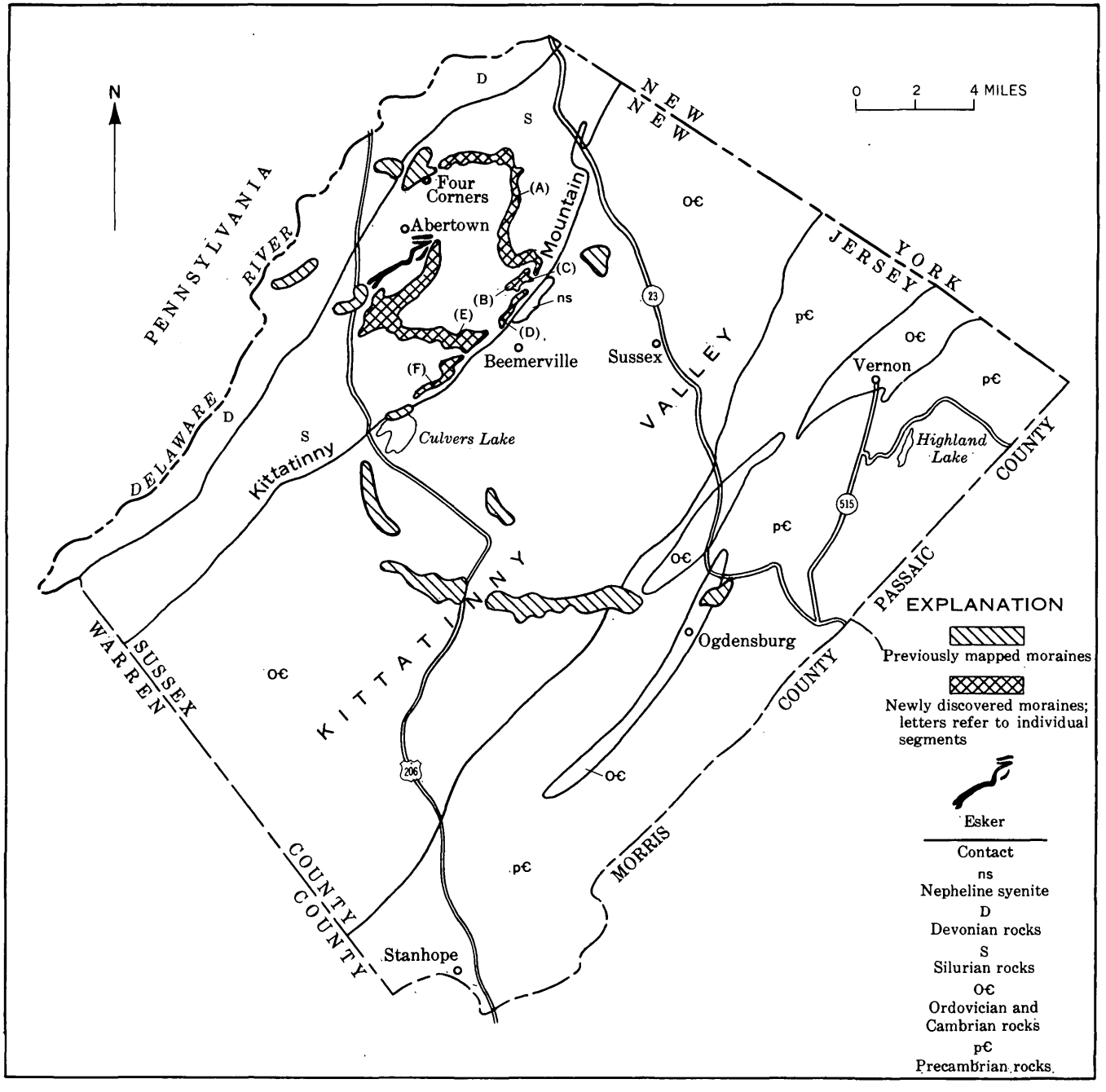

FIGURE 172.1.—Map of Sussex County, N.J., showing the location of end moraines and eskers on Kittatinny Mountain and their relations to moraines in the valleys on either side. Letters in parentheses are explained in text.

and deposits of stratified drift cover much of the bedrock elsewhere.

The surfaces of the moraines consist of irregular hummocks, parallel ridges, and many kettleholes, all in sharp contrast to the relatively smooth surface of the adjacent ground. The moraine ridges are partly convex, partly transverse, and partly parallel to the general southwestward movement of the ice. The many kettleholes range from 10 feet to 300 feet across and are as much as 40 feet deep.

The presence in the moraines of boulders of nepheline syenite and (or) fragments from the Martinsburg shale, indicates that ice moved westward from Kittatinny Valley up over the mountain, probably as overflow tongues from the major ice mass which flowed down the broad valley.

The northern morainal belt consists of 4 separate segments which extend across the mountain from an altitude of 800 feet on the bottom of the valley on the northwest (occupied by Flat Brook and its west

tributary) across the secondary ridge and intermontane valley to the crest of the main ridge (altitude more than 1,500 feet, fig. 172.2). A small glacial lake, 1½ miles long, was dammed behind a prominent morainal ridge (A) in the valley of Big Flat Brook (fig. 172.2). A power-auger hole in the bed of the former lake penetrated 5 feet of iron-oxide-mottled gray silt and clay underlain by at least 35 feet of gray sand and gravel. The sand is mostly quartz and the gravel a mixture of quartz, quartzite, sandstone, and conglomerate pebbles from the High Falls formation and Shawangunk conglomerate, and shale fragments from the Martinsburg.

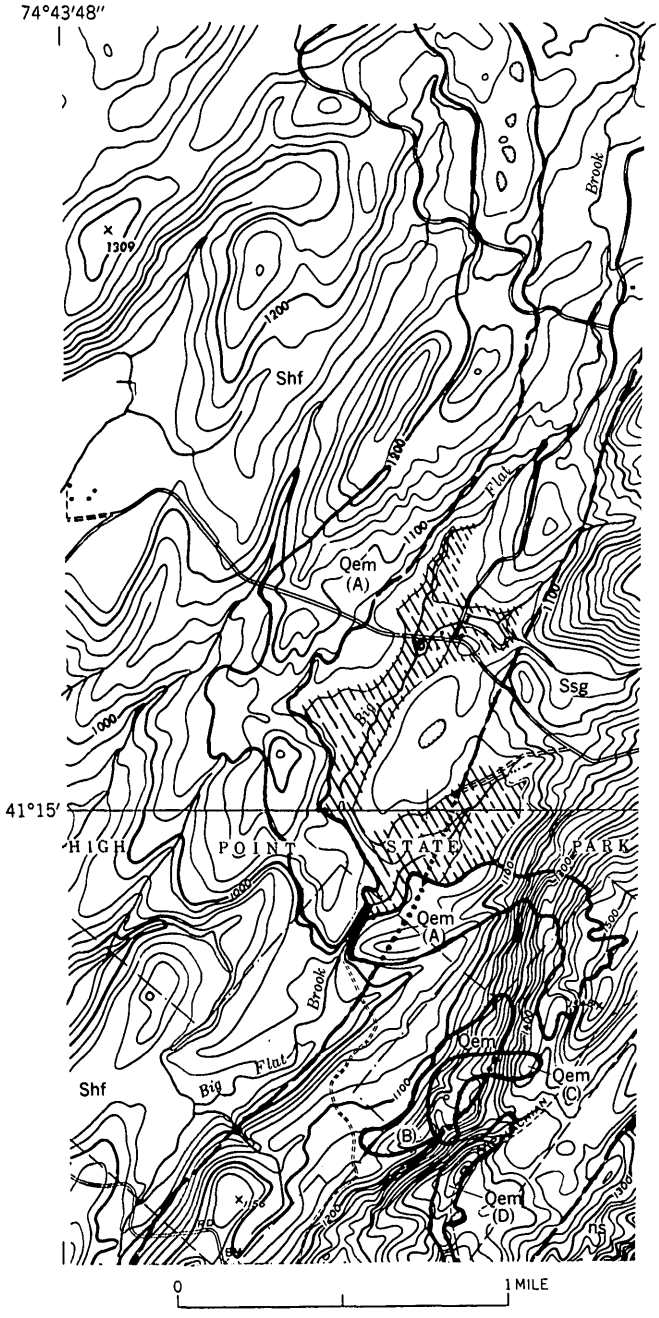

FIGURE 172.2.—Geologic map of part of the northern belt of end moraines on Kittatinny Mountain. Glacial lake bed (Quaternary), diagonal lines; end moraine (Quaternary), Qem; nepheline syenite, ns; High Falls formation (Silurian), Shf; Shawangunk conglomerate (Silurian), Ssg. Letters in parentheses are explained in text.

Morainal segment (C) lies on morainal segment (B) at the west base of the main ridge (fig. 172.2). The composition of segment (B) suggests that the Shawangunk conglomerate was the main source, whereas segment (C) contains an abundance of rock debris from the Martinsburg shale and nepheline syenite. This latter moraine apparently was deposited at the end of a lobe that extended westward from the glacier in the main valley, through the col in the crest of the mountain, and terminated on morainal segment (B). Segment (D), lying along the crest of the main ridge, was deposited at the margin of a large glacier in Kittatinny Valley to the southeast. Abundant shale fragments from the Martinsburg and, particularly, abundant nepheline syenite cobbles and boulders in this moraine, were carried as much as several hundred feet up the ridge from the valley below.

The southern belt of moraines extends southerly and easterly along the lower northwest ridge of the mountain, across the intermontane valley (east tributary of Flat Brook), and along the crest of the main ridge. Morainal segment (E) was deposited along the front and sides of an ice lobe in the intermontane valley. Most of the material in it was derived from the underlying High Falls formation and the Shawangunk conglomerate, but some syenite boulders are present. Numerous kettleholes, hummocky heaps of rock debris, boulder fields, and curved ridges characterize the surface of this distinctive end moraine. Segment (F) (fig. 172.1) lies along the crest of the main ridge. It was deposited at the margin of the main glacier in the valley to the southeast, as is evidenced by abundant fragments from the Martinsburg shale, carried up from the valley below.

Several esker ridges lie on the High Falls formation south of Abertown. The main esker is a sinuous, narrow ridge 1½ miles long, and as much as 40 feet high, extending diagonally down the dip slope of the mountain. It is gravelly sand at the base, and contains some well-rounded cobbles of sandstone and quartzite, in the upper part.

The moraines, eskers, and lakebed contain large amounts of sand and gravel suitable for construction purposes, unsorted material for fill, and resistant

quartzite slabs suitable for riprap. All these deposits store large quantities of water during the fall and winter and supply the streams during the spring and summer.

REFERENCES

Minard, J. P., Holman, W. W., and Jumikis, A. R., 1954, Engineering soil survey of New Jersey, Report no. 11, Sussex County: Rutgers Univ. Engineering Research Bull. 25, 76 p.

Salisbury, R. D., 1902, The glacial geology of New Jersey: New Jersey Geol. Survey, Final Rept. State Geol., v. 5, 802 p.

Spencer, A. C., Kummel, H. B., Wolff, J. E., Salisbury, R. D., and Palache, Charles, 1908, Description of the Franklin Furnace quadrangle [New Jersey]: U.S. Geol. Survey Geol. Atlas, Folio 161, 27 p.

173. REDEFINITION OF THE MOUNT LAUREL SAND (UPPER CRETACEOUS) IN NEW JERSEY

By JAMES P. MINARD, JAMES P. OWENS, and RUTH TODD, Washington, D.C.

In New Jersey the location of the boundary between the Matawan and Monmouth groups of Late Cretaceous age (correlative with the Taylor and Navarro groups of Texas) has long been controversial. Most workers place the boundary between the Wenonah formation and Mount Laurel sand. These two formations, however, are shown as a single unit on previous maps because of an apparent lithologic similarity. Therefore, the contact between the two formations, which coincides with the Matawan-Monmouth boundary, has not been mapped but was located paleontologically by Weller (1907, p. 23–24) on the basis of the *Belemnitella americana* and *Terebratula* (*Choristothyris*) *plicata* zone, and by Stephenson and others (1942, p. 438–439) on the basis of the *Exogyra costata* and *E. cancellata* zone. These zones are in the upper part of the Mount Laurel sand as defined in this report.

During detailed mapping southeast of Trenton we examined this boundary and found that the two formations could be distinguished lithologically. We have mapped the Wenonah formation and Mount Laurel sand as distinct lithologic units from near Walnford, where the aggregate thickness is about 40 feet, to Springville 21 miles to the southwest, where the aggregate thickness is nearly 100 feet. Both units thicken southwestward.

The entire Mount Laurel sand crops out in a gully system 1.1 miles south of Walnford, and its relation to the underlying Wenonah and overlying Navesink formations can be determined in good exposures. This is the same locality cited by Spangler and Peterson as locality 662 (1950, p. 35, 38). A composite section at this locality is shown on figure 173.1.

The Wenonah formation here is a dark-gray nonfossiliferous massive fine- to very fine-grained sand and is mainly well sorted (fig. 173.2). Quartz, mica (both green and colorless), feldspar (10 to 15 percent), and glauconite (greater than 5 percent) are the major sand constituents. Sand-sized fragments of carbonaceous matter and finely crystalline pyrite are locally abundant. The formation is characterized by much colorless and green mica, abundant sand-sized carbonaceous fragments, and a uniform texture throughout. The Wenonah grades upward into the Mount Laurel sand with no perceptible interruption.

The Mount Laurel sand is a fossiliferous dark-gray (reddish-brown where weathered) massive sand that coarsens from a medium-fine sand at the base to a medium-coarse sand containing gravel at the top (fig. 173.2). Sorting is not as good as in the underlying Wenonah. Quartz and feldspar (10 to 15 percent) are the major minerals, and glauconite occurs in moderate amounts in the lower and upper few feet. Small ovoid brown pellets of apatite and other organically derived remains, such as shark teeth, are common. Coarse carbonaceous matter, mica, and pyrite are characteristically less abundant than in the Wenonah. The diagnostic features of the Mount Laurel are its relatively coarse texture, gravel at the top, and occurrence of fossils. The contact with the overlying Navesink formation is distinct, although this boundary is locally interrupted by numerous cyclindrical borings that extend down into the Mount Laurel and are filled with glauconite derived from the overlying Navesink. This feature imparts a mottled appearance to the upper part of the formation. The overlying Navesink formation is a dark greenish-gray very fos-

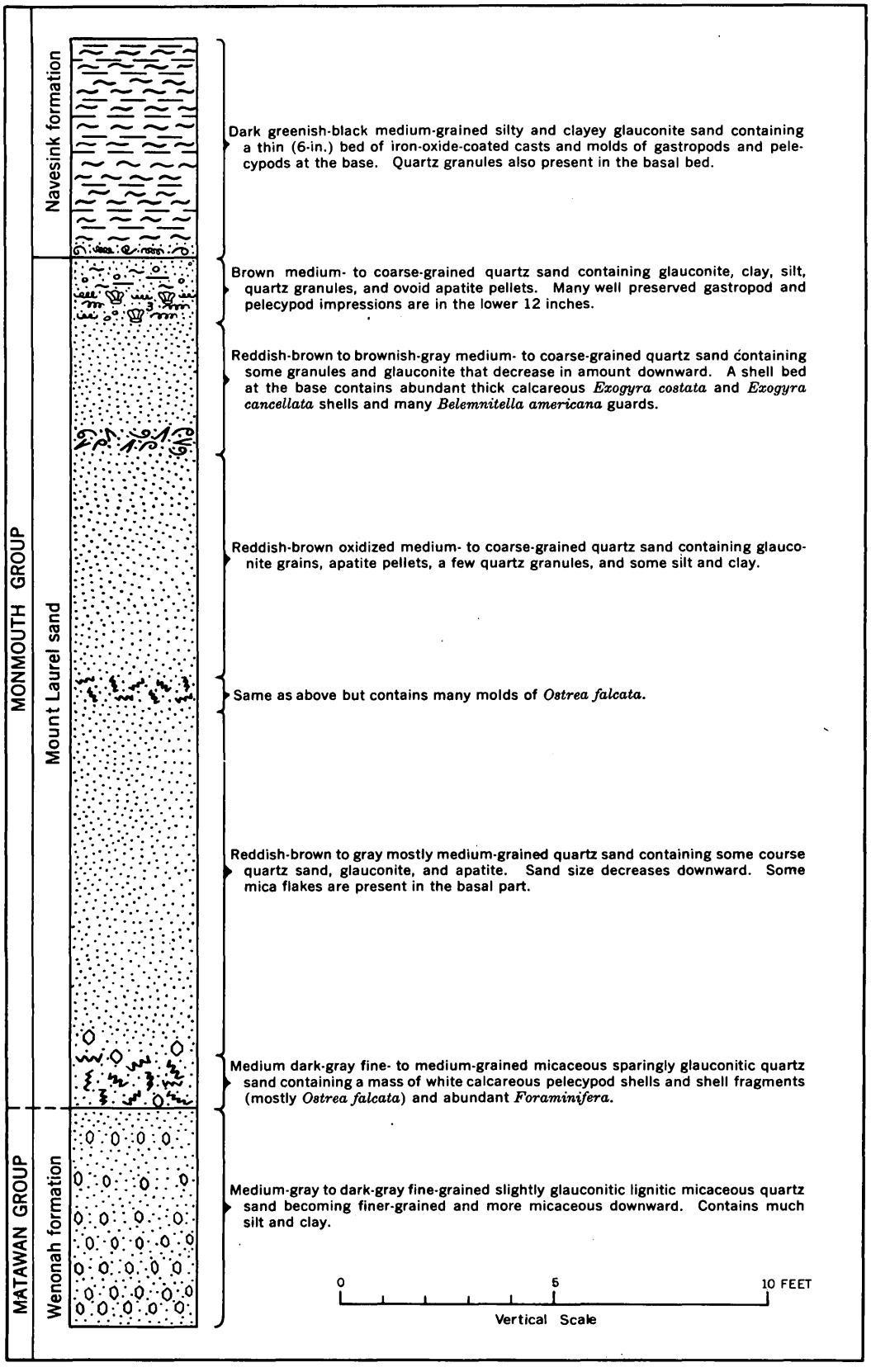

FIGURE 173.1.—Stratigraphic section of the Mount Laurel sand, including the basal part of the Navesink and upper part of the Wenonah formations, at locality 662 of Spangler and Peterson (1950).

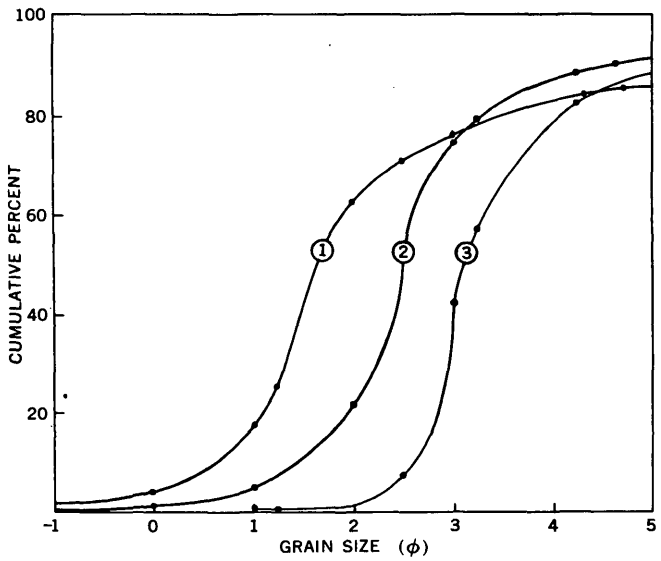

FIGURE 173.2.—Variation in size distribution in the upper 5 feet of the Wenonah formation (curve 3), and the basal and upper 5 feet of the Mount Laurel sand (curves 2 and 1, respectively). Each curve represents a composite sample from about 5 feet of beds.

siliferous massive clayey glauconite sand. Pyrite, quartz, mica, and finely comminuted carbonaceous matter are minor constituents. It can readily be distinguished from the underlying Mount Laurel on the basis of its abundant glauconite, and, locally, by a shell bed at its base (fig. 173.1).

As shown on figure 173.1, the Mount Laurel contains two distinctly different types of shell beds. The lower shell beds are characterized by *Ostrea falcata* whereas the upper beds contain *Exogyra costata* and *Exogyra cancellata*, *Gryphaea convexa*, *Belemnitella americana*, *Choristothyris plicata*, and unidentified species of gastropods. A macrofaunal suite similar to that in the Navesink is present in the upper part of the Mount Laurel. Previously reported faunal studies of the Mount Laurel were restricted to the upper *Exogyra* beds; consequently the formation was grouped with the Navesink as a single biostratigraphic unit (Weller, 1907, p. 103). Spangler and Peterson (1950, p. 38) noted the lower shell beds and placed the lowest one at the top of the Wenonah, but apparently made no attempt to identify the fossils. Unfortunately, *Ostrea falcata*, the macrofossil present in the greatest abundance, is a wide-ranging Cretaceous form of little value for precise correlation.

Microfossils in the *Ostrea* beds (table 173.1) were found by Ruth Todd to be mixed, having both Taylor (=Matawan) and Navarro (=Monmouth) affinities, whereas those in the *Exogyra* beds (table 173.2) have dominant Navarro affinities. It is concluded that the lower beds of the Mount Laurel are a mixed or transitional paleontological zone. Stephenson and others (1942, p. 438–439) noted a similar relation between units of Taylor and Navarro ages in Texas.

TABLE 173.1.—*Foraminifera identified from lowest* Ostrea falcata *shell beds*

Foraminifera	Recorded age range [1]
Anomalina cf. *A. rubiginosa* Cushman.	----------
Arenobulimina americana Cushman, juv.	Austin, Taylor, and Navarro.
Cibicides compressus Olsson	Mt. Laurel and Hornerstown (Paleocene).
Cibicides coonensis (Berry)	Taylor or Navarro.
Citharina sp. (striate)	----------
Dentalina basiplanata Cushman	Taylor and Navarro.
Dentalina gracilis d'Orbigny	Austin, Taylor, and Navarro.
Frondicularia glabrans Cushman	Taylor or Navarro.
Globulina lacrima Reuss	Upper Cretaceous and Paleocene.
Guttulina adhaerens (Olszewski)	Navarro and Paleocene.
Neobulimina spinosa Cushman and Parker.	Taylor and Navarro.
Nodosaria affinis Reuss	Long-ranging.
Pyrulina cylindroides (Roemer)	Long-ranging.
Robulus pseudo-secans Cushman [possibly a synonym of *R. navarroensis* (Plummer)].	Austin, Taylor, and Navarro.
Vaginulina taylorana Cushman	Taylor.

[1] Mostly as given in Cushman, 1946.

TABLE 173.2.—*Foraminifera identified from* Exogyra costata *and* Exogyra cancellata *shell beds*

Foraminifera	Recorded age range [1]
Anomalina nelsoni Berry	Taylor and Navarro.
Anomalina cf. *A. rubiginosa* Cushman.	----------
Arenobulimina americana Cushman.	Austin, Taylor, and Navarro.
Bolivina (*Loxostomum*) *gemma* Cushman.	Navarro.
Buliminella carseyae plana Cushman and Parker.	Navarro.
Cibicides compressus Olsson	Mt. Laurel and Hornerstown (Paleocene).
Cibicides coonensis (Berry)	Taylor or Navarro.
Dentalina gracilis d'Orbigny	Austin, Taylor, and Navarro.
Dorothia bulletta (Carsey)	Austin, Taylor, and Navarro.
Fissurina spp	----------
Gaudryina stephensoni Cushman	Austin, Taylor, and Navarro.
Globigerina (*Rugoglobigerina*) *rugosa* Plummer.	Navarro.
Globigerinella aspera (Ehrenberg)	Upper Cretaceous and Paleocene.
Globotruncana fornicata Plummer	Taylor and Navarro.
Guembelina globulosa (Ehrenberg)	Taylor and Navarro.
Guembelina pulchra Brotzen	Austin and Taylor.
Gyroidina depressa (Alth)	Austin, Taylor, and Navarro.
Neoconorbina sp	----------
Nodosaria lonqiscata d'Orbigny	Long-ranging.
Nonionella anasata Cushman	Navarro.
Planoglobulina carseyae (Plummer).	Navarro.
Plectina watersi Cushman	Navarro.
Pseudotextularia elegans (Rzehak)	Austin, Taylor, and Navarro.
Pseudouvigerina plummerae Cushman.	Austin, Taylor, and Navarro.
Pullenia americana Cushman	Taylor and Navarro.
Pulsiphonina prima (Plummer)	Navarro.
Robulus macrodiscus (Reuss)	Upper Cretaceous and Paleocene.
Spiroplectammina semicomplanata (Carsey).	Taylor and Navarro.

[1] Mostly as given in Cushman, 1946.

REFERENCES

Cushman, J. A., 1946, Upper Cretaceous Foraminifera of the Gulf Coastal region of the United States and adjacent areas: U.S. Geol. Survey Prof. Paper 206.

Spangler, W. B., and Peterson, J. J., 1950, Geology of Atlantic Coastal Plain in New Jersey, Delaware, Maryland and Virginia: Am. Assoc. Petroleum Geologists Bull., v. 34, p. 1–99.

Stephenson, L. W., King, P. B., Monroe, W. H., and Imlay, R. W., 1942, Correlation of the outcropping Cretaceous formations of the Atlantic and Gulf Coastal Plain and Trans-Pecos, Texas: Geol. Soc. America Bull., v. 53, p. 435–448.

Weller, Stuart, 1907, A report on the Cretaceous paleontology of New Jersey: New Jersey Geol. Survey, Paleont. ser., v. 4.

174. THE BREVARD FAULT IN NORTH AND SOUTH CAROLINA

By John C. Reed, Jr., Henry S. Johnson, Jr., Bruce Bryant, Henry Bell III, and William C. Overstreet, Denver, Colo., Columbia, S.C., and Washington, D.C.

A belt of rocks of low metamorphic grade extends along a pronounced topographic lineament from the coastal plain in Alabama northward at least 375 miles to Mt. Airy, N. C. (fig. 174.1). This belt has a maximum width of only a few miles. It has been known as the Brevard belt and many of the rocks in it have been mapped as Brevard schist (Keith, 1905, 1907; Stose and Smith, 1939; Crickmay, 1952).

The Brevard schist was interpreted by Keith (1905, 1907) as Cambrian rock resting unconformably on schist, gneiss, and granite of Precambrian age and folded into a narrow syncline. Crickmay (1952) regarded the Brevard schist in Georgia as part of the Carolina gneiss, and thought that it was intruded by granite gneiss of Precambrian age. Jonas (1932) recognized the rocks of the belt as retrogressively metamorphosed and interpreted them as marking a major thrust fault of late Paleozoic age which she connected with the Martic thrust in Pennsylvania. Later this fault was called the Brevard overthrust (King and others, 1944). Hamilton (1957) showed that the fingers mapped as Brevard schist by Keith (1905) west of Old Fort, N. C., are retrogressively metamorphosed schists derived from adjacent schist and gneiss. The authors believe, as a result of recent reconnaissance observations in North and South Carolina, that the Brevard belt is a fault zone. The authors agree with Jonas' interpretation that the low metamorphic rank in the belt results from retrogression.

Detailed study in the Table Rock and Lenoir quadrangles, North Carolina, has shown that rocks within the Brevard belt are polymetamorphic and consist of phyllonite and blastomylonite (recognized by Stose and Stose, 1951) derived from adjacent mica schist, gneiss, and granitic rock (Reed and Bryant, 1960).

In the Table Rock and Lenoir quadrangles and at all the other places where we have seen the Brevard belt, the rocks generally strike parallel to the trend of the belt and dip from 40° to 60° SE. In a segment of the belt west and north of Lenoir, vertical to steep westerly dips are characteristic. Elongate mineral grains and aggregates in almost all the cataclastic rocks are nearly horizontal and trend northeasterly.

We have made a reconnaissance of the Brevard belt between northern Georgia and Mt. Airy, N.C. At all places visited, the rocks (except for apparently exotic lenses of dolomitic limestone) consist of polymetamorphic schist, phyllonite, blastomylonite, and some graphitic phyllonite. One common rock type is "fish scale" schist or gneiss containing deformed porphyroclasts of muscovite 1 cm in diameter. These porphyroclasts are altered to aggregates of sericite where retrogressive metamorphism is most complete. In less intensely retrogressively metamorphosed rock, pods of pegmatite and relict kyanite and garnet are found. The low-grade rocks are derived by intense shearing and partial to complete recrystallization of the rocks on either side of the Brevard fault. These relations are particularly well exposed east of Rosman, N.C., on

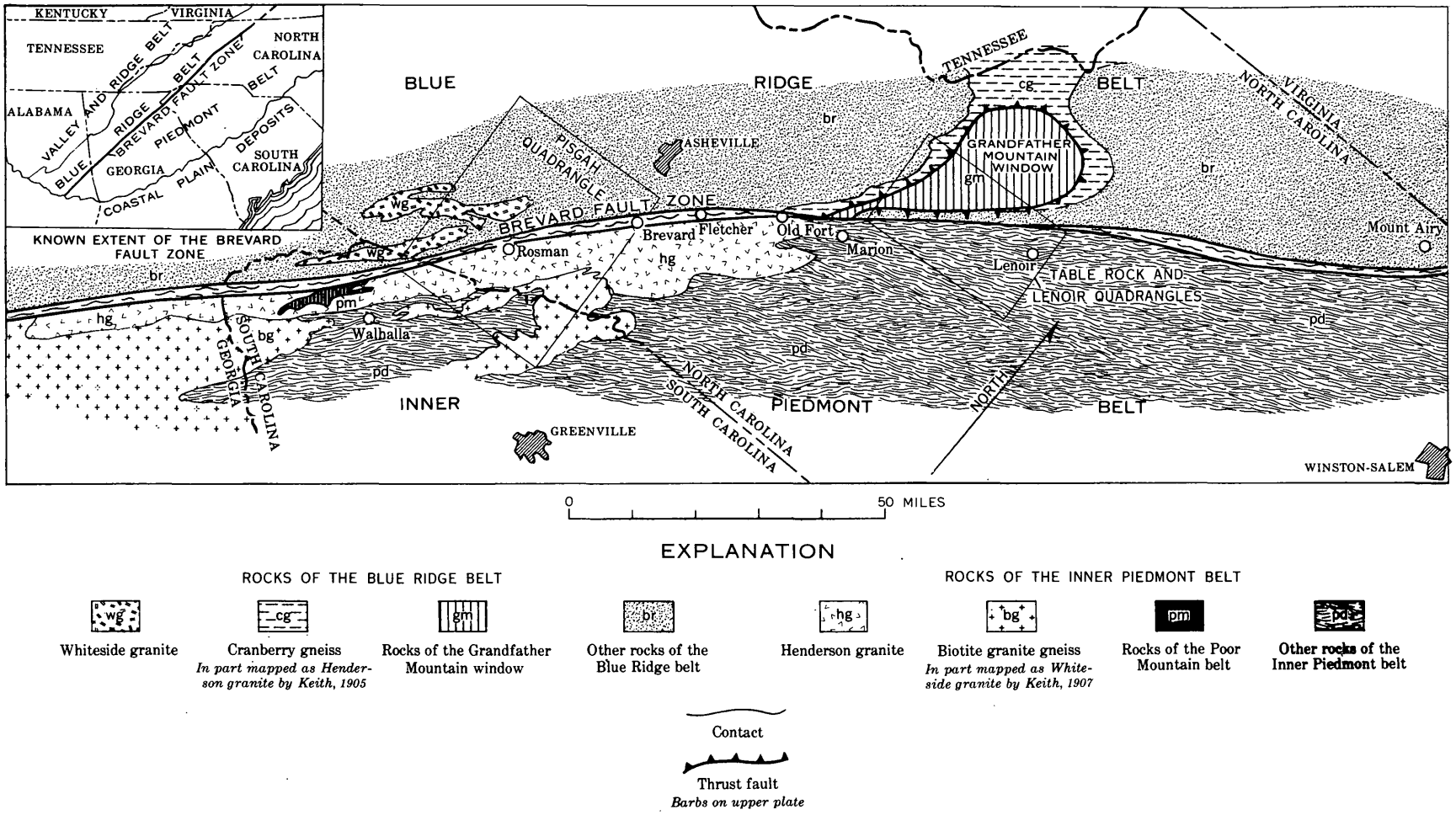

FIGURE 174.1.—Sketch map of the Brevard belt in North and South Carolina from published geologic maps and reconnaissance observations.

U.S. Highway 64. There is a transition westward from Henderson granite through sheared Henderson granite to blastomylonite of the Brevard belt. On the west side of the belt, layered mica schist and gneiss of the Blue Ridge show a transition southeastward to phyllonite in the Brevard belt.

The occurrence of limestone in the Brevard belt has been cited as evidence of a unique stratigraphic unit. Lenticular beds of marble are more common in Piedmont rocks than is usually supposed (Sloan, 1908; Conrad, 1960; Clarke, 1957, 1958, written communication, 1958). These marbles are mostly coarsely crystalline; grain size of 2 to 5 mm is common and locally is as much as 1 cm. The marble is found at scattered localities in the Piedmont, and some localities such as those near Marion, N.C., and in the Poor Mountain belt near Walhalla, S.C., are almost adjacent to the Brevard belt. One limestone inside the belt at Fletcher, N.C., is fine-grained recrystallized white and gray dolomite containing phyllitic partings. It closely resembles the Shady dolomite in the Grandfather Mountain window, where the dolomite was metamorphosed under greenschist facies conditions and displays no evidence of having been at higher grade. Limestone at Fletcher is highly disordered and most likely it is faulted into the adjacent phyllonite rather than included as a simple sedimentary lens or an infold of a younger formation.

Mapping in the Grandfather Mountain area has revealed gross differences between the rocks of the Blue Ridge and those of the Inner Piedmont. Rocks of the Blue Ridge have a higher proportion of mica schist and amphibolite, more gneisses of migmatitic aspect, granitic rocks of different character and structural habit, and pegmatites of a different composition than rocks of the Inner Piedmont. The Henderson granite mapped by Keith (1905) northwest of the Brevard belt is part of the Cranberry gneiss (Eckelmann and Kulp, 1956), and is markedly different from Henderson granite at its type locality southeast of the belt. The Cranberry gneiss is a layered gneiss containing numerous granitic layers and lenses of contrasting composition, layers of biotite schist, amphibolite, and plagioclase porphyroclast schist, whereas the Henderson granite is a relatively uniform augen gneiss of quartz monzonite composition.

Farther south, Whiteside granite at the type locality northwest of the Brevard belt is coarser, more contorted, and richer in inclusions and pegmatite dikes than the biotite granite gneiss called the Whiteside granite by Keith (1907) southeast of the belt.

In South Carolina the Poor Mountain zone of Sloan (1908) has been considered a part of the Brevard belt (King and others, 1944). One of us (Johnson) has found that the rocks in the Poor Mountain zone consist of coarsely crystalline marble associated with hornblende gneiss and Henderson granite—rocks typical of the Inner Piedmont. The lithologic units are truncated by phyllonite and blastomylonite in the Brevard belt, which in this area was called the Chauga zone by Sloan. Rocks within the Chauga zone have a strong, subhorizontal cataclastic lineation that trends toward the northeast, parallel to the strike of the rocks. The lineation was observed by Clarke (written communication, 1958), but he did not recognize its cataclastic origin. Mapping by Keith (1907) in the Pisgah quadrangle shows different rock types on either side of the Brevard schist.

Overstreet and others (Art. 45, Prof. Paper 424–B) conclude that most rocks of the Piedmont of North and South Carolina are of probable Paleozoic age except, perhaps, for some rocks of late Precambrian age near the base. They find no evidence of earlier Precambrian rocks in the Piedmont. No Precambrian ages have been obtained for minerals from rocks east of the Brevard belt (Long, Kulp, and Eckelmann, 1959; Overstreet and others, Art. 45, Prof. Paper 424–B). However, isotopic determinations on zircon are lacking. Geologic and mineral age data show that much of the rock of the Blue Ridge west of the Brevard belt is of earlier Precambrian age and is unconformably overlain by late Precambrian rocks, all of which were metamorphosed to medium grade at least once during the Paleozoic.

We conclude that the Brevard belt marks a major fault because of the retrogressive metamorphism of the rocks in it, the differences in rocks on either side, and truncation of the Grandfather Mountain window and stratigraphic units in the Poor Mountain area. The extension of the belt traced by Jonas (1932) into Virginia is uncertain (Brown, 1958; Espenshade, 1954). We have found no rocks on one side of the fault which can be definitely matched with rocks on the other, so the direction and amount of displacement are unknown. Intense cataclastic lineation in the fault zone suggests important lateral movement, whereas regional geologic considerations indicate that some vertical component was involved.

In the Grandfather Mountain area the Brevard fault truncates the southern edge of the Grandfather Mountain window and the fault zone contains unmetamorphosed diabase dikes of Triassic(?) age, showing

that the fault was active after large-scale Paleozoic thrusting and before Triassic(?) igneous activity.

REFERENCES

Brown, W. R., 1958, Geology and mineral resources of the Lynchburg quadrangle, Virginia: Virginia Div. Mineral Resources Bull. 74, 99 p.

Clarke, J. W., 1957, Contact metamorphism in Laurens County, South Carolina: South Carolina Div. Geology, Mineral Industries Lab. Monthly Bull., v. 1, no. 4, p. 2–7.

——— 1958, A normal fault in Cherokee County, South Carolina: South Carolina Div. Geology, Mineral Industries Lab. Monthly Bull., v. 2, no. 3, p. 20–22.

Conrad, S. G., 1960, Crystalline limestones of the Piedmont and mountain regions of North Carolina: North Carolina Dept. Conserv. Devel. Bull. 74, 56 p.

Crickmay, G. W., 1952, Geology of the crystalline rocks of Georgia: Georgia Geol. Survey Bull. 58, p. 1–54.

Eckelmann, F. D., and Kulp, J. L., 1956, The sedimentary origin and stratigraphic equivalence of the so-called Cranberry and Henderson granites in western North Carolina: Am. Jour. Sci., v. 254, p. 288–315.

Espenshade, G. H., 1954, Geology and mineral deposits of the James River-Roanoke River manganese district, Virginia: U.S. Geol. Survey Bull. 1008, 115 p.

Hamilton, W. B., 1957, Polymetamorphic rocks of the Blue Ridge front near Old Fort, North Carolina: Am. Jour. Sci., v. 255, p. 568–573.

Jonas, A. I., 1932, Structure of the metamorphic belt of the southern Appalachians: Am. Jour. Sci., 5th ser., v. 24, p. 228–243.

Keith, Arthur, 1905, Description of the Mt. Mitchell quadrangle: U.S. Geol. Survey Geol. Atlas, Folio 124.

——— 1907, Description of the Pisgah quadrangle [N. C.–S. C.]: U.S. Geol. Survey Geol. Atlas, Folio 147.

King, P. B., and others, 1944, Tectonic map of the United States: Am. Assoc. Petroleum Geologists.

Long, L. E., Kulp, J. L., Eckelmann, F. D., 1959, Chronology of major metamorphic events in the southeastern United States: Am. Jour. Sci., v. 257, no. 8, p. 585–603.

Reed, J. C., Jr., and Bryant, B. H., 1960, A major topographic lineament in western North Carolina and its possible structural significance, *in* Short papers in the geological sciences: U.S. Geol. Survey Prof. Paper 400–B, p. B195–B197.

Sloan, B. E., 1908, Catalogue of the mineral localities of South Carolina: South Carolina Geol. Survey, ser. 4, Bull. 2, 505 p.

Stose, G. W., and Smith, R. W., 1939, Geologic map of Georgia: Georgia Div. Mines, Mining and Geology.

Stose, G. W., and Stose, A. J., 1951, Blue Ridge Front—a fault scarp: Geol. Soc. America Bull., v. 62, p. 1371–1373.

175. ANNUAL MINIMUM STREAMFLOWS IN A PERMEABLE BASIN IN OHIO

By William J. Schneider, Washington, D.C.

The magnitude of annual minimum streamflows during the summer and fall in permeable basins is governed by the extent that ground water is released to the streams from storage, and by the precipitation. These factors have been related for the Mad River drainage basin, which includes 485 square miles near Springfield, Ohio. The Mad River basin is described by Cross and Bernhagen (1949) as follows:

> The Mad River occupies a broad, trough-like valley of preglacial and interglacial origin, and most of its course lies between the morainal ridges deposited by the Miami and Scioto lobes of the Wisconsin glacier. The surface material in the interlobate areas consists of extensive permeable drift such as kames, kame terraces, and end-moraines accompanied by high-level outwash in the uplands and valley train in the main valleys. At no other place in the state is there such an accumulation of permeable material and as a result the Mad River has the highest index of flow of all the streams in Ohio.

Annual minimum flows for the period 1922 to 1956 were used for this study. The annual minimum flow is defined as the average flow for the minimum seven consecutive days of streamflow in the hydrologic year ending April 30. The seven-day period rather than a shorter period is used in order to dampen out or minimize any unnatural low flow which might occur in a shorter period from temporary storage or other causes in the basin.

Annual minimum flows of the Mad River usually occur in the fall coincident with the normal seasonal lows of ground-water levels. During the 35 years of record, 17 of the annual minimum flows occurred in September and October, 2 in late July, 4 in August, 2 in November, 7 in December, and 3 in January and February. None occurred from late February to late July.

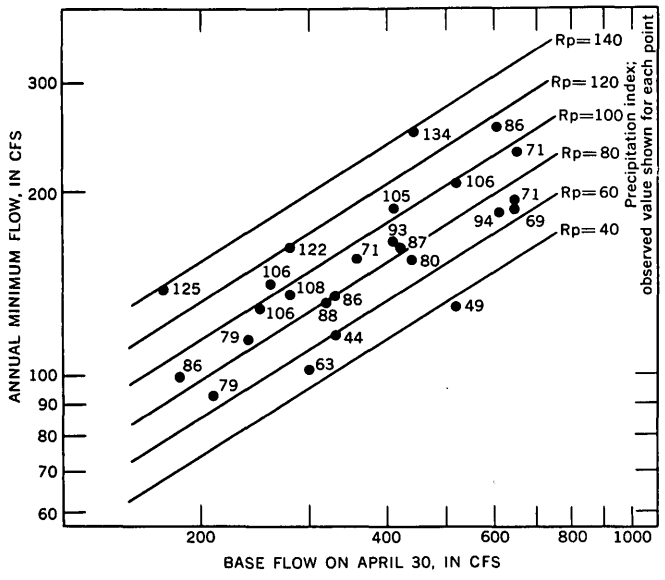

FIGURE 175.1.—Relation of base flow and precipitation to annual minimum flows of Mad River near Springfield, Ohio, occurring during summer and fall.

The magnitude of the ground-water supply at the beginning of the ground-water depletion season in the summer and fall is represented in this study by the base flow of the Mad River near Springfield, Ohio, on April 30. The measure of precipitation was taken as the percent of normal precipitation at Urbana, Ohio, for the period beginning May 1 and ending on the last date of 7-day period of annual minimum stream flow.

Preliminary graphical analyses indicated a difference in the relations for summer-fall and for winter minimums. Therefore, the final analysis, shown by figure 175.1, was limited to the 25 annual minimum flows that occurred prior to December 1. The relation is computed as:

$$\log Q_m = 0.284 + 0.63 \log Q_b + 0.32 R_p \qquad (1)$$

where Q_m is the annual minimum flow in cfs, Q_b is base flow in cfs on the preceding April 30, and R_p is the ratio of precipitation for the period May 1 to date of low flow to the normal precipitation for that period. The regression coefficients in equation 1 are statistically significant at the 0.1 percent level; the standard error is +10, −9 percent.

REFERENCES

Cross, W. P., and Bernhagen, R. J., 1949, Ohio stream-flow characteristics, Part 1, Flow duration: Ohio Dept. Nat. Resources, Div. Water, Bull. 10, 40 p.

176. CLASSIFICATION OF GLACIAL DEPOSITS IN THE KILLBUCK LOBE, NORTHEAST-CENTRAL OHIO

By GEORGE W. WHITE, Urbana, Ill.

Work done in cooperation with the Ohio Department of Natural Resources, Division of Water

Deposits of the Killbuck glacial lobe, which occur in several counties in northeast-central Ohio in the Allegheny plateau (fig. 176.1), can now be divided into several rock-stratigraphic units (table 176.1) as has been done with the deposits of the Grand River lobe in eastern Ohio (White, 1960) and northwestern Pennsylvania (Shepps and others, 1959).

MILLBROOK TILL

The Millbrook till is named for the village of Millbrook in southwestern Wayne County, Ohio. The following section was measured 1¼ miles north-northeast of Millbrook in the SE¼SE¼ sec. 25, Plain

TABLE 176.1—*Glacial deposits of the Killbuck lobe*

Epoch	Stage	Substage	Unit	Material
Pleistocene	Wisconsin	Cary	Hiram till	Brown clay till
			Hayesville till	Brown silty clay till
			Navarre till	Yellow-brown sandy till
	---(?)---- Wisconsin (?) Illinoian (?)		Millbrook till	Olive-brown sandy till; in places has weathered zone at top

Township, Wayne County, in a steep road bank and ditch:

	Thickness (Ft.	in)
Quaternary system:		
Pleistocene series:		
Wisconsin stage:		
Cary substage:		
Hayesville till:		
Soil and weathered dark-brown till; sparingly pebbly; poorly exposed	4	0
Navarre till:		
Till, yellow-brown, noncalcareous	1	0
Till, yellowish-brown (10YR 5/6); calcareous; sandy, pebbly; sand, 48 percent; silt, 35 percent; clay, 17 percent	2	6
Silt, olive-brown, calcareous (ranges from 1 to 4 feet in thickness)	3	0
Illinoian(?) or Wisconsin(?) stage:		
Millbrook till:		
Till, olive to light olive-brown (2.5Y 4/4–5/6), with dark stains along partings; calcareous; sandy, pebbly; sand, 49 percent; silt, 38 percent; clay, 13 percent	3	0
Till, dark-gray (5Y 4/1); hard, platy; sand, 44 percent; silt, 41 percent; clay, 15 percent	1	6
	15	0

Bottom of ditch.

The Millbrook till is sandy and pebbly, and is characteristically olive brown.

The Millbrook till overlies the Paleozoic bedrock. At many localities the upper part of the Millbrook till is leached and severely weathered.

The Millbrook till extends across most of Wayne, the central part of Ashland, northern Holmes, and western Stark Counties. Outcrops are common in many of the valleys tributary to Killbuck Creek northwest, north, and northeast of Wooster, and especially in cuts of the Pennsylvania Railroad 2 to 4 miles east of Wooster. It is well exposed in strip mines in Paint Township, southeastern Wayne County, where the overlying till is thin or absent.

The Millbrook till may be Illinoian or very early Wisconsin in age. The latter age has been proposed for a till in western Ohio having a buried weathered zone (Forsyth, 1957).

NAVARRE TILL

The Navarre till is named for the village of Navarre, southwestern Stark County. The following section was measured 2 miles south of Navarre and 50 feet north of the highway bridge in a deep cut of the Nickel Plate Road, SW¼ sec. 16, Bethlehem Township:

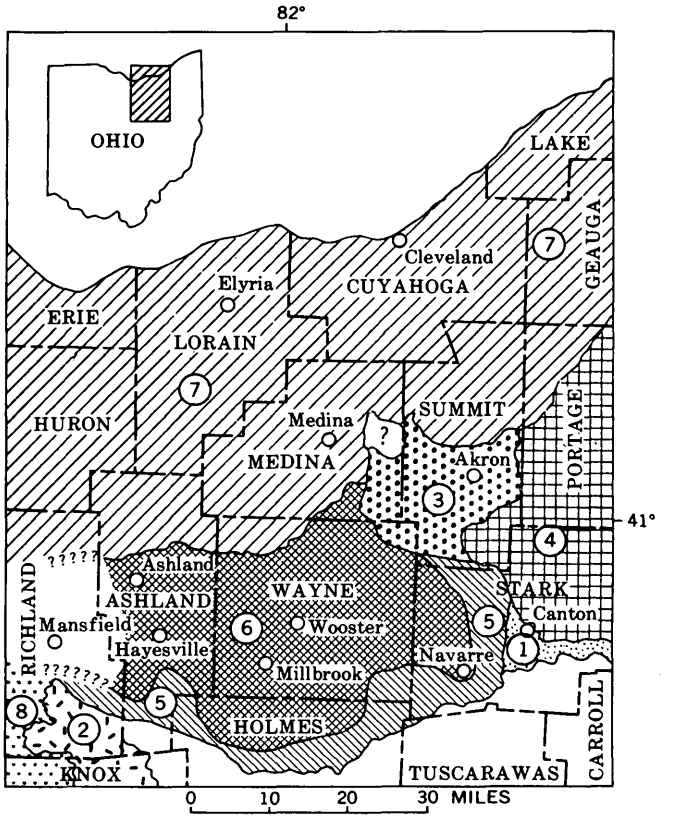

FIGURE 176.1.—Map showing areal extent of rock-stratigraphic units in Killbuck glacial lobe, Ohio. (1) Illinoian drift of Grand River lobe; (2) Illinoian drift of Scioto lobe; (3) Mogadore till; (4) Kent till of Grand River lobe; (5) Navarre till; (6) Hayesville till; (7) Hiram till; (8) Wisconsin till of Scioto lobe.

	Thickness (Ft	in)
Quaternary system:		
Pleistocene series:		
Wisconsin stage:		
Cary substage:		
Navarre till:		
Loam, dark gray-brown	0	7
Loam, yellow-brown	0	4
Silt loam, brownish-yellow	1	1
Till, much weathered; yellow-brown and gray; some manganese stains	2	0
Till, noncalcareous; dark yellow-brown	2	0
Till, calcareous; dark yellow-brown (10YR 4/4); sandy, moderately pebbly; irregular horizontal fracture; sand, 46.3 percent; silt, 37.9 percent; clay, 15.8 percent	4	8
Till, calcareous; yellow-brown mixed with gray	2	0
Till, calcareous; gray (10YR 4/1); sandy, moderately pebbly; sand, 53.8 percent; silt, 33.0 percent; clay, 13.2 percent	5	0
Pennsylvanian system:		
Shale, limestone, coal, and clay	27	0
	44	6

Level of track.

The Navarre till is sandy to moderately pebbly, and contains scattered cobbles and a few boulders. It is yellow brown where oxidized. The Navarre till unconformably overlies bedrock or the Millbrook till.

The Navarre till occurs at the surface in west-central and southwestern Stark County, a very small area in extreme southern Summit County, and in a belt extending across central Holmes County and southern Ashland County. It forms knolls around the margin of the Killbuck lobe in Stark County in the prominent Buck Hill end moraine.

The Navarre till is the same age as the Kent till of the Grand River lobe in eastern Ohio (White, 1960, p. 5) and northwestern Pennsylvania (Shepps and others, 1959, p. 31), and is correlative with the "early Cary" drift of the Scioto and Miami lobes (Goldthwait, 1952, p. 2a, map).

HAYESVILLE TILL

The Hayesville till is named from the village of Hayesville in southern Ashland County. The following section was measured in a road cut and ditch at a road corner 1½ miles northeast of the center of Hayesville. The locality is at the top of the south wall of the valley of Oldtown Run in the center of sec. 11, Vermillion Township:

	Thickness (Ft	in)
Quaternary system:		
Pleistocene series:		
Wisconsin stage:		
Cary substage:		
Hayesville till:		
Silt loam, dark gray-brown	0	7
Silt loam, yellowish-brown	0	5
Silty clay loam, coarse, yellow-brown	1	0
Silty clay loam (much weathered till), mottled gray, brown, and yellow	0	11
Till, noncalcareous, weathered, dark-brown (10YR 4/3), with black manganese stains	1	4
Till, calcareous, dark-brown; secondary calcite splotching	1	0
Till, calcareous dark-brown, silty, sparingly pebbly; sand, 20.4 percent; silt, 47.6 percent; clay, 32.0 percent	1	9
	7	0
Bottom of ditch.		

In auger holes on the east side of the road the Hayesville till overlies brown gravel, beneath which is weathered Millbrook till. The Hayesville till crops out in road cuts 1 mile south of Hayesville, for several miles along an east-west road 2 miles north of Hayesville, and at a crossroad 2½ miles south-southeast of Hayesville.

The Hayesville till is silty, sparingly to very moderately pebbly, and contains a few cobbles and fewer boulders. It is dark brown where oxidized, and contrasts with the light yellow-brown or olive-brown color of older tills.

At many places the Hayesville till lies unconformably upon sand and gravel or Navarre till. Where the Navarre till is missing, the Hayesville till overlies the Millbrook till.

The Hayesville till forms the surface in northwestern Stark County, a small part of southeastern Medina, almost all of Wayne, central and southern Ashland and northern Holmes Counties, and it extends an unknown distance into Richland County.

In most of the area the Hayesville till is less than 10 feet thick and at some places it is only 1 or 2 feet thick. It is thickest in the northern part of the area.

The Hayesville till is correlated with the Lavery till of the Grand River lobe (White, 1960, p. 6: Shepps and others, 1959, p. 38), and with drift of the Scioto lobe called "middle Cary" by Goldthwait (1952, p. 2a, map).

HIRAM TILL

The Hiram till was named from its type locality in the Grand River lobe (White, 1960). It has now been traced into the Killbuck lobe in northwestern Wayne and northern Ashland Counties where it has the same characteristics as previously described by White (1960, p. 8).

REFERENCES

Forsyth, J. L., 1957, "Early" Wisconsin drift in Ohio [abs.]: Geol. Soc. America Bull., v. 68, p. 1728.

Goldthwait, R. P., 1952, Guidebook for the 1952 field conference of friends of the Pleistocene: Ohio Geol. Survey.

Shepps, V. C., White, G. W., Droste, J. B., and Sitler, R. F., 1959, Glacial geology of northwestern Pennsylvania: Pennsylvania Geol. Survey Bull. G–32.

White, G. W., 1960 Classification of Wisconsin glacial deposits in northeastern Ohio: U.S. Geol. Survey, Bull. 1121–A, 12 p.

601530 O—61——6

177. ROTATIONAL BLOCK OF THE CUMBERLAND OVERTHRUST SHEET IN SOUTHEASTERN KENTUCKY AND NORTHEASTERN TENNESSEE

By KENNETH J. ENGLUND, Washington, D.C.

The Cumberland overthrust sheet is a northeast-trending rectangular area approximately 125 miles long by 25 miles wide which is located in southwestern Virginia and adjacent parts of Kentucky and Tennessee. This sheet has moved to the northwest on the Pine Mountain overthrust fault an estimated 2 miles at its northeast end and about 10 miles at its southwest end (Wentworth, 1921, p. 368). The resulting rotation by pivoting on the northeast end of the overthrust sheet was confirmed by Butts (1927), who discovered fensters in the center of the sheet that indicated an intermediate distance of movement of about 7 miles. This measurement was later modified to about 6 miles by Miller and Fuller (1954, p. 260).

In addition to the Pine Mountain and associated faults on the periphery of the Cumberland overthrust sheet, faults and associated folds have been reported at several places within the sheet. The most conspicuous of these is the Rocky Face fault (Ashley and Glen, 1906, p. 47–50), which strikes northward across the Middlesboro syncline in the west-central part of the overthrust sheet (fig. 177.1). This fault has been described as having both strike-slip (Rodgers, 1953, fig. 5) and vertical displacement (Hauser and others, 1957, fig. 6). The genetic and structural relations of the Rocky Face fault to the entire overthrust sheet have received little attention.

Observations made during detailed mapping of the Rocky Face fault confirm previous reports that the displacement of the west side of the nearly vertical fault plain is predominantly strike-slip to the south (fig. 177.1). The direction of displacement is substantiated by the drag of beds. The amount of displacement is from 1 to 2 miles, as indicated by the offset of lithologic units in Carboniferous rocks cropping out on opposite sides of the fault. At its south end, the Rocky Face fault intersects a zone of northwestward dipping thrust faults that contains several previously unrecognized fault slices involving rocks as old as the Chattanooga shale. This fault zone strikes southwestward from the Rocky Face fault at Cumberland Gap and is herein designated the Doublings thrust-fault zone, named after the creek which flows in the valley along the trace of the fault between Powell and Cumberland Mountains. The minimum displacement on the Doublings thrust-fault zone is a little less than 2 miles, as shown on the structure section (fig. 177.2); this measurement is about the same as the amount of strike-slip displacement on the Rocky Face fault. Southwestward along the Doublings thrust-fault zone, beyond the area of detailed mapping (fig. 177.1), the fault slices thin and the displacement appears to be confined to one fault plane near the base of the Chattanooga shale. Considering the amount of displacement in the area of detailed mapping, the Doublings fault probably extends several miles southwestward, possibly changing into a bedding plane fault.

The relations described here between the Rocky Face and Doublings faults are similar in many respects to those between the Jacksboro and Pine Mountain faults at the southwest corner of the Cumberland overthrust sheet. The Jacksboro fault, like the Rocky Face fault, is a strike-slip fault with the northeast side displaced to the northwest (fig. 177.1). The Jacksboro fault, at its northwest end, also intersects a belt of imbricate faults at the trace of the Pine Mountain overthrust fault which, like the Doublings fault, also converges to a single fault plane to the northeast.

The relative directions of movement on the Jacksboro, Pine Mountain, Rocky Face, and Doublings faults resulted in clockwise rotation of the block bounded by these faults relative to the remainder of the Cumberland overthrust sheet. This clockwise rotation of the block probably was facilitated by a distribution of movement to the imbricate fault slices at the east and west corners of the main block, and it explains movement to the southeast along the Doublings thrust-fault zone in an area where the major thrusting was to the northwest.

REFERENCES

Ashley, G. H., and Glenn, L. C., 1906, Geology and mineral resources of part of the Cumberland Gap coal field, Kentucky: U.S. Geol. Survey Prof. Paper 49, 239 p.

Butts, Charles, 1927, Fensters in the Cumberland overthrust block in southwestern Virginia: Virginia Geol. Survey Bull. 28, p. 1–12.

Hauser, R. E., Walker, F. H., and Nelson, V. E., 1957, Itinerary: Some stratigraphic and structural features of the Middlesboro basin, Kentucky Geol. Soc. and Appalachian Geol. Soc. Ann. Field Conf. Guidebook: 35 p.

Miller, R. L., and Fuller, J. O., 1954, Geology and oil resources of the Rose Hill district, the fenster area of the Cumberland overthrust block, Lee County, Virginia: Virginia Geol. Survey Bull. 71, 383 p.

Rodgers, John, 1953, Geologic map of east Tennessee with explanatory text: Tennessee Div. Geol. Bull. 58, 168 p.

Wentworth, C. K., 1921, Russell Fork fault of southwest Virginia: Jour. Geology, v. 29, p. 351–369.

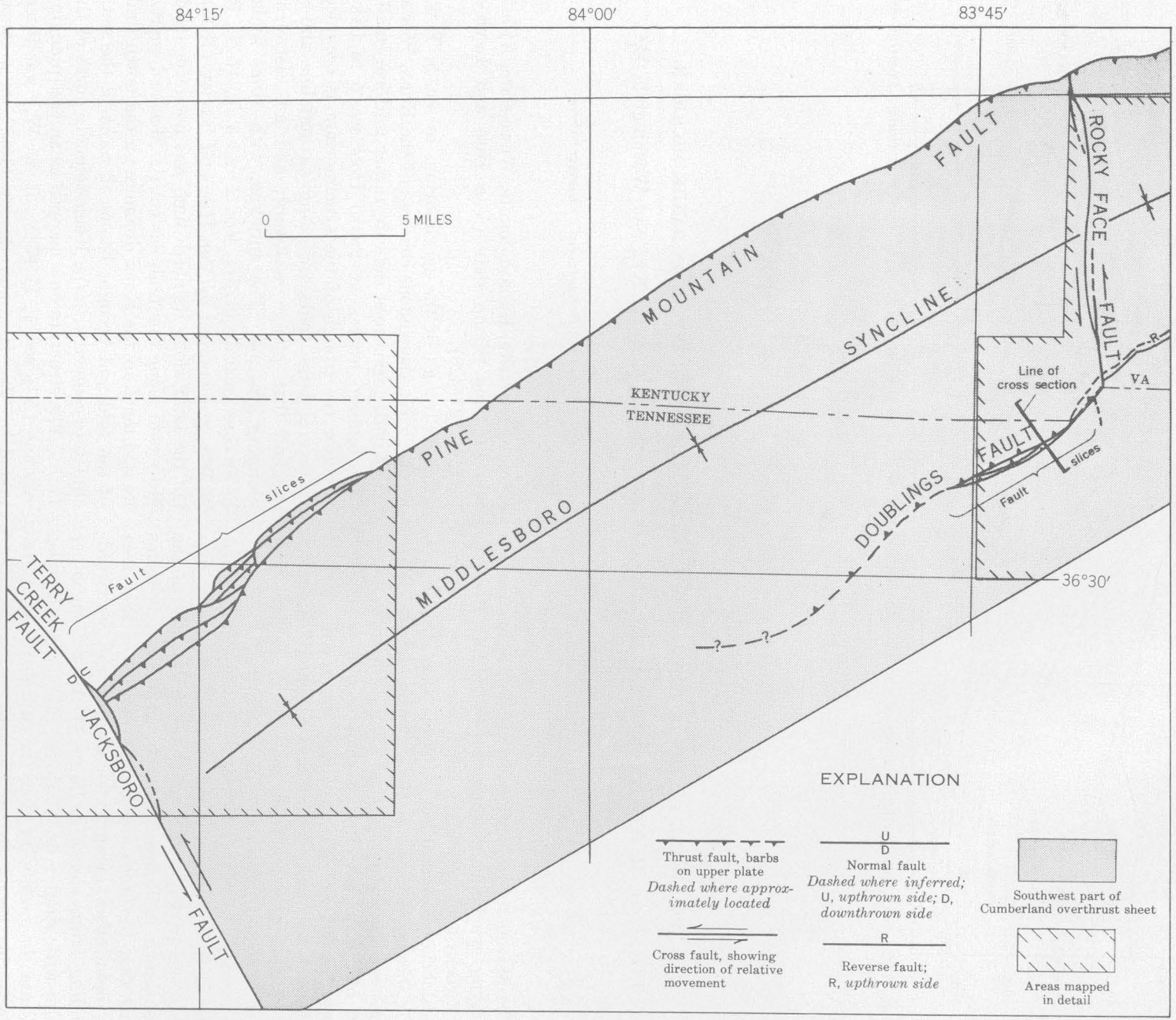

FIGURE 177.1.—Generalized map of the southwest part of the Cumberland overthrust sheet showing relations of major faults.

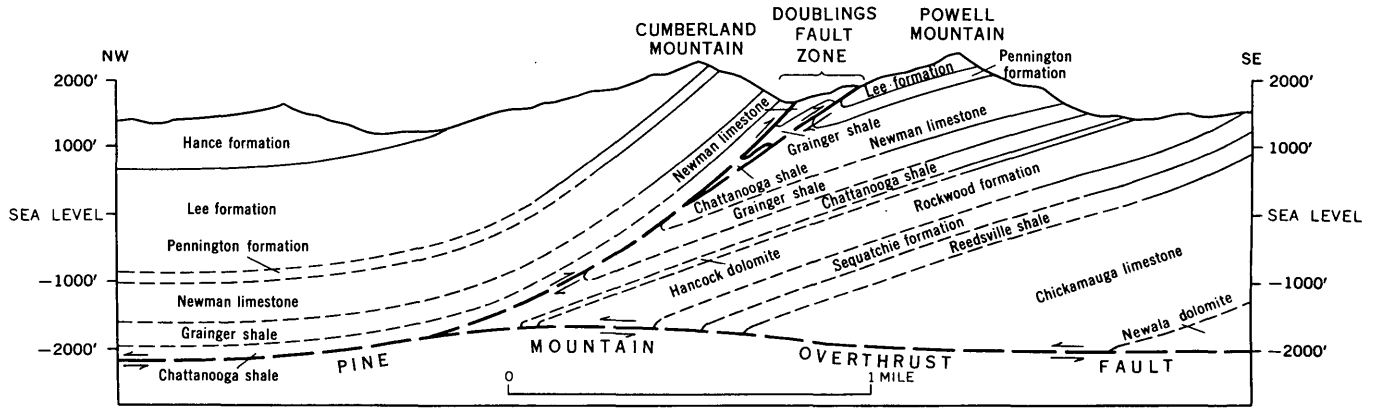

FIGURE 177.2.—Section showing relation of the Doublings thrust fault zone to the Pine Mountain overthrust fault. Position of section indicated on map.

178. FOLDS AND FAULTS IN THE EASTERN PART OF THE MARQUETTE IRON RANGE, MICHIGAN

By J. E. GAIR, R. E. THADEN, and B. F. JONES, Denver, Colo., Columbia, Ky., and Washington, D.C.

Work done in cooperation with the Geological Survey Division of the Michigan Department of Conservation

The Marquette iron range, Michigan, is on a west-plunging synclinorium composed of middle Precambrian rocks bounded on the north and south by lower Precambrian basement rocks (Van Hise and Bayley, 1897; James, 1958, p. 28–30). Recent detailed mapping near the east end of the range, where the lower part of the middle Precambrian section is exposed across the nose of the synclinorium, reveals several faults not previously known and has modified the interpretation of some folds mapped in earlier work (Van Hise and Leith, 1911, pl. 17, fig. 1).

These structures are noteworthy because similar patterns of folds and faults may exist in the main iron-producing part of the range a few miles west of the area shown in figure 178.1. In particular, it seems likely that the Negaunee iron-formation of that area has been offset along extensions of the westward-trending faults shown in figure 178.1, or along other faults with similar orientations. The structures also indicate the possibility that the Marquette stratigraphic section recurs east of the area.

The major rock units involved in the folding and faulting near the east end of the range are, in sequence, the basement of Mona schist and granitoid-gneissic rocks overlain in profound unconformity by Mesnard quartzite, Kona dolomite, Wewe slate, Ajibik quartzite, and Siamo slate (Van Hise and Bayley, 1897, p. 221–328).

In the trough of the synclinorium in sec. 5, T. 47 N., R. 25 W., the sinuous contacts of the Kona, Wewe, and Ajibik formations indicate rather uniform small-scale folding, whereas eastward from sec. 5 to Lake Superior the trough of the synclinorium is occupied by several large folds, including an anticline and a syncline that plunge westward, and an eastward-plunging syncline. The anticline, with Mona schist in its core (mainly in N½ secs. 2 and 3, T. 47 N., R. 25 W.), was mapped by Van Hise and Bayley (1897), but the fault along its north limb was not recognized. Movement along this fault cut out the Mesnard quartzite and much of the Kona dolomite on the north limb of the fold and brought basement rocks in the anticline into contact with the Kona dolomite north of the fault. The structure now mapped as an east-plunging syncline (N½ sec. 1, T. 47 N., R. 25 W.) was interpreted by Van Hise and Bayley (1897) as a canoe-shaped fold, with the east end located west of the lake shore. Detailed mapping, however, revealed no evidence of closure at the east end or of a west plunge of the fold axis west of the lake shore. It is therefore

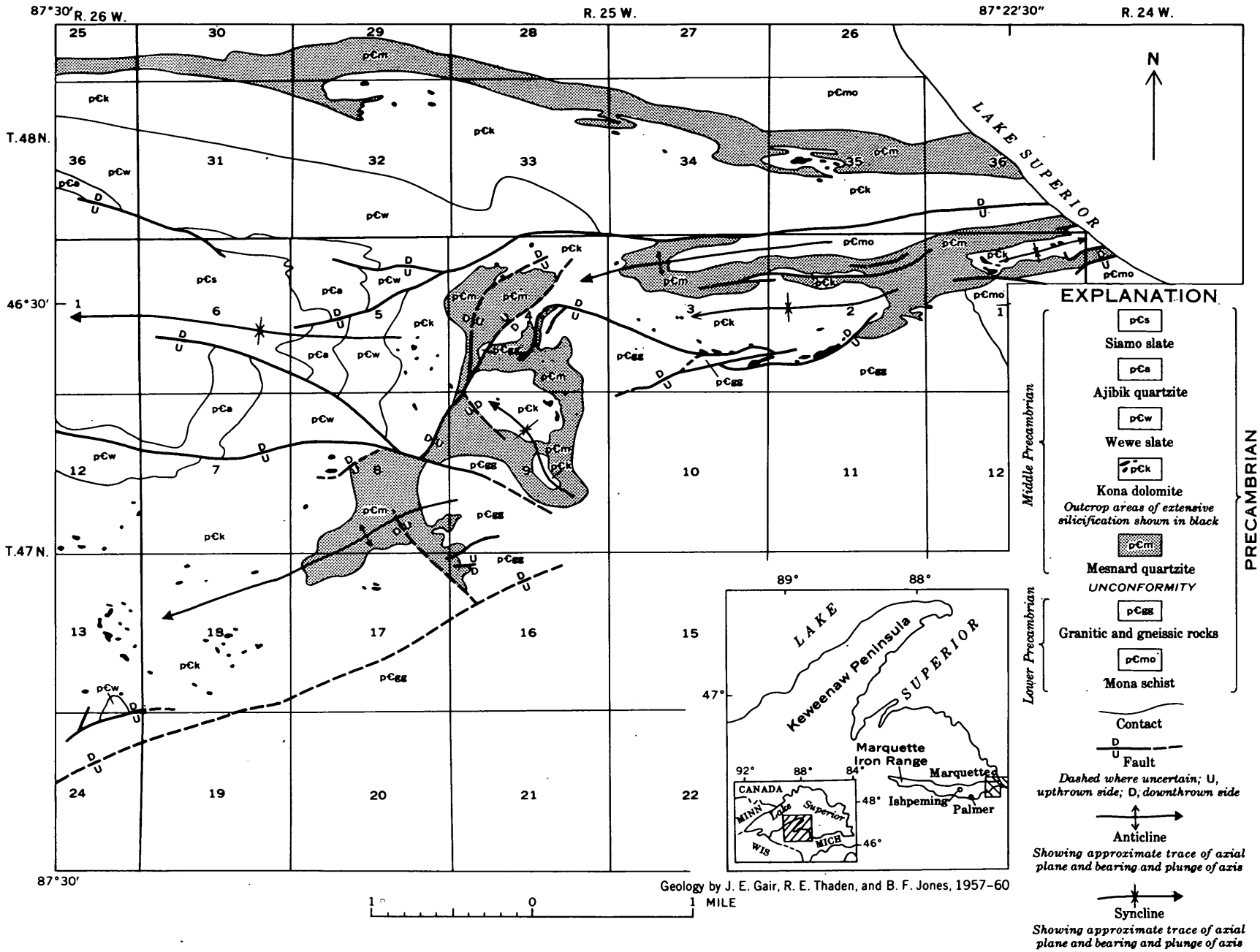

FIGURE 178.1.—Map of Precambrian geology near east end of Marquette iron range, Michigan.

possible that the syncline is open to the east and may portend a major reversal of plunge for the Marquette synclinorium. If this interpretation is valid, the middle Precambrian rocks found west of Lake Superior along the Marquette range would recur beneath the lake and adjacent land areas that have Paleozoic rocks at the surface.

Fault surfaces are rarely exposed, and for the most part the existence and position of the faults are inferred from (a) anomalous thickness changes of formations, (b) juxtaposition of formations normally separated by one or more formations, (c) offsets in formations or dikes, (d) unusual shear zones or breccias, generally marked by secondary quartz—in conjunction with (a), (b), or (c)—and (e) long straight narrow clefts in areas of granitoid-gneissic rocks, when such clefts are also in accord with or are alined with faults inferred from other criteria.

Most of the faults mapped near the east end of the range trend generally westward, approximately parallel with the synclinorium. The major westward-trending faults are in or adjacent to the trough of the synclinorium, or along the south margin of the synclinorium. The disposition of these faults in relation to the synclinorial structure suggests that the faults are related genetically to the folds. Accordingly, the deduction is made that movement on the faults was mainly dip slip, roughly perpendicular to the major axis of folding. The apparent right lateral offsets along the faults therefore indicate that the displacement on virtually all the westward-trending faults was north-side downward. During the downfolding near the east end of the Marquette synclinorium the relative uplifting of the basement as a part of the folding process probaby was greater on the south side of the synclinorium than on the north side, thereby accounting for the upthrow of blocks south of the faults. The faults trending north-northeastward and northwestward in secs. 4, 8, 9, 16, and 17, T. 47 N., R. 25 W., formed earlier than the major westward-trending faults, and their location along or close to the prominent southward bend of the Mesnard and Kona formations suggests that they were related to the folding that produced the change in trend.

A few miles west of the area shown on figure 178.1, near Palmer, displacement along the Volunteer fault (Tyler and Twenhofel, 1952, p. 120–121) was south-side down. The Volunteer fault trends toward and may well be an extension or branch of the fault entering the map area in sec. 24, T. 47 N., R. 26 W. Therefore, it appears that the general rule regarding relative movement on westward-trending faults at the east end of the range does not apply to all faults west of the area shown on figure 178.1.

REFERENCES

James, H. L., 1958, Stratigraphy of pre-Keweenawan rocks in parts of northern Michigan: U.S. Geol. Survey Prof. Paper 314–C, p. 27–44.

Tyler, S. A., and Twenhofel, W. H., 1952, Sedimentation and stratigraphy of the Huronian of Upper Michigan: Am. Jour. Sci., v. 250, pt. 1, no. 1, p. 1–27; pt. 2, no. 2, p. 118–151.

Van Hise, C. R., and Bayley, W. S., 1897, The Marquette iron-bearing district of Michigan: U.S. Geol. Survey Mon. 28, 608 p.

Van Hise, C. R., and Leith, C. K., 1911, The geology of the Lake Superior region: U.S. Geol. Survey Mon. 52, 641 p.

179. SILICIFICATION OF THE KONO DOLOMITE IN THE EASTERN PART OF THE MARQUETTE IRON RANGE, MICHIGAN

By J. E. Gair, R. E. Thaden, and B. F. Jones, Denver, Colo., Columbia, Ky., and Washington, D.C.

Work done in cooperation with the Geological Survey Division of the Michigan Department of Conservation

The Precambrian Kona dolomite (equivalent to the Randville dolomite in the lower part of the Animikie series of James, 1958, p. 35) is widely exposed in the eastern part of the Marquette iron range, Michigan. It conformably overlies the Mesnard quartzite and is overlain conformably by the Wewe slate.

The most comprehensive description of the Kona has been given by Van Hise and Bayley (1897, p. 240–256). The Kona dolomite consists predominantly of dolomite and laminated cherty dolomite, but also locally of interlayered slate and quartzite. Chert layers in the laminated cherty dolomite are generally less

than ½ inch thick, and alternate with dolomite layers that are generally less than 2 inches thick. Because of the uniform thickness of most individual chert layers in the laminated cherty dolomite and their smooth and sharply defined interfaces with dolomite, we believe that such chert layers are primary rather than replacements of dolomite along bedding surfaces.

Parts of the Kona dolomite are silicified and parts are both brecciated and silicified. Van Hise and Bayley (1897) noted this, but they did not map the silicified parts of the Kona. Our recent mapping has indicated that they included some silicified and quartzitic parts of the Kona in the Mesnard quartzite.

The distribution of silicified parts of the Kona is shown in figure 178.1 of the previous article. As only areas of substantial exposure are indicated, the real distribution is probably not as "spotty" or discontinuous as the map suggests.

Partial silicification of dolomite results in (a) cherty layers retaining buff to yellowish streaky zones of dolomite; (b) cherty masses along cross joints in the carbonate layers of laminated cherty dolomite, commonly merging with the chert laminae; and (c) isolated masses of dolomite surrounded by massive chert or vein quartz. Occurrences such as (b) and (c) indicate postconsolidation replacement of the dolomite.

Silicified Kona dolomite most typically consists of thick laminated masses of fine-grained quartz (chert). The laminations are reddish or bluish black to white, depending on variations in minor amounts of different iron oxides from layer to layer. Massive siliceous rock consisting of fragments of white chert in a reddish-brown hematitic cherty matrix apparently resulted from postbrecciation silicification of the dolomitic portion of laminated cherty dolomite. Thin sections of silicified dolomite generally show a fine-grained mosaic of cherty quartz with small loose clusters of very fine-grained carbonate particles.

Fine- to coarse-grained white vein quartz in masses of irregular shape and trend commonly cuts the banded chert. One large area of secondary silica in the Kona consists almost entirely of vein quartz, but along strike this becomes a mixture of cherty silicified Kona and vein quartz. Although massive vein quartz in the Kona is generally associated spatially with cherty silicified Kona, it is unknown whether the quartz is a product, under differing physico-chemical conditions, of essentially the same solutions that produced the cherty silicification, or a product of later solutions which brought in new silica or remobilized the chert.

Slate, slate-quartzite, slate-dolomite, and quartzite-dolomite in the Kona have also been silicified. The slate has been invaded by lenses, pods, or cross-cutting masses of coarse-grained vein quartz; in places it has been rather thoroughly impregnated both by coarse- and fine-grained quartz and retains only streaky remnants of mica. Alternating layers or lenses of purple, locally brecciated, quartzite and reddish-brown chert are interpreted by us as silicification of interbedded quartzite and dolomite.

The silicification of dolomite in several localities in northern Michigan has been discussed by Leith (1925) and by Gair and Wier (1956, p. 34). Leith pointed out a widespread relation between silicification and erosion surfaces (unconformities) and concluded that such silicification resulted from weathering along erosion surfaces prior to deposition of unconformably overlying rocks. Although Leith referred specifically to unconformities within the Precambrian stratigraphic section, it seems implicit that his concept also included possible silicification along the Precambrian-Cambrian unconformity, or on the erosion surface representing the Cambrian-Pleistocene interval.

Most of the silicified Kona in the central and western parts of the area, that is in secs. 5, 8, 17, and 18, T. 47 N., R. 25 W., and in secs. 12 and 13, T. 47 N., R. 26 W., may well have developed on the post-Precambrian erosion surface, in accordance with Leith's hypothesis. In the eastern part of the area in figure 178.1 (previous article), however, most silicification of the Kona dolomite or replacement of the dolomite by massive vein quartz occurred either close to the contact with the subjacent Mesnard quartzite (as in secs. 32, 34, 35, T. 48 N., R. 25 W., the N½ sec. 1, the northwest part of sec. 3, the NW¼ sec. 4, and the NE¼ sec. 9, T. 47 N., R. 25 W.) or along faults where the Mesnard quartzite is displaced from the stratigraphic section (as in SW¼ sec. 2 and the SE¼ sec. 3, T. 47 N., R. 25 W.). From the fault in the SW¼ sec. 2, wedgelike quartz veins, from ½ to 3 inches in thickness, extend a short distance into the granitic basement. In the eastern part of figure 178.1, silica-bearing solutions evidently moved along the faults, along slippage zones between the Mesnard and the Kona, or along shears in the lower part of the Kona that were related to slippage in the Kona-Mesnard contact zone. All of these structures probably formed during the major folding at the end of middle Precambrian time.

We have no firm basis for determining whether the silica-bearing solutions moved upward, downward, or laterally along the slippage zones or faults. One might readily deduce from Leith's conclusions that

such solutions moved downward from an erosion surface that existed at some distance above the present surface, and that silicified material on that surface has been eroded away, leaving only the downward extensions of silicified material along faults or slippage zones. However, the types of silicification described above (particularly the thorough bed-by-bed replacement of thick masses of dolomite, the lenticular knots of coarse-grained quartz along foliation in slates of the Kona, as well as the wedgelike quartz veins in the basement a few feet from a massive white vein quartz replacement of the Kona) seem to us better explained by introduction of silica laterally or from below rather than from an overlying erosion surface.

REFERENCES

Gair, J. E., and Wier, K. L., 1956, The geology of the Kiernan quadrangle, Iron County, Michigan: U.S. Geol. Survey Bull. 1044, 88 p.

James, H. L., 1958, Stratigraphy of pre-Keweenawan rocks in parts of northern Michigan: U.S. Geol. Survey Prof. Paper 314–C, p. 27–44.

Leith, C. K., 1925, Silicification of erosion surfaces: Econ. Geology, v. 20, no. 6, p. 513–523.

Van Hise, C. R., and Bayley, W. S., 1897, The Marquette iron-bearing district of Michigan: U.S. Geol. Survey Mon. 28, 608 p.

180. THICKNESS TRENDS IN THE HARTSHORNE SANDSTONE AND THE McALESTER FORMATION IN NORTHWESTERN ARKANSAS

By Boyd R. Haley, Denver, Colo.

Work done in cooperation with the Arkansas Geological and Conservation Commission

Geologic information obtained since 1953 from mapping Pennsylvanian rocks in Arkansas and from earlier published and unpublished reports gives fairly detailed information on the thickness and source area of the Hartshorne sandstone, the thickness and source area of the McAlester formation, and the stratigraphic relations between these two rock units.

The Hartshorne sandstone of Pennsylvanian age, ranging in thickness from a featheredge to 345 feet, is the first continuous sandstone unit beneath the Lower Hartshorne coal bed in Arkansas, and it is equivalent to the lower sandstone unit of the Hartshorne sandstone in Oklahoma. It unconformably overlies the Atoka formation of Pennsylvanian age and conformably underlies the McAlester formation of Pennsylvanian age. The Hartshorne sandstone in Arkansas contains minor amounts of siltstone and shale and, in a few places, thin beds of coal. The deepest part of the sedimentary basin during the deposition of the Hartshorne sandstone extended through Sebastian, Franklin, Logan, Yell, and Conway Counties, Ark. (fig. 180.1). Sediments were supplied to this basin from the north across Franklin County, from the northeast across Pope County, from the east across Conway County, and from the south across Yell County as attested to by the thickness trends shown on figure 180.1, and by measurements of the dip direction of crossbeds and other features indicating current directions.

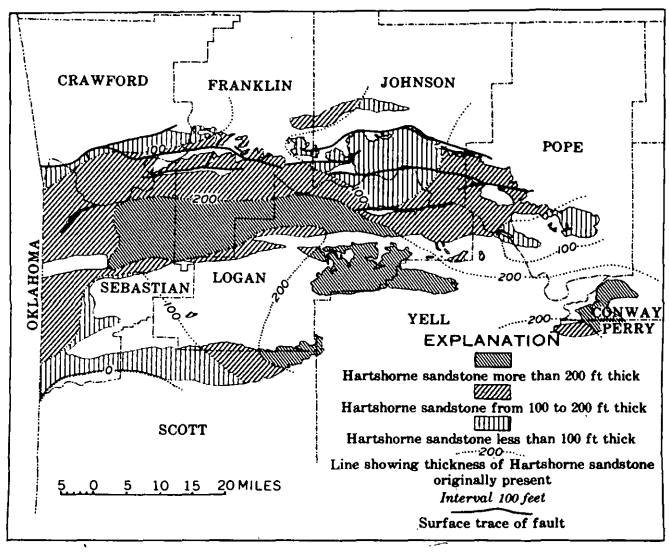

FIGURE 180.1.—Distribution and thickness of the Hartshorne sandstone in northwestern Arkansas. Formation present only in patterned areas.

The McAlester formation, ranging in thickness from 500 to 2,000 feet, is predominantly shale, but contains subordinate amounts of sandstone and siltstone, a few thin beds of limestone, and 8 coal beds. The formation was deposited in a sedimentary basin having two troughs. The shallower trough extended across Sebastian and Franklin Counties, and the deeper trough extended across Sebastian, Scott, Logan, and Yell Counties (fig. 180.2). Sediments were supplied to this basin probably from areas to the north and south. In southwestern Sebastian County and northern Scott County the McAlester formation contains a coal bed and a sandstone unit that are equivalent to the Upper Hartshorne coal bed and the upper sandstone unit of the Hartshorne sandstone in Oklahoma. These pinch out to the north and east in south-central Sebastian County.

The Lower Hartshorne coal bed, near the base of the McAlester formation, has a depositional history that is related to the depositional history of the underlying Hartshorne sandstone. In general, where the Hartshorne sandstone is thick the coal bed is thin or absent, and where the sandstone is thin or absent the coal bed is thick (figs. 180.1 and 180.3). This relation is particularly notable in Franklin, Johnson, Pope,

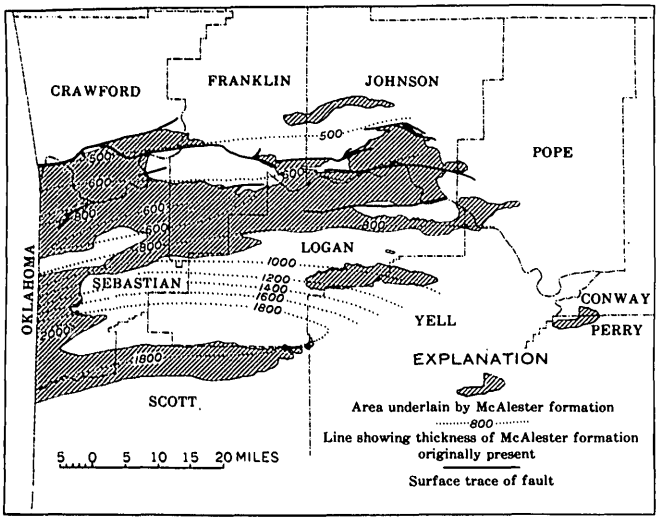

FIGURE 180.2.—Distribution and thickness of the McAlester formation in northwestern Arkansas.

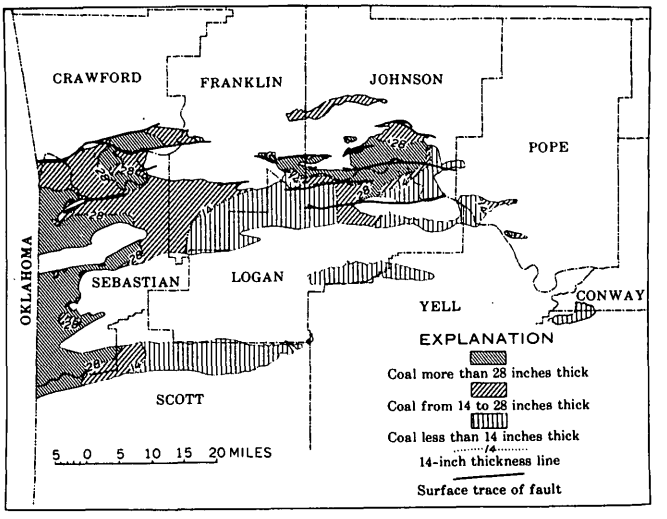

FIGURE 180.3.—Distribution and thickness of the Lower Hartshorne coal bed in northwestern Arkansas.

Yell, and eastern Logan Counties. Hendricks (1937) suggested that belts of thick and thin coal in a small part of west-central Sebastian County, where he had detailed control, tend to parallel major structural axes. The area of his observations was so small that regional relations of coal thickness could not be determined. In some areas the Lower Hartshorne coal bed was deposited contemporaneously with sandstone beds that are lithologically similar to the sandstone beds in the Hartshorne sandstone. These sandstone beds are mapped as a part of the Hartshorne sandstone because of their lithologic characteristics, but they were deposited during early McAlester time, probably by the same streams that had supplied sediments to the Hartshorne sedimentary basin. In many areas, the inverse thickness relation of the Lower Hartshorne coal bed to the Hartshorne sandstone can be explained by the continuation or noncontinuation of Hartshorne-like sedimentation during early McAlester time.

REFERENCE

Hendricks, T. A. 1937, Pennsylvanian sedimentation in Arkansas coal field: Am. Assoc. Petroleum Geologists Bull., v. 21, no. 11, p. 1403–1421.

181. POSSIBLE BENTONITE BEDS IN THE ATOKA FORMATION IN ARKANSAS AND OKLAHOMA

By Sherwood E. Frezon and Leonard G. Schultz, Denver, Colo.

The Atoka formation, of Pennsylvanian age, in the Arkoma basin of western Arkansas and eastern Oklahoma locally contains as many as four beds of light-gray or greenish-gray soft generally flaky shale that has a soapy or pearly luster. The physical characteristics of this shale contrast sharply with the characteristics of harder darker gray micaceous shale common in the formation. Although data concerning the distribution of this atypical shale are incomplete, the authors hope that the information presented here will call attention to the beds and to their potential usefulness in stratigraphic studies of the Atoka formation.

Light-colored shale, tentatively identified as bentonite, has been observed in the Atoka formation in samples from 36 wells, and in a bed 2 inches thick at 1 outcrop (fig. 181.1 and table 181.1). Lithologic descriptions of the bentonite(?) beds in selected wells, and the stratigraphic interval between these beds and the base of the Atoka formation are presented by table 181.2.

Where found in well samples, fragments of light-colored shale comprise less than 5 percent of the individual sample. Inasmuch as the samples generally represent 5- to 10-foot drilled intervals, the small amount in most samples suggests that the beds of light shale in the wells are comparable in thickness to the 2-inch thick bed at the outcrop (lo-

Table 181.1.—*List of wells and outcrop section shown on figure 181.1*

Map locality number (fig. 181.1)	Well name and location of well or outcrop
1	Phillips Petroleum Co. 1 C. W. Mandler, SE¼SW¼SW¼ sec. 1, T. 6 N., R. 10 E., Hughes County, Okla.
2	Superior Oil Co. 1 Allred, NW¼SE¼NE¼ sec. 18, T. 8 N., R. 20 E., Haskell County, Okla.
3	Carter Oil Co. 1 C. L. Follansbee, SW¼NW¼SW¼ sec. 18, T. 9 N., R. 15 E., McIntosh County, Okla.
4	Carter Oil Co. 1 Graham C–309, NW¼SE¼NE¼ sec. 3, T. 9 N., R. 16 E., McIntosh County, Okla.
5	Phillips Petroleum Co. 1 Sammons CSE¼NE¼ sec. 22, T. 9 N., R. 21 E., Haskell County, Okla.
6	Arkansas-Oklahoma Gas Co. 1 G. D. Cloud, SE¼NW¼SE¼ sec. 27, T. 9 N., R. 24 E., Le Flore County, Okla.
7	Phillips Petroleum Co. 1 Ruby, CNW¼SW¼ sec. 30, T. 10 N., R. 16 E., McIntosh County, Okla.
8	Edwin D. Pauley 1 Dyton Bennett CSE¼NE¼ sec. 18, T. 10 N., R. 18 E., McIntosh County, Okla.
9	I.T.I.O. Co. 1 John J. Blake, CSW¼NW¼ sec. 3, T. 10 N., R. 21 E., Haskell County, Okla.
10	L. A. Chudacaff 1 Tabor, NE¼NW¼SE¼ sec. 11, T. 11 N., R. 16 E., McIntosh County, Okla.

Table 181.1.—*List of wells and outcrop section shown on figure 181.1*—Continued

Map locality number (fig. 181.1)	Well name and location of well or outcrop
11	Midco Oil Co. 1 Mary Dunagan, SE¼SE¼NE¼ sec. 31, T. 11 N., R. 19 E., Muskogee County, Okla.
12	Diamond Drilling Co. 1 James Mullen, CNW¼ sec. 5, T. 11 N., R. 23 E., Sequoyah County, Okla.
13	Arkansas-Oklahoma Gas Co. 1 Binnie Barry, CN½SW¼NE¼ sec. 23, T. 11 N., R. 25 E., Sequoyah County, Okla.
14	Residue Co. 1 Mansfield Gas Co., NW¼SE¼NW¼ sec. 6, T. 4 N., R. 30 W., Scott County, Ark.
15	Post Petroleum Co. (Carter) 1 H. E. Turner, CSW¼SE¼ sec. 15, T. 6 N., R. 28 W., Logan County, Ark.
16	Gulf Oil Corp. 1 F. R. Borum, SW¼SW¼SW¼ sec. 18, T. 6 N., R. 28 W., Logan County, Ark.
17	Blackwell Oil & Gas Co. 1 G. A. Scroggin, SW¼NW¼SE¼ sec. 14, T. 7 N., R. 16 W., Conway County, Ark.
18	Shell Oil Co. 1 T. V. Jones, NW¼NW¼NW¼ sec. 19, T. 7 N., R., 21 E., Yell County, Ark.
19	Western Natural Gas Co. 1 W. B. Bergkamp, S½SE¼NW¼ sec. 1, T. 7 N., R. 30 W., Sebastian County, Ark.
20	Arkansas-Oklahoma Gas Co. 1 George Bieker, CNW¼SE¼ sec. 2, T. 7 N., R. 32 W., Sebastian County, Ark.
21	Gulf Oil Corp. 1 Tackett, CSW¼NE¼ sec. 2, T. 8 N., R. 22 E., Johnson County, Ark.
22	Gulf Oil Corp. 1 S. W. Roberts, NE¼NW¼ sec. 33, T. 8 N., R. 22 W., Logan County, Ark.
23	Western Natural Gas Co. 1 Roy Gray, CSW¼NE¼ sec. 25, T. 8 N., R. 24 W., Logan County, Ark.
24	Gulf Oil Corp. 1 Hembree, NW¼NW¼SW¼ sec. 13, T. 8 N., R. 26 W., Logan County, Ark.
25	Western Natural Gas Co. 1 Lucy Chapman, NW¼ NE¼NW¼ sec. 14, T. 9 N., R. 12 W., Cleburne County, Ark.
26	Carter Oil Co. 1 C. T. Williams, W½SE¼SE¼ sec. 1, T. 9 N., R. 16 W., Conway County, Ark.
27	Cosden Oil Co. 1 Shackleford, NW¼SE¼ sec. 13, T. 9 N., R. 19 W., Pope County, Ark.
28	Gulf Oil Corp. 1 J. J. Bauman, CNE¼SW¼ sec. 13, T. 9 N., R. 22 W., Pope County, Ark.
29	Gulf Oil Corp. 1 Ragon, CSE¼SW¼ sec. 28, T. 9 N., R. 23 W., Logan County, Ark.
30	Gulf Oil Corp. 1 Arkansas Real Estate Co., Inc., E½NE¼NW¼ sec. 32, T. 9 N., R. 23 W., Logan County, Ark.
31	Arkansas-Louisiana Gas Co. 1 R. S. Barton, SE¼ SE¼NW¼ sec. 27, T. 9 N., R. 28 W., Franklin County, Ark.
32	Stephens Production Co., Inc., 1 Taylor Landthrip, NW¼SE¼NW¼ sec. 22, T. 10 N., R. 23 W., Johnson County, Ark.
33	Carter Oil Co. 1 Boyer Heirs, SW¼SW¼NE¼ sec. 18, T. 10 N., R. 24 W., Johnson County, Ark.
34	Le Flore County Gas & Electric Co. 4A Low Gap Unit, SE¼SW¼SE¼ sec. 6, T. 11 N., R. 23 W., Johnson County, Ark.
35	Carter Oil Co. 1 Federal Government, CNE¼SW¼ sec. 12, T. 11 N., R. 26 W., Franklin County, Ark.
36	Cities Service Co. 1 W. R. Bruce, SW¼SE¼NW¼ sec. 4, T. 11 N., R. 32 W., Crawford County, Ark.
37	West side of State Highway 2, north of the hairpin turn in NE¼ sec. 3, T. 3 N., R. 19 E., Latimer County, Okla.

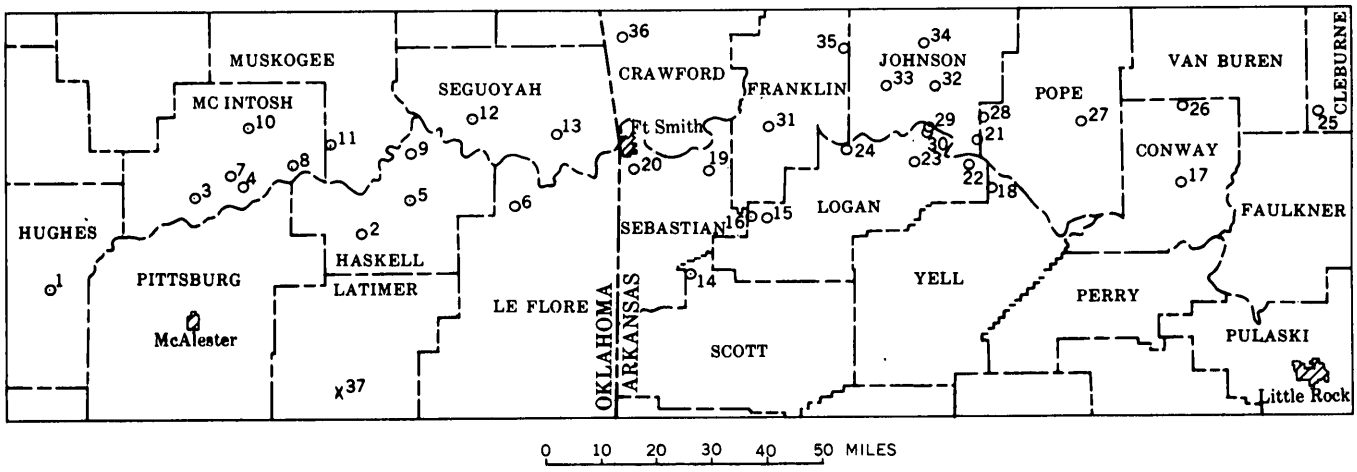

FIGURE 181.1.—Location of 36 wells and 1 outcrop (X) in Arkansas and Oklahoma having possible bentonite beds in the Atoka formation. Numbers refer to wells and outcrop listed in table 181.1.

TABLE 181.2.—*Information on possible bentonite beds in selected wells and in the outcrop section*

Map locality No. (fig. 181.1)	Description of possible bentonite bed(s)	Distance between base of bed and base of Atoka formation (feet)
2	Olive-gray flaky shale; unidentified clear mineral grains and orange, flaky mineral (mica?)	53
3	Olive-gray to light olive-gray, soft shale; scattered fine to medium grains of unidentified clear mineral	102
4	Light brownish-gray to pale-yellow brown shale; brown mica and unidentified clear mineral grains	105
	Very light gray to yellow-gray flaky shale; unidentified clear mineral grains	21
11	Light-gray soft flaky shale; brown mica	145
	Light-gray to very light gray flaky shale; fine round grains of unidentified clear mineral	60
13	Light olive-gray to yellowish-gray flaky shale; scattered fine grains of unidentified clear mineral	413
	Light-gray to very light gray dolomitic soapy flaky shale; scattered unidentified clear mineral grains	46
14	Pale reddish-brown and grayish-yellow waxy shale; red pinpoint inclusions	[1] 6, 777
	Grayish-orange flaky soapy shale; grayish-red platy inclusions (mica?)	[1] 5, 443
17	Yellowish-orange shale	404
	Dusky yellowish-gray flaky dolomitic shale	219
	Light-gray slightly flaky compact shale	59
	Light-gray compact soapy shale	12
20	Light-gray to white shale; some unidentified clear mineral grains	61
21	Light-gray waxy flaky shale; fine dolomite crystals; trace of dark-gray mica(?)	1, 098

TABLE 181.2.—*Information on possible bentonite beds in selected wells and in the outcrop section*—Continued

Map locality No. (fig. 181.1)	Description of possible bentonite bed(s)	Distance between base of bed and base of Atoka formation (feet)
	Very light gray flaky shale; dolomite rhombs, unidentified clear mineral grains, and brownish-gray mica	148
29	Gray granular and flaky shale; unidentified clear mineral aggregates containing trace of dolomite	207
30	Light-gray to very light gray shale, very slightly dolomitic; trace of unidentified clear mineral aggregates; trace of black biotite	193
31	Very light gray to yellowish-gray, granular and flaky shale; dolomite rhombs	27
35	Yellowish-gray soft flaky shale with dolomite rhombs; trace of brown mica; trace of black mica	568
	Light-gray flaky shale; one piece contains 1 large grain of unidentified clear mineral	148
36	Yellowish-gray soft flaky shale; dolomite rhombs and trace of black mica	325
	Light-gray soft flaky shale; dolomite rhombs	15
37	Youngest: light-gray hard nonfissile shale; trace of very fine mica flakes; breaks with rough surface	--------
	Very light gray granular limestone; weathers white; iron stains; a single irregular bed having maximum thickness of ½ inch	--------
	Very light gray, smooth shale: soapy luster: weathers to mud; 2 inches thick	[1] 400
	Oldest: light-gray hard nonfissile shale; breaks with rough surface	--------

[1] Estimated.

cality 37, fig. 181.1). Such small amounts can easily be overlooked in sample examination or may be mistaken for pieces of drilling-mud cake. The light-colored shale readily disintegrates in water and possibly in some samples the small quantity of shale from the thin beds is partly or totally removed by water-base drilling muds and sample washing. The shale beds have not been detected on electrical or radioactivity logs.

X-ray diffraction analyses were made of samples of light-colored shale and of darker colored shale from adjacent beds from locality 37 and from wells 29 and 30 (fig. 181.1), and the results are shown in table 181.3. As the 2 wells are only 1 mile apart and the light-colored shale beds are about 200 feet above the base of the Atoka formation in both wells, the well samples probably are from the same bed; the light-colored shale bed at locality 37 is believed to be a different bed.

TABLE 181.3.—*Mineralogy of some samples of shale and bentonite(?) from the Atoka formation, determined by X-ray diffraction*

[Estimated to nearest 5 percent of total sample; (?), mineral possibly present]

Locality No. (fig. 181.1)	Sample	Montmorillonite	Mixed-layer montmorillonite-illite	Illite	Chlorite	Kaolinite	Quartz
Darker shale adjacent to or near the bentonite(?)							
29	b	--------	35	25	10	10	20
30	b	--------	25	35	10	10	20
37	a	20	15	20	------	10	35
	b	30	25	5	------	5	35
Bentonite(?)							
29	a	--------	60	------	------	30	10
30	a	--------	75	------	------	20	5
37	c	--------	75	(?)	------	5	20

Samples of the darker shale contain mixed-layer montmorillonite-illite, illite, kaolinite, quartz, and, in some samples, montmorillonite and chlorite (table 181.2); the absence of chlorite in the outcrop (loc. 37) samples is probably due to its having been destroyed during weathering. Samples of the light-colored shale are predominantly mixed-layer montmorillonite-illite, and contain some kaolinite and quartz; a trace amount of illite may be present in one sample from the outcrop. Unlike the mixed-layer clay in the darker shale, the mixed-layer clay in the light-colored shale shows regular mixed-layering, as indicated by a superorder reflection at a spacing of 30 A after glycol treatment of the samples. Megascopic examination of the light-colored bentonitic(?) shale from many wells indicates that it contains colored mica—probably biotite—that generally is much coarser than the normal detrital mica in the other shales of the Atoka.

Clear-cut shard or other volcanic textures have not been observed in samples of the light-colored shale. The mineralogy of the light-colored shale beds suggests, but does not prove, that they are of volcanic origin. The predominance of a single clay mineral, the absence of chlorite, and only a questionable trace of illite indicate that the original sediments of these beds differed significantly from those of the darker shale beds. The light-colored shale beds in the Atoka are not composed of montmorillonite, as many typical bentonite beds are, but the mixed-layer clay dominant in the light-colored shale of the Atoka formation is common to some Paleozoic metabentonites (Weaver, 1953). Kaolinite like that in the light-colored shale of the Atoka may form as a result of alteration of volcanic ash.

Incomplete studies show that some of the light-colored shale beds in the Atoka formation can be correlated over areas of at least 1,200 square miles. Their wide areal extent, apparent thinness, and mineralogical and lithological differences as compared to adjacent darker shale beds indicate that these light-colored beds represent brief, abrupt, and relatively widespread changes in the type of sediment deposited. Such changes are reasonably attributed to ash falls. If these beds represent altered volcanic ash, they may serve as useful time markers within the Atoka formation.

REFERENCE

Weaver, C. E., 1953, Mineralogy and petrology of some Ordovician K-bentonites and related limestones [Pa.]: Geol. Soc. America Bull., v. 64, no. 8, p. 921–943.

182. THICKENING OF THE ATOKA FORMATION IN THE CENTRAL PART OF THE ARKANSAS VALLEY, NORTHWESTERN ARKANSAS

By E. A. Merewether, Denver, Colo.

Work done in cooperation with the Arkansas Geological and Conservation Commission

The Atoka formation of Pennsylvanian age increases in thickness from a featheredge on the Ozark uplift in southern Missouri to as much as 20,000 feet in the Ouachita Mountains in Arkansas 140 miles to the south. This increase in thickness was recognized by some of the first geologists concerned with this region (Collier, 1907; Croneis, 1930).

Recent geologic mapping and drilling on the north limb of the Arkansas Valley basin in the Arkansas Valley give information on some of the details of thickening of the Atoka. In a distance of about 28 miles in a southerly direction, the Atoka formation increases in thickness from about 3,100 feet at the Pure Oil Co. Low Gap well 4-A in central Johnson County to about 10,750 feet at the Shell Oil Co. T. V. Jones well 1 in northern Yell County (fig. 182.1). Between these two wells the Atoka can be divided into five unnamed units and the average rates of thickening for these units range from 1.87 percent per mile to 7.55 percent per mile. In addition, the percentage of shale in the Atoka as shown by table 182.1, increases greatly from the Low Gap well to the Jones well.

The Atoka formation in the central part of the Arkansas Valley consists of interbedded shale, siltstone, and sandstone; a few thin lenticular beds of coal and limestone in the upper part of the formation; and a few thin lenticular beds of limestone in the lower part. Coal and limestone beds comprise less than 1 percent of the Atoka and are not included in table 182.1.

TABLE 182.1.—*Percentages of sandstone, siltstone, and shale, and thickness (in feet) of sandstone in the Atoka formation at six localities in northwestern Arkansas*

Locality	Atoka formation							
	Whole formation				Lower three units			
	Percentage of—			Thickness of sandstone (feet)	Percentage of—			Thickness of sandstone (feet)
	Sandstone	Siltstone	Shale		Sandstone	Siltstone	Shale	
A					45	30	25	804
B	27	34	39	1,222	28	46	26	768
C	20	28	52	1,070	22	34	44	688
D	26	23	51	1,393	26	31	43	896
E	12	21	67	877	10	25	65	465
F	17	19	64	1,762	13	25	62	951

The Atoka formation is divided into 5 units by the top and base of the formation, and by 4 widespread beds within the formation that can be identified in drill cuttings, electric logs of drill holes, and at outcrops (fig. 182.1). Surface and subsurface stratigraphic information has been projected to a line trending S. 5° E. across part of the north limb of the Arkansas Valley basin. The resulting cross section (fig. 182.1) illustrates a thickening of the entire Atoka formation in a southerly direction at an average rate of 4.67 percent per mile.

An isopach map of the Atoka formation in the Arkansas Valley indicates that, if the top of the Atoka is taken as a horizontal datum, the base of the Atoka in the direction of maximum thickening closely approximates an exponential curve expressed as $Y=(1+p)^x$ (E. E. Glick, oral communication, 1961). In this formula, p is the rate of thickening per mile in percent, x is the distance in miles, and Y is the ratio of the thickness of a unit to that of a correlative thinner unit. The Atoka formation in this area doubles in thickness approximately every 15 miles in the direction of maximum thickening. Within the Atoka the maximum rate of thickening (7.55 percent per mile) is in the unit between the bentonite(?) bed (Frezon and Schultz, Art. 181) and the sandstone that produces gas in the Knoxville gas field, in the lower part of the Atoka (fig. 182.1). The minimum rate of thickening (1.87 percent per mile) is in the lowest unit of the formation. The rates of thickening per mile for the units delineated on figure 182.1 are evidence that the basin subsided, relative to the shelf, at the slowest rate in very early Atoka time, at a maximum rate during early to middle Atoka time, and at intermediate rates in late Atoka time.

The percentages of sandstone and siltstone in the Atoka formation (table 182.1) in general decrease to the south along the line of the cross section, but the total thicknesses of sandstone and siltstone stay nearly the same. The percentage and amount of shale in general increase in a southerly direction, and most of the thickening of the Atoka formation in the area along the line of the cross section (fig. 182.1) is a result of the increase in the amount of the shale.

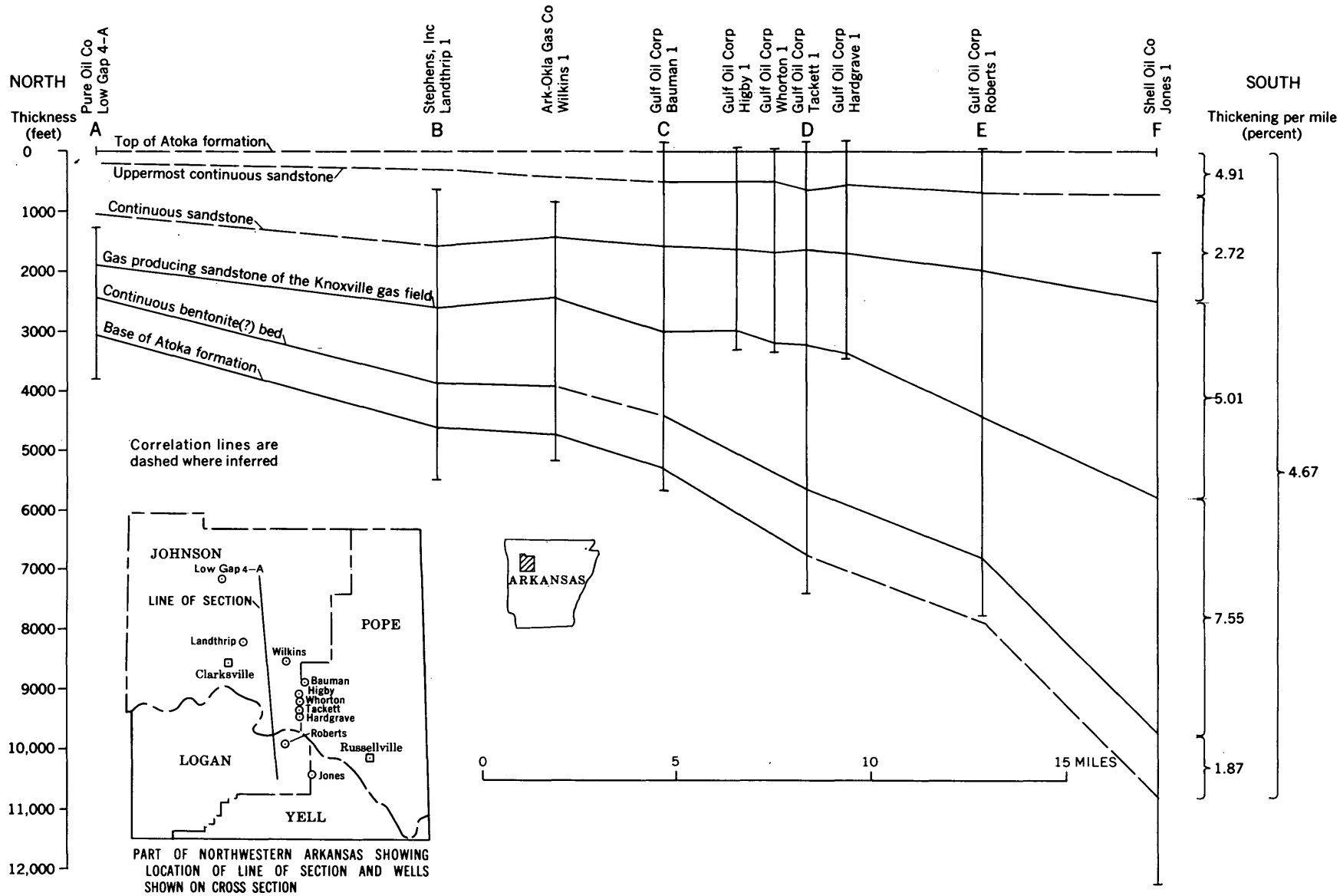

PART OF NORTHWESTERN ARKANSAS SHOWING LOCATION OF LINE OF SECTION AND WELLS SHOWN ON CROSS SECTION

FIGURE 182.1.—Correlation of stratigraphic units in the Atoka formation, Johnson County to Yell County, Ark. Wells projected to line of section.

The pronounced thickening of the Atoka formation was probably caused by the rate of generally continuous deposition keeping pace with the rate of subsidence in a basin. Sandstone and siltstone in the lower and middle part of the Atoka represent periodic influxes of fine-grained clastic material from a distant northern source into a gently sloping shallow largely marine basin in which organic-rich shales were accumulating. Sediments in the upper part of the Atoka were probably deposited near a shoreline that oscillated across the basin, as suggested by the alternation of marine shale units, channeling sandstone units, and coal beds.

REFERENCES

Collier, A. J., 1907, The Arkansas coal field: U.S. Geol. Survey Bull. 326, 158 p.

Croneis, C. G., 1930, Geology of the Arkansas Paleozoic area, with special reference to oil and gas possibilities: Arkansas Geol. Survey Bull. 3, 457 p.

GEOLOGY AND HYDROLOGY OF WESTERN CONTERMINOUS UNITED STATES

183. THE QUARTZ DIORITE LINE IN NORTHWESTERN NORTH AMERICA

By James G. Moore, Arthur Grantz, and M. C. Blake, Jr., Menlo Park, Calif.

Buddington (1927) demonstrated that the granitic rocks of southeastern Alaska show a regional zonation in composition: they pass progressively from quartz diorite on the west, through granodiorite, to quartz monzonite on the east. A similar relation has been described in the western conterminous United States (Moore, 1959) where it is possible to delineate a line (called the quartz diorite line) roughly parallel to the Pacific Coast, which separates a western zone in which quartz diorite is the dominant granitic rock from an eastern zone in which granodiorite or quartz monzonite is the dominant granitic rock. The granitic rocks considered are chiefly of Jurassic and Cretaceous age, but they include some Tertiary intrusives and possibly some Paleozoic intrusives. In the present paper the quartz diorite line is extended across Alaska and the significance of the regional chemical differences that it helps to outline is explored.

Data regarding the dominant granitic rock type in each of approximately 100 mapped areas in Alaska and Canada (British Columbia and Yukon) are shown on figure 183.1. In order to compare the data, the same system is used in classifying the granitic rocks of all the mapped areas, even if the author of a published report used a different system. The classification system is the same system used in the earlier compilation of data on granitic rocks of the western conterminous United States (Moore, 1959). On figure 183.1 symbols are used for three main groups of granitic rocks: (a) quartz diorite, (b) granodiorite, and (c) quartz monzonite or granite.

The granitic rocks of Alaska show an increase in the proportion of K-feldspar relative to plagioclase inland from the southern continental margin; this change is very similar to that found in the granitic rocks of California, Oregon, and Washington. In each area the granitic rocks become progressively richer in K and Si, and poorer in Na, Fe, and Mg inward from the continental margin.

The quartz diorite line drawn across Alaska (fig. 183.1) separates a zone adjacent to the southern coast in which quartz diorite is the dominant granitic rock from a zone to the north where granodiorite, quartz monzonite, or granite is the dominant granitic rock. The quartz diorite line does not mark an abrupt change in composition; and its position is dependent on the classification system employed.

From the latitude of Ketchikan to that of Skagway, the line is close to the international boundary between Alaska and Canada. It trends northwestward from Skagway on the north side of the St. Elias and Wrangell Mountains. The line reaches its farthest north point about 70 miles south of Fairbanks from where it curves to the southwest and ultimately passes out to sea at Bristol Bay. The line remains north of the Aleutian Islands, many of which are underlain by

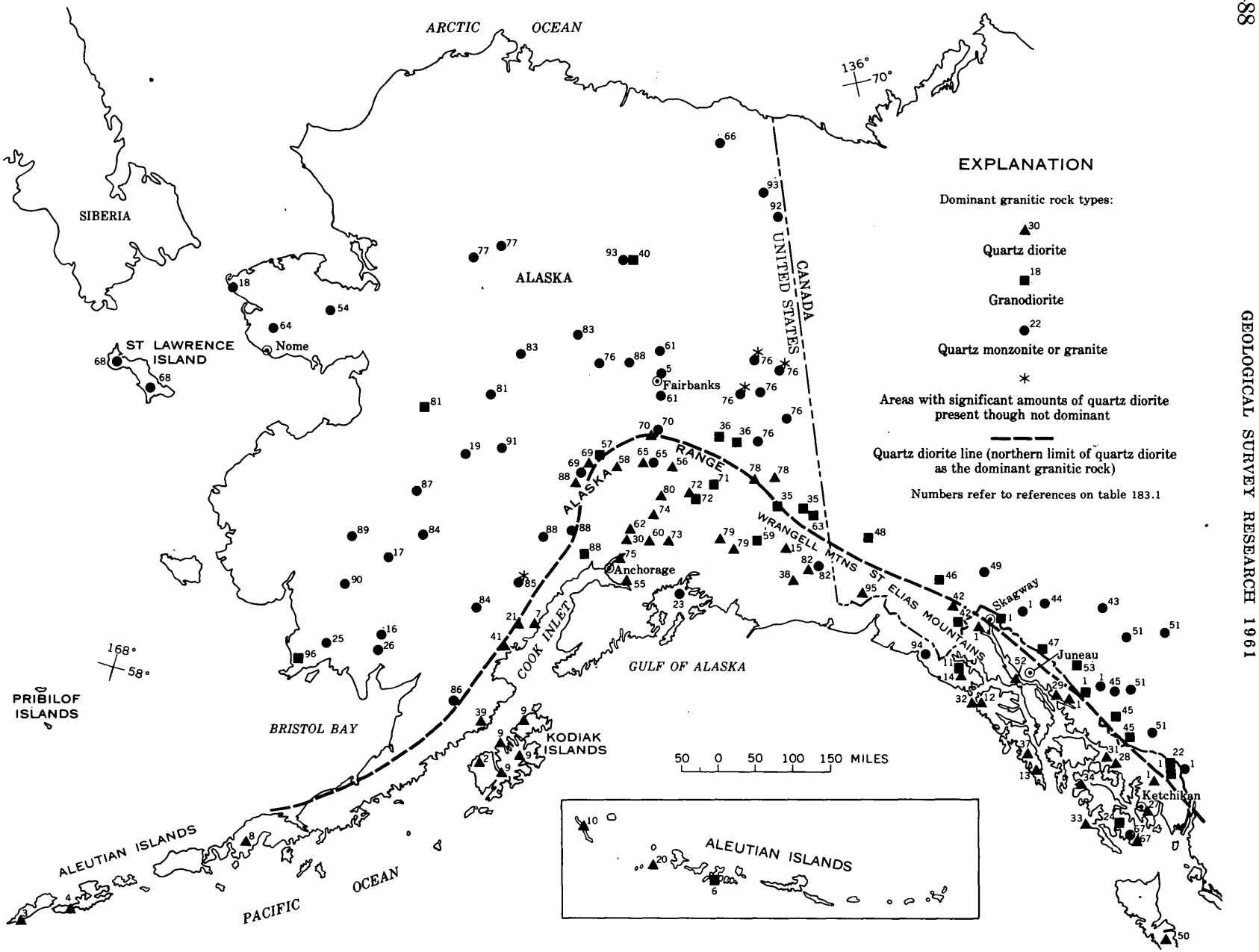

FIGURE 183.1.—Dominant granitic rock types in some mapped areas of Alaska and adjoining parts of Canada.

quartz diorite, but is probably south of the Pribilof Islands. The line is subparallel to the arcuate pattern of the regional structural elements of southern Alaska.

By combining all the data on the position of the quartz diorite line in northwestern North America, the line can be traced for more than 3,500 miles from the Gulf of California to Bristol Bay in the Bering Sea (fig. 183.2). The quartz diorite line is approximately parallel to the west coast of North America, and especially to the inner edge of the continental slope. On the average, it is about 150 miles inland from the inner edge of the continental slope.

Two prominent landward embayments are present in the trend of the quartz diorite line. In Alaska the line curves northward 300 miles from the continental slope, and in Oregon and Washington, the line curves eastward more than 400 miles. Both embayments are reflected in more subdued landward curves in the trend of the edge of the continental shelf.

Although the embayment in Oregon and Washington is only faintly reflected by the configuration of the coast line or of the inner edge of the continental slope, it is paralleled more closely by coast lines of the geologic past. The line representing the greatest transgression of seas of early Tertiary age (dotted line, fig. 183.2) is deflected markedly into the embayment in Washington and Oregon. Moreover, some evidence suggests that the continental slope within this embayment may have been farther east than at present during early Tertiary time. Eocene rocks of the Olympic Peninsula in northwestern Washington are marine throughout; chiefly pillow basalt, thin-bedded graywacke, argillite, and red foraminiferal limestone with associated manganese deposits. Such an assemblage of rocks, and the absence of shallow-water sedimentary structures in them, suggest deposition in deep water, possibly on or beyond the continental slope.

The quartz diorite line is approximately parallel to major Mesozoic and Cenozoic tectonic elements, such as elongation of granitic intrusives, foliation of metamorphic rocks, axes of folds, and strike of large faults. Major Quaternary volcanoes are alined parallel to, and slightly on the seaward side of the line (see fig. 183.2).

It is evident from the relations described above and shown on figure 183.2 that the quartz diorite line is a fundamental feature of the western continental margin of North America. It trends approximately parallel to the edge of the continent as indicated today by its relation to the shore line and to the continental slope, and as indicated in the past by its relation to early Tertiary shore lines. The difference in chemical

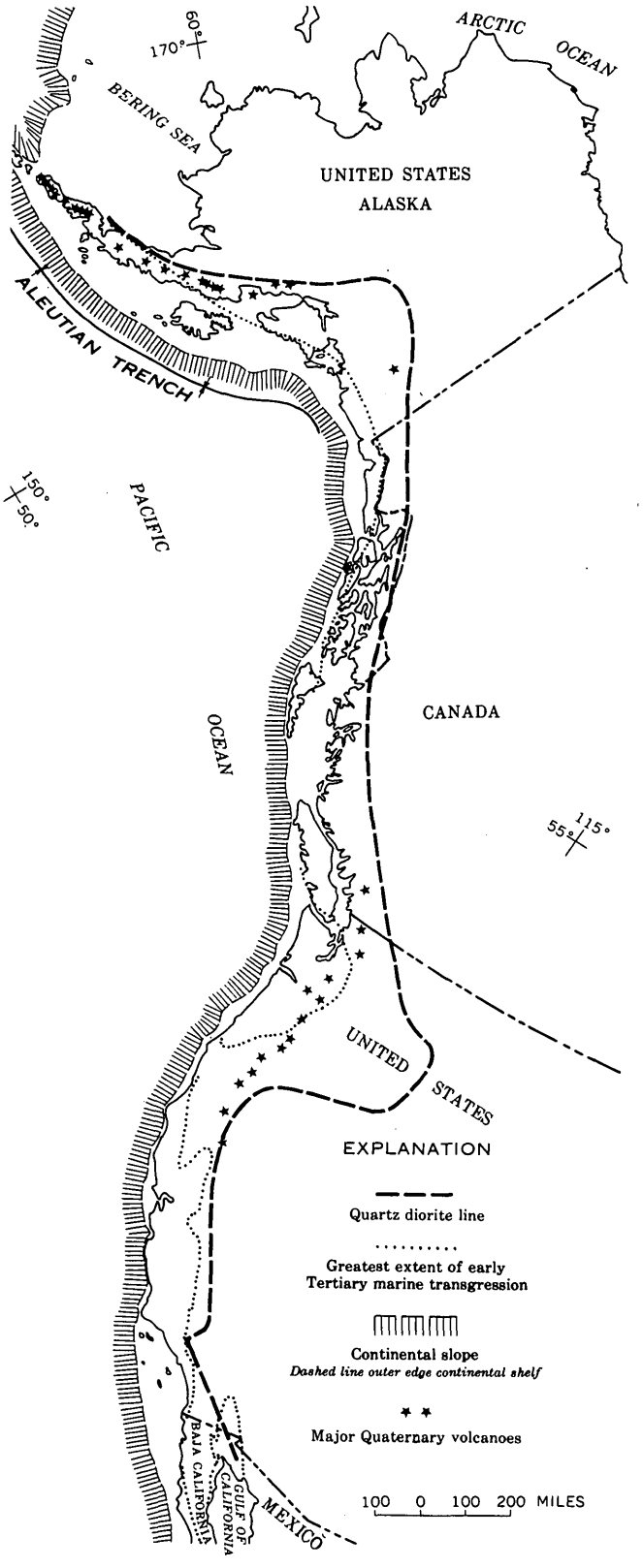

FIGURE 183.2.—The position of the quartz diorite line in northwestern North America and its relation to other features of the continental margin.

601530 O—61——7

composition of granitic rocks on each side of the line is presumably inherited from chemical differences in the crust, which existed before the granitic rocks were emplaced (Moore, 1959). A possible explanation of this difference is that west of the quartz diorite line the crust was thinner than in the area east of it and composed of a larger percentage of eugeosynclinal sediments and volcanic rocks that are relatively rich in sodium. The character of the Precambrian rocks west of the line is little known because exposures are extremely rare. However, the authors believe that Precambrian granitic rocks are practically nonexistent west of the line. If this is true, then the Mesozoic and Cenozoic granitic rocks there are largely in their first cycle, that is, they were emplaced in a basement containing nc older granitic rock.

East of the quartz diorite line, before emplacement of the Mesozoic granitic rocks, the crust was probably thicker and was composed of a larger percentage of platform-type sediments as well as great volumes of granitic rock. Thus, east of the line the crust was relatively rich in potassium relative to sodium. The Mesozoic and Cenozoic granitic rocks generated in this crust therefore contain a larger proportion of potassium feldspar relative to sodium-calcium feldspar than the granitic rocks of the continental border.

Quartz diorite appears to be the dominant granitic rock encircling the entire Pacific basin. A detailed search has not been made of the literature to establish the position of the line in the southern or western Pacific. However, evidence at hand suggests that the line passes west of Kamchatka and between Japan and Korea. A similar change in composition of granitic rocks seems to occur slightly north of New Guinea, and in northern New Zealand. The quartz diorite line probably lies from 200 to 600 miles on the outside (landward side) of the andesite line (Marshall, 1911, and Macdonald, 1949), and consequently the island arcs of the Pacific border are between the andesite line and the quartz diorite line.

REFERENCES

Buddington, A. F., 1927, Coast Range intrusives of southeastern Alaska: Jour. Geology, v. 35, p. 224.

Macdonald, G. A., 1949, Hawaiian petrographic province: Geol. Soc. America Bull., v. 60, p. 1541–1596.

Marshall, Patrick, 1911, Oceania: Handb. der Regionalen Geologie, v. 7, no. 2, 36 p.

Moore, J. G., 1959, The quartz diorite boundary line in the western United States: Jour. Geology, v. 67, no. 2, p. 198–210.

184. PRODUCTION AND USE OF FRESH WATER FROM THE ASHLEY VALLEY OIL FIELD, UINTAH COUNTY, UTAH

By R. D. Feltis and H. D. Goode, Salt Lake City, Utah

Work done in cooperation with the Utah State Engineer and the Utah Oil and Gas Conservation Commission

Water produced in association with oil from wells in the Ashley Valley field, Uintah County, Utah, contains only 500 to 2,000 parts per million (ppm) dissolved solids—much lower than the total in typical oil-field brines. At this relatively low salinity the water from the Ashley field is used for irrigation in and near the field, whereas typical oil-field brines must be disposed of by other means to prevent harm to plants and soils.

The Ashley Valley oil field is on a 300-foot closure on the axis of the westward-plunging Section Ridge anticline in the north-central Uinta Basin (fig. 184.1). Oil is produced from the highly fractured Weber sandstone of Pennsylvanian age and the Phosphoria formation of Permian age at a depth of about 4,200 feet. In 1960 the field contained 27 producing wells in about 1½ square miles. The field is under sufficient hydrostatic pressure to maintain flowing wells.

The amount of water produced from the oil field has increased from 0 in 1948 to more than 18,700,000 barrels (2,400 acre-feet) in 1960. The maximum water yield for an individual well during 1960 was about 2,920,000 barrels (about 380 acre-feet). Since 1950, when the field became fully developed, the oil pro-

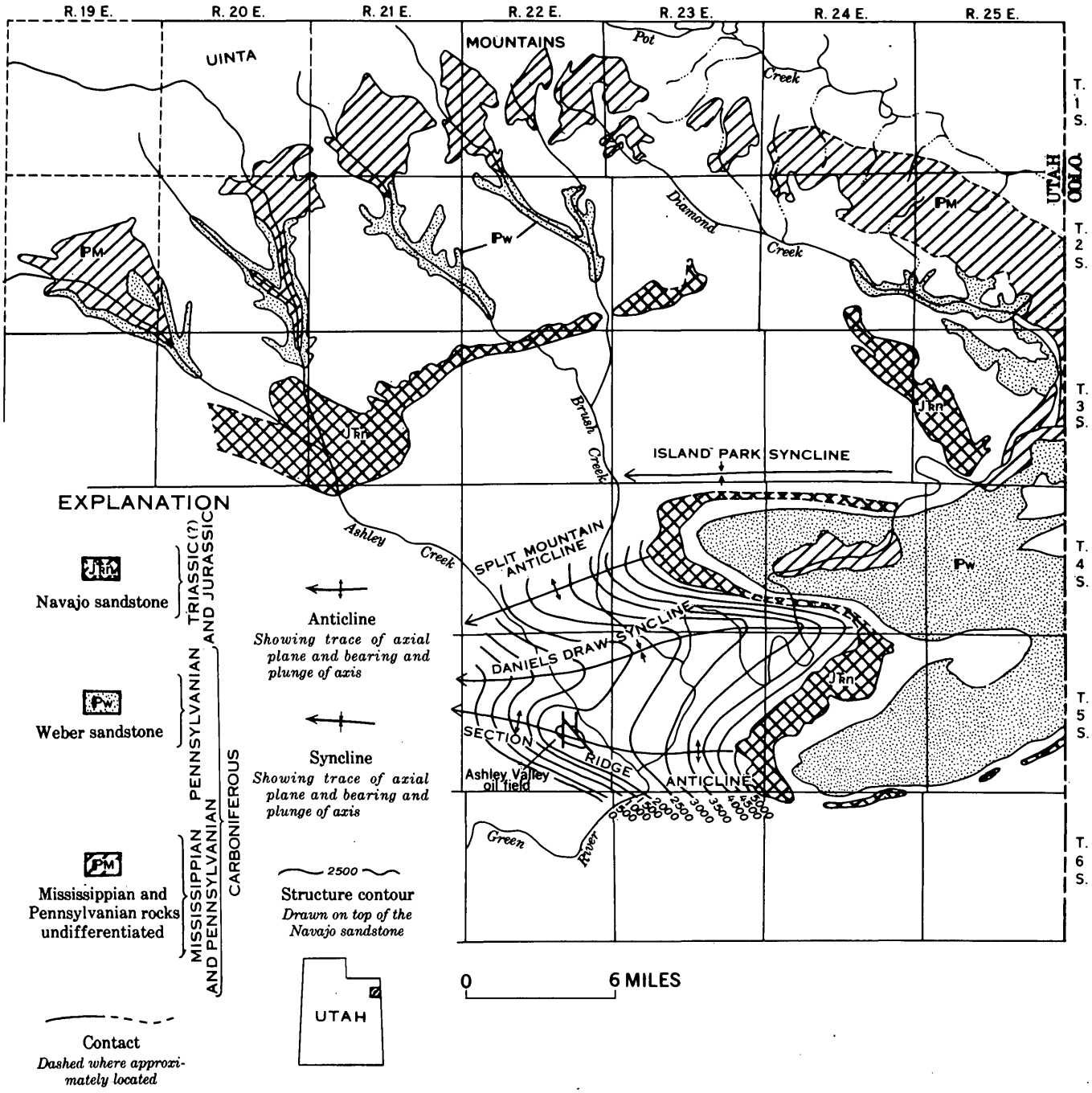

FIGURE 184.1.—Generalized geologic map of part of northeastern Utah, showing structure in the vicinity of the Ashley Valley oil field (T. 5 S., R. 22 E.). Geology in ranges 19E–23E adapted largely from Kinney (1955, pl. 1), that in ranges 24E–25E in part from Goodhue (1957, pl. 1, sheet 1).

duction has remained between 730,000 and 1,400,000 barrels per year, although the ratio of water to oil, and hence the water production, has increased. In 1953 the water-to-oil ratio was 1.2 to 1 and by 1960 the ratio had increased to 13 to 1. Pumps were installed in several wells in 1959 and 1960 to increase oil production but their effect on the ratio of water-to-oil production is not known.

The water-drive of the oil field is probably sustained by surface recharge in outcrop areas north and east of the field. Possibly the water comes not only from the oil-bearing strata but also from a sequence of underlying Pennsylvanian and Mississippian limestones. Thomas (1952, p. 12), in describing springs observed in Split Mountain Canyon said, "These springs rise from cavernous beds near the top of the Madison

TABLE 184.1.—*Chemical analyses of water samples from selected sources in Ashley Valley, Utah.*

[Analyses by the U.S. Geological Survey and U.S. Bureau of Reclamation]

Source of sample	Location: Section	T.S.	R.E.	Date collected	pH	Temperature (degrees Fahrenheit)	Specific conductance in micromhos at 25° C	Constituents in parts per million (ppm): Silica (SiO_2)	Iron (Fe)	Calcium (Ca)	Magnesium (Mg)	Na+K: Sodium (Na)	Na+K: Potassium (K)	Bicarbonate (HCO_3)	Sulfate (SO_4)	Chloride (Cl)	Boron (B)	Nitrate (NO_3)	Dissolved solids (sum)	Hardness as $CaCO_3$: Carbonate	Hardness as $CaCO_3$: Noncarbonate	Percent sodium	Sodium-adsorption-ratio
Selected oil wells																							
Pan American Petroleum 10	NE¼SW¼SE¼ 22	5	22	Nov. 3, 1959	8.1	112	829	19	------	85	27	52		238	227	4.0	------	0.5	532	324	129	26	1.3
Pan American Petroleum 1	SE¼SW¼NE¼ 22	5	22	Nov. 4, 1960	7.8	115	975	----	34	103	28	38	20	386	244	104	0.28	3.2	[1] 1,060	372	55	17	.9
Pan American Petroleum 1	NE¼SW¼SW¼ 23	5	22	Nov. 3, 1959	7.9	120	1,860	20	------	155	38	198		340	519	108	------	3.3	1,210	544	265	44	3.7
Equity Oil 7	SW¼SE¼NW¼ 23	5	22	Nov. 3, 1959	8.5	112	1,330	21	------	112	30	158		[2] 300	379	76	------	.6	925	404	158	46	3.4
Equity Oil 1-9 (composite)	23	5	22	Nov. 3, 1959	8.4	--------	1,350	19	------	116	36	152		[3] 283	399	86	------	.0	947	438	206	43	3.2
Equity Oil 1 [4]	NE¼NW¼SW¼ 23	5	22	Nov. 3, 1959	8.6	110	1,590	20	------	93	27	253		[5] 337	362	170	------	.5	1,090	344	68	62	5.9
Hollandsworth 1	NW¼SW¼SE¼ 23	5	22	Nov. 3, 1959	8.0	--------	2,560	27	------	109	31	547		518	615	372	------	2.6	1,960	400	0	75	12
Robert Six 1M	SW¼SE¼SW¼ 24	5	22	Nov. 3, 1959	7.7	--------	2,340	23	------	338	74	163		280	1,120	77	------	.3	1,930	1,150	920	24	2.1
Pan American Petroleum 2	NW¼NW¼NE¼ 26	5	22	Nov. 3, 1959	8.0	115	2,460	22	------	242	56	261		317	874	162	------	4.1	1,780	834	574	41	3.9
Pan American Petroleum 3	NW¼NE¼NW¼ 26	5	22	Nov. 4, 1960	7.4	120	1,830	20	.05	192	43	171	27	270	681	116	.44	.2	1,410	656	435	35	2.9
Oil-field drainage and irrigation ditches																							
Irrigation ditch	NE¼NE¼ 22	5	22	Nov. 4, 1960	7.7	--------	1,340	18	0.03	128	31	117	23	256	441	72	0.26	0.0	[1] 950	446	236	35	2.4
Union Irrigation Co. canal	SE¼SE¼NW¼ 25	5	22	Nov. 4, 1960	8.0	--------	2,940	10	.01	293	172	263	9.3	322	1,590	72	.57	19	[1] 2,770	1,440	1,170	28	3.0
Oil-field drainage ditch	NE¼ 26	5	22	Nov. 3, 1959	7.8	--------	2,350	17	------	208	65	279		249	877	190	------	8.3	1,770	784	580	44	4.3
Natural surface drainage																							
Ashley Creek	NE¼ 31	3	21	Mar. 14, 1956	----	--------	335	----	------	45	13	1.8	1.2	[6] 151	40	3.6	------	------	[1] 197	------	------	2	--------
				May 24, 1956	----	--------	102	----	------	15	2.3	1.4	.8	45	13	.4	------	------	[1] 75	------	------	6	--------
				July 9, 1956	----	--------	165	----	------	23	4.3	2.3	.8	89	6.7	.4	------	------	[1] 100	------	------	6	--------
				Aug. 7, 1956	----	--------	195	----	------	27	5.0	1.2	.8	102	6.7	--------	------	------	[1] 113	------	------	3	--------
				Sept. 17, 1956	----	--------	224	----	------	24	8.2	2.1	.8	120	--------	--------	------	------	[1] 141	------	------	5	--------
	NE¼ 26	5	22	Mar. 14, 1956	----	--------	2,000	----	------	227	117	104	3.5	[7] 314	940	28	------	------	[1] 1,668	------	------	18	--------
				May 25, 1956	----	--------	581	----	------	61	26	22	2.3	[8] 139	182	5.0	------	------	[1] 413	------	------	15	--------
				Aug. 7, 1956	----	--------	5,300	----	------	361	376	567	9.8	[9] 320	3,130	115	------	------	[1] 5,500	------	------	33	--------
				Sept. 18, 1956	----	--------	4,385	----	------	326	311	427	8.2	[10] 306	2,560	81	------	------	4,584	------	------	31	--------

[1] Residue on evaporation at 180° C.
[2] Includes 20 ppm CO_3
[3] Includes 10 ppm CO_3
[4] Water from this well is included in the preceding sample
[5] Includes 23 ppm CO_3
[6] Includes 10 ppm CO_3
[7] Includes 22 ppm CO_3
[8] Includes 2 ppm CO_3
[9] Includes 3 ppm CO_3
[10] Includes 26 ppm CO_3

limestone, or possibly at the base of the Morgan formation." He considered these " * * * to be artesian springs, dependent on this high outcrop area [in the Uinta Mountains (fig. 184.1)] for recharge."

In the Ashley Valley area these sources of water are about 2,000 feet deeper than the bottoms of the oil wells. Peterson (1957, p. 191) has described normal faults of 150 feet displacement that could have formed conduits between the Madison and Morgan formations, and the overlying oil-bearing rocks.

Analyses of water from the Ashley Valley field are shown in table 184.1. It is principally a calcium–sodium–sulfate water with bicarbonate as an additional important constituent. Few samples of water were collected for analysis before 1959, so it is not possible to determine whether a secular change has occurred in the dissolved solids or in the percent of chemical constituents.

Although the sodium content of the Ashley Valley oil field water might preclude its use for irrigation in many areas, this water can be used in Ashley Valley because the local soil contains gypsum derived from the underlying Mancos shale. Base exchange of sodium ions from the oil-field water with calcium ions in the soil prevents deflocculation of the soil and maintains its tilth.

The water of Ashley Creek (table 184.1) is high in calcium, magnesium, and sulfate, presumably leached from the gypsum-bearing soils by irrigation water. Thus, the water from the oil field, with its high content of sodium, may be used successfully either mixed with the water of Ashley Creek or used directly on soil containing gypsum. In some parts of the area the oil field waters contain less dissolved solids than water from the creek.

It is possible that irrigation of gypsiferous soils with relatively fresh oil-field waters may be found practicable in other areas—particularly in the Rocky Mountain region, where this combination of conditions is more likely to occur or be approached than in most other parts of the county.

REFERENCES

Goodhue, Betty, 1957, Geologic map of the Uinta Basin, Utah, *in* Intermountain Assoc. Petroleum Geologists Guidebook 8th Ann. Field Conf., 1957.

Kinney, D. M., 1955, Geology of the Uinta River—Brush Creek area, Duchesne and Uintah Counties, Utah: U.S. Geol. Survey Bull. 1007, 185 p., 6 pls., 13 figs.

Peterson, V. E., 1957, The Ashley Valley oil field, *in* Intermountain Assoc. Petroleum Geologists Guidebook 8th Ann. Field Conf., 1957, p. 191–192.

Thomas, H. E., 1952, Hydrologic reconnaissance of the Green River in Utah and Colorado: U.S. Geol. Survey Circ. 129, 32 p.

185. RELATION OF THE DEEP AND SHALLOW ARTESIAN AQUIFERS NEAR LYNNDYL, UTAH

By R. W. Mower, Fillmore, Utah

Work done in cooperation with the Utah State Engineer

Ground water occurs in several aquifers in the vicinity of Lynndyl, Utah. There is one shallow perched water-table aquifer and at least two artesian aquifers. The perched aquifer is not related to the artesian aquifers and, because it is relatively unimportant, is not discussed here. This investigation shows also that the artesian aquifers are not related.

Well logs indicate that the many alternating beds of gravel, sand, and clay form two general aquifer groups (shallow and deep artesian aquifers), separated by an aquiclude consisting of about 400 to 500 feet of clay, silt, sand, and lenses of gravel (fig. 185.1). The upper group (shallow artesian aquifer) consists of 200 to 250 feet of saturated material, about 75 to 150 feet of which is sand and gravel. The lower group (deep artesian aquifer) consists of about 200 to 300 feet of saturated material, about 75 to 135 feet of which is sand and gravel. The relation of the shallow and deep aquifers to the sand and gravel lenses in the aquiclude is not known, although well logs indicate that they probably are not related.

The irrigation wells drilled in the vicinity of Lynndyl during 1951–58 were completed in the shallow artesian aquifer. Water levels in the wells declined progressively during that period. In the fall of 1958 an irrigation well was drilled into the deep artesian aquifer. Limited testing at that time indicated the presence of a considerable ground-water reservoir that apparently was not related to the shallow artesian aquifer.

Pumping tests and an extensive observation program began in the fall 1959 and continued through 1960 to determine the relation of the shallow artesian aquifer to the deep artesian aquifer and to determine if all shallow wells actually were completed in the same aquifer.

The deep artesian well (C–15–5)26baa–1 (fig. 185.2) was pumped continuously for 27 days during November and December 1959, and water-level measurements were made in selected wells completed in the shallow aquifer within a radius of 8 miles. Water-level measurements for the pumped well and for several representative wells are plotted on figure 185.3. These hydrographs show no measurable decline of water levels in wells completed in the shallow aquifer, caused by pumping the deep well. The slight irregularities in the hydrographs are due chiefly to fluctuating atmospheric pressure. After correcting for atmospheric pressure changes and this rising water-level trend, a maximum of 0.03 foot of decline remains to be accounted for. This amount is within the limits of accuracy of the water-level measurements, the corrections for atmospheric pressure changes, and data plotting.

Interpretation of the recovery data for the deep well indicates that the coefficient of transmissibility (T) in the vicinity of the deep aquifer is 57,000 gpd/ft (gallons per day per foot). In another deep well (C–16–5)19cbd–1, about 6 miles to the southwest of (C–15–5)26baa–1, the coefficient of transmissibility was 34,000 gpd/ft. The coefficient of storage (S) could not be determined in either test of the two deep wells because there were no deep observation wells. Tests in the shallow aquifer show an average T of 300,000 gpd/ft and an average S of 3.3×10^{-4}. A consideration of the differences in the material in the two aquifers suggests that the coefficient of storage for the deep aquifer should be less than for the shallow aquifer, and for purposes of argument S for the deep aquifer is assumed to be about 10^{-4}. Calculations using aquifer constants T equals 57,000 gpd/ft and S equals 10^{-4} suggest that if the observation wells and the pumping well (C–15–5)26baa–1 had been completed in the same or connected aquifers, the water levels in the observation wells should have declined 17 to 23 feet after 27 days of pumping. The hydrographs in figure 185.3 show no decline in water levels in the observation wells during the period Nov. 24 to Dec. 22, when well (C–15–5)26baa–1 was being pumped.

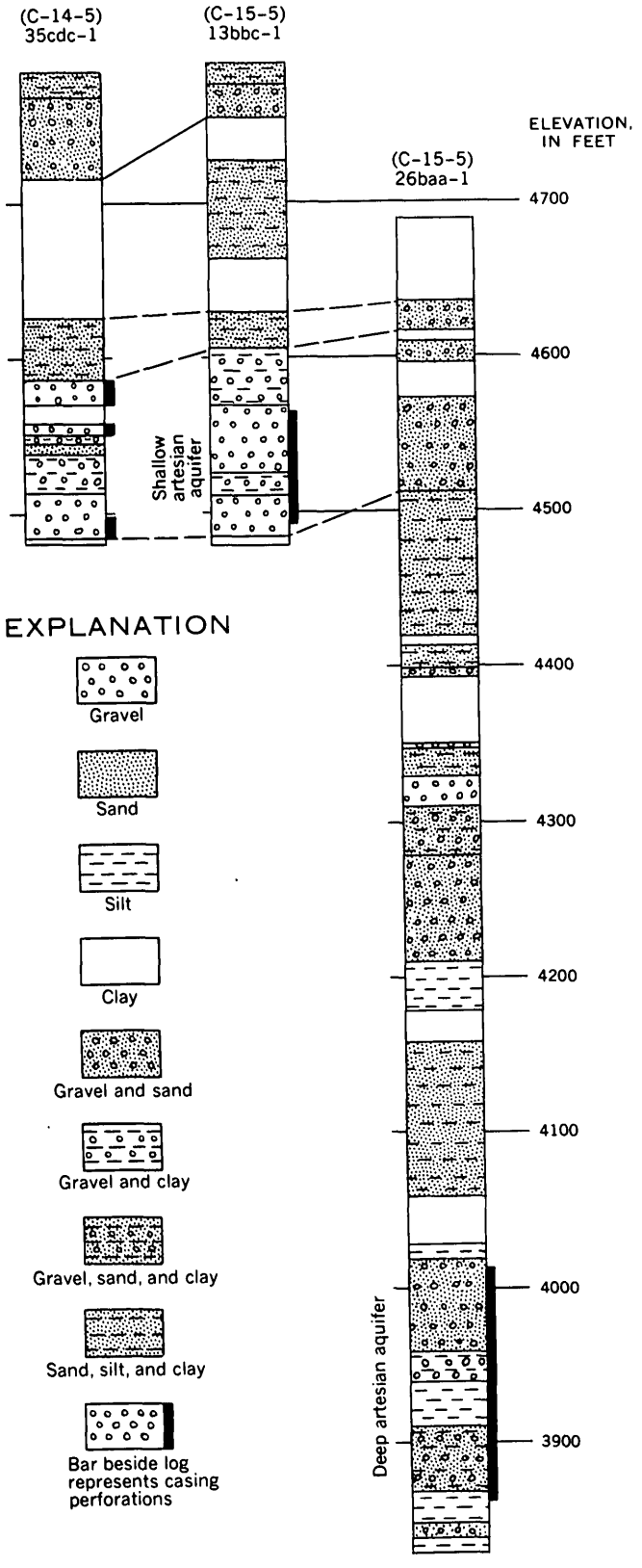

FIGURE 185.1.—Graphic logs of representative wells.

A pumping test was made in the shallow aquifer during April 1960, using well (C–15–5)2ddc–1 as the pumped well and observing water levels in the other shallow wells and in the deep well (C–15–5)26baa–1. No measurable effect was observed in the deep well but within 2 hours measurable effects were observed in all the shallow wells within a radius of 3½ miles.

Water levels in 16 wells were measured at least monthly during 1960. Hydrographs for 5 selected wells are shown in figure 185.4. The shallow irrigation wells were pumped intermittently during the 1960 irrigation season, April to September. Water levels in the shallow wells reacted to the intermittent pumping, as shown by the fluctuation of the hydrographs in figure 185.4. The deep well was turned off purposely for 2 weeks during July to make additional measurements of possible interference between it and the shallow artesian wells. Again no measurable effects were noted.

It is concluded that if the deep and the shallow aquifers are related, it is to such a small degree that interference between them can be considered nil, and that the deep aquifer can be developed with no detrimental effect on the shallow aquifer, at least within a radius of 8 miles of well (C–15–5)26baa–1.

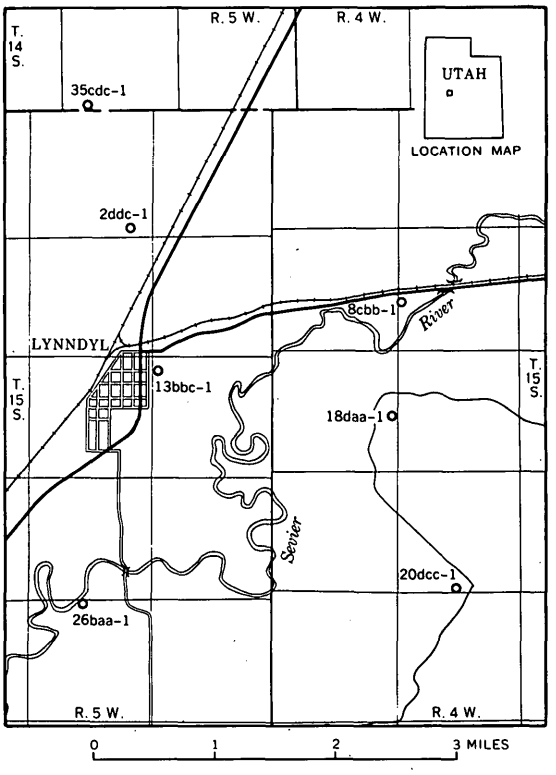

FIGURE 185.2.—Map showing locations of selected wells in the Lynndyl area, Utah.

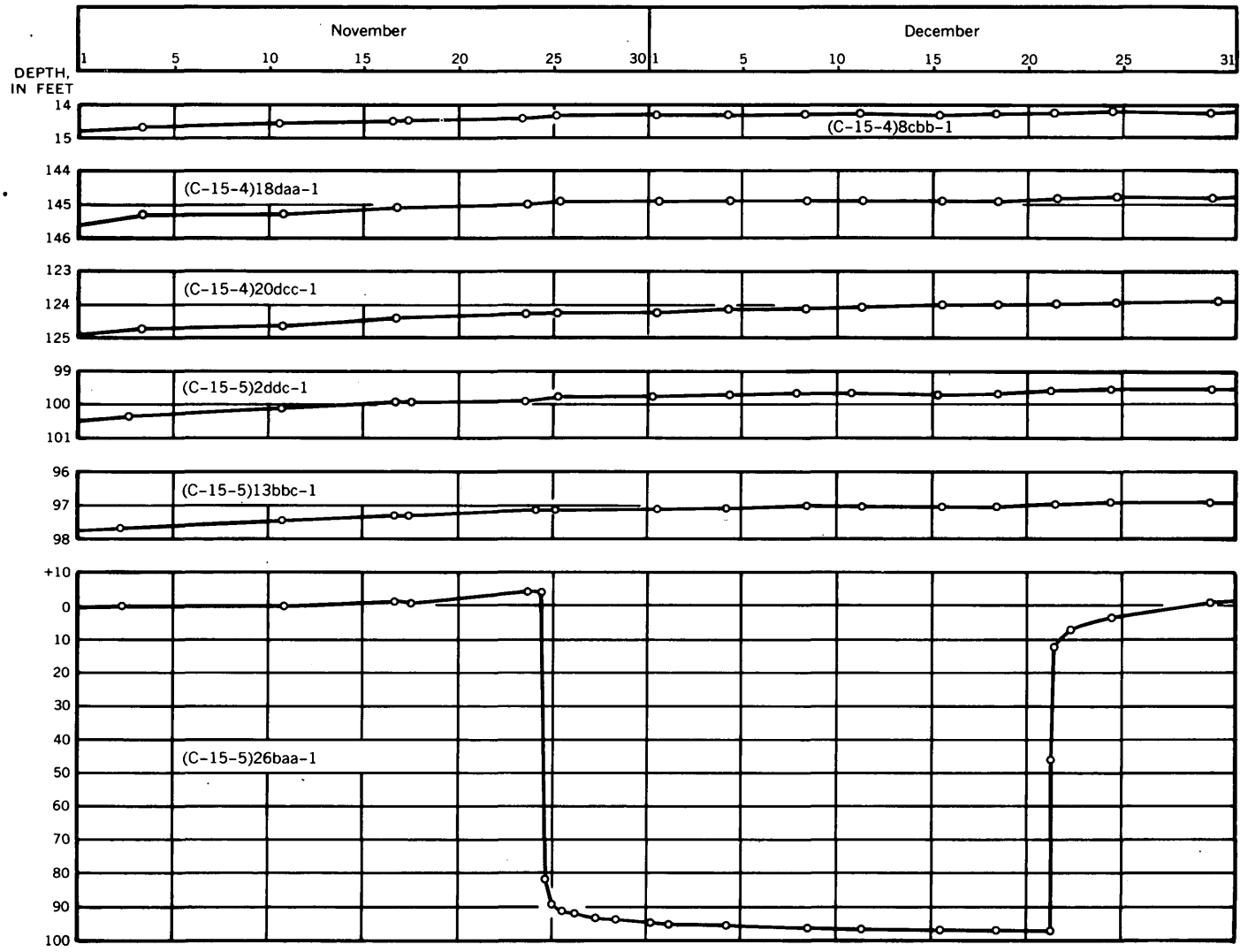

FIGURE 185.3.—Hydrographs of selected observation wells, November and December, 1959. (Locations of wells shown on figure 185.2.)

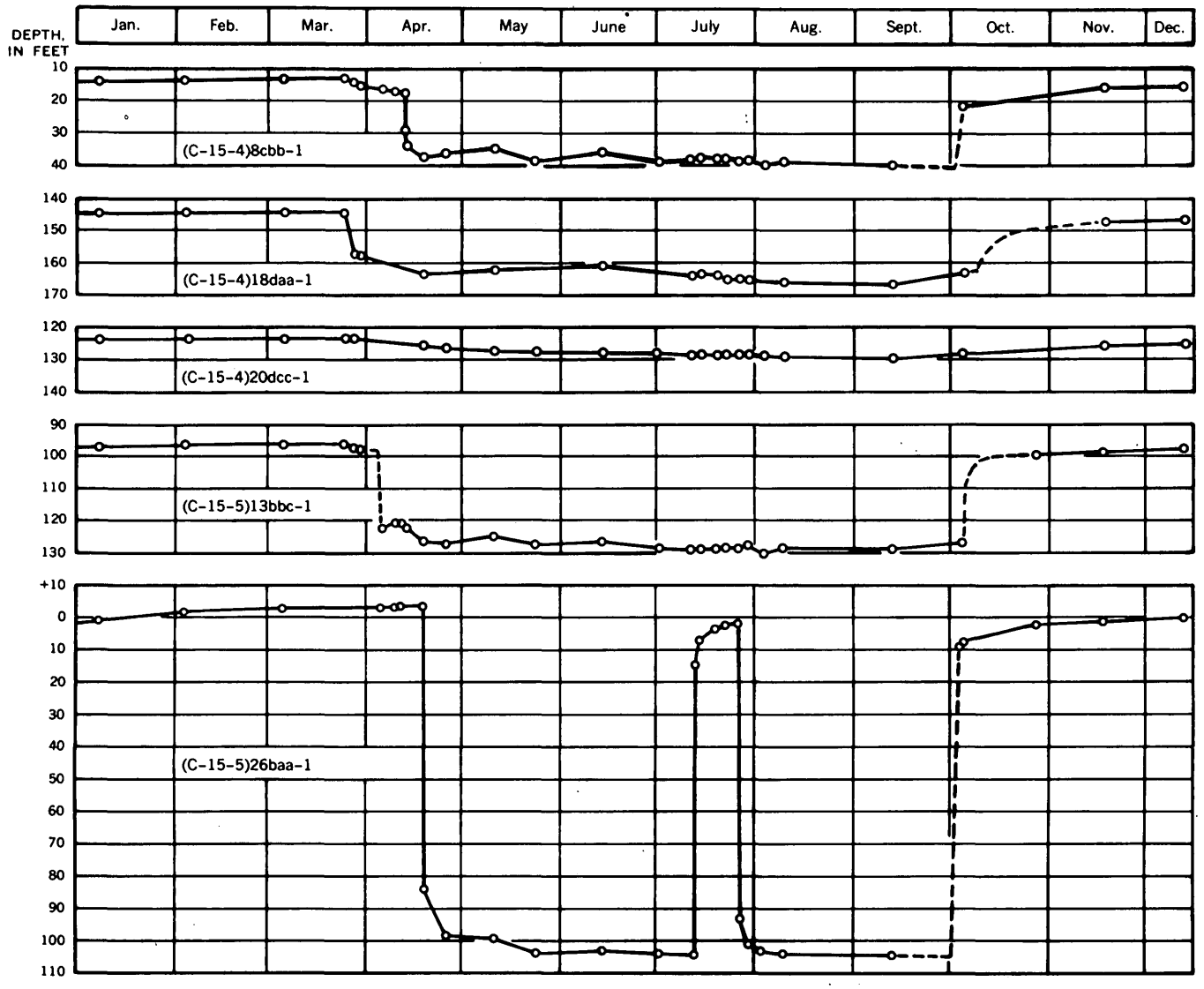

FIGURE 185.4.—Hydrographs, dashed where inferred, of selected observation wells, 1960. (Locations of wells shown in figure 185.2.)

186. A REINTERPRETATION OF TWO OF G. K. GILBERT'S LAKE BONNEVILLE SECTIONS, UTAH

By David J. Varnes and Richard Van Horn, Denver, Colo.

Unconformities generally are not well displayed within the deposits of Pleistocene Lake Bonneville. Therefore, the history of the lake, especially its early part, must be inferred from isolated fragments of positive evidence. Perhaps a dozen or so definitive areas of exposures are now known. Some were first studied by G. K. Gilbert, and several of these localities are still of prime interest 70 years after his classic work.

Gilbert (1890, p. 188–200, 259–262) based a reconstruction of the principal oscillations of the lake largely upon interpretation of the stratigraphic record at three critical localities in west-central Utah. These are the exposures of lake beds at (a) Leamington, where the Sevier River issues westward from the Canyon Range, and at (b) the upper and (c) the lower parts of the Old River Bed. The Old River Bed is a northwest-sloping valley, 25 to 60 miles northwest of Leamington, that once connected the Sevier body of Lake Bonneville with the main body. The lake cycles inferred from these stratigraphic sections were shown schematically in Gilbert's figure 30.

Reexamination of the Leamington and lower Old River Bed localities has led us to conclusions that differ somewhat from those of Gilbert. The upper Old River Bed section is informative but complex, and we believe that it deserves detailed study before Gilbert's interpretation can either be confirmed or revised.

Dark-colored sandy gravel is exposed sporadically for about 8 miles along the east side of the Old River Bed from just north of the Shutoff, shown on the Coyote Springs, Utah topographic sheet, northwestward to the southern boundary of the Dugway Proving Ground, Tooele County, Utah. This gravel caps remnants of a strath terrace along the valley. Trenching done by us in 1957, and in company with R. B. Morrison in 1960, demonstrated the presence of similar sandy gravel in place, at the level of the terrace, but within the adjacent Lake Bonneville deposits. The gravel fills a channel cut in and covered by fine-grained beds that Gilbert called Yellow Clay, and which we regard as equivalent to part of the Alpine formation.

The base of the gravel in the Yellow Clay is 4,455 feet above sea level, where trenched in the NE¼SE¼ sec. 1, T. 10 S., R. 10 W. (Table Mountain, Utah topographic sheet). It drops to an altitude of 4,420 feet 3½ miles to the northwest, and appears to rise to an altitude of about 4,520 feet 4 miles to the southeast.

The gravel is typically 5 to 15 feet thick, is cross-bedded, and contains a few cobbles as much as 4 inches in diameter, although more than one-half the material is medium to coarse sand. The pebbles are mostly of volcanic rocks, quartzite, and chert. The sandy gravel rests on olive to gray silty clay and grades upward into sand. The sand is overlain by silty clay and interbedded silt and sand, on which lies about 5 feet of typical White Marl. The base of the White Marl at the locality of the trench is about at altitude 4,493 feet and is in many places marked by an unconformity and a few inches of pebble and cobble gravel. The marl is overlain by 6 or 7 feet of gray silt, overlain in turn by 10 to 15 feet of gravelly sand that has been reworked into dunes.

At some places the present Old River Bed lies outside of the older gravel-filled channel. Here the gravel within the Yellow Clay is missing, and Gilbert evidently recorded his typical lower Old River Bed section in one of these areas. He mentions, however, that "In this [the Yellow Clay] are occasional passages of sand, but these are local and discontinuous" (Gilbert, 1890, p. 190). Gilbert's field notes covering several visits to the Old River Bed indicate that he observed and dug out gravels in the Yellow Clay near the upper Old River Bed section, but he interpreted the larger bodies downstream as terrace cappings of post-White Marl age.

Stratigraphic studies at and near Leamington disclosed two gravels, rather than one, within the Lake Bonneville sediments that were deposited prior to the White Marl or its equivalents. (See fig. 186.1). At Leamington the thicker and lower wedge, at an altitude of 4,955 feet, is the gravel that Gilbert (1890, p. 192, fig. 28, unit 3) placed between the Yellow Clay and White Marl. We believe that this gravel lies wholly within the upper part of the Yellow Clay or Alpine formation, and that a similar but thinner and higher gravel at altitude 5,002 feet marks the drop in the lake between the epochs of the Yellow Clay and the White Marl. The upper gravel at Leamington is overlain by a few feet of light-colored diatomaceous and calcareous sand that contains a layer of black basaltic ash. This is overlain by sand, and the de-

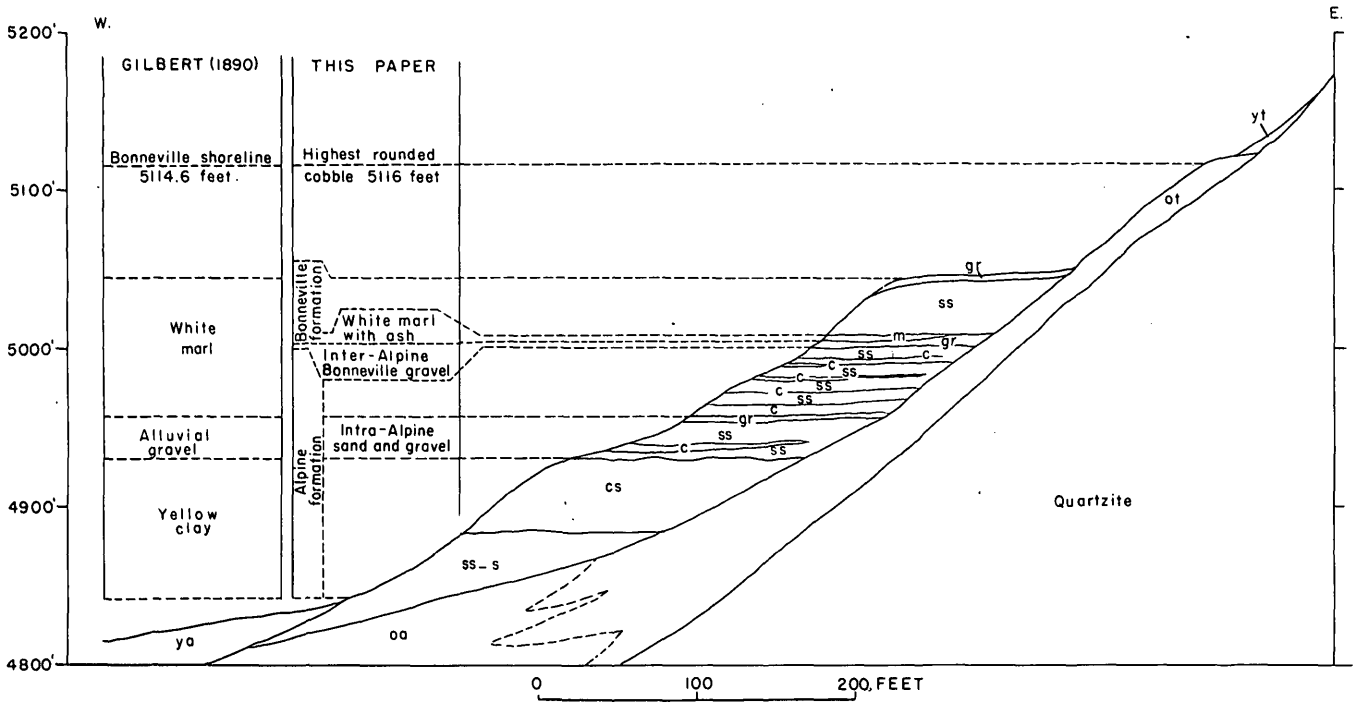

FIGURE 186.1.—Diagrammatic sketch of Lake Bonneville deposits adjacent to the mountain front northeast of Leamington, Utah, showing the differing interpretations of Gilbert and the authors. Pre-Lake Bonneville deposits are quartzite; ot, old talus; and oa, old alluvial fan. Lithology of lake deposits is indicated by gr, gravel; ss, sand; m, diatomaceous sandy marl; c, clay; cs, clayey silt; and ss-s, interbedded sand and silt. Post-Lake Bonneville young talus and alluvium are shown by yt and ya. Gilbert's altitude for the Bonneville shoreline is derived by adding his difference in elevation from the railroad at Leamington, determined by spirit level, to the modern U.S.C.&G.S. altitude of the rails.

posits are capped by beach gravel at altitude 5,046 feet. The ash, which has been found associated with White Marl at many places in the Leamington-Lynndyl-Oak City area, occurs not only in beach deposits but also in the upper part of the basin sediments. We believe that the White Marl and ash were deposited during the rise of the lake from the Alpine-Bonneville recession to the highest or Bonneville level.

It is not possible to demonstrate conclusively that the gravel within the Yellow Clay at the lower Old River Bed and the lower of the two gravels at Leamington are equivalent, because exposures are not continuous between the two localities. The general sequence of beds is quite similar, although the Leamington section is somewhat coarser owing to its position at the head of a major delta. The gravel in the Alpine at Leamington can be traced about 3 miles westward, away from the shoreline, by a discontinuous thin line of well-rounded beach pebbles and cobbles within the enclosing beds of silt and clay.

The Yellow Clay or Alpine formation generally comprises more than three-fourths of the Lake Bonneville deposits. The lake apparently had no outlet during this long early period. Fluctuations in water level in response to imbalance between inflow and evaporation were inferred by Gilbert from a study of the Intermediate embankments. These fluctuations are confirmed by the stratigraphic record in the Leamington-Delta area, which indicates three periods of high water prior to the recession between the deposition of Yellow Clay (or Alpine formation) and White Marl. We believe that one of the recessions in Alpine time, perhaps the fall between the second and third high-water stages, may be of a magnitude comparable to the Alpine-Bonneville and later major recessions.

REFERENCE

Gilbert, G. K., 1890, Lake Bonneville: U.S. Geol. Survey Mon. 1, 438 p.

187. REVISION OF STRATIGRAPHIC NOMENCLATURE OF CAMBRIAN ROCKS, NEVADA TEST SITE AND VICINITY, NEVADA

By HARLEY BARNES and ALLISON R. PALMER, Denver, Colo., and Washington, D.C.

Work done in cooperation with the U.S. Atomic Energy Commission

Re-evaluation of lithologic data and consideration of new paleontologic data suggest that stratigraphic units in a thick sequence of rocks of Cambrian age exposed on the Nevada Test Site (fig. 187.1) have been miscorrelated with units in other parts of southern Nevada. Therefore, a revision of the stratigraphic nomenclature used by Johnson and Hibbard (1957) is desirable. Figure 187.2 gives a generalized geologic section and a comparison of stratigraphic names.

WOOD CANYON FORMATION

The oldest rock known to crop out on the test site is a sequence of quartzite and shale correlated by Johnson and Hibbard (1957, p. 336) with the Stirling quartzite of Nolan (1929, p. 463) but in the present report correlated with the Wood Canyon formation of Nolan (1929, p. 463, 464). Our decision to correlate these rocks with the Wood Canyon formation is based on a comparison of their lithology with that of the corresponding sequence of rocks in the Desert Range, 45 miles southeast of Banded Mountain, and with the lithology of the Stirling quartzite and Wood Canyon formation at the type locality in the northwest Spring Mountains (fig. 187.1). At its type locality, the Stirling includes thick sequences of quartzite containing abundant lenses of pebble and cobble conglomerate; the Wood Canyon at its type locality also contains much quartzite but with little conglomeratic material, essentially none of cobble size. In addition, the Wood Canyon contains more quartzitic sandstone and sandy shale than the Stirling. It also contains a few thin limestone beds, whereas the Stirling does not. The rocks that crop out on the test site 2 miles north of Banded Mountain are chiefly quartzite with a few lenses of pebble conglomerate, much interbedded sandy shale, and a few thin beds of limestone.

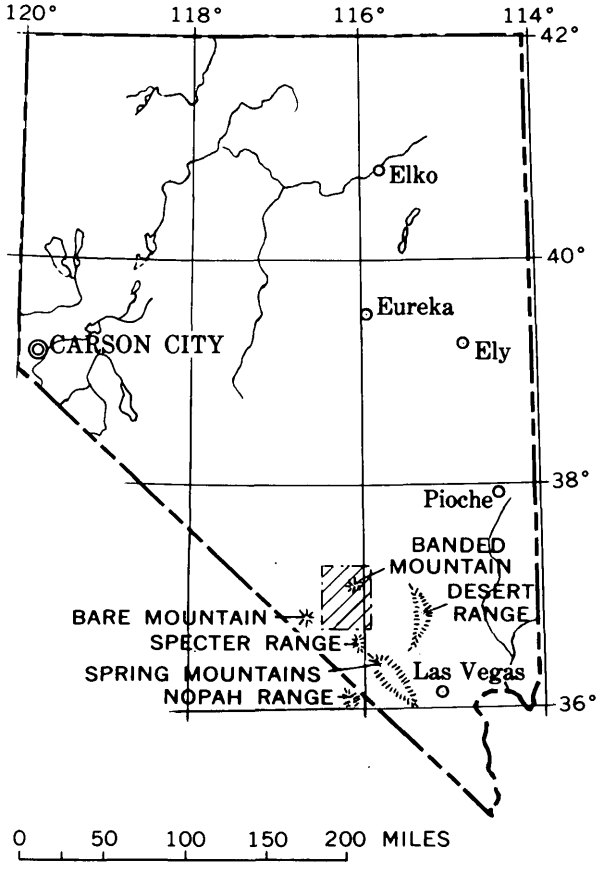

FIGURE 187.1.—Index map of Nevada showing Nevada Test Site and other localities.

Because of faulting the thickness of the Wood Canyon formation cannot be determined on the test site, but a thickness of more than 1,200 feet is exposed. Nolan (1929, p. 463, 464) reports 2,100 feet in the northwestern Spring Mountains, and Clark Burchfiel (oral communication, 1960) reports 2,200 feet in the Specter Range.

CADIZ, CHAMBLESS, AND LATHAM FORMATIONS

Above the Wood Canyon formation is a 1,000-foot sequence of interbedded shale and limestone with a few thin sandstone beds in the lower part. Johnson and Hibbard (1957, p. 337–340) correlated the lower part of this sequence with the upper part of the Pioche shale, the Lyndon limestone, and the Chisholm shale of the Pioche district (fig. 187.1); they named the next higher 275 feet the Jangle limestone; and they placed the top of the sequence, a silty and shaly limestone unit 50 feet thick, in the lower part of their newly defined Yucca Flat formation.

This sequence is faulted and poorly exposed on the test site where it crops out 2 miles east of Banded Mountain, but fossils recently collected from these beds indicate that the Chisholm shale, Lyndon lime-

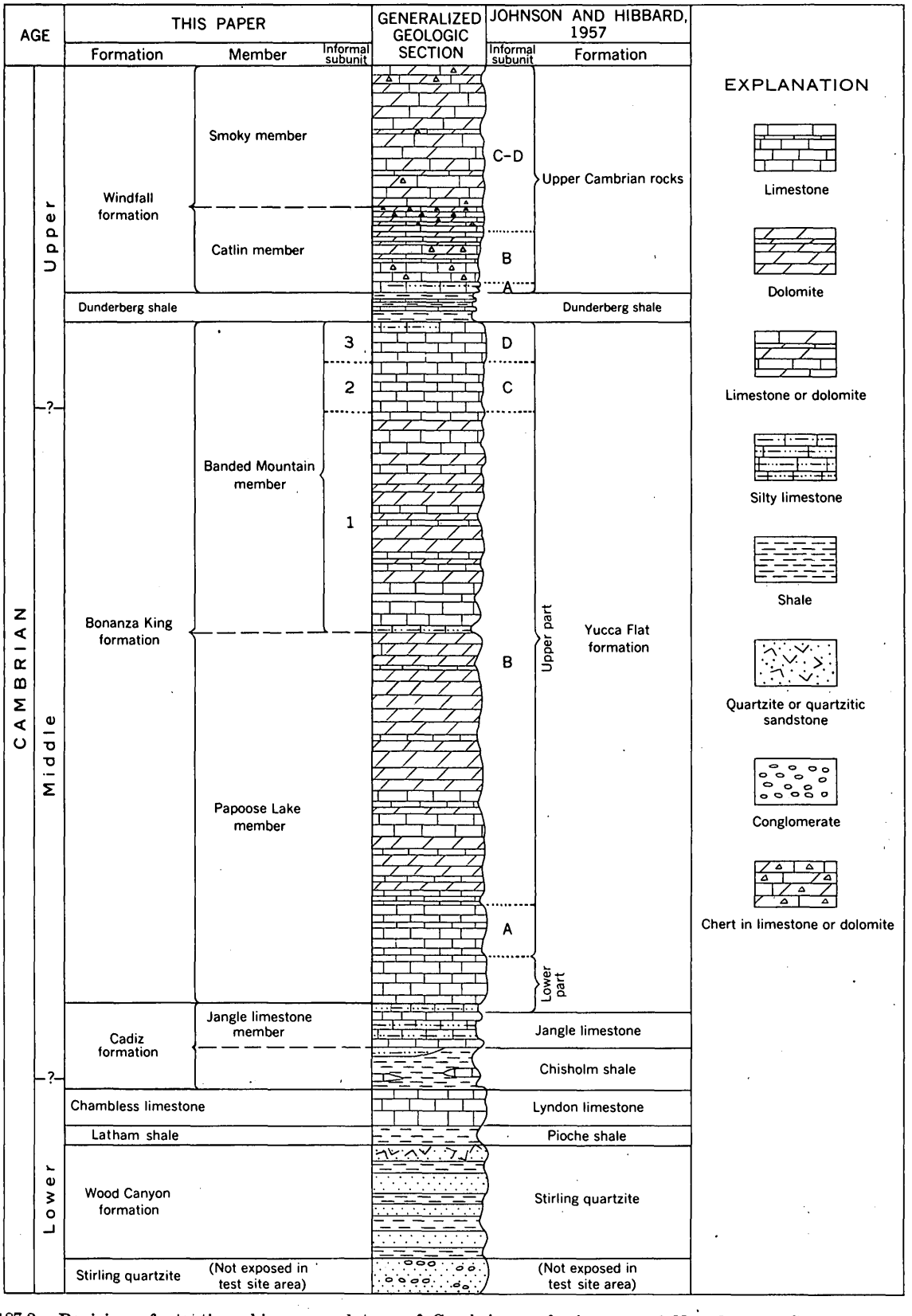

FIGURE 187.2.—Revision of stratigraphic nomenclature of Cambrian rocks in area of Nevada Test Site, southern Nevada.

stone, and upper part of the Pioche shale of Johnson and Hibbard are older than, and do not correlate with, the corresponding units in the Pioche district. Shale in the lower part contains the olenellid trilobite *Bristolia* and is of late Early Cambrian age. It correlates with the Latham shale (Hazzard, 1954) in the Providence Mountains, California. This shale, mapped as the upper part of the Pioche by Johnson and Hibbard, is chronologically equivalent to the lower part of the Pioche in the Pioche district. The Lyndon limestone of Johnson and Hibbard is miscorrelated and as mapped seems to include limestone of more than one age. A thick lower limestone with abundant *Girvanella* is probably of late Early Cambrian age and correlates with the Chambless limestone (Hazzard, op. cit.) and the Combined Metals member of the Pioche shale in the Pioche district. A thinner limestone also mapped as Lyndon is of earliest Middle Cambrian age. It contains trilobites of the *Kochaspis-Plagiura* zone, a fauna found in limestone beds just above the Combined Metals member of the Pioche shale at Pioche. Both of these limestones are older than the Lyndon limestone at Pioche. The overlying Chisholm shale of Johnson and Hibbard at the test site contains an *Albertella* zone fauna of early Middle Cambrian age which is characteristic of the upper part of the Pioche shale at Pioche. Above the Jangle limestone as mapped by Johnson and Hibbard is a 50-foot brown-weathering sequence of silty limestone that Johnson and Hibbard included in the lower part of their Yucca Flat formation. *Glossopleura*, characteristic of the upper part of the Cadiz formation elsewhere in the region, and of the true Chisholm shale, has been found in this brown-weathering silty sequence, which is here included with the Jangle limestone and the underlying "Chisholm shale" in the Cadiz formation. The Jangle limestone as mapped by Johnson and Hibbard is recognized as a member of the Cadiz formation in the Nevada Test Site.

The Wood Canyon and overlying Latham shale compose a lithologically transitional sequence and their contact is therefore arbitrary. We suggest the contact should separate the lower sequence of interbedded shale, quartzite, and sandstone from the upper sequence of interbedded shale and limestone. Therefore, we place the contact at the top of the highest thick quartzite or quartzitic sandstone in the sequence. This is the approximate horizon at which Nolan (1929, p. 463, 464) placed the top of the Wood Canyon in the northwestern Spring Mountains, except that he put the uppermost 20-foot bed of quartzite in an overlying formation correlated with the Bright Angel shale. Because of the transitional nature of the contact the upper part of the Wood Canyon formation includes some thin beds of limestone and the lower part of the overlying Latham shale includes some thin beds of sandstone.

BONANZA KING FORMATION

Between the Cadiz formation and the Dunderberg shale is a carbonate sequence about 5,150 feet thick called by Johnson and Hibbard (1957, p. 340) the Yucca Flat formation and here correlated with the Bonanza King formation of Hazzard and Mason (1936, p. 234, 235) as redefined by Palmer and Hazzard (1956). The Yucca Flat formation on the test site and the Bonanza King formation in the Nopah Range (fig. 187.1) are lithologically similar and occupy essentially the same stratigraphic interval. In view of this and in view of the fact that the term Bonanza King has priority, we are substituting Bonanza King formation for Yucca Flat formation as the name for the carbonate sequence on the test site. The term Yucca Flat, is therefore, abandoned.

The Bonanza King formation on the test site consists of limestone and dolomite, parts of which are silty and sandy. A persistent brown-weathering siliceous carbonate sequence about 40 feet thick occurs

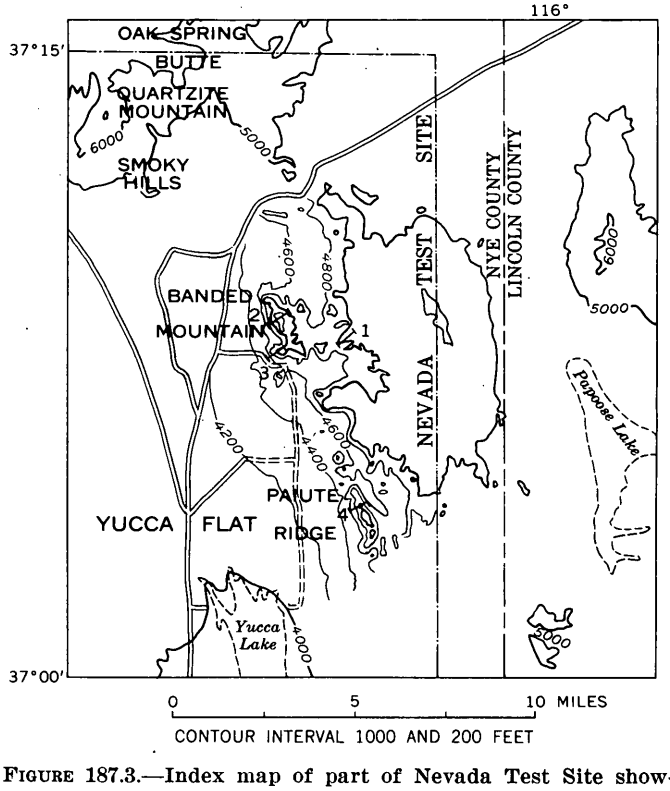

FIGURE 187.3.—Index map of part of Nevada Test Site showing location of measured sections: 1, 2, Bonanza King formation; 3, Dunderberg shale and Windfall formation; 4, Windfall formation.

about 2,400 feet below the top of the formation and is here used as the lithologic basis for subdividing the unit into two members. The lower member is here named the Papoose Lake member (fig. 187.3), after the playa 9 miles east of Banded Mountain, and the upper member is named the Banded Mountain member, after the area of its most conspicuous exposure. The location of measured sections is shown on figure 187.3. The brown-weathering siliceous carbonate sequence is included in the Banded Mountain member and is believed to be the equivalent of a regional key unit that contains the trilobite "*Ehmania?*" in the Desert Range, Spring Mountains, and Nopah Range. This key unit is correlated with unit 7A of Hazzard (1937, p. 277) in the Nopah Range. Most of the Bonanza King formation is of Middle Cambrian age but at least the top 300 feet, and probably the top 700 feet, is of Late Cambrian age.

DUNDERBERG SHALE

The Dunderberg shale was described by Johnson and Hibbard (1957, p. 342) as "brown and reddish-brown hard, fissile, nonresistant shale" with interbedded dark-gray fine-grained fossiliferous limestone. It is a distinctive lithologic unit, here 223 feet thick.

WINDFALL FORMATION

The rocks between the Dunderberg shale and the Pogonip group of Ordovician age are a previously unnamed carbonate sequence about 1,785 feet thick. This sequence is here correlated with the Windfall formation of Nolan, Merriam, and Williams (1956, p. 20) in the Eureka district. The formation is divided into Catlin and Smoky members. It is described in greater detail by Barnes and Byers (Art. 188, this volume).

REFERENCES

Hazzard, J. C., 1937, Paleozoic section in the Nopah and Resting Springs Mountains, Inyo County, California: California Jour. Mines and Geology, Rept. 33, State Mineralogist, p. 273–339.

——— 1954, Rocks and structure of the northern Providence Mountains, San Bernardino County, California; *in* Geology of southern California: California Div. Mines Bull. 170, p. 27–35.

Hazzard, J. C., and Mason, J. F., 1936, Middle Cambrian formations of the Providence and Marble Mountains, California: Geol. Soc. America Bull., v. 47, no. 2, p. 229–240.

Johnson, M. S., and Hibbard, D. E., 1957, Geology of the Atomic Energy Commission Nevada Proving Grounds area, Nevada: U.S. Geol. Survey Bull. 1021–K, p. 333–384.

Nolan, T. B., 1929, Notes on the stratigraphy and structure of the northwest portion of Spring Mountain, Nevada: Am. Jour. Sci., 5th ser., v. 17, p. 461–472.

Nolan, T. B., Merriam, C. W., and Williams, J. S., 1956, The stratigraphic section in the vicinity of Eureka, Nevada: U.S. Geol. Survey Prof. Paper 276, 77 p.

Palmer, A. R., and Hazzard, J. C., 1956, Age and correlation of Cornfield Springs and Bonanza King formations in southeastern California and southern Nevada: Am. Assoc. Petroleum Geologists Bull., v. 40, no. 10, p. 2494–2499.

188. WINDFALL FORMATION (UPPER CAMBRIAN) OF NEVADA TEST SITE AND VICINITY, NEVADA

By Harley Barnes and F. M. Byers, Jr., Denver, Colo.

Work done in cooperation with the U.S. Atomic Energy Commission

The sequence of carbonate rocks lying between the Dunderberg shale and the Goodwin limestone on the Nevada Test Site (fig. 187.1 of Barnes and Palmer, Art. 187) is correlated with the Windfall formation that was originally described by Nolan, Merriam, and Williams (1956, p. 19–22) for the Eureka district. These rocks crop out in the Smoky Hills north of Yucca Flat, on Teapot Ridge and Paiute Ridge east of Yucca Flat, in the Specter Range in the southern part of the test site, and at Bare Mountain west of the site. Johnson and Hibbard (1957, p. 343) referred to these beds on the test site as unnamed Upper Cambrian rocks and assigned to them an estimated thickness of 2,660 feet. More recent detailed measurements, however, show a total thickness of about 1,785 feet (fig. 188.1).

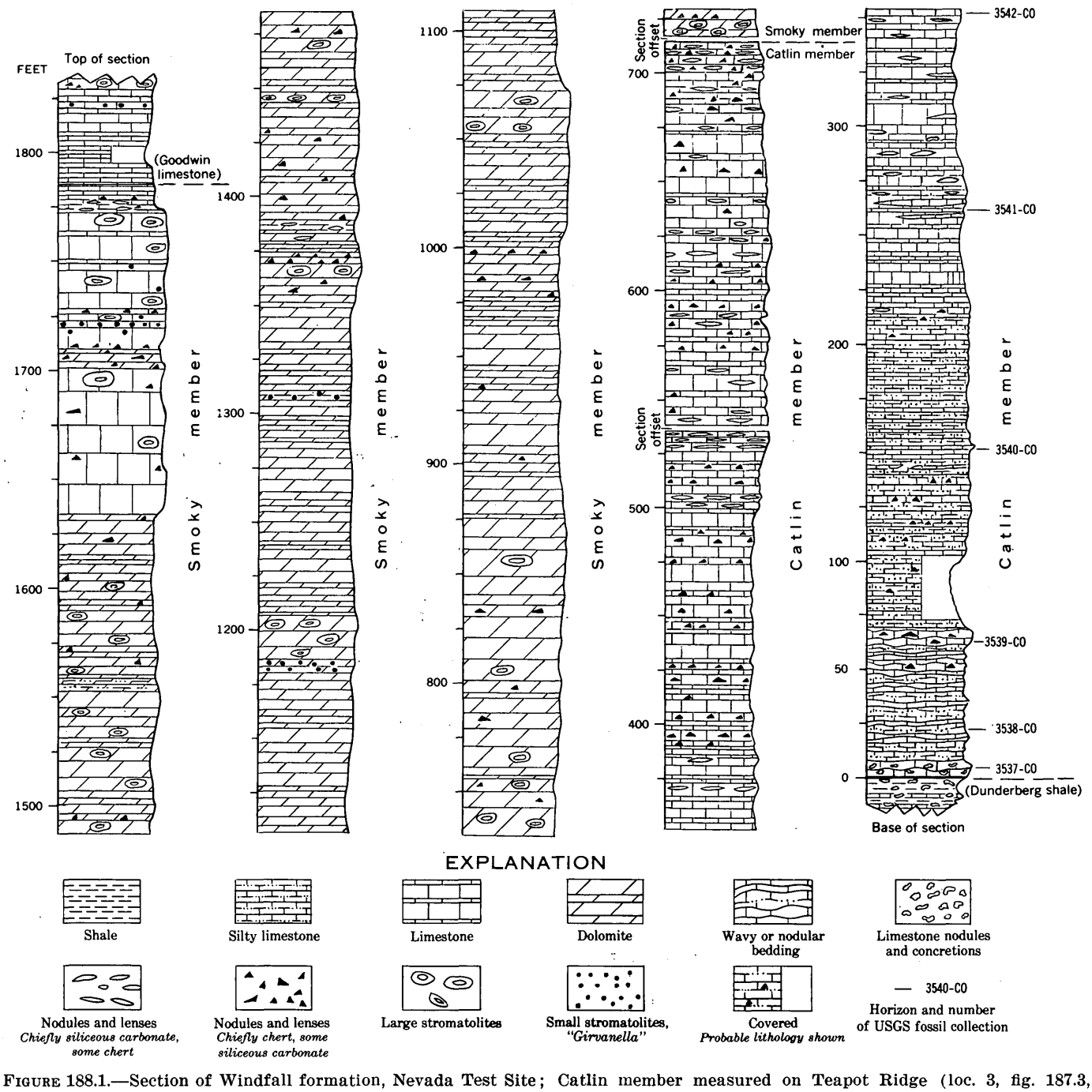

FIGURE 188.1.—Section of Windfall formation, Nevada Test Site; Catlin member measured on Teapot Ridge (loc. 3, fig. 187.3, Art. 187), Smoky member measured on Paiute Ridge (loc. 4, fig. 187.3, Art. 187).

The lower part of the Windfall formation at the test site is about 715 feet thick and is considered to be the Catlin member because of its lithologic similarity to the type Catlin, which is about 250 feet thick at Eureka. At Eureka the Catlin is characterized by thin-bedded platy and sandy limestone alternating with ledge-forming thicker bedded limestone, and by an abundance of thin-bedded chert in the lower part (Nolan, Merriam, and Williams, 1956, p. 20). At the test site the Catlin is characterized by very thin bedded flaggy-splitting limestone and dolomite intercalated with laminae of silty limestone and dolomite, and very thin beds of chert (fig. 188.1).

The upper part of the Windfall formation at the test site is distinctly different from the upper part in the Eureka district. At Eureka the upper part is 400

feet thick and has been named the Bullwhacker member (Nolan, Merriam, and Williams, 1956, p. 21). It is composed of slope-forming, thin-bedded platy or shaly limestone that weathers to a distinctive yellowish-tan color.

At the test site the upper part of the Windfall formation is a cliff- and ledge-forming carbonate about 1,070 feet thick that weathers to several shades of gray. Because of these differences it seems best to adopt a new name that will distinguish these beds from the Bullwhacker member of the Eureka district. Accordingly, the upper part of the Windfall formation on the test site is here named the Smoky member after the Smoky Hills at the north end of Yucca Flat (fig. 187.3, Art. 187). The member is well exposed in the Smoky Hills and on Paiute Ridge. In contrast with the underlying Catlin, the Smoky member is characterized by thicker beds that tend to split into blocks and massive fragments, and by less abundant chert that occurs as scattered nodules. The base of the Smoky member is placed where the unusually high concentration of chert lenses and siliceous carbonate concretions in the thin beds of the Catlin are overlain by thick- to thin-bedded dolomite and limestone with only scattered nodules of chert. Dolomite is predominant in the Smoky member, but a stratigraphic sequence may be dolomite at one locality and limestone at another. On Paiute Ridge the lower 920 feet is chiefly dolomite and the upper 150 feet is cliff-forming massive-splitting very thick bedded limestone with smaller amounts of slope-forming, thin-bedded limestone. Cross-lamination of beds occurs locally throughout the member. Predominant colors of the Smoky member are various shades of gray, and outcrops in many places are marked by conspicuous broad contrasting bands of very light and dark gray from 20 to several hundred feet wide.

Large and small stromatolites are conspicuous in the Smoky member. Individual algal "heads" 1 to 2 feet wide and 2 to 4 feet high are crowded together in thick-bedded strata throughout the member, as well as in the overlying Goodwin limestone. The "heads" are irregular but generally concentric ovoids that are outlined in various shades of gray. "*Girvanella*" 1 to 2 inches in diameter occur in sequences of thin-bedded strata 6 inches to 3 feet thick, especially in the upper part of the member, where they are conspicuously embossed by weathering.

The contact of the Windfall formation with the overlying Goodwin limestone is gradational and is determined primarily on the basis of color. The basal beds of the Goodwin limestone are laminated to thin bedded and weather to a characteristic pale yellowish brown or light brown, but the uppermost beds of the Windfall formation weather gray. This contrast in color is readily mappable both in the field and on aerial photographs.

Most of the Windfall formation in the test site area is thought to be of Late Cambrian age. A. R. Palmer (written communication, 1960) has determined that collections 3537–CO and 3538–CO, 3 and 22 feet respectively, above the base of the Windfall (fig. 188.1 and table 188.1), contain trilobites of the lower *Elvinia* zone of Franconia age. Collection 3539–CO,

TABLE 188.1.—*Fossils identified from localities 3 and 4 (fig. 187.3, Art. 187), Nevada Test Site*

[Collections D733–CO from west side of Paiute Ridge identified by R. J. Ross, Jr.; collections 3537–CO to 3542–CO from northeast side of Teapot Ridge identified by A. R. Palmer]

D733–CO (about 200 feet above base of Goodwin limestone):

Xenostegium cf. *X. franklinense* Ross
Symphysurina? sp.
Parabellefontia cf. *P. concinna* Hintze

3542–CO (about 350 feet above base of Windfall formation):

Richardsonella sp.
Loganellus sp.
Drumaspis sp.
Idahoia? sp.
Homagnostus sp.
Pseudagnostus sp.

3541–CO (about 260 feet above base of Windfall formation):

Homagnostus sp.
Loganellus? sp.
Pseudagnostus cf. *P. convergens* Palmer
Hungaia sp.
Richardsonella sp.
Lotagnostus sp.
Prosaukia? sp.

3540–CO (about 150 feet above base of Windfall formation):

Idahoia sp.
Richardsonella sp.
Loganellus sp.
Wilbernia? sp.
Pseudagnostus sp.

3539–CO (63 feet above base of Windfall formation):

Irvingella major Ulrich and Resser
Elvinia roemeri (Shumard)
Pterocephalia sanctisabae Roemer
Homagnostus sp.
Pseudagnostus sp.

3538–CO (22 feet above base of Windfall formation):

Irvingella angustilimbatus Kobayashi
Pterocephalia sanctisabae Roemer
Elvinia? sp.
Homagnostus sp.
Pseudagnotus sp.

3537–CO (3 feet above base of Windfall formation):

Dokimocephalus pernasutus (Walcott)
Irvingella angustilimbatus Kobayashi
Elvinia roemeri (Shumard)
Pseudagnostus sp.
Homagnostus sp.

63 feet above the base, contains trilobites of the upper *Elvinia* zone. Collections 3540–CO, 3541–CO, and 3542–CO (150, 260, and 350 feet above base) contain a related fauna from the *Ptychaspis-Prosaukia* zone of late Franconia age. Comparable faunas are found in the Catlin member in its type area at Eureka, Nevada (Nolan, Merriam, and Williams, 1956, p. 22). No identifiable fossils have been found between this fauna and one about 200 feet above the base of the Goodwin limestone, where R. J. Ross, Jr. (written communication, 1960) identified a fauna equivalent to the zone "B" fauna in the Pogonip-Garden City sequence, which is of earliest Ordovician age. The Cambrian-Ordovician boundary in the rock sequence at the Nevada Test Site is therefore at an unknown position between these two points, which are about 1,600 feet apart stratigraphically.

REFERENCES

Johnson, M. S., and Hibbard, D. E., 1957, Geology of the Atomic Energy Commission Nevada Proving Grounds area, Nevada: U.S. Geol. Survey Bull. 1021–K, p. 333–384.

Nolan, T. B., Merriam, C. W., and Williams, J. S., 1956, The stratigraphic section in the vicinity of Eureka, Nevada: U.S. Geol. Survey Prof. Paper 276, 77 p.

189. REVISED SUBDIVISION OF ORDOVICIAN SYSTEM AT THE NEVADA TEST SITE AND VICINITY, NEVADA

By F. M. Byers, Jr., Harley Barnes, F. G. Poole, and R. J. Ross, Jr., Denver, Colo.

Work done in cooperation with the U.S. Atomic Energy Commission

Mapping of Ordovician rocks in the Papoose Lake and Frenchman Lake quadrangles at the Nevada Test Site (fig. 189.1) has shown that the lithologic units mapped by Johnson and Hibbard (1957, pl. 32) are not in sufficient detail for hydrologic and geophysical studies in Yucca and Frenchman Valleys. They divided rocks of the Ordovician system into the Pogonip group at the base, overlain in turn by the Eureka quartzite and "dolomite of middle Paleozoic age, undifferentiated." The last named unit also included Silurian and probably Lower Devonian rocks. We propose to subdivide the Pogonip group in the vicinity of the test site into the three formations defined by Nolan, Merriam, and Williams (1956, p. 25–29) in the vicinity of Eureka, Nev. (inset, fig. 189.1): the Goodwin limestone, the Ninemile formation, and the Antelope Valley limestone. The subdivision is based on the close similarity in lithology and faunal content between these formations in the two areas. Johnson and Hibbard (1957, p. 352) correlated the lower part of the "dolomite of middle Paleozoic age, undifferentiated" with the Ely Springs dolomite of Late Ordovician age (Westgate and Knopf, 1932, p. 15–16) in the vicinity of Pioche, Nev. (inset, fig. 189.1), but they made no attempt to locate the Ordovician-Silurian boundary. It is now possible on the basis of additional fossils to locate the Ordovician-Silurian boundary within a stratigraphic interval of 190 feet. The new subdivisions of Ordovician rocks at the Nevada Test Site are given on table 189.1.

The Antelope Valley limestone of the Pogonip group is here further subdivided into the Paiute Ridge, Ranger Mountains, and Aysees members named from exposures at Paiute Ridge, Ranger Mountains, and Aysees Peak, respectively (fig. 189.1). The stratigraphic descriptions and thicknesses are mostly from a well-exposed section at Aysees Peak (loc. 2, fig. 189.1). The three members are exposed at all type localities and show only minor lithologic variation from one locality to another. Correlation of these members with the informal lettered units of Johnson and Hibbard (1957, p. 345–349) is shown in table 189.1.

The contact between the Cambrian and Ordovician systems is placed about 175 feet stratigraphically

TABLE 189.1—*Generalized stratigraphic chart of Ordovician system at the Nevada Test Site and vicinity*

[Locality of measured section includes initials of persons who measured sections: FMB, F. M. Byers, Jr.; HB, Harley Barnes; and FGP, F. G. Poole. Fauna identified by R. J. Ross, Jr., except where footnoted. Informal unit designations as used by Johnson and Hibbard (1957, p. 33)]

System or series	Formation	New member name	Informal unit[1]	Lithology (sequence conformable except where noted)	Thickness (feet)	Fauna	Locality of measured section (fig. 189.1)
Silurian			E	Dolomite, olive-gray; 50-foot thick massive yellowish-gray bed in middle of unit; upper part of unit thin and poorly bedded; a few shaly partings, lenticular chert, and silicified horn corals near top; lower part thick bedded, faintly mottled.	[2] 205	*Halysites* or *Cystihalysites*.[3]	Ranger Mountains (loc. 4, FMB).
				Dolomite and chert, ratio 80:20, very thin to thin bedded; slope forming, but otherwise similar to unit below. Corals collected 20 ft below top of unit.	[2] 60	*Favosites*(?) sp., Dissepimented horn coral cf. *Pilophyllum* sp., Nondissepimented horn coral cf. *Rhegmaphyllum* sp., massive stromatoporoid.[4]	
——?——	——?——						
Upper Ordovician	Ely Springs dolomite		E	Dolomite and chert, ratio 70:30; dolomite is medium dark gray, weathers olive gray; chert is medium light gray to pale yellowish brown, weathers orange and brown, very thin bedded to thin bedded; cliff forming. Brachiopods (*Dinorthis* sp.) 20 ft above base.	170	*Dinorthis* sp.	
			D	Dolomite, light olive gray, largely massive; slabby to blocky splitting prominent in upper part; small vuggy cavities, some lined with coarsely crystalline dolomite; cliff forming.	275		
			C	Dolomite, olive-black; bedded olive-gray chert especially abundant in lower 20 ft; very thin bedded in lower 20 ft grading upward to thin bedded; cliff forming.	115		
			B	Dolomite, light olive gray; silty in lower 25 ft; very thin bedded to thin bedded; slope forming. Relations with unit above obscured by minor faulting.	160 ± 20	*Favosites* sp., *Austinella* sp., *Holtedahlina* sp., *Thaerodonta* sp., *Sowerbyella*? sp., *Leptaena* sp., *Zygospira*? sp.	
			A	Dolomite, olive-gray, slightly darker in upper part; sparse lenticular very thin bedded chert; indistinctly thin bedded in lower part grading upward to thick bedded with rare sand grains; slope forming.	105	Streptelasmatoid coral[4], *"Lambeophyllum"* sp.[4]	
——?——				Quartzite, orange, red, and brown in lower 171 ft; mostly white and sandy in upper 132 ft; fine grained; mostly thick bedded; cross-bedded in basal 20 ft; forms ledges and low cliffs.	300		

See footnotes at end of table.

TABLE 189.1—*Generalized stratigraphic chart of Ordovician system at the Nevada Test Site and vicinity*—Continued

System or series	Formation	New member name	Informal unit [1]	Lithology (sequence conformable except where noted)	Thickness (feet)	Fauna	Locality of measured section (fig. 189.1)
Middle Ordovician	Eureka quartzite			Limestone; dolomitic in upper part; olive gray, mottled and weathered in shades of orange and brown; very thin bedded, flaggy splitting; ledge forming.	35	*Valcourea* cf. *V. plana*, *Sowerbyella*? sp., *Bronteopsis* sp., *Lonchodomas* sp., *Homotelus*? sp., Unidentified ostracods.	
				Quartzite, light-gray; weathers brown; very fine grained to fine grained, indistinctly thin bedded; ledge and cliff forming.	60		
Middle and Lower Ordovician	Antelope Valley limestone (Pogonip group)	Aysees member	I	Limestone, medium-gray to dark-gray; weathers medium light gray and light olive gray to yellowish gray; contains thin-bedded siliceous and laminated silty limestone that weathers shades of orange and brown; two pink ledges in lower middle; laminated to thin bedded; forms varicolored stairstep slope. Fossiliferous.	440	"*Lichenaria*" sp.[4], *Eofletcheria* sp.[4], *Orthambonites paucicostata*, *Anomalorthis oklahomensis*, *Desmorthis*? cf. *D. nevadensis*.	Ranger Mountains (loc. 3, HB, FGP, FMB).
			H	Limestone, medium-gray to dark-gray, thick bedded to very thick bedded; upper contact gradational and intertonguing, possibly through a large stratigraphic interval; cliff forming. Gastropods and *Receptaculites* abundant in upper part.	330	*Palliseria robusta*, *Receptaculites* sp.	Aysees Peak (loc. 2, HB, FGP, FMB).
		Ranger Mountains member	G	Silty limestone, olive-gray, mottled yellow and red along silty layers; dominantly very thin bedded; thin-bedded brachiopod-bearing limestone in upper 50 ft; ledge forming. Abundantly fossiliferous.	215	*Orthambonites eucharis*, *Orthidiella* 2 spp., *Ingria cloudi*, *Ectenonotus* cf. *E. connemaricus*, *Paracybeloides*? sp., *Bathyurellus feitleri*, *Remopleurides*? sp., *Illaenus* sp., *Carolinnites* sp., *Trinodus* sp., *Leperditia* sp.	
		Paiute Ridge member	F and E	Limestone, gray; laminae and etched irregular network of silty limestone that weathers brown; etched network forms "chicken-wire" pattern; thin to thick bedded; cliff forming. Many straight-coned cephalapods.	370	*Orthambonites* cf. *O. subalata*, *Lachnostoma latucelsum*, *Kirkella decliviita*, *Goniotellina* or *Bathyurus* sp.	
	Ninemile formation (Pogonip group)		D	Claystone and limestone (ratio 80:20) interstratified; claystone is light olive to greenish gray, fissile weathering; limestone is gray, nodular, very thin bedded becoming thin bedded and more abundant in uppermost 50 to 100 ft; forms gentle slope, largely covered.	335	*Archaeorthis elongata*, *Hesperonomia* cf. *H. antelopensis*, *Pseudocybele* cf. *P. nasuta*, *Kirkella* cf. *K. declivita*, *K.* cf. *K. vigilans*, *Trinodus* sp., *Pseudomera*? sp., *Lachnostoma* cf. *L. latucelsum*, *Asaphellus*? cf. *A. eudocia*.	

See footnotes at end of table.

TABLE 189.1—*Generalized stratigraphic chart of Ordovician system at the Nevada Test Site and vicinity*—Continued

System or series	Formation	New member [1] name	Informal unit [1]	Lithology (sequence conformable except where noted)	Thickness (feet)	Fauna	Locality of measured section (fig. 189.1)
Lower Ordovician	Goodwin limestone (Pogonip group)		C	Limestone, medium light gray to light olive gray; upper 50 ft weathers olive gray to brown; nodular chert in lower part becoming sparse upward; limestone-pebble conglomerate common, especially in upper part; thin bedded; silty laminae common in basal and upper 50 ft; ledge-forming.	[5] 415+	*Ampyx* sp., *Protopresbynileus* sp., *Lannacus*? sp., *Pseudoclelandia*? sp.	Aysees Peak (loc. 2) and Paiute Ridge (loc. 1) (HB, FMB).
			B	Silty limestone, medium light gray with abundant grayish-yellow silty partings; laminated to very thin-bedded; limestone plates weather out on gray-yellow slope; gradational and apparently intertonguing contacts above and below; forms swale. Fossiliferous.	85	*Nanorthis*? sp.	
			A	Limestone, light olive gray; brownish-weathering siliceous limestone laminae; about 200 to 300 ft above base is very thin bedded silty fossiliferous limestone; cherty near base; thin bedded; lower contact placed at base of brownish-weathering thin-bedded olive-gray limestone; ledge forming.	405	*Xenostegium* cf. *X. franklinensis*, *Parabellefontia* cf. *P. concinna*, *Symphysurina* sp.	Paiute Ridge (loc. 1, HB, FMB).
——?——							
Upper Cambrian	Windfall [6] formation (upper part)	Smoky [6] member (upper part)	[7] A	Limestone, mainly light gray in lower part grading upward to medium gray and medium dark gray; dolomitic in lower 35 ft; mainly thick bedded to massive; upper part contains common very thin layers of lenticular chert and large ovoid algal structures; conspicuous "Girvanella" beds in middle of unit; cliff-forming.	[2] 175		
	Approximate total thickness of Ordovician rocks				3, 800		

[1] Informal units of Johnson and Hibbard (1957).
[2] Footage not included in total thickness of rocks of Ordovician age.
[3] Helen Duncan *in* Johnson and Hibbard (1957, p. 352).
[4] Corals identified by W. A. Oliver, Jr. (written communication, 1961).
[5] Faulted; estimated 500 feet.
[6] See Barnes and Byers, Art. 188.
[7] Pogonip unit A of Johnson and Hibbard (1957, p. 346) extends about 175 feet below contact of Goodwin limestone and Windfall formation as shown in table.

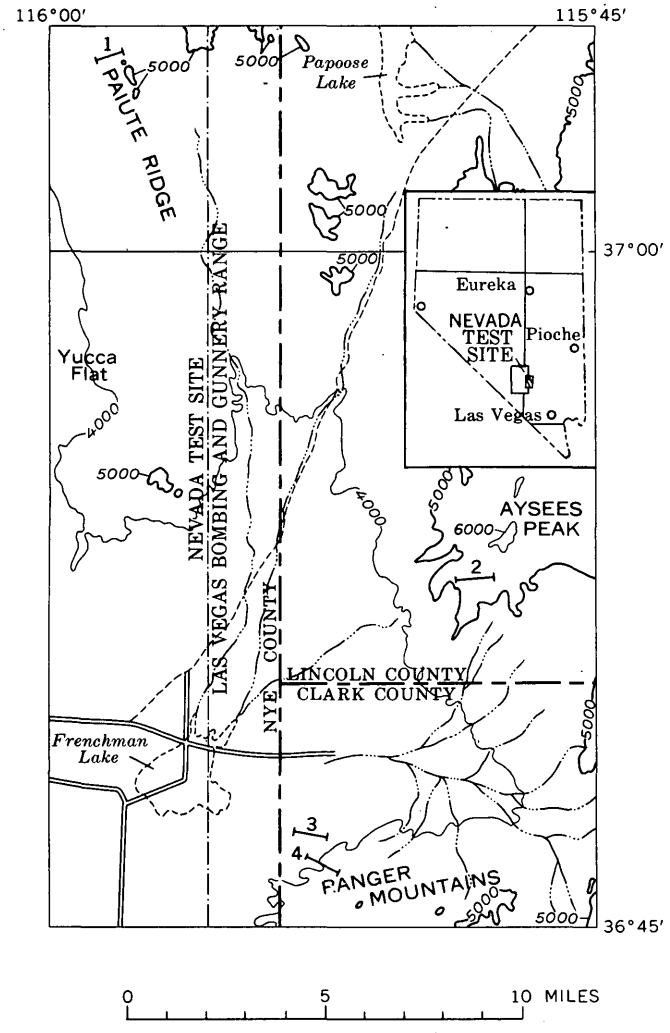

FIGURE 189.1.—Map of Frenchman Lake and southern one-third of Papoose Lake 15-minute quadrangles, Nevada Test Site and vicinity, showing location of stratigraphic sections of Ordovician rocks (table 189.1).

higher than that defined by Johnson and Hibbard (1957, p. 346). This contact is mapped at a color change within a 40-foot thick transitional sequence. The basal beds of the Ordovician Goodwin limestone are laminated to thin bedded and weather to a characteristic pale yellowish brown or light brown, but the uppermost beds of the Cambrian Windfall formation weather gray (Art. 188). Thin lenticular chert is common both above and below the contact as herein defined.

The top of the Ordovician system is placed tentatively at a seemingly minor lithologic break 170 feet above the base of Johnson's and Hibbard's (1957, p. 351) unit E, "dolomite of middle Paleozoic age, undifferentiated" or about 830 feet above the top of the Eureka quartzite. The exclusively Middle and Late Ordovician brachiopod genus *Dinorthis* occurs 20 feet above the base of unit E, within a 170-foot thick cliff-forming dolomite and chert sequence. Corals of unquestioned Silurian age (W. A. Oliver, oral communication) occur 210 feet above the base of unit E (865 feet above the top of the Eureka quartzite) or about 190 feet above the stratigraphic position of the Ordovician *Dinorthis*. Therefore, the Ordovician-Silurian boundary must lie within this 190-foot-thick interval.

REFERENCES

Johnson, M. S., and Hibbard, D. E., 1957, Geology of the Atomic Energy Commission Nevada Proving Grounds area, Nevada: U.S. Geol. Survey Bull. 1021–K, p. 333–384.

Nolan, T. B., Merriam, C. W., and Williams, J. S., 1956, The stratigraphic section in the vicinity of Eureka, Nevada: U.S. Geol. Survey Prof. Paper 276, 77 p.

Westgate, L. G., and Knopf, Adolf, 1932, Geology and ore deposits of the Pioche district, Nevada: U.S. Geol. Survey Prof. Paper 171, 79 p.

190. LITHOLOGIC CHARACTER OF THE DIAMOND PEAK FORMATION (MISSISSIPPIAN) AT THE TYPE LOCALITY, EUREKA AND WHITE PINE COUNTIES, NEVADA

By DAVID A. BREW, Menlo Park, Calif.

The type locality of the "Diamond Peak quartzite" was established by Arnold Hague (1880, p. 34; 1882, p. 28; 1883, p. 252–253; and 1892, p. 85 and 158) in a series of reports dealing with the geology of the Eureka mining district. He described the formation on the slopes of Diamond Peak as follows (1883, p. 268): "* * * conglomerates firmly cemented together lie next to the argillaceous shales of the White Pine epoch, but quickly give place to a more massive, uniformly vitreous quartzite, with a characteristic grayish-brown color, and breaking with an irregular flinty fracture. Near the summit the beds pass into thinly

laminated green and brown schists and shales." In 1892 Hague expanded this description slightly, noting (p. 85) that "Intercalated black cherty bands, * * * occur near the middle portion of the horizon." He also states (p. 158) that the upper shale unit was about 500 feet thick whereas the lower 2,500 feet consisted of "Dark gray quartzites, compact conglomerates, with interbedded layers of jasper and siliceous grits. Near the base narrow belts of blue limestone * * *."

This concept of the Diamond Peak formation as an almost wholly coarse clastic unit has persisted, although Dott (1955, p. 2233, 2265–2266) and Nolan and others (1956, p. 56–61) called attention to the occurrence of significant amounts of shale and siltstone in the lower part of the formation.

Recent mapping has shown that the Diamond Peak formation on the southern and eastern slopes of Diamond Peak is cut by numerous high-angle faults and at least one large low-angle thrust fault (Brew, Art. 191, fig. 191.1), and that some of the formation is absent. Mapping elsewhere in the Eureka quadrangle, and study of apparently complete and relatively undisturbed exposures of the Diamond Peak formation on the northwestern slope of Diamond Peak in secs. 7 and 18 (unsurveyed), T. 20 N., R. 55 E. (between lat 39°36′ N. and lat 39°37′ N. and between long 115°48′30″ W. and long 115°50′ W.) show that the amount of conglomerate and silicified sandstone is small relative to other rock types. Only about 12 percent of the formation is conglomerate, 20 percent is sandstone and silicified sandstone, 6½ percent limestone, 5½ percent limestone phenoplast conglomerate, 9½ percent claystone, and 45 percent siltstone.

In the newly studied section about 3,525 feet of strata, divided informally into eight map units, are assigned to the Diamond Peak formation (fig. 190.1). These units have been mapped on all the slopes of Diamond Peak and throughout the Eureka quadrangle. The map units vary in thickness and character from place to place and probably are not regionally persistent.

Conformably underlying the Diamond Peak formation are laminated and very thin bedded medium-gray to medium dark-gray siltstone, clayey siltstone, claystone, and fine-grained sandstone that weather olive gray and light olive gray and belong to a relatively coarse facies of the Chainman shale, also of Mississippian age. Lenses and beds of conglomerate occur

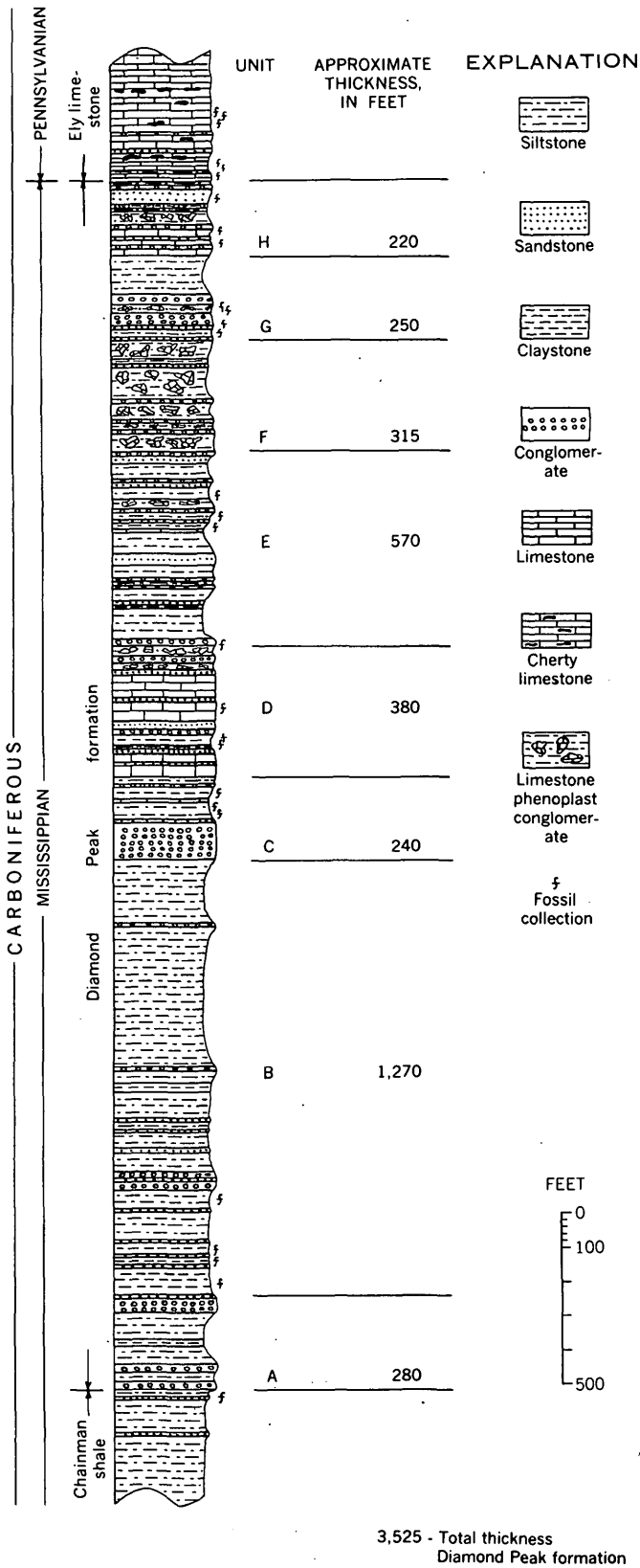

FIGURE 190.1.—Generalized columnar section of the Diamond Peak formation in the vicinity of Diamond Peak, showing approximate thickness and dominant lithologic types for 8 units, A to H.

in the Chainman, but are much more common in the overlying basal unit of the Diamond Peak formation.

Unit A, at the base of the Diamond Peak formation, is characterized by interstratified thick-bedded and very thick bedded gray-weathering chert, quartzite, and limestone-pebble and cobble conglomerate; siltstone similar to that of the underlying Chainman shale; claystone; and thin-bedded gray, brown-weathering, fine- to medium-grained silicified sandstone. The unit is about 280 feet thick, forms prominent ledges, and, although discontinuous in detail, has been traced throughout the area north of Diamond Peak.

Unit B consists of about 1,270 feet of slope-forming thin to very thin bedded siltstone interbedded with silicified sandstone, claystone, and minor lenticular conglomerate. In general, the unit closely resembles the Chainman shale, but forms steeper slopes.

Unit C has at the base a prominent ledge of very thick bedded chert and quartzite cobble and pebble conglomerate that weathers gray and brownish-gray. This bed is overlain by steep slope forming very thin bedded siltstone, claystone, and sandstone. The upper one-third of unit C contains some conglomerate and very thin bedded gray limestone beds that become more numerous upward. The unit is about 240 feet thick.

Unit D is a resistant cliff- and ledge-forming sequence of thick and very thick bedded gray and blue-gray limestone interstratified with limy gray and brown sandstone, olive-gray claystone and siltstone, and gray and brown chert and quartzite cobble and pebble conglomerate. This unit also includes some limestone phenoplast conglomerate, an unusual rock consisting of irregularly shaped nodule-like fragments of gray limestone ranging from 0.5 to 10.0 cm in maximum diameter in a matrix that commonly is siltstone. The relative proportion of matrix and phenoplasts varies considerably both vertically and laterally. The limestone fragments are interpreted as intraformational in origin and are believed to have been plastic at the time of deposition with the siltstone. Unit D is about 380 feet thick.

Unit E is about 570 feet thick and consists of alternating beds of siltstone, sandstone, conglomerate, claystone, limestone, and limestone phenoplast conglomerate that form steep slopes and scattered resistant ledges. Limestone and siltstone diminish upward, and sandstone and conglomerate are prominent in the upper half of the unit.

Unit F is characterized by distinctive alternating purple and green siltstone and claystone, pale-green silicified sandstone, pale-green chert-cobble conglomerate, and purple, green, and gray limestone phenoplast conglomerate. The unit is about 315 feet thick and probably is the base of the upper shaly part of the Diamond Peak formation noted in previous reports.

The lower half of unit G contains thick-bedded dark chert-pebble and cobble conglomerate and subsidiary interstratified siltstone, silicified sandstone, and limestone phenoplast conglomerate and it forms ledges; the upper half is poorly exposed and probably consists mainly of siltstone. The unit is about 250 feet thick.

Unit H is 220 feet thick and represents the beginning of deposition of the thin- to thick-bedded blue-gray limestone that characterizes the conformably overlying Ely limestone of Pennsylvanian age. The transition to the Ely occurs by the alternation of thick bedded blue-gray noncherty limestones with silicified sandstone, limestone phenoplast conglomerate, conglomerate, and minor siltstone.

The upper contact of the Diamond Peak formation is placed about at the base of the lowest sequence of cherty blue-gray limestone. Limestone abruptly becomes the dominant lithologic type at about this horizon, although siltstone, silicified siltstone, and conglomerate of the Diamond Peak type occur in minor amounts through a thickness of about another 140 feet at the base of the Ely.

REFERENCES

Dott, R. H., Jr., 1955, Pennsylvanian stratigraphy of Elko and northern Diamond Ranges, northeastern Nevada: Am. Assoc. Petroleum Geologists Bull., v. 34, no. 11, p. 2211–2305.

Hague, Arnold, 1880, Preliminary report on field-work in the Eureka district: U.S. Geol. Survey, 1st Ann. Rept., p. 32–35.

——— 1882, Administrative report of Mr. Arnold Hague: U.S. Geol. Survey, 2d Ann. Rept., p. 21–34.

——— 1883, Abstract of report on the geology of the Eureka district, Nevada: U.S. Geol. Survey, 3d Ann. Rept., p. 237–290.

——— 1892, Geology of the Eureka district, Nevada: U.S. Geol. Survey Mon. 20, 419 p.

Nolan, T. B., Merriam, C. W., and Williams, J. S., 1956, The stratigraphic section in the vicinity of Eureka, Nevada: U.S. Geol. Survey Prof. Paper 276, 77 p.

191. RELATION OF CHAINMAN SHALE TO BOLD BLUFF THRUST FAULT, SOUTHERN DIAMOND MOUNTAINS, EUREKA AND WHITE PINE COUNTIES, NEVADA

By David A. Brew, Menlo Park, Calif.

The Bold Bluff thrust fault extends from near Poison Spring north of Newark Summit northeastward to the base of the range at a point north of the mouth of Sadler Canyon (fig. 191.1). The existence of this thrust within the Carboniferous strata of the southern Diamond Mountains had long been suspected by T. B. Nolan (oral communication, 1956) and it has been delineated in recent detailed mapping.

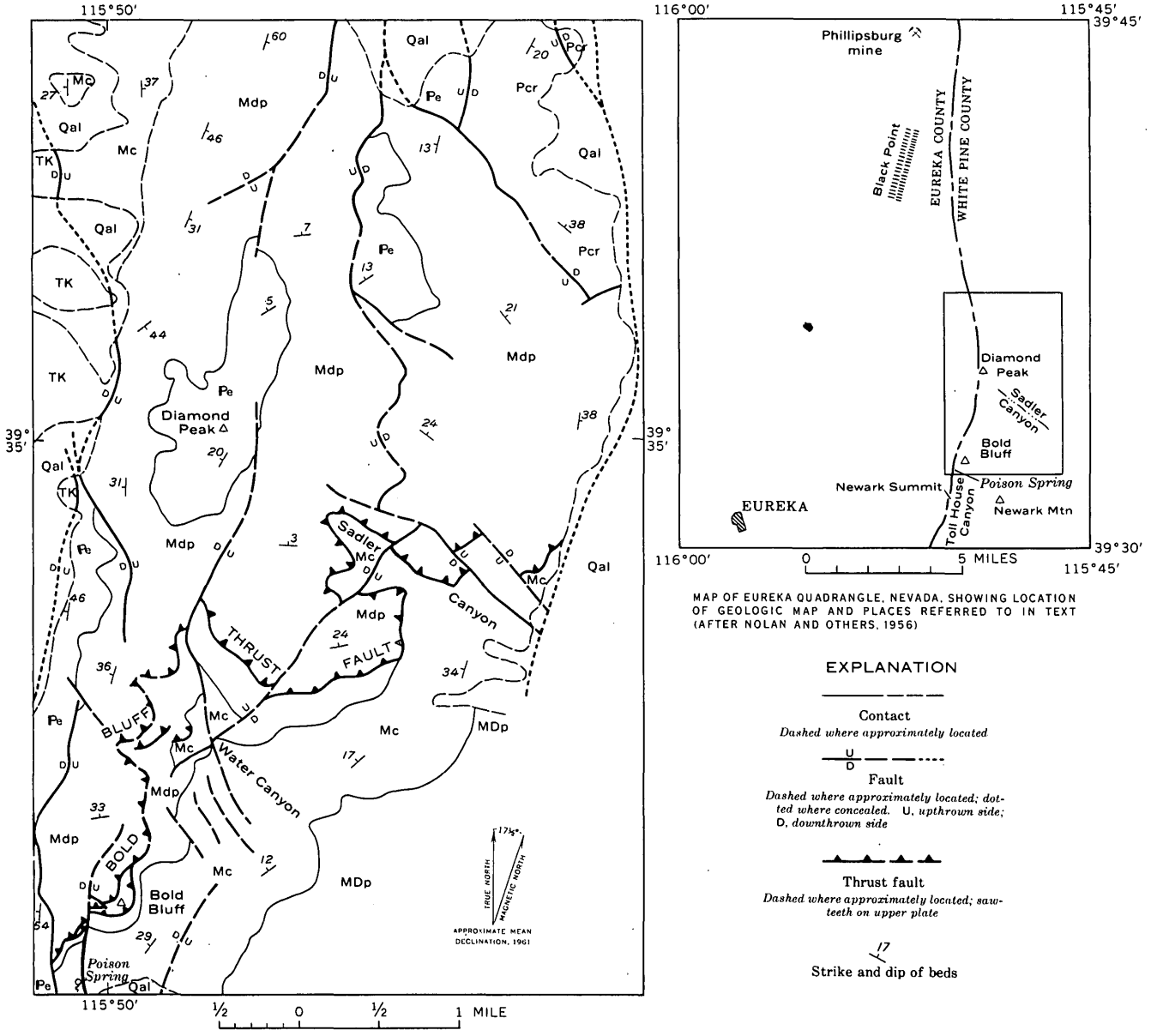

FIGURE 191.1.—Generalized geologic map of part of the southern Diamond Mountains, Eureka quadrangle, Nevada. Formations exposed within the map area are: MDp, Pilot shale of Devonian and Mississippian age; Mc, Chainman shale of Mississippian age; Mdp, Diamond Peak formation of Late Mississippian age; Pe, Ely limestone of Pennsylvanian age; Pcr, Carbon Ridge formation of Permian age; TK, undifferentiated Newark Canyon formation of Cretaceous age and megabreccias of Tertiary(?) age; and Qal, alluvium and colluvium of Quaternary age. Inset map shows other localities outside of the map area.

In the locality where it has been recognized, the thrust has brought siltstone, sandstone, conglomerate, and limestone of the Diamond Peak formation of Late Mississippian age over correlative siltstone and sandstone and also over highly deformed very dark claystone and siltstone ("black shales") of the Chainman shale of Mississippian age.

The thrust surface dips in general less than 10° to the west, but is locally horizontal and near Sadler Canyon dips about 13° north. The main thrust surface is not exposed but was located by the mapping of lithologic units within both the Chainman shale and Diamond Peak formation. Extensive slickensided surfaces, minor thrusts, and overturned folds in the lower part of the upper plate indicate that the relative movement of the upper plate was toward the southeast.

In the lower plate of the thrust are exposed (although not all are within the boundaries of fig. 191.1) the Nevada formation and Devils Gate limestone (Devonian); the Pilot shale (Devonian and Mississippian); the Joana limestone, Chainman shale, and the lower part of the Diamond Peak formation (Mississippian). In the upper plate within the map area are exposed the upper part of the Chainman shale; a complete section of the Diamond Peak formation; the Ely limestone (Pennsylvanian); the Carbon Ridge formation (Permian); and younger units. To the north of the map area, but within the upper plate of the thrust, are exposed the Lone Mountain dolomite

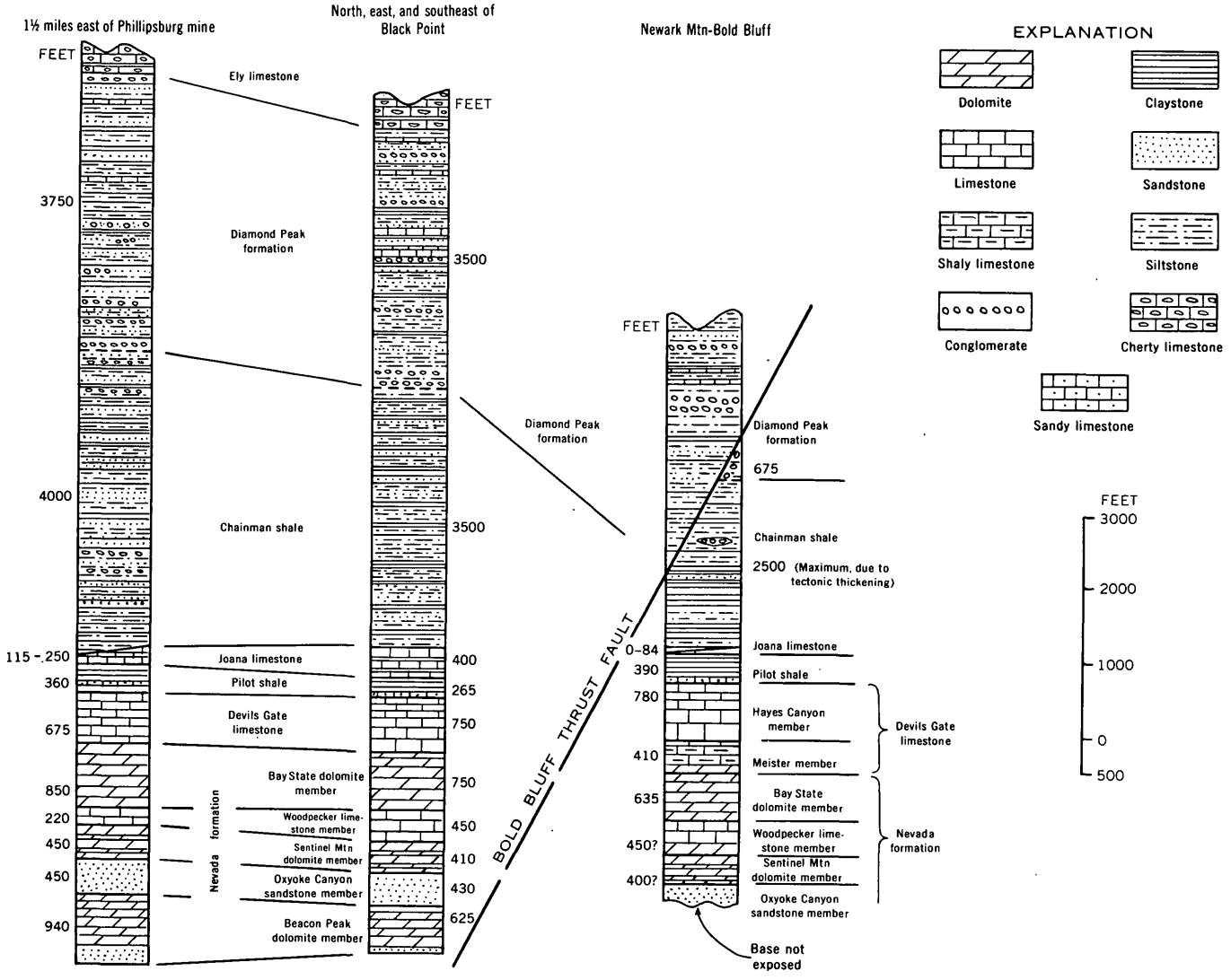

FIGURE 191.2.—Thickness and lithologic character of Devonian and Mississippian sections in the upper and lower plates of the Bold Bluff thrust fault. (Modified in part from Nolan and others, 1956.)

(Silurian) and all of the formations noted previously as occurring in the lower plate of the thrust. Nolan and others (1956) have discussed the stratigraphy of all these rocks.

All formations involved in the Bold Bluff thrust that are exposed in both plates show contrast in thickness, but the contrasts in thickness and lithologic character of the Chainman shale are the most striking (fig. 191.2). These differences were first commented on by Nolan and others (1956, p. 57–58). Possibly some of the variations in thickness are due to unrecognized low-angle faulting, folding, or both.

The difference in thickness of the Chainman shale, as shown on figure 191.2, is approximate because the Tollhouse Canyon section in the lower plate was obtained in an area of intense deformation and, as Nolan and others (1956, p. 57) point out, probably is tectonically thickened. In general, this "black shale" variety of Chainman, where known from less deformed exposures to the south of the area of figure 191.1 (Nolan and others, 1956, p. 57–58), is markedly thinner than in the Newark Summit area.

The thicker Chainman shale of the upper plate is exposed only 1½ miles west of the thinner section below the Bold Bluff thrust (fig. 191.1).

The Chainman shale and Diamond Peak formation of the upper plate of the Bold Bluff thrust have been differentiated on the basis of the relative proportions of conglomerate, sandstone, and siltstone, and by the presence of discontinuous, but nevertheless stratigraphically restricted, lithologic units. Nolan, Merriam, and Williams (1956, p. 57) did not separate the formations where they occur in the upper plate.

The contrast in lithologic character of the Chainman shale above and below the Bold Bluff thrust fault is as striking as the contrast in thickness described earlier. The Chainman of the upper plate consists of about 2 percent chert and quartzite pebble and cobble conglomerate, 24 percent brown and gray sandstone, 39 percent olive-gray and brown-weathering gray siltstone, and 35 percent dark-gray siltstone and claystone, which is lithologically similar to the Chainman of the lower plate. Any one section of the Chainman of the upper plate shows variations from these averages, with conglomerate most likely to be missing. Sandstone everywhere makes up at least 15 percent of the section and siltstone predominates over claystone in every section.

The Chainman shale of the lower plate of the Bold Bluff thrust, as exposed in the vicinity of Newark Summit, consists of about 90 percent pyritiferous claystone and clayey siltstone, with claystone dominant, and about 10 percent sandstone and conglomerate. The characteristic claystone and siltstone are uniformly medium dark gray to grayish black and weather to form distinctive angular brownish pencil-like fragments as much as 8 inches long and an inch in maximum diameter.

The contrast in lithologic character and thickness of the Chainman shale above and below the Bold Bluff thrust fault indicates that a somewhat coarser facies, deposited near the source area, has been thrust over a finer grained facies and suggests further that the coarser grained facies was originally significantly thicker than the more easterly, finer grained facies. Recognition of this shortening may assist in explaining some of the differences that exist between other formations that are present in both plates of the thrust.

REFERENCE

Nolan, T. B., Merriam, C. W., and Williams, J. S., 1956, The stratigraphic section in the vicinity of Eureka, Nevada: U.S. Geol. Survey Prof. Paper 276, 77 p.

192. MAJOR WESTWARD THRUSTING OF POST-MIDDLE TRIASSIC AGE IN NORTHWESTERN NEVADA

By RONALD WILLDEN, Menlo Park, Calif.

Work done in cooperation with the Nevada Bureau of Mines

A major thrust fault, here called the Quinn River thrust, on which the upper-plate rocks have been displaced westward at least 40 miles has been recognized at the south end of the Kings River Range in Humboldt County, Nev. (fig. 192.1). The fault is well exposed and is marked by a thick brecciated zone above the thrust plane. The upper-plate rocks are nonmetamorphosed limestone and fine-grained clastic rocks of Permian and Triassic age, which are lithologically quite different from rocks of the same age in the surrounding area. The lower-plate rocks are part of the mildly metamorphosed Happy Creek volcanic series of Permian or older age that is widely exposed in western Humboldt County.

Most of the Kings River Range is made up of middle Tertiary volcanic rocks, but pre-middle Tertiary intrusive rocks are exposed beneath the volcanics at the north end of the range and Permian and Triassic rocks are exposed on a low hill west of the range at its south end (fig. 192.2). Three of the four pre-Tertiary units recognized at the south end of the Kings River Range are in the upper plate of the Quinn River thrust. These upper-plate rocks include an unnamed fossiliferous limestone formation of Early Permian age about 1,000 feet thick. The limestone is overlain by about 400 feet of unfossiliferous mudstone, chert, and graywacke; this is in turn overlain by the Quinn River formation, which consists of silty shale with thin chert and carbonate beds and scattered thin gypsum beds. The Quinn River formation has an exposed thickness of about 600 feet and contains Middle Triassic pelecypods and ammonites.

Permian and, to a lesser extent, Triassic rocks in nearby areas are quite different from those in the Kings River Range (fig. 192.3, p. C–119). In the Jackson Mountains, Permian fossils have been collected from a siliceous recrystallized limestone in a thick sequence of interbedded graywacke, intermediate and mafic volcanic rocks, silty and cherty phyllite, pebble conglomerate, and some silty and sandy limestone. This sequence rests conformably on the Happy Creek volcanic series and grades upward into a thick unit, of probable Late Triassic age, consisting of phyllite and thin recrystallized chert and carbonate beds. In the Pine Forest Range a carbonate-clastic unit about 1,000 feet thick rests on the Happy Creek volcanic series. Fossils found in the lowermost limestone of this unit include *Isastraea*-like colonial hexacorals and radially ribbed carditoid pelecypods that indicate an early Mesozoic age (N. J. Silberling, written communication, 1956). This carbonate-clastic unit is overlain by a sequence of dark phyllite with abundant interbedded fine-grained quartzite. Rocks of Late Permian age, consisting of volcanic sediments with varying amounts of limestone, have recently been reported from Black Rock at the south end of the Black Rock Range by Gianella and Larson (1960).

Permian rocks are not exposed in the Trout Creek Mountains, the Slumbering Hills, and the Santa Rosa Range. The Triassic rocks in these ranges consist of phyllite, slate, and fine-grained quartzite, with some thin limestone beds.

Several formations of Permian age or partly of Permian age, which are essentially contemporaneous but have widely different lithologies, have been recognized in southeastern Humboldt County. These formations have been involved in repeated periods of deformation which are not yet completely understood. Thrust faults separate most of these formations from older and younger units, and their original sites of deposition can only be guessed, but all these Permian formations with the exception of the Koipato formation, which is probably at least in part younger than Permian (Roberts and others, 1958; Wallace and others, 1959) are completely lacking in volcanic material, just as are the Permian rocks of the upper plate in the Kings River Range. The Osgood Mountains section (fig. 192.3) illustrates the heterogeneity of the southeastern Humboldt County Permian formations.

All the pre-Cretaceous rocks in Humboldt County west of the line shown on figure 192.1 as the eastern limit of regional metamorphism have been metamorphosed to the greenschist facies or higher, except those on the upper plate of the Quinn River thrust. The volcanic rocks and the Jurassic diorite intrusives contain abundant chlorite, clinozoisite, epidote, and albite or sodic oligoclase. The shales have been converted to phyllites and slate with secondary cleavage that cuts across the bedding. In contrast, the shales of the Quinn River formation are not phyllitic and they lack secondary cleavage. The pebbles in the Permian and Triassic conglomerates in the western part of Humboldt County, particularly those in the

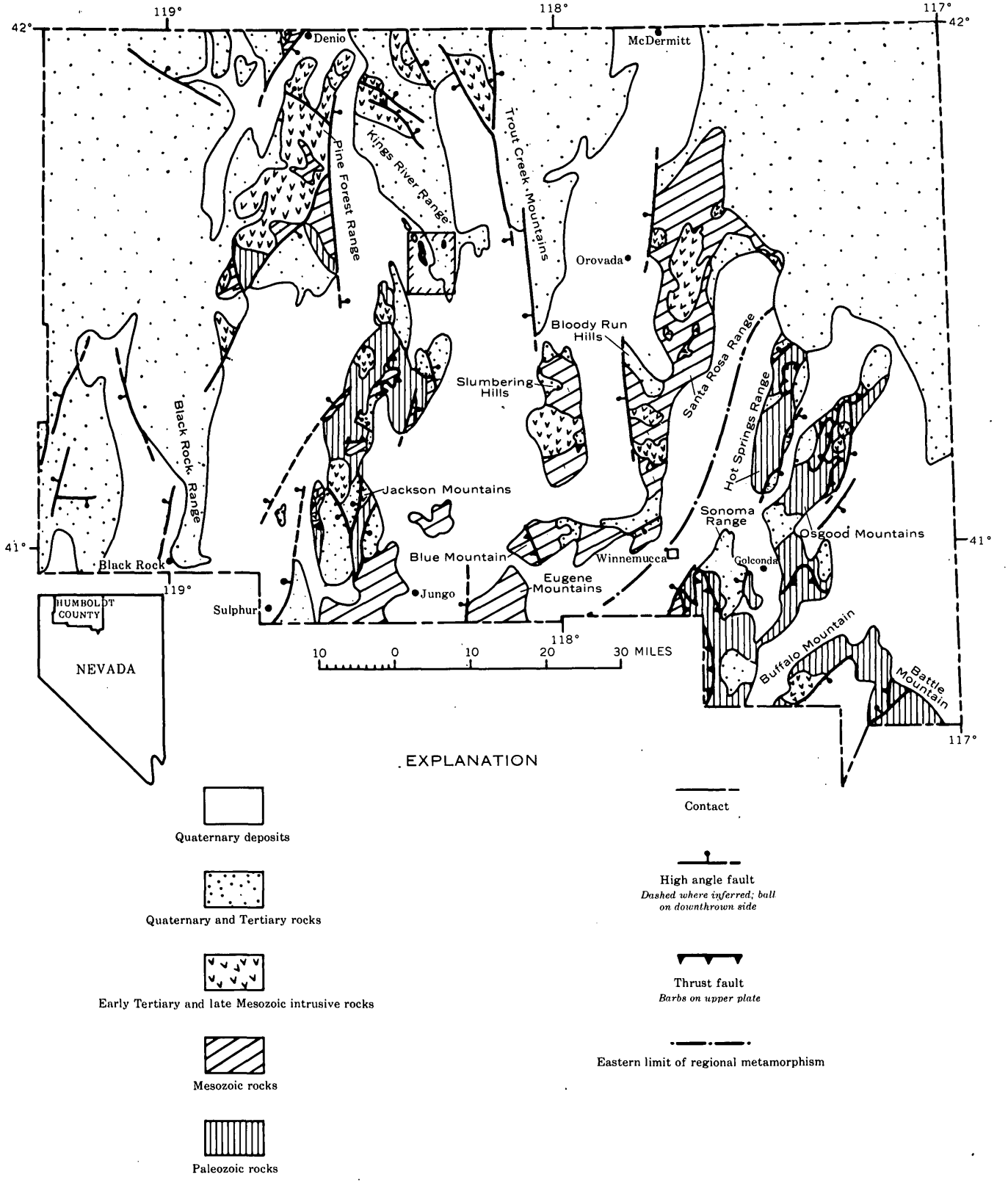

FIGURE 192.1.—Generalized geology of Humboldt County, Nevada, showing location of area shown on figure 192.2 at south end of Kings River Range.

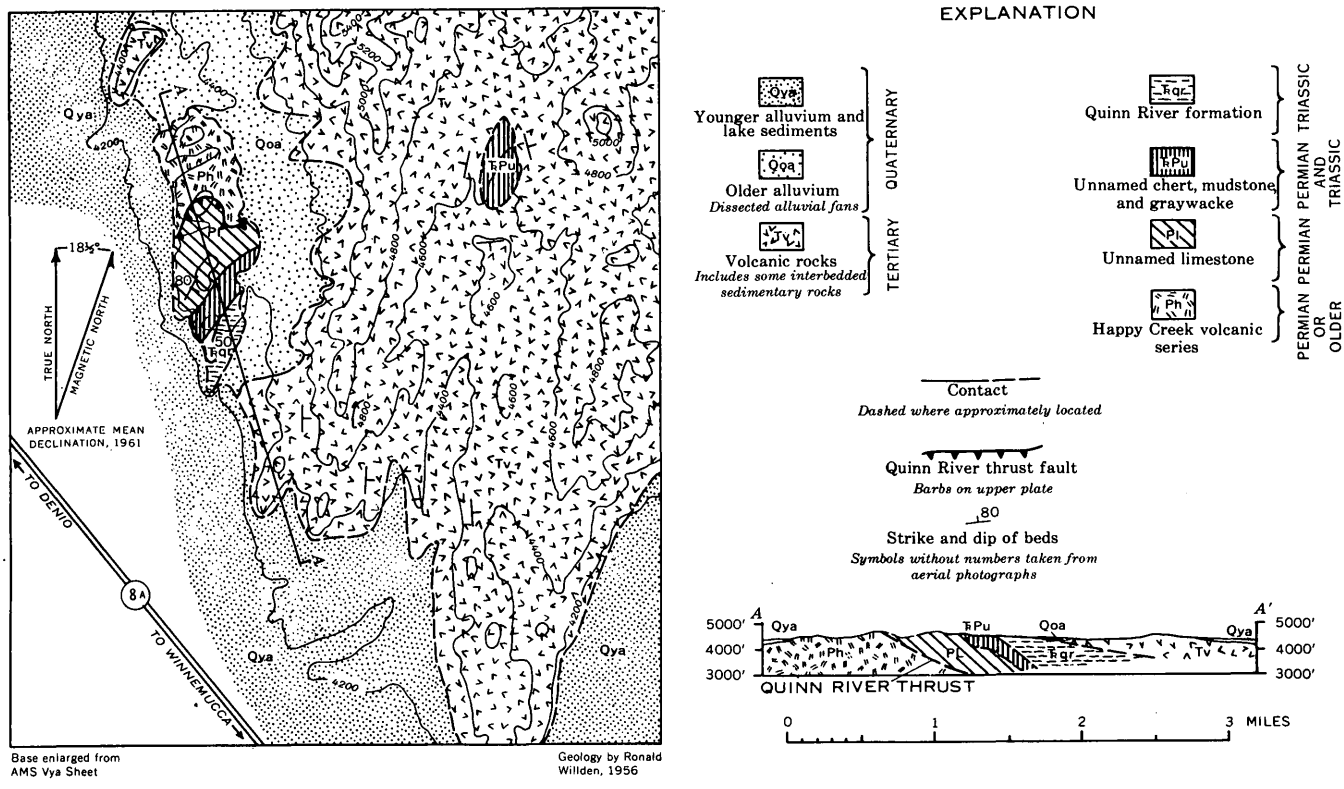

FIGURE 192.2.—Geology of the south end of the Kings River Range.

Jackson Mountains, have been flattened and stretched; whereas the conglomerates in the unnamed limestone unit in the Kings River Range are not deformed. At the Kings River Range locality, the limestones are not recrystallized, and they contain fairly well preserved fossils—in contrast to their usual recrystallized unfossiliferous condition elsewhere in western Humboldt County.

The lithologic similarities of the Permian rocks in the Kings River Range to those in southeastern Humboldt County—in particular the absence of volcanic material in the two areas and the absence of metamorphic effects in the Kings River Range rocks—indicate that rocks on the upper plate of the Quinn River thrust have been displaced westward at least 40 miles and possibly as much as 50 miles. The volcanic material and degree of metamorphism in the Permian section to the west in northern California seem to preclude the possibility that the displacement on the thrust has been from west to east.

The age of the thrusting can be fixed as younger than the regional metamorphism, which is younger than the intrusion of some diorites of probable Jurassic age in the Jackson Mountains, and older than the nonmetamorphosed King Lear formation of Early Cretaceous age (Willden, 1958). The Quinn River thrust probably developed as one phase of the orogenic episode that produced the mountainous terrane which was eroded to form the Cretaceous sediments of the King Lear formation.

Muller (1949) has postulated westward overthrusting of substantial magnitude—on the order of tens of miles—involving Upper Triassic rocks in the Sonoma Range one-degree quadrangle. Later Muller, Ferguson, and Roberts (1951) assigned this thrusting to a Jurassic orogeny. The Quinn River thrust is probably of the same age and has about the same direction and amount of displacement as postulated by these workers for some thrusts in the Sonoma Range.

REFERENCES

Ferguson, H. G., Muller, S. W., and Roberts, R. J., 1951, Geologic map of the Winnemucca quadrangle, Nevada: U.S. Geol. Survey Geol. Quad. Map GQ-11.

Gianella, V. P., and Larson, E. R., 1960, Marine Permian at Black Rock, Nevada [abs.]: Geol. Soc. America Bull., v. 71, p. 2061.

Muller, S. W., 1949, Sedimentary facies and geologic structures in the Basin and Range province, *in* Longwell, C. R., chm., Sedimentary facies in geologic history (symposium): Geol. Soc. America Mem. 39, 171 p.

Muller, S. W., Ferguson, H. G., and Roberts, R. J., 1951, Geology of the Mount Tobin quadrangle, Nevada: U.S. Geol. Survey Geol. Quad. Map GQ-7.

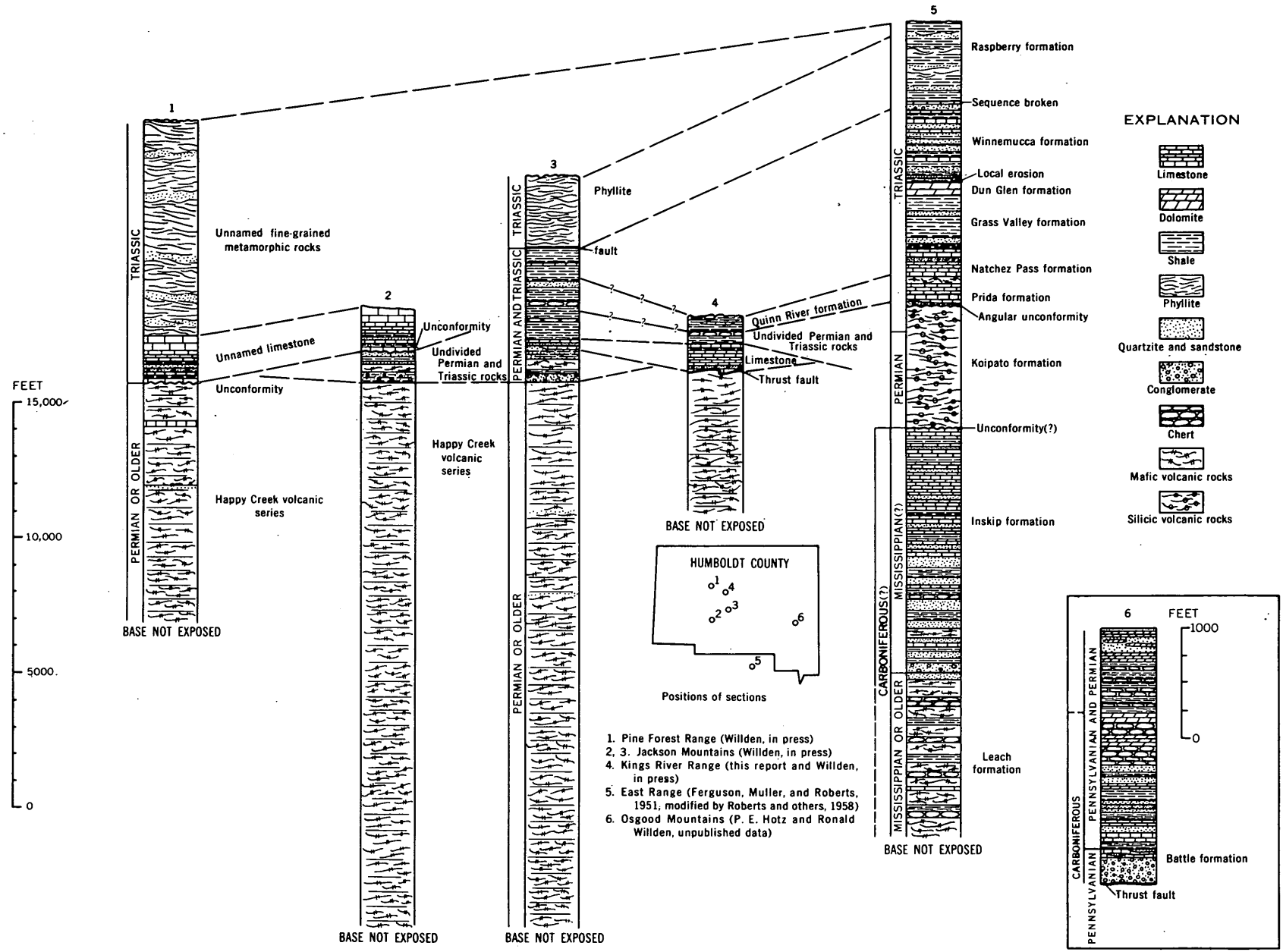

FIGURE 192.3.—Suggested correlation of the Permian and Triassic rocks of the Kings River Range with those in nearby areas.

Roberts, R. J., Hotz, P. E., Gilluly, James, and Ferguson, H. G., 1958, Paleozoic rocks of north-central Nevada: Am. Assoc. Petroleum Geologists Bull., v. 42, p. 2813–2857.

Wallace, R. E., Silberling, N. J., Irwin, W. P., and Tatlock, D. B., 1959, Preliminary geologic map of the Buffalo Mountain quadrangle, Nevada: U.S. Geol. Survey Min. Inv. Field Studies Map MF–220.

Willden, Ronald, 1958, Cretaceous and Tertiary orogeny in Jackson Mountains, Humboldt County, Nevada: Am. Assoc. Petroleum Geologists Bull., v. 42, p. 2378–2398.

——— in press, Geology of Humboldt County, Nevada: Nevada Bur. Mines Bull. 59.

193. GEOLOGY OF THE MOUNT WHEELER MINE AREA, WHITE PINE COUNTY, NEVADA

By Donald H. Whitebread and Donald E. Lee, Menlo Park, Calif.

Work done in cooperation with the Nevada Bureau of Mines

The occurrence of the beryllium minerals phenacite, bertrandite, and beryl at the Mount Wheeler mine in the Snake Range, White Pine County, Nev., has been described by Stager (1960). During the past year there have been additional discoveries of beryllium minerals and fluorite more than a mile north of the mine. This paper presents information on the areal geology, with particular emphasis on the limestone that is host to the beryllium minerals.

The area is underlain by the Prospect Mountain quartzite, Pioche shale, and Pole Canyon limestone, all of Cambrian age, which are folded into a broad anticline that plunges gently to the south; a quartz monzonite stock is exposed about three miles north of the Mount Wheeler mine (fig. 193.1).

The distribution and lithology of the Pioche shale are of particular interest because the known deposits of phenacite and bertrandite are in a limestone unit, locally known as the "Wheeler limestone," in the lower part of the Pioche. At the Mount Wheeler mine the beryllium is localized along quartz veinlets in the "Wheeler limestone" (Stager, 1960, p. 71). The deposit of phenacite, bertrandite, and beryl a mile north of the mine and several deposits of fluorite also are in this limestone.

The Pioche shale is chiefly yellowish brown to dark greenish gray, micaceous silty shale with minor limestone and quartzite in the lower part; fine-grained calcareous quartzite and interbeds and lenses of limestone make up the upper one-fourth of the formation. The Pioche is 450 feet thick on the north side of Pole Canyon and 330 feet thick on the south side of Dry Canyon; both sections are poorly exposed, and probably both are cut by faults. The contact between the Pioche shale and the underlying Prospect Mountain quartzite is gradational through a sequence of alternating quartzite and shale; the contact is mapped at the top of the uppermost light gray, resistant quartzite. Because of lateral variations in lithology, however, the contact may not be everywhere at the same horizon.

The "Wheeler limestone" unit of the Pioche shale is medium gray to dark bluish gray, thin- to thick-bedded limestone; some beds are bioclastic, and in places there are beds of sandy limestone. The limestone is commonly recrystallized, as at the portal of the Mount Wheeler mine, where it is light gray, coarsely crystalline marble. The limestone ranges in thickness from 8 feet to about 25 feet, and Stager (1960, p. 70) states that it is as much as 50 feet thick in the Mount Wheeler mine. Near the mine the "Wheeler limestone" is about 45 to 65 feet above the base of the Pioche, about 1 mile west of the mine it is 27 feet above the base, and in several places it is less than 20 feet above the base. An excellent exposure of the basal part of the Pioche on the crest of the range shows 11 feet of sandy limestone with irregularly interbedded shale about 10 feet above the base, and several beds and lenses of limestone and sandy limestone as much as 4 feet thick over an interval of 70 feet above the base. The variations described above raise the possibility that the "Wheeler limestone" as

601530 O—61—9

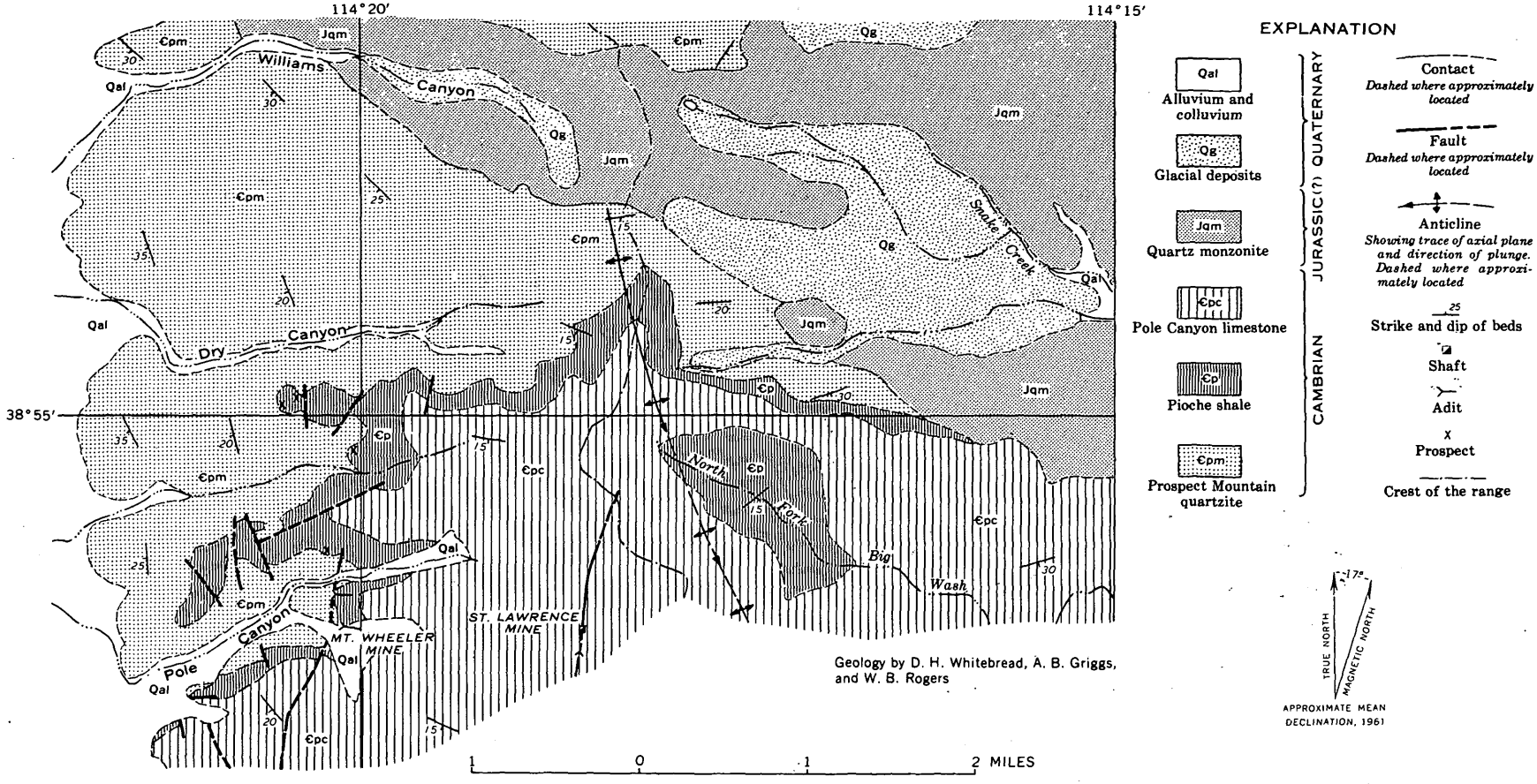

FIGURE 193.1.—Simplified geologic map of the area in the vicinity of the Mount Wheeler mine, Snake Range, White Pine County, Nev.

mapped may not be a continuous unit, but actually may consist of discrete lenses of limestone that may differ slightly in stratigraphic position, but that all occur within about a 70-foot zone above the base of the Pioche. A lateral change in the "Wheeler limestone" may be indicated along the adit of the Mount Wheeler mine, where Stager (1960, p. 70) reported that the limestone is almost completely silicified beyond 3,800 feet east of the portal. A thin section of one sample of this "silicified" rock shows it is fine-grained micaceous quartzite. The field relations have not been observed by the writers because poor ventilation prevented access to that part of the mine.

A possible source of the beryllium is the quartz monzonite stock, which is exposed as a westward-trending band 1 to 3 miles wide (fig. 193.1). On the west side of the range it intrudes the Prospect Mountain quartzite, but to the east it intrudes the Prospect Mountain, Pioche, and the lower part of the Pole Canyon formations. Cross sections based on surface maps indicate that the intrusive may extend to the south roughly concordant to the bedding in the overlying sedimentary rocks, and, if so, the intrusive may be on the order of 1,000 feet below the Mount Wheeler mine. No direct relation is apparent, however, between the mineralization of the limestone and the proximity of the intrusive. Throughout most of the area contact minerals are absent from the "Wheeler limestone"; but on the crest of the range, where the limestone is about 1,500 feet horizontally from the intrusive, light-green amphibole and light-green pyroxene are developed locally, and scheelite is disseminated in some beds. Quartz veinlets in recrystallized limestone probably will serve as the most useful guide to additional mineral deposits in the "Wheeler limestone." Prospecting in outcrop areas of this limestone is hindered, however, by the rubble that characteristically covers slopes underlain by the Pioche shale.

The search for beryllium minerals has been mainly confined to the "Wheeler limestone," but the possibility of beryllium minerals in other rocks should not be overlooked. Limestone apparently is the most favorable host rock for the beryllium minerals, as well as for the fluorite and scheelite. Perhaps the "Wheeler limestone" is a good host rock because, being the lowest limestone in the stratigraphic section, it would be the first to be encountered by ascending mineralizing solutions. Prospecting might be rewarding in younger limestones, particularly where the Wheeler is absent.

REFERENCE

Stager, H. K., 1960, A new beryllium deposit at the Mount Wheeler mine, White Pine County, Nevada, *in* Short papers in the geological sciences: U.S. Geol. Survey Prof. Paper 400–B, p. B70–B71.

194. TRITIUM-AGE OF GROUND WATER AT THE NEVADA TEST SITE, NYE COUNTY, NEVADA

By Alfred Clebsch, Jr., Washington, D.C.

Work done in cooperation with the U.S. Atomic Energy Commission

Estimates of the residence time of water in an aquifer are important to several problems in hydrology, particularly to questions concerning the movement of medium- and long-lived fission products in ground water. Methods of estimating the residence time by utilizing the natural distribution and radioactive decay rate of tritium, and increases in the tritium concentrations resulting from the testing of hydrogen bombs have been described by Libby (1953), Kaufman and Libby (1954), von Buttlar and Libby (1955), and von Buttlar and Wendt (1958).

Tritium in the ground water from the Nevada Test Site and vicinity suggests a much shorter residence time for water in perched aquifers than for water in the main aquifer. Analyses of water samples collected in 1958 and 1959 from a tunnel, a spring, and five wells (fig. 194.1) are reported in table 194.1. The samples from the tunnel and the spring are from perched aquifers.

In estimating the residence time for the water (underground or in the aquifer), an average pre-hydrogen bomb tritium concentration of greater than 8

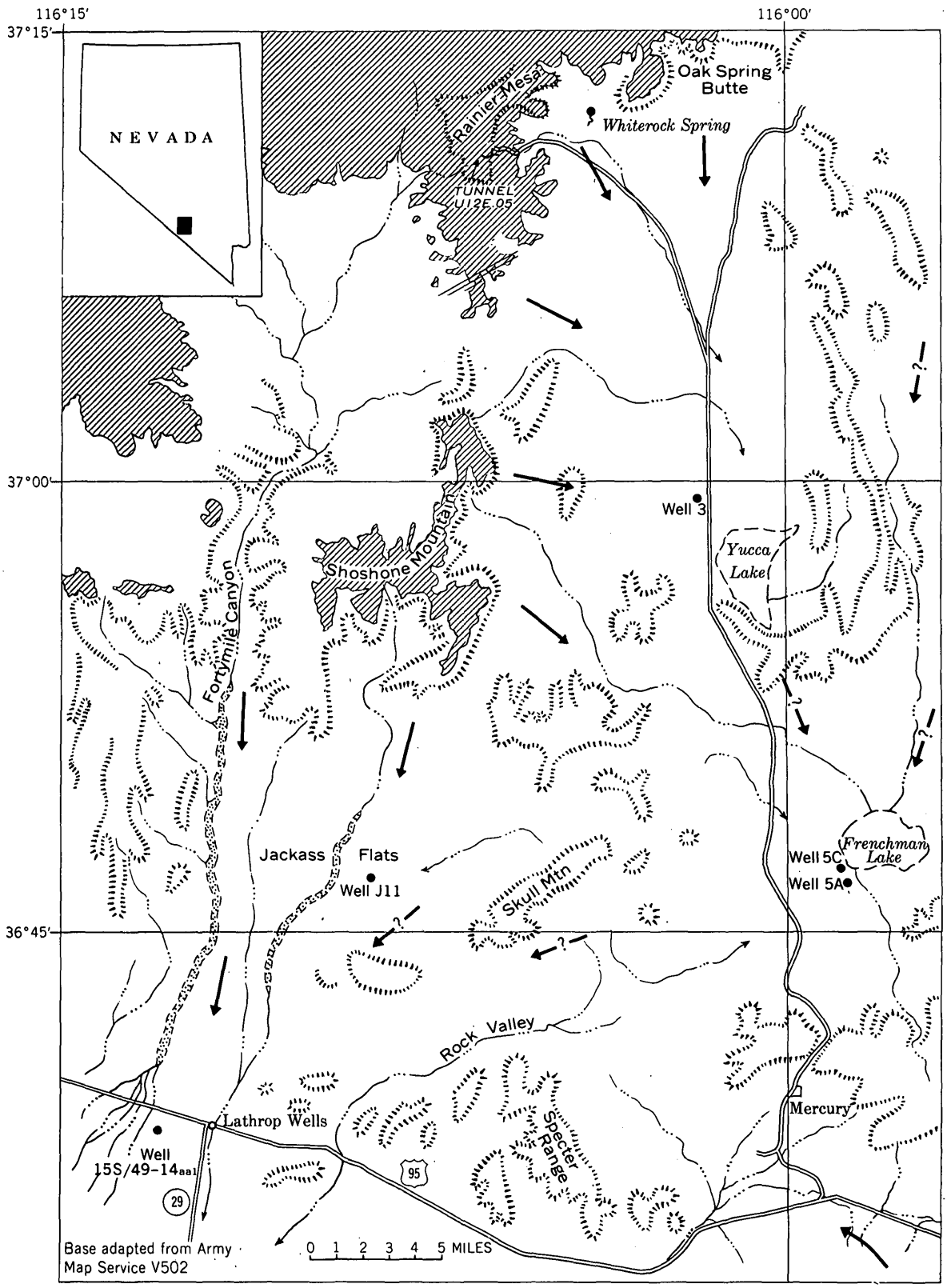

FIGURE 194.1.—Map of the Nevada Test Site and vicinity showing tunnel, wells, and springs sampled for tritium analysis, and inferred directions of ground-water movement. Shaded areas are higher than 6,000 feet above sea level. Hachures indicate steep slopes.

TABLE 194.1.—*Tritium analyses of water samples from the Nevada Test Site and vicinity*

[Analyses by L. L. Thatcher, U.S. Geological Survey; analyses completed June 28, 1960]

Sample location	Aquifer	Date of sampling	Concentration (T units)[1]	Estimated residence time[2] (years)
Well 3	Oak Spring formation	8- 7-58	<0.5	>50
Do	do	4-21-59	<.5	>50
Well 5A	Alluvium	2-26-59	<.5	>50
Well 5C	do	2-26-59	<.5	>50
Well J 11	Oak Spring formation	8- 7-58	<.5	>50
Do	do	4-21-59	<.5	>50
Well 15S/49-14aa1	Alluvium	1-28-59	<.5	>50
Whiterock Spring	Oak Spring formation	8- 7-58	34	< 6 >0.8
Tunnel U12e.05	do	9-12-58	36	< 6 >0.8

[1] One tritium unit equals 1 atom of tritium per 10^{18} atoms of protium.
[2] Based on an average pre-1952 tritium concentration in precipitation of >8 <35 T units.

T-units (tritium units; one T-unit equals 1 atom of tritium per 10^{18} atoms of protium) and less than 35 T-units is assumed, based on analyses of Chicago precipitation by Kaufman and Libby (1954) and von Buttlar and Libby (1955). The only pre-hydrogen bomb tritum analyses of precipitation available are those made at Chicago.

The tritium analyses (table 194.1) indicate that water in the aquifers tapped by supply wells on the Nevada Test Site and one nearby off-site well had an apparent residence time of more than 50 years. If the natural tritium level was higher than 8 T-units, water from all the wells sampled would be older than indicated in table 194.1. On the other hand, water in perched aquifers in the high areas has been recharged since 1952, as indicated by the tritium samples from Whiterock Spring and tunnel U12e.05 (site of the Blanca explosion of October 30, 1958).

Since the fall of 1952 the tritium content of atmospheric water has been highly variable as a result of hydrogen-bomb tests. The first increase in tritium concentration due to bomb testing resulted in a concentration of tritium in precipitation of 66±1 T-units at Chicago on November 18, 1952. In the periods March-July 1954 and March-September 1956, tritium in Chicago rainfall exceeded about 100 T-units and between December 18, 1957, and July 29, 1958, the tritium level in Chicago rain and snow (and presumably in Nevada precipitation) ranged from a minimum of 54.0 T-units to a maximum of 2160.0 T-units (Barrett and Huebner, 1960). Between these "peaks" the tritium level decreased considerably, sometimes to less than 10 T-units.

Many different mixtures of old water with water that entered the aquifer since 1952 might result in the tritium concentration shown by the samples of perched water, but if the aquifers had been recharged significantly during one of the "peaks," the tritium concentration should have been higher.

The above interpretations are somewhat tentative because they are based almost entirely on the tritium concentration in Chicago precipitation, and there may have been geographic variations that would invalidate the interpretations (C. W. Carlston, U.S. Geol. Survey, written communication, January 16, 1961). Geographic variations seem unlikely, however, in view of the general agreement found by von Buttlar and Wendt (1958) between their analytical data for precipitation in New Mexico, and the analytical data for precipitation in Chicago.

Underground nuclear tests in Rainier Mesa (fig. 194.1) produced strontium–90 that has been taken into solution by perched ground water (Clebsch and Barker, 1960). It is important to know whether the contaminated water is likely to reach wells that are utilized for water supplies and what the concentration of contaminants might be when the ground water reaches the wells. This requires a knowledge of the rates and directions of ground-water movement, both of which are poorly known at present. The tritium-age interpretations, however, provide a basis for estimating the minimum time required for movement—and certain inferences can be drawn about the directions of movement.

One may infer that the Rainier Mesa-Shoshone Mountain highland is an area of ground-water replenishment, inasmuch as orographic effects should result in appreciably greater precipitation on the mountains than that measured in the adjacent valleys and closed basins. In 1960 the precipitation was 8–9 inches on Rainier Mesa and 4–5 inches in Yucca Valley and Jackass Flats. One may also infer that much of the perched water ultimately reaches the main aquifer, because of the scarcity and small discharge of nearby springs and virtual absence of vegetation dependent upon ground water. The natural discharge area for this hydrologic system probably is the Ash Meadows-Death Valley Junction area south of Lathrop Wells (Clebsch, 1960). A generalized interpretation of the probable flow pattern is shown on figure 194.1.

If perched water contaminated with strontium–90 moves to one of the wells sampled, 40 years or more will be required for travel. In this time, the strontium–90 activity would have been reduced to about 35 percent of its concentration at the site of the explosion by radioactive decay alone. Physical and chemical

processes such as diffusion, dispersion, and ion exchange should further reduce the concentration of activity, possibly by several orders of magnitude.

REFERENCES

Barrett, E. W., and Huebner, Leonid, 1960, Atmospheric tritium analysis: Chicago Univ., Tech. Progress Rept. No. 2, Contract AT (11–1)–636, Feb. 16.

Clebsch, Alfred, Jr., 1960, Ground water in the Oak Spring formation and hydrologic effects of underground nuclear explosions at the Nevada Test Site: U.S. Geol. Survey TEI 759, 29 p. (Available from Office of Tech. Services, U.S. Dept. Commerce, Washington 25, D.C.)

Clebsch, Alfred, Jr., and Barker, F. B., 1960, Analyses of ground water from Rainier Mesa, Nevada Test Site, Nye County, Nevada: U.S. Geol. Survey TEI 763 (open-file rept.) 22 p.

Kaufman, Sheldon, and Libby, W. F., 1954, The natural distribution of tritium: Phys. Rev., v. 93, no. 6, p. 1337–1344, March 15.

Libby, W. F., 1953, The potential usefulness of natural tritium: [U.S.] Natl. Acad. Sci. Proc., v. 39, p. 245–247.

von Buttlar, Haro, and Libby, W. F., 1955, Natural distribution of cosmic-ray produced tritium II: Inorg. Nucl. Chem. Jour., v. 1, no. 1, p. 75–91.

von Buttlar, Haro, and Wendt, Immo, 1958, Ground-water studies in New Mexico using tritium as a tracer: Am. Geophys. Union Trans., v. 39, no. 4, p. 660–668.

195. PROPOSED CLASSIFICATION OF GROUND-WATER PROVINCES, HYDROLOGIC UNITS, AND CHEMICAL TYPES OF GROUND WATER IN THE UPPER COLORADO RIVER BASIN

By David A. Phoenix, Salt Lake City, Utah

In 1958, the Geological Survey started the Upper Colorado River hydrologic studies project to gather and analyze information about the water resources of the upper basin in order to provide a basis for intelligent planning of future water developments in the basin.

Work on the phases of the project concerned with ground water has resulted in (a) the division of the upper basin into 6 ground-water provinces; (b) a broad grouping of the rocks into 7 hydrologic units, each defined in terms of its potential ground-water yield; and (c) a classification of ground waters from springs, and from wells mostly less than 1,500 feet deep, by their content of dissolved solids.

The six ground-water provinces (fig. 195.1) recognized in the upper basin facilitate descriptions of the occurrence and chemical character of the ground water. The provinces, which differ from those of Meinzer (1923, p. 309–310), are based mainly upon the geology, and are separated in most places by ground-water divides. Four of the provinces, the Green River-Washakie, the Uinta-Piceance, the San Juan, and the Black Mesa are large structural basins in which the general occurrence and quality of ground water are similar and relatively uniform. Permeable beds receive ground-water recharge in the peripheral areas of these provinces and contain mineralized ground water under artesian pressure in the central areas. In the Canyon Lands province the strata are more complexly folded and locally are intruded by igneous rocks. In the Rocky Mountain province, granite, metamorphic, and volcanic rocks yield small supplies of excellent water, largely from joints. The sedimentary rocks in this province yield water to springs along the outcrops and to wells near the outcrops.

The water-bearing rocks in the upper basin, including the consolidated rocks in almost 200 formations and the alluvium along the flood plains and stream terraces, can be grouped into seven major units according to their geologic and hydrologic properties.

Unit 1, the alluvium which is found in all the provinces, is recharged during periods of high stream flow, and during the irrigation season much of this water returns to the streams laden with sodium, chloride, and sulfate, and in some areas nitrate. Three of the seven hydrologic units, units 2, 3, and 5, consist chiefly of thick deposits of shale and siltstone, which cover about 70 percent of the region to great depths. They yield but little water and serve mainly to confine artesian water in underlying aquifers. In some places shallow wells in these units yield small amounts of water for livestock, but the water generally is highly mineralized except near recharge areas. The sandstone of

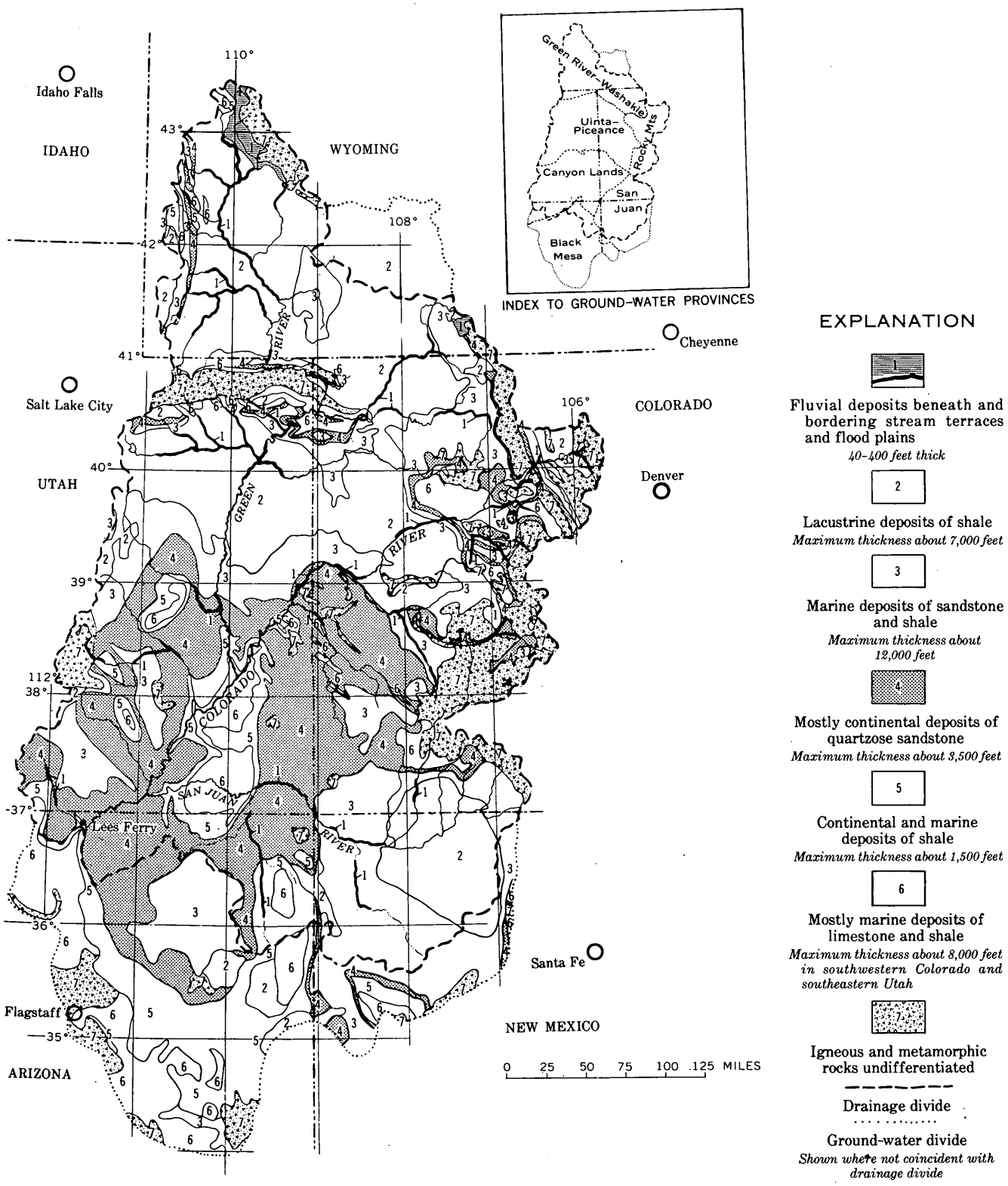

FIGURE 195.1.—Maps showing ground-water provinces and major hydrologic units in the Upper Colorado River Basin.

unit 4 yields water to flowing artesian wells in many parts of the Canyon Lands, Black Mesa, San Juan and Uinta-Piceance provinces. The water generally is of good quality within a few miles of the recharge areas, but at greater distance from the outcrop the water locally is too highly mineralized for most uses. Over large areas, particularly in the Canyon Lands province, the sandstones are deeply dissected and much or all of the water is drained out. The oldest sedimentary rocks in the region, in unit 6, comprise aquifers that differ greatly from place to place. In parts of the Canyon Lands province where the rocks contain saline minerals they yield only brine; but in the Rocky Mountain and Black Mesa provinces, where limestone or sandstone is the dominant rock, they locally yield supplies of water suitable for domestic, stock, and municipal needs. Unit 7, composed of igneous and metamorphic rocks, is restricted mostly to mountainous areas in all the provinces. In places where they are weathered or jointed, these rocks yield small supplies of excellent water; elsewhere they are generally unproductive.

The rocks of the Rocky Mountain province contribute water of excellent quality to the streams. The rocks in most other provinces, particularly those including shales of marine origin, contribute considerable amounts of dissolved solids to the streams. Thus, during periods of low streamflow, when the flow of the Colorado River and its tributaries consists almost wholly of ground-water discharge, the water becomes progressively harder and more concentrated in dissolved solids toward the mouth of the upper basin.

The water-bearing strata in each of the hydrologic units yield water that differs chemically from place to place, depending upon the source of supply, distance, and rate of ground-water movement, and the mineralogy of the aquifers. However, a study of about 1,000 analyses of ground water indicates that the waters in all the units are characterized by the dominance of one cation and one anion, and the sequence of chemical types is almost the same for all seven units. In order of increasing concentration of dissolved solids the dominant ions are: less than 300 ppm (parts per million) of dissolved solids, calcium and bicarbonate; 300–700 ppm, sodium and bicarbonate; 700–3,500 ppm, sodium and sulfate; and more than 3,500 ppm, sodium and chloride. Bicarbonate also is present in waters having total concentrations up to about 5,500 ppm, but is not a major constituent, and sulfate also is present in waters having total concentrations up to 10,000 ppm. This progressive increase of total dissolved solids in the water results in chemical changes that ultimately make the water unfit for use.

The aquifers in the Upper Colorado River Basin are not highly productive, so the larger cities and towns must rely on surface-water supplies. However, the limited supplies of ground water are of considerable value for domestic and stock supplies and small industrial or town needs, and additional supplies can be developed in many places where supplies of surface water are not available.

REFERENCE

Meinzer, O. E., 1923, The occurrence of ground water in the United States, with a discussion of principles: U.S. Geol. Survey Water-Supply Paper 489, 321 p.

196. METAMORPHISM AND STRUCTURAL HISTORY OF THE COAL CREEK AREA, FRONT RANGE, COLORADO

By JOHN D. WELLS, DOUGLAS M. SHERIDAN, and ARDEN L. ALBEE, Denver, Colo., and Pasadena, Calif.

Three periods of deformation and metamorphism during Precambrian time, one of which was accompained by igneous intrusion, produced the quartzite, schist, and gneiss of the Coal Creek area (fig. 196.1).

A simplified geologic map of the Coal Creek area (fig. 196.2) shows the major lithologic groups. The metasedimentary rock units included in table 196.1 are combined into groups, as shown in the explanation of figure 196.2, that have similar gross lithologic features. The igneous rocks are grouped as one unit. Rocks are grouped into the cataclastic rock unit where cataclasis is so extreme that the original unit cannot be recognized.

The quartzite and schist in quartzite occur in the central and northern parts of the area and outline the northeast-plunging Coal Creek syncline. South of

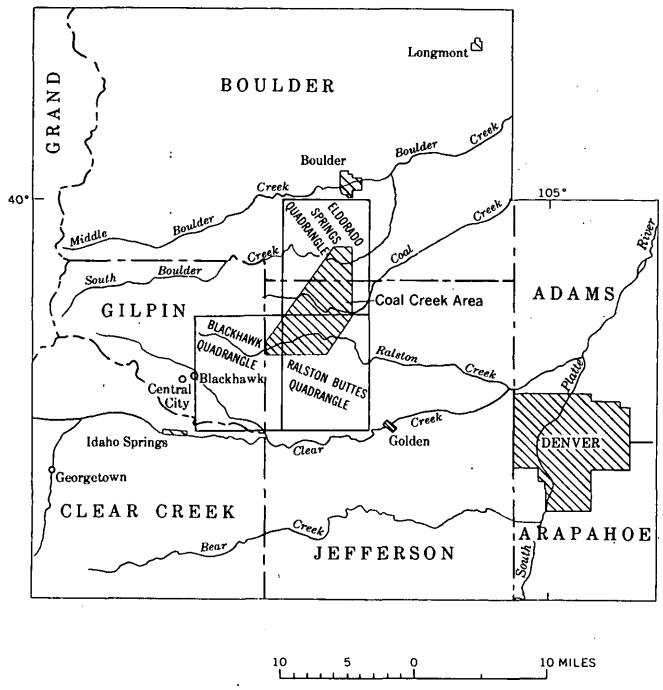

FIGURE 196.1.—Index map showing location of the Coal Creek area, Colo.

this quartzite and schist mass is a succession including biotite-quartz-plagioclase gneiss, microcline-quartz-plagioclase-biotite gneiss, lime silicate rocks, amphibolite, and schist typical of the Idaho Springs formation.

The igneous rocks consist almost exclusively of two units: a part of the Boulder Creek batholith and a younger quartz monzonite. These are present southeast and northwest of the Coal Creek syncline. Very small amounts of pegmatite, aplite, and hornblendite and associated hornblende diorite are present, but these are not significant in this discussion and will not be considered further.

The rocks of the Boulder Creek batholith are medium grained and gray, ranging in composition from quartz monzonite to quartz diorite, and consisting essentially of quartz, feldspar, and biotite. The quartz monzonite unit is fine grained and tan, ranging in composition from granite to granodiorite, and consisting essentially of quartz, feldspar, biotite, and muscovite. The quartz monzonite contains inclusions of the Boulder Creek rocks and, therefore, is younger. These rocks, however, are intimately mixed with irregular mutual contacts and interdiking relations, and both units have about the same structural history. These factors indicate that these rocks are closely associated in time and origin.

The igneous and metasedimentary rocks have been granulated in varying degrees of intensity in the northeast-trending cataclastic zone (fig. 196.2), which is as much as 1.5 miles wide. This cataclastic zone is considered to be part of the Idaho Springs-Ralston shear zone (Tweto and Sims, 1960).

Upturned Paleozoic and Mesozoic sedimentary rocks flank the area on the east side. The northwest-trending faults show Laramide movement.

The earliest recognized period of Precambrian deformation was plastic folding which formed mineral lineations that plunge predominantly south-southwest. These lineations are in the metasedimentary rocks but not in the igneous rocks. The second recognized period was plastic folding that (a) warped the south-southwest plunging mineral alinements, (b) formed the Coal Creek syncline which plunges east-northeast and minor folds that locally plunge west-southwest, and (c) formed mineral lineations in the metasedimentary and igneous rocks that plunge nearly south.

The intrusion of the igneous rocks accompanied the second period of folding. These rocks cut the folded quartzite and schist and engulfed large bodies of them; Boulder Creek rocks intruded the Coal Creek syncline and formed a phacolith. The igneous rocks were deformed by pervasive, minor cataclasis, possibly as a result of differential movement near the quartzite contact and were folded to a minor extent. The parallelism of the nearly south-plunging mineral alinements in the metasedimentary and igneous rocks indicates that alinements in both rocks were formed by the same deformation.

The third period of deformation formed the cataclastic zone south of the axis of the Coal Creek syncline. The foliation formed by this deformation cuts layering in the metasedimentary rocks and earlier formed foliation in the igneous rocks. This deformation obilterated all preexisting structures in some areas and modified structures in others.

Metamorphism of the Coal Creek area is believed to be closely related to the structural and intrusive history. The metamorphic rocks fall into three categories that are correlative with the three periods of structural deformation: (a) rocks containing mineral assemblages of high-grade regional metamorphism formed during the first two periods of deformation; (b) rocks containing new high-grade mineral assemblages in part superimposed on earlier assemblages, suggesting fluctuations in pressure, temperature, and other variables during a complex history of folding and intrusion; and (c) rocks in which the earlier high-grade mineral assemblages were modified texturally and structurally by cataclasis, and variably recrystallized but with only minor retrogression.

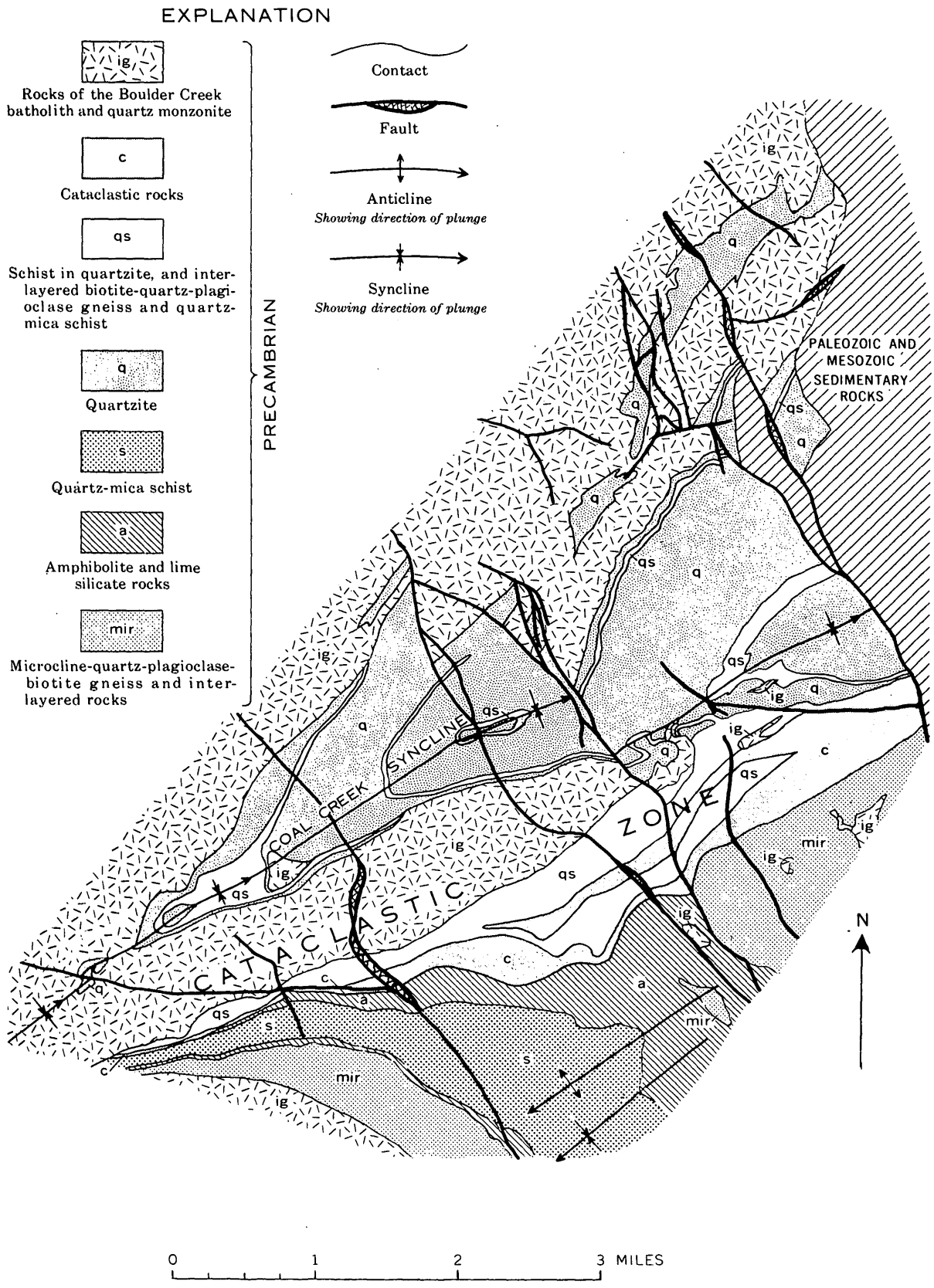

FIGURE 196.2.—Simplified geologic map of the Coal Creek area.

Most of the mineral suites of the Coal Creek area are typical of the gneiss and schist of the Idaho Springs formation and are common and widespread in the east-central Front Range. These mineral suites and the relatively uncommon suites from the quartzite and schist in the Coal Creek area are shown in table 196.1, which lists the significant minerals in each metasedimentary rock type followed by notes on their paragenetic relations.

The common mineral suite of muscovite with sillimanite (category 1) is correlative with the lower sillimanite zone (Heald, 1950, and Thompson, 1957)

TABLE 196.1.—*Suites of significant minerals in each metasedimentary rock type with notes on paragenesis*

[Note: Quartz is present in all specimens except amphibolite]

Microline-quartz-plagioclase-biotite gneiss and interlayered rocks: Microcline, plagioclase (oligoclase), biotite, epidote. (hornblende, garnet—from Ralston Buttes quadrangle)

Amphibolite and lime silicate rocks:
- Hornblende, plagioclase (andesine), epidote, clinopyroxene, calcite. (garnet, cummingtonite, tremolite, microcline, scapolite, vesuvianite—from Ralston Buttes quadrangle)

Quartz-mica schist:
- Muscovite, biotite, plagioclase (oligoclase), sillimanite, garnet (mostly almandine), andalusite, microcline.
  - Sillimanite needles in microline and muscovite.
  - Sillimanite needles replacing biotite.
  - Fine-grained muscovite replacing sillimanite glomeroporphyroblasts.
  - Biotite and muscovite pseudomorphous after staurolite.
  - Sillimanite, instead of andalusite, common south of Coal Creek area.

Interlayered biotite-quartz-plagioclase gneiss and quartz-mica schist:
- Muscovite, biotite, plagioclase (oligoclase), microcline, sillimanite, andalusite.
  - Sillimanite needles in muscovite and microcline.

Quartzite:
- Muscovite, andalusite, plagioclase, microcline (detrital), sillimanite, biotite.
  - Muscovite replacing biotite in specimen with andalusite.
  - Sillimanite replacing muscovite a fraction of a millimeter from andalusite.

Schist in quartzsite:
- Muscovite, biotite, plagioclase (oligoclase), cordierite, andalusite, garnet (spessartite and almandine), staurolite.
  - Andalusite, younger; poikilitically includes staurolite and some biotite and muscovite; almandine garnet nearby.
  - Cordierite about same age as andalusite, both of which are younger than early folding inasmuch as cordierite poikilitically includes folds.
  - Transverse orientation of biotite.

Lime silicate-quartz rock in schist in quartzite (in bodies too small to be shown on figure 196.2):
- Epidote, plagioclase (oligoclase-andesine), microcline, tremolite, garnet.

while the local occurrence of the critical assemblage sillimanite with microcline (category 1) indicates that the highest metamorphic grade reached is correlative to the higher sillimanite zone. Inasmuch as sillimanite is both replaced by and replaces micas, multiple generations of these minerals must have occurred. The earliest crystallization of sillimanite cannot be determined with certainity, but it must have occurred as early as the second and possibly the first deformation. During the second deformation andalusite and cordierite (category 2) crystallized poikiloblastically. Poikilitic inclusions of staurolite (category 1), as well as opaque minerals, quartz, and muscovite that outline microfolds, are probably relicts of the first deformation. It seems likely that the andalusite and cordierite were formed at the time that the igneous rocks were intruded. The position of andalusite relative to sillimanite and kyanite (Thompson, 1955, fig. 3, p. 97) suggests that this period was characterized by relatively lower pressure and (or) relatively lower temperature than during metamorphism when sillimanitic schist was formed.

There seems to be some spatial relation between the distribution of andalusite, sillimanite, and quartz monzonite. Andalusite is abundant in the quartzite and schist along Coal Creek, where both the quartz monzonite and the Boulder Creek rocks are abundant, but sillimanite rather than andalusite is found where only Boulder Creek rocks are exposed farther south in the Ralston Buttes quadrangle.

Despite this spatial relation, these rocks are not true contact metamorphic rocks; no typical contact metamorphism is noted at the igneous contacts. Only a thin micaceous selvage is formed along the contact with the quartzite and no effect is seen in other rock types. The various "contact" and "regional" suites are interlayered, and they extend over rather large areas. We suggest that the observed mineralogic differences are caused by different metamorphic environments, probably related to the syntectonic intrusive activity.

The late Precambrian cataclastic deformation mechanically deformed part of the metasedimentary and igneous rocks. The cataclasis reduced the grain size and changed the texture; some rocks were recrystallized (category 3). Late poikilitic muscovite crystallized with biotite and a few needles of sillimanite. Potassic feldspar became more perthitic and all feldspars became less well-twinned than before. Late microcline filled small fractures. Only minor retrogression accompanied cataclasis, more muscovite was formed and, locally, chlorite replaced biotite.

REFERENCES

Heald, M. T., 1950, Structure and petrology of the Lovewell Mountain quadrangle, New Hampshire: Geol. Soc. America Bull., v. 61, p. 43–89.

Thompson, J. B., Jr., 1955, The thermodynamic basis for the mineral facies concept: Am. Jour Sci., v. 253, no. 2, p. 65–103.

——— 1957, The graphical analysis of mineral assemblages in pelitic schists: Am. Mineralogist, v. 42, p. 842–858.

Tweto, Ogden, and Sims, P. K., 1960, Relation of the Colorado Mineral Belt to Precambrian structure, *in* Short papers in the geological sciences: U.S. Geol. Survey Prof. Paper 400–B, p. B8–B9.

197. EARLY AND LATE GROWTH OF THE GYPSUM VALLEY SALT ANTICLINE, SAN MIGUEL COUNTY, COLORADO

By E. R. Landis, E. M. Shoemaker, and D. P. Elston, Denver, Colo., and Menlo Park, Calif.

Work done in cooperation with the Division of Research, U.S. Atomic Energy Commission

The Gypsum Valley salt anticline in southwestern Colorado is one of the major salt anticlines of the Paradox basin (fig. 197.1). Detailed structural, stratigraphic, and paleontologic investigations in southeastern Gypsum Valley indicate that the earliest stages of growth of the salt structure occurred in Middle Pennsylvanian (Des Moines) time, and that the latest stages of growth appear to have occurred in Late Cretaceous (upper Carlile and Niobrara) time. Unconformable relations between the leached cap of the

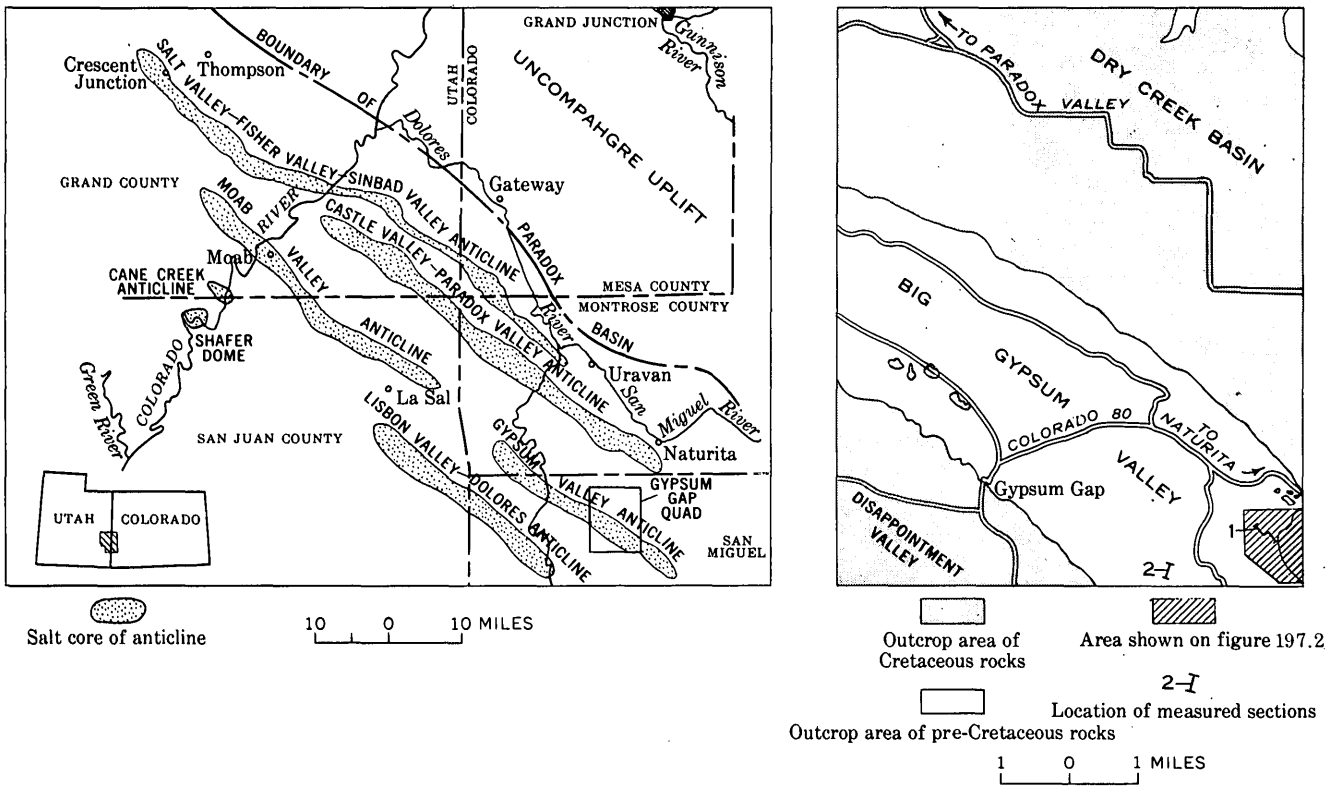

FIGURE 197.1.—Index maps of salt anticline region, Utah and Colorado, and the Gypsum Gap quadrangle, Colorado.

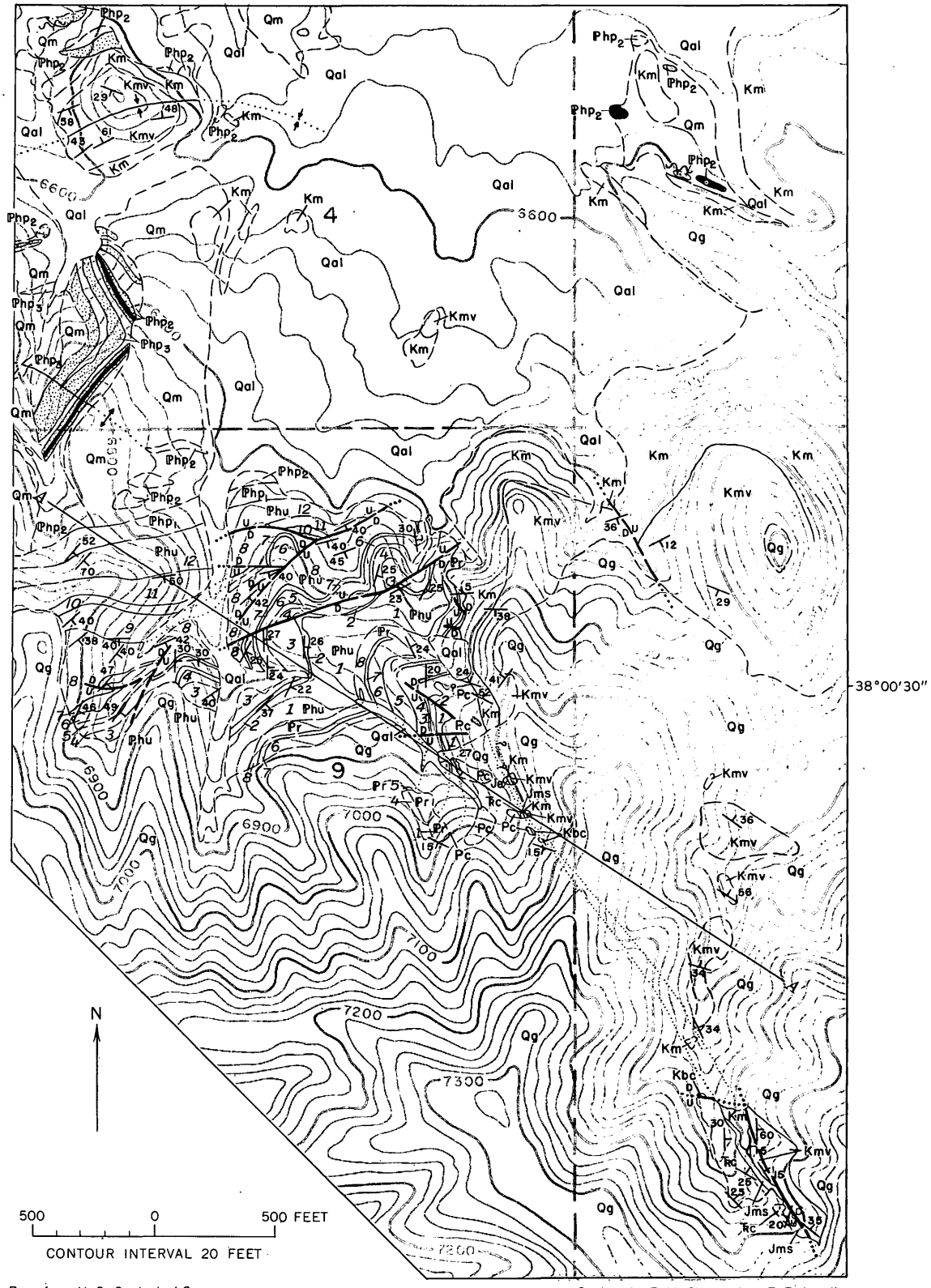

FIGURE 197.2.—Geologic map of part of southeastern Gypsum Valley, San Miguel County, Colo. Numbers on map refer to section (fig. 197.3).

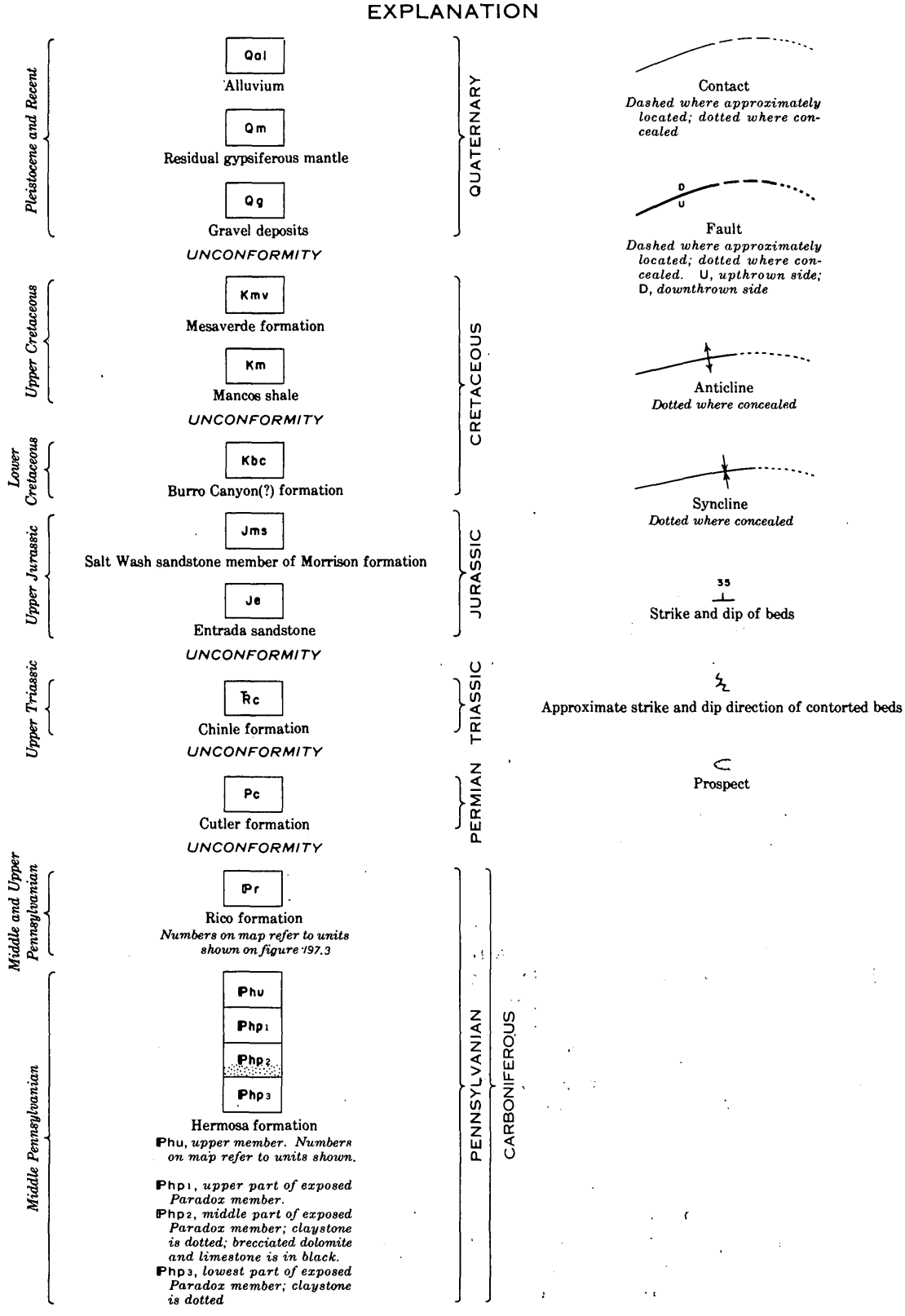

Explanation for figure 197.2.

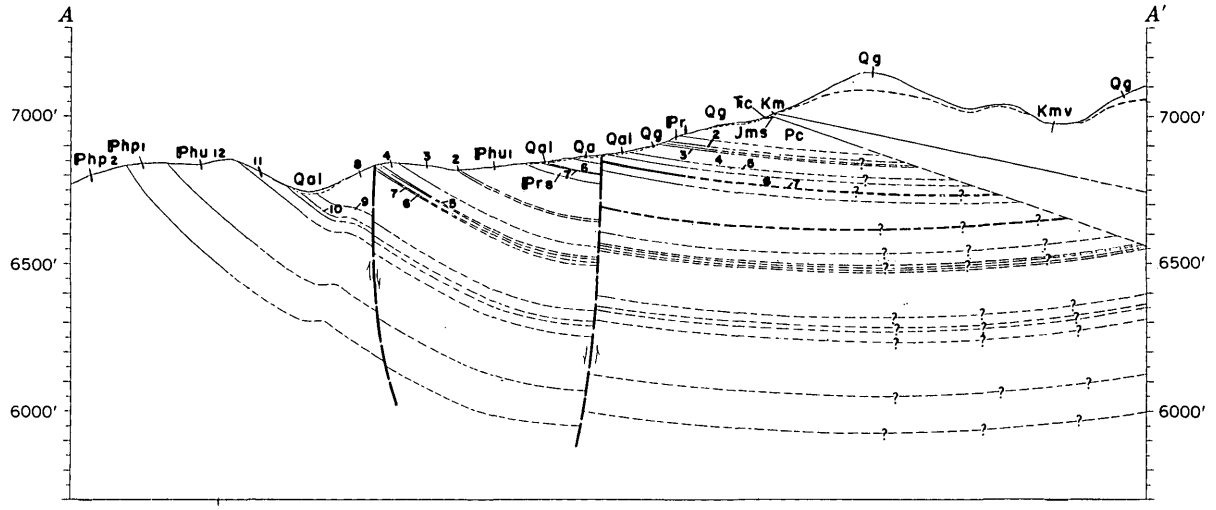

FIGURE 197.3.—Section *A–A'* across part of southeastern Gypsum Valley. Symbols explained on map (fig. 197.2) and measured sections (fig. 197.4).

salt-bearing Paradox member and the limestone-bearing upper member of the Hermosa formation of Middle Pennsylvanian age indicate that growth of the Paradox Valley and Gypsum Valley anticlines began prior to the end of deposition of the Hermosa formation (Elston and Landis, 1960; Elston and Shoemaker, 1960). The salt anticlines apparently grew gradually during Middle and Late Pennsylvanian, and Permian time, and a thick sequence of "post-salt" Paleozoic rocks was deposited adjacent to the salt structures.

The Gypsum Valley anticline is underlain by a thick elongate northwest-trending salt core, about 2 to 3 miles wide, more than 25 miles long, and more than 10,000 feet thick. The salt core, and an overlying leached cap that crops out on the valley floor, are rocks of the Paradox member of the Hermosa formation of Middle Pennsylvanian age (Bass, 1944; Cater, 1955a). Deep drill holes have penetrated about 4,000 feet of "post-salt" Paleozoic rocks beneath the south flank of the anticline, and about 8,500 feet of "post-salt" Paleozoic rocks beneath the north flank. These rocks thin and pinch out against the salt structure, and Mesozoic strata directly overlie the leached cap of the salt core.

Although structurally complex in detail, the leached cap in southeast Gypsum Valley is structurally simple in gross view; the units of the Paradox are folded into a broad anticlinal flexure upon which smaller folds are superimposed. Rocks of the Paradox member directly underlying the upper member of the Hermosa in southeast Gypsum Valley (figs. 197.2 and 197.3) have been traced for a distance of about 1 mile to the northwest, across the crest of the anticline, where the lower two of the three exposed map units of the Paradox are overlain unconformably by the Salt Wash member of the Morrison formation of Jurassic age. The relations here indicate that no great extrusion of the caprock occurred during growth of the salt structure, although leaching of salt from the anticlinal core has resulted in the development of internally disrupted units interbedded in gypsum. Similary, a gross simplicity of the cores also exists in Paradox Valley (mapped by Elston) and in Sinbad Valley (mapped by Shoemaker).

In southeast Gypsum Valley, the lowest exposed unit (fig. 197.2) of the Paradox member consists dominantly of gypsum with discontinuous dark-gray claystone beds, the middle unit (fig. 197.2) consists of interbedded gypsum and greenish-gray to dark-gray claystone, and some dark-gray limestone and dolomite beds at the top, and the upper unit (fig. 197.2) consists of light-gray to yellowish-gray dolomite, dark- to light-gray claystone and siltstone, and subordinate sandstone. The upper unit, which generally is transitional into the upper member of the Hermosa formation, locally appears to be separated from it by an unconformity that possibly is equivalent to unconformities mapped beneath the upper member in northwest Gypsum Valley (Elston and Landis, 1960), and in Paradox Valley. Fossils indicate a late Middle Pennsylvanian (Des Moines) age for the upper member of the Hermosa formation and for most of the overlying Rico formation on the south flank of the Gypsum Valley anticline (Hunt's Hole section, fig. 197.4 and table 197.1); the remainder of the Rico formation is Late Pennsylvanian in age. The Hunt's Hole section (fig. 197.4) correlates lithologically with the section in the map area (fig. 197.2) where the

fauna are generally sparse and are not critically diagnostic of age.

Growth of the salt structure is recorded by the pinchout of rock units of late Paleozoic to Late Jurassic age against the salt structure. Locally, in southeast Gypsum Valley, rocks of Late Jurassic and Early Cretaceous age, and some rocks of Late Cretaceous age, also appear to thin and pinch out over the salt structure. In and adjacent to the map area (fig. 197.2) the Mancos shale of Late Cretaceous age overlies rocks ranging in age from Middle Pennsylvanian to Early Cretaceous. Near Gypsum Valley the Mancos is about 3,000 feet thick (Stokes and Phoenix, 1948; Cater 1955a), but in the mapped area (fig. 197.2) the maximum exposed thickness is about 200 feet. The contact of the Mancos with older rocks is generally poorly exposed, but where seen it seems to be depositional. The Mesaverde formation of Late Cretaceous age, which conformably overlies the Mancos, crops out in the eastern part of the area mapped, and extends 6 miles to the southeast in an asymmetrically downwarped area (Vogel, 1960). The authors interpret this feature to be a syncline formed by subsidence over the salt core of the Gypsum Valley anticline. This feature appears to be similar to the Coke Ovens syncline that overlies the southeast end of the Paradox Valley salt structure (Cater, 1955b; Shoemaker and others, 1958). The southern margin of the salt core of the Gypsum Valley structure apparently is delimited in the southeast part of the

TABLE 197.1.—*Fossils collected from Hunt's Hole measured section, southeastern Gypsum Valley, Colo.*

[Fossils identified by E. L. Yochelson, aided by David Delo, Jr., I. G. Sohn; L. G Henbest, and Helen Duncan]

U.S. Geological Survey locality	Fossils	Age assigned to diagnostic fossils
19130–PC	*Linoproductus meniscus* Dunbar and Condra. *Neospirifer* cf. *N. latus* Dunbar and Condra. *Juresania*? sp. indet. *"Dictyoclostus"* cf. *"D" hermosanus* (Girty). *Composita subtilita* (Hall) Crinoid stems	Early Late Pennsylvanian.
19129–PC	*Composita subtilita* (Hall) *Phricodothyris perplexa* (McChesney). Terabratuloid? indet. *Allorisma* cf. *A. terminale* (Hall) *Bairdia* spp. *Rectobairdia* sp. *Earlandia perparva* Plummer *Osagia* sp. Calcitornellids *Apterrinella*? sp. *Spiroloculina* sp. *Climacammina* sp. *Tetrataxis* sp.	

TABLE 197.1.—*Fossils collected from Hunt's Hole measured section, southeastern Gypsum Valley, Colo.*—Continued

U.S. Geological Survey locality	Fossils	Age assigned to diagnostic fossils
19129–PC	*Bradyina magna* Roth and Skinner. *Millerella* sp. *Fusulina lonsdalensis* Dunbar and Henbest.	Late Middle Pennsylvanian.
19128–PC	*"Dictyoclostus" hermosanus* (Girty). *Composita subtilita* (Hall) *Phricodothyris* sp. indet.	Middle Pennsylvanian.
19127–PC	Algae? Crinoid stems and plates Incrusting bryozoan Rhomboporoid bryozoan Linoproductid brachiopod *Composita* sp. *Nuculana*? sp. indet. *Permophorus*? sp. indet. *Allorisma* sp. indet. Small pelecypods indet. Bellerophontacean indet. *"Strobeus"* sp. indet. Gastropod with spiral lirae indet.	Middle Pennsylvanian.
19126–PC	Horn coral indet. Crinoid stems Rhomboporoid bryozoan Ramose and incrusting bryozoans. *Meekella striatocostata* (Cox) *Derbyia* cf. *D. crassa* (M and H.) *Linoproductus meniscus* Dunbar and Condra. *"Dictyoclostus" hermosanus* (Girty). *Juresania nebrascensis* (Owen) *Composita subtilita* (Hall) *Neospirifer* sp. indet. *Nuculana* sp. indet. *Permophorus*? sp. indet. *Septimyalina*? sp. indet. *Aviculopecten* cf. *A. occidentalis* (Shumard). *Bellerophon* sp. indet. *Neritacean*? indet. High-spired gastropod indet.	Middle Pennsylvanian.
19125–PC	Plant scraps indet. *Sansabella* sp.	Late Paleozoic.
19124–PC	Crinoid stems Echinoid debris *Prismopora triangulata* (White) *Composita* sp. *Crurithyris* sp. Spiriferoid brachiopod (fragment). Pectenoid pelecypod (fragment)	Middle Pennsylvanian.
19123–PC	*Linoproductus* sp. indet. *Cancrinella*? sp. indet. *"Dictyoclostus" hermosanus* (Girty). *Neospirifer*? sp. indet. *Composita subtilita* (Hall) *Spirifer* cf. *S. boonensis* Swallow *Allorisma*? sp. indet. *Fasciculopecten* cf. *F. knighti* Newell. Myalinid pelecypod indet. *Metoptoma* sp. indet.	Middle Pennsylvanian.

map area by thin wedges of Mesozoic strata against which the Mancos was deposited.

Fossils collected from the lowermost Mancos, where it rests directly on the Paradox in the northeastern part of the map area, were identified as Niobrara in age (W. A. Cobban, oral communication, 1960). In the valley floor, about 1,000 feet north of the map area, fossils of late Carlile age (W. A. Cobban, oral communication, 1959) were collected from near the base of the Mancos. The Mancos and underlying Upper Cretaceous Dakota sandstone, which crop out in the valley floor within 500 feet of the north edge of the area mapped, are downfaulted relative to the Paradox member, and also apparently are downfaulted relative to the Mancos (fig. 197.2).

Stokes and Phoenix (1948) show the Mancos in the mapped area (fig. 197.2) in sedimentary contact with Paleozoic rocks. The authors concur with this interpretation. The overall distribution of the Mancos and Mesaverde relative to the salt structure appears to be best explained by a pinchout of pre-Mancos Cretaceous rocks and a thinning of the Mancos on the salt structure. Faunal evidence suggests that the core of the Gypsum Valley salt structure in southeast Gypsum Valley was not completely buried until Niobrara time.

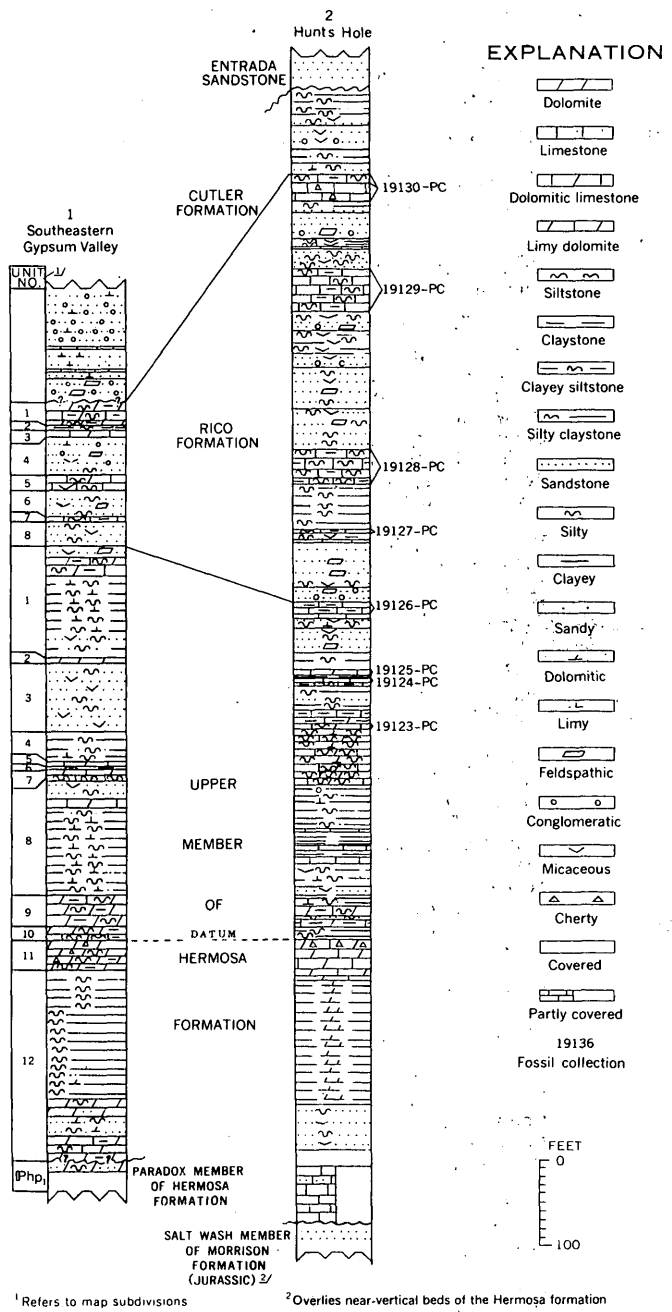

FIGURE 197.4.—Measured sections in eastern part of Gypsum Valley, Colo. Location of sections shown on index map of Gypsum Gap quadrangle (fig. 197.1).

REFERENCES

Bass, N. W., 1944, Paleozoic stratigraphy as revealed by deep wells in parts of southwestern Colorado, northwestern New Mexico, northeastern Arizona, and southeastern Utah: U.S. Geol. Survey Oil and Gas Inv. Prelim. Chart 7, with accompanying text.

Cater, F. W., Jr., 1955a, Geology of the Gypsum Gap quadrangle, Colorado: U.S. Geol. Survey Geol. Quad. Map GQ–59.

——— 1955b, Geology of the Naturita NW quadrangle, Colorado: U.S. Geol. Survey Geol. Quad. Map GQ–65.

Elston, D. P., and Landis, E. R., 1960, Pre-Cutler unconformities and early growth of the Paradox Valley and Gypsum Valley salt anticlines, Colorado, *in* Short papers in the geological sciences: U.S. Geol. Survey Prof. Paper 400–B, art. 118, p. B261–B265.

Elston, D. P., and Shoemaker, E. M., 1960, Late Paleozoic and early Mesozoic structural history of the Uncompahgre front, *in* Four Corners Geol. Soc. Guidebook Field Conf. No. 3, Geology of the Paradox basin fold and fault belt, 1960: p. 47–55.

Shoemaker, E. M., Case, J. E., and Elston, D. P., 1958, Salt anticlines of the Paradox basin, *in* Intermountain Assoc. Petroleum Geologists Guidebook, 9th Ann. Field Conf., Guidebook to the Geology of the Paradox basin, 1958: p. 39–59.

Stokes, W. L., and Phoenix, D. A., 1948, Geology of the Egnar-Gypsum Valley area, San Miguel and Montrose Counties, Colorado: U.S. Geol. Survey Oil and Gas Inv. Prelim. Map 93.

Vogel, J. D., 1960, Geology and ore deposits of the Klondike Ridge area, Colorado: U.S. Geol. Survey open-file report, 205 p.

198. EMPLACEMENT OF THE WILSON PEAK STOCK AND ASSOCIATED INTRUSIVE ROCKS, SAN MIGUEL MOUNTAINS, COLORADO

By Calvin S. Bromfield, Denver, Colo.

During the Tertiary period, probably in post-Oligocene time, the Wilson Peak stock and the Black Face and Ames intrusives were emplaced in the Upper Cretaceous and Tertiary sedimentary rocks and overlying Tertiary volcanic rocks in the San Miguel Mountains, the westernmost prong of the San Juan Mountain region of southwest Colorado (fig. 198.1). The Wilson Peak stock underlies an area of about 5 square miles and is exposed through a vertical distance of over 4,000 feet. It is a composite stock composed of microgranogabbro, medium-grained granodiorite, and porphyritic quartz monzonite, intruded in that order. The Black Face intrusive, southeast of the stock, is a smaller, westward trending mass. The Ames intrusive, east of the stock, is connected with the stock by a narrow discordant west-trending arm. The Ames and Black Face intrusives are both identical seriate porphyritic granodiorite, and probably are exposures of a single saucer-shaped mass. These igneous bodies were all emplaced at relatively shallow depths; in the terminology of Buddington (1959, p. 677) they are epizonal intrusives. No accurate figure can be given for the cover of rocks originally present above the existing level of exposure, but perhaps not more than 5,000 feet of volcanic and sedimentary rocks were present, and probably much less.

Where not disturbed by intrusions, the Mancos shale of Late Cretaceous age, and the Telluride conglomerate and the overlying volcanic series, both of Tertiary age, are generally flat-lying with only minor undulations superposed on a gentle southerly to southwesterly rise of strata toward the Rico dome, which is approximately 10 miles to the southwest. The intrusion of the Wilson stock and the associated Black Face and Ames intrusive rocks produced two contrasting effects on the nearly flat-lying strata, depending on the mode of emplacement. The Black Face and Ames intrusives apparently made room for themselves primarily by forceful doming of their roof rocks and by pushing aside strata; the later Wilson Peak stock was emplaced, at least in its final stage, primarily by piecemeal stoping, and adjacent flat-lying strata were not appreciably disturbed.

Parts of the sedimentary roof rocks are still preserved on the Black Face intrusive (fig. 198.1, section *A–A'*). Along the north side of the intrusive the contact of the igneous and sedimentary rocks dips north and is essentially concordant. Along the south side, however, the strata have been crowded aside, and near the edge of the intrusive they are commonly vertical to overturned, and probably are locally faulted. Strata on the south side of the intrusive probably were first stretched and faulted, and later crumpled as the magma expanded laterally and vertically.

A belt of folded strata connects the west end of the Black Face intrusive with the Wilson Peak stock. Sedimentary rocks in this belt are sharply bent into an asymmetric anticline that is locally overturned to the southwest and probably faulted (fig. 198.1, section *B–B'*). The axial trace of the fold describes a roughly crescent-shaped arc open to the northeast. At its west end, the fold is transected by the Wilson Peak stock; eastward, the fold is continuous with the fold occupied by the Black Face intrusive. The fold was probably formed by a buried extension of the Black Face intrusive as shown by the structural relations, and the presence of several dikes and small irregular intrusives of the Black Face type which cut the anticline and in part are parallel to it.

The Ames intrusive, near the Wilson Peak stock, is a discordant body adjacent to which the strata are domed and crumpled. The intrusive grades northeastward into a sill 600 to 800 feet thick that made room for itself by separating the adjacent rocks. The Ames and Black Face intrusive rocks probably connect in subsurface.

The Wilson Peak stock is inferred to be younger than the Black Face and Ames intrusive rocks because the stock truncates at approximately right angles the belt of rocks structurally deformed by the Black Face intrusive, and because east-northeast trending dikes that cut the deformed belt do not cut the stock (fig. 198.1). Some evidence suggests that these dikes may be essentially contemporaneous with the stock.

The Wilson Peak stock, in contrast to the Black Face and Ames intrusive rocks, appears to have been emplaced, at least in its final phase, by a process of piecemeal stoping. Some doming may have occurred near the northeast edge of the stock during intrusion of an early granogabbro, but if this mode of emplacement was widespread the evidence has been obliterated

601530 O—61——10

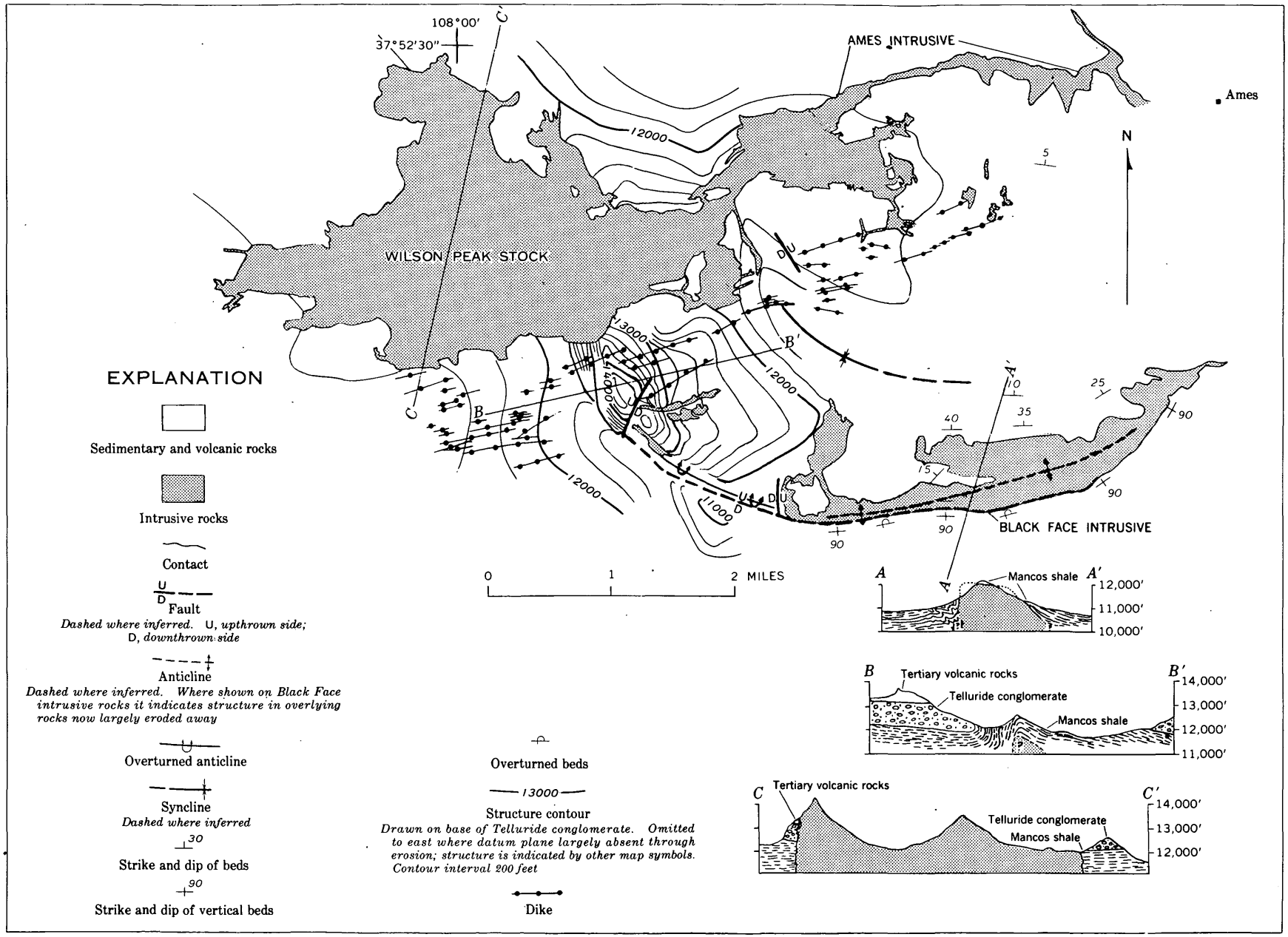

FIGURE 198.1.—Generalized structure map and sections of the Wilson Peak stock area, San Miguel Mountains, Colo.

during the final intrusion. Several lines of evidence suggest piecemeal stoping was the important intrusive mechanism. Along much of the stock contact the flat-lying strata are essentially undisturbed and the relation of the sedimentary rocks to the stock indicates that a considerable volume of country rock has disappeared (fig. 198.1, section *C–C'*). In plan the outline of the stock is irregular (fig. 198.1). The contacts of the stock with the country rocks are sharp, essentially vertical, irregular in detail, and discordant. In addition, piecemeal stoping is strongly suggested by irregular apophyses, dikes, and sills which may have acted as levers to pry off blocks of country rocks; by reentrants of the stock along bedding planes and fracture surfaces in the country rocks, resulting at places in a steplike pattern of outcrop both laterally and vertically; and by the presence locally of angular inclusions of wall rock near the contacts. These features are observed through a vertical interval of at least 2,000 feet.

REFERENCE

Buddington, A. F., 1959, Granite emplacement with special reference to North America: Geol. Soc. America Bull., v. 70, no. 6, p. 671–747.

199. STREAM DIRECTIONS IN TRIASSIC ROCKS OF THE COLORADO PLATEAU

By F. G. Poole, Denver, Colo.

Work done in cooperation with the U.S. Atomic Energy Commission

The cross-stratified fluvial units of Triassic age are here grouped into four major stratigraphic units. These units are: Moenkopi formation of Early and Middle(?) Triassic age; lower part of Chinle formation of Late Triassic age; upper part of Chinle formation of Late Triassic age; and Kayenta formation and upper part of the underlying Moenave formation of Late Triassic(?) age.[1]

These units are interpreted as fluvial because in their lithology and sedimentary structures they are physically similar to modern stream deposits. Two major types of cross-strata sets are recognized in fluvial units on the Colorado Plateau—trough and planar (McKee and Weir, 1953). Nearly all cross-strata measurements used to determine the directions of stream flow shown on figure 199.1 were made on trough sets. The direction of dip was measured at the closed end of the trough set. At each locality 50 to 150 of these measurements were taken within a particular stratigraphic unit and averaged to obtain a resultant stream-flow direction. Each arrow shown on figure 199.1 represents the resultant dip direction of cross-strata in one or more subunits in the four major stratigraphic units at a particular locality. No correlation or stratigraphic position of these subunits is implied within the four major stratigraphic units. The resultant dip orientations indicate that drainage trends are closely related to the positions of major Triassic highlands and that the regional drainage direction shifted from dominantly northwest to dominantly southwest during Triassic time in response to shifting areas of uplift and subsidence.

[1] The Kayenta formation is now considered as Late Triassic(?) in age (Lewis, Irwin, and Wilson, in press).

MOENKOPI FORMATION

The fluvial part of the Moenkopi consists of reddish sandstone, siltstone, and local conglomerate that are believed to represent deposits on alluvial plains and tidal flats.

Cross-strata dip orientation measurements were made in the "lower massive sandstone" of McKee (1954), Holbrook member, and a sandstone in Arizona; a ledge-forming sandstone in southeastern Utah; the conglomeratic Ali Baba member in west-central Colorado and east-central Utah; and conglomeratic units in west-central New Mexico and east-central Arizona (fig. 199.1*A*). The averages of these measurements indicate that the streams that deposited the fluvial sediments of the Moenkopi formation flowed most commonly northwestward and less commonly toward the north, west, and northeast (fig. 199.1*A*).

The Mogollon and Uncompahgre highlands were probably the principal source areas for the Moenkopi

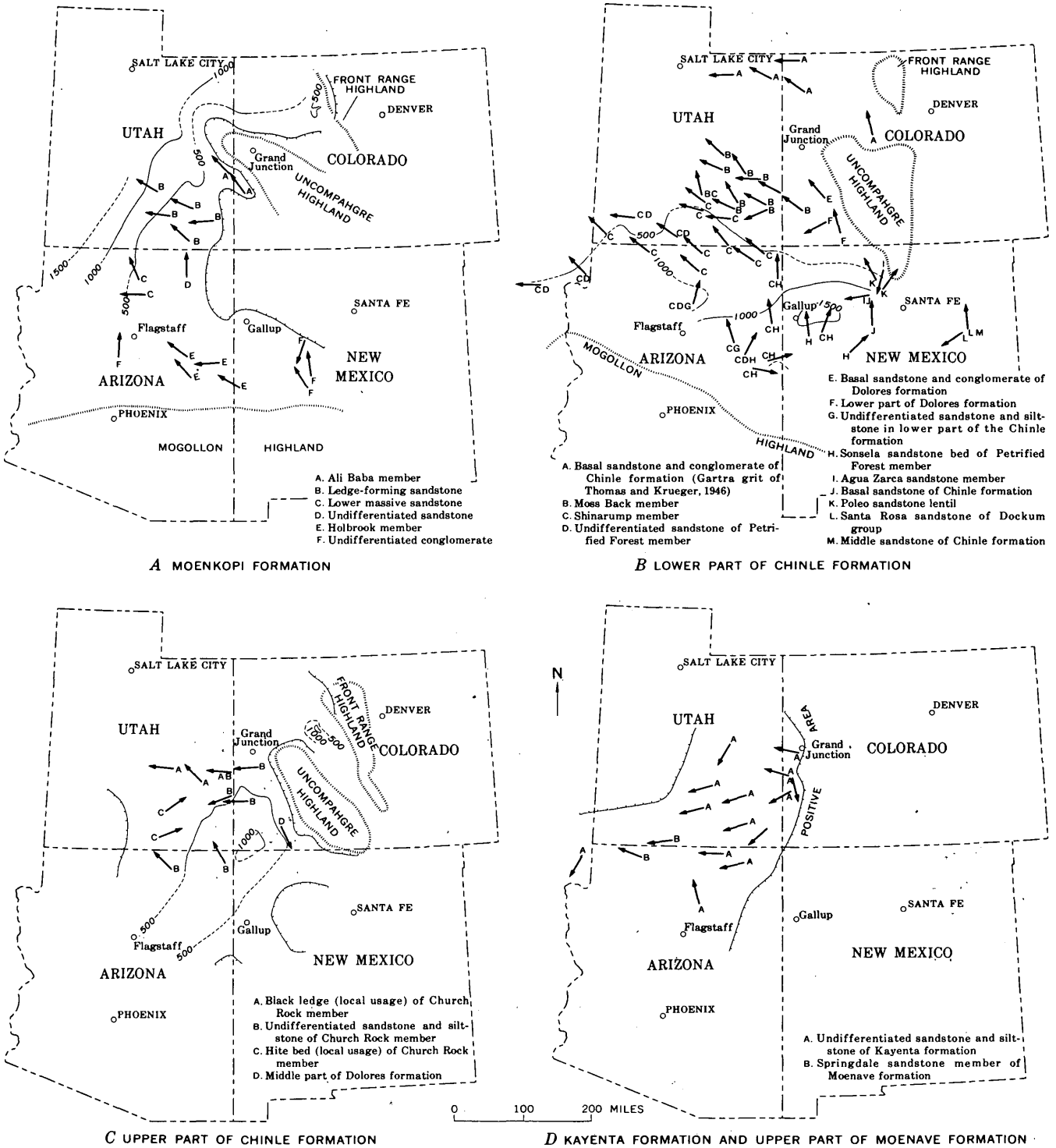

A MOENKOPI FORMATION

B LOWER PART OF CHINLE FORMATION

C UPPER PART OF CHINLE FORMATION

D KAYENTA FORMATION AND UPPER PART OF MOENAVE FORMATION

EXPLANATION

Approximate limit of deposition
Barbs on side of non deposition or erosion

Isopach line
Dashed where inferred. Interval 500 feet

Generalized direction of streamflow

FIGURE 199.1.—Stream directions during deposition of Triassic rocks, Colorado Plateau.

sediments on the Colorado Plateau although some sediments were derived from the Front Range highland. In addition to the flow direction of streams, further evidence that the source areas for Moenkopi sediments were northeast, east, and southeast of the formation is that the average grain size of the rock is progressively smaller and cross stratification is less common to the west and north. Regional stratigraphic relations of the units studied indicate that the fluvial sandstones derived from the Uncompahgre and Front Range highlands are older than those derived from the Mogollon highland.

LOWER PART OF CHINLE FORMATION

The lower part of the Chinle formation consists of variegated bentonitic claystone, siltstone, clayey sandstone, and persistent sandstone and conglomerate beds that have physical characteristics of stream channel and flood plain deposits.

The members and units studied in this part of the formation are given on figure 199.1*B*. Cross-strata dip directions indicate that the streams that deposited the sediments in the members and units studied flowed mainly north, northwest, and west (fig. 199.1*B*). The Mogollon highland was probably the main source area for lower Chinle sediments; the Uncompahgre and Front Range highlands contributed a minor amount of detritus. Sediments of the lower part of the Chinle become coarser southward toward the Mogollon highland and eastward toward the Uncompahgre and Front Range highlands.

UPPER PART OF CHINLE FORMATION

The upper part of the Chinle formation consists of red sandstone and siltstone, and subordinate gray conglomerate and limestone that are believed to represent fluvial, flood-plain, deltaic, and lacustrine deposits. It includes the Owl Rock and Church Rock members of the Chinle in southeastern Utah and northeastern Arizona, the red siltstone part of the Chinle in northwest Colorado, and the upper part of the Dolores formation of southwestern Colorado. The Owl Rock member, which is predominantly limestone and structureless siltstone, was not studied.

Cross-strata dip directions in sandstone units of the upper part of the Chinle indicate that the sediment was derived from positive areas adjacent to the depositional basin (fig. 199.1*C*). The red siltstone and sandstone in the upper part of the Chinle were probably derived largely from older sedimentary rocks exposed on and adjacent to the Uncompahgre and Front Range highlands. Cross-strata orientations in the upper part of the Dolores formation of southwest Colorado, and a local sandstone bed, the Black Ledge, of the Church Rock member in southeast Utah, indicate a source in the Uncompahgre highland. An additional minor source to the west of the west margin of the upper part of the Chinle is suggested by dip orientations in the Hite bed, a local unit in the Church Rock member of southeast Utah.

KAYENTA FORMATION AND UPPER PART OF THE MOENAVE FORMATION

The Kayenta formation consists primarily of red-brown sandstone, siltstone, and claystone that have physical characteristics typical of fluvial and flood plain deposits. The Springdale sandstone member of the underlying Moenave formation is included with the Kayenta in this report because it is similar in lithology and depositional environment. R. F. Wilson (oral communication, 1961) believes that the Springdale sandstone member is laterally equivalent to most of the Kayenta formation of northeastern Arizona.

Cross-strata orientations indicate that the regional drainage in Kayenta and Springdale time was mainly to the west and southwest (fig. 199.1*D*). The Kayenta sediments were probably derived mainly from older sedimentary rocks uplifted along the east margin of the formation. Sediments of the Kayenta formation, in general, decrease in coarseness southwestward from western Colorado.

REFERENCES

Lewis, G. E., Irwin, J. H., and Wilson, R. F., in press, Changes in age assignment for the Glen Canyon group (Triassic and Jurassic) on the Colorado Plateau: Geol. Soc. America Bull.

McKee, E. D., 1954, Stratigraphy and history of the Moenkopi formation of Triassic age: Geol. Soc. America Mem. 61, 133 p.

McKee, E. D., and Weir, G. W., 1953, Terminology for stratification and cross-stratification in sedimentary rocks: Geol. Soc. America Bull., v. 64, no. 4, p. 381–389.

Thomas, H. D., and Krueger, M. L., 1946, Late Paleozoic and early Mesozoic stratigraphy of the Uinta Mountains, Utah: Am. Assoc. Petroleum Geologists Bull., v. 30, no. 8, p. 1255–1293.

200. SODA RHYOLITE (PANTELLERITE?) FROM LAKE COUNTY, OREGON

By George W. Walker, Menlo Park, Calif.

Reconnaissance mapping has disclosed several widely separated masses of sodium-rich volcanic rocks of middle to late Cenozoic age in south-central Oregon, a region characterized by large volumes of calcic-alkalic volcanic rocks. The most extensive exposures of these rocks are on the flanks of Hart Mountain (secs. 1, 9, and 12, T. 36 S., R. 25 E.) in southeastern Lake County; other masses of sodium-rich rocks, exposed in the upper drainage of Deep Creek (sec. 2, T. 41 S., R. 21 E.) southeast of Crane Mountain, Lake County, probably are extensions of the silicic intrusive and extrusive volcanic rocks of the High Grade district of California (Hill, 1915; Gay and Aune, 1958).

The sodium-rich volcanic rocks occur both as near-surface intrusive masses as much as a mile long and several hundreds of feet wide and as restricted thick flows that emanated from the intrusive centers. All of these rocks are porphyritic, the phenocrysts being enclosed in a fine-grained holocrystalline groundmass (fig. 200.1); commonly the flows are strongly flow banded and locally autobrecciated suggesting a magma of high viscosity.

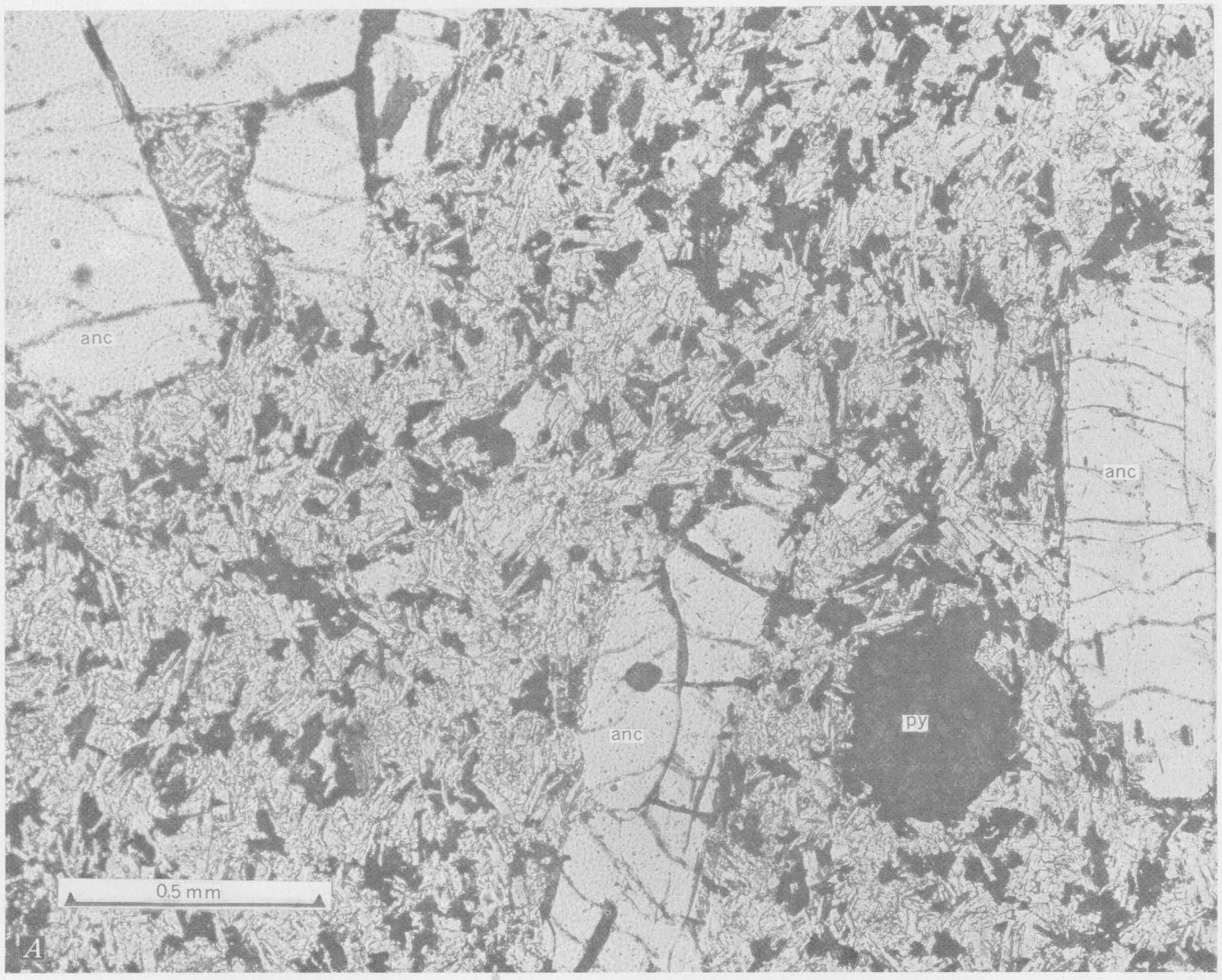

A

Analyses of two samples of these sodium-rich rocks are presented in table 200.1. Sample 1 was collected from a large intrusive at the west base of Hart Mountain and sample 2 from a brecciated flow on the east flank of the mountain. The alkali content of these rocks, totaling about 10.5 percent, is higher than normal for rhyolite, and the ratio of Na_2O to K_2O is approximately 6 to 5. In both rocks analyzed the content of Al_2O_3, CaO, and MgO is noticeably low. Both samples are characterized by a slight molar excess of $Al_2O_3 + Fe_2O_3$ over $Na_2O + K_2O$. Standard minerals of the norm, which for both specimens includes quartz, orthoclase, albite, acmite, and diopside, also are presented in table 200.1. Even though the groundmass of both samples is too fine grained to permit accurate and complete modal analyses, an approximate modal analysis has been made of sample 1 (table 200.1) using a standard point count method (Chayes, 1949).

The sodium-rich rocks of Hart Mountain contain many phenocrysts of alkali feldspar ($2V(-)=47°\pm2°$), fewer phenocrysts of a pleochroic green diopsidic pyroxene (variable $2V(+)=65°\pm5°$; $n_\beta \approx 1.77$) with slightly darker green reaction rims, and scattered rare phenocrysts of quartz and oxyhornblende in a fine-grained groundmass. The groundmass consists of anhedral grains of quartz and alkali feldspar, small prisms and shreds of acmite ($n_\alpha \approx 1.76$; $n_\gamma \approx 1.80$; $X\Lambda c = 0°-5°$), a pleochroic blue amphibole (riebeckite?, $n_\beta \approx 1.69$; $X\Lambda c = 4°$), a pleochroic brown mineral ($n_\beta \approx 1.76$; $Z\Lambda c \approx 43°$)

B

FIGURE 200.1.—Photomicrographs of thin sections of soda rhyolite intrusive, *A*, and flow-banded and autobrecciated flow, *B*. Phenocrysts of anorthoclase (anc) and diopsidic pyroxene (py) in fine-grained groundmass of quartz and alkali feldspar (light colored minerals) and acmite, riebeckite?, aenigmatite-rhönite?, and magnetite (dark colored minerals).

TABLE 200.1.—*Rapid rock analyses (in weight percent), calculated norms, and an approximate mode of two samples of soda rhyolite from Hart Mountain, Lake County, Oreg.*

[Analysts: P. L. D. Elmore, I. H. Barlow, S. D. Botts, Gillison Chloe, U.S. Geological Survey]

Sample Field number	1 GWW-3-60	2 GWW-4-60
SiO_2	68. 6	69. 4
Al_2O_3	13. 5	13. 2
Fe_2O_3	3. 1	3. 2
FeO	1. 8	1. 8
MgO	. 03	. 05
CaO	. 52	. 30
Na_2O	5. 8	5. 8
K_2O	4. 7	4. 6
H_2O	1. 0	1. 0
TiO_2	. 37	. 35
P_2O_5	. 03	. 05
MnO	. 17	. 18
Total	99. 6	99. 9
CO_2	<. 05	<. 05
Norm[1]		
Quartz	16. 6	18. 2
Orthoclase	27. 8	27. 2
Albite	43. 0	42. 0
Acmite	5. 5	6. 5
Diopside	2. 2	1. 2
Hypersthene	1. 1	1. 7
Magnetite	1. 6	1. 4
Ilmenite	. 8	. 8
Total	98. 6	99. 0

Approximate mode[2]

Phenocrysts[3]		35. 2
Anorthoclase	32. 0	
Diopsidic pyroxene	3. 0	
Oxyhornblende	. 2	
Magnetite		2. 0
Groundmass		62. 4
Quartz and alkali feldspar	48. 0	
Riebeckite?, acmite, and aenigmatite-rhönite?	14. 0	
Orange-brown alteration mineral	. 4	

[1] Calculated by C.I.P.W. system.
[2] Based on a 350-point traverse in each of three thin sections, sample 1. Color index 20.
[3] A few crystals of quartz present in some sections.

probably transitional in the rhönite-aenigmatite series, magnetite, and an unidentified orange-brown alteration mineral.

The alkali feldspar phenocrysts commonly are faintly zoned and exhibit either fine grid-twinning or poorly developed simple twinning. A cryptoperthitic intergrowth of the albite and orthoclase components in this alkali feldspar is suggested by the complex diffraction pattern obtained from the phenocrysts (fig. 200.2*A*). To simplify the diffraction pattern and allow an estimate of composition, the phenocrysts were heated in a muffle furnace for 6 hours at 1,000°C to homogenize the albite-orthoclase components into one feldspar. A diffraction pattern of the homogenized feldspar (fig. 200.2*B*) is similar to the pattern (fig. 200.2*C*) given for a high temperature synthetic alkali feldspar whose composition is $Ab_{71}Or_{29}$ (Donnay and Donnay, 1952, fig. 4). The normative feldspar shows about $Ab_{60}Or_{40}$ which suggests that this compositional estimate is the right order of magnitude. The moderately large axial angle ($47°\pm2°$) of the natural feldspar is comparable to those given by Tuttle (1952, table 1) and by Carmichael (1960, table 3, spec. 3112F) for anorthoclase of compositions ranging from about $Ab_{76}Or_{23}$ to $Ab_{63}Or_{36}$. An X-ray diffraction pattern of the light fraction (sp gr <2.88+) of the groundmass suggests that the groundmass feldspar also is anorthoclase.

Some mineralogic differences exist between the sodium-rich rocks exposed on Hart Mountain and those southeast of Crane Mountain. Sanadine, as phenocrysts, is an important constituent of the rocks near Crane Mountain. Also, quartz (as phenocrysts and crystal fragments), oxyhornblende, and aenigmatite or rhönite are more abundant, whereas diopsidic pyroxene and acmite are rare or lacking.

According to the classification of Rittman (1952), these volcanic rocks chemically are soda rhyolite, close to his alkali rhyolite. They have many chemical and mineralogical characteristics in common with varieties of pantellerite (Washington, 1913), but contain slightly less $Na_2O + K_2O$, less $Fe_2O_3 + FeO + TiO_2$, and more Al_2O_3 than those on the island of Pantelleria.

The geologic occurrence of these rocks as intrusive and flow units within large andesitic and basaltic volcanic piles suggests that they are late volcanic differentiates. As yet, no data are available as to the characteristics of the parent magma or the type of pre-Tertiary bedrock intruded; consequently, there is no evidence either for or against sodium enrichment of the magma by contamination.

REFERENCES

Carmichael, I. S. E., 1960, The feldspar phenocrysts of some Tertiary acid glasses: Mineralog. Mag., v. 32, p. 587–608.

Chayes, Felix, 1949, A simple point counter for thin section analysis: Am. Mineralogist, v. 34, p. 1–11.

Donnay, Gabrielle, and Donnay, J. D. H., 1952, The symmetry change in the high-temperature alkali-feldspar series: Am. Jour. Sci., Bowen Volume, pt. 1, p. 115–132.

Gay, T. E., Jr., and Aune, Q. A., 1958, Geologic map of California, Alturas Sheet: California Div. Mines.

Hill, J. M., 1915, Some mining districts in northeastern California and northwestern Nevada: U.S. Geol. Survey Bull. 594, 200 p.

Rittman, A., 1952, Nomenclature of volcanic rocks: Volcanol. Bull., ser. 2, v. 12, p. 75–102.

Tuttle, O. F., 1952, Optical studies on alkali feldspars: Am. Jour. Sci., Bowen Volume, pt. 2, p. 553–567.

Washington, H. S., 1913, The volcanoes and rocks of Pantelleria, Part II: Am. Jour. Sci., v. 21, p. 683–713.

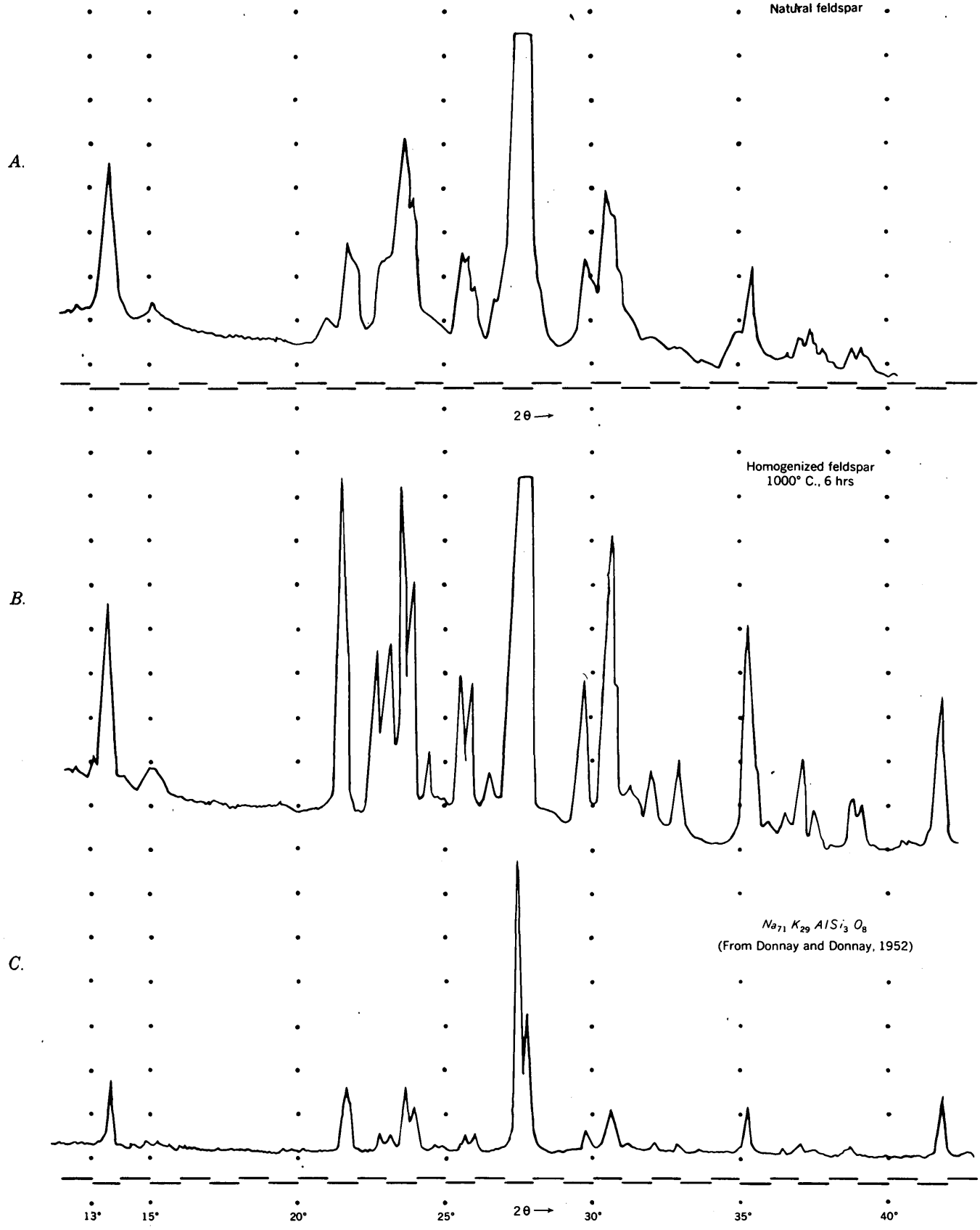

FIGURE 200.2.—Powder diffraction patterns. *A*, Unmodified natural feldspar phenocrysts; *B*, homogenized feldspar phenocrysts; and *C*, high-temperature synthetic alkali feldspar.

201. PREHNITE-PUMPELLYITE METAGRAYWACKE FACIES OF UPPER TRIASSIC ROCKS, ALDRICH MOUNTAINS, OREGON

By C. Ervin Brown, Washington, D.C.

In east-central Oregon a thick sequence of Upper Triassic rocks, briefly described by Thayer and Brown (1960), contain authigenic mineral assemblages characteristic of the prehnite-pumpellyite metagraywacke facies and the laumontite stage of the zeolite facies of Coombs (1960). The lithology and authigenic alteration are similar to those of a sequence of rocks in Southland, New Zealand, in which the lower grade mineral facies were first recognized (Coombs, 1954).

The rocks in Oregon, which make up most of the Aldrich Mountains, have a composite thickness of 40,000 to 50,000 feet and comprise conglomerate, graywacke, shale, siltstone, tuffaceous graywacke, andesitic tuff, rhyolitic vitric tuff, and basaltic lava. These are unconformably overlain by as much as 14,000 feet of similar Jurassic rocks present south of this area (Lupher, 1941).

Intraformational unconformities, differences in trends of folds, and faults that cut only the older rocks of the sequence show that deformation recurred during deposition. Eastward thickening of younger units in the sequence indicates successive eastward shifts of the basin of deposition. Absence of foliation suggests that the strongly folded sedimentary rocks were only partly indurated and possibly well lubricated by connate water during folding and deep burial.

Many of the rock types contain large amounts of authigenic chlorite, albite, and quartz, and also minor quantities of sphene, epidote, and rutile that possibly are not authigenic. Authigenic pumpellyite, prehnite, and laumontite occur chiefly in volcanic rocks or rocks rich in volcanic debris.

Albite is the most abundant detrital plagioclase throughout the stratigraphic section. Although some fragments are obviously from albitic rocks, I believe most of them were albitized in places. Albite also forms fine-grained mosaics of twinned laths intergrown with quartz that replace the matrix of tuffaceous graywackes and tuffs. In one specimen of bedded vitric tuff, the shard structure is well preserved despite complete recrystallization of the glass to a felt of intergrown albite laths and quartz. Albitic plagioclase too fine for microscopic identification also has been indicated in devitrified tuffs by X-ray diffraction.

Authigenic quartz likewise occurs throughout the stratigraphic section, both intergrown with albite as a devitrification product and as cryptocrystalline clots associated with laumontite. Greenstones near the base of the section contain secondary quartz; and pillow basalts about 4 miles southwest of Canyon City are veined by quartz, pumpellyite, and calcite. Fine-grained quartz veinlets are numerous in siliceous mudstone and chert in the lower part of the sequence.

Chlorite is most abundant as an alteration product of basic volcanic fragments in graywackes and basaltic lithic tuffs. It forms much of the yellowish-green cryptocrystalline matrix in graywacke, tuff, and greenstone. In places chlorite forms flaky spherulitic aggregates, some of which show an anomalous blue interference color.

Prehnite occurs most commonly as wispy patches in tuffaceous rocks, but also forms idioblastic prisms as much as 0.5 mm long in mudstone and siltstone and veins in shattered rock near early faults. The wispy patches are as much as 10 mm in diameter and weather to light-gray spots.

Pumpellyite has been found mainly in basaltic lavas in the lower part of the stratigraphic section and in the pillow lavas southwest of Canyon City. It occurs with chlorite in amygdules and also forms veinlets with calcite and quartz. Pumpellyite also occurs in coarse lithic tuffs.

Authigenic laumontite occurs as spots in siltstones of Jurassic age south of the Aldrich Mountains and almost completely replaces some rhyolitic or dacitic vitric tuffs of Triassic age. Laumontitized tuff is present in 2-inch layers in the upper part of the section and in beds as much as 10 feet thick in the lower part. Irregular optically continuous patches as much as 5 mm across generally include several hundred relict shard forms. Laumontite has replaced interstitial material in dacitic volcanic breccia and in a conglomerate near the base of the section.

Celadonite occurs as thin green bands, mainly in tuffaceous rocks that constitute most of the peaks of the Aldrich Mountains. In thin section this mineral is seen as irregular blue-green pleochroic blebs localized in layers. Celadonite is also present in greenstones near the base of the sequence and in finely cross-bedded tuffaceous siltstones near its top.

Epidote, sphene, and rutile are found throughout

the section as extremely fine grains or granular aggregates. Commonly, these cannot be distinguished one from another nor can their authigenic origin be established because of the small grain size.

The assemblages of authigenic minerals in the Aldrich Mountains are characteristic of rocks in the zeolitic facies, named by Fyfe and others (1958) as a result of Coombs' study in New Zealand (1954). This facies is characterized by authigenic zeolites, albite, adularia, and quartz, all stable at low temperature in an aqueous environment. Coombs and others (1959) studied other occurrences reported in the literature and interpreted the zeolitic facies according to results of hydrothermal syntheses. They found that the stability of some zeolites is affected by the availability of free silica and consequently redefined it as a zeolite mineral facies, an assemblage formed under physical conditions that produce quartz-heulandite, quartz-analcime, or quartz-laumontite. Analcime and heulandite are indicative of a lower grade stage and laumontite of a higher grade. A non-zeolitic transition zone between the zeolite facies and the greenschist facies was also recognized and was named the prehnite-pumpellyite metagraywacke facies by Coombs (1960). This mineral facies is characterized by prehnite or pumpellyite, generally with quartz, albite, and chlorite. Most of the altered rocks of the Aldrich Mountains are in this facies.

The zeolitic alteration in the rocks of Southland, New Zealand, is attributed to elevated temperature and pressure related to deep burial (Coombs, 1954). The authigenic minerals in the Aldrich Mountains rocks do not span enough of the lower grade mineral facies to determine whether depth of burial was significant in controlling the mineral associations that appear in various parts of the section. Detrital plagioclase does seem to be more completely albitized in the lower units than in the upper; laumontite occurs in the upper part of the Triassic sequence and in basal Jurassic rocks, but it is also present in the lower part of the Triassic section. These older rocks may not have been deeply buried, however, because of the eastward shift of the basin of deposition.

The rocks under consideration are thicker and more intensely folded than those in New Zealand, and consequently were probably plunged into an environment where temperature and pressure were above the stability range of the more hydrated zeolites. The generally selective occurrence of laumontite in silicic vitric tuffs, prehnite in tuffaceous rocks, and pumpellyite in basaltic lavas indicates the influence of original rock composition on the authigenic mineral assemblage.

REFERENCES

Coombs, D. S., 1954, The nature and alteration of some Triassic sediments from Southland, New Zealand: Royal Soc. New Zealand Trans., v. 82, p. 65–109.

——— 1960, Lower grade mineral facies in New Zealand: Internat. Geol. Cong., 21st, Copenhagen 1960, sec. 13, pt. 13, p. 339–351.

Coombs, D. S., Ellis, A. J., Fyfe, W. S., and Taylor, A. M., 1959, The zeolite facies, with comments on the interpretation of hydrothermal syntheses: Geochim. et Cosmochim. Acta, v. 17, p. 53–107.

Fyfe, W. S., Turner, F. J., and Verhoogen, John, 1958, Metamorphic reactions and metamorphic facies: Geol. Soc. America Mem. 73, 259 p.

Lupher, R. L., 1941, Jurassic stratigraphy of central Oregon: Geol. Soc. America Bull., v. 52, p. 219–270.

Thayer, T. P., and Brown, C. E., 1960, Upper Triassic graywackes and associated rocks in the Aldrich Mountains, Oregon, *in* Short papers in the geological sciences: U.S. Geol. Survey Prof. Paper 400–B, p. B300–B302.

202. COMPUTATION OF THE TOTAL FLOW OF THE COLUMBIA RIVER AT THE MOUTH

By Hollis M. Orem, Portland, Oreg.

Gaging the flow of Columbia River is not feasible in the tidal reach, which extends from the mouth 145 miles upstream to Bonneville Dam. Therefore, requests for information on the total flow at the mouth can be answered only by estimating flow from the ungaged areas and adding these estimates to the gaged flows. Such requests are of two kinds, those for estimates of monthly discharge for previous years and those for estimates made currently within a few days after the end of each calendar month. This paper describes the way both kinds of estimates are made.

The first step in estimating the monthly discharge for previous years is to estimate the annual inflows for the period 1943 to 1957 from the various ungaged areas downstream from all stream-gaging stations on the basis of a map showing average annual runoff. This map was developed by Harry Hulsing and Nick Kallio (written communication, 1961) from an isohyetal chart furnished by the Corps of Engineers and from Geological Survey runoff data. The amount of annual flow from each ungaged area is estimated from the gaged flow of a nearby area and from the ratio of runoffs, as defined by the map, for the two areas. The annual flows so obtained are then distributed by calendar months on the basis of the distribution of flows from gaged areas having similar elevation, exposure, and position. The estimated average runoff from ungaged areas for the period 1943 to 1957 is 5.0 percent of the estimated total flow of Columbia River at the mouth. Figure 202.1 shows the drainage area of Columbia River below The Dalles and the locations of gaging stations.

Monthly runoff measured at gaging stations for which reports are available a few days after each month are added to the runoff estimated for ungaged areas to give the total estimated monthly runoff. Estimates of current monthly inflow below The Dalles include estimates for three main reaches of the Columbia River as follows:

Inflow reach	*Measured runoff*
Columbia River from The Dalles to Vancouver	Wind River near Carson plus Hood River near Hood River
Willamette River at mouth (adjusted for change in storage)	Willamette River at Salem (adjusted for change in storage)
Columbia River below Willamette River (adjusted for change in storage)	Lewis River at Ariel (adjusted for change in storage) and Cowlitz River at Castle Rock

A preliminary value of the monthly flow of Columbia River at the mouth is obtained by adding the estimates for the three inflow reaches to the measured flows at the following stations:

Gaging station records available each month	Drainage area (square miles)	
	Index area	Total area
Columbia River at The Dalles		237,000
Klickitat River near Pitt	1,290	
Hood River near Hood River (includes conduit)	329	
Wind River near Carson	225	
Willamette River at Salem	7,280	
Cowlitz River at Castle Rock	2,238	
Lewis River at Ariel	731	
Subtotal of areas below The Dalles	12,093	21,000
Columbia River at the mouth		258,000

The preliminary value is corrected for precipitation on 400 square miles of river, slough, pond, and island area below The Dalles and below Salem, and for evaporation from the same area. All of the precipitation which falls on water surfaces is assumed to become runoff. Evaporation is taken as 2.0 feet per year (U.S. Weather Bureau, 1959) and is distributed among the months according to the average pattern for Seattle (U.S. Weather Bureau, 1950).

For months when the flows at The Dalles and at Salem are changing, a correction for time-of-travel is applied to the estimates of flow at the mouth.

Finally, the estimated mean flow at the mouth is adjusted, without consideration of time lag, for aggregate storage change in 8 major power reservoirs on the Columbia River, 5 reservoirs in the Willamette River basin, and 3 reservoirs in the Lewis River basin, and for the pumped diversion at Grand Coulee.

Data on the mean flow of record and the adjusted flow at the mouth of the Columbia River is published monthly in the Pacific Northwest Water Resources Summary.[1]

REFERENCES

U.S. Weather Bureau, 1950, Mean monthly and annual evaporation from free water surface for the United States, Alaska, Hawaii, and West Indies: U.S. Weather Bur. Tech. Paper 13.

——— 1959, Evaporation maps for the United States: U.S. Weather Bur. Tech. Paper 37.

[1] Summary prepared by U.S. Geological Survey Current Records Center, Portland, Ore., and released by the U.S. Geological Survey in collaboration with the Canada Department of Northern Affairs and Natural Resources Water Resources Division.

FIGURE 202.1.—Map of lower Columbia River basin showing location of gaging stations.

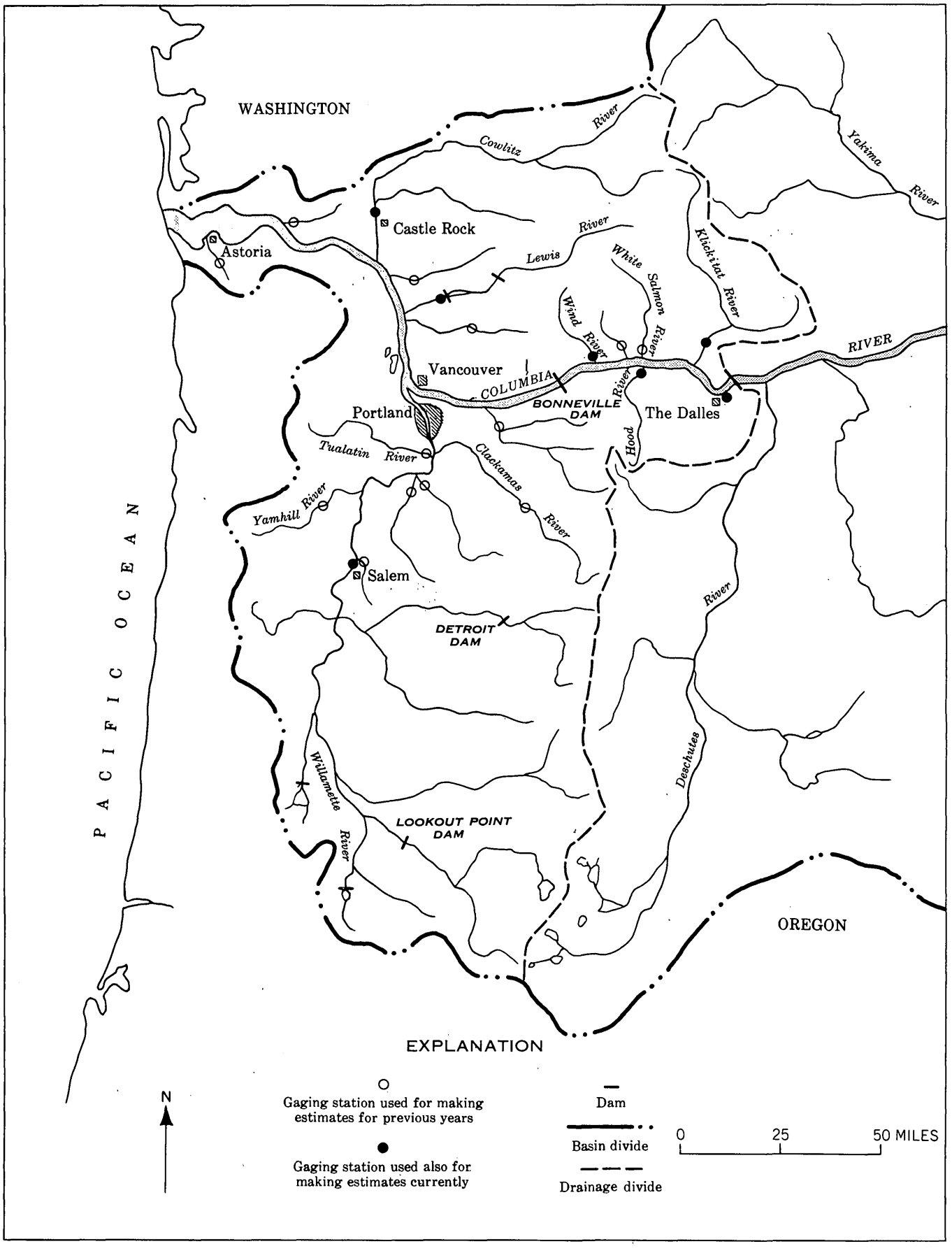
WASHINGTON
OREGON
PACIFIC OCEAN
Cowlitz River
Yakima River
Castle Rock
Astoria
Lewis River
White Salmon River
Wind River
Klickitat River
Vancouver
COLUMBIA RIVER
BONNEVILLE DAM
Portland
The Dalles
Hood River
Tualatin River
Clackamas River
Yamhill River
Salem
DETROIT DAM
Deschutes River
Willamette River
LOOKOUT POINT DAM
EXPLANATION
N
Gaging station used for making estimates for previous years
Gaging station used also for making estimates currently
Dam
Basin divide
Drainage divide
0 25 50 MILES

203. DEFORMED BASALTIC CAPROCK AS AN AQUIFER AT COW VALLEY, OREGON

By Bruce L. Foxworthy, Portland, Oreg.

Work done in cooperation with the office of the Oregon State Engineer

In parts of the Basin and Range province (Fenneman, 1931), and to a lesser extent in the flanking mountains and plateaus, a layer of lava caps older rocks exposed on the slopes of buttes, mountains, and plateaus. At places, the effectiveness of these caprocks as aquifers is greater than has been commonly appreciated. Much of the caprock lava is massive in appearance and creates the illusion of impenetrability, but shrinkage joints, vesicular zones, and local breccia layers may give it considerable permeability. In parts of the area of their occurrence, the lava beds have been deformed so that they extend below the level of the water table, where they may constitute a permeable reservoir for ground water.

Basaltic caprock of this type is the main aquifer for the irrigation wells in Cow Valley, a small upland basin in Malheur County, in the semiarid part of Oregon (fig. 203.1). Studies being made in that area (Brown and Newcomb, 1956) indicates that this type of aquifer may be fairly common in that region and in regions of similar geologic setting.

In the northern part of the lower Malheur River basin, and in adjacent drainage basins northwest of Ontario, Oreg. (fig. 203.1), a widespread layer of basaltic lava caps sedimentary rocks of Pliocene and Pleistocene age, and sedimentary, metamorphic, and granitic rocks of Mesozoic(?) age. The lava ranges from about 10 to 300 feet in thickness, and it caps the older rocks in upland areas north and south of Cow Valley. Folding and faulting in the Cow Valley area

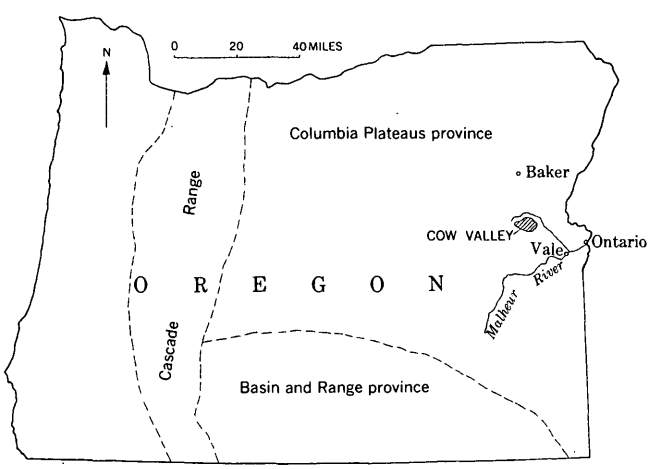

FIGURE 203.1.—Cow Valley in relation to major physiographic provinces in Oregon.

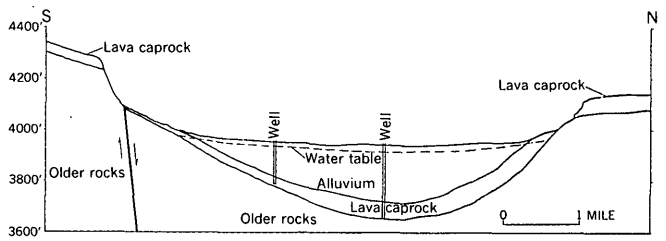

FIGURE 203.2.—Diagrammatic section across Cow Valley, Oreg., showing the position of the caprock lava where it constitutes the major aquifer.

have lowered it to and below the present valley floor. Within the valley it overlies relatively impervious sedimentary and partly metamorphosed rocks, and is overlain by alluvium and colluvium. The maximum thickness of the alluvium is about 300 feet near the center of the valley floor. Figure 203.2 shows the general stratigraphic relations and position of the water table within the valley.

The first test wells for irrigation in the valley obtained water from the alluvium, but problems of sand entering the wells and excessive drawdown of water level during pumping caused later wells to be drilled deeper into the underlying basalt. The basalt affords much greater yields and sand-free water; consequently, it has been tapped by the latest 14 of the 18 irrigation wells in the area.

The lava consists principally of joined massive basalt in which layers of rubbly breccia are interspersed. Drillers' logs show that toward the south side of the valley the bottom part of the lava zone consists of red sandy and scoriaceous tuff. Other tuff layers are intercalated in the lava. The maximum thickness of basalt penetrated thus far is 314 feet; however, where it was penetrated completely by one well it had a thickness of only 45 feet.

The wells that tap the basalt have an average pumping yield of about 1,100 gpm (gallons per minute) and less than 100 feet of drawdown. Aquifer tests on some of those wells indicate coefficients of transmissibility ranging from about 85,000 to 300,000 gpd/ft (gallons per day per foot). The ground water in the lava rock and in the overlying alluvium is a hydraulically continuous body. Pumping from a well that taps either aquifer eventually causes some lowering of ground-water levels throughout the reservoir.

The great demand for ground water in the valley, which lacks other dependable supplies for irrigation, resulted in a progressive lowering of ground-water levels during the period 1951–60, and led to studies to determine the average annual recharge to the ground-water body. Data now available indicate that the recharge may be only about 5,000 acre-feet per year for the entire drainage basin, which covers about 60 square miles. The estimated recharge is about two-thirds of the annual pumpage during recent years.

Chemical analyses of ground water from the alluvium and from the lava indicate that the waters from the two aquifers are similar in character and are of generally good quality for most uses.

REFERENCES

Brown, S. G., and Newcomb, R. C., 1956, The ground-water resources of Cow Valley near Ironside, Malheur County, Oregon: U.S. Geol. Survey open-file rept.

Fenneman, N. M., 1931, Physiography of Western United States: New York, McGraw-Hill Book Co., Inc., 534 p.

204. FACIES DISTRIBUTION AND HYDROLOGY OF INTERMONTANE BASIN FILL, SAFFORD BASIN, ARIZONA

By Edward S. Davidson, Tucson, Ariz.

Work done in cooperation with the University of Arizona

The Safford basin includes about 1,350 square miles in southeastern Arizona (fig. 204.1). Reconnaissance mapping in this area shows that the extent of permeable gravels may have been significantly overestimated. Previous descriptions of the basin sediments have been made by G. K. Gilbert (1875), Schwennesen (1919, 1921), and Knechtel (1938).

The Safford basin is a northwest-trending depression lying between the Gila and Whitlock Mountains to the northeast and the Pinaleno and Santa Teresa Mountains and Mount Turnbull to the southwest. Peaks in the mountains to the northeast average about 5,500 feet in altitude, and those to the southwest range from 10,000 feet in the Pinaleno Mountains to 7,000 feet in the Santa Teresa Mountains and at Mount Turnbull. The central part of the basin has an altitude of about 2,800 feet. The Gila River drains the basin, entering from the east and leaving to the west at Coolidge Dam.

The basin is a typical basin-and-range downfaulted sediment-filled trough lying between the uplifted ranges. The maximum displacement and thickness of sediment are not known, but a well near Pima (fig. 204.1) was drilled to a depth of more than 3,700 feet without reaching bedrock.

The mountains to the northeast are composed of mafic lava flows, agglomerate, and tuff; those to the southwest consist of granite and assorted metamorphic and indurated sedimentary rocks, including granitic gneiss, limestone, and conglomerate.

Sediments in the basin are classified in this report as (a) terrace gravel and alluvium, (b) deformed conglomerate or gravel, and (c) basin fill. The basin fill unconformably overlies the deformed conglomerate or gravel beds and is erosionally overlain by the terrace gravels and alluvium. The terrace gravels and alluvium are not distinguished on figure 204.1.

Terrace gravels and alluvium were deposited by the Gila and its tributaries. The terrace gravels mantle slopes extending from the mountain fronts to the present stream flood plain. The alluvium fills valleys of the present streams.

The deformed conglomerate or gravel beds crop out in a closely limited area, and are apparently derived from local sources. The beds are moderately to firmly cemented and moderately folded and faulted. These rocks are exposed only on the basin margins; a finer grained facies may occur in the central part of the basin, but this is not yet definitely known. The deformation of the beds probably occurred during a major pulse of block faulting preceding deposition of the unconformably overlying basin-fill sediments.

The basin-fill sediments are thick extensive deposits of flat-lying unconsolidated sediment forming the bulk

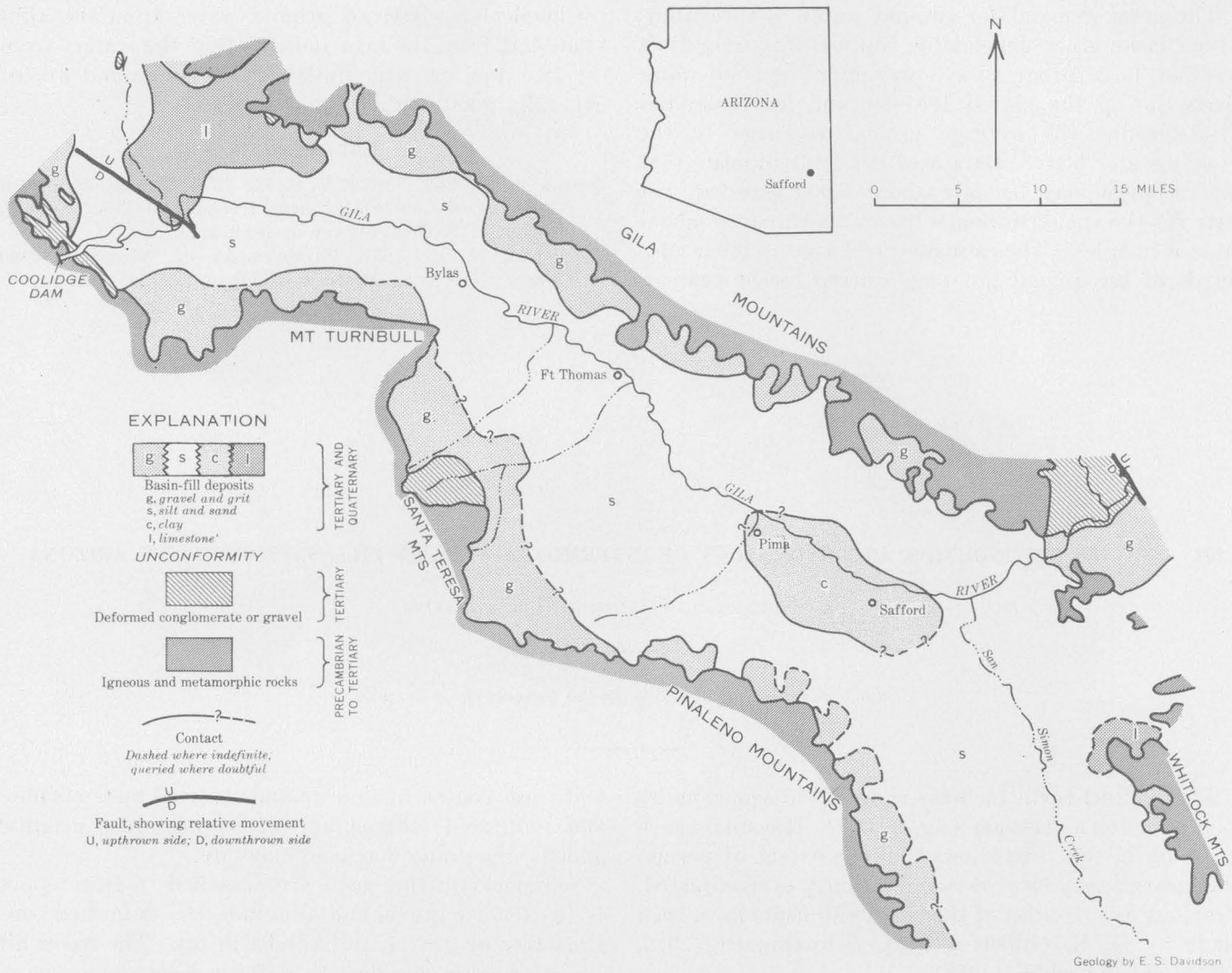

FIGURE 204.1.—Geologic map of the Safford basin, Arizona, showing distribution of basin-fill deposits.

of fill in the basin. They range in age from Pliocene to middle Pleistocene (Knechtel, 1938; Wood, 1960; Lance, 1960). Four principal types of basin-fill sediments can be distinguished: (a) gravel and grit—spread out from the mountains basinward, but deposited in substantial amounts only where large streams entered the basin; (b) silt and sand—deposited over much of the basin by running water, probably in poorly defined stream courses; (c) green and black clay—probably deposited mainly in marshes or swamps; and (d) limestone—deposited in fresh-water lakes. Tuff and diatomite beds and lava flows are interbedded in the sediments and in most areas provide the only convenient means of correlating units from place to place.

The distribution of the several facies of the basin fill and their sedimentary structures suggest that the sediments were deposited by streams heading in the mountains and converging in two low areas represented by extensive limestone and clay facies. Thus, at the time of deposition of the basin-fill sediments, the drainage was largely centripetal, and not throughgoing as at present.

Fanlike gravel beds did not coalesce to form the continuous gravelly basin edge seen in many generalized maps of western basins. The gravel deposits are notably small and sporadic northeast of Safford, at the Whitlock Mountains, and along the edge of the Pinaleno Mountains. Most individual gravel beds do not extend basinward in tongues; instead they grade rather abruptly basinward to silt and fine sand. At some places, particularly north of Fort Thomas to north of Pima, the gravels appear to be relatively thin, and may represent only a thin mantle of gravel

on a bedrock surface. North of the Pinaleno Mountains, gravel in the fans is very poorly sorted, and the fans contain considerable clay.

The basinward edge of the gravel facies is not more than 2 or 3 miles from the older rocks along the basin margin except in a few places where the gravels extend 6 to 8 miles inward from the point where the streams of Tertiary and Quaternary age entered the basin. One of these places is a well-known locality, the site of Gilbert's (1875) type section of the Gila conglomerate, where the present Gila River enters the Safford basin. A similar large stream entered the basin from the south; its mouth is about 10 miles southeast of Coolidge Dam.

Ground water in basin-fill sediments similar to those described is recharged primarily by runoff from rain and snowmelt in adjacent mountains. The most effective channelway for this recharge is the coarse-gravel facies that occurs near the margin of the basin. This gravel margin is not everywhere present, nor is it everywhere highly permeable; thus, water wells drilled in the marginal areas may not everywhere be good producers. Moreover, a thin mantle of gravel over bedrock, clay-rich gravel, silt, or other fine sediment where gravel normally is expected, and a shorter basinward extension of gravel than is commonly expected, all reduce the effective recharge to the basin-fill sediments.

REFERENCES

Gilbert, G. K., 1875, Report on the geology of portions of Nevada, Utah, California, and Arizona: U.S. Geog. and Geol. Surveys W. 100th Meridian Rept., v. 3, p. 17–187.

Knechtel, M. M., 1938, Geology and ground-water resources of the valley of the Gila River and San Simon Creek, Graham County, Arizona: U.S. Geol. Survey Water-Supply Paper 796–F, p. 181–222.

Lance, J. F., 1960, Stratigraphic and structural position of Cenozoic fossil localities in Arizona: Arizona Geol. Soc. Digest, v. 3, p. 155–159.

Schwennesen, A. T., 1919, Ground water in San Simon Valley, Arizona and New Mexico: U.S. Geol. Survey Water-Supply Paper 425–A, p. 1–35.

——— 1921, Geology and water resources of the Gila and San Carlos Valleys in the San Carlos Indian Reservation, Arizona: U.S. Geol. Survey Water-Supply Paper 450–A, p. 1–27.

Wood, P. A., 1960, Paleontological investigations in the 111 Ranch area: Arizona Geol. Soc. Digest, v. 3, p. 141–143.

205. MIOCENE AND PLIOCENE HISTORY OF CENTRAL ARIZONA

By F. R. Twenter, Phoenix, Ariz.

The Mogollon Rim separates the Basin and Range province from the Colorado Plateaus province in central Arizona. Southwest of the Mogollon Rim, Cenozoic rocks fill many basins and valleys, some of which are indicated on figure 205.1. The geological history of this region is shown diagrammatically on figure 205.3, and is summarized below.

A thick series of volcanic rocks, chiefly tuffaceous sediments, pyroclastic deposits, and basaltic lavas, occur throughout much of the Basin and Range province, and part of the Colorado Plateaus province in central Arizona. Volcanic rocks in one area may not be strictly correlative with those in another; however, the major period of Cenozoic volcanic activity in central Arizona probably started in Miocene time and lasted to early Pliocene time.

601530 O—61——11

Basaltic lavas, and pyroclastic and tuffaceous rocks underlain by conglomerate, are called the Hickey formation in the Black Hills (Anderson and Creasey, 1958). Volcanic rocks in the Hickey can be traced into, and correlated with, other volcanic rocks in surrounding areas, and most tuffaceous sediments, pyroclastic rocks, and basaltic lavas in the basins, valleys, and intervening mountains of central Arizona are believed to be equivalent to the Hickey.

The volcanic rocks of the Hickey, and the equivalent volcanics accumulated during a period of recurrent diastrophism. Gradual tilting of large fault blocks produced low-lying areas in which tuffaceous sediments and pyroclastics were deposited. In Rock Springs Valley, Bloody Basin, Seven Springs Basin, lower Verde Valley, and Sunflower Basin, tuffaceous

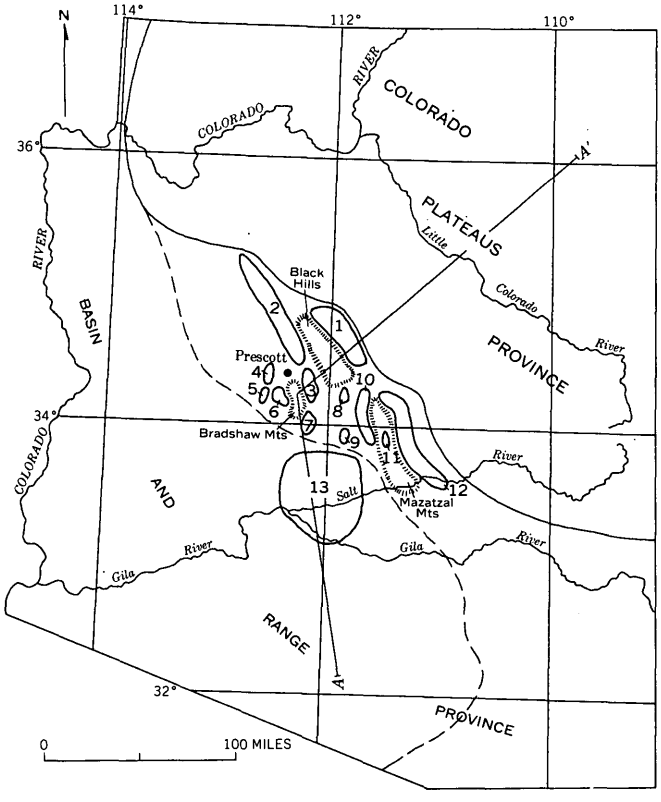

FIGURE 205.1.—Index map of Arizona. Section *A*–*A*' shown on figure 205.3. 1, Verde Valley; 2, Chino Valley; 3, Lonesome Valley; 4, Skull Valley; 5, Peeples Valley; 6, Walnut Grove Basin; 7, Rock Springs Valley; 8, Bloody Basin; 9, Seven Springs Basin; 10, Lower Verde Valley; 11, Sunflower Basin; 12, Tonto Basin; and 13, Phoenix area. The solid line separates the physiographic provinces, the dashed line separates the Mountain Region on the north from the Desert Region on the south.

and pyroclastic rocks equivalent to the Hickey make up the major part of the Cenozoic rocks.

In Verde Valley, volcanic rocks equivalent to the Hickey overlie erosional remnants composed chiefly of conglomerate and lesser amounts of sandstone, mudstone, and limestone; these rocks are referred to here as Dry Beaver Creek rocks. Included with the Dry Beaver Creek rocks are the oldest alluvial materials of Mahard (1949), the Cenozoic sediments of Mears (1950), and the type A gravels of Price (1950). The Dry Beaver Creek rocks are exposed at altitudes ranging from about 3,500 to 6,500 feet and were probably laid down during a continuous cycle of deposition.

After development of the ancestral Mogollon Rim and excavation of a deep, broad valley in the area now occupied by Lonesome, Chino, and Verde Valleys, Dry Beaver Creek rocks were deposited in the Verde Valley area until the accumulated materials were more than 3,000 feet thick. Later erosion removed most of the Dry Beaver Creek rocks; only remnants remained when Hickey-equivalent volcanic deposits accumulated. Similar geologic events may have occurred in much of Arizona's Basin and Range province.

In Verde Valley, Chino Valley, Lonesome Valley, Tonto Basin, Walnut Grove Basin, Peeples Valley, and Skull Valley, volcanic rocks equivalent to the Hickey are overlain by lacustrine and fluviatile rocks that in their lower parts appear to interfinger with or conformably overlie the volcanics; in their upper parts the lacustrine and fluviatile rocks unconformably overlie tilted Hickey equivalents (fig. 205.2). No major break in deposition occurred between the deposition of the volcanic materials and the lacustrine and fluviatile rocks.

Fossiliferous lacustrine and fluviatile rocks in Tonto and Walnut Grove Basins interfinger with or conformably overlie volcanic rocks equivalent to the Hickey. Fossils in the upper part of beds in the Tonto Basin are "no older than lower Pliocene and possibly as young as middle Pliocene" (J. F. Lance, oral communication, 1960). In Walnut Grove Basin, the upper member of Hook's Milk Creek formation,[1] which overlies tuffaceous rocks equivalent to volcanic rocks in the Hickey formation, contains "* * * diagnostic fossils of lower Pliocene age" (Lance, 1960, p. 156). These fossils indicate that deposition of the lacustrine and fluviatile rocks that overlie volcanic rocks equivalent to the Hickey formation began in lower Pliocene time, and that the Hickey formation and equivalent volcanic rocks accumulated in Miocene and earliest Pliocene time. They indicate, also, that the Dry Beaver Creek rocks are no younger than

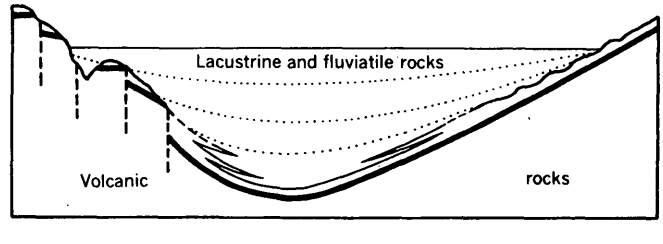

FIGURE 205.2.—Diagrammatic section of typical basin or valley, showing relation of volcanic rocks (equivalent to the Hickey formation) to lacustrine and fluviatile rocks. Black line in volcanic rocks and dotted lines in lacustrine and fluviatile rocks are hypothetical marker beds.

[1] Hook, D. L., 1956, Late Cenozoic stratigraphy and structure of part of the Walnut Grove Basin, Yavapai County, Arizona: Unpub. M.A. thesis, Arizona Univ.

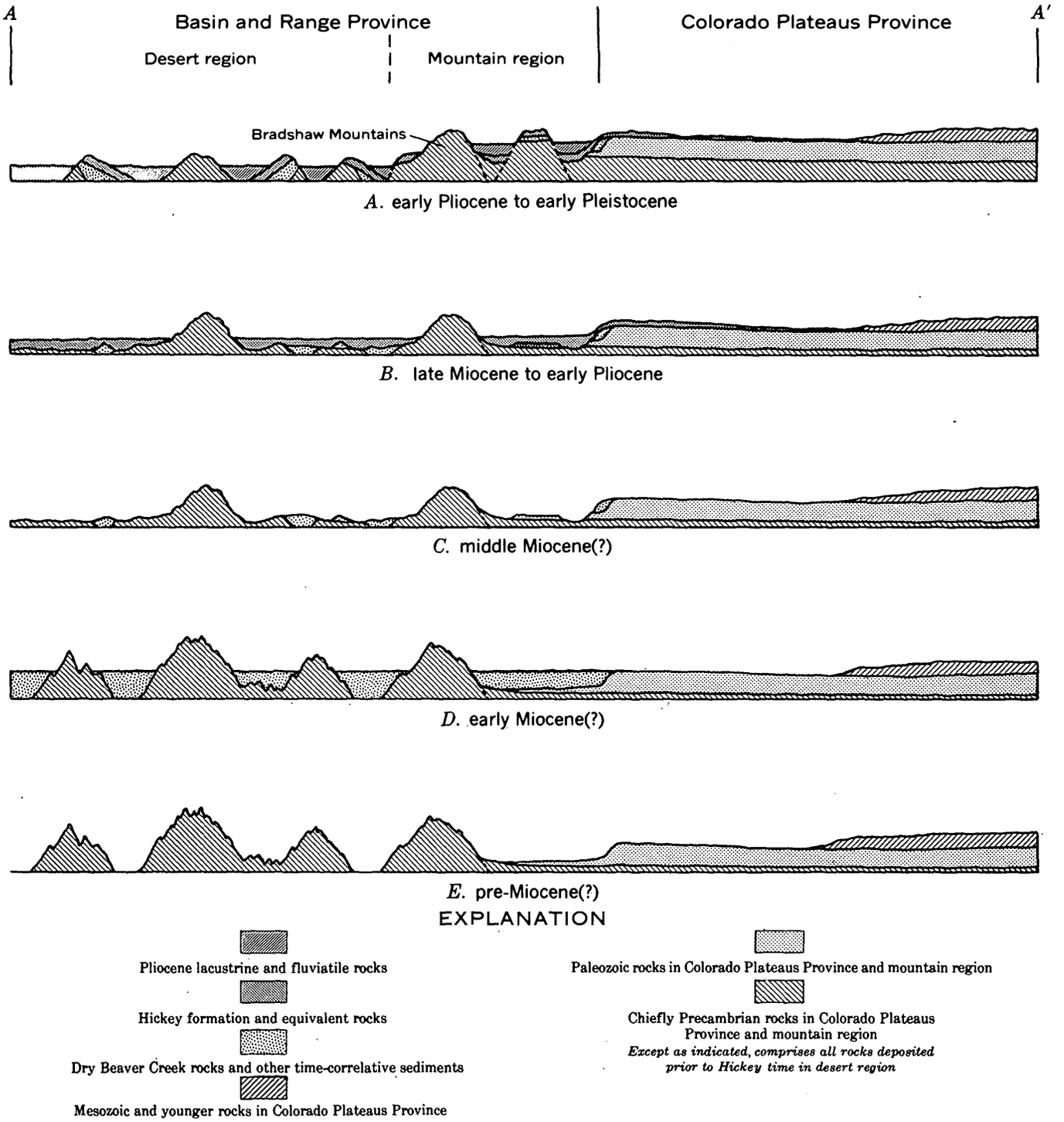

FIGURE 205.3.—Diagrammatic sections showing relations of rocks along section *A–A'*, figure 205.1.

Miocene, and that the Mogollon Rim is Miocene or older.

Recurrent structural movement during and following deposition of the Hickey and equivalent rocks elevated the Colorado Plateaus and produced the present mountain ranges of the Basin and Range province. Thereafter, the uplifted areas were eroded and the basins alluviated.

Deposits correlative with the fossil-bearing rocks in Walnut Grove and Tonto Basins are covered by later deposits in much of the desert region, especially in the Phoenix area; however, tilted blocks of rocks equivalent to the Hickey protrude above the alluviated desert floor locally.

REFERENCES

Anderson, C. A., and Creasey, S. C., 1958, Geology and ore deposits of the Jerome area, Yavapai County, Arizona: U.S. Geol. Survey Prof. Paper 308, 185 p.

Jenkins, O. P., 1923, Verde River lake beds near Clarkdale, Arizona: Am. Jour. Sci., 5th ser., v. 5, no. 25, p. 65–81.

Lance, J. F., 1960, Stratigraphic and structural position of Cenozoic fossil localities in Arizona: Arizona Geol. Soc. Digest, v. 3, p. 155–159.

Mahard, R. H., 1949, Late Cenozoic chronology of the Upper Verde Valley, Arizona: Denison Univ., Sci. Lab. Bull., v. 41, art. 7, p. 97–127.

Mears, Brainerd, Jr., 1950, Cenozoic geomorphic history of the Oak Creek Canyon region, Arizona [Abs.]: Geol. Soc. America Bull., v. 61, no. 12, pt. 2, p. 1557.

Price, W. E., Jr., 1950, Cenozoic gravels on the rim of Sycamore Canyon, Arizona: Geol. Soc. America Bull., v. 61, no. 5, p. 501–508.

206. CORRELATION OF PERMIAN ROCKS IN NORTHEASTERN ARIZONA AND ADJOINING PARTS OF NEW MEXICO AND UTAH

By Charles B. Read and A. A. Wanek, Albuquerque, N. Mex., and Menlo Park, Calif.

The Permian rocks that crop out in the Monument Valley upwarp and Defiance uplift, Arizona and Utah, the Mogollon Rim, Arizona, and the Zuni Mountains of New Mexico, have been studied by one or both of us at various times during the last 15 years. This report is a résumé of our present opinions regarding the correlation of these strata and will be supplemented at a later date by a more detailed account. The accompanying index map, figure 206.1, shows the location of all the areas discussed except the Mogollon Rim, which lies south of the map in Arizona at a latitude of approximately 34°15′ N.

The Zuni uplift in New Mexico is an oval eroded dome locally complicated by faults. Permian rocks are exposed widely in the central part of the dome and rest directly on rocks of Precambrian age, or on marine rocks that may be of Pennsylvanian or Permian age. The stratigraphic sequence in the Zuni uplift is shown in table 206.1, column 1 (Read, 1950).

The Mogollon Rim is an east-trending escarpment in central Arizona. It has been studied by Huddle and Dobrovolny (1945) and by one of us in the vicinity of Carrizo Creek and the canyon of Salt River. The stratigraphic sequence is shown in table 206.1, column 2.

The Defiance uplift is an asymmetrical anticline that trends north along the New Mexico-Arizona line from about the latitude of Gallup almost to the Four Corners. Permian rocks as shown in table 206.1, columns 3 and 4, rest on Precambrian rocks in the southern and central parts of the uplift, but elsewhere the base of the section has not been observed (Read, 1950).

The Monument Valley upwarp is a major structural feature in the central part of the Colorado Plateau province and lies athwart the Arizona-Utah boundary line. In this area, rocks of Permian age rest conformably on strata assigned to the Rico and Hermosa formations. The stratigraphic sequence in the Monument Valley upwarp is shown in table 206.1, columns 5 and 6 (Baker and Reeside, 1929; Baker, 1936).

Figure 206.1.—Index map of parts of Arizona, New Mexico, and Utah showing locations of the Zuni uplift, Defiance uplift, and Monument Valley. Arrows indicate the dominant direction of inclination of crossbedding in (M) Meseta Blanca member of the Yeso formation; (G) Glorieta sandstone; (LD) lower member of the De Chelly sandstone; (UD) upper member of the De Chelly sandstone; (C) Cedar Mesa sandstone member of the Cutler formation; and (CO) Coconino sandstone.

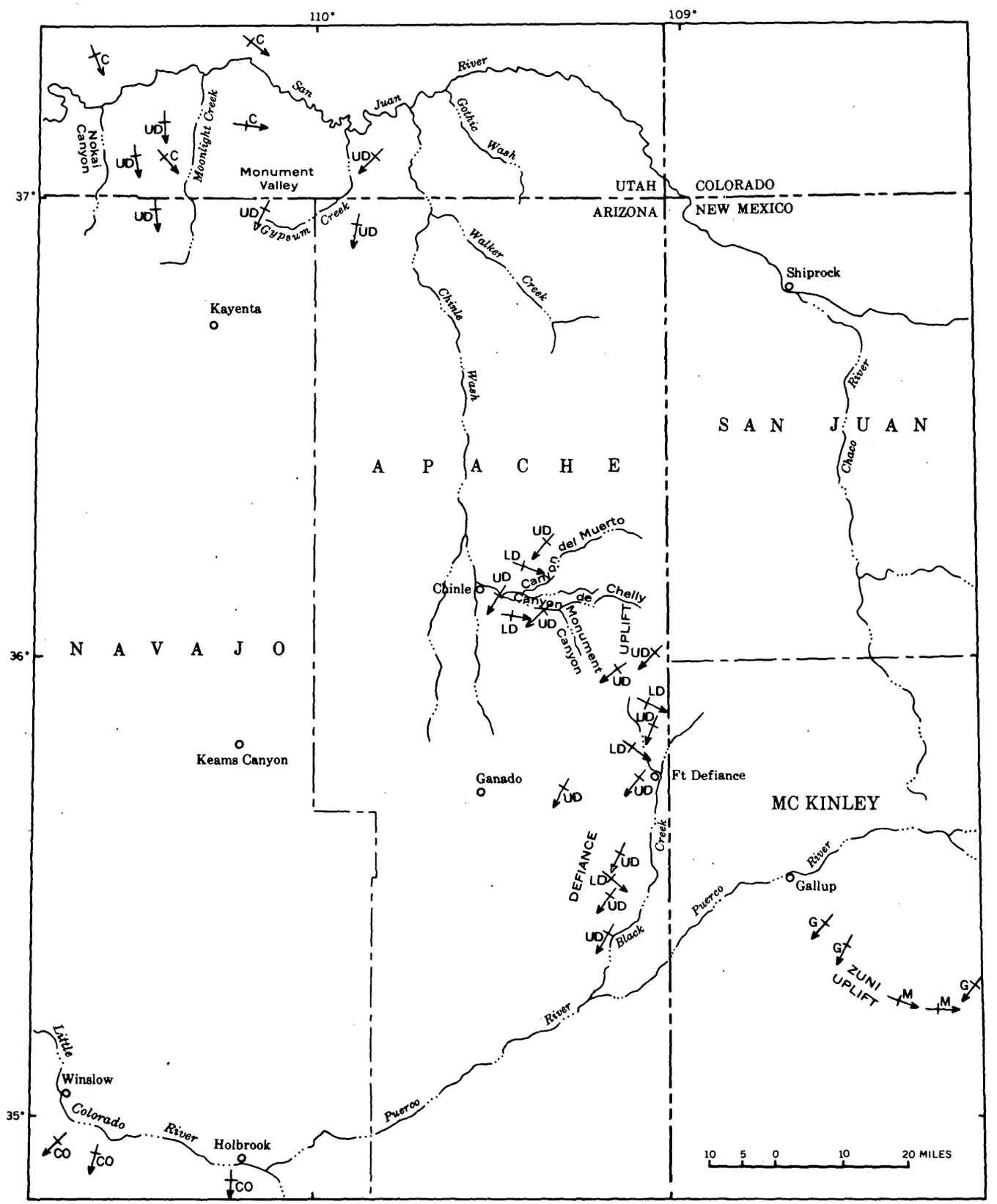
110°
109°
37°
36°
35°
UTAH
COLORADO
ARIZONA
NEW MEXICO
Nokai Canyon
Moonlight Creek
Monument Valley
San Juan River
Gothic Wash
Gypsum Creek
Walker Creek
Chinle Wash
Kayenta
Shiprock
Chaco River
SAN JUAN
APACHE
NAVAJO
Chinle
del Muerto Canyon
de Chelly Canyon
Monument Canyon
UPLIFT
Keams Canyon
Ganado
Ft Defiance
MC KINLEY
DEFIANCE
Black Creek
Puerco River
Gallup
ZUNI UPLIFT
Little Colorado River
Winslow
Holbrook
10 5 0 10 20 MILES

TABLE 206. 1.—*Nomenclature and correlation of Permian sequences in parts of New Mexico, Arizona, and Utah*

[Equivalence is not necessarily implied in the "Triassic and younger" and "Pennsylvanian and Permian?" brackets where formations or members are placed opposite]

SYSTEM	1 Zuni uplift, New Mexico	2 Mogollon Rim, Arizona	3 Defiance uplift, Arizona — Southern part	4 Defiance uplift, Arizona — Northern part	5 Monument Valley, Utah and Arizona — Eastern part	6 Monument Valley, Utah and Arizona — Western part
TRIASSIC AND YOUNGER	Shinarump member of Chinle formation	Various Mesozoic and Cenozoic formations	Shinarump member of Chinle formation	Shinarump member of Chinle formation	Moenkopi formation	Moenkopi formation
TRIASSIC (?)					Hoskinnini tongue	Hoskinnini tongue
PERMIAN	San Andres limestone / Glorieta sandstone	Kaibab limestone / Coconino sandstone	De Chelly sandstone — Upper member	De Chelly sandstone — Upper member	De Chelly sandstone member	De Chelly sandstone member
	Yeso formation — San Ysidro member	Supai formation — Upper member	Lower member	Lower member	Organ Rock tongue	Organ Rock tongue
	Yeso formation — Meseta Blanca sandstone member	Supai formation — Middle member	Supai formation	Supai formation	Cedar Mesa sandstone member	Cedar Mesa sandstone member
	Abo formation	Supai formation — Lower member			Halgaito tongue	Halgaito tongue
PENNSYLVANIAN AND PERMIAN(?)	Madera formation (Pennsylvanian) — Red Tanks member	(Beds of Pennsylvanian age may be included in the Supai formation)			Rico formation (May contain beds of both Permian(?) and Pennsylvanian ages)	Rico formation (May contain beds of both Permian(?) and Pennsylvanian ages)
	Madera formation (Pennsylvanian)	Naco formation (Pennsylvanian)			Hermosa formation (Pennsylvanian)	Hermosa formation (Pennsylvanian)

The general correlation of the Permian strata based on both physical and paleontologic data as interpreted by the writers is also shown in table 206.1. We are of the opinion that the Abo formation of the Zuni Mountains correlates with the lower member of the Supai formation along the Mogollon Rim in the vicinity of Carrizo Creek. The lower part of the Supai formation in the Defiance uplift, and part or all of the Halgaito tongue of the Cutler formation in Monument Valley, also seem to be equivalent to the Abo formation.

The Yeso formation in the Zuni uplift consists of the Meseta Blanca and the San Ysidro members and is equivalent to the middle and upper members of the Supai in the Mogollon Rim. Equivalent strata in the Defiance uplift are the upper part of the Supai and the lower member of the De Chelly sandstone. The Cedar Mesa sandstone member of the Cutler formation in Monument Valley is believed to be the approximate correlative of the Meseta Blanca sandstone member of the Yeso formation; the Organ Rock tongue seems to correlate with the San Ysidro member of the Yeso formation, and with the upper part of the Supai formation and the lower member of the De Chelly sandstone.

The Glorieta sandstone and the San Andres limestone are correlated on paleontological evidence with the Coconino sandstone and Kaibab limestone, respectively, of the Mogollon Rim. The upper member of the De Chelly sandstone in the Defiance uplift is correlated with the Glorieta sandstone and the Coconino sandstone. Except for one report of its occurrence in the subsurface south of Fort Defiance, Ariz., the Kaibab limestone is believed to be absent from the uplift (Peirce, 1958).

The upper member of the De Chelly sandstone in the Defiance uplift seems to correlate with the De Chelly sandstone member of the Cutler formation in Monument Valley.

The Hoskinnini tongue of the Cutler formation, as defined by Baker (1936) and Baker and Reeside (1929), is of uncertain age. Physical evidence suggests that it may be a part of the Moenkopi formation and it is so shown in table 206.1.

Of interest in connection with the correlation of the Permian strata are the dominant directions of the foreset beds in the thick tangentially crossbedded sandstones that are present in all the areas examined. These are shown in figure 206.1. (See also Reiche, 1938.) The dominant directions were determined by measuring 100 or more directions of maximum inclination of crossbedding at places shown on the map, and plotting these in 5° and 10° classes.

Two preferred directions of inclination were observed, one trending southeast and east, and the other south and southwest. The southeast-east directions of inclination are characteristic of the Meseta Blanca sandstone in the Zuni Mountains, the lower member of the De Chelley sandstone in the Defiance uplift, and the Cedar Mesa sandstone member of the Cutler in Monument Valley. Observations on the direction of inclination of foreset beds in the middle member of the Supai formation on the Mogollon Rim have not been made.

South to southwest directions of inclination are characteristic of the Glorieta sandstone in the Zuni uplift, the upper member of the De Chelly sandstone in the Defiance uplift, and the De Chelly member of the Cutler formation in Monument Valley. In the area of Holbrook and Winslow, Ariz., south to southwest directions of inclination of foreset beds were observed in the Coconino sandstone. Observations have not been made at more southerly places.

These thick tangentially crossbedded sandstones have been referred to by some as having been deposited under aeolian conditions (Opdyke and Runcorn, 1960). Others have ascribed their origin to beach and nearshore marine environments, thus interpreting them as transgressive sandstones (Read and others, 1945; Read, 1950). At the present time we prefer this interpretation.

Whether the rocks were deposited in aeolian or in transgressive beach and bar environments, there is evidence that the wind or the water, or both, moved toward the south and southeast during transportation and deposition of the sediments of the lower group of sandstones. The sediments of the upper group of sandstones were transported by wind or water, or both, moving to the south and southwest.

Explanation of these changes in directions of currents as indicated by the direction of crossbedding is conjectural. They may be related, however, to differences in direction of marine transgression.

REFERENCES

Baker, A. A., 1936, Geology of the Monument Valley-Navajo Mountain region, San Juan County, Utah: U.S. Geol. Survey Bull. 865, p. 24–40.

Baker, A. A., and Reeside, J. B., Jr., 1929, Correlation of the Permian of southern Utah, northern Arizona, and southwestern Colorado: Am. Assoc. Petroleum Geologists Bull., v. 13, no. 11, p. 1413–1449.

Huddle, J. W., and Dobrovolny, Ernest, 1945, Late Paleozoic stratigraphy and oil and gas possibilities of central and northeastern Arizona: U.S. Geol. Survey Oil and Gas Inv. Prelim. Chart 10.

Opdyke, N. D., and Runcorn, S. K., 1960, Wind direction in the western United States in the late Paleozoic: Geol. Soc. America Bull., v. 71, p. 959–971.

Peirce, H. W., 1958, Permian sedimentary rocks of the Black Mesa basin area, *in* New Mexico Geol. Soc. Guidebook of the Black Mesa basin, 9th Field Conf.: p. 82–87.

Read, C. B., 1950, Stratigraphy of the outcropping Permian rocks around the San Juan Basin, *in* New Mexico Geol. Soc. Guidebook of the San Juan Basin, New Mexico and Colorado: p. 62–66.

Read, C. B., Wilpolt, R. H., Andrews, D. A., and others, 1945, Geologic map and stratigraphic sections of Permian and Pennsylvanian rocks of parts of San Miguel, Santa Fe, Sandoval, Bernalillo, Torrance, and Valencia Counties, north-central New Mexico: U.S. Geol. Survey Oil and Gas Inv. Map OM–21.

Reiche, Parry, 1938, An analysis of cross-lamination; the Coconino sandstone: Jour. Geology, v. 46, no. 7, p. 905–932, 6 figs. incl. index maps.

207. TROY QUARTZITE (YOUNGER PRECAMBRIAN) AND BOLSA AND ABRIGO FORMATIONS (CAMBRIAN), NORTHERN GALIURO MOUNTAINS, SOUTHEASTERN ARIZONA

By Medora H. Krieger, Menlo Park, Calif.

Recent detailed mapping in the northern end of the Galiuro Mountains, Pinal County, Ariz., has solved some problems that have long puzzled stratigraphers. Many geologists have considered the Troy quartzite to be correlative with the Cambrian Bolsa quartzite and Abrigo limestone farther south. Thick diabase sills in the area have been variously considered to be post-Pennsylvanian to pre-Troy in age. Mapping in the Holy Joe Peak quadrangle (fig. 207.1) in southern Arizona has proved that rocks formerly called Troy quartzite include units of Precambrian and Cambrian age and that these units are separated by a major unconformity. The older of these two units, to which the name Troy is here restricted, rests disconformably on the Dripping Spring quartzite of the Precambrian Apache group and has been extensively injected by diabase also of Precambrian age. The Cambrian beds compose the Bolsa and overlying Abrigo formations; the Bolsa rests from place to place on the Apache group, on Troy, and on deeply weathered diabase.

Ransome (1915, p. 384–385) named the Troy quartzite and used the name at Ray and in the Sierre Ancha; he included it in the Apache group, which he considered to be Cambrian in age. He found that the upper part locally contains shaly and silty sandstone. Cambrian fossils had already been discovered in similar beds farther east (Campbell, 1904). Diabase sills were considered to be post-Paleozoic by Ransome (1903, p. 86). Darton (1925, p. 36) recognized that—

* * * the "Troy" in most places includes in its upper part or is overlain by a much younger sandstone, doubtless equivalent to the Tapeats and Bolsa-Abrigo beds.

Darton (1925, p. 34 and 254) found that the Troy locally rests with sedimentary contact on diabase and concluded that small diabase dikes in younger Paleozoic limestones are not of the same age as the large diabase sills. Stoyanow (1936, p. 472–481) extended the name Troy southward to the Santa Catalina Mountains, where it conformably underlies the Abrigo. Farther south the Abrigo overlies the Bolsa quartzite. Stoyanow placed the Apache group, minus the Troy, in the Precambrian. Shride (1958 and oral communications) recognized the pre-diabase and Precambrian age of the Troy in the Sierra Ancha and concluded that it was separated from Cambrian sedimentary rocks farther south by a long time interval; the two formations, however, had not been definitely recognized in contact until the present study.

In the Holy Joe Peak quadrangle Cambrian rocks rest at most places on the Dripping Spring quartzite of the Apache group or on diabase, but in local areas Cambrian rocks rest on the Troy quartzite, which has been preserved in grabens and intruded by diabase in the same manner as the Apache. The best exposures are in the Zapata Mountain-Holy Joe Peak area (fig. 207.1), where as much as 700 feet of the formation is preserved. The Troy, which is mainly conglomerate and sandstone in a lower member and quartzite in an upper member, is overlain by about 700 feet of Cambrian sandstone, shale, and mudstone, consisting of two cliff-forming units alternating with two slope-forming units (fig. 207.2, top). The lower, cliff-forming unit is the Bolsa quartzite; the upper three units are assigned to the Abrigo formation, which here contains carbonate beds at the top.

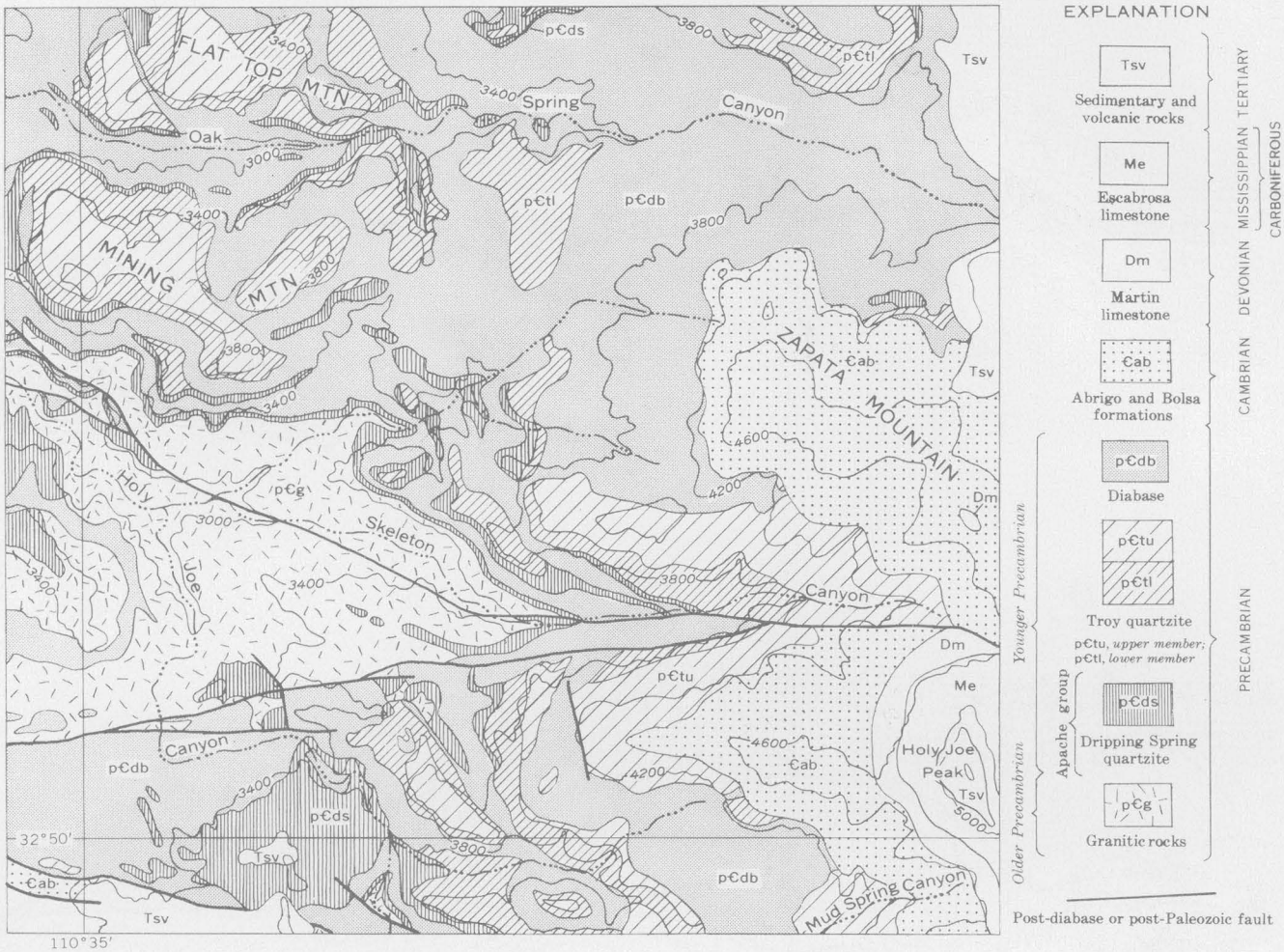

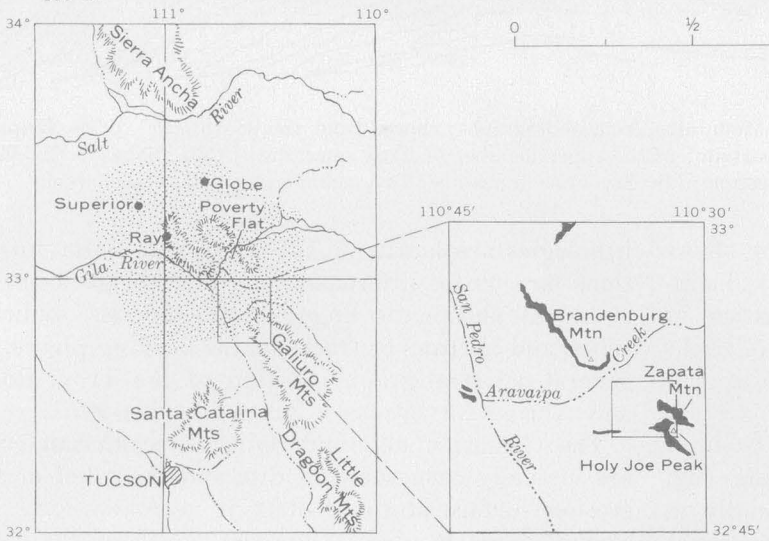

INDEX MAP OF SOUTHEASTERN ARIZONA

HOLY JOE PEAK QUADRANGLE SHOWING LOCATION OF DETAILED GEOLOGIC MAP

Index map of the quadrangle shows in black the outcrops of Cambrian formations. Troy quartzite only locally underlies the Cambrian rocks on Zapata and Brandenburg Mountains and west of the San Pedro

The index map of southeastern Arizona shows location of areas cited and the area (stippled) within which both the younger Precambrian Troy and the Cambrian formations are known to occur; north of the area only Troy remains; south of it only Cambrian formations are present

FIGURE 207.1.—Geologic map of the Zapata Mountain-Holy Joe Peak area.

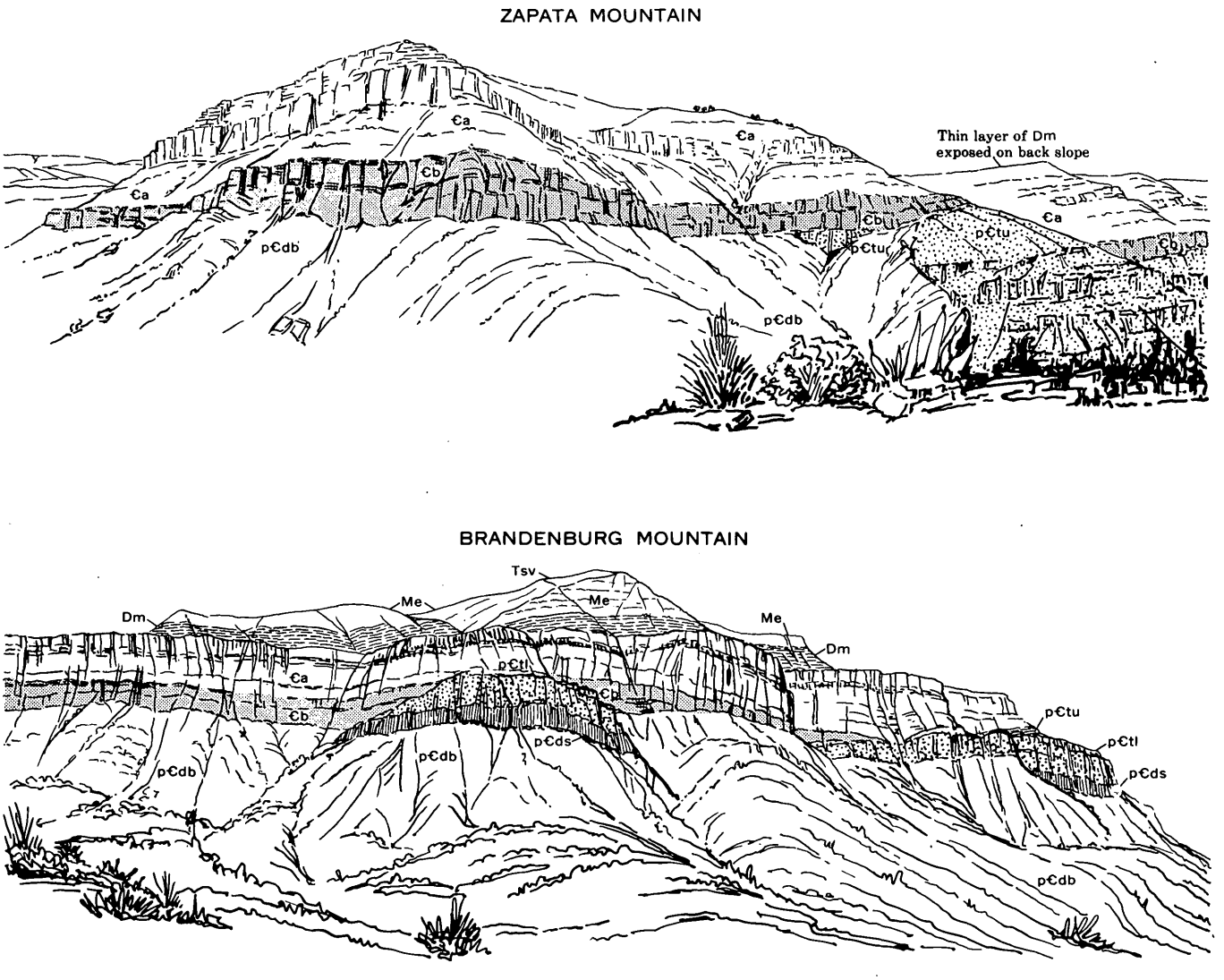

FIGURE 207.2.—Sketches of Zapata and Brandenburg Mountains, from photographs; viewed from the southwest. p€ds, Dripping Spring quartzite; p€tl, lower member of Troy quartzite; p€tu, upper member of Troy quartzite; p€db, diabase; €b, Bolsa quartzite; €a, Abrigo formation; Dm, Martin limestone; Me, Escabrosa limestone; Tsv, sedimentary and volcanic rocks.

In the Holy Joe Peak quadrangle the Troy shows no significant lateral variations and is readily distinguished from the Bolsa and Abrigo by differences in color, composition, and bedding, and by the relations to diabase. The lower member of the Troy is generally dark brownish gray, the upper member is white or light gray; the Cambrian rocks are pale or light brown. Channeling and very irregular bedding (fig. 207.3*A*) are characteristic of the Troy, especially in the lower member, which is probably of terrestrial origin; bedding in the overlying Cambrian rocks is much more regular (fig. 207.3*B*). Wherever the base of the Troy is exposed, it includes conglomerate, light bluish-gray sandstone, and arkosic conglomerate; conglomerates in the basal part of the Bolsa locally resemble conglomerate in the basal Troy, but the other lithologies are lacking. The Troy and Bolsa formations are unfossiliferous, but the Abrigo contains abundant phosphatic linguloid brachiopods, scolithus tubes, and burrows or tracks on the bedding planes. A generalized stratigraphic section of the Troy, Bolsa, and Abrigo formations is given in table 207.1.

The Cambrian and underlying Precambrian rocks are virtually concordant in dip, and the relief on the erosion surface at the contact is generally low. At Brandenburg Mountain, however, much of the Cambrian pinches out against monadnocks of the Troy (fig. 207.2, bottom). The Troy is assigned to the Precambrian because of the long time interval that probably is represented by its complete removal from large areas, and by deep weathering of the diabase prior to deposition of the Bolsa. Isotope analyses of ura-

nium- and thorium-bearing minerals in differentiates in diabase in the Sierra Ancha indicate a minimum age of about 1,200 million years (Silver, 1960) for the diabase.

Stratigraphic sections between the Little Dragoon Mountains and the Sierra Ancha show that the Cambrian rocks become thinner and the Abrigo becomes progressively more sandy northward; hence, the term Abrigo formation seems more appropriate than Abrigo limestone in and north of the Santa Catalina Mountains. Cambrian stratigraphic units in the Santa Catalina Mountains and in the Holy Joe Peak quadrangle are similar to and are correlative with the Bolsa and Abrigo farther to the south. Near Poverty Flat on the Gila River, and near Superior, undifferentiated Cambrian beds rest on the Troy quartzite; near Globe Cambrian rocks rest on the Apache group. No Cambrian rocks have been recognized in the Sierra Ancha where sandstone of Devonian age fills deep channels in the Troy quartzite. The Troy in that area includes three members; the lowest pinches out southward. The middle member is primarily a sandstone that has large-scale crossbedding and thus differs lithologically from the lowest member in the

TABLE 207.1.—*Generalized stratigraphic section of Troy, Bolsa, and Abrigo formations*

	Thickness (feet)
Abrigo formation:	
Upper slope-forming unit. Sandstone, shale, mudstone, and quartzite; some cliff-forming; tracks and trails common; brown quartzite and sandstone that contain phosphatic linguloid brachiopods at base of upper 100 feet, overlain by interbedded sandstone, glauconitic beds, intraformational conglomerate, and minor amounts of carbonate; dolomite and limestone that contain silicified *Billingsella* brachiopods near top	248
Upper cliff-forming unit. Sandstone and quartzite, similar to Bolsa quartzite, but thicker bedded and contain scolithus tubes and horizontal markings	126
Lower slope-forming unit. Sandstone, shale, mudstone, and thin interbedded quartzite; contains abundant fragments of phosphatic linguloid brachiopods especially in lower part, and vertical scolithus tubes and horizontal tracks or burrows higher up	155
Total Abrigo formation	529
Bolsa quartzite:	
Cliff-forming, unfossiliferous, even-grained, evenly bedded sandstone and quartzite, locally crossbedded, thinly bedded and very thinly laminated at top; purplish pebble- to small boulder-conglomerate, as much as 25 feet thick, at base where it rests on diabase, but absent where it rests on Troy	158
Total Cambrian	687
Troy quartzite:	
Upper member. Quartzite and some sandstone, mostly cliff-forming, white, quite pure, locally slightly arkosic (white feldspar or clay from feldspar), in part pebbly (quartz pebbles), thicker bedded than lower unit and irregularly bedded; base is white quartzite about 6′ thick with 6″ quartz-pebble conglomerate beds	523
Lower member. Sandstone, conglomerate, a few beds of quartzite, and thin silty layers; mostly cliff-forming; dark brownish-gray-weathering; thin and very irregular bedding, abundant channelling; two conglomerate beds and intervening light bluish-gray sandstone at base; abundant large pink fragments of feldspar and quartz porphyry in upper conglomerate; light-colored quartzite beds more abundant upward	208
Total Troy quartzite	731

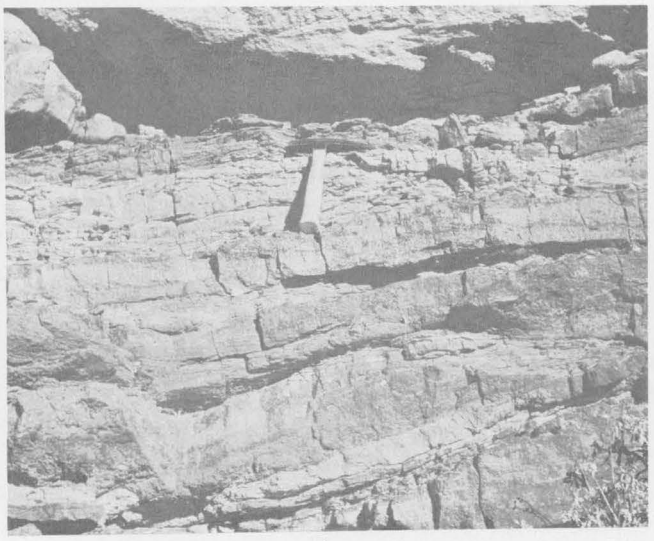

A

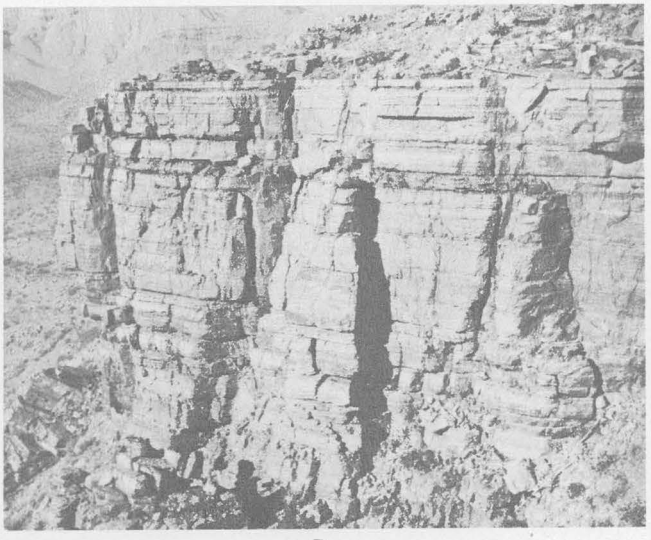

B

FIGURE 207.3.—Contrasting bedding features in the Troy and Bolsa quartzites. *A*, Details of channeling and very irregular bedding in lower member of Troy quartzite. *B*, Thin regular bedding in top of Bolsa quartzite.

Holy Joe Peak area, but the two units can be correlated as shown by progressive changes between the two areas.

REFERENCES

Campbell, M. R., 1904, The Deer Creek coal field, Arizona: U.S. Geol. Survey Bull. 225, p. 240–258.

Darton, N. H., 1925, A résumé of Arizona geology: Ariz. Bur. Mines Bull. 119, 298 p.

Ransome, F. L., 1903, Geology of the Globe copper district, Arizona: U.S. Geol. Survey Prof. Paper 12, 168 p.

Ransome, F. L., 1915, The Paleozoic section of the Ray quadrangle, Arizona: Washington Acad. Sci. Jour., v. 5, p. 380–388.

Shride, A. F., 1958, Younger Precambrian geology in southeastern Arizona [abs.]: Geol. Soc. America Bull., v. 69, p. 1744.

Silver, L. T., 1960, Age determinations on Precambrian diabase differentiates in the Sierra Ancha, Gila County, Arizona [abs.]: Geol. Soc. America Bull., v. 71, p. 1973–1974.

Stoyanow, A. A., 1936, Correlation of Arizona Paleozoic formations: Geol. Soc. America Bull., v. 47, p. 459–540.

208. TRAP-DOOR INTRUSION OF THE CAMERON CREEK LACCOLITH, NEAR SILVER CITY, NEW MEXICO

By Walden P. Pratt and William R. Jones, Denver, Colo.

The Silver City region of southwestern New Mexico contains a variety of intrusive igneous masses—dikes, sills, laccoliths, and stocks—in a terrane characterized also by a complex pattern of normal faults (Art. 150). Recent mapping in the Hurley West quadrangle, on the southern edge of the Silver City region, has revealed details of intrusion of the Cameron Creek laccolith, once regarded as a stock (Paige, 1916) but now known to have a concordant roof and floor. The laccolith made room for itself by lifting its roof like a trap-door; the fault that represents the open side of the "trap-door" was then stoped out by the magma and is no longer exposed. Interpretation of the development of the laccolith and the structures around it, which involve two periods of faulting earlier than the laccolith, is facilitated by the presence of segments of an older sill that postdated the first period of faulting but predated the second. The present distribution of formations and the shape of the laccolith are shown on the geologic map (fig. 208.1) and cross sections (fig. 208.2). Our interpretation of the stages of development is shown on figure 208.3 as successive maps, somewhat generalized, at the level of the present ground surface. This interpretation is summarized as follows:

1. Pre-Late Cretaceous tilting and normal faulting of the Oswaldo formation, with dominantly right-lateral apparent offset. Erosion to an irregular surface, followed by deposition of the Beartooth quartzite in Late(?) Cretaceous time and the Colorado formation in Late Cretaceous time (fig. 208.3*A*).
2. Emplacement of Chino Quarry sill within the Oswaldo formation, at different distances above the base because of the earlier faulting. Roof rocks are raised uniformly. Southernmost of earlier faults is locus of feeder channel (fig. 208.3*B*).
3. Minor folding of Oswaldo and Beartooth formations, and renewed faulting, with left-lateral apparent offset. Major movement is on Indian Village fault, which splits westward into two (or more) faults, southernmost of which is later to coincide with part of Cameron Creek fault (fig. 208.3*C*).
4. Intrusion of Cameron Creek laccolith along surface indicated by dotted line in figure 208.3*C*. Room for laccolith is created by vertical uplift of roof rocks along a new fault, the Cameron Creek fault (which represents the open side of the "trap-door"), so that the entire block north of fault is apparently offset to east (fig. 208.3*D*). (Hinge of "trap-door" is represented by point where laccolith wedges out to north—now concealed under Gila conglomerate.) Laccolith magma then partly engulfs rocks south of fault so that western part of fault now appears stoped. Rocks within Indian Village fault zone—Lake Valley limestone, Oswaldo formation, and Chino Quarry sill—are severely faulted by drag along Cameron Creek fault (fig. 208.3*D*).

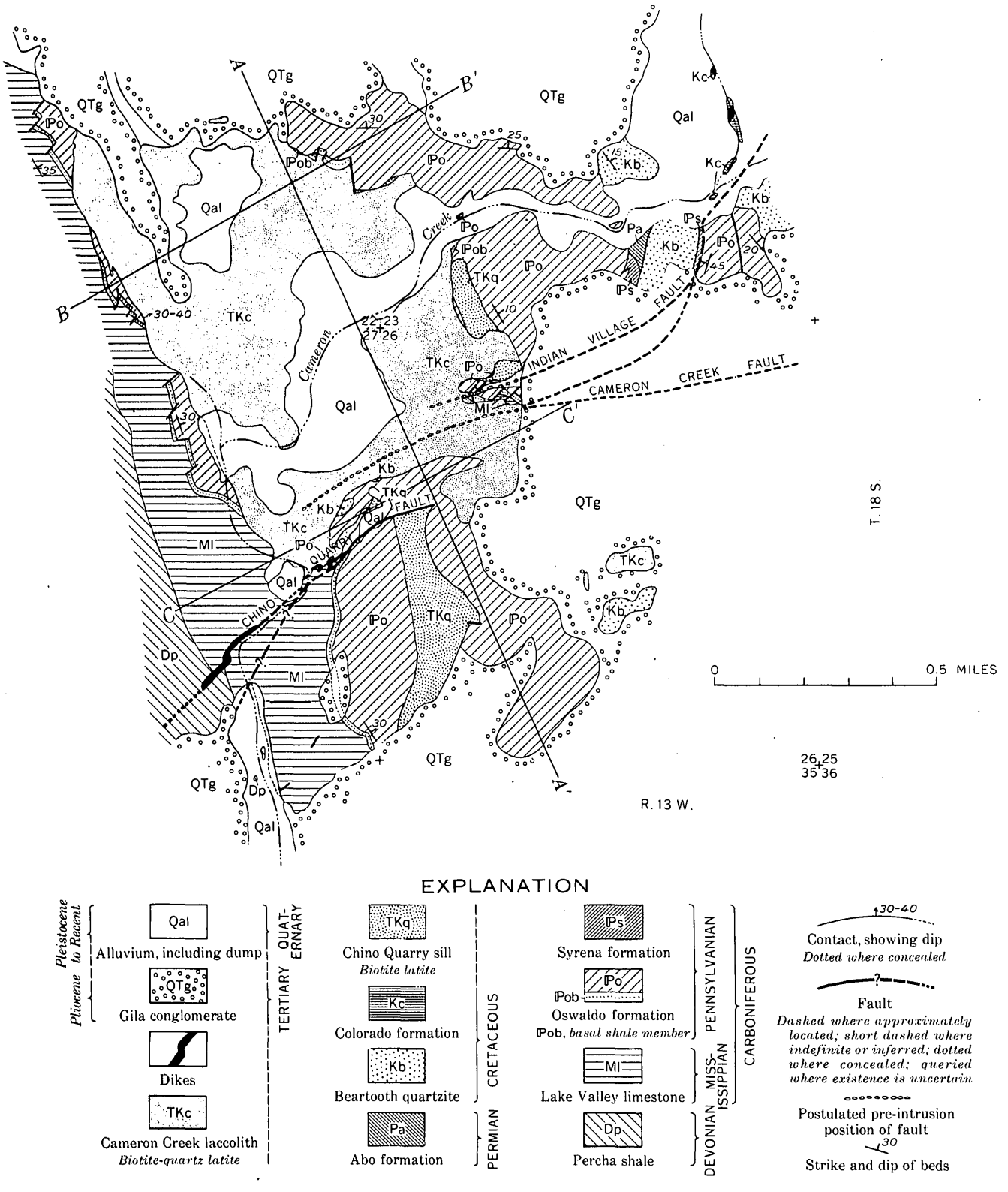

FIGURE 208.1.—Geologic map of part of Hurley West quadrangle, Grant County, N. Mex.

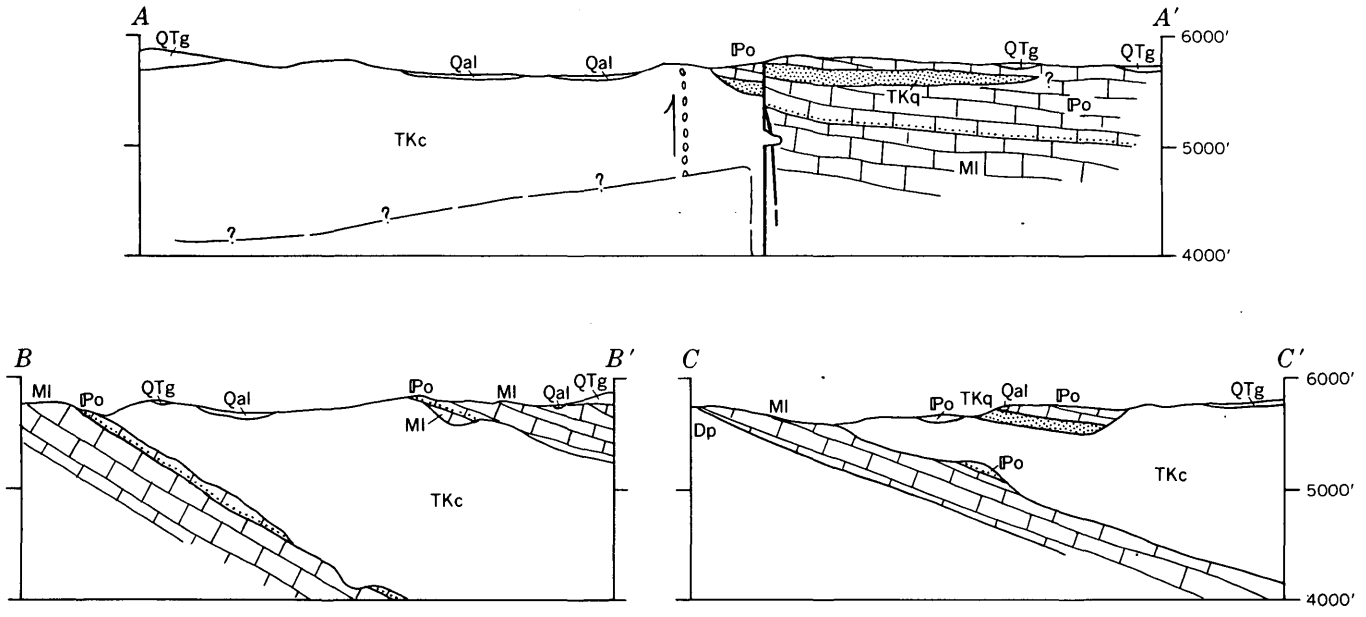

FIGURE 208.2.—Cross sections through Cameron Creek laccolith. (Compare fig. 208.1.)

5. Erosion; deposition of Gila conglomerate; later erosion to present surface (fig. 208.1).

Evidence that the Chino Quarry fault preceded, and in part limited, emplacement of the Cameron Creek laccolith, is found in the fault zone in the NE¼SE¼ sec. 27, T. 18 S., R. 13 W., where the laccolith intrudes the rock of the fault zone. The presence in the fault zone of dark-green latite like that of the Chino Quarry sill suggests that the original fault acted as a feeder for the sill—as it did later for the Cameron Creek laccolith. According to this interpretation, renewed movement on the fault after emplacement of the sill (fig. 208.3*C*) deformed the feeder dike and left the isolated remnants now exposed.

The geologic age of the faults and the intrusive rocks is known only as post-middle Late Cretaceous and pre-late Miocene(?); within these limits they can be dated only with respect to each other and therefore cannot be correlated certainly with any specific epoch of the Tertiary.

REFERENCE

Paige, Sidney, 1916, Description of the Silver City quadrangle, New Mexico: U.S. Geol. Survey Geol. Atlas, Folio 199.

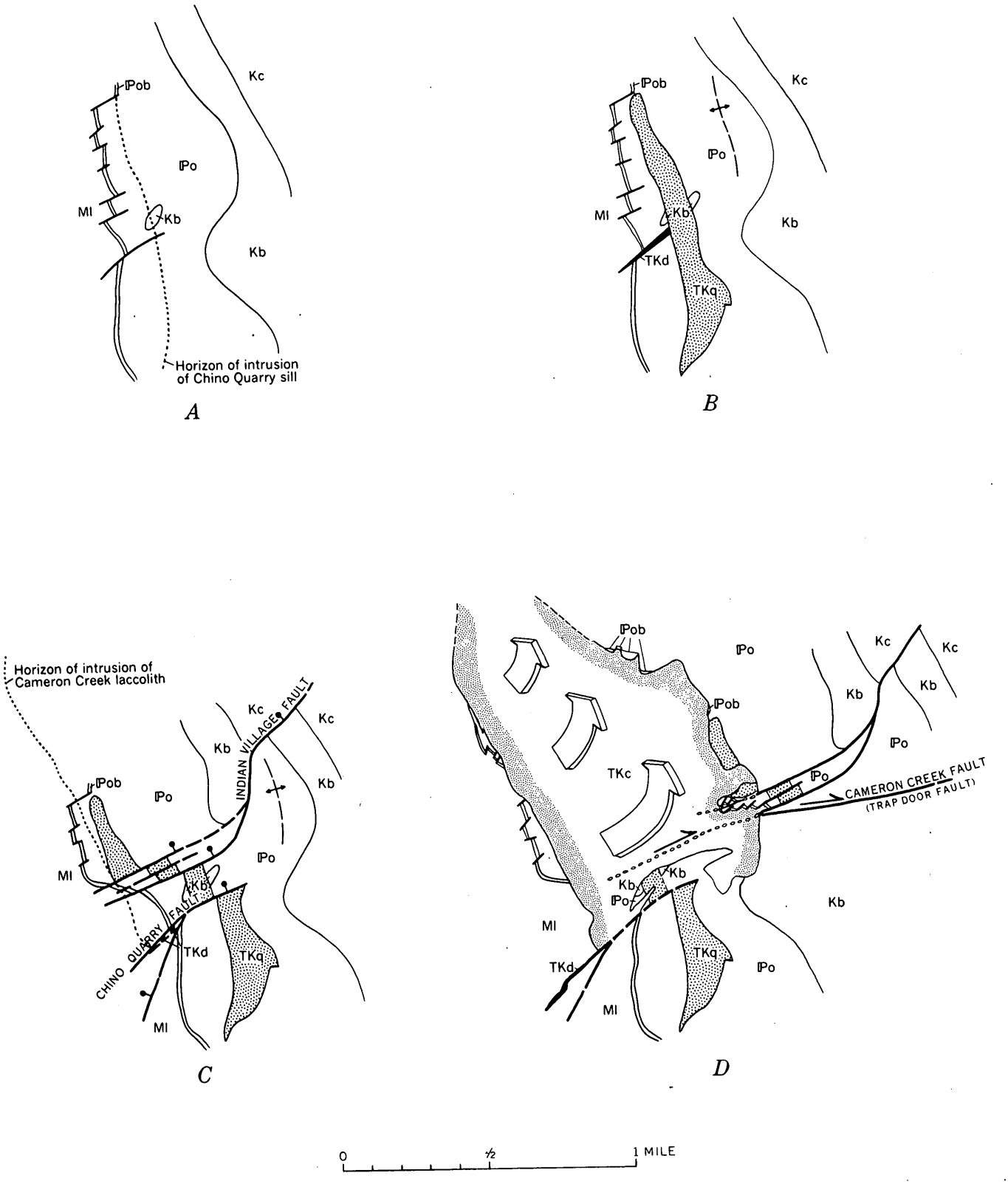

FIGURE 208.3.—Inferred history of deformation in the vicinity of the Cameron Creek laccolith, shown as successive maps at level of present ground surface (compare fig. 208.1.) TKc, Cameron Creek laccolith; TKq, Chino Quarry sill; Kc, Colorado formation; Kb, Beartooth quartzite; Po, Oswaldo formation; Pob, basal shale member of Oswaldo formation; Ml, Lake Valley limestone; feeder dikes shown in solid black. Large arrows in *D* suggest relative uplift of roof by intrusion of laccolith.

209. MIDDLE AND UPPER TERTIARY ROCKS OF SOUTHEASTERN WYOMING AND ADJOINING AREAS

By N. M. Denson and M. H. Bergendahl, Denver, Colo.

Tuffaceous continental deposits of middle and late Tertiary age unconformably overlie the truncated edges of older rocks in western Nebraska, southeastern Wyoming, and northeastern Colorado. The thickness of these Tertiary rocks ranges from about 600 feet in the western and southern parts of the area to about 1,900 feet in the northeastern part. In general, the younger rocks are coarser grained than the older ones —the Oligocene rocks are chiefly claystone and siltstone; the Miocene rocks, very fine grained sandstone; and the Pliocene rocks, medium- to coarse-grained sandstone and conglomerate. Lenticular beds of bentonite and fresh water limestone occur locally.

Middle and upper Tertiary rocks contain large quantities of volcanic ash. Where they are underlain by arkosic and carbonaceous rocks, suitable reducing conditions may exist for the precipitation and concentration of uranium leached from the ash by ground water. Northwest of the Hartville uplift, in southeastern Wyoming, small deposits of uranium occur along gravity faults of small displacement in the Arikaree formation of Miocene age.

The data from numerous test wells for oil and gas, and from areal mapping are adequate to determine structure and thicknesses of the rocks, and the general configuration of the erosion surface upon which they were deposited.

The writers are indebted to Laura W. McGrew for information on the Fort Laramie-Wheatland area and for sample logs of several wells. R. F. Gantnier, J. A. Thomas, and T. S. Sterrett made size analyses and prepared slides and thin sections of the Tertiary rocks for petrographic studies.

Stratigraphy.—The stratigraphic succession and nomenclature for the middle and upper Tertiary rocks in western Nebraska, southeastern Wyoming, and northeastern Colorado have been described by Lugn (1939), McGrew (1953), and Galbreath (1953). In this report only the names of the chief rock units are used, without reference to the subordinate units recognized by the foregoing authors. In the region shown in figures 209.1 and 209.3, the Tertiary rocks are assigned to the White River formation of Oligocene age, the Arikaree formation of Miocene age, and the Ogallala formation [1] of Pliocene age. These units can be recognized and mapped over wide areas and are particularly useful for regional studies.

Figure 209.1 shows the areal distribution of the Tertiary rocks and their present total thickness as determined from electric, gamma ray, and sample logs.

Paleogeography and geologic history.—As indicated by the schematic diagram, figure 209.2, erosion followed uplift at the close of the Oligocene and again at the end of the Miocene and removed much of the Tertiary sequence in the southwestern part of the region. The Ogallala in the southwestern part of the area rests on the bevelled edges of the White River and Arikaree formations. Northward and northeastward the White River thickens from about 300 feet to 850 feet, and the Arikaree from a feather edge to about 600 feet. Both units are reported to contain younger beds in areas to the northeast than they do in areas to the southwest.

Figure 209.3 shows the reconstructed thickness of the White River formation immediately preceding deposition of the Arikaree or Ogallala formations. As shown on this map the White River formation generally increases in thickness toward the northeast. Local areas of greater thickness probably represent topographic lows or valleys formed by a pre-Oligocene drainage system. In some areas the present-day streams are parallel to valleys developed on the land surface at the beginning of Oligocene time, although in other areas the present-day and ancient valleys trend in different directions. Stream piracy, perhaps preceded by regional uplift in post-Pliocene time, is suggested by a change in the trend of present-day Horse and Bear Creeks. The upper reaches of these streams are alined with two conspicuous pre-Oligocene topographic lows in Scottsbluff and Banner Counties, Nebr. (fig. 209.3). These topographic lows at one time may have formed the lower courses of Horse and Bear Creeks; the two streams now turn abruptly north at their "elbow of capture" in southeastern Goshen County, Wyo., and flow north and northeastward through Goshen Hole to the North Platte River.

Possible source of sediments.—The surface upon which the Oligocene rocks were deposited now slopes northeastward from an elevation of about 6,600 feet in northeastern Larimer County, Colo., to about 3,600 feet in northwestern Nebraska. This is partly the result of tilting subsequent to deposition of the White River formation. A southwesterly source for the sediments comprising the Oligocene and Miocene rocks

[1] The lower part of the Ogallala at a few places is reported to contain vertebrate fossils which some paleontologists regard as late Miocene in age.

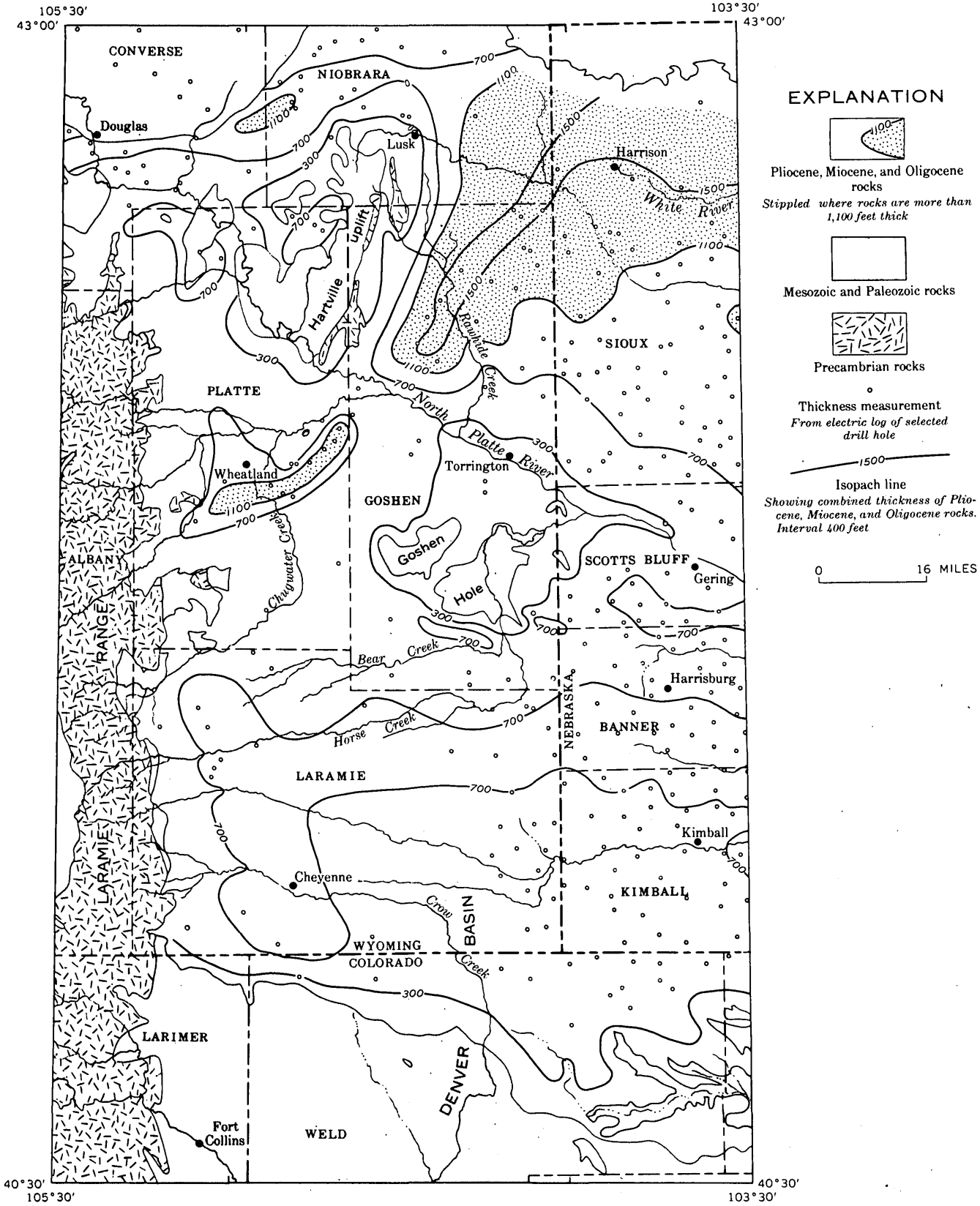

FIGURE 209.1.—Map showing combined thickness of Oligocene, Miocene, and Pliocene rocks in test wells in southeastern Wyoming and adjoining areas.

601530 O—61——12

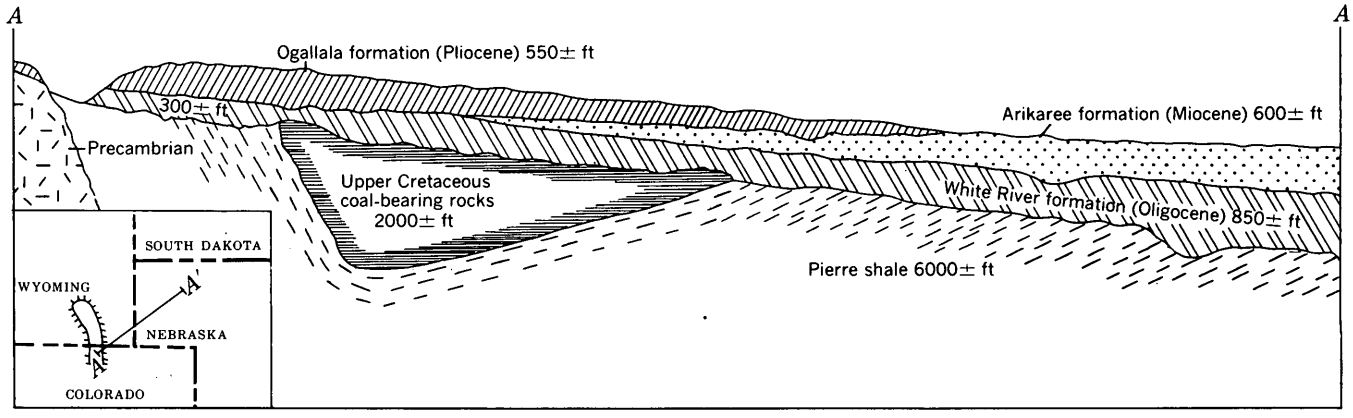

FIGURE 209.2.—Schematic diagram showing stratigraphic relations of middle and upper Tertiary rocks from east side of Laramie Range northeastward to the Nebraska panhandle.

is suggested in areas away from the major uplifts by the following: (a) direction of crossbedding observed over large areas in the Arikaree formation indicate transportation and deposition by northeasterly flowing stream, (b) northeasterly axial trends of "pipy" concretions in Miocene rocks (Schultz, 1941, p. 74, 77) indicate northeasterly direction of flow of underground water shortly after or contemporaneous with deposition, and (c) a small but general increase in the average percentage of heavy minerals occurs in the Oligocene rocks towards the southwest (table 209.1).

Petrography of Oligocene rocks.—The average of size analyses of about 100 samples from 10 measured sections of the White River formation in the region (table 209.1) indicate that these rocks are remarkably uniform in grain size over wide areas and contain relatively insignificant amounts of locally derived materials. To the unaided eye most of the samples appear similar in color, texture, and composition, but preliminary studies of thin sections show considerable variation in component minerals. In general, these rocks consist of 65 to 85 percent silt and 5 to 25 percent very fine grained sand embedded in a matrix of clay-size particles. The silt and very fine grained sand fractions consist of glass shards and angular to subrounded fragments of quartz, potassium feldspar (microcline and orthoclase), plagioclase, and small amounts of detrital minerals. The clay-size fraction consists of montmorillonitic clay, clay-size carbonate flakes, and fine volcanic ash. Shards are present in nearly every sample and comprise from less than 10 percent to at least 50 percent of the rock. The glassy components of some samples are partially devitrified, showing feeble birefringence. Samples in which many of the shards are devitrified also are marked by a relatively large content of montmorillonitic clay. It is inferred that

TABLE 209.1.—*Average grain size distribution, calcium carbonate content, and heavy mineral content for grab samples of Oligocene rocks (White River formation) from southeastern Wyoming and some adjacent areas*

[vfg, very fine grained; fg, fine grained]

Locality No. on map (fig. 209.3)	Locality	Location			County	State	Thickness of stratigraphic unit sampled, in feet	Number of samples	Average grain-size distribution of insoluble light fraction, in percent				Average percent $CaCO_3$	Average percentage of heavy minerals in vfg sand
									Clay	Silt	Sand			
		Sec.	T.N.	R.W.							vfg	fg		
1	Young Woman Creek	N½ 35	35	64	Niobrara	Wyo	300	11	14	64	20	2	30	0.06
2	Monroe Canyon	SE¼ 17	33	56	Sioux	Nebr	200	8	16	80	4	----	20	.06
3	Slater	SE¼ 19	22	66	Platte	Wyo	190	10	8	66	26	----	24	.11
4	Bear Mountain	S½ 17	20	62	Goshen	Wyo	235	11	14	80	6	----	22	.20
5	Eagles Nest	22, 26	21	58	Scottsbluff	Nebr	200	8	13	81	6	----	23	.09
6	Scottsbluff	N½ 12	21	56	Scottsbluff	Nebr	280	12	8	86	6	----	21	.08
7	Horse Creek	E½ 32	17	69	Laramie	Wyo	300	11	16	70	13	1	24	.16
8	Terry Ranch	27, 34	12	69	Larimer	Colo	280	11	17	68	14	1	31	.18
9	Chalk Bluffs	8, 17	11	65	Weld	do	225	9	13	63	23	1	23	.12
10	Stony Buttes	2, 3	11	55	Logan	do	300	11	12	67	20	1	23	.06

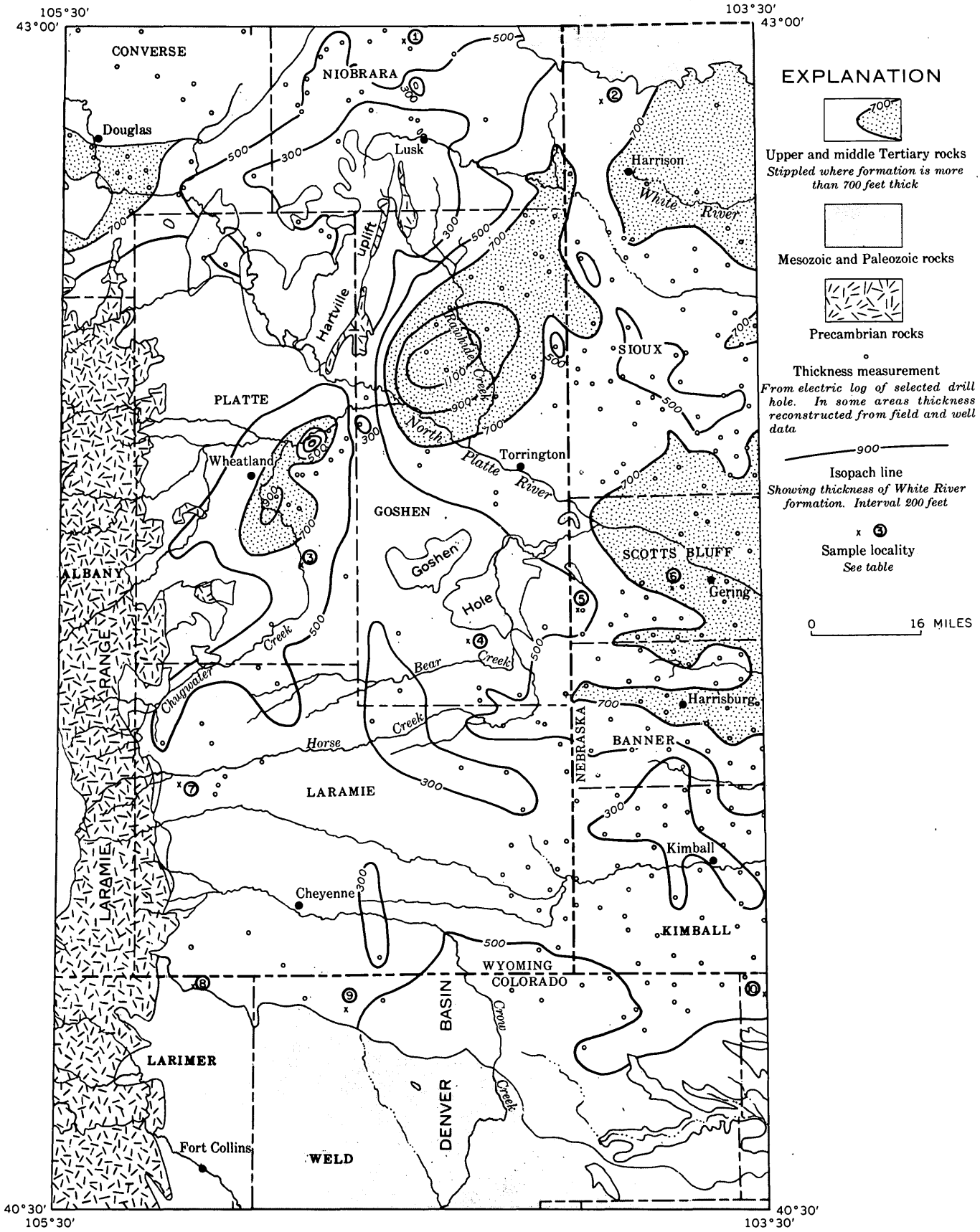

FIGURE 209.3.—Map of southeastern Wyoming and adjoining areas showing thickness of White River formation (Oligocene).

both devitrification and formation of montmorillonitic clay in these rocks are produced by post-depositional alteration.

The dominant heavy minerals in these rocks are hornblende (both blue-green sodic and red-brown basaltic varieties) and biotite, and lesser amounts of zircon, garnet, rutile, epidote, orthopyroxene, and gold. Most of this assemblage indicates a mixed igneous and metamorphic terrane as a source for the detrital portion of these rocks; the dominant basaltic hornblende and possibly the biotite suggest a volcanic source for some of the heavy minerals compatible with the large amount of volcanic matter in the light fraction.

No pattern, either stratigraphic or areal, has yet been recognized in the petrographic variations among these samples. The distribution of gold, for example, is not related to the position of the present mountain front. It occurs in greatest amounts in the Slater, Young Woman Creek, and Stony Buttes sections, far east of all present known sources of gold. The significance of this is not completely understood at present, but it may be related to a drainage system developed during Oligocene time.

REFERENCES

Galbreath, E. C., 1953, A contribution to the Tertiary geology and paleontology of northeastern Colorado: Kansas Univ. Paleont. Contrib., art. 4, 120 p.

Lugn, A. L., 1939, Classification of the Tertiary system in Nebraska: Geol. Soc. America Bull., v. 50, p. 1245–1276.

McGrew, P. O., 1953, Tertiary deposits of southeastern Wyoming, *in* Wyoming Geol. Assoc. Guidebook 8th Ann. Field Conf., Laramie Basin, Wyoming, and North Park, Colorado, 1953: p. 61–64.

Schultz, C. B., 1941, The pipy concretions of the Arikaree: Nebraska State Mus. Bull., v. 2, no. 8, p. 69–82.

210. CLAYS IN THE INYAN KARA GROUP (CRETACEOUS), BLACK HILLS, WYOMING AND SOUTH DAKOTA

By Leonard G. Schultz and William J. Mapel, Denver, Colo.

The Inyan Kara group of Early Cretaceous age consists of the Lakota and overlying Fall River formations, and crops out on the flanks of the Black Hills in Wyoming and South Dakota. About 110 samples of Inyan Kara rocks, taken from 5 outcrop sections and from the cores of 2 drill holes, were analyzed for their clay minerals to provide information that might be useful in subdividing and correlating stratigraphic units, and in interpreting the history of deposition. The rocks sampled are mostly siltstone, claystone, and shale. They represent most parts of the Fall River formation, but only the upper part of the Lakota except for a section at Cabin Creek. The stratigraphic relations of the Inyan Kara group are summarized in table 210.1 and the lithology of the formations and composition of the clays at the sample localities are shown on figure 210.1.

STRATIGRAPHIC RELATIONS

The Lakota formation is a nonmarine deposit laid down in swampy areas and on flood plains of streams in an area of low relief. The Fall River formation is probably a marginal marine deposit laid down on tidal flats, in coastal swamps, or in marine deltas (Waagé, 1959, p. 63–64). An unconformity separates the two formations everywhere in the Black Hills. Stream channels outlined by Brobst (1956, p. 103–105) and the dip directions of crossbeds suggest that sediments in both formations were supplied from the southeast.

Claystone and siltstone in a unit several feet thick at the top of the Lakota formation generally are mottled shades of gray, purple, red, and yellow, and the rocks contain numerous ferruginous spherules commonly about 1 mm in diameter. Fresh spherules are reported by Waagé (1959, p. 55) to consist of siderite. Ferruginous spherules are also found in a mottled zone below a thin tongue of variegated mudstone that crops out near the middle of the Fall River formation at Angostura Reservoir and elsewhere on the east side of the Black Hills. Although the significance of the siderite is equivocal, similar siderite spherules in some other areas have been interpreted

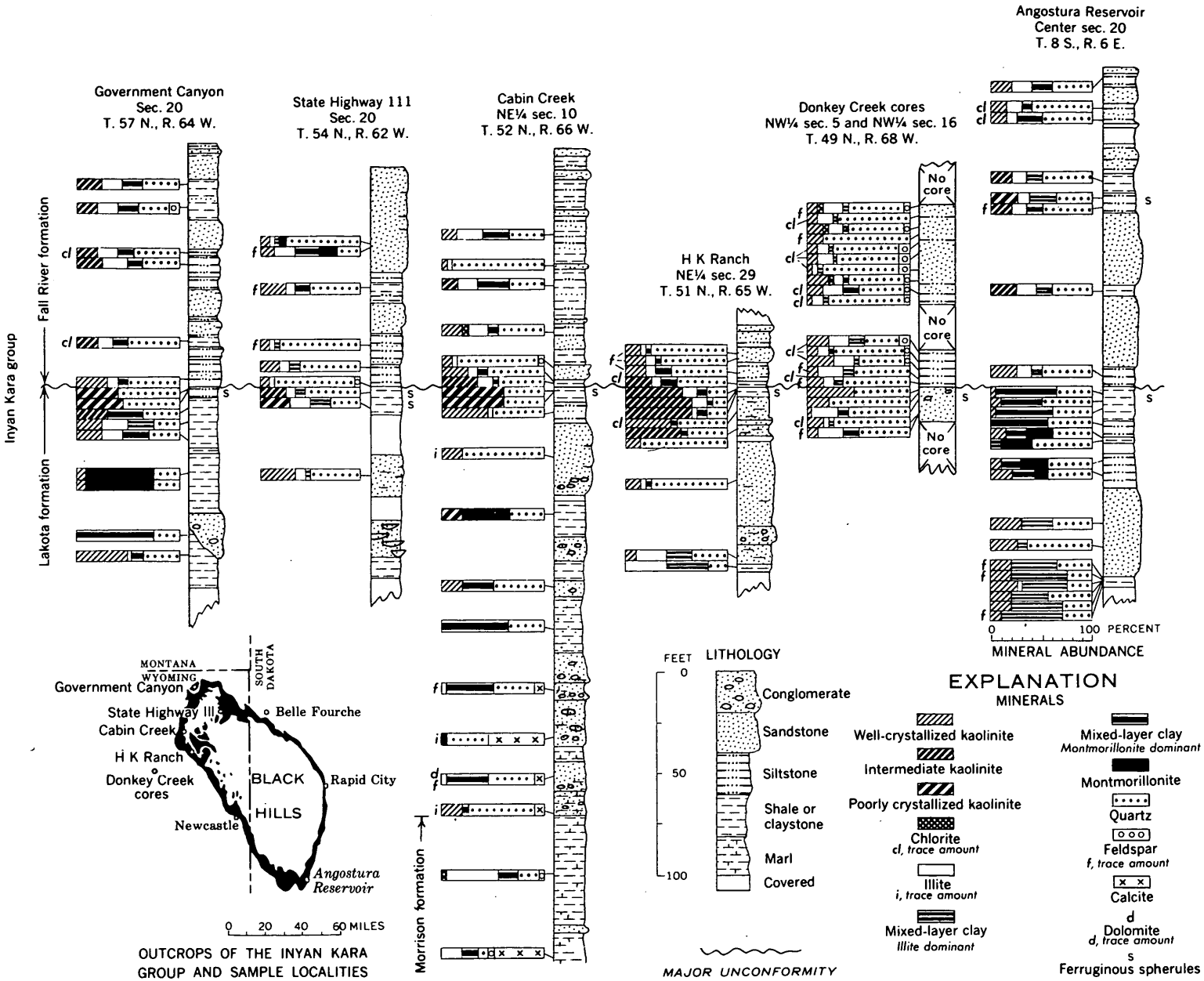

FIGURE 210.1.—Principal minerals in samples from the Inyan Kara group, Black Hills.

TABLE 210.1.—*Generalized description of the Inyan Kara group and adjacent formations, Black Hills*

Age	Group and formation		Thickness (feet)	Description
Early Cretaceous		Skull Creek shale	200–260 (thins southeastward)	Fissile black shale; a few ferruginous concretions; thin siltstone seams in the lower part; rare marine fossils.
	Inyan Kara group	Fall River formation	120–160 (thickens southeastward)	Interbedded brown-weathering sandstone, light- to dark-gray siltstone, and dark-gray silty shale; locally carbonaceous. Thin tongue of variegated mudstone about the middle of the formation in the eastern part of the Black Hills; nonmarine pelecypods locally at the base; contains more sandstone to the southeast.
		Unconformity		
		Lakota formation	100–550 (thickens southeastward)	Light-gray locally conglomeratic sandstone, and variegated claystone and sandy claystone; local lenses of coal and carbonaceous shale in the lower part; nonmarine fossils.
Late Jurassic		Morrison formation	100±	Greenish-gray and grayish-red claystone and marl; a few thin beds of grayish-white sandstone; nonmarine fossils.

as a product of a long period of subaerial leaching and oxidation (Waagé, 1959, p. 56–57).

CLAY MINERALS

Abundance of clay minerals in samples studied during this investigation is estimated to the nearest 5 percent on the basis of X-ray diffraction intensities. The clay minerals include kaolinite, illite, montmorillonite, mixed-layer clays, and trace amounts of chlorite. Well-crystallized, intermediate, and poorly crystallized kaolinite and two types of mixed-layer clay have been distinguished—one mixed-layer clay has illite and the other has montmorillonite as the dominant layer. Nonclay minerals, consisting mainly of quartz and minor amounts of feldspar, make up from 20 to 90 percent and average about 50 percent of individual samples.

The Lakota and Fall River formations have the same clay minerals but in different proportions. Illite was found in nearly all of the Fall River samples, but was found in less than half of the Lakota samples. This distribution of illite may indicate conversion of some mixed-layer clay to illite in brackish or marine waters of the Fall River sea, or it might indicate local destruction of illite by weathering during deposition of the Lakota.

Montmorillonite is locally abundant in the Lakota formation, and the montmorillonitic variety of mixed-layer clay is fairly common in both formations. The montmorillonitic variety of mixed-layer clay appears to be slightly more prevalent at the northernmost outcrops of both formations, but this mineralogic distribution is less marked in the Lakota than in the Fall River. The occurrence of montmorillonitic clays suggests contamination by volcanic material, and possible additional evidence of volcanism during depositon of the Inyan Kara group is found in the local occurrence of trace amounts of apatite in euhedral crystals and some biotite in heavy-mineral concentrates from the Fall River formation (W. A. Chisholm, written communication, 1957).

The most consistent variation in the distribution of clay minerals is the abundance of poorly crystallized kaolinite at several localities in the mottled unit at the top of the Lakota formation. At Government Canyon and Cabin Creek, poorly crystallized kaolinite is the only clay mineral present in this interval. In the Donkey Creek cores, kaolinite is the only clay mineral present, but it is a well-crystallized variety. At Angostura Reservoir, clay in the uppermost Lakota sample (which is about 5 feet stratigraphically below the top of the formation) contains only a small amount of kaolinite; however, the kaolinite zone may be present in the overlying part of the Lakota, or it may have been eroded away before deposition of the Fall River formation. At Angostura Reservoir a fairly large amount of poorly crystallized kaolinite occurs in a sample from the mottled zone near the middle of the Fall River formation.

In all samples from the mottled zones of both formations, chlorite and feldspar—minerals that are relatively easily destroyed by weathering—are absent. Concentrations of kaolinite associated with ferruginous material, and the absence of chlorite and feld-

spar, are consistent with an interpretation of the mottled zones at the top of the Lakota and in the Fall River formations as zones that have undergone severe weathering; they perhaps represent ancient soils. The poor crystallization in most of the kaolinite in these zones might indicate degradation of the clay during soil leaching.

REFERENCES

Brobst, D. A., 1956, Channel sandstone, southern Black Hills, *in* Geologic investigations of radioactive deposits—Semiannual progress report, June 1 to Nov. 30, 1956: U.S. Geol. Survey TEI–640, p. 102–108, issued by U.S. Atomic Energy Comm. Tech. Inf. Service, Oak Ridge, Tenn.

Waagé, K. M., 1959, Stratigraphy of the Inyan Kara group in the Black Hills: U.S. Geol. Survey Bull. 1081–B, p. 11–87.

211. COBERN MOUNTAIN OVERTHRUST, LEWIS AND CLARK COUNTY, MONTANA

By Robert George Schmidt and Peter Zubovic, Washington, D.C.

The Cobern Mountain overthrust is in western Montana, in the southeastern part of Lewis and Clark County, near the towns of Wolf Creek and Craig (fig. 211.1). The fault extends from the Dearborn River southeastward for many miles along the western margin of the Adel Mountain volcanic field, which forms the northern end of the Big Belt Range, and was partly mapped by Lyons (1944, pl. 1) in a reconnaissance study of this area. In the course of detailed geologic mapping in 1960, we traced this fault northward from the Missouri River, recognized that it has a large displacement and the characteristics of an overthrust, and named it after Cobern Mountain, a prominent peak approximately 6 miles north of Craig.

The overthrust lies in the eastern part of the so-called Disturbed Belt, a zone of intensely folded and faulted rocks that extends along the eastern front of the Northern Rocky Mountains in western Montana and southern Alberta. The Disturbed Belt includes rocks of Mississippian, Jurassic, and Cretaceous age in the area shown in figure 211.1. (See Lyons, 1944, pl. 1.) The trace of the overthrust is within rocks of Late Cretaceous age. The sequence of Upper Cretaceous strata in the general vicinity of the fault is as follows:

Upper Cretaceous:
- Adel Mountain volcanics of Lyons (1944)
- St. Mary River formation (lowermost part)
- Two Medicine formation
- Virgelle sandstone
- Telegraph Creek formation

Colorado group:
- Marias River shale.

Along the fault, older rocks are thrust northeastward upon younger rocks, and the fault plane cuts upward gradually across the stratigraphic section. North of the Missouri River, the fault brings rocks of the Two Medicine formation, rocks assigned to the St. Mary River formation, and overlying rocks at the base of the Adel Mountain volcanics over younger rocks of the Adel Mountain volcanics. At the Missouri River, where erosion has exposed the fault plane at a deeper stratigraphic level, the Virgelle sandstone forms the hanging wall of the fault. South of the Missouri River, as shown by Lyons (1944, pl. 1), the fault brings rocks of the Two Medicine formation over the Adel Mountain volcanics.

In places, north of the Missouri River, the overthrust is deformed. Along the upper part of Dog Creek and in the vicinity of Cobern Mountain, the fault plane is folded into an anticline and syncline and its trace is very sinuous. In this region, the dip of the fault plane ranges from near horizontal to 50° and the net slip along the fault is more than 2 miles. Cobern Mountain, which forms part of the overthrust block, and a small klippe to the south of Cobern Mountain (fig. 211.1) lie along the axis of the syncline. Other klippen, too small to show on the accompanying map, occur along the axis of the anticline on hill tops adjacent to Dog Creek. West of Cobern Mountain, the trace of the overthrust is offset by a high-angle fault. At its northern limit, the plane of the overthrust steepens and the fault trace passes into rocks of the Two Medicine formation. Beneath the Cobern Mountain overthrust, rocks of the Adel Mountain volcanics are intensely crushed

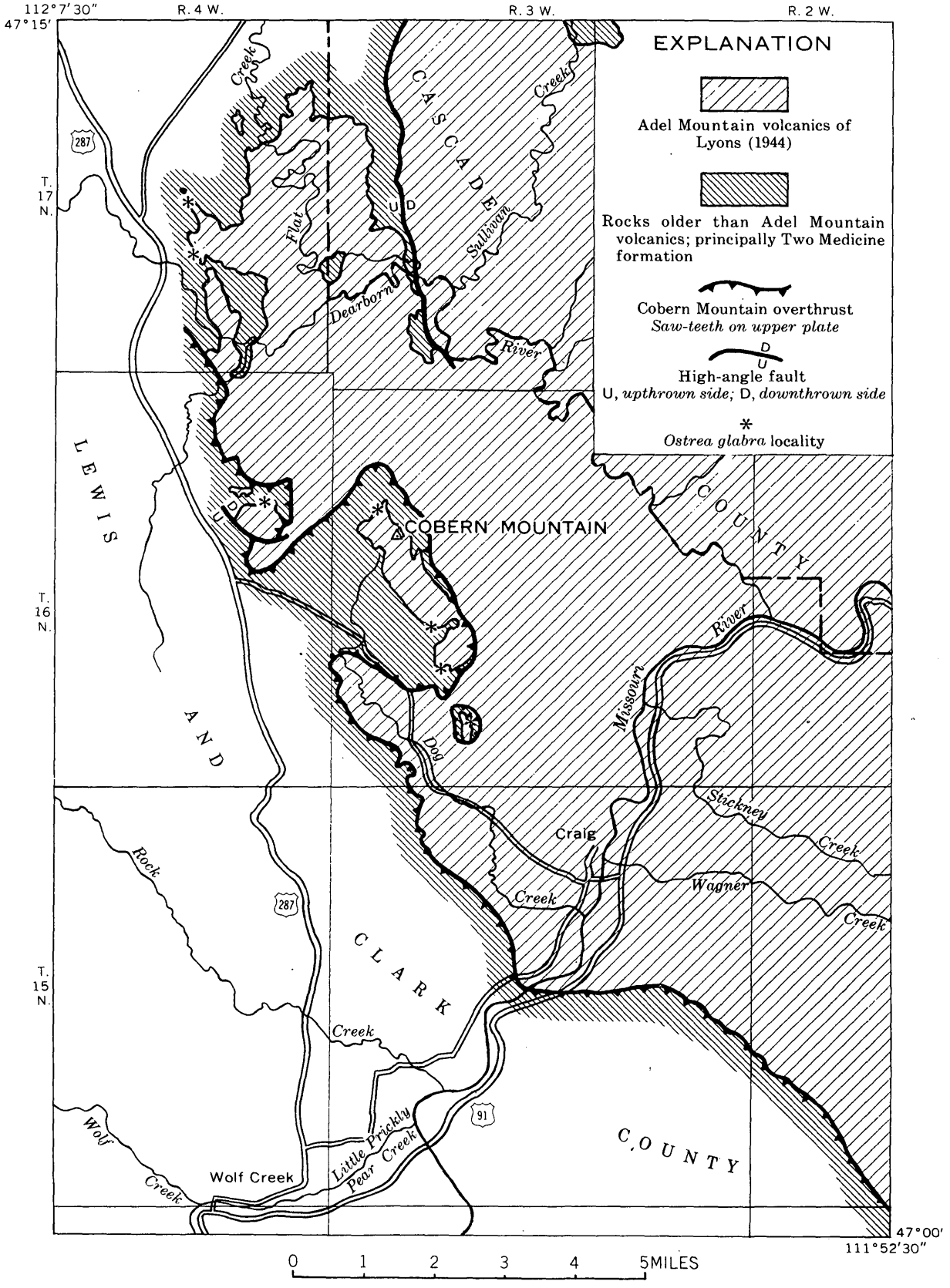

FIGURE 211.1.—Map showing geologic relations along northern trace of Cobern Mountain overthrust, Montana.

and fractured as a result of the thrust movement. The zone of crushing and fracturing in the footwall is as much as 200 feet thick. The rocks in the hanging wall of the fault, principally sedimentary rocks of the Two Medicine formation, are greatly deformed by drag folding and shearing, but they are not so intensely crushed as the volcanic rocks in the footwall. The zone of deformation above the fault is as much as 300 feet thick. The structural interpretation presented above differs considerably from that of Lyons (1944, pl. 1; p. 453).

At several places within the overthrust sheet, pyroclastic breccias in the lower part of the Adel Mountain volcanics lie unconformably on beds of sandstone and mudstone that contain abundant shells of the oyster *Ostrea glabra* (identified by W. A. Cobban of the U.S. Geological Survey), and a similar relation is found in the block beneath the fault north of the Dearborn River. These beds are confined to the northwest margin of the Adel Mountain volcanic field. The principal occurrences of *Ostrea glabra* are shown in figure 211.1 According to Cobban (oral communication), this oyster also occurs in the Horsethief sandstone of Late Cretaceous age, and the species seems to be restricted to that horizon in this part of Montana although it has a known range throughout Montana time. The Horsethief sandstone occurs north of the area shown in fig. 211.1; there it rests conformably on the Two Medicine formation and underlies the St. Mary River formation. The beds of sandstone and mudstone beneath the Adel Mountain volcanics are therefore believed to be of Horsethief age, although they are assigned to the lowermost part of the St. Mary River formation on the basis of lithology. Elsewhere the Adel Mountain volcanics rest on a surface eroded across the Two Medicine formation, the Virgelle sandstone, and the upper part of the Colorado group, and plant fossils indicate that the volcanics are of Late Cretaceous age (Lyons, pl. 1; p. 465). From these relationships it follows that the Adel Mountain volcanics are of latest Cretaceous age and equivalent to part of the St. Mary River formation.

REFERENCE

Lyons, J. B., 1944, Igneous rocks of the northern Big Belt Range, Montana: Geol. Soc. America Bull., v. 55, no. 4, p. 445–472.

212. A REDEFINITION AND RESTRICTION OF THE TERM CHALLIS VOLCANICS

By Clyde P. Ross, Denver, Colo.

Early in my work in south-central Idaho the masses of Tertiary volcanic rocks there were grouped as the Challis volcanics (Ross, C. P., 1927, p. 79; 1934, p. 46) in a definition that was necessarily broad. The rocks with which I was immediately concerned are widespread in the region that is centered around Challis, so that name was applied to them. They were then regarded as of Oligocene or, at the youngest, early Miocene age. Only the readily recognizable Snake River basalt and Columbia River basalt were excluded from the formation.

Later studies have demonstrated that, as expected, the Challis volcanics of the region around Challis are a coherent, thick, and widespread (fig. 212.1) unit. There are some volcanic and sedimentary rocks in distant parts of south-central Idaho that are now recognized as so different from the Challis volcanics that they should be excluded from that formation. Furthermore, confusion has arisen as to the relation of certain sedimentary beds in the Challis volcanics to the formation as a whole.

I here propose that the term Challis volcanics be restricted to dominantly volcanic strata of early Tertiary age within the part of central Idaho north of the Snake River Plain and south of the westward-flowing segment of the Salmon River (near lat 45°30′). Tuff and sedimentary beds intercalated with the lava flows are included in the formation. Essentially, this restricted definition limits use of the name to the rocks so designated on figure 212.1, although, of course, future mapping will produce modifications and extensions in detail.

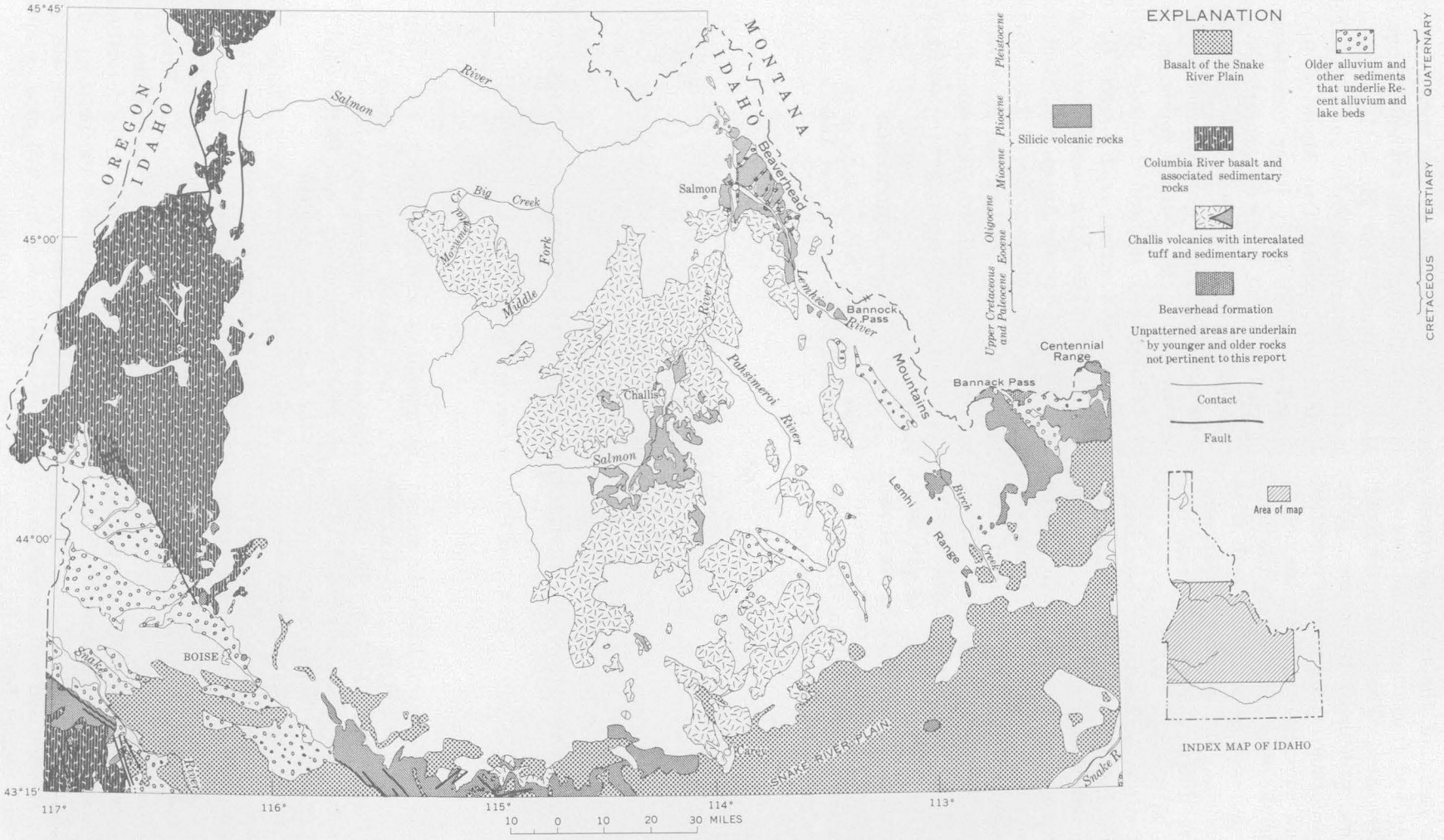

FIGURE 212.1.—Map of south-central Idaho showing distribution of Tertiary volcanic and related strata. Geology taken from geologic map of Idaho by C. P. Ross and J. D. Forrester, 1947, with numerous modifications based on unpublished maps by C. P. Ross, H. E. Malde, and C. M. Marshall.

The Challis volcanics consist mainly of flows and flow breccias of a wide range of composition, but sedimentary rocks (in part with little or no contained volcanic matter) and tuff are locally present. In places members of the formation have been distinguished. These include, among others, the Yankee Fork rhyolite, the Germer tuffaceous member, and various clastic units near the town of Salmon. The last are being studied and subdivided by Anderson (1956, p. 28–30; 1957, p. 16–18; 1959, p. 25–28), who believes that the various members are separated by unconformities. However, neither the unconformities discussed by Anderson nor those recognized earlier (Ross, 1937, p. 49) are believed to have regional significance. They record interruptions in eruption and deposition such as are to be expected in volcanic strata with intercalated sediments.

The Challis volcanics represent the lower part of the Tertiary deposits of south-central Idaho. The formation was originally regarded as possibly or probably of Oligocene age and not younger than early Miocene (Ross, 1937, p. 65–68; Brown, 1937, p. 164). R. W. Brown (written communication, 1956) has revisited plant fossil localities near Salmon and near Monumental Creek. The deposits near Monumental Creek were originally thought by Ashlee (Carpenter, 1932, p. 59) to be Oligocene and by Brown (1937, p. 164–165) to be early Miocene in age. Brown now says that they "could well be late Oligocene." He found little in common between collections from near Monumental Creek and those from the Germer tuffaceous member near Challis, although he regarded both as components of the Challis volcanics. He now regards the rocks near Salmon, including the youngest of Anderson's units (1956, p. 28–30), as Oligocene and those near Challis as Eocene. His revision of opinion as to the beds west of Challis is based on leaves determined as *Ficus densifolia* that resemble some from Yellowstone National Park regarded as of Eocene age. My collections made in 1959 near Salmon are regarded by J. A. Wolfe (written communications, 1959 and 1960) as of Oligocene age. He also reported my collections made in 1960 west of Challis as Oligocene, but the new collections add nothing to the information previously available for either the Salmon or the Challis area. These collections do not include *Ficus densifolia* and have little bearing on the possibility of an Eocene age for the rocks west of Challis. Thus, the Challis volcanics, as here restricted, may range in age from Eocene into, at the most, early Miocene. Probably most of the formation is Oligocene.

Late Tertiary strata within and on the borders of the mountains of the eastern part of south-central Idaho have long been known but available details are scanty. These strata include volcanic rocks and some sedimentary beds, exposed fairly continuously from the western part of the Centennial Range past Bannack Pass to the southern end of the hills bordering Birch Creek. Other scattered exposures are known at the southern tip of the Lemhi Range and along slopes northwest of Birch Creek. Available data (Scholten and others, 1955, p. 369–379, 376–377; Ross, 1961), including a reconnaissance in 1960, suggest that large parts of these rocks may be Pliocene and possibly younger. Clastic beds on both sides of the divide between Lemhi River and Birch Creek may also be Pliocene. Sedimentary beds in Bannock Pass may be of late Miocene age (Scholten and others, 1955, p. 369–370). The possibility that some volcanic and sedimentary rocks in the eastern part of south-central Idaho are as old as middle Miocene cannot be excluded on present evidence. If any exist, they do not belong to the Challis volcanics as redefined.

The Beaverhead formation in the southeastern part of the Beaverhead Mountains (Scholten and others, 1955, p. 368) is nonvolcanic. Much of it is conglomerate sufficiently like that locally present in the Challis volcanics so that confusion is possible. Conceivably future work may show that some beds now mapped as Beaverhead are equivalent to basal conglomerate in the Challis volcanics.

The intermontane valleys contain large amounts of poorly consolidated somewhat deformed coarse alluvial material, including the Donkey fanglomerate in the upper drainage basin of the Pahsimeroi River (Ross, 1947, p. 1122–1124). These are Pliocene and younger. All of the varied strata commented upon above are younger than (and different from) the Challis volcanics of the areas around Challis and Salmon.

In the western part of south-central Idaho the Challis volcanics are not known and the Tertiary strata differ from those cited above. Most are younger. From near Carey westward near the northern border of the Snake River Plain there are silicic rocks broadly similar to those mentioned above. Lack of definite age criteria introduces some uncertainty but all the post-Oligocene silicic rocks in this area would now be excluded from the Challis volcanics. The western part of south-central Idaho contains extensive exposures of the Columbia River basalt and of associated sedimentary rocks and some strata that

may be younger. All of these are obviously different from the Challis volcanics as here defined. Suggested ages for the rocks in western areas range from early Miocene to late Pliocene and Pleistocene with the more recent assignments favoring the later age. (H. A. Powers and H. E. Malde, written communications, 1961).

REFERENCES

Anderson, A. L., 1956, Geology and mineral resources of the Salmon quadrangle, Lemhi County, Idaho: Idaho Bur. Mines and Geology Pamph. 106.

——— 1957, Geology and mineral resources of the Baker quadrangle, Lemhi County, Idaho: Idaho Bur. Mines and Geology Pamph. 112.

——— 1959, Geology and mineral resources of the North Fork quadrangle, Lemhi County, Idaho: Idaho Bur. Mines and Geology Pamph. 118.

Brown, R. W., 1937, Additions to some fossil floras of the western United States: U.S. Geol. Survey Prof. Paper 186–J, p. 163–206.

Carpenter, J. T., 1932, A tentative correlation of northwestern Tertiary strata: Northwest Sci., v. 6, no. 2, p. 54–55.

Ross, C. P., 1927, Ore deposits in Tertiary lava in the Salmon River Mountains, Idaho: Idaho Bur. Mines and Geology Pamph. 25.

——— 1934, Geology and ore deposits of the Casto quadrangle, Idaho: U.S. Geol. Survey Bull. 854.

——— 1937, Geology and ore deposits of the Bayhorse region, Custer County, Idaho: U.S. Geol. Survey Bull. 877.

——— 1947, Geology of the Borah Peak quadrangle, Idaho: Geol. Soc. America Bull., v. 58, no. 12, pt. 1, p. 1085–1160.

——— 1961, Geology of the southern part of the Lemhi Range, Idaho: U.S. Geol. Survey Bull. 1081–F.

Scholten, Robert, Keenmon, K. A., and Kupsch, W. O., 1955, Geology of the Lima region, southwestern Montana and adjacent Idaho: Geol. Soc. America Bull., v. 66, no. 4, p. 345–404.

213. UPPER PALEOZOIC ROCKS IN THE DEEP CREEK MOUNTAINS, IDAHO

By WILFRED J. CARR and DONALD E. TRIMBLE, Denver, Colo.

More than 11,000 feet of Mississippian, Pennsylvanian, and lower Permian rocks are exposed in the Deep Creek Mountains 25 miles southwest of Pocatello, Idaho (fig. 213.1). Parts of this stratigraphic sequence are correlated with the Lodgepole limestone, Great Blue limestone, Manning Canyon shale, and Oquirrh formation. The last three names, first applied by Gilluly (1932) in the Oquirrh Range, Utah, and the Lodgepole limestone of Montana and Utah have not previously been used in Idaho by the Geological Survey. Fine-grained clastic beds and thin-bedded cherty limestone lie below the Great Blue and above the Lodgepole in the Deep Creek section; these rocks are here named the Deep Creek formation.

Upper Paleozoic rocks in the Deep Creek Mountains compare closely with equivalent rocks to the south (fig. 213.1), but, with one exception noted later, they are generally unlike upper Paleozoic rocks in southeastern Idaho to the north and east. The Brazer limestone (Mississippian) and Wells formation (Pennsylvanian) of southeastern Idaho are not separated by shale equivalent to the Manning Canyon shale of Late Mississippian and earliest Pennsylvanian age. Moreover, the Brazer in some areas includes rocks of Pennsylvanian, Early Mississippian, and Permian age, whereas the age of the Great Blue is Late Mississippian. Restriction of the name Brazer has been suggested by Sando, Dutro, and Gere (1959), who showed that the type Brazer is a dolomite of limited geographic distribution. The Oquirrh formation, although partly equivalent to the Wells, is thicker and less sandy.

Lowermost Mississippian rocks in the Deep Creek Mountains (fig. 213.1) are limestone and dolomite assigned to the Lodgepole limestone. These carbonate rocks contain fossils of Early Mississippian age.

The Deep Creek formation is here named from the mountains where it is typically exposed. In the type section (measured in SW1/4NE1/4 sec. 35, T. 9 S., R. 31 E.), and elsewhere in the region, the formation is divisible into two mappable members; a lower siltstone, and an upper limestone. The lower member, 750 feet thick, consist mainly of light-gray to brown or black siltstone that weathers brown to purplish and is interbedded with subordinate amounts of silty limestone and shale. The upper member, 1,500 feet thick, is gray to blue-gray, mostly thin- to medium-bedded limestone that contains much dark chert, and locally is silty, platy, and weathers purplish. The lower contact of the formation is the base of the first shale or siltstone above the Lodgepole limestone; the upper contact, normally gradational, is placed at the change from thin-bedded cherty limestone to the more massive ledges of the Great Blue limestone.

Fossils are rare in the Deep Creek formation and the present age assignment is based mostly on the stratigraphic position of the formation between fossil-bearing beds in the Lodgepole and Great Blue limestones. From near the top of the Deep Creek, J. T. Dutro and W. J. Sando (written communication, 1961) have identified the coral *Rhopalolasma*, and brachiopods that "show some similarities with forms that occur in the Moorefield shale (early Late Mississippian) of the Mid-Continent region." They conclude that "although the age of the Deep Creek formation is uncertain, it may include beds of both late Osage and early Meramec age." J. T. Dutro (written communication, 1960) also identified *Leiorhynchus* cf. *L. carboniferum* Girty from the lower member on Paps Mountain near American Falls, Idaho. He stated that "this species is common in the Chainman shale (Meramec equivalents) in Utah." On Bannock Peak, 5 miles east of the measured section, the Deep Creek is present in the upper plate of a thrust fault, and there part of the lower member resembles the Chainman shale of western Utah and eastern Nevada. Sadlick and Schaeffer (1959, p. 1786) believe that the Chainman of northwestern Utah ranges in age from Middle Mississippian to Early Pennsylvanian. The Deep Creek formation (fig. 213.1) is also approximately equivalent to the Humbug formation and possibly the Deseret limestone in Utah, to parts of the Milligen formation in central Idaho, and to the lower part of the Brazer limestone as it has been used in central and southeastern Idaho. In the Mackay quadrangle, Idaho (Ross, 1960) an unnamed formation (fig. 213.1) that intertongues with the Milligen, Brazer, and Wood River formations, locally resembles the lower member of the Deep Creek, and at Timbered Dome, west of Arco, (Skipp, Art. 236) the rocks exposed are remarkably similar to the Deep Creek formation. *Leiorhynchus carboniferum* Girty has been reported by C. P. Ross (written communi-

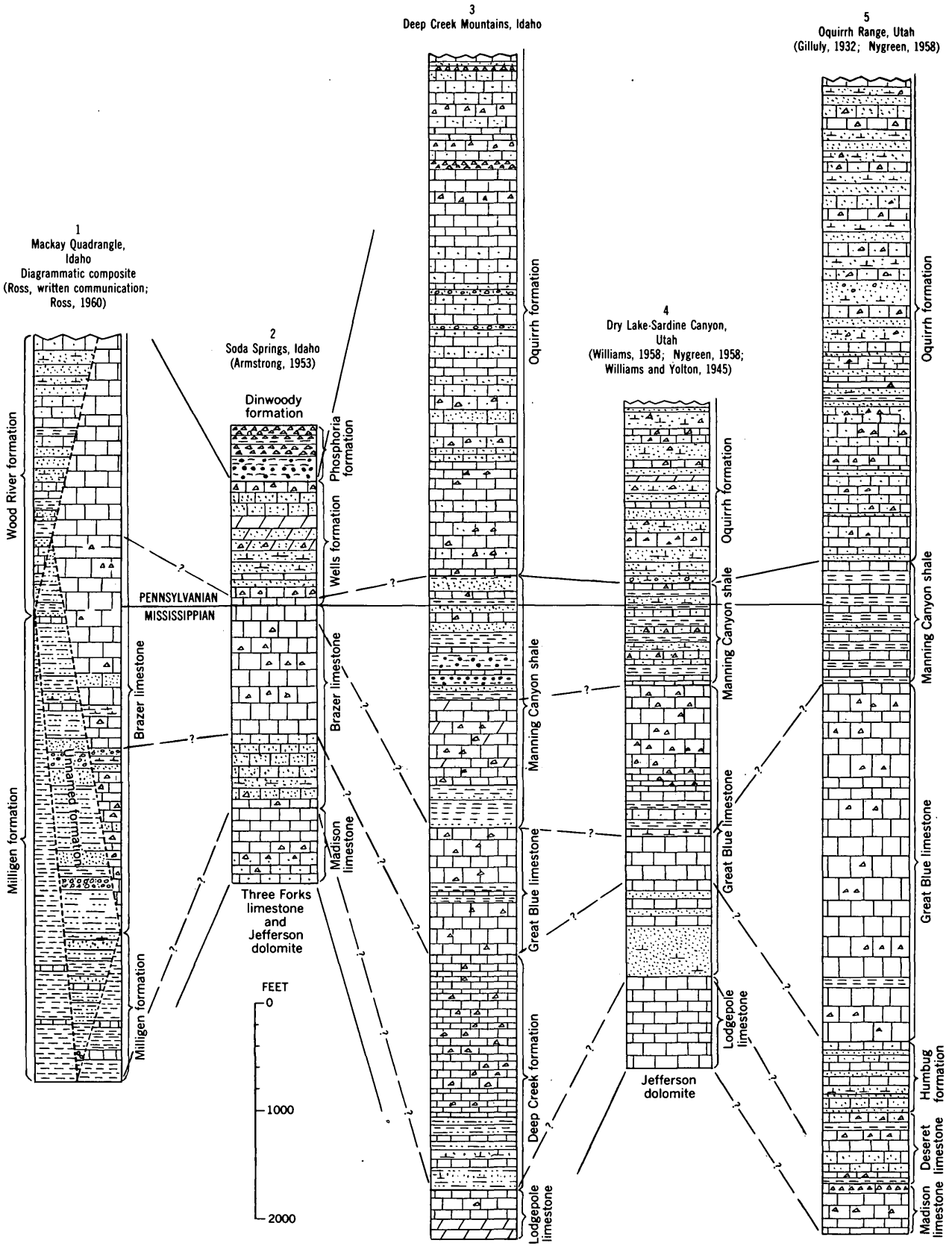

FIGURE 213.1.—Tentative correlation of upper Paleozoic section, Deep Creek Mountains, Idaho, with selected upper Paleozoic sections in Idaho and Utah. Interfingering of formations shown diagrammatically for the Mackay quadrangle, Idaho. See explanation on facing page.

cation, 1961) from Upper Mississippian rocks in that area.

The Upper Mississippian Great Blue limestone of the Deep Creek Mountains (fig. 213.1) is like the type Great Blue, even to the presence of a medial shale zone at the same position above the base of the formation in both sections. The Great Blue in the Deep Creek Mountains contains fossils of probable late Meramec age near the base.

The Manning Canyon shale of Mississippian and Pennsylvanian age is divisible into 3 distinct members (fig. 213.1) in the Deep Creek Mountains. A similar tripartite Manning Canyon shale is suggested by Williams' and Yolton's (1945, p. 1145) section southwest of Logan, Utah (fig. 213.1). We examined this section and believe that, despite uncertainties caused by faulting, Williams' units 3, 4, and 5 correspond to our members of the Manning Canyon. Thick shales that probably correlate with the Manning Canyon shale or Milligen formation occur in the Sublett and Black Pine Ranges southwest of the Deep Creek Mountains; however, much more work is needed to determine the relations of Mississippian and Pennsylvanian shales in southern Idaho.

Probably more than 8,000 feet of rocks assigned to the Oquirrh formation overlie the Manning Canyon shale in the Deep Creek Mountains; a minimum of nearly 5,000 feet of Oquirrh, including rocks of Lower Permian age perhaps 600 feet thick, has been measured. Four units of the Oquirrh have been mapped in the Deep Creek Mountains but it is unlikely that these units can be mapped in adjacent areas.

Fusulinids from the Oquirrh formation in the Deep Creek Mountains, identified by R. C. Douglass, include assemblages of probable Atoka, Des Moines, Missouri, Virgil, and Wolfcamp age. E. L. Yochelson (written communication, 1960) recognized *Omphalotrochus* from the Permian part of the section. No equivalents of the Park City or Phosphoria formations have been found, although rocks of this age are present (Cheney and others, 1956) in the Sublett Range 20 miles southwest of the section described here. Youngquist and Haegele (1955) described Pennsylvanian and Permian rocks in the Sublett Range that are about the same age as upper Paleozoic rocks in the Deep Creek Mountains but are different in lithology.

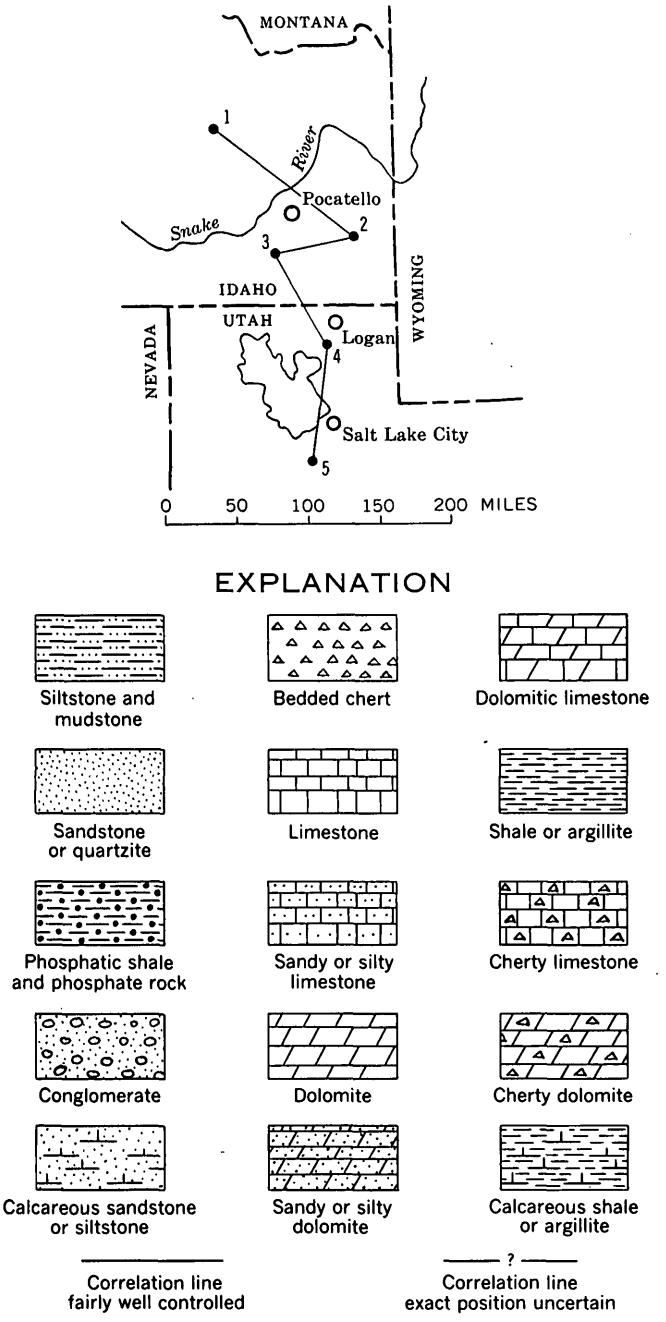

Explanation for figure 213.1.

REFERENCES

Armstrong, F. C., 1953, Generalized composite stratigraphic section for the Soda Springs quadrangle and adjacent areas in southeastern Idaho, *in* Intermountain Assoc. of Petroleum Geologists, Guide to the geology of northern Utah and southeastern Idaho, 4th Ann. Field Conf., 1953: pl. in pocket.

Cheney, T. M., McKelvey, V. E., and Gere, W. C., 1956, Fusulinid-bearing rocks in Sublett Range, southern Idaho —a discussion: Am. Assoc. Petroleum Geologists Bull., v. 40, no. 7, p. 1716–1719.

Gilluly, James, 1932, Geology and ore deposits of the Stockton and Fairfield quadrangles, Utah: U.S. Geol. Survey Prof. Paper 173, 171 p.

Nygreen, P. W., 1958, The Oquirrh formation, stratigraphy of the lower portion in the type section and near Logan, Utah: Utah Geol. and Mineralog. Survey Bull. 61, 67 p.

Ross, C. P., 1960, Diverse interfingering Carboniferous strata in the Mackay quadrangle, Idaho, *in* U.S. Geological Survey, Short papers in the geological sciences: U.S. Geol. Survey Prof. Paper 400–B, p. B232–B233.

Sadlick, Walter, and Schaeffer, F. E., 1959, Dating of an Antler orogenic phase (Middle Mississippian) in western Utah [abs.]: Geol. Soc. America Bull., v. 70, no. 12, pt. 2, p. 1786.

Sando, W. J., Dutro, J. T., Jr., and Gere, W. C., 1959, Brazer dolomite (Mississippian) Randolph quadrangle, northeast Utah: Am. Assoc. Petroleum Geologists Bull., v. 43, no. 12, p. 2741–2769.

Williams, J. S., 1958, Geologic atlas of Utah, Cache County: Utah Geol. and Mineralog. Survey Bull. 64, 98 p.

Williams, J. S., and Yolton, J. S., 1945, Brazer (Mississippian) and lower Wells (Pennsylvanian) section at Dry Lake, Logan quadrangle, Utah: Am. Assoc. Petroleum Geologists Bull., v. 29, no. 8, p. 1143–1155.

Youngquist, Walter, and Haegele, J. R., 1955, Fusulinid-bearing rocks in Sublett Range, southern Idaho: Am. Assoc. Petroleum Geologists Bull., v. 39, no. 10, p. 2078–2084.

214. TIDE-AFFECTED FLOW OF SACRAMENTO RIVER AT SACRAMENTO, CALIFORNIA

By Franklin C. Craig, Sacramento, Calif.

Work done in cooperation with the California Department of Water Resources

The Sacramento River at Sacramento is subject to tidal influence when the flow is less than about 35,000 cfs (cubic feet per second). Questions regarding the accuracy of flows computed by a method that was not designed specifically for unsteady flow conditions prompted a study of the factors to be considered in establishing a rating between stage and discharge on a tide-affected stream. The study has been in progress intermittently since 1952.

The tide in the vicinity of Sacramento usually consists of a large tide and a small tide each lunar day and has a maximum range of about 3 feet. Sacramento is more than twenty miles upstream from the zone of flow reversal and a hundred miles from the ocean. Tidal patterns are shown by the inserts on the map on figure 214.1. The tidal action at San Francisco is complex and a pattern results that is a mixture of the diurnal and semi-diurnal types of tides. The mixed tidal pattern is characterized by succeeding tides that frequently vary considerably in magnitude and that do not oscillate about mean sea level.

Characteristics of tides vary considerably from day to day throughout fortnightly, monthly, and other tide cycles. Furthermore, the characteristics change as the tides move upstream; differences in tide range become less, but differences between the rate of change in stage in the rising and falling phases become greater. The rate of depletion of tidal energy depends, in part, upon the magnitude of the tide, the depth of the stream, and the initial elevation of the water surface. Some small-range tides suffer a depletion of only a few tenths of a foot in range between San Francisco and Sacramento while large-range tides always suffer a depletion of many feet.

The result of the depletion of tide energy as the tide moves upstream becomes apparent in several ways, such as by changes in the rate of rise or fall. Most striking are differences in the gradients of the tide troughs between San Francisco and Sacramento, the gradient of the trough of a large-range tide being much greater than that of a small-range tide. There is not a great deal of difference between the gradient of tide crests.

Brown (1932, p. 749) has stated that water rushing into the mouth of an estuary induces a wave of translation which transmits force and energy upstream until it is finally depleted by friction and the force of the downflowing stream. Likewise as the tide recedes and water rushes out of the estuary a negative wave of translation is induced that also transmits force upstream until its energy is dissipated.

It is evident at Sacramento that an active force is present. It has been observed many times that the rate of flow tends to decrease toward the end of the falling phase. Before the end of the phase is reached,

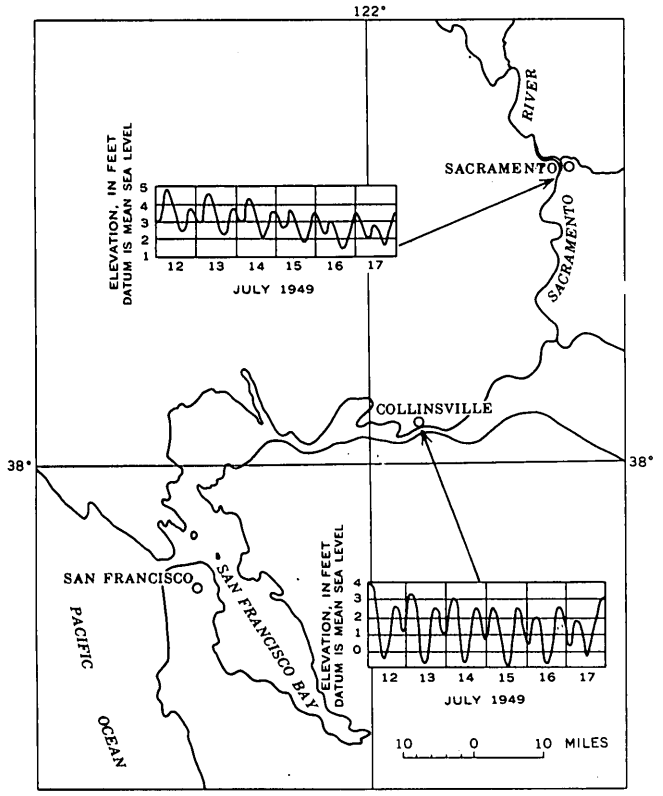

FIGURE 214.1.—Map of lower Sacramento River and San Francisco Bay, showing tide pattern at Sacramento and Collinsville, Calif.

however, there is a marked increase in the rate of flow followed by a second decrease. Such phenomena could only occur as a result of an active force.

It is evident, too, from the pattern of depletion of tide range that waves of translation induced in the falling phase (ebb tide) lose their energy much more rapidly than those induced during the rising phase (flood tide). There is, of course, much more work to be done during the falling phase because the water that enters the estuary during the rising phase plus the water from upland sources must be accelerated and moved out of the estuary during the falling phase. As the tidal energy in this phase is insufficient to move this amount of water, a head must be created to accomplish the task. The head is created from the energy of the tide in the rising phase and from the force of the downflowing stream.

The net effect of this head is to cause the mean water surface elevation of a tide-affected stream to tend to assume the shape of a long flat arch extending from the ocean to the point of depletion of tide effect. The shape of the arch is, of course, dependent upon the geometry of the stream.

The extent of the arching action varies with tide range, water depths, volume of upland flow, and other factors. The arching action, or head, is considered to be largely an acceleration head although velocity and friction heads are contributing factors. Velocity observations have shown that with acceleration, deceleration, and the movement of water at varying elevations there is considerable variation in velocity distribution throughout the cross section of the stream. Hence, there is more internal friction present than there is in a stream flowing under steady flow conditions.

The problem of developing a rating between stage and discharge for the Sacramento River at Sacramento becomes one of evaluating the effect of variable head. This evaluation becomes difficult because, for example, an increase in head may be caused either by an increase in tide range or by an increase in the upland flow. Variations in head as a result of variation in tidal activity have increasingly greater effect as flows decrease below 10,000 cfs and decreasing effect for greater flows. Techniques used in rating other streams subject to variable backwater effects have proved to be satisfactory in rating the higher flows, but are not dependable for low flows when applied to the Sacramento River. A technique developed for rating tide-affected streams in Florida has proved to be usable when flows are low, and changes in the variable head are mainly the result of changes in tidal activity. The method proved to be weak when the rate of flow from upland sources was changing rapidly. The technique makes use of the depletion in tide range from the lower to the upper end of the rating reach as a factor in adjusting the rating. Since the variation in head, insofar as it relates to changes in tidal activity, is associated with depletion in tide range, the method is usable under limited conditions. A technique developed by the present author, also based upon the depletion of tide range in the rating reach, has proved to be usable over a wider range of flow.

Techniques such as these, which are based on stage readings many miles apart, produced good results when limited to the conditions to which they are adapted but are not the final solution to the problem. The weakness of these techniques lies in the fact that they take into consideration only partly the varying characteristics of individual tides. New developments in instrumentation promise to make it practical to apply complex mathematical relationships that are involved in a rigid analysis of a tide-affected stream, and hence permit using these relations to compute discharge on

601530 O—61——13

a day to day basis. Digital punches, which are now installed at both ends of the rating reach, will make stage, fall, and rate of change in stage over short intervals of time available to an electronic computer. Research is now being carried on by the Geological Survey to bring all of the essential factors into a computer program for analyzing the characteristics of every type of tide.

REFERENCE

Brown, E. I., 1932, Flow of water in tidal canals: Am. Soc. Civil Engineers Trans., v. 96, p. 749.

215. INTERCHANGE OF SURFACE WATER AND GROUND WATER ALONG TRIBUTARY STREAMS IN THE CENTRAL VALLEY, CALIFORNIA

By S. E. Rantz and Donald Richardson, Menlo Park, Calif., and Tacoma, Wash.

Work done in cooperation with the California Department of Water Resources

The seepage rates along the lower reaches of 21 streams traversing the alluvial plain of the Central Valley provide a basis for estimating potential rates of ground-water recharge through these stream channels under conditions of conjunctive use of surface- and ground-water storage. From 1952 to 1958 streamflow was measured periodically to determine seepage rates, but no concurrent observations of ground-water elevation were made. Discharge measurements were made at each end of several reaches on each stream, the measuring sites being selected at locations where the geology indicated that a definite change in the rate of gain or loss in streamflow might be expected. The streams investigated are listed in table 215.1 and are shown on figures 215.1 and 215.2. Ten streams are tributary to the San Joaquin River and flow intermittently; the other eleven are tributary to the Sacramento River and flow perennially.

Emphasis was placed on determining maximum seepage rates for each reach of channel. These maximum rates occur under the optimum combination of ground-water elevation and maximum streambed permeability. Because of the lack of information on ground-water, it was impossible to determine these optimum conditions independently, but their occurrence was indicated by observing the greatest seepage rate per acre of wetted channel. High recharge rates would probably be maintained if surface- and ground-water reservoirs are to be maintained in conjunction. The seepage rate per acre of wetted channel may vary widely during the course of a year as a result of the deposition of relatively impermeable silt on the streambed during the recession of a stream and the removal of this silt during a rise. However, under conditions of conjunctive storage, a high degree

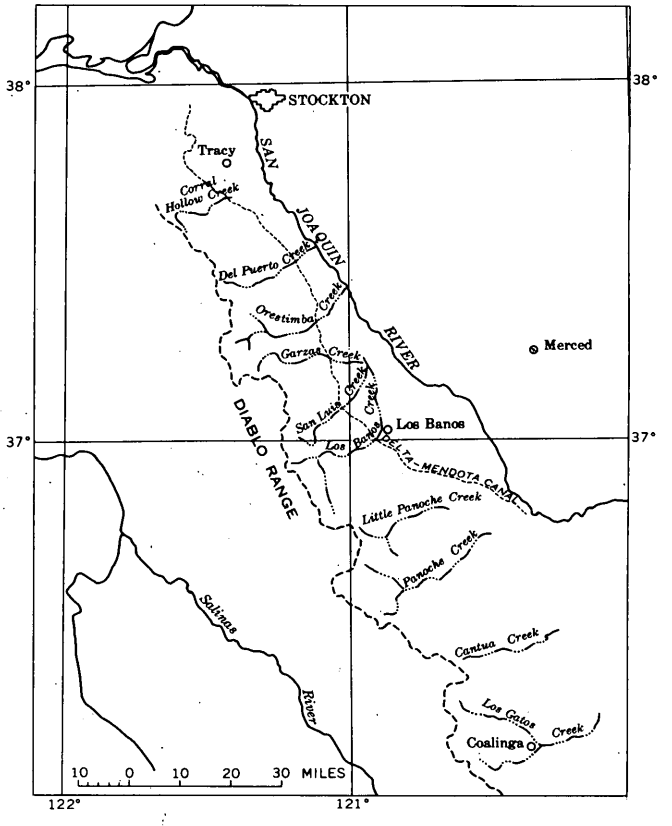

FIGURE 215.1.—Tributary streams investigated in the San Joaquin Valley.

of channel permeability could be maintained by mechanically scarifying or removing the more impermeable surface material on the streambed. The water table could probably be maintained at levels conducive to high recharge rates by the judicious pumping of ground-water, and water-table gradients might be reversed by pumping to permit recharge of the ground-water reservoir through the beds of some channels that now receive effluent ground-water seepage.

Table 215.1 gives the range of unit seepage rates observed during the period of investigation at the 21 Central Valley streams. The plus sign indicates seepage gain to the stream; the minus sign represents seepage loss from the stream. Expressing the seepage rate in terms of cubic feet per second per acre of wetted channel permits direct comparison of the various channels, because this unit rate is independent of discharge, channel geometry, and length of reach. Doubling this unit rate gives the seepage in terms of acre-feet per day per wetted acre, a unit that is numerically equivalent to seepage expressed in feet of water (depth) per day. For example, the highest unit seepage rate observed, 3.5 cfs per wetted acre, which occurred on Orestimba Creek, is equivalent to a seepage rate of 7 feet of water per day.

TABLE 215.1.—*Summary of observed unit seepage rates*

[+, seepage into the channel; −, seepage out of the channel]

Creek	Range in unit seepage rates (cfs per acre of wetted channel)
San Joaquin Valley	
Los Gatos	+0.03 to −0.6
Cantua	+.10 to −1.7
Panoche	+.06 to −2.3
Little Panoche	−.12 to −.8
Los Banos	+.3 to −1.6
San Luis	0 to −2.7
Garzas	+.2 to −2.5
Orestimba	0 to −3.5
Del Puerto	+.07 to −1.2
Corral Hollow	0 to −.8
Sacramento Valley	
Clear	+0.18 to −0.15
Cottonwood	+1.8 to −.4
Red Bank	+.3 to −.8
Antelope	+2.0 to −.9
Elder	+.04 to −2.5
Mill	+3.0 to −2.4
Thomes	+.8 to −.4
Deer	+2.5 to −1.5
Pine	+.5 to −1.5
Big Chico	+.6 to −2.3
Cache	+1.8 to −3.0

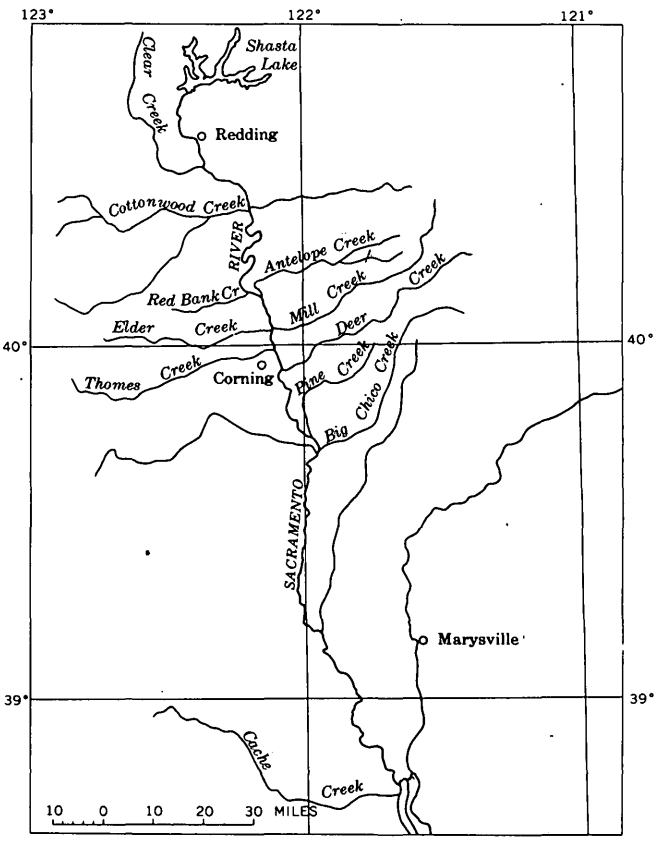

FIGURE 215.2.—Tributary streams investigated in the Sacramento Valley.

Of the 10 intermittent San Joaquin Valley streams, only Del Puerto Creek contributes a large percentage of its flow directly to the San Joaquin River. In years of average rainfall virtually all the runoff from the other streams is absorbed by permeable alluvial fan deposits before reaching the valley trough. Although a small part of this runoff is lost by evapotranspiration, and a small part is used for irrigation, most of the water passes downward through the soil zone and eventually reaches the water table in the upper water-bearing zone. It is estimated that the average annual runoff of streams on the west side of the San Joaquin Valley is 60,000 acre-feet, and that 60 to 80 percent of this runoff reaches the groundwater body.

216. SILURIAN AND DEVONIAN ROCKS OF THE KLAMATH MOUNTAINS, CALIFORNIA

By C. W. MERRIAM, Washington, D.C.

Paleozoic and Mesozoic rocks of the Klamath Mountains are disposed in arcuate north-south belts (fig. 216.1) as shown by W. P. Irwin (1960, p. 15). In the southern and eastern parts of this region fossiliferous rocks ranging from Silurian to Permian in age crop out widely. Elsewhere in this region the fossil record is meager.

WESTERN KLAMATH BELT OF PALEOZOIC AND TRIASSIC ROCKS

Supposedly Devonian Prolecanitidae were collected by Diller (1903, p. 345) northwest of North Yolla Bolly Mountain (locality 13). Restudy indicates that these ammonoids are probably Triassic arcestids (N. J. Silberling, written communication, 1958). Limestones along the southwest margin of this belt contain structures resembling *Chaetetes* and *Solenopora;* these deposits may be of Paleozoic or early Mesozoic age.

Limestone on Knownothing Creek (locality 7) near the center of this belt yields calcareous algae, stromatoporoids, and *Cladopora*, suggesting a Silurian and Devonian age.

SOUTHEASTERN KLAMATH BELT OF MIDDLE DEVONIAN ROCKS

This belt of Paleozoic rocks, otherwise known as the Redding-McCloud belt, (localities 19, 20, 21, 22) in-

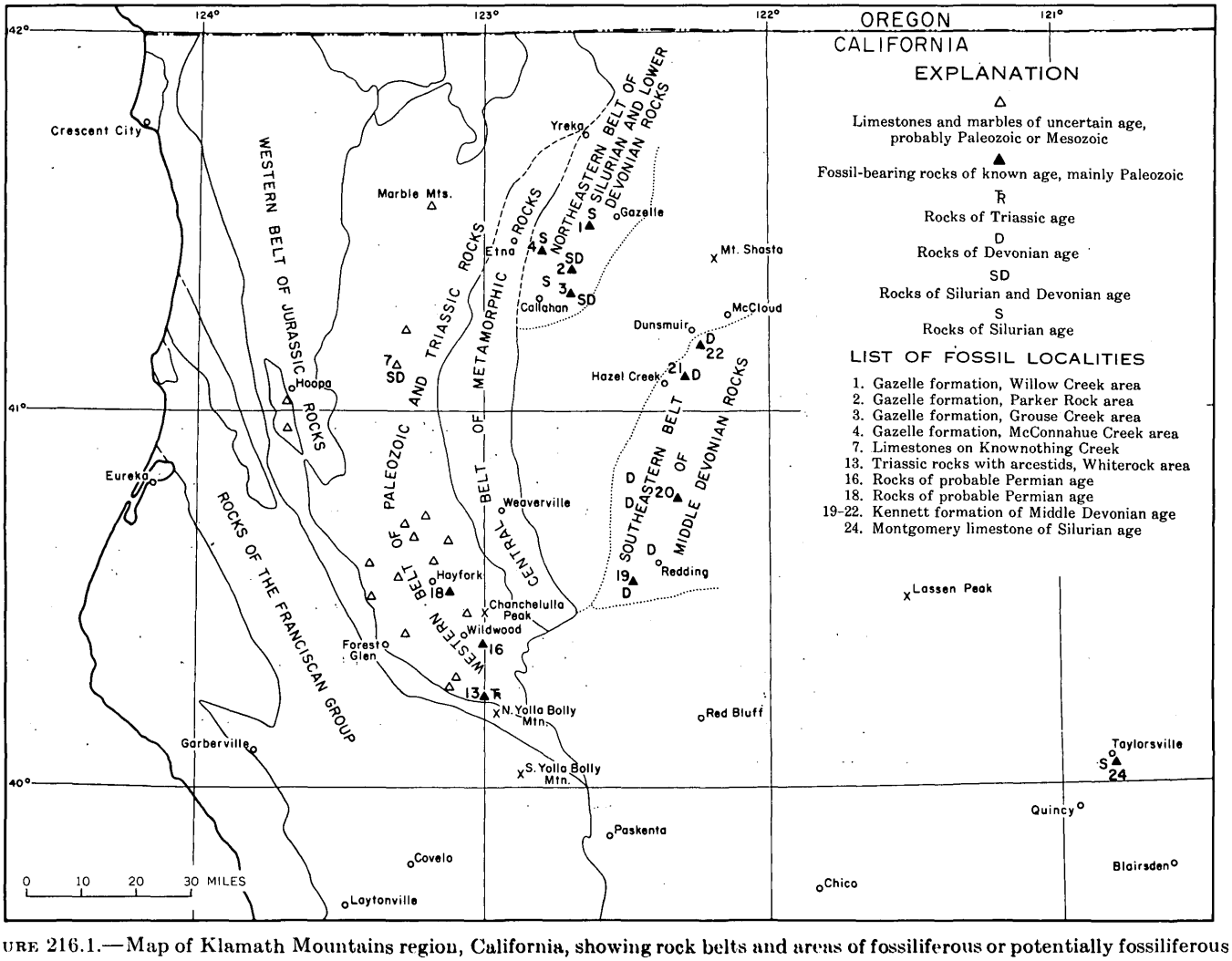

FIGURE 216.1.—Map of Klamath Mountains region, California, showing rock belts and areas of fossiliferous or potentially fossiliferous outcrops. Adapted from map by W. P. Irwin (1960, fig. 3).

cludes the Middle Devonian Kennett formation (Diller, 1903, p. 347). The Kennett rests upon the Balaklala rhyolite which overlies the Copley greenstone (Kinkel, Hall and Albers, 1956, p. 32). The Kennett of the type area includes three members: a lower 75-foot siliceous shale, a middle bluish limestone 200 feet thick and an upper mudstone-tuff-sandstone unit about 325 feet thick. Overlying the Kennett is the Bragdon formation of supposed Mississippian age.

The limestone member (Stauffer, 1930, p. 95), largely a coral facies, contains abundant favositids, *Heliolites, Alveolites*, *Cladopora*, cyathophyllids, cystiphyllids and *Phillipsastraea?* The abundant stromatoporoids include *Amphipora*. Among the brachiopods are *Atrypa*, a large robust *Schizophoria*, and *Cryptonella*. Faunas of the mudstone in the upper part of the Kennett include *Productella*, *Martiniopsis? Schizophoria*, *Cyrtina*, *Atrypa* and *Cladopora*. *Heliolites* and complex cyathophyllids like those just below *Stringocephalus* in Nevada suggest a late Middle Devonian age.

NORTHEASTERN KLAMATH BELT OF SILURIAN AND LOWER DEVONIAN ROCKS

The northeastern Klamath or Scott River belt includes the Gazelle formation (Wells, Walker, and Merriam, 1959) now considered to be of Silurian and Early Devonian age. The Gazelle comprises gray, greenish and reddish shale, gritty sandstone and graywacke, siliceous conglomerate, bedded chert, and massive gray limestone. Tuffaceous interbeds are present. The limestone beds are lenticular; some lenses were small reefs on a sea bottom where accumulation was mainly graywacke and other silicious sediments.

Significant faunas have been collected from argillaceous beds just below the upper limestone of the Gazelle on Willow Creek (locality 1) and from the limestone itself (Diller and Schuchert, 1894; Stauffer, 1930, p. 98). These include *Chonophyllum*, *Heliolites*, cystiphyllids, *Conchidium*, *Stricklandia?*, *Gypidula* cf. *G. galeata* (Dalman), *Atrypa*, *Atrypella* cf. *A. dunbari* Kirk and Amsden, *Encrinurus*, and *Bumastus*. A distinctive trilobite assemblage from shale in the Gazelle of the Willow Creek area (Churkin, 1961) comprises species of *Leonaspis*, *Dicranopeltis*, *Trochurus*, *Scutellum*, *Cheirurus*, *Encrinurus*, and *Proetus*.

Parker Rock (locality 2) is another massive limestone (Gazelle) of probable reef origin, near the base of which occur abundant favositids, *Halysites* and *Chonophyllum*. Other Silurian fossils from the Parker Rock vicinity include *Heliolites*, *Conchidium*, *Atrypella?*, cheirurid trilobites, and *Calymene*. Coral-bearing limestones at Gregg Ranch east of Parker Rock have yielded *Skenidioides?*, *Howellella*, and the large cap-shaped gastropod *Hercynella*.

Dark-gray carbonaceous limestone bodies at Grouse Creek (locality 3) contain *Cladopora*, *Diversophyllum?*, *Schizophoria* sp cf. *S. bisinuata* Weller, *Stropheodonta* sp. cf. *S. varistriata* (Conrad), *Cyrtina*, *Ambocoelia*, and *Proetus*. These appear to be the youngest Paleozoic rocks of the northeast belt, and are regarded as Helderberg Lower Devonian.

The oldest Silurian beds of the Gazelle formation occur on McConnahue Creek (locality 4), 8 miles north of Callahan, where they contain *Cladopora*, *Halysites*, *Heliolites* or *Plasmopora*, and *Schizoramma?*.

CORRELATION

The Silurian rocks of the northeastern Klamath belt are correlative with those of the Taylorsville area, California (locality 24) where the Montgomery limestone fauna with *Halysites*, *Plasmopora*, *Schizoramma?*, and *Bilobites* suggests faunas in the lower part of the Gazelle.

Higher Gazelle strata of the Willow Creek area (locality 1) were long regarded as Devonian (Diller and Schuchert, 1894, p. 417; Stauffer, 1930, p. 98) and equivalent to the Kennett formation of the southeastern Klamath belt. This interpretation now appears untenable (Merriam, 1940, p. 48). It is not, however, unlikely that the Gazelle formation with its tuffaceous interbeds is correlative with the Copley greenstone and Balaklala rhyolite which underlie the Kennett.

The Gazelle strata containing distinctive *Atrypella* faunas are correlative with *Atrypella*-bearing Upper Silurian beds of southeast Alaska (Kirk and Amsden, 1952, p. 53–55) and with beds carrying similar faunas in the Ural Mountains (Khodalevich, 1939, p. 90–125). Trilobites, from the Gazelle formation, described by Churkin (1961) reveal affinity to Middle and Upper Silurian trilobites of Bohemia.

Heliolites and large complex cyathophyllids of the limestone in the middle part of the Kennett resemble those of the *Heliolites* subzone in the central Great Basin Nevada formation (Merriam, 1940, p. 9). This subzone lies at the base of the *Stringocephalus* zone in the Great Basin and is of late Middle Devonian age.

REFERENCES

Churkin, Michael, Jr., 1961, Silurian trilobites from the Klamath Mountains, California: Jour. Paleontology, v. 35, no. 1, p. 168–175.

Diller, J. S., 1903, Klamath Mountain section, California: Am. Jour. Sci., 4th ser., v. 15, p. 342–362.

Diller, J. S., and Schuchert, C., 1894, Discovery of Devonian rocks in California: Am. Jour. Sci., 3d ser., v. 47, p. 416–422.

Irwin, W. P., 1960, Geologic reconnaissance of the northern Coast Ranges and Klamath Mountains, California: California Div. Mines Bull. 179.

Khodalevich, A. N., 1939, Upper Silurian Brachiopoda of the eastern Urals: Trans. Ural Geol. Service (Geol. Service of U.S.S.R.), p. 1–135.

Kinkel, A. R., Hall, W. E., and Albers, J. P., 1956, Geology and base-metal deposits of West Shasta copper-zinc district, Shasta County, Calif., U.S. Geol. Survey Prof. Paper 285.

Kirk, Edwin and Amsden, T. W., 1952, Upper Silurian brachiopods from southeastern Alaska: U.S. Geol. Survey Prof. Paper 233–C.

Merriam, C. W., 1940, Devonian stratigraphy and paleontology of the Roberts Mountains Region, Nevada: Geol. Soc. America Spec. Paper no. 25.

Stauffer, C. R., 1930, The Devonian of California: California Univ. Dept. Geol. Sci. Bull., v. 19, no. 4, p. 81–118.

Wells, F. G., Walker, G. W., and Merriam, C. W., 1959, Upper Ordovician(?) and Upper Silurian formations of the northern Klamath Mountains, California: Geol. Soc. America Bull., v. 70, p. 645–650.

217. CITY COLLEGE FAULT, SAN FRANCISCO, CALIFORNIA

By M. G. Bonilla, Menlo Park, Calif.

A fault that separates two distinct bedrock assemblages and is marked by a wide zone of sheared rock was discovered in the southwest part of San Francisco. The fault is here named the City College fault after the City College of San Francisco, which is in the fault zone. The dimensions of the zone of sheared rock and the differences in the adjacent rocks indicate that the fault has a large displacement. The sheared rock presents special problems in engineering construction.

The location and known extent of the fault are shown on figure 217.1. The zone of sheared rock that marks the fault has a maximum width of about half a mile and is exposed discontinuously for 4½ miles along the strike. This is probably only a small part of the total length of the fault, but possible extensions are concealed by San Francisco Bay on the southeast and by Quaternary deposits on the northwest.

Several kinds of rocks are exposed north of the fault but only two varieties are exposed in the area just south of it. The northern assemblage consists of sandstone (graywacke), shale, chert, greenstone, and schists of the Franciscan formation and serpentine, whereas the southern assemblage consists only of sandstone (graywacke) and shale.

The rocks of the southern assemblage are less faulted and sheared than those in the northern assemblage. The rocks of the southern assemblage commonly show graded bedding and bedding-plane structures such as flow- and load-casts, and they contain appreciable quantities of K-feldspar whereas these features are scarce or absent in the sediments of the northern assemblage.

The difference in the K-feldspar content of the two groups is very striking. Staining tests were made on 51 widely distributed samples from the area shown on figure 217.1 using the technique described by Bailey and Irwin (1959, p. 2802–2803). None of the 17 samples taken north of the fault zone contains K-feldspar. Of the 12 samples from the area south of the fault, 1 sample has no K-feldspar, 1 has 1 percent, and the rest range from 2 to 8 percent. Sandstones from both the northern and southern groups occur in the zone of sheared rock along the fault. About one-third of the 22 samples from the zone of sheared rock contain 1 to 6 percent K-feldspar and the rest contain a trace or none. The faultline shown on the map was drawn so as to bisect the zone of sheared rock; the line also separates all 51 of the samples into two groups, the northerly group having no K-feldspar or only a trace.

The sediments of the southern assemblage were designated by Lawson (1914) as Cahil sandstone, the oldest formation of his Franciscan group. However, the work of Bailey and Irwin (1959) suggests that because of the high K-feldspar content the southern assemblage should perhaps be excluded from the Franciscan formation. The other differences between the two assemblages strengthens this belief; for the purposes of this report, however, the term Franciscan is retained for the southern assemblage.

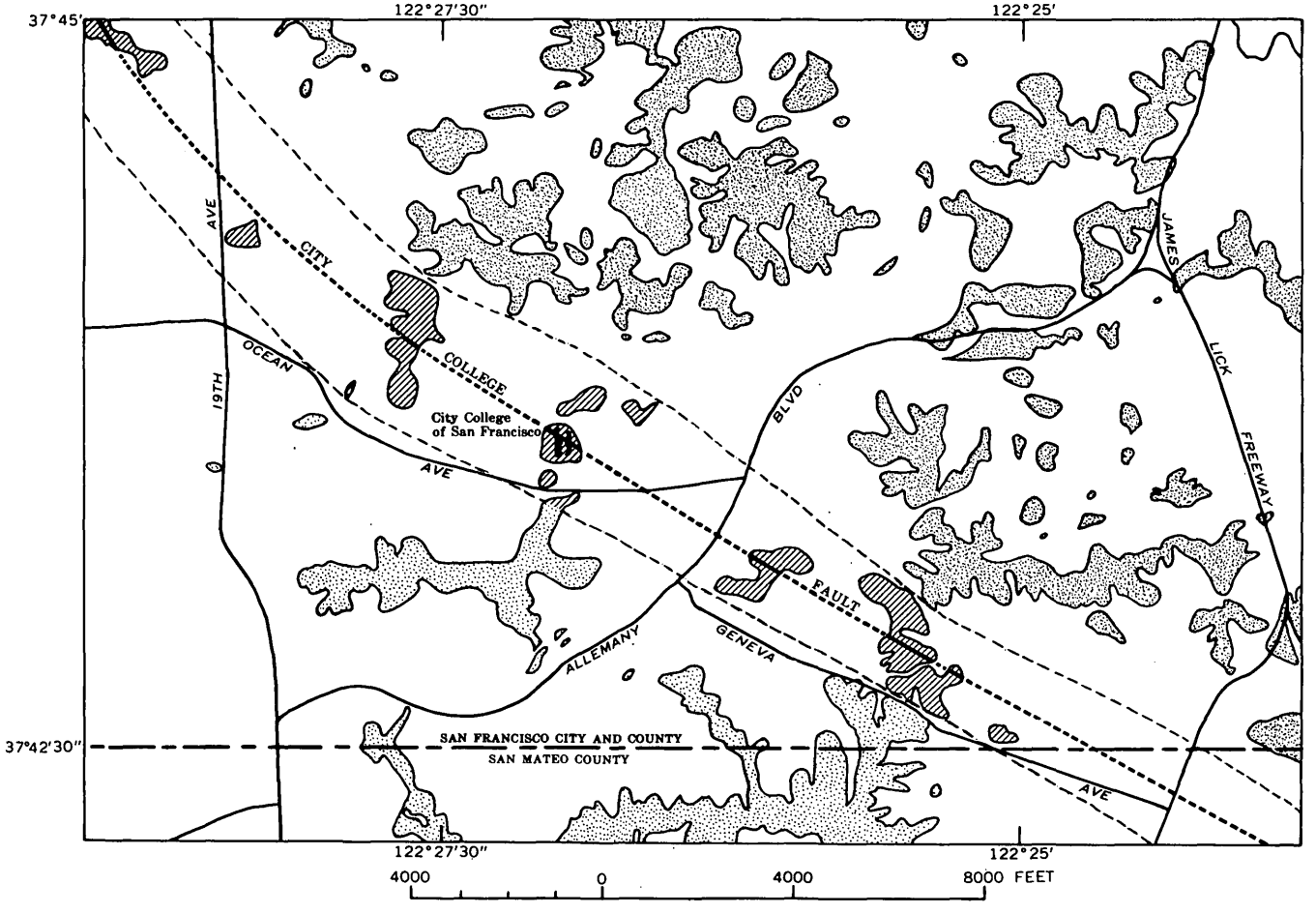

FIGURE 217.1.—Generalized geologic map showing location of City College fault. Fault is dotted where concealed. Dashed lines show approximate limits of zone of sheared rock where zone is concealed by Quaternary deposits. Quaternary deposits, undifferentiated (blank areas). Franciscan formation, sandstone and shale (light stippling, south of fault); sandstone contains potassium feldspar. Franciscan formation and serpentine, undifferentiated (dense stippling, north of fault); Franciscan includes sandstone, shale, chert, greenstone, and schist; sandstone contains no potassium feldspar. Sheared rocks derived from second and third groups above (diagonal ruling).

The surface expression of the zone of sheared rock consists of isolated blocks of resistant rock protruding from the soil. The resistant blocks range from a few feet to many tens of feet in longest dimension and, where they are large or numerous, they form the cores of small hills. Several kinds of rocks may crop out in a small area. One hill has exposures of sandstone, shale, chert, greenstone, schist, and serpentine in an area that is about 800 feet long and 500 feet wide. In contrast to some shear zones in the Coast Ranges, this one contains little serpentine. Artificial cuts show that the resistant rock is generally surrounded by sheared fine-grained rock that is brown and moderately soft where weathered but dark gray and moderately tough where fresh. Within the sheared material are sound pieces of various sizes, many of them elliptical or lenticular in cross section. No plastic, claylike gouge was seen in the fault zone.

Neither the dip of the City College fault nor the relative ages of the adjacent rocks are known, and one can only speculate as to what type of fault it is. The fault is roughly parallel to the San Andreas fault, which lies about 4 miles to the southwest, and the Hayward fault, which lies about 15 miles to the northeast. Both the San Andreas and Hayward are strike-slip faults and the City College fault may be one also.

It is not known whether the fault is active. No scarps or other evidence of faulting have been seen in the late Pleistocene and younger sediments that overlie the fault, but such evidence could easily escape notice or be quickly destroyed in the soft sediments. Two of the epicenters shown on a map published by Byerly (1951, fig. 20) may indicate recent activity on the fault. One epicenter is shown on the extension of the fault and southeast of the area shown on fig-

ure 217.1, and the other is about two-thirds of a mile northeast of the fault. The proximity of the epicenters to the City College fault may be the result of the inaccuracies inherent in locating epicenters rather than the result of recent activity along the fault; the earthquakes may have originated along the nearby San Andreas fault. The question of the activity of the City College fault can probably be answered when more seismological data are accumulated.

The sandstone near Point Lobos, about 3 miles northwest of the area of figure 217.1, contains appreciable quantities of K-feldspar (J. Schlocker, oral communication, 1961). The City College fault may, therefore, join the faults near Lands End that are shown on the San Francisco North quadrangle (Schlocker and others, 1958).

The significance of the City College fault to engineering lies chiefly in the foundation characteristics, slope stability, and excavation properties of the zone of sheared rock. Test borings that encounter the inclusions of hard rock give a false impression of the soundness and configuration of the "bedrock." Piles or caissons may have a great range in length at a particular building site because they rest on the erratically distributed hard blocks. The sheared rock can generally be removed with earthmoving equipment but the large blocks require blasting or other special handling. Slopes cut in the sheared rock, particularly where it is weathered, are generally less stable than similar slopes in sound rock. As indicated on figure 217.1, much of the sheared rock is concealed by Quaternary deposits, and the line that represents the fault was drawn merely to bisect the zone of sheared rock. No one should infer that the rock along this line is more intensely faulted than elsewhere in the shear zone.

REFERENCES

Bailey, E. H., and Irwin, W. P., 1959, K-feldspar content of Jurassic and Cretaceous graywackes of northern Coast Ranges and Sacramento Valley, California: Am. Assoc. Petroleum Geologists Bull., v. 43, no. 12, p. 2797–2809.

Byerly, Perry, 1951, History of earthquakes in the San Francisco Bay area, *in* Geologic guidebook of the San Francisco Bay counties: California Div. Mines Bull. 154, p. 151–160.

Lawson, A. C., 1914, San Francisco folio: U.S. Geol. Survey Geol. Atlas, Folio 193, 24 p.

Schlocker, J., and Bonilla, M. G., and Radbruch, D. H., 1958, Geology of the San Francisco North quadrangle, California: U.S. Geol. Survey Misc. Geol. Inv. Map I–272.

GEOLOGY AND HYDROLOGY OF ALASKA AND HAWAII

218. ORIENTATION OF PHENOCLASTS IN LAMINATED GLACIOLACUSTRINE DEPOSITS, COPPER RIVER BASIN, ALASKA

By Henry R. Schmoll, Washington, D.C.

Pleistocene sediments in the intermontane Copper River Basin of south-central Alaska are dominantly deposits of Wisconsin age (Ferrians and Schmoll, 1957) and of older proglacial lakes and associated glaciers. They range from till through till-like deposits with various degrees of bedding, sorting, and stone content to rhythmically bedded (varved) deposits referred to here as laminated silt. The last-named deposits also contain clay, fine sand, and scattered phenoclasts. Among other types of analyses, macrofabric studies of 80 100-stone samples are being undertaken to differentiate the deposits and to determine their origin.

Field and laboratory methods for analysis of fabric are essentially those of Karlstrom (1952) modified by Schmoll and R. H. Bennett. The axes, of the stones are as follows: A, longest dimension; B, longest dimension perpendicular to A; C, longest dimension normal to the plane parallel to A and B. In the present studies, A-axis lengths are limited to the 32 to 128 mm range. Contour diagrams were constructed by an independently derived method similar to that of Mellis (1942).

Three samples (fig. 218.1) were collected at localities spaced about 0.6 mile apart within a laminated silt deposit of Wisconsin age exposed along the Cop-

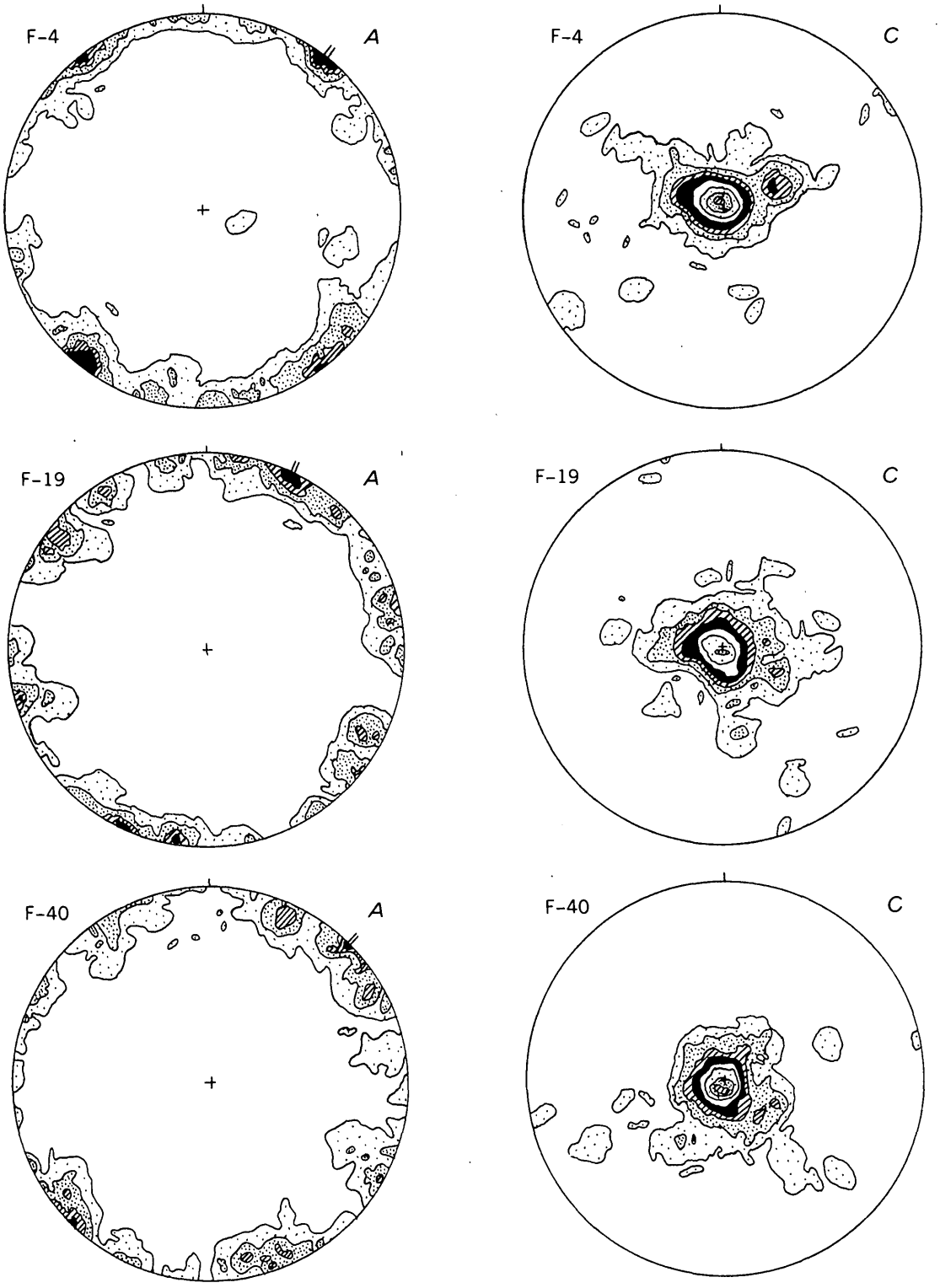

FIGURE 218.1.—Contour diagrams of *A*-axis and *C*-axis distribution of 3 100-stone samples of phenoclasts from a laminated silt deposit of Wisconsin age. Sample numbers appear at the upper left of each diagram, axis designations at the upper right. North is indicated by a single line at the circumference. On *A*-axis diagrams, the azimuth of maximum point concentration is indicated by a double line at the circumference. Contoured areas, in percent per 1 percent of area, are as follows (values in parentheses apply at the centers of the *C*-axis diagrams within the solid unit): blank, 0–2 (10–15); lightly stippled, 2–4 (15–20); heavily stippled, 4–6 (20–25); diagonally lined, 6–8 (25–28); solid, 8–10.

per and Gakona Rivers near Gakona, Alaska. Two other samples (fig. 218.2) are from older deposits in the same area.

Both *A*-axis and *C*-axis diagrams reveal a strongly preferred orientation. The *A* axes lie close to a horizontal plane and *C* axes approach vertical. The *B* axes must therefore also lie nearly horizontal, and a field observation that the stones tend to lie "flat" is confirmed.

Two features of the *A*-axis diagrams were rather unexpected: the high concentrations of points within the horizontal girdle, and the close azimuth agreement of maximum point concentrations among all three coeval samples (fig. 218.1). This agreement is not found in samples of different ages. (Compare figs. 218.1 and 218.2.)

To determine whether point concentrations as high as those obtained would result from random distribution, artificial diagrams (Flinn, 1958, p. 531) were constructed so that they would resemble the "natural" diagrams. Randomly selected "azimuth" values were randomly combined with "plunge" values distributed similarly to the plunges in the "natural" samples. Diagram R-1 (fig. 218.2) is typical of the results obtained. Concentrations of points are as high as those in the "natural" diagrams. Two types of chi-square significance tests (Flinn, 1958, p. 534, 536) compare each of the "natural" distributions with an "expected" distribution derived from means of the artificial distributions. The "area test," comparing the grouping of points, indicates that the "natural" distributions do not differ significantly from a random distribution. The "frequency test," comparing the spatial distribution of points, shows, however, a significant difference for each "natural" distribution at the 0.04 probability level or below.

A further comparison of the distribution of areas of high concentration of points around the horizontal girdle indicates that for all three diagrams from laminated silt of Wisconsin age, when considered collectively and when the maximum point concentrations are alined at an arbitrary zero azimuth, there is a higher-than-expected secondary maximum concentration at approximately 100 degrees in the clockwise direction. Similar relations are not obtained from the random diagrams, nor from a group of natural

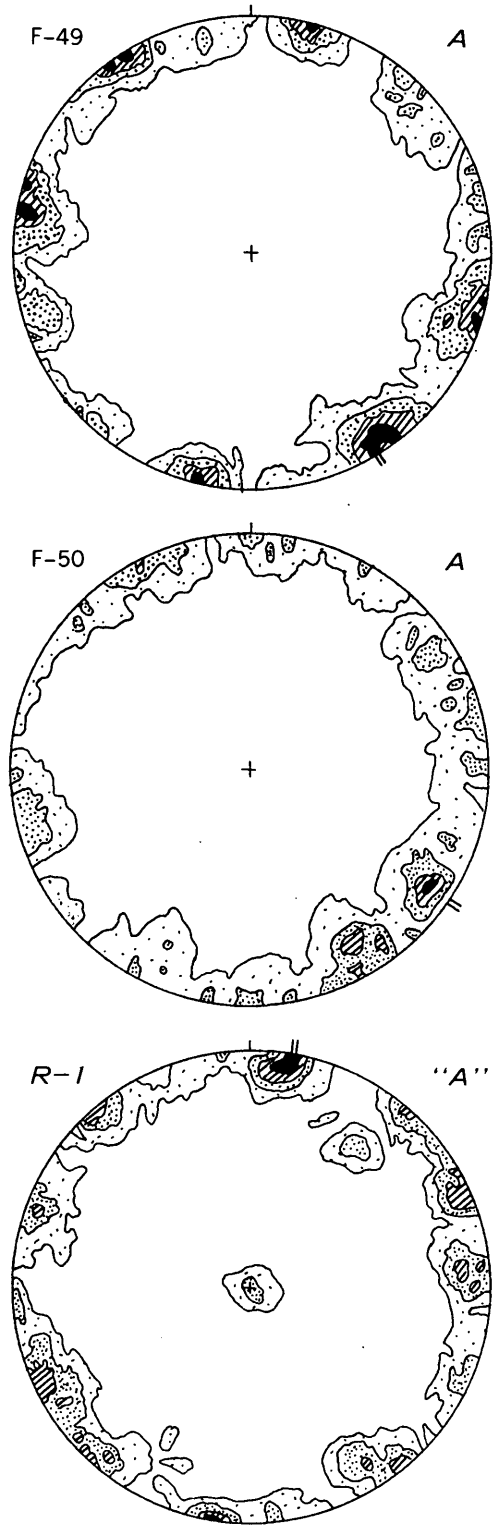

FIGURE 218.2.—Contour diagrams of *A*-axis distributions of samples of phenoclasts from two noncoeval laminated silt deposits of pre-Wisconsin age, and artificial "*A*-axis" distribution *R*–1. Diagrammed as in figure 218.1.

diagrams from noncoeval deposits, which suggests a nonrandom distribution.

Near alinement of areas of maximum point concentration of three coeval samples, value of chi-square in the "frequency test," and distribution of areas of high concentration around the girdle in coeval samples thus seem to indicate that the orientation of *A* axes within the horizontal girdle is not random but preferred. This preferred orientation is weak however, and requires more widespread sampling for confirmation.

The *C*-axis concentration centers do not seem to depart sufficiently from the center of the diagram to indicate any significant or consistent imbrication of the stones. The slightly noncircular shape of most of these point concentrations may be a manifestation of the secondary element of the fabric which is better expressed in the *A*-axis diagrams.

Assuming that the stones arrived in the midst of otherwise fine-grained sediments by ice-rafting on the lake, any orienting force would then act upon each stone (a) when still in the ice; (b) while falling through the water; (c) upon contact with the bottom; or (d) after initial deposition. The primary element of the preferred orientation is most likely the result of the stone's coming to its natural rest position on the flat, relatively firm floor with the two longest axes (*A* and *B*) essentially parallel to the floor. The cause of the secondary fabric element is more problematical. Proposition (a) seems unreasonable, especially for a time-space range as wide as the samples represent. Proposition (c) is improbable because any surface features which might guide the *A*-axes to a preferred azimuth would probably also remove the *A-B* plane from the horizontal. Proposition (d) is similarly discarded, inasmuch as most post-depositional movement would also alter the primary fabric element more than is apparent, and compaction itself is not considered competent. In addition, other evidence for the factors involved in (c) and (d) is lacking at the sample sites. Proposition (b) remains, and forces such as currents that acted on the sinking stones are tentatively considered the cause of the secondary fabric element.

REFERENCES

Ferrians, O. J., Jr., and Schmoll, H. R., 1957, Extensive proglacial lake of Wisconsin age in the Copper River Basin, Alaska [abs.]: Geol. Soc. America Bull., v. 68, p. 1726.

Flinn, Derek, 1958, On tests of significance of preferred orientation in three-dimensional fabric diagrams: Jour. Geology, v. 66, p. 526–539.

Karlstrom, T. N. V., 1952, Improved equipment and techniques for orientation studies of large particles in sediments: Jour. Geology, v. 60, p. 489–493.

Mellis, Otto, 1942, Gefügediagramme in sterographischer Projektion: Zeitschr. Min. Pet. Mitt., v. 53, p. 330–353.

219. WEATHERED BASALT IN THE EASTERN PART OF KAUAI, HAWAII

By Sam H. Patterson and C. E. Roberson, Beltsville, Md., and Menlo Park, Calif.

Work done in cooperation with Hawaii Department of Land and Natural Resources

Alumina-rich soil and deeply weathered basalt occur in several extensive areas in the eastern part of Kauai, Hawaii (fig. 219.1). The richest deposits are restricted to the upper parts of a group of lava flows mapped as the Koloa volcanic series by Macdonald, Davis, and Cox (1960). The most deeply weathered rocks are on gently rolling uplands that were formed through modification of original flow surfaces by erosion. Land surfaces are younger in numerous stream valleys cut into the flows, and the least weathered rocks are in the deepest valleys.

Depth of weathering, more than 60 feet in most places and locally more than 100 feet, is controlled chiefly by differences in ages of flows within the Koloa series, to a lesser extent by rainfall of 80 to 150 inches a year, and by drainage and other factors.

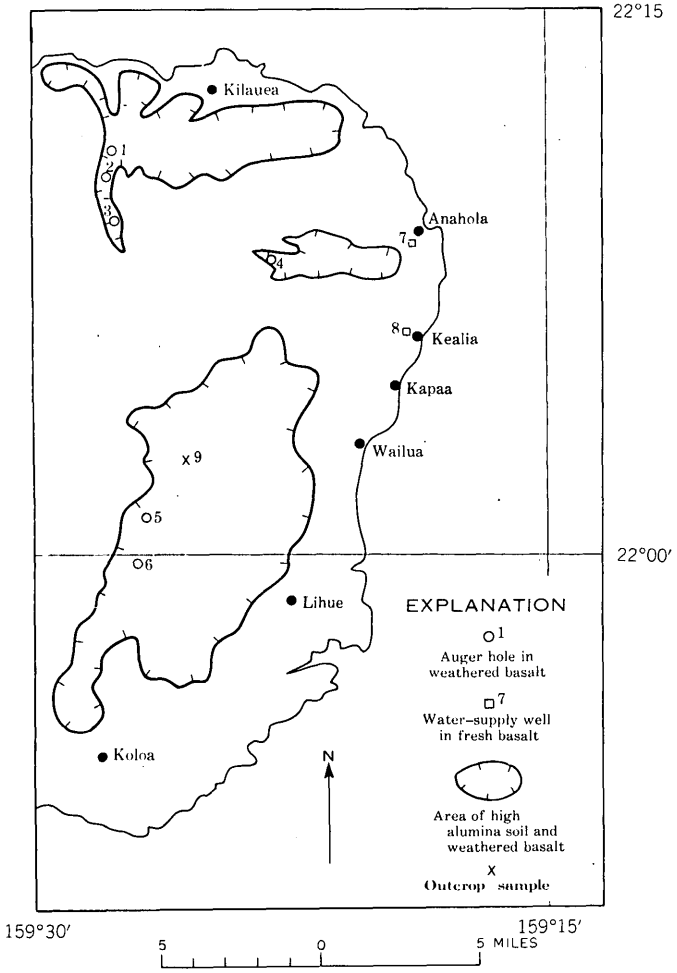

FIGURE 219.1.—Areas of deeply weathered basalt in the eastern part of Kauai, Hawaii, showing water-sample localities.

Most of the fresh basalt is dark gray to black. Pale shades of gray develop with weathering. As the rock loses its hardness, colors change to dark brown, grayish brown, and finally to various shades of reddish brown. Nearly all the weathered rock is saprolite in which much of the basaltic structure and texture has been preserved; however, all but very small amounts of the original constituents have been replaced by secondary minerals.

Deeply weathered rocks at the surface consist mainly of alumina and oxides and hydroxides of iron. Minor constituents include titanium oxides and clay minerals, and the concentration of minerals varies with depth. The rock at the surface is 25 to 40 percent gibbsite by weight, and 40 to 50 percent iron minerals. Clay minerals, titanium oxides, organic matter, and miscellaneous minerals make up the remainder. At depths of 15 or 20 feet clay minerals become abundant, a condition reported by Holmes, Takahashi, and Sherman (1960). At greater depths clays ordinarily make up more than 50 percent of the volume of the rocks, and gibbsite is present only in minor amounts. As there is little loss of volume except in the very advanced stages of weathering, the greater concentration of gibbsite close to the surface indicates that gibbsite is formed in a late stage of weathering by alteration of clay minerals. Essentially all of the clay minerals belong to the kaolin group, and halloysite is the most common, if not the only member present.

Iron minerals tend to be concentrated by weathering and to decrease in amounts with depth, but more gradually than does gibbsite. Goethite and hematite are the most commonly secondary iron minerals. Fine-grained magnetite occurs sparsely throughout the weathered rocks, and traces of ilmenite are common. Both magnetite and ilmenite are residual from the basalt. Amorphous materials, including iron and alumina gels, are present (Bates, 1960, p. 5), but their importance has not been evaluated because they have no diagnostic X-ray characteristics—the principal method used for mineral identification.

The saprolite near the surface is in a very advanced stage of weathering; that at depth is in an intermediate stage of weathering. The analyses (table 219.1) are of samples from an auger hole (fig. 219.1, hole 9) at a point where fresh rock was several feet below the bottom of the hole, as inferred from deeper holes nearby, and of a sample of essentially fresh basalt from an outcrop (fig. 219.1). They show the chemical gradation from the thoroughly weathered rock at the surface toward fresh rock at depth and indicate that most of the rock is in intermediate stages. Nearly all of the alkalies are removed before the intermediate stages of weathering are reached; however, small amounts do remain even in the advanced stages. Roughly half of the silica is removed early and the other half initially remains in the form of clay minerals, and then is gradually lost as clays are leached and altered to gibbsite.

Concentration of secondary iron minerals begins early and continues into the advanced stages. A large part of the iron concentration is due to the removal of silica. Alumina is not concentrated as much as iron in the weathering process, though concentrations at different depths and at different localities vary much more than shown (table 219.1). Apparently some alumina is lost as clays are altered to gibbsite. In the early stages manganese remains in about the same proportions as in the basalt, and is leached very gradually as weathering progresses. Secondary manganese minerals are intimately associated with halloysite and gibbsite. Titanium is also concentrated pro-

TABLE 219.1.—*Chemical and spectrographic results, in percent, of analyses of samples of weathered basalt from an auger hole and of a sample of essentially fresh basalt in the eastern part of Kauai, Hawaii*

[Chemical wet analyses by Paul L. D. Elmore, Samuel D. Botts, Ivan H. Barlow, and Gillson Chloe, using rapid rock analysis method described by Shapiro and Brannock, 1956. Spectrographic analyses by Sol Berman.]

Depth in feet	Chemical analysis													Spectrographic analysis		
	SiO_2	Al_2O_3	Fe_2O_3	FeO	CaO	MgO	Na_2O	K_2O	H_2O	TiO_2	P_2O_5	MnO	CO_2	Sum	Cr	V	Ca
0–4	5.7	25.6	40.2	0.40	<.10	0.65	0.04	.12	18.6	5.6	0.27	0.12	<.05	[1] 97	0.16	0.069	0.08
4–10	8.6	25.5	39.1	.37	<.10	.72	.05	.09	17.8	5.6	.30	.14	<.05	[1] 98	.15	.059	.08
10–14	11.4	24.6	37.8	.82	<.10	.91	.06	.05	17.2	5.7	.36	.20	<.05	99	.17	.077	.09
14–19	17.1	26.2	32.7	.58	<.10	.83	.06	.03	15.8	5.1	.31	.25	<.05	99	.13	.065	.08
19–24	19.7	25.8	32.1	.50	<.10	1.0	.06	.03	15.0	4.9	.32	.27	<.05	100	.11	.052	.07
24–34	21.5	25.1	30.7	.53	<.10	1.0	.06	.03	14.6	4.9	.36	.27	<.05	99	.12	.058	.08
34–39	25.3	24.4	29.1	.44	<.10	.87	.06	.03	13.9	4.5	.38	.27	<.05	99	.14	.060	.08
A [2]	45.0	11.8	4.3	9.3	9.7	12.0	1.8	.62	3.1	1.9	.30	.26	.09	100	.064	.031	>1.0

[1] Sample contained appreciable amounts of organic matter.
[2] Essentially fresh basalt from outcrop (fig. 219.1, location 9).

gressively with advancing weathering. As only trace amounts of ilmenite are present, probably most of the titanium is in very fine grained anatase, but this has not been confirmed.

The soil and weathered rocks at the surface are highly porous and permeable. Permeability decreases with depth, however, as the percentage of clay minerals increases, and local perched bodies of water have been found. The highly porous surface absorbs ordinary rainfall, and runoff takes place only during very heavy rains. In augering, most of the perched bodies of water were penetrated at depths of 30 to 50 feet. At a few places, nearly dry rock was present below the water. The size of the water bodies varies appreciably with the wet and dry seasons. Several were encountered at the end of an uncommonly dry season, and some are inferred to be permanent features. The perched water passes slowly downward into the basal ground water and laterally where it spills over the edge of the local perching clay-rich zone into streams.

The water in weathered basalt is weakly acidic and that in fresh rock is slightly alkaline. Oxidation, hydrolysis, and leaching in the presence of ground water appear to be the principal agents in the weathering process. Probably the weakly acidic water in weathered rock is neutralized as it passes through the zone where alkalies are released during the initial weathering of the basalt. Measurements of pH were made of perched water immediately after it was bailed from 36 auger holes and of two samples from town water-supply wells which penetrate fresh basalt of the Koloa volcanic series. The samples from weathered basalt ranged in pH from 4.0 to 5.9, the average pH being 4.9. The cause of the low pH is probably due to both organic acids and to carbon dioxide produced by oxidation of organic matter in the soil.

The two samples from fresh basalt had a pH of 7.6 and 7.8. The samples from the two types of rock may not be directly comparable because the two water-supply wells may be slightly contaminated by sea water. The sodium and chloride in the water from weathered basalt (table 219.2) is probably due chiefly to the concentration of salt in rainwater. The content of sodium and chloride in the well-water samples is approximately three times that of the water from weathered basalt.

TABLE 219.2.—*Chemical analyses of water samples from weathered and fresh basalt of the Koloa volcanic series, Kauai, Hawaii*

[Analysts, A. S. VanDenburgh and C. E. Roberson. Samples are from weathered basalt, except those from holes 7 and 8, which are from fresh basalt.]

Hole No.	Parts per million																					Cation total	Anion total	Dissolved solids calculated (ppm)	Hardness as $CaCO_3$ (ppm)	N.C. hardness as $CaCO_3$ (ppm)	Specific conductance (microhms at 25° C)	pH
	SiO_2	Al	Fe	Mn	Cr	Ca	Mg	Na	K	Li	NH_4	HCO_3	CO_3	OH	SO_4	Cl	F	I	NO_2	NO_3	PO_4	B							
1	2.9	0.11	0.00	0.26	0.000	0.8	1.9	11	0.6	0.00	0.02	1	0	0	2.7	19	0.1	0.008	0.00	0.6	0.02	0.04	0.70	0.64	41	10	9	90	4.6
2	1.2	.00	.18	.13	-----	.9	1.9	6.3	.6	.00	.02	6	0	0	4.0	9.1	.1	.006	.00	.7	.04	.02	.49	.46	28	10	5	60	5.1
3	4.1	.01	.00	.07	.000	1.0	1.2	6.9	.3	.00	.03	3	0	0	2.3	12	.1	.003	.00	.4	.03	.03	.46	.46	30	7.4	5	56	5.6
4	3.0	.04	.00	.12	.000	.4	.7	7.2	.0	.00	.02	2	0	0	3.2	12	.2	.006	.00	.1	.02	.03	.39	.45	28	4.0	2	54	4.8
5	2.6	.03	.06	.54	.000	1.0	2.3	8.6	.6	.00	.01	6	0	0	6.5	16	.1	.004	.00	.9	.02	.05	.63	.71	42	12	7	78	5.3
6	2.5	.12	.00	.11	.000	.6	1.5	8.5	.5	.00	.02	0	0	0	2.7	13	.1	.002	.00	.8	.00	.05	.53	.45	30	7.6	8	67	4.7
7	32	.03	.00	.00	-----	13	14	30	1.3	.00	-----	96	0	0	37	30	.2	.002	-----	2.0	.43	.05	3.13	3.23	207	92	12	331	7.8
8	42	.06	.00	.00	.00	13	11	21	.8	.00	.01	78	0	0	5.2	34	.1	.001	.00	1.5	.16	.01	2.48	2.38	167	77	14	265	7.6

Smaller contents of dissolved solids were present in the water of lower pH from weathered rock than in the water from fresh rocks (table 219.2). Probably, this is because the water in the weathered zone moves rather fast and has less time to react with its host, and because during its history of downward migration it was in contact only with rocks that were already thoroughly leached. The water in fresh basalt has passed both through a weathered zone and through a second zone where the minerals in the basalt are actively being weathered; therefore, the water has had ample opportunity to pick up alkalies and silica.

REFERENCES

Bates, T. F., 1960, Rock weathering and clay formation in Hawaii: Mineral Industries [Pa. State Univ.], v. 8, p. 1, 4–6.

Holmes, W. E., Takahashi, M., and Sherman, G. D., 1960, Distribution of gibbsite and kaolinite with depth in a gibbsitic soil on Kauai: Hawaii Agr. Expt. Sta., Tech. Prog. Rept. 125, Univ. of Hawaii.

Macdonald, G. A., Davis, D. A., and Cox, D. C., 1960, Geology and ground-water resources of the island of Kauai, Hawaii: Hawaii Div. of Hydrography Bull. 13, p. 1–212.

Shapiro, Leonard, and Brannock, W. W., 1956, Rapid analysis of silicate rocks: U.S. Geol. Survey Bull. 1036–C, p. 19–56.

220. SORTING OF BEACH SEDIMENT, NORTHWESTERN ALASKA

By George W. Moore, Menlo Park, Calif.

Work done in cooperation with the U.S. Atomic Energy Commission for the Plowshare Program, Project Chariot

Beach sediment is well sorted partly because the finest fractions are carried to sea in suspension, leaving only the larger particles having more rapid settling velocities. The beach environment differs, for example, from that of rivers, where ever-present silt and clay may settle with the sand in local areas of quiet water. The sediment remaining on a beach after the fine material has been winnowed away may range from very fine grained sand to boulders, depending chiefly on the size range of the material being supplied. This material is sorted by wave action into grain-size belts disposed as follows: moderately coarse on the unsubmerged part of the beach; very coarse on a bar directly below the break point of the waves; and progressively finer offshore from the break-point bar. The results of the present investigation suggest that much of this typical beach sorting, and perhaps most of it, occurs not during the prolonged periods of uniform surf conditions when the beach profile is in equilibrium, but during relatively brief periods when the waves are changing from one set of characteristics to another.

Field observations were made at Ogotoruk Beach, a pebble-gravel beach at lat 68°0′ N., long 165°41′ W., in northwestern Alaska. This area is especially suitable for studies of wave action because the mean tide range is only 0.4 meter. The data were collected jointly with David W. Scholl and Reuben Kachadoorian.

Wave and sediment characteristics of Ogotoruk Beach during a 35-hour period on July 19–20, 1960, are presented on figure 220.1. The observation period included the crestal and waning parts of a storm. During the first half of the period, which was chiefly characterized by waves over a meter high, the beach underwent very slow erosion. At approximately 2:00 a.m. on July 20, deposition began, and the surface of the beach rose at a rate of about 10 centimeters an hour to the end of the observation period.

The wave height remained about constant during the shift from erosion to deposition, but the wave period and wave length shortened appreciably. Probably deposition began because the waves with shorter wave length felt bottom at a shallower depth and began to erode the outer face of the break-point bar. The abundant new supply of material thrown into suspension by this erosion resulted in deposition on the face of the beach.

Grain-size analyses of beach samples collected during the period of change from erosion to deposition

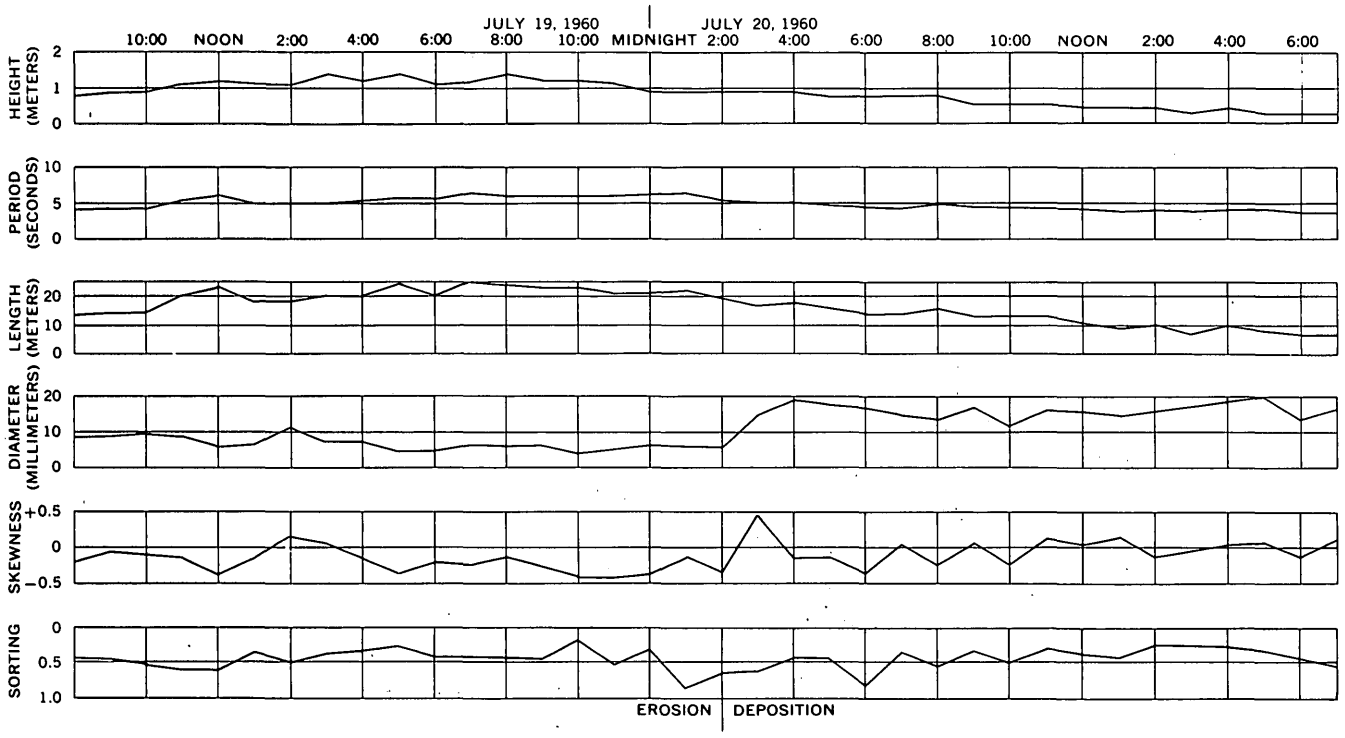

FIGURE 220.1.—Wave characteristics (upper three graphs) and sediment properties (lower three graphs) at Ogotoruk Beach, Alaska, during the crestal and waning parts of a storm. Sediment samples were collected from the midpoint of the zone alternately covered and uncovered by the waves wash; the grain-size properties follow the conventions of Inman (1952).

show that the debris remaining on the beach during erosion is much finer than that added to the beach during deposition. When deposition began at about 2:00 a.m. on July 20, the median diameter of the beach material increased in an hour from about 6 to 15 mm (fig. 220.1). The grain-size distribution of four sets of beach samples, collected at 2-hour intervals from 11:00 p.m., July 19, to 5:00 a.m., July 20, are shown on figure 220.2. During the period of erosion, represented by the frequency curve at 11:00 p.m., the sediment had a single grain-size mode near 6 mm. About an hour before the start of actual net deposition, the grain-size distribution became bimodal. As represented by the mode at 6 mm, residual beach sediment existed for several hours but steadily decreased, and the addition of new sediment is indicated by another mode near 15 mm. As deposition became dominant, and the eroded beach surface was completely covered by new sediment with a median diameter averaging 15 mm, the frequency curve retains only a single mode at the larger grain size as shown by the curve at 5:00 a.m. on figure 220.2. The two modes suggest that the material being deposited was derived from a new source in the beach system, rather than merely representing a reversal in the direction of movement of material formerly being eroded.

The skewness of the sediment curve also changed during the transition from erosion to deposition. Negative skewness values characterize samples collected during erosion (fig. 220.1) and illustrate an excess of coarse sizes in the residual sediment. This is typical of sediment undergoing erosion (Ellis, 1960) as the coarser fractions tend to lag behind. The skewness of the deposited material became less negative, as might be expected. If the deposited material was derived directly from the material formerly being eroded, without additional sorting, it would have a smaller median diameter than the residual sediment because of the earlier lag of the coarser sizes. The opposite is actually true, however, further indicating a separate source for the two materials.

The following mechanism is proposed to explain the relations observed at Ogotoruk Beach, and it is suggested that the process may have general application. During the rise of abnormally high, long waves, the beach is stripped down, and a large bar is built at the break point of the waves (fig. 220.3). The material being eroded from the beach face accumulates at the break-point bar because it is stopped there by an opposing landward traction that is generated by the wave train beyond the break point where

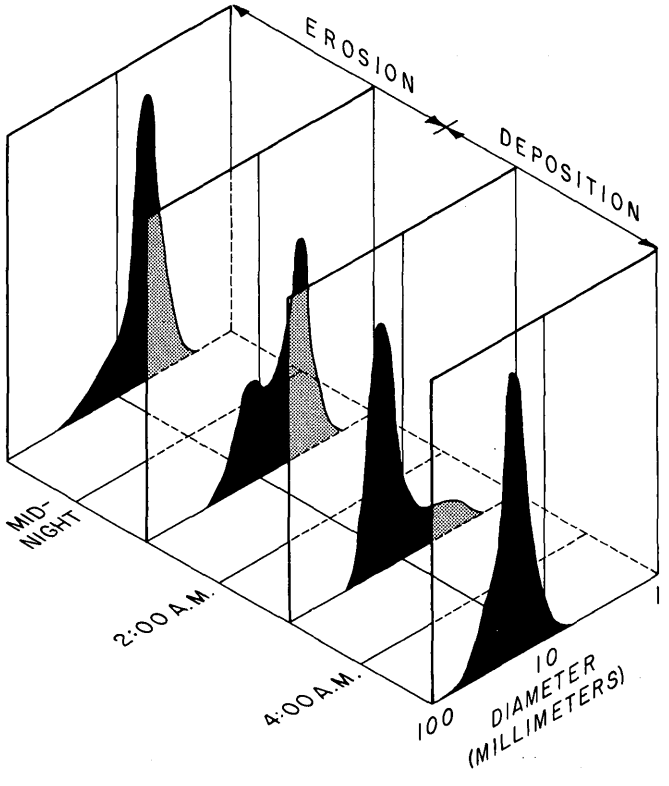

FIGURE 220.2.—Frequency diagrams showing bimodal character of beach sediment during transition from net erosion to net deposition, suggesting that the deposited material was derived from a different part of the beach system than the eroded material.

the waves drag on the bottom as they begin to transform into breakers. As soon as this landward transporting force is met, the coarse fractions derived from the eroding face of the beach are deposited because of their rapid settling velocity. The finer fractions disperse farther seaward in suspension because of the enormous turbulence in the breaker zone. This process causes a selective concentration of the coarse fractions on the break-point bar.

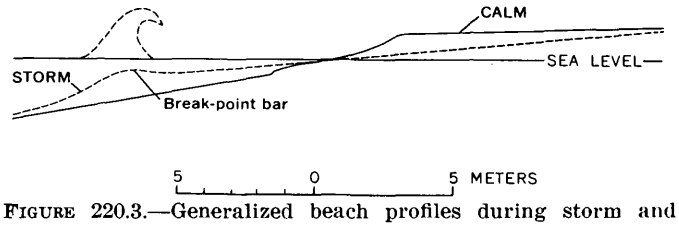

FIGURE 220.3.—Generalized beach profiles during storm and calm periods.

Later, as the waves become smaller after the storm, they break nearer to shore, erode the outer face of the break-point bar, and move its crest landward. During this transportation, the coarse sediment from the bar is deposited on the exposed part of the beach.

The classical view that most beach sorting is accomplished by the action of waves on beaches whose profiles are in equilibrium seems insufficient because at such times only a thin layer on the surface of the beach is moving and, consequently, being sorted. The alternative mechanism outlined in this report is believed to be the chief one because a large percent of the beach sediment is processed, and the well-sorted coarse-grained sediment is stored close to shore where it can be moved quickly toward the unsubmerged part of the beach during the depositional stage.

If fresh material is supplied from outside the beach system, it is quickly sorted by the nonequilibrium process outlined above. At other times, the grossly uniform increase in grain size toward the land is maintained by the balance between retention of coarse sizes near the unsubmerged beach during waxing-waning surf conditions, and movement of the remaining sizes landward to the breaker zone during steady surf conditions.

REFERENCES

Ellis, C. W., 1960, Marine sedimentary environments in the vicinity of the Norwalk Islands, Connecticut: Geol. Soc. America Bull., v. 71, p. 1857–1858.

Inman, D. L., 1952, Measures for describing the size distribution of sediments: Jour. Sed. Petrology, v. 22, p. 125–145.

GEOLOGY AND HYDROLOGY OF PUERTO RICO, PACIFIC ISLANDS, AND ANTARCTICA

221. WATER-BEARING PROPERTIES OF THE ROCKS IN THE ARECIBO-BARCELONETA AREA, PUERTO RICO

By Ted Arnow, Salt Lake City, Utah

Prepared in cooperation with the Commonwealth of Puerto Rico

Large quantities of ground water have been developed from wells and springs in both consolidated and unconsolidated formations in the Arecibo and Barceloneta 7½-minute quadrangles, north-central Puerto Rico (fig. 221.1). Most of the water is potable, but without treatment is excessively hard for many industrial uses. Wells close to the coast eventually may be intruded by salt water.

The geology of the Arecibo and Barceloneta area has been mapped in detail by R. P. Briggs (written communication). The southern two-thirds of the area is underlain by formations of Oligocene and Miocene age, which dip gently toward the north and crop out in strips extending across the area from east to west. The formations are predominately limestone and have been eroded into a karst topography. Most of the drainage is subsurface, but the area is crossed by two major northward-flowing streams, the Río Grande de Manatí and the Río Grande de Arecibo. The northern third of the area is a relatively flat coastal plain dotted with limestone hills. The Río Grande de Manatí and the Río Grande de Arecibo meander across the plain in wide alluvial valleys.

The Lares limestone (Oligocene), which does not crop out in the area, has a maximum thickness of about 1,650 feet in the northern part of the area, and is the oldest water-bearing formation. A well in the extreme southwestern corner of the area penetrated the Lares. It produced 50 gpm (gallons per minute) of water under artesian pressure.

The Cibao formation (Oligocene or Miocene), which overlies the Lares limestone, has weathered to a subdued karst topography. It has a maximum thickness of about 1,000 feet in the northern part of the area. Few wells have been drilled in the area of outcrop. West of the Río Grande de Arecibo, chalk and marl form a dominant part of the formation, and the Cibao yields little water. East of the Río Grande de Arecibo, where the formation consists almost entirely of limestone, the average yield of two wells in the Cibao

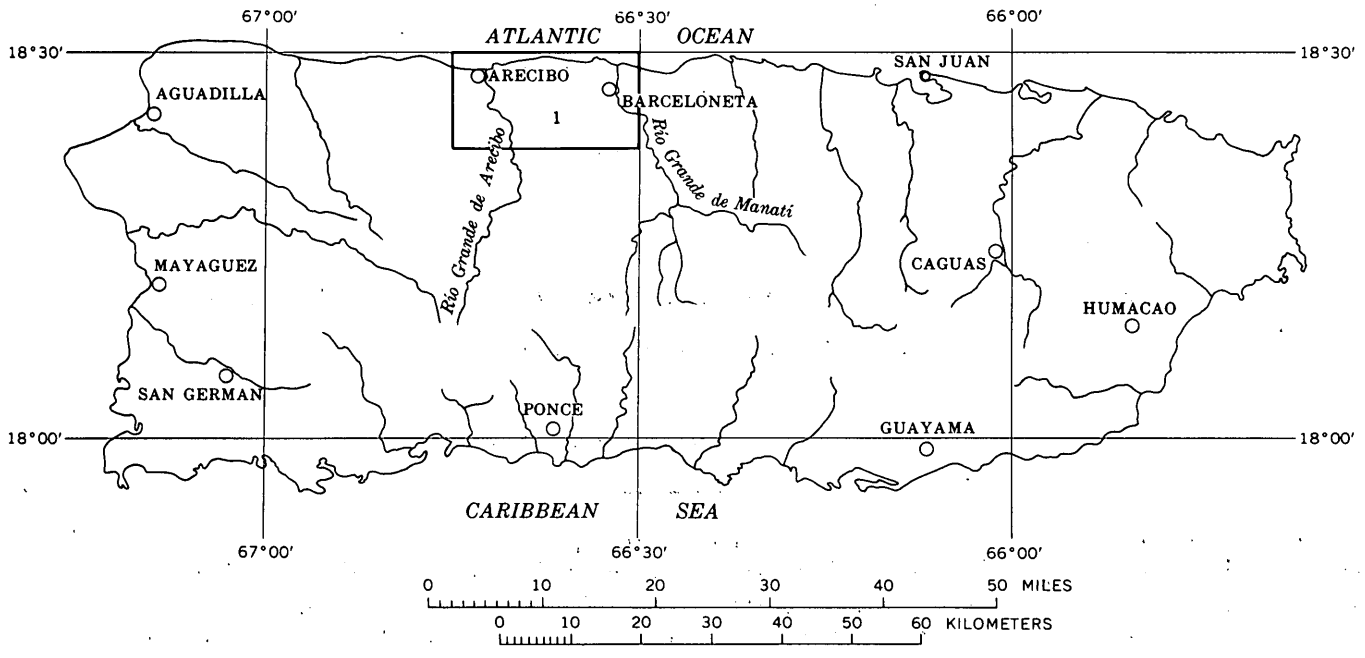

FIGURE 221.1.—Map of Puerto Rico showing outline of Arecibo-Barceloneta area.

601530 O—61——14

is 155 gpm. Two large springs issue from the Cibao on the west wall of the valley of the Río Grande de Arecibo. The average yield of each spring is about 2,000 gpm, but the yield fluctuates greatly depending upon rainfall.

The Aguada limestone (Miocene), which overlies the Cibao formation, has a maximum thickness of about 580 feet in the northern part of the area. Relatively few wells have been drilled in the area of outcrop, and none of them has a large yield. The best well had a specific capacity of about 2. The formation has weathered to a mature karst terrain, however, attesting to its great overall permeability. The small yields of the wells suggests that they were not drilled deep enough to reach the main water table, which is close to sea level.

The Aymamón limestone (Miocene) overlies the Aguada limestone and has a maximum thickness of about 1,240 feet in the northern part of the area. The formation yields much water to wells. Data from tests of 13 wells in the Aymamón show an average yield of 935 gpm and a range from 40 to 3,600 gpm. The specific capacity of 5 of the wells ranged from 36 to 4,500. The water in the Aymamón is under water-table conditions, and most of the wells with the largest yields are close to the large river valleys.

Tertiary and Quaternary surficial deposits consisting of alluvium, beach deposits, dunes, marine terrace deposits, swamp deposits, and landslide debris overlie the Oligocene and Miocene formations. Except for the alluvium, the surficial deposits are thin and do not yield large quantities of water to wells. In the northern part of the area driven wells in the marine terrace deposits commonly yield small supplies of water for domestic use.

The alluvium, which reaches known depths of 220 and 266 feet in the valleys of Río Grande de Arecibo and the Río Grande de Manatí, respectively, yields large quantities of water to wells. Data from tests of 13 wells in alluvium indicate an average yield of 1,540 gpm and a range from 300 to 4,000 gpm. The specific capacity of 8 of the wells averaged 158 and ranged from 26 to 500. No significant difference was observed between yields of wells in the valleys of the Río Grande de Arecibo and the Río Grande de Manatí.

All the formations in the Arecibo and Barceloneta area yield water that is similar in chemical quality; the water being of the calcium bicarbonate type typical of limestone aquifers. Analyses of 21 samples from 6 different aquifers indicated a range in dissolved solids from 176 to 954 ppm (parts per million), with an average of 388 ppm; a range in hardness from 120 to 390 ppm, with an average of 251 ppm; and a range in silica content from 3.6 to 48 ppm, with an average of 12 ppm. Several deep wells close to the coast or in the low lying alluvial valleys yield salt water, whereas nearby shallower wells yield fresh water.

The temperature of the ground water, as observed at 11 wells and springs, ranged from 74° to 81°F. Temperatures higher than 76°F were recorded at wells in the reatively low lying northern third of the Arecibo and Barceloneta area.

222. GROUND-WATER CONDITIONS IN THE LOWER TALLABOA VALLEY, PUERTO RICO

By I. G. Grossman, San Juan, P.R.

Work done in cooperation with the Commonwealth of Puerto Rico

Favorable hydrologic and geologic conditions have permitted the establishment of a burgeoning petrochemical industrial complex and an extensive irrigation system in the relatively small Río Tallaboa valley on the southwest coast of Puerto Rico. The upper part of the Río Tallaboa consists of two branches that drain a hilly area having an annual rainfall averaging about 65 inches. The junction of the two branches is the northern boundary of the lower Tallaboa Valley.

The lower valley is about 4 miles long and generally less than 1 mile wide. River water rapidly recharges permeable unconsolidated deposits of the flood plain at some places, and this recharge is augmented by irrigation water leaking from canals and lateral ditches. Rain falling directly on the lower valley is a comparatively small source of recharge, even though the average annual rainfall here is about 40 inches. Unconsolidated deposits on the valley flood plain are made up of particles ranging in size from fine clay to boulders. The deposits of sand and gravel, which supply most of the ground water used in the area, range in thickness from less than 1 foot at the valley sides to at least 52 feet near the center. The yields of 52 wells tapping sand and gravel average about 245 gpm (gallons per minute) and range from 20 to 1,200 gpm.

Correlation of hydrographs of river stage with fluctuations of water levels in wells on both sides of the valley shows a hydrologic continuity between the river and the underlying alluvium. Water in shallow sand and gravel is under water-table conditions. Deeper sand and gravel, separated from the shallow aquifer by relatively impermeable clay, contains water under artesian conditions.

Underlying the alluvium are three bedrock units: the Ponce limestone of late Oligocene and early Miocene age; the Juana Díaz formation of middle Oligocene age; and an older complex that is principally of late Cretaceous age (Zapp, Bergquist and Thomas, 1948). The older complex, which may contain some beds of early Tertiary age, is exposed only in the northeastern part of the area. There it consists principally of intrusive and extrusive igneous rocks and some beds of partly metamorphosed limestone.

The Ponce limestone, which underlies most of the area, is the only bedrock that is an important source of water. Of 4 wells tapping the limestone, 2 in the upland area east of the lower Tallaboa Valley yield 2.5 and 3.5 gpm and 2 in the valley yield 10 and 100 gpm. The higher yields in the valley are in part the result of more extensive fractures and solution openings in the limestone and in part the result of the more favorable location for recharge from the river and river gravels. Locally water passes freely between the limestone and the overlying sand and gravel. The yields of 9 wells reportedly drawing water from both the limestone and the overlying sand and gravel range from about 100 to 2,500 gpm and average about 1,300 gpm.

The water table in the alluvial plain of the lower Tallaboa Valley slopes southward toward the sea with a gradient of about 50 feet per mile in the northern part of the plain and less than 10 feet per mile in the southern part of the plain. Static water levels measured in 1959 and 1960 show pronounced seasonal fluctuations. The maximum decline in the principal dry season (December to March) amounted to about 5 feet, and occurred in the northern part of the area; the minimum decline during the same season in the same 2-year period was about 0.5 foot and occurred in the southern part. Water returned to its former level during the principal rainy season (August to November). No large-scale downward trend in static water levels was detected in spite of the large increase in pumping for industrial use in recent years.

Throughout most of the lower valley, ground water is rather uniform in chemical quality and is of the calcium-bicarbonate type. Hardness ranges from about 200 to 350 ppm (parts per million), chloride content from about 10 to 20 ppm, and silica content from about 20 to 30 ppm. The quality of water generally is satisfactory for agricultural, municipal, and most other uses, but treatment is necessary for some industrial uses. Near the coast, fresh ground water is underlain by saline water which is at progressively greater depths to the north. At least 14 wells drilled less than a mile from the Caribbean have yielded brackish or saline water at fairly shallow depths. A well drilled to a depth of 325 feet, slightly more than a mile north of the Caribbean, yielded water that contained 1,430 ppm chloride. After being plugged back to 145 feet it yielded water containing only 22 ppm of chloride, which is suitable for industrial use without extensive treatment.

REFERENCE

Zapp, A. D., Bergquist, H. R., and Thomas, C. R., 1948, Tertiary geology of the coastal plains of Puerto Rico: U.S. Geol. Survey Oil and Gas Inv. (Prelim.) Map 85.

223. VOLCANIC SUITE OF PAGAN, MARIANA ISLANDS

By GILBERT CORWIN, Washington, D.C.

Pagan, largest of the northern Mariana Islands, western Pacific Ocean, consists predominantly of Quaternary volcanic rocks erupted from several volcanoes and numerous subsidiary centers, most of which are alined along the north-northeast-trending axis of the island. The rocks are made up of two major successions: an older precaldera succession of lava flows and pyroclastic deposits erupted prior to formation of two calderas (situated near the north and south ends of the island), and a younger post-caldera succession of lava flows and pyroclastic deposits concentrated in the caldera depressions (Corwin and others, 1957, p. 111; Fosberg and Corwin, 1958, p. 3). Rocks of the two successions are not significantly different petrographically or chemically, although the variety of precaldera rock types is somewhat greater.

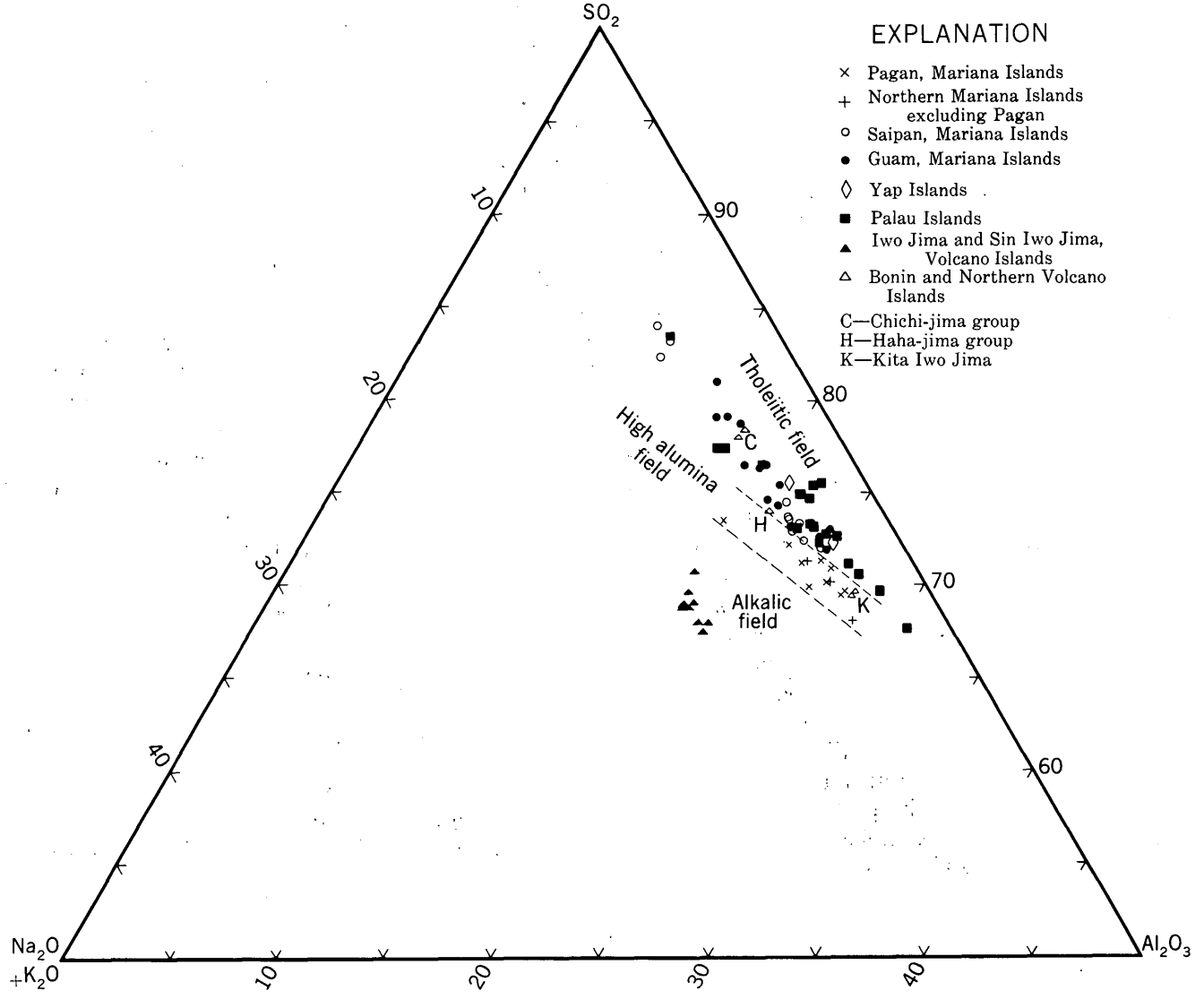

FIGURE 223.1.—Silica-alumina-total alkali diagram for volcanic rocks from Pagan and other northern Mariana Islands, and from the Bonin, Volcano, southern Mariana, Yap, and Palau Islands. Chemical analyses of rocks that show evidence in thin sections of appreciable hydrothermal alteration or weathering of feldspars have been excluded. Sources of data: Schmidt (1956, p. 151, 157); Macdonald (1948, p. 1015, 1016); Tsuya (1937, p. 224, 227, 284); and unpublished analyses of Gilbert Corwin, C. G. Johnson, and J. T. Stark.

The most abundant rock variety of the island is olivine-augite basalt, which has 50 to 52 weight-percent silica. The range of rock types extends from augite-olivine basalt that has about 49 percent silica to hypersthene-augite andesite that has about 62 percent silica. No silicic andesites or dacites are known. Fragments of gabbro were found in precaldera tuff breccias but are scarce.

Mineral assemblages of the volcanic rocks are relatively simple. Plagioclase is generally the dominant mineral, both as phenocrysts and as a groundmass constituent. Plagioclase phenocrysts range in composition from nearly pure anorthite (approximately An_{98}), sodic anorthite and bytownite, to labradorite and andesine; zoned groundmass plagioclase has average compositions of sodic labradorite or andesine. Mafic phenocrysts include olivine and augite in most specimens, and hypersthene and magnetite in a few basalts and most andesites. Augite, subcalcic augite, and pigeonite are the most abundant ferromagnesian minerals and magnetite is common in the groundmass of all well-crystallized specimens. Other groundmass constituents include scarce to common olivine in most basalts and basaltic andesites; scarce hypersthene in a few andesites; late cristobalite, tridymite, and potassic feldspars in most well-crystallized rocks; and, in a few specimens, phlogopitic biotite, probable pargasite, zeolites, and other late deuteric and hydrothermal minerals.

Petrographically, all specimens belong to a pigeonitic rock series as defined by Kuno (1950, p. 992). Subcalcic augite and pigeonite are final primary ferromagnesian crystallization products of all well-crystallized lavas on Pagan, with the exception of a few augite-olivine basalts in which olivine appears to have been stable throughout groundmass crystallization, and a few andesites in which scarce late biotite and pargasite crystallized after the clinopyroxenes. Compared to basaltic and andesitic rocks of volcanic suites on Guam, Palau, and other islands to the south and southwest, the rocks of Pagan are much richer in olivine and slightly richer in plagioclase. The high calcium content of the plagioclase contrasts with sodic plagioclase reported for rocks of Iwo Jima in the Volcano Islands to the north.

Chemically, the Pagan volcanic suite belongs to the high alumina basalt type as defined by Kuno (1960, p. 121) with properties that are intermediate between those of tholeiitic and alkalic suites (figs. 223.1 and 223.2). Compared to tholeiitic suites of the southern Mariana, Palau, and other island groups within the island system extending southward from Honshu, Japan, the Pagan volcanic suite has high proportions

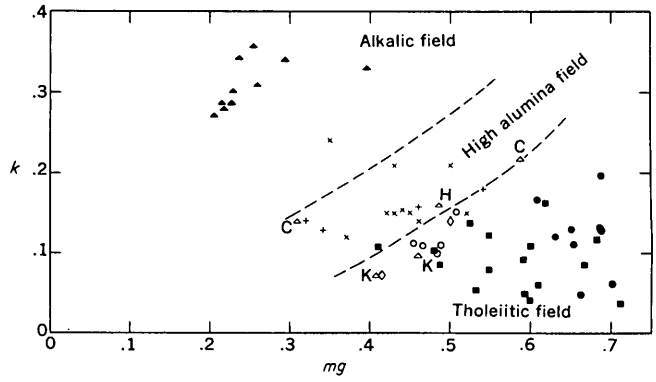

FIGURE 223.2.—Niggli *k-mg* diagram for volcanic rocks from Pagan and other northern Mariana Islands, and from the Bonin, Volcano, southern Mariana, Yap, and Palau Islands. Chemical analyses of dacites (more than 65 percent silica) and rocks that show evidence in thin sections of appreciable alteration are excluded. Explanation and sources same as figure 223.1.

of total alkalis and alumina to silica and of potash to total alkalis, and a low proportion of magnesia to total ferromagnesian oxides. The opposite relations exist with respect to the alkalic suite of Iwo Jima and Sin Iwo Jima in the Volcano Islands.

Chemical analyses and petrographic descriptions of several samples from Kita Iwo Jima in the Volcano Islands and from the Bonin Islands (Tsuya, 1937, p. 223–225, 284–285) suggest existence of high alumina volcanic suites, similar to that of Pagan, within island groups to the north of the Mariana Islands. Data for these islands are insufficient, however, and satisfactory comparison of the suites with those of the northern Mariana Islands is not now feasible.

The Mariana Islands are arranged along two concentric axes on the crest of the Mariana ridge, one of the prominent, dominantly submarine arcuate structures forming the east margin of the Philippine Sea. Tholeiitic volcanic suites of the southern Mariana Islands lie along the outer eastern axis; the high-alumina suites of the northern Mariana Islands, including Pagan, along the inner western axis. The Volcano Islands are situated near the intersection of the Mariana ridge and a broad, gently curving submarine ridge that extends southward west of the Mariana structure. Alkalic suites of Iwo Jima and Sin Iwo Jima appear related to the western ridge; the high-alumina or tholeiitic suite of Kita Iwo Jima to northward extension of the Mariana ridge. Distribution of tholeiitic suites on the outer side of the Mariana ridge, high-alumina suites on the inner side, and alkalic suites related to a structure to the west is comparable to distribution of similar volcanic suites in

the Japanese Islands which have been described and interpreted by Kuno (1960, p. 133–135, 142).

REFERENCES

Corwin, Gilbert, Bonham, L. D., Terman, M. J., and Viele, G. W., 1957, Military Geology of Pagan, Mariana Islands: U.S. Army, Chief of Engineers, Intelligence Div., Headquarters U.S. Army Pacific, 259 p.

Fosberg, F. R., and Corwin, Gilbert, 1958, A fossil flora from Pagan, Mariana Islands: Pacific Science, v. 12, p. 3–16.

Kuno, Hisashi, 1950, Petrology of Hakone Volcano and the adjacent areas, Japan: Geol. Soc. America Bull., v. 61, p. 957–1020.

——— 1960, High-alumina basalt: Jour. Petrology, v. 1, p. 121–145.

Macdonald, G. A., 1948, Petrography of Iwo Jima: Geol. Soc. America Bull., v. 59, p. 1009–1018.

Schmidt, R. G., 1956, Geology of Saipan, Mariana Islands, Petrology of the volcanic rocks: U.S. Geol. Survey Prof. Paper 280–B, p. 127–175 [1957].

Tsuya, Hiromichi, 1937, On the volcanism of the Huzi volcanic zone with special reference to the geology and petrology of Idu and the Southern Islands (Nanpo Shoto): Tokyo Univ. Earthquake Research Inst. Bull., v. 15, pt. 1, p. 215–357.

224. STRUCTURE OF LOWER TAYLOR GLACIER, SOUTH VICTORIA LAND, ANTARCTICA

By Warren Hamilton and Philip T. Hayes, Denver, Colo.

Work done with the support of the National Science Foundation

The Ross Sea and Ross Ice Shelf are bounded on the west by a system of high mountains, which dams the ice of the continental interior ice plateau. The Taylor Glacier flows eastward, through one of the passes in this mountain system, from the plateau into Taylor Valley (fig. 224.1). Although in the recent geologic past the glacier reached the sea, it has receded so that the lower part of the valley (Taylor Dry Valley) is free of ice except for small alpine glaciers coming into it from the sides. As part of our geologic study of the Taylor Valley region (Hamilton and Hayes, 1960), we examined structures in Taylor Glacier.

Taylor Glacier is 40 miles long, and its surface drops from an altitude of about 6,000 feet near the interior ice plateau to about 250 feet in Taylor Dry Valley. The cross profile of the glacier is gently convex upward, the slope increasing near the margins; the sides of the glacier for most of its length are near-vertical ice cliffs 20 to 50 feet high. Most of the glacier is free of snow during at least the summer months: precipitation, although entirely in the form of snow, is light, and most of the snow is swept away by wind. Air temperatures are below freezing all year except near the snout of the glacier, where on occasional summer days it is as warm as 35°F.

Longitudinal flow lines, a few of which are marked by sparse trains of rock debris, are conspicuous on the surface of the glacier (fig. 224.1) and in a few

Figure 224.1.—View westward over Taylor Valley. Taylor Glacier flows from interior ice plateau (upper right) into upper Taylor Valley, and makes a sharp bend (upper center) into lower Taylor Valley. Frozen Bonney Lake in bottom of picture, Kukri Hills in left foreground, and Ferrar Glacier in left middle distance. The circle on Taylor Glacier marks the area where velocity was measured, 8 miles from the snout of the glacier; distance from foreground to mountains in upper right is 40 miles. U.S. Navy photograph.

places have been folded or sheared apart in plan by differential flow. The scarcity of rock material within or on the surface of the glacier even at its snout (figs. 224.1 and 224.2) is in marked contrast to the character of most temperate-latitude glaciers, and only small moraines have formed at the present ice front. Moraines of more extensive past glaciations are widespread, but are of relatively small volume. Perhaps 75 percent of the volume of the till is silt and sand.

Lines of vertical aerial photographs made by the U.S. Navy in December 1956 and in November 1959 cross on Taylor Glacier 8 miles above its terminus. Along a flow line about 3,700 feet from the south side of the glacier, which, at that point, is 12,000 feet wide, rocks clearly recognizable on both sets of pictures moved about 300 feet in the 3 years, or 100 feet per year. Nearer the edge, 1,200 to 2,000 feet from the south side of the glacier, moraine-fold axes moved about half as far.

Two sets of vertical photographs of the snout of the glacier were taken only a year apart, in December 1956 and January 1958. These pictures show no apparent change in position of the ice front, and no detectable movement of points on the ice; changes of 50 feet should have been easily detectable had they occurred.

The ice in Taylor Glacier is strongly foliated, the layers revealed by varying color (white to bluish white) in thick masses, or by varying transparency where thin. Where thin pinnacles of ice are backlighted by the sun, individual folia can be seen to be from a fraction of an inch to several inches thick, and to be continuous for tens of yards. Foliation produces the faint horizontal layering in the shaded ice cliff in the right part of figure 224.2. The foliation has a nearly horizontal trace along the side of the glacier near the snout, and dips gently toward the glacier edge in at least some places, apparently indicating obliquely outward flow of nearsurface ice.

Discontinuous layers of dark silty ice, parallel to foliation, are conspicuous near the base of the glacier at its snout (fig. 224.2) and along the sides near the snout. Such layers are not exposed along the upper part of the glacier, near the interior ice plateau. The layers are nearly parallel and undulate gently, anastomosing at slight angles. At the snout of the glacier

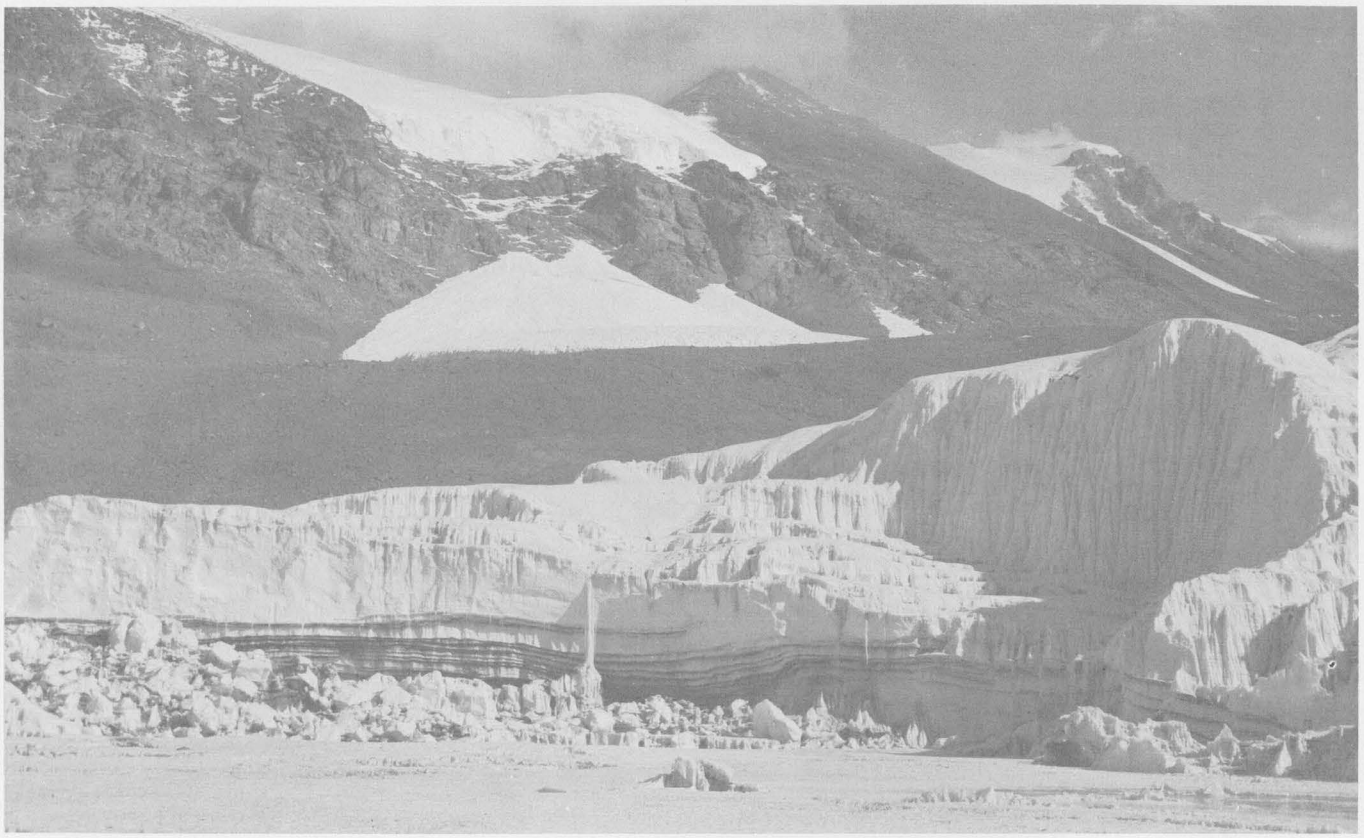

FIGURE 224.2.—Snout of Taylor Glacier, seen across solidly frozen Bonney Lake. The ice overhangs above many of the dark silty shear planes. Foliation planes, parallel to the shear planes, are visible in the ice cliff on the right. Ice at right is about 100 feet high. Below the cliffs, in the center background, fragments fallen from a hanging glacier have been rewelded into an apron glacier.

(fig. 224.2) the ice above many of these planes overhangs that beneath, indicating that these layers are planes of active laminar shear, along which the upper ice slid out over the lower. Similar shear planes have been described by Klebelsberg (1948). The overhanging ice breaks off in blocks that form an ice talus. As the ice foliation is parallel to these obvious shear planes, we conclude that pervasive laminar shear operates also throughout the glacier, but at rates generally too slow to be expressed by frontal overhangs.

Similar shear planes of silty ice—parallel to glacier bases and to ice foliation, and overhung by faster-moving ice—were seen also near the bases of a number of small glaciers, including some (for example, fig. 224.2) that reach their termini only after being fragmented over ice falls and rewelded into glaciers from ice taluses. Despite thicknesses locally less than 100 feet, these re-formed glaciers flow smoothly by laminar shear. Motion by flow rather than fracture seems to operate at even very shallow depths in these glaciers.

A large part of the glaciological literature (for example, Wright and Priestley, 1922, writing about the Taylor Glacier and others in this same region) treats foliation and shear planes as bedding layers, somehow preserved from original layers of snow despite many miles of complexly differential flow interrupted by ice falls and even by complete fragmentation and rewelding.

The silty shear planes are confined to the basal part of the glacier, rather than curving upward to the surface as is often the case with temperate-latitude glaciers. Presumably, most of the upward increase in velocity in the glacier takes place within the basal zone with its conspicuous shear planes. These planes must reach the base of the ice at some stages, and thus pick up the rock debris that colors them (a chemical analysis of the silt showed a granodioritic composition similar to that of the local bedrock), but there may be relatively little movement of the ice in direct contact with the rock floor.

FIGURE 224.3.—Silty layers deformed by isoclinal drag fold. Man below center gives scale. South side of Taylor Glacier, about one-half mile from snout.

The silty shear layers exposed along the sides of the lower part of the glacier are deformed in many places into spectacular isoclinal drag folds (fig. 224.3) whose axes are nearly perpendicular to the trend of the glacier and whose axial planes are parallel to the active shear layers. These drag folds are due to laminar shear, for there are no open folds, but only isoclinal ones. The axial planes of these folds must mark velocity discontinuities, the ice above having moved considerably farther than the ice beneath, and the fold front migrating down-glacier at a speed midway between that of the ice above and beneath (fig. 224.4). Each drag fold remains isoclinal throughout its history. Similar structures were attributed to longitudinal compression of ice by Shumskii (1955, p. 334–335),

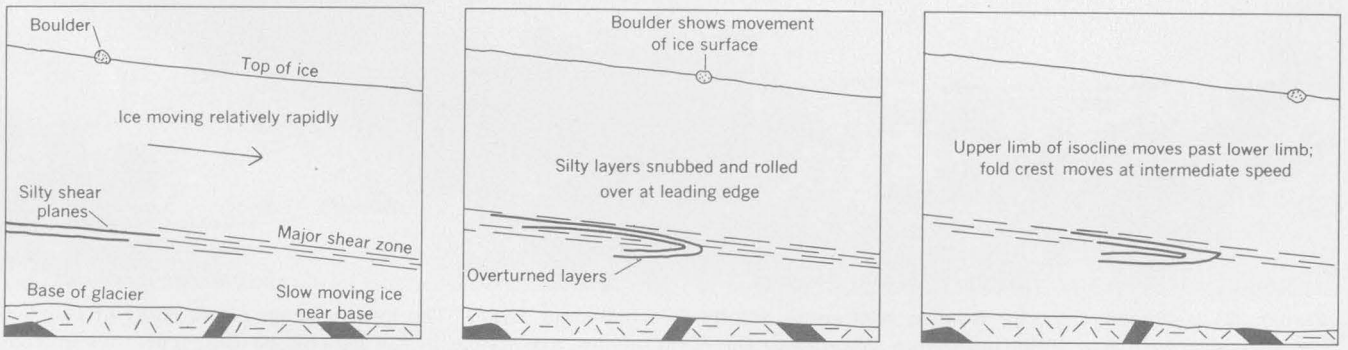

FIGURE 224.4.—Mechanism of isoclinal folding by differential flow. Longitudinal sections of glacier, in sequence from oldest (left) to youngest (right), at the same bedrock position.

despite a geometry which requires an origin by shear. Some isoclines point down-glacier, like the one in the photograph, but at least as many point up-glacier. Also present are sheared-off limbs of isoclines, lenses bounded by active shear planes, in which the fold structures are now relic rather than actively developing. To the right of the isoclinal axis of figure 224.3, there is no silty layer or other obvious discontinuity, even though the axial plane must project into a thin zone of rapid shear.

Probably most isoclinal folds in metamorphic rocks are formed by a similar mechanism of drag accompanying laminar shear whereby folds are isoclinal at all stages of their development rather than being formed by progressive tightening of initially open folds. Where, as is commonly the case, even thin formations in rocks deformed by intense isoclinal folding are planar sheets parallel to foliation and to axial planes, shear folding by differential laminar flow is required, because folding by compressive tightening of flexure folds would also fold formation contacts.

REFERENCES

Hamilton, Warren, and Hayes, P. T., 1960, Geology of Taylor Glacier-Taylor Dry Valley region, South Victoria Land, Antarctica, *in* Short papers in the geological sciences: U.S. Geol. Survey Prof. Paper 400–B, p. B376–B378.

Klebelsberg, R. V., 1948, Handbuch der Gletscherkunde und Glazialgeologie, v. 1: Springer-Verlag, Vienna, 403 p.

Shumskii, P. A., 1955, Osnovy strukturnogo ledovedeniya [Principles of structural ice study]: Akad. Nauk SSSR, 492 p.

Wright, C. S., and Priestley, R. E., 1922, Glaciology: London, British Antarctic Exped. 1910–13, 581 p.

225. PETROCHEMISTRY OF PROBABLE PALEOZOIC GRANITIC ROCKS FROM THE ROSS SEA REGION, ANTARCTICA

By Warren Hamilton, Denver, Colo.

Work done with the support of the National Science Foundation

Between the large Precambrian shield of East Antartica and the Cretaceous (or early Tertiary?) granitic rocks of Palmer Peninsula lies a broad region of metasedimentary and granitic rocks of inadequately known age. Although these intervening rocks have long been assumed to belong in part to the shield and in part to the Mesozoic orogen, I (1960) interpret them, on the basis of much newly available information, to belong instead to Paleozoic orogens, the ages of whose sediments, deformations, and granites all become progressively younger from the shield toward Palmer Peninsula (fig. 225.1). The recent finding of Lower Cambrian fossils by New Zealand geologists in prebatholithic metasedimentary rocks near Beardmore Glacier (fig. 225.2) (Bernard M. Gunn, written communication, 1961) confirms the most important element of this new interpretation.

The Precambrian shield is characterized by charnockites—gneisses and granites containing orthopyroxene—and by polymetamorphic rocks. The Palmer Peninsula, which contains all of the certainly known Cretaceous (or early Tertiary?) granitic rocks, is characterized by quartz diorite intrusive into metavolcanic rocks. Between the shield and Palmer Peninsula is a broad region of sedimentary rocks, metamorphosed at low, middle, or high grades, and intruded by batholiths of granitic rocks that are at least partly of Paleozoic age.

The batholithic granitic rocks of early Paleozoic, probably Cambrian or Ordovician, age are known particularly well in South Victoria Land (for example, Hamilton and Hayes, 1960), west of the Ross Sea. The granites interpreted as being of middle or late Paleozoic age are best known in western Marie Byrd Land (for example, Warner, 1945), east of the Ross Sea.

A total of 29 new chemical analyses (fig. 225.3) have been made of granitic rocks from these and other areas within the Paleozoic(?) orogens. Of the 15 probable Cambrian or Ordovician rocks analyzed, 12 were collected by P. T. Hayes and me in the McMurdo Sound region, two were collected by L. M. Gould in the

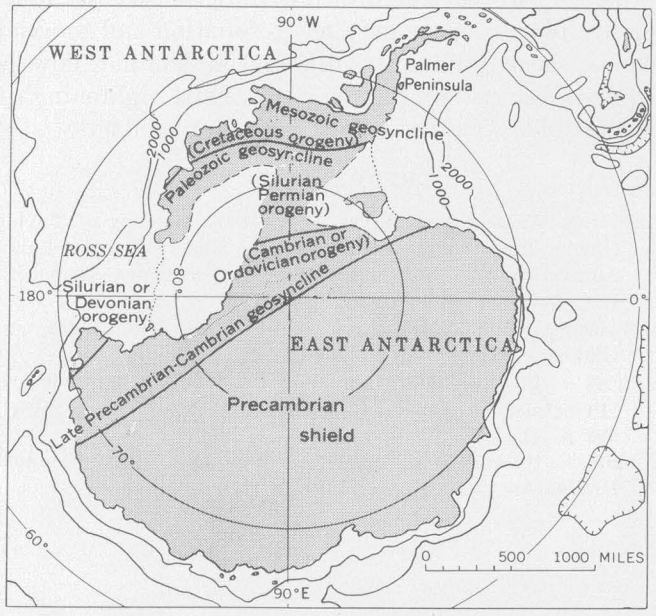

FIGURE 225.1.—New interpretation of major tectonic elements of Antarctica. Submarine contour interval 1,000 fathoms.

Queen Maud Mountains (and obtained from the University of Michigan collection, through the courtesy of E. W. Heinrich), and one was collected in the Horlick Mountains by W. E. Long. Of the 14 analyzed samples of granitic rocks of likely Silurian to Permian age, 9 were collected by L. A. Warner in western Marie Byrd Land (and obtained from the U.S. National Museum); 1 each was collected from the same region by E. L. Boudette and by Col. Dan Crozier; and 1 each was collected from isolated nunataks in the deep interior of west Antarctica, in the region of long 90° W., lat 82° S., by J. C. Craddock, J. Pirrit, and W. E. Long. Three new analyses were made also of granitic rocks from the Palmer Peninsula region, collected by the Expedition Antarctique Francaise, 1903–05, and obtained from the University of Michigan collection. Most relevant American collections are represented in this small suite of specimens, and it is a pleasure to acknowledge the assistance of the geologists who supplied them. These new analyses include all of the minor-element determinations known to me of granites from the Paleozoic terrane as shown in figure 225.3. (The published major-oxide analyses of granitic rocks from these regions are not considered here because most of them are of poor quality.) Despite the small number of samples, trends and distinctions are suggested by the data.

Most of the new analyses plot near the same variation curves. The obvious exceptions, those with SiO_2 lower than 63 percent, are of probable Cambrian or Ordovician rocks collected within a few miles of extensive outcrops of silicated carbonate rocks, so that these aberrant granitic rocks may owe their character to loss of magmatic silica to the carbonate rocks and to accompanying diffusion of alkalis. The proportion of FeO to MgO is much higher in this same suite than in the others. Relative to SiO_2 content, the Cretaceous(?) rocks from Palmer Peninsula appear higher in CaO and lower in K_2O than the others; the more silicic of the analyses of Palmer Peninsula rocks by Adie (1955) show the same pattern. Other such contrasts are suggested within and between the suites of samples, and more analyses are desirable to test their validity.

Frequency distributions of rock types are quite different in the several provinces, as is shown by the varying ranges and groupings of their components. The probable Cambrian or Ordovician granitic rocks include quartz diorite, granodiorite, and quartz monzonite. The later Paleozoic(?) rocks include some granodiorite, but are mostly quartz monzonite and granite, so that their bulk composition is considerably more silicic and potassic. The Cretaceous(?) rocks of Palmer Peninsula are dominantly quartz diorite (Adie, 1955).

Differences in abundances of some of the minor elements appear to have significance in characterizing petrologic provinces. As the minor elements vary with abundances of other components within each

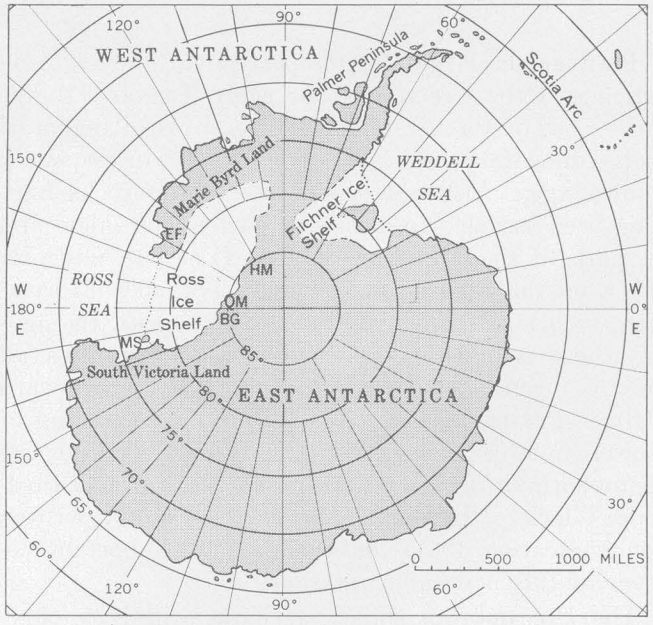

FIGURE 225.2.—Geographic map of Antarctica, showing place names. BG, Beardmore Glacier; EF, Edsel Ford Ranges; HM, Horlick Mountains; MS, McMurdo Sound; QM, Queen Maud Ranges.

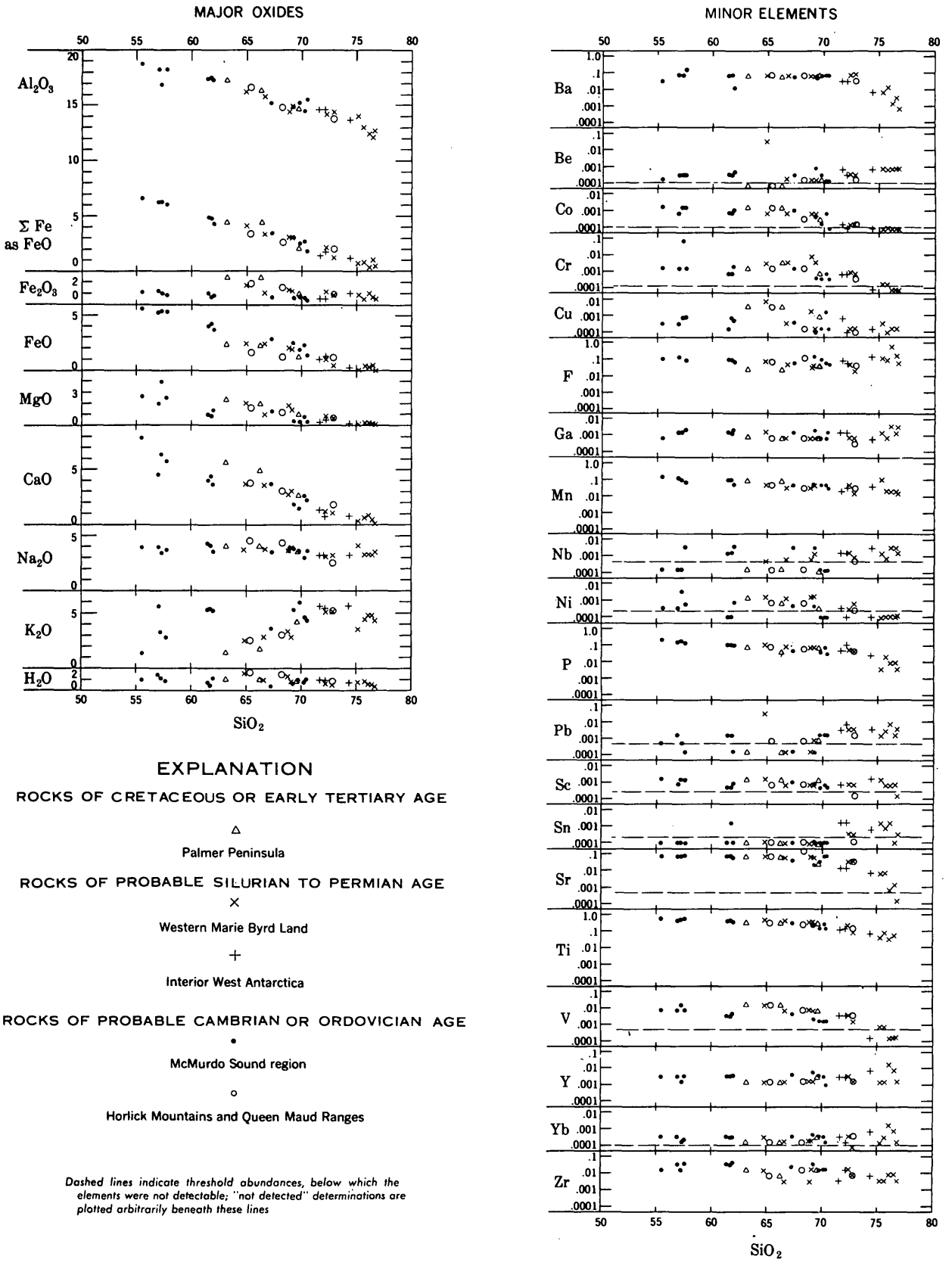

FIGURE 225.3.—Silica-variation diagrams of major oxides and minor elements in granitic rocks from Antarctica. Major oxides plotted on arithmetic scale; minor elements plotted on logarithmic scale.

province, these distinctions must be considered relative to accompanying amounts of other components; SiO_2, a good indicator of other variables, is used as the major reference here. Considered relative to SiO_2, chromium, nickel, and vanadium, and probably copper, tin, and titanium, appear to be less abundant in the probable Cambrian or Ordovician rocks than in the later Paleozoic(?) rocks, whereas zirconium, and possibly gallium, niobium, ytterbium, and yttrium, are apparently more abundant. The earlier Paleozoic(?) rocks thus appear considerably richer in rare earths, but poorer in ore metals, than the later Paleozoic(?) rocks. This consistency shown by groups of related trace elements supports the suggestion that the apparent contrasts are real rather than being mere illusions due to inadequate sampling.

Within the probable Cambrian or Ordovician group, there are marked differences between the 12 analyses of rocks from the McMurdo Sound region and the 3 from the Queen Maud Ranges and Horlick Mountains. The latter sample of 3 is so small that only a sampling inadequacy may be demonstrated—as is suggested by the virtual petrographic identity of Horlick Mountains rocks and some McMurdo Sound ones—but the data suggest conspicuous differences in Be, Nb, V, Y, and possibly other elements.

Similarly, within the later Paleozoic(?) group, there are apparent differences between western Marie Byrd Land (11 analyses) and interior West Antarctica (3 analyses) in several elements; but again, larger suites of samples are needed to evaluate such possible distinctions.

In many provinces of igneous rocks, barium varies systematically with potassium. Here, however, determinations of barium in the probable Cambrian or Ordovician rocks yielded nearly constant values, near 0.05 percent, regardless of potassium contents, whereas determinations in the later Paleozoic rocks showed the opposite pattern of widely variable barium with nearly constant potassium. This is perhaps related to desilication of the Cambrian or Ordovician magmas, in the low SiO_2 rocks, and to decreasing feldspar contents in the most silicic rocks.

Fluorine is higher, relative to SiO_2 content, in the probable Cambrian or Ordovician rocks than in the later Paleozoic(?) ones, and much higher in those than in the Cretaceous(?) rocks of Palmer Peninsula.

REFERENCES

Adie, R. J., 1955, The petrology of Graham Land, II, The Andean granite-gabbro intrusive suite: Falkland Islands Dependencies Survey, Sci. Rept. 12, 39 p.

Hamilton, Warren, 1960, New interpretation of Antarctic tectonics, *in* Short papers in the geological sciences: U.S. Geol. Survey Prof. Paper 400–B, p. B379–B380.

Hamilton, Warren, and Hayes, P. T., 1960, Geology of Taylor Glacier-Taylor Dry Valley region, South Victoria Land, Antarctica, *in* Short papers in the geological sciencies: U.S. Geol. Survey Prof. Paper 400–B, p. B376–B378.

Warner, L. A., 1945, Structure and petrography of the southern Edsel Ford Ranges, Antarctica: Am. Philos. Soc. Proc., v. 89, p. 78–122.

GEOLOGY AND HYDROLOGY OF OTHER COUNTRIES

226. INVESTIGATION OF THE PRINCIPAL FLUORSPAR DISTRICTS OF MEXICO

By Ralph E. Van Alstine, Washington, D.C.

Work done in cooperation with the Consejo de Recursos Naturales No Renovables, Secretaria del Patrimonio Nacional, Mexico, D.F., and the Office of Minerals Mobilization, U.S. Department of the Interior

Since 1956 Mexico has been the world's largest producer and exporter of fluorspar. In the past 4 years Mexico has supplied more than 60 percent of the fluorspar imported into the United States, averaging about 330,000 tons a year. Twelve major fluorspar districts in 9 states of Mexico were visited in April–June 1960, by the writer accompanied by Samuel Estrada and Ernesto de la Garza of the Consejo de Recursos Naturales No Renovables. The survey indicates that Mexican reserves are adequate for many

TABLE 226.1.—*Districts and mining companies visited*

State	District	Mining company or mine	Affiliate
Chihuahua	Parral	Industriale de Fluorita	General Chemical Div., Allied Chemical Corp.
Coahuila	El Tule	Minera Rosala	E. I. du Pont de Nemours & Co.
Do	Encantada-Buenavista.	Fluorita de Mexico	Continental Ore Co.
Do	do	El Camaron mine	
Do	do	Minera Rosala	E. I. du Pont de Nemours & Co.
Do	Paila-San-Marcos	Minera Nacional	American Smelting and Refining Co.
Do	do	San Marcos y Pinos	Reynolds Metals Co.
Do	do	Minera Julieta	St. Lawrence Corp. of Newfoundland, Ltd.
Do	do	Minera La Valenciana	
Do	Pico Etereo	La Domincia	Dow Chemical Co.
Do	do	Mal Abrigo mine	
Durango	Villa Union	Impulsora Minera	Mexus Minerals.
Guanajuato	Rio Verde	Minera Rio Colorado	General Chemical Div., Allied Chemical Corp.
Guerrero	Taxco	Restauradora de Minas	Minerales y Productos Derivados, Spain.
Do	do	Minas del Norte	La Consolidada.
Mexico	Zacualpan	Mexicana de Minas y Beneficios	
San Luis Potosi	Zaragoza	Minera Las Cuevas	Noranda Mines, Ltd., and others.
Do	do	Minerales Pennsalt	Pennsalt Chemicals Corp.
Do	Rio Verde	Minera La Valenciana	
Do	do	Fluorita de Rio Verde	Continental Ore Co.
Sonora	Esqueda	Fluoresqueda	San Luis Mining Co.
Zacatecas	Frio	Josefina mine	Aluminium Laboratories, Ltd.

TABLE 226.2.—*Processing plants visited*

No. on fig. 226.1	Location	Operating company	Process	Approximate daily capacity (tons of concentrates)
1	Esqueda, Sonora	San Luis Mining Co	Flotation	125
2	Heath Crossing, Coahuila	Dow Chemical Co	do	100
3	Eagle Pass, Tex	Reynolds Metals Co	do	100
4	El Tule, Coahuila	E. I. du Pont de Nemours & Co	Air separation pilot plant	30
5	Muzquiz, Coahuila	Fluorita de Mexico	Flotation	200
6	Agujita, Coahuila	American Smelting and Refining Co	do	150
7	Frausto, Coahuila	St. Lawrence Corp. of Newfoundland, Ltd	Heavy media	100+
8	Zaragoza district, San Luis Potosi.	Minerales Pennsalt	Crushing and sizing	300
9	San Luis Potosi, San Luis Potosi.	Noranda Mines, Ltd., and others	do	200
10	Rio Verde, San Luis Potosi	Minera La Valenciana	Washing and sizing	75
11	Zacualpan, Mexico	Mexicana de Minas y Beneficios	Flotation	70

years at the present rate of production. Brief visits were made to more than 30 fluorspar mines to obtain information on the deposits and their geologic settings. The deposits and the processing plants visited are listed in tables 226.1 and 226.2 and are shown on the index map (fig. 226.1).

More than two-thirds of the deposits examined are in limestone of Early Cretaceous age. The other deposits are mainly in shale or volcanic rocks that overlie the limestone and are within or next to Tertiary rhyolite.

The deposits are found as nearly flat manto bodies or as steeply dipping veins, pipes, conical bodies, tabular and irregular replacement bodies, and filled sink holes and collapse breccias. The manto deposits are generally smaller but contain higher grade ore than the veins, pipes, and conical bodies; they are abundant in several widely separated areas of limestone in northern and southern Coahuila.

The ore consists predominantly of fluorite, calcite, and quartz or chalcedony. The fluorite is highly variable in texture, grain size, and color. In some deposits the calcite content increases with depth; in others it decreases below a superficial caliche zone. Small quantities of barite, celestite, gypsum, native sulfur, pyrite, sphalerite, galena, chalcopyrite, iron oxides, or manganese oxides are present in most of the ores.

Although detailed sample data were not available for most of the deposits being worked, the average grade

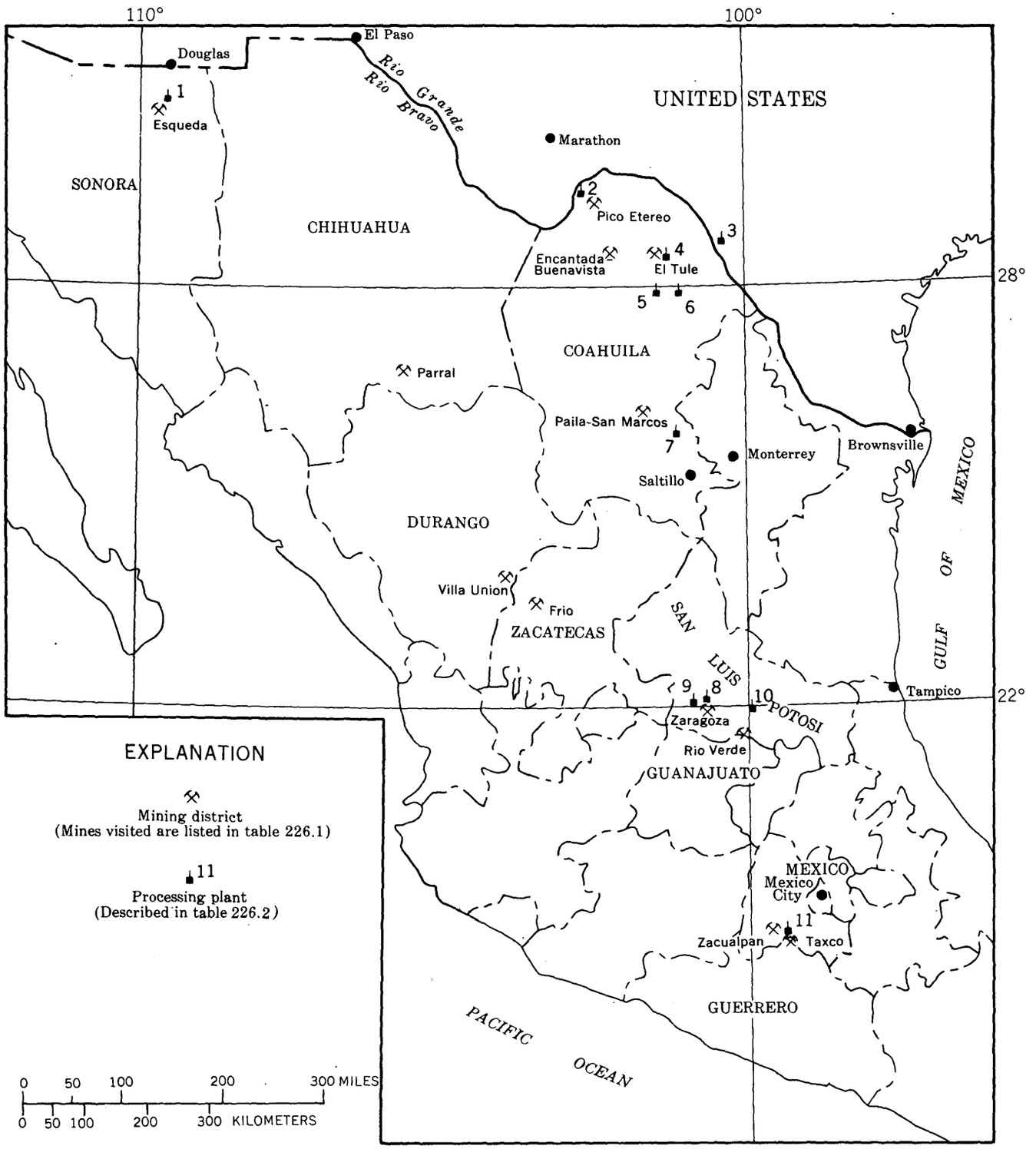

FIGURE 226.1.—Sketch map of part of Mexico showing fluorspar mining districts and processing plants visited, April–June 1960.

of ore, estimated at about 65 percent CaF_2, seems to be higher than that of fluorspar deposits in the United States. However, the overall range in grade from less than 40 to more than 90 percent CaF_2 is similar in the two countries. The silica content of the ore is commonly less than 10 percent and in some deposits is less than 1 percent; other deposits contain more than 30 percent calcite. The high quality of fluorspar shipped from some Mexican districts is the result of selective mining in lower grade deposits and repeated handpicking at the mines and mills.

Fluorspar reserves in the twelve districts visited are estimated at about 5 million tons of measured and indicated ore and about 10 million tons of inferred ore, averaging about 65 percent CaF_2. Individual deposits containing these reserves range in size from less than 10,000 tons to more than 1 million tons. An additional potential reserve of about 5 million tons of acid-grade fluorspar is contained in about 45 million tons of tailings that have accumulated from the flotation of zinc-lead-copper ore in the Parral area, Chihuahua. Undoubtedly additional fluorspar reserves will be found in the districts visited, especially in Coahuila and San Luis Potosi.

The fluorspar deposits are mined chiefly by shrinkage stoping, modified cut-and-fill system, room-and-pillar method, and benching in opencuts. Some of the larger mines are highly mechanized; at most of the smaller deposits, however, modern mining techniques are not used, and only the highest grade, thickest, or most readily accessible ore is mined by hand and packed to the surface on the backs of the miners. High-grade fluorspar as little as 4 inches thick is mined profitably from one manto deposit.

Water for mine use must be hauled to most of the districts. Because of this lack of water near the mines, ore is hauled as much as 150 miles to a mill.

As a result of the increasing need for fluorspar, especially in the United States, Canada, and Mexico, the Mexican fluorspar industry has expanded greatly and has become very profitable within the last 8 years. The mining and milling methods at the larger deposits are becoming more efficient, and the industry is continuing to flourish.

227. EVIDENCE FOR LOCAL GLACIER STAGNATION IN EAST GREENLAND

By JOSEPH H. HARTSHORN, Boston, Mass.

Work done in cooperation with the U.S. Air Force Cambridge Research Laboratories

Several glaciers on the islands and forelands of Greenland north of Scoresby Sund (fig. 227.1) show collapsed glacial stream deposits or ablation moraine that clearly indicate downwastage and stagnation during glacial retreat. Kettled glacial stream deposits that are now many miles from the nearest glacier were found as far north as the Haystack.

During an older more extensive glaciation, a glacier extended southeast toward Moskusoksefjord and Loch Fyne from the mountains of Hudson Land. This ancient glacier, here called the Stordal Glacier, reached eastward nearly to Loch Fyne. The general eastward slope of the glacier surface is shown by marginal channels (fig. 227.2).

The radiating pattern of former stream channels on the largest remaining uncollapsed outwash plains show that meltwater from Stordal Glacier flowed south and east and buried the terminus of the glacier under large quantities of glaciofluvial sediments. The collapsed part of the stream deposits shows the position of the stagnant ice. The forms of the ridges and hollows (fig. 227.2) lead to the conclusion that general downwastage and thinning had reduced the glacier front to a thin hummocky discontinuous mass. Aggrading streams flowed either on the ice or on the subglacial floor. Deposition in the lower parts of the irregular ice topography and on the ground took place in areas where there is little or no collapse. In places where ice blocks or high knobs on the nearly buried ice protruded through the blanket of sediments, however, there are now low spots produced by the inversion of relief.

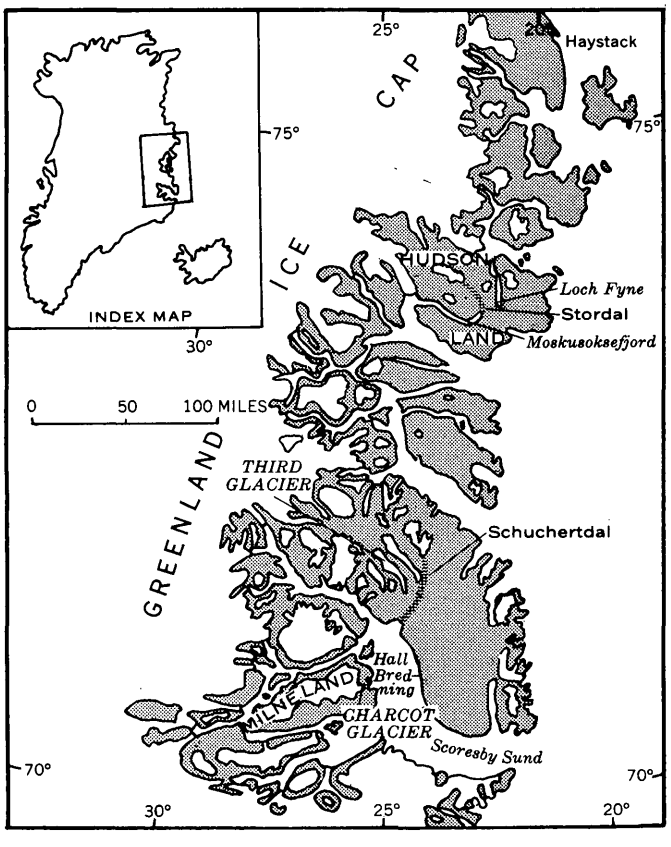

FIGURE 227.1.—Map of East Greenland.

Large flat-topped masses of stratified drift are bounded on all or nearly all sides by ice-contact slopes. Ridges of stratified drift that in many places completely surround depressions now filled with water indicate that erosion could have played no part in forming the features. The numerous mounds, ice-channel fillings, and rimmed kettles are evidently remnants of a once extensive plain deposited on irregular stagnant ice. The ice melted away after the streams from the Stordal Glacier had stopped flowing here and had begun to cut down to a new base level farther south, and after the glacier itself had retreated to some position farther back in the valley in the mountains. The pattern of collapse is similar to that in the better mapped area of the southern New England States, where ice retreated by stagnation.

Charcot Glacier (unofficial name) is a small valley glacier about 11 miles long that extends eastward from the ice cap covering the center of Milne Land, an island on the west side of Hall Bredning. It has a relatively clean surface, but it carries a heavy subglacial load that can be seen coming up along shear planes at the end of the glacier. The glacial streams flow at or near the base of the glacier near the terminus, and the heavy load of subglacial debris is picked up by the streams and delivered beyond the terminus.

The topography in front of Charcot Glacier (fig. 227.3) shows striking evidence of stagnation. Thin ice with an irregular upper surface was buried by

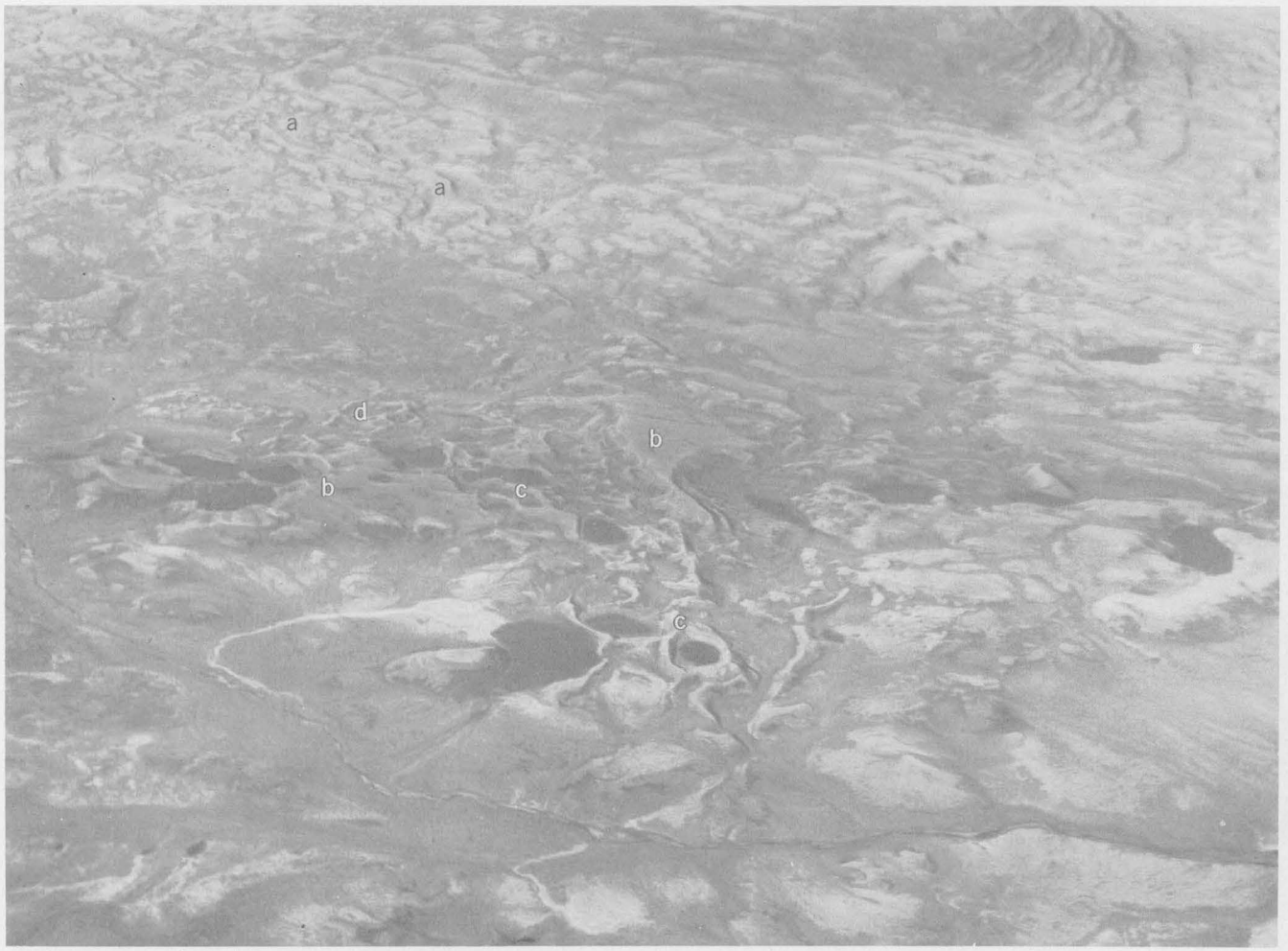

FIGURE 227.2.—Collapsed glaciofluvial deposits near Loch Fyne. View north from approximately 5,000 feet altitude. Area of marginal channels in bedrock (*a*), uncollapsed portions of outwash plains (*b*), kettle lakes (dark gray), and braided drainage (*c*), and reticulate ice-channel fillings (*d*). Ice moved from left to right.

glacial stream deposits from the last ice advance. The upper surface of these collapsed glaciofluvial deposits was once a smoothly aggraded plain. Collapse of areas underlain by thicker parts of the ice has destroyed the smooth surface by creation of numerous irregularities, small pits, and large circular kettles. The water-filled kettle in the center of figure 227.3 shows very steep sides and a fresh slump scarp along the left edge, indicating that collapse is still going on. The numerous ridges have formed from deposition of early channel deposits in low parts of the irregular ice sheet, later aggradation to a generally level upper surface, and final melting of the buried ice. The flat surfaces of parts of the ridges can be traced into uncollapsed outwash; elsewhere the narrower ridges have slumped below the general surface level.

On the west side of Schuchertdal, a valley about 43 miles long, are five glaciers that formerly must have been tributary to a large glacier in the main valley. The five glaciers are informally numbered in order from south to north; only the Third Glacier will be discussed.

Third Glacier terminates well out on the main valley floor in an expanded ice foot and encircling drift deposits. A trimline and some small concentric arcuate moraines show that the glacier pushed almost all the way across the valley floor at some very recent time. A semicircular pattern of deposits was left behind after the retreat of the ice to its present position. Next to the present glacier margin is a semicircular belt of knobby topography composed of superglacial moraine let down onto the ground. At the outer edge of the belt, deformed deposits of stratified sand and fine-grained gravel show a series of arcuate concentric ridges with central cracks, parallel to and between the present ice margin and the outer limit of the last advance. It is possible that the deformed outwash

601530 O—61——15

FIGURE 227.3.—Aerial view of collapsed stratified drift in front of Charcot Glacier, Milne Land; taken from an altitude of about 150 feet. Breached end moraine (*a*), modern sandy outwash plain (*b*), older collapsed outwash (*c*), ice-channel filling at same elevation as uncollapsed part of older outwash (*d*), and recent slump scarp (*e*) on edge of kettle.

was laid down in front of an advancing glacier and crumpled by advancing ice. An alternative possibility is as follows: the sediments were deposited as an outwash apron on a thin marginal zone of ice, consisting of alternate concentric arcuate bands of fast melting clean ice and slowly melting moraine-covered ice with a concentric pattern parallel to the snout of the glacier; as the last remnants of the thin ice melted, the clean bands formed shallow valleys and the dirty bands remained as small ridges; outwash deposited on this irregular surface consisted of thick belts over the valleys and thin belts over the moraine-covered ridges; when the ice finally melted completely, the thicker sections of outwash over the ice bands became low ridges and developed cracks owing to lateral slumping toward the areas of minimum outwash deposition, the present lows. Most of the ice buried under the superglacial deposits has melted away, but the presence of ponds with water clouded by rock flour shows that there is still some ice beneath these deposits.

At Third Glacier, as at Stordal Glacier and Charcot Glacier, a relatively recent expansion of ice has been followed by stagnation and burial of the glacier terminus.

228. THERMAL REGIME DURING THE THAW OF CENTRUM SØ, NORTHEAST GREENLAND

By D. B. Krinsley, Washington, D.C.

Work done in cooperation with Air Force Cambridge Research Laboratory

During May 1960, and prior to the thaw, two cables containing Western Electric thermistors were placed in Centrum Sø (lake), northeast Greenland. The cables, supported by floats resting on the ice surface, extended through 1 foot of snow and 6 feet of ice to the lake bottom where they rested on fine-grained sediments. The suspended cables were located near each end of a trough-shaped deep which lay along the longitudinal section of the lake (fig. 228.1). The thermistors in each cable were at approximately 10, 100, 200, and 260 feet below the ice surface. Readings accurate to 0.1°C were made at intervals of from 1 day to 3 weeks. During a 24-hour period beginning at noon May 29, thermistors in cable 2 were read hourly.

Overflow from Saefaxi Elv (river) spread over a quarter-mile square area adjacent to the river mouth, at noon on May 20. This overflow, resulting from increased flow because of higher air temperatures, initiated a general melt of the subjacent snow cover. By May 29, isolated ponds had developed on the lake ice and a moat 8 inches deep and 20 feet wide extended eastward along the north shore to point A (fig. 228.1). These changes at the surface and periphery of the lake were recorded on May 31 when the thermistor at 10 feet in cable 1 indicated a rise of 0.1°C, and thermistors at 200 and 207 feet in cable 2 each indicated a decrease of 0.1°C (fig. 228.2).

During the period from May 31 through June 6, Saefaxi Elv and Graeselven (river) eroded channels through the stream ice and a large volume of warmer water (3.0° to 8.0°C) poured into the adjacent moats and under the lake ice which had broken away from the shore bottom. The water which had accumulated on the surface of the lake ice drained into the rapidly widening moats. Firm ice that had characterized the frozen surface had been transformed to candle ice which extended to a depth of 14 inches. On June 6, the thermistor at 110 feet in cable 1 indicated a decrease of 0.1°C in the water temperature. Thermistors at 6.5, 10, 200, and 207 feet in cable 2 indicated a rise of 0.5°, 0.4°, 0.1°, and 0.1°C, respectively.

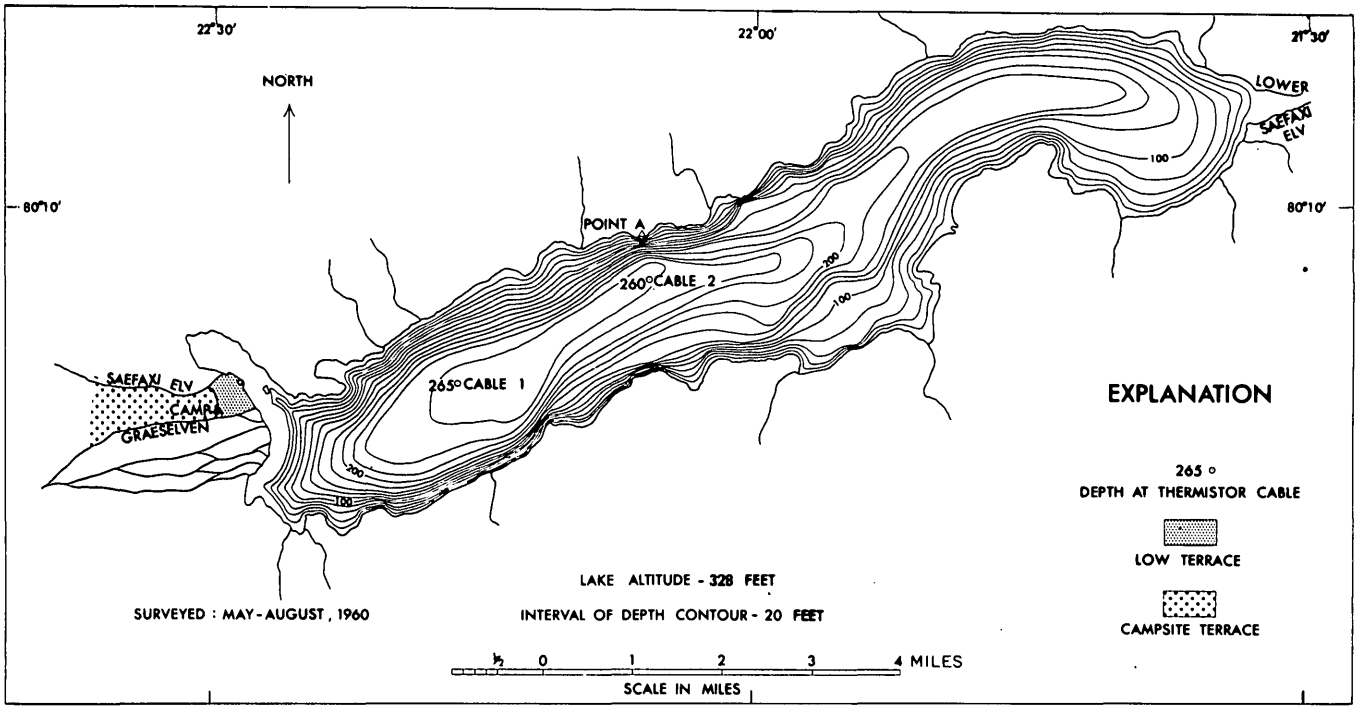

FIGURE 228.1.—Hydrographic map of Centrum Sø, northeast Greenland.

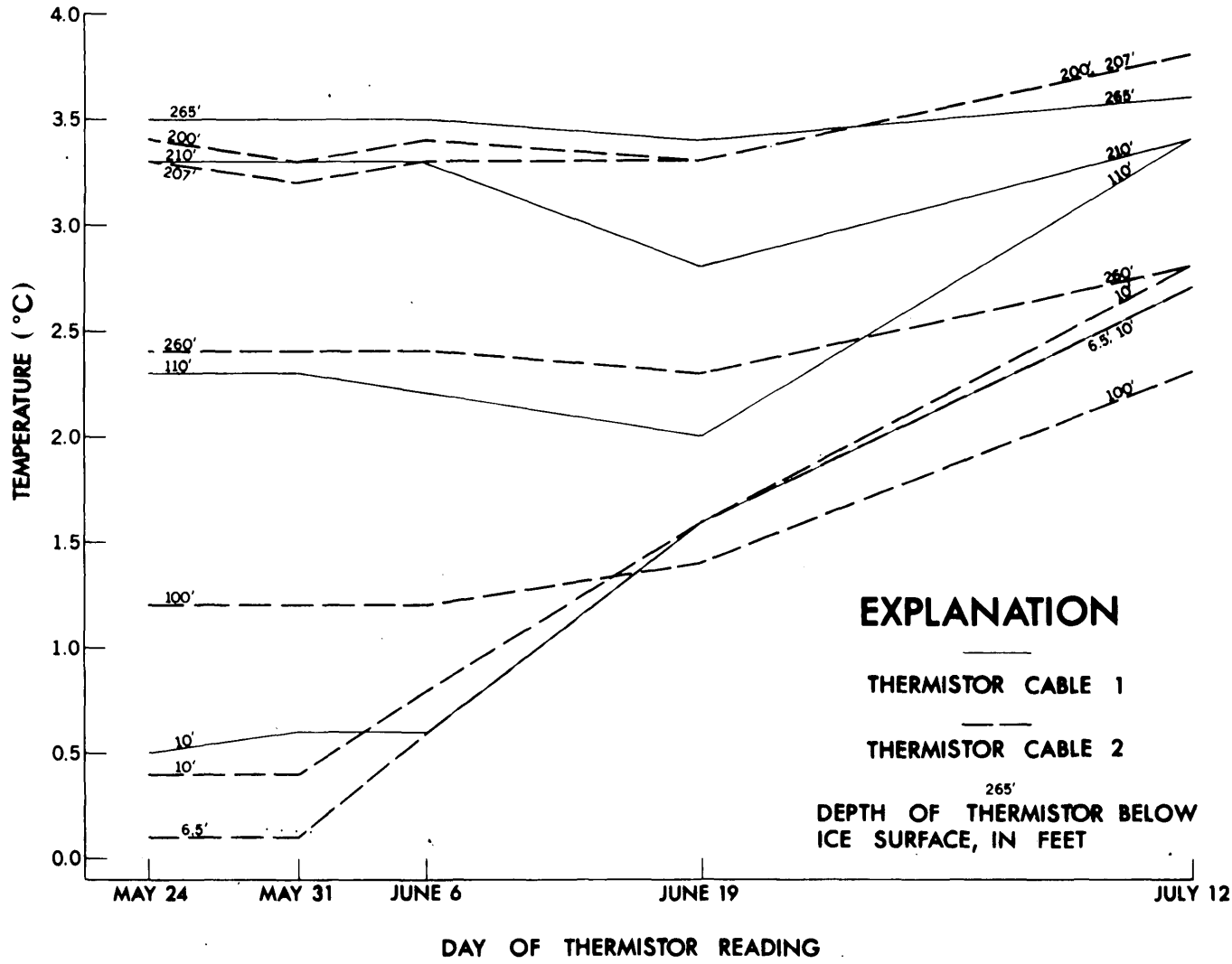

FIGURE 228.2.—Water temperature during the thaw at Centrum Sø.

A staff gauge for measuring the lake level was installed on June 7 as the water surface started to rise. Three days later, the lake had risen one foot, which was sufficient to neutralize the current in Saefaxi Elv. The lake ice deteriorated rapidly by candling but by late June the level of the lake had stabilized. On June 19 the thermistor at 10 feet in cable 1 indicated a 1.0°C rise in water temperature although all other thermistors in the cable recorded a decrease in water temperature (fig. 228.2). At cable 2 the upper three thermistors recorded a rise of 1.0°, 0.8°, and 0.2°C. As at cable 1, the lower thermistors of cable 2 indicated a decrease in water temperatures.

During the first week in July, the lake rose 3.5 feet and a 15-foot wide crack opened in the vicinity of cable 2. The ice in this area had thinned from 72 inches to 48 inches. The moat was continuous around the entire lake but it closed locally with shifting wind directions. By July 9, the lake had risen a total of 8.3 feet, and water 2.5 feet deep flooded a low terrace adjacent to the campsite (fig. 228.1). The lake receded from this maximum flooding the next day. The moat was now from 25 to 50 feet wide around the lake, and several cracks formed near the center of the lake ice. On July 12, prior to their removal because of possible ice damage, the thermistors were read for the last time. At cable 1, all thermistors recorded a significant rise in water temperature; the maximum rise of 1.4°C occurred at a depth of 110 feet. At cable 2, all thermistors recorded a significant rise in water temperature; the maximum rise of 1.2°C occurred at a depth of 10 feet. During the period July 10 to 25, the lake ice melted so rapidly that by July 26 all lake ice had disappeared except for scattered floating remnants at the north side of Centrum Sø.

The temperature data indicate that although water temperatures near the surface and on the lake bottom changed in the same direction, there were significant temperature differences between cables, in the same horizon at the same time. Temperature differences between the 10-foot thermistors (4 feet below the bottom of the ice) were not due to differences in the local environment because both instrument platforms were covered by a white canvas, and snow and ice cover were identical. Small temperature fluctuations along the lake bottom could not have been caused by different radiative properties of the sediments as suggested by Brewer (1958) because of the uniformity of the fine-grained sediments (red silt) at both cable ends. Temperature changes between cables were in the same direction in the 200- to 210-foot horizon but were in opposite directions in the 100- to 110-foot horizon during the period June 6 through June 19 (fig. 228.2).

The water temperature differences between levels were greater prior to melting of the insulating snow cover and they diminished during the thaw period. During a critical 24-hour period (May 30–31), on the threshold of the lake thaw, when the air temperature fluctuated 5.0°C and the snow cover was reduced to slush, there was not more than a 0.03°C (4 ohms resistance) fluctuation in water temperature and this occurred at a depth of 200 to 207 feet.

Solar radiation, even differentially applied, as in the case of sunlight and shadow alternately produced by a low arctic sun on topographic obstacles, cannot affect water temperatures prior to the removal of the snow cover. The principal tributaries of Centrum Sø freeze to the bottom so that they cannot add heat to the lake until they break up (June 1).

Prior to the thaw, heat may enter the system from the flow of ground water beneath the streams, from sublimnol springs, and from the bottom sediments. These potential heat sources are capable of generating local convective systems that could account for the horizontal temperature differences as well as the temperature anomaly which occurred at the 260-foot thermistor of cable 2 (fig. 228.2).

During the breakup of the principal tributaries the persistence of the horizontal temperature differences at depth appears to be the result of local displacement by the warmer denser water which may flow in currents controlled by the bottom configuration.

REFERENCES

Barnes, D. F., and Hobbie, J. E., 1960, Rate of melting at the bottom of floating ice, *in* Short papers in the geological sciences: U.S. Geol. Survey Prof. Paper 400–B, p. B392–B394.

Brewer, M. C., 1958, Thermal regime of an Arctic lake: Am. Geophys. Union Trans., v. 39, no. 2, p. 278–284.

Hobbie, J. E., 1960, Limnological studies on Lakes Peters and Schrader, Alaska: Air Force Cambridge Research Center—TN–60–261, Scientific Report no. 5.

229. FACIES CHANGE IN NEOCOMIAN ROCKS OF THE TERESITA-CHULO AREA, ATACAMA PROVINCE, CHILE

By Kenneth Segerstrom, Santiago, Chile

Work done in cooperation with the Instituto de Investigaciones Geológicas, Santiago

Recent detailed mapping in the Teresita-Chulo area, 10 to 15 km northeast of Copiapó, Chile, shows major changes in facies in northerly and westerly directions from marine calcareous rocks of the Chañarcillo group (Segerstrom and Parker, 1959) to predominantly continental volcanic and clastic rocks of the Bandurrias formation (Segerstrom, 1960a). Interfingering of the Bandurrias formation and the Chañarcillo group is most convincingly shown along the crest and on both limbs of the Tierra Amarilla anticline, a large fold that extends south of the area for at least 200 km. (See fig. 229.1.) Both facies are truncated with angular discordance by the continental clastic and volcanic Cerrillos formation.

The Chañarcillo group comprises a sequence of four marine formations, Abundancia, Nantoco, Totoralillo, and Pabellón, which were named and defined by Biese (1942). The sequence, chiefly limestone, was named

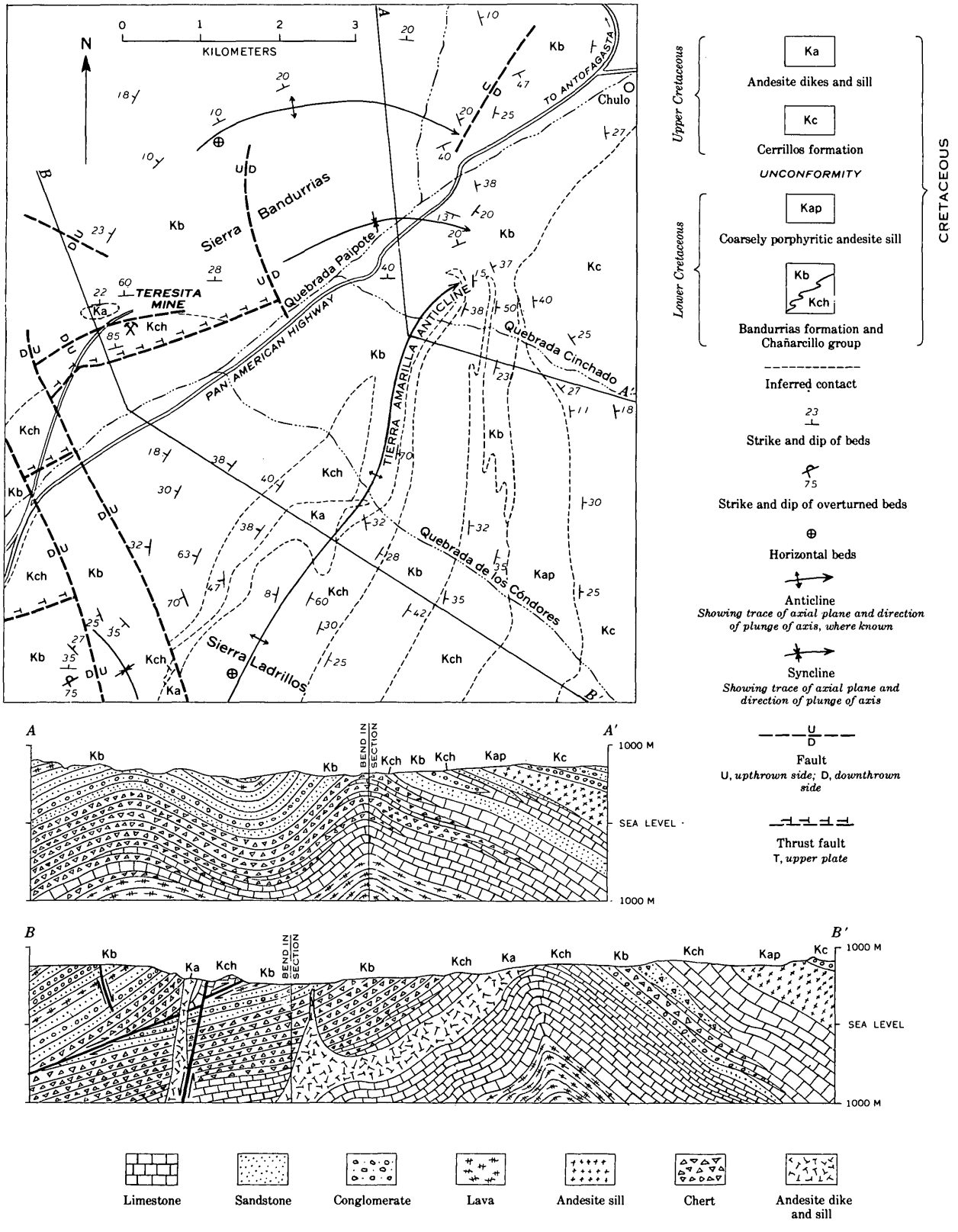

FIGURE 229.1.—Bedrock map and structure sections of Teresita-Chulo area, Atacama Province, Chile.

Chañarcillo formation by Whitehead (1919) and Chañarcillo group by Segerstrom and Parker (1959). The group is prominently exposed from the Teresita-Chulo area to the region of Vallenar about 145 km to the south.

A complete section of the Chañarcillo group is exposed in Quebrada Meléndez, 16.3 km south of Teresita mine, where it overlies massive lava of the older Punta del Cobre formation. At that place, general lithologic succession from oldest to youngest is as follows: The basal Abundancia formation consists of 30 m of alternating limestone and graywacke succeeded by 175 m of limestone with intercalated chert, sandstone, and conglomerate. The Nantoco formation consists of about 500 m of limestone overlain by 225 m of interbedded limestone and calcareous shale and topped by 125 m of gypsiferous limestone. The Totoralillo formation is about 255 m thick and contains abundant marl and calcareous shale, as well as limestone. The Pabellón formation, which is the uppermost member of the group consists of 430 m of limestone with abundant intercalations of chert, conglomerate, and breccia and is intruded by several small sills of andesite. According to Corvalán and Perez (1958) on the basis of paleontological evidence this group of four formations ranges in age from late Valanginian to the Barremian substage of Neocomian (Early Cretaceous) time.

The Bandurrias formation, composed principally of clastic and pyroclastic material, interfingers with the calcareous rocks of the Chañarcillo group along the crest and flanks of the Tierra Amarilla anticline in the central part of the Teresita-Chulo area. The lower and middle parts of the formation occupy approximately the same stratigraphic position as the Chañarcillo group, and the upper part occupies a higher position. The oldest beds in the formation that are exposed in the Teresita-Chulo area—those immediately north of Teresita mine—consist of lava and marine breccia, sandstone, and conglomerate. These rocks totaling about 1,000 m in thickness are overlain by about 1,000 m of red crossbedded conglomerate and sandstone, siltstone (all of continental origin), and lava. Some of the lava beds are coarsely porphyritic and are similar lithologically to the great andesite sill along the eastern edge of the area.

The continental sequence is cut out completely along the unconformity at the base of the Cerrillos formation, in the Llampos quadrangle, about 13 to 40 km north of the area. The marine sequence thickens to about 3,000 m in the Llampos quadrangle and contains lenses of limestone and chert. About 1.2 km north of the quadrangle, ammonites of the genera *Acanthodiscus* and *Holcostephanus* are contained in one of the limestone lenses (Segerstrom, 1960b). The ammonites indicate that the lower part of the Bandurrias formation, north of the Teresita-Chulo area, is of late Valanginian age (Corvalán and Perez, 1958) and is correlative with the Chañarcillo group. The continental part of the formation is probably correlative with the lithologically similar Veta Negra and Colimapu formations of central Chile that are believed to be of Aptian to Turonian (mid-Cretaceous) age (Thomas, 1958), and which are younger than any formation in the Chañarcillo group.

Limestone beds at the Teresita mine belong to the Chañarcillo group and have been thrust up from the west limb of the Tierra Amarilla anticline. These beds contain the ammonites, *Thurmannia quintucoensis* Weaver var., *Acanthodiscus* aff. *A. radiatus* Bruggen var. (Juan Tavera, written communication, 1951), as well as *Liticoceras* sp. and *Simbirskites*? sp. (R. W. Imlay, written communication, 1958). These ammonites have been assigned to the late Valanginian substage of Neocomian time by Tavera and to the late Valanginian and early Hauterivian substages by Imlay.

Overlying the limestone at the Teresita mine are clastic and pyroclastic rocks, assigned to the Bandurrias formation, that contain the late Hauterivian ammonite, *Crioceras andinum* (Corvalán and Perez, 1958). The same species is found 4 km to the southeast in the core of the Tierra Amarilla anticline in beds of limestone of the Chañarcillo group.

REFERENCES

Biese, W. A., 1942, La distribución del Cretáceo inferior al sur de Copiapó: Santiago, Anales del Primer Congreso Pan-americano de Ingeniería de Minas y Geología, v. 2, p. 429–466.

Corvalán, D., José, and Pérez D'A., Ernesto, 1958, Fósiles guías chilenos, Titoniano-Neocomiano: Santiago, Instituto de Investigaciones Geológicas, Manual No. 1, 48 p.

Segerstrom, Kenneth, 1960a, Geología del cuadrángulo Quebrada Paipote: Santiago, Instituto de Investigaciones Geológicas, Carta Geológica de Chile, v. 2, no. 1, 35 p.

——— 1960b, Geología del cuadrángulo Llampos: Santiago, Instituto de Investigaciones Geológicas, Carta Geológica de Chile, v. 2, no. 2, 40 p.

Segerstrom, Kenneth, and Parker, R. L., 1959, Geologíc del cuadrángulo Cerrillos: Santiago, Instiuto de Investigaciones Geológicas, Carta Geológica de Chile, v. 1, no. 1, 33 p.

Thomas, Herbert, 1958, Geología de la Cordillera de la Costa, entre el valle de La Ligua y la Cuesta de Barriga: Santiago, Instituto de Investigaciones Geológicas, Bol. 2, 86 p.

Whitehead, W. L., 1919, The veins of Chañarcillo, Chile: Econ. Geology, v. 14, p. 1–45.

230. RHYOLITE TUFF, A SOURCE OF THE SALTS OF NORTHERN CHILE

By GEORGE E. ERICKSEN, Santiago, Chile

Work done in cooperation with the Instituto de Investigaciones Geológicas, Santiago

Although many investigators have described the well-known nitrate deposits of northern Chile and have advanced theories to explain their origin, few have considered the more general field of the saline deposits of which nitrates are a small but closely related fraction. Geologic field investigations in northern Chile, made by the writer since 1955, have led to the conclusion that geologic, physiographic, and climatic conditions of today are similar to those prevailing since the saline deposits started to accumulate, probably during the Pleistocene, and that any explanation for the origin and accumulation of the salts must be in terms of these known factors.

Field evidence leads to the conclusion that the salts came from erosion and leaching of rocks, chiefly rhyolite tuffs, in those areas of the high Andes and the western Andean slopes where rainfall is sufficient. Average annual rainfall above an altitude of 4,000 meters is on the order of 200 to 300 mm per year and this decreases progressively at lower altitudes until at 1,000 m altitude rainfall is almost nil. The salts were and still are carried by surface and ground water and precipitated in closed basins or broad flat areas in the high Andes, the coastal range, and the intervening lower lying region (fig. 230.1). The nitrate deposits, in contrast to other saline deposits, are along the lower eastern slopes of the coastal range and the lower hillslopes bordering salt pans within the coastal range in the region extending from near Iquique southward to Taltal.

Rhyolite tuff covers extensive areas in the Andean cordillera and is interstratified with unconsolidated piedmont sediments that extend as far westward as the western limit of the Pampa del Tamarugal (fig. 230.1). The tuff is considered to be of late Tertiary age (R. J. Dingman and C. A. Galli, written communication). A considerable quantity of the rhyolite tuff is welded, indicating deposition from gaseous, high-temperature ash flows, or nuees ardentes.

The writer, in attempting to explain the number, size, and distribution of the saline deposits of northern Chile, was led to postulate that the rhyolite tuffs contained soluble salts as primary constituents.

To test for soluble salt, samples of rhyolite welded tuff were collected from two areas, one a quarry near Mamiña and the other a roadcut near Pachica (fig. 230.1); the localities are well-drained areas in which

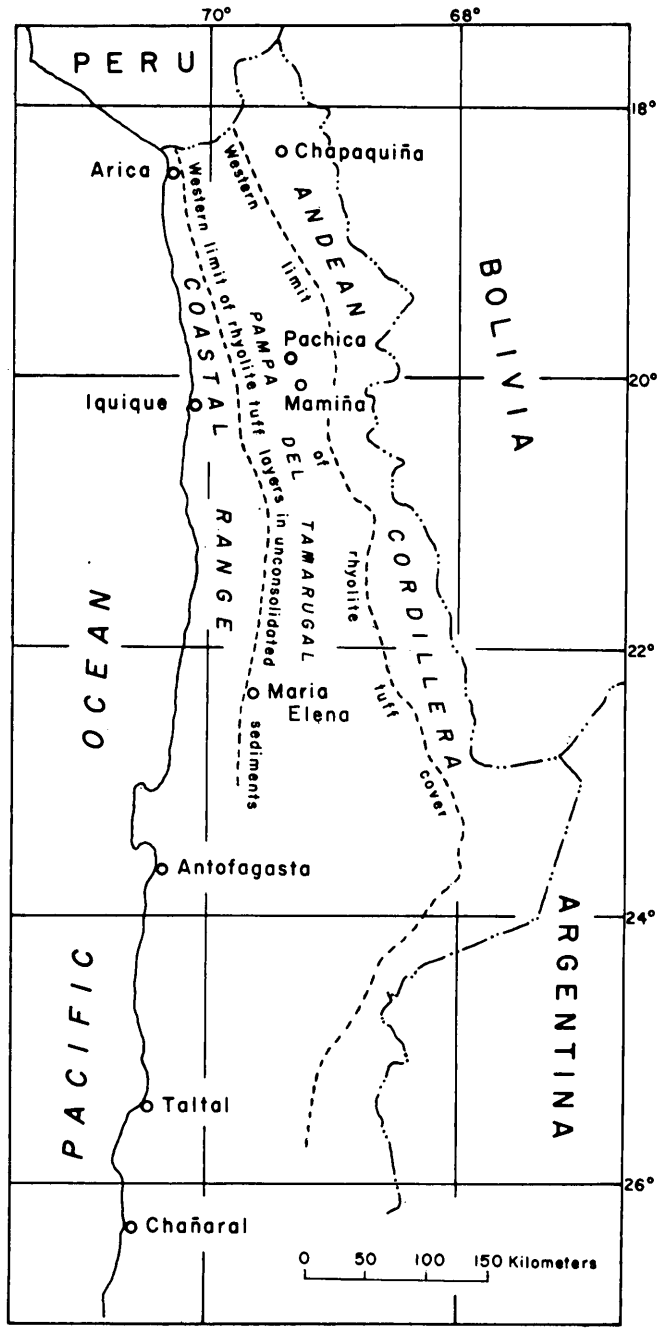

FIGURE 230.1.—Index map of northern Chile.

TABLE 230.1.—*Partial analyses of soluble salts contained in samples of rhyolite tuff, Mamiña and Pachica*

[In weight percent of entire specimen]

	Mamiña sample		Pachica sample	
	[1] 1	[2] 2	[3] 1	[2] 2
Total soluble salt	0. 1930	0. 2705	0. 1250	0. 1935
NO_3	. 0014	. 0055	. 0018	. 0055
Cl	. 0317	. 0367	. 0213	. 0332
SO_3[4]	. 0660	. 1171	. 0428	. 0484
F	--------	--------	. 0004	--------
B	--------	--------	. 0003	--------
CO_3	--------	--------	. 0009	--------
SiO_2	. 0036	. 0081	. 0014	. 0159
Fe_2O_3 and Al_2O_3	. 0003	. 0025	--------	. 0032
CaO	. 0066	. 0448	. 0029	. 0026
Na_2O	--------	--------	. 0510	--------
K_2O	. 0005	. 0110	. 0036	. 0048
MgO	trace	trace	trace	trace

[1] Analyses by laboratory of the Superintendencia del Salitre, Iquique.
[2] Analyses by laboratory of the Cia. Salitrera Anglo-Lautaro, Maria Elena.
[3] Analyses by laboratory of the Instituto de Investigaciones Geológicas of Chile, Santiago.
[4] Sulphate is reported as SO_3 in conventional analyses of nitrate ore.

rainwater would tend to leach soluble salts rather than deposit them. The sample from Mamiña is a pink, porous tuff, welded only to a slight degree; that from Pachica is a light-tan, dense welded tuff that has a very high percentage of glass. Portions of these samples were analyzed by three different laboratories to give the results listed in table 230.1.

The analytical techniques used by the laboratories of the Superintendencia del Salitre and Compañia Salitrera Anglo-Lautaro were those used in the analyses of nitrate ores; the laboratory of the Instituto de Investigaciones Geológicas employed the techniques of standard water analyses. Analyses were made of the salts in solutions prepared by leaching pulverized rock with distilled water kept at constant boiling temperature. The laboratory of the Instituto de Investigaciones Geológicas made a single 10-minute leaching and obtained a solution of less than one liter; the other laboratories made separate leachings and washings of a 4-kilogram sample over a period of several hours and obtained a solution of several liters. The leach solutions had a pH of approximately 8.5.

Any conclusions drawn from data based on analyses of samples from only two localities are at best tentative; perhaps most important is that this work shows the need of testing certain volcanic rocks for soluble salts that may be residual from late-stage magmatic fluids. However, the analyses do show that the rhyolite tuffs from these areas contain the principal ions (Cl, SO_4, NO_3, Ca, Na, and K) that occur in the saline deposits of northern Chile. Soluble salts in the amounts indicated by the analyses, contained in the rhyolite tuffs that have been eroded or leached, would be more than sufficient to supply the existing saline deposits, including nitrates.

The soluble salt was evidently a wide-spread constituent of the tuff at the time of extrusion and not the result of later contamination. It is possible that the nitrate formed by oxidation of nitrogen or ammonia, perhaps in the presence of minerals that acted as catalysts, within the hot gaseous ash flows. The problem remains of accounting for the formation of anions of high redox potential such as chromate, iodate, and perchlorate, which occur in the nitrate deposits. Additional information is needed to determine whether the salts are primary magmatic constituents or whether they were contained in sediments incorporated into the magma as it moved to the surface.

PALEONTOLOGY, GEOMORPHOLOGY, AND PLANT ECOLOGY

231. CORRELATION OF THE ARCTIC PERMIAN

By J. THOMAS DUTRO, Jr., Washington, D.C.

Arctic Permian faunas have attracted the attention of paleontologists and stratigraphers since Toula (1873, 1874, 1875) first described fossils from Spitzbergen. George Girty and James Steele Williams spent many years studying Permian collections from Alaska and assisting other geologists with problems involving ages and stratigraphic correlations of the various rock units. Extensive lists of the faunas of the Tahkandit limestone and the Mankomen formation were published long ago (Mertie, 1930, and Moffit, 1938, among others), but the rich faunas have never been described.

Several taxonomic papers in the past few years have stimulated interest in the Arctic Permian. In 1955, Dunbar described the brachiopods of east-central Greenland. Faunas from Grinnell peninsula in the Canadian Arctic were recently treated by Harker and Thorsteinsson (1960). A fauna from Oregon related to the Arctic Permian fauna was the subject of a paper by Cooper (1957). In addition, the monograph on the Productoidea by Muir-Wood and Cooper (1960) prepared the way for extensive taxonomic work on the late Paleozoic brachiopod faunas everywhere.

ARCTIC PERMIAN FAUNAS

A study of the Permian brachiopods of northwestern Alaska has led me to examine, among other things, the age significance of a peculiar group of spiriferoid brachiopods including the distinctive genus *Licharewia*. This brachiopod has a shell that is wider than long with simple rounded ribs and a broad, relatively flat, unmodified fold and sulcus. The genus is considered a guide to the Upper Permian of the U.S.S.R. (Sarycheva and Sokolskaya, 1952; Likharev, 1959) and is represented in the well-known Zechstein fauna of western Europe. Similar brachiopods have been reported from Spitzbergen, east-central Greenland, the Grinnell peninsula, Novaya Zemlya, and elsewhere.

Many specimens of *Licharewia* occur among the brachiopods collected from the Permian clastic sequence in the DeLong Mountains, Alaska (Tailleur and others, 1958). Associated genera are typical of Permian faunas elsewhere in the Arctic, but I consider the total assemblage to indicate an early Late Permian age (probably a Kazanian equivalent). With *Licharewia* are: *Derbyia* sp., *Linoproductus* sp., *Stepanoviella* sp., *Waagenoconcha* aff. *W. payeri* (Toula), *Antiquatonia* spp., *Kochiproductus* cf. *K. freboldi* (Stepanow), *Horridonia* cf. *H. horrida* (Sowerby), *Muirwoodia* cf. *M. greenlandica* Dunbar, *Choristites* spp., *Neospirifer* sp., *Spiriferella* cf. *S. keilhavii* (von Buch), *Spiriferella* sp., *Stenoscisma* sp., *Squamularia* sp., *Spirigerella* sp., *Rhynchopora* cf. *R. kochi* Dunbar, and *Dielasma* spp.

The correlations of the Arctic Permian fauna suggested by Harker and Thorsteinsson (1960) place this important assemblage too low in the Permian. On the other hand, the position of the Greenland fauna indicated by Dunbar and others (1960) is probably much too high. The beds in Alaska, and their correlatives, probably are assignable to the Kamian stage as defined by Likharev (1959) to include the Ufimian and Kazanian substages in the Upper Permian. A suggested revision of these correlations is indicated in figure 231.1, which shows related sequences in the Arctic region. My interpretations of how the Arctic Permian fits into the type Russian Permian and the west Texas sequences are also shown.

CORRELATION OF WEST TEXAS AND RUSSIAN SEQUENCES

The correlation of the west Texas sequence with the Russian type area differs from both that shown by Dunbar and others (1960) and that adopted by the U.S. Geological Survey (Cohee, 1960). This is due, in part, to my acceptance of the Kamian as suggested by Likharev (1959). However, I interpret faunal evidence from the west Texas region differently from Dunbar. As a basis for correlations, the faunal ranges of the fusulinids, ammonites, and brachiopods are considered together and compared with generic ranges recently defined by Miklukho-Maklay and others (1958), Ruzhentsev (1960), and Likharev (1959).

Fusulinid genera found in the higher beds in west Texas, for which ranges were given by the Russian workers, include *Codonofusiella*, *Leella*, *Rausserella*, *Polydiexodina*, and *Yabeina*. All except the last are shown starting at the base of the Upper Permian. *Yabeina* is shown to range only through the upper part of the Upper Permian. Taken together with the ranges given on the Permian chart of Dunbar and others (1960), these data suggest a Lower-Upper Permian boundary most likely near the Word-Capitan boundary or, at most, no lower than the base of the Cherry Canyon equivalents.

Ammonite ranges suggest that the base of the Kamian (as I would interpret it) might be placed at least as low as the South Wells limestone member of the Cherry Canyon formation, perhaps as low as the base of the Getaway limestone member of the Cherry Canyon formation.

There seems to be no question that all the Bone Springs is an Artinskian equivalent and Cooper (1957, p. 19) has suggested that the brachiopod faunas of the lower part of the Word formation of the Glass Mountains are upper Artinskian equivalents.

For these reasons I am suggesting that the Word straddles the Lower-Upper Permian boundary. Perhaps it is roughly the equivalent of the Kungurian-Ufimian interval.

As regards the top of the Kazanian equivalents, the occurrence in the Lamar limestone member of the Bell Canyon formation of both *Strigogoniatities* (Newell and others, 1953, p. 232) and *Yabeina* (Skinner and Wilde, 1955) suggests that the Lamar is Kazanian in age. I interpret the entire span of the

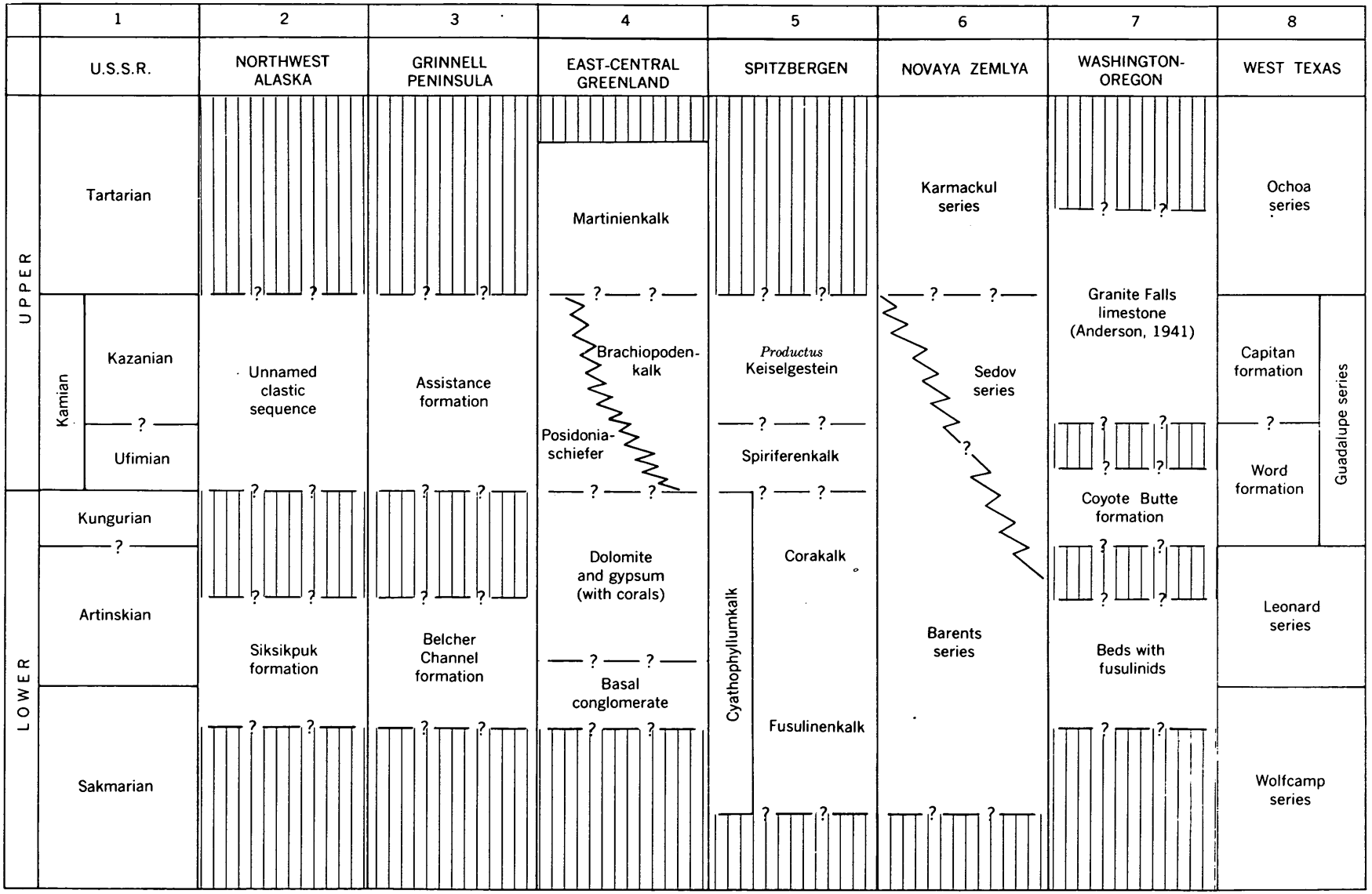

FIGURE 231.1.—Suggested correlation of some Permian formations in western North America and the Arctic regions. Vertical-lined pattern indicates probable absence of beds. Columns 3 to 6 modified from Harker and Thorsteinsson (1960).

Capitan formation and its equivalents to be correlative with the Kazanian.

REFERENCES

Anderson, R. A., 1941, Fusulinids of the Granite Falls limestone and their stratigraphic significance: Washington State Coll. Research Studies, v. 9, no. 3, p. 189–202.

Cohee, G. V., 1960, Series subdivisions of Permian system: Am. Assoc. Petroleum Geologists Bull., v. 44, no. 9, p. 1578–79.

Cooper, G. A., 1957, Permian brachiopods from central Oregon: Smithsonian Misc. Coll., v. 134, no. 12, 79 p., 12 pls.

Dunbar, C. O., 1955, Permian brachiopod faunas of central east Greenland: Meddelelser om Grønland, v. 110, no. 3, 169 p., 32 pls.

Dunbar, C. O., and others, 1960, Correlation of the Permian formations of North America: Geol. Soc. America Bull., v. 71, p. 1763–1806, 1 pl.

Harker, P., and Thorsteinsson, R., 1960, Permian rocks and faunas of Grinnell Peninsula, Arctic Archipelago: Canada Geol. Survey Mem. 309, 89 p., 25 pls.

Likharev, B. K., 1959, On the boundaries and principal subdivision of the Permian system: Sovietskaya Geologiya, no. 6, p. 13–30. [Translation by G. Rabchevsky, Dec. 1959.]

Mertie, J. B., Jr., 1930, Geology of the Eagle-Circle district, Alaska: U.S. Geol. Survey Bull. 816, 168 p.

Miklukho-Maklay, A. D., Rauzer-Chernousova, D. M., and Rozovskaya, S. E., 1958, Sistematika i filogenija Fuzulinidej: Voprozy Mikropaleontologii, v. 2, p. 5–21, figs. 1, 2. [French translation, 1960.]

Moffit, F. H., 1938, Geology of the Slana-Tok district, Alaska: U.S. Geol. Survey Bull. 904, 54 p.

Muir-Wood, H. M., and Cooper, G. A., 1960, Morphology, classification and life habits of the Productoidea (Brachiopoda): Geol. Soc. America Mem. 81, 447 p., 135 pls.

Newell, N. D., and others, 1953, The Permian reef complex of the Guadalupe Mountains region, Texas and New Mexico: 236 p., San Francisco, W. H. Freeman and Co.

Ruzhentsev, V. E., 1960, Systematic principles, classification, and phylogeny of Paleozoic ammonites: Akad. Nauk. SSSR, Paleont. Inst., Trudy, v. 83, 331 p. [In Russian]

Sarycheva, T. G., and Sokolskaya, A. N., 1952, Guide de détermination des brachiopodes Paléozoiques de la dépression de Moscou: Akad. Nauk. SSSR, Paleont. Inst., Trudy, v. 38, 307 p., 71 pls. [French translation S. I. G. no. 1814, 1956]

Skinner, J. W., and Wilde, A. L., 1955, New fusulinids from the Permian of west Texas: Jour. Paleontology, v. 29, no. 6, p. 927–940, pl. 89–96.

Tailleur, I. G., and others, 1958, Unusual upper Paleozoic rock sequence in northern Alaska [abstract]: Geol. Soc. America Bull., v. 69, no. 12, p. 1746–1747.

Toula, Franz, 1873, Kohlenkalk-Fossilien von der Südspitze von Spitzbergen: Akad. Wiss. Wien, Sitzungsber., v. 68, p. 267–291, pls. 1–5.

——— 1874, Kohlenkalk und Zechstein-Fossilien aus dem Hornsund an der Sud-Westküste von Spitzbergen: Akad. Wiss. Wien, Sitzungsber., v. 70, p. 133–156, 1 pl.

——— 1875, Permo-Carbon-Fossilien von der Westküste von Spitzbergen: Neues Jahrb. Mineralogie, Geologie, u. Paläeontologie, p. 225–264, pls. 5–10.

232. AGE OF THE KEECHELUS ANDESITIC SERIES OF THE CASCADE RANGE, WASHINGTON

By Jack A. Wolfe, Menlo Park, Calif.

The Keechelus andesitic series of Smith and Calkins (1906) is a thick sequence of andesitic lava, tuff, and breccia cropping out in an extensive area of the Cascade Range of Washington. The age of these rocks has previously been determined almost entirely by their stratigraphic position with respect to other rock units whose ages are uncertain. The one fossil previously reported from the Keechelus was determined as *Eporeodon* sp. by R. A. Stirton (Grant, 1941), but both the stratigraphic position within the Keechelus and the specific identity of the specimen are unknown.

Attempts to date the Keechelus andesitic series by its stratigraphic relations prove unsatisfactory because of the general lack of accurate knowledge of the age of the underlying units. The Keechelus rests conformably on rocks of the Puget group and unconformably on those of the Guye formation. The latter unit was dated as probably late Eocene on the basis of plants by R. W. Brown (Foster, 1960). The plants from the Guye formation identified by Brown definitely indicate an Eocene age, although Foster (1960) reevaluated the significance of Brown's determinations and concluded that the plants could equally well indicate a Paleocene age. The age of the Puget group has also been in doubt, but recent work demonstrates an early through latest Eocene age (Art. 233).

Conclusive evidence on age of the lower part of the Keechelus andesitic series has been obtained by analy-

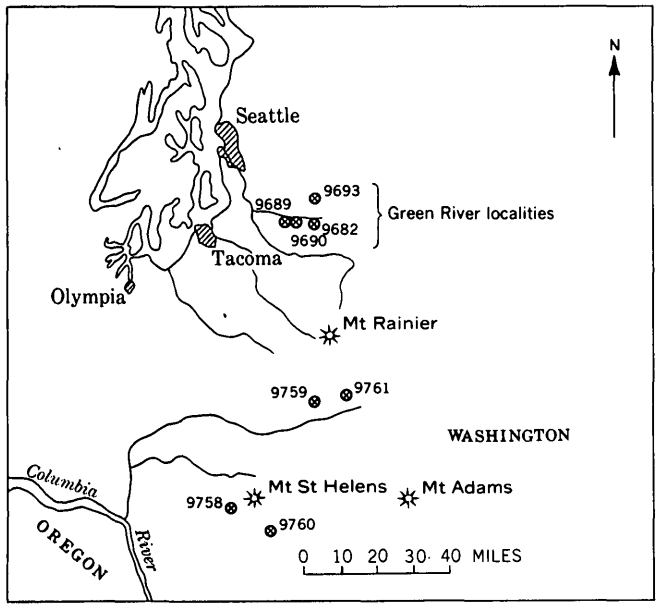

FIGURE 232.1.—Map of western Washington showing source of fossil plants in the Keechelus andesitic series. The numbers are U.S. Geological Survey paleobotanical locality numbers, listed below.

sis of fossil plants from eight new localities. These localities (fig. 232.1) lie in a continuous belt of andesitic volcanic rocks assigned to the Keechelus andesitic series (Waters, 1955) that extends south from the area east of Seattle (Warren and others, 1945) to the Mount St. Helens area.

The stratigraphic position of the plants at all of the localities is not precisely known, but those in the Green River valley east of Tacoma are almost certainly lower than those south of Mount Rainier (H. D. Gower, oral communication, 1961). The Green River localities occur 200 to 700 feet stratigraphically above the contact of the Keechelus with the underlying Puget group. The localities south of Mount Rainier are a few thousand feet higher stratigraphically and taken together may represent a stratigraphic range of considerable thickness.

Keechelus fossil localities in the Green River valley contain elements which superficially appear to represent different ages. Species characteristic of the Eocene flora are: *Macclintockia* sp., *Cryptocarya presamarensis* Sanborn, *Asplenium hurleyensis* of Sanborn, and *Aralia taurinensis* of Sanborn. Another group of species suggests an Oligocene age: *Cordia rotunda* Chaney and Sanborn, *Cupania oregona* Chaney and Sanborn, *Ocotea eocernua* Chaney and Sanborn, and *Tetracera oregona* Chaney and Sanborn. A third group of species is represented by *Laurophyllum raminervum* Rotbury and *Phyllites alchorneopsis* Potbury. This last group and the mixed character of the flora indicate a correlation with the La Porte flora of California (Potbury, 1935) and other floras of the same age as the informal Keasey "stage" of the invertebrate paleontologists. The flora from the uppermost part of the Puget group east of Seattle is essentially identical with that from the Keechelus in the Green River valley localities, but is not similar to the uppermost Puget flora of the Green River area. Thus, paleontologic evidence indicates that the uppermost part of the Puget group east of Seattle is correlative with the lowermost part of the Keechelus east of Tacoma.

The Keechelus localities south of Mt. Rainier have a flora differing from that of the Keechelus in the Green River valley. The former contains: *Cercidiphyllum crenatum* (Unger) Brown, *Prunus franklinensis* Sanborn, *P. pristina* Brown, *Ficus quisumbingi* Chaney and Sanborn, *F. plinerva* Chaney and Sanborn, *Meliosma aesculifolia* Chaney and Sanborn, *Alangium thomae* (Chaney and Sanborn) Lakhanpal, and other species that occur in the Goshen (Chaney and Sanborn, 1933) and Scio (Sanborn, 1947) floras of Oregon. These last two floras occur in nonmarine rocks equivalent to the lower and upper parts of the Lincoln "stage," respectively. Floras from two of the Keechelus localities (9758, 9759) appear to correlate with the Goshen flora, but the floras from localities 9760 and 9761 correlate with the Scio flora.

The evidence cited thus indicates that the lower part of the Keechelus andesitic series is the nonmarine equivalent of the Keasey and Lincoln "stages." This correlation was suggested by Waters (1955) on petrographic evidence. In turn, the upper part of the Keechelus can be no older than late Oligocene and may be as young as early Miocene.

PLANT FOSSIL LOCALITIES

9682. NW¼NW¼ sec. 36, T. 21 N., R. 7 E.
9689. SE¼NW¼ sec. 36, T. 21 N., R. 6 E.
9690. SE¼NW¼ sec. 36, T. 21 N., R. 6 E.
9693. NE¼NW¼ sec. 13, T. 21 N., R. 7 E.
9758. NW¼NW¼ sec. 32, T. 8 N., R. 4 E.
9759. SW¼NE¼ sec. 17, T. 13 N., R. 7 E.
9760. 6700 feet N., 30° W. from summit of Timbered Peak.
9761. 2500 feet N. of SW cor. sec. 9, T. 13 N., R. 9 E.

REFERENCES

Chaney, R. W., and Sanborn, E. I., 1933, The Goshen flora of west central Oregon: Carnegie Inst. Washington Pub. 439, 103 p.

Foster, R. J., 1960, Tertiary geology of a portion of the central Cascade Mountains, Washington: Geol. Soc. America Bull., v. 71, p. 99–126.

Grant, R. Y., 1941, A John Day vertebrate fossil discovered in the Keechelus series of Washington: Am. Jour. Sci., v. 239, p. 590–593.

Potbury, S. S., 1935, The La Porte flora of Plumas County, California: Carnegie Inst. Washington Pub. 465, p. 31–81.

Sanborn, E. I., 1947, The Scio flora of western Oregon: Oregon State College Mon., Studies in Geology, no. 4, 47 p.

Smith, G. O., and Calkins, F. C., 1906, Description of the Snoqualmie quadrangle, Washington: U.S. Geol. Survey Geol. Atlas, Folio 139.

Warren, W. C., Norbisrath, H., Grivetti, R. M., and Brown, S. P., 1945, Preliminary geologic map and brief description of the coal fields of King County, Washington: U.S. Geol. Survey Prelim. Map.

Waters, A. C., 1955, Volcanic rocks and the tectonic cycle: Geol. Soc. America Spec. Paper, No. 62, p. 702–722.

233. AGE AND CORRELATION OF THE PUGET GROUP, KING COUNTY, WASHINGTON

By JACK A. WOLFE, HOWARD D. GOWER, and JAMES D. VINE, Menlo Park, Calif.

Work done in cooperation with the Division of Mines and Geology of the Washington Department of Conservation

The Puget group, a thick sequence of predominantly continental coal-bearing sedimentary rocks, is one of the most widespread stratigraphic units in the Pacific Northwest. These rocks underlie a large area in the western foothills of the Cascade Range and in the Puget Sound lowlands of western Washington.

Fossil leaves are well preserved and abundant in the Puget group and, during the course of recent geologic investigations in King County, many of these leaves were collected from known stratigraphic positions. The localities where the fossils were collected are shown on figure 233.1, and the stratigraphic positions of the fossil collections are shown on figure 233.2.

In King County, the Green River has cut a canyon 200 to 300 feet deep, exposing an almost continuous section of about 5,600 feet of strata of the Puget group. The base of the Puget group is not exposed in the canyon, but its upper contact with the overlying Keechelus andesitic series of Warren and others (1945) is exposed. Coal beds, which crop out within the canyon and can be traced through underground mine workings into the adjacent hills, provide stratigraphic control for determining the position of floral zones within the Puget group. All of the 17 fossil flora localities shown in figure 233.1 south of the Cedar River can therefore be related with confidence to the stratigraphic section exposed in the canyon of

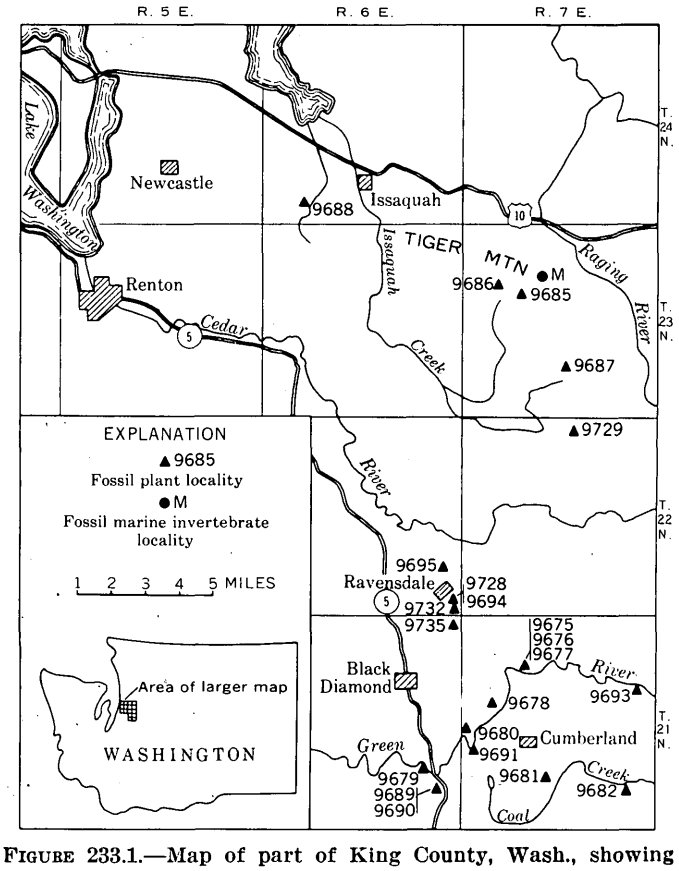

FIGURE 233.1.—Map of part of King County, Wash., showing localities where fossils were collected.

Green River. Fossil-leaf collections from these localities are within the Puget group and the lower part of the Keechelus andesitic series, and they can be grouped into 7 floral zones.

The characteristic species and correlative floras of each zone are summarized in table 233.1. The zones are established by means of two widely-used methods of biostratigraphy: detailed analysis of selected phylads to determine phylogenetic sequences, and overlap of ranges of selected species. The floral differences between any two successive zones are slight, and most of the species range through two or more zones; thus, species listed as characteristic of a particular zone are not necessarily restricted to it. Although most of the zones can be recognized elsewhere in the western United States, additional studies may prove them to be zonules.

The several floras known in the predominantly marine rocks of Eocene age in Washington, Oregon, and California permit a tentative correlation of the plant zones with the standard West Coast invertebrate megafossil chronology. The Comstock flora (Sanborn, 1935), which is placed in zone 6, occurs in the basal part of the Keasey and uppermost part of the "Tejon" stages (Vokes and others, 1951). The undescribed Cowlitz flora, which is in zone 5, is in beds assigned, as a bulk unit, to the "Tejon" stage (Weaver and others, 1944). Zone 3 has been recognized near Elkton, Ore., in predominantly marine beds assigned to the upper part of the "Domengine" stage. The Chalk Bluffs flora (zone 1) is in a nonmarine facies of the Ione formation of California (MacGinitie, 1941) which is part of the "Capay" stage (early Eocene). The floral zones in the Puget group can also be recognized in the nonmarine Clarno formation of Oregon and in beds near La Porte, California (table 233.1).

Leaf fossils were also collected from several localities near Tiger Mountain and Issaquah, 10 to 15 miles north of the Green River area. The oldest rocks in the Tiger Mountain area are a thick sequence of marine sedimentary rocks that contain marine mollusks of middle Eocene age (F. Stearns MacNeil, written communication, Nov. 9, 1960). These rocks are probably equivalent in part to the nonmarine rocks of floral zones 2 and 3 in the Green River area.

Overlying the marine rocks in the Tiger Mountain area are continental coal-bearing sedimentary rocks 1,000 to 2,000 feet thick that are in turn overlain by volcanic rocks more than 8,000 feet thick, the Eocene volcanic series of Warren and others (1945). The volcanic rocks contain a flora similar to that in zone 4, and are therefore considered to be laterally equivalent to the part of the coal-bearing sedimentary se-

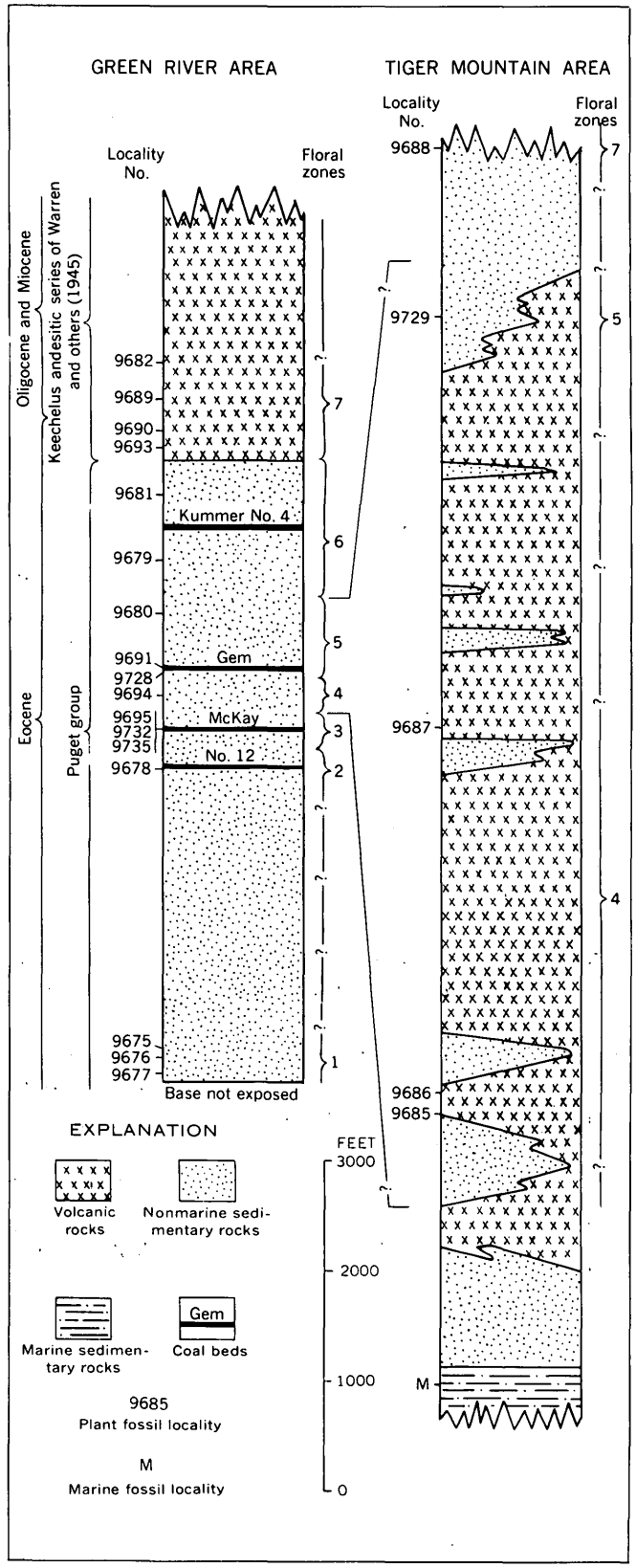

FIGURE 233.2.—Stratigraphic sections in King County, Wash., showing positions of fossil collections and floral zones.

TABLE 233.1.—*Summary of floral zones in the Puget group*

Series	Pacific Coast standard marine megafaunal stages [1]	Floral zones	Characteristic species in the Green River area [h.o. denotes highest known occurrences and l.o. denotes lowest known occurrence of species present in more than one zone]	Correlative floras
Oligocene	Keasey	7	*Macclintockia* sp.; *Tetracera oregona*, l.o.; *Cryptocarya presamarensis*, h.o.; *Ocotea eocernua*, l.o.; *Laurophyllum raminervum*; *Phyllites alchorneopsis*.	La Porte
		6	*Mallotus oregonensis*; *Cinnamomum dilleri*, h.o.; *Platanophyllum angustiloba*, h.o.; *Cryptocarya presamarensis*, l.o.; *Laurophyllum* aff. *L. litseafolia* h.o.; *Cercidiphyllum elongatum*, h.o.; *Alnus* sp. "B", h.o.	Comstock (Sanborn, 1935) Clarno (in part)
	"Tejon"	5	*Carya* sp., h.o.; *Alnus* sp. "A", l.o.; *Rhus* sp., h.o.; *Castanopsis longietiolata*, h.o.; *Laurophyllum* aff. *L. litseafolia*, l.o.; *Viburnum* sp.	Cowlitz
	------? ------			
Eocene	"Transition" beds	4	*Ardisia* sp.; *Hemitelea pinnata*, h.o.; *Triumfelta* sp., h.o.; *Platanophyllum angustiloba*, l.o.; *Laurophyllum litseafolia*, h.o.; *Ulmus* sp. "B", h.o.; *Machilus* sp., h.o.; *Cupania* sp.; *Alnus* sp. "B", h.o.; *Anemia eocenica*, h.o.	(None known)
	------? ------			
	"Domengine"	3	*Ficus omballi*; *Alnus* sp. "B", l.o.; *Machilus* sp. l.o.; *Carya* sp., l.o.; *Ulmus* sp. "B", l.o.; *Engelhardtia nevadensis*, h.o.	Elkton
		2	*Microcos* sp.; *Phytocrene* sp.; *Triumfelta* sp., l.o.; *Juglans* sp.; *Rhus* sp., l.o.; *Ulmus* sp. "A", h.o.; *Pericampylus* sp.; *Rhamnus plena*, h.o.; *Stephania* sp.	Clarno (in part)
	------? ------			
	"Capay"	1	*Laurophyllum litseafolia*, l.o.; *Mallotus riparius*; *Ulmus* sp. "A", l.o.; *Rhamnus plena*, l.o.; *Gordonia egregia*.	Chalk Bluffs (MacGinitie, 1941)

[1] Weaver and others (1944).

quence assigned to zone 4 in the Green River area. South of Tiger Mountain, at locality 9729, the volcanic rocks are overlain by coal-bearing sedimentary rocks that contain the flora of zone 5.

The volcanic rocks of the Tiger Mountain area extend westward nearly to Lake Washington. They are overlain on the north by nonmarine coal-bearing sedimentary rocks of the Puget group which are about 3,000 feet thick. Locality 9688 near Issaquah is in the Puget group, and is about 1,000 feet stratigraphically above the contact with the volcanic rocks. The rocks at this locality contain a zone 7 flora, which in the area of the Green River is in the lower part of the Keechelus andesitic series of Warren and others (1945). The paleobotanical evidence, therefore, indicates that the upper part of the Puget group northwest of Tiger Mountain is equivalent to strata in the lower part of the Keechelus along the Green River.

REFERENCES

MacGinitie, H. D., 1941, A middle Eocene flora from the central Sierra Nevada: Carnegie Inst. Washington Pub. 534, 178 p.

Sanborn, E. I., 1935, The Comstock flora of west central Oregon: Carnegie Inst. Washington Pub. 465, p. 1–28, 10 pls.

Vokes, H. E., Snavely, P. D., Jr., and Myers, D. A., 1951, Geology of the southern and southwestern border area, Willamette Valley, Oregon: U.S. Geol. Survey Oil and Gas Inv. OM–110.

Warren, W. C., Norbisrath, Hans, Grivetti, R. M., and Brown, S. P., 1945, Preliminary geologic map and brief description of the coal fields of King County, Washington: U.S. Geol. Survey Prelim. Map.

Weaver, C. E., and others, 1944, Correlation of the marine Cenozoic formations of western North America (chart 11): Geol. Soc. America Bull., v. 55, no. 5, p. 569–598.

234. EARLY MISSISSIPPIAN FAUNAS IN SOUTHWESTERN ELKO COUNTY, NEVADA

By MACKENZIE GORDON, Jr., and HELEN DUNCAN, Washington, D.C.

Early Mississippian faunas under study occur in rocks along the western flanks of the Pinyon and Sulphur Springs Ranges in the Carlin and Pine Valley quadrangles and at two localities on the east side of the ranges in the Dixie Flats and Robinson Mountain quadrangles. These four 15-minute quadrangles are being mapped by J. F. Smith and K. B. Ketner, who have established the general stratigraphic sequence and areal relations of the units, and found and collected fossils from the localities shown on figure 234.1. The rocks are dark brown and gray shale and yellow siltstone, marl, and calcareous sandstone, locally intercalated with conglomerate in beds and lenses as much as 500 feet thick. This facies resembles that of the Diamond Peak formation at its type locality in the Eureka district, about 40 miles south of the southern-most outcrop studied, but the fossils show that the Elko County beds are mostly Early Mississippian in age, whereas those of the Diamond Peak formation are Late Mississippian.

The Early Mississippian beds, except where faulted locally against Late Mississipian and Pennsylvanian rocks (particularly in the northern part of the area) are overlain unconformably by Permian rocks. The beds immediately beneath the unconformity are of somewhat different ages at different localities, the older ones occurring at the southern end of the belt of outcrop.

The oldest Mississippian assemblage occurs in the Pine Valley quadrangle about a mile south of Papoose Canyon. Approximately 35 species occur in gray limestone pods in shale and include fragmentary corals, together with brachiopods and many mollusks. The important fossils at one locality include *Menophyllum*? sp. B, *Cyathaxonia* sp., *Tetracamera*? cf. *T. subtrigona* (Meek and Worthen), *Spirifer* aff. *S. grimesi* Hall, *Dimegelasma* cf. *D. plenum* (Hall), and *Protocanites lyoni* (Meek and Worthen). The brachiopods resemble Osage species, but the goniatite *P. lyoni* has long been considered to be confined to a relatively narrow stratigraphic zone in the late Kinderhook of the United States and the late Tournaisian of northwestern Europe.

A dominantly brachiopod assemblage similar to that of the beds with *Protocanites* is found at several localities in the Pine Valley quadrangle between Papoose Canyon and Trout Creek. The principal species are *Leptagonia* cf. *L. analoga* (Phillips), *Setigerites* sp., *Labriproductus* cf. *L. wortheni* (Hall), *L.* aff. *L. keokuk* (Hall), *Spirifer* aff. *S. grimesi* Hall, *S.* aff. *S. marionensis* Shumard, *S.* aff. *S. missouriensis* Swallow, *Dimegelasma* cf. *D. plenum* (Hall), and *Cleiothyridina* aff. *C. tenuilineata* (Rowley). A similar fauna occurs in the Dixie Flats quadrangle 4 miles southwest of the summit of Grindstone Mountain in rocks mapped by Dott (1955, fig. 5) as "White Pine-like shale and quartzite."

The southeasternmost occurrence of this fauna is in the Robinson Mountain quadrangle 4 miles south and about half a mile east of the summit of Robinson Mountain. Echinoid spines, brachiopods, and pelecypods occur in light-gray siliceous siltstone, the more common species being *Chonetes* aff. *C. illinoisensis* Worthen, *Labriproductus* cf. *L. wortheni* (Hall), *Rhipidomella* aff. *R. theimei* (White), *Spirifer* aff. *S. shepardi* Weller, *S.* aff. *S. missouriensis* Swallow, and *Torynifer* aff. *T. cooperensis* (Swallow).

What appears to be the youngest faunule of this shale sequence in the Pine Valley quadrangle occurs about ¾ mile north of Papoose Canyon. A collection from 75 feet of dark-gray shale with scattered thin limestone pods contain some significant corals associated with brachiopods. Thirty feet higher is a conglomerate overlain by limestone of Permian age. The fossils include *Menophyllum*? cf. sp. A., *Trochophyllum* sp., *Permia* sp., *Amplexizaphrentis* cf. *A. welleri* (Grove), "*Amplexus*" sp., *Cyathaxonia* sp., *Leptagonia* cf. *L. analoga* (Phillips), *Setigerites* sp., *Schizophoria* sp. A, *Spirifer* aff. *S. imbrex* Hall, *S.* aff. *S. floydensis* Weller, *Cleiothyridina* cf. *C. incrassata* (Hall), *Straparollus* (*Euomphalus*) sp., and *Loxonema* sp. The corals in this faunule resemble those of the New Providence shale at Buttonmould Knob, Ky.

In the Carlin quadrangle all the Early Mississippian fossils occur in light creamy gray shale and yellow calcareous siltstone and sandstone. These beds probably are slightly younger than those previously discussed, the fauna resembling that of the late Osage shale beds of north-central Kentucky. Collections were made through 250 feet of section on Ferdelford Creek. The lower 100 feet contains an assemblage of corals, bryozoans, brachiopods, and ostracodes along with several mollusks. The principal fossils are *Menophyllum*? sp. A, *Leptagonia* cf. *L. analoga* (Phillips), *Setigerites* n. sp. A, *Schizophoria* sp. A, *Spiriffer* aff. *S. imbrex* Hall, *S.* aff. *S. floydensis* Weller, *Dimegelasma* cf. *D. neglectum* (Hall), *Cleiothyridina* cf. *C.*

601530 O—61——16

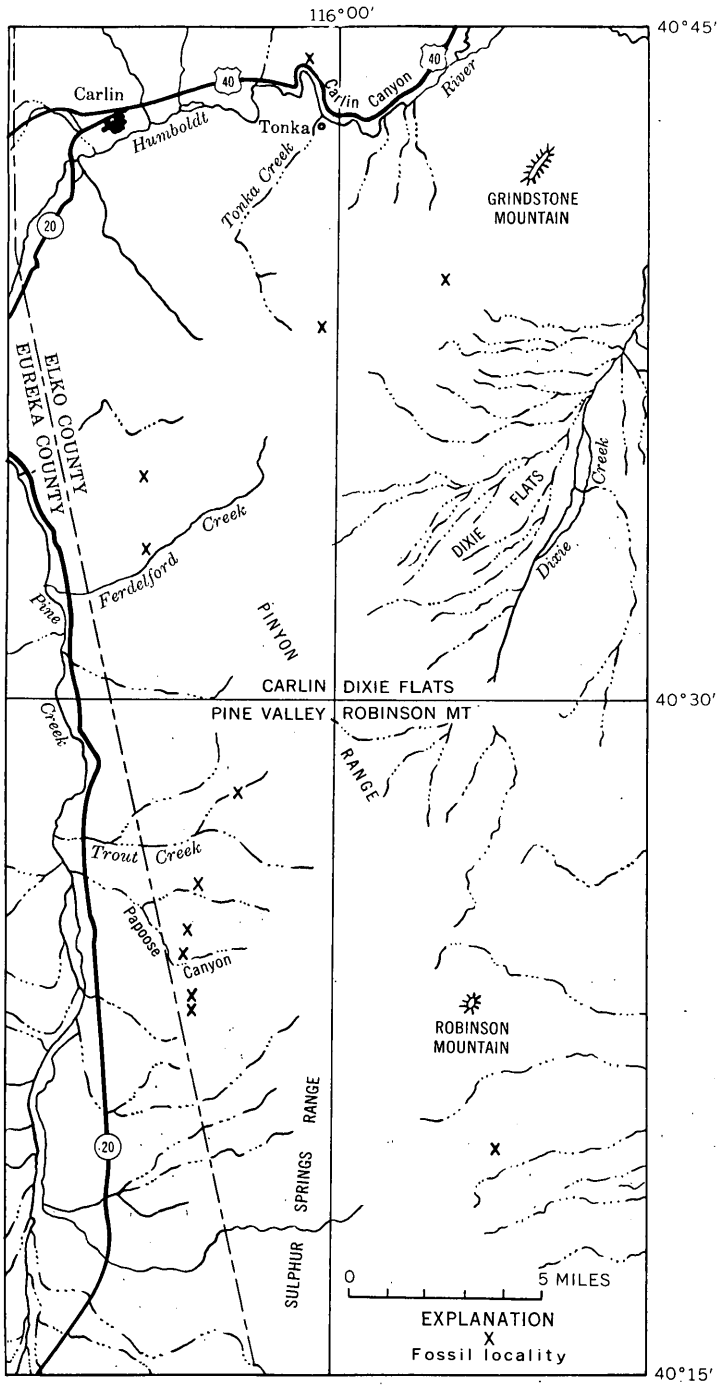

FIGURE 234.1.—Map showing Early Mississippian localities in southwestern Elko County, Nev.

glenparkensis Weller, *Composita* cf. *C. pentagona* Weller, *Straparollus* (*Euomphalus*) sp., and *Loxonema* sp. These are mostly Osage forms.

In a 22-foot zone 90 feet higher, the beds contain compound and solitary corals, bryozoans, brachiopods, and ostracodes. The fauna includes "*Menophyllum*" sp., *Siphonodendron* n. sp., *Diphyphyllum* sp., *Spirifer* aff. *S. floydensis* Weller, *S.* aff. *S. subaequalis* Hall, and *Cleiothyridina* cf. *C. glenparkensis* Weller.

The uppermost fossiliferous bed, 24 feet higher, is an 8-foot marl containing a distinctive large ramose stenoporoid bryozoan. With it occur *Lithostrotionella* sp., *Spirifer* aff. *S. floydensis* Weller, and *Composita* cf. *C. pentagona* Weller.

The phaceloid lithostrotionoid corals in the 22-foot zone described above suggest a possible early Meramec age for the uppermost beds here. Moreover, collections made for microfossils believed to have come from the upper part of this section contain such Late Mississippian elements as *Worthenopora* cf. *W. spinosa* Ulrich, *Coryellina* sp., and *Bairdiolites* sp. (the ostracodes identified by I. G. Sohn).

Near the western end of Carlin Canyon, a similar faunule occurs in rocks of similar lithology. The lower 100 feet of a measured section contains about the same species as the lower 100 feet of the Ferdelford Creek section. The occurrence near the top of this zone of a new species of the Keokuk bryozoan genus *Cyclopora* is of particular interest.

Fossils from a 15-foot zone 150 feet above the base of the same section include another distinctive large ramose stenoporoid bryozoan together with *Menophyllum*? sp., new genus aff. *Canadiphyllum*, and *Dimegelasma* cf. *D. neglectum* (Hall).

Dott (1955, fig. 3) mapped the yellow calcareous siltstone in west Carlin Canyon with his Tonka formation but he pointed out (p. 2232) that it may be below the Tonka or interbedded with the lower part. The Tonka type section (Dott, 1955, p. 2222, 2292, 2293), however, contains beds of Late Mississippian and Early Pennsylvanian age only, equivalent to the upper part of the Diamond Peak formation and the lower part of the Ely limestone in the Eureka district.

Possible wider distribution in Elko County of this Lower Mississippian fine clastic facies is indicated by Dott's mention of a similar faunule in black shale 5 miles northwest of Elko (Dott, 1955, p. 2230) and by the occurrence of *Protocanites lyoni* (Meek and Worthen), identified by Furnish, Miller, and Youngquist (1955), in black shale in the Pequop Range, 20 miles east of Wells, Nev.

REFERENCES

Dott, R. H., Jr., 1955, Pennsylvanian stratigraphy of Elko and northern Diamond Ranges, northeastern Nevada: Am. Assoc. Petroleum Geologists Bull., v. 39, no. 11, p. 2211–2305.

Furnish, W. M., Miller, A. K., and Youngquist, Walter, 1955, Discovery of the Early Mississippian goniatite *Protocanites* in northeastern Nevada: Jour. Paleontology, v. 29, no. 1, p. 186.

235. CONTINENTAL VERTEBRATES AND THEIR STRATIGRAPHIC CORRELATION WITH MARINE MOLLUSKS, EASTERN CALIENTE RANGE, CALIFORNIA

By C. A. Repenning and J. G. Vedder, Menlo Park, Calif.

Five and possibly six North American provincial (mammalian) ages, as defined by Wood and others (1941), are represented by vertebrate faunas in upper Tertiary rocks of the eastern part of the Caliente Range. This record of superimposed mammalian assemblages is equalled at few places in the world. By tracing fossiliferous beds, faunas representing three of these ages can be correlated with assemblages of abundant marine mollusks in this same area.

The eastern part of the Caliente Range is composed primarily of clastic sedimentary rocks of Miocene and Pliocene age that attain a thickness of over 16,500 feet near Caliente Mountain (fig. 235.1). These rocks have been mapped in detail from the Caliente Mountain area eastward for a distance of about 16 miles to the eastern end of the range, where they apparently are less than 2,500 feet thick. The Miocene part of the thick stratigraphic succession grades eastward from a dominantly marine facies into largely nonmarine deposits.

The continental deposits into which the marine beds grade, and some of the overlying nonmarine beds that have no marine equivalents in the eastern Caliente Range, have been described as the Caliente formation by Hill, Carlson, and Dibblee (1958). The Caliente formation in this area contains vertebrate faunas referable to the Arikareean, Hemingfordian, Barstovian, Clarendonian, and Hemphillian ages of Wood and others.[1] Continental beds about 2,300 feet stratigraphically above the top of the Caliente formation contain vertebrates that suggest a Blancan age.

Arikareean age.—Vertebrate fossils of Arikareean age, listed in table 235.1, have been found only in the eastern part of the Caliente Range, from the area indicated by section 2, figure 235.2, to a point about 3 miles east of section 3 where fossil mammals occur as low as 700 feet above the base of the Soda Lake member[2] of the Vaqueros formation. Two thousand feet to the west of these stratigraphically lowest vertebrate localities the mammal-bearing beds intertongue with marine sandstone in the upper part of the Soda Lake member. This sandstone contains *Turritella inezana* and *Lyropecten magnolia*, forms that presumably are restricted to strata of early Miocene age.

[1] The United States Geological Survey has not adopted the North American provincial (mammalian) ages of Wood and others for official usage.

[2] Nomenclature of Hill, Carlson, and Dibblee, 1958.

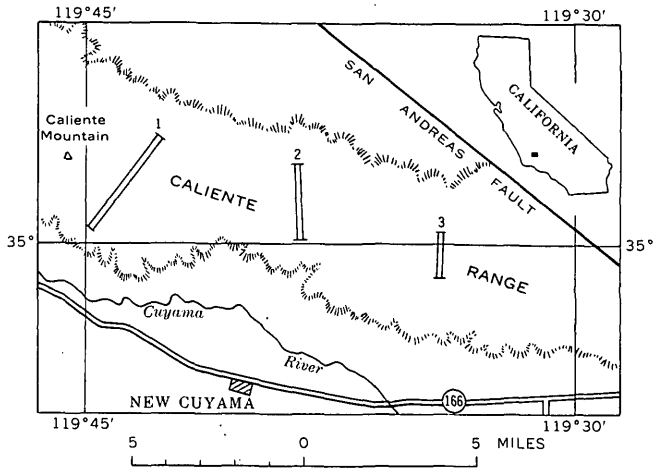

FIGURE 235.1.—Eastern Caliente Range showing location of sections in figure 235.2.

The youngest mammals believed to be of Arikareean age are from beds that can be traced into the top of the Painted Rock sandstone member[2] of the Vaqueros formation, which locally contains *Turritella inezana*, *Rapana vaquerosensis*, *Lyropecten miguelensis*, and "*Crassatella*" *granti*. These mollusk species also are present in the lower 500 feet of the Saltos shale member[2] of the Monterey shale in the central and western parts of the eastern Caliente Range between section 2 and Caliente Mountain.

Mammalian faunas from beds that are laterally equivalent to the basal part of the Saltos shale member are tentatively assigned an Arikareean age. From these nonmarine beds east of section 2, D. E. Savage of the University of California collected a small dromomerycine at a point about 200 feet stratigraphically above the highest Arikareean fanna and an equal distance below the lowest known Hemingfordian fauna. Dougherty (1940, fig. 3, C.I.T. loc. 325) lists "Merycoidodont" from about the same position in the section.

If the small dromomerycine is of Arikareean age, the Arikareean-Hemingfordian boundary falls close to the boundary between the early and middle Miocene as based upon the larger marine invertebrates; if this deerlike animal is of Hemingfordian age, there is, in the Caliente formation only slight disagreement about the boundary.

The stratigraphically lowest beds of Arikareean age have not been determined in the Caliente Range.

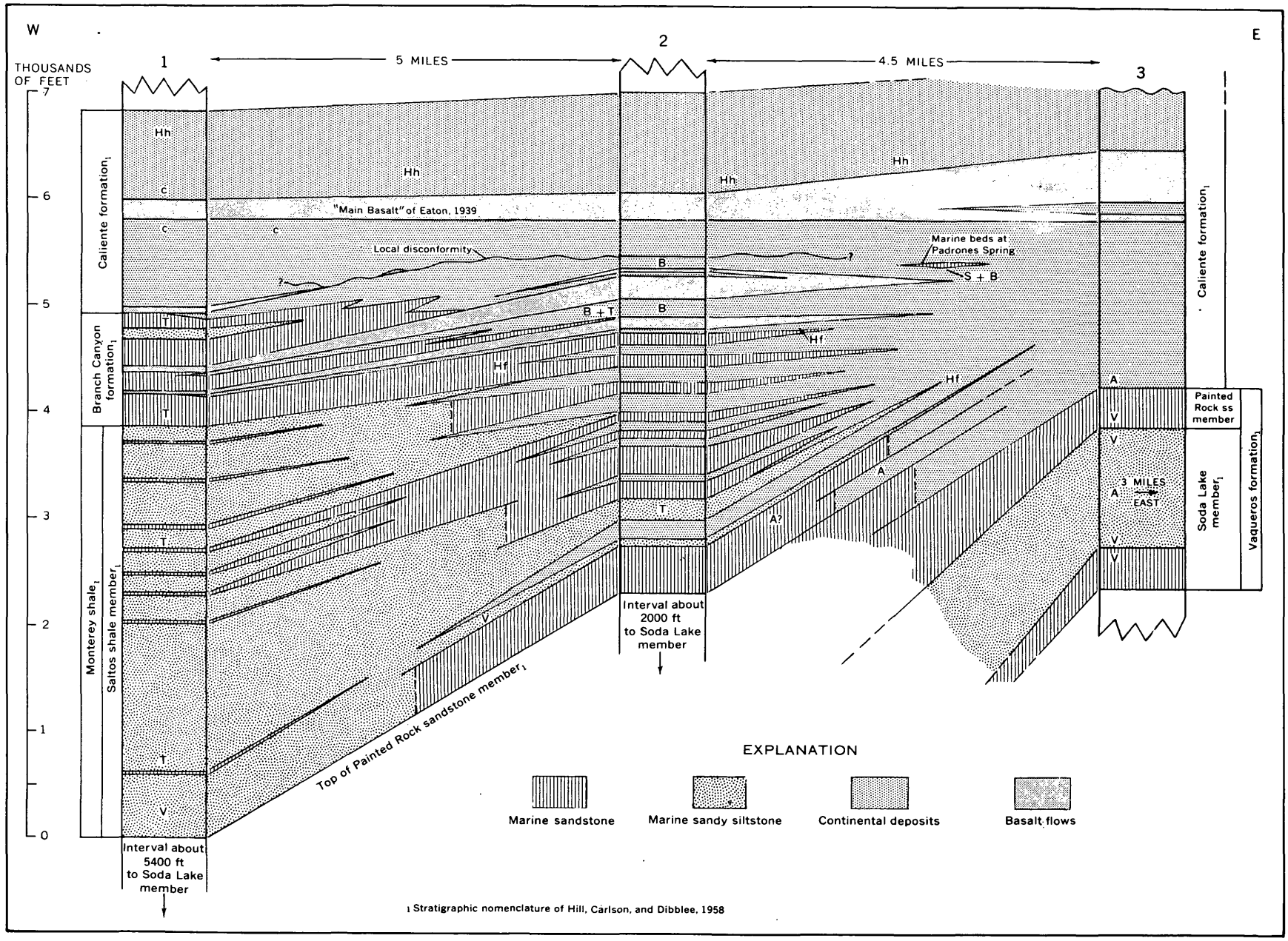

FIGURE 235.2.—Stratigraphic diagram of rocks of Miocene and Pliocene age in the eastern Caliente Range. Vertical dashed line marks arbitrary boundary in area of intricate intertonguing. B, Hh, and the like show approximate stratigraphic location and also indicate age of collections of diagnostic fossils; explanation given on table 235.1.

TABLE 235.1.—*Correlation of faunal divisions based upon vertebrates and mollusks from the eastern Caliente Range showing discrepancies between continental and marine age assignments*

Faunal divisions and age assignments based upon vertebrates			Faunal divisions and age assignments based upon mollusks			
Age names applied to continental beds in North America and their correlation with Lyellian epochs as proposed by Wood and others (1941) [1]		Continental vertebrates collected from the Caliente formation of the eastern Caliente Range (Identifications by C. A. Repenning)	Selected common mollusk species from assemblages that suggest faunal divisions in marine strata of the eastern Caliente Range (Identifications by J. G. Vedder)		Informal stage names based upon marine megafaunas of the Pacific Coast and their correlation with Lyellian epochs as proposed by Weaver and others (1944) [2] and Durham (1954) [2]	
Middle Pliocene	Hemphillian Hh[3]	megalonychid[5] leporid felid[5] *Pliohippus* cf. *P. osborni* Frick camelid *Capromeryx* cf. *C. altidens* (Matthew)	Marine faunas not known to be present			
Early Pliocene	Clarendonian C[3]	felid[5] *Pliohippus* cf. *P. tehonensis* (Merriam) *Pliohippus* cf. *P. leardi* (Drescher)[5]	---?---			
Late Miocene	Barstovian B[3]	crocodilian[6] *Tomarctus* sp.[6] rhinocerotid[9] *Archaeohippus mourningi* (Merriam)[6] *Hypohippus* sp.[9] *Merychippus brevidontus* Bode *Merychippus sumani* Merriam[6] *Merychippus* sp. *Dyseohyus* sp. *Ticholeptus calimontanus* (Dougherty)[7 9] *Protolabis*? sp. *Dromomeryx* sp. or *Rakomeryx* sp.	*Turritella carisaensis padronesensis* Grant and Eaton[10] *"Siphonalia" danvillensis* Clark *Lyropecten* cf. *L. estrellanus* (Conrad)[11]		"Neroly" "Cierbo" "Briones"[4] S[3]	Late Miocene
Middle Miocene	Hemingfordian Hf[3]	*Amphicyon* aff. *A. frendens* Matthew *Archaeohippus ultimus* (Cope) *Parahippus*? sp. *Merychippus carrizoensis* Dougherty *Merychippus* cf. *M. seversus* (Cope) *Hesperhys vagrans* Douglass *Prosthennops*? sp. *Ticholeptus calimontanus* (Dougherty) camelid *Dromomeryx*? sp.[7 8]	*Ficus (Trophosycon) ocoyana* (Conrad)[12] *Kelletia posoensis* (Anderson and Martin) *Macron merriami* Arnold *Bruclarkia barkerianum* (Cooper) [?= *B. geniculata* (Conrad)] [12] *"Phos" dumbleanus* Anderson *in* Hanna *Nassarius antiselli* (Anderson and Martin) *Oliva californica* Anderson [12] *"Cancellaria" condoni* Anderson [12] *Conus owenianus* Anderson [12] *Megasurcula keepi* (Arnold) *Turricula wilsoni* (Anderson and Martin) [12] *Strioterebrum cooperi* (Anderson) *Anadara osmonti* (Dall) *Saccella ochsneri* (Anderson) *Aequipecten andersoni* (Arnold) *Dosinia mathewsonii* (Gabb) *Chione temblorensis* (Anderson)[12] *Chione panzana* Anderson and Martin	Age range of *Turritella ocoyana* Conrad and *Turritella ocoyana topangensis* Merriam in the eastern Caliente Range	"Temblor" T[3]	Middle Miocene
Early Miocene	Arikareean A[3]	*Archaeolagus* sp. *Miohippus* sp. or *Archaeohippus* sp. *Parahippus* sp. chalicotheriid oreodont *Oxydactylus brachyodontus* Peterson [?= *Paratylopus cameloides* (Wortman)] *Parablastomeryx* aff. *P. falkenbachi* Frick dromomercine [5]	*Turritella inezana* Conrad *Turritella inezana hoffmannii* Gabb *Turritella inezana altacorona* Loel and Corey *Rapana vaquerosensis* (Arnold) *"Lyropecten" magnolia* (Conrad) *Lyropecten miguelensis* (Arnold) *"Crassatella" granti* (Wiedey)		"Vaqueros" V[3]	Early Miocene

[1] These age names not officially used by the U.S. Geological Survey.
[2] These informal stage names not officially used by the U.S. Geological Survey.
[3] Symbol used on figure 235.2 to indicate approximate stratigraphic location of selected diagnostic collections.
[4] These three "stages" often are collectively referred to the "Santa Margarita stage" in southern California.
[5] Collected by University of California (D. E. Savage, oral communication, 1960).
[6] Vertebrates found with a middle Miocene marine mollusk fauna which includes: *Melongena californica* Anderson and Martin, *Anadara topangaensis* Reinhart, *Crassostrea* cf. *C. altatemblorensis* Grant and Eaton, *Crassostrea* aff. *C. ashleyi* Hertlein.
[7] Collected by J. F. Dougherty (1940).
[8] Resembles *Dromomeryx borealis* (Cope) according to Dougherty (1940).
[9] Vertebrates found with or stratigraphically near the late Miocene marine mollusk fauna at Padrones Spring.
[10] The typical form of *Turritella carisaensis* locally ranges down into strata of middle Miocene age in the eastern Caliente Range.
[11] This species ranges into strata of middle Miocene age at localities outside the eastern Caliente Range.
[12] These species range into strata of early Miocene age in the eastern Caliente Range but are uncommon or rare in rocks of this age.

Hemingfordian age.—The oldest vertebrate assigned a Hemingfordian age was collected from the Caliente formation 2 miles east of section 2 about 100 feet above a conspicuous marine tongue that contains the stratigraphically highest occurrence of diagnostic early Miocene mollusks in the area of section 2. The youngest mammals assigned to the Hemingfordian are from a locality near section 2 and about 30 feet below the lowest of three basalt flows called the "triple basalts" by Eaton (1939, pl. 4). These basalt flows form prominent markers throughout most of the eastern Caliente Range. All Hemingfordian mammal localities are from beds that intertongue with the marine Saltos shale member of the Monterey shale or with the Branch Canyon formation.[2] These marine units contain large mollusk assemblages similar to faunas from other areas that are assigned a middle Miocene age in California.

The Hemingfordian fauna of the Caliente formation shown on table 235.1 contains four species of horses. All four have been found in one quarry in a 3-foot-thick bed, the type locality of *Merychippus carrizoensis* (Dougherty, 1940, p. 130–133). Although *M. carrizoensis* is generally considered indicative of a Hemingfordian age, its occurrence with the other horses suggest that the entire fauna should be considered late Hemingfordian or possibly even early Barstovian. The few specimens referred to *Merychippus* cf. *M. seversus* are indistinguishable from individuals of this species from the Mascall formation of late Miocene age in eastern Oregon. *Archaeohippus ultimus* is also a Mascall form.

The generic assignment of the horse called *Parahippus?* sp. is debatable although it is represented by a large number of specimens. It is morphologically intermediate between a large and progressive parahippine as *Parahippus leonensis* Sellards and *Merychippus brevidontus* Bode. The enamel pattern of the upper cheek teeth is nearly identical to that of *M. brevidontus* from the overlying beds of Barstovian age. It is less hypsodont than *M. brevidontus* and has less or no cementation, being quite variable in this respect.

Barstovian age.—Vertebrate fossils of Barstovian age (table 235.1) are relatively abundant in the Caliente formation. They have been found through the section from about 10 feet above the lowest flow of the "triple basalts" to about 200 feet above the middle of these flows in the area of section 2 on figure 235.2. Near Caliente Mountain, in the area of section 1 of figure 235.2, the "triple basalts" are in the Branch Canyon formation, which is laterally continuous with the Caliente formation. In this area the highest typical middle Miocene mollusk fauna is about 35 feet below the highest flow of the "triple basalts" (about 960 feet above the middle of the three flows). Except at Padrones Spring, all Barstovian faunas of the Caliente formation are from beds that have been traced into marine rocks that contain mollusk assemblages assigned a middle Miocene age. At Padrones Spring, a marine lens with a meager molluscan fauna (including *Turritella carisaensis padronsensis* and "*Siphonalia*" *danvillensis*, which suggest a late Miocene age) contains mammals of Barstovian age. These youngest marine beds of the eastern Caliente Range are not continuous with marine rocks to the west but presumably represent a northward extension of a marine basin that lay chiefly to the south.

The apparent upper limit of beds of Barstovian age in the Caliente formation is marked locally by a disconformity. The disconformity has been recognized only in the central part of the eastern Caliente Range where the upper flow of the "triple basalts" has been cut out (fig. 235.2). Near section 1, figure 235.2, strata about 600 feet thick separate the upper flow of the "triple basalts" from the lowest fossils of Clarendonian age. No mammals have been found in these intervening beds, and they may be deposits of Barstovian age in part younger than the disconformity.

Clarendonian age.—Few vertebrate fossils of Clarendonian age have been found in the Caliente formation of the eastern Caliente Range (table 235.1). In most of the area the part of the formation that is of this age contains a conspicuous unit composed of several flows. This unit was called the "main basalt" by Eaton (1939, pl. 4). Fossils of Clarendonian age have been found in beds about 150 feet below to about 30 feet above the "main basalt" in the area between sections 1 and 2. In the Pacific Coast region faunas of Clarendonian age have been separated into two groups; in some areas the lower group is generally found interbedded with strata containing late Miocene mollusks, and the upper group with strata containing Pliocene mollusks (Savage, 1955). The known mammalian fauna of the Caliente formation is not adequate to identify upper and lower parts of the Clarendonian fauna.

Hemphillian age.—The stratigraphically lowest occurrences of fossil vertebrates of Hemphillian age in the Caliente formation are about 100 feet above the "main basalt" and the highest about 400 feet above the same unit. In the area of section 1, figure 235.2, the youngest fossils of Hemphillian age are found about 250 feet below the top of the Caliente formation.

REFERENCES

Dougherty, J. F., 1940, A new Miocene mammalian fauna from Caliente Mountain, California: Carnegie Inst. Washington Pub. 514, p. 109–140.

Durham, J. W., 1954, The marine Cenozoic of southern California, Pt. 4, *in* Chap. III of Jahns, R. H., ed., Geology of southern California: California Div. Mines Bull. 170, p. 23–31.

Eaton, J. E., 1939, Geology and oil possibilities of Caliente Range, Cuyama Valley, and Carrizo Plain, California: California Jour. Mines and Geology, v. 35, no. 3, p. 255–274.

Hill, M. L., Carlson, S. A., and Dibblee, T. W., Jr., 1958, Stratigraphy of Cuyama Valley-Caliente Range area, California: Am. Assoc. Petroleum Geologists Bull., v. 42, no. 12, p. 2973–3000.

Savage, D. E., 1955, Nonmarine lower Pliocene sediments in California: California Univ. Pub. Geol. Sci., v. 31, no. 1, p. 1–26.

Weaver, C. E., and others, 1944, Correlation of the marine Cenozoic formations of western North America: Geol. Soc. America Bull., v. 55, p. 569–598.

Wood, H. E., and others, 1941, Nomenclature and correlation of the North American continental Tertiary: Geol. Soc. America Bull., v. 52, p. 1–48.

236. STRATIGRAPHIC DISTRIBUTION OF ENDOTHYRID FORAMINIFERA IN CARBONIFEROUS ROCKS OF THE MACKAY QUADRANGLE, IDAHO

By Betty A. L. Skipp, Denver, Colo.

Preliminary studies of Carboniferous endothyrid Foraminifera from three measured sections in the Mackay quadrangle, Idaho (fig. 236.1) indicate that the endothyrids are valuable for the interpretation of gross stratigraphic relations in the thick sequence of miogeosynclinal sedimentary rocks of the area. The measured sections (fig. 236.2) contain rocks presently assigned to the Brazer limestone (Sando and others, 1959, p. 2768) and to an unnamed formation that interfingers with the Brazer limestone and which is described by Ross (1960, p. B–232–233) as containing lithologic equivalents of the Milligen and Wood River formations and the Brazer limestone, with detrital rocks predominant over limestones. Endothyrid Foraminifera indicate that both formations, as represented in the three measured sections, range in age from Early Mississippian (Osage, possibly Kinderhook) to at least Early Pennsylvanian (Morrow).

Studies of megafossils from the Mackay quadrangle indicate that the Brazer and associated beds are Late Mississippian in age at most places, and are Pennsylvanian in age at a few (Anderson, 1929, p. 11; Umpleby, 1917, p. 28; Ross, 1960, p. B232; Skipp, 1961).

Girty (*in* Anderson, 1929, p. 11) identified an upper Mississippian fauna from beds stratigraphically equivalent to the mudstone beds 350–750 feet above the dolomite of the Timbered Dome section. He also assigned a collection of fossils from the limestones above the lower zone of jasperoid of the same section to the Upper Mississippian, but with some doubt. No fossils were found in the more than 650 feet of light-gray weathering dolomite and quartzitic sandstone at

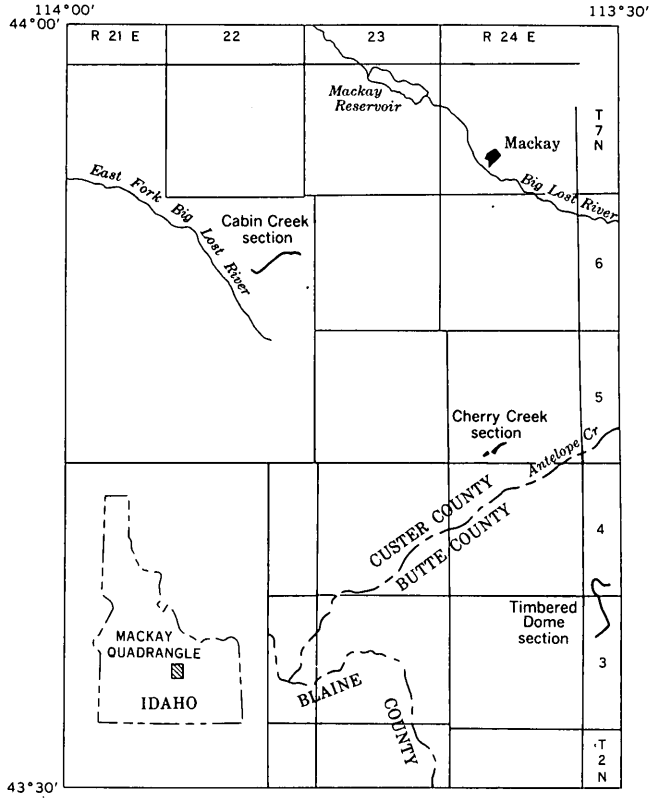

Figure 236.1.—Index map of Mackay quadrangle.

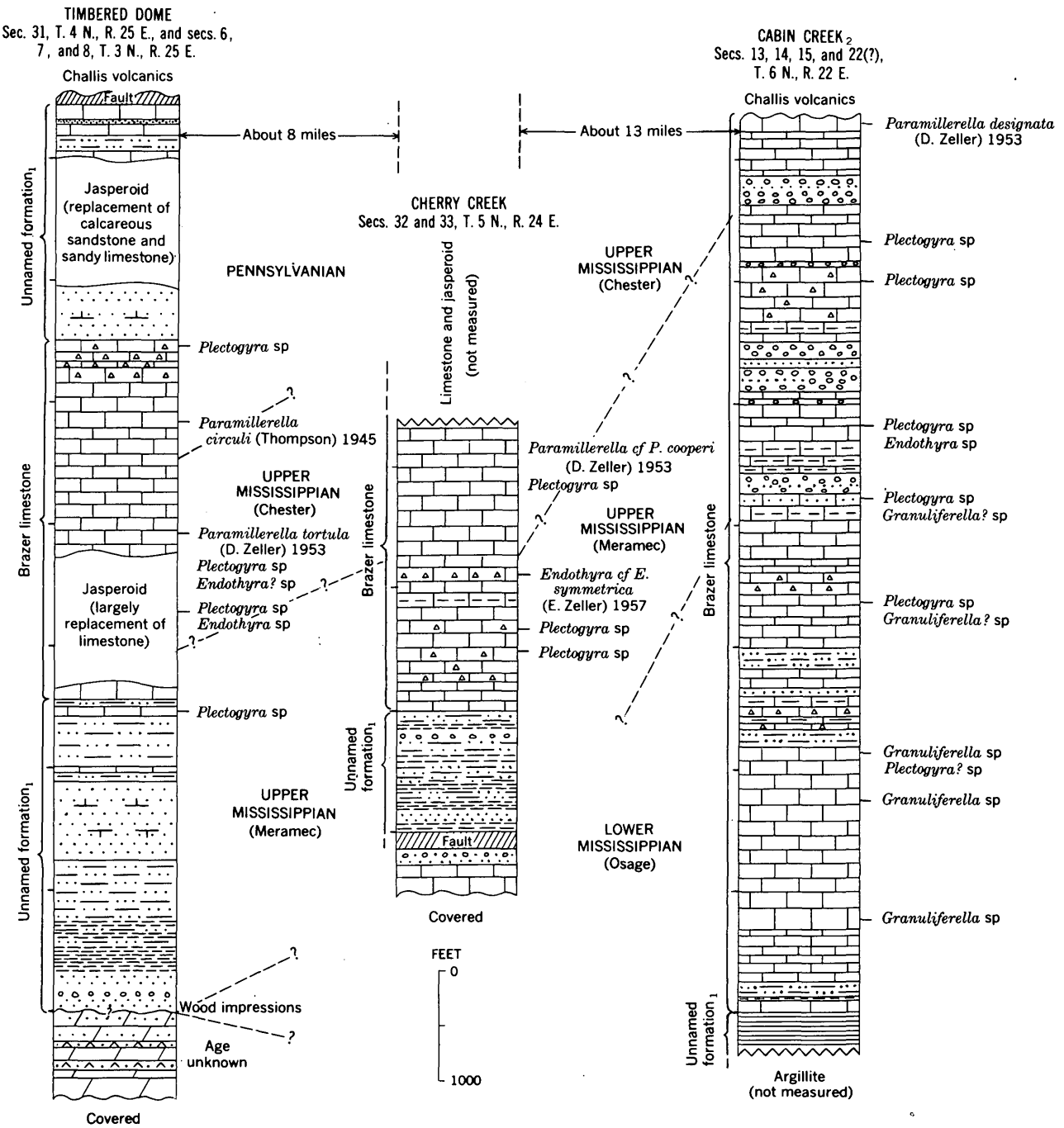

EXPLANATION

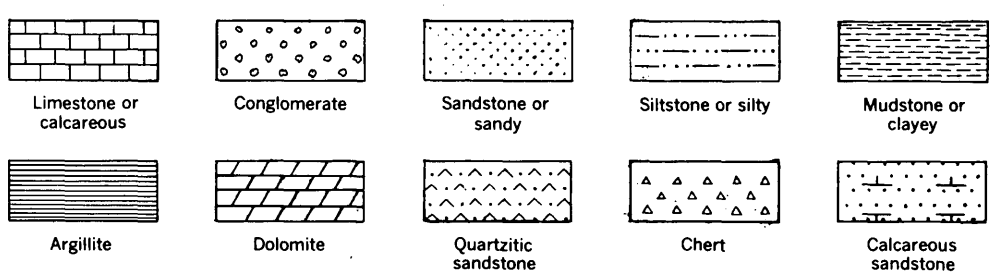

1. Described by C. P. Ross (1960)
2. This section described in detail by Skipp (1961)

the base of the Timbered Dome section, and therefore stratigraphic relations are in doubt.

Girty (*in* Umpleby, 1917, p. 28) regarded all the collections he saw from the Brazer and associated beds in the vicinity of the Cabin Creek section as Late Mississippian in age, but with varying degrees of confidence. Preston Cloud, David Dunkle and I (*in* Skipp, 1961, p. 385) also suggest a Middle or Late Mississippian age for the upper part of this section.

An Upper Mississippian fauna similar to that described by Girty from the mudstone of the Timbered Dome section, containing the distinctive brachiopod, *Leiorhynchus carboniferum* var. *polypleurum* Girty, was recognized by me approximately 250 feet above the fault at the base of the Cherry Creek section. Beds probably stratigraphically higher in the Brazer limestone contain fusulinids of Pennsylvanian age near the Cherry Creek section, as identified by R. C. Douglass (written communication, 1958).

In general, the age assignments based on the endothyrid Foraminifera support age assignments based on available megafossils, but suggest two important modifications:

1. The Mississippian-Pennsylvanian boundary lies in the thick sequence of limestones above the lower zone of jasperoid in the Timbered Dome section.
2. The Cabin Creek section contains a minimum of 3,500 feet of Lower Mississippian limestone and interbedded siltstone.

Tentative correlations of the three sections are given in figure 236.2. Meramec time is represented by sandstone, siltstone and mudstone in the Timbered Dome area and by quartzose conglomerate and clastic limestone in the Cabin Creek area (Skipp, 1961) just 20 miles to the northwest. Both appear to be shallow water deposits. Chester time appears to be represented mainly by limestone in all three areas. During Pennsylvanian time quartzose clastic rocks interbedded with limestone accumulated in the Timbered Dome area.

ENDOTHYRID ANATOMY AND STRATIGRAPHIC DISTRIBUTION

Endothyrid Foraminifera are minute calcareous forms commonly found in pure limestones ranging in age from Devonian to Triassic. In the Mackay region, they are best preserved in medium- to coarse-grained clastic limestones that have finely crystalline matrices and are not recrystallized to any appreciable extent. They are commonly associated with corals, brachiopods, gastropods, ostracods, echinoids, and crinoids. At places, they are also found in oolitic limestones.

Figure 236.3 illustrates the stratigraphic succession of the endothyrids in the Mackay quadrangle. Early Mississippian forms, *Granuliferella* sp., are characterized by a homogeneous single-layered wall and a plectogyrid coil (Zeller, 1950, p. 3) and appear contemporaneous with the ubiquitous Carboniferous form, *Plectogyra* sp. This form is characterized by a heterogeneous wall structure composed of three primary layers; a fourth, secondary layer of variable characteristics (Zeller, 1957, p. 693); and a plectogyrid coil. *Endothyra* sp. is characterized by a layered wall, distinctive secondary deposits, and a planispiral coil, and is a common form in Upper Mississippian rocks, but it may also be present in Lower Mississippian rocks. *Paramillerella* sp. of Late Mississippian and Pennsylvanian age has a layered wall structure, dominantly a planispiral coil, and rudiments of chomata which characterize true fusulinids. The distinctions between endothyrid populations of different ages in the Mackay quadrangle are those recognized by me, but the bases for this work were developed by Thompson (1942, 1944, 1945, 1951), E. J. Zeller (1950, 1957), D. E. N. Zeller (1953), Woodland (1958), and others.

Osage forms:

Granuliferella sp. is the most abundant form. Walls are homogeneous, single layered, and variable in thickness. Coil is plectogyrid. Specimens are generally small, averaging 0.2–0.3 mm in length. (Fig. 236.3, *Q* to *U*.)

Plectogyra sp. is rare. Wall layering is indistinct, total rotational distortion is small, and rare secondary deposits consist of small generally rounded nodes on chamber floors and no, or very thin, connecting layers. Specimens are generally small. (Fig. 236.3, *P*.)

Endothyra? sp. is very small and rare.

Meramec forms:

Plectogyra sp. is very abundant. Wall layering is distinct, secondary deposits are common and consist of hamuli, acanthi, nodes, thin to thick layers on chamber floors, and deposits on septa. Amount of rotational distortion and size of specimens ranges from small to large, although very large forms, up to 1.2 mm across, are more usual. (Fig. 236.3, *K* to *N*.)

Endothyra sp. is common. It is very closely related to *Paramillerella* and *Millerella* but secondary deposits are restricted to hamuli, acanthi, and nodes in final chamber in contrast to the rudimentary chomata which characterize the other genera. Other, less diagnostic differences are stubby septa, strong anterior direction of septa, and generally fewer chambers per volution. (Fig. 236.3, *O*.)

Chester forms:

Paramillerella sp. is abundant. It is characterized by rudimentary chomata in early volutions and is differentiated from *Millerella* sp. in having a more nearly spherical shell (Thompson, 1951). (Fig. 236.3, *G* to *J*.)

FIGURE 236.2.—Columnar sections of Carboniferous rocks.

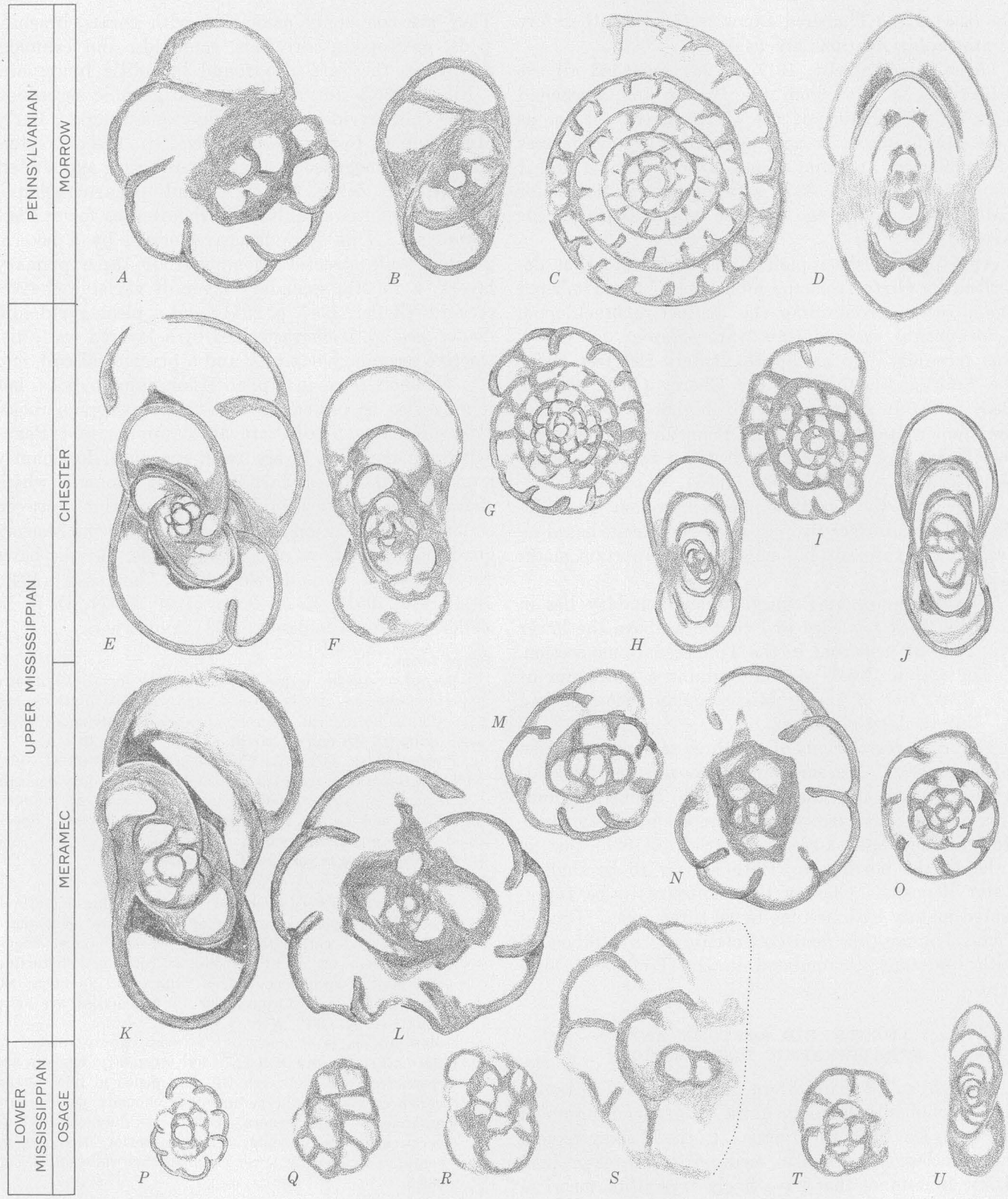

FIGURE 236.3.—Representative endothyrid Foraminifera from the Mackay quadrangle, Idaho. Morrow, Chester, Meramec, and Osage are correlative provincial series in the Mississippi Valley and Mid-continent region.

Chester forms—Continued

Plectogyra sp. is common and is largely indistinguishable from Meramec forms on the basis of present work. (Fig. 236.3, *E*, *F*.)

Endothyra? sp. is present.

Pennsylvanian forms:

Paramillerella circuli (Thompson) 1945 was first described by Thompson (1945, p. 47) from the Belden formation of Pennsylvanian age in Colorado and Utah, and is here used as a Pennsylvanian indicator. It is larger, has more volutions, more chambers per volution, and better developed chomata than related Chester forms. (Fig. 236.3, *C*, *D*.)

Plectogyra sp. is common but is not presently recognized as diagnostic. (Fig. 236.3, *A*, *B*.)

CONCLUSIONS

Generic and specific divisions of endothyrid Foraminifera in the Carboniferous rocks of the Mackay quadrangle are recognizable in sufficient detail to show that they have limited stratigraphic range and are useful for age determination. Although specific divisions of *Plectogyra* are recognized, their nomenclature has not yet been determined in the Mackay region because many of the original descriptions of species are incomplete, and limits of specific variables are not stated. Size differences have been emphasized in past descriptions although the size varies with environment and with megalospheric and microspheric forms of the same species. The coiling habit has not been described fully for most species. The degree of rotational distortion (Zeller, 1950, p. 3) is useful as a basis for classification although in some specimens it changes from volution to volution and has never been calibrated more precisely than the individual worker's estimate—small, moderate, large—and these vary. The same holds true for rate of coiling.

REFERENCES

Anderson, A. L., 1929, Geology and ore deposits of the Lava Creek district, Idaho: Idaho Bur. Mines and Geology Pamph. 32, 70 p.

Ross, C. P., 1960, Diverse interfingering Carboniferous strata in the Mackay quadrangle, Idaho, *in* Short papers in the geological sciences: U.S. Geol. Survey Prof. Paper 400–B, p. B232–B233.

Sando, W. J., Dutro, J. T., Jr., and Gere, W. C., 1959, Brazer dolomite (Mississippian), Randolph quadrangle, northeast Utah: Am. Assoc. Petroleum Geologists Bull., v. 43, no. 12, p. 2741–2769.

Skipp, B. A. L., 1961, Interpretation of sedimentary features in the Brazer limestone near Mackay, Custer County, Idaho: Am. Assoc. Petroleum Geologists Bull., v. 45, no. 3, p. 376–387.

Thompson, M. L., 1942, New genera of Pennsylvanian fusulinids: Am. Jour. Sci., v. 240, no. 6, p. 403–420.

——— 1944, Pennsylvanian Morrowan rocks and fusulinids of Kansas: Kansas State Geol. Survey Bull. 52, pt. 7, p. 409–431.

Explanation for figure 236.3

[All drawings of photographs ×100]

A, *B*, *Plectogyra* sp., showing extensive secondary deposits; 4,850 feet above dolomite at base of Timbered Dome section. *A*, oblique axial section, USNM 628595; *B*, oblique axial section; USNM 628596.

C, *D*, *Paramillerella circuli* (Thompson), 1945, showing numerous chambers and well developed chomata; 4,850 feet above dolomite at base of Timbered Dome section. *C*, sagittal section, USNM 628596; *D*, axial section missing proloculus, USNM 628595.

E, *F*, *Plectogyra* sp., showing large size, secondary deposits, and angular rotation; not in direct line of section, but considered to be about 3,300 feet above dolomite at base of Timbered Dome section. *E*, oblique axial section, USNM 628597; *F*, vertical axial section, USNM 628597.

G, *H*, *Paramillerella tortula* (D. Zeller), 1953, showing small size, uneven coiling and rudimentary chomata; 3,950 feet above dolomite at base of Timbered Dome section. *G*, sagittal section, USNM 628598; *H*, axial section missing proloculus, USNM 628598.

I, *J*, *Paramillerella designata* (D. Zeller), 1953, showing evolute final volution and rudimentary chomata; 7,300 feet above argillite of Cabin Creek section. *I*, sagittal section, USNM 628599; *J*, axial section missing proloculus, USNM 628599.

K, *L*, *Plectogyra* sp., showing large size and extensive secondary deposits; *K*, vertical axial section; USNM 628600; 6,000 feet above argillite of Cabin Creek section: *L*, horizontal axial section; USNM 628601; 4,800 feet above argillite of Cabin Creek section.

M, *Plectogyra* sp., oblique section showing small size and node in final chamber; USNM 628602; 2,500 feet above dolomite at base of Timbered Dome section.

N, *Plectogyra* sp., horizontal axial section, partly recrystallized; USNM 628603; 2,100 feet above base of Cherry Creek section.

O, *Endothyra* cf. *E. symmetrica* E. Zeller, 1957, sagittal section; USNM 628603; 2,100 feet above base of Cherry Creek section.

P, *Plectogyra* sp., horizontal axial section showing small size, small rotational distortion and lack of secondary deposits; USNM, 628604; 4,200 feet above argillites of Cabin Creek section.

Q–U, *Granuliferella* sp., showing homogeneous wall and small rotational distortion; all specimens from Cabin Creek section: *Q*, oblique section, USNM 628605, 4,200 feet above argillites; *R*, oblique axial section, USNM 628606, 2,200 feet above argillites; *S*, partial oblique section, USNM 628607, 1,800 feet above argillites; *T*, oblique section, USNM 628608, 1,800 feet above argillites; *U*, *Granuliferella*? sp., vertical axial section, USNM 628609, 800 feet above argillites.

Thompson, M. L., 1945, Pennsylvanian rocks and fusulinids of east Utah and northwest Colorado correlated with Kansas section: Kansas Univ. Geol. Survey Bull. 60, pt. 2, p. 17–84.
——— 1951, New genera of fusulinid Foraminifera: Cushman Found. Foram. Research Center, v. 2, pt. 4, p. 115–119.
Umpleby, J. B., 1917, Geology and ore deposits of the Mackay region, Idaho: U.S. Geol. Survey Prof. Paper 97, 129 p.
Woodland, R. B., 1958, Stratigraphic significance of Mississippian endothyroid Foraminifera in central Utah: Jour. Paleontology, v. 32, no. 5, p. 791–814.
Zeller, D. E. N., 1953, Endothyroid Foraminifera and ancestral fusulinids from the type Chesteran (Upper Mississippian): Jour. Paleontology, v. 27, no. 2, p. 183–199.
Zeller, E. J., 1950, Stratigraphic significance of Mississippian endothyroid Foraminifera: Kansas Univ. Paleont. Contri., Protozoa, art. 4, 23 p.
——— 1957, Mississippian endothyroid Foraminifera from the Cordilleran geosyncline [Rocky Mountains]: Jour. Paleontology, v. 31, no. 4, p. 679–704.

237. ANCIENT EROSIONAL CYCLES OF THE LITTLE COLORADO RIVER, ARIZONA AND NEW MEXICO

By Maurice E. Cooley and Jay P. Akers, Tucson, Ariz.

Work done in cooperation with the Arizona State Land Department and the Navajo Tribe

The Little Colorado River drains most of the southern part of the Colorado Plateau. It flows in a large valley carved in soft strata in the northwest-trending Tusayan downwarp, which has been described by Gregory (1917, p. 112). The Tusayan downwarp and the surrounding highlands are shown on figure 237.1.

Recurrent movements of the highlands and periods of accelerated regional upwarping throughout middle and late Tertiary time have controlled the erosional stages of the Little Colorado River system, as shown on figure 237.2. Four distinct erosional surfaces have been recognized: the Valencia surface, named in this report after Valencia County, N. Mex.; the Hopi Buttes and Zuni surfaces, undifferentiated, named and described, respectively, by Gregory (1917) and McCann (1938); the Black Point surface, named and described by Gregory (1917); and the Wupatki surface, named and described by Childs (1948). The discussion in this report is confined principally to the Valencia and Hopi Buttes and Zuni surfaces and the related deposits.

Early studies of the Colorado Plateau by Dutton (1882), Davis (1901), Robinson (1907 and 1910), and Gregory (1947) led them to postulate a general entrenchment and development of the Colorado River system from a widespread erosion surface formed in middle and late Tertiary time. This period of erosion has been known generally as the "Great Denudation" (Dutton, 1882) and the "Plateau Cycle" (Davis, 1901). The following cycle, during which the river system was entrenched in canyons, was called the "Canyon Cycle." In the Little Colorado River area the Valencia and Hopi Buttes and Zuni cycles are correlative roughly with the Great Denudation and the Plateau Cycle, and the Black Point and Wupatki cycles are equivalent to the Canyon Cycle.

After the northeastward retreat of the Late Cretaceous seas from the Arizona part of the Colorado Plateau, it seems likely that early Tertiary streams flowed in a northward direction as postulated by Hunt (1956, p. 73–77). Evidence for northward flow at this time is found in a sequence of nonvolcanic rocks believed to be correlative with the Baca formation of Eocene(?) age, which contains pebbles of quartzite, granite, and fossiliferous chert and limestone derived from the Central Mountains beyond the southern border of the Colorado Plateau.

The Baca formation is overlain conformably by the Datil formation (Oligocene), which is largely of volcanic origin (Winchester, 1921, p. 4). The Datil seems to have been deposited in the vicinity of the Arizona-New Mexico State line northward from the rim of the Colorado Plateau. Deposition of these volcanic rocks was probably accompanied by slow regional upwarping that caused a shift westward of the earlier northward flowing streams.

These streams constituted the initial stages of the Little Colorado system. Differential uplift of the

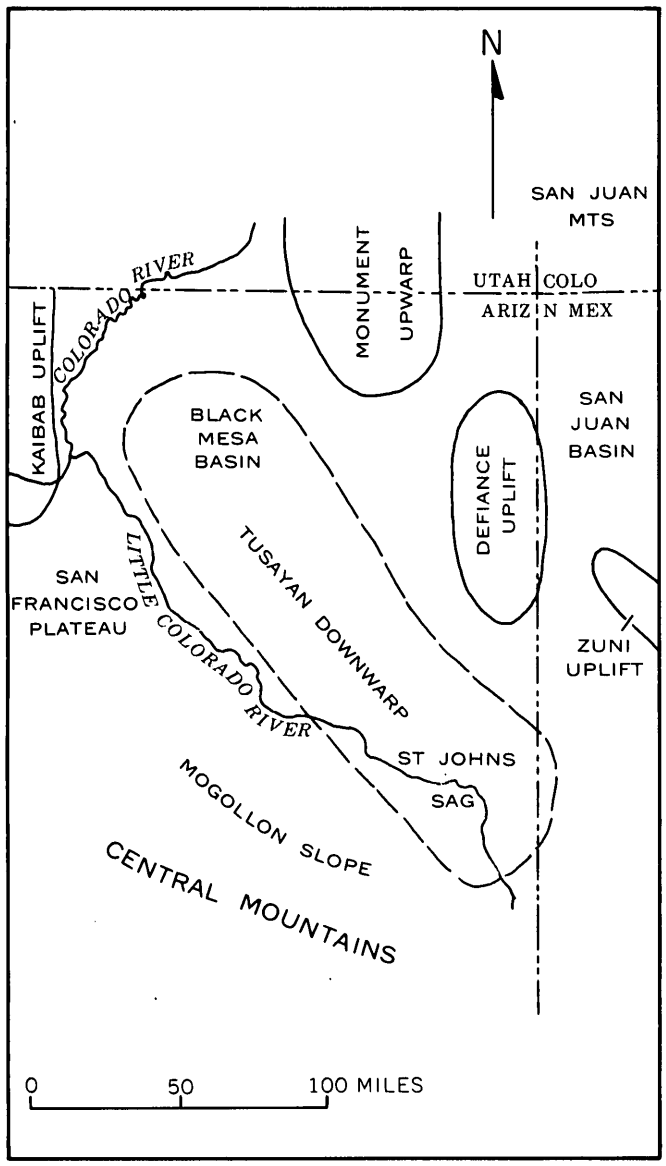

FIGURE 237.1.—Index map of the southern part of the Colorado Plateau showing structural elements that control the Little Colorado River drainage system.

Central Mountains and of the Zuni–Defiance–Monument uplift area confined the newly developed stream system to the Tusayan downwarp–Mogollon slope region. This new drainage, here assigned to the Valencia cycle, flowed generally westward and carved an open valley 50 to 125 miles wide. Evidence for this ancient valley is preserved on the relatively flat North Plains at altitudes between 7,000 and 7,500 feet (fig. 237.3), and on the general accordance of summits on Black Mesa at altitudes above 7,000 feet. Erosion surfaces of the Valencia cycle are present at altitudes of more than 7,500 feet beneath lavas capping Red Butte near the Grand Canyon and on other buttes and small mesas in the White Mountains volcanic field.

The reconstruction of the Valencia cycle stream pattern, shown on figure 237.3, was based on contours drawn on the Hopi Buttes and Zuni surfaces representing the succeeding cycle (fig. 237.3) and on the Valencia surfaces preserved beneath volcanic caprocks. The amount of downcutting that occurred during the Valencia cycle was nearly 2,000 feet near the Arizona–New Mexico State line, as indicated by the removal of much of the Datil formation and some of the underlying Mesozoic rocks.

Accelerated downcutting during the early part of the Hopi Buttes–Zuni cycle entrenched the ancestral Little Colorado system to an average depth of about 1,200 feet below the level of the Valencia surface. Subsequently, the lacustrine lower member of the Bidahochi formation (Reagan, 1924; Repenning and Irwin, 1954) was deposited within this valley. Later, after through-flowing drainage was re-established, eruptions in the Hopi Buttes field, represented by the volcanic member of the Bidahochi formation, blocked this old valley and caused the accumulation of the upper member of the Bidahochi only in the upstream reaches. The volcanism also diverted the ancestral Little Colorado River southward around the Hopi Buttes field to nearly its present position. The upper member of the Bidahochi completely filled the valley and overlapped for short distances upon broad terraces that represented the level of the Valencia surface.

The Hopi Buttes and Zuni surfaces on which the Bidahochi formation was deposited were contoured from data obtained from about 50 drilled wells and from altitudes of the outcrops (fig. 237.3). The contours indicate that an integrated drainage system was present and that the Defiance uplift–Chuska Mountains and the Zuni Mountains formed a divide between the ancestral Little Colorado system and the drainage in the San Juan Mountains area. The closure of the 5,800- to 6,600-foot contour lines downstream from the Hopi Buttes suggests at least 700 feet of differential uplift between these two areas since Bidahochi time. The contours indicate also that the "rim gravel" near Show Low and some of the volcanics on the San Francisco Plateau are part of the Hopi Buttes–Zuni cycle and presumably are a lateral equivalent of the Bidahochi formation. In addition, the contours confirm a correlation of gravel and volcanic rocks at altitudes of about 7,000 feet near Fence Lake, N. Mex., with the Bidahochi formation.[1]

Vigorous downcutting caused by regional uplift of the Colorado Plateau region during late Cenozoic time

[1] G. K. Sirrine, 1958, Geology of the Springerville-St. Johns area, Apache County, Ariz.: Texas Univ., Austin, unpublished doctoral thesis.

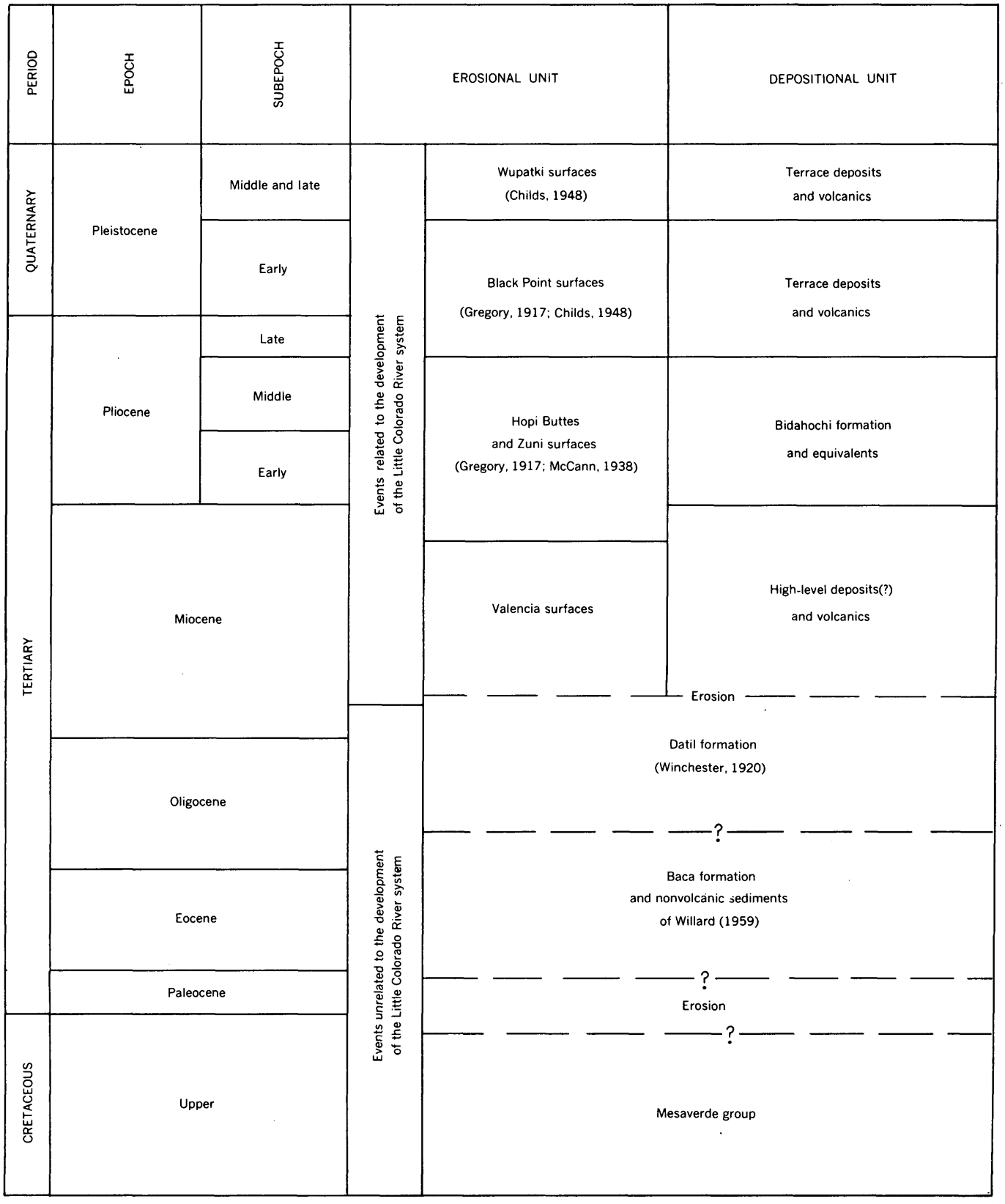

FIGURE 237.2.—Chart showing the deposits and surfaces in the valley of the Little Colorado River.

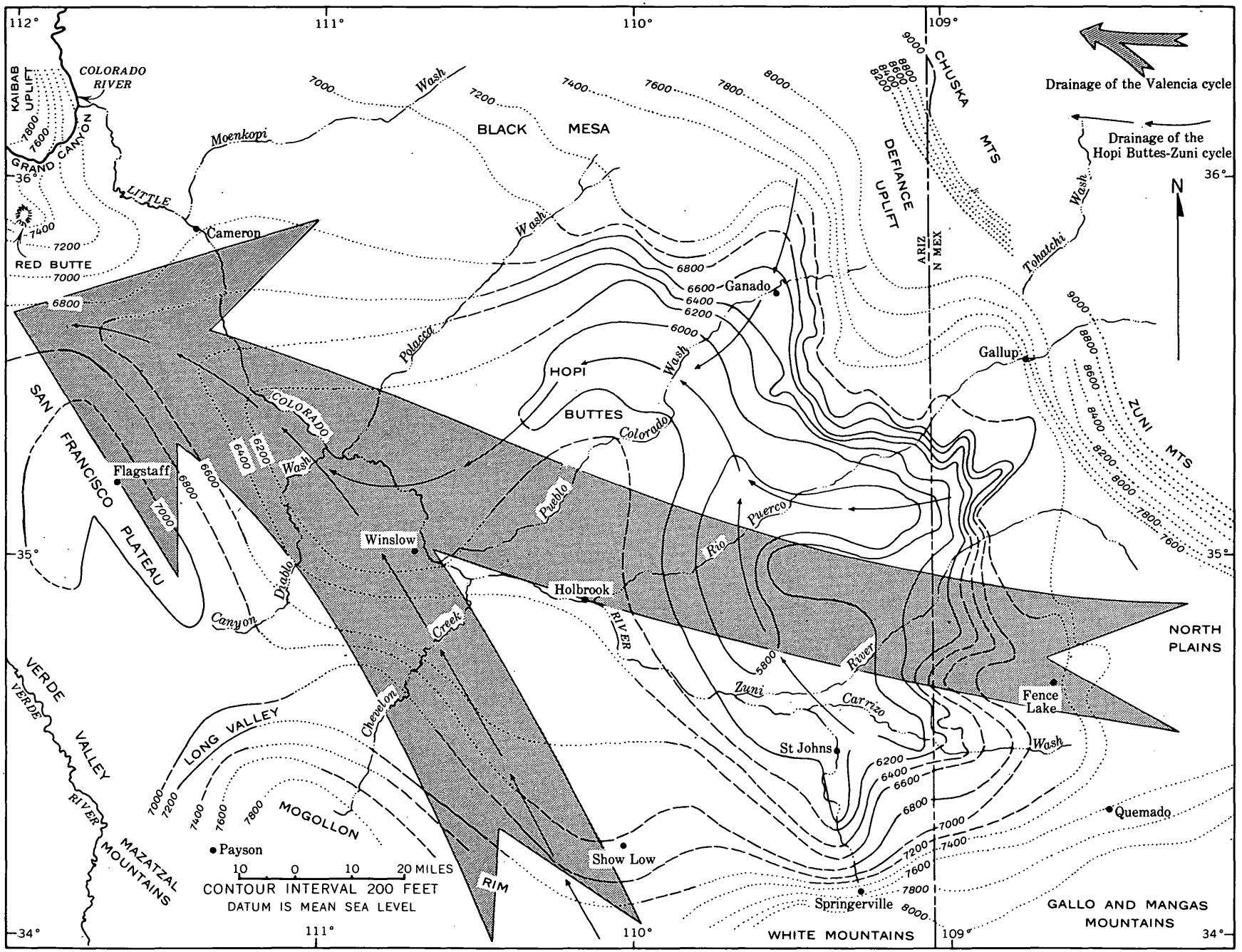

FIGURE 237.3.—Map showing the configuration of the base of the Bidahochi formation and the Hopi Buttes and Zuni erosion surfaces, drainage of the Hopi Buttes-Zuni cycle, and approximate drainage of the Valencia cycle.

ended the Hopi Buttes–Zuni cycle, and during the following Black Point and Wupatki cycles all the present Little Colorado drainage system was outlined and entrenched. In the vicinity of Holbrook, Ariz., the valley of the Little Colorado River was excavated about 800 feet below the base of the Bidahochi formation. Downstream, the cutting was more severe, but upstream between St. Johns and Springerville it was less than 200 feet.

REFERENCES

Childs, O. E., 1948, Geomorphology of the valley of the Little Colorado River, Arizona: Geol. Soc. America Bull., v. 59, p. 353–388.

Davis, W. M., 1901, An excursion to the Grand Canyon of the Colorado: Harvard Coll. Mus. Comp. Zoology Bull. 38, p. 108–200.

Dutton, C. E., 1882, Tertiary history of the Grand Canyon district, with atlas: U.S. Geol. Survey Mon. 2, 264 p.

Gregory, H. E., 1917, Geology of the Navajo country: U.S. Geol. Survey Prof. Paper 93, 161 p.

——— 1947, Colorado drainage basin: Am. Jour. Sci., v. 245, p. 694–705.

Hunt, C. B., 1956, Cenozoic geology of the Colorado Plateau: U.S. Geol. Survey Prof. Paper 279, 99 p.

McCann, F. T., 1938, Ancient erosion surface in the Gallup-Zuni area, New Mexico: Am. Jour. Sci., v. 235, p. 260–278.

Reagan, A. B., 1924, Stratigraphy of the Hopi Buttes volcanic field, Arizona: Pan-Am. Geologist, v. 41, no. 5, p. 355–366.

Repenning, C. A., and Irwin, J. H., 1954, Bidahochi formation of Arizona and New Mexico: Am. Assoc. Petroleum Geologists Bull., v. 38, p. 1821–1826.

Robinson, H. H., 1907, The Tertiary peneplain of the plateau district, and adjacent country, in Arizona and New Mexico: Am. Jour. Sci., ser. 4, v. 24, p. 109–129.

——— 1910, A new erosion cycle in the Grand Canyon district, Arizona: Jour. Geology, v. 18, p. 742–763.

Willard, M. E., 1959, Tertiary stratigraphy of northern Catron County, New Mexico: New Mexico Geol. Soc. Field Conf., 10th, 1959, Guidebook of west-central New Mexico, p. 92–99.

Winchester, D. E., 1921, Geology of Alamosa Creek valley, Socorro County, New Mexico, with special reference to the occurrence of oil and gas: U.S. Geol. Survey Bull. 716–A, p. 1–15.

238. VEGETATION IN RELATION TO FLOOD FREQUENCY NEAR WASHINGTON, D.C.

By Robert S. Sigafoos, Washington, D.C.

Vegetation along the Potomac River near Washington, D.C., is being studied to determine the relationship between the form and distribution of plants and the magnitude and frequency of floods. Flood-plain vegetation has long been recognized as being different from upland vegetation (Cain and Castro, 1959; Curtis, 1959; Dansereau, 1957; Putnam and others, 1960; and Wistendahl, 1958). The zonation of vegetation from the river bank to adjoining uplands is considered by many to represent a normal succession or change in the development of vegetation with time. That is, the belief is held that the type of vegetation in the zone along the bank will be replaced by vegetation in the adjoining zone, and it in turn by the vegetation in the next zone toward the upland. In contrast to this view, preliminary results of this study show that the form and kind of trees growing on flood plains are determined in large part by the magnitude and frequency of floods.

The study area, upon which this report is based, is a small section of the flood plain of the Potomac River at Little Falls, a few hundred yards upstream from the Washington, D.C.–Maryland boundary, between the Chesapeake and Ohio canal and the left bank of the low water channel. The flooded area is, for the most part, a bedrock surface, which nearest the canal is covered with alluvium of undetermined thickness. The forest is composed of typical flood-plain species. Twenty-four wood species were identified in the plots. Of these willow (*Salix* L.),[1] eastern cottonwood (*Populus deltoides* Bartr.), river birch (*Betula nigra* L.), swamp white oak (*Quercus bicolor* Willd.), slippery elm (*Ulmus rubra* Muhl.), American sycamore (*Platanus occidentalis* L.), box-elder (*Acer negundo* L.), silver maple (*Acer saccharinum* L.), and ash (*Fraxinus L.*) are predominant. Shingle oak (*Quercus imbricaria* Michx.) is present outside the plots, and it, along with swamp white oak, grows only on bedrock.

Seven 2,500-square-foot plots were distributed in an area where the vegetation and topography differ with distance away from the river bank. Within each plot

[1] Nomenclature follows Little (1953).

all living stems were counted, and those larger than 0.3 inch in diameter were measured. From these data, the total basal area (or the total cross-sectional area of the stems at the point of measurement) was calculated for each plot. From this the diameter of a circle having an area equivalent to the mean basal area was determined (Spurr, 1952, p. 14). This diameter combined with the number of stems per plot is the basis for describing quantitatively three types of vegetation. These data are plotted on figure 238.1 (p. C–250), along with the elevations of the crests of 3 floods. The 3 types of vegetation suggested by the graphical representation are as follows—

1. Trees about 15 inches in diameter. Plot 15 has 14 tree species and 1 vine species.
2. Trees about 3 to 5 inches in diameter. Plots 14a, 14b, 16, and 17 have 7 to 13 tree species and 1 vine species.
3. Trees growing as shrubs having stems less than 1 inch in diameter. Plots 21 and 22 have 3 and 4 species respectively, of woody plants.

The trees were inundated by floods of varying magnitude during the period of study from January 1, 1958, to January 1, 1961. The records of all floods during the period, March 1, 1930 to December 31, 1960, were examined to determine the average number of floods per year that (a) inundated the shrubby vegetation, (b) inundated small trees, and (c) inundated lower parts of the large trees. Elevation of the crest of each flood was measured on a crest-stage gage (Ferguson, 1942) located within the area, and peak discharge was determined from U.S. Geological Survey gaging-station records. High-water marks of some floods were mapped on aerial photographs soon after the water receded.

During the period of study the highest flood occurred May 10, 1960. The peak discharge was 124,000 cfs (cubic feet per second) and covered all types of vegetation except the large trees. The depths to which each type of vegetation was inundated by this flood are shown in figure 238.1 During the period of record, 31 years and 10 months, 17 floods equalled or exceeded this discharge. A flood equal to or exceeding this discharge thus occurs 0.5 times per year or has a recurrence interval of 2.0 years (Darling, 1959) based on the annual flood series methods described by Dalrymple (1960).

The shrubby vegetation was covered by the flood that occurred January 25, 1958, during which the mean discharge for the day was 33,100 cfs, and by the flood of March 1, 1958, with a peak discharge of 49,000 cfs. The lower flood of January 25, 1958, covered the vegetation to depths of 1 to 6 feet. The higher flood of March 1, 1958, covered it to depths of 3 to 8 feet and barely covered the bases of some of the small trees.

During the period of record, the shrubby vegetation has been flooded 155 times, or on an average of 4.8 times per year. The small trees have been flooded 17 times or approximately once every 1.8 years. The larger trees have been flooded less frequently.

The shrubby vegetation is scarred by occasional minor ice floes like one that occurred on January 20, 1958, but these floes are of minor extent and are not recorded. It is not known whether 155 floods plus occasional ice floes and jams are more important in determining the shrubby form of these plants than are the higher stream velocities and greater depths during 17 floods greater than 124,000 cfs that occurred during the same period.

The 3 types of vegetation that occur on the flood plain of the Potomac River in the study area are thus flooded at different frequencies, and the vegetation at lower elevations is flooded at greater depths. The form and species composition of these types are related to the magnitude and frequency of flooding. An analysis of flood history would aid in any study of flood-plain vegetation, and conversely a study of flood-plain vegetation will aid in the analysis of flood frequency of selected areas.

REFERENCES

Cain, S. A., and Castro, G. M. de O., 1959, Manual of vegetation analysis: New York, Harper and Brothers, 325 p.

Curtis, J. T., 1959, The vegetation of Wisconsin: Madison, Univ. Wisconsin Press, 657 p.

Dalrymple, Tate, 1960, Flood-frequency analyses: U.S. Geol. Survey Water-Supply Paper 1543–A, p. 1–80.

Dansereau, Pierre, 1957, Biogeography: New York, The Ronald Press, 394 p.

Darling, J. M., 1959, Floods in Maryland—magnitude and frequency: U.S. Geol. Survey open-file report, 9 p.

Ferguson, G. E., 1942, Gage to measure crest stages of streams: Civil Eng., v. 12, p. 570–571.

Little, E. L., Jr., 1953, Check list of native and naturalized trees of the United States: U.S. Forest Service Agr. Handb. 41, 472 p.

Putnam, J. A., Furnival, G. M., and McKnight, J. S., 1960, Management and inventory of southern hardwoods: U.S. Forest Service Agr. Handb. 181, 102 p.

Spurr, S. H., 1952, Forest inventory: New York, The Ronald Press, 476 p.

Wistendahl, W. A., 1958, The flood plain of the Raritan River, New Jersey: Ecol. Mon., v. 28, p. 129–153.

601530 O—61——17

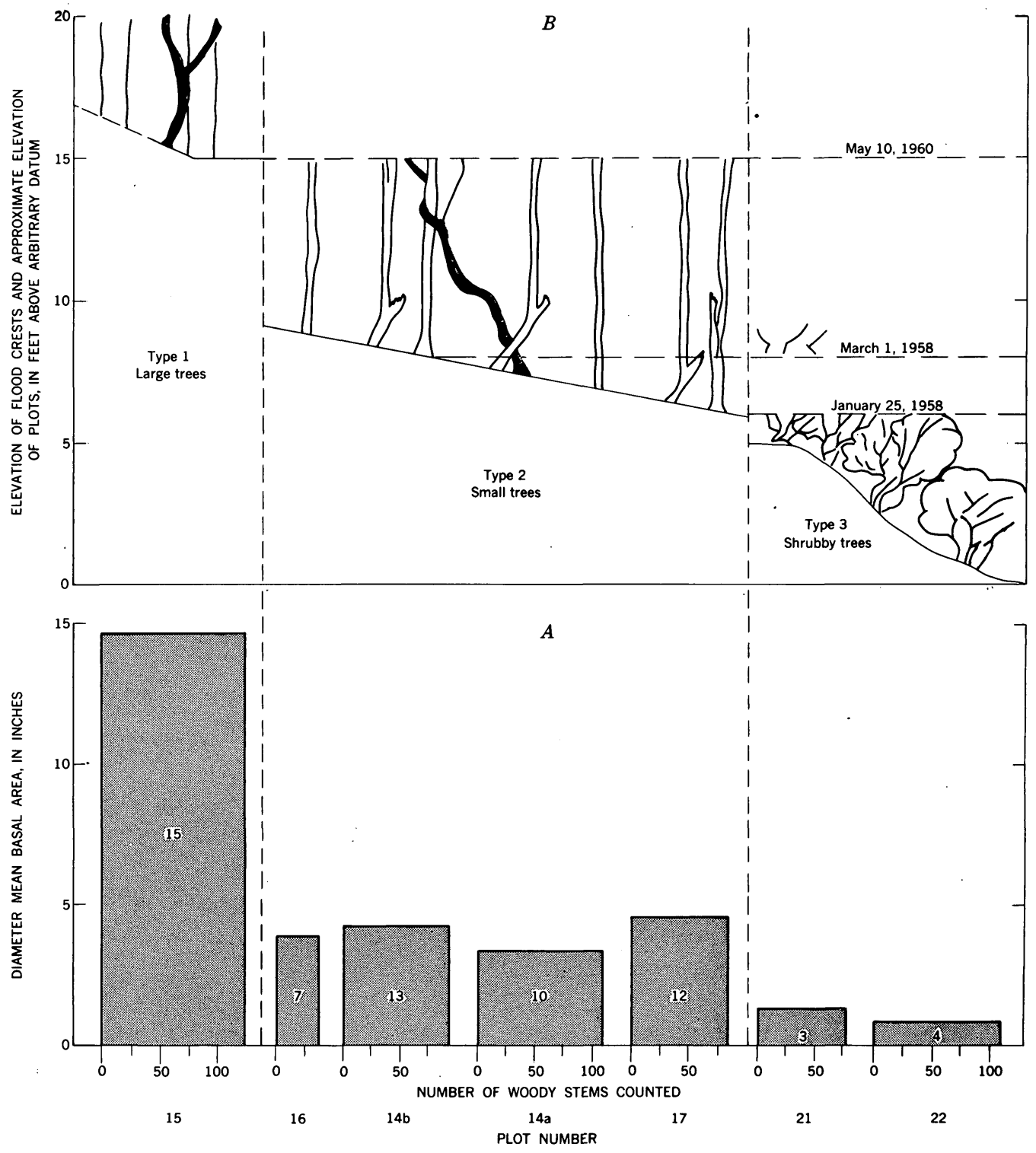

FIGURE 238.1.—Graphical representation of flood and botanical data. Three vegetation types are separated by vertical dashed lines. *A*, Number in bar is number of woody species counted. *B*, Diagrammatic representation of plots and vegetation types. Dashed horizontal lines indicate crests of observed floods.

239. SOIL-WATER AVAILABILITY AND USE BY GRASSLANDS ON ADJACENT STONY AND SHALE-DERIVED SOILS IN COLORADO

By F. A. Branson, R. F. Miller, and I. S. McQueen, Denver, Colo.

Work done in cooperation with U.S. Soil Conservation Service

Adjacent to the foothills of the Rocky Mountains in Colorado the number and variety of plants growing on stony soil are greater than the number and variety growing on shale-derived soil. A study of the causes of this difference was carried out at two nearby sites about 8 miles north of Golden, Colo.

One study site is on a stony soil that has developed on a pediment surface locally known as Rocky Flats (fig. 239.1). The gravel capping on Rocky Flats is from 1 to 50 feet thick and averages about 10 feet thick (Malde, 1955). This deposit is believed to be of Pleistocene age and has been named Rocky Flats alluvium (Scott, 1960). The other site is nearby on a soil derived from the Pierre shale of Late Cretaceous age (fig. 239.2) (Van Horn, 1957).

The Rocky Flats site is 6,250 feet in altitude; the Pierre shale site is 300 feet lower at 5,950 feet. This difference is negligible in effect on the plant communities.

The climate in the area of the study sites is similar to that of other parts of the central Great Plains in that dry cool winters and moist warm summers are characteristic. The average annual precipitation at Boulder, Colo., about 11 miles north of Rocky Flats, is 18.3 inches. The precipitation probably is slightly greater on the study sites, which are 700 to 1,000 feet higher in altitude. About 66 percent of the precipitation occurs during the growing season of April 1 to September 30. Average monthly temperature at Boulder ranges from 32.5°F in January to 73.6°F in July and the average annual temperature is 50.8°F.

FIGURE 239.1.—Vegetation on stony soil. Mountain muhly and big bluestem are the dominant grasses shown.

FIGURE 239.2.—Vegetation on soil derived from the Pierre shale. The conspicuous midgrasses are western wheatgrass and Japanese brome. The shortgrass in the foreground is buffalograss. The rock outcrop in the background is sandstone of the Laramie formation.

The data in table 239.1 show that most of the species occurring on the two soils are different and that the few species common to both sites are present in different amounts. The numbers of species present are also greatly different on the two soils. As shown in table 239.2, many more species of forbs and grasses and fewer species of shrubs are present on the stony soil than on the shale-derived soil.

Most of the species present on the shale-derived soil are those commonly found at altitudes of 1,500 to 6,000 feet on the central and northern Great Plains. They are classified as the mixed prairie association of the grassland formation (Weaver and Clements, 1938). Western wheatgrass (*Agropyron smithii* Rydb.), blue grama (*Bouteloua gracilis* (H.B.K.) Lag.), and buffalograss (*Buchloe dactyloides* (Nutt.) Engelm.) are the most abundant perennial plants on the shale-derived soil.

Most of the species present on the stony soil are those usually found at altitudes above 6,000 feet in the Rocky Mountains. The plant assemblage on the

stony soil is remarkable, however, because it contains relatively large quantities of a few true prairie species typical of grasslands of eastern Nebraska and Iowa (Weaver and Fitzpatrick, 1934). Big bluestem (*Andropogon gerardi* Vitman.), little bluestem (*A. scoparius* Michx.), and Indian grass (*Sorghastrum nutans* (L.) Nash.) are the dominant species in true prairie and are a significant part of the vegetation of Rocky Flats. Livingston (1952) proposed that true prairie species occurring in and near the Black Forest of Colorado have persisted on high mesas since the retreat of the continental glaciers about 10,000 years ago, and this may be true of the species found at the Rocky Flats site. Although these true prairie grasses are abundant on Rocky Flats, they are of minor importance in terms of numbers of species present (table 239.3).

TABLE 239.1.—*Vegetation and surface features on a stony soil and an adjacent shale-derived soil as determined by the all-contacts point-quadrat method (Levy and Madden, 1933)*

Vegetation	Stony soil		Shale-derived soil	
	Percent composition	Hits per 100 pins	Percent composition	Hits per 100 pins
Grasses				
Muhlenbergia montana (Nutt.) Hitchc. Mountain muhly	26. 0	23. 6	------	--------
Schedonnardus paniculatus (Nutt.) Trel. Tumblegrass	------	--------	1. 7	1. 7
Sitanion hystrix (Nutt.) J. G. Smith Squirreltail	1. 2	1. 1	------	--------
Sorghastrum nutans (L.) Nash. Indiangrass	3. 2	2. 9	------	--------
Sporobolus cryptandrus (Torr.) A. Gray Sand dropseed	0. 1	0. 1	1. 0	1. 0
Other grasses	0. 6	0. 6	1. 1	1. 1
Forbs				
Arenaria fendleri A. Gray Sandwort	3. 0	2. 8	------	--------
Artemisia ludoviciana Nutt. Sagewort	1. 6	1. 4	------	--------
Carex heliophila Mack. Sun sedge	0. 5	0. 5	1. 9	1. 9
Erigeron strigosus Muhl. ex Willd. Fleabane	1. 3	1. 2	------	--------
Liatris punctata Hook. Blazing star	2. 5	2. 3	------	--------
Paronychia jamesii T. & G. Whitlow-wort	2. 5	2. 3	------	--------
Petalostemon purpureum (Vent.) Rydb. Purple prairie clover	1. 1	1. 0	------	--------
Chrysopsis villosa (Pursh) Nutt. Hairy gold aster	1. 7	1. 6	------	--------
Other forbs	8. 3	7. 3	2. 5	2. 4
Shrubs				
Gutierrezia sarothrae (Pursh) Britt. Snakeweed	------	--------	4. 4	4. 3
Other shrubs	0. 1	0. 1	1. 1	1. 1
Mulch	34. 9	65. 1	50. 1	99. 8
Rock	12. 0	22. 3	------	--------
Bare	4. 3	8. 1	3. 3	6. 5
Total hits	------	1, 545. 0	------	1, 793. 00
Total pins	------	830. 0	------	900. 0

TABLE 239.2.—*Numbers of species of grasses, forbs, and shrubs on stony soil and on shale-derived soil*

Plant group	Stony soil	Shale-derived soil
Grasses	25	13
Forbs	56	21
Shrubs	2	4
Total	83	38

Different rates of percolation into the two soils affect the quantities of soil moisture available for plant use. In table 239.4 infiltration rates for two plant types on each of the two soils are shown. The highest rate measured on the shale-derived soil was 1.90 inches per hour, which was less than one-half the lowest rate measured on the stony soil. The higher rates of infiltration on the stony soil permit greater storage of moisture for use by vegetation (fig. 239.2).

Other factors that may explain the presence of contrasting plant communities on the two soils include soil-moisture percentage, soil-moisture tension, and soil temperature (fig. 239.3).

Based on the assumption that soil moisture would not be retained by fine and coarse gravel, soil-moisture percentages were computed only for the smaller than 2 mm fraction of the stony soil. Soil-moisture percentages were considerably greater in the stony soil early in the growing season and remained higher during the entire growing season.

TABLE 239.3.—*Relationships of numbers of species present on stony and shale-derived soils near Golden, Colo., to other vegetation associations and geographic locations*

Vegetation type or geographic origin	Stony soil	Shale-derived soil
True prairie	6	----------
Montane	31	3
Mixed prairie	24	24
Mixed prairie and true prairie	6	1
Mixed prairie and montane	11	4
Introduced	4	4
Mixed prairie, true prairie, and montane	1	2
Total	83	38

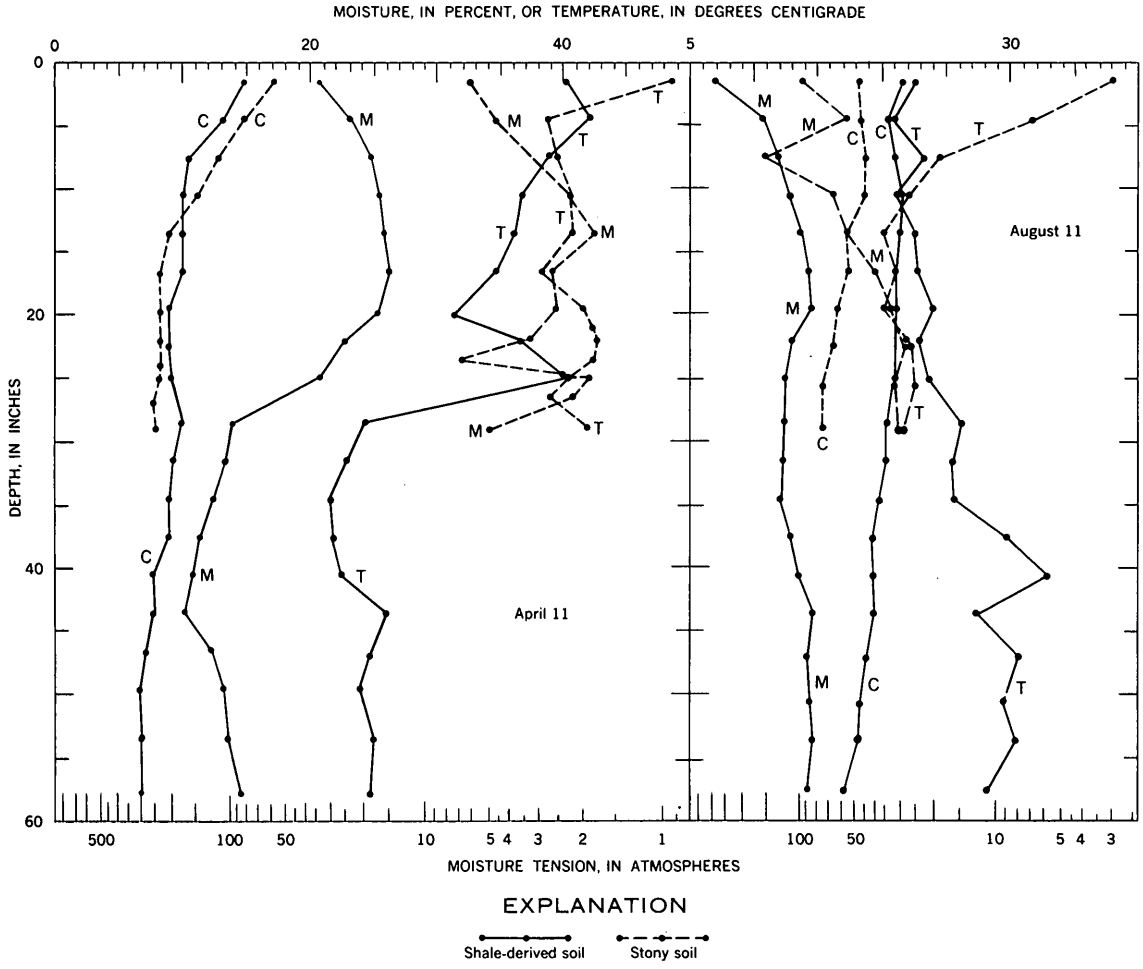

FIGURE 239.3.—Soil moisture (M), soil-moisture tension (T), and soil temperature (C), in adjacent stony- and shale-derived soils for samples obtained April 11 and August 11, 1960.

TABLE 239.4.—*Infiltration rates of simulated rainfall on shale-derived and stony soils under given kinds of vegetation*

[Two 1-hour measurements were made on each plant-soil type]

Rate of rainfall	Infiltration rate (inches per hour)			
	Shale-derived soil		Stony soil	
	Buffalo-grass	Western wheatgrass	Big bluestem Blue grama	Cheatgrass brome
High	1. 90	1. 10	4. 80	7. 35
Low	1. 87	. 40	3. 90	4. 60
Average	1. 89	. 75	4. 35	5. 98

Soil-moisture tensions were generally higher in the shale-derived soil than in the stony soil.

Early in the growing season (April 11) soil temperatures in the upper 10 inches of the stony soil exceeded those of the shale-derived soil, but near the end of the growing season soil temperatures were higher at all depths in the shale-derived soil (August 11).

These results indicate that the greater quantities of available soil moisture in the stony soil apparently is the major causative factor for the presence of the more varied flora on this soil.

REFERENCES

Levy, E. B., and Madden, E. A., 1933, The point method of pasture analysis: New Zealand Jour. of Agriculture, v. 46, p. 267–279.

Livingston, R. B., 1952, Relict true prairie communities in central Colorado: Ecology, v. 33, no. 1, p. 72–86.

Malde, H. E., 1955, Surficial geology of the Louisville quadrangle, Colorado: U.S. Geol. Survey Bull. 996–E, p. 217–257.

Scott, G. R., 1960, Subdivision of the Quaternary alluvium east of the Front Range near Denver, Colorado: Geol. Soc. America Bull., v. 71, p. 1541–1544.

Van Horn, Richard, 1957, Bedrock geology of the Golden quadrangle, Colorado: U.S. Geol. Survey Geol. Quad. Map GQ–103.

Weaver, J. E., and Clements, F. E., 1938, Plant ecology: New York, McGraw-Hill Book Co., Inc., 601 p.

Weaver, J. E., and Fitzpatrick, T. J., 1934, The prairie: Ecol. Mon., v. 4, no. 2, p. 112–259.

GEOPHYSICS

240. A SEISMIC RECORD OF MESOZOIC ROCKS ON BLOCK ISLAND, RHODE ISLAND

By CURTIS R. TUTTLE, WILLIAM B. ALLEN, and GLENN W. HAHN, Boston, Mass., and Providence, R.I.

Work done in cooperation with the Rhode Island Water Resources Coordinating Board

In June 1960, six refraction seismic traverses were made on Block Island, R. I.; three of these were reversed. Seismic travel times have been compared with drillers' logs from 4 borings made in June 1960, and 6 borings from existing water wells. The location of seismic and boring sites and the profile made from the physical measurements are shown on figure 240.1.

Four subsurface geologic units, based on longitudinal wave speeds (V_0, V_1, V_2, and V_3) were found: a weathered zone (V_0), an underlying unconsolidated zone (V_1), a semi-consolidated zone (V_2), and a crystalline zone (V_3). This nomenclature is defined by Ewing and others (1937).

The seismic low-velocity layer (weathered zone of Ewing and others, 1937) is mostly drift of Pleistocene age 16 to 153 feet thick and it has an average longitudinal wave speed (V_0) of 3,200 feet per second. All material above the base of brown sediments shown on figure 240.1 is of Pleistocene age; some light-colored sediments below this line are probably of Pleistocene age. Clearly the V_0–V_1 discontinuity (fig. 240.1) does not represent a sharp lithologic or age boundary except at boring 62 where a change in wave speed, a change in color, and a change in lithology occur at the same horizon.

Fenneman (1938, p. 14–15) implies that Block Island has a Cretaceous substratum which is the crest of a cuesta whose inner lowland is submerged in Block Island Sound. The presence of a subsurface zone of Cretaceous age is verified by the presence of an unconsolidated zone that is 408 to 856 feet thick and extends beneath the entire profile shown on figure 240.1. This zone has an average longitudinal wave speed of 6,270 feet per second. It is believed to be represented in part by white clay exposed in the northern Cretaceous outcrop, figure 240.1, and identified as the Magothy clay by Woodworth (1934). At this locality, sediments of Cretaceous age are unconformably overlain by brown Pleistocene drift. Further, boring 62 penetrated 35 feet of white clay and 135 feet of red clay similar to that described as Cretaceous by Woodworth. At points 4 *A* and 4 *C* (fig. 240.1) only the minimum thickness of the unconsolidated zone is recorded because a much shortened traverse was necessitated by topography and culture. The maximum wave speed at this site ranges from 5,900 feet per second to 6,600 feet per second.

The unconsolidated zone is probably correlative with other geologic units found nearby. Suter and others (1949) list Cretaceous rocks from well 189 in Suffolk County, Long Island, N.Y. This well is about 35 statute miles west of Block Island. Offshore from 7 to 21 statute miles southeast of the island is 600 feet of so-called "semiconsolidated" material with a longitudinal wave speed of 6,470 feet per second (Oliver and Drake, 1951). This layer is thought to be correlative with the unconsolidated zone on Block Island. At a second offshore site, 36 to 37 statute miles east of Block Island, Ewing and others (1950) measured a layer with a longitudinal wave speed of 5,800 feet per second.

The semiconsolidated zone has a thickness of 755 feet and an approximate average longitudinal wave speed of 12,200 feet per second at point 3 *A*. This traverse was unreversed; however, the maximum speed computed for traverses 2 *A* to 2 *D* and 5 *A* to 5 *D* ranges from 11,300 to 12,900 feet per second. The short traverses required by the topography and the culture did not allow measurement of the entire thickness of this zone. This material may be of Cretaceous age, as suggested by the wave speed of 9,750 to 11,500 feet per second of a semiconsolidated layer reported offshore east of the Island by Ewing and others (1950). Or, the semiconsolidated zone on Block Island may be sandstone of Triassic age, similar to the Longmeadow sandstone—which has a wave speed of 13,000 feet per second in the Connecticut River valley as measured by Tuttle and others (1960). Stetson (1949) reports sandstone of Cretaceous age obtained in place from tows along submarine canyons on Georges Bank.

The crystalline zone at point 3 *A* has a speed of 19,700 feet per second and is inferred to consist of Paleozoic or older rocks similar to the bedrock ex-

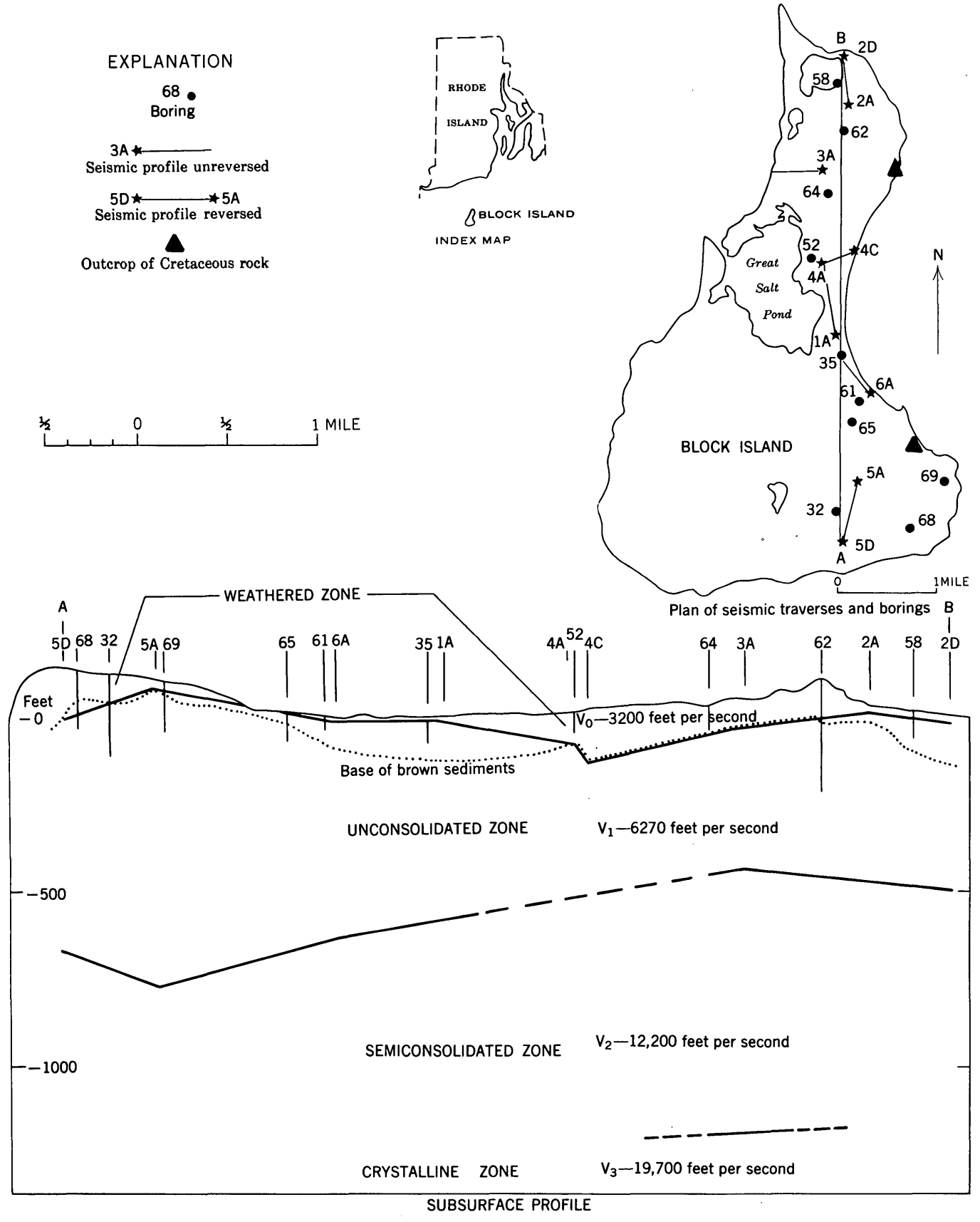

FIGURE 240.1.—Map showing seismic traverses and borings, and subsurface profile, Block Island, R.I.

posed on the mainland of eastern Connecticut and western Rhode Island. Speeds of 18,625 to 19,450 feet per second were measured by Oliver and Drake (1951) offshore 7 to 21 miles southeast of the island and are of the same order of magnitude.

The identification of subsurface geologic units of Cretaceous age and of possible Triassic age are similar to findings of other geophysicists along the coast of New York and New England. No sediments of Tertiary age were recognized in the zones measured; however, speed discontinuities do not occur everywhere at age or lithologic boundaries. Tertiary rocks may be present inasmuch as Eocene rocks have been reported by Zeigler and others (1960) from eastern Cape Cod. The speed of seismic waves in these Eocene silt and sand units is 4,900 to 5,900 feet per second (C. R. Tuttle and R. N. Oldale, written communication, 1960).

REFERENCES

Ewing, Maurice, Crary, A. P., and Rutherford, H. M., 1937, Geophysical investigations in the emerged and submerged Atlantic Coastal Plain, Part I, methods and results: Geol. Soc. America Bull., v. 48, p. 763–764.

Ewing, W. M., Worzel, J. L., Steenland, N. C., and Press, Frank, 1950, Geophysical investigations in the emerged and submerged Atlantic Coastal Plain, Part V, Woods Hole, New York, and Cape May sections: Geol. Soc. America Bull., v. 61, no. 12, pt. 2, p. 877–892.

Fenneman, N. M., 1938, Physiography of eastern United States: New York, McGraw-Hill Book Co., Inc., 714 p.

Oliver, J. E., and Drake, C. L., 1951, Geophysical investigations in the emerged and submerged Atlantic Coastal Plain, Part VI, the Long Island area: Geol. Soc. America Bull., v. 62, p. 1287–1296.

Stetson, H. C., 1949, The sediments and stratigraphy of the east coast continental margin; Georges Bank to Norfolk Canyon: Massachusetts Inst. Technology and Woods Hole Oceanog. Inst. Papers in Physical Oceanography and Meteorology, v. 11, no. 2, p. 33, table 1.

Suter, Russell, deLaguna, Wallace, and Perlmutter, N. M., 1949, Mapping of geologic formations and aquifers of Long Island, New York: New York Water Power and Control Comm., Bull. GW–18, p. 117.

Tuttle, C. R., Koteff, Carl, and Hartshorn, J. H., 1960, Seismic investigations in the Connecticut River valley, southern Massachuetts [abs.]: Geol. Soc. America Bull., v. 71, no. 12, p. 1994.

Woodworth, J. B., 1934, Geology of Block Island, *in* Woodworth, J. B., and Wigglesworth, Edward, Geography and geology of the region including Cape Cod, the Elizabeth Islands, Nantucket, Martha's Vineyard, No Man's Land, and Block Island: Harvard College Mus. Comp. Zoology Mem. v. 52, p. 212–219.

Zeigler, J. M., Hoffmeister, W. S., Giese, Graham, and Tasha, Herman, 1960, Discovery of Eocene sediments in subsurface of Cape Cod: Sci., v. 132, no. 3437, p. 1397–1398.

241. ELECTRICAL PROPERTIES OF SULFIDE-MINERALIZED GABBRO, ST. LOUIS COUNTY, MINNESOTA

By C. J. Zablocki, Denver, Colo.

During geophysical exploration of the Duluth gabbro, the Bear Creek Mining Co. discovered extensive conductive areas that were later drilled in the search for sulfide ore. The holes penetrated the Duluth gabbro and older sedimentary rocks. All the rocks are of Precambrian age. Sulfides, predominantly pyrrhotite, and some disseminated graphite occur in an olivine-rich gabbro, in hornfels, and in a dense fine-grained gabbro containing hornfels. In-hole measurements have been made of self-potential, resistivity, conductivity, induced polarization, and magnetic susceptibility. The logging devices used are described by Zablocki and Keller (1957). Typical logs obtained in the study are shown on figure 241.1. The Bear Creek Mining Co. kindly gave permission to make the study, and Mr. James Mancuso provided core logs and assay data.

Very large potential differences, as great as 0.5 volt, were recorded on the self-potential logs; potentials opposite sulfide-bearing rocks were positive relative to potentials opposite barren gabbro. These large potential differences are caused by electrochemical reactions within the sulfides.

The resistivity of rocks containing neither graphite nor sulfide minerals in large amounts is moderately large, about 2,000 ohm-meters. Rocks containing more

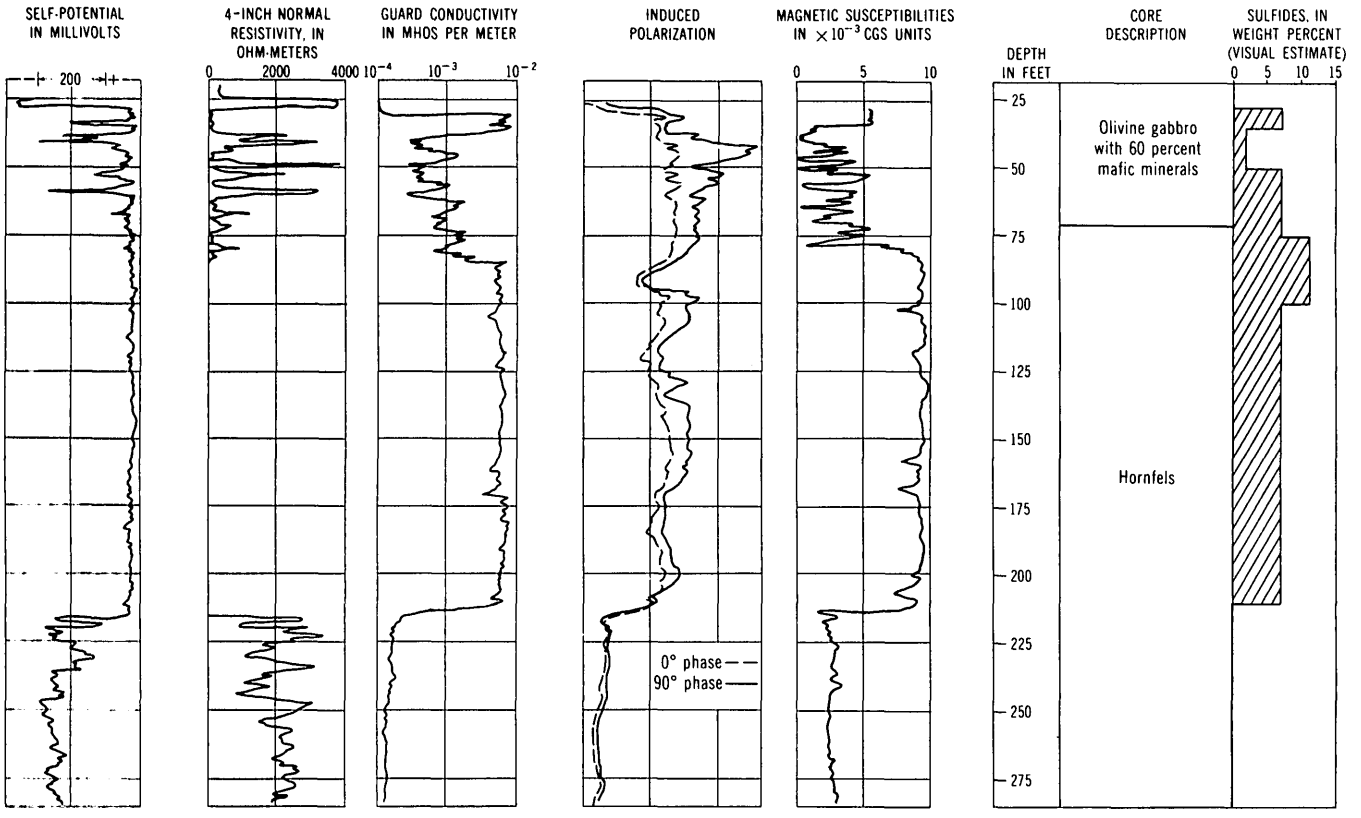

FIGURE 241.1.—Geophysical borehole logs in sulfide-mineralized gabbro and hornfels, near Babbitt, Minn. The guard conductivity log is plotted on a nonlinear scale; the induced polarization logs are plotted in relative units.

than 7 percent sulfides by weight are highly conductive, and have resistivities less than 0.1 ohm-meter. Certain hornfels were found to have a low resistivity regardless of whether they contained large amounts of sulfide minerals. Apparently the sulfide-free hornfels contain a high enough concentration of graphite to render them conductive.

Induced-polarization logs were made using the repeating pulse method. A standard normal resistivity array was used, except that the current electrodes were powered by a series of current pulses rather than by a continuous current. The voltage at the pickup electrodes during the current pulses is separated electronically from the voltage at the pickup electrodes during the intervals between current pulses. These two voltages were recorded separately as the in-phase and out-of-phase signals, as indicated on figure 241.1. The amplitude of the induced polarization is proportional to the ratio of the out-of-phase voltage to in-phase voltage.

The largest ratios, and thus the greatest induced polarization, were recorded in gabbro containing only a few percent of sulfide minerals. The highly mineralized conductive zones exhibit much lower induced polarization. This behavior is typical of rocks in which the conductive minerals occur in continuous chains rather than as disseminated particles.

TABLE 241. 1.—*Average values of the properties measured.*

Rock description	Resistivity (ohm-meters)	Induced polarization, ratio of out-of-phase to in-phase (percent)	Magnetic susceptibility (10^{-6} cgs units)
Olivine gabbro (barren)	>4, 000	<1	1, 000
Olivine gabbro (≈2.5 percent sulfides)	>2, 000	3 to 5	1, 500
Olivine gabbro (>10 percent sulfides)	<. 1	1 to 3	4, 000
Hornfelsic gabbro (barren, fine-grained, hornfelsic texture)	2, 500	----	<1, 000
Hornfelsic gabbro (<7 percent sulfides)	<.01 to >2, 000	----	5, 000
Hornfelsic gabbro (>7 percent sulfides)	<. 1	----	15, 000
Iron formation (10 to 15 percent Fe_3O_4)	<2, 500	----	45, 000
Hornfels (disseminated graphite and quartzite)	<0.1 to >4, 000	----	<500
Hornfels (>7 percent sulfides)	<. 1	1 to 3	10, 000

The magnetic susceptibility appears to be determined by the amount of pyrrhotite in the rock. Very little magnetite was observed in the core samples.

The susceptibility of the hornfels is about twice as high as that of the gabbro, even though both rocks contain about the same amount of pyrrhotite. However, the pyrrhotite appears to form continuous chains in the hornfels and not in the gabbro. The same amount of magnetic material may well have a higher susceptibility when it is continuous than when it is disseminated.

The average values of the properties measured are tabulated in table 241.1 according to rock type.

REFERENCE

Zablocki, C. J., and Keller, G. V., 1957, Borehole geophysical logging methods in the Lake Superior district, *in* Seventh annual drilling symposium, exploration drilling: Minnesota Univ. Center for Continuation Study, p. 15–24.

242. STRUCTURE OF PLUTONS FROM GRAVITY MEASUREMENTS

By Martin F. Kane, Washington, D.C.

Detail gravity measurements made in 1959 show the subsurface shape of two outcropping mafic intrusives, one in Maine and one in Pennsylvania. Mafic intrusives were chosen for study because their high density usually causes large positive gravity anomalies. The outcrops form the upper surface of the gravitating bodies, which makes interpretation much more certain than usual. The stations were placed along traverses normal to the outcrop pattern and were spaced short distances apart compared to the width of the outcrop. Closer spacing was used in the immediate vicinity of the surface contacts. The measured gravity profiles and best-matching theoretical values for hypothetical bodies are shown in figures 242.1 and 242.2. The theoretical values were computed graphically, using the densities of representative rock samples from each area.

One of the intrusives is a gabbro body (fig. 242.1) near the south end of Moosehead Lake in Maine. It has an east-trending linear outcrop pattern and intrudes highly compacted sedimentary rocks of Paleozoic age. The measured and computed gravity anomalies show that the boundaries of the gabbro are marked by steep gravity gradients; the dip is shown by the direction of offset in the peak amplitude. The best-matching computed values indicate that the body is dikelike in shape, dips east about 60°, and extends to a depth of a few miles. The small departures between the two profiles are probably caused by small changes in density or by a slight widening or curvature of the body with depth. A series of profiles were computed for different shapes, and in all the profiles the steep gradients noted above occur over the contacts and therefore can be used to locate them. For dikelike bodies, the direction of offset in the peak amplitude indicates the direction of dip; however, the depth extent of the bodies can only be expressed approximately because the resolving power of gravity decreases sharply with depth.

A diabase sill (fig. 242.2) that forms Solebury Mountain in Bucks County, Pa., was also studied. The sill and the sedimentary rocks it intrudes are Triassic in age. As with the gabbro, the contacts and direction of dip are shown by the characteristic steep gradients and the offset in the peak amplitude. The best-matching computed values indicates that the sill dips about 20° and extends at least half a mile deep. A comparison of the gravity profiles in figures 242.1 and 242.2 shows a marked difference in the shape of the profiles. The difference is caused by the change in dip, indicating that a rough estimate of the amount of dip can be obtained by simply inspecting the measured gravity profile.

Comparison of several computed profiles suggested that the range of density contrasts that give a good definition of the intrusive is limited. In Maine, profiles made over irregularly shaped felsic plutons that are less dense than the rock into which they were intruded gave much information on location of contacts, and on size and shape of the intrusives, but the profiles are less helpful than profiles over dikelike bodies.

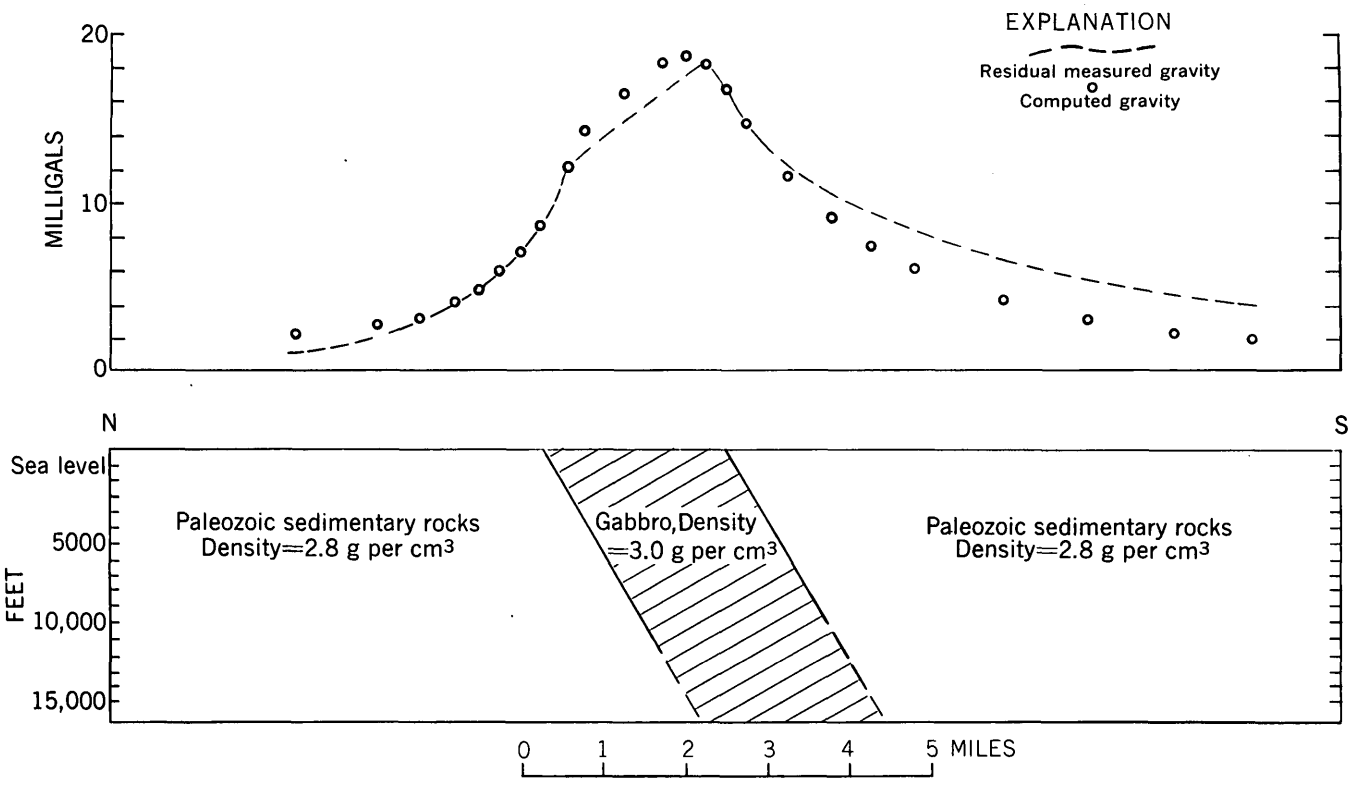

FIGURE 242.1.—Gravity profile and section over gabbro body near south end of Moosehead Lake, Maine.

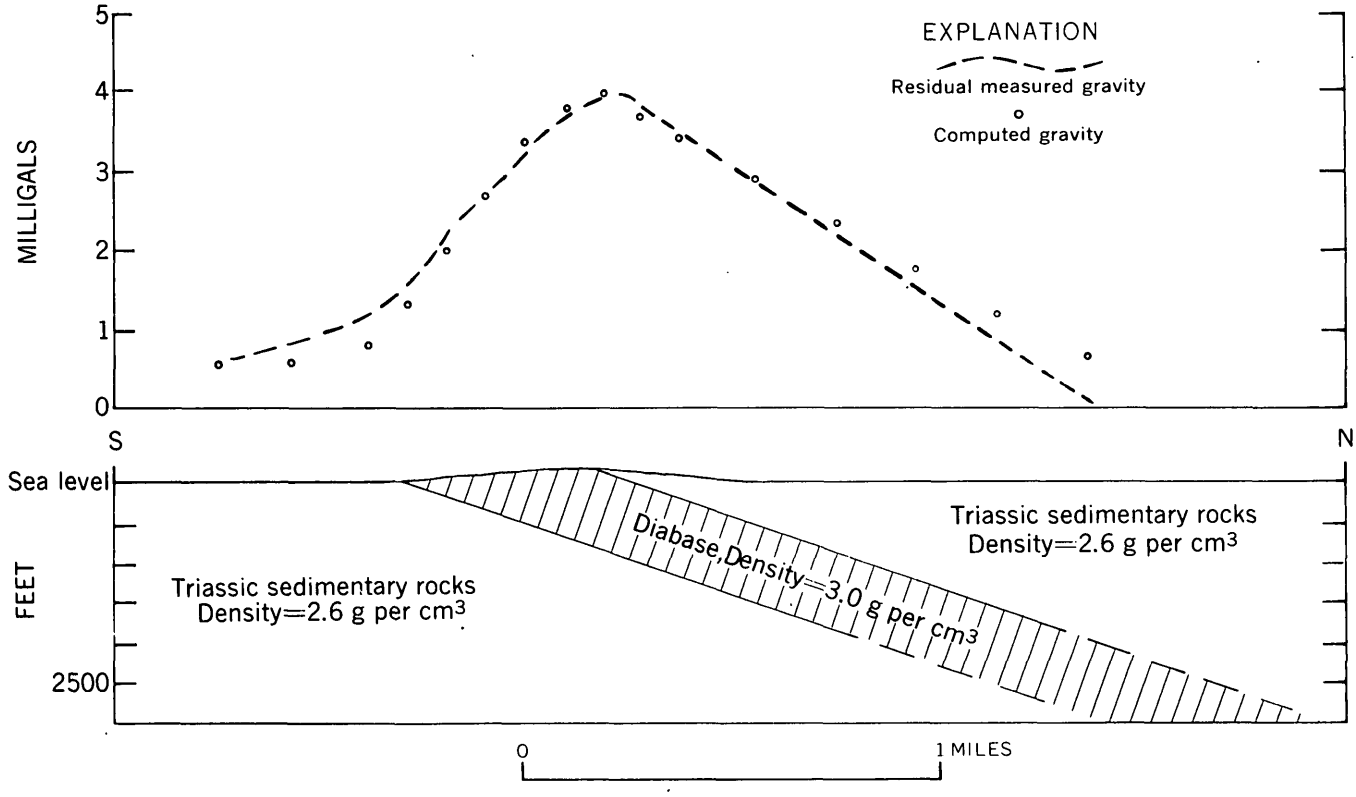

FIGURE 242.2.—Gravity profile and section over diabase sill, Solebury Mountain, Bucks County, Pa.

243. RELATION BETWEEN GRAVITY AND STRUCTURE OF PART OF THE WESTERN FLANK OF THE BLACK HILLS, SOUTH DAKOTA AND WYOMING

By R. A. Black and J. C. Roller, Denver, Colo.

Work done in cooperation with the U.S. Atomic Energy Commission

A regional gravity survey delineates the major structural features of part of the west flank of the Black Hills in the area between lat 43°30′ and 44°00′ and long 103°52½′ and 104°30′, South Dakota and Wyoming (figs. 243.1 and 243.2). Results are presented in this report.

The Black Hills are described by Darton and Paige (1925) as an irregular dome-shaped anticline, elongated northwest and southeast, asymmetrical with the steep side on the west, and covering an area about 125 miles long and 60 miles wide. Bartram (1940) states that the Black Hills were formed during the Laramide Revolution in Late Cretaceous to early Eocene time. Noble (1952) regards the Black Hills as consisting of two uplifted blocks, the main one with its axis trending nearly north, and the other with an axis trending northwest. The uplift is most abrupt on the western flank of the Black Hills near the town of Newcastle, Wyo., where the two blocks join. Noble (1952) proposed that predominantly vertical forces

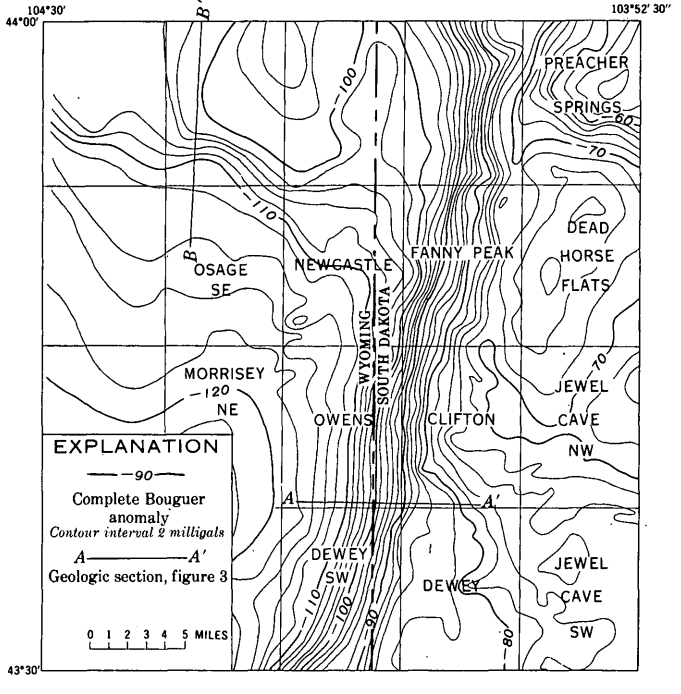

FIGURE 243.1.—Complete Bouguer gravity map of part of the western flank of the Black Hills.

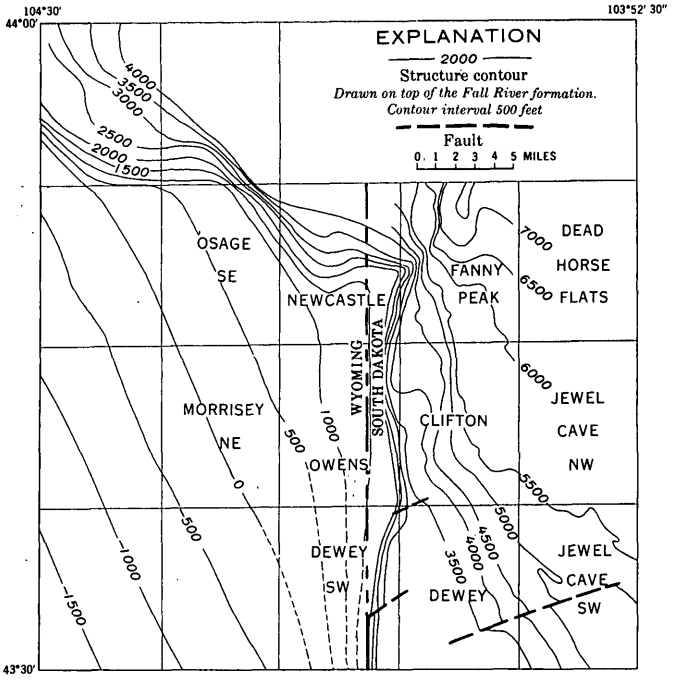

FIGURE 243.2.—Structural contour map of part of the western flank of the Black Hills.

associated with igneous intrusion are responsible for the main structural features of the Black Hills. Chamberlin (1945) suggested that compression in a northeast-southwest direction may have produced north and west-northwest shear zones that determined the outline of the Black Hills and perhaps produced the uplift. Whatever the origin of the uplift, it is of sufficent magnitude to be reflected in the regional gravity measurements, especially near Newcastle.

Standard gravity field methods and reduction techniques were used in the work. Stations were occupied at intervals of about 1 to 1½ miles. Where available, 7½-minute topographic maps were used to locate gravity stations at points where elevations were known to the nearest foot. Altimeters and county road maps were used in areas where topographic maps were not available.

Observed gravity was based on a value of 980,145 milligals for pendulum station 270 at Newcastle, Wyo. (Duerksen, 1949). The gravity data were reduced to

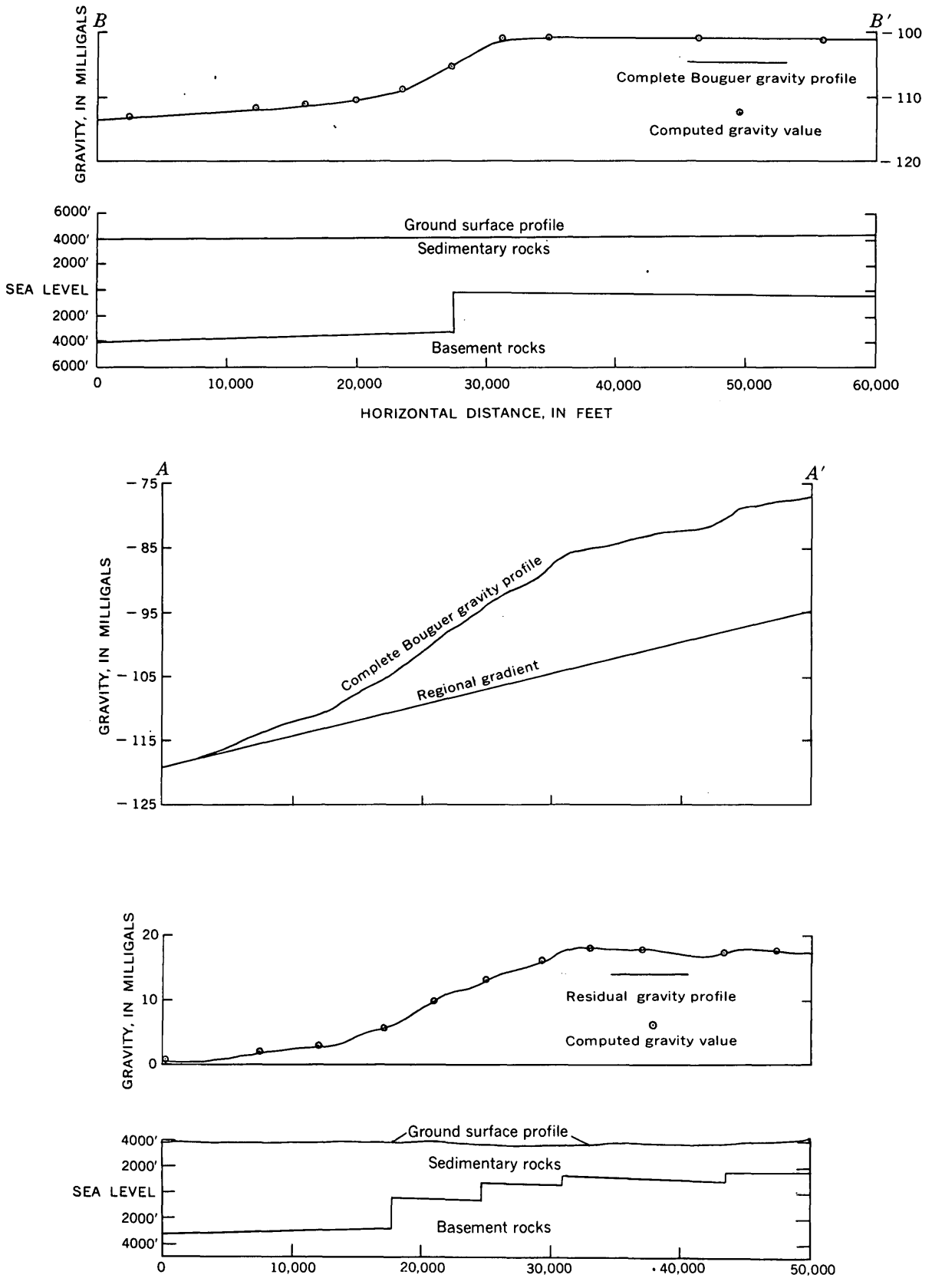

FIGURE 243.3.—Generalized geologic sections along lines A–A' and B–B' determined by two-dimensional graticule analysis.

a sea level datum by using an elevation correction factor of 0.063 milligal per foot, which corresponds to a density of 2.43 grams per cubic centimeter. This value was computed as the weighted average of the densities of the sedimentary section in the southern Black Hills, and the Bouguer anomaly values therefore represent changes in configuration of the more dense basement rocks.

The complete Bouguer anomaly map of the area discussed is shown on figure 243.1. The contour interval is 2 milligals and all gravity values are negative. The most prominent feature of the gravity map is a north-trending zone having a steep east-west gravity gradient that extends from the southwest corner of the Dewey SW 7½-minute quadrangle to north of the Fanny Peak quadrangle. A second zone of steep gravity gradient, less pronounced than the north-trending zone, extends northwest to southeast and intersects the north-trending zone in the Fanny Peak quadrangle.

Figure 243.2 is a structure contour map of the area drawn on the top of the Fall River formation. The structure data are from Dobbin and others (1957) and from unpublished data by D. A. Brobst, N. C. Cuppels, and W. A. Braddock. The map shows two monoclines, one trending north and the other trending northwest, which intersect in the western part of the Fanny Peak quadrangle. A structural terrace is formed between the two monoclines in the Dewey quadrangle. The uniform slope in the southwest part of the map represents regional dip into the Powder River basin.

Comparison of figures 243.1 and 243.2 shows a good general correlation between the monoclines and the zones of steep gravity gradient. In detail, the tightening of the monoclinal gradient just north of the Osage SE quadrangle is reflected by an increase in the gravity gradient at this point; the intersection of the two monoclines at the western edge of the Fanny Peak quadrangle, and the apparent offset of the northwest-trending monocline is reflected by the gravity contours. The terrace in the Dewey quadrangle is clearly shown by the gravity data.

Two gravity profiles, *A-A′* and *B-B′* (fig. 243.1), were selected for theoretical analysis using a two-dimensional graticule. These gravity profiles, assumed geologic cross sections, and computed gravity values are shown on figure 243.3. A density contrast of 0.35 grams per cubic centimeter was used between the sedimentary and basement rocks. On profile *A-A′*, 3 faults or steep folds with a combined throw of approximately 4,000 feet provide a close fit to the residual gravity profile in the zone of north-striking gravity gradient; the fault or steep fold with a throw of approximately 900 feet at the horizontal distance of 43,500 feet (fig. 243.3) is related to the northwesterly trending zone. Although the gravity data are insensitive to the dip of fault planes, it seems probable, from reverse slopes of the basement surfaces on the upthrown blocks, that the faults are reverse faults. No faults parallel to the monoclines break the surface rocks and the assumed reverse faults, if present, die out upward. Gravity profile *B-B′* (fig. 243.2) is essentially perpendicular to the regional gradient. A single fault or steep fold with a throw of approximately 3,200 feet provides a close fit to the observed gravity profile. The gravity data thus indicate that there has been greater vertical movement along the north-south direction than has occurred along the northwest-southeast direction. This is shown also by the structure map, figure 243.2.

REFERENCES

Bartram, J. G., 1940, The stratigraphy and structure of eastern Wyoming and the Black Hills area, *in* Kansas Geol. Soc. Guidebook, 14th Ann. Field Conf., Aug. 26 to Sept. 1: p. 113–120.

Chamberlin, R. T., 1945, Basement control in Rocky Mountain deformation: Am. Jour. Sci., v. 243–A (Daly Volume), p. 98–116.

Darton, N. H., and Paige, Sidney, 1925, Central Black Hills: U.S. Geol. Survey Geol. Atlas, Folio 219.

Dobbin, C. E., Cramer, W. B., and Horn, G. H., 1957, Geologic and structural map of the southeastern part of the Powder River Basin: U.S. Geol. Survey Oil and Gas Inv. Map OM–185.

Duerksen, J. A., 1949, Pendulum gravity data in the United States: U.S. Coast and Geodetic Survey Spec. Pub. 244.

Noble, J. A., 1952, Structural features of the Black Hills and adjacent areas developed since pre-Cambrian time: Billings Geol. Soc. Guidebook, 3rd Ann. Field Conf., Sept. 1952: p. 31–37.

244. GRAVITY PROFILE ALONG ROBERTS TUNNEL, COLORADO

By Donald Plouff, Denver, Colo.

During 1960 gravity stations were established in the Harold D. Roberts Tunnel as part of a regional gravity survey of the Colorado Rocky Mountains. This tunnel was built to transport water for 23 miles from the western to the eastern slope of the Continental Divide. The Roberts Tunnel penetrates three major groups of rocks: granite and schist (Precambrian), sedimentary rock (Mesozoic), and quartz monzonite (Tertiary) (fig. 244.1).

Roberts Tunnel affords a unique opportunity to establish a closely spaced line of gravity stations across the Rocky Mountains, without entailing extensive surveying or time-consuming access to the area. Gravity measurement at two levels—in the tunnel and at the surface—provides data for study of the density of the intervening rocks and the variation of the vertical gradient of gravity with depth and location.

The gravity values for 10 stations at the surface, established near the tunnel line, are compared with gravity values at stations in the tunnel. The surface stations are near bench marks or points whose elevations were determined photogrammetrically. The elevations in the tunnel were surveyed by Tipton and Kalmbach, Inc., supervising engineers, on behalf of the Denver Board of Water Commisioners. The stations at the surface are no more than 730 feet horizontally from the tunnel line. Errors in latitude correction and in location relative to the Bouguer gravity anomaly caused by this offset are considered negligible.

The values of observed gravity were established relative to a value of 979,633.0 milligals at Stapleton Municipal Airfield in Denver, (Woollard, 1958, p. 532). The accuracy of the measurement of the observed gravity within the limits of this survey is believed to be about 0.3 milligals. Corrections for terrain were calculated through zone "O" of the U.S. Coast and Geodetic Survey system (Swick, 1942), corresponding to a distance of 104 miles from the station. Corrections also were made for the small second-order term in the free-air correction and the effect of curvature on the Bouguer correction (Swick, 1942, p. 64, 67).

Terrain corrections for gravity stations at the surface ranged from 3.1 milligals at Dillon, where the elevation is 8,832 feet, to 25.8 milligals along the Continental Divide, where the elevation is 13,180 feet above sea level. Terrain corrections for gravity stations in the tunnel ranged from 33.6 milligals about midway between the access shaft and the West Portal,

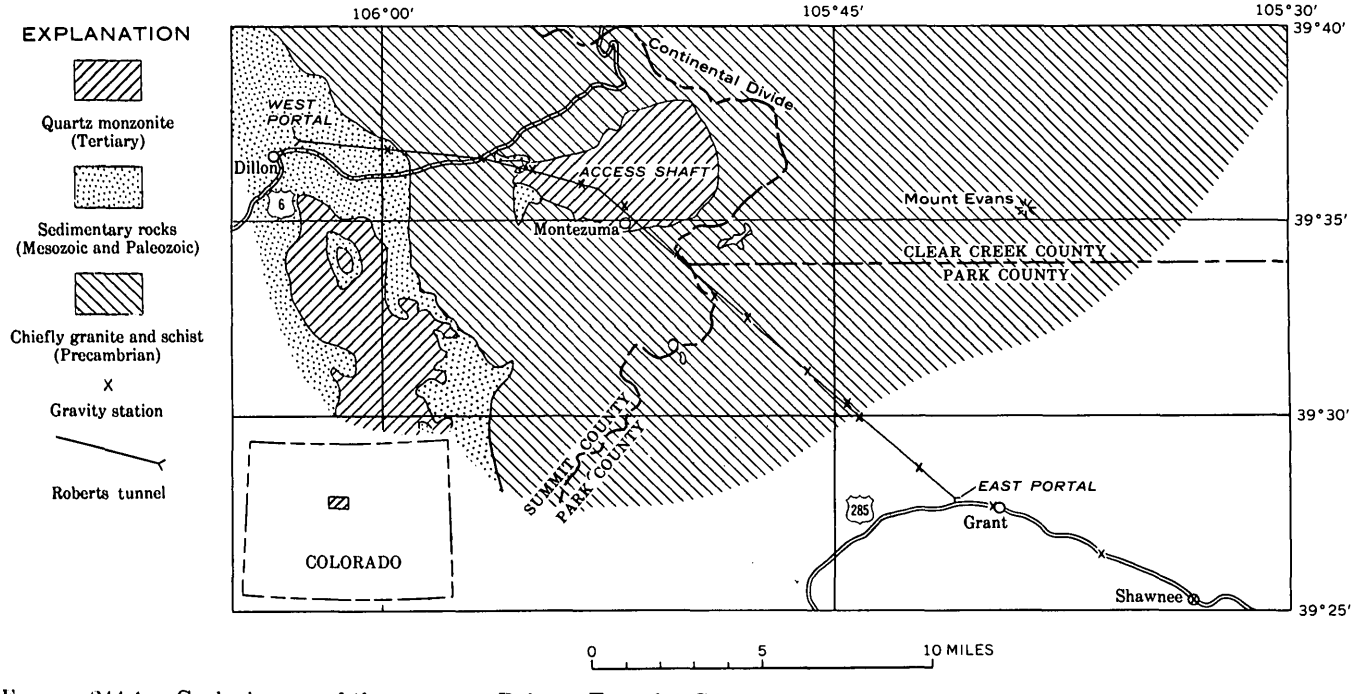

Figure 244.1.—Geologic map of the area near Roberts Tunnel. Geology generalized from Lovering and Goddard (1950, pl. 2).

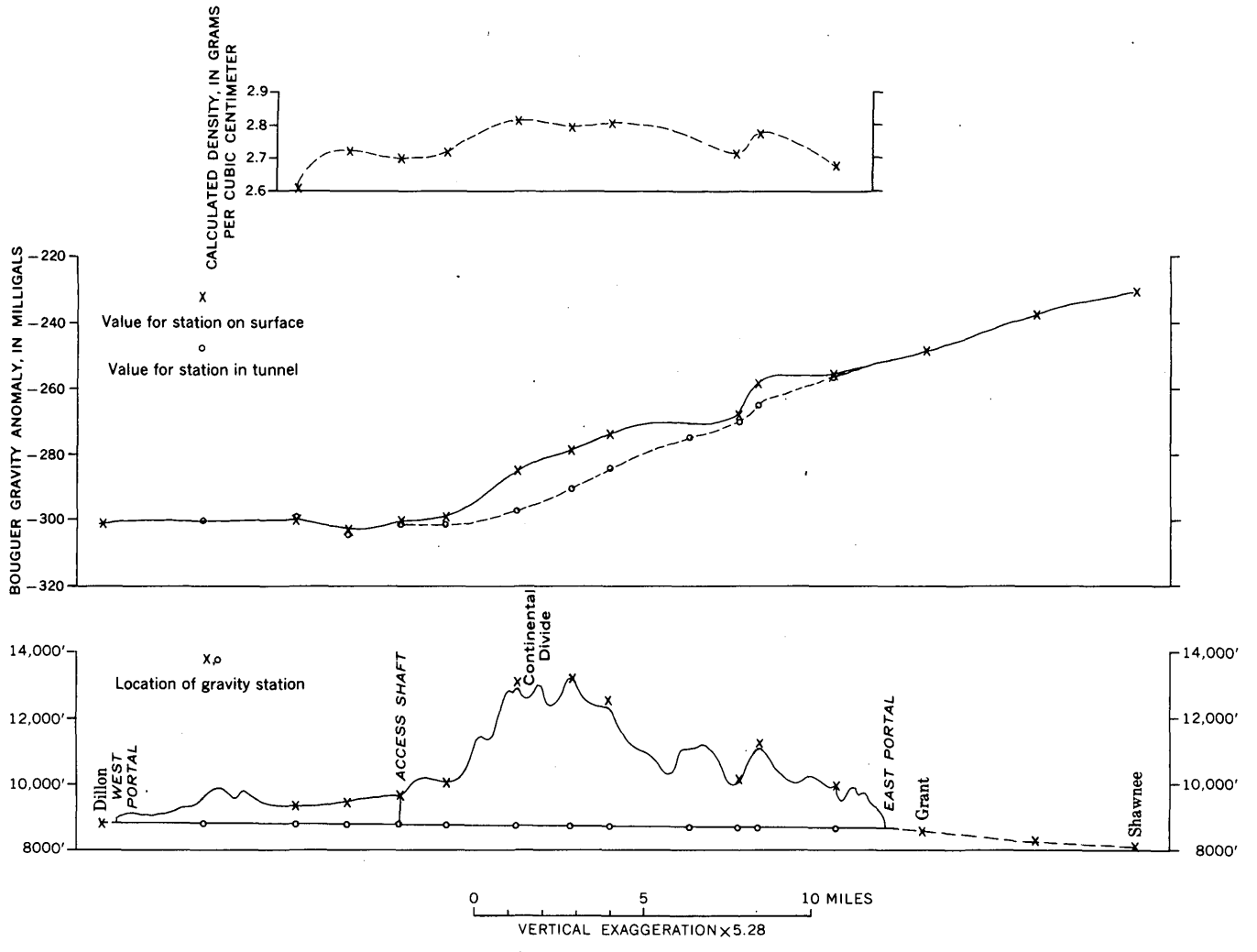

FIGURE 244.2.—Bouguer gravity anomaly and calculated densities along Roberts Tunnel.

where the tunnel is 544 feet beneath the surface, to 110.6 milligals where the tunnel is 4,497 feet beneath the surface. Thus an error as small as 1 percent in terrain correction will limit the accuracy of the Bouguer anomaly to 0.3 milligal at the surface and 1.1 milligals in the tunnel. The correction for material excavated from the tunnel is 0.1 milligal and that for the shaft is 0.0 milligals.

The Bouguer gravity anomaly has a relief of about 70 milligals (fig. 244.2) along a line extending from Dillon southeastward to Shawnee via the Roberts Tunnel. An average density of 2.67 g per cm^3 for the rocks between the surface and sea level has been assumed for these calculations. The most negative point along the gravity profile is west of the access shaft, rather than in the vicinity of the Continental Divide, as would be expected if the density of underlying rocks is inversely related to elevation.

The difference between the Bouguer gravity anomaly along the Roberts Tunnel, as measured at the surface and in the tunnel, is largely caused by variation from the assumed average density of 2.67 g per cm^3 in the density of the intervening rocks, incompleteness or inaccuracy of the terrain correction, and variation of the vertical gradient of gravity with depth and location. If the difference is entirely caused by the effect of the density variations, the density is given by:

$$D=(G_{BA}+Fh_{BA}+f_{BA})/(Mh_{BA}-T_{BA}),$$

where D is the average density of the intervening rocks calculated from gravity data, G_{BA} is the difference of observed gravity at the surface and in the tunnel, F is the free-air correction factor (0.09406 milligals per foot), h_{BA} is the difference in elevation between the two stations, f_{BA} is the difference of second-order free-air corrections between the two stations taken from a nomograph (Swick, 1942), M is the Bouguer correction

factor (0.01276 milligals per foot per unit density), and T_{BA} is the difference of terrain and curvature corrections between the two stations for unit density. The densities calculated with this formula show a positive correlation with topography (fig. 244.2). The range is from 2.61 to 2.81 g per cm^3. Carrying the terrain correction beyond 104 miles tends slightly to increase the calculated densities.

The mean density for 144 representative samples of Precambrian rock collected from the Alva B. Adams Tunnel, about 45 miles north of the Roberts Tunnel, is 2.67 g per cm^3 (Birch, 1950, p. 608). The mean densities for granite and quartz monzonite (78 samples), quartz diorite gneiss (18 samples), and injection schist and gneiss (48 samples) are 2.63, 2.67, and 2.73 g per cm^3, respectively. Variations in density alone do not account for the difference of the Bouguer gravity anomaly, as calculated at stations in the tunnel and on the surface.

Near the Roberts Tunnel, the most negative gravity values of the gravity low that is associated with the deficiency of mass deep in the crust beneath the Rocky Mountains (Woollard, 1943, p. 768–769; Qureshy, 1960; Stuart and Wahl, Art. 245, are near the west end of Roberts Tunnel. The vertical gradient of gravity, F, is less than 0.09406 milligals per foot—the value usually assumed for free-air corrections—in this area of anomalously negative gravity. Hence the calculated densities are consistently too high and increase with the thickness of cover, h_{BA}, over the tunnel. The general correspondence of calculated density with topography is attributed largely to the decrease of the vertical gradient of gravity near the major gravity low associated with the Rocky Mountains.

REFERENCES

Birch, Francis, 1950, Flow of heat in the Front Range, Colorado: Geol. Soc. America Bull., v. 61, p. 567–630.

Lovering, T. S., and Goddard, E. N., 1950, Geology and ore deposits of the Front Range, Colorado: U.S. Geol. Survey Prof. Paper 223, 319 p.

Qureshy, M. N., 1960, Airy-Heiskanen anomaly map of Colorado, *in* Guide to the geology of Colorado: Geol. Soc. America, Rocky Mountain Assoc. of Geologists, and Colorado Scientific Soc., Denver, p. 8–9.

Swick, C. H., 1942, Pendulum gravity measurements and isostatic reductions: U.S. Coast and Geod. Survey Spec. Pub. 232, 82 p.

Woollard, G. P., 1943, Transcontinental gravitational and magnetic profile of North America and its relation to geologic structure: Geol. Soc. America Bull., v. 54, no. 6, p. 747–790.

——— 1958, Results for a gravity control network at airports in the United States: Geophysics, v. 23, no. 3, p. 520–535.

245. A DETAILED GRAVITY PROFILE ACROSS THE SOUTHERN ROCKY MOUNTAINS, COLORADO

By David J. Stuart and Ronald R. Wahl, Denver, Colo.

Gravity measurements discussed in this paper are part of a gravity survey that will provide a network across Colorado between the 39th and 40th parallels of latitude. Earlier, less detailed work in the area has been described by Woollard (1943), Holmer (1954), and Qureshy (1958).

A LaCoste and Romberg portable geodetic gravity meter with a scale value of about 0.01 mgal (milligal) per dial division was used to make the measurements. Stations were established at bench marks and spot elevations shown on U.S. Geological Survey maps, and at locations where elevations could be obtained from road profiles of the Colorado Department of Highways. Observed gravity values are referred to a series of 10 U.S. Geological Survey base stations that are tied to airport gravity network stations at Denver and Colorado Springs (Woollard, 1958). Instrumental readings, corrected for drift, have been reduced to sea level on the assumption that rocks between stations and sea level have an average density of 2.67 g per cm^3. Terrain corrections, through Hayford letter-zone "O," have been added to all the stations (Swick, 1942). Suitable maps for the estimation of terrain effects of the inner zones were available for most of the stations; however, terrain corrections for 23 stations were made from Army Map Service 1/250,000 sheets. An attempt was made to locate these stations at points where the effect of nearby topography would be small.

Gravity values at 261 stations were projected at right angles onto seven straight-line segments that generally follow U.S. Highway 6 west of Denver

601530 O—61——18

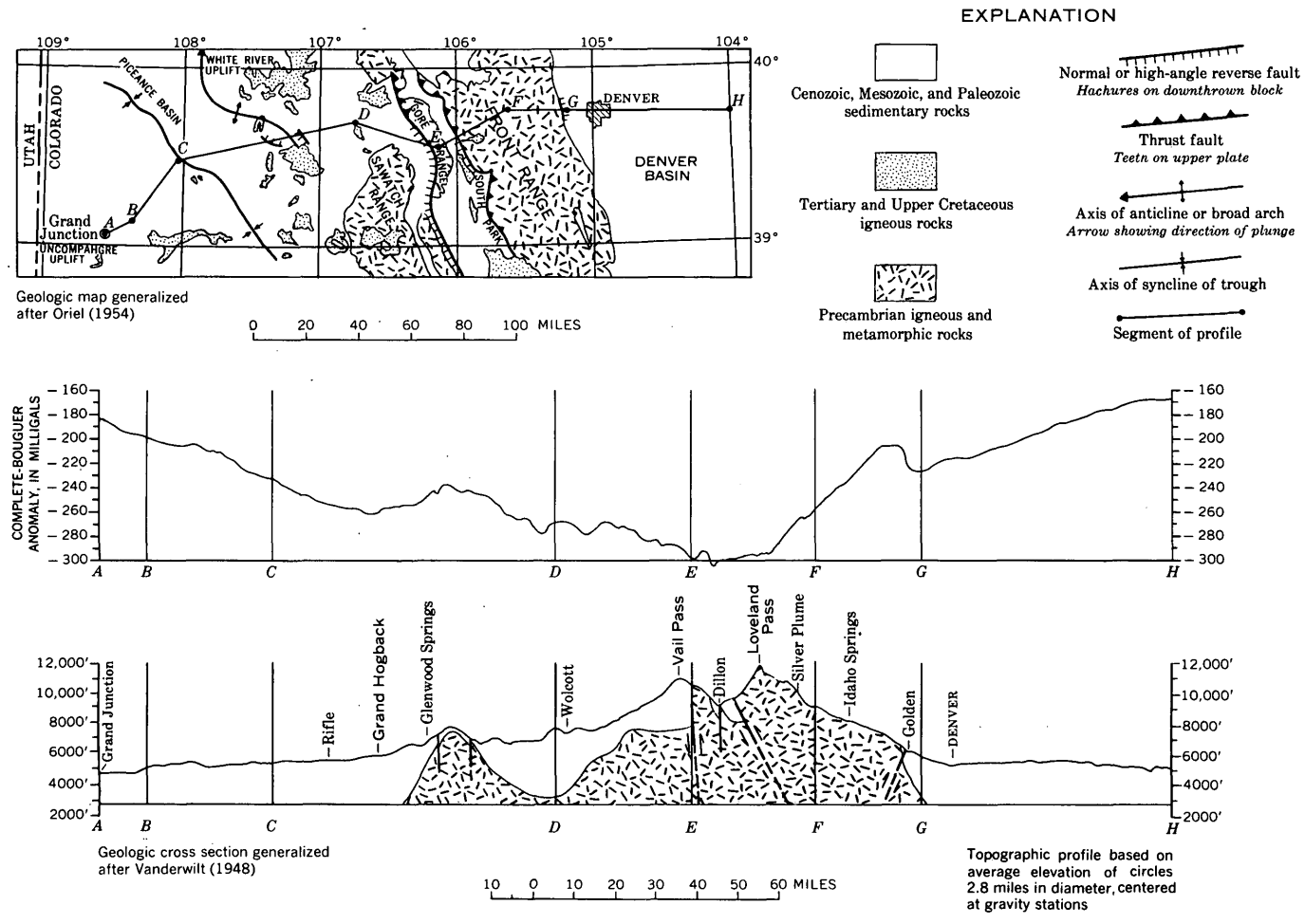

FIGURE 245.1.—Bouguer-gravity profile and generalized geology across the Southern Rocky Mountains, Colorado.

and extend due east from Denver (fig. 245.1). None of these stations is more than 4 miles from the profile segments, and most stations are within 2 miles. Total length of the profile is 264 miles, so average spacing is nearly one station per mile.

The broad gravity low, extending from one end of the profile to the other, demonstrates that the Southern Rocky Mountains are, to some extent at least, isostatically compensated on a regional scale. Absence of gravity lows associated with the White River uplift and other prominent topographic highs suggests that large but geographically limited loads are not locally compensated. Qureshy (1960) has observed that isostatic equilibrium prevails only on a broad scale in Colorado.

Superimposed on the broad regional low are anomalies that show some relation to the configuration of the upper surface of Precambrian basement rocks. At the eastern end of the profile (fig. 245.1), the gravity field decreases westward at a fairly uniform rate to about the area near Denver where contact between the basement rock and overlying sedimentary rocks dips westward to its greatest depth. Gravity values become more positive across steep gradients on approaching the more dense metamorphic rocks of the Front Range. Westward toward the Continental Divide, the gravity field decreases with steep gradients as a result of the deep-seated mass deficit which tends to compensate the mass excess of the mountains. Little gravity relief is observed in traversing the Colorado mineral belt between Idaho Springs and Silver Plume. A gravity high of 7 mgals amplitude, based on 8 stations near Silver Plume, may bear some relation to the mineral belt. The 10-mgal high immediately west of Dillon corresponds to a sequence of relatively dense Precambrian metasedimentary rocks.

It is difficult to distinguish, without additional data, whether the anomalous gravity lows on either side of Wolcott are the expression of density contrasts within the sedimentary basin or within the underlying Precambrian basement rocks.

Precambrian basement rocks are exposed east of Glenwood Springs where the gravity profile crosses the White River uplift. These rocks are more dense than the rocks to the east and to the west, so they give rise to a gravity high about 35 miles wide and of about 25 mgals amplitude (fig. 245.1). Slight gravity relief superimposed on this high is probably the result of inaccuracy in the terrain corrections. Terrain corrections of more than 30 mgals were computed for some stations in this area of strong topographic relief. The gravity low west of the White River uplift is probably related to the Piceance basin; however, the largest negative values do not occur near the structural axis of the basin west of Rifle, but are displaced eastward to a point near Grand Hogback, as was noted by Holmer (1954).

The increase in gravity field level west of Grand Hogback is caused, in part, by increased distance from the region of maximum gravity influence of the Rocky Mountain compensating mass, and to a decrease in thickness of the sedimentary-rock section on the western flank of the Piceance basin.

REFERENCES

Holmer, R. C., 1954, A regional gravity survey of Colorado: Colorado School Mines Thesis 801, 94 p.

Oriel, S. S., 1954, Major tectonic elements of Colorado: a review, *in* Oil and gas fields of Colorado: Rocky Mountain Assoc. Geologists, Denver, p. 41–48.

Qureshy, M. N., 1958, Gravity anomalies and computed variations in thickness of the earth's crust in Colorado: Colorado School Mines Thesis 862, 41 p.

——— 1960, Airy-Heiskanen map of Colorado, *in* Guide to the geology of Colorado: Geol. Soc. America, Rocky Mountain Assoc. Geologists, and Colorado Sci. Soc., Denver, p. 8–9.

Swick, C. H., 1942, Pendulum gravity measurements and isostatic reductions: U.S. Coast and Geod. Survey Spec. Pub. 232, 82 p.

Vanderwilt, J. W., 1948, Field trip no. 3, Denver, Glenwood Springs, Rifle, Leadville, South Park, *in* Guide to the geology of central Colorado: Colorado School Mines Quart., v. 43, no. 2, p. 73–116.

Woollard, G. P., 1943, Transcontinental gravitational and magnetic profile of North America and its relation to geologic structure: Geol. Soc. America Bull., v. 54, no. 6, p. 747–790.

——— 1958, Results for a gravity control network at airports in the United States: Geophysics, v. 23, no. 3, p. 520–535.

246. AFTERSHOCK-ENERGY RELEASE VERSUS TIDAL EFFECTS, HEBGEN LAKE EARTHQUAKE, MONTANA

By Renner B. Hofmann, Denver, Colo.

Distance, magnitude, and energy were calculated from 876 seismograms of aftershocks which followed the Hebgen Lake, Montana, earthquake of 1959. Two portable seismic stations, approximately 40 km southwest and 130 km south of the epicentral area, recorded the aftershocks for about 2½ days (Stewart and others, 1960).

Only shocks of magnitude 2.2 and greater, obtained from 475 seismograms, were used. During 90 percent of the recording time, instrument gains and background noise in the epicentral area were such that all shocks of magnitude 2.2 and greater should have been recorded.

Chester Glenn, meteorologist at Stapleton Airfield, Denver, Colo., and Roy L. Fox, Director, and Gerald L. Barger of the National Weather Records Center, Asheville, N. C., provided meteorological data and barograms for the Yellowstone Park area.

ENERGY CALCULATIONS

The magnitude of each aftershock and the energy released were calculated from formulas developed by Gutenberg for California earthquakes near a depth of 18 km (Richter, 1958). Uncertainties caused by focal depth, polarization, and ground character at the station are unavoidable, but are not believed to be serious for the purposes of this study. Continuous operation at the stations was not possible. Interruptions in recording were caused by changing recording paper, instrumental difficulties, and field testing the seismic systems.

Energies released by aftershocks recorded during 0.1-day intervals were summed, and each sum was divided by the fraction of the interval during which the instruments were operating. The resulting number, shown on figure 246.1, is assumed to be the energy that would have been recorded during the interval

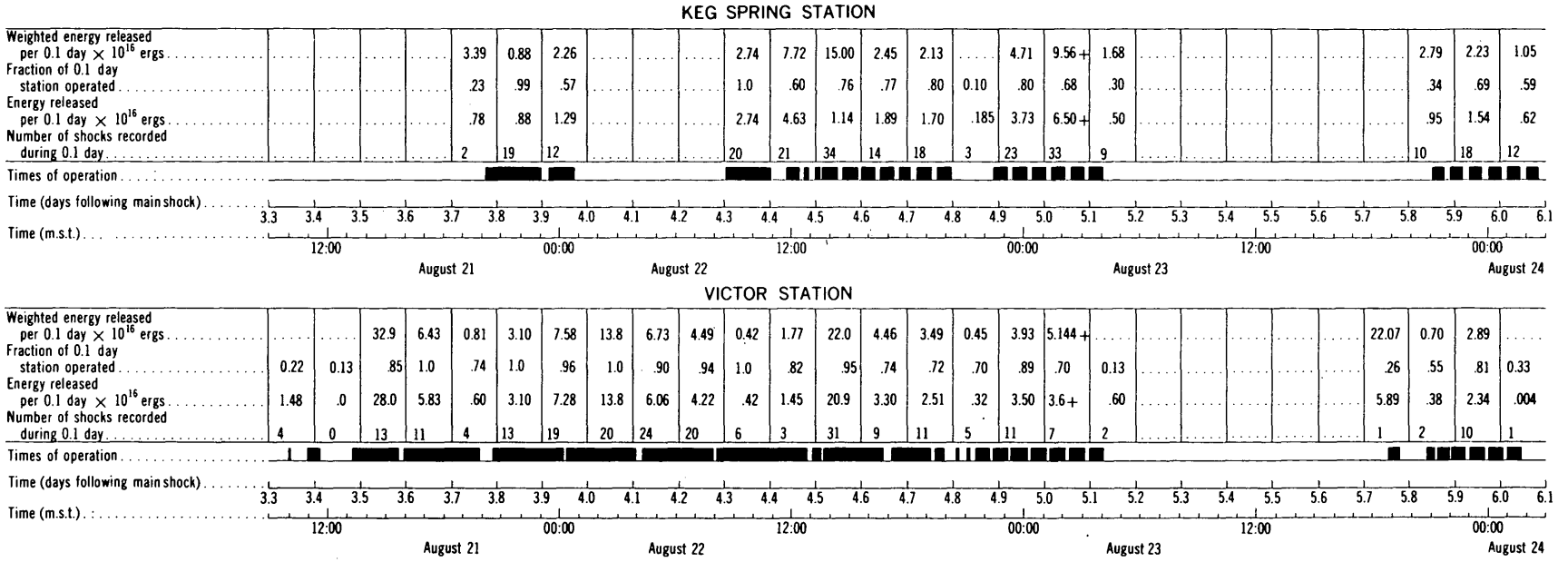

FIGURE 246.1.—Times of station operation and energy-release data for aftershocks of magnitude 2.2 and greater.

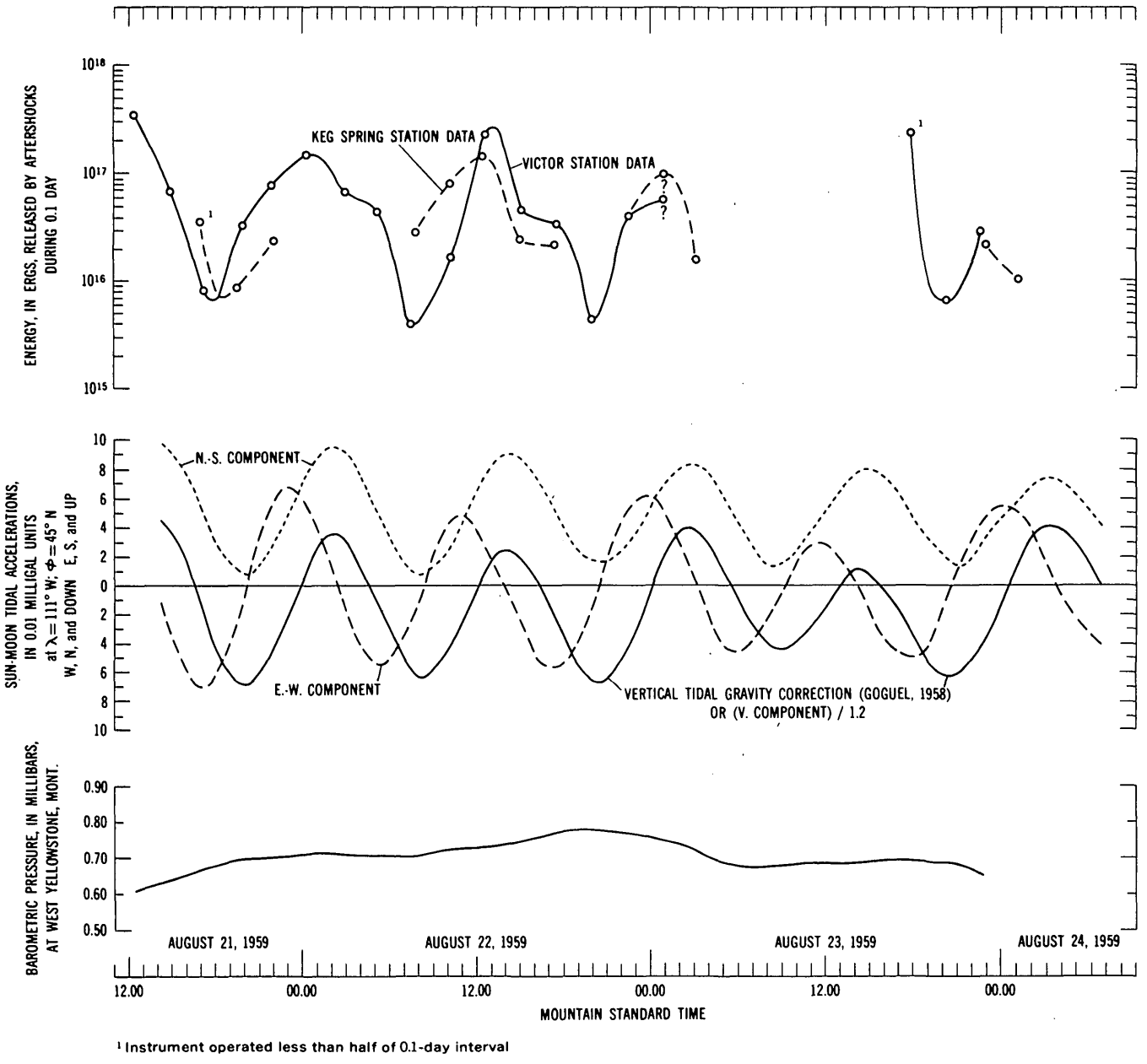

FIGURE 246.2.—Comparison of aftershock-energy-release with barometric pressure and components of tidal acceleration caused by the sun and moon.

if the station had been in continuous operation. For most intervals, the correction caused by inoperative time is small. Any inoperative time, however, may contribute a significant error because the sample size is inherently limited and most of the energy is contributed by the larger aftershocks. Curves were plotted from the weighted energies released per 0.1 day (fig. 246.1). These aftershock-energy-release curves seem to have a smoother shape for times when recording was continuous; however, the proportion of time the stations were operating seems unrelated to the maxima and minima of the energy-release curves.

With the exception of two values (figs. 246.1 and 246.2), energy was plotted only for those intervals during which the instruments operated more than half of the 0.1-day interval. Points labeled with a question mark (fig. 246.2) represent a sequence of aftershocks that ran together and whose amplitudes were sufficient to cause clipping on records from both stations. The energy could not be estimated as accu-

rately for this period as for the others, but the values shown are believed to be at least the minimum. Except for the weighting procedure, there is no normalization or other statistical process applied to the data. Other 0.1-day intervals could have been used.

TIDAL ACCELERATIONS AND BAROMETRIC PRESSURE

The vertical tidal gravity correction (fig. 246.2) was taken directly from Goguel (1958). The horizontal components of tidal acceleration (force per unit mass at the surface) for each hour were computed using the stereographic nomogram method of Doodson and Warburg (1941). The attractions of both the sun and the moon were taken into account. The predominant period of the tidal accelerations, in the epicentral region of the aftershock sequence during the time of recording, is semidiurnal. The energy released (fig. 246.2) also has a semidiurnal period, and the maxima and minima correspond closely in time with maxima and minima of tidal accelerations. Tidal accelerations are not the same over large areas and are not exactly periodic, so a better correlation might be expected if the actual tidal accelerations for a given latitude, longitude, and time were used.

The barogram from West Yellowstone, Mont., does not have a semidiurnal period (fig. 246.2). The barogram is somewhat irregular but seems to have a predominant period of about one day. Barograms from Cody, Wyo., and Livingston, Mont., for the same time have similar shapes. Changes in atmospheric loading, therefore, had no obvious relation to the variation of aftershock-energy release.

Diurnal variations in numbers of earthquakes at other places have been reported by Cotton (1922), Davison (1934), Stetson (1935), and Romana and Lobato (1948). Nishimura (1950) found that at the times of smallest observed strain "* * * seismic activity was nearly zero * * *." These and similar studies, however, have been concerned mainly with earthquakes or aftershocks occurring over large areas and over long time intervals.

REFERENCES

Cotton, L. A., 1922, Earthquake frequencies with special reference to tidal stresses in the lithosphere: Seismol. Soc. America Bull., v. 12, p. 47–198.

Davison, Charles, 1934, The diurnal periodicity of earthquakes: Jour. Geology, v. 42, no. 5, p. 449–468.

Doodson, A. T., and Warburg, H. D., 1941, Admiralty manual of tides: His Majesty's Stationery Office, London, Chapter 3, 270 p.

Goguel, Jean, 1958, Tidal gravity corrections for 1959: Geophys. Prosp., v. 6, Suppl. 1.

Nishimura, Eiichi, 1950, On earth tides: Am. Geophys. Union Trans., v. 31, no. 3, p. 357–376.

Richter, C. F., 1958, Elementary seismology: San Francisco, W. H. Freeman and Co., 768 p.

Romana, Antonio (S. J.) and Lobato, Aurora, 1948, Sur la periode annuelle et diurne des tremblements de terre: Internat. Union Geodesy and Geophysics, Series A, v. 17, p. 205–215.

Stetson, H. T., 1935, The correlation of deep-focus earthquakes with lunar angle hour and declination: Science, v. 82, no. 29, p. 523–524.

Stewart, S. W., Hofmann, R. B., and Diment, W. H., 1960, Some aftershocks of the Hebgen Lake, Montana, earthquake of August 1959, *in* Short papers in the geological sciences: U.S. Geol. Survey Prof. Paper 400–B, p. B219–B221.

247. DETERMINATION OF THICKNESS OF A BASALT FLOW BY ELECTRICAL RESISTIVITY METHOD ON BUCKBOARD MESA, NEVADA TEST SITE, NYE COUNTY, NEVADA

By J. C. Roller and R. A. Black, Denver, Colo.

Work done in cooperation with the U.S. Atomic Energy Commission

As part of the selection and evaluation of a test site for a nuclear cratering experiment in basalt, the electrical resistivity method was used by the Geological Survey to determine the thickness of a basalt flow on Buckboard Mesa at the Nevada Test Site, Nye County, Nev.

Buckboard Mesa, in the western part of the Nevada Test Site, is approximately 5 miles long and 2 miles wide. The surface is relatively flat except at the northern end where a cinder cone rises 500 feet above the mesa and a low ridge extends southeastward several thousand feet from the cone. The basalt, which ranges in thickness from 50 feet on the rim to more than 200 feet in the center of the mesa, is underlain by alluvium and a soft bedded tuff of the Oak Spring formation, Miocene(?) or younger. A welded tuff about 50 feet thick is present approximately 100 feet below the base of the basalt. Technical criteria for the proposed nuclear cratering experiment required knowledge of the thickness of unweathered basalt in the immediate vicinity of the point of burst. Comparison of the known physical properties of the bedded tuff with average physical-property values published for basalt indicated that a large contrast in seismic velocity and electrical resistivity could be expected across the interface between the basalt and the underlying bedded tuff. The seismic velocity of the basalt is greater than that of the bedded tuff, and the resulting velocity inversion prohibits the use of the refraction seismic method to determine the thickness of unweathered basalt. Because of the large electrical contrast between the basalt and bedded tuff the electrical resistivity method was used.

The electrical resistivity of the bedded tuff was known to be about 50 ohm-meters (Keller, 1960) and tabulated values for unaltered basalt (Slichter and Telkes, 1950) range from 1,000 to 10,000 ohm-meters. Therefore, it was expected that field curves obtained with the electrical resistivity method would exhibit at least three electrical layers as follows: a low-resistivity surface layer, presumably representing weathered basalt; a high-resistivity layer representing the unweathered basalt; and a low-resistivity layer representing the bedded tuff.

The resistivity measurements were made with standard direct current equipment and nonpolarizing electrodes. The field technique used was that of depth profiling with the Lee-partitioning configuration. The location of the stations are given on figure 247.1.

The field data were interpreted by superposition of theoretical two- and three-layer curves and by partial curve matching. The field curve obtained at station 4 (fig. 247.2), plotted on a log-log scale, shows six distinct electrical layers. The top layer has a resistivity of 80 ohm-meters, is 1.7 feet thick, and represents alluvium. The second and third layers have thicknesses of 5 and 32 feet, resistivities of 3,120 and 50 ohm-meters, and are presumed to represent dry and partially saturated weathered basalt or cinders, respectively. Under these three layers lies a thick layer of

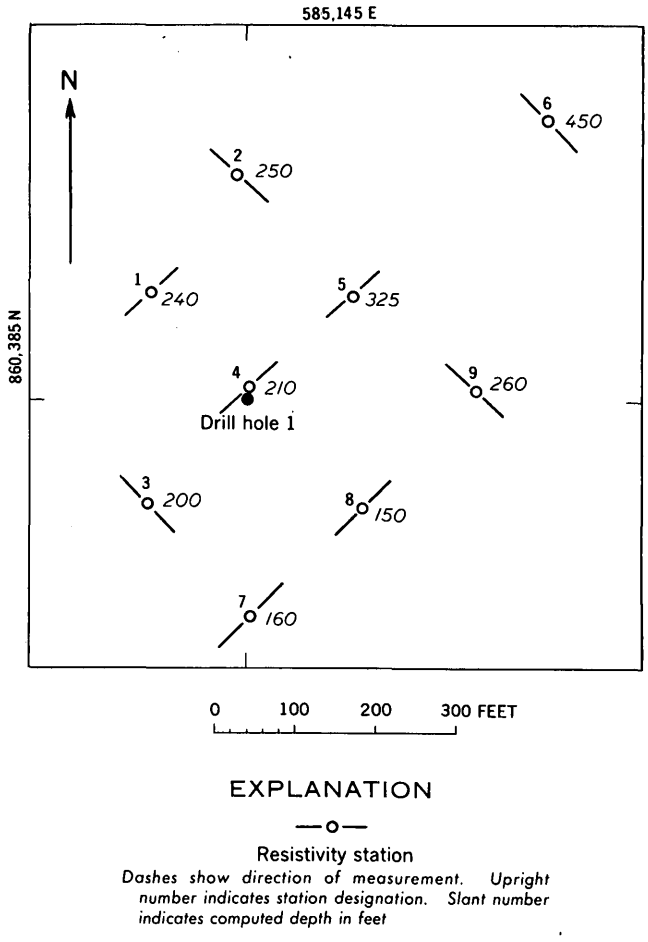

FIGURE 247.1.—Locations of resistivity stations (Nevada Test Site coordinates).

material having a resistivity of 1,260 ohm-meters interpreted to be unweathered unsaturated basalt. The depth to the base of this layer, as computed from the resistivity curve for station 4, is 210 feet. This agrees very closely with the depth of 211 feet as determined by drilling at hole 1, which is near station 4 (fig. 247.1). The low resistivity layer beneath the basalt is presumed to represent alluvium and bedded tuff. The rise in the resistivity curve beginning at an electrode spacing of approximately 350 feet is presumed to be caused by the layer of welded tuff, which has a high resistivity.

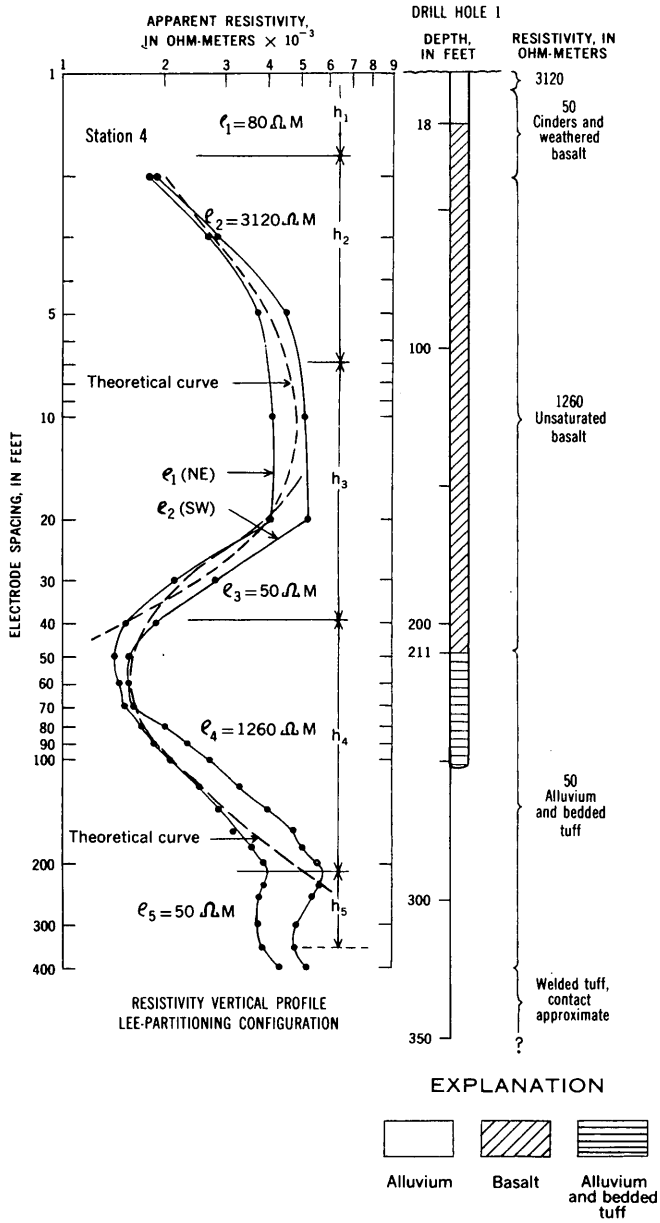

FIGURE 247.2.—Resistivity depth curve at station 4 and lithologic log of drill-hole 1.

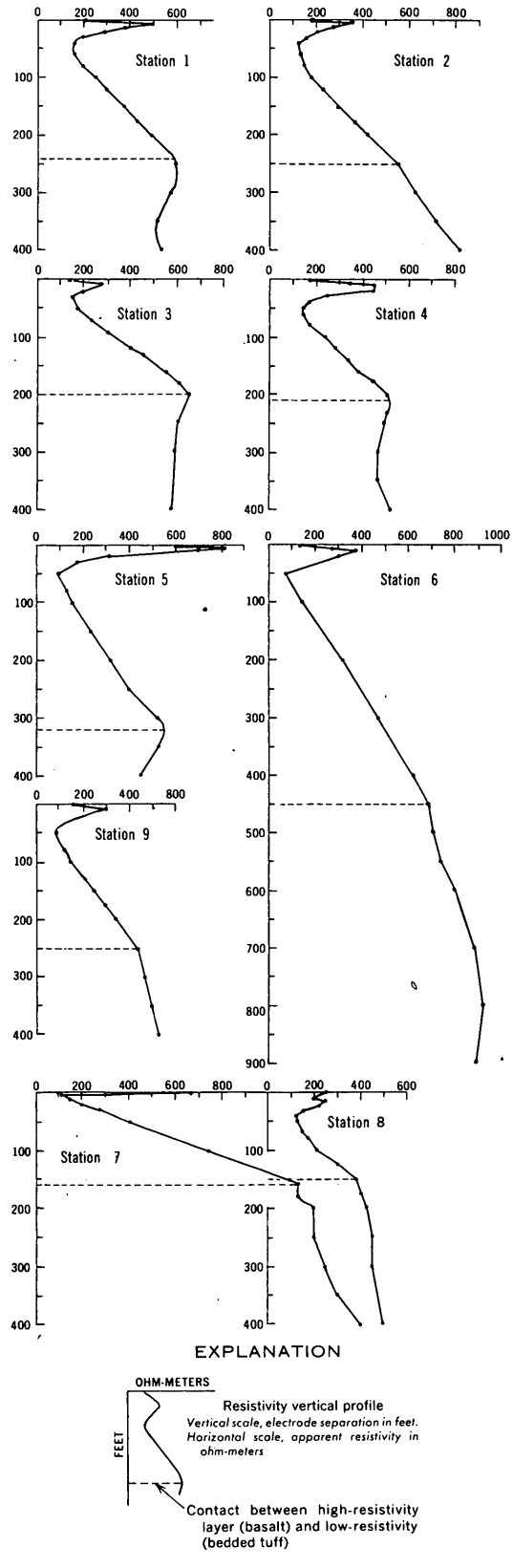

FIGURE 247.3.—Resistivity depth curves for stations shown on figure 247.1.

The curves computed from the field data are shown on figure 247.3 for nine resistivity stations in the vicinity of the proposed test site. These curves and the numbers on figure 247.1 show depths to the base of the unweathered basalt.

The computed thickness of the basalt is much greater at stations 5 and 6 than at the other stations. There are at least two possible explanations for the anomalously large values for the basalt thickness at stations 5 and 6. The first is that the low ridge extending southeastward from the volcanic cone is the surface expression of a fissure from which the basalt flowed to cover the mesa. In this event, stations 5 and 6, which lie on a line perpendicular to the ridge (with station 6 closest to the ridge), could be expected to show increased thicknesses of basalt. A second possibility is that the basalt is underlain by welded tuff in the vicinity of stations 5 and 6, and as both the welded tuff and basalt have a high resistivity, their contact could not be determined. In support of this explanation, the curves for stations 2, 8, and 9 indicate a thinning of the bedded tuff layer that lies between the basalt and the welded tuff.

REFERENCES

Keller, G. V., 1960, Physical properties of tuffs of the Oak Spring formation, Nevada, *in* Short papers in the geological sciences: U.S. Geol. Survey Prof. Paper 400–B, p. B396–B400.

Slichter, L. B., and Telkes, Maria, 1950, Electrical properties of rocks and minerals, *in* Handbook of physical constants: Geol. Soc. America Spec. Paper 36, p. 299–319.

248. GRAVITY STUDY OF CRUSTAL STRUCTURE IN WESTERN WASHINGTON

By David J. Stuart, Denver, Colo.

A gravity survey of western Washington was made during the period 1956 to 1959 to investigate the relations of the gravity field to major structural units and to study the configuration of Tertiary basins. About 2,100 gravity stations were established in an area of approximately 25,000 square miles bounded on the east by the western foothills of the Cascade Range, and on other sides by the Washington State boundaries (fig. 248.1). Topographic altitudes within this region range from sea level to nearly 8,000 feet.

Drift-corrected instrument readings were reduced to a common datum on the assumption that material between station altitude and sea level has a density of 2.67 g per cm ^{3}. Measurements were reduced to an absolute datum by reference to Seattle, Wash., and Portland, Oreg., airport gravity network stations (Woollard, 1958). Topographic corrections, through Hayford letter-zone "O," were added to only those Olympic Mountains stations having topographic effects greater than 3 milligals.

The most conspicuous feature of the gravity field is its correlation with lower and middle Eocene volcanic rocks (fig. 248.1). Where these dense rocks are at or near the surface, gravity values are relatively high, and where they are absent or deeply buried the gravity field is lower. A continuous gravity high forms a westward-opening U-shaped pattern around the Olympic Mountains, along the limbs of what appears to be a southeast-plunging anticlinorium. The southeast-plunging nose of this eroded fold is clearly outlined by the gravity high between Seattle and Tacoma. These gravity maximums and also the intensely negative anomalies such as those associated with the thick Tertiary sedimentary sections at Seattle and Everett, are superimposed upon a broad gravity minimum of about −35 milligals. A general lack of correlation between elevation and Bouguer anomaly value indicates that individual highs and lows are not a response to local isostatic conditions. An exception is in the Olympic Mountains where the Bouguer anomaly level changes to significantly greater negative values with increase in elevation, thus indicating some degree of compensation for the mass of the mountains.

A gravity anomaly alone does not give enough information to determine uniquely the mass distribution responsible for the variation; however, some information concerning the size and depth or thick-

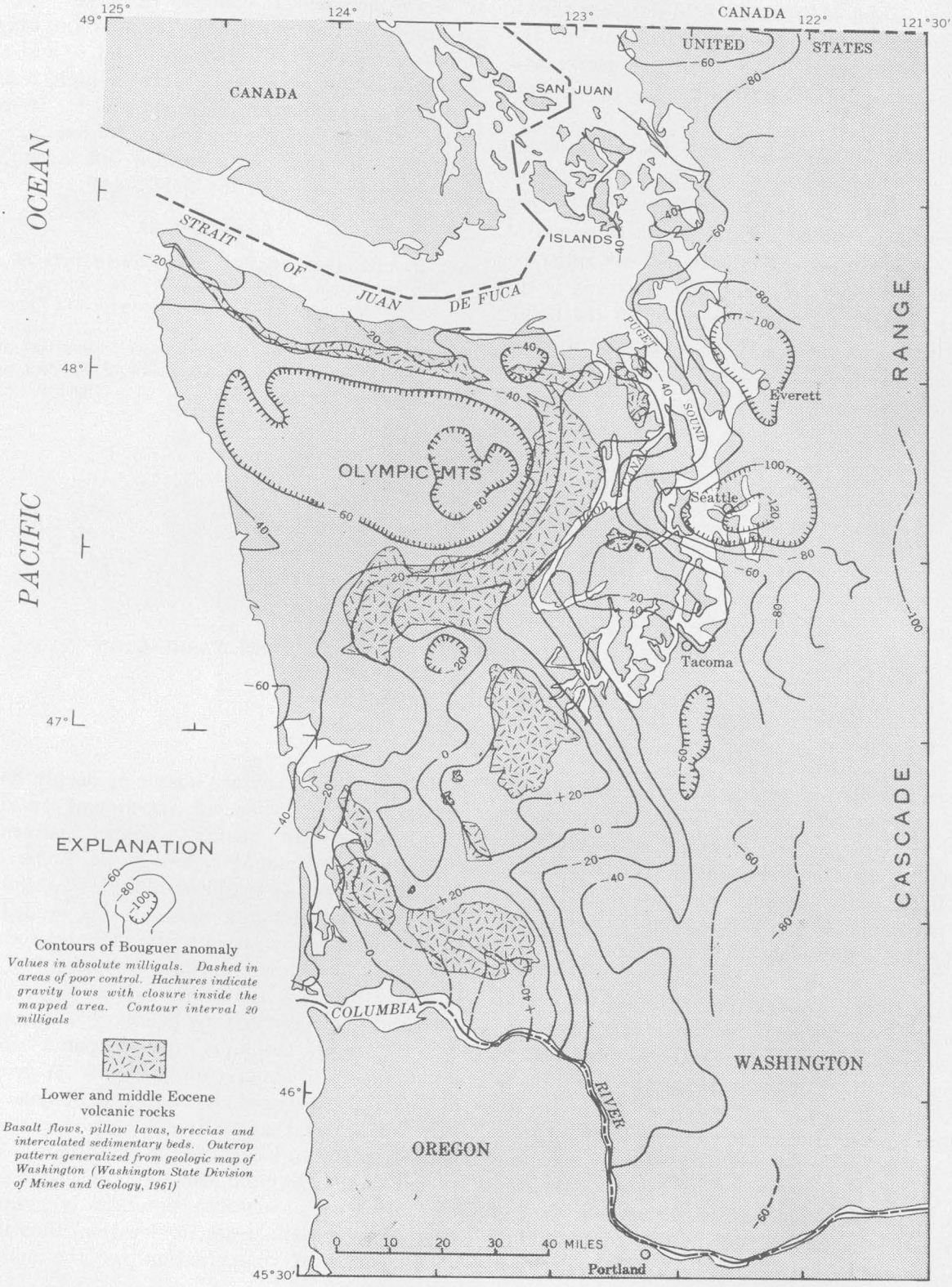

FIGURE 248.1.—Bouguer anomaly and generalized outcrop pattern of lower and middle Eocene volcanic rock in western Washington.

ness of the disturbing body can be estimated from the amplitude, gradient, and width of the anomaly variation. For a first approximation, the Seattle low might be considered the gravitational expression of a hemisphere of low-density material enclosed in a higher density medium. The difference between the regional field level and the most negative Bouguer value near Seattle is about −95 milligals. If the density contrast is assumed to be 0.3 g per cm,^{3} the radius or depth to the bottom of the hemisphere will be about 50,000 feet. Little reliance should be placed on the precise magnitude of this figure because the density contrast and the approximation of the structure by a hemisphere are merely assumptions; however, this result does show that the thickness of low-density material underlying Seattle is measurable in tens of thousands of feet.

The gravity lows in Puget Sound and the Olympic Mountains are separated by a high over the lower and middle Eocene volcanic rock outcrop west of Hood Canal. Bouguer anomaly values in the Olympic Mountains are influenced by a deep-seated mass deficiency which tends to compensate for the mass of the mountains. In order to remove or reduce this influence, Airy-Heiskanen isostatic reductions (T = 30 km) were made for several stations in the mountains and for some stations established on the lower and middle Eocene volcanic rocks (Heiskanen, 1938). Isostatic reductions for the first group averaged about −32 milligals and for the second, about +33 milligals. The average of 5 published Airy-Heiskanen values (T = 40 km) for stations in Puget Sound is −26 milligals (Heiskanen, 1939). These three gravity levels, which define the amplitude of the isostatic anomaly, have been connected by reasonable gradients to form a composite or average profile extending from the Olympic Mountains into Puget Sound (fig. 248.2).

Some conception of the amount of high-density material required to produce this high can be obtained from a two-dimensional mass distribution capable of giving rise to the composite profile (fig. 248.2). An

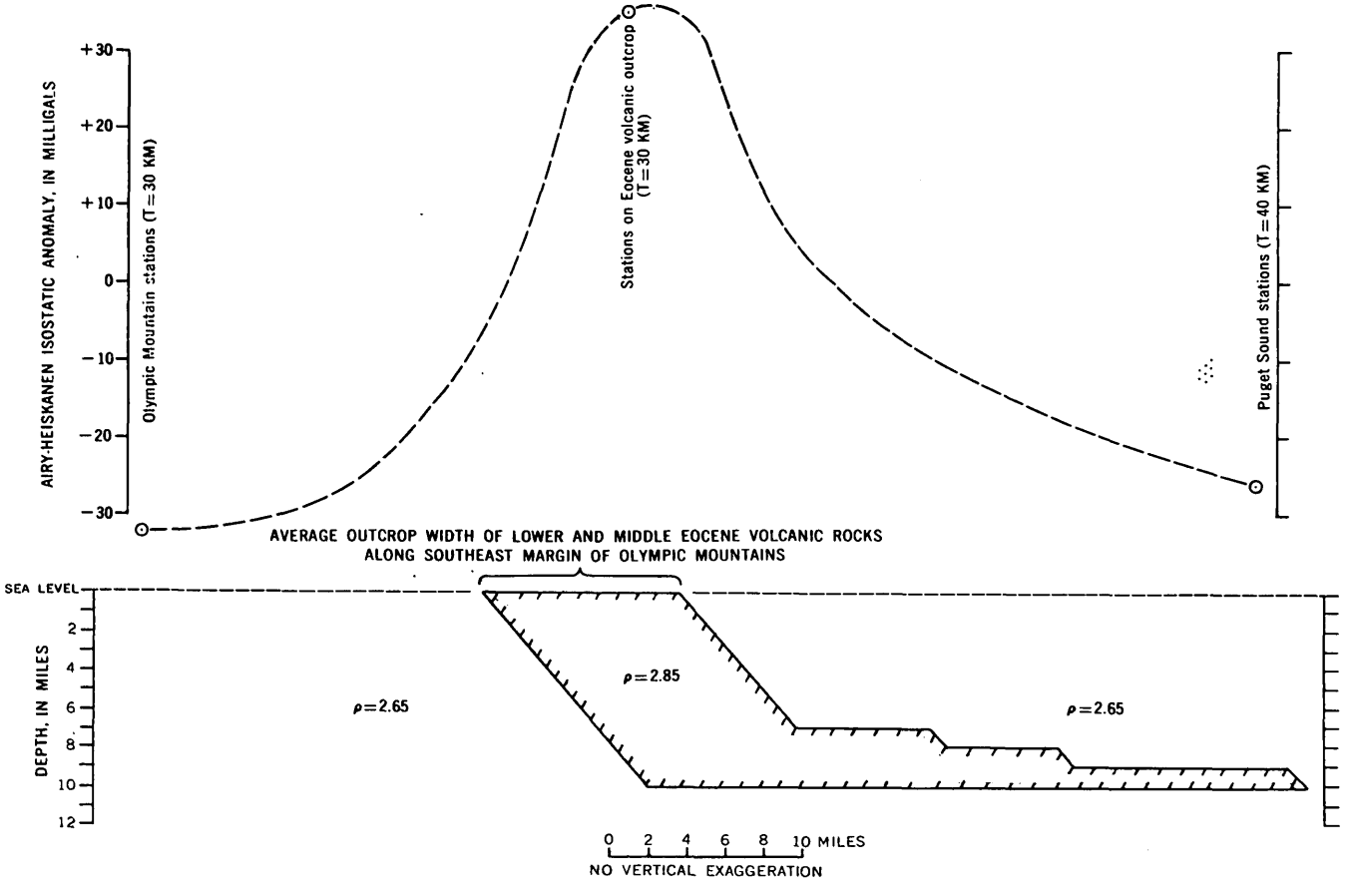

FIGURE 248.2.—Two-dimensional mass distribution capable of producing the composite gravity profile extending from the Olympic Mountains into Puget Sound, Wash. On the gravity anomaly profile, circles represent the average value of reduced data collected at the indicated locations. The dashed line represents gravity values computed from the mass distribution shown on the lower part of the figure.

assumed density contrast of 0.2 g per cm^3 between dense rock and the less dense surrounding material was used in deriving the section. Use of one crustal thickness, $T = 40$ km, for isostatic reductions in the Puget Sound group of stations and use of another, $T = 30$ km, for the other groups will introduce only a slight error in the solution. The same is true for use of a two-dimensional mass distribution which assumes an infinite length of structure normal to the section. Other sections could explain the profile equally well but as long as geologically reasonable densities are assigned to rocks involved, the thickness of the volcanic rocks or dense crustal rocks associated with them will always be measured in tens of thousands of feet and the depth to the base of the dense rocks will be of the same order of magnitude.

REFERENCES

Heiskanen, W. A., 1938, New isostatic tables for the reduction of gravity values calculated on the basis of Airy's hypothesis: Suomalainen Tiedeakatemia, Annales Acad. Sci. Fennicae, ser. A, v. 51, no. 9, p. 1–42.

——— 1939, Catalogue of the isostatically reduced gravity stations: Suomalainen Tiedeakatemia, Annales Acad. Sci. Fennicae, ser. A, v. 51, no. 10, p. 1–140.

Washington State Division of Mines and Geology, 1961, Geologic map of Washington.

Woollard, G. P., 1958, Results for a gravity control network at airports in the United States: Geophysics, v. 23, no. 3, p. 520–535.

249. REGIONAL MAGNETIC AND GRAVITY ANOMALIES IN THE DARWIN AREA, CALIFORNIA

By Don R. Mabey, Menlo Park, Calif.

Work done partly in cooperation with the California Division of Mines

In eastern California, between the southern end of the Inyo Mountains and the north end of the Argus Range, lies an upland area with moderate local relief (fig. 249.1*A*). This upland area has an average altitude of about 5,000 feet above sea level. The slope from the upland through Lower Centennial Flat into Owens Valley is relatively gentle, but there is an abrupt front on the Panamint Valley side. Several canyons over 1,000 feet deep are cut through this front.

GENERAL GEOLOGY

The oldest rocks in the area are sedimentary rocks of Paleozoic age which are intruded by plutonic rocks of Mesozoic age. Volcanic rocks of late Cenozoic age cover much of the area, and about half of the area is overlain by late Cenozoic sedimentary rocks.

The plutonic rocks exposed in the northeast part of the map (fig. 249.1*A*) are part of an extensive batholith around Hunters Mountain in the Panamint Range which consists mainly of the Hunter Mountain quartz monzonite (McAllister, 1956). Those exposed extensively in the southwest corner of the map (fig. 249.1*A*) are part of a large batholith, also chiefly quartz monzonite, that forms part of the Coso and Argus Ranges.

Near plutonic rocks the Paleozoic sedimentary rocks commonly have been altered to calc-hornfels and, in Darwin Canyon northwest of Zinc Hill mine, to a body of diorite, gabbro, epidote amphibolite, and amphibolite. Hall and MacKevett (1958, p. 12) report that this body grades into calc-hornfels. The average density determined for 9 samples of this rock, which is the densest large rock mass sampled in the region, was 3.15 g per cm.^{3} The density of the calc-hornfels near this body covers a wide range but is generally higher than either the quartz monzonite or the unaltered sedimentary rocks. The area contains numerous mines and prospects, mainly for lead, zinc, and silver, or for talc.

The late Cenozoic volcanic rocks described by Hall and MacKevett (1958) consist of older basalt pyroclastics with interbeds of andesite and pumice in the upper part and younger olivine basalt flows. The pyroclastic rocks reach a thickness of about 1,000 feet near local vents. The basalt, which covers much of

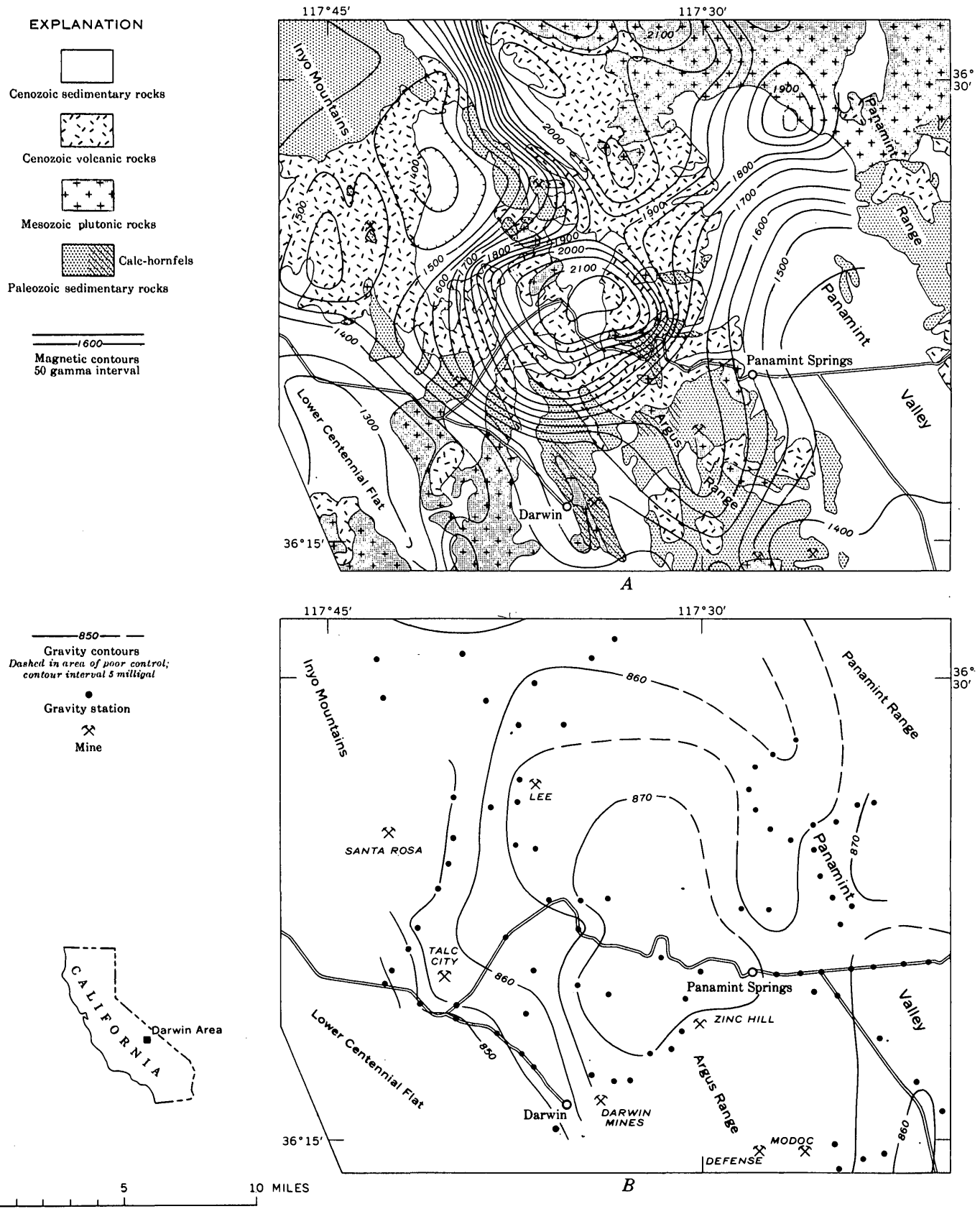

FIGURE 249.1.—*A*, Aeromagnetic and generalized geologic map of the Darwin area. The magnetic data were obtained along east-west flight lines 2 miles apart at 10,000 feet above sea level. The geology is generalized from the Death Valley sheet of the geologic map of California (Jennings, 1958) with supplemental data from Hall and MacKevett (1958). *B*, Complete Bouguer gravity anomaly map of the Darwin area, with terrain corrections through zone O of Hayford-Bowie charts.

the surface, occurs in flows 10 to 100 feet thick. The maximum aggregate thickness of the flows is about 600 feet.

GEOPHYSICAL SURVEYS

Figure 249.2 shows gravity and magnetic profiles from the Sierra Nevada at Owens Lake to the east side of Death Valley near Badwater. The largest magnetic feature on the profile is a high of about 700 gammas in the Darwin area. The dominant gravity feature is a westward decrease of the Bouguer anomaly values corresponding to a westward rise in the average elevation of the land surface. Superimposed on this regional anomaly is a gravity high in the Darwin area. The gravity high, which is offset to the east of the magnetic high, is difficult to isolate from the regional anomaly, but it appears to have an amplitude of more than 10 milligals.

The Cenozoic sedimentary rocks, which cover much of the area of figure 249.1, are generally less than a few hundred feet thick and do not have a major effect on the magnetic and gravity anomalies.

The volcanic rocks are not believed to show a major effect on the magnetic and gravity maps. The volcanic rocks range from very light pumice to moderately dense basalt; however, the average density of any thick accumulation of volcanic rocks is probably less than that of the pre-Tertiary rocks. The warping of the gravity contours 6 miles west and slightly north of Panamint Springs may be produced by volcanic rocks. The magnetic effect of the volcanic rocks is harder to evaluate. Ground profiles over the basalt flows show that the basalt is highly magnetic; however, the anomalies produced by the basalt are alternating highs and lows that probably do not have a large net effect on the magnetic field several thousand feet above the surface. The ground data, an inspection of profiles from airborne data, and comparison with data over similar volcanic rocks in the region indicate that the larger magnetic anomalies are not produced by the volcanic rocks. The volcanic rocks probably do not produce much more than 100 gammas variation in the magnetic field at the flight level.

In the northeast part of the magnetic contour map (fig. 249.1*A*) is an area of high magnetic intensity that includes five local magnetic highs. Three of these highs are certainly produced by the plutonic rock, and others are also probably produced by plutonic rock. Much of the southwest edge of the exposure of Hunter Mountain quartz monzonite is bordered by volcanic rocks; however, the steep magnetic gradients which flank the area of the extensive magnetic high in the northeast part of the map are between out-

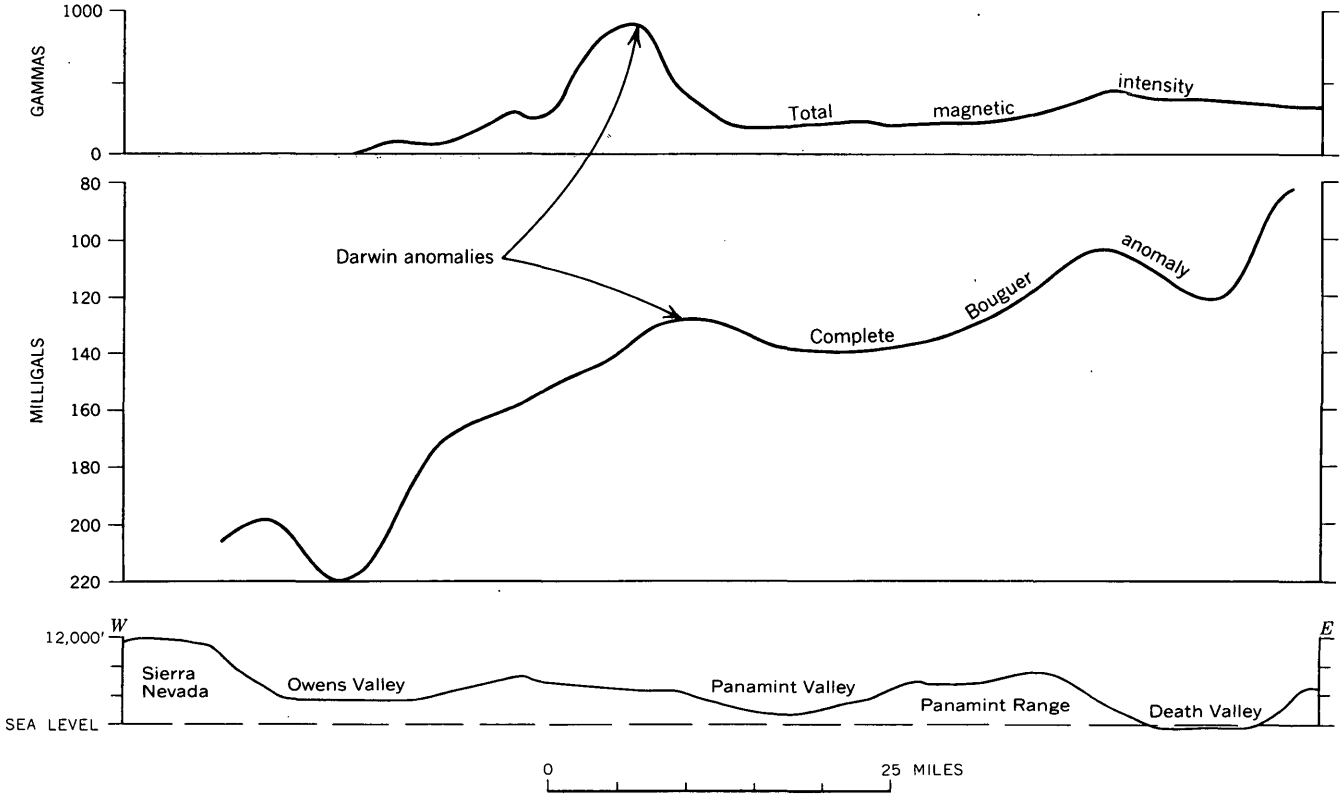

FIGURE 249.2.—Total magnetic intensity and complete Bouguer gravity anomaly along a profile from the Sierra Nevada at Owens Lake to the east side of Death Valley near Badwater. The flight level of the aeromagnetic profile was 10,000 feet above sea level. Gravity data in Owens Valley from Kane and Pakiser (1961).

crops of the pre-Tertiary sedimentary rock and the plutonic rock. Clearly this extensive magnetic high is produced by the quartz monzonite.

The magnetic high near the center of the map is in an area covered extensively by Cenozoic alluvium and volcanic rocks; however, intrusive rock is exposed in the deep canyons in the area of the anomaly and at two places on the highland. Thus it is inferred that this magnetic high is produced by a large intrusive body that is only partly exposed. Two magnetic noses extend south and southeast from the main high. One of these is over the intrusive outcrops near the town of Darwin and the other is over the intrusive outcrop at Zinc Hill mine. The general level of the magnetic field is low over the batholith that crops out in the southwest corner of the map. The intrusive rock underlying the magnetic high in the central part of the map appears to have magnetic properties more like the batholith of Hunter Mountain to the north than like the batholith of the Coso Range immediately to the south.

The gravity high, along the east side of the large magnetic high, is in an area of extensive exposures of calc-hornfels. The gravity high is probably produced by dense rocks formed by the alteration of sedimentary rocks along the east side of the intrusive body that produces the large magnetic high.

A small magnetic high was observed in the area of the Santa Rosa mine. This anomaly could be produced by the volcanic rock, which is within 2,300 feet of the flight elevation in the south end of the Inyo Mountains. The two exposures of Paleozoic rock in the area of the anomaly are calc-hornfels, however, and a small exposure of intrusive rock occurs at the south edge of the anomaly. This small magnetic high may be produced by a body of intrusive rock underlying the area of the Santa Rosa mine.

REFERENCES

Hall, W. E., and MacKevett, E. M., 1958, Economic geology of the Darwin quadrangle, Inyo County, California: California Div. Mines Spec. Rept. 51, 73 p.

Jennings, C. W., 1958, Geologic map of California, Death Valley sheet: California Div. Mines.

Kane, M. F., and Pakiser, L. C., 1961, Geophysical study of the subsurface structure in southern Owens Valley, California: Geophysics, v. 26, no. 1, p. 12–26.

McAllister, J. F., 1956, Geology of the Ubehebe Peak quadrangle, Inyo County, California: U.S. Geol. Survey Quad. Map GQ–95.

MINERALOGY, GEOCHEMISTRY, AND PETROLOGY

250. VANADIUM AND ASSOCIATED ELEMENTS IN THE PHOSPHORIA FORMATION IN THE AFTON AREA, WESTERN WYOMING

By J. D. Love, Laramie, Wyo.

Work done partly in cooperation with the U.S. Bureau of Mines

Vanadium in phosphate rock in the Phosphoria formation of Permian age in western Wyoming and Idaho has been known since 1911 (Mansfield, 1927, p. 212, 299–300), and W. W. Rubey has discovered shale and mudstone beds that contain more vanadium than the phosphate rock (Rubey, 1943). During 1942 and 1943, the Paris-Bloomington area in Idaho (McKelvey and Strobell, 1955) and the Sublette Ridge and Afton areas in Wyoming (fig. 250.1) were sampled in detail in trenches and adits.

The Phosphoria formation in the Afton area is composed of three members: (a) At the base is the Meade Peak phosphatic shale member, which consists of 90 to 120 feet of soft, black and gray, slightly to moderately vanadiferous shale, mudstone, siltstone, and oolitic phosphate (fig. 250.2). The phosphate beds are in two zones, one near the top and the other near the base of the member. (b) Above the Meade Peak is the Rex chert member, 112 to 150 feet thick, composed of gray and black massive to bedded and

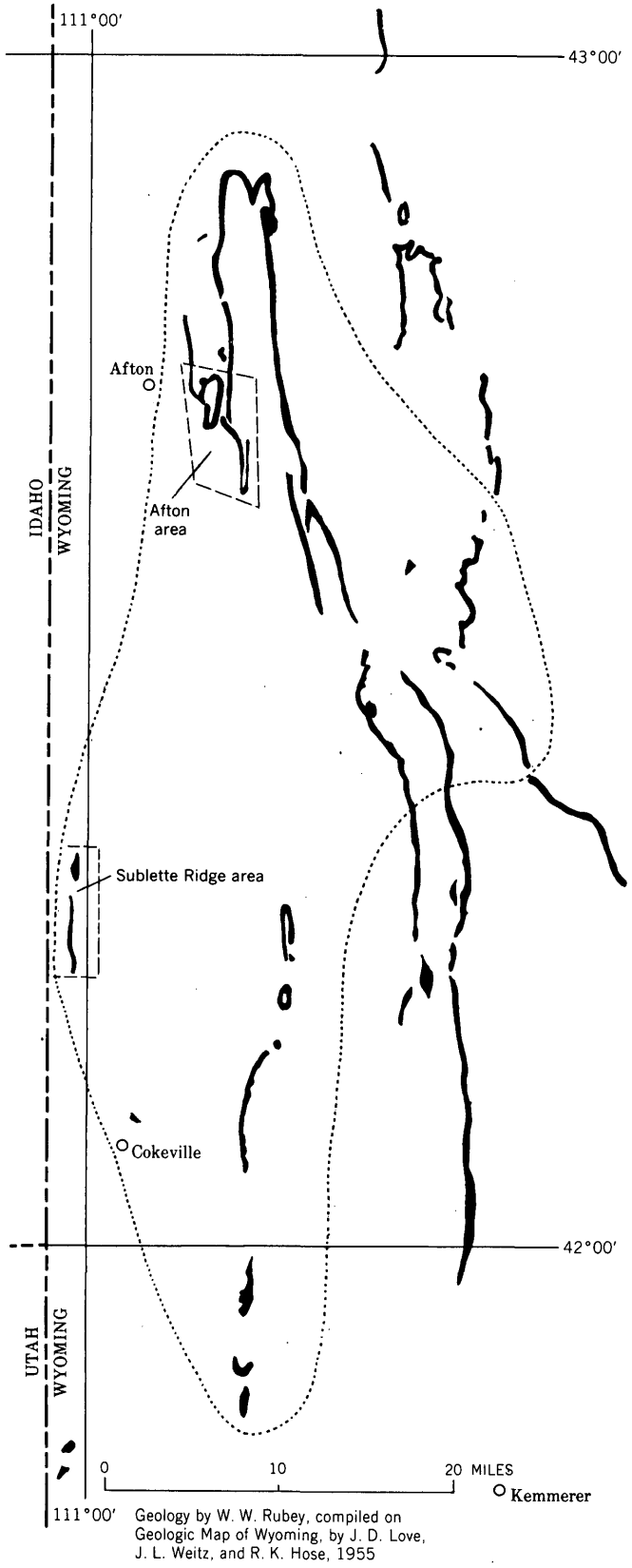

nodular chert, cherty and locally phosphatic gray limestone, and thin beds of gray quartzite. (c) The uppermost is the Retort phosphatic shale member (McKelvey and others, 1959, fig. 5), which consists of 0 to 20 feet of non-vanadiferous black to dark gray shale, siltstone, and phosphatic limestone. Underlying the Phosphoria formation is the Grandeur member of the Park City formation, which consists of 25 to 50 feet of hard gray limestone, and which in turn overlies the sandstone and quartzite of the Wells formation.

Although several vanadiferous zones were found by sampling, only one has sufficient thickness, grade, and continuity to be of possible economic interest. It is a 3- to 5-foot zone of black shale and dark gray mudstone about 5 to 10 feet below the upper phosphate in the Meade Peak member and 15 to 40 feet below the top of the member. Within the Afton area, the zone averages 4.15 feet in thickness and consists of 6 beds of shale and mudstone. Chemical analyses show that (a), a central shale bed 0.5 to 1 foot thick is richest, averaging 1.6 percent V_2O_5 (maximum 2.5 percent); (b), beds abve and below the richest one are successively lower grade toward the margins of the zone; (c), the full zone averages 0.7 percent V_2O_5; and (d), the vanadium content of the richest 3 feet of the zone varies from a minimum of 0.7 percent V_2O_5 in the northern part of the area to a maximum of 1.0 percent V_2O_5 in the central part.

The delimitation of this zone, and the determination of grade and tonnage of vanadium in the Afton area, are based on nearly 2,000 field tests (Axelrod, 1946) and more than 1,000 chemical analyses for vanadium of samples from 89 trenches and 6 adits on 4 lines of outcrop of the Meade Peak member within an area of less than 10 square miles (fig. 250.2). Except in the vicinity of faults, the continuity of the zone is such that the average grade and thickness can be predicted with some confidence. It is estimated that within the area shown on figure 250.2, reserves classed as indicated total 45 million tons of rock having an average grade of 0.9 percent V_2O_5 and an average thickness of 3 feet, between the outcrops and a depth of 500 feet below major drainage level (35 million tons above drainage level, 10 million tons from drainage level to 500 feet below). Excluded from this estimate are areas where

FIGURE 250.1.—Map of part of western Wyoming showing outcrops of Phosphoria formation (black), outline of area within which the Phosphoria formation was sampled at widely separated intervals (black dots), and the Afton and Sublette Ridge areas within which the formation was studied and sampled in detail (enclosed by dashes).

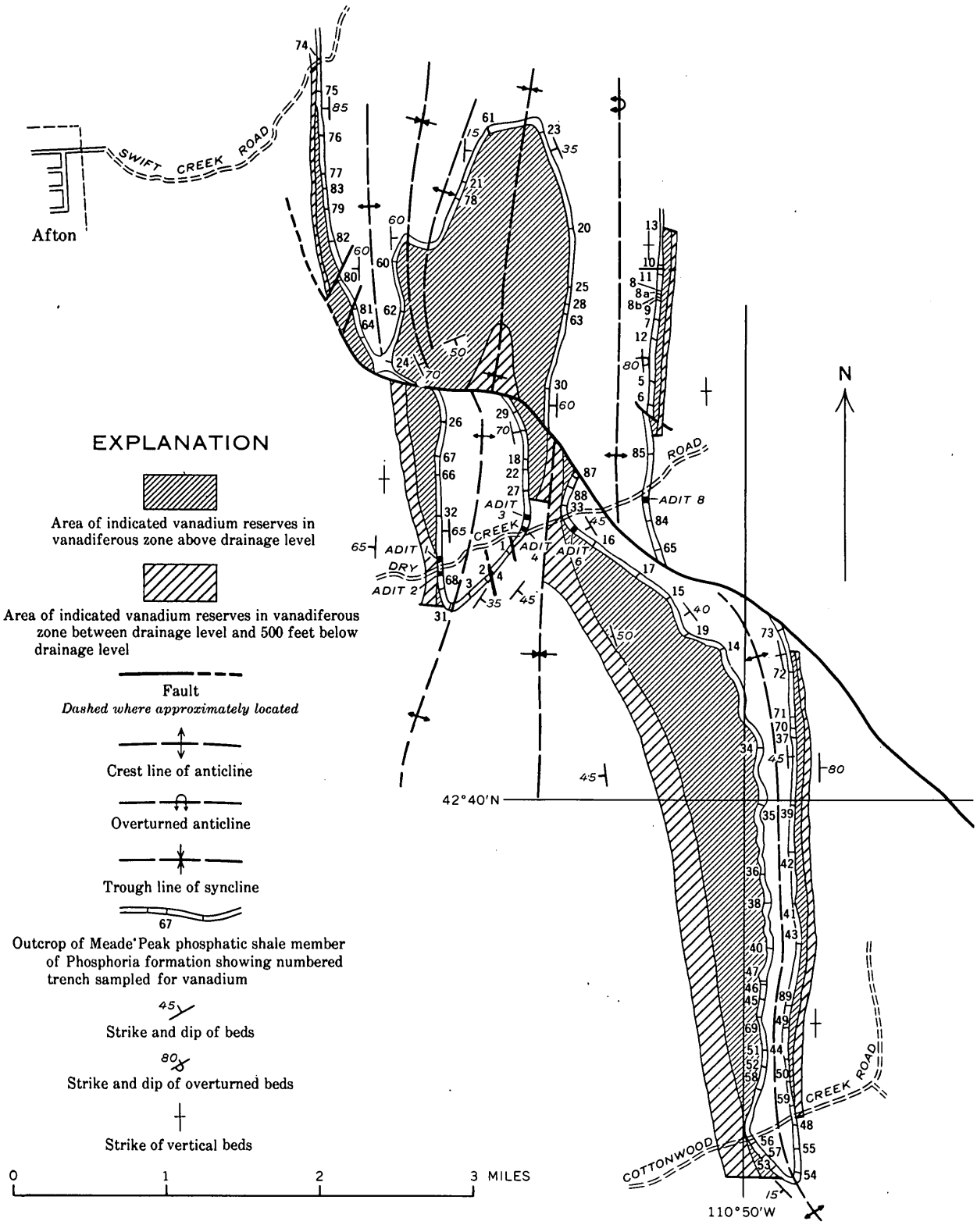

Geology by W. W. Rubey, slightly modified by J. D. Love and L. E. Smith

FIGURE 250.2.—Geologic map of Afton area showing outcrops of Meade Peak phosphatic shale member of Phosphoria formation, generalized structure, and location of computed reserves of vanadiferous rock.

601530 O—61——19

faulting is intense or where mining difficulties can be expected.

Small amounts of selenium, molybdenum, zinc, nickel, cobalt, titanium, and cadmium are present in the six beds comprising the vanadiferous zone. The middle beds that contain the most vanadium likewise contain the greatest concentration of these elements. Chromium is also present, but unlike the other metals, is apparently concentrated in the upper and lower beds of the zone.

The selenium content of the vanadiferous zone in the Afton area as a whole has not been accurately established. The maximum quantity obtained (from adit 2, fig. 250.2) is 0.068 percent selenium in a 0.8-foot bed containing 2.12 percent V_2O_5 (Beath, Hagner, and Gilbert, 1946, p. 14–15). At this locality, the vanadiferous zone has a weighted average of 0.042 percent selenium and 0.94 percent vanadium for 3.85 feet of strata.

The highest chemical analysis of MoO_3 is 0.1 percent. However, selected samples from the most vanadiferous middle part of the zone (containing 1.3 to 2 percent V_2O_5) in unweathered sections from several adits average 0.02 to 0.05 percent MoO_3. The highest chemical analysis of ZnO is 1.3 percent, that of TiO_2 is 1.0 percent, of NiO, 0.3 percent, and of Cr_2O_3, is 0.5 percent. Semiquantitative spectrographic analyses of samples obtained by D. F. Davidson in 1960 (Art. 267) from adits 1, 6, and 8 (fig. 250.2) show maximum cadmium content of 0.02 percent.

The upper and lower phosphate beds in the Meade Peak member contain small quantities of uranium, with maximum known content ranging from 0.01 to 0.02 percent. One phosphatic shale 5.7 feet thick in the middle of the member contains 0.009 percent uranium (Rubey, 1958).

It is the writer's belief that the vanadium, uranium, molybdenum, selenium, nickel, zinc, titanium, chromium, cadmium, and probably other trace elements, were deposited contemporaneously with the rocks of the Meade Peak member as precipitates from solution in a unique marine environment, the nature of which is not fully understood. There is little evidence of leaching or secondary concentration of these elements, with minor localized exceptions in the near-surface zone of weathering.

REFERENCES

Axelrod, J. M., 1946, A field test for vanadium, *in* Contributions to geochemistry, 1942-45: U. S. Geol. Survey Bull. 950, p. 19-23.

Beath, O. A., Hagner, A. F., and Gilbert, C. S., 1946, Some rocks and soils of high selenium content: Geol. Survey of Wyoming Bull. 36.

McKelvey, V. E. and others, 1959, The Phosphoria, Park City, and Shedhorn formations in the western phosphate field: U. S. Geol. Survey Prof. Paper 313-A, p. 1-47.

McKelvey, V. E., and Strobell, J. D., Jr., 1955, Preliminary geologic maps of the Paris-Bloomington vanadium area, Bear Lake County, Idaho: U. S. Geol. Survey Mineral Inv. Field Studies Map MF-41.

Mansfield, G. R., 1927, Geography, geology, and mineral resources of part of southeastern Idaho: U. S. Geol. Survey Prof. Paper 152.

Rubey, W. W., 1943, Vanadiferous shale in the Phosphoria formation, Wyoming and Idaho [abs.]: Econ. Geology, v. 38, no. 1, p. 87.

——— 1958, Geology of the Bedford quadrangle, Wyoming: U. S. Geol. Survey Geol. Quad. Map GQ-109.

251. SOME GEOCHEMICAL ASPECTS OF GROUND WATER IN NORTHERN ST. LAWRENCE COUNTY, NEW YORK

By Ralph C. Heath and Edward H. Salvas, Albany, N.Y.

Work done in cooperation with the New York State Power Authority and the New York Water Resources Commission

In 1957, the U.S. Geological Survey began an investigation of the ground-water resources of 480 square miles of area bordering the St. Lawrence River near Massena, N. Y. The bedrock of the area consists, from oldest to youngest, of crystalline rocks of Precambrian age and the Potsdam sandstone, Theresa dolomite and Beekmantown group, all of early Paleozoic age. The crystalline rocks and Potsdam sandstone crop out at a few places in the southern part of the area. The Theresa formation, which consists of alternating beds of sandstone and dolomite, is the uppermost unit of bedrock in most of the southern part of the area. The Beekmantown group, which is a gypsiferous dolomite more than 500 feet thick at Massena, is the uppermost bedrock unit in the central and northern parts of the area. The bedrock in the Massena area dips north toward the center of a structural basin in Ontario, Canada. Pleistocene deposits, most of which were deposited by continental ice sheets but which include some marine and lake sediments, form an almost continuous blanket, in places more than 100 feet thick, over the bedrock. Ground water occurs in a continuous zone of saturation that extends downward from the water table, which is in the Pleistocene deposits in nearly the whole area, into the crystalline rocks.

Data on the chemical quality of the ground water provide significant information on the following aspects of the geochemistry: (a) the occurrence in the area of two distinctly different types of ground water, and (b) evidence of ion exchange.

The differences in chemical composition of the two types of ground water are shown graphically in figure 251.1. For convenience in discussion, these waters may be referred to as fresh water and saline water. The fresh water contains a relatively low concentration of sodium and chloride ions, but these ions are dominant constituents in the saline water. Fresh water is in the upper part of the zone of saturation in the recharge areas between streams, and the saline water is in the lower part of the bedrock. Because there are no extensive impermeable beds in the bedrock, the fresh and saline waters are in contact and are rather thoroughly mixed in the zones of ground-water discharge along the principal streams. Several analyses which show the intermediate chemical content of mixtures of fresh and saline water also are presented on figure 251.1. (See, for example, analyses of water from wells 455-452-4 and 440-459-1).

Areal variations in chloride content of water from the upper part of the bedrock are shown in figure 251.2 (p. C–285). The areas of higher chloride in the midst of low-chloride areas reflect the few available analyses from wells penetrating the deeper rock. Conversely, areas of low chloride in the midst of higher chloride areas reflect the influence of localized recharge through northeast-southwest elongated hills. An important feature of the map is the discontinuous areas of high chloride adjacent to the principal streams, which are believed to show areas where saline water is moving upward from the deeper zones, mixing with fresh ground water and discharging into the streams. The upper part of the bedrock in the intervening areas of low chloride content along the streams is believed to have such a low vertical permeability that little, if any, saline water is moving upward and being discharged.

Differences in the fresh and saline waters, as reflected by changes in the ratio of chloride to dissolved solids, are shown in figure 251.3 (p. C–286). The analyses in the lower left-hand part of the graph show the relation of chloride to dissolved solids in the fresh water. The values at the extreme left-hand side of the graph are believed to reflect the chemical content of water at the time it reaches the water table—that is a chloride content of 1 ppm (part per million), which is present in the precipitation, and a dissolved solids content of 280 ppm, most of which is calcium and magnesium bicarbonate dissolved from the materials above the water table. Higher values on the graph show principally the addition of chloride to the initial composition. The additional chloride is believed to be derived largely from saline water but some, particularly in the lower concentrations, may be derived from salts used to deice roads, from fertilizers, and the effluent from septic tanks. The relation of chloride to dissolved solids for

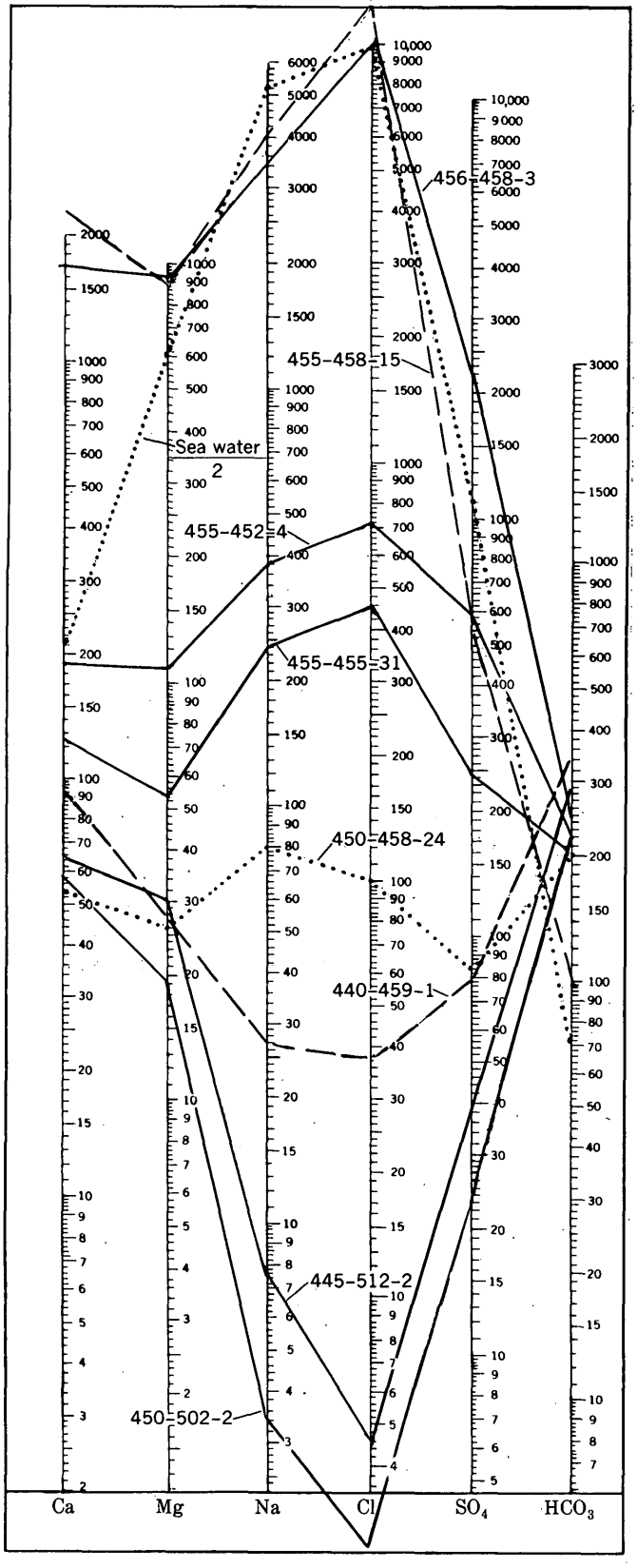

the saline water is shown by the steeply sloping trend line. Because of natural mixing of the fresh and saline waters a larger number of water samples having intermediate chloride contents (from about 20 to about 200 ppm) would doubtless have shown a merging of the two trends shown on figure 251.3 into a smooth curve. Ratios of chloride to dissolved solids for water samples from mineral springs and wells in eastern Ontario (Elworthy, 1918, p. 22-63) also are shown on figure 251.3. These analyses, which plot along the trend of the Massena analyses, are of waters from the bedrock in the northern part of the basin.

The fresh water is derived from precipitation falling on the area. The saline water probably is sea water that entered the ground when the area was covered by the Champlain Sea, an arm of the Atlantic Ocean that covered the area for a period of about 2,500 years following the melting of the last ice sheet, about 7,000 years ago. Salt beds and connate water are also possible sources of the saline water, although supporting evidence is lacking. If the Champlain Sea were the source of the saline water, the present distribution of the water reflects the extent to which flushing has taken place. It is noteworthy that salty water has been reported in some of the marine clays deposited in the Champlain Sea in eastern Ontario (John Terasmae, Geological Survey of Canada, written communication, June 29, 1960).

The analyses in figure 251.1 show differences in the behavior of certain ions brought in by sea water during the processes of dilution and flushing. Chloride is not adsorbed appreciably by the minerals in the aquifers. However, sodium is adsorbed to some extent by minerals having ion-exchange capacity. During early stages of dilution the saline water contains a high amount of chloride as compared to sodium. During later stages when the chloride concentration has reached a low level the sodium that had been adsorbed is gradually displaced by calcium and magnesium from the fresh water. Hence, the ratio of chloride to sodium is lower in the fresh water than in the saline water.

REFERENCE

Elworthy, R. T., 1918, Mineral springs of Canada, *in* The chemical character of some Canadian mineral springs, Pt. 2: Canada Dept. Mines Bull. 16, 173 p.

FIGURE 251.1.—Analyses, in parts per million, of ground water in the Massena area, as plotted on logarithmic nomograph. Serial numbers identify wells sampled.

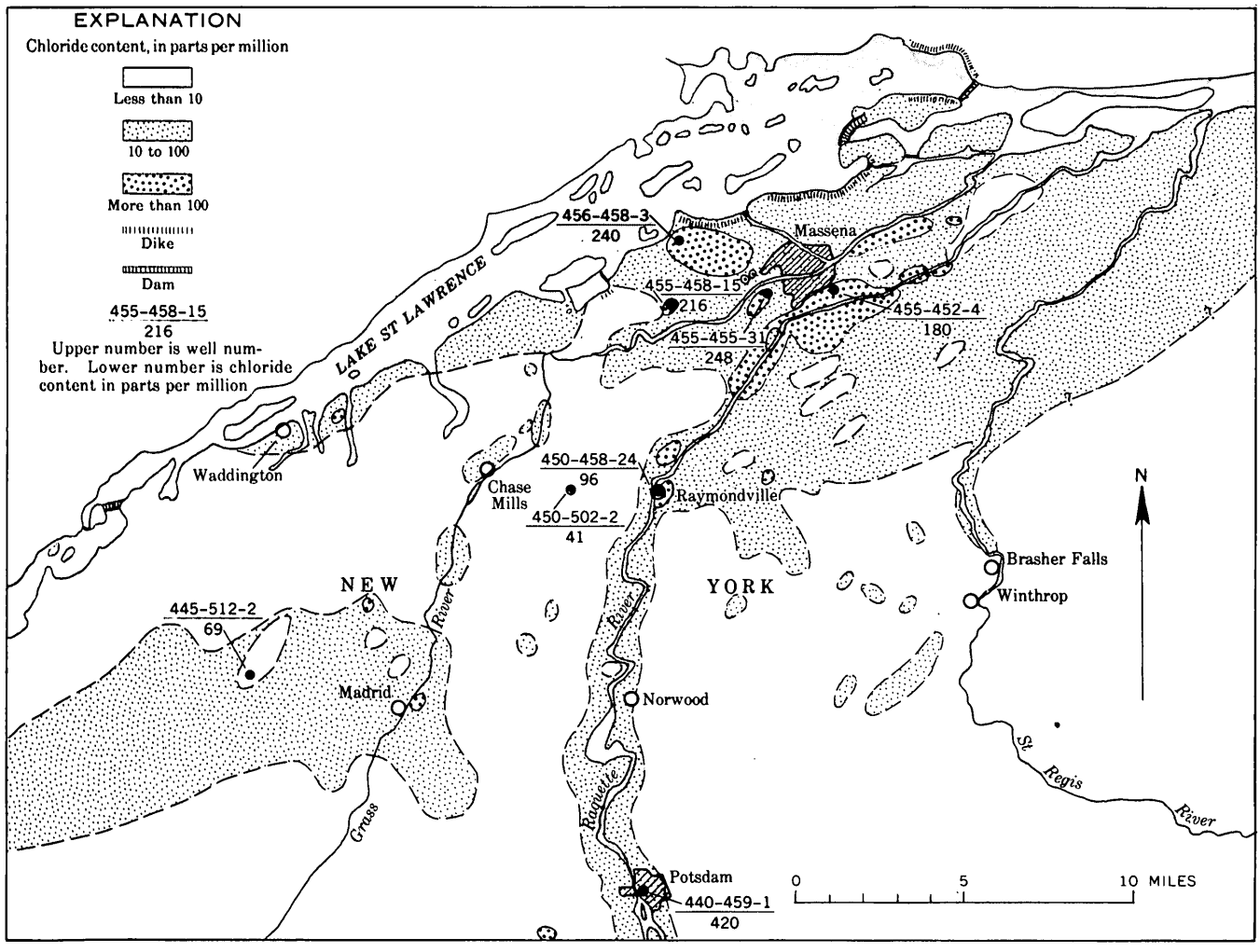

FIGURE 251.2.—Areal distribution of chloride in ground water in the upper part of the bedrock in the Massena area, New York.

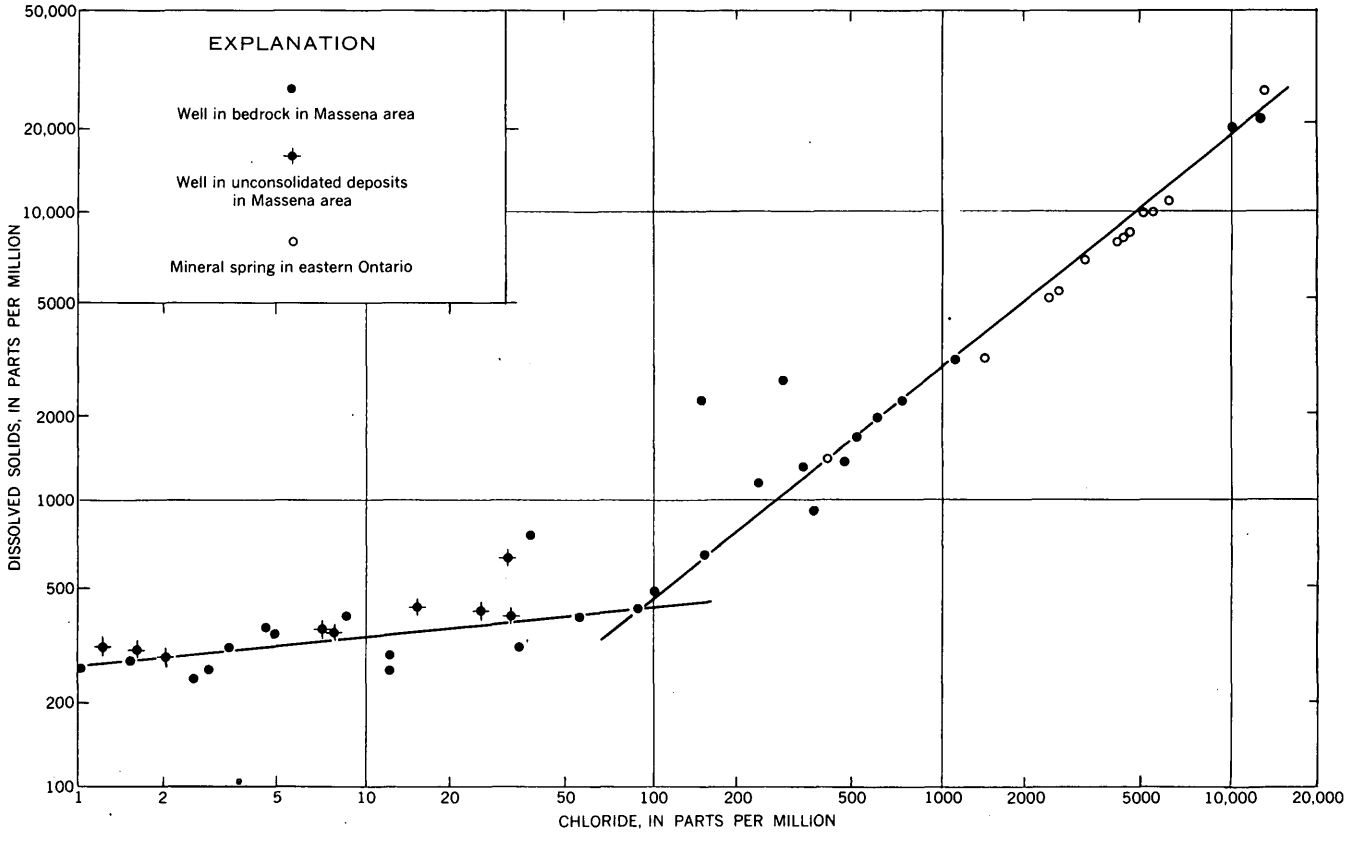

FIGURE 251.3.—Graph of chloride versus dissolved solids of fresh and saline ground water in the Massena area and saline ground water in eastern Ontario.

252. X-RAY DETERMINATIVE CURVE FOR SOME NATURAL PLAGIOCLASES OF COMPOSITION An_{60-85}

By EVERETT D. JACKSON, Menlo Park, Calif.

The usefulness of X-ray powder diffraction methods for estimating An content of natural plagioclase has been seriously questioned in a number of recent publications on grounds that diffraction parameters are strongly influenced by structural state and degree of inversion of the plagioclase.[1] Smith and Yoder (1956), while cautioning against indiscriminate use of X-ray diffraction curves for plagioclases from diverse environments, suggested that such curves might be useful for suites of plagioclases of closely similar origins and thermal histories. In particular, they suggested that plagioclases of the Bushveld type formed such a suite. However, Smith and Gay (1958) saw no reason to attach special importance to plagioclases from thick layered intrusions, nor to exclude them from their reservations about the usefulness of diffraction measurements for determinative purposes.

In order to determine whether a useable determinative curve could be constructed for use within a single layered intrusion, the 2θ (131)-($1\bar{3}1$) and 2θ ($1\bar{3}1$)-(220) reflection separations of 12 analyzed plagioclases from the Basal and Ultramafic zones of the Stillwater complex, Montana, were measured and plotted against

[1] The plagioclase X-ray determinative curve of Overkott (1958) is based on an absorption method and is not sensitive to structural factors.

An content. The resulting curve appears to be linear over the investigated range and to have sufficiently narrow confidence limits to warrant its use to estimate the composition of plagioclases from the lower part of the complex.

Plagioclase concentrates from 5 specimens of plagioclase-bearing rocks from the Ultramafic zone and 5 specimens from the Basal zone were crushed to —325 mesh and cleaned by centrifuging in dilute bromoform. Optical grain counts indicate that the samples thus obtained are more than 99 percent pure plagioclase. Two of the samples were split to make hidden duplicates, which were then treated as separate samples. All 12 samples were analyzed by a spectrogravimetric method devised by Stevens and others (1960), and the An content was calculated as 100 times the atomic ratio of Ca and Sr to Ca, Sr, Na, and K. Three subsamples were split from each of the samples prior to analysis for X-ray examination. These 36 subsamples were assigned random numbers to determine run order, prepared as slurrys on circular cover glasses, placed in a rotating sample holder, and allowed to oscillate twice up and twice down between 28° and 32° 2θ on a Norelco diffractometer using unfiltered Cu Kα radiation. A one-degree divergent slit, one-quarter degree scatter slit, and 0.006-inch receiving slit were used; the scan speed was one-quarter degree per minute; the chart scale was 2 inches per degree 2θ. The distances between (131) and ($1\bar{3}1$) peaks and between the ($1\bar{3}1$) and (220) peaks were measured directly in degrees from the charts and compiled, and means and standard deviations of $\Delta\ 2\theta$ were calculated from them. The Γ parameter of Smith and Gay (1958, p. 748) was obtained by subtracting the ($1\bar{3}1$)-(220) separation from the ($1\bar{3}1$)-(131) separation. An content, calculated from the analyses, and X-ray data are summarized in table 252.1.

TABLE 252.1.—*An content and X-ray diffraction measurements (using Cu Kα radiation) of 12 plagioclase samples from the Stillwater complex*

Field no.	Lab. no.	An [1] (percent)	$\Delta 2\theta$(131)-($1\bar{3}1$) (degrees, 12 readings)		$\Delta 2\theta$($1\bar{3}1$)-(220) (degrees, 12 readings)		Γ [$\Delta 2\theta$(131)-($1\bar{3}1$)-$\Delta 2\theta$($1\bar{3}1$)-(220)] (degrees)
			Mean	Standard deviation	Mean	Standard deviation	
53IN-2	21	59.9	1.857	±0.0025	1.246	±0.0010	+0.611
53NB-11	16	60.0	1.889	.0030	1.199	.0025	+.690
55MV-29	20	68.5	2.012	.0019	1.080	.0010	+.932
55NB-1 [2]	17	70.1	2.039	.0028	1.053	.0021	+.986
52BE-35	13	70.3	2.027	.0031	1.060	.0037	+.967
55BE-2	23	70.3	2.029	.0016	1.058	.0021	+.971
55BE-4	14	72.0	2.071	.0014	1.018	.0016	+1.053
55MV-32	25	73.0	2.073	.0018	1.016	.0034	+1.057
55NB-2 [3]	24	73.6	2.066	.0022	1.019	.0021	+1.047
52BE-29	22	76.6	2.121	.0024	0.956	.0027	+1.165
55BE-7	15	76.9	2.138	.0028	0.947	.0037	+1.191
55BE-1	19	83.3	2.206	.0009	0.875	.0011	+1.331

[1] Atomic ratio of Ca+Sr/Ca+Sr+Na+K×100
[2] Hidden duplicate of 52BE-35
[3] Hidden duplicate of 55MV-32

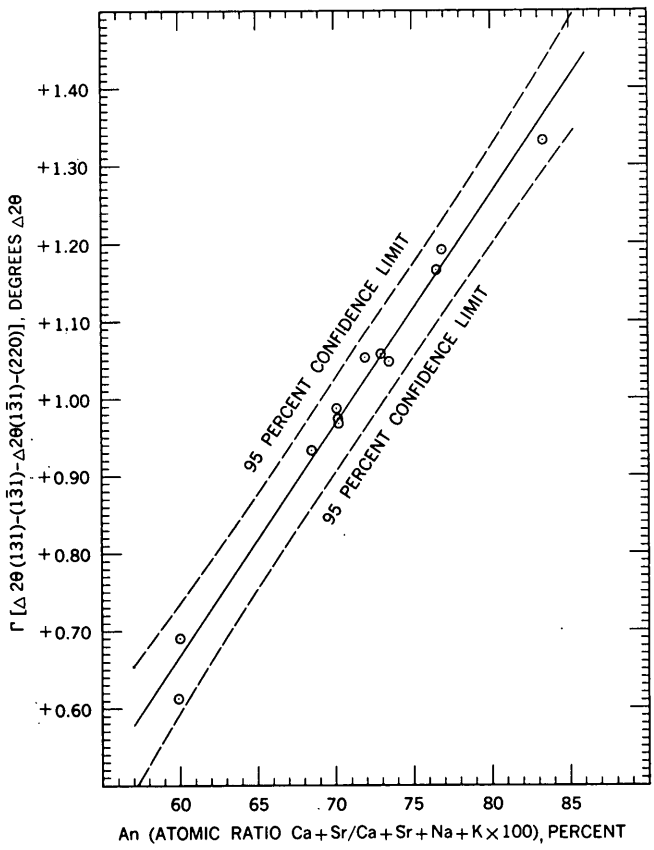

FIGURE 252.1.—X-ray determinative curve for plagioclase from the lower part of the Stillwater complex.

The information in table 252.1 forms the basis for the determinative curve in figure 252.1. The value Γ is plotted directly as degrees $\Delta 2\theta$ on the ordinate, the An value on the abscissa. A regression analysis was made considering the 12 measurement sets to represent individual samples, using the average X-ray parameter Γ as the dependent variable, and taking the chemically derived value of An as the independent variable. The equation for the straight line curve is:

$$\Gamma = .029868\ \mathrm{An} - 1.1268$$

The 95 percent confidence intervals (based on assumed normal distribution) for the regression equation are $\pm 0.064°2\theta$ at 70 percent An and $\pm 0.070°2\theta$ at 60 and 80 percent An. These limits correspond to an uncertainty of about ±2.1 percent An at the center of the curve and ±2.4 percent An at the ends of the curve. This uncertainty is considerably larger than that obtained in much the same way for estimating composition of olivines (Jackson, 1960), although the standard deviations of the X-ray data and the differences in reported chemical constituents between hidden duplicates are of the same order of magnitude in both sets of data.

No marked displacement of the curve is noted in the interval An_{70-75} in response to the abrupt structural change in plagioclases within that compositional range (Bown and Gay, 1958). Furthermore, there seem to be no systematic differences between samples from the Basal and Ultramafic zones. The entire curve, however, lies an average of about 0.08°Γ above one constructed in the same manner from data given by Smith and Yoder (1956, p. 637). The analyses on which these authors' An values are based are systematically poorer in K_2O than those analyzed for the present study, and it may be that the displacement is at least partly due to different analytical methods of K_2O determination.

It is concluded that the determinative curve is useful over a limited range of compositions of plagioclases from a restricted environment, and that its use within that environment should lead to An values at least as precise as those usually obtained by optical methods. Additional data will be needed to determine whether or not the curve can be applied to other plagioclases of the Bushveld type.

REFERENCES

Bown, M. G., and Gay, P., 1958, The reciprocal lattice geometry of the plagioclase feldspar structures: Zeitschr. Krist., v. 111, p. 1-14.

Jackson, E. D., 1960, X-ray determinative curve for natural olivine of composition Fo_{80-90}, *in* Short papers in the geological sciences: U.S. Geol. Survey Prof. Paper 400-B, p. B432-B434.

Overkott, E., 1958, Eine röntgenographische Methode zur Bestimmung der An-Gehalte von Plagioklasen: Neues Jahrb, Mineralogie Monatsh., v. 5, p. 113-120.

Smith, J. R., and Yoder, H. S., Jr., 1956, Variations in X-ray powder diffraction patterns of plagioclase feldspars: Am. Mineralogist, v. 41, p. 632-647.

Smith, J. V., and Gay, P., 1958, The powder patterns and lattice parameters of plagioclase feldspars. II: Mineralog. Mag., v. 31, p. 744-762.

Stevens, R. E., Chodos, A. A., Havens, R. G., Godijn, E., and Neil, S. T., 1960, Combination of gravimetric and spectrographic methods in the analysis of silicates, *in* Short papers in the geological sciences: U.S. Geol. Survey Prof. Paper 400-B, p. B499-B501.

253. BORON IN BENTONITE AND SHALE FROM THE PIERRE SHALE, SOUTH DAKOTA, WYOMING, AND MONTANA

By Harry A. Tourtelot, Leonard G. Schultz, and Claude Huffman, Jr., Denver, Colo.

The boron content of shale has been of interest since Landergren (1945) noted that boron in fine-grained sedimentary rocks is proportional to the amount of clay-size material and to the salinity of the water in which each rock was deposited. (See also Degens, Williams, and Keith, 1957.) Frederickson and Reynolds (1960) reported that the illite contains nearly all of the boron in shale samples. Harder (1959) also considered micaceous clay minerals the principal carrier of boron in most sedimentary rocks.

The Pierre shale is entirely marine. Bentonite samples are nearly pure montmorillonite and their boron content ranges widely (fig. 253.1). Other rocks are mixtures of montmorillonite, mixed-layer illite-montmorillonite, illite, quartz, and generally minor amounts of kaolinite, chlorite, and other minerals; carbonate minerals are abundant in a few samples. The boron content of individual samples shows little relation to the total clay or organic carbon content.

Five samples of bentonite and five of other rocks were selected from those previously analyzed (fig. 253.1) to represent a range of boron content convenient to work with and a range of mineralogical composition. Two splits of each sample were separated into fractions coarser than 1 micron and finer than 1 micron by repeated disaggregation in distilled water and centrifuging. The coarse and fine fractions of one split intended for boron analysis were handled in plastic containers to avoid any possible contamination with boron dissolved from glassware (Wichers and others, 1941). A blank sample of distilled water was run to monitor possible contribution of boron by distilled water or the sodium metaphosphate dispersing agent. The two fractions of the split for mineralogical analysis by X-ray were stored in glass containers. A third unfractionated split of each sample represents the original sample.

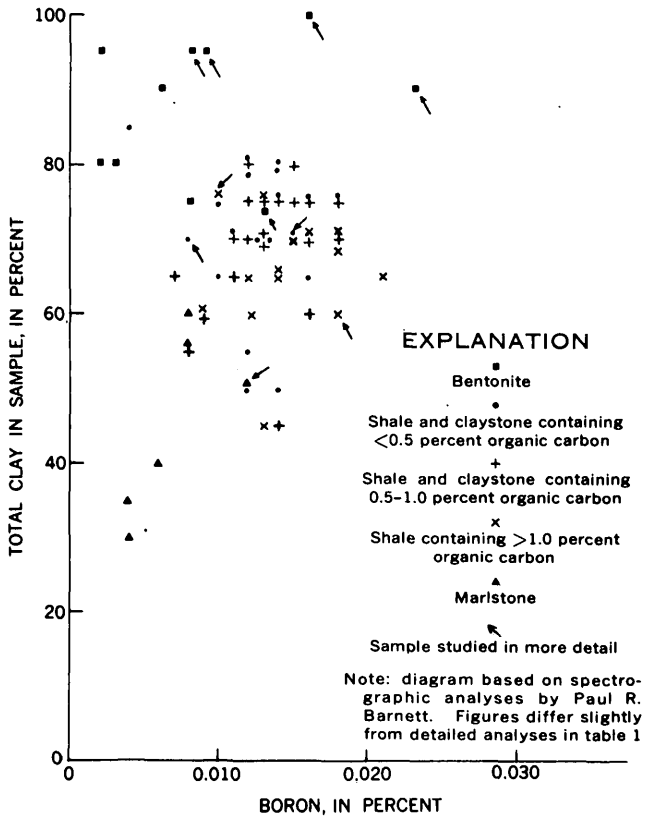

FIGURE 253.1.—Relations between boron and clay contents in 69 samples of Pierre shale from South Dakota and parts of adjacent States.

Boron was determined by the carminic acid method of Hatcher and Wilcox (1950). The precision indicated by 20 duplicate runs made of 10 solutions of our samples is ±0.001 percent boron. The sum of the boron in the two fractions of each sample is systematically higher than the boron in the original, unfractionated sample (table 253.1), but differences are within the precision of the determinations. No boron was found in the reagent blank.

X-ray analyses (table 253.1) of the mineralogy have a precision of about 10 percent (Schultz, 1960, and written communication). Total clay is reported to the nearest 5 percent. The amount of each clay mineral in the total rock was calculated by multiplying the relative proportion of each clay mineral by the percentage of total clay.

The boron contents of the fine and coarse fractions of 3 of the 5 bentonite samples are very similar (fig. 253.2), apparently because both fractions are almost entirely montmorillonite. The fine fraction of bentonite sample 259548 contains less boron than the coarse fraction. This relation is reversed in sample 259588, apparently because the coarse fraction contains abundant feldspar and jarosite which probably contain little boron. The most important factor controlling the boron content of the different size fractions of the bentonite is the total amount of clay minerals rather than the particle size of the clay.

Boron content of the fine fraction of all 5 shale samples is greater than that of the coarse fraction by 20 to 100 percent (fig. 253.2). The principal nonclay mineral is quartz (table 253.1), with appreciable carbonate and sulfate minerals in two samples. These minerals characteristically contain little boron (Harder, 1959). On calculating percent boron to 100 percent clay (table 253.1), the boron content of the coarse and fine fractions is about the same within the limits of analytical techniques. The boron content of the size fractions of the shale as well as the bentonite from the Pierre shale thus is related to the total clay content and apparently is independent of the clay particle size.

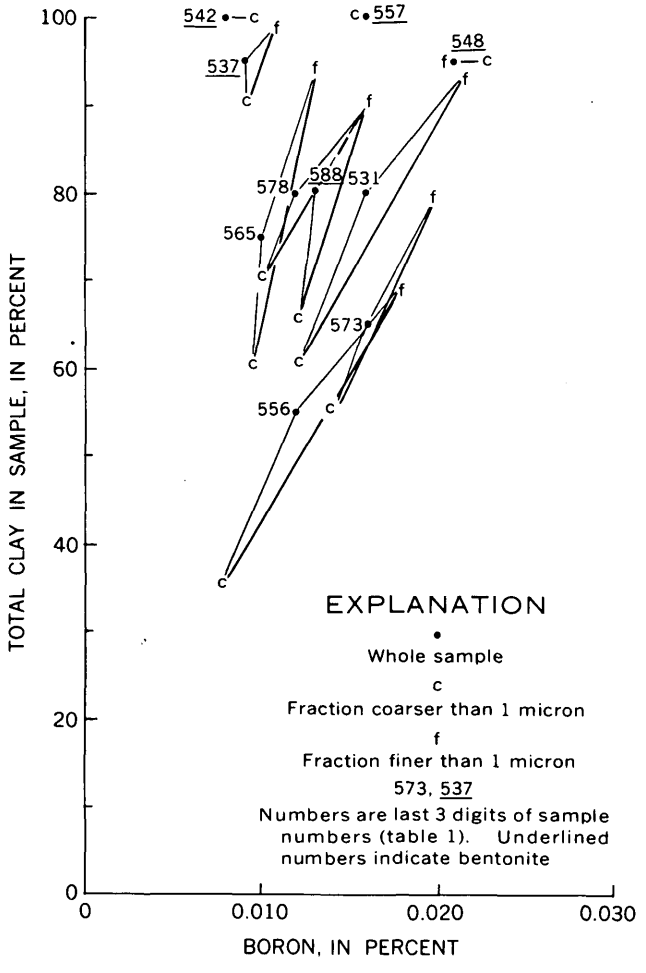

FIGURE 253.2.—Boron and total clay contents in whole sample and size fractions.

TABLE 253.1—*Boron content and mineralogical composition of 10 samples of bentonite, claystone, shale, and marlstone from the Pierre shale in South Dakota, Wyoming, and Montana*

[Chemical analyses for boron by Claude Huffman, Jr.; X-ray mineralogical analyses by L.G. Schultz. Mineralogical data for whole samples obtained by multiplying data on fractions by weight percent of the fractions]

Number	Location	Description of material	Stratigraphic unit	Fraction [1]	Weight in grams	Percent	Boron: Percent	Boron: Micrograms [2]	Boron: Percent recalculated to 100 percent	Relative proportions of clay minerals in total clay: Montmorillonite	Mixed-layer, illite-montmorillonite	Illite	Chlorite	Kaolinite	Total clay	Whole rock: Clay minerals: Montmorillonite	Mixed-layer, illite-montmorillonite	Illite	Chlorite	Kaolinite	Other minerals: Quartz	Feldspar	Calcite	Dolomite	Jarosite	Pyrite	Total
Bentonite																										
[Samples are in numerical order]																										
259537	NW¼ sec. 1, T. 111 N., R. 80 W., Hughes County, S. Dak.	Bentonite, very light gray, biotitic.	Agency shale member (Russel, 1930).	Coarse	1.23	42.1	0.0090	111	0.010	100	----	----	----	----	90	90	----	----	----	----	----	8	----	----	----	----	98
				Fine	1.69	57.9	.011	185	.011	100	----	----	----	----	100	100	----	----	----	----	----	----	----	----	----	----	100
				Whole	------	100.0	.009	(296) 262	.009	100	----	----	----	----	95	95	----	----	----	----	----	3	----	----	----	----	99
259542	Sec. 30, T. 6 N., R. 31 E., Stanley County, S. Dak.	Bentonite, light greenish-gray.	Upper part of Virgin Creek member.	Coarse	1.23	38.3	.0098	120	.010	100	----	----	----	----	100	100	----	----	----	----	----	[3] ?	----	----	----	----	100
				Fine	1.97	61.7	.0098	193	.010	100	----	----	----	----	100	100	----	----	----	----	----	----	----	----	----	----	100
				Whole	------	100.0	.0080	(313) 256	.008	100	----	----	----	----	100	100	----	----	----	----	----	----	----	----	----	----	100
259548	NW¼NE¼ sec. 17, T. 104 N., R. 71 W., Lyman County, S. Dak.	Bentonite, yellowish-gray with abundant jarosite.	Sharon Springs member.	Coarse	1.27	42.2	.023	292	.024	100	----	----	----	?	95	95	----	----	----	?	----	5	----	----	----	----	100
				Fine	1.74	57.8	.020	348	.021	97	----	----	----	3	95	92	----	----	----	3	----	----	----	----	7	----	102
				Whole	------	100.0	.021	(640) 632	.022	98	----	----	----	2	95	93	----	----	----	2	----	2	----	----	4	----	101
259557	SW¼NE¼ sec. 18, T. 96 N., R. 67 W., Gregory County, S. Dak.	Bentonite, white, jarositic.	Lower part of Virgin Creek member.	Coarse	2.75	80.7	.016	440	.016	100	----	----	----	----	100	100	----	----	----	----	----	----	----	----	----	----	100
				Fine	.65	19.3	(4)	(4)	-------	100	----	----	----	----	100	100	----	----	----	----	----	----	----	----	----	----	100
				Whole	------	100.0	.016	(4) 544	.016	100	----	----	----	----	100	100	----	----	----	----	----	----	----	----	----	----	100
259588	SE¼SE¼ sec. 21, T. 7 S., R. 56 E., Carter County, Mont.	Bentonite, pale grayish-orange.	Lower part of Mitten black shale member.	Coarse	1.00	33.6	.012	120	.018	100	----	----	----	----	65	65	----	----	----	----	----	10	----	----	25	----	100
				Fine	1.97	66.4	.016	315	.018	100	----	----	----	----	90	90	----	----	----	----	----	----	----	----	7	----	97
				Whole	------	100.0	.013	(435) 386	.014	100	----	----	----	----	80	80	----	----	----	----	----	3	----	----	13	----	96
Shale, claystone, and marlstone																											
[Samples are in order of decreasing montmorillonite content]																											
259578	SE¼NE¼ sec. 22, T. 38 N., R. 62 W., Niobrara County, Wyo.	Shale, medium dark-gray.	Middle unnamed member.	Coarse	1.74	55.4	0.0099	172	0.014	28	30	30	8	4	70	19	21	21	6	3	25	5	----	----	----	?	100
				Fine	1.40	44.6	.016	224	.018	67	24	8	0	1	90	60	22	7	0	1	7	?	----	----	----	----	97
				Whole	------	100.0	.012	(396) 377	.015	47	28	19	4	2	80	39	22	15	3	2	17	3	----	----	----	----	100
259565	SE¼SE¼ sec. 31, T. 7 N., R. 11 E., Meade County, S. Dak.	Claystone, yellowish-gray, silty.	Upper part of Pierre shale, equivalent to Mobridge (?) member.	Coarse	1.70	59.7	.0094	160	.016	10	22	49	12	7	60	6	13	30	7	4	36	5	----	----	----	----	101
				Fine	1.15	40.3	.013	150	.014	40	40	15	2	3	95	38	38	14	2	3	5	1	----	----	----	----	101
				Whole	------	100.0	.010	(310) 285	.013	26	31	32	7	4	75	19	23	25	5	3	23	3	----	----	----	----	101
259573	NE¼NE¼ sec. 31, T. 7 S., R. 7 E., Fall River County, S. Dak.	Shale, brownish-gray, platy, with fish remains.	Gammon member	Coarse	1.73	53.3	.014	242	.020	10	35	45	0	10	55	6	19	24	0	6	35	3	----	----	----	2	95
				Fine	1.52	46.7	.020	304	.025	26	54	18	?	2	80	21	43	14	?	2	8	1	----	----	----	9	98
				Whole	------	100.0	.016	(546) 520	.025	19	45	30	0	6	65	13	29	19	0	4	23	2	----	----	----	5	95
259531	NE¼SE¼ sec. 34, T. 124 N., R. 79 W., Walworth County, S. Dak.	Shale, medium-gray, calcareous.	Mobridge member	Coarse	.88	43.7	.012	105	.020	?	?	70	15	15	60	?	?	42	9	9	35	3	----	----	----	----	98
				Fine	1.13	56.3	.022	248	.023	19	37	26	6	12	95	18	35	25	6	12	5	----	?	----	----	----	100
				Whole	------	100.0	.016	(353) 321	.020	13	25	40	9	13	80	10	20	33	7	10	18	1	----	----	----	----	99
259556	SW¼SW¼ sec. 18, T. 96 N., R. 67 W., Gregory County, S. Dak.	Marlstone, medium gray.	Mobridge member	Coarse	1.53	48.8	.0078	119	.022	3	21	49	18	9	35	1	7	17	6	3	21	3	27	2	----	10	98
				Fine	1.61	51.2	.018	290	.026	15	50	19	5	11	70	11	35	13	3	8	5	----	22	----	----	----	97
				Whole	------	100.0	.012	(409) 377	.022	11	42	28	9	10	55	6	23	15	5	6	13	1	24	1	----	5	99

[1] Coarse fraction is >1 micron; fine fraction is <1 micron; whole means whole sample.
[2] Based on weight of samples and fractions multiplied by boron content in percent. Figures in parentheses are sums of micrograms of boron in fractions.
[3] The symbol "?" indicates that presence of the mineral is doubtful.
[4] Insufficient sample for analysis.

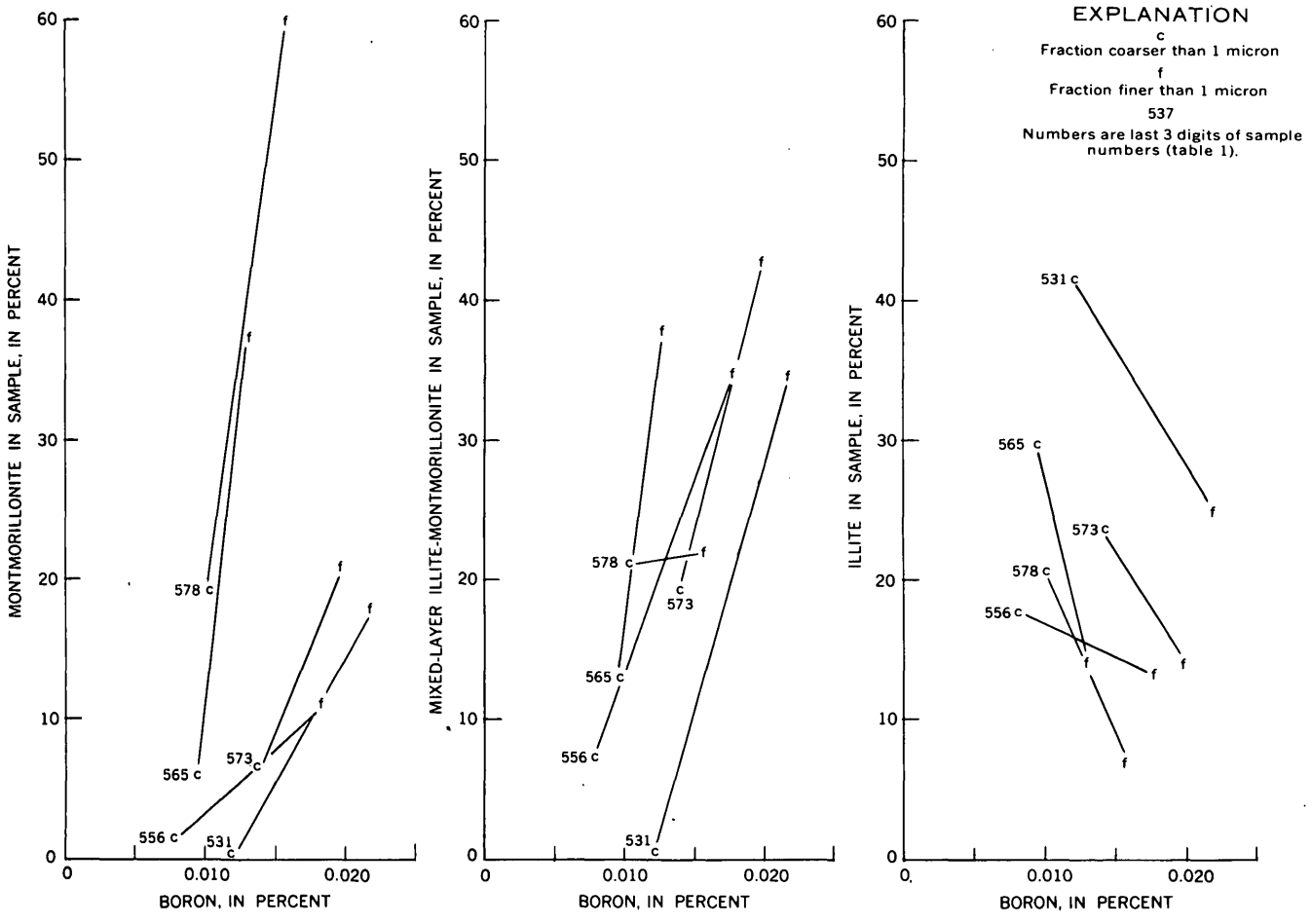

FIGURE 253.3.—Boron and clay mineral contents in size fractions of 5 samples of shale, claystone, and marlstone.

Montmorillonite and mixed-layer illite-montmorillonite are strongly concentrated in the fine fraction of the shale samples (fig. 253.3); illite and other minerals are concentrated in the coarse fraction. Amounts of kaolinite and chlorite generally are too small to influence the boron content appreciably. Without considering dilution by nonclay minerals, the greater abundance of boron in the fine fraction might suggest that boron is contained preferentially in the montmorillonite and (or) mixed-layer clay. Illite, however, is the only clay mineral in the coarse fraction of sample 259531 that can account for its boron content, just as montmorillonite is the only clay mineral that can account for the boron content of bentonite. This relation and those between the fractions of the other shale samples indicate little difference in the amount of boron that these individual clay minerals can contain.

Tourmaline, if present in significant amounts in the Pierre shale, almost certainly would be concentrated in fractions coarser than 1 micron (Harder, 1959, tables 4-9). As illite also is concentrated in the coarse fraction, tourmaline would decrease the amount of boron inferred in illite rather than montmorillonite.

Stability of boron in clays subjected to strong acid treatment (Harder, 1959; Frederickson and Reynolds, 1960) indicates the boron is in the clay structure rather than in exchange positions. Boron ions are small. Cation positions in the tetrahedral clay layers are appreciably smaller than cation positions in the octahedral layers. Thus, substitution of boron for silicon in the tetrahedral layer seems most likely. Such a substitution is reported by Eugster and Wright (1960) for micas and by Stubican and Roy (1960) for saponite (Mg-montmorillonite). Stubican and Roy also report that substitution of aluminum in the silicon tetrahedrons limits substitution of boron, possibly because substitution of the relatively large aluminum ions expands the lattice, and thus a poorer fit for the small boron ions is provided. Generally greater tetrahedral substitution of aluminum in illite than in montmorillonite should make illite a less favorable host for boron.

Montmorillonite and mixed-layer clay apparently contain as much boron as illite in the Pierre shale. In fractionated samples, the boron content is related to total abundance of clay minerals rather than abundance of specific clay minerals. The wide range of boron content of samples of Pierre shale (fig. 253.1) indicates, however, that other factors must also be involved. Such factors may include composition of source material, the boron content of sea water and, possibly, the rates of sedimentation that controlled the length of time the clay minerals were in contact with sea water.

REFERENCES

Degens, E. T., Williams, E. G., and Keith, M. L., 1957, Environmental studies of Carboniferous sediments: Am. Assoc. Petroleum Geologists Bull., v. 41, no. 11, p. 2427-2455; v. 42, p. 981-997.

Eugster, H. P., and Wright, T. L., 1960, Synthetic hydrous boron micas, *in* Short papers in the geological sciences: U.S. Geol. Survey Prof. Paper 400-B, p. B441-B442.

Frederickson, A. F., and Reynolds, R. C., Jr., 1960, How measuring paleosalinity aids exploration: Oil and Gas Jour., v. 58, no. 5, p. 154-158.

Harder, Hermann, 1959, Beitrag zur Geochemie des Bors, Pt. I, Bor in Mineralen und magmatischen Gesteinen; Pt. II, Bor in sedimenten: Akad. der Wiss. Göttingen Nachr., Math.-Phys. Kl., Pt. I, v. 1959, no. 5, p. 67-122; Pt. II, v. 1959, no. 6, p. 123-183.

Hatcher, J. T., and Wilcox, L. V., 1950, Colorimetric determination of boron using carmine: Anal. Chemistry, v. 22, p. 567-569.

Landergren, Sture, 1945, Contribution to the geochemistry of boron. II, The distribution of boron in some Swedish sediments, rocks, and iron ores. The boron cycle in the upper lithosphere: Arkiv för Kemi, Mineralogi och Geologi, v. 19 A, no. 5, paper no. 26, 31 p.

Russell, W. L., 1930, South Dakota Geol. Nat. History Survey Rept. Inv. 7, p. 5.

Schultz, L. G., 1960, Quantitative determinations of some aluminous clay minerals in rocks, *in* Swineford, Ada, ed., Natl. Clay Conf. on clays and clay minerals, 7th, Washington, 1958, Proc.: London, Pergamon Press, p. 216-224.

Stubican, V., and Roy, Rustum, 1960, Boron substitution in clays [abs.]: Natl. Clay Conf., 9th, Lafayette, Ind., 1960, Program and abstracts.

Wichers, Edward, Finn, A. N., and Clabaugh, W. S., 1941, Comparative tests of chemical glassware: Indust. and Eng. Chemistry, Anal. Ed., v. 13, p. 419-422.

254. ACCESSORY BASTNAESITE IN THE PIKES PEAK GRANITE, COLORADO

By John W. Adams and Edward J. Young, Denver, Colo.

During an examination of rare-earth pegmatites in the vicinity of Raleigh Peak in southern Jefferson County, Colo., specimens of the surrounding Pikes Peak granite were found to contain bastnaesite. Further sampling of the granite has shown that it may contain from 0.006 to 0.19 percent bastnaesite that is apparently unrelated to the pegmatites.

Bastnaesite, a fluocarbonate of dominantly cerium group rare earths, was until recently considered to be a very rare mineral. Its best known occurrences, which have been summarized by Glass and Smalley (1945), are in contact metamorphic zones, pegmatites, and fluorite deposits. In 1949, however, bastnaesite was recognized as an abundant mineral in the carbonatite and related veins at Mountain Pass, Calif. (Olson and others, 1954), a discovery that has raised bastnaesite to the status of an important ore mineral.

The new bastnaesite occurrence is at the north end of the Pikes Peak batholith in coarse- to medium-grained granite that contains either biotite or hornblende as the dominant mafic mineral, and which probably belongs to the outer zone rocks that Hutchinson (1960) concludes are older than the other rock types that comprise the batholith. Biotite is the only mafic mineral in the samples from the Raleigh Peak area, but about equal proportions of hornblende and biotite are present in bastnaesite-bearing granite collected 6 miles to the northwest.

In the granites that were sampled, the bastnaesite is associated with monazite, wholly or partially metamict allanite, or both. The bastnaesite appears invariably to be a constituent of impure microcrystalline aggregates that may be seen in some hand specimens as irregular yellow-brown areas surrounding grains of black glassy allanite. The aggregates have a waxy luster and, when examined with the microspectroscope, show weak but characteristic neodymium absorption bands, a property not shown by allanite.

In thin section the bastnaesite-bearing aggregate may have sharp boundaries with the residual allanite or may pervade the allanite, commonly in lath-shaped areas that probably represent compositional zones of the host. This replacement is complete in some grains, with only the crystal outline of the allanite remaining. The bastnaesite in the aggregates appears as minute birefringent fibers in a groundmass of an isotropic to weakly birefringent material of variable index of refraction. The minute size of the fibers and their enclosure in the other material prevent the determination of most of the optical properties of the bastnaesite. However, uniaxial positive interference figures, which are characteristic of bastnaesite, were seen in some aggregate areas that contain fibers in parallel growth.

Positive identification of the bastnaesite has been possible only by X-ray methods. X-ray diffraction patterns of the aggregate show bastnaesite lines accompanied by generally weaker lines ascribable to one or more other minerals including allanite, quartz, zircon, monazite, and hematite. The isotropic to weakly birefringent groundmass of the aggregate is probably largely allanite that for the most part is amorphous from metamictization and chemical alteration but which locally is sufficiently crystalline to produce weak X-ray diffraction lines.

It is concluded from the mode of occurrence of the bastnaesite in the Pikes Peak granite that it was formed from allanite by reaction with late-stage magmatic solutions. These solutions, containing fluorine and carbon dioxide, were sufficiently reactive to attack the earlier formed allanite and partly replace it by the fluocarbonate.

Where the bastnaesite-bearing aggregate occurs in granite in which no allanite was found, its origin from monazite might be considered—particularly because monazite occurs in the allanite-free rocks, and monazite lines are present in the X-ray diffraction pattern of one such aggregate. In thin section, however, the aggregate from these rocks shows relict zonation and general appearance similar to that clearly derived from allanite. Also, no megascopic or microscopic relations comparable to those found between the aggregate and allanite have been seen between the aggregate and monazite. Although the evidence is still equivocal, it appears more probable that in such rocks the bastnaesite aggregates are the residuals of complete allanite alteration.

The first reported occurrence of bastnaesite as an accessory mineral of granitic rocks was in the Redstone granite of Rhode Island (Smith and Cisney, 1956), where it is estimated to make up 0.02 percent of the rock. There the bastnaesite is found as irregular aggregates or as prismatic forms, both of which are made up of minute crystallites. W. L. Smith (oral communication, 1960) considers that the crystal forms may be those of an earlier mineral now replaced by the bastnaesite. A very small amount of monazite is found in the granite, but no allanite. Allanite, however, is reported as an accessory mineral elsewhere in the Narragansett Pier granite with which the Redstone granite has been correlated (Moore, 1959), so that this occurrence may well represent a further example of complete allanite alteration.

Bastnaesite has also been found in granites of the Elberton area of southeast Georgia as a constituent of fine-grained aggregates that pseudomorphically replace allanite (Silver and Grunenfelder, 1957). The allanite, which originally made up 0.3 percent of the rock, appears to have been largely converted to bastnaesite, huttonite(?), hematite, and a pale yellow isotropic, or nearly isotropic, mineral. The alteration is thought by Silver and Grunenfelder to be the result of reactive solutions, probably deuteric, that attacked the allanite along crystal and zonal boundaries.

Sverdrup and others (1959) recently described four occurrences of bastnaesite in Norway. In one of these, the Lapplaegret pegmatite, the bastnaesite has replaced allanite in a manner that appears identical with that in the Pikes Peak granite and shows the same microcrystalline habit and poorly defined optical properties.

In contrast to what is probably the deuteric alteration of allanite to bastnaesite is the weathering alteration of allanite studied by Watson (1917). Using material from pegmatites in Virginia, Watson made comparative chemical analyses of relatively unaltered allanite and the reddish-brown alteration rinds so commonly found on allanite masses. These analyses showed the alteration product to be variable in composition, but to consist in general of hydrated ferric oxides, alumina, and silica. The rare-earth elements were essentially absent except for cerium, which, while generally present to a lesser amount than in the allanite, was found in one instance to be actually enriched in the outermost layer of the rind. The persistence of cerium in the alteration product may well be due to its ready oxidation to Ce (IV), a property that allows it to be separated from other members of the rare earth group in analytical procedures.

This supergene alteration characterized by oxidation, leaching, and hydration differs from the deuteric process by which bastnaesite is formed. The development of bastnaesite from allanite involves chemically active solutions such as might expectably be residual in fluorine-rich intrusive rocks.

The metamict character shown by much of the allanite in the Pikes Peak granite is probably entirely unrelated to the bastnaesite alteration, which may be assumed to have been completed at a time when the allanite was entirely crystalline. Supergene alteration, on the other hand, would be accelerated by metamictization through radiochemical effects and by the physical disruption of the allanite and the enclosing rock.

REFERENCES

Glass, J. J., and Smalley, R. G., 1945, Bastnäsite [Gallinas Mts., N. Mex.]: Am. Mineralogist, v. 30, p. 601-615.

Hutchinson, R. M., 1960, Structure and petrology of north end of Pikes Peak batholith, Colorado *in* Guide to the geology of Colorado: Geol. Soc. America, Rocky Mtn. Assoc. Geologists, Colo. Sci. Soc., p. 170-180.

Moore, G. E., Jr., 1959, Bedrock geology of the Carolina and Quonochontaug quadrangles, Rhode Island: U.S. Geol. Survey Geol. Quad. Map GQ-117.

Olson, J. C., Shawe, D. R., Pray, L. C., and Sharp, W. N., 1954, Rare earth mineral deposits of the Mountain Pass District, San Bernardino County, California: U.S. Geol. Survey Prof. Paper 261, 75 p.

Silver, L. T., and Grunenfelder, Marc, 1957, Alteration of accessory allanite in granites of the Elberton area, Georgia: Geol. Soc. America Bull., v. 68, p. 1796.

Smith, W. L., and Cisney, E. A., 1956, Bastnaesite, an accessory mineral in the Redstone granite from Westerly, Rhode Island: Am. Mineralogist, v. 41, p. 76-81.

Sverdrup, T. L., Bryn, K. Ø., and Saebø, P. C., 1959, Bastnäsite a new mineral for Norway: Norsk geol. tidsskr., v. 39, p. 237-247.

Watson, T. L., 1917, Weathering of allanite: Geol. Soc. America Bull., v. 28, p. 463-500.

255. TUNELLITE, A NEW HYDROUS STRONTIUM BORATE FROM THE KRAMER BORATE DISTRICT, CALIFORNIA

By Richard C. Erd, Vincent Morgan, and Joan R. Clark,
Menlo Park, Calif.; U. S. Borax & Chemical Corporation, Boron, Calif.; and Washington, D. C.

Tunellite was first noted by Erd in some samples collected in 1957 from a ventilating shaft in the Jenifer mine, Kramer borate district, California, by Daniel M. Cooper of the U. S. Borax & Chemical Corporation. Initial mineralogical determinations showed that the optical properties of tunellite nearly matched those of hydroboracite, $MgO{\cdot}CaO{\cdot}3B_2O_3{\cdot}6H_2O$, but its X-ray powder pattern could not be identified. Later Morgan analyzed material collected from the newly opened pit of the company and established the composition of tunellite, $SrO{\cdot}3B_2O_3{\cdot}4H_2O$. In 1959 the mineral was discovered in the Furnace Creek borate area, Death Valley region, California, by James F. McAllister, U.S. Geological Survey, who kindly supplied material for comparison. Goniometric and X-ray crystallographic studies by Clark corroborated the chemical analysis and confirmed tunellite as a new species isostructural with nobleite (tables 255.1 and 255.2).

The name tunellite (pronounced tŭn nĕl′ īt) is in honor of Dr. George Tunell, Professor of Geology, University of California, Los Angeles.

The geology of the Kramer borate district has been described by Schaller (1930) and Gale (1946); more recent data are given by Smith (1960). In the western part of the deposit, where the initial open pit was excavated, a prominent fault has displaced the borate beds. Near this fault there is an angular discordance between the sodium borate ore and overlying borate-bearing mudstone beds; this discordance may have been the result of subsurface solution (Smith, 1960, p. 113). A 6-foot zone above the sodium borate-mudstone con-

TABLE 255.1.—*Crystallographic data for tunellite,* $SrO{\cdot}3B_2O_3{\cdot}4H_2O$

	[1] Space Group $P2_1/a-C_{2h}^5$	[1][2] Space Group $P2_1/n-C_{2h}^5$
a	14.36 ± 0.05 A	13.75 A
b	$8.19_8\pm0.02$	8.19_8
c	$9.93_0\pm0.02$	9.93_0
$a:b:c$	1.752:1:1.211	1.677:1:1.211
β	$113°55'\pm10'$	107°23′
Cell volume		1068 A^3
Cell contents		$4[SrO{\cdot}3B_2O_3{\cdot}4H_2O]$
Density (calculated)		2.39_1gcm^{-3}
Specific gravity (measured, D^{20}_4)		[2] 2.40 ± 0.01

[1] Transformation, $P2_1/a$ to $P2_1/n$: $\bar{1}0\bar{1}/010/001$.
[2] Determined using the sink-float method with a mixture of bromoform and carbon tetrachloride.

TABLE 255.2.—*Comparison of crystallographic, optical, and physical data for tunellite and nobleite*

	Tunellite	Nobleite [1]
Cell contents	$4[SrO{\cdot}3B_2O_3{\cdot}4H_2O]$	$4[CaO{\cdot}3B_2O_3{\cdot}4H_2O]$
Crystal system	Monoclinic	Monoclinic
Space group	$P2_1/a$	$P2_1/a$
a	14.36 ± 0.05A	14.56 ± 0.05A
b	$8.19_8 \pm 0.02$	$8.01_6 \pm 0.02$
c	$9.93_0 \pm 0.02$	$9.83_8 \pm 0.02$
β	$113°55' \pm 10'$	$111°45' \pm 10'$
Cell volume	1068 A^3	1066 A^3
Density (calculated)	$2.39_1 gcm^{-3}$	$2.09 gcm^{-3}$
Specific gravity (meas., D_4^{20})	2.40 ± 0.01	2.09 ± 0.01
Indices of refraction, sodium light:		
α	1.519 ± 0.003	1.500 ± 0.003
β	1.534 ± 0.002	1.520 ± 0.002
γ	1.569 ± 0.002	1.554 ± 0.002
2V (calculated)	68°	76°
Dispersion	$r>v$, weak	$r>v$, weak
Optical orientation	$X \wedge a = 29°$ $Y = b$ $Z \wedge c = -5°$	$X \wedge a = 29°$ $Y = b$ $Z \wedge c = -7°$
Cleavage	{100} perfect {001} distinct	{100} perfect {001} indistinct
Hardness	2½	3

[1] Data from Erd and others, 1961.

tact is disturbed and within this zone tunellite formed as a disseminated secondary mineral.

The first material found consisted of white compact fine-grained nodules associated with lenses of inderite and kurnakovite (the monoclinic and triclinic polymorphs of $2MgO{\cdot}3B_2O_3{\cdot}15H_2O$; Schaller and Mrose, 1960) and nodular ulexite in a greenish to black montmorillonitic clay. Subsequently individual long prismatic [001] and flat tabular {100} crystals of tunellite up to 1.5 cm in length were found in the clay. As the open pit was developed, Morgan discovered a large vuggy mass of hydroboracite lined with splendid equant crystals of tunellite up to 1 cm in diameter. Figure 255.1 shows idealized prismatic and equant habits, common forms, and optical orientation of the tunellite crystals from the open pit. Other minerals associated with tunellite in these occurrences are realgar, stibnite, several undescribed iron sulfides, adularia, and analcime.

Most of the physical and optical properties of tunellite are summarized in table 255.2. It is colorless, transparent, nonfluorescent, and has a subvitreous luster, except that the {100} and cleavage surfaces parallel to {100} are pearly. Thin crystals are flexible, inelastic, and sectile. Faces of the form {0kl} are striated parallel to [001], notably so in specimens from the Furnace Creek area. Faces of {100} are relatively smooth, lustrous, and soft, whereas {110} and {001} faces are rough, pitted, and hard. X-ray powder diffraction data for tunellite are given in table 255.3.

Determinations of SrO and B_2O_3 were made using separate 0.5-gram samples. The SrO sample was dissolved in dilute HCl, neutralized with NH_4OH, and combined with sufficient dilute H_2SO_4 to precipitate all of the strontium. An equal volume of methanol was added, the solution was mixed, and was allowed to stand overnight. The $SrSO_4$ precipitate was filtered into a dried and tared Gooch crucible and weighed after washing and drying. B_2O_3 was determined by titration with NaOH and manitol. Water was determined by loss on ignition of 1-gram samples. Redetermination of B_2O_3 on the residue proved that there was no loss of B_2O_3 due to volatilization during ignition. Calcium was not detected. The results of the analysis are given in table 255.4.

The synthetic $SrO{\cdot}3B_2O_3{\cdot}4H_2O$ was prepared by adding 3 g H_3BO_3 in 50 ml of water to a solution of 10 g recrystallized borax in 100 ml of water at 80° C. Three-fourths of a gram of $SrCO_3$ was added and the solution was stirred for one day. After six days, when most of the precipitate was found to be $SrCO_3$, 10 g more H_3BO_3 in 50 ml of water was added. An extremely fine-grained precipitate of $SrO{\cdot}3B_2O_3{\cdot}4H_2O$ had formed after two days, and rhomb- and octagonal-shaped plates 0.02 mm in diameter developed after standing for one month at room temperature. (See analysis, table 255.4.) We found no previous report

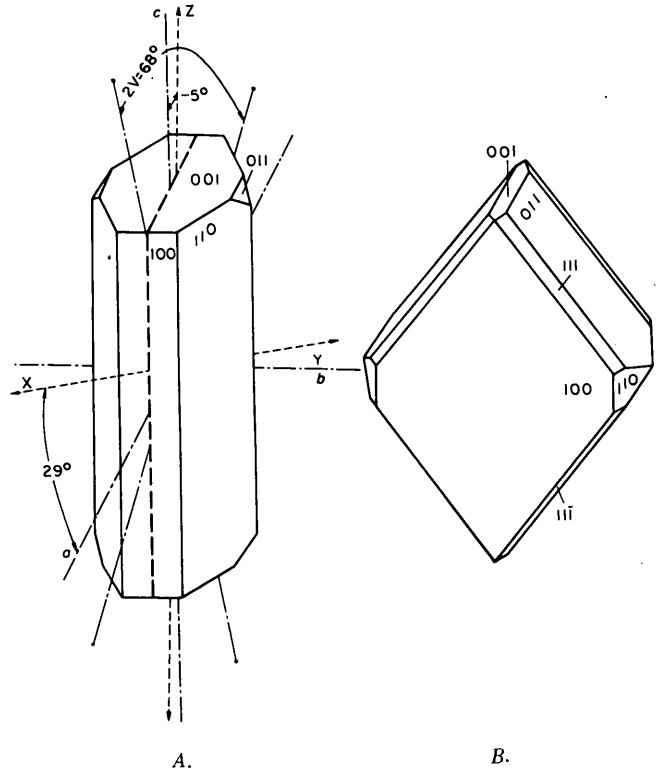

FIGURE 255.1.—Prismatic (*A*) and equant (*B*) habits and optical orientation of tunellite crystals from the Kramer borate district.

TABLE 255.3.—*X-ray diffraction data for tunellite*

Measured [1]						Calculated [2]	
Mineral [3]				Synthetic compound [4]		Indexing for space group $P2_1/a$ (table 255.1)	
Boron, Calif.		Death Valley region, California					
I	d_{hkl}	I	d_{hkl}	I	d_{hkl}	d_{hkl}	*hkl*
				1	9.10	9.078	001
3	6.97	4	6.97	24	6.97	6.954	110
4	6.79	7	6.78	11	6.79	6.783	$\bar{2}01$
100	6.58	100	6.57	100	6.57	6.564	200
2	6.22	3	6.21	15	6.21	6.200	$\bar{1}11$
						6.084	011
1	5.231	2	5.215	2	5.231	5.226	$\bar{2}11$
6	5.138	8	5.138	32	5.135	5.124	210
						5.024	111
1	4.750	1	4.745	11	4.750	4.738	$\bar{2}02$
6	4.531	11	4.525	18	4.529	4.539	002
						4.520	201
						4.240	$\bar{1}12$
						4.123	$\bar{3}11$
						4.102	$\bar{2}12$
<1	4.112	----	----	3	4.112	4.099	020
<1	3.972	<1	3.969	3	3.969	3.971	012
						3.958	211
1	3.924	1	3.914	8	3.922	3.913	120
7	3.872	9	3.867	21	3.867	3.860	310
						3.762	$\bar{1}21$
<1	3.741	<1	3.743	8	3.743	3.736	021
						3.656	$\bar{3}12$
4	3.597	8	3.592	9	3.596	3.586	401
1	3.513	1	3.513	17	3.517	3.508	$\bar{2}21$
2	3.486	2	3.484	16	3.484	3.477	220
						3.475	112
						3.445	121
1	3.399	1	3.399	3	3.399	3.391	$\bar{4}02$
						3.304	$\bar{2}03$
						3.285	$\bar{4}11$
2	3.290	5	3.286	2	3.288	3.282	400
2	3.175	2	3.175	8	3.175	3.179	202
				14	3.163	3.168	311
						3.158	$\bar{1}22$
						3.134	$\bar{4}12$
<1	3.110	<1	3.113	9	3.106	3.109	$\bar{3}21$
<1	3.100	<1	3.099			3.100	$\bar{2}22$
						3.064	$\bar{2}13$
						3.047	410
4	3.052	7	3.045	19	3.046	3.042	022
						3.036	221
2	3.028	5	3.028	18	3.025	3.026	003
						3.022	$\bar{1}13$
1	3.001	2	2.993	10	2.996	2.991	320
						2.964	212
1	2.955	1	2.954	7	2.952	2.948	$\bar{3}13$
1	2.898	1	2.898	9	2.898	2.893	$\bar{3}22$
1	2.889	1	2.887	11	2.887	2.882	$\bar{4}03$
1	2.841	1	2.840	11	2.840	2.839	013
<1	2.805	----	----	6	2.804	2.801	122
1	2.755	3	2.751	3	2.751	2.750	401
<1	2.724	----	----	4	2.722	2.719	$\bar{4}13$
						2.699	$\bar{4}21$
3	2.700	4	2.696	8	2.697	2.691	$\bar{5}11$
						2.675	130
		<1	2.673	3	2.673	2.668	$\bar{5}12$
						2.633	321
						2.626	$\bar{1}31$
1	2.622	----	----	13	2.619	2.617	031
						2.613	$\bar{4}22$
		1	2.609	----	----	2.607	411
						2.579	113
						2.572	$\bar{2}23$
1	2.568	1	2.565	7	2.566	2.562	420
						2.547	$\bar{1}23$
						2.535	$\bar{2}31$
<1	2.536	<1	2.536	6	2.536	2.528	312
						2.523	230
				6	2.514	2.512	222
						2.511	$\bar{1}31$
						2.502	$\bar{3}23$
4	2.507	8	2.503	11	2.505	2.500	510
<1	2.481	<1	2.479	4	2.479	----	----
<1	2.438	----	----	3	2.436	----	----
2	2.390	3	2.388	4	2.390	----	----
<1	2.378	----	----	3	2.375	----	----
2	2.362	5	2.359	5	2.361	----	----
1	2.322	----	----	6	2.320	----	----
4	2.268	6	2.266	13	2.266	----	----
3	2.207	7	2.202	8	2.204	----	----
<1	2.192	2	2.190	2	2.191	----	----
<1	2.178	----	----	4	2.176	----	----
1	2.145	<1	2.141	7	2.143	----	----
2	2.122	2	2.119	19	2.120	----	----
1	2.106	1	2.101	11	2.102	----	----
1	2.076	<1	2.071	11	2.073	----	----
1	2.053	2	2.051	11	2.051	----	----
1	2.032	2	2.024	13	2.026	----	----

See footnotes at end of table.

TABLE 255.3.—*X-ray diffraction data for tunellite*—Continued

Measured [1]						Calculated [2]	
Mineral [3]				Synthetic compound [4]		Indexing for space group $P2_1/a$ (table 255.1)	
Boron, Calif.		Death Valley region, California					
I	d_{hkl}	I	d_{hkl}	I	d_{hkl}	d_{hkl}	*hkl*
<1	1.985	<1	1.981	4	1.983	----	----
2	1.949	4	1.948	7	1.948	----	----
1	1.936	2	1.931	6	1.931	----	----
1	1.904	2	1.903	6	1.896	----	----
<1	1.885	----	----	4	1.885	----	----
				1	1.858	----	----
<1	1.822	<1	1.819	3	1.821	----	----
1	1.805	1	1.802	4	1.804	----	----
				2	1.789	----	----
				1	1.772	----	----
<1	1.765	----	----	1	1.761	----	----
<1	1.748	1	1.744	3	1.745	----	----
<1	1.710	----	----	2	1.708	----	----
		←plus additional lines					
all with I≤1		all with I≤2		all with I≤3			

[1] *X*-ray diffractometer data; Cu/Ni radiation, λ CuK_α=1.5418 A. Aluminum powder used as internal standard. Scanned at ¼° per minute from 8°–55°2θ; at 1° per minute from 55°–101°2θ.

[2] All calculated spacings listed for $d_{hkl} \geq 2.500$ A. Indexing assigned on basis of comparison with single-crystal precession photographs. Computation of the *d*-spacings by Daniel L. Appleman.

[3] Diffractometer charts X–1935 (Boron, Calif.) and X–1934 (Death Valley region, California) of the mineral show strong preferred orientation effects.

[4] Synthetic material prepared by R. C. Erd; analyzed by V. Morgan. Diffractometer chart X–1929.

TABLE 255.4.—*Chemical analyses of tunellite*

	Weight percent [1]		Molecular proportions		Ratios		Calculated composition for $SrO \cdot 3B_2O_3 \cdot 4H_2O$ (percent)
	Mineral [2]	Synthetic [3]	Mineral	Synthetic	Mineral	Synthetic	
SrO	27.71	27.02	0.2674	0.2607	1.023	0.988	26.94
B_2O_3	53.70	52.88	.7711	.7593	2.951	2.877	54.32
H_2O	18.71	20.04	1.0385	1.1123	3.974	4.214	18.74
Total	100.12	99.94					100.00

[1] Analyst, Vincent Morgan, U.S. Borax & Chemical Corporation.

[2] Material from U.S. Borax & Chemical Corporation open pit, Boron, Calif. Figure for SrO includes approx. 0.3 percent BaO determined using *X*-ray spectrochemical analysis.

[3] Material synthesized by R. C. Erd (Expt. 58–3).

of this compound, although the compound $SrO \cdot 3B_2O_3 \cdot 5H_2O$ was synthesized by Gode and Kesans (1953, p. 36).

Tunellite is soluble in cold dilute acid or strong alkaline solutions, but is unaffected by treatment with glycerol or methanol; a coating of $SrSO_4$ impedes further solution in H_2SO_4.

The differential thermal analysis curve of the mineral shows two endothermic troughs with initial temperatures of 200° C and 405° C and trough temperatures of 255° C and 430° C. An exothermic peak with initial temperature of 625° C and peak temperature of 670° C appeared near the end of the run which was discontinued at 700° C to prevent fusion of the sample in the block.

Heated in a closed tube tunellite exfoliates perpendicular to the cleavage, turns silvery white (resembling

muscovite), then turns chalky white. Water driven off has a pH of 4 and probably indicates some loss of B_2O_3 due to rapid heating. On prolonged heating a clear glass forms from which an anhydrous strontium borate crystallizes. The melting point of tunellite has not been determined.

In late 1960, large crystals (some nearly 4 cm in length) were found in the open pit by M. L. Speckels, who kindly gave them to us for study. Some of these crystals have a specific gravity of 2.46 and contain up to 15.0 percent BaO. The presence of barium in tunellite suggests the possibility that $BaO{\cdot}3B_2O_3{\cdot}4H_2O$, synthesized by Gode and Kesans (1953, p. 36), may be isostructural with tunellite but data for this compound are not available. Tunellite is isostructural with nobleite (table 255.2) but the extent of any solid solution is unknown. There is no simple dehydration-hydration relation between tunellite, veatchite ($SrO{\cdot}3B_2O_3{\cdot}2H_2O$), and the $SrO{\cdot}3B_2O_3{\cdot}5H_2O$ of Gode and Kesans. Tunellite and veatchite have not been found as associated minerals, although both have been found in the Kramer area (Benda and others, 1960, p. 330).

REFERENCES

Benda, W. K., Erd, R. C., and Smith, W. C., 1960, Core logs from five test holes near Kramer, California: U.S. Geol. Survey Bull. 1045-F, p. 319-393.

Erd, R. C., McAllister, J. F., and Vlisidis, A. C., 1961, Nobleite, another new hydrous calcium borate from the Death Valley region, California: Am. Mineralogist, v. 46, p. 560–571.

Gale, H. S., 1946, Geology of the Kramer Borate District, Kern County, California: California Jour. Mines and Geology, v. 42, p. 325-378.

Gode, H. K., and Kesans, A. D., 1953, Sintezy boratov v vodnykh rastvorakh (Syntheses of borates in aqueous solutions), *in* Khimiia boratov (Chemistry of the borates): Akad. Nauk Latv. SSR, Izdatelstvo, p. 29-43, Riga.

Schaller, W. T., 1930, Borate minerals from the Kramer district, Mohave Desert, California: U.S. Geol. Survey Prof. Paper 158, p. 137-170.

Schaller, W. T., and Mrose, M. E., 1960, The naming of the hydrous magnesium borate minerals from Boron, California—a preliminary note: Am. Mineralogist, v. 45, p. 732-734.

Smith, W. C., 1960, Borax and borates, *in* Industrial minerals and rocks: New York, Am. Inst. Mining Metall. Petroleum Engineers, 3d ed., p. 103-122.

256. HYDROZIRCON FROM THE WIND RIVER FORMATION, WYOMING

By R. G. Coleman and R. C. Erd, Menlo Park, Calif.

Work done partly in cooperation with the U. S. Atomic Energy Commission

A high concentration of zirconium (1 to 5 weight percent) was discovered in a uranium-bearing arkose submitted for spectrographic analysis and uranium assay (table 256.1). This sample was collected as part of a geologic study of the Gas Hills uranium district in Wyoming (Zeller, 1957) and represented the mineralized zone within a nonproductive uranium prospect along the eastern border of the district (SW1/4SE1/4 SW1/4 sec. 15, T. 35 N., R. 89 W., Arminta SW quadrangle, Natrona County, Wyoming).

Zirconium-uranium mineralization is restricted to an area of less than 300 square yards within a small bench rising several feet above the nearly flat terrain and occurs below an iron gossan caprock within a coarse-grained arkose of the Wind River formation of early Eocene age. A series of samples was obtained in vertical sequence from the face of the prospect pit

TABLE 256.1.—*Chemical and spectrographic analyses of hydrozircon-bearing arkose, Wind River formation, Wyoming*

[Analysts: J. C. Hamilton (spectrographic); Lorraine M. Lee, E. J. Fennelly, G. T. Burrow (chemical)]

	ZW-120	ZW-121	$4929A_{30}$
Chemical analyses (weight percent)			
U	0.16	0.11	0.25
As	0.052	0.12	Not determined
Se	0.0005	<0.0005	Not determined
Semiquantitative spectrographic analyses (weight percent)			
>10	Si	Si	Si
5–10	Al	Al K	Al Na
1–5	K Na Zr	Na Fe Zr	Zr Fe K
0.5–1.0	Fe	----------	Ca P
0.1–0.5	Ca Mg	As	As
0.05–0.1	Ti As Ba	Ca Mg Ba	Ba Mg
0.01–0.05	Mn Mo Sc	Ti	B Tl Mn Sr
0.005–0.01	Sr Cr Y	Mn Mo Sr Y	Pb La Ni Y
0.001–0.005	Ga B V La Cu Pb Yb	Ga Sc Cr V La Pb Yb	Ge Cr Mo Cu Ga Sc V
0.0005–0.001	----------	Cu	Be Yb

601530 O—61——20

10 feet deep (fig. 256.1). The arkose sampled contains from 60 to 80 percent quartz, 20 to 40 percent feldspar (perthite and microcline), and minor amounts of plagioclase and mica. These clastic grains are angular and poorly sorted, and the potassium feldspar shows only minor alteration. The sampled section was divided into zones according to the dominant intergranular cement within the arkose (fig. 256.1).

X-ray determinations on the purified hydrozircon (fig. 256.2) shows that its diffraction pattern is similar to that of zircon, but considerable water and minor amounts of arsenic, uranium, and iron were found by chemical analysis (table 256.2). The hydrozircon is transparent and nearly isotropic with only a faint aggregate birefringence and is characterized by a complete lack of crystalline form. The X-ray pattern demonstrates the similarity to zircon; however, the low density and index of refraction combined with a high water content clearly show hydration. Razumnaya and others (1958) have described a metacolloid

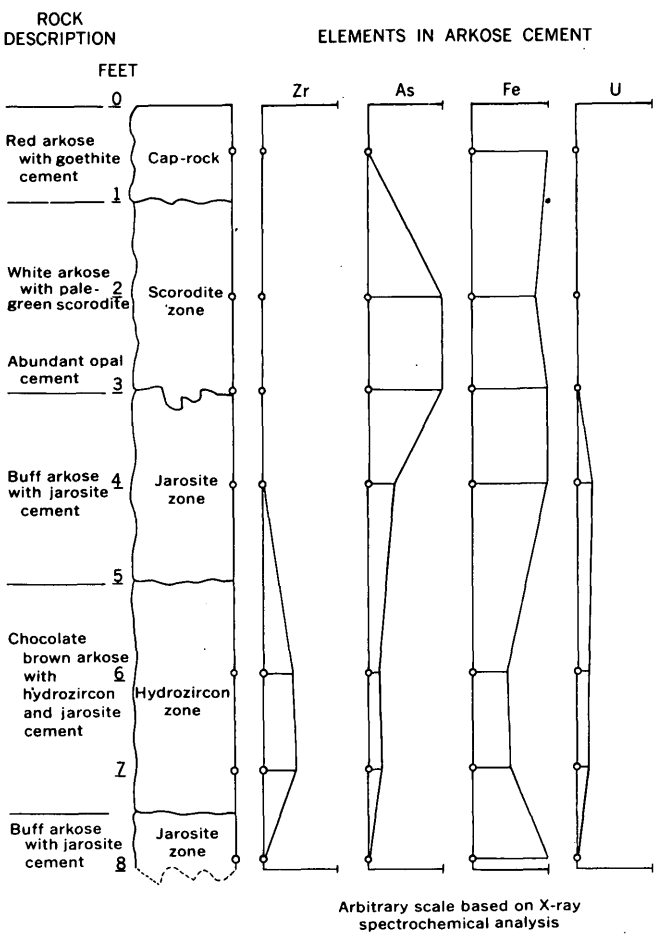

FIGURE 256.1.—Mineralogic and chemical variations in the zirconium-bearing arkose of the Wind River formation, Gas Hills uranium district, Wyoming.

TABLE 256.2.—*Some chemical and physical properties of hydrozircon from Wyoming*

Partial analysis (weight percent)						Mean index of refraction	Density	Intensity ratio Zr/Si [4]
Si [1]	Zr [1]	Fe [2]	As [2]	U [3]	H_2O [3]			
>10	>10	1.1	0.68	0.11	16.6	1.70–1.72	3.0–3.2	2.68

[1] Semiquantitative spectrographic analysis, by K. V. Hazel.
[2] X-ray spectrochemical analysis using GeO as internal standard, by J. M. Axelrod.
[3] Estimated by loss on ignition at 950° C for two hours.
[4] Determined by X-ray spectrochemical methods using the ZrLα/SiKα peaks, by Harry J. Rose and Francis J. Flanagan.

variety of zircon from the U.S.S.R. similar in many respects to the Wyoming hydrozircon, except that the Russian variety is soluble in dilute HNO_3 and HCl whereas the Wyoming material studied is resistant even to concentrated HNO_3 and HCl.

Prior to the discovery of hydrozircon from Wyoming and the U.S.S.R., metamict zircons derived from igneous and metamorphic rocks were the only natural zircons known to contain minor amounts of water. Frondel (1953) has proposed the general formula $Zr(SiO_4)_{1-x}(OH)_{4x}$ for hydrozircons, but Mumpton and Roy (1961) present experimental evidence, combined with 43 analyses of natural metamict zircons, that suggests the formula $ZrSiO_4 \cdot xH_2O$. As the Zr/Si intensity ratio of the Wyoming hydrozircon (table 256.2) is similar to that of normal zircon, it is possible that its formula is more nearly like that suggested by Mumpton and Roy. The X-ray pattern of the Wyoming hydrozircon is diffuse with a_0 larger and c_0 smaller than zircon; however on heating the hydrozircon for two hours at 950° C the pattern is identical with that of well crystallized zircon and neither ZrO_2 nor SiO_2 were detected (fig. 256.2). The arsenic, iron, and uranium revealed by analysis must be part of the compound. If we assume iron is present as Fe^{+3} (ionic radius 0.67A) and arsenic as $(AsO_4)^{-3}$ then it is possible to substitute Fe^{+3} for Zr^{+4} (ionic radius 0.87A) and $(AsO_4)^{-3}$ for $(SiO_4)^{-4}$. Maintaining a 1:1 ratio for $(AsO_4)^{-3}$ and Fe^{+3} would satisfy the valence requirements and a possible formula for the Wyoming hydrozircon would then be as follows:

$$[(Zr^{+4}, U^{+4})_{1-x}Fe^{+3}{}_x]\ [(SiO_4)^{-4}{}_{1-x}(AsO_4)^{-3}{}_x] \cdot 2H_2O.$$

Further complete analyses will be needed to confirm this tentative formula.

Hydrozircon deposited as a secondary intergranular cement in an unaltered arkose and lacking crystalline form is clear evidence that this material was formed at low temperatures and transported to the point of deposition as a soluble zirconium compound. Experimental work on the stability of zircon demonstrates that corrosion may take place in alkaline environments, and that a stable zirconium carbonate complex can

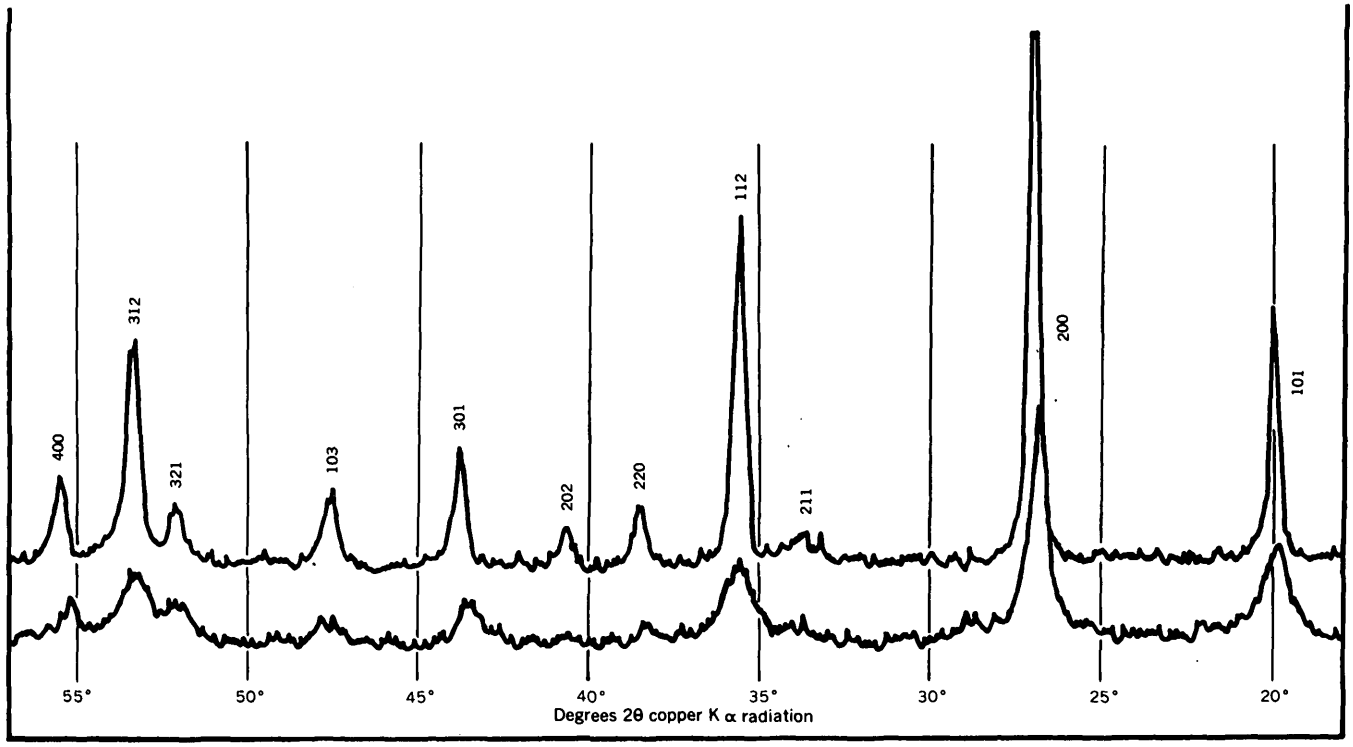

FIGURE 256.2.—Diffractometer traces for natural hydrozircon (lower trace) and for hydrozircon heated two hours at 950°C (upper trace).

exist in solutions whose pH is not excessively alkaline (Blumenthal, 1958, p. 210–213, p. 37–39). Zircons from the granite in the vicinity of the Sweetwater River, source rock for the arkosic facies of the Wind River formation, are partly metamict, and a lead-alpha age determination on these same zircons shows them to be Precambrian in age.[1] Detrital zircons, within the arkose and derived from these granites, are also partially or completely metamict and show evidences of corrosion. Evidence for alkaline leaching of the alkali-soluble constituents in the Wind River formation has been given by Coleman (1957), and the well-known fact that metamict zircons are susceptible to corrosion (Pabst, 1952) leads to the conclusion that zirconium could have been mobilized by these same alkaline solutions. The association of uranium with the secondary zirconium indicates that leaching of the detrital zircon was contemporaneous with the leaching that gave rise to the high-grade uranium deposits of the Gas Hills district. Precipitation of the zirconium as $Zr(OH)_4$ may have been concomitant with the deposition of iron sulfides in an alkaline reducing environment. Later surface oxidation of the pyrite produced the oxide, arsenate, and sulfate zones of iron, and the silica released in this acid environment may have reacted with the zirconium hydrate to form the hydrozircon.

Radiochemical studies by Rosholt (1958; 1959) on the Gas Hills uranium ores and the hydrozircon-bearing arkose disclose a Pleistocene(?) age for the mineralization with some ores giving ages of 12,000 years.

[1] Sample ZW-263 shows the following: α/mg-hr 816, Pb 800 ppm, and an age of 2000±225 my. Lead-alpha determination by T. W. Stern, lead determination by H. J. Rose, Jr., and H. W. Worthing. Age calculation by methods similar to those given by Gottfried and others (1959).

TABLE 256.3.—*Radiochemical analyses of hydrozircon-bearing arkose, Wyoming*

[Analyst: J. N. Rosholt, Jr. Analyses made according to methods described by Rosholt (1959)]

Sample	Percent			Percent equivalent			Radioisotope ratios			
	eU	U	Th^{232}	Pa^{231}	Rn^{222}	Pb^{210}	eU/U	ePa^{231}/U	eRn^{222}/U	ePb^{210}/U
ZW–120	0. 12	0. 16	0. 015	0. 12	0. 09	0. 10	0. 75	0. 75	0. 56	0. 62
ZW–121	. 083	. 11	. 003	. 080	. 06	. 046	. 75	. 72	. 55	. 42

The hydrozircon samples have a time-related daughter-product deficiency suggesting that the zirconium and uranium are of Recent origin (table 256.3). If this zirconium has been derived by leaching of Precambrian metamict zircons, it has to be in the soluble form and transported to allow a separation from the daughter products contained in the metamict zircon.

This unusual concentration of zirconium as a secondary cement in sedimentary rocks reveals that, under certain conditions, zirconium deposits may form by processes hitherto unrecognized.

REFERENCES

Blumenthal, W. B., 1958, The chemical behavior of zirconium: New York, Van Nostrand, 398 p.

Coleman, R. G., 1957, Mineralogy and geochemistry of uranium deposits in the Gas Hills district, Wyoming, *in* Geologic investigations of radioactive deposits—Semiannual progress report, Dec. 1, 1956 to May 31, 1957: U. S. Geol. Survey TEI-690, book 2, p. 508-512, issued by U. S. Atomic Energy Comm. Tech. Inf. Service Ext., Oak Ridge, Tenn.

Frondel, C., 1953, Hydroxyl substitution in thorite and zircon: Am. Mineralogist, v. 38, p. 1007-1018.

Gottfried, D., Jaffe, H. W., and Senftle, F. E., 1959, The lead-alpha (Larsen) method of determining the age of igneous rocks from their accessory minerals: U. S. Geol. Survey Bull. 1097-A, 64 p.

Mumpton, F. A., and Roy, R., 1961, Hydrothermal stability studies of the zircon-thorite group: Geochim. et Cosmochim. Acta, v. 21, p. 217-238.

Pabst, A., 1952, The metamict state: Am. Mineralogist, v. 37, p. 137-157.

Razumanya, E. G., Smolianskaya, K. G., Korolev, K. G., and Pakulpis, G. V., 1958, Arshinovite as a metacolloid variety of uranium-containing zircon: United Nations Internat. Conf. on Peaceful Uses of Atomic Energy, 2d. Geneva, 1958, Proc., v. 2, Survey of Raw Materials, p. 307-308.

Rosholt, J. N., Jr., 1958, Radioactive disequilibrium studies as an aid in understanding the natural migration of uranium and its decay products: United Nations Internat. Conf. on Peaceful Uses of Atomic Energy, 2d. Geneva, 1958, Proc., v. 2, Survey of Raw Materials, p. 230-236.

——— 1959, Natural radioactive disequilibrium of the uranium series: U. S. Geol. Survey Bull. 1084-A, 30 p.

Zeller, H. D., 1957, The Gas Hills uranium district and some probable controls for ore deposition: Wyoming Geol. Assoc. Guidebook, 12th Ann. Field Conf., p. 156-160.

257. MICROTEXTURE OF ARTIFICIALLY CONSOLIDATED ARAGONITIC MUD

By JOHN C. HATHAWAY and EUGENE C. ROBERTSON,
Denver, Colo., and Silver Spring, Md.

The aragonitic muds of the Bahama Banks have long been considered to be one type of sediment from which aphanitic limestones, so widespread in the geologic column, may have formed. Our laboratory experiments on the diagenesis of this carbonate mud show that aphanitic limestone can indeed be formed from such mud. Previous investigations of the Bahama muds, for example, those by Smith (1940), Black (1933), and Illing (1954), were field studies concerned primarily with the origin of the sediment itself and only secondarily with diagenesis.

We have examined replicas of fractured surfaces of experimentally consolidated products and of natural aphanitic limestone with the electron microscope to compare characteristics of the two. Our observations confirm suggestions by Black (Hatch, Rastall, and Black, 1938, p. 173–174), and by Bramlette (1958, p. 125) that the fine mosaic texture of tiny interlocking crystals in very fine grained limestones, as seen in thin sections, was probably formed by recrystallization of original particles of all shapes.

In the electron microscope technique that is used, a piece of each sample is broken into small fragments a few millimeters across, and each is cemented to a glass slide with a nearly flat surface facing upward. A replica of the surface of each fragment is formed in an evacuated chamber: the surface is first shadowed with platinum at a high angle (about 60°), and carbon is then evaporated vertically onto it. Next, the replicated surfaces are coated with household cement to protect and support the carbon-platinum film while the original carbonate is dissolved away by HCl. After washing, each replica is placed gently on a copper electron-microscope grid, and its cement coating removed with acetone. After it is dry, electron micrographs, usually at a magnification of about 30,000 diameters, are taken of representative areas of the replica for closer examination.

More than 200 consolidation experiments on mud from the Bahama Banks have been performed under various conditions of temperature, pressure, and time, but only pertinent ones will be described here; the experimental work will be discussed more completely later. Briefly, mud in very nearly its natural state is compressed under a constant load in a cylinder, fitted so as to permit escape of the water, and the cylinder and mud are heated at a controlled temperature; lengths of most runs were from 1 day to 4 weeks.

In one type of apparatus, a large porous alundum sleeve was used as a cylinder, although its low tensile strength placed a limit of 1,000 psi on pressure; densities of the consolidated mud of about 1.9 g per cm^3 were obtained. In a second type of apparatus, a steel cylinder was used, so that apparent pressures up to 50,000 psi could be obtained. Probably owing to friction of the piston and the mud against the wall, the pressure inside the mud was reduced by as much as 20 percent from the nominal value so that the highest density obtained in the products was only about 2.1 g per cm^3. Hydrostatic pressures up to 50,000 psi were applied in a third apparatus to mud samples contained in gold tubing, and densities up to 2.4 g per cm^3 were obtained.

As neither the chemical composition of the sea water in the mud nor that of the vapor driven off was analyzed, there was no control of the chemical environment of the mud; this important variable is not accounted for in any of the experiments. Furthermore, the fact that the aragonite seems to be stable as deposited but metastable under our experimental conditions introduces another intangible in determining how much recrystallization occurred upon inversion to calcite. (X-ray diffraction patterns were made to determine the degree of inversion.) Due to these uncertainties, the experiments were controlled only roughly; the accuracies are pressure ± 20 percent, temperature $\pm 10°$ C, and time ± 2 hours.

The needle shape of the original unconsolidated grains, 1 to 3 μ long, is depicted in an electron micrograph on figure 257.1. The needles are broken up at pressures above 10,000 psi, as shown on figure 257.2.

The effect of increasing time of experiment on samples under low pressure and at a temperature near 400°C is shown by the micrographs on figures 257.3-5. (The effect of pressure is unimportant at 400°C.) In all three runs, the aragonite inverted completely to calcite; recrystallization is probably speeded up by the inversion, but actual grain growth is a rate process, as shown by comparison of the textures and times. On figure 257.3, the needle shape of the grains is still quite evident, but the originally square and ragged ends of the grains (fig. 257.1) have become rounded, and some of the shorter grains have become globular as a result of rounding. The sample shows considerable open space, which accounts for its moderately low density. On figure 257.4, the remains of one rela-

FIGURES 257.1–4.—ELECTRON MICROGRAPHS OF ARAGONITE NEEDLES AND COMPRESSED ARAGONITIC MUD

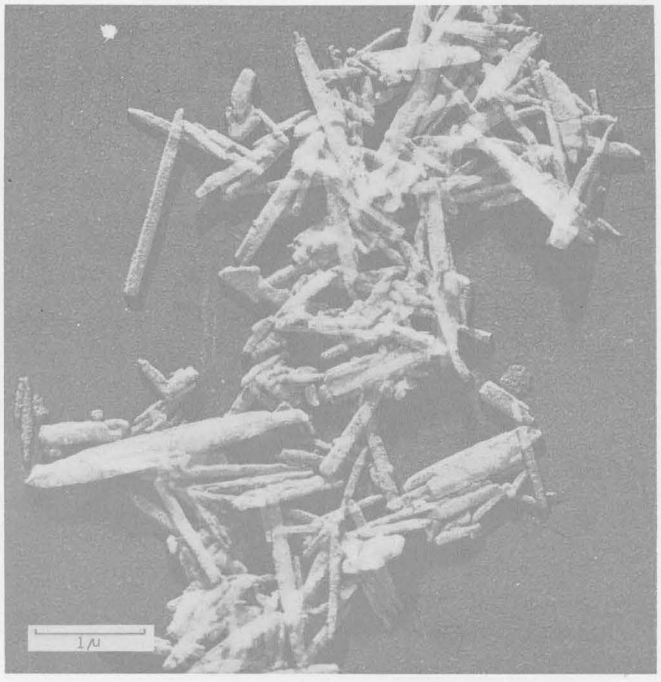

FIGURE 257.1.—Aragonite needles from mud from the Bahama Banks before consolidation. 5 to 10 percent calcite.

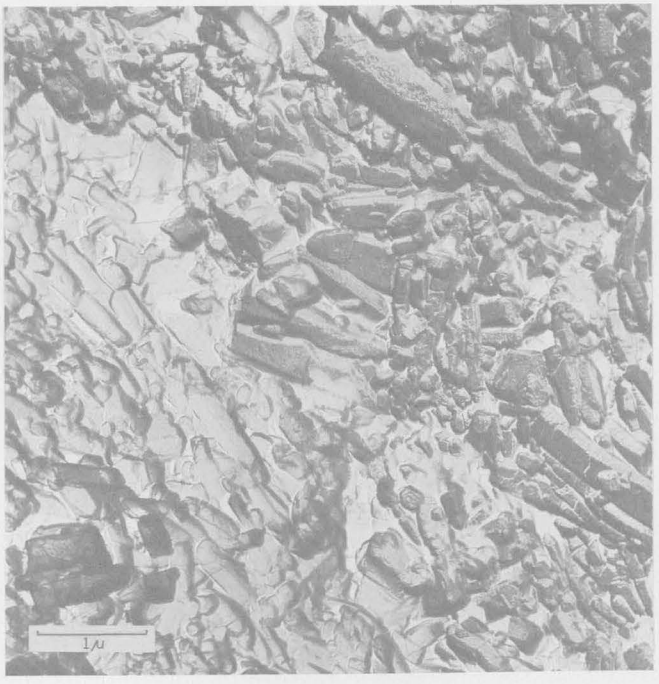

FIGURE 257.2.—Sample D169. Aragonitic mud from the Bahama Banks compressed for 7 days at 20,000 psi and 200°C. 8 percent (original) calcite. Density—2.1 g per cm^3.

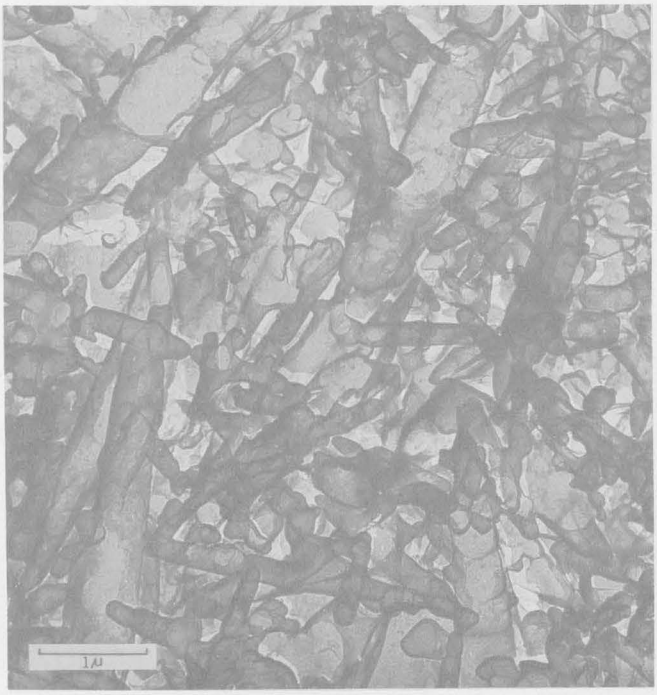

FIGURE 257.3.—Sample D103. Aragonitic mud from the Bahama Banks compressed for 5 hours at 1,000 psi and 430°C. 100 percent calcite. Density—1.6 g per cm^3.

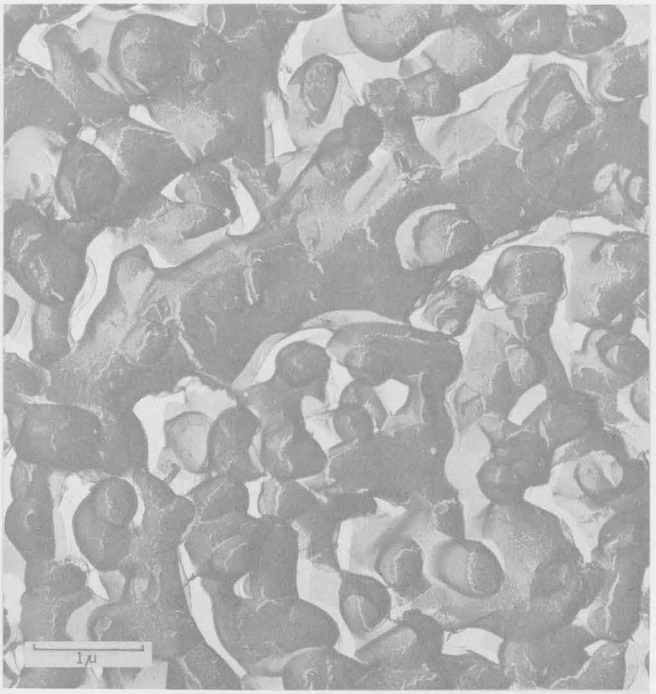

FIGURE 257.4.—Sample D118. Aragonitic mud from the Bahama Banks compressed for 1.0 days at 500 psi and 400°C. 100 percent calcite. Density—1.95 g per cm^3.

FIGURES 257.5–8.—ELECTRON MICROGRAPHS OF COMPRESSED ARAGONITIC MUD AND SOLENHOFEN LIMESTONE.

FIGURE 257.5.—Sample D119. Aragonitic mud from the Bahama Banks compressed for 2.6 days at 180 psi and 400°C. 100 percent calcite. Density—1.35 g per cm³.

FIGURE 257.6.—Sample D163. Aragonitic mud from the Bahama. Banks compressed for 14 days at 5,000 psi and 300°C. 100 percent calcite. Density—1.85 g per cm³.

FIGURE 257.7.—Sample D162. Aragonitic mud from the Bahama Banks compressed for 63 days at 5,000 psi and 200°C. 100 percent calcite. Density—1.9 g per cm³.

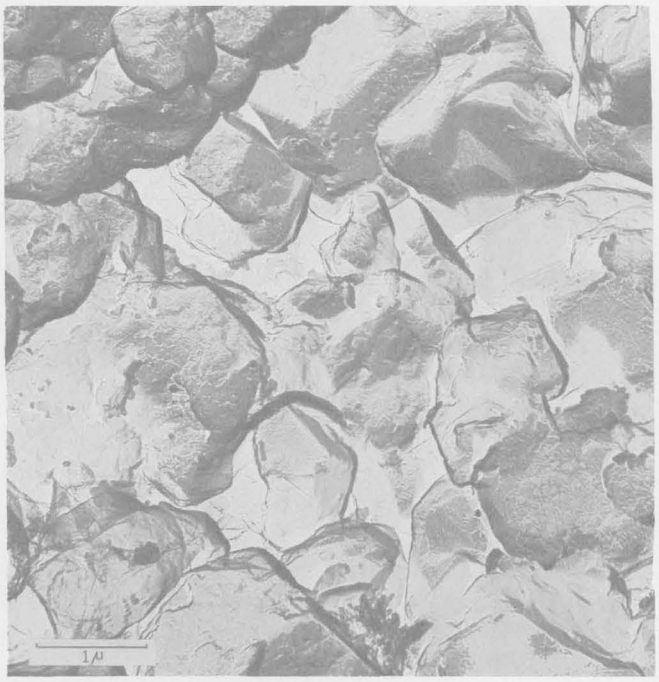

FIGURE 257.8.—Solenhofen limestone, Bavaria. 100 percent calcite. Density—2.6 g per cm³.

tively large needle can be seen, but the rest of the grains are rounded and are beginning to coalesce to form larger, continuous masses; considerable open space is still visible. On figure 257.5, the grains are very rounded, and coalescence is far advanced. Owing to the relatively low pressure, the density of the sample is quite low.

Longer time and higher pressure than in the preceding experiments offset a lower temperature in recrystalling the consolidated product, as figure 257.6 shows. The grains have intergrown to give a mosaic texture and have begun to show rudimentary crystal faces on some surfaces. The globular appearance of the grains shown on figure 257.5 is modified to more angular outlines in the sample on figure 257.6, and there is no suggestion of the original needle shape. Even longer time under a moderately high pressure offsets the low temperature of 200°C in causing a subhedral mosaic texture to be formed in the sample replicated on figure 257.7. The similarity of the textures of the artificial products on figures 257.6 and 257.7 to that of the natural limestone from Solenhofen, Bavaria, on figure 257.8 is striking.

The pressures in our experimental conditions are probably much the same as those in nature at a depth of 5,000 feet or less. On the other hand, the relatively high temperatures are not those expected in the earth's crust near the surface, and the lengths of the experiments are very short. However, it seems reasonable that, given geologic time, recrystallization of a calcium carbonate mud to an aphanitic limestone would occur in nature in a manner similar to that described here.

We are grateful to Preston E. Cloud, Jr., who supplied the aragonite mud samples and who stimulated our interest in this problem in conjunction with his own studies of calcium carbonate deposition on the Bahama Banks. Acknowledgment is due Paul Blackmon for making the X-ray determinations of calcite-aragonite ratios in the samples.

REFERENCES

Black, Maurice, 1933, The precipitation of calcium carbonate on the Great Bahama Bank: Geol. Mag., v. 70, no. 10, p. 455-466.

Bramlette, M. N., 1958, Significance of coccolithophoride in calcium carbonate deposition: Geol. Soc. America Bull., v. 69, p. 121-126.

Hatch, F. H., Rastall, R. H., and Black, Maurice, 1938, The petrology of the sedimentary rocks: London, Thomas Murby & Co., 383 p.

Illing, L. V., 1954, Bahaman calcareous sands: Am. Assoc. Petroleum Geologists Bull., v. 38, p. 1-95.

Smith, C. L., 1940, The Great Bahama Banks: Jour. Marine Research, pts. 1 and 2, v. 3, no. 2, p. 147-189.

258. FLUORINE DURING HYDRATION OF RHYOLITIC GLASS

By Irving Friedman and Joseph Harris, Washington, D. C.

During a study of the amount of water bound in glassy rhyolites and their relative deuterium-hydrogen concentrations, the authors became curious as to the role of fluorine in such glasses. Harris made determinations of fluorine of glasses whose water contents had been determined by Friedman.

The fluorine content was determined colorimetrically after fusion of the sample in a flux and distillation of the SiF_4. The method has been described by Grimaldi and others (1955).

Water content was determined by heating the rock in a vacuum, converting the extracted water to hydrogen gas, and measuring the quantity of hydrogen gas volumetrically. The technique was described by Friedman and Smith (1958).

Most of the samples of rhyolitic glasses include both obsidian and perlite that were separated from the same hand sample. The perlite in these samples is believed to have been formed by hydration of obsidian under surficial conditions (Ross and Smith, 1955). Thus, the only alteration has been the addition of water to the glass. The paper of Friedman and Smith (1958) discusses the formation of such perlite in more detail.

Table 258.1 lists the water and fluorine content of the samples analyzed. The data show a remarkable

TABLE 258.1.—H_2O and F analyses of rhyolitic glass samples

[Precision of analyses is ±5 percent of the amount present]

Location	Sample	Description	H_2O (percent)	F_2 (percent)
Canovas Canyon, Valles Mts., N. Mex.	20–2	obsidian	0. 21	0. 021
	20–1	perlite	2. 9	. 023
Bland Canyon, Valles Mts., N. Mex.	67–8	black perlite	2. 5	. 035
Do	65–7A	gray perlite	2. 9	. 029
	65–7B	blue perlite	2. 9	. 034
Do	65–6A	gray perlite	3. 6	. 036
	65–6B	black perlite	4. 4	. 023
Superior, Ariz	3024–7	obsidian	. 23	. 037
	3024–6	perlite	3. 4	. 041
Olancha, Calif	[1] 53–9	obsidian	. 95	. 072
	53–11	pumice	3. 5	. 072
Mono Craters, Calif	52–23	gray glass	. 31	. 060
	53–7	obsidian	. 36	. 065
Do	39–3	pumice	1. 9	. 060
Clear Lake, Lake County, Calif.	52–21	obsidian	. 09	. 056
	52–22	perlite	3. 1	. 060
Big Glass Mountain, Calif.	2–5	obsidian	. 10	. 028
	47–14	pumice	. 26	. 031
Pueblo, Mex	67–5	obsidian	. 98	. 081
	67–6	perlite	3. 1	. 075
Prestahnukur, Iceland	3023–3	obsidian	. 17	. 11
	3023–2	perlite	3. 7	. 079
Mayor Island, New Zealand.	70–9	obsidian	. 10	. 13
	70–10	perlite	3. 7	. 11
Ongarato, New Zealand.	70–11	obsidian	. 10	. 028
	70–12	perlite	2. 6	. 025

[1] From single outcrop; all others are single specimens.

constancy to the weight percent fluorine in a given igneous province. This fact was noted by R. R. Coats (1956). Howard Powers (Art. 111, Prof. Paper 424-B) has found that most samples from the same bed of volcanic ash have a similar content of fluorine, regardless of the water content of the shards.

This suggestion differs from the view expressed by Ross and Smith (1955) on the basis of the work of Shepherd (1938). Ross and Smith stated that "hydration has had the effect of flushing CO_2, Cl_2, and F_2 from the system and replacing them by H_2O in the hydrated glasses." However, careful consideration of Shepherd's results shows the fallacy of this interpretation. Shepherd reported the constituents of the gases extracted from his samples in volume percent. If the fluorine content of the glass remains constant, but the water content increases, the relative volume percent of fluorine in the extracted gas will be decreased. This is demonstrated in table III in Shepherd's paper, where the analyses of the rocks, both fresh and hydrated, are reported in weight percent.

Our data show that during hydration the fluorine content of the glass remains relatively constant in the samples that we analyzed. From this it may be inferred that the amount of fluorine found in the hydrated glass shards of a bed of volcanic ash represents the original fluorine content of the material and not an accidental fraction that remains after variable degrees of hydration. The constancy of the fluorine content during hydration then permits the fluorine content of hydrated glasses to be used as an index of place of origin of volcanic ash.

We do not wish to give the impression that fluorine cannot be released during extensive alteration of rhyolitic ash. We prefer to divide the alteration process into two steps. The first step discussed in this paper is the diffusion of water into the glass. This water can come from groundwater, meteoric water, or atmospheric water vapor. The diffusion is fairly rapid and results in a glass containing about 3.5 percent water by weight from glass usually containing originally less than 0.35 percent water (Friedman and Smith, 1960). During this process, fluorine is not lost from the glass.

The next step in the alteration of the glass is probably the devitrification of the hydrated glass, during which clay minerals are formed and fluorine may be lost. As yet, we have no data on the movement of fluorine during devitrification, but it is probably during this process that many elements present in the glass are released to the groundwater.

REFERENCES

Coats, R. R., 1956, Uranium and certain other trace elements in felsic volcanic rocks of Cenozoic age in western United States: U.S. Geol. Survey Prof. Paper 300, p. 75-78.

Friedman, Irving, and Smith, R. L., 1958, The deuterium content of water in some volcanic glasses: Geochim et Cosmochim. Acta, v. 15, p. 218-228.

——— 1960, A new dating method using obsidian, Pt. I, The development of the method: Am. Antiquity, v. 25, p. 476-522.

Grimaldi, F. S., Ingram, Blanche, and Cuttitta, Frank, 1955, Determination of small and large amounts of fluorine in rocks: Anal. Chemistry, v. 27, p. 918-921.

Ross, C. S., and Smith, R. L., 1955, Water and other volatiles in volcanic glasses: Am. Mineralogist, v. 40, p. 1071-1089.

Shepherd, E. S., 1938, The gases in rocks and some related problems: Am. Jour. Sci., 5th ser., v. 35A, p. 311-351.

259. A CRITICAL REVIEW OF ANALYSES OF CHLORITOID

By MARGARET D. FOSTER, Washington, D. C.

Chloritoid, so named by G. Rose (in Dana, 1892, p. 642) from its superficial similarity to chlorite, closely resembles the mica minerals physically and chemically. It is commonly included in the group of brittle micas, which are generally presumed to be similar to the true micas in structure but to have greater substitution of Al for Si in the tetrahedral layers, and, in margarite and xanthophyllite, to have Ca instead of K in interlayer positions. In chloritoid, as generally formalized,

$$4[(Fe^{+2},Mg)_2(Al,Fe^{+3})_2(Si_2Al_2)O_{10}(OH)_4],$$

the deficiency in charge in the tetrahedral group is balanced by an excess of charge in the octahedral group because of the trivalent cations present. The unit layers neutralize each other and there is no need for interlayer cations as in the true micas, and in margarites and xanthophyllites.

Machatschki and Mussgnug (1942) proposed a structure for chloritoid based on that of muscovite, with K being replaced by $1(Fe^{+2},Mg)$ and $2(OH)$ forming a close-packed arrangement between the silicate layers. The remaining Fe^{+2},Mg, and Fe^{+3}, and any Al not required to complete the tetrahedral layers, occupy octahedral positions. Octahedral Al and Fe^{+3} are together close to 2.00, as is also tetrahedral Al; consequently the silicate layers are neutral, as is also the interlayer $(Fe^{+2},Mg)(OH)_2$, and there is no charge binding the silicate layers and the interlayer $(Fe^{+2},Mg)(OH)_2$, as in the true micas. Machatschki and Mussgnug expressed their structure by the formula

$$^{2}_{\infty}Fe^{+2}(OH)_2\{(OH)_2(Fe,Al,Mg)_3[(Si,Al)_4O_{10}]\}.$$

Presumably Fe in the octahedral group in this formula represents both Fe^{+3} and Fe^{+2}. In this formula and that previously given for chloritoid, (Si,Al) occupy four positions, with Si and Al usually occupying about two positions each, with some variation in the relative amounts of Si and Al permissible. Thus Milne (1949) found $(Si+Al)_4$ ranging from $(Si_{1.93}Al_{2.07})$ to $(Si_{2.27}+Al_{1.73})$.

More recent work by Brindley and Harrison (1954) indicates, however, that chloritoid does not have a mica-like structure but a type of layer lattice structure not reported heretofore. They found that in a Fourier synthesis the electron content of the "Si" peak is only half the usual value, 2Si in place of the usual 4(Si,Al) at this level in the structure. The peak heights also suggested $2(Fe^{+2},Mg)+1Al$ within the silicate sheets, in the octahedral positions, and 3Al between the sheets, where K occurs in muscovite. The Si atoms do not form continuous silicate sheets as in the micas, but occur within distinct (SiO_4) groups. Brindley and Harrison expressed this structure in the formula, $[(Fe^{+2}Mg)_2Al](OH)_4Al_3[O_2(SiO_4)_2]$. In this structure there are only 2 Si ions. Thus, the upper limit of the number of Si ions in a chloritoid is strictly defined. This limitation on the number of Si ions, and the other atomic proportions indicated for chloritoid by Brindley and Harrison, suggested the desirability of a review of published analyses of chloritoid.

ATOMIC PROPORTIONS IN CHLORITOID ANALYSES CITED BY DANA

Some of the chloritoid analyses cited by Dana (1892) with their calculated atomic proportions, are given in table 259.1 The atomic proportions were calculated on the basis of the theoretical O(OH) content, $O_{10}(OH)_4$, by a method adapted from that used for calculating the formulas of micas (Foster, 1960) by using the number 48 instead of 44 to convert gram-equivalents of cationic constituents to cationic valences per unit cell. In the allocation of Al, which occupies two different sites in the Brindley and Harrison structure, three Al ions were assigned to positions between the silicate groups and the remainder was assigned to octahedral positions. The atomic proportions for a few of the analyses, particularly analyses 10 and 3, agree quite satisfactorily with Brindley and Harrison's suggested proportions of 2Si:1 octahedral $(Al+Fe^{+3})$: $2R^{+2}$, but those of most of the others do not agree as well.

In five analyses, (10, 6, 3, 8, and 4) the number of positions occupied by Si is 2.00 ± 0.04, but in the others Si is either deficient by 0.10 or more positions (as in 2, 11, and 9), or is excessive by 0.06 to 0.24 positions (as in 13, 9, 12 and 1). In those in which Si is excessive, the high Si is probably due to occluded quartz.

Brindley and Harrison (1954) did not state whether Al can substitute for Si if Si is somewhat deficient, as in analyses 2, 11, and 7. In analyses 2 and 11, in which Si is only 1.89, octahedral R^{+3} is also low, 0.90 and 0.68, respectively, and allocation of some Al ions to tetrahedral positions only increases the deficiency in R^{+3} ions. In no. 7, however, octahedral R^{+3} is high, 1.18, and allocation of 0.10 Al to tetrahedral positions to bring

TABLE 259.1.—*Analyses of chloritoids cited by Dana (1892), and atomic proportions*

[Numbers of analyses are those of Dana (1892, p. 641)]

	2 Kosoibrod	11 Asia Minor	7 Vielsalm	10 Zermatt	6 Shetland	3 Pregratten	8 St. Marcel	4 Ile de Groix	13 Virginia	9 St. Marcel	12 Leeds, Canada	1 Kosoibrod
Chemical analyses												
SiO_2	23.01	23.91	22.52	24.40	24.47	24.90	26.03	24.90	25.03	25.50	26.30	27.48
Al_2O_3	40.26	39.52	39.60	42.80	41.34	40.99	42.33	40.36	39.75	38.13	37.10	35.57
Fe_2O_3			3.97		.38	.55	4.09					
FeO	27.40	28.05	15.35	19.17	18.52	24.28	14.32	26.17	22.92	23.58	25.92	27.05
MgO	3.97		2.10	6.17	6.80	3.33	7.30	2.54	3.32	5.19	3.66	4.29
MnO			8.40		.91				1.30		.93	.30
CaO			.35		.30		.35		.21			
H_2O	6.34	7.08	7.44	6.90	6.98	7.82	6.56	6.23	6.64	6.90	6.10	6.95
Total	100.98	98.56	[1] 99.78	99.44	99.70	101.87	100.98	100.20	[2] 99.31	99.30	100.01	101.64
Atomic proportions												
Si	1.89	1.89	1.90	1.96	1.97	2.02	2.02	2.04	2.06	2.10	2.16	2.24
R^{+3}	.90	.68	1.18	1.04	.95	.94	1.12	.89	.86	.70	.59	.42
Al	.90	.68	.93	1.04	.93	.91	.88	.89	.86	.70	.59	.42
Fe^{+3}			.25		.02	.03	.24					
R^{+2}	2.37	2.69	1.94	1.98	2.13	2.04	1.77	2.10	2.08	2.26	2.29	2.39
Fe^{+2}	1.88	1.86	1.08	1.24	1.25	1.64	.93	1.79	1.58	1.62	1.78	1.85
Mg	.49	.83	.26	.74	.82	.40	.84	.31	.41	.64	.45	.52
Mn			.60		.06				.09		.06	.02
$R^{+3}+R^{+2}$	3.27	3.26	3.02	3.02	3.08	2.98	2.89	2.99	2.94	2.96	2.88	2.81
Al (interlayer)	3.00	3.00	3.00	3.00	3.00	3.00	3.00	3.00	3.00	3.00	3.00	3.00

[1] Includes 0.05 percent CoO.
[2] Includes 0.14 percent alkalies.

the total to 2.00, would reduce the number of R^{+3} ions to 1.08. In this analysis the number of R^{+2} ions is only 1.94, slightly deficient of the 2.00 R^{+2} ions indicated by Brindley and Harrison. The slightly high octahedral R^{+3} and slightly low R^{+2} in the atomic proportions of this analysis may be due to error in the relative amounts of Fe_2O_3 and FeO reported.

A correct determination of the ferrous iron content of rocks and minerals is generally beset with great difficulties, of which one of the greatest is preparation of the sample. Grinding the sample in air tends to lower the FeO and to increase the Fe_2O_3 in a rock or mineral that contains FeO. This oxidizing effect was not realized until after about 1900; consequently, nearly all mineral analyses made prior to that date are apt to contain more or less serious errors with respect to the relative amounts of Fe_2O_3 and FeO reported. For example, a chlorite was reported by Clarke (1910) to contain 2.86 percent Fe_2O_3 and 17.77 percent FeO. Recent values for Fe_2O_3 and FeO on a sample from the same hand specimen are 0.72 and 20.25 percent, respectively. Total iron as Fe_2O_3 are 22.61 and 23.23, respectively. Thus, the slightly high octahedral R^{+3} and slightly low R^{+2} content of analysis 7 may well be due to error in the relative proportions of Fe_2O_3 and FeO reported in the analysis. This may also be the reason for the high octahedral R^{+3} and low R^{+2} content of analysis 8.

In eight of the analyses in table 259.1 no value is given for Fe_2O_3; only FeO is reported. This suggests that the total iron in these samples was reported as FeO, and that FeO was not determined as such; it was simply assumed that all the iron was present as ferrous iron. However, the low octahedral R^{+3} and high R^{+2} contents of seven of these analyses (2, 11, 4, 13, 9, 12 and 1) suggest that the samples must have contained more or less Fe_2O_3. If it is assumed, for example, that 5 percent of the FeO reported (23.58 percent) was actually present as Fe_2O_3, and the atomic proportions recalculated on that basis, Si decreases from 2.10 to 2.07 positions, octahedral R^{+3} increases from 0.70 to 0.98 positions, R^{+2} decreases from 2.08 to 1.89 positions and octahedral (R^{+3} and R^{+2}) decreases from 2.94 to 2.87 positions—a considerably better agreement with the atomic proportions suggested for chloritoid by Brindley and Harrison (1954). In only one analysis (10) in which FeO only is reported do the atomic proportions of octahedral R^{+3} and R^{+2} indicate that all the iron was probably present as ferrous iron.

From this review of 12 of the analyses of chloritoid cited by Dana it may be concluded that error in the relative amounts of Fe_2O_3 and FeO reported, and failure to differentiate Fe_2O_3 and FeO (reporting all iron as FeO), which are characteristic of many analyses of rocks and minerals made before the beginning of the twentieth century, are important reasons for lack of agreement between the atomic proportions calculated from these analyses and those indicated for

chloritoid by Brindley and Harrison. Another reason for lack of agreement in those analyses in which Si occupies an excessive number of positions is probably failure to remove impurities, especially quartz, before analysis, or to adjust the analysis to allow for such impurities.

ATOMIC PROPORTIONS OF SELECTED RECENT ANALYSES OF CHLORITOID

Selected analyses of chloritoid published since 1925 and the calculated atomic proportions are given in table 259.2. In calculating the atomic proportions for analyses 1, 2, and 7, the CaO reported is considered extraneous to the chloritoid structure, in which there is no likely place for an ion as large as Ca. The atomic proportions of these analyses, with the exception of those of analysis 7, agree very well with those suggested for chloritoid by Brindley and Harrison; Si 2.00, octahedral R^{+3} 1.00, R^{+2} 2.00, with 3 Al ions between the silicate sheets. Analysis 1 is slightly low in Si, 1.92. However, octahedral R^{+3} and $(R^{+3}+R^{+2})$ are both slightly high, 1.07 and 3.12, respectively, and allocation of 0.08 Al to tetrahedral positions, if permissible, would bring these values close to the ideal. Analysis 7 is high in Si, and low in octahedral R^{+3} and $(R^{+3}+R^{+2})$, suggesting incomplete separation of the analyzed sample from occluded impurities such as quartz.

The analyses in table 259.2 were made after the oxidizing effect of fine grinding on FeO was realized, and after more refined methods for determining FeO had been developed. The good agreement of the atomic proportions of analyses 1 to 6 with those indicated by the new structure for chloritoid, compared with the poor agreement of the atomic proportions calculated from the older analyses, especially in octahedral R^{+3} and R^{+2}, demonstrates the importance of correct values for Fe_2O_3 and FeO in calculating atomic proportions not only for chloritoid but also for all other minerals containing Fe_2O_3 and FeO. Nearly all mineral analyses that were made before the effect of fine grinding was considered are affected by more or less serious errors in respect to the oxides of iron.

The analyses in table 259.2 also demonstrate the extremely narrow limits permitted for SiO_2 in the new structure. In analysis 1 with 22.67 percent SiO_2, the number of Si ions is low, only 1.92, in analysis 5, with less than 2.5 percent more SiO_2, the number of Si ions is slightly high, 2.04, and in analysis 7, with only 2.31 percent more SiO_2 than analysis 1, the number of Si positions is 2.12. These two analyses (5 and 7), illustrate the effect of other constituents present in calculating the number of positions occupied by Si.

TABLE 259.2.—*Selected analyses of chloritoids published since 1925, and atomic proportions* [1]

	1	2	3	4	5	6	7
Chemical analyses							
SiO_2	22. 67	23. 74	24. 31	24. 20	25. 12	24. 4	24. 98
Al_2O_3	38. 86	39. 01	39. 18	40. 46	40. 25	39. 6	35. 07
Fe_2O_3	2. 98	3. 04	3. 56	------	3. 22	2. 4	4. 81
FeO	25. 46	23. 98	22. 64	24. 24	19. 62	23. 0	26. 84
MgO	1. 96	1. 61	2. 70	2. 60	3. 89	1. 8	. 67
MnO	------	. 49	1. 51	------	1. 05	. 2	. 79
CaO	. 93	1. 02	Tr	------	none	Tr	. 58
H_2O	7. 14	7. 72	6. 65	7. 30	6. 76	7. 3	6. 34
Total	100. 00	100. 61	100. 55	98. 80	99. 91	98. 7	100. 08
Atomic proportions							
Si	1. 92	2. 00	2. 00	2. 02	2. 04	2. 04	2. 12
R^{+3}	1. 07	1. 04	1. 01	. 97	1. 04	1. 05	. 82
Al	. 88	. 87	. 79	. 97	. 84	. 90	. 51
Fe^{+3}	. 19	. 17	. 22	------	. 20	. 15	. 31
R^{+2}	2. 05	1. 93	1. 99	2. 01	1. 87	1. 85	2. 04
Fe^{+2}	1. 80	1. 69	1. 55	1. 69	1. 33	1. 61	1. 90
Mg	. 25	. 20	. 33	. 32	. 47	. 22	. 08
Mn	------	. 04	. 11	------	. 07	. 02	. 06
$R^{+3}+R^{+2}$	3. 12	2. 97	3. 00	2. 98	2. 91	2. 90	2. 86
Al (interlayer)	3. 00	3. 00	3. 00	3. 00	3. 00	3. 00	3. 00

[1] Analyses as follows:
1, Lemhi County, Idaho, Shannon, 1926; analysis adjusted for about 3 percent cobaltiferous arsenopyrite; 2, Kalgoorie, Western Australia, Simpson, 1931; analysis corrected for occluded quartz; 3, Vampi, Western Australia, Simpson, 1931; 4, El Cardosa (Somosierra) Guadalajara, Spain, Recarte, 1951; 5, Rawlinsville, Lancaster County, Pa., Hietanen, Anna, 1951; also reported 0.09 percent K_2O; analysis adjusted for 0.63 percent TiO_2 (rutile); 6, Clove Valley, Dutchess County, N.Y., Barth and Balk, 1934; also reported 1,3 percent TiO_2; analysis adjusted for impurities; 7, Rhode Island, Koch, 1935.

Analyses 5 and 7 have almost the same SiO_2 content, 25.12 and 24.98 respectively. Yet the calculated number of Si positions is 0.08 greater in the analysis having the lower SiO_2 content because of its higher FeO and lower Al_2O_3 and MgO content. It is for this reason that precise limits cannot be set on the amount of SiO_2 to be found in chloritoid. However, it would be expected that in analyses reporting less than 22.0 or more than 26.0 percent SiO_2, Si would occupy either too few or too many positions to fit the new structure for chloritoid.

REFERENCES

Barth, T. F. W., and Balk, Robert, 1934, Chloritoid from Dutchess County, New York: Am. Mineralogist, v. 19, p. 348.

Brindley, G. W., and Harrison, F. W., 1954, The structure of chloritoid, *in* Swineford and Plummer, eds., Clays and clay minerals, Natl. Research Council Pub. 327, p. 360-363.

Clarke, F. W., 1910, Analyses of rocks and minerals from the Laboratories of the United States Geological Survey, 1880 to 1903: U.S. Geol. Survey Bull. 419, p. 294.

Dana, E. S., 1892, The system of mineralogy, 6th ed., New York, p. 641.

Foster, Margaret D., 1960, Interpretation of the composition of trioctahedral micas: U.S. Geol. Survey Prof. Paper 354–B, p. 13.

Hietanen, Anna, 1951, Chloritoid from Rawlinsville, Lancaster County, Pennsylvania: Am. Mineralogist, v. 36 p. 867.

Koch, Gottfried, 1935, Chemische und physikalisch-optische Zusammenhänge innerhalb der Sprödglimmergruppe: Chemie der Erde, v. 9, p. 460-461.

Machatschki, F., and Mussgnug, F., 1942, Über die Kristallstruktur des Chloritoids: Naturwissenschaften, v. 30, p. 106.

Milne, I. H., 1949, Chloritoid from Megantic County, Quebec: Am. Mineralogist, v. 34, p. 422–434.

Recarti, A. B., 1951, Nota acerca del mineral clasificado como "diasporo" de El Cardosa (Somosierra) Guadalajara: Inst. Geol. España, Notas Comun., no. 23, p. 66.

Shannon, E. V., 1926, The minerals of Idaho: U.S. Natl. Museum Bull. 131, p. 378.

Simpson, E. S., 1931, Contributions to the mineralogy of Western Australia, Series V: Royal Soc. Western Australia Jour., v. 16, p. 29.

260. X-RAY CRYSTALLOGRAPHY AND OPTICAL PROPERTIES OF SYNTHETIC MONOCLINIC $KFeSi_3O_8$ IRON-SANIDINE

By DAVID R. WONES and DANIEL E. APPLEMAN, Washington, D.C.

In a study of the phase equilibria involving the mica $KFe_3FeSi_3O_{10}(OH)_2$, Wones (1959) found one of the reactants to be potassium-iron feldspar, $KFeSi_3O_8$. Single-crystal techniques have shown that this monoclinic feldspar forms in the system K_2O–SiO_2–Fe–O–H_2O from the reaction of mica with gas to form feldspar, hematite, and magnetite:

$$\underset{\text{mica}}{2\,KFe_3FeSi_3O_{10}(OH)_2} + \underset{\text{oxygen}}{5/4\,O_2} \rightarrow \underset{\text{feldspar}}{2KFeSi_3O_8} + \underset{\text{magnetite}}{Fe_3O_4} + \underset{\text{hematite}}{3/2\,Fe_2O_3} + \underset{\text{steam}}{2H_2O}.$$

The best crystals of the monoclinic polymorph formed from an aggregate of mica held at 750° C, 2000 bars total pressure and 10^{-10} bars oxygen fugacity for 4 hours, then held at 650° C, 2000 bars total pressure and 10^{-12} bars oxygen fugacity for 48 hours. The runs were made in standard hydrothermal apparatus using the oxygen-buffer technique described by Eugster (1957). The resultant feldspar crystals are thin and tabular, ranging up to 0.5 mm in diameter, with well-developed {010} forms; carlsbad-type twins are frequent.

A comparison of the X-ray powder diffraction pattern of the monoclinic feldspar with those of feldspars obtained in other runs in the same study shows that a triclinic polymorph can be synthesized under different experimental conditions. The crystals formed are very small, exhibit some "triclinicity", and show the "grid-iron" twinning characteristic of microcline.

The space group and unit-cell parameters of the monoclinic potassium-iron feldspar were determined from an untwinned crystal with approximate dimensions of 0.2×0.2×0.05 mm. Zero- and first-level photographs were taken of the *h0l* and 0*kl* zones, using a quartz-calibrated Buerger precession camera with MoK_α radiation; zero- and first-level photographs of the *hk*0 zone, taken on a Weissenberg camera using MoK_α and FeK_α radiations, were used only to check the space group. The values found from precession photographs are as follows: monoclinic, $C2/m$; $a = 8.68_9 \pm 0.01$A; $b = 13.12 \pm 0.02$; $c = 7.31_9 \pm 0.01$; $\beta = 116°06' \pm 5'$; cell contents: 4[$KFeSi_3O_8$]; cell volume: 749.3 ± 2.0 A^3; specific gravity (calculated): 2.72. Using these cell parameters, the values of the *d*-spacings were computed; they are compared in table 260.1 with the observed *d*-spacings, measured from an X-ray powder-diffraction film taken with a Debye-Scherrer camera (114.59 mm diameter) using the Straumanis technique with manganese-filtered FeK_α radiation ($\lambda = 1.9373$A). The agreement is considered adequate.

TABLE 260.1.—*X-ray powder data for synthetic monoclinic $KFeSi_3O_8$, iron-sanidine*

[Monoclinic, $C2/m$ [1]; $a = 8.68_9 \pm 0.01$ A; $b = 13.12 \pm 0.02$; $c = 7.31_9 \pm 0.01$; $\beta = 116°06' \pm 5'$]

Measured [2]		Calculated	
I	d_{hkl}	d_{hkl}	hkl
		6.70_6	110
		6.57_3	001
10	6.5_5B	6.56_1	020
<1	5.9_4	5.95_2	$\bar{1}11$
		4.64_3	021
30	4.28_2	4.28_2	$\bar{2}01$
15	3.99_4	3.99_9	111
		3.90_1	200
40	3.81_5	3.81_5	130
		3.65_9	$\bar{1}31$
		3.58_6	$\bar{2}21$
20	3.52_3	3.52_4	$\bar{1}12$
60	3.37 to 3.34 B	3.35_3	$\bar{2}20$
		3.340	$\bar{2}02$

See footnotes at end of table.

TABLE 260.1.—*X-ray powder data for synthetic monoclinic* $KFeSi_3O_8$, *iron-sanidine*—Continued

Measured [2]		Calculated	
I	d_{hkl}	d_{hkl}	hkl
100	3. 27_9	3. 28_6	002
		3. 28_0	040
30	3. 02_6	3. 02_9	131
15	2. 978	2. 976	$\bar{2}22$
		2. 938	022
30	2. 934	2. 935	041
		2. 850	201
		2. 825	$\bar{3}11$
13	2. 803	2. 806	$\bar{1}32$
20	2. 653	2. 642	$\bar{3}12$
		2. 614	221
8	2. 60 to 2. 58 B	2. 604	$\bar{2}41$
		2. 589	112
		2. 551	310
		2. 511	240
<1	2. 463D	2. 487	150
		2. 442	$\bar{1}51$
		2. 418	$\bar{2}03$
5	2. 411	2. 413	$\bar{3}31$
		2. 363	$\bar{1}13$
		2. 340	$\bar{2}42$
		2. 322	042
15	2. 289	2. 296	$\bar{3}32$
		2. 268	$\bar{2}23$
		2. 261	132
		2. 236	330
		2. 225 [3]	151
15	2. 183	2. 187	060
5	2. 148	2. 151	241
		2. 145	$\bar{4}01$
<1	2. 117	2. 106	$\bar{1}33$
<1	2. 076D	2. 078	023
		2. 075	061
8	2. 033	2. 035	$\bar{4}22$
2	1. 995D	1. 999	222
8	1. 880	1. 881	$\bar{3}52$
<1	1. 866D	1. 870	420
15	1. 823	1. 823	170

[1] Space group assumed to be centrosymmetric because of the crystal morphology, lack of piezoelectric properties, and analogy with sanidine.

[2] Films corrected for expansion. Camera diameter 114.59 mm. Manganese-filtered iron radiation. (λ=1.9373A). Lower limit of 2θ measurable: approximately 7° (15.9A). B=broad. D=diffuse.

[3] All smaller *d*-spacings not corresponding with observed reflections were omitted beyond this arbitrarily chosen *d*-spacing.

The optical data of the monoclinic potassium-iron feldspar are as follows: $\alpha=1.584\pm0.001$, $\beta=1.595\pm0.001$, $\gamma=1.605\pm0.001$, $2V_\alpha\sim85°$ (observed), $2V_\alpha=86.5°$ (calculated); $Y=b$, $Z\wedge c=16°\pm4°$. Optical measurements were made with a sodium light source, using immersion oils calibrated on an Abbé refractometer at the time of measurement. The orientation of the indicatrix is comparable to that found for "high sanidine" (Tuttle, 1952). These values differ from those quoted by Faust (1936) for the measurements by Hautefeuille and Perrey, Niggli, and Gaubert on synthetic iron feldspar prepared by Hautefeuille and Perrey, using a potassium vanadate flux. The discrepancy is not unexpected, considering the vanadium content of their material. Faust reported that the material he prepared was unsuited for precise optical measurements. The data presented in this paper strengthen the view that the phase referred to as "Fe-sanidine" by Wones (1959) is structurally analogous to monoclinic potassium-aluminum feldspar (high sanidine).

The authors thank H. T. Evans, Jr., for preliminary single-crystal measurements, and Mary E. Mrose, for preparing the X-ray powder-diffraction film.

REFERENCES

Eugster, H. P., 1957, Heterogeneous reactions involving oxidation and reduction at high pressures and temperatures: Jour. Chem. Physics, v. 26, no. 6, p. 1760-1761.

Faust, G. T., 1936, The fusion relations of iron orthoclase: Am. Mineralogist, v. 21, p. 735-763.

Tuttle, O. F., 1952, Optical studies on alkali feldspars: Am. Jour. Sci., Bowen volume, p. 553-567.

Wones, D. R., 1959, Biotites, Phase relations of the $K_2O{\cdot}6FeO{\cdot}Fe_2O_3{\cdot}6SiO_2{\cdot}2H_2O$ end member [abs.]: Jour. Geophys. Research, v. 64, no. 8, p. 1131.

261. A REVIEW OF THE CHEMICAL COMPOSITION OF GASES FROM VOLCANIC FUMAROLES AND IGNEOUS ROCKS

By DONALD E. WHITE and G. A. WARING, Menlo Park, Calif., and Palo Alto, Calif.

VOLCANIC GASES

Careful systematic work on the composition of volcanic gases has been attempted at only a few volcanoes and generally for short periods of time; nevertheless, some conclusions can be reached from a review of the geologic literature. The extensive studies of Kamchatkan volcanoes have been reviewed by Naboko (1959a; 1959b). Other recent studies have been made at Shōwa-Shinzan, Japan (Nemoto, Hayakawa, Takahashi, and Oana, 1957, p. 121-123); Nasu, Japan (K. Hayase, written communication, 1957); O-shima, Japan (Iwasaki, 1951, p. 140-143); Vulcano, Italy (Sicardi, 1956); White Island, New Zealand (Wilson, 1959, p. 42, 45); and Hekla, Iceland (Baldur Lindal, written communication, 1957).

The principal generalizations that can be made for chemical analyses of gases from volcanic fumaroles are:

1. Steam, where determined, is with few exceptions the greatly dominant gas, generally exceeding 90 percent of the total in volume percent.
2. Total air, when reported, commonly exceeds the "active" gases and may be greatly dominant even when much effort is made to exclude it (the "active" gases are considered to include all gases other than H_2O, air, excess N_2, and the inert gases, and are here recomputed to equal 100 percent).
3. CO_2 is generally the dominant "active" gas, particularly at low temperatures.
4. H_2 is highly erratic in amount; it is commonly absent but exceeds 40 percent in some analyses. CH_4 and NH_3 are erratic in amount, but seldom exceed 1 percent.
5. HCl commonly increases with increasing temperature, but some high-temperature fumaroles contain little HCl, and some low-temperature fumaroles contain much.
6. HF, seldom determined, is generally less than 10 percent of reported HCl but may be higher in silicic volcanism.
7. H_2S seldom exceeds 20 percent of the "active" gases, and its proportion is commonly not clearly related to temperature.
8. SO_2 is nearly always the dominant oxidized sulfur gas; it exceeds 20 percent of total "active" gases in nearly one-third of the samples in which it was determined, but is commonly not clearly related to temperature.
9. SO_3 has seldom been determined in addition to SO_2 in whole gases. In fumarolic condensates, SO_3 dissolves as H_2SO_4, which commonly exceeds HCl in weight percent.
10. The content of H_3BO_3 generally ranges from 1/1,000 to 1/20 that of HCl.
11. Bromine has been determined in only a few fumarolic condensates; the Br/Cl ratio generally ranges from about that of sea water (0.0034) to less than one-tenth that of sea water.
12. Components of low volatility (SiO_2, Na, Ca, Mg, and others) have been found in condensates from low-temperature fumaroles in much larger quantities that can be accounted for by their volatilities. Transport in droplets of water or aerosols in wet steam is suspected (Naboko, 1959, p. 127).
13. The same low-volatile components as well as significant quantities of minor metals also occur in high-temperature fumarolic vapors.

Zn, As, Sn, and Ag are present in especially large quantities at Showa-Shinzan (table 261.1). These analyses constitute the most extensive search that has been made for minor components in fumarolic gases.

TABLE 261.1.— *"Complete" chemical analyses of gas from volcanic fumaroles Showa-Shinzan, Japan*

[From Nemoto, Hayakawa, Takahashi, and Oana, 1957, p. 122-123, recomputed to parts per million; fumaroles associated with eruption of extrusive dome of hypersthene dacite]

	Sample 9081	Sample 9051	Sample 9063
	Temperature 760° C	Temperature 525° C	Temperature 220° C
SiO_2	253	289	48
Al	15	14	1. 3
Fe	1. 3	1. 2	5. 9
Ca	4. 6	4. 3	21
Mg	32	14	7. 9
Na	22	22	13
K	15	11	1. 7
CO_2	29, 200	25, 800	13, 000
CO	50	34	----------
SO_2	1, 490	716	716
SO_3	21	11	2. 7
H_2S	8. 0	42	1, 080
S	3. 7	1. 8	----------
Cl	728	420	433
F	238	169	35
Br	1. 1	. 9	1. 2
B	39	21	5. 6
PO_4	2. 8	3. 0	. 8
NO_2	. 01	. 001	. 008
O_2	51	47	23
H_2	685	381	20
NH_3	1. 3	. 8	17
N_2	567	676	1, 250
A^{40}	. 6	----------	1. 5
CH_4	1. 5	18	----------
[1] Ni	<. 01	. 0007	. 0007
[1] Cu	. 03	. 03	. 004
[1] Zn	. 5	. 4	. 02
[1] Ge	<. 01	. 003	. 0007
[1] As	. 7	. 3	. 007
[1] Mo	Trace	Trace	Trace
[1] Ag	. 003	. 0007	<. 0001
[1] Sn	. 03	. 006	. 001
[1] Sb	<. 1	<. 01	<. 005
[1] Pb	. 03	. 03	. 005
[1] Bi	<. 05	<. 005	<. 002
[2] Rn	1.3×10^{-7}	2.1×10^{-7}	12.6×10^{-7}

[1] Semiquantitative spectrographic analysis of solids in condensate computed to ppm in total gases; intermediate value of range.
[2] Curies.

GASES IN ROCKS

Recent analyses of gases in rocks have been published by Nikogosyan (1940) and Iwasaki, Katsura, and Sakato (1955, p. 70). Special studies have been made of specific components, the principal one of which is water, which is absorbed by natural glass with time (Friedman and Smith, 1960).

Shepherd's summary (1938) of his careful work on gases in rocks contains few general conclusions. Selected analyses that contain all major components and that are apparently of gases from fresh unaltered rocks (Shepherd, 1938, p. 326-337, analyses, 1-6, 8, 10-12, 16-19, 22-27) have been recomputed on a water-free basis, greatly decreasing the percentage variations. Generalizations for gases other than water that are suggested from these few recomputed analyses are:

1. The gases other than water are rather consistent in quantity, ranging from a little more than 0.1 to 6 cc per gram. Rhyolitic obsidians seem to have the lowest contents and granites the highest; basaltic lavas are relatively consistent, generally with a little more than 1 cc per gram.
2. CO_2 is generally near 50 percent of total gases other than H_2O in basalts, but is generally low in rhyolites and intermediate in granites and andesites.
3. H_2 is the dominant gas of the granites, but is highly variable in other rocks; CO, N_2, and Ar do not show systematic differences.
4. Sulfur, reported as S_2, is generally 2 to 9 percent of "other" gases in basalts, is also high in some andesites, but is generally low in obsidians and granites.
5. Cl_2 is commonly 10 to 30 percent in rhyolites and some andesites, is less than 10 percent in basalts and less than 1 percent in the two granites.
6. F_2 is the dominant gas in most obsidians and in some basalts, and ranges from 10 to 30 percent in most other rocks.

The data suggest that more interest should be shown in the gases contained in rocks. Extensive geochronologic and isotope studies now being made on specific volatile elements in rocks could be broadened with relatively little effort to include quantitative study of other gases driven off in the extraction process. The data also indicate that gases are consistently retained during extrusion of volcanic rocks, and that K/Ar age determinations of whole rocks should be corrected for Ar^{40} that was retained.

REFERENCES

Friedman, I., and Smith., R. L., 1960, A new dating method using obsidian—Pt. 1, The development of the method: Am. Antiquity, v. 25, p. 476-522.

Iwasaki, Iwaji, 1951, The 1950-51 eruption of Mihara-yama, Geochemical investigation of the volcano: Jour. Geology [Japan], v. 60, p. 140-143.

Iwasaki, Iwaji; Katsura, Takashi; and Sakato, Naoyuki, 1955, Geochemical investigations of volcanoes in Japan, 30, Volatile components of igneous rocks: Chem. Soc. Japan Jour., Pure Chem. Sec., v. 76, p. 778-782.

Naboko, S. I., 1959a, Volcanic exhalations and the products of their reactions: Akad. Nauk SSSR, Vulkanol. Trudy Lab., v. 16, p. 1-301.

——— 1959b, Volcanic exhalations and products of their reactions as exemplified by Kamchatka-Kuriles volcanoes: Bull. Volcanol., v. 20, p. 121-136.

Nemoto, Tadahiro; Hayakawa, Masami; Takahashi, Kiyoshi; and Oana, Shinya, 1957, Report on the geological, geophysical, and geochemical studies of Usu volcano (Shōwa-Shinzan): Japan Geol. Survey Rept. 170, 149 p.

Nikogosyan, K. S., 1940, Investigation of gaseous components of rocks: Akad. Nauk SSSR, Inst. Geol. Nauk, Trudy Tret'ego Soveshchaniya Eksptl. Min. i Petrog., p. 55-64.

Sheperd, E. S., 1938, The gases in rocks and some related problems: Am. Jour. Sci., ser. 5, v. 35a, p. 311-351.

Sicardi, Ludovico, 1956, Dell'esalazione solfidrico-sofforosa nella attvale face solfatarica dell'attivita dell'isla di Vulcano e di alcune questioni ad essa increnti: Bull. Vulcanol. ser. 2, v. 18, p. 159-168.

Wilson, S. H., 1959, Physical and chemical investigations 1939-1955 (of White Island, New Zealand): New. Zealand Dept. Sci. and Indust. Research Bull. 127, p. 32-50.

262. VARIATIONS IN PROPERTIES OF HORNBLENDES FORMED DURING PROGRESSIVE METAMORPHISM OF AMPHIBOLITES, NORTHWEST ADIRONDACK MOUNTAINS, NEW YORK

By A. E. J. Engel, Celeste G. Engel, and R. G. Havens,
La Jolla, Calif., and Denver, Colo.

Work done in cooperation with the University of California, La Jolla, Calif., and the National Science Foundation.

Hornblendes in amphibolite rocks of the northwest Adirondacks show systematic variations in composition and color clearly related to the progressive metamorphism of the rock system. Other properties of the hornblendes such as density, and dimensions of unit cell do not show measurable, systematic changes.

Maximum temperatures of reconstitution of the hornblende-bearing amphibolites have increased uniformly from at least 525°C or higher at Emeryville, N. Y., to 625°C or higher near Colton, N. Y., at the edge of the central Adirondack massif (fig. 262.1). The chemical composition of the amphibolite rock changes with increasing temperature and pressure from that of a typical saturated basalt to olivine basalt or pyroxene granulite (table 262.1). The mineralogy of the rock also shows systematic changes. At Emery-

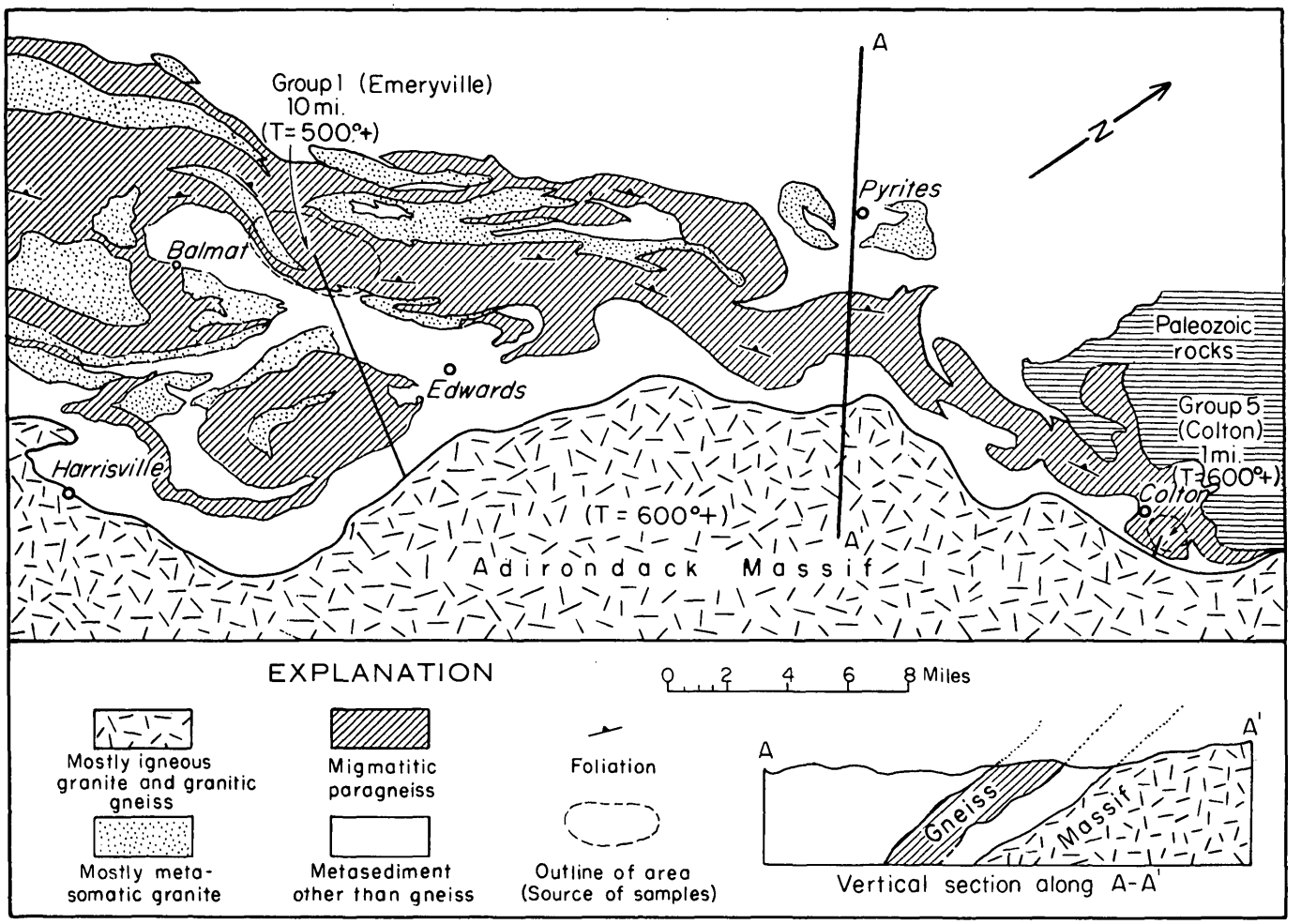

FIGURE 262.1.—Sketch may of the northwest Adirondack Mountains showing the relations of the several major rock types. The hornblendes described in the text occur in amphibolites within the paragneiss complex. The lines drawn approximately normal to the perimeter of the massif indicate the relative distances of the Emeryville and Colton areas from the massif.

601530 O—61——21

ville (almandite-amphibolite facies) bluish-green hornblende is the dominant mineral, averaging about 60 volume percent of the rock. Associated minerals are (in order of abundance) andesine, quartz, and accessory ilmenite and sphene. At Colton (hornblende-granulite facies) near the perimeter of the Adirondack massif, the hornblende is brownish green in body color and decreases in abundance to about 25 volume percent of the rock. Sodic labradorite, clinopyroxene, and orthopyroxene are coexisting phases (Engel and Engel, 1960b, p. B467, fig. 212.3). Sphene is absent and ilmenite is the only significant accessory mineral.

The average composition and mean deviations of the hornblendes in amphibolites at opposed ends of the belt of progressive metamorphism are shown in table 262.2 along with the structural formulae. Inspection of table 262.2 and figure 262.2 shows that with increasing temperature and pressure the variations in chemical composition of the hornblendes include a very marked increase in amounts of Ti, and lesser increases in Na, K, and F. There are also increases in the concentrations of the trace elements Cr, V, Sc, and probably Co and Ni (table 262.3). The concentrations of Mn, Zn, OH+F+Cl, as well as the ratios Fe_2O_3/FeO and Fe/Mg decrease with increasing grade of metamorphism.

TABLE 262.1.—*Chemical composition and C.I.P.W. norms of average amphibolite rock in the Emeryville and Colton areas, New York*

	Emeryville area (almandite-amphibolite facies, 7 samples)	Colton area (hornblende-granulite facies, 9 samples)
Chemical composition (percent)		
SiO_2	48. 20	47. 89
TiO_2	1. 89	1. 56
Al_2O_3	14. 45	14. 63
Fe_2O_3	3. 50	1. 85
FeO	10. 53	11. 20
MnO	. 25	. 25
MgO	6. 62	7. 41
CaO	10. 25	11. 54
Na_2O	1. 94	2. 19
K_2O	. 96	. 58
H_2O^+	1. 31	. 72
H_2O^-	. 01	. 03
P_2O_5	. 18	. 14
Total	100. 09	99. 99
C.I.P.W. Norm		
Quartz	. 38	----
Orthoclase	5. 67	3. 45
Albite	16. 40	18. 50
Anorthite	27. 88	28. 36
Diopside	17. 87	23. 03
Hypersthene	21. 38	8. 54
Olivine	----	11. 29
Magnetite	5. 08	2. 69
Ilmenite	3. 65	3. 01
Apatite	. 44	. 34

TABLE 262.4.—*Chemical composition and structural formulae of hornblendes from amphibolite rocks in the Emeryville and Colton areas, N.Y.*

	Emeryville area, almandite-amphibolite facies, 7 samples		Colton area, hornblende-granulite facies, 9 samples	
Chemical composition (weight percent)				
	Mean	Mean deviation	Mean	Mean deviation
SiO_2	42. 46	0. 56	42. 16	0. 40
TiO_2	1. 32	. 05	2. 40	. 15
Al_2O_3	12. 53	. 51	12. 19	. 39
Fe_2O_3	4. 94	. 22	3. 36	. 45
FeO	13. 71	. 47	14. 36	. 53
Mno	. 31	. 009	. 17	. 014
MgO	9. 04	. 59	9. 42	. 20
CaO	11. 64	. 17	11. 49	. 05
Na_2O	1. 33	. 04	1. 51	. 09
K_2O	1. 03	. 08	1. 39	. 16
H_2O^+	1. 83	. 03	1. 50	. 08
F	. 11	. 04	. 18	. 03
Cl	. 03	. 002	. 03	. 02
Fe_2O_3/FeO	. 36	. 014	. 23	. 040
Fe/Mg [1]	2. 59	----	2. 38	----
Mg/Mg+Fe [1]	. 278	----	. 295	----
Structural formulae [2]				
(W) K	. 20		. 27	
(W) Na	. 38	2. 45	. 43	2. 56
(W) Ca	1. 87		1. 86	
(X) Mg	2. 01		2. 12	
(X) Fe^{++}	1. 72	3. 77	1. 78	3. 92
(X) Mn	. 04		. 02	
(Y) Al	. 57		. 52	
(Y) Fe^{+++}	. 56	11. 28	. 42	1. 21
(Y) Ti	. 15		. 27	
(Z) Si	6. 36	8. 00	6. 35	8. 00
(Z) Al	1. 64		1. 65	
OH	1. 83		1. 50	
F	. 05	1. 89	. 08	1. 59
Cl	. 01		. 01	

[1] Atomic weight percent ratios.
[2] The structural type is taken as $W_{2-3}(XY)_5(Z_4O_{11})_2(OH,F,Cl)_2$

Total Si, Ca, and Al in the hornblendes remain essentially constant throughout the probable difference in temperature of metamorphism of 100°C or more (Engel and Engel, 1958). The ratio Mg/Mg+Fe increases only slightly between Emeryville and Colton (table 262.2).

The increase in Na, K, and Ti in solid solution in the hornblendes formed at the highest measured temperature and pressure must be near the maximum possible under the prevailing physical conditions. This interpretation for Ti follows from the facts that

FIGURE 262.2.—Variations in chemical composition of hornblendes plotted as a function of increasing grade of metamorphism between Emeryville and Colton, N. Y. Total analyses of the average hornblendes are listed in tables 262.2 and 262.3.

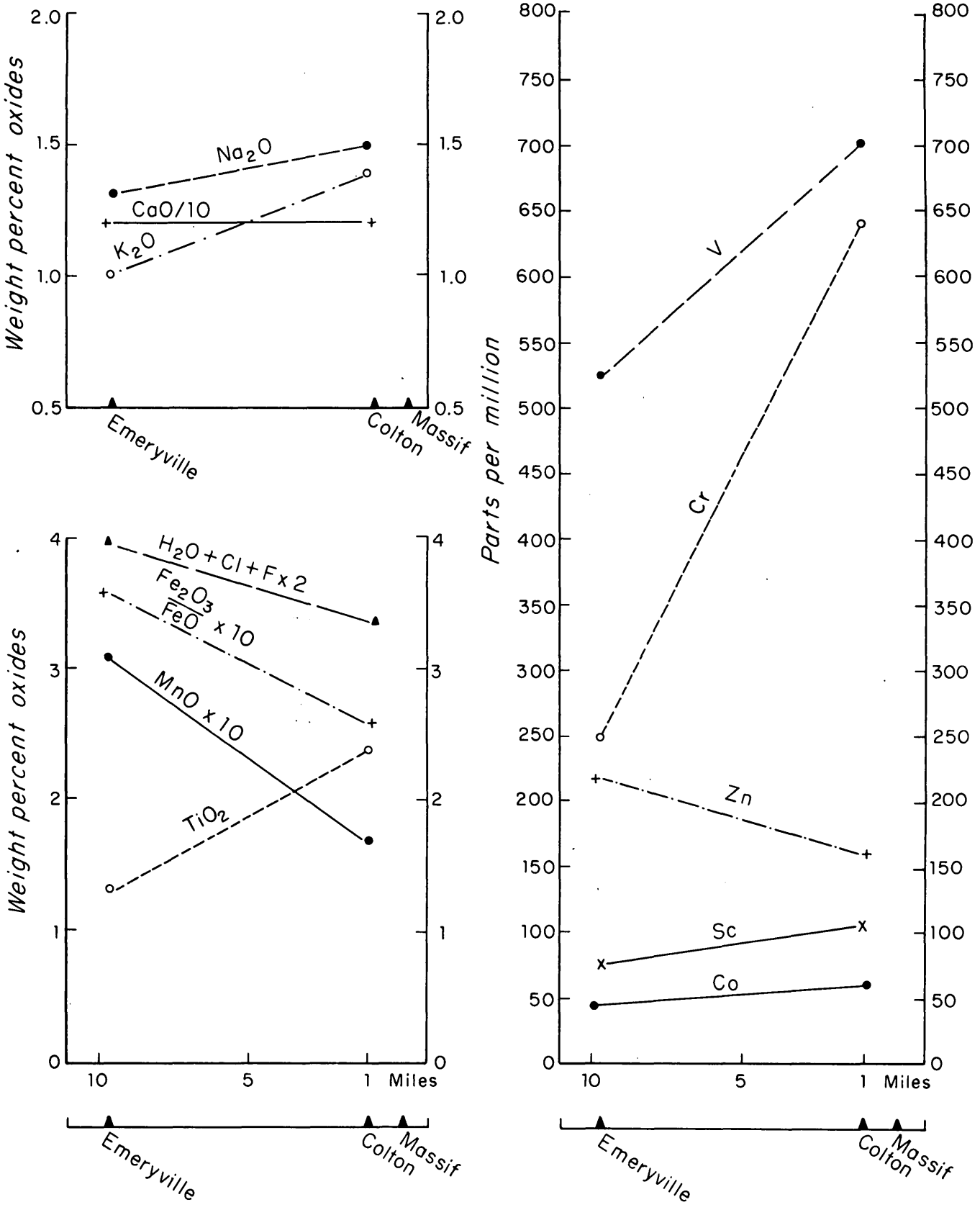
Weight percent oxides
2.0
1.5
1.0
0.5
Na_2O
CaO/10
K_2O
Emeryville
Colton
Massif
Weight percent oxides
4
3
2
1
0
$H_2O + Cl + F \times 2$
Fe_2O_3
FeO x 10
MnO x 10
TiO_2
10
5
1 Miles
Emeryville
Colton
Massif
Parts per million
800
750
700
650
600
550
500
450
400
350
300
250
200
150
100
50
0
V
Cr
Zn
Sc
Co
10
5
1 Miles
Emeryville
Colton
Massif

TABLE 262.3.—*Trace-element analyses and mean deviations of hornblendes from amphibolite rocks, Emeryville and Colton areas, N.Y.*

[In parts per million; analyses of Pb are colorimetric analyses by N. L. Nieman all other analyses are quantitative spectrographic analyses by R. G. Havens]

	Emeryville area, almandite-amphibolite facies, 7 samples		Colton area, hornblende-granulite facies, 9 samples	
	Mean	Mean deviation	Mean	Mean deviation
B	<40		<40	
Ba	86	32	106	40
Co	47	3	60	2
Cr	249	95	737	131
Cu	17	6	7	4
Ga	18	2	19	2
Ni	57	11	76	13
Pb	6	1	7	3
Sc	77	2	109	8
Sr	46	12	42	12
V	527	66	811	81
Y	72	22	118	22
Yb	9	2	13	2
Zn	216	32	163	21
Zr	97	26	75	9

ilmenite is invariably present in the rock as a common accessory mineral, and Ti, in addition, tends to be emitted from the amphibolite rock system as it is reconstituted at Colton (Engel and Engel, 1960b). Potassium is also emitted and this emission undoubtedly is because there is no other phase capable of incorporating more than a few tenths of one percent of K except the rapidly diminishing amounts of hornblende.

The decrease in OH+F+Cl in the hornblendes with increasing temperature and pressure is accompanied by a decrease in the ratio Fe_2O_3/FeO in both hornblendes and total rock. An analogous relation exists in the enclosing paragneiss. There the decrease in OH+F+Cl in biotites (with increasing temperature and pressure) is also accompanied by a decrease in the ratio Fe_2O_3/FeO in both biotite and total rock (Engel and Engel, 1960a). In addition, both rocks are profoundly dehydrated. The paragneiss commonly contains magnetite. Magnetite and other iron oxides are, however, uncommon constituents of the amphibolite rocks due to the abundance of ferrophile hornblende. The combined reduction and dehydration of constituent mafic minerals and total rock systems needs further study to evaluate the mobility of O and H in progressive metamorphism.

The lack of significant variations in concentrations of Si, Al, in the ratio Al/Al+Si and hence in amounts of Al in the Y structural site (table 262.2) is in contradiction to most published generalizations and predictions. Considering the range of temperature and pressure involved, the increases in the ratio Mg/Mg+Fe also seem remarkably small.

The near constancy of CaO content in the hornblendes at about 11.5 weight percent appears to be consistent with concentrations of CaO in carefully analyzed hornblendes from many mafic igneous and metamorphic rocks. Inasmuch as both Na and K increase with increasing temperature and pressure, the total value for the W structural site (Ca,Na,K) increases at Colton (table 262.2).

The systematic variations in minor elements in the hornblendes, especially Co, Ni, Sc, V, and Zn, do not appear to bear simple relations to the variations in the presumed chemical cogeners such as Fe and Mg, which have high concentrations in the hornblendes but show relatively small variations with temperature and pressure (tables 262.2 and 262.3, fig. 262.2). Chromium seems to be the trace element most responsive to the changes in the ratio Fe/Mg.

The average density of hornblendes at both Emeryville and Colton is about 3.26 to 3.27. As might be predicted, the most obvious fluctuations in density are induced by the largest variations in Fe/Mg. A hornblende from a slightly granitized amphibolite at Emeryville shows an Fe/Mg ratio some 50 percent higher than the average and has a density of 3.32. This increase in the ratio Fe/Mg and in density is accompanied by a tenfold decrease in the amount of Cr in the hornblende.

Unit cell parameters a sin β, b, c sin β were determined for all 16 hornblendes. Any systematic variations which may result from changes in composition, temperature, and pressure are within the limits of the errors of the measurements.

REFERENCES

Engel, A. E. J., and Engel, Celeste G., 1958, Progressive metamorphism and granitization of the major paragneiss, northwest Adirondack Mountains, New York, part 1, total rock: Geol. Soc. America Bull., v. 69, p. 1369-1414.

——— 1960a, Progressive metamorphism and granitization of the major paragneiss, Northwest Adirondack Mountains, New York, part 2, mineralogy: Geol. Soc. America Bull., v. 71, p. 1-58.

——— 1960b, Migration of elements during metamorphism in the northwest Adirondack Mountains, New York, *in* Short papers in the geological sciences: U.S. Geol. Survey Prof. Paper 400-B, p. B465-B470.

263. DISTRIBUTION OF CLAY-SIZED SEDIMENTS IN THE COASTAL PLAIN FORMATIONS NEAR TRENTON, NEW JERSEY

By James P. Owens, James P. Minard, and Paul D. Blackmon,
Washington, D.C., and Denver, Colo.

A general relation between environment of deposition and rock type has been observed in formations of the Coastal Plain near Trenton, N. J. The clay-sized particles in these formations are particularly sensitive indicators of depositional conditions.

Three major environments of deposition are recognized on the basis of lithology, bedding, shape of deposit, and fossil content (table 263.1). These are marine, depth generally less than 100 fathoms; transitional between marine and nonmarine; and nonmarine, including fluvial, lacustrine, paludal, and beach environments. A characteristic assemblage of clay-sized minerals typifies each environment, although there are some exceptions.

The marine formations are composed of dark unconsolidated quartz sand containing 5 to 15 percent feldspar; green glauconite-bearing sand; or mixtures of both types. The clay-sized sediment in these formations occurs as finely dispersed cement, except in the Woodbury clay—in which clay is a major constituent. In most of the marine formations, the clay-sized fraction is a complex mixture of many clastic and authigenic minerals (table 263.2). Each formation generally has its own diagnostic suite. Detrital minerals identi-

Table 263.1.—*Characteristics of pre-Quaternary formations near Trenton, N.J.*

Age	Formation	Depositional environment	Characteristics		
			Bedding	Fossils	Rock type
Miocene(?)	Cohansey sand	Transitional (beach)	Well-stratified.	None.	Quartz sand (orthoquartzite).
Miocene	Kirkwood	Marine (inner neritic)	Massive.	None.	Feldspathic quartz sand (subgraywacke).
Eocene	Manasquan	Marine (inner to outer neritic)	Massive.	Rare.	Glauconite sand.
		Marine (inner neritic)		Common.	Feldspathic quartz sand.
Paleocene	Vincentown	Marine (inner neritic)	Stratified.	Very abundant.	Calcarenite (spergenite).
		Marine (inner neritic)	Massive.	Rare.	Feldspathic quartz sand.
	Hornerstown sand	Marine (inner neritic?)	Massive.	Rare.	Glauconite sand.
Late Cretaceous	Red Bank sand	Marine (inner neritic)	Massive.		Feldspathic quartz sand.
		Marine (inner neritic)	Massive.	Rare.	Glauconite sand.
	Navesink	Marine (outer neritic)	Massive.	Very abundant.	Glauconite sand.
	Mount Laurel sand	Marine (outer neritic?)	Massive.	Locally abundant.	Feldspathic quartz sand.
	Wenonah	Marine (inner neritic)	Massive.	Rare.	Feldspathic quartz sand.
	Marshalltown	Marine (outer neritic)	Massive.	Rare.	Glauconite sand.
	Englishtown	Transitional (beach, lagoon)	Well-stratified.	Very rare.	Interbedded sand and clay (feldspathic quartz sand).
	Woodbury clay	Marine (inner neritic-lagoon)	Massive.	Common to rare.	Clay.
	Merchantville	Marine (outer to inner neritic)	Massive.	Common to rare.	Glauconitic quartz silt to sand.
	Magothy	Transitional (beach, lagoon)	Well-stratified.	Rare.	Interbedded sand and clay (orthoquartzite).
	Raritan	Nonmarine (fluvial, beach(?), paludal, lacustrine)	Well-stratified.	None.	Interbedded gravel, sand and clay; mainly quartz sands (orthoquartzite).

TABLE 263.2.—*Composition of clay-sized sediment concentrated by water elutriation from pre-Quaternary formations near Trenton, N.J.*

[M, major constituent; C, common; R, rare; Tr, trace. Constituents identified by X-ray analysis, P. D. Blackmon, analyst]

Formation	Sample No.	Quartz	Kaolinite	Montmorillonite	Mica (mostly muscovite)	Glauconite	Chlorite	Mica-glauconite mixture	Glauconite-montmorillonite mixed layer	Glauconite-chlorite-montmorillonite mixed layer	Mica-chlorite-montmorillonite mixed layer	Mica-montmorillonite mixed layer	Mica-chlorite mixed layer	Feldspar	Pyrite	Calcite	Carbonaceous matter	Remarks
Cohansey sand	Bm 34	C	C									C						Light.
	Bm 39	C	C		C										R		C	Dark.
Kirkwood	Co 178	M	M		C													Light.
	Bm 9	M	C		C		C										C	Dark.
Manasquan	NE 67	C		C	C	M			C?			C?			C			
	PEm 35	C	C				C	M		C?	C?				Tr			
	PEm 11	C	C	C				C	C?			C?					C	Quartz sand.
	PEm 3			M														
Vincentown	PEm 26	C	Tr	C				M	C?			C?					C	Quartz sand member.
	Co 196	C	Tr	Tr				M	C?			C?					C	Quartz sand member.
	NE 59	C														M		Calcarenite member.
	PEm 28	C	Tr													M		Calcarenite member.
Hornerstown sand	PEm 49	Tr				M												
	PEm 57	Tr						M										
	Co 160					M												
Red Bank sand	NE 119	C	C	C	M		Tr							Tr	C		C	Glauconite member.
	NE 29	M	Tr		Tr												C	Glauconite member.
	NE 56	C	C	C				C									R	Quartz sand member.
Navesink	PEm 57	C	C	C	M	Tr?	C				C				C		C	
	NE 13B	M	C		C							C+					C	
	Co 181	Tr	Tr			M									Tr		C	
Mount Laurel sand	PEm 9	C	C				Tr	M	C?			C?					C	
Wenonah	Co 182	C	C		C						Tr-R			Tr			C	
	NE 18B	C	Tr	Tr	M		C				C			Tr	C		C	
Marshalltown	Co 74	C	C	Tr	M		C				C				C		C	Dark.
Englishtown	Co 22	M	C	C	C							Tr					C	Dark.
	Co 34	M	C		C													Light.
	BR 24A	M	C	C	C												C	Dark.
Woodbury clay	Co 1	C	C		C							C						Light brown.
	Co 53	C	C	C	M		C				C			Tr	C		C	
	TE 22	M	C	Tr	M							Tr					C	
Merchantville	Co 25	C	C		M		C						C	Tr	C		C	
Magothy	TE 20	M			C						R						C	
	BC 1	M	R		C							R					C	
	CB 1	M	C		C		C										C	
Raritan	TE 21	M	C		C							Tr						

fied include kaolinite, montmorillonite, and mixed-layered clays having montmorillonite or chlorite as one layer. Quartz and muscovite also are abundant, and small amounts of feldspar are locally present. Abundant authigenic minerals, mainly glauconite and chlorite, characterize the marine formations. Authigenic apatite, pyrite, siderite, and vivianite also have been found in small amounts. Finely comminuted carbonaceous matter amounts to as much as 7 percent by weight in some units, but whether it is authigenic or detrital is not known. It is the major coloring agent in almost all the marine formations.

Probably the most diagnostic mineral in the marine formations of the New Jersey Coastal Plain, as compared with most other marine formations, is glauconite, which occurs abundantly either as discrete grains or interlayered with other minerals (table 263.2). It is most abundant in the Hornerstown sand, in which both the sand and clay fractions are almost totally glauconite. A large quantity of authigenic glauconite in the marine beds indicates that a high degree of chemical alteration has taken place in the marine environment.

Other particularly prominent minerals are kaolinite in the older marine formations and montmorillonite in the younger ones. Some writers suggest that the relatively coarse grained kaolinite is deposited in shallow water and the finer grained montmorillonite in deep water. Others, including us, regard the difference in mineralogy as the result of a change with time in the type of sediment supplied from the source area.

Carbonate cement in the calcarenite member of the Vincentown formation is unusual in this sequence of formations, which is largely characterized by siliceous cements. Apparently the Vincentown represents the only time from the lower Upper Cretaceous to the middle Miocene during which environmental conditions favored the accumulation of clay-sized calcite.

The transitional formations are beach-lagoon deposits and include the Magothy, Englishtown, and Cohansey formations. These formations can be distinguished from the marine formations by their more common intercalation of thin beds of sand and clay. The composition of the sand in these units is variable; the Magothy and Cohansey are chiefly quartz sands, and the Englishtown a quartz sand or subgraywacke containing 10 or 15 percent feldspar. The clay beds are dark. Carbonaceous matter is not everywhere as finely dispersed as in the marine deposits; locally it occurs as large woody pieces as much as several feet long, particularly in the Magothy formation. The clay-sized mineral assemblage is relatively simple, consisting of quartz, kaolinite, and mica. Mixed-layered mica montmorillonite and(or) chlorite are present in small amounts, except in some of the beds in the Englishtown, which have complex assemblages resembling those in the marine formations. Glauconite is absent, and the amount of authigenic minerals, except for pyrite, is sharply reduced.

The only known nonmarine formation on the Coastal Plain near Trenton is the Raritan, the oldest and thickest Coastal Plain formation. The Raritan has the same bedding characteristics as the transitional beds; however, the clayey beds are typically lighter colored, mainly red and white, and considerably thicker. The clay-sized mineral assemblage is quartz, kaolinite, and mica; authigenic minerals, except for local concentrations of siderite, are virtually absent. The associated sand is mainly quartz sand.

264. A HEULANDITE-LIKE MINERAL ASSOCIATED WITH CLINOPTILOLITE IN TUFFS OF OAK SPRING FORMATION, NEVADA TEST SITE, NYE COUNTY, NEVADA

By A. O. SHEPARD, Denver, Colo.

Work done in cooperation with the U. S. Atomic Energy Commission

Zeolites which make up as much as 45 percent of some of the tuffs of the Oak Spring formation (Miocene(?) or younger) at the Nevada Test Site have been studied extensively using thermal and X-ray diffractometer methods. Botinelly and Hinrichs (1959, p. 20) reported the principal zeolite in the tuff as heulandite but later reclassified it as clinoptilolite (Wilmarth, Botinelly, and Wilcox, 1960, p. 150). These two minerals have virtually the same X-ray diffraction pattern, but Mumpton (1960, p. 368) pointed out they can be distinguished by a simple thermal test. Heulandite is decomposed on long heating at 450°C, whereas clinoptilolite is stable to temperatures of 750°C or above. This difference in thermal stability affords a simple means of distinguishing the two minerals, but special heat treatment is required to detect either heulandite or a heulandite-like mineral in mixtures of the heulandite-clinoptilolite type of zeolites.

The criterion used in this study for identifying the heulandite or heulandite-like zeolites is a phase change which occurs in heulandite but not in clinoptilolite when the minerals are heated to certain critical temperatures. The higher temperature form of heulandite (the "B" modification mentioned by Mumpton (1960, p. 367) as characterizing heulandite) appears at about 250°C, and the X-ray pattern is so distinctly different from that of heulandite that a fundamental change in structure is indicated (fig. 264.1). The X-ray diffraction pattern obtained from a mixture of heulandite and clinoptilolite which has been heated to critical temperatures shows the heulandite "B" pattern together with the persistent clinoptilolite pattern.

Most of the zeolites in the tuff of the Oak Spring formation are clinoptilolite, although mixtures of clinoptilolite and heulandite-like mineral have been found in a tuffaceous sandstone bed by X-ray diffractometer analysis of samples subjected to special heat treatment (fig. 264.2). This treatment consists of heating a sample for 10 minutes at 250°C and at 50°C increments until the heulandite-like mineral is destroyed. After each heating, the sample is analyzed by X-ray diffractometer methods as soon as it is cool enough to handle, because the critical phase change is not permanent when produced by short heating at low temperatures. In some of the samples a sluggish phase change indicated by peak asymmetry is often found. If upon heating at next 50°C temperature increase, the phase change is not complete, another sample is heated at the lower temperature for a longer period. In general, the zeolites of the Oak Spring formation required additional heat treatment at 350°C.

The heulandite-like mineral in the tuffaceous sandstone can be distinguished from heulandite by its slower phase change and by the higher temperatures required for phase change and destruction (table 264.1). Moreover, before the temperature at which the mineral is destroyed is reached, the strongest reflection undergoes an additional change in *d* spacing not observed in heulandite. The heulandite-like mineral has an average refractive index that varies from 1.483 to 1.486 (heulandite near 1.500; clinoptilolite, 1.480), and its birefringence is lower than that of heulandite.

Thin sections of the tuffaceous sandstone show that the heulandite-like mineral fills the interstitial spaces of the rock, and rims or fills vesicles in the pumice lapilli. X-ray diffraction analysis reveals the presence of the heulandite-like mineral in both the sandstone cement and the pumice lapilli. Silt and less than two micron fractions were compared for differences in the amounts of clinoptilolite and heulandite-like mineral.

TABLE 264.1.—*Thermal behavior and optical properties of heulandite- and clinoptilolite-type minerals after heating for 10 minutes*

Changes in the 020 peak	Heulandite [1]	Heulandite-like mineral [2]	Clinoptilolite [2]
Temperature, in degrees centigrade			
First appearance of 8.35A peak	250	350–400	----------
Change to 8.35A complete	300	400	----------
Maximum intensity at 8.35A	350	400	----------
Change to 8.19A	400	400	----------
Change to 7.90–7.76A	----------	550–700	----------
Destruction	500	500–750	850–900
Optical properties			
Refractive index	near 1. 500	1. 483–1. 486	1. 480
Birefringence	near 0. 005	low	very low

[1] Beruflord, Iceland.
[2] Oak Spring formation, Nevada Test Site, Nye County, Nev.

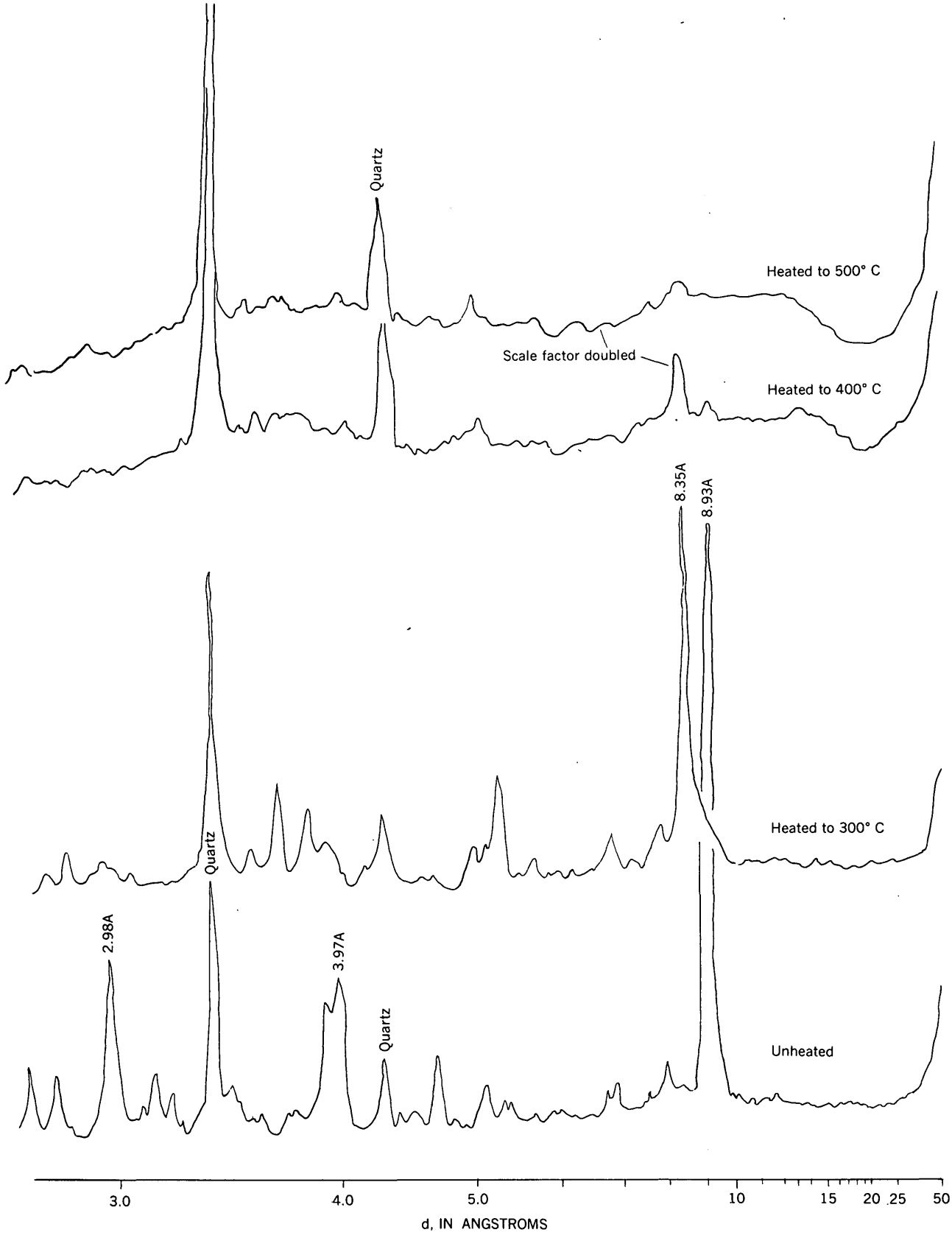

FIGURE 264.1.—X-ray diffractograms of heulandite from Berufiord, Iceland, after heating to various temperatures.

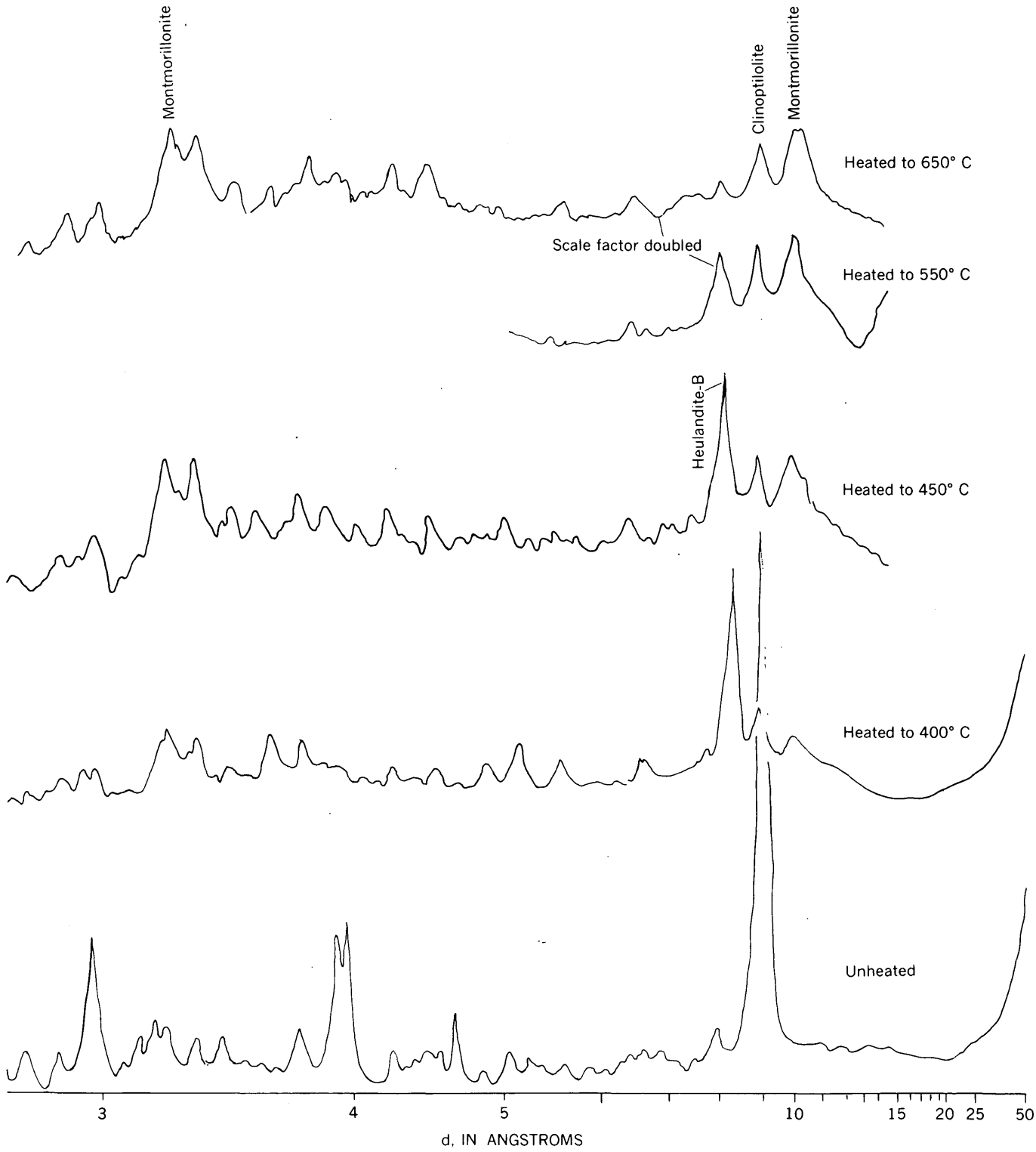

FIGURE 264.2.—X-ray diffractograms of a mixture of heulandite-like mineral and clinoptilolite heated to various temperatures. Samples from Nevada Test Site, Nye County, Nev.

Although clinoptilolite is typically finer grained than the heulandite-like mineral, analysis of the two fractions showed the two minerals in approximately the same proportions. No evidence was found to indicate the two minerals are of different generations.

The heulandite-like zeolite in the Oak Spring formation is not unique. Similar mixtures of clinoptilolite and a heulandite-like mineral have been identified in volcanic rocks from Arizona and Oregon. This mineral may be more common than would be inferred from the absence of any published reference to it because evidence of it is destroyed by the usual thermal tests.

REFERENCES

Botinelly, Theodore, and Hinrichs, E. N., 1959, Part 3, Petrology, *in* Diment, W. H. and others, Geological Survey investigations in the U12b.01 tunnel, Nevada Test Site: U. S. Geol. Survey TEM–998, open-file report.

Mumpton, F. A., 1960, Clinoptilolite redefined: Am. Mineralogist, v. 45, p. 351-369.

Wilmarth, V. R., Botinelly, Theodore, and Wilcox, R. E, 1960, Alteration of tuffs by Rainier underground nuclear explosion, Nevada Test Site, Nye County, Nevada, *in* Short papers in the geological sciences: U. S. Geol. Survey Prof. Paper 400-B, p. B149-B151.

265. PARTICLE-SIZE DISTRIBUTION OF STREAM BED MATERIAL IN THE MIDDLE RIO GRANDE BASIN, NEW MEXICO

By Carl F. Nordin, Jr., and James K. Culbertson, Albuquerque, N. Mex.

Samples of channel-bed material at eight sites on the Rio Grande between Otowi Bridge near San Ildefonso and San Marcial, N. Mex., a reach of about 190 miles, were used to prepare average particle-size distribution curves for sediment transport studies. All samples of bed material are from the top inch or two of the bed. Three to fifteen samples were collected along a cross section at equal centroids of flow and were analyzed separately by sieves or by the visual accumulation tube method. The results of the individual samples were averaged to obtain the size-distribution curve for the cross section.

Two parameters describe particle-size distribution in this discussion, the median diameter, d, and the geometric standard deviation, σ. The median diameter is the midpoint in the size distribution of a sample of which one half of the sample weight is composed of particles larger in diameter than the median, and one half of particles smaller in diameter. The slope of the log-normal plot of the cumulative size distribution is a measure of the geometric standard deviation, and is approximated as follows:

$$\sigma = 1/2(d/d_{16} + d_{84}/d)$$

where the subscript indicates percentage finer.

Table 265.1 summarizes the statistical analysis of bed material. The analysis indicates the dispersion of the observed values of d and σ for individual observations about mean values. For example, between discharges of 4 and 10,100 cfs at the Rio Grande near Bernalillo station, the average median diameter of bed material for 139 observations is 0.29 mm, and 68 percent of the values fall between 0.27 and 0.31 mm. Similarly, the average slope of the log-normal plots of size distribution is 1.68, and 68 percent of the values fall between 1.39 and 1.97.

The 3 upstream stations show large variations in bed-material characteristics when compared to the other 5 stations, and there is a systematic change in bed-material characteristics in a downstream direction.

The arithmetic averages of all observations for each station were used to determine average size-distribution curves (fig. 265.1). All of the curves approximate a log-normal distribution. However, the curves for three upstream stations, Otowi, Cochiti, and San Felipe, indicate a skewed distribution toward the coarser material, whereas the curve for San Marcial shows a skewed distribution toward the finer material. The curves for Bernalillo, Belen, Socorro, and San Antonio most closely approach a log-normal distribution.

The values of d and σ from the curves of figure 265.1 do not agree with the average values listed in table 265.1 In preparing the average curves, values of percentages finer than a given size were averaged; whereas in the table, values of diameters that represent a specific percentage were averaged. The values in

TABLE 265.1.—*Statistical analyses of bed material, Middle Rio Grande basin, New Mexico*

[Upstream stations listed at top]

Rio Grande station	Number of observations	Range of discharge rate (cubic feet per second)	Median diameter, d					Geometric standard deviation, σ				
			Minimum value (millimeters)	Maximum value (millimeters)	Mean value (millimeters)	Standard deviation (millimeters)	Coefficient of variation (percent)	Minimum value	Maximum value	Mean value	Standard deviation	Coefficient of variation (percent)
At Otowi	11	1, 130–10, 100	0. 20	10. 4	1. 45	3. 00	207	1. 50	14. 7	3. 97	3. 82	96
At Cochiti	102	24–9, 810	. 18	3. 10	. 44	. 32	73	1. 23	25. 8	2. 71	3. 07	113
At San Felipe	102	71–9, 720	. 17	5. 10	. 45	. 48	107	1. 36	42. 0	3. 24	4. 90	151
Near Bernalillo	139	4–10, 100	. 11	. 45	. 29	. 02	7	1. 37	3. 44	1. 68	. 29	17
Near Belen	85	520–8, 270	. 08	. 37	. 23	. 06	26	1. 38	2. 10	1. 55	. 16	10
Near Socorro	10	697–3, 600	. 15	. 25	. 19	. 03	16	1. 36	1. 65	1. 52	. 09	6
At San Antonio	14	368–8, 500	. 15	. 25	. 20	. 03	15	1. 38	1. 64	1. 48	. 08	5
At San Marcial	9	1, 990–8, 680	. 13	. 16	. 14	. 01	7	1. 32	1. 55	1. 43	. 08	6

table 265.1 and the average curves in figure 265.1 show that the median particle size and the standard deviation both tend to decrease downstream.

The changes that occur in the characteristics of the bed material in the reach between Otowi and San Marcial may be seen more readily by plotting d and σ against distance downstream from Otowi (fig. 265.2). The values of d and σ were taken from the average curves. The elevations of channels are also plotted. There is a discontinuity in the slope of the channel profile between the San Felipe and Bernalillo stations. Downstream from this discontinuity the channel elevation, the average water-surface slope, and the median diameter of bed material decrease systematically. The geometric standard deviation attains a near-constant value of about 1.6.

Culbertson and Dawdy (written communication, 1961) indicate that downstream from the discontinuity in channel slope resulting from the steep reach of

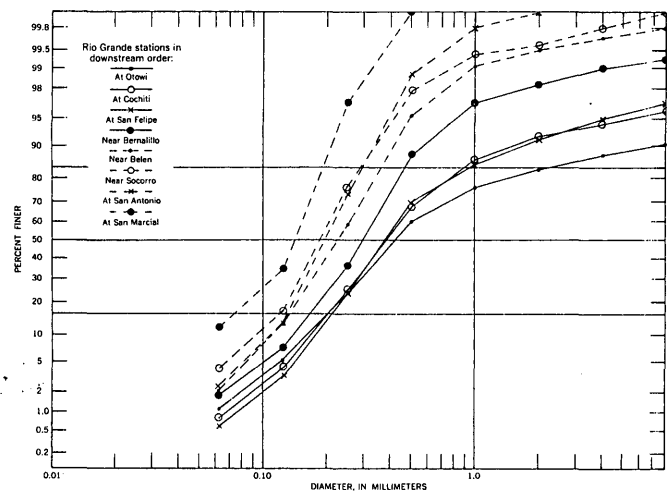

FIGURE 265.1.—Average particle-size distribution of bed material for eight localities in the Middle Rio Grande basin, New Mexico.

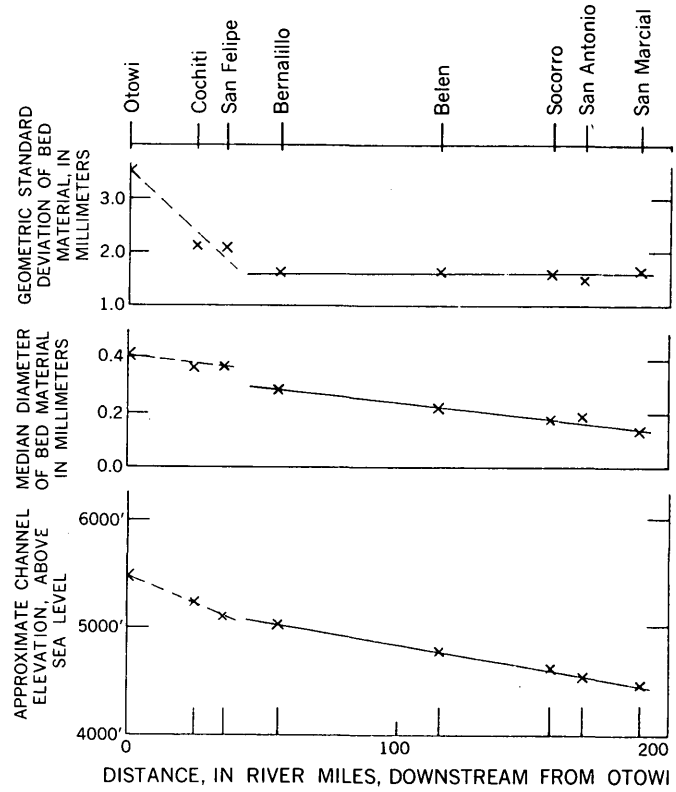

FIGURE 265.2.—Variations in elevation and bed-material characteristics for the Middle Rio Grande basin, New Mexico.

White Rock Canyon, the Rio Grande is a sand-channel stream; that is, an unlimited supply of sand-size particles in the bed is available for transport. They also show that the water-surface slope remains approximately constant at a station over a wide range of discharge and may be assumed equal to the slope of the energy gradient for most purposes.

The sand-bed channel of the Middle Rio Grande has median diameters of bed material between 0.14 and 0.30 mm, geometric standard deviations between 1.49

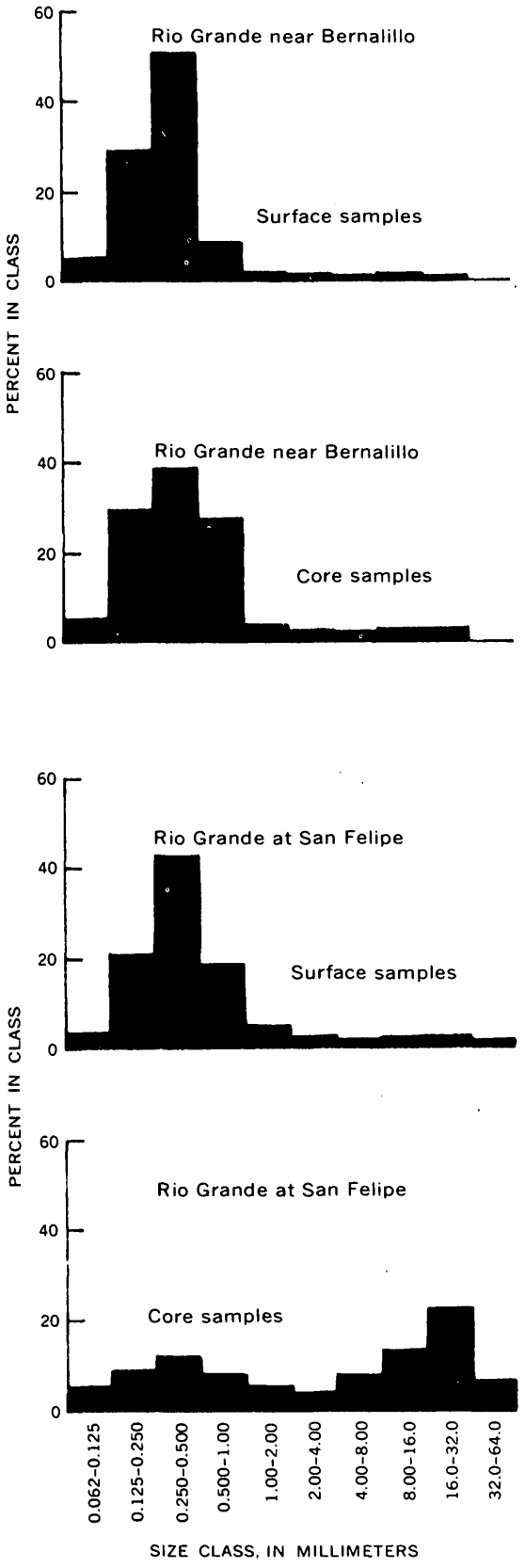

FIGURE 265.3.—Comparison of particle-size distribution between core samples and surface samples of bed material for the Rio Grande near Bernalillo and at San Felipe, N. Mex.

and 1.66, and slopes ranging from 0.0004 to about 0.001. On the other hand, the channel bed of the three upstream stations is composed of material ranging in size from fine sand to gravel. The water-surface slope varies appreciably with rate of discharge, apparently due to a pool-and-riffle condition which is flooded out at high rates of discharge. The characteristics of bed material show a wide range of values as indicated in the statistical analysis.

The median diameter of bed material at the three upstream stations shown on figures 265.1 and 265.2 is in the sand-size range, and is only slightly coarser than the medians for the sand-bed channels. The values, however, represent the average of only the top few inches of the bed material. Figure 265.3 shows histograms of the size distribution of the surface samples from the average curves of figure 265.1 and of core samples furnished by the U. S. Bureau of Reclamation for two of the stations. The histogram for Bernalillo represents the average of 17 cores, average depth 6.4 feet; for San Felipe, 3 cores, average depth 4.0 feet. The particle-size distributions in surface and core samples for the Rio Grande near Bernalillo are similar, but for the Rio Grande at San Felipe, the core samples exhibit a definite bimodal distribution.

The significance of bimodal distributions of sediments has been discussed in detail by Pettijohn (1949). Relations similar to those shown in figure 265.2 between the channel-profile discontinuity (fig. 265.2) and an abrupt change in channel bed material from sand to gravel, or to the bimodal distribution with a deficiency of material in the size range from 1 to 8 mm, have been investigated by Yatsu (1955) and Sundborg (1956). It is significant that the surface samples, which represent the material available for transport, show a log-normal distribution as an average condition even though the material at greater depths in the bed has a bimodal distribution.

A basic difference in behavior between the sand-bed channels and the sand-gravel channels of the Rio Grande is illustrated in figure 265.4 For the range of discharge shown, which represents a frequency of discharge rates equalled or exceeded between about 95 percent and 2 percent of the time, the characteristics of the bed material at all the sand-bed channels show no relation to discharge. The values plotted for San Felipe are typical of the three stations upstream from the discontinuity in channel profiles. Above a certain discharge rate (about 2,000 cubic feet per second for all three sand-gravel stations), the median diameter and the geometric standard deviation of the bed material increase with discharge; in general, the highest values are associated with falling stages. It

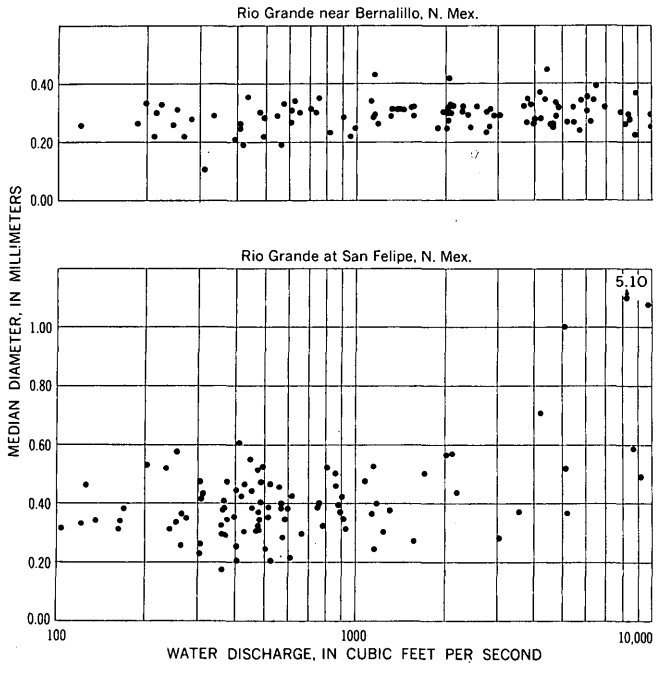

FIGURE 265.4.—Relation of median diameter of bed material to water discharge for the Rio Grande near Bernalillo and at San Felipe, N. Mex.

may be assumed that at these higher stages, the capacity of the stream to transport sand-size particles exceeds the supply of these particles. Below this discharge rate the sections behave as sand-bed channels. The rate of sediment supply to the sections approximately equals the rate of sediment transport, and the d and σ of the bed material show no relation to discharge, but vary around a mean value with approximately the same degree of dispersion as the sand-bed channels. The coefficient of variation at San Felipe for the median diameters of bed material below the discharge of 2,000 cubic feet per second is 25 percent, about the same as at Belen.

The changing characteristics of the bed material for the sand-gravel channels are reflected in the resistance to flow at these sections, which tends to increase with increasing discharge above 2,000 cubic feet per second. For the sand-bed channels, the resistance to flow remains about constant or decreases with increasing discharge rate.

It may be concluded that the characteristics of the bed material for sand-bed channels show no change with change of discharge rate, and that an average bed-material size distribution may be assumed subject to the random deviations indicated in table 265.1. Below a certain definable stage, the sand-gravel channels behave essentially as sand-bed channels; above this stage, the characteristics of the bed material change appreciably with rate of discharge.

REFERENCES

Pettijohn, F. J., 1949, Sedimentary rocks: New York, Harper & Brothers, 526 p.

Sundborg, A., 1956, The river Klarälven, a study of fluvial processes: Stockholm, Geogr. Ann., v. 38, p. 191-195.

Yatsu, E., 1955, On the longitudinal profile of the graded river: Am. Geophys. Union Trans., v. 36, p. 655-663.

266. WORLDWIDE RUNOFF OF DISSOLVED SOLIDS

By W. H. DURUM, S. G. HEIDEL, and L. J. TISON,
Washington, D. C. and University of Ghent, Belgium

A study of the size and nature of the load of dissolved solids carried by the large rivers of the world is in progress by the Geological Survey and the International Union of Geodesy and Geophysics. (See Durum, Heidel, and Tison, 1960). Measurements of dissolved solids in waters of major rivers of the world reveal gross loads discharged to the oceans range from about 17 tons per square mile per year for the arid Colorado River basin to about 695 tons per square mile per year for the humid Rhine River basin. Some of the results obtained for individual countries or continents are summarized below.

The rivers of conterminous United States drain about 3.02 million square miles and discharge water to the oceans at a rate of about 1.8 million cfs (cubic feet per second). For this study, 2.75 million square miles of drainage area was included, for which streamflow averages 1.73 million cfs. Table 266.1 summarizes some

TABLE 266.1—*Summary of rates of dissolved solids runoff and water discharge in conterminous United States*

Basin	Area drained [1] (sq mi)	Precipitation (inches)	Runoff			Drainage area covered			Gross dissolved solids (ppm)		Gross yield of dissolved solids			
											Thousand tons per year		Tons per square mile	
			Mean annual discharge (cfs)	Discharge (cfs per sq mi)	Inches	Area (sq mi)	Mean discharge (cfs)	Cfs per sq mi	Weight average in area covered	Entire basin	Dole and Stabler (1909)	Present study	Dole and Stabler (1909)	Present study
(1)	(2)	(3)	(4)	(5)	(6)	(7)	(8)	(9)	(10)	(11)	(12)	(13)	(14)	(15)
North Atlantic slope	148,000	40.2	210,000	1.42	19.3	88,100	134,000	1.52	89	90	20,800	18,600	130	126
South Atlantic slope	144,000	49	143,000	.99	13.4	72,900	61,700	.85	56	55	11,700	7,760	94	54
Eastern Gulf of Mexico	140,000	52	182,000	1.30	17.7	80,000	104,000	1.30	83	83	16,600	14,900	117	106
Mississippi River	1,244,000	29	634,000	.51	6.9	1,244,000	634,000	.51	196	196	136,400	123,000	108	99
Western Gulf of Mexico	413,000	24.6	56,000	.14	1.9	307,600	36,800	.12	240	235	14,900	13,000	36	31
Colorado River	246,000	12.6	5,500	.02	.30	243,000	5,500	.02	750	750	11,700	4,070	51	17
Pacific Slope in California	117,000	26.7	80,000	.68	9.2	57,700	66,900	1.16	95	120	12,800	9,470	177	81
Columbia River and North Pacific Slope	302,000	31.6	419,000	1.39	18.9	252,000	248,000	.90	99	82	30,200	33,900	100	112
Total	2,754,000		1,729,500			2,345,000	1,291,000				[2] 255,100	[3] 224,700		
Average		30		.63	8.6			.55	149	131			[2] 94	[3] 82

[1] Excludes area of Great Basin, St. Lawrence River basin, and Hudson Bay, and includes Columbia River basin in Canada and Rio Grande basin in Mexico.

[2] Value computed by Dole and Stabler (1909) adjusted to comparable area $\frac{255{,}100{,}000 \text{ tons}}{2{,}708{,}000 \text{ square miles}} = 94$ tons per square mile.

[3] $\frac{\text{Col. 13}}{\text{Col. 2}} = \frac{225{,}000{,}000 \text{ tons}}{2{,}754{,}000 \text{ square miles}} = 82$ tons per square mile.

of the hydrologic and chemical load data for eight basins in the United States. The total annual yield of dissolved solids in streams draining these basins is about 224.7 million tons, ranging from about 4.0 to 123 million tons for individual basins. The largest yields are in streams from the North Atlantic slope basins, where 19.3 inches of runoff to the Atlantic Ocean annually contains about 126 tons of dissolved solids for each square mile of drainage area. The humid Eastern Gulf of Mexico basin, with 17.7 inches of runoff, yields annually about 106 tons per square mile. The Mississippi River basin, intermediate between the arid regions of the west and the humid regions of the east, yields 99 tons per square mile per year to the Gulf of Mexico. The bulk of the dissolved solids transported from the United States (about 55 percent) is discharged by the Mississippi River. Thus the Gulf of Mexico receives annually about 151 million tons or 67 percent of the total 225 million tons average annual chemical load from conterminous United States. About 47 million tons, or 21 percent of the total, reaches the Pacific Ocean, and the remainder, about 26 million tons, or 12 percent of the total, reaches the Atlantic Ocean.

The entire North American Continent, covering 8.24 million square miles and discharging 5.35 million cfs of river water, yields about 611 million tons of dissolved solids annually. This is equivalent to about 116 parts per million or 74 tons per square mile of drainage. Other gross values (uncorrected for salts in precipitation) in North America are as follows:

Area	*Annual runoff (inches)*	*Gross yield of dissolved solids*	
		(ppm)	*(tons per square mile per year)*
Alaska	8.9	94	68
Canada	8.5	91	57

The weighted-mean loads of dissolved solids for major North American rivers generally is related to the modulus of runoff. For example, a log-log plot of annual runoff in inches versus annual load in tons per square mile for rivers and principal drainage basins of North America (fig. 266.1) shows a direct increase in load with increase in runoff up to the maximum observed—about 21 inches runoff and 199 tons per square mile per year (Hudson River). There is considerable

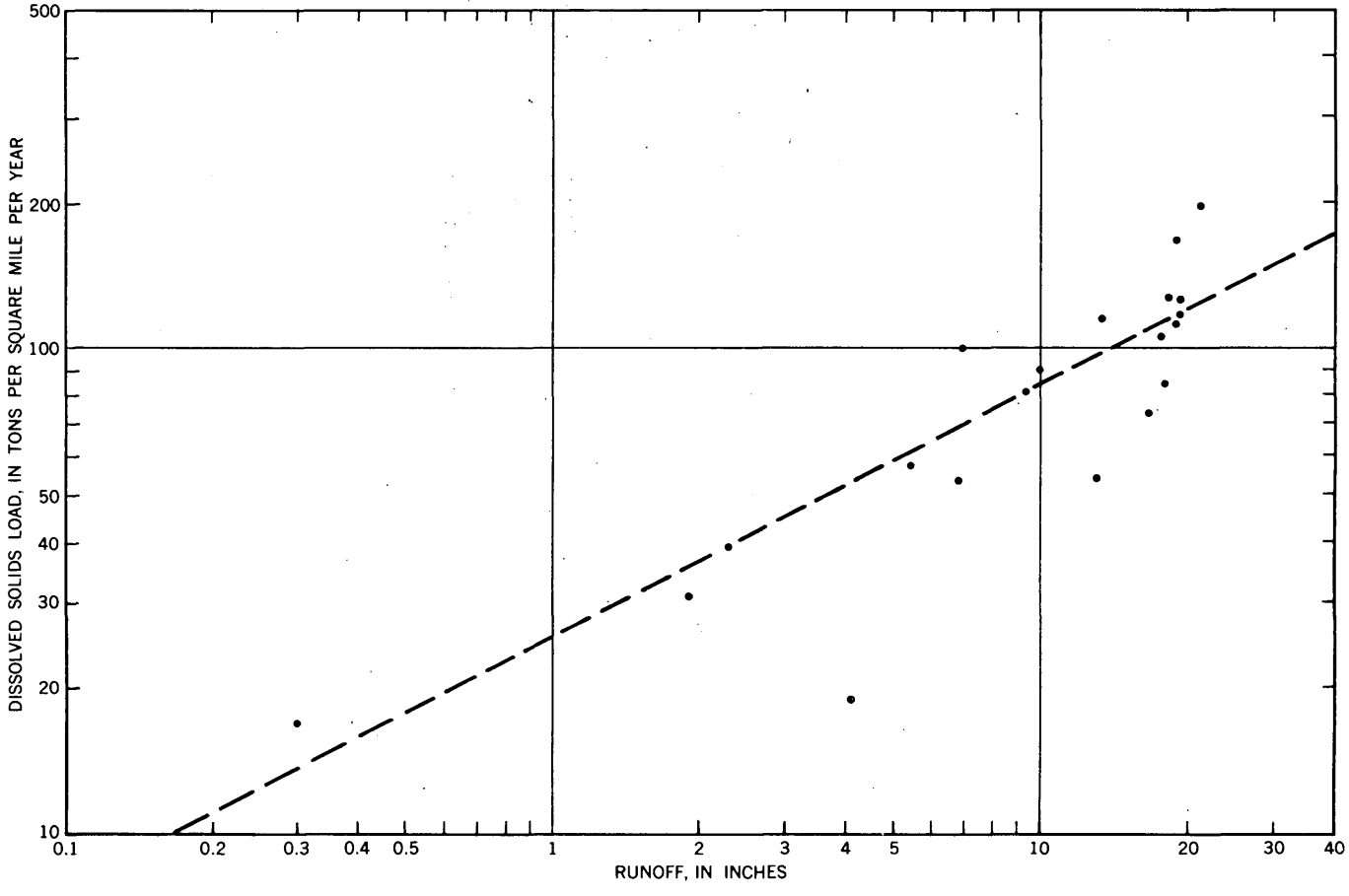

FIGURE 266.1.—Runoff and loads of dissolved solids at mouths of large rivers and drainage basins, North America.

scatter about the curve of relationship, which has a slope of about 0.5.

The excellent work of Alekin and Brazhnikova (1957) has enabled us to compute the ionic (principal cations and anions) discharge from the territory of the USSR. For an area of 6.4 million square miles of drainage, having an average stream flow of about 4.0 million cfs, about 287 million tons of dissolved solids are discharged annually to the oceans. Thus, for all the territory of the USSR, the annual discharge of ionic substance is about 44.5 tons per square mile. The largest load, about 205 million tons, is carried to the Arctic Ocean. Alekin and Brazhnikova (1957) report that about 25.5 million tons and 78.5 million tons of nonionic and organic substances, respectively, drain from the USSR, giving a total of about 390.9 million tons annually or about 61 tons per square mile.

The following examples of hydrologic data for selected rivers show the wide range of observed conditions that enter into continental averages:

River	Drainage area (thousands of square miles)	Annual runoff (inches)	Gross yield of dissolved solids	
			(ppm)	(tons/square mile/year)
Rhine, Holland	56	19.0	503	695
Glomma, Norway	15	21.7	30	47
Mekong, Thailand	310	17.1	124	154
Congo, Congo	1,550	12.4	50	45

The load of dissolved solids includes small quantities of many minor elements of which iron, aluminum, strontium, barium, manganese, boron, titanium, copper, chromium, nickel, and phosphorus are the most abundant. Lesser amounts of about 15 other minor elements are also present. Quantitative data on most of these minor elements can be obtained through use of emmission spectrography techniques described by Haffty (1960).

Of the alkaline earth metals, barium occurs in all waters examined in concentrations of as much as 150 micrograms per liter, and, strontium occurs in concentrations of as much as 800 micrograms per liter. Undoubtedly these values are exceeded at very low flows, although barium concentrations seem to be independent of the rate of streamflow.

Generally, there is no well-defined relation between strontium content and streamflow, except for samples from the Mississippi and Atchafalaya Rivers. In these streams strontium content and the ratio of strontium to barium decrease when streamflow increases. Also, ratios of calcium to strontium and calcium to barium in samples from these two streams tend to be high at high flow stages and low at low flow.

REFERENCES

Alekin, O. A., and Brazhnikova, L. V., 1957, New data on the discharge of dissolved substances from the Territory of the USSR: USSR Acad. Sci. Proc., v. 114, no. 1-6.

Dole, R. B., and Stabler, Herman, 1909, Denudation, *in* Papers on the conservation of water resources: U. S. Geol. Survey Water-Supply Paper 234, p. 78-93.

Durum, W. H., Heidel, S. G., and Tison, L. J., 1960, World-wide runoff of dissolved solids: Internat. Assoc. Hydrology, Surface Waters Comm. Pub. 51, Gen. Assembly of Helsinki, p. 618-628.

Haffty, Joseph, 1960, Residue method for common minor elements: U. S. Geol. Survey Water-Supply Paper 1540-A, p. 1-9.

267. METAL CONTENT OF SOME BLACK SHALES OF THE WESTERN UNITED STATES

By D. F. Davidson and H. W. Lakin, Denver, Colo.

The high metal content of black shale beds in the Permian Phosphoria formation in western Wyoming and southeastern Idaho, and in an unnamed Paleozoic formation exposed in the Fish Creek Range near Eureka, Nev., has led to a search for, and study of, other similar rocks in the western United States. The metal concentrations in some of these rocks probably will be considered ore deposits in the relatively near future.

In this paper are presented partial analyses for some samples from the Phosphoria formation, the unnamed Paleozoic formation referred to above, and from four other stratigraphic units: the Comus formation (Ordovician) exposed in the Edna Mountains, Nev.; the Chainman shale (Mississippian) exposed in the Schell Creek Range, Nev.; the Deseret limestone (Mississippian) at Mercur Dome, Utah; and the Minnelusa formation (Pennsylvanian) exposed in Hot Brook

601530 O—61——22

TABLE 267.1—*Analyses of carbonaceous marine shale samples from six geologic formations of the western United States*

[Semiquantitative spectrographic analyses by R. G. Havens, Uteana Oda, and E. F. Cooley; chemical analyses by H. L. Neiman; X=1 to 9]

No. on map	Collector	Sample Nos.	Source of samples	Number of samples	Semiquantitative spectrographic analyses (parts per million)									
					Pb		Mn		Cu		Zn		Ni	
					Range	Average	Range	Average	Range	Average	Range	Average	Range	Average
1	C. C. Hawley	D–78831 to D–78834	Minnelusa formation, Hot Brook Canyon, S. Dak.	4	X0		X0		70–1,500		<500		70–1,500	
2	D. F. Davidson and H. W. Lakin.	60–4581 to 60–4603	Phosphoria formation, Dry Creek Canyon Wyo.	23	10–50	20	100–300	180	100–300	150	700–10,000	2,800	150–1,500	500
3	T. S. Lovering	52517, 52520 to 52521, 52527–52530.	Deseret limestone, Mercur Dome, Utah.	7	0	0	X0–X00	X00	X0	X0	X00–X000	X00	X0–X00	X00
4	Harald Drewes	60–5087S	Chainman shale, Schell Creek Range, Nev.	1	30		300		200		2,000		100	
5	D. F. Davidson	60–3416 to 60–3441.	Unnamed Paleozoic formation, Fish Creek Range, Nev.	26	<10–20	10	20–500	180	15–100	40	<150–5,000	1,430	10–100	55
6	do	60–3445 and 60–3543.	Comus formation, Edna Mountains, Nev.	2	30		100–150		200–500		2,000–3,000		150–700	

No. on map	Collector	Sample Nos.	Source of samples	Number of samples	Semiquantitative spectrographic analyses (parts per million)										Chemical analysis (parts per million)	
					V		Mo		Ag		Cr		Fe		Se	
					Range	Average	Range	Average	Range	Average	Range	Average	Range	Average	Range	Average
1	C. C. Hawley.	D–78831 to D–78834.	Minnelusa formation, Hot Brook Canyon, S. Dak.	4	1,500–3,000		70–3,000		0–X00		150–300		X000–X0000		130–150	
2	D. F. Davidson and H. W. Lakin.	60–4581 to 60–4603.	Phosphoria formation, Dry Creek Canyon, Wyo.	23	500–7,000	2,500	50–500	150	2–30	7	500–5,000	2,000	10,000–20,000	17,000	100–675	277
3	T. S. Lovering	52517, 52520 to 52521, 52527–52530.	Deseret limestone, Mercur Dome, Utah.	7	X000	X000	X–X0	X0	X0	X0	X00	X00	X000	X000	24–110	65
4	Harald Drewes.	60–5087S	Chainman shale, Schell Creek Range, Nev.	1	1,000		50		20		1,000		30,000		20	
5	D. F. Davidson.	60–3416 to 60–3441.	Unnamed Paleozoic formation, Fish Creek Range, Nev.	26	200–2,000	1,000	5–50	28	<1–2	1.5	50–150	90	5,000–20,000	8,000	7–290	79
6	do	60–3445 and 60–3543.	Comus formation, Edna Mountains, Nev.	2	3,000		<2–10		5–30		200–300		15,000		<1–1	

Canyon, S. Dak. The locations of the sample sites are shown on figure 267.1, and the collector, description, and analyses are listed in table 267.1.

All samples are of carbonaceous marine "shales." Most are from beds intercalated in thick sequences of carbonate rocks, and probably represent a part of a "shelf facies" of marine sediments.

The thicknesses of rock represented by these samples vary greatly. The samples from the unnamed shale in the Fish Creek Range represent a thickness of 135 feet, but the samples from the Minnelusa formation represent thicknesses of only 0.5, 0.6, 1.25, and 3.3 feet of rock, and are from different stratigraphic horizons. The 2 samples from the Comus formation each repre-

FIGURE 267.1.—Locations at which samples were collected. 1, Hot Brook Canyon, S. Dak.; 2, Dry Creek Canyon, Wyo.; 3, Mercur Dome, Utah; 4, Schell Creek Range, Nev.; 5, Fish Creek Range, Nev.; 6, Edna Mountains, Nev.

sent a thickness of 5.0 feet and are from different horizons, as are the 3 from the Deseret limestone, which represent thicknesses of 2.6, 6.1, and 15.5 feet. The samples from the Phosphoria formation are from the same stratigraphic horizon at three different localities in Dry Creek Canyon and are of thicknesses of rock of 3.6, 4.8, and 5.0 feet. (See J. D. Love, Art. 250). The sample of Chainman shale is a grab sample.

The metal contents of these shales tend to be as high as or higher than those reported by Krauskopf (1955, p. 417) as shown by table 267.2.

Reconcentration of metals may have occurred locally during diagenesis or structural deformation of the rocks, which presents the possibility that shales containing even larger amounts of metals may be discovered.

TABLE 267.2.—*Comparison of metal contents, in parts per million, of shales discussed, with content in black shales reported by Krauskopf (1955)*

[X=1–9]

Metal	Metal content in black shales according to Krauskopf		Metal content of black shales discussed in this paper	
	Average	Maximum	Average	Maximum
Lead	20–400	700	0–30	50
Manganese	----------	----------	X0–180	500
Copper	20–300	1,000	X0–540	1,500
Zinc	100–1,000	10,000	X00–2,800	10,000
Nickel	20–300	2,400	55–540	1,500
Vanadium	50–2,000	14,000	1,000–3,000	7,000
Molybdenum	10–300	1,000	5–840	3,000
Silver	5–50	800	1.5–15	30
Chromium	10–500	5,000	90–2,000	5,000
Iron	----------	----------	X000–17,000	30,000
Selenium	----------	----------	<1–277	675

REFERENCE

Krauskopf, K. B., 1955, Sedimentary deposits of rare metals: Econ. Geology, 50th Anniv. Volume, pt. 1, p. 411-463.

268. CORDIERITE HORNFELS FROM LITCHFIELD, CONNECTICUT

By FRED BARKER, Washington, D. C.

Cordierite hornfels of argillaceous composition is found at the northwest margin of the Mount Prospect igneous complex in Litchfield, Conn. This hornfels has formed from regionally metamorphosed Berkshire schist of Middle Ordovician age. Its mineral assemblage is biotite, cordierite, garnet (metastable), magnetite, orthoclase, plagioclase, quartz, sillimanite. Pleonaste is present with cordierite and sillimanite in pseudomorphs that have formed from staurolite. This is a new occurrence of cordierite in Connecticut.

The Berkshire schist consists of intensely folded interlayered mica schist, gneiss, and quartzite of middle to high metamorphic grade (Agar, 1927, p. 26-28; Cameron, 1951, p. 8-9). The igneous rocks adjacent to the cordierite hornfels are quartz norite, biotite-hornblende diorite, and other rocks (Cameron, 1951, p. 31-33, pl. 2).

The hornfels lies about 1.6 miles northwest of Bantam, Conn., at the sharp bend where Prospect Road changes direction from northwesterly to northeasterly.

The locality is 1.55 miles S. 54.5° W. from the northeast corner of the New Preston quadrangle, Connecticut. Blocks of hornfels lie about 10 feet east of the sharp bend in Prospect Road, and about 10 feet farther east is a small outcrop of hornblendite of the Mount Prospect complex. Exposures of the hornfels are scarce, and the thickness of hornfelsed schist is only about 10 or 15 feet. There are no exposures here of schist unaffected by thermal metamorphism.

PETROGRAPHY

The hornfels is bluish gray and is fine grained in hand specimen, except for easily visible garnet, biotite, and orthoclase. The rock is not fissile, although original laminae of the schist are well preserved. In thin section one sees two types of laminae: one of red-brown biotite, equant cordierite, felted masses of sillimanite, irregular grains of magnetite, scattered garnet, and occasional quartz and feldspar; and another of quartz, orthoclase, and andesine, and small quantities of biotite, cordierite, and sillimanite. The first type of laminae are 1 to several mm thick, the second mostly 5 to 25 mm thick. Most of the minerals have maximum dimensions of ¼ to ½ mm. The orthoclase is partly perthitic, and myrmekite is often found between it and the plagioclase. Pleochroic haloes around the zircons in cordierite are exceptionally conspicuous. The rock is fresh, and the only retrograde minerals are in a fine felt of sillimanite and biotite that rims many of the grains of cordierite. Andalusite and muscovite were not seen in 14 thin sections.

In one thin section a rectangular pseudomorph, 8 by 25 mm in size, contains about 75 percent of sillimanite, 15 percent of biotite, 5 percent of cordierite, and the remainder magnetite, pleonaste, and plagioclase; pleonaste is in contact with only sillimanite and cordierite. This is a local assemblage free of K_2O. The composition of the pseudomorph suggests that the original mineral was staurolite. Minor exchange of alkalies, lime, and silica between the original constituents of the staurolite and the surrounding rock resulted in the formation of biotite, orthoclase, and plagioclase. The infiltration of K_2O, however, was not complete, as evidenced by the presence of pleonaste. Other sillimanite-rich pseudomorphs are present, but have less regular outlines.

Garnet is veined by biotite and magnetite (both singly and together), is deeply embayed by these minerals and also by cordierite, and commonly shows very ragged boundaries where in contact with aggregates of biotite, cordierite, and magnetite. These features imply that it is metastable.

Compositions of the biotite, cordierite, and garnet may be estimated approximately from their indices of refraction. These minerals are too impure to be easily separated for chemical analysis. Biotite, like plagioclase, is slightly zoned; the γ index in sodium light ranges from 1.637 to 1.642, suggesting roughly equal amounts of ferrous and magnesian end members. Cordierite has relatively high indices; α, 1.547; β, 1.552; and γ, 1.557. Leake's graph (1960, p. 289) indicates a composition of about half Mg-cordierite and half Fe-cordierite. The index of garnet is 1.793, which is in the usual range of garnet of regionally metamorphosed rocks; it is mainly almandine, perhaps 15 or 20 percent is pyrope, and only small amounts are lime-bearing end members. Plagioclase is mostly sodic andesine; some grains are zoned outward from sodic oligoclase, left from the original schist, to calcic andesine, which formed during thermal metamorphism.

PHASE RELATIONS

The hornfels formed during thermal metamorphism consists of an assemblage of 7 minerals—biotite, cordierite, magnetite, orthoclase, plagioclase, quartz, and sillimanite. The breakdown of staurolite alone yielded cordierite, pleonaste, and sillimanite, and expelled water. Components of the rock may be chosen as Al_2O_3, CaO, Fe, H_2O, K_2O, MgO, Na_2O, O_2, and SiO_2. The fugacity of H_2O probably was uniform throughout the hornfels. Magnetite formed from ferrous silicates indicates relative variations in FeO and Fe_2O_3, so Fe and O_2 are taken as components. The fugacity of O_2 may have been defined internally in the hornfels by temperature, total pressure, fugacity of water, and the mineral assemblage (Wones and Eugster, 1959, p. 130-132), or it may have been set externally by the fugacity of O_2 in the adjacent magma. One cannot tell from the assemblage whether O_2 is an inert component or has its fugacity externally determined. The remaining 7 components are inert; that is, their activities are determined by their relative amounts. The phase rule allows at least 7 and perhaps 8 phases to coexist stably for a given total pressure and temperature (Thompson, 1955, p. 81). The hornfels consists of 7 phases and so does not violate the phase rule, which suggests (but does not prove) that equilibrium was reached. The phase pleonaste is stable only with cordierite and sillimanite, and this mineral is not a part of the 7-phase assemblage that forms most of the hornfels.

Formation of the hornfels from the original garnet-staurolite schist involved several related reactions.

The most probable ones are, written without stoichiometric coefficients:

(1) Muscovite + quartz → Sillimanite + Orthoclase + H_2O
(2) Staurolite + orthoclase + quartz + H_2O → biotite + cordierite + magnetite + sillimanite + H_2
(3) Garnet + orthoclase + H_2O → biotite + cordierite + magnetite + quartz + H_2
(4) orthoclase + oligoclase + andesine → orthoclase perthite + labradorite.

The simple breakdown of staurolite is the reaction:

(5) staurolite → cordierite + pleonaste + sillimanite + H_2O,

where the ratio FeO/(FeO + MgO) in the staurolite probably is less than that in the pleonaste and greater than that in the cordierite. Staurolite may be considered as a system of 4 inert components, Al_2O_3, FeO, MgO, and SiO_2. The coexistence of only these 3 phases, cordierite, pleonaste, and sillimanite, at given total pressure, temperature, and fugacity of water, necessitates that the ratios FeO/(FeO + MgO) of the cordierite and pleonaste be fixed.

The formation of similar cordierite-bearing hornfels from schist has been described by Harker (1939, p. 324-329).

REFERENCES

Agar, W. M., 1927, The geology of the Shepaug Aqueduct Tunnel, Litchfield County, Connecticut: Connecticut Geol. Nat. History Survey Bull. 40, 38 p.

Cameron, E. N., 1951, The geology of the Mount Prospect complex: Connecticut Geol. Nat. History Survey Bull. 76, 44 p.

Harker, A., 1939, Metamorphism: New York, E. P. Dutton and Co., 362 p.

Leake, B. E., 1960, Compilation of chemical analyses and physical constants of natural cordierites: Am. Mineralogist, v. 45, p. 282-298.

Thompson, J. B., 1955, The thermodynamic basis for the mineral facies concept: Am. Jour. Sci., v. 253, p. 65-103.

Wones, D. R., and Eugster, H. P., 1959, Biotites on the joins phlogopite ($KMg_3AlSi_3O_{10}(OH)_2$)-annite ($KFe_3AlSi_3O_{10}(OH)_2$): Carnegie Inst. Washington Yearbook 58, p. 127-132.

269. FIELD MEASUREMENTS OF SILICA IN WATER FROM HOT SPRINGS AND GEYSERS IN YELLOWSTONE NATIONAL PARK

By G. W. Morey, R. O. Fournier, J. J. Hemley, and J. J. Rowe, Washington, D. C.

The geochemistry of the hot springs and geysers of Yellowstone Park has been of interest ever since their discovery. The first study was that of Gooch and Whitfield (1888) on a series of 43 water samples collected during the field seasons of 1883 to 1886 under the direction of Mr. Arnold Hague (1899). Allen and Day (1935) published an exhaustive monograph describing the physical and chemical nature of many of the hot springs in the area. In all the above work, the analyses were made on samples collected some time previous to analysis and accordingly any changes which could take place with time had taken place.

White, Brannock, and Murata (1956) found that the dissolved silica content of waters from hot springs may change with the age of the sample—the dissolved, presumably monomeric, silica changing to polymerized and colloidal silica. In Yellowstone, White measured the dissolved silica contents of several springs at the time of sample collection, using the colorimetric silicomolybdate method. The analytical uncertainty ranged from ±10 to ±30 ppm (parts per million).

For our investigation, water samples were collected in 500 ml polyethylene bottles from the hottest regions of pools and as near the vents as possible. Immediately after each sample was collected, the dissolved silica content was measured in the field by means of the colorimetric molybdenum blue method, using a portable photoelectric colorimeter. Many samples were analyzed a second time the day after collection and some samples were analyzed a third time on the third or fourth day after collection. Several weeks later, all the samples were again analyzed for dissolved silica and also for total silica. The results are tabulated in table 269.1. To determine total silica, it was necessary to evaporate a measured amount of the sample to dryness, fuse the residue with NaOH, leach with water, and acidify to assure the complete conversion of highly polymerized silica to the monomeric form.

The precision of the field analyses ranged from about ±1 ppm for the most dilute silica-bearing waters to about ±5 ppm for the more concentrated waters.

TABLE 269.1.—*Silica content of water of Yellowstone Park springs and geysers, 1960*

[Samples collected September 1960 by G. W. Morey and others. R. O. Fournier made field analyses (0 to 2 days elapsed); J. J. Rowe made laboratory analyses (more than 2 days elapsed)]

Locality	Temperature (°C)	pH	Approximate time elapsed (days)	Dissolved silica (ppm)	Total silica (ppm)
Mammoth Hot Springs					
Jupiter Terrace	72	6.7	0	52	
			26	52	
			88		51
Opal Spring	69	6.5	0	50	
			1	52	
			26	51	
			88		51
New spring, north of Opal			88		55
Norris Basin					
Cinder Pool	86	3.8	0	316	
			36	322	
			73	322	
			88		348
Echinus Geyser [1]	87	3.4	0	280	
			36	283	
			73	286	
			88		287
Green Dragon	71	2.9	0	428	
			1	422	
			25	430	
			73	420	
			87		441
"Little Scald", SW side of Porcelain Terrace	91	7.7	0	573	
			35	126	
			87		608
Opalescent Pool	40	7.7	0	358	
			1	262	
			25	142	
			73	118	
			87		492
Pinwheel Geyser	85	2.9	0	456	
			35	460	
			87		460
Porcelain Terrace, near road	91	2.3	0	179	
			35	184	
			73	191	
			87		189
"Pork Chop" Pool, 200' SW of Pearl	71	7.5	0	428	
			36	131	
			73	114	
			88		435
Steamboat Geyser [2]	81	7.7	0	550	
			1	155	
			36	129	
			73	115	
			88		570
West of Norris drill hole	66	2.3	0	204	
			36	202	
			73	198	
			88		205
Beryl Pool					
Beryl Pool	91	6.8	0	269	
			33	149	
			85		268
Lower Basin					
Black Warrior	92	8.1	0	209	
			33	145	
			85		211
Great Fountain Geyser	95	8.7	0	324	
			33	160	
			85		325
Narcissus Geyser [1]	90	6.8	0	331	
			33	160	
			85		354
Midway Basin					
Excelsior Geyser	76	8.4	0	283	
			1	207	
			28	145	
			90		303

See footnotes at end of table.

TABLE 269.1.—*Silica content of water of Yellowstone Park springs and geysers, 1960*—Continued

Locality	Temperature (°C)	pH	Approximate time elapsed (days)	Dissolved silica (ppm)	Total silica (ppm)
Upper Basin					
Artemisia Geyser [1]	95	3.45	0	267	
			1	234	
			2	185	
			29	147	
			91		275
Daisy Geyser [1]	91	7.8	0	306	
			1	247	
			2	179	
			29	131	
			91		304
Pool SW of Daisy and Splendid Geysers	71	4.3	0	270	
			1	272	
			2	271	
			29	272	
			91		278
Giantess Geyser	95	8.9	0	384	
			1	163	
			28	145	
			90		417
Hillside spring	86	7.0	0	222	
			1	179	
			28	132	
			90		190
Iron Spring	95	3.5	0	455	
			29	463	
			91		456
Old Faithful [2]	90	9.3	0	356	
			33	205	
			85		381
Small spring N of Old Faithful	78	8.9	0	313	
			33	167	
			85		318
Riverside Geyser [1]	95	8.9	0	226	
			1	190	
			2	152	
			28	150	
			90		268
Sapphire Pool	92	9.2	0	348	
			1	233	
			2	179	
			28	175	
			90		352
Turban [1]	89	8.5	0	315	
			32	184	
			84		318
Pool near Upper Basin drill hole	93	9.7	0	361	
			1	316	
			2	282	
			29	251	
			91		374
At Continental Divide 7 miles west of Old Faithful					
"Contrary Spring" in stream gully	91	6.9	1	246	
			2	240	
			27	252	
			89		252
Cloudy spring in stream gully	82	6.3	1	254	
			27	259	
			89		264
Boiling pool S of trail	92	2.3	1	262	
			27	302	
			89		300
West Thumb					
Abyss Pool	91	8.5	0	282	
			1	152	
			28	139	
			90		297
Occasional geyser [1]	94	8.6	0	262	
			1	163	
			28	139	
			90		283
Mud Volcano area					
Churning Cauldron	55	2.0	0	297	
			1	300	
			28	327	
			90		321

[1] Sampled before eruption, during preliminary overflow.
[2] Sampled during eruption.

Only one sample, from Hillside, showed evidence of flocculation and settling of silica to the bottom of the container between the time of field analysis and the laboratory analysis because the total silica measured in the laboratory was 32 ppm less than the dissolved silica measured at poolside. For most of the samples, dissolved silica determined immediately after collection and total silica values are identical, within the limits of accuracy of the method. Analyses from 14 pools showed 10 to 35 ppm more total silica than initially dissolved silica. These differences may be the result of polymerization taking place in the few minutes between the sample collection and the completion of analyses, or they may even be due to the presence of a few small solid particles swept up in the waters from the bottom of the pool. The only large discrepancy between total silica and dissolved silica was registered for water taken from an opalescent pool in Norris Basin. The opalescence of the water, at the time of collection, was due to dispersed colloidal silica. However, even though colloidal silica was forming, this pool was still greatly supersaturated with dissolved silica in respect to silica gel. The hottest part of the pool was 40°C. At this temperature the solubility of silica gel is about 175 ppm, while the water in the pool contained 358 ppm. The pool had a slow but continuous overflow, and water coming up from hotter regions presumably was adding dissolved silica at too fast a rate for equilibrium between dissolved and colloidal silica to be attained.

White and others (1956, p. 42–43) observed that acid waters tend to maintain high degrees of supersaturation of dissolved silica at room temperature and pressure for long periods of time. On the other hand, in alkaline waters dissolved silica tends to convert rapidly to polymerized silica until the equilibrium solubility with silica gel is approximated. This effect may be seen in table 269.1, where for given springs the pH and dissolved and total silica values are compared.

Of the springs analyzed, Little Scald contains the most dissolved silica. It lies on the southwest side of Porcelain Terrace, in the Norris Basin. The dissolved silica content was 573 ppm and the total silica 608 ppm. If the solubility of quartz or chalcedony in hot regions at depth controls the quantity of silica in the waters issuing from rapidly discharging springs and geysers, then, using data from Kennedy (1950), the temperature at which equilibrium between dissolved silica and quartz was last attained in the water of Little Scald was about 275°C. More commonly, springs and geysers in Yellowstone contain 250 to 350 ppm dissolved and total silica. At pool temperatures of 90°C, such solutions are unsaturated in respect to silica gel. They are saturated, however, with respect to quartz at temperatures ranging from 175°C to 225°C, assuming pressures equal to the vapor pressure of water (Fournier, 1960). Indeed, it is likely that quartz and chalcedony deposit in hot spring areas at relatively shallow depths and at temperatures ranging from 175°C to 275°C. Secondary quartz has been reported by Fenner (1936) in drill core from both Norris Basin and the Upper Basin. The maximum temperature encountered in the Norris drill hole was 205°C at a depth of 246½ feet and in the Upper Basin drill hole 180°C at a depth of 406 feet. Also, in experimental work at 1,000 bars H_2O pressure, quartz was precipitated from initially supersaturated solutions within three days at 125°C.

In stagnant and slowly discharging springs, the dissolved silica content of the water may be fixed in great part by the formation of colloidal and gelatinous silica, or even by silica dissolving from the immediate borders of the spring pools, as suggested for acid sulfate pools by White and others (1956, p. 43).

One of the objectives of this study is to determine what chemical changes, if any, have taken place in the waters from springs and geysers previously analyzed. Of the 36 springs reported here, waters from 21 had been sampled one or more times and analyzed by other workers. Waters from 8 springs show no change in silica content, within the limits of accuracy of the measurements. Four previous analyses are higher in silica and 15 are lower in silica.

Abnormally intense discharge was reported for many of the springs and geysers of Yellowstone Park the night of the 1959 Hebgen Lake earthquake (Marler, 1960; and personal communication, 1960). Other springs became markedly less active. Some of these changes have persisted up to the present (spring 1961). The frequencies of eruption of both Artemisia and Great Fountain geysers have greatly increased since the earthquake, yet their silica and chlorine contents remain practically unchanged. Sapphire Pool changed from a minor to a major geyser with all aspects of its former function greatly altered. The silica content of its water has also increased from 320 ppm in 1947 to 350 ppm now.

The greatest change in the chemical nature of a spring was found at Porcelain Terrace in Norris Basin. There, one spring, known to have been an alkaline chloride type, had changed to an acid sulfate type with a pH of 2.3. The total silica has decreased from about 700 ppm measured both in 1930 and 1947 to 189 ppm now. Chlorine has dropped from 748 ppm to 20 ppm. Since the Hebgen Lake earthquake, the spring has ceased overflowing and the water level has ebbed.

The old water supply to the spring was probably diverted to other channels as ground shifted during the earthquake. In agreement with the views of White, Sandberg, and Brannock (1953, p. 493) for the origin of acid sulfate pools, it is probable that now only steam, rich in acid-forming gases, rises to the vicinity of the spring, there condensing and mixing with ground waters already present to produce an acid sulfate pool. Steam at 108°C perpetually roars from a small vent adjacent to the pool.

Unfortunately, at most places it cannot be determined with certainty what chemical changes have been brought about in various spring waters due to the catastrophic effects of the earthquake and what changes we now see were due to slow continuous processes operative before the earthquake. Five years elapsed between the time of the last collection of samples for analyses (White and others, 1956, p. 34) and the time of the earthquake. There is a definite need to obtain more chemical data at Yellowstone to achieve a better understanding of the extent of chemical variations in thermal waters in one area and to provide a broader base to judge when, why, and how chemical changes take place.

REFERENCES

Allen, E. T., and Day, A. L., 1935, Hot springs of the Yellowstone Park: Carnegie Inst. Washington Pub. 466, 524 p.

Fenner, C. N., 1936, Bore-hole investigations in the Yellowstone Park: Jour. Geology, v. 44, p. 282-310.

Fournier, R. O., 1960, The solubility of quartz in water in the temperature interval 25°C to 300°C [abs.]: Geol. Soc. America Bull., v. 70, p. 1604.

Gooch, F. A., and Whitfield, J. E., 1888, Analyses of waters of the Yellowstone National Park: U.S. Geol. Survey Bull. 47.

Hague, Arnold, and others, 1899, Geology of the Yellowstone Park: U. S. Geol. Survey Mon. 32, pt. 2, 893 p.

Kennedy, G. C., 1950, A portion of the system silica-water: Econ. Geology, v. 45, p. 629-653.

Marler, G. D., 1960, The 1959 Hebgen Lake earthquake alters Yellowstone's hot springs, *in* Billings Geol. Soc. Guidebook 11th Ann. Field Conf., 1960: p. 61-66.

White, D. E., Brannock, W. W., and Murata, K. J., 1956, Silica in hot spring waters: Geochim. et Cosmochim. Acta, v. 10, p. 27-59.

White, D. E., Sandberg, C. H., and Brannock, W. W., 1953, Geochemical and geophysical approaches to the problems of utilization of hot-spring water and heat: Pacific Sci. Cong., 7th, New Zealand, 1949, Proc., v. 2, p. 491-493.

270. ANTHOPHYLLITE-BIOTITE-HYPERSTHENE-RHODOLITE ASSEMBLAGE, MASON MOUNTAIN, NORTH CAROLINA

By Fred Barker, Washington, D. C.

Rhodolite, a pyrope-rich variety of garnet, is associated with aluminous anthophyllite, hypersthene, biotite, quartz, and sillimanite at Mason Mountain, Macon County, N. C., about 6 miles north of Franklin. The rhodolite locality is a small quarry 1.18 miles N. 82° W. of the southeastern corner of the Alarka quadrangle, as shown on figure 270.1.

RHODOLITE-BEARING ROCK

Rhodolite garnet was described and named by Hidden and Pratt (1898a). Henderson (1931) described the quarry where fresh rhodolite-rich rock crops out. He gave analyses of the anthophyllite and hypersthene, checked Pratt's determination of FeO in rhodolite, and analyzed biotite for FeO and Fe_2O_3. The quarry was later enlarged, and Heinrich (1950) made a detailed petrographic study of the rhodolite-bearing rocks.

The body of rhodolite-bearing rock is exposed only in the quarry. It is about 15 to 40 feet in width, is at least 100 feet long, and has steep contacts with the wallrocks. An abundance of rhodolite in the gravels of the lower part of Mason Branch suggests that the body is much longer than 100 feet. It probably is a dike. Decomposed gneiss and schist are exposed along both sides of the rhodolite-bearing rock; their foliation is truncated by the dike.

The rhodolite-bearing rock is coarsely crystalline, mostly rudely banded, and composed of variable proportions of anthophyllite, biotite, rhodolite, hypersthene, quartz, sillimanite, ferriferous rutile, and graphite. Henderson (1931, p. 564) pointed out that anthophyllite formed from an original rhodolite-

hypersthene rock. Heinrich (1950) gave a detailed sequence of mineral growth, which is confirmed by my own petrographic work. Rhodolite and hypersthene are the earliest minerals. They are corroded and veined by anthophyllite, biotite, and quartz. These minerals are transected by veinlets of sillimanite and quartz. Anthophyllite and sillimanite are rarely associated. The rutile contains patches of ilmenite. Flakes of graphite are associated with biotite, rhodolite, and rutile. Analyses of the mafic minerals are given in table 270.1.

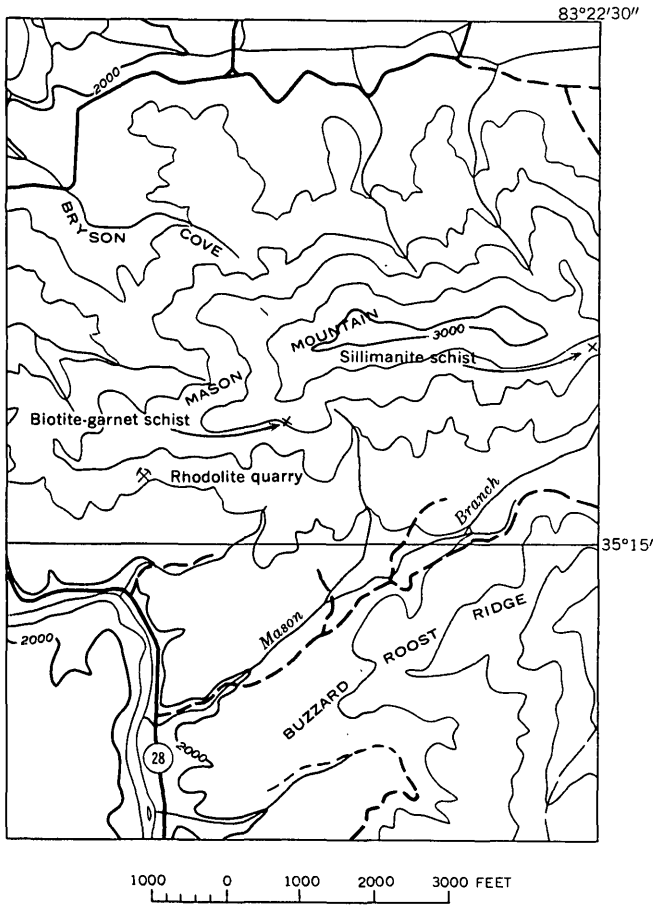

FIGURE 270.1.—Mason Mountain and vicinity, showing locations of rhodolite quarry, and outcrops of biotite-garnet schist and twice-metamorphosed sillimanite schist.

TABLE 270.1.—*Chemical analyses of minerals, rhodolite deposit, Mason Mountain, Macon County, N.C.*

[In percent]

	Rhodolite [1]			Antho-phyllite [2]	Hyper-sthene [2]	Biotite [3]
SiO_2	41.54	41.65	.....	44.22	52.36	38.9
TiO_2	.....	.....	.....	.....	.....	2.9
Al_2O_3	.....	23.26	23.10	23.79	4.29	17.7
Fe_2O_3	1.88	1.92	.....	.20	.....	.72
FeO	15.48	15.63	.....	9.21	16.90	6.2
MnO	.....	.....	.....	.16	.....	.....
MgO	.....	16.90	17.48	20.69	25.89	20.2
CaO	1.02	.86	.....	.62	.44	.....
Na_2O	.....	.....	.....	.....	.....	.54
K_2O	.....	.....	.....	.....	.....	8.7
H_2O	.....	.....	.....	1.42	.34	3.5
F	.....	.....	.....	.....	.....	.54
Total	100.22			100.31	100.22	99.90

[1] Analyst: J. H. Pratt (Hidden and Pratt, 1898a, p. 295).
[2] Analyst: E. P. Henderson (1931, p. 566 and 568).
[3] Analyst: B. L. Ingram. Spectrochemical analysis of the biotite shows: Ca 0.003 percent, and Mn 0.015 percent.

Henderson (1931, p. 565, 568) obtained an average of 16.06 percent of FeO in rhodolite from two determinations, and 5.78 percent of FeO and 0.72 percent of Fe_2O_3 in biotite. He measured (1931, p. 565–568) the indices of refraction of the mafic materials as follows:

	n	α	β	γ	Limit of error
Rhodolite	1.758	.....	.....	.....	.....
Anthophyllite	.....	1.642	1.655	1.661	±0.003
Hypersthene	.....	1.658	1.696	1.699	± .003
Biotite	.....	1.565	1.607	1.607	± .003

Measurements by the author agree.

The molar ratios MgO: (MgO+FeO) of these minerals are: rhodolite 0.66, hypersthene 0.73, anthophyllite 0.81, and biotite 0.85. The formula of biotite may be written:

$$\begin{bmatrix} K_{1.55} \\ Na_{0.15} \end{bmatrix} \begin{bmatrix} Mg_{4.29} \\ Fe^{+2}_{0.73} \end{bmatrix} \begin{bmatrix} Al_{0.55} \\ Ti_{0.31} \\ Fe^{+3}_{0.08} \end{bmatrix} \begin{bmatrix} Si_{5.57} \\ Al_{2.43} \end{bmatrix} \cdot \begin{bmatrix} O_{20.44} \\ (OH)_{3.32} \\ F_{0.24} \end{bmatrix}$$

ADJACENT SCHIST

Hidden and Pratt (1898b, p. 468) found a garnet that they called impure rhodolite that occurs with biotite near the summit of Mason Mountain. About 1,600 feet southwest of the western summit of the mountain a small pit exposes weathered biotite-garnet-oligoclase-quartz-sillimanite schist. The garnet in this rock is violet as is rhodolite; however, as its index ranges from 1.793 to 1.798, ±0.004, it is an almandine-rich variety. The β and γ indices of the biotite are 1.635, ±0.003, which is much higher than those of the biotite found with rhodolite. This rock is a typical regionally metamorphosed argillaceous schist.

Twice-metamorphosed schist crops out south of the saddle that lies ¼ mile east of the eastern summit of Mason Mountain. This rock consists of corroded garnets and tabular pseudomorphic masses of intergrown sillimanite in a matrix of sillimanite, biotite, quartz, perthitic microcline, cordierite, magnetite, and leucoxene. The original elongated tabular mineral, in crystals as large as 1 inch in length, is judged to have been kyanite. Garnet has partly reacted to biotite, cordierite, sillimanite, and iron oxides. Fine-grained microcline and sillimanite in the matrix probably formed from muscovite and quartz. An initial metamorphism apparently produced the garnet, kyanite, muscovite, and the staurolite found in placer deposits

(Hidden and Pratt, 1898a, p. 294). These minerals are typical of middle-rank regional metamorphism. The second metamorphism produced biotite-cordierite-oligoclase-quartz-sillimanite-Fe, Ti oxides. Garnet may be unstable in this environment, or the original garnet may have reacted to form a mineral that contains more magnesium and is stable with cordierite; the petrographic relations do not indicate which alternative is correct. The second metamorphism was either the result of very high rank regional metamorphism or of thermal metamorphism by plutonic intrusives.

ORIGIN

The mineral pair rhodolite-hypersthene is an unusual one; its origin is unknown. These minerals may have been part of a rare igneous rock, such as a pyrope-bearing peridotite, or the hypersthene may be a relict from a normal ultramafic igneous body, and the rhodolite may have formed in the initial, middle-rank metamorphism. Anthophyllite, biotite, and quartz, and the younger veinlets of sillimanite and quartz as well, probably formed during the second, high-rank metamorphism.

Compositions of the mafic minerals and sillimanite are shown on figure 270.2. Alteration of hypersthene and rhodolite to anthophyllite and biotite involved addition of H_2O and K_2O and probably Al_2O_3. Breakdown of muscovite during the second metamorphism of the adjacent schist may have forced a solution of $KAlO_2$, saturated with SiO_2, into the rhodolite rock. Anthophyllite and biotite have higher ratios of $MgO:(MgO+FeO)$ than the hypersthene and rhodolite; this could be the result either of addition of MgO to the system, or of subtraction of FeO. The proportions of ferrous iron in anthophyllite and biotite were complex functions of fugacities of oxygen and water, pressure, and temperature, as well as composition of the original rock. Thus, exact equations for the transformation of hypersthene and rhodolite to anthophyllite and biotite cannot be written, even though the compositions of these minerals are known.

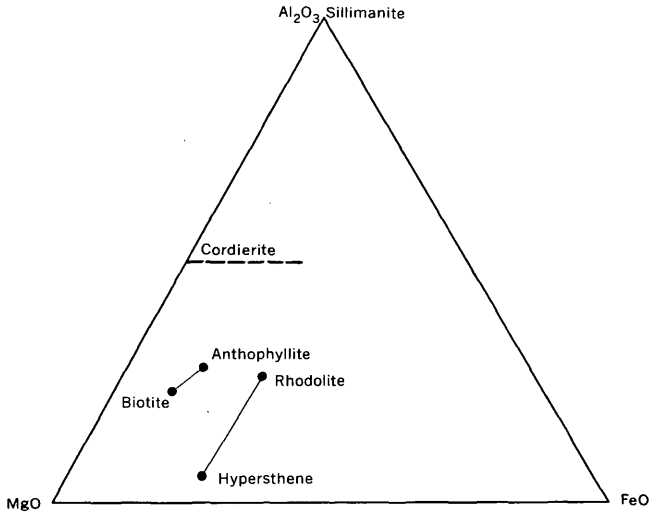

FIGURE 270.2.—Compositional plot of Al_2O_3–FeO–MgO in moles of mafic silicates from Mason Mountain, N. C. Composition of cordierite is not known.

Sillimanite in the late veinlets may be due to leaching by hot water that percolated along fractures. Solution of the more soluble constituents of the four mafic silicates would leave Al_2O_3, which, with the excess SiO, would crystallize as sillimanite. This mode of origin was suggested to the author by Werner Schreyer (oral communication, 1961).

REFERENCES

Heinrich, E. W., 1950, Paragenesis of the rhodolite deposit, Mason Mountain, North Carolina: Am. Mineralogist, v. 35, p. 764-771.

Henderson, E. P., 1931, Notes on some minerals from the rhodolite quarry near Franklin, North Carolina: Am. Mineralogist, v. 16, p. 563-568.

Hidden, W. E., and Pratt, J. H., 1898a, On rhodolite, a new variety of garnet: Am. Jour. Sci., v. 5, p. 294-296.

———1898b, On the associated minerals of rhodolite: Am. Jour. Sci., v. 6, p. 463-468.

271. TWO OCCURRENCES OF THORIUM-BEARING MINERALS WITH RHABDOPHANE-LIKE STRUCTURE

By J. R. Dooley, Jr., and John C. Hathaway, Denver, Colo.

Recently Bowie (1959, p. 306) reported a thorium-bearing phosphate with a rhabdophanelike structure from the Mtoko district of Southern Rhodesia independently, Fisher (*in* McKelvey, 1960, p. A60) and Phair (written communication, 1960) found similar material in a sample from the Wet Mountains of Colorado. Two additional occurrences of similar material, one from Wyoming and one from near Gunnison, Colo., are here described.

We wish to acknowledge the initial work and analyses of the material from Gunnison, Colo., by J. W. Adams and R. P. Marquiss. F. H. Hildebrand furnished the X-ray pattern of rhabdophane from Salisbury, Conn.

WYOMING OCCURRENCE

Radioactive samples of the limestone member of the Pliocene Moonstone formation were found in Fremont County, Wyo. (sec. 25, T. 30 N., R. 90 W.) by J. D. Love in 1951 and H. D. Zeller and J. D. Love in 1955. Autoradiographs of polished specimens of limestone showed the radioactive material to be distributed throughout the limestone, but the highest concentrations were in crack fillings. Formic acid was used to concentrate the insoluble residue from the limestone, as hydrochloric acid tended to dissolve a considerable amount of thorium from the sample.

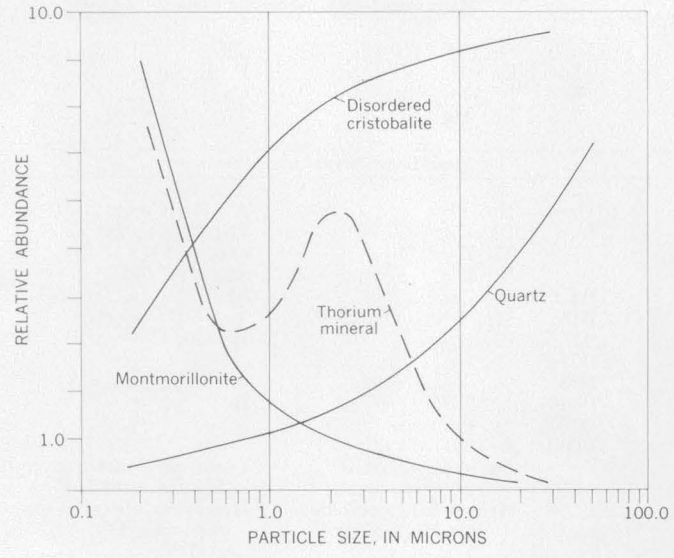

FIGURE 271.1.—Schematic diagram showing the distribution of insoluble minerals as a function of particle size. Samples 265110A and 265112.

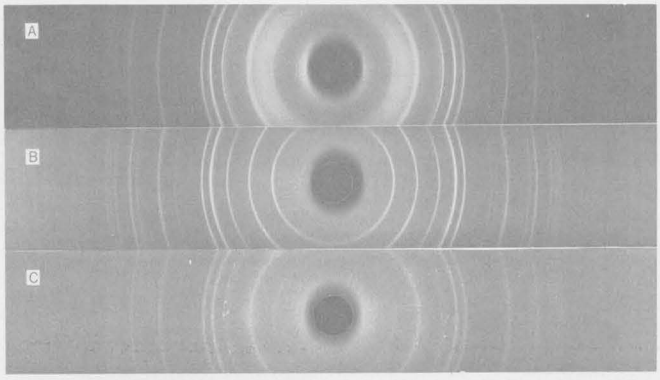

FIGURE 271.2.—X-ray powder diffraction patterns of the thorium-bearing minerals and rhabdophane. *A*, thorium-bearing mineral, Fremont County, Wyo.; *B*, rhabdophane, Salisbury, Conn.; *C*, thorium-bearing mineral, Gunnison, Colo.

The highest concentrations of thorium were in the finer sized materials; these fractions were concentrated by wet sieving and centrifuging, then analyzed by X-ray powder diffraction techniques. Disordered cristobalite (Flörke, 1955a, 1955b), quartz, montmorillonite, and the thorium-bearing mineral, in order of decreasing abundance, were identified. A schematic representation of the mineral distribution versus particle size that was compiled from both X-ray and radioactivity measurements of the various size fractions is presented on figure 271.1.

A particle size of about 1 micron showed the greatest concentration of the thorium mineral and the smallest amount of impurities. A few milligrams of the thorium-bearing mineral were obtained from this size fraction by solution of the disordered cristobalite in strong NaOH. It was not possible to determine physical or optical properties on so small an amount of very fine grained material, but X-ray powder photographs and diffraction data showed the material to have a structure closely resembling that of rhabdophane (fig. 271.2 and table 271.1).

Further similarity of the mineral to rhabdophane was noted on ignition of the sample at 800° to 900°C. The ignited material gave an X-ray pattern closely resembling that of monazite (fig. 271.3) as does rhabdophane after ignition (Muto and others, 1959, p. 648).

TABLE 271.1.—*X-ray powder diffraction data for two thorium-bearing minerals and for rhabdophane*

[CuKα radiation; 114.59 mm powder camera; d in Angstrom units]

Material from Wyoming before heating. Film 457		Material from Gunnison before heating. Film D-2449		Rhabdophane, Salisbury, Conn. (Muto and others, 1959, p. 644)	
d	I[1]	d	I[1]	d	I[1]
7. 14	f[2]				
6. 04	w	6. 05	w	6. 07	m
4. 47	vw[3]				
4. 35	w	4. 35	m	4. 40	s
4. 26	vw[4]	4. 26	f[4]		
3. 90	f[6]				
3. 56	f[2]				
3. 41	w	3. 46	vw	3. 49	m
3. 33	m[4]	3. 33	vw[4]		
3. 21	w				
3. 04	vs[5]	3. 03	vs	3. 02	vsb
2. 96	vw				
2. 82	s	2. 82	s	2. 83	s
2. 71	f				
2. 56	f				
2. 45	f[4]	2. 45	f[4]		
2. 37	w	2. 36	vw	2. 36	w
2. 28	w	2. 27	f	2. 28	vw
2. 21	f				
2. 14	s	2. 15	s	2. 15	s
2. 10	vw[6]			2. 02	f
1. 914	w	1. 914	vw	1. 920	w
1. 856	m	1. 856	m	1. 859	m
1. 821	w				
1. 788	vw				
1. 749	w	1. 748	vw	1. 743	vwb
1. 697	w	1. 704	vw	1. 704	vw
1. 667	vw	1. 667	vw	1. 675	vw

[1] vs, very strong; s, strong; m, medium; w, weak; vw, very weak; f, faint; b, broad.
[2] Kaolinite(?).
[3] Montmorillonite.
[4] Quartz.
[5] Includes trace of calcite.
[6] Calcite.

Semiquantitative spectrographic analysis of the same fraction that was analyzed by X-rays is shown in table 271.2. It is noteworthy that the material contains less than 0.5 percent rare earths. The silicon, aluminum, iron, and magnesium among the major constituents are probably the result of failure to remove all the montmorillonite and quartz from the fraction, although it is possible that some silicon may substitute for phosphorus in the rhabdophane structure. The calcium shown may occur in the rhabdophanelike structure but some is undoubtedly the result of failure to remove all the calcite from the sample by acid treatment.

GUNNISON, COLO., OCCURRENCE

A second occurrence of a thorium-bearing material having a rhabdophane structure was found in a small vein in Precambrian rocks southwest of Gunnison, Colo. (sec. 24, T. 49 N., R. 2 W.) in 1955 by R. C. Derzay and R. C. Maylan. Both the vein material and the surrounding rock are oxidized and friable. The original sample of relatively fresh material consisted principally of potassium feldspar, chiefly microcline, and subordinate quartz. Analyses showed thorium to be the principal source of the radioactivity; uranium was present only in minor amounts. The same structure was observed in the X-ray powder patterns of both the Wyoming and Gunnison material.

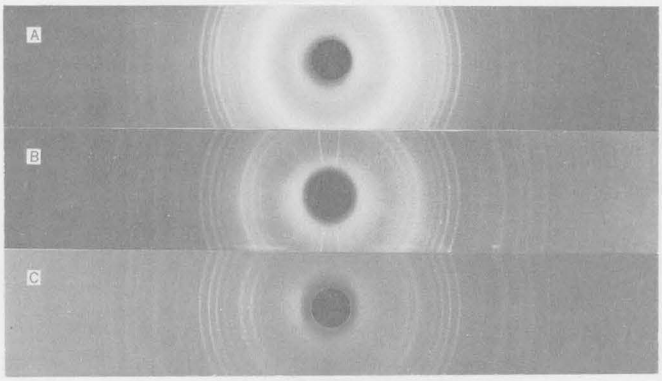

FIGURE 271.3.—X-ray powder diffraction patterns of the thorium-bearing minerals after heating at 800° to 900°C and monazite, unheated. *A*, thorium-bearing mineral, Fremont County, Wyo.; *B*, monazite, locality unknown; *C*, thorium-bearing mineral, Gunnison, Colo.

TABLE 271.2.—*Semiquantitative spectrographic data on concentrate containing thorium-bearing mineral*

[Analyst: N. M. Conklin; in percent to nearest number in the series 7, 3, 1.5, 0.7, 0.3, 0.15, and so forth]

Percent group	Wyoming occurrence. Mineral concentrate 0.5–1.0 micron size. Sample 265110A–plate II–1986	Gunnison occurrence. Mineral concentrated from heavy fraction. Sample 231219–plate 1348
Major constituents and contaminants		
>10. 0	Si, Th	Th
7.	Ca	P, Si, Fe
3.	P, Al	Ca
1. 5	Fe, Mg	Ti
Minor impurities and trace elements		
0. 7	Na, Pb	Al, Ba, Ce
. 3	Ba, Cu, Sr	La, Nd, Y, Zr
. 15	Ti, Y	Cu
. 07	Ni, V	Mg, Dy, Gd
. 03	Sn, Zr, Yb	Mn
. 015	Mn	Yb
[1]<. 01	Bi	Bi, Co, Cr
. 007	Co, Cr	
. 003	B	
. 0015		Be
. 0007	Ag, Ga	
. 0003	Be	
([2])	Light rare earths	Light rare earths except La, Ce, and Nd
([2])	Heavy rare earths except Yb and Y	Heavy rare earths except Gd, Dy, Yb, and Y
([3])	U	U

[1] Lower limit of detection is 0.01 percent.
[2] The lower limits of detection from 10 ppm to 500 ppm depending upon each particular element.
[3] The lower limit of detection is 0.05 percent.

A heavy-mineral fraction of the sample contained the thorium-bearing mineral together with iron-bearing opaque minerals, and minor amphibole and rutile. A few milligrams of the thorium mineral were concentrated by hand picking. The mineral was dark reddish brown and occurred in cryptocrystalline aggregates. Lighter colored material grading into red and reddish-orange grains was abundant but optical and X-ray analyses of these grains showed considerable amounts of intimately admixed quartz.

Some physical and optical properties of the mineral, as determined from the hand-picked grains, are as follows:

Physical and optical properties

Color	Reddish brown
Fracture	Conchoidal
Luster	Resinous
Hardness	3 to 4
Specific gravity	3.7 to 4.3
Average index of refraction	1.66 to 1.69
Birefringence	Moderate

The similarity of this mineral to the Wyoming material described above and to rhabdophane can be seen in the X-ray data given in table 271.1 and figure 271.2. The Gunnison mineral also shows a monazite-like structure on ignition at 800° to 900° C (fig. 271.3).

A semiquantitative spectrographic analysis of the heavy-mineral concentrate is compared in table 271.2 with that of the Wyoming material; in the Gunnison mineral the rare-earth content is relatively higher but is nevertheless below 2 percent. Some silicon, iron, calcium, and titanium in the analysis undoubtedly are due to amphibole, rutile, and iron-bearing opaque minerals that were not removed during concentration of the samples. It is possible that some of the silicon may substitute for phosphorus in the rhabdophane-like structure.

In both the occurrences rare-earth elements are minor as compared to thorium and calcium. This low rare-earth content contrasts with the usually moderate and high rare-earth content of rhabdophane and monazite.

Phosphorus appears among the major elements in samples from both occurrences but the material available was insufficient for complete chemical analysis. Presumably the thorium-bearing minerals, like rhabdophane and ningyoite (Muto and others, 1959), are fundamentally hydrated phosphates and like rhabdophane and ningyoite, they alter to a monazite structure through dehydration upon ignition.

REFERENCES

Bowie, S. H. U., 1959, Note on uranium and thorium occurrences in the Federation of Rhodesia and Nyasaland: Chronique des Mines d'Outre-Mer de la Recherche Miniere, no. 279, p. 304-309.

Flörke, O. W., 1955a, Zur Frage des "Hoch"—Cristobalit in Opalen, Bentoniten und Gläsern: Neues Jarhb. Mineralogie Monatsh., no. 10, p. 217–223.

———1955b, Structuranomalien bei Tridimyt und Cristobalit: Deutschen Keramischen Gesell. Ber., v. 32, p. 364-381.

McKelvey, V. E., compiler, 1960, Geological Survey research, 1960, synopsis of geologic results: U.S. Geol. Survey Prof. Paper 400-A, 136 p.

Muto, Tadashi, Meyrowitz, Robert, Pommer, A. M., and Murano, Toru, 1959, Ningyoite, a new uranous phosphate mineral from Japan: Am. Mineralogist, v. 44, nos. 5 and 6, p. 633–650.

272. EFFECTS OF IMPACT ON THERMOLUMINESCENCE OF YULE MARBLE

By C. H. Roach, G. R. Johnson, J. G. McGrath, and F. H. Spence, Denver, Colo.

Impact experiments are being made on various rock types as a part of a general study of the physical effects of high energy shock in rocks. Yule marble from Marble, Colo., was selected for investigation because of the large amount of physical, chemical, and petrofabric data available for this rock (Balsley, 1941; Griggs and Miller, 1951; Griggs and others, 1951; Handin and Griggs, 1951; Knopf, 1949; Lepper, 1941; Turner, 1949; Turner and Ch'ih, 1950; Turner and Ch'ih, 1951; and Turner and others, 1950).

A sawed block of unfractured Yule marble about 6 inches thick and with a target surface area of about 1 square foot was used for an experiment. A 30-caliber armor-piercing bullet was fired into the block of marble in a direction normal to the target surface. The point of impact was 46.0 feet from the gun muzzle, impact velocity of the projectile was estimated at 2,700 feet per second, and the bullet weighed 10.92 grams.

The impact formed a crater having an average diameter of about 5 inches and a depth at the center of about 1 inch (fig. 272.1). A well-defined radial fracture system intersects the crater. Marble in the central part of the crater has a white opaque appearance apparently related to intense microbrecciation caused by shock produced by the impacting projectile. The intensity of microbrecciation decreases progressively with distance from the center of the crater. Along the rim of the crater, single pieces of marble up to 1 square inch in area and about 0.1 inch thick spalled loose but were not ejected from the crater. Apparently the marble failed mainly by shear in the zone of microbrecciation, whereas tensional failure was more important along the rim of the crater.

Shock produced by the impact caused significant changes in thermoluminescence characteristics of the marble (fig. 272.1). Comparison of glow curves (fig. 272.1) of samples CS-1, CS-2, CS-3, CS-4, S-4″, and S-6″ taken from the target surface and crater surface after the impact with a sample taken before impact shows that the total thermoluminescence of the marble was increased. The amount of shock-induced thermoluminescence is greatest at the center of the crater and generally decreases with distance outward. Glow curves of pre-impact samples of Yule marble have a lower peak amplitude at 270°C than at 325°C. The effect of the shock in the intensely microbrecciated region was to reverse the relative heights of the 270°C and 325°C peaks in samples CS-1 and CS-2. This "reversed peak" relation has been observed in shocked carbonate rocks from other impact experiments and in rocks associated with meteorite craters, and may be a common characteristic of intensely shocked rocks.

The block of marble was sawed perpendicular to the target surface and one-quarter of an inch from the projectile hole in order to evaluate the effect of shock below the crater (fig. 272.2). The top of the steel projectile penetrated to a depth coinciding with the horizontal fracture shown in figure 272.2, and is about one-quarter of an inch behind the sawed surface. The fracture system is roughly symmetrical with respect to the crater axis. Fractures above the projectile are concave upward, whereas fractures below the projectile are concave downward. Other cross sections show that the fracture surfaces are approximately paraboloids.

The impact increased the total thermoluminescence of the marble below the crater; the greatest increase occurred in sample V-1 and the sample that formed a coating on the bullet (fig. 272.2). The amount of shock-produced thermoluminescence decreases with increasing distance below the crater. Glow curves of sample V-1 and the bullet coating do not have the "reversed peaks" expected in the intensely brecciated zone. The lack of "reversed peaks" in these samples might be attributed to thermal decay of the 270°C peak as a result of frictional heating close to the path of penetration of the projectile.

Splits of sample V–2 and the pre-impact sample were preheated at 400° C for 16 hours and subsequently exposed to short-wave (λ=2537 A) ultraviolet radiation for 4 hours. Significant low temperature thermoluminescence was induced in the post-impact sample but not in the pre-impact sample (fig. 272.3). The two ultraviolet-induced peaks of sample V–2 decay rapidly at room temperature (fig. 272.4); the 70° C peak has the fastest rate of decay. The 70° C peak decayed approximately according to the equation $\log Y = -0.92 \log X + 1.719$ (where Y is the peak height in relative thermoluminescence units and X is the time, in minutes, elapsed since the sample was removed from the radiation source). The 140° C peak decayed approximately according to the equation $\log Y = -0.38 \log X + 2.054$.

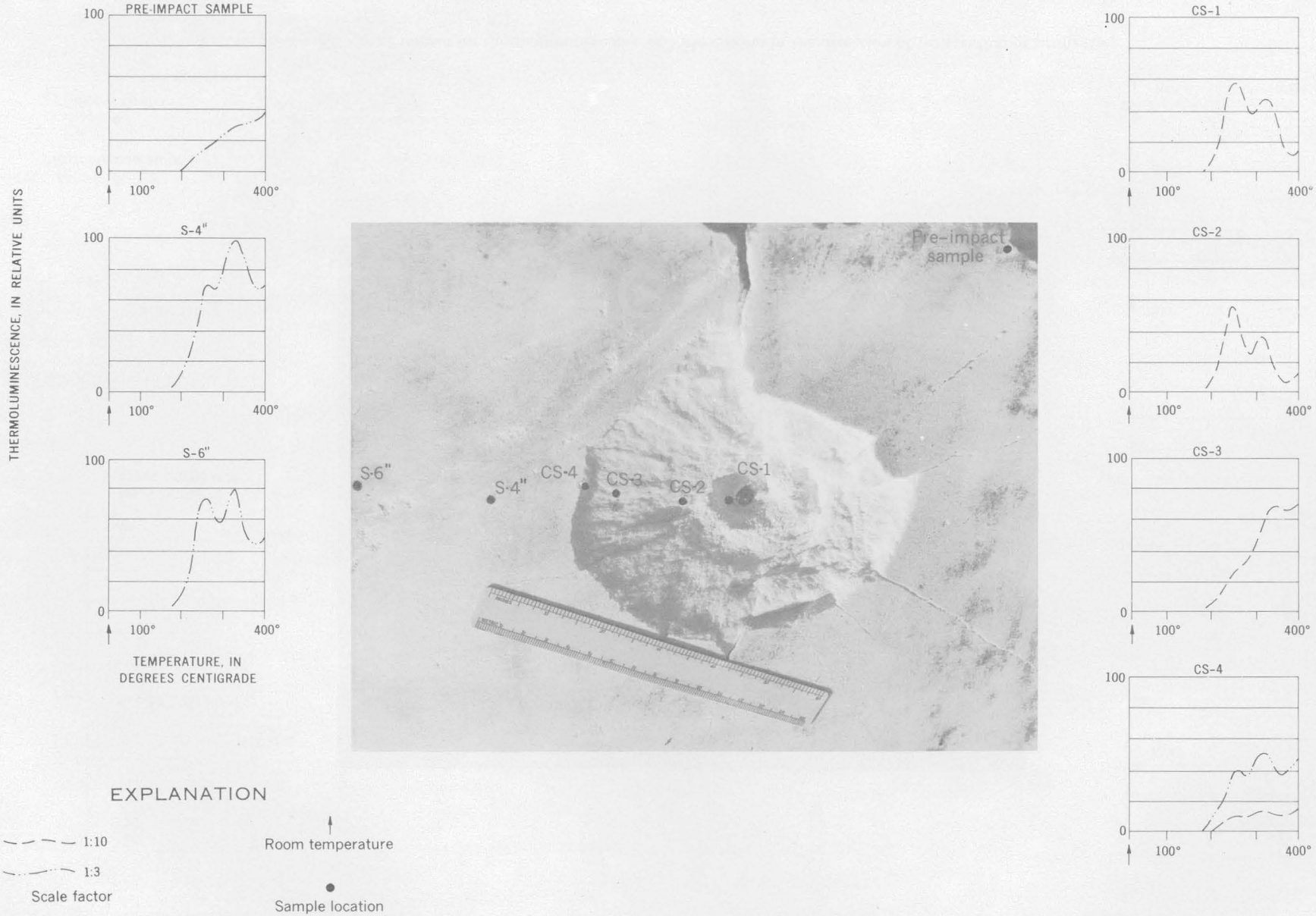

FIGURE 272.1.—Effects of impact on thermoluminescence of Yule marble along crater surface and original surface.

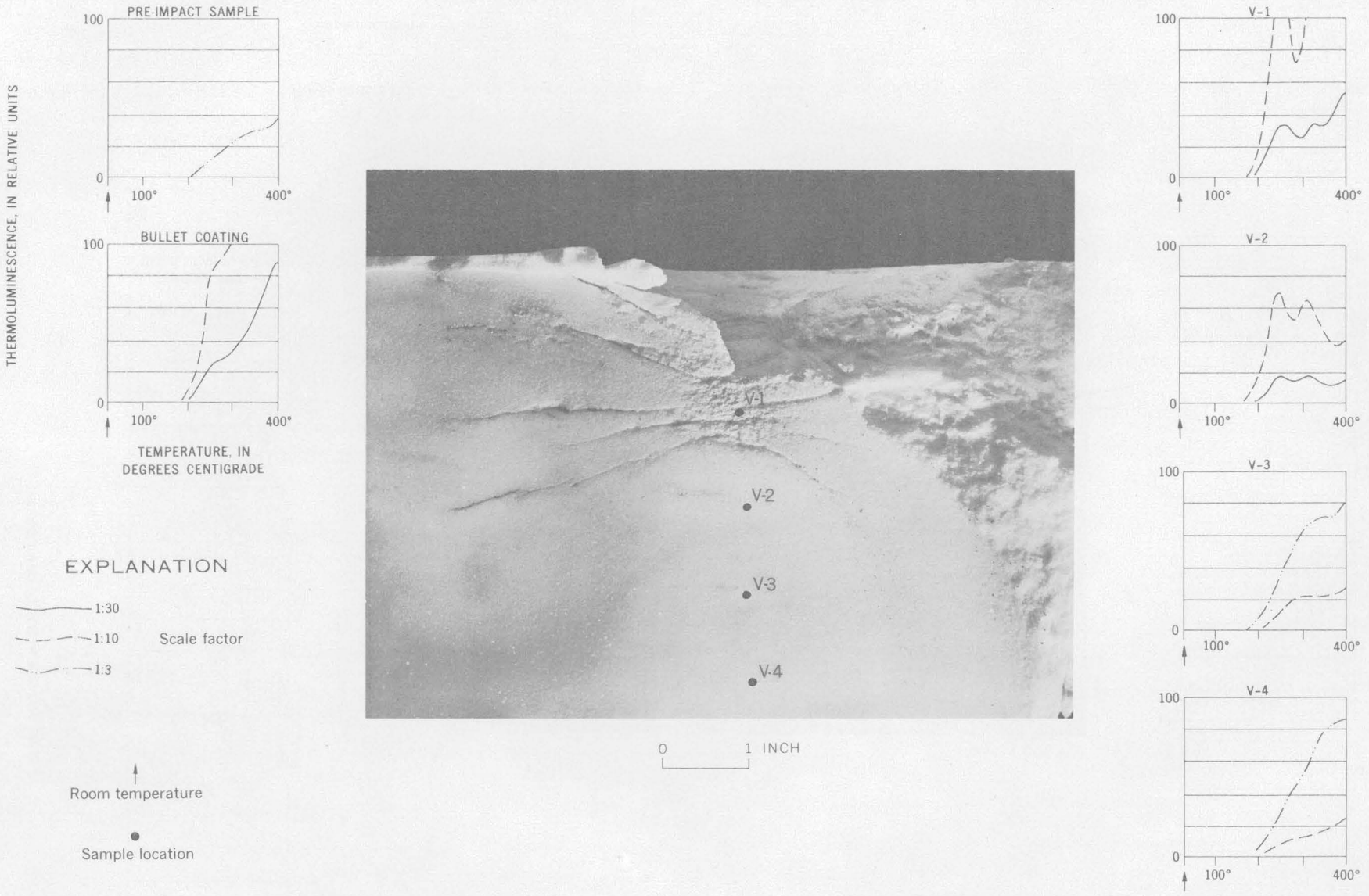

FIGURE 272.2.—Effects of impact on thermoluminescence of Yule marble in the direction of penetration of projectile.

The thermoluminescence was not completely destroyed in either the pre-impact sample or sample V-2 by preheating the samples to 400°C for 16 hours before obtaining their glow curves (fig. 272.3). This persistence of thermoluminescence is of interest because heating of samples at 400°C for less time has been considered standard treatment for completely destroying the thermoluminescence of any sample (Angino, 1959).

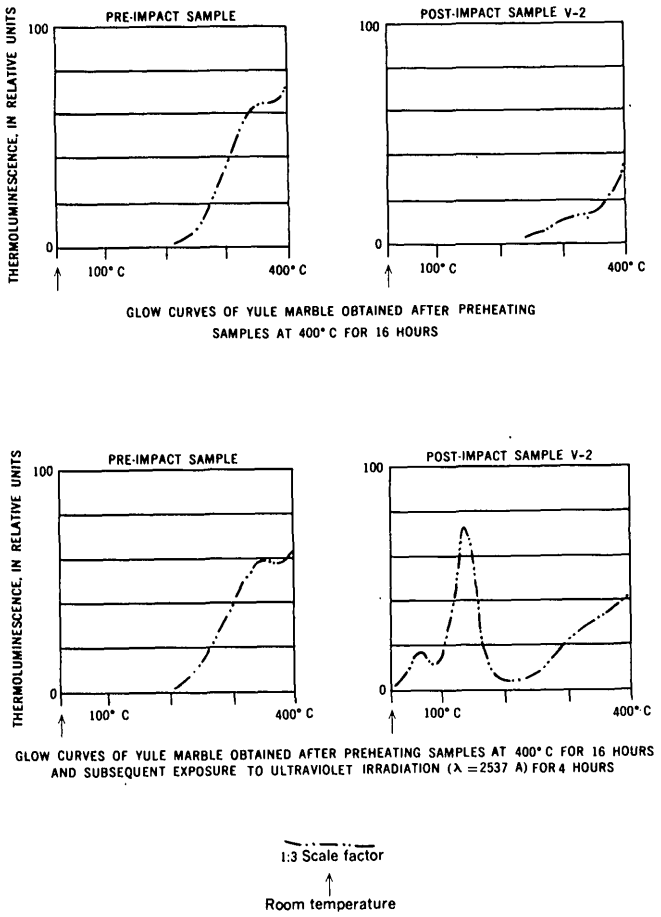

FIGURE 272.3.—Effects of preheating and short-wave ultraviolet irradiation on thermoluminescence of pre- and post-impact samples of Yule marble.

A comparison of selected calcite X-ray diffraction peaks of the bullet coating and pre-impact samples shows that the impact-produced shock caused changes in lattice structure of the calcite coating the bullet (fig. 272.5). The effect of the impact was to decrease the amplitude of the peaks and to dull or chop off some peaks. The shock produced by impact of the bullet in the Yule marble thus caused changes in the crystal structure of the calcite that may account for some of the observed changes in the thermoluminescence.

601530 O—61——23

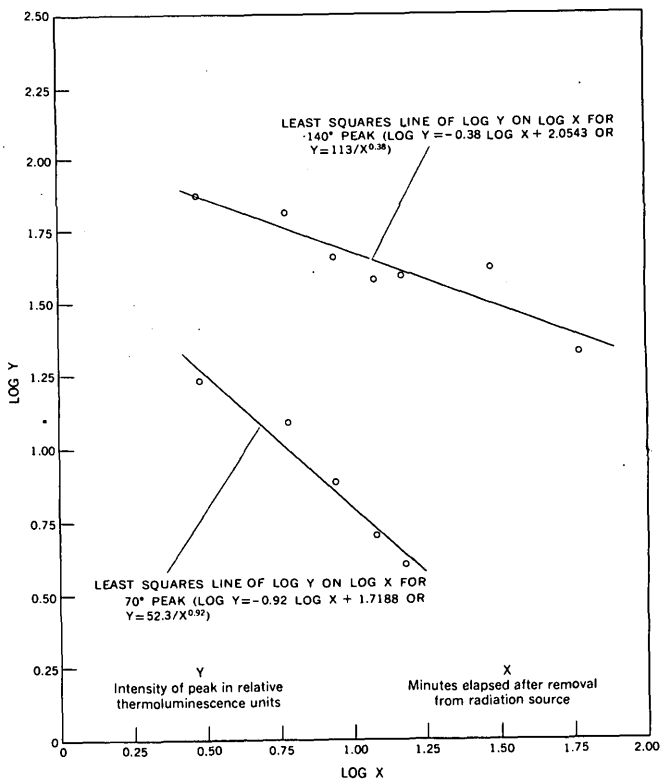

FIGURE 272.4.—Decay rate of ultraviolet-induced thermoluminescence peaks of post-impact sample V–2.

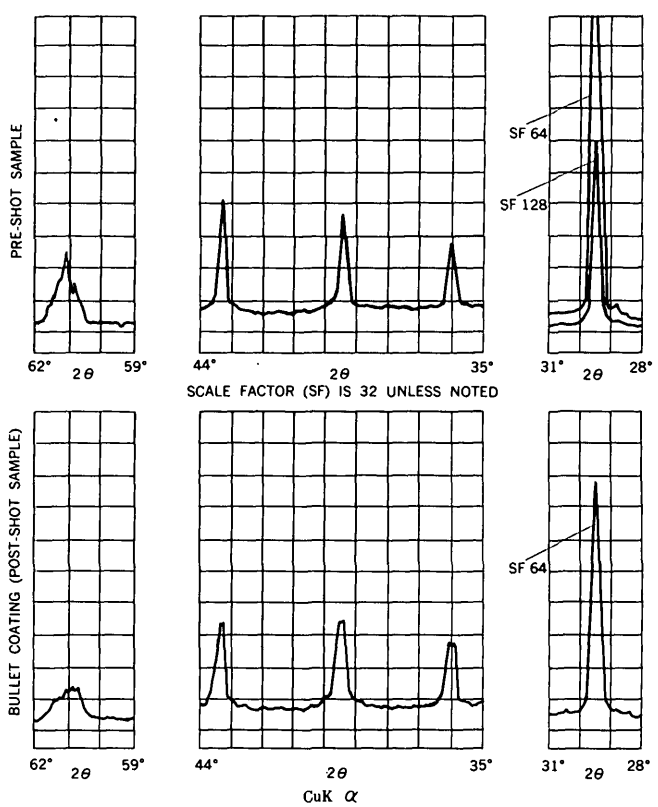

FIGURE 272.5.—Effects of impact on X-ray diffraction patterns of Yule marble.

REFERENCES

Angino, E. E., 1959, Pressure effects on thermoluminescence of limestone relative to geologic age: Jour. Geophys. Research, v. 64, no. 5, p. 569-573.

Balsley, J. R., 1941, Deformation of marble under tension at high pressure: Am. Geophys. Union Trans., v. 22, p. 519-525.

Griggs, D. T., and Miller, W. B., 1951, Compression and extension experiments on dry Yule marble at 10,000 atmospheres confining pressure, room temperature, pt. 1 *of* Deformation of Yule [Colo.] marble: Geol. Soc. America Bull., v. 62, p. 853-862.

Griggs, D. T., Turner, F. J., Borg, Iris, and Sosoka, John, 1951, Effects at 150°C, pt. 4 *of* Deformation of Yule [Colo.] marble: Geol. Soc. America Bull., v. 62, no. 12, p. 1385-1405.

Handin, J. W., and Griggs, D. T., 1951, Predicted fabric changes, pt. 2 *of* Deformation of Yule [Colo.] marble: Geol. Soc. America Bull., v. 62, no. 8, p. 863-885.

Knopf, E. F. B., 1949, Fabric changes in Yule marble after deformation in compression: Am. Jour. Sci., v. 247, p. 433-461, 537-569.

Lepper, H. A., Jr., 1941, Compression tests on oriented specimens of Yule marble: Am. Jour. Sci., v. 247, no. 8, p. 570-574.

Turner, F. J., 1949, Preferred orientation of calcite in Yule marble: Am. Jour. Sci., v. 247, no. 9, p. 593-621.

Turner, F. J., and Ch'ih, C. S., 1950, Note on survival of fabric characters in Yule marble after heating at 700°C: Am. Jour. Sci., v. 248, no. 5, p. 347-352.

———1951, Observed fabric changes due to deformation at 10,000 atmospheres confining pressure, room temperature, dry, pt. 3 *of* Deformation of Yule [Colo.] marble: Geol. Soc. America Bull., v. 62, no. 8, p. 887-905.

Turner, F. J., Griggs, D. T., and Ch'ih, C. S., 1950, Fabric of Yule marble deformed experimentally at ordinary temperatures in absence of water [abs.]: Geol. Soc. America Bull., v. 61, no. 12, pt. 2, p. 1512.

273. X-RAY POWDER DATA FOR HERZENBERGITE, TEALLITE, AND TIN TRISULFIDE

By Shirley Mosburg, Daphne R. Ross, Philip M. Bethke, and Priestley Toulmin 3d, Washington, D.C.

As a preliminary step in an investigation of the phase relations and crystallographic properties of phases in the system Pb–Sn–S, the X-ray powder diffraction data for synthetic SnS (herzenbergite), $PbSnS_2$ (teallite), and Sn_2S_3 (tin trisulfide) have been indexed. The three phases were prepared from the elements by heating in evacuated sealed silica tubes for several days. Synthesis temperatures were 600°C for SnS, 750°C for $PbSnS_2$, and 700°C for Sn_2S_3. Analyses of the lead and sulfur used are reported by Bethke and Barton (Art. 114, Prof. Paper 424–B). The tin used is standard sample 42e of the National Bureau of Standards; semiquantitative spectrographic analysis by K. V. Hazel revealed only the following impurities (in weight precent): iron, 0.003; silver, 0.001; copper, 0.001; nickel, 0.001; and vanadium, 0.0001.

The crystals of SnS and $PbSnS_2$ are platy and the crystals of Sn_2S_3 are acicular. Both of these habits cause preferred orientation of the materials on a diffractometer slide. No attempt was made to decrease preferred orientation as it does not affect the problem of indexing the materials. Because it does affect peak intensity, however, the intensities can be reported only approximately. All three materials, but particularly SnS and $PbSnS_2$, are malleable and have a tendency to smear when ground, resulting in poor resolution of the peaks. Therefore, SnS and $PbSnS_2$ were first ground to a size suitable for X-ray diffraction and then annealed in evacuated sealed silica tubes at 600° C for 2 hours and 24 hours, respectively, in order to improve their crystallinity. The diffractometer slides were then prepared without further grinding.

The indexing was accomplished by comparing observed and calculated $\sin^2\theta$ values for the reflections. The lower limit of observed 2θ was 5°. Observed $\sin^2\theta$ values were determined from reflections measured from a diffractometer chart made on a Norelco wide range diffractometer, using Ni-filtered CuK radiation (λ=1.54050A). Scanning speed was ¼° (2θ) per minute; chart speed was 30 inches per hour. The difference between observed and calculated $\sin^2\theta$ was then minimized by successive least squares approximations on well-resolved low-angle peaks, most of which had been measured against either fluorite or silicon as an internal standard. The uncertainty reported for the cell edge is the root mean square percentage deviation calculated from observed d-spacings of the peaks used in the final least squares analysis.

From Buerger precession photographs, D. R. Ross determined the unit cell of Sn_2S_3 to be orthorhombic with space group *Pnam* and approximate axes a=8.84A, b=14.02A, and c=3.71A. These values have been refined by powder measurements to a=8.79±.03A, b=14.02±.05A, c=3.74±.01A.

All reflections of SnS and $PbSnS_2$ can be indexed on the basis of Hofmann's earlier work (1935). Hofmann

TABLE 273.1.—*Indexed powder pattern of herzenbergite* (SnS)

[Spacings d_{hkl} calculated for unit cell in space group *Pbnm* with a=4.328±0.002A, b=11.190±0.004A, c=3.978±0.001A. Intensity ratio based on measurements of height above background]

$\frac{I \times 100}{I_{max.}}$	d_{hkl} A		hkl
	Observed	Calculated	
5	4. 036	4. 037	110
10	3. 421	3. 425	120
15	3. 243	3. 243	021
5	2. 929	2. 929	101
25	2. 831	2. 834	111
		2. 826	130
100	2. 793	2. 798	040
15	2. 305	2. 304	[1] 131
1	2. 123	2. 125	210
10	2. 024	2. 023	[1] 141
10	1. 988	1. 988	[1] 150
5	1. 874	1. 874	022
		1. 874	211
5	1. 778	1. 779	[1] 151
1	1. 721	1. 720	122
5	1. 713	1. 712	[1] 240
1	1. 694	1. 694	231
5	1. 689	1. 689	[1] 061
5	1. 622	1. 621	[1] 042
5	1. 454	1. 452	212
5	1. 451	1. 449	251
1	1. 403	1. 403	171
70	1. 399	1. 399	[1] 080
1	1. 320	1. 320	[1] 081
1	1. 286	1. 286	[1] 270
5	1. 262	1. 262	[1] 181
5	1. 195	1. 195	[1] 190
5	1. 145	1. 145	[1] 191
1	1. 084	1. 084	1·10·0
5	1. 081	1. 081	063
5	1. 078	1. 078	342
		1. 078	290
1	1. 041	1. 041	[1] 291
1	1. 025	1. 024	192
1	. 9741	. 9741	450
		. 9738	381
1	. 9613	. 9610	1·11·1
1	. 9521	. 9514	1·10·2
15	. 9326	. 9326	[1] 0·12·0
1	. 9238	. 9231	273
1	. 9212	. 9207	2·11·0
1	. 9082	. 9080	0·12·1
1	. 8892	. 8894	154
1	. 8887	. 889	2·10·2
5	. 8792	. 8793	[1] 283
5	. 8444	. 8444	0·12·2
		. 8443	1·13·0

[1] Reflections measured against fluorite internal standard and used in final least squares computation.

TABLE 273.2.—*Indexed powder pattern of teallite* ($PbSnS_2$).

[Spacings d_{hkl} calculated for unit cell in space group (*Pbnm* with $a=4.266\pm0.003$A, $b=11.419\pm0.007$A, $c=4.090\pm0.002$A. Intensity ratio based on measurements of height above background]

$\frac{I\times100}{I_{max.}}$	d_{hkl} A		*hkl*
	Observed	Calculated	
5	3. 993	3. 999	[1] [2] 110
10	3. 416	3. 417	[1] [2] 120
15	3. 327	3. 324	[1] [2] 021
5	2. 952	2. 951	[1] [2] 101
100	2. 856	2. 859	[1] 111
		2. 855	040
10	2. 334	2. 333	[1] [2] 131
1	2. 096	2. 097	210
10	2. 052	2. 052	[1] [2] 141
5	2. 014	2. 011	[1] 150
5	1. 861	1. 861	[2] 230
5	1. 8077	1. 8064	[1] [2] 151
1	1. 7551	1. 7546	122
5	1. 7390	1. 7379	[2] 160
5	1. 7250	1. 7254	[2] 061
1	1. 6926	1. 6936	231
5	1. 6620	1. 6622	[2] 042
		1. 4293	222
10	1. 4282	1. 4280	171
		1. 4274	080
2	1. 2161	1. 2162	[2] 190
1	1. 1719	1. 1704	082
5	1. 1663	1. 1665	191
		1. 1656	262
1	1. 1031	1. 1030	1. 10. 0
5	1. 1004	1. 0999	0. 10. 1
		1. 0997	233
1	1. 0536	1. 0537	291
1	1. 0457	1. 0453	192
1	0. 9793	0. 9796	124
		0. 9793	1. 11. 1
1	. 9707	. 9709	1. 10. 2
		. 9706	441
1	. 9520	. 9516	0. 12. 0
1	. 9340	. 9334	2. 11. 0
1	. 9271	. 9269	0. 12. 1
1	. 9060	. 9057	1. 12. 1
1	. 8630	. 8627	0. 12. 2
1	. 8606	. 8603	1. 13. 0
1	. 8421	. 8426	373
		. 8419	1. 13. 1

[1] Reflections measured against fluorite internal standard.
[2] Reflections used in final least squares computation.

TABLE 273.3.—*Indexed powder pattern of tin trisulfide* (Sn_2S_3).

[Spacings d_{hkl} calculated for unit cell in space group *Pnam* with $a=8.79\pm0.03$A, $b=14.02\pm0.05$A, $c=3.74\pm0.01$A. Intensity ratio based on measurements of height above background]

$\frac{I\times100}{I_{max.}}$	d_{hkl} A		*hkl*
	Observed	Calculated	
40	7. 003	7. 011	[1] [2] 020
75	5. 495	5. 481	[1] [2] 120
10	4. 433	4. 394	[1] [2] 200
100	4. 131	4. 126	[1] [2] 130
35	3. 740	3. 723	[1] [2] 220
15	3. 346	3. 344	[1] [2] 111
30	3. 257	3. 256	[1] [2] 140
25	3. 215	3. 201	[1] [2] 230
5	3. 095	3. 091	[1] [2] 121
25	2. 890	2. 921	[1] [2] 031
5	2. 859	2. 868	[1] [2] 310
		2. 849	201
15	2. 801	2. 792	[2] 211
35	2. 747	2. 740	[2] 240
45	2. 670	2. 672	[2] 150
5	2. 646	2. 640	[2] 221
5	2. 495	2. 482	[2] 330
5	2. 460	2. 455	[2] 141
20	2. 368	2. 364	[2] 250
5	2. 334	2. 337	[2] 060
25	2. 257	2. 259	[2] 160
		2. 248	[1] 340
10	2. 244	2. 244	051
5	2. 215	2. 211	[2] 241
10	2. 112	2. 097	420
		2. 069	331
10	2. 065	2. 063	260
10	2. 002	1. 999	[2] 251
10	1. 952	1. 953	[2] 170
		1. 934	[2] 161
10	1. 933	1. 927	341
		1. 878	411
5	1. 873	1. 871	002
5	1. 841	1. 827	360
		1. 756	431
5	1. 751	1. 753	080
		1. 744	510
5	1. 6568	1. 6535	[2] 370
10	1. 5813	1. 5808	[2] 511
5	1. 5616	1. 5620	181
10	1. 4771	1. 4802	[2] 470
		1. 3765	471
10	1. 3772	1. 3755	390
		1. 3746	352

[1] Reflections measured against silicon internal standard.
[2] Reflections used for final least squares computation.

determined the space group as *Pmcn*; we have chosen the alternate setting *Pbnm*, in agreement with the isostructural GeS (Smithells, 1955, p. 216–217). The axes have been refined as follows: SnS $a=4.328\pm.002$A, $b=11.190\pm.004$A, $c=3.978\pm.001$A; $PbSnS_2$ $a=4.266\pm.003$A, $b=11.419\pm.007$A, $c=4.090\pm.002$A.

Tables 273.1, 273.2, and 273.3 present the indexed powder patterns. For SnS, there are 143 additional permissible reflections in the range 5° to 140° 2θ, 98 of which are above 80° 2θ. For $PbSnS_2$ there are 159 additional permissible reflections in the range 5° to 140° 2θ, 105 of which are above 80° 2θ. For Sn_2S_3, there are 77 additional permissible reflections in the range 5° to 70° 2θ.

REFERENCES

Hofmann, Wilhelm, 1935, Ergebnisse der Strukturbestimmung komplexer sulfide: Zeitschr. für Kristallographie, v. 92, p. 161-185.

Smithells, C. J., 1955, Metals reference book, v. 1: London, Butterworths Scientific Pub., 531 p.

GEOLOGY AND HYDROLOGY APPLIED TO ENGINEERING AND PUBLIC HEALTH

274. DEFORMATION AND STRESS DISTRIBUTION AROUND COAL MINE WORKINGS IN SUNNYSIDE NO. 1 MINE, UTAH

By FRANK W. OSTERWALD, Denver, Colo.

Work done in cooperation with the U.S. Bureau of Mines

Ribs, floors, and roofs in the Sunnyside No. 1 mine, Utah, show evidence of premining and postmining deformation indicating that the coal and surrounding rocks are highly stressed.

Small deformational features in the mine, and the distribution and intensity of rock failures provide an insight into the stress distribution around the mine workings. These small features include fracture zones, joints, cleavage, curved shear fractures and faults in coal, faults and joints in rock, and deformed roof bolts, bent landing mats, broken crossbars, bent, broken, and tilted timbers, and bent track. Although the surface topography is rugged and coal is mined from depths as great as 2,500 feet, deformation (structural) features in the mine indicate that compressional deformation resulting from lateral stress components is greater than deformation from vertical stress (load). Tensional deformation of mine workings is clearly superficial and appears to result from components of the predominantly compressional stress. Deformation of workings strongly indicates high lateral stress, and the strong deformation of southeast ribs of slopes and northeast ribs of entries (fig. 274.1) indicates asymmetric stress distribution.

Most of the joints, cleavage, fracture zones, and faults in the ribs are of premining age because their orientation is closely parallel to that of the regional joint and fault pattern at the surface. Curved shear fractures commonly observed in ribs are of postmining age. Ribs are also deformed by movement of coal into the workings, commonly along contacts with shale above and coal below. Such contacts become shear planes along which coal is "underthrust" into openings. The top of the coal commonly is in contact with shale and other argillaceous rocks and slips much more readily than the bottom, which commonly is in contact with coarse-grained siltstone. Slight expansion of coal that is thrust into openings causes numerous tension fractures to form. If fracture zones are present, the expansion causes individual fractures to open slightly. The slow movement of coal, which is loosened because of expansion, produces many slivers and columns of coal that separate from ribs and fall into workings (fig. 274.2). Coal also moves into some workings by creep, which amounted to as much as 2 feet in 4 years as measured from roof bolts that are now covered by coal from the ribs (fig. 274.3). Some ribs bulge outward into the workings and buckle near the middle. Bulged and buckled ribs apparently result from friction between siltstone roofs and coal (fig. 274.6).

Deformation of floors commonly produces domes and anticlines in siltstone below the coal beds. Anticlines are as much as 100 feet long and have a structural relief of as much as 1 foot. Tension along the crests of some anticlines produced small cross fractures, some of which have as much as 2 inches vertical displacement (fig. 274.4) because of gravitational collapse of the crests. Cores of the domes and anticlines are commonly hollow, suggesting that the folds formed by slipping along bedding planes or along thin coal splits within the siltstones. High vertical compressional stress in pillars adjacent to workings probably produces lateral stress in the uppermost bed of the floor that causes upward folding.

Deformation of unsupported roofs, or of roofs supported lightly, commonly produces "synclines" that are parallel to the mine openings. Such "synclines" result from lateral components of compressive stress in the lowermost beds of the roof. Tensional components of stress along the troughs of the "synclines" commonly produce small fractures parallel to the mine workings. The fractures allow blocks of rock to loosen and to fall into the workings.

Deformation of roofs that are strongly supported by timber, crossbars, and roof bolts is different from that of lightly supported roofs. Such crossbars are commonly bent downward and snapped off (fig. 274.5). The bending and breaking are not the result of downward pressure, but of horizontal stress against the ends of the crossbars and against the rocks above them, thus forcing the timber and rocks downward into the openings. The breaks in some crossbars can be traced upward into shear fractures in the roof.

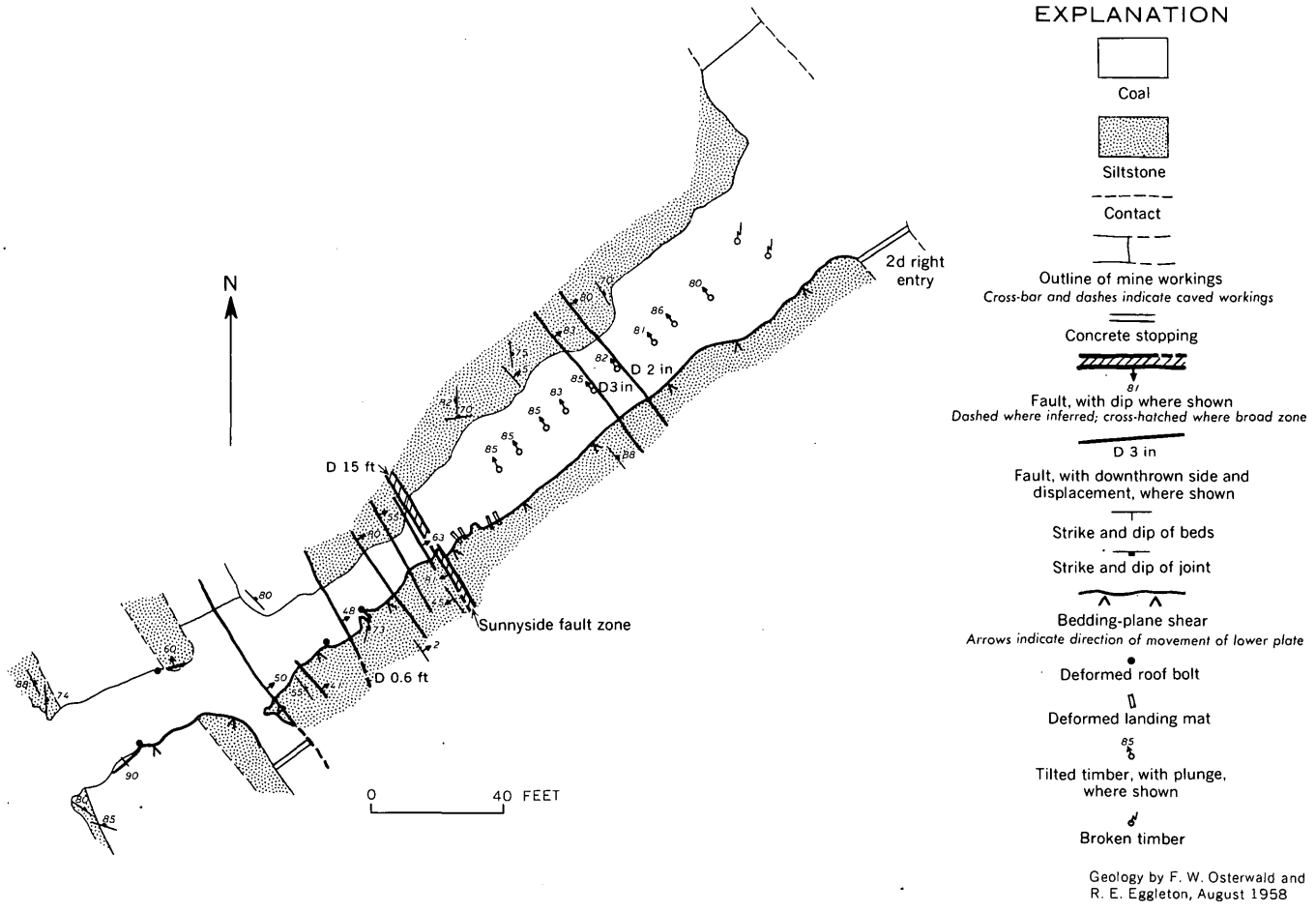

FIGURE 274.1.—Underground geologic map of right-hand air course at Sunnyside fault zone, main slopes, Sunnyside No. 1 mine, Utah. Plane mapped is roof.

Whenever an opening is made in a rock, the vertical load formerly supported by the removed rock is added to the adjacent rocks. Lateral stress formerly transmitted by the removed rock will be added to the rocks above and below the opening, and, in addition, lateral stress components of vertical stress cause strong deformation of ribs. The tensional deformation of workings in the Sunnyside No. 1 mine resulting from strong lateral and vertical compressive stress produces a narrow zone of reduced stress around mine workings similar to "yielded" or "destressed" zones observed in other mines (Holland and Thomas, 1954, p. 7–15; Spackeler, 1958, p. 316; Serata and Gloyna, 1960, p. 2981–2986). Analysis of observed directions of movement along shear planes indicates that inclinations of principal stress directions range from vertical in the roof to near 45° in the ribs (fig. 274.6). Although differing degrees of adhesion between coal and

FIGURE 274.2.—Arcuate slabs of coal in rib resulting from movement along curved shear fractures that flatten in dip upward and probably downward. Fracture zone striking into rib at high angle causes splinters, slabs, and columns of coal to separate and fall into working. Photograph by J. C. Witt.

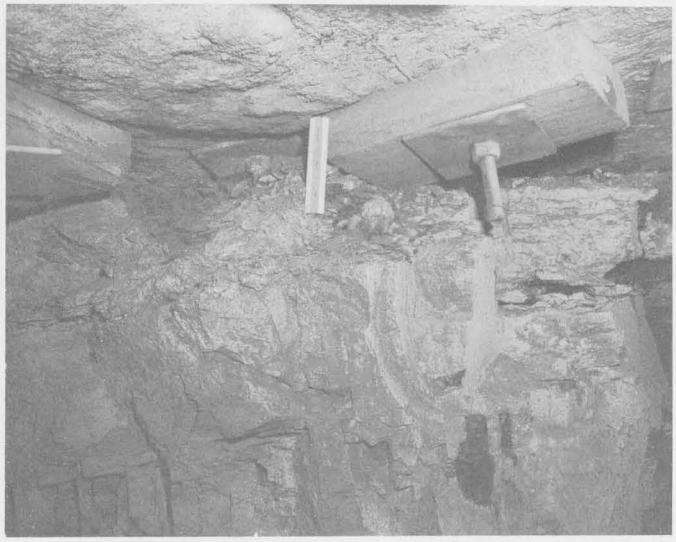

FIGURE 274.3.—Rib coal moving by creep into right-hand manway at first right entry, Sunnyside No. 1 mine, Utah. Coal is deforming and covering roof bolt to left of scale. Photograph by J. C. Witt.

FIGURE 274.4.—Floor anticline (heave) in thin-bedded siltstone in left-hand air course near main parting, Sunnyside No. 1 mine, Utah. Crest of anticline, marked by irregular longitudinal fault, trends obliquely to direction of mine working. Cross faults with as much as 2 inches of displacement cut crest. Photograph by J. C. Witt.

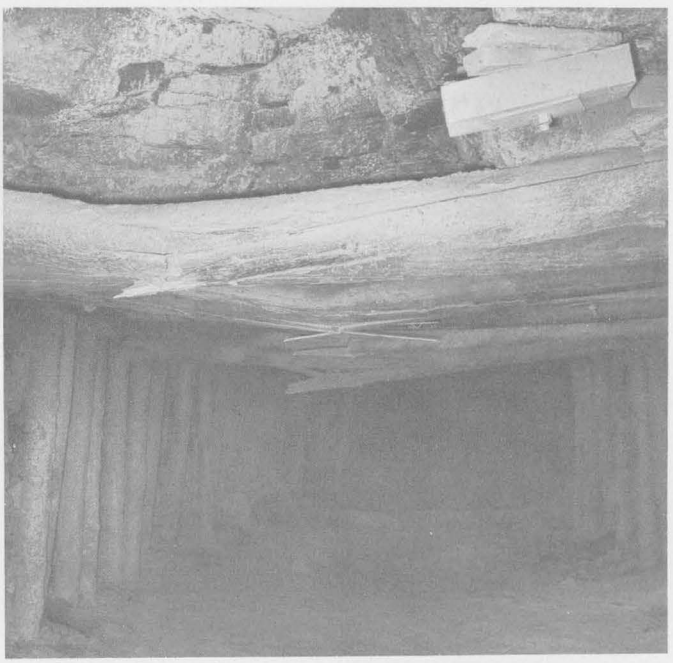

FIGURE 274.5.—Broken timber crossbars, in incoming air course, main slopes above main parting, Sunnyside No. 1 mine, Utah. Horizontal stress from ribs has broken timbers, and horizontal stress in roof created shear fracture in rocks above break in timbers. Another shear fracture extends upward in roof from intersection with left rib.

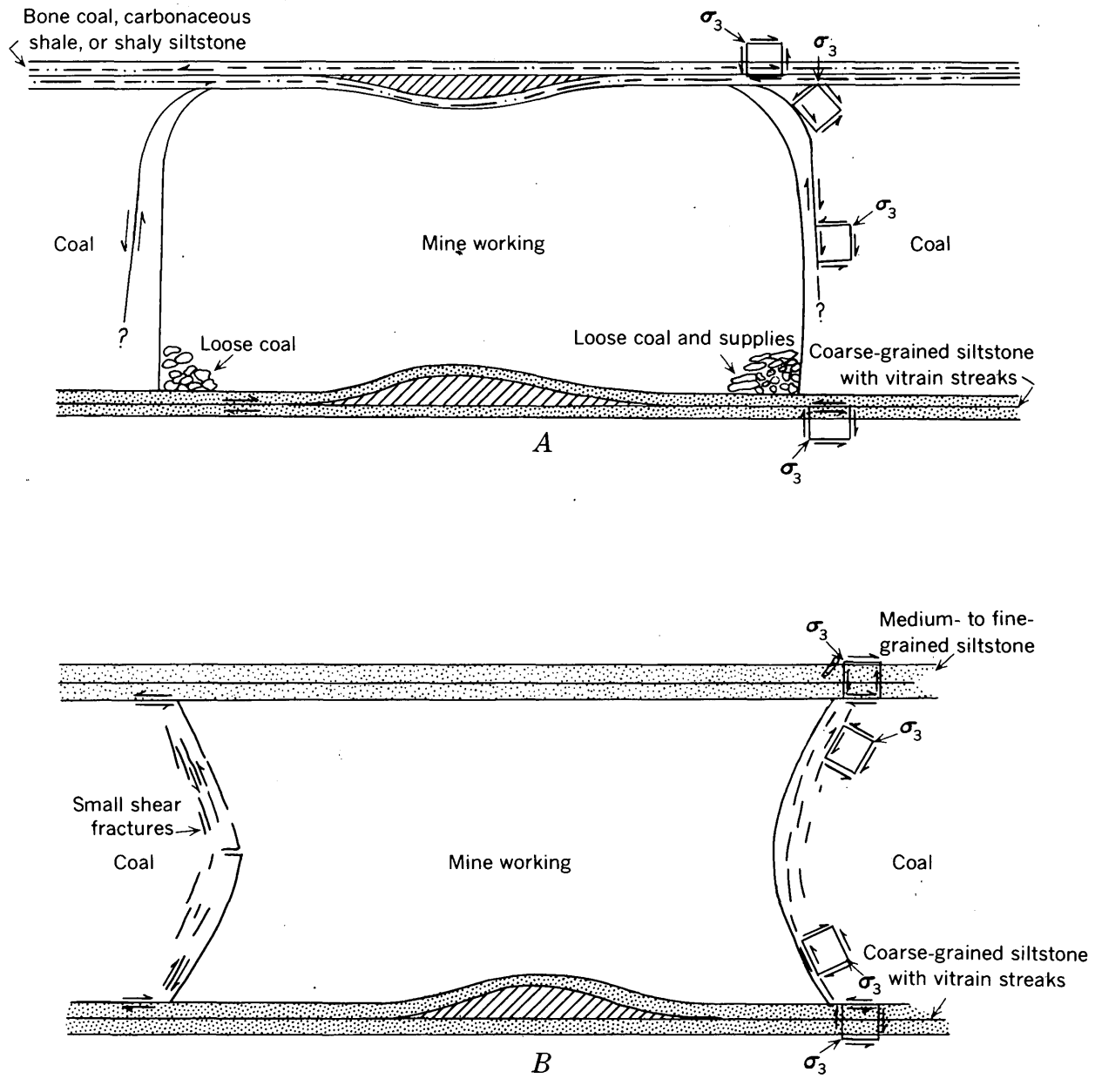

FIGURE 274.6.—Diagrammatic sections showing deformation and stress distribution around workings in Sunnyside No. 1 mine, Utah. Diagonally lined areas are hollow. *A*, Roof synclines, floor anticlines, curved shear fractures, and resolution of principal stress components (σ_3, where coal slips along clayey roof but adheres to coarse-grained siltstone floor. *B*, Bulged and buckled ribs where coal adheres to roof and floor.

floor causes differences in the type of deformation observed in ribs, orientations of stress components are the same (fig. 274.6). Because lateral stress causes roofs to act as prestressed beams (Corlett and Emery, 1959), roof control measures should be adequate to resist both the movement of coal and rock into mine openings and the superficial tensional deformation due to bending in order to preserve the beams. Thus the rocks themselves can support much of the superincumbent load.

Geologic examination of small deformational features in mines will reveal what types of deformation are present and will permit the stress distribution around openings to be predicted. Mining engineers can take advantage of such geologic features for more effective design of mine layouts and artificial supports.

Studies of deformation in salt mines enabled Dellwig (1958) to suggest remedial measures for buckling of floors. Studies of postmining deformation should aid similarly in the designing of many other kinds of underground openings.

REFERENCES

Corlett, A. V., and Emery, C. L., 1959, Prestress and stress redistribution in rocks around a mine opening: Canadian Mining Metall. Bull., v. 52, p. 372-384.

Dellwig, L. F., 1958, Flowage in rock salt at Lyons, Kansas: Kansas Geol. Survey Bull. 130, p. 166-175.

Holland, C. T., and Thomas, Edward, 1954, Coal-mine bumps; some aspects of occurrence, cause and control: U. S. Bur. Mines Bull. 535, 37 p.

Serata, Shosei, and Gloyna, E. F., 1960, Principles of structural stability of underground salt cavities: Geophys. Research Jour., v. 65, p. 2979-2987.

Spackeler, Georg., 1958, Observations on the distribution of stress around coal and salt workings: Akad. Wiss., Berlin, Section für Bergbau, [Internat. Strata Control Cong., 1958, Leipzig, English translation p. 305-319].

275. HYDROLOGIC EFFECTS OF URBAN GROWTH—SOME CHARACTERISTICS OF URBAN RUNOFF

By Arvi O. Waananen, Menlo Park, Calif.

The concentration of two-thirds of our population in urban and suburban areas, and the accelerated development of suburban centers and strip cities with associated improvement in highways gives rise to growing concern about storm drainage from those areas.

Hydrographs of runoff from natural areas reflect the influence of topographic characteristics, geology, vegetation, infiltration and percolation, evaporation and transpiration, land use, and related hydrologic and meteorologic factors. The physical changes associated with urban growth modify the surface characteristics and drainage patterns. As a result, the timing, intensity, and distribution of runoff, and the shape of the flood hydrograph are affected. The effects on individual storm-drainage systems may be evaluated using procedures and data now available. Few data are available, however, to define cumulative impact of urban growth on downstream receiving channels and streams.

The impact of urban development on streamflow is demonstrated in figure 275.1, which presents runoff hydrographs of Onondaga Creek at two locations in Syracuse, N. Y. These hydrographs demonstrate runoff characteristics evident in records for many streams flowing through developed areas. Records for the Dorwin Avenue gage (drainage area, 88.9 square miles) at the southern edge of the city define characteristics of runoff from a predominantly rural area. Runoff at the Temple Street gage 4.9 miles downstream (from stage records collected by the Syracuse City Engineer's Office) is affected by drainage from substantial areas of development in the city. The drainage area at the Temple Street gage is approximately 103 square miles, but the actual area contributing storm runoff is not known. High flows from 68.1 square miles of the drainage basin have been regulated since 1949 by Onondaga Reservoir (18,200 acre-feet capacity) on Onondaga Creek at Nedrow, N.Y.

The sharp peak at the Temple Street gage preceding the usual flood peak from upstream illustrates a significant characteristic of urban runoff. Short-duration, high-intensity summer storms (such as those that occur in central New York), may in urban areas cause sharp flood peaks that are considerably higher than flood peaks generally in the basin. The hydrograph of the flood of August 1953, for example, indicates an urban flood peak of 860 cfs, as contrasted to only 132 cfs from upstream flows. Although individual flood peaks vary in magnitude, the average of 16 peaks representing urban runoff in Syracuse was nearly three times greater than the average of corresponding peaks representing regulated flow from Onondaga Reservoir plus natural storm runoff between the reservoir and Syracuse. These runoff events were the result of summer storms during the period 1952-1958. The increase in runoff at the Temple Street gage during the storm periods appeared to be greater than the amount normally attributable to the intervening area and reflects differences in overland flow, retardation, depres-

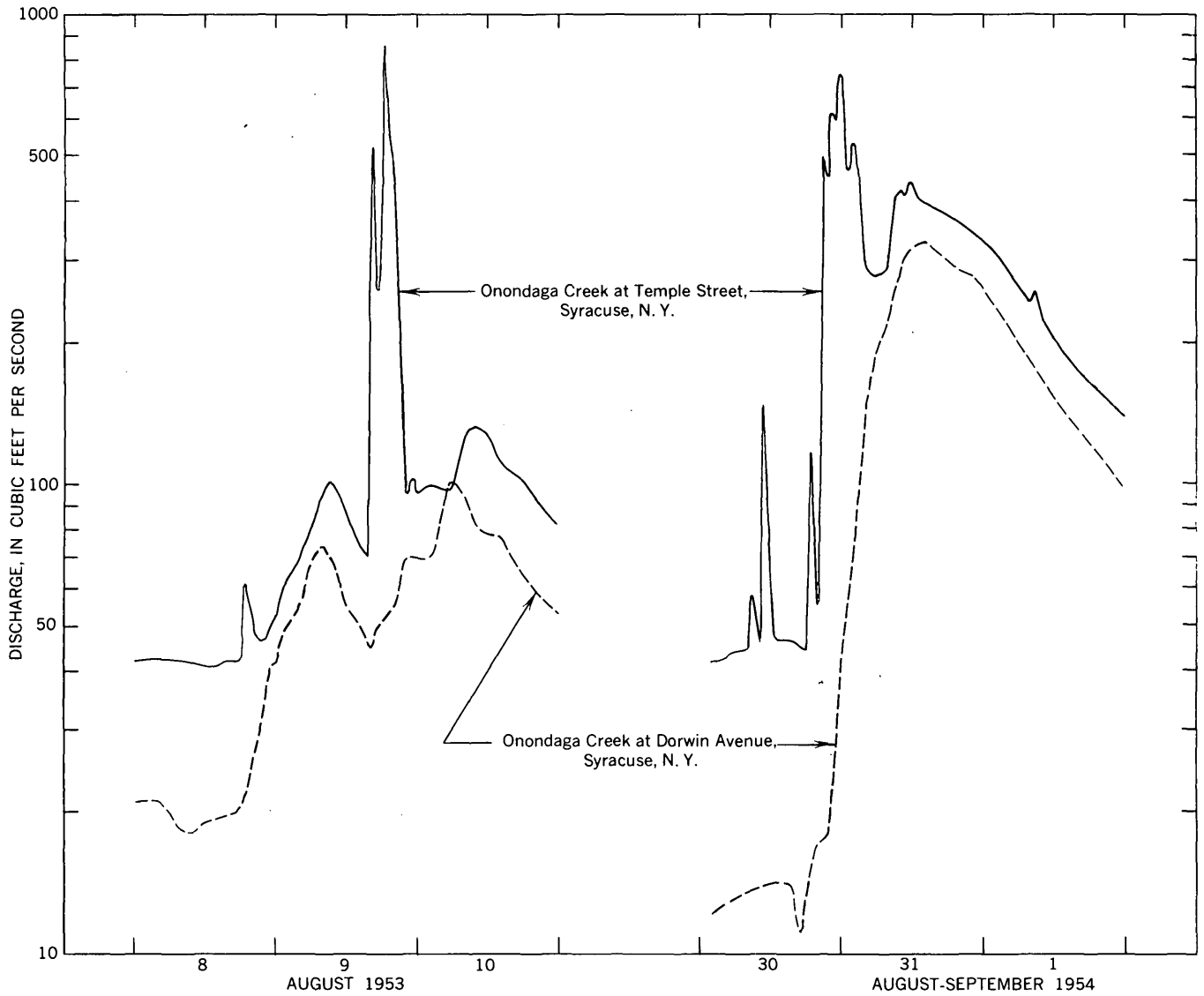

FIGURE 275.1.—Hydrographs of storm runoff in Onondaga Creek basin, Syracuse, N.Y., comparing flows at the Dorwin Avenue and Temple Street gages during storms of August 8 to 10, 1953, and August 30 to September 1, 1954.

sion and subsurface storage, and seepage, a result of urbanization.

The principal floods in Onondaga Creek usually result from substantial and sustained basin-wide rainfall. Urban runoff from such storms usually is nearly proportional to basin runoff. Maximum discharge at the Dorwin Avenue gage during the period 1951 to 1959, for example, was 1,960 cfs on January 22, 1959 (probably about two-thirds of the unregulated peak). An unregulated peak flow of 3,980 cfs occurred December 30, 1942 at a former gage on Onondaga Creek (drainage area, 98.2 square miles) 2.2 miles downstream. Although these peaks exceed those from local runoff, the accelerated and rapid runoff from urban areas following thunderstorms creates significantly large peaks and raises the magnitude of floods of a given frequency.

Available records for streams that drain natural and urbanized areas in northern New Jersey, Michigan, Pennsylvania, and Virginia indicate that peak runoff from developed areas on the average is three to four times those from upstream or adjacent natural areas.

The degree of change may be illustrated further by several examples. Tholin and Kiefer (1959), in their computation of urban runoff at Chicago using the "Chicago Hydrograph Method", show that industrial and commercial areas may produce flood peaks up to 3½ to 4 times greater than those from single-family residential suburban areas. Ramey (1959), in his

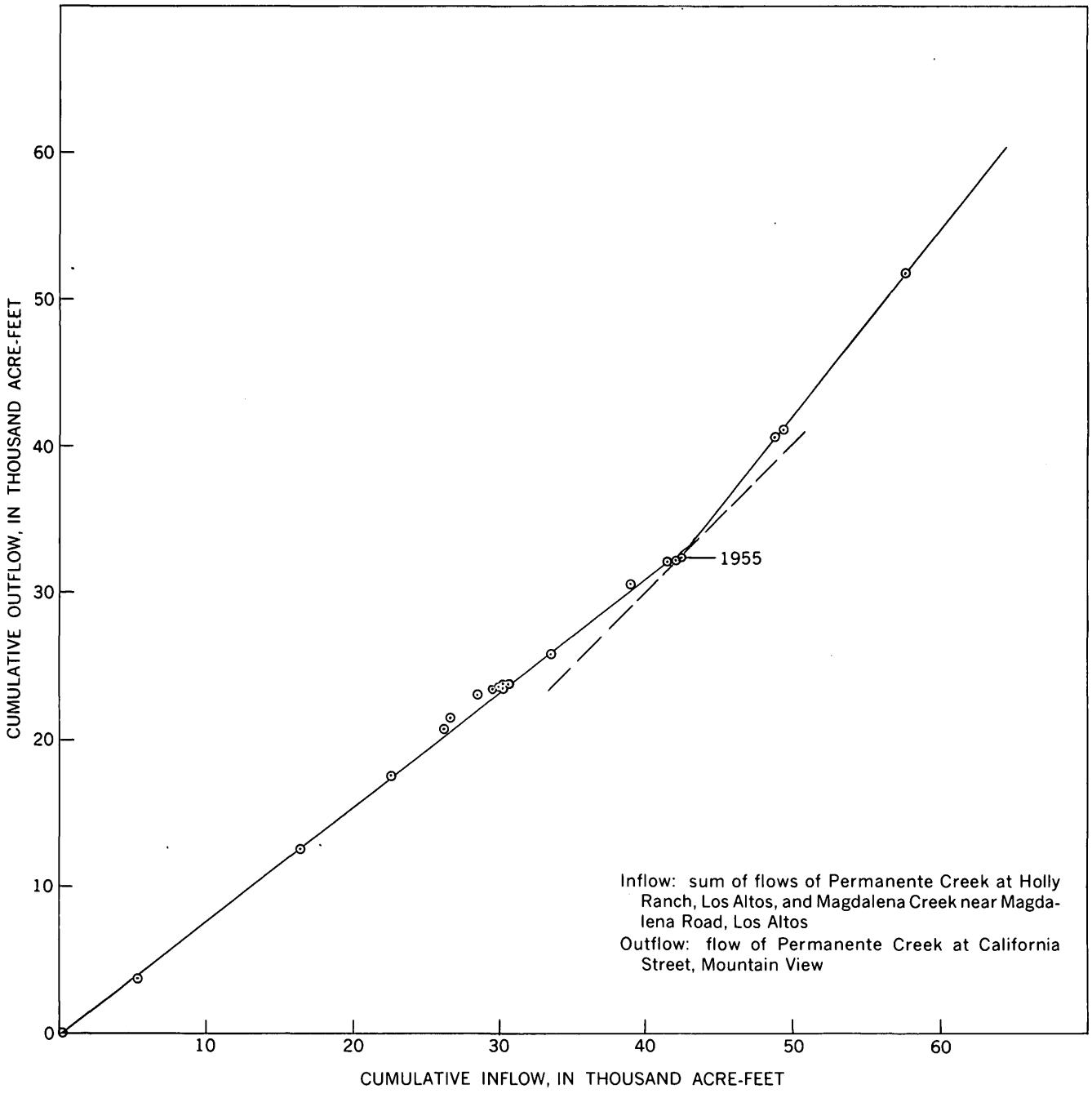

FIGURE 275.2.—Double-mass curve of inflow and outflow, Permanente Creek basin, Los Altos and Mountain View, Calif., 1939–58, comparing inflow (the sum of flows of Permanente Creek at Holly Ranch, Los Altos, and Magdalena Creek near Magdalena Road, Los Altos) with the outflow, Permanente Creek at California Street, Mountain View.

analysis of flows in the Chicago Drainage Canal states, "* * * in the Chicago area, within the past 30 years the runoff, from one cause or another, has increased two and a half times", and reports that several floods exceeding 25,000 cfs occurred since 1948 in a canal originally designed to carry 10,000 cfs. The Bigwood and Thomas (1955) formula for determination of mean annual discharge of floods in Connecticut is $Q_M = C_B A S$ in which A is the effective area, S the basin slope, and C_B the watershed coefficient. C_B is only 0.85 for the state as a whole, but it is 3.0 for urban-residential areas.

Urban development thus may affect flood flows substantially. It has been postulated that the annual runoff from developed areas should not differ materially from that occurring before development. The timetable for runoff, however, differs significantly. A substantial part of the flow from urban areas will occur during a short period following the storm, primarily as overland flow to streets, gutters and sewers that discharge promptly into the receiving channels and streams. The quick runoff reduces evaporation and transpiration opportunity, as well as infiltration and percolation.

Figure 275.2 illustrates a change in runoff characteristics following urban development. A double-mass curve of inflow and outflow in a portion of the Permanente Creek basin in Los Altos and Mountain View, Calif., in which ground-water recharge occurs, based on records obtained by the Santa Clara Valley Water Conservation District during the period 1939-1958, shows a sharp change in the relationship in 1955. Intensive urban residential development took place in the intervening area between 1953 and 1955 and is continuing. The physical changes include installation of streets, gutters, other paved areas, and short storm sewers discharging into Permanente Creek. Outflow from this recharge reach was only 76 percent of the inflow during the period 1939-1955, but increased to 123 percent of the inflow during 1956-1958, thus demonstrating the change in the relationship of infiltration, recharge, and local runoff since 1955.

A few other appropriate streamflow records indicate increases in total runoff from developed areas. Analysis of mean annual flows in Connecticut, using the same parameters as for the flood-flow formula, indicates coefficients of 0.017 for normal and 0.036 for urban areas in the formula $Q_A = C(AS)^{1.2}$, or a twofold increase.

There is a paucity of information about urban runoff characteristics. A few studies by federal, state, and local agencies of urban flood hydrology are underway, including the project of the Geological Survey in San Francisquito Creek basin at Menlo Park, Calif., for evaluation of hydrologic changes as lands are converted from rural to urban residential use.

REFERENCES

Bigwood, B. L., and Thomas, M. P., 1955, A flood flow formula for Connecticut: U.S. Geol. Survey Circ. 365, 16 p.

Ramey, H. P., 1959, Storm water drainage in the Chicago area: Am. Soc. Civil Engineers Proc., v. 85, HY4, Paper 1995.

Tholin, A. L., and Kiefer, C. J., 1959, The hydrology of urban runoff: Am. Soc. Civil Engineers Proc., v. 85, SA2, Paper 1984.

276. ENGINEERING GEOLOGY AND THE CHILEAN EARTHQUAKES OF 1960

By Ernest Dobrovolny and Richard W. Lemke, Ashland, Ky., and Denver, Colo.

Work done in cooperation with the Chilean Instituto de Investigaciones Geologico

The authors spent most of the month of July 1960 doing geologic investigations of the cities of Concepcion, Valdivia, and Puerto Montt. During this time they worked closely with geologists of the Chilean Instituto de Investigaciones Geologico and with other geologists of the U.S. Geological Survey stationed in Chile. This paper incorporates the work of all these geologists.

REGIONAL EARTHQUAKE EFFECTS

Earthquakes of high magnitudes shook southern Chile in May and June 1960. The first shock, of magnitude 7.5 (Richter scale), occurred May 21. The main shock, of magnitude approximately 8.5 (Duke, 1960) and epicenter south of Lebu (Pierre St. Amand, written communication), came May 22 at 3:15 p.m. local time. Other significant shocks occurred as late as June 20. Depth of focus of the shocks was about 50 km (Duke, 1960). Highest intensities, reaching XI on the Mercalli scale, were along the coast from Lebu to south of Ancud (St. Amand, 1960).

Surface faulting attributable to the earthquakes was not observed, although altitude changes, probably due to movement along a north-trending pre-existing fault zone, occurred along the coast. In the vicinity of Lebu the land rose 1½ m; from Puerto Saavedra to south of Ancud (fig. 276.1) the coast sank 1 to 2 m (St. Amand, 1960). Landslides, debris flows, fissures caused by lateral displacement, liquification of deposits, and subsidence resulting from compaction were common. Large landslides of glaciofluvial and lacustrine deposits dammed the outlet of Lake Rinihue.

A tsunami followed the major shock; waves 10 m high (St. Amand, 1960) swept the shoreline in the vicinity of Ancud causing great loss of life. The tsunami traveled across the Pacific Ocean at nearly 500 mph reaching Hilo, Hawaii about 14 hours later where it caused much loss of life and property (Murata, 1961). Disastrous effects reached as far as Japan.

Volcano Puyehue started a flank eruption on May 24. It threw cinders, ash, vapor, and gas for several weeks, terminating in an eruption of a small quantity of viscous lava (Pierre St. Amand, oral communication).

About 4,000 people were killed by the earthquakes and tsunami (Duke, 1960). Property damage, estimated at about $400 million, was particularly high in the cities of Concepcion, Valdivia, and Puerto Montt.

EARTHQUAKE EFFECTS IN CONCEPCION

Concepcion, a city of about 40,000 people on the north side of the Bio Bio River, is built mostly on Quaternary alluvium about 30 m thick (Galli O. and Sanchez R., 1960), on terraces of sand, clay, silt and gravel, and on artificial fill. Hills composed of marine and continental sediments of Cretaceous or Tertiary age locally project through the alluvium. Granitic rocks of Jurassic or Cretaceous age and metamorphic rocks of Paleozoic age underlie low hills along the edge of the city.

Earthquake intensities were between VIII and IX on the Mercalli scale (Duke, 1960; Watanabe and Karzulovic, 1960). Ground motion of the May 21 shock was north-south; the May 22 shock movement was first north-south and then east-west (Fred K. Coleman, oral communication).

A direct relation between ground conditions and amount of damage to buildings was not demonstrable from field studies in this city. There is, however, a direct relation between damage and the kind of material that was used in construction. This relation was scaled for many types of building materials (Galli O. and Sanchez R., 1960). Reinforced concrete buildings generally sustained little or no damage whereas adobe buildings or brick buildings with mud mortar and tile roofs sustained almost complete to complete damage. Wooden buildings sustained little damage even where located on alluvium or artificial fill. Concrete roadbeds on artificial fill, such as the approach to the bridge over the Bio Bio River, however, were fractured and differentially displaced.

The earthquake shocks caused landslides in surficial materials, differential compaction in alluvial deposits and artificial fill, and eruption of water, sand, and mud from fissures. The landslides were generally small. Local differential compaction in alluvial deposits and in artificial fill was estimated to be as much as 40 cm; however, the total regional amount of settlement of the alluvium due to compaction is unknown (Galli O. and Sanchez R., 1960). Water, sand, and mud erupted from fissures in tidal flats and cultivated fields near the mouth of the Bio Bio River; ridges and cones of

sand as much as 10 cm high and 5 to 70 cm across were formed (Segerstrom, 1960).

EARTHQUAKE EFFECTS IN VALDIVIA

Valdivia, a city of about 60,000 persons, lies on both sides of the estuary of the Rio Calle Calle, which has its principal source in Lake Rinihue. The city is built on alluvium and eolian deposits of Tertiary and Quaternary age as much as 150 m thick. Metamorphic rocks of undetermined age underlie these deposits (Watanabe and Karzulovic, 1960, p. 52).

FIGURE 276.2.—Street in Valdivia showing destruction of houses built on artificial fill and alluvium.

Highest shock intensity in the city was X on the Mercalli scale on May 22 (Duke, 1960). Ground motion was undulatory and slow; there was no unanimity of opinion as to the direction of the movement (Doyel, Moraga B., and Falcon M., 1960).

Principal effects and resulting damage to man-made structures of the earthquake shocks were settlement of the land surface as much as 2 m below mean sea level along the estuary of the river in the city, fracturing and differential settlement in Quaternary deposits and artificial fill, and slumping. Settlement and resulting damage caused by compaction of artificial fill and alluvium in an abandoned watercourse are illustrated on figure 276.2. Slumping and associated fracturing of Quaternary deposits and artificial fill occurred along the banks of the Rio Calle Calle (fig. 276.3). Evidence of faulting was not observed. Subsidence appears to be due to both tectonic down-warping and to compaction of unconsolidated materials. The amount attributable to either cause cannot be determined until first-order levels are rerun.

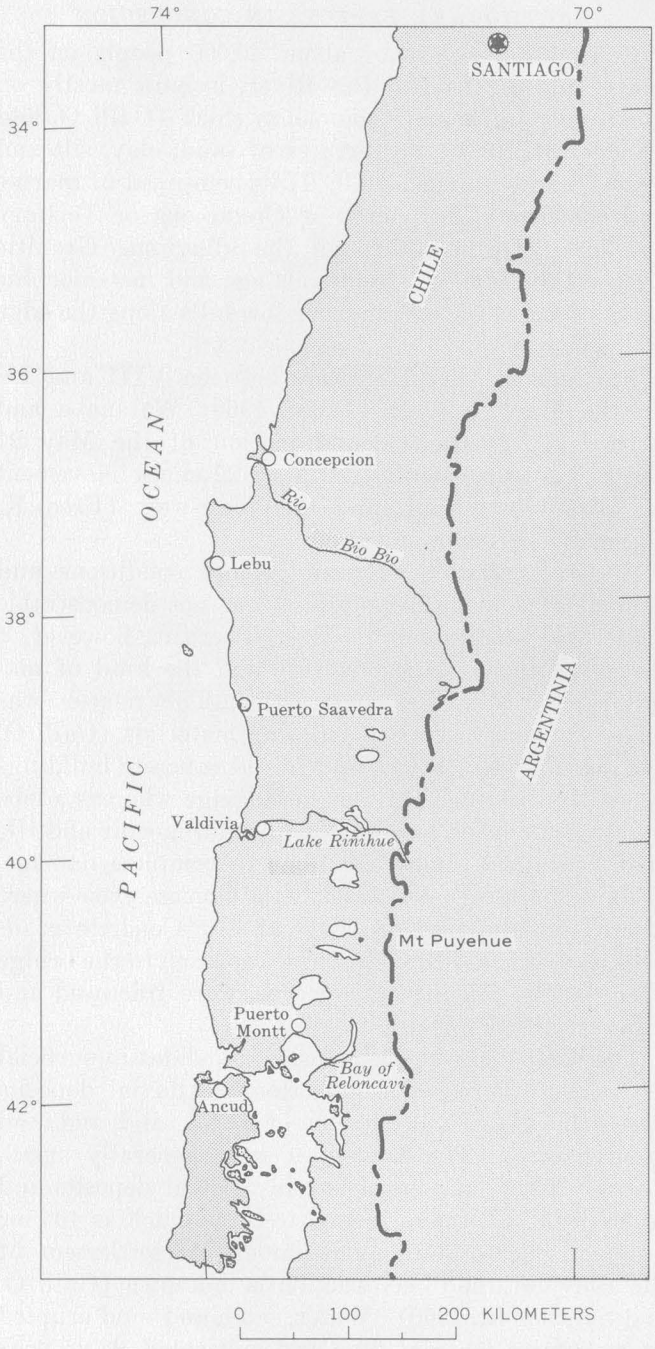

FIGURE 276.1.—Index map of southern Chile.

EARTHQUAKE EFFECTS IN PUERTO MONTT

Puerto Montt, a city of approximately 33,000 persons, lies on the north edge of the Bay of Reloncavi. No bedrock is exposed in the city. Stratified glacial deposits of sand and gravel, more than 30 m thick, form steep cliffs and well-defined terraces that flank the bay in most places.

The residential part of the city lies mostly on two terraces at altitudes of 45 m and 107 m; the business district is built mostly on alluvium, debris flows, and artificial fill along the bay shoreline. Thinly stratified glaciolacustrine silt and clay are locally exposed un-

FIGURE 276.3.—Street in Valdivia showing results of slumping and fracturing in underlying Quaternary deposits and artificial fill.

derlying the glaciofluvial deposits in the southwest part of the dock area. End moraines roughly rim the city.

Maximum shock intensities in the city ranged from VII on the two terrace levels to XI in areas underlain by artificial fill (Pierre St. Amand, oral communication). Ground motion reportedly was a slow rocking movement. No tsunami was produced in the bay.

Ground effects of the earthquakes were expressed by surficial fractures, landslides and debris flows, and slumping on steep hillsides. Man-made structures built on artificial fill, alluvium, and colluvium were most heavily damaged. Those built on outwash in broad terraces and on till in end moraines were least damaged.

The dock area, underlain by artificial fill consisting of gravel, sand, brick, wood, and muck, possibly as much as 4 m thick, was heavily damaged. Here numerous fractures and scarps, with vertical displacements of as much as 1 m, were formed by subsidence due to differential compaction and to lateral displacement.

Three conspicuous landslides and debris flows were triggered by the earthquakes in the city. The largest, involving mostly fine to medium sand, moved rapidly down a steep slope of a terrace 45 meters high and formed a toe of debris several meters thick. A second debris or mud flow, originating in a debris flow active in 1957, swept across two city blocks and destroyed all houses in its path with loss of life. Open fractures in the deposits at the head of the slide scarp indicate that additional sliding can be expected. The third and smallest slide originated in colluvial material along a steep terrace scarp.

Many small fractures showing displacement of material downslope were formed along colluvial covered terrace scarps. Had the ground been saturated at the time of the major earthquake, as it is during the rainy season, these incipient slides might well have become destructive landslides or mudflows.

REFERENCES

Doyel, W. W., Moraga B., A., and Falcon M., E., 1960, Relaciones entre la geologia de Valdivia (Chile) y los danos causados por los terremotos del 22 de Mayo de 1960 [informe preliminar]: Santiago de Chile, Inst. de Inv. Geologicas, 15 p.

Duke, C. M., 1960, The Chilean earthquakes of May 1960: Science, v. 107, p. 1797-1802.

Galli O., C., and Sanchez R., J., 1960, La geologia y los effectos de los terremotos de Mayo de 1960 en Concepcion y alrededores [informe preliminar]: Santiago de Chile, Inst. de Inv. Geologicas, 22 p.

Murata, K. J., 1961, Vigil for disaster: GeoTimes, v. 5, no. 5, p. 12-13.

St. Amand, Pierre, 1960, South Chile earthquake swarm of 1960 [abs.]: Geol. Soc. America Bull., v. 71, no. 12, pt. 2, p. 1964.

Segerstrom, Kenneth, 1960, Eruption of water, sand, and clay resulting from the earthquake of May 21, 1960, near Concepcion, Chile [abs.]: Geol. Soc. America Bull., v. 71, no. 12, pt. 2, p. 1972.

Watanabe, Takeo and Karzulovic, Ivan K., 1960, Los movimientos sismicos del mes de Mayo de 1960 en Chile *in* Anales de la Facultad de Ciencias Fisicas y Matemáticas: Univ. de Chile, Pub. 14, v. 17.

277. EFFECT OF TUNNEL CONSTRUCTION ON FLOW OF SPRINGS AND SMALL STREAMS IN THE TECOLOTE TUNNEL AREA OF SANTA BARBARA COUNTY, CALIFORNIA

By S. E. Rantz, Menlo Park, Calif.

Work done in cooperation with Santa Barbara County Water Agency

The effect of the construction of Tecolote Tunnel in southern Santa Barbara County, Calif., on the flow of springs and spring-fed streams in the vicinity of the tunnel has been evaluated by monthly measurements of discharge at 125 places in the area from late 1948 to 1961. Construction of the tunnel began in March 1950 and was completed in January 1956. By late 1951 water was seeping into the tunnel at a rate of 9 cubic feet per second. An analysis of the effect of tunnel construction on discharge is complicated by the occurrence of the Arvin-Tehachapi earthquake on July 21, 1952, and the Refugio brush fire in early September 1955.

The earthquake, whose epicenter was located 65 miles northwest of Tecolote Tunnel, abruptly increased the flow at 18 measuring sites. Because the earthquake occurred in July during the usual summer drought, the increase in discharge was strikingly noticeable. At 15 of the 18 sites, the increased discharge continued for several months, and at the other 3 sites it continued for several years. It is doubtful that the earthquake had any permanent effect on recharge areas or on the permeability of any of the aquifers. The increase in discharge was most likely due to disturbance of the unconsolidated material in the discharge areas, resulting in the clearing of existing ground-water outlets and the opening of new ones.

The Refugio brush fire of September 1955 may have caused an increase in the summer flow of springs and streams because of decreased evapotranspiration, but the evidence is inconclusive. The possibility of such an increase, however, adds a complication to the task of interpreting the discharge data.

Many complex and interrelated factors influence the discharge of springs and spring-fed streams and make it difficult to isolate the effect of the tunnel on the flow. A complicating element, also, is the short period of record before construction of the tunnel. This calibration period was only 3 years, 1948 to 1951, during all 3 of which the precipitation was deficient. At all but one spring, discharge was greater in the years after 1951 than in the preceding 3 years. Available data concerning water quality and water temperature, however, are helpful in evaluating the effect of tunnel construction.

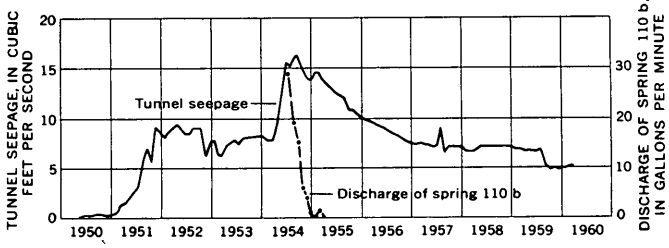

FIGURE 277.1.—Hydrographs of seepage into Tecolote Tunnel and discharge of spring 110b.

Seepage appeared in the tunnel a month after excavation began. When the tunneling progressed into areas of faults, inflow into the tunnel increased sharply and reached a peak of 16.7 cfs in September 1954. Seepage has more or less steadily declined ever since. Figure 277.1 shows the discharge hydrograph of seepage; the irregular shape of the graph indicates the effect of grouting, which was used in an effort to control the seepage. The tunnel inflows were under a static head of about 500 feet, and water temperatures were as high as 113°F. These high temperatures may be a result of heating along active faults in the area, or may be an indication that the flows originate at considerable depth. The great volume of water discharged seems to indicate that a large underground water reservoir had been tapped. The chemical quality of the water and the decline of inflow into the tunnel strongly suggest that the ground water is meteoric in origin.

For the flow of a spring to be adversely affected by the tunnel, both the spring discharge and the tunnel inflow would have to be supplied from the same aquifer. To determine positively the existence of a common aquifer for both flows is very difficult, but sufficient evidence shows that one spring, designated as spring 110b, was affected by construction of the tunnel. Spring 110b, now dry, is about 1.8 miles east of the tunnel. Its water was chemically similar to water that seeped into the tunnel and dissimilar to water discharged from the other springs in the area. The tunnel seepages are predominantly sodium waters, whereas the springs other than spring 110b, discharge

calcium waters. Hardness, fluoride concentration, and the presence of sulfides were also similar in the waters discharged by spring 110b and the seepage into the tunnel. Water temperatures at spring 110b ranged from 105°F to 112°F, equaling the water temperatures observed in the tunnel; at the other springs and streams the temperature ranged from 45°F to 75°F. Although the elevation of spring 110b is 400 feet above the tunnel, tunnel inflows were under a static head of about 500 feet, thus making it possible that both spring and tunnel are supplied from the same aquifer.

The flow of spring 110b was first measured in July 1954 and a discharge of 29 gallons per minute was observed. The discharge receded rapidly, as shown on figure 277.1, and by March 1955 the spring was dry. Although springs and streams in the area normally show little time lag between precipitation and discharge, spring 110b was not recharged by precipitation in the following years. All evidence indicates that the failure of spring 110b was a result of seepage into Tecolote Tunnel. Construction of the tunnel seems not to have affected the flow of any other spring or stream.

278. INFLUENCE OF NATURAL FRACTURES ON THE SHAPE OF EXPLOSION-PRODUCED CRATERS

By D. D. Dickey and Ross B. Johnson, Denver, Colo.

Work done in cooperation with the U.S. Atomic Energy Commission

Explosion-produced craters in basalt and alluvium at the Nevada Test Site, Nye County, Nev., show that natural (preexplosion) fractures in the rock influence the shape of the craters and the pattern of ejecta. Five small craters in basalt, each made by the detonation of 1,000 pounds of high explosive, and three large craters in basalt, each made by the detonation of 40,000 pounds of high explosive, were mapped to determine the geologic factors affecting the size and shape of the craters and ejecta patterns. Control of the crater shape and the pattern of ejecta by preexplosion fractures are especially evident in the small craters. The cratering experiments were performed by the Sandia Corp. on Buckboard Mesa in the northwestern part of the test site.

Buckboard Mesa is capped by 50 to 200 feet of nearly flat lying olivine basalt of probable Quaternary age. Although the basalt is cut by only one fault, it is extensively jointed. The joints seem to be randomly oriented at most places on the mesa. Many joints are arcuate or wavy. Dip of the joints ranges from horizontal to vertical, but straight and slightly arcuate joints less than 50 feet long that dip from 75° to 90° are most common. The basalt is black and dense, and has a uniform chemical composition. Vesicles make up as much as 20 percent by volume of the upper 2 or 3 feet of the rock but generally make up less than 2 percent below 3 feet. Locally some of the vesicles are partly or completely filled by calcite.

The influence of fractures on cratering is clearly shown in craters 8 and 11 (fig. 278.1). The craters were formed by detonation of spherical charges of high explosive weighing 1,000 and 40,000 pounds, and centered at depths of 15 and 25.5 feet, respectively.

The maximum depth of crater 8 below the original surface is 9.4 feet, and maximum width is 45 feet. Conspicuous nearly vertical joints that form much of the north and south edges of the crater are coated with caliche and obviously existed before the explosion. The long dimension of the crater roughly parallels the direction of these joints, and ejecta are sparse in the directions parallel to the joints. The long narrow area covered by ejecta north of the crater is oriented nearly normal to the strike of the joint along the south rim. The size and shape of the ejecta-covered area that extends north of the crater apparently were controlled by the joint on the south rim, and by the spatial relation of the joint to the explosive charge.

Crater 11 (fig. 278.1) has a maximum width of 115 feet and a maximum depth of 24.8 feet below the

601530 O—61——24

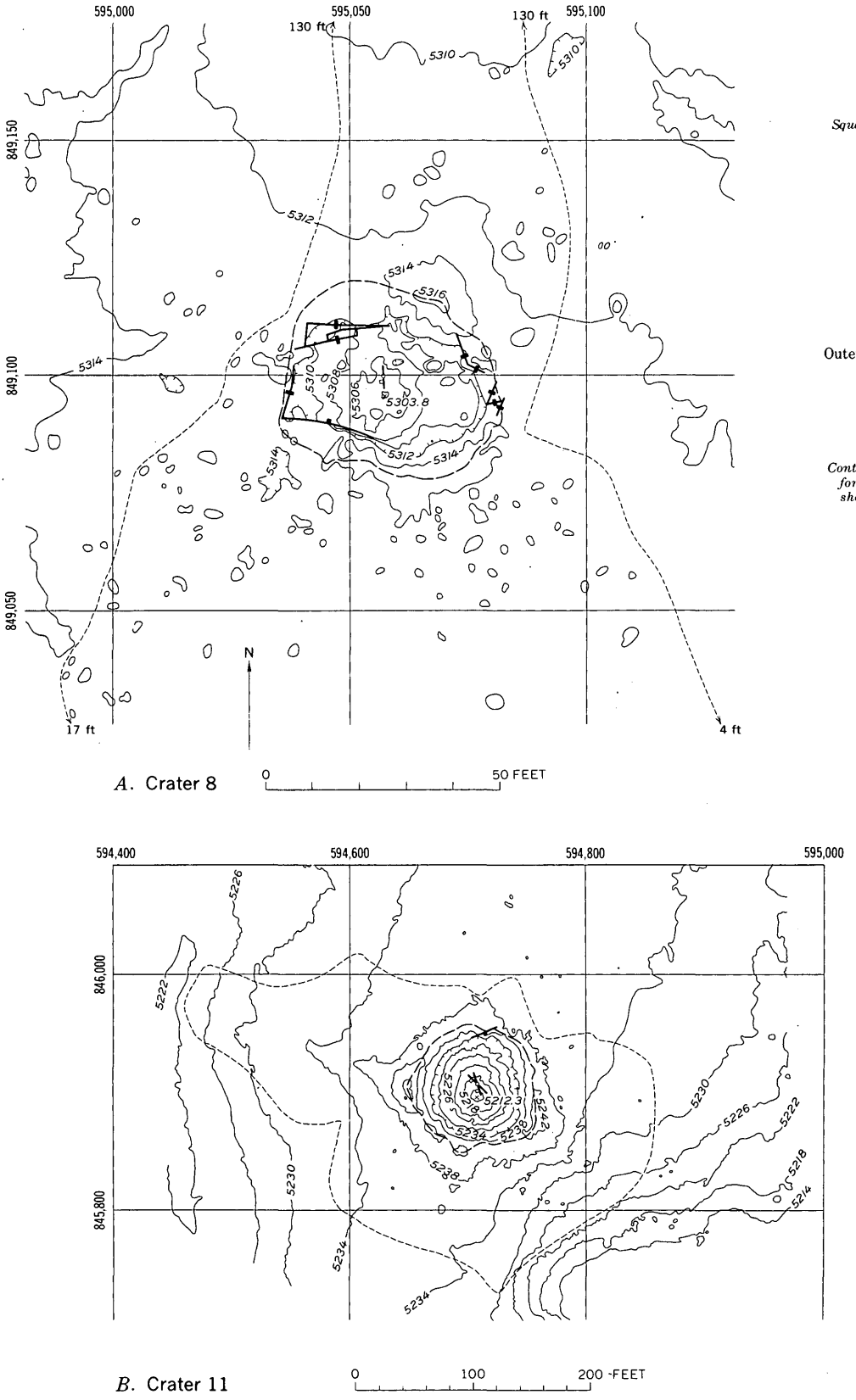

EXPLANATION

Dominant pre-explosion joints mapped in drill hole
Square shows direction of dip; circle shows position of drill hole

Post explosion surface joints

Crest of crater rim

130 ft
Outer limit of area mostly covered by ejecta
Number indicates distance in feet to farthest limit

5310
Topographic contours
Contour interval 2 feet for Crater 8 and 4 feet for Crater 11. Datum is sea level. Hachures show depression

FIGURE 278.1.—Maps of craters 8 and 11, Nevada Test Site.

FIGURE 278.2.—Meteor Crater, Ariz. Photograph by Army Air Service.

original surface of the mesa. The overall shape of crater 11 is more circular than that of crater 8. The crater rim locally parallels preexplosion joints for as much as 10 feet. The ejecta pattern, as shown on figure 278.1, is elongate to the northwest; however, the pattern is more nearly circular than the ejecta pattern for crater 8 and suggests less control by joints. Crater 11 is so large and encompasses so many randomly oriented joints that a nearly circular crater formed.

The influence of fractures on crater shape and ejecta distribution is also apparent at Meteor Crater, Ariz. (fig. 278.2). This crater is about 400 feet deep, 4,000 feet across, and is "square" in plan. The shape apparently was controlled by two strong regional joint sets (Shoemaker, 1959) that are oriented parallel to the diagonals of the "square".

Presumably a crater produced by an explosion in homogeneous material would be circular and have a circular distribution of ejecta. Explosion-produced craters in unjointed alluvium are circular. In structurally anisotropic rocks, however, the distribution of energy from an explosion is controlled by physical discontinuities such as fractures. Fractures act as reflectors and attenuators of kinetic energy, and therefore the greatest amount of energy is transmitted in those directions which intersect the fewest fractures. This results in removal of more material in these directions. The "square" shape of Meteor Crater can be explained by this process. The shape of crater 8 on the other hand was largely controlled by a few large fractures limited to the immediate crater area.

In large-scale excavations produced by explosion cratering, the structural anisotropy of the rocks may be an economically important factor. Adequate knowledge of the natural fractures could aid in predicting the shape of the crater and the distribution of ejecta, or artificially crested fractures could be used to control these effects of cratering.

REFERENCE

Shoemaker, E. M., 1959, Impact mechanics at Meteor Crater, Arizona: U.S. Geol. Survey open-file report.

EXPLORATION AND MAPPING TECHNIQUES

279. NEW EQUIPMENT FOR MEASUREMENTS IN THE UNSATURATED ZONE

By R. W. STALLMAN and R. P. MOSTON, Denver, Colo.

Field applications of even the simpler equations of isothermal liquid flow in the unsaturated zone (Richards, 1931) have not been made on any significant scale. This lack of application may be ascribed partly to a lack of instrumentation for field measurement of the flow variables. Most instruments now in field use have been developed through agricultural research wherein interest has been centered on qualitative measurements to depths of only a few feet. Of the equipment now available, only the nuclear probe devices (Stone and others, 1955) for measuring moisture content and bulk soil density, and thermistors or thermocouples for measuring temperature, seem to fit the broader requirements in hydrology for reasonably accurate measurement at greater depths. Standard laboratory techniques, such as the use of the manometer for measuring liquid head (a tensiometer in soils parlance), have very limited application be-

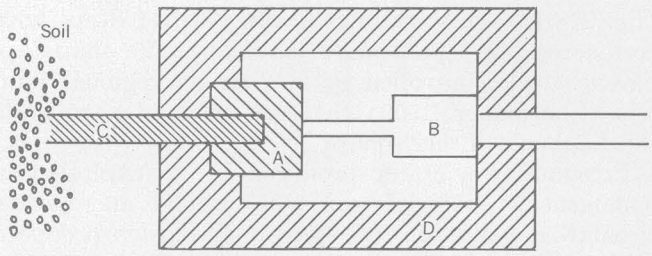

FIGURE 279.1.—Schematic diagram of an electrical tensiometer. *A*, sensor; *B*, transducer; *C*, flexible wick; and, *D*, rigid support frame.

cause of placement or reading difficulties under field conditions.

Liquid heads in the unsaturated zone range from zero to several atmospheres and are negative with respect to atmospheric pressure. Measurements of negative heads with a liquid column are impossible above one atmosphere, and generally are impracticable above 0.5 atmosphere. Use of head-indicating devices based on other than manometric principles is required. In a search for a suitable device, preliminary tests have been made using the concept illustrated in figure 279.1. The liquid phase comes into equilibrium with a sensor material, *A*, through a flexible porous wick, *C*. Material *A* is an annulus of wood which swells appreciably with increased content of liquid, and causes displacement of the sensing arm of transducer *B*. The form of electrical measurement depends upon the type of transducer used; for example, one might measure a change in resistance or a change in elapsed time between pulses.

A system like the one shown in figure 279.1 would have the advantage of easy installation at great depths. With the use of available transducers, however, the overall accuracy will be limited to less than 1 percent of full range. Hysteresis effects due to the sensor material *A* have not yet been evaluated.

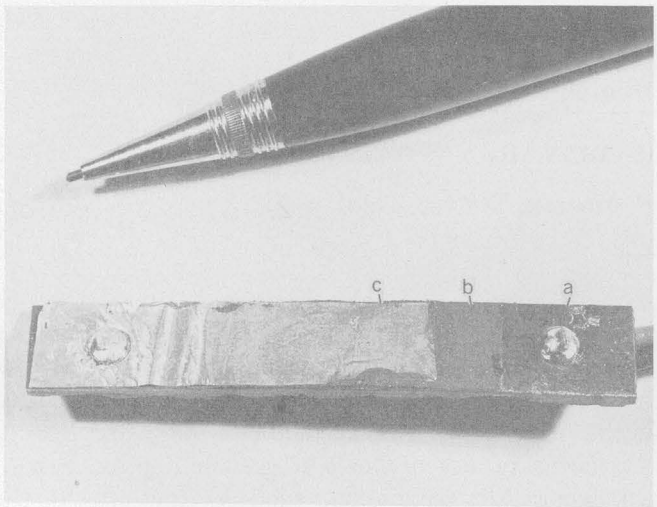

FIGURE 279.2.—Test strip using Celab: *a*, first conductor; *b*, Celab; *c*, second conductor.

Pronounced hysteresis effects in standard transducers, which are due largely to loose mechanical coupling between the sensed and sensing elements, have prompted a search for materials which would reduce or eliminate defective coupling. A "paint" that changes resistance as pressure is applied is now being studied for possible use as the transducer of figure 279.1. A test strip, made for observing the electrical characteristics of the paint, is shown in figure 279.2.

The pressure-sensitive paint used is sold by Clark Electronic Laboratories, Palm Springs, Calif., under the registered trade name Celab. The test strip shown was prepared by painting Celab on one conductor bonded to phenolic, drying at room temperature for 48 hours, wetting with a second coat of Celab over which the second conductor was pressed lightly, and curing at room temperature for about 30 days. Changes in resistance of the test strip observed in the laboratory under atmospheric conditions over a short period of time are shown at the top of figure 279.3. The sensitivity to pressure changes was not great enough to ascribe the resistance fluctuations noted to atmospheric-pressure fluctuations; and, because the period of observation was short, effects due to temperature changes were small. The results from this test strip indicate that the Celab paint has an inherent instability over short periods of time. However, other tests have shown that stability can be improved by high-temperature cures at a cost of decreased sensitivity. Short-period fluctuations of resistance can be smoothed by adding electrical capacity in parallel with the resistive paint. Figure 279.3 also shows that Celab cured at room temperatures has resistance versus current characteristics nearly identical with those of commercial elements commonly referred to as varistors. Resistance increases markedly with decreased current. This relation increases the problem of attaining stability and reproducible measurements in the field.

Direct measurement of vapor content in comparatively dry soils is a prerequisite to evaluation of the role of vapor movement in the unsaturated zone. Electrical hygrometers, "borrowed" from climatology, have been used for this purpose (Fukuda, 1955). However, after a few hours in the highly humid pore space, they become ineffective because the thin element film is contaminated or partly washed off (Wexler and others, 1955). The thermocouple described by Monteith and Owen (1958) for measuring dewpoint depression seems more promising for vapor-content

determinations. The Humistor, produced by Conrad-Carson, Inc., San Diego, Calif., is a device which changes resistance markedly in a changing environment of any gas or vapor having a strong dipole moment. The Humistor is reported to have a temperature coefficient of zero over the range 0–100° C and, according to the manufacturer, can be cleaned without affecting its calibration by heating to a cherry red in a clean flame. A sample Humistor is shown in figure 279.4, and a characteristic curve of humidity versus electrical resistance is shown in figure 279.5. Its small size, purported durability and stability, and high sensitivity qualify the Humistor element as a prospect for extensive application in unsaturated zone measurements; particularly because the usual soil gases, with the exception of water vapor, have a very weak or no dipole moment. The Humistor could easily be installed underground because of its small size, and its present cost is only $10. Preliminary tests indicate that each element will require individual calibration. Detailed and closely controlled tests of these elements are being set up currently by W. N. Palmquist and the junior author in the U.S. Geological Survey's Hydrologic Laboratory, Denver, Colo.

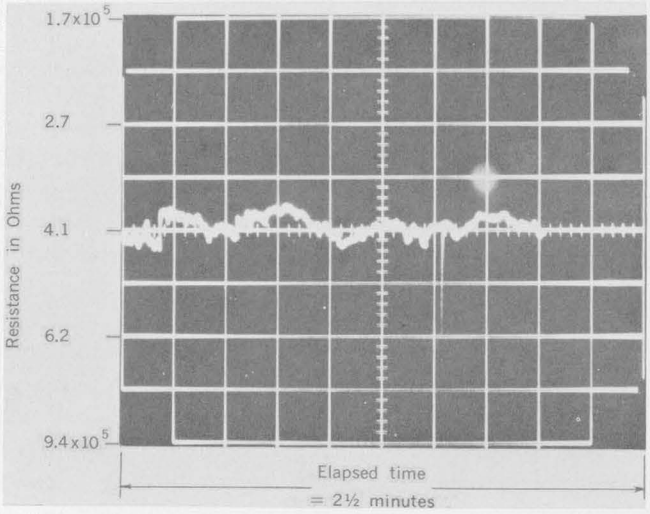

FIGURE 279.3.—Electrical characteristics of Celab. Top, resistance versus time; bottom, resistance and voltage versus current.

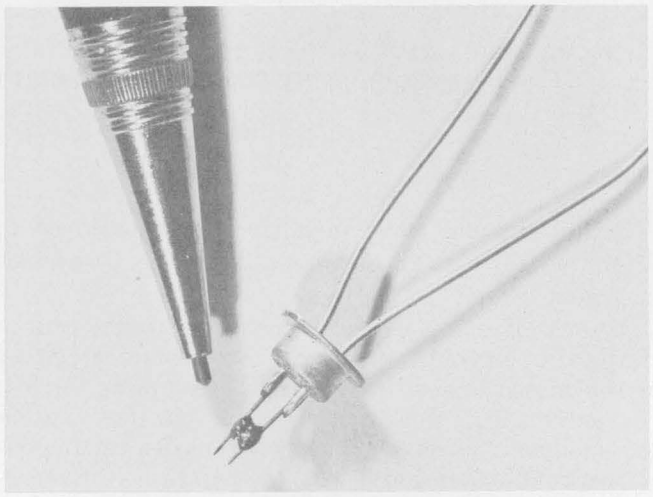

FIGURE 279.4.—The Humistor.

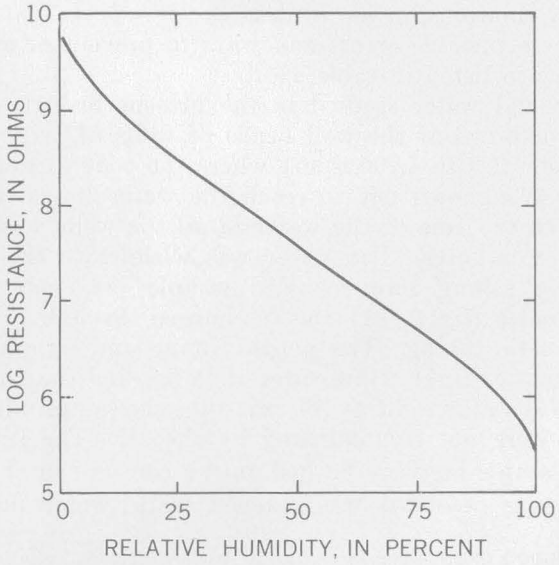

FIGURE 279.5.—Resistance of the Humistor versus relative humidity in clean air.

REFERENCES

Fukuda, Hitoshi, 1955, Air and vapor movement in soil due to wind gustiness: Soil Sci. v. 79, p. 249-256.

Monteith, J. L., and Owen, P. C., 1958, A thermocouple method for measuring relative humidity in the range 95-100%: Jour. Sci. Instr., v. 35, p. 443-446.

Richards, L. A., 1931, Capillary conduction of liquids through porous mediums: Physics, v. 1, p. 318-333.

Stone, J. F., Kirkham, Don, and Read, A. A., 1955, Soil moisture determination by a portable neutron scattering moisture meter: Soil Sci. Soc. Am. Proc., v. 19, p. 419-423.

Wexler, Arnold, and others, 1955, A fast responding electric hygrometer: Jour. Res., Natl. Bur. Standards, v. 55, no. 2, p. 71-78.

280. EQUIPMENT FOR FIELD MEASUREMENT OF ELECTROCHEMICAL POTENTIALS

By WILLIAM BACK and IVAN BARNES, Washington, D. C.

Equipment and techniques have been developed to determine in the field certain electrochemical variables in ground water.

Sources of error in electrochemical studies can be classified in 4 groups: (a) electrical interference, either in the measuring system or in the sampling device; (b) mechanical work, either done on the solution (electrokinetic effects) or on the electrodes (analogous to work of expansion); (c) temperature differences among reference samples, study samples, and electrode; and (d) contamination of reference solutions, study solutions, or electrodes.

These possible errors and ways to prevent or assess them are listed in table 280.1.

Ground water studied in the present investigation was obtained at the well heads of wells of large discharge (200 to 1,200 gpm) where the cone of depression was known not to reach the water intake area. The travel time of the water in all the wells was less than 8 minutes. The water was withdrawn through plastic tubing into a sealed sample jar containing electrodes (fig. 280.1) and discharged through 15 feet of plastic tubing. The plastic tubing and sample jar were water tight at pressures of 15 psi, and the sample jar was water tight at 100 psi; thus the samples probably were not contaminated by the air. The tubing and sample jar were flushed until a constant or slowly changing potential was reached while water flowed

TABLE 280.1.—*Sources of error in electrochemical studies*

Nature of error	Source of error	Prevention
Static charge	Proximity of personnel.	Electrical shielding.
Electric current	Wind, friction	Do.
Electric current (AC pickup).	Power lines and motors.	Do.
Electrokinesis	Motion of sample	Static measurements.
Osmotic work	Sample pressure higher than atmospheric.	Sample pressure brought to atmospheric pressure.
Contamination	From previous sample, washing, and stagnant water in the casing.	High capacity pumps. Long flow period for complete flushing of sample jar and casing.
Contamination	From the atmosphere.	Closed sample jar.
Thermal differences.	Temperature of electrodes not the same as the sample.	Long flow period, sampling when ambient temperature is that of ground water; heating and cooling of reference solutions.

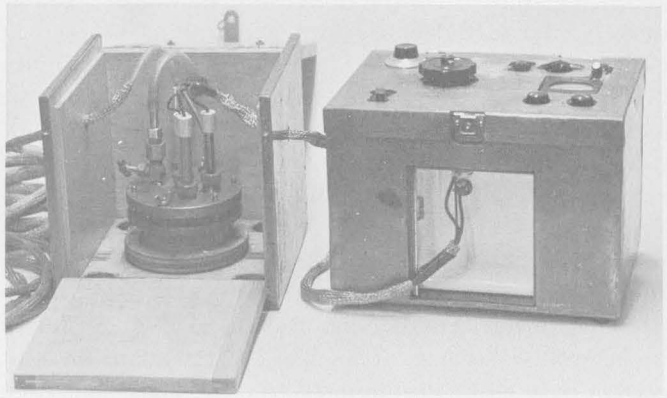

FIGURE 280.1.—Equipment used to measure electrochemical potentials in the field. Shielded plastic intake and discharge tubing and three electrodes (reference, platinum, and a third electrode of any material such as glass or gold) are mounted in a brass lid for a jar, which is enclosed in a copper-clad box. The electrodes are wired to a potentiometer (pH meter) which is shielded.

in the system (3/4 hour to 8 hours). A constant potential was assumed to mean that all the oxygen and all traces of earlier samples were flushed from the system, and that the system was filled with uncontaminated ground water.

Time-potential curves for three wells are shown in figure 280.2. These examples are representative of curves plotted for 42 wells. The potential measured in the field between the platinum and saturated calomel electrodes is plotted against time of sampling. Zero time is when the water began flowing through the system.

After a reasonably steady potential was obtained in flowing samples, the flow was stopped and the potential in the static samples was recorded as a function of time. The water level in the discharge tube was brought to the level of the top of the sample jar to avoid pressure on the saturated calomel electrode. Owing to electrokinetic effects a potential difference was always observed between flowing and static samples (fig. 280.2). The lowest (or in a few tests the highest), constant static potential was presumably the potential of the ground-water sample. The curves for most samples that had a final potential lower than about 100 millivolts had a downward trend, whereas

FIGURE 280.2.—Time-potential curves for three wells in the Atlantic Coastal Plain.

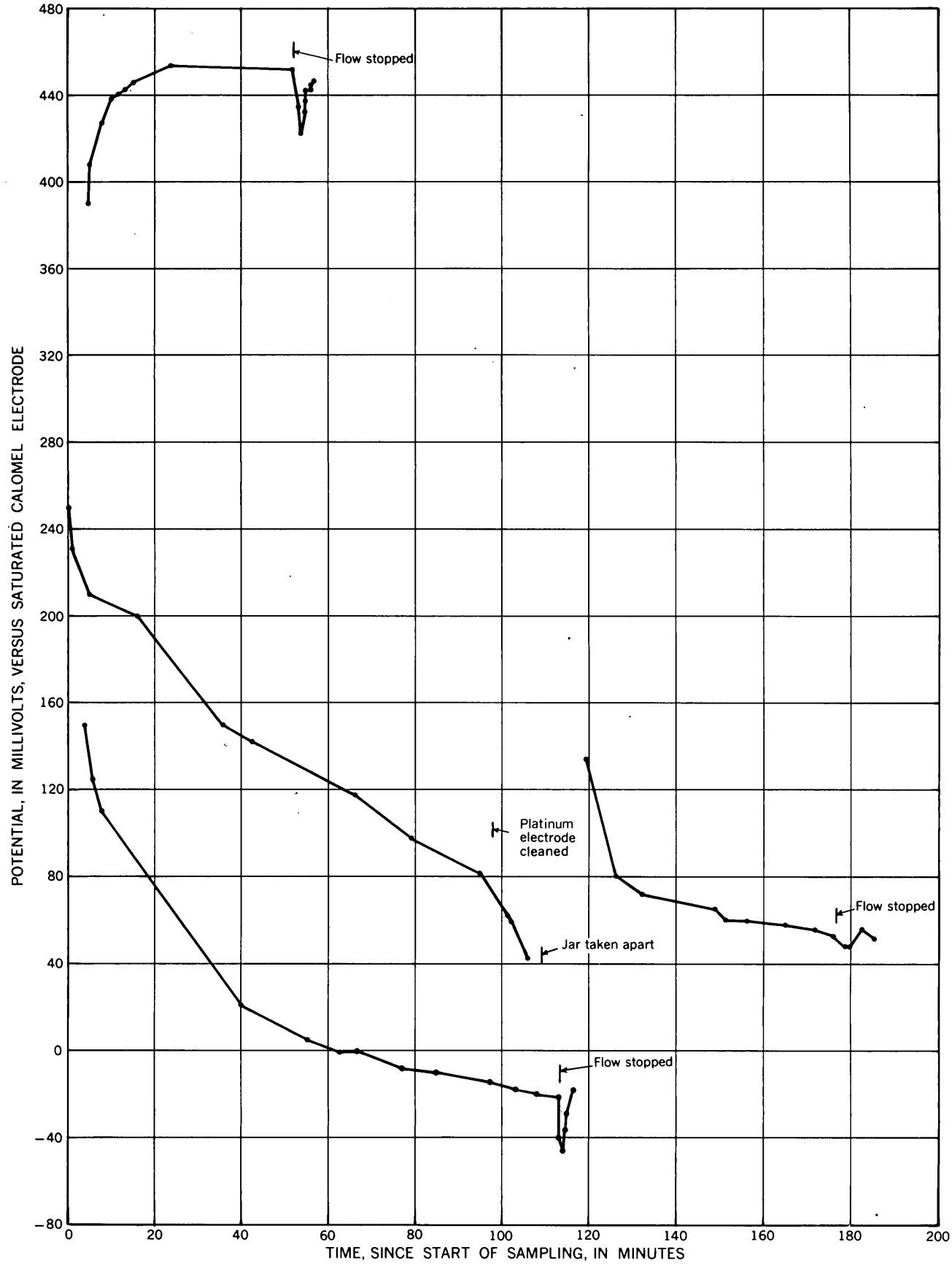
480
440
400
360
320
280
240
200
160
120
80
40
0
−40
−80
0
20
40
60
80
100
120
140
160
180
200
POTENTIAL, IN MILLIVOLTS, VERSUS SATURATED CALOMEL ELECTRODE
TIME, SINCE START OF SAMPLING, IN MINUTES
Flow stopped
Platinum electrode cleaned
Jar taken apart
Flow stopped
Flow stopped

curves for samples having a potential of more than about 400 mv generally had an upward trend, as shown in the top curve, figure 280.2. The middle curve shows the effect of cleaning the electrode with washed sea sand and the contamination of the sample with air when the jar was later taken apart for a minor repair. After the electrode was cleaned the potential decreased at a more rapid rate. Later with the admittance of air the potential increased as shown (fig. 280.2).

In the calibration of the electrodes for pH determination, the temperature of the reference solutions (standard buffers) were brought to within 2°C of the temperature of the electrodes, which were brought to the temperature of ground-water sample by immersion in the discharge water.

To avoid electrical interference, the meter, sample jar, electrodes, electrode leads, inlet and discharge tubes were electrically shielded. Two copper shields were added outside the built-in shield of the meter. The outside shields were connected in series and grounded to a stake, the well casing, or some other true earth ground. No difference was observed among any of these ground connections. The shielding and grounding assured that potentials where unaffected by blowing wind, movement of people in the vicinity of the meters, transporting the equipment, a physical connection of the water inlet tube to the water main, and 60 horsepower motors and pumps operating in the vicinity. It was observed that without the shielding any of the disturbances listed above could cause rapidly fluctuating erratic measurements or significant errors in sluggishly changing measurements.

The techniques outlined here have permitted a maximum precision of measurement of pH to ± 0.03 pH unit and Eh to ± 10 mv in waters that are essentially unbuffered and unpoised, and that contained total dissolved solids of 50 to 200 ppm.

281. TRANSFER OF GEOLOGIC DATA FROM AERIAL PHOTOGRAPHS TO TOPOGRAPHIC MAPS BY DIRECT TRACING

By Russell H. Campbell, Menlo Park, Calif.

Direct tracing of geologic data from vertical aerial photographs to a transparent topographic map prepared at an average of the scales of a set of aerial photographs covering the same area can provide a rapid and accurate method of field compilation. Tracing requires no cumbersome plotting instruments and can be done in even the most primitive field camp. Except in areas of high ground relief, tracing offers greater accuracy than transfer by inspection, particularly where relatively featureless plains are cut by enough drainage lines for good registry. In addition, many features in areas of poor tone contrast on the photographs are more clearly visible and sharply defined than are their images as projected through an optical system.

The fit between the transparent base map and individual photographs of the set depends on the amount by which the scales of the photos differ from their average, which is determined by the uniformity of the flying height above the ground surface. For most modern aerial photographs the plotting error introduced by these scale variations is small. The chief sources of error in the tracing method are those common to any method of transfer from a single nonorthographic photo print. Ray (1956, p. 15-16) discusses the sources of error in methods using reflecting projectors and the vertical sketchmaster. For modern commercial photographs the source of greatest plotting error is the radial displacement of photographic images imposed by the ground relief. Of particular advantage is the ease with which the map can be shifted to register with specific parts of a photograph such as stream intersections and hill and ridge tops to adjust for scale variations.

A few simple preliminary computations will determine the maximum plotting errors to be expected due

to scale variations and local relief for a particular set of photos and maps. With these various sources of error in mind, a sample area in northwestern Alaska having generally low ground relief and a large number of recognizable points for local registry was studied to determine the practical problems involved in the application of the direct tracing method. Preliminary computations indicated that the maximum expectable errors were small. In addition, experience showed that virtually all plotting errors caused by scale variations between photo prints and map, and much of the error within individual prints caused by radial displacement due to relief, can be eliminated in tracing by adjusting to local points of registry within segments of a photograph. Moreover, as pointed out by C. L. Pillmore (oral communication, 1961), the stereo model may be observed in relation to the topography by using one print of a stereoscopic pair above the transparent map and the other below it. By this technique photographic distortions of the form of lines on hillsides were found to be easily adjustable to their correct map expression.

In the sample area the fit between the photographs and an enlarged topographic base map was found to be very good. In only a few small areas did plotting errors approach the computed maxima. Contacts and fault traces could be traced directly from the photographs with confidence, and map symbols could be accurately located.

DETERMINING SCALE FOR TRANSPARENT BASE MAPS

Where a known distance is represented on the original map by D inches and on a photograph by d inches, and the map scale is $\frac{1}{M}$ and the photo scale is $\frac{1}{P}$, then since $Pd=MD=$the distance on the ground, then

$$P=\frac{MD}{d}. \tag{1}$$

For each photograph determine P for two lines diagonal to the flight line approximately through the photo center as defined by four points of registry at about the same ground elevation. The mean of these two scales is used for the scale of the photograph. (Variations in the scales of the two diagonals are due chiefly to tilt, and are commonly small.) The map is then photographically enlarged on a transparent medium to a scale of $\frac{1}{S}$, the average scale of the individual photos.

DETERMINING EXPECTABLE ERRORS

To determine the plotting error, Δx, in tracing from a photo of scale $\frac{1}{P}$ to a map of scale $\frac{1}{S}$, let x_m be the distance on the map from a *point of registry* to a point to be plotted, and x_p be the distance on the photo between the same two points. Then the error is represented by

$$\Delta x=x_m-x_p. \tag{2}$$

Now, using equation (1), $x_m=\frac{x_pP}{S}$ and substituting in equation (2), the error is $\Delta x=x_p\left(\frac{P-S}{S}\right)$. For each individual photograph $\frac{P-S}{S}$ is a constant, K, and a family of lines can be drawn for different K's along which the maximum expected plotting error due to scale variation can be determined as a function of the distance from a point of registry (fig. 281.1). In the sample area the average photo scale, $\frac{1}{S}$, is $\frac{1}{41{,}450}$ and the constant K was found to be 0.010 or less for most of the photographs of the covering set and exceeded 0.012 for only two photo prints. In practice, the distance from a point of registry did not exceed 2 inches; therefore, the plotting error resulting from the difference in scale between the map and photographs may be expected to be less than 0.025 inch (fig. 281.1).

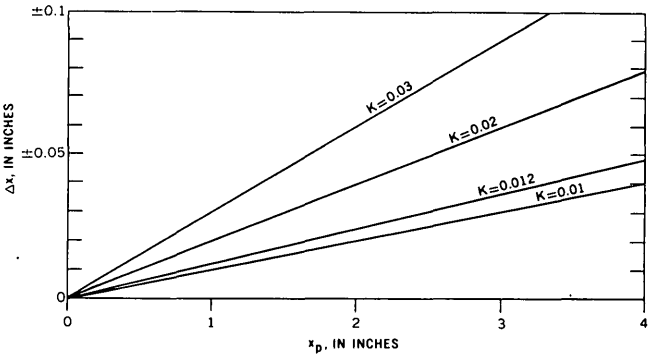

FIGURE 281.1.—Family of lines showing plotting error Δx as a function of the distance x_p of the point to be plotted from a point of registry and the constant $K=\frac{P-S}{S}$ for an individual photo print, where $\frac{1}{P}$ is print scale and $\frac{1}{S}$ is map scale.

A complete evaluation of the effects of radial displacement caused by ground relief is beyond the scope of this paper. Several textbooks concerning the applications of aerial photographs cover their characteristics in detail (for example, Smith, 1943, p. 36–39). The general formula for computation of this displacement is $\Delta r=\frac{rh}{H}$ where Δr is the radial displacement, h is

the difference in ground elevation between the center of a strictly vertical photograph and a point at a distance r from the photo center, and H is the altitude above the mean ground surface from which the photo was taken. The flying height, H, and the contact print scale, $\frac{1}{P}$, are related by the formula $P=\frac{H}{f}$ where f is the focal length of the camera, thus $\Delta r=\frac{rh}{Pf}$. Figure 281.2 shows a family of lines that may be conveniently compared with those on figure 281.1. They show the expectable displacement due to relief of points at a distance of 3 inches from a photo center for several common scales as computed for a camera focal length (6 inches) in common use. In the sample area in northwestern Alaska the approximate photo scale is 1:40,000 and the local relief averages 500 to 700 feet with one hill rising to 1,500 feet. The ground relief between photo centers and peripheral points is commonly less than 500 feet and the resulting radial displacement is commonly less than 0.1 inch (fig. 281.2).

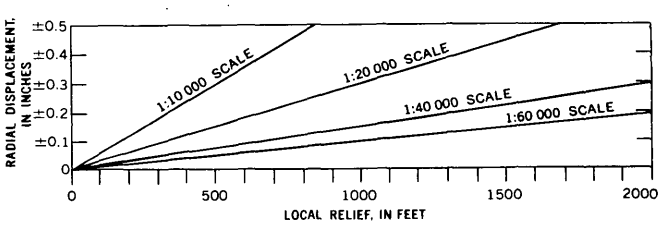

FIGURE 281.2.—Family of lines showing maximum radial displacement due to relief of a peripheral point 3 inches from the center of a vertical photograph. Displacement is a function of the contact print scale (in this example computed for a camera focal length of 6 inches) and the difference in altitude between the photo center and the peripheral point.

REFERENCES

Ray, Richard G., 1956, Photogeologic procedures in geologic interpretation and mapping: U. S. Geol. Survey Bull. 1043-A, p. 1-21.

Smith, H. T. U., 1943, Aerial photographs and their applications: New York, Appleton-Century-Crofts, Inc., 372 p.

282. A REMANENT MAGNETOMETER AND MAGNETIC SUSCEPTIBILITY BRIDGE

By LENNART A. ANDERSON, Denver, Colo.

A dual-purpose instrument, using separate detecting and common amplifying systems, precisely measures remanent magnetism and magnetic susceptibility of rock samples. The instrument was developed with the assistance of J. A. Graham and P. F. Michelsen of the Department of Terrestrial Magnetism of the Carnegie Institution of Washington from unpublished designs of equipment of that organization.

REMANENT MAGNETOMETER

Remanent magnetization is magnetization that exists within a material independent of any external magnetic field. The remanent magnetization of a rock sample is given in terms of intensity and its orientation with respect to magnetic north and the horizontal plane.

A functional diagram of the remanent magnetometer is shown on figure 282.1. A cylindrical core, one inch in diameter and length, is cut from a rock sample marked to indicate its orientation. The sample is placed in an air-driven, cylindrical, lucite turbine and rotated within a vertically mounted pickup coil at 280 cycles per second. The horizontal component of the alternating magnetic field generated by the rotating

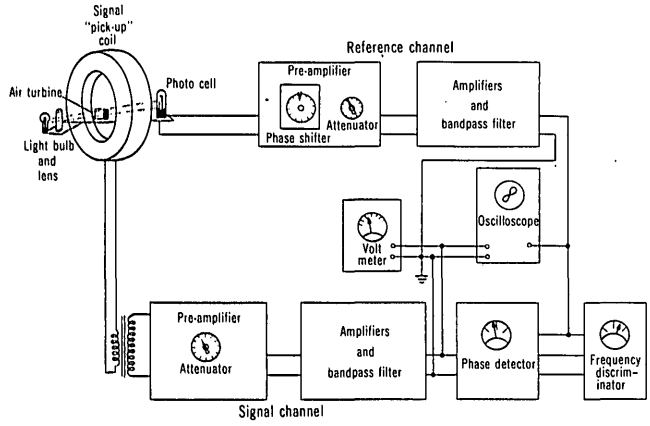

FIGURE 282.1.—Functional diagram of the remanent magnetometer.

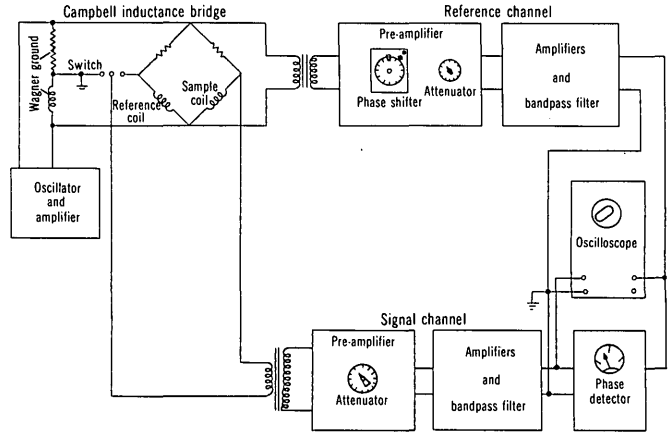

FIGURE 282.2.—Functional diagram of the magnetic susceptibility bridge.

sample induces a small alternating voltage in the coil windings. This voltage is amplified and measured, and its phase is compared with a synchronous reference voltage.

The reference signal is produced by focusing a light beam on a photoelectric cell and interrupting the beam with an opaque 105-degree sector of the rotating sample holder. The phase angle between the reference signal and the induced signal depends on the angular displacement between the leading edge of the opaque sector of the turbine and the component of magnetization of the sample in the horizontal plane. The speed of the turbine is adjusted by varying the air pressure until a null reading is obtained at the output of the frequency discriminator.

The values for intensity and phase determine the length and direction of one particular component of the remanent magnetization vector. The sample is spun on three mutually perpendicular axes in order to determine three components of the total vector. By plotting these components on an equal area projection net, the direction of the remanent magnetization of the sample is determined. Its total intensity is found by taking the square root of one-half the sum of the squares of the three average intensities.

MAGNETIC SUSCEPTIBILITY BRIDGE

Magnetic susceptibility is the ratio between the intensity of the induced magnetization of a substance in an external magnetic field and the intensity of the field.

The magnetic susceptibility bridge utilizes the same amplification channels as the remanent magnetometer but differs in the system of detection. As indicated on figure 282.2, two sets of identical coils and resistances are arranged to form a Campbell inductance bridge. An additional inductance and resistance arm, called a Wagner ground, is used to bring the signal output side of the bridge to ground potential. The resistance arms are made of coiled manganin wire. An oscillator set for 280 cps (cycles per second) drives the bridge and also feeds a signal into the reference channel through an isolation transformer. The reference signal is amplified and sent through a phase shifting circuit which is adjusted so that the phase detector will be sensitive to only the inductive component of the bridge unbalanced voltage.

Initial balance of the bridge inductance is obtained by moving a ferrite slug near the balancing coil. The effective resistance of the reference coil, and hence the resistive balance, is adjusted by changing the position of a closed loop of manganin wire that acts as a resistance-loaded secondary transformer winding. The Wagner ground arm is balanced in the same manner. In addition to the balancing controls, the reference coil has a control using a slug of ferrite with enough permalloy to match the resistive unbalanced component due to the conductivity of magnetite. This control varies the resistive and inductive components as seen by the reference coil. The slug is mounted on a screw and enters the core of the coil. It is in the shape of a long cone so that the susceptibility can be measured to two significant figures from 10^{-6} to 0.5 cgs units per cc.

The mode of operation requires that the sample coil be balanced first with respect to the Wagner ground and then with respect to the reference arm with the

screw control set at zero. A rough balance is achieved by obtaining a horizontal line on the oscilloscope. The phase shifter is adjusted so that a small change of the resistive control will not unbalance the bridge. Fine balance is achieved by adjusting the controls for zero output of the phase detector.

When a rock is inserted into the sample coil its inductance will become greater if the rock is paramagnetic, and smaller if the rock is diamagnetic. The resulting off balance is compensated for by varying the reference coil screw control until the phase meter reads zero. The position of the screw control is read on a scale that has been calibrated previously by using as standards ferric chloride solutions of various susceptibilities, and cores of magnetite and plaster whose susceptibilities were determined by measuring the anomaly they produce in a known field.

REFERENCE AND SIGNAL AMPLIFICATION CHANNELS

The reference and signal channels are common to the remanent magnetometer and the magnetic susceptibility bridge. The reference channel consists of a pre-amplifier, an attenuator, a phase shifter, two a-c amplifiers, and a narrow bandpass filter. The output of the reference channel feeds a phase detection circuit and the horizontal input of an oscilloscope. The signal channel has essentially the same components without a phase shifter. The outputs feed the vertical input of the oscilloscope, the phase detector, and an a-c voltmeter.

The outputs of the signal and reference channels are fed into an oscilloscope to form a single-loop Lissajous figure. When used with the susceptibility bridge, the oscilloscope is useful in making rapid course balances of the bridge because a relatively small unbalance will cause the phase meter to go off scale. The oscilloscope also serves to detect saturation of the amplifier.

The limit of reliable sensitivity is of the order of $1x10^{-6}$ cgs units per cc, although sensitivities of $1x10^{-8}$ cgs units per cc are possible for the susceptibility bridge when the external noise level is sufficiently low. The signal channel has an overall gain of $1x10^{8}$ and has a noise level of approximately $1.2x10^{-8}$ volts.

ANALYTICAL AND PETROGRAPHIC METHODS

283. A METHOD FOR DETERMINING THE SPECIFIC GRAVITY OF SAND AND GROUND ROCK OR MINERALS

By Joseph J. Fahey, Washington, D. C.

The determination of the specific gravity of sand, or samples of rock or minerals ground to pass a 100 mesh sieve and to be retained on a 200 mesh sieve is usually made by one of several pycnometer methods. Each of these procedures entails successive weighing on the analytical balance of the pycnometer, the pycnometer plus the sample, the pycnometer plus the liquid (usually water), and the pycnometer plus sample plus liquid. From these data the specific gravity of the sample at the temperature of the room is computed. By applying a suitable factor the specific gravity at 4°C can be obtained.

Appreciable errors may occur in the pycnometer method due to the difficulty encountered in weighing the pycnometer plus liquid, and the pycnometer plus sample plus liquid. Duplicate determinations may differ by as much as 10 mg due to variations in temperature, humidity, time on the balance pan, and the adjustment of the stopper of either the truncated cone with a capillary, or the plane surface top of the Adams-Johnston pycnometer. These errors are eliminated in the procedure described in this paper.

Suspend an unstoppered Erlenmeyer flash of about 5 ml capacity or a 5 ml pycnometer with truncated stopper removed, on about 10 cm of fine platinum wire from the arm of the analytical balance. Record the weight in air and also the weight in water, which is obtained by immersing the suspended flask in a beaker

of water that rests on a bridge over the balance pan. The height of the water in the beaker should be marked to assure constant depth of immersion in successive determinations. This is necessary to avoid a small error that would result from the immersion of varying lengths of the fine platinum wire. The weight in air and the weight in water of the flask are constants for a given flask and need not be repeated when determining the specific gravity of a sample.

After drying the flask well, place about 0.5 to 1.5 grams of the sample into the flask. The weight of the flask plus the sample is recorded. Remove the suspended flask plus sample from the balance arm and add water until it is about three-fourths full. Tap the flask until all bubbles are exhausted. Fill the flask with water and suspend it from the balance arm in a beaker of water as described above. The weight in water of the flask plus sample is recorded.

The specific gravity is computed from the following relation:

$$\text{Specific gravity} = \frac{\text{Wt. of sample in air}}{\text{Wt. of sample in air} - \text{wt. of sample in } H_2O}$$

The weight of the sample in air equals the combined weight of flask and sample in air less the weight of flask in air, and the weight of the sample in water is determined similarly from corresponding measurements in water.

A sample of quartz (Ottawa sand) was ground to pass a 100-mesh sieve. That portion retained on a 200-mesh sieve was allowed to remain in (1+1) HCl on the steam bath over night. After washing and drying, this sample of quartz was used to check the accuracy and precision of the results obtained by this method for the determination of specific gravity.

Four determinations were made, each requiring about 15 minutes. The results recorded were: 2.649, 2.652, 2.654, 2.654.

Tiny liquid inclusions, readily visible under the microscope, may account for the slightly lower figures than the 2.653 to 2.660 given by Dana and Ford (1945, p. 471).

The specific gravity of water-soluble minerals can be determined by this method using toluene that has been saturated with the mineral being examined. The specific gravity of the mineral-saturated toluene can be determined easily by weighing in a 50 ml volumetric flask on the analytical balance.

REFERENCE

Dana, E. S., and Ford, W. E., 1945, A textbook of mineralogy: New York, John Wiley and Sons, 851 p.

284. MEASUREMENT OF SODIUM ACTIVITIES IN CLAY SUSPENSIONS WITH CATIONIC-SENSITIVE ELECTRODES

By Alfred M. Pommer, Washington, D. C.

Work done in cooperation with the U.S. Atomic Energy Commission

Millivolt readings obtained with sodium-sensitive glass electrodes are useful in clay titrations (Pommer, 1960). Such electrodes measure activities rather than concentrations. The difficulties of measuring pH in clay suspensions (Jenny and others, 1950; Marshall, 1951; Eriksson, 1951; Mysels, 1951; Overbeek, 1953; Low, 1954) apply equally to measurements with cationic-sensitive glass electrodes in such suspensions (Bower, 1961). It is essential, therefore, to consider the difficulties involved. Although the work of Low (1954) vitiates the statement by Feldman (1956) that "pH measurements on suspensions of highly charged particles are meaningless," many of Feldman's comments pertaining to the "use and abuse of pH measurements" may be applied profitably to sodium determinations with sodium-sensitive glass electrodes. To visualize the dangers inherent in an uncritical utilization of sodium electrode readings as a measure

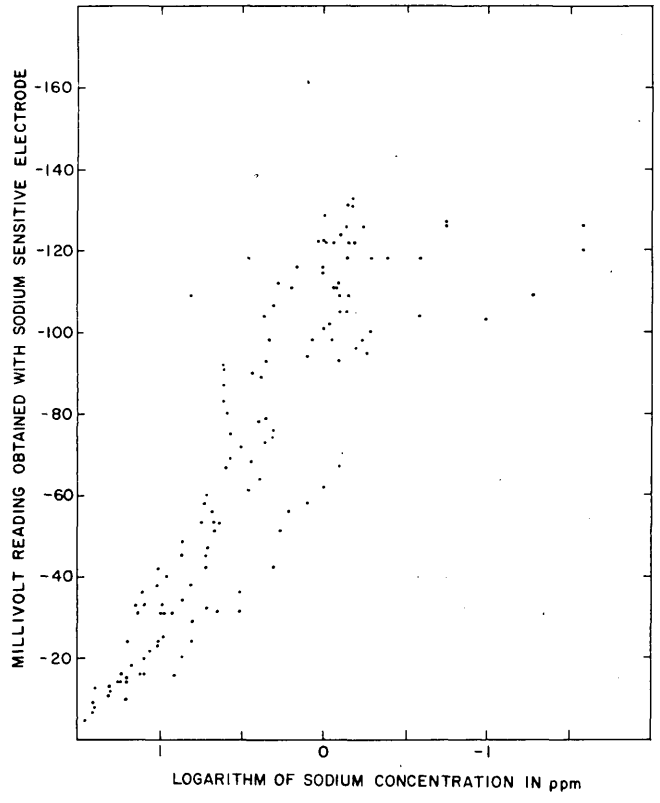

FIGURE 284.1.—A comparison of sodium values in 143 unselected determinations with sodium electrode readings.

of sodium content, the first 143 sodium electrode readings obtained in this laboratory were plotted against sodium content. Electrode readings were obtained from a single Beckman cationic-sensitive glass electrode (Spec. Electrode No. 78137V) using either a Beckman Model GS or Zeromatic pH meter. Analytical sodium values were obtained either with a Beckman Model DU spectrophotometer with flame photometer attachment and photomultiplier attachment or (in the case of pure NaCl solutions) were computed from the nominal composition of the solutions. As the sodium-sensitive glasses yield electrode potentials which are a linear function of the logarithm of the cation activity (Eisenman, Rudin, and Casby, 1958), the logarithm of the sodium concentration was plotted against the millivolt readings obtained with the electrode. Figure 284.1 clearly shows that an uncritical substitution of electrode readings for analytical values gives unsatisfactory results.

Eisenman, Rudin, and Casby (1957) give the following empirical equation for the performance of a glass electrode in a mixture of any two univalent cations:

$$E=E^{\circ}+\frac{RT}{F}\,ln\left[(A^{+})^{\frac{1}{n_{AB}}}+K_{AB}^{\frac{1}{n_{AB}}}(B^{+})^{\frac{1}{n_{AB}}}\right]^{n_{AB}} \quad (1)$$

wherein:

E=measured emf
E°=standard potential
R=ideal gas equation constant
T=Temperature
F=Faraday constant
(A^{+}) and (B^{+})=activity of the ionic species A^{+} and B^{+}
n_{AB} and K_{AB}=empirical constants for a given glass composition
and ionic pair A^{+} and B^{+}

It should be noted that E°, the "standard potential," is not the potential of the electrode if all activities are unity, and the term "standard" does not carry the customary thermodynamic connotation. It is simply the measured emf whenever the logarithmic term drops out, and depends on all the sources contributing to this emf in the cell chain, such as the potential of the reference electrode, the potential contributed by the silver–silver chloride wire dipping into a sodium acetate–hydrochloric acid solution inside the glass electrode (Isard, 1959), and asymmetry, contact, and liquid junction potentials (Bates, 1954).

In the case of a solution containing H^{+} and Na^{+} ions only, n_{HNa} is unity (Eisenman, Rudin, and Casby, 1957), and equation (1) reduces to

$$E=E^{\circ}+\frac{RT}{F}\,ln\,[(H^{+})+K_{HNa}(Na^{+})] \quad (2)$$

an equation which indicates that in a plot of log (Na^{+}) against E, a straight line is possible only if $(Na^{+})\gg H^{+}/K_{HNa}$. Figure 284.2 shows millivolt readings obtained with a sodium-sensitive glass electrode at 22° C plotted against sodium activities of sodium chloride solutions. These were prepared by dissolving in distilled water NaCl dried in an oven and diluting to yield a series of solutions ranging in molarity from 0.05 to 0.000165. Sodium ion activities were calculated using the Debye-Hückel formula. The straightness of the line indicates that $H^{+}/K_{HNa}\ll Na^{+}$. Figure 284.2 clearly shows the applicability of the method to sodium solutions under carefully controlled conditions.

Figure 284.3 relates the millivolt readings obtained with a sodium-sensitive glass electrode (Pommer, 1960) during the titration of a hydrogen montmorillonite with sodium hydroxide to the sodium values determined with a flame photometer (Dorothy Carroll, analyst). As the ionic strength of the solution was not uniquely defined by the conditions of the experiment and could not be determined experimentally, the activity corrections required by the Debye-Hückel theory could not be made. In spite of this, the plot gives a rather straight line in the region where the sodium concentration exceeds 2.5 millimoles per liter.

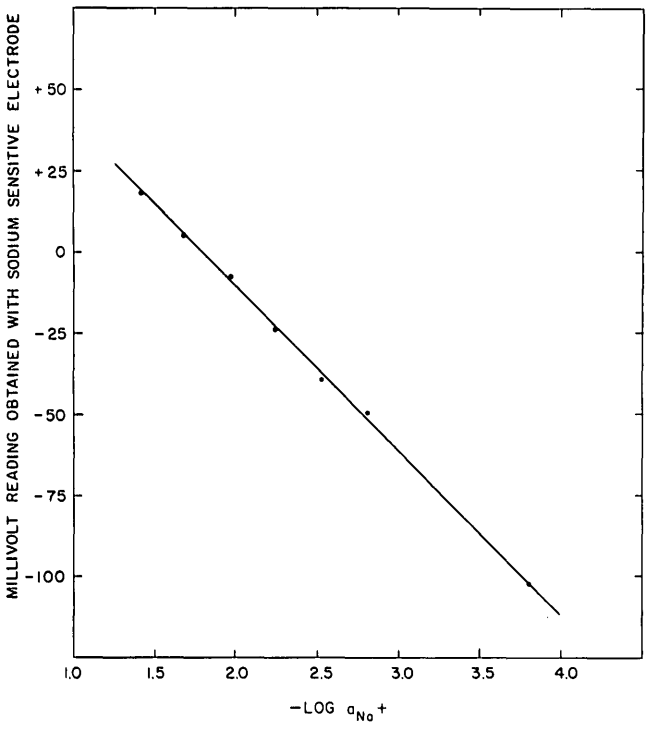

FIGURE 284.2.—Relation between sodium-electrode emf and calculated sodium activity in sodium chloride solutions. Data by M. M. Schnepfe.

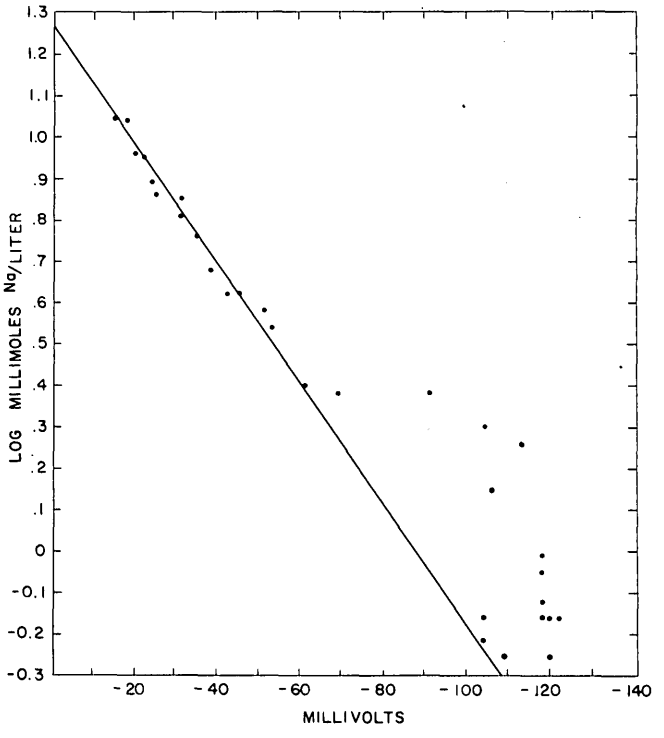

FIGURE 284.3.—Relation betwen flame photometric and potentiometric sodium values in a discontinuous montmorillonite titration.

The deviation of the slope from unity can be explained by the failure to make corrections for activity coefficients. The bulge in the graph at a concentration of less than 2.5 millimoles indicates that the electrometric sodium values are lower than those obtained by flame photometry. The reason for the discrepancy between the flame photometry and electrometric sodium values is not yet known. It is generally accepted that the analysis of alkali metals tends to give high values, and this may be the reason. The possibility of colloidal clay particles passing through the filter paper and, during flame photometry, being aspirated and vaporized, thus contributing excess sodium, must be borne in mind. Microscopic examination of a clay suspension filtrate (by E. Zen) indicated the presence of some clay particles, though aspiration of the filtrate through a flame photometer capillary failed to deposit particles on a slide which could be detected on microscopic examination. This is not necessarily conclusive, since the extremely small amount of particulate matter necessary to give discrepant results may be missed on microscopic examination. Since the clay suspensions containing higher sodium concentrations were better coagulated, it is still tempting to ascribe the deviations in the low-sodium region to this effect.

It is also possible that the deviations result from the presence of sodium in a form other than Na^+. Gregor (1951) has reported on ion-pair formation in ion-exchange systems, and it is conceivable that this phenomenon may account for the apparent lowering of sodium activity. Another possibility is uptake of carbon dioxide from the atmosphere which may result in the formation of $NaCO_3^-$ ion (Garrels, Thompson, and Siever, 1961), thus lowering the amount of sodium available for formation of Na^+. However, insufficient information is available at this time to settle the point.

REFERENCES

Bates, R. G., 1954, Electrometric pH determinations: New York, John Wiley and Sons, 330 p.

Bower, C. A., 1961, Studies on the suspension effect with a sodium electrode: Soil Science Soc. America Proc., v. 25, p. 18-21.

Eisenman, George, Rudin, D. O., and Casby, J. U., 1957, Glass electrode for measuring sodium ion: Science, v. 126, p. 831-834.

———1958, Glass electrode for measuring sodium ion: U.S. Patent No. 2,829,090.

Eriksson, Erik, 1951, The significance of pH, ion activities, and membrane potentials in colloidal systems: Science, v. 113, p. 418-420.

Feldman, Isaac, 1956, Use and abuse of pH measurements: Anal. Chemistry, v. 28, p. 1859-1866.

Garrels, R. M., Thompson, M. E., and Siever, Raymond, 1961, Control of carbonate solubility by carbonate complexes: Am. Jour. Sci., v. 259, p. 24-45.

Gregor, H. P., 1951, Ion-pair formation in ion exchange systems: Am. Chem. Soc. Jour., v. 73, p. 3537-3538.

Isard, J. D., 1959, Alkali ion determinations by means of glass electrodes: Nature, v. 184, p. 1616-1618.

Jenny, Hans, Nielsen, T. R., and Coleman, N. T., 1950, Concerning the measurement of pH, ion activities, and membrane potentials in colloidal systems: Science, v. 112, p. 164-167.

Low, P. F., 1954, Ion activity measurements in heterogeneous systems: Soil Science, v. 77, p. 29-41.

Marshall, C. E., 1951, Measurements in colloidal systems: Science, v. 113, p. 43-44.

Mysels, K. J., 1951, (Potentiometric) measurements in (some) colloidal systems: Science, v. 114, p. 424-425.

Overbeek, J. T. G., 1953, Donnan-emf and suspension effect: Jour. Colloid Science, v. 8, p. 593-605.

Pommer, A. M., 1960, Sodium-sensitive glass electrodes in clay titrations *in* Short papers in the geological sciences: U.S. Geol. Survey Prof. Paper 400-B, p. B502-B504.

285. EVALUATION OF THE USE OF DICHROMATE OXIDATION TO ESTIMATE THE ORGANIC CARBON CONTENT OF ROCKS

By I. C. Frost, Denver, Colo.

The determination of organic matter in sedimentary rocks and associated ores presents some challenging and difficult analytical problems. The complex chemical nature of the organic matter and its intimate association with inorganic minerals makes separation into organic and inorganic fractions difficult if at all possible. Organic matter in sedimentary rocks may range from none to several percent. As contrasted with the analysis of samples for their organic matter, the determination of organic carbon is much easier to obtain and serves well as an index to the amount of organic matter.

The reducing capacity of the organic matter as measured by the dichromate oxidation is used routinely in many soil studies to approximate soil organic matter. The method was originally proposed by Schollenberger (1927), and later modified by Walkley (1945, 1947). The method used in this study is that of Walkley as adapted and described by the U.S. Dept. of Agriculture (1954). A weighed sample not exceeding 10 g and containing from 10 to 25 mg of organic carbon is treated in a 500-ml Erlenmeyer flask with 10 ml of 1 N potassium dichromate and 20 ml of concentrated sulfuric acid containing 25 g per liter of silver sulfate. The flask is heated gently to a temperature of 150°C in a period of 1 minute, then allowed to cool. The excess potassium dichromate is measured after dilution by titration with 0.5 N ferrous sulfate using orthophenanthroline as an indicator.

It is recognized that dichromate oxidation cannot distinguish reduction due to organic matter from that due to sulfides, ferrous iron, or other reducing agents. The method was investigated, however, to see if it might satisfy the demand for a quick, simple, and approximate means for determining the organic carbon

TABLE 285.1.—*Comparative data used to evaluate a rapid field method for organic carbon in Pierre shales*

[In percent]

Sample No.	Organic carbon		Carbonequivalent by dichromate oxidation	Sulfur [1]	Carbonequivalent by dichromate oxidation corrected for sulfur
	Modified combustion method	Gasometric method			
Range 0.10 to 0.49 percent					
259557	0.10	----------	0.06	0.09	0.02
528	.12	----------	.16	.02	.16
539	.15	----------	.32	.23	.19
542	.16	----------	.40	.39	.17
583	.18	----------	.22	.02	.22
559	.21	----------	.21	.01	.21
534	.23	----------	.26	[2].10	.21
536	.24	----------	.27	.01	.27
550	.24	----------	.24	.06	.21
598	.24	----------	.30	[2].10	.25
565	.25	----------	.27	.02	.27
600	.27	----------	.28	.04	.27
540	.28	----------	.52	.27	.37
551	.30	----------	.29	.01	.29
580	.32	----------	.26	.01	.26
586	.36	----------	.30	.02	.30
566	.36	----------	.43	.02	.43
605	.37	----------	.54	.01	.54
531	.39	----------	.43	[2].14	.35
538	.41	----------	.63	.31	.45
584	.41	----------	.38	.14	.30
546	.41	----------	.40	.07	.37
535	.43	----------	.46	[2].19	.35
529	.46	----------	.46	.01	.46
530	.48	----------	.48	.09	.44

See footnotes at end of table.

TABLE 285.1.—*Comparative data used to evaluate a rapid field method for organic carbon in Pierre shales*—Continued

[In percent]

Sample No.	Organic carbon: Modified combustion method	Organic carbon: Gasometric method	Carbonequivalent by dichromate oxidation	Sulfur [1]	Carbonequivalent by dichromate oxidation corrected for sulfur
Range 0.50 to 0.99 percent					
259576	0.50	----------	0.64	0.17	0.51
552	.52	----------	.60	.02	.59
575	.55	----------	.80	.43	.46
590	.57	----------	.58	.03	.57
589	.58	----------	1.08	.45	.73
587	.59	----------	.65	.02	.64
533	.59	----------	1.14	.60	.67
597	.64	----------	1.12	.61	.65
577	.66	----------	.63	.09	.57
569	.67	----------	1.13	.41	.81
259560	.73	----------	.92	.27	.72
581	.75	----------	.69	.02	.68
594	.75	----------	.84	[2] 1.11	.76
564	.78	----------	1.42	.87	.74
585	.78	----------	.65	.02	.64
601	.79	----------	1.23	.42	.91
592	.80	----------	1.14	[2] 1.14	1.04
545	.82	----------	1.02	.29	.80
558	.82	----------	.76	.02	.75
568	.89	----------	1.05	.42	.73
570	.96	----------	1.14	.40	.83
532	.96	----------	1.23	.56	.80
Range 1.00 to 8.08 percent					
259543	----------	1.00	1.60	0.84	1.15
555	----------	1.10	1.02	.02	1.15
547	----------	1.32	2.14	1.02	1.56
574	----------	1.81	2.43	.99	1.87
604	----------	2.43	4.25	2.00	2.97
562	----------	2.48	3.61	1.64	2.59
571	----------	2.49	3.42	1.76	2.31
553	----------	2.58	4.09	1.93	2.86
556	----------	2.87	3.40	.92	2.89
563	----------	3.18	3.36	.87	2.88
526	----------	4.73	4.75	.25	4.72
595	----------	4.93	5.51	1.17	4.82
561	----------	5.40	5.75	.45	5.58
591	----------	5.70	6.28	.85	5.82
582	----------	6.50	10.15	4.46	7.11
602	----------	7.15	10.53	5.67	6.63
[3] 549	----------	8.23	14.96	9.83	8.08

[1] The difference between the sulfur oxidizable with (1+3) nitric acid and that soluble in dilute (10 percent) hydrochloric acid.
[2] Total sulfur values.
[3] Composite samples.

content of shales and to determine its applicability as a field reconnaissance method.

The reducing capacities of 64 selected samples of the Pierre shale were determined by the described method and calculated as organic carbon. The samples selected had organic carbon contents greater than 0.10 percent. The values of organic carbon for different ranges of concentration are given in tables 285.1 and 285.2. Organic carbon was determined by methods described by Frost (1960). The modified combustion method was used for those samples having less than 1.00 percent organic carbon and a gasometric method for those having more.

TABLE 285.2.—*Mean carbon content of 64 samples of Pierre shale and their standard deviations before and after sulfur corrections*

Number of samples	Organic carbon (percent): Range	Organic carbon (percent): Mean	Standard deviation between organic carbons and dichromate carbon equivalents: Uncorrected	Standard deviation between organic carbons and dichromate carbon equivalents: Corrected for sulfur
25	0. 10–0. 49	0. 29	0. 10	0. 06
22	. 50–0. 99	. 71	. 30	. 10
17	1. 00–8. 23	3. 76	2. 2	. 27

The samples are arranged in the tables in three groups according to their organic carbon contents. The reducing capacities, calculated as organic carbon, were mostly greater than the determined carbon values. Those samples having the larger amounts of oxidizable sulfur show the greatest differences. The effect of the oxidizable sulfur was determined for each range of organic carbon by the method of least squares. Standard deviations between the corrected values and the values determined directly can be obtained by multiplying the oxidizable sulfur by 0.7 and subtracting the result from the carbon equivalent of the reducing capacities.

The reducing capacities determined by dichromate oxidation are quick and easy to obtain and can be carried out in field reconnaissance studies.

REFERENCES

Frost, I. C., 1960, Comparison of three methods for the determination of total and organic carbon in geochemical studies, *in* Short papers in the geological sciences: U.S. Geol. Survey Prof. Paper 400-B, p. B480-B483.

Schollenberger, C. J., 1927, A rapid approximate method for determining soil organic matter: Soil Science, v. 24, p. 65-68.

U.S. Department of Agriculture, 1954, Diagnosis and improvement of saline and alkaline soils: Agriculture Handbook No. 60, p. 105-106.

Walkley, A., 1945, An examination of methods for determining organic carbon and nitrogen in soil: Jour. of Agr. Sci. (England), v. 25, p. 598-609.

———1947, A critical examination of a rapid method for determining organic carbon in soil—effect of variations in digestion conditions and of inorganic soil constituents: Soil Science, v. 63, p. 251-264.

601530 O—61——25

286. DETERMINING THE DISTRIBUTION OF BERYLLIUM IN ROCKS BY A CONTACT-PRINT METHOD

By Wallace R. Griffitts and Lorraine E. Patten, Denver, Colo.

During a mineralogic study of beryllium ores from Spor Mountain, Utah, we wished to determine the distribution of beryllium in siliceous nodules and other coherent lumps of rock. Staining with quinalizarin (Jedwab, 1957) was unsatisfactory because the reagent stained the porous surfaces and because the purple fluorite in many specimens made the color distinctions difficult. We found that beryllium could easily be dissolved from the surfaces of the specimens and transferred to paper, on which it could be rendered visible with suitable reagents. This technique has long been used in the study of sulfide ores.

To make the print, a flat, smooth, but not polished, rock surface is pressed for about 15 seconds against a piece of fine filter paper moistened with 3 normal sulfuric acid. The paper is then dried, sprayed with a 0.01 percent solution of morin in ethyl alcohol, and suspended in a closed container over concentrated ammonium hydroxide. The ammonia fumes neutralize the acid that remains in the paper and makes the paper alkaline; the beryllium-morin compound then fluoresces under ultraviolet light. The intensity of the fluorescence varies with the amount of beryllium. For permanent record the fluorescent image can be photographed or the areas with different intensity of fluorescence can be outlined on the paper with a pencil, as was done with the samples shown on figure 286.1.

Beryllium is dissolved from the Spor Mountain ore because of the extremely fine grain size of the bertrandite. Sulfuric acid does not readily dissolve coarse beryl or bertrandite unless the specimen is first briefly etched with sodium hydroxide. This preliminary treatment consists of dipping the cold specimen into fused NaOH for a few seconds, withdrawing it, and washing off the coating of solidified hydroxide with water. After drying, the specimen can be treated in the same manner as the Spor Mountain ore.

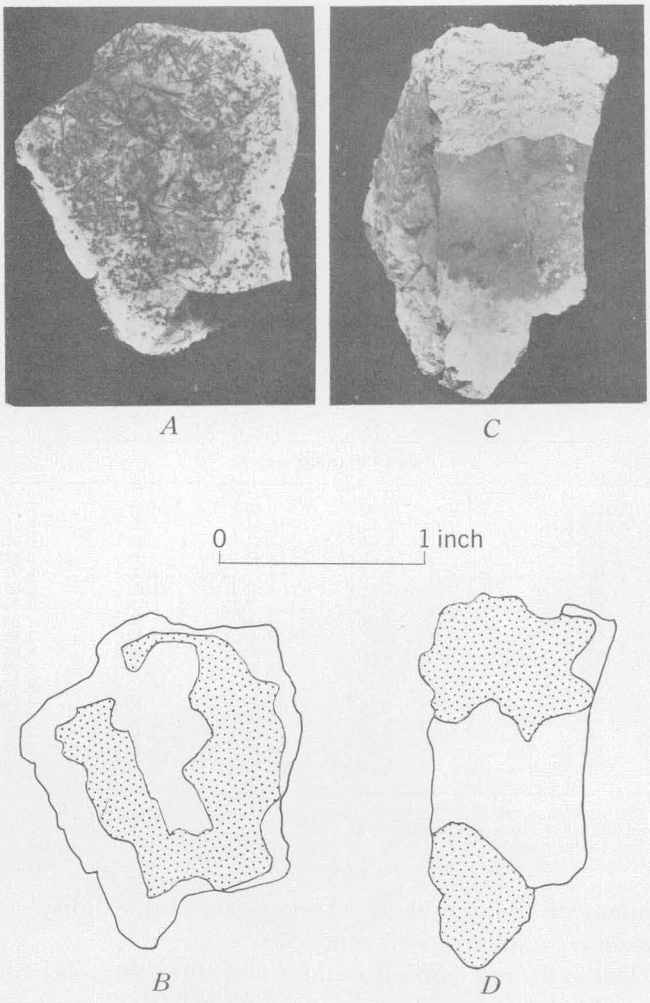

Figure 286.1.—Distribution of beryllium in two specimens from Spor Mountain, Utah. *A*, nodule that contains blades of purple fluorite and a white rind; *B*, outline of smooth surface of specimen *A* (stippled area is strongly fluorescent indicating that beryllium is most concentrated in rock with medium-sized fluorite blades); *C*, specimen having pale-purple center and mottled white ends; *D*, outline of smooth surface of specimen *C* (stippled area is strongly fluorescent, indicating that beryllium is most concentrated in the white terminal parts of the specimen).

REFERENCE

Jedwab, J., 1957, Coloration du surface du beryl: Soc. Geol. Belgique Bull., v. 66, no. 1, p. 133-136.

287 SOME FACTORS AFFECTING THE DETERMINATION OF BERYLLIUM BY THE GAMMA-RAY ACTIVATION METHOD

By Wayne Mountjoy and H. H. Lipp, Denver, Colo.

A gamma-ray activation analysis instrument for the detection and determination of beryllium has been described by Vaughn and others (1960). This instrument activates a beryl sample by exposure to the gamma radiation from antimony-124. The activated beryllium nuclei emit neutrons according to the reaction: $Be^9+\gamma \rightarrow Be^8+n$. These neutrons are moderated by a block of paraffin and counted with a scintillation type detector and a scaler. The reaction is specific for beryllium except for deuterium, which has a negligible effect in rock samples (Bowie and others, 1960).

The relative efficiency of the instrument using sample holders of different sizes and shapes was determined for the following types of sample holders: (a) half-pint, cylindrical ice cream cartons, 8.7 cm in diameter and 5.5 cm high, which are commonly used for storing samples, (b) shallow cylindrical plastic dishes, 8.7 cm in diameter and 2.0 cm high, having a capacity of about 115 cc, (c) cone shaped dishes, 6 cm in diameter at the top, 3 cm in diameter at the bottom, 2.0 cm high, and having a capacity of about 40 cc.

Both the cylindrical and conical dishes rest in the sample well of the instrument almost in contact with the capsule containing the radioactive antimony when the capsule is raised for counting. Dishes with low sides permit the neutron detector to be lowered quite close to the samples. The cartons however, have both the top and bottom recessed about 1 cm. This spacing holds the sample farther away from both the source and detector and creates a less efficient counting geometry than that obtained with the other two containers.

The relation between sample size, sample-container shape, and count rate is shown on figure 287.1. The cone-shaped dish is superior to the cylindrical dish and to the paper cartons when less than 100 grams of sample are available for analysis. The count rate of 10 grams of sample in the conical dish is about twice that obtained with the cylindrical dishes and nearly 4½ times that obtained with the cartons. An advantage of the conical dishes, not apparent from the graph, is the greater accuracy obtained by their use because of the difficulty of distributing a small sample evenly over the bottom of larger dishes. However, when both are filled to capacity, the cylindrical dishes give an approximately 45 percent greater count-rate than the conical ones.

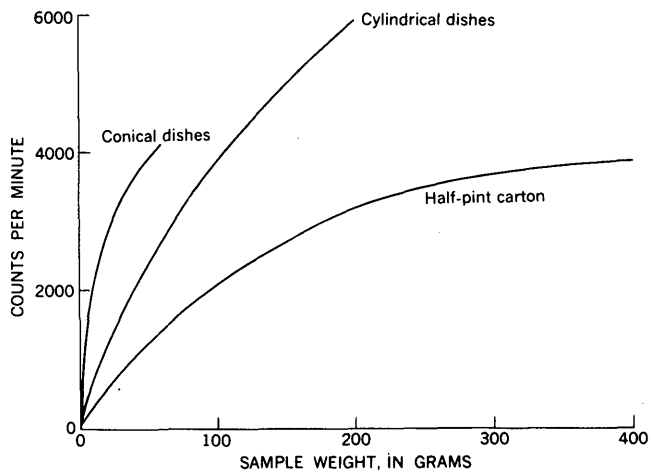

Figure 287.1.—Difference in count rate for different sample weights for 3 types of sample containers.

The radioactive source is rod shaped, and more efficient counting geometry would be obtained on small samples if the dishes were elongate. Modeling clay containing about 4 percent BeO was molded into various shapes of the same volume as the conical dish and were analyzed by the counter. All models were flat at top and bottom. The most efficient model tested was wedge shaped in section and had rounded ends. This model gave an 11-percent greater count-rate than the conical one.

In order to determine the effect of particle size on the count rate, a rough crushed sample containing about 10.3 percent BeO was split into three parts. One part was ground very fine, the second medium fine, and the third not ground.

The count-rate per gram for a constant weight of sample was virtually the same for all three samples. The rough crushed sample had a greater apparent density than the fine material and therefore gave a slightly greater count-rate for an equal volume of sample.

Table 287.1 shows a comparison of the results obtained by activation analysis to those obtained by the direct reading spectrograph. Calibration factors were calculated for both the conical dishes and the cartons as sample holders. These factors, based on the average percent BeO obtained by direct reading spectrograph, were used to calculate the activation-analysis percent BeO. The average standard deviations between the spectrographic analysis and the activation analysis in

the range from 0.1 to 2.3 percent BeO were found to be 0.08 percent BeO for 11 weighed samples in conical dishes and 0.04 percent BeO for 7 samples in filled paper cartons. It is obvious that these standard deviations are a measure of the precision of the calibration rather than the accuracy, which depends on the standard used.

TABLE 287.1.—*Comparison of the activation analysis with the direct reading spectrographic determination of beryllium for 12 samples from Spor Mountain, Utah*

Laboratory No.	Activation analysis counts per minute		Sample weight in cartons (grams)	BeO, percent		
	Conical[1] dishes	Paper cartons		By direct reading spectrograph	By activation analysis	
					Conical dishes	Paper cartons
648	684	718	246	2.36	2.32	2.37
643	[2] 643	----------	----------	2.22	2.17	----------
701	[2] 645	----------	----------	2.19	2.17	----------
623	[2] 639	----------	----------	2.08	2.15	----------
864	[2] 631	----------	----------	1.91	2.13	----------
809	461	505	254	1.66	1.55	1.67
613	358	365	198	1.25	1.21	1.21
649	281	311	256	.94	.95	1.03
737	141	129	253	.44	.47	.43
645	112	124	256	.42	.38	.41
632	37	36	251	.014	.13	.12
741	35	28	270	.11	.12	.09

[1] Sample weight, 40 grams.
[2] Replicate splits.

Table 287.1 also shows that the cartons gave results in agreement with those obtained with the conical dishes even though the sample weights ranged from 198 grams to 270 grams. An explanation is that samples in cartons may be considered to approach infinite size in their effect on count rate.

It was concluded from this study that full cartons of sample material, when available for analysis, give reliable results without removing the sample from the half-pint storage container. For smaller amounts of material, the sample should be weighed in one of the plastic sample holders for the most precise determination of beryllium by activation analysis. In this case, the cylindrical holder may be used to advantage if the sample weight is over 100 grams, but the conical holder should be used if less than that amount is available.

REFERENCES

Bowie, S. H. V., Bisby, H., Burke, K. C., and Wale, F. H., 1960, Electronic instruments for detecting and assaying beryllium ores: Inst. Mining Metall. Trans., v. 69, no. 7, p. 345-359.

Vaughn, W. W., Wilson, E. E., and Ohm, J. M., 1960, A field instrument for quantitative determination of beryllium by activation analysis: U.S. Geol. Survey Circ. 427.

288. DETERMINATION OF BERYLLIUM WITH A DIRECT-READING SPECTROGRAPH

By ARMIN W. HELZ and CHARLES S. ANNELL, Washington, D. C.

A spectrographic method has been developed for determining beryllium quantitatively and rapidly in concentrations ranging from a few parts per million to a few percent in a large variety of silicate rocks and beryllium ores without special attention to the types of samples being analyzed. A spark-pellet technique is used similar to that described by Tingle and Matocha (1958) for the determination of the major elements in nonmetallic samples.

APPARATUS

A low voltage spark source (Multisource) with a mechanical rotary interrupter is used with the following sets of circuit parameters:

Capacitance	10	2.
Inductance	Residual	Residual.
Resistance, ohms	Residual	Residual.
Voltage	940	940.

Ten microfarads capacitance are used for the lower concentration range (0.0003 to 0.026 percent), two microfarads for the higher concentration range (0.026 to 4.2 percent).

Vibration or shaking type of grinding and mixing equipment is used, a mechanical shaker aided by manual brushing for sieving, a pellet press giving 40,000 pounds force, a furnace heating to 1000°C, Plattner mortar, a 4-inch mortar and a pestle, and special pellet holders as shown on figure 288.1.

The spectrograph is a grating spectrograph having a reciprocal linear first-order dispersion of about 5 angstroms per millimeter and may be used either for photographic or photoelectric recording. An entrance slit of 50 microns and exit slits of 100 microns wide are used for this work. Receiving or exit slits are set

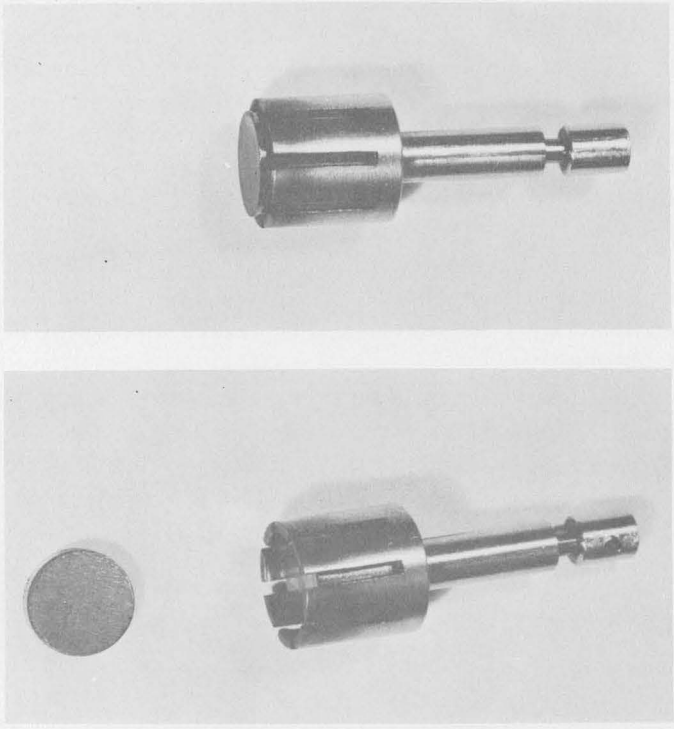

FIGURE 288.1.—Pellet holder; pellet to the left.

on the following lines, second order spectrum: beryllium 3131.07A, beryllium 2348.6A, lithium 3232.61A and boron 3451.41A.

The lithium line is used as the time monitoring line; that is, the apparatus is so arranged that all recording is cut off when the lithium photomultiplier has received a set amount of radiation. A simultaneous check with the boron line showed a different reaction to excitation changes than beryllium 3131.07A and thus eliminated its use as a possible monitor in place of the lithium line. The beryllium 3131.07A line was selected for the analysis because it was more intense and less diffuse than the beryllium 2348.6A line with the excitation conditions used. The spectra of several samples containing 1 percent concentrations of thorium, tantalum, and molybdenum, and 0.5 to 5 percent concentrations of chromium were recorded photographically and studied for possible interferences with beryllium lines and also for selecting the most favorable type of discharge.

ANALYTICAL PROCEDURE

Silicate rock and beryl concentrates, chemically analyzed for beryllium, are used to prepare standards covering a concentration range from 0.00026 percent to 4.22 percent beryllium. An additional 1.06 percent beryllium standard are used for the high concentrations.

One hundred mg of the sample or standard and 800 mg of lithium tetraborate are lightly mixed in a mortar and transferred to graphite crucibles. The crucibles are placed in a nickel tray designed to hold 12 crucibles and are heated in a muffle furnace for 8 minutes at 1,000°C. The lithium tetraborate fusions form clear beads which are easily removed after cooling because there is no wetting of the graphite by the molten lithium tetraborate.

The cool bead is crushed in a Plattner mortar and then pulverized with an automatic grinding apparatus. A 12 mm tungsten carbide ball strikes tungsten carbide plates in the caps at either end of an alumina cylinder 4.4 cm long and 1.9 cm inside diameter. The mechanical vibrator is run for 3 minutes and provides about 2000 impacts per minute. The powdered material is passed through a 325-mesh stainless steel screen by means of a mechanical shaker aided by manual brushing. The small amount of coarser material remaining is ground by hand in a boron carbide mortar until it passes 325 mesh.

A 300 mg portion of the powdered sample bead and 600 mg of briquetting graphite are weighed into a 2.6 cm glass vial of 1.5 cm inside diameter, which holds a 5 mm nylon ball. The vial is capped with a plastic cover and placed in a small vibrator which mixes the material for 3 minutes. The sample-graphite mixture is then placed in a ½-inch hydraulic press die and subjected to 40,000 pounds force for 20 seconds. The pellet is placed in a labeled powder box and stored in a desiccator until ready for analysis.

The pellet is pressed into a stainless steel pellet holder (fig. 288.1) and the surface of the pellet is then cleaned by rubbing over a piece of filter paper on a flat surface. The surface is rubbed clean between each sparking. The dial readings for at least three "runs" are averaged for each pellet. The pellet constitutes the lower electrode of the discharge gap which is kept at a 3 mm spacing throughout the recording time. The upper electrode is a pointed ¼-inch graphite rod. A horizontal cylindrical lens at the slit focuses the source on the collimator and a vertical cylindrical lens focuses the source on the slits. No filtering is used.

The capacitance used for the source, and the multiplier phototube potential are adjusted to give approximately 40-second exposures and 3 analytical ranges from 0.0003 percent to 4 percent beryllium.

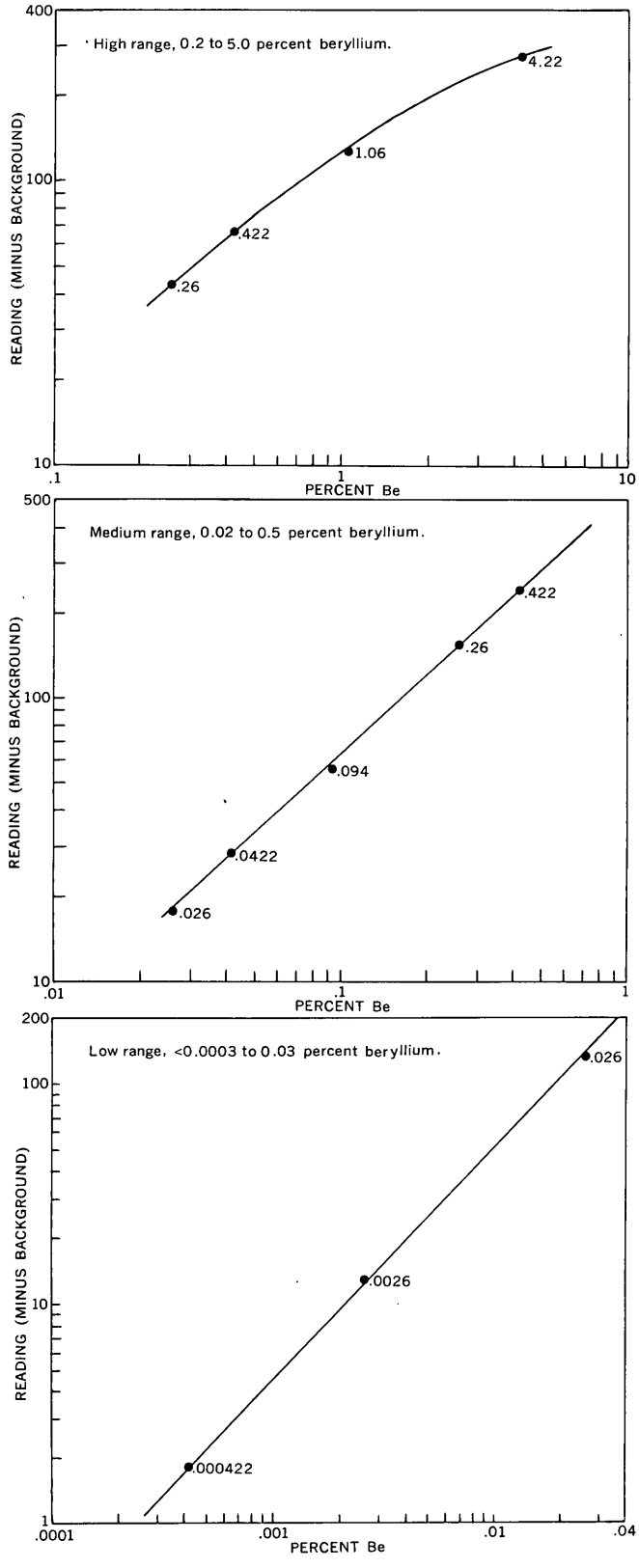

FIGURE 288.2.—Analytical curves for the determination of beryllium in three concentration ranges, using a direct-reading spectrograph.

In a continuous period of analysis a group of 3 or 4 standards and a lithium tetraborate blank are sparked at the beginning of the period and after each group of 8 sample pellets. This procedure corrects for any slight curve shift caused by electronic variations. The beryllium concentrations are read from curves relating the average readings of the standard pellets to concentration (fig. 288.2).

A preliminary check of the accuracy of the method was made with 4 samples which had been chemically analyzed by 7 laboratories. The results are shown in table 288.1.

Additional comparisons were made with analyses using a general spectrographic method devised by Bastron and others (1960), and with fluorimetric analyses using a method developed by I. May and F. S. Grimaldi (oral communication, 1960). The results are given in table 288.2.

TABLE 288.1.—*Comparison of results from direct-reading spectrograph with chemical analyses*

Sample	Beryllium (percent), determined by method indicated	
	Chemical analysis	Direct-reading spectrograph
Beryl concentrate	4. 04	4. 0
Medium-grade beryl ore	1. 99	1. 9
Low-grade beryl ore	. 50	. 42
Tailing waste	. 094	. 086

TABLE 288.2.—*Comparison of results from direct-reading spectrograph with analyses using general spectrographic and fluorimetric methods*

[Spectrographic analyses by H. Bastron; fluorimetric analyses by I. May and F. Grimaldi]

Sample	Beryllium (percent), determined by method indicated		
	General spectrographic	Fluorimetric	Direct-reading spectrographic
60–ASN–53	0. 0002	0. 0002	0. 0003
60–ASN–84	. 0008	. 0016 (avg of 3)	. 0010
60–ASN–96	. 0011	. 0015 (avg of 3)	. 0011
60–ASN–69C	. 18	. 15	. 15
60–ASN–141	. 22	. 21	. 18
Blue Jay–1	----------	. 83	. 79
Boomer–1	----------	4. 2	4. 2

REFERENCES

Bastron, Harry, Barnett, P. R., and Murata, K. J., 1960, Method for the quantitative spectrochemical analysis of rocks, minerals, ores, and other materials by a powder d-c arc technique: U.S. Geol. Survey Bull. 1084-G, p. 165-182.

Tingle, W. H., and Matocha, C. K., 1958, Spectrochemical analysis of non-metallic samples: Anal. Chemistry v. 30, p. 494-498.

289. USE OF BATHOPHENANTHROLINE FOR DETERMINING TRACES OF IRON IN ZIRCON

By Frank Cuttitta and Jesse J. Warr, Washington, D .C.

Some studies involving measurements of magnetic susceptibility require the determination of trace amounts of iron in zircon. This paper describes the use of 4, 7–diphenyl–1, 10-phenanthroline commonly called bathophenanthroline (Smith and others, 1952) in the spectrophotometric determination of trace amounts of iron in zircon. Previous work by other investigators (Smith and others, 1952; Peterson, 1953; Seven and Peterson, 1958) has shown that the optimum pH for full color development is from 2 to 9. Our data show further that in the presence of their recommended buffer (acetic acid-sodium acetate, resulting in a pH of 4.5), a white gelatinous hydrous oxide of zirconium precipitates when the sample size exceeds 5 to 8 milligrams of zircon. Amounts of zircon in excess of 5 to 8 mg require a complexing agent to keep zirconium in solution. Hydroxy organic acids such as citric, tartaric, salicylic, and sulfo-salicylic acids are the best materials to prevent the precipitation of zirconium at elevated pH. From past experience, the choice of complexing agent was limited to tartrates and citrates. Meso-tartaric acid was selected as the complexing agent to prevent the precipitation of zirconium in the pH range recommended for full chelate formation.

When sodium acetate is used as the buffer salt in the estimation of iron with bathophenanthroline, complete color is attained after the solutions have stood at room temperature for 15 minutes. However, when tartrates are used to complex zirconium the color of the iron chelate does not reach a maximum value until at least an hour and a half after preparation of the solution. The inhibition of the color development can be overcome by allowing the solution to stand for at least half an hour at 60°C in a water bath or by adding N,N′–dimethylformamide (DMF) in an amount not less than 20 percent (v/v). The latter practice was adopted because DMF also obviates the turbidity (opalescence) often experienced in using bathophenanthroline for the spectrophotometric determination of iron.

In the course of this investigation, the following observations were made: (a) reagents must be added in the order given; (b) absorbance due to 10 μg (micrograms) of iron in 25 ml was stable (0.815 ± 0.005) for a period of 6 days; (c) iron in zircons is determined with errors less than 0.05 μg of iron per 25 ml; (d) development of the pink color of the ferrous-bathophenanthroline complex is complete within 15 minutes at room temperature in the presence of dimethylformamide (at least 20 percent v/v); (e) boron (from flux used in the decomposition of zircon) has no effect on the color system; (f) extraction of the red iron complex into solvents such as n-amyl alcohol, iso-amyl alcohol, n-hexyl alcohol, or nitrobenzene permits the determination of less than 1 ppm of iron when using a 1-g sample.

The high sensitivity of 4, 7-diphenyl-1, 10-phenanthroline (molar absorptivity=22,400) plus the use of carefully purified "iron-free" reagents makes it possible to measure smaller amounts of iron than can be measured with other iron reagents.

REAGENTS

Bathophenanthroline, 0.0015M.—Dissolve 99.7 mg of the reagent ($C_{24}H_{16}N_2$, mol wt 334) in 50 ml N,N′–dimethylformamide (DMF) and dilute the solution to 200 ml with DMF.

Hydroxylamine hydrochloride, 10 percent w/v solution.—Reagent grade $NH_2OH \cdot HCl$ contains appreciable amounts of iron. Prepare 100 ml of a 10 percent aqueous solution of $NH_2OH \cdot HCl$ and add 5 ml of the 0.0015M bathophenanthroline solution. The solution has a pH of 1.5 to 1.8. Place the solution in a 25-ml plastic-stoppered (Teflon) separatory funnel and extract twice by shaking with 15 ml portions of iso-amyl alcohol (alternately, n–amyl alcohol, n–hexyl alcohol, or nitrobenzene can be used).

Meso-tartaric solution.—Dissolve 62.5 g of meso-tartaric acid in 100 ml of water. Add 50 ml of ammonium hydroxide (prepared from cylinder ammonia) to the tartaric solution and transfer the solution to a 250-ml plastic-stoppered (Teflon) separatory funnel. Add 10 ml of the hydroxylamine hydrochloride solution to reduce the iron present and 20 ml of the bathophenanthroline solution. Extract the red iron complex by adding 20 ml of iso-amyl alcohol and shaking the contents of the separatory funnel thoroughly. When the two phases have separated completely (2 to 3 minutes), draw off the lower tartrate layer into a second separatory funnel and repeat the extraction to insure complete removal of iron. After the second extraction, draw off the tartrate layer, add an additional 50 ml of the ammonium hydroxide, and make up to 250 ml with water. Store the tartrate solution in a polyethylene bottle. A 5 ml aliquot of this solution contains 1.25 g of tartaric acid and enough NH_4OH to produce a pH of 5 in the recommended procedure.

PROCEDURE

Preparation of sample solution.—Grind the sample to an impalpable powder in a boron carbide mortar and mix thoroughly. Small particle size is necessary to insure complete fusion in a reasonable time. Weigh out a 50-mg sample (should contain 15 to 50 μg of iron) into a 10-ml platinum crucible and add half a gram of carbonate-borate flux prepared by mixing equal portions by weight of anhydrous sodium carbonate and anhydrous sodium borate (Ampt, 1935). Mix thoroughly. Cover the crucible, place it in a furnace, and heat to 150° or 200° C, to drive off any moisture. Gradually increase the temperature until the mass is a viscous liquid (approximately 925° C.) Keep the crucible at this temperature for 20 to 30 minutes. Cool to room temperature and place the crucible and melt in a 50-ml beaker, add 5 ml water, cover, and digest on a steam bath until the melt has completely disintegrated to a fine "silt". Then add 12.4 ml 1:1 HCl, cover, and digest on a steam bath until the "silt" just dissolves. Transfer the solution quantitatively to a 25-ml volumetric flask, remove and wash the crucible. Adjust volume to 25 ml. The final HCl concentration is 20 percent v/v. Process a reagent blank with the samples.

Spectrophotometric determination.—Transfer a 5-ml aliquot (contains from 2 to 10 μg of iron) to a 25-ml flask. Add 2 ml of hydroxylamine hydrochloride solution. Add 5 ml bathophenanthroline solution. This will make the final solution at least 25 percent v/v DMF. Add 5 ml of the tartrate solution gradually shaking the flask vigorously during the addition of the reagent. The pH is now between 4.8 and 5.0. Allow solutions to cool to room temperature. Adjust the volume to 25-ml with water, stopper the flask, and mix thoroughly. Read absorbance at 535 μ in a 5-cm cell against water as a reference solution. Process reagent blanks and iron standards used in preparing the standard curve along with the samples.

REFERENCES

Ampt, G. A., 1935, Determination of zirconium: Australian Chem. Inst. Jour. and Proc., v. 2, p. 321-334.

Peterson, R. E., 1953, Improved spectrophotometric procedure for determination of serum iron: Anal. Chemistry v. 25, p. 1337.

Seven, M. J., and Peterson, R. E., 1958, Spectrophotometric determination of iron in urine using bathophenanthroline: Anal. Chemistry v. 30, p. 2016.

Smith, G. F., McCurdy, W. H., Jr., and Diehl, H., 1952, Bathophenanthroline. Use in the determination of iron in raw and treated water: Analyst, v. 77, p. 418.

290. DITHIZONE MIXED-COLOR METHOD FOR DETERMINING SMALL AMOUNTS OF THALLIUM IN MANGANESE ORES

By Frank Cuttitta, Washington, D. C.

The determination of thallium is often required in a variety of materials undergoing geochemical studies. This paper describes an application of the thallium-dithizone mixed-color system (Clarke and Cuttitta, 1958) for determining small amounts of thallium in manganese ores. The dithizone data summarized by Sandell (1959) show that manganese and iron are major interferences. Manganese (II) forms a primary dithizonate complex in alkaline media, which is unstable (air oxidation) and forms brown flocs in chloroform. In addition, thallium dithizonate is also accompanied by dithizonates of lead, bismuth (III), tin (II), and indium. The thallium value so obtained is in error to an extent equivalent to the amount of tin, bismuth, lead, or indium present. The modified procedure eliminates any increase of thallium values due to lead, bismuth, tin, or indium. It also provides a means for the total separation of large amounts of manganese and iron which interfere in the extraction of thallium with dithizone.

Several investigators (Bock and others, 1953; Irving and Rossotti, 1952; Reith and Gerritsma, 1946; and Wada and Ishii, 1934, 1938) have made intensive studies of the extraction of metal halides from aqueous halogen acid solution by ethyl ether. This procedure utilizes ether extraction of thallium (I or III) bromide as a preliminary separation of interfering metallic ions. Irving and Rossotti (1952) reported that the

ether extraction of thallium (I or III) bromide provides a better separation of thallium than does extraction of the chloride. At 0.5 to 1N HBr ferric iron, gallium, or indium are extracted. Very small amounts of tellurium, zinc, mercury, molybdenum, and antimony are also extracted. These elements are removed from the ether layer by shaking the organic phase with 1N HBr. Gold (III) follows thallium quantitatively. Reith and Gerritsma (1946) found in their experiments that the extractability of thallium (I or III) bromides into ethyl ether is greater than 99.9 percent at room temperature using equal volumes of phases and multiple extractions. My investigation confirms this and shows that microgram quantities can be separated satisfactorily in this way.

The organic content of the thallium-bearing extracts is destroyed by wet-ashing with HNO_3. The thallium is then determined spectrophotometrically with dithizone as described by Clarke and Cuttitta (1958). A standard curve was prepared from known amounts of thallium carried through the ether extraction of the bromides and dithizone steps. Results obtained on a few samples of manganese ores agree with those obtained by X-ray fluorescence (H. Rose, oral communication, 1960).

Preparation of solution. — A sample containing approximately 100 to 500 μg of thallium is weighed into a 100-ml plastic beaker. (Platinum is not used because of the solvent action of ferric iron in strong HBr.) Ten ml 1:1 HBr and 2 ml HF are added. The beaker is covered with a plastic disc and left on the steam bath for 1½ hours. The cover is removed and the solution is evaporated to dryness. The salts are converted to bromides by evaporation to dryness several times with HBr. Sixteen ml of 1:1 HBr are added and the covered solution is heated on the steam bath until all salts are dissolved. The solution is transferred quantitatively to a 50-ml volumetric flask and the volume adjusted to 50 ml with water. The final acid concentration is 1.5 N HBr. A reagent blank is processed along with the samples.

Elimination of interferences.—A 5-ml aliquot of the stock solution (containing 10 to 50 μg of thallium) is transferred to a 60-ml plastic-stoppered (Teflon) separatory funnel. This is diluted with 5 ml water. The acidity is now 0.75 N HBr. Ten ml of chilled ethyl ether and 5 drops of alizarin indicator (used to dye the ether layer so that a sharp separation of the phases can be made) are added to the solution in the separatory funnel. The thallium is then extracted as thallium bromide into the ether from the 0.75 N HBr solution by vigorous shaking for 2 minutes. The lower aqueous layer is then transferred to a second separatory funnel. The ether extraction of thallium bromide is repeated three more times and all four ether extracts are combined in the first separatory funnel. Entrained interfering elements are back-stripped with 10 ml of 1N HBr by shaking the two phases for 2 minutes. The aqueous HBr layer is discarded. The ether extracts are transferred quantitatively to a 100-ml beaker, and the funnel washed 3 times with 3-ml portions of fresh ether. The ether washings are combined with the ether extracts in the beaker. The ether extracts are evaporated to dryness on a steam bath using a petri dish as a platform. The organic residue is wet-ashed with two 10-ml portions of 1:1 HNO_3, evaporating the solution to dryness after each addition. The remaining residue is dissolved with 1 percent HCl and transferred quantitatively to a 125-ml plastic-stoppered separatory funnel. The resulting volume of solution and rinsings is about 30 to 35 ml.

Spectrophotometric determination.—The thallium is determined by the dithizone procedure as described by Clarke and Cuttitta (1958) using chloroform as the solvent. The samples, reagent blanks, and thallium standards used in the preparation of the standard spectrophotometric curve are processed (ether extraction and dithizone separation-determination steps) simultaneously.

REFERENCES

Bock, H., Kusche, H., and Beck, E., 1953, On the separation of inorganic mixtures by extraction: Zeitschr. Anal. Chemie, v. 138, p. 167.

Clarke, R. S., Jr., and Cuttitta, Frank, 1958, Determination of thallium by a dithizone mixed-color method: Anal. Chim. Acta, v. 19, p. 555-562.

Irving, H. M., and Rossotti, F. J. C., 1952, The solvent extraction of Group III B metal halides: Analyst, v. 77, no. 920, p. 801-812.

Reith, J. F., and Gerritsma, K. W., 1946, A combined microgravimetric and titrimetric microdetermination of thallium and other toxicological material: Rec. trav. chim., v. 65, p. 770.

Sandell, E. B., 1959, Colorimetric determination of traces of metals: 3d ed, New York, Interscience Publishers, Inc., p. 139-176.

Wada, I., and Ishii, R., 1934, Extraction of thallium as bromide from its hydrobromic acid solution by ether: Inst. Phys. Chem. Research (Tokyo) Bull., v. 13, p. 264.

———1938, Separation and detection of the elements of the silver and thallium group: Inst. Phys. Chem. Research (Tokyo) Sci. Papers, v. 34, p. 787.

291. DETERMINATION OF FERROUS IRON IN MAGNETITE AND ILMENITE IN THE PRESENCE OF AMPHIBOLES AND PYROXENES

By Joseph J. Fahey, Washington, D. C.

The analysis of amphibolites and pyroxenites for their content of magnetite, hematite, and ilmenite must be preceded by a heavy-liquid separation of these oxides. If a Clerici solution having a specific gravity of 4.2 is used, magnetite, hematite, and ilmenite can be completely separated from the silicates provided intergrowths do not cause some of the silicates to be carried down with the heavy oxides. However, because of intergrowths, grinding to pass a 200-mesh sieve generally does not effect a complete separation of the oxides from the silicates.

In one common method, FeO is determined by using a solution of hydrofluoric acid and sulfuric acid in an inert atmosphere to liberate the ferrous iron, which is then titrated by a standard permanganate solution. This procedure obviously cannot be used to determine FeO in magnetite or ilmenite that is associated with ferrous iron silicates, because it would yield a figure for total FeO that would include the ferrous iron from the silicates. This difficulty was avoided by breaking up the magnetite and ilmenite in a nonoxidizing environment by hot (1+1) HCl that does not attack many of the minerals of the amphibole and pyroxene groups.

A ½-gm sample of heavy oxides obtained by a Clerici separation, including intergrown silicates, is placed in an Erlenmeyer flask of 50-ml capacity. After displacing the air with CO_2, 10 ml of (1+1) HCl is added and the flask is immediately tightly closed with a rubber stopper and placed in a steam bath. The stopper is held in place against increasing pressure within the flask by an inverted 250-ml beaker. The time during which the flask is allowed to remain in the steam bath is not critical. Usually over night (16 to 24 hours) was found to be sufficient for the decomposition of the oxides. The steam bath is then turned off and after about ½ hour the flask is chilled in cold water.

The contents of the flask are quickly transferred to a large beaker (800 ml) containing 300 ml of 5 percent H_2SO_4 plus 25 ml of Reinhardt's solution by keeping the mouth of the flask below the surface of the sulfuric acid solution, thereby allowing a minimum contact with the air. Ferrous chloride is quickly oxidized on contact with air. The flask is held inverted in this position while the solution is titrated with permanganate. The flask is used instead of a stirring rod to agitate the solution. When the end point of the titration is reached, the flask is quickly filled with some of the solution from the beaker. The solution in the flask is then returned to the beaker and the end point again attained. In using permanganate to titrate a solution containing hydrochloric acid and Reinhardt's solution, the color of the end point does not persist as long as it does when sulfuric acid alone is present. However, when the end point is reached, the color of the permanganate will not fade within thirty seconds.

Complete decomposition of samples of magnetite and hematite (minus 200 mesh) is attained by one overnight treatment in (1+1)HCl as described above. Most samples that are very high in ilmenite are similarly decomposed. However, a small percentage of ilmenite samples require a second overnight treatment with the (1+1)HCl. This is done by decanting the titrated solution and transferring the undecomposed opaque material that has settled to the bottom of the 800-ml beaker to the 50-ml flask. A stream of water from the wash bottle readily moves the remaining oxide to the flask. The water is then carefully decanted, the air displaced by CO_2, and the procedure repeated as described above.

In order to demonstrate that there is no measurable amount of oxidation of the ferrous iron prior to titration, 10 ml of a ferrous iron sulfate solution (10 ml ≏ 5.8 ml permanganate solution ≏ 0.0432 gm FeO) was pipetted into the 50-ml Erlenmeyer flask, the air was displaced by CO_2, 10 ml (1+1)HCl was added, and after tightly stoppering the flask it was allowed to remain in the steam bath over night. The next morning a titer of 5.8 ml of permanganate was required, showing that no oxidation had taken place during the 18 hours on the steam bath.

A sample of magnetite from Franklin Furnace, N. J., yielded 30.57 percent FeO by the conventional hydrofluoric acid and sulfuric acid procedure. By the method described in this paper the figure 30.49 percent FeO was obtained. The theoretical figure for magnetite is 31.0 percent FeO.

The analysis of the magnetite and the nonmagnetite fractions obtained from a sample of amphibolite from the Adirondacks is given in table 291.1.

The low totals (table 291.1) for the analysis of the magnetite and nonmagnetite fractions are due to the presence of nonopaque minerals, mostly amphiboles, that contain ferrous iron. A determination of FeO in the nonmagnetite fraction by the conventional hydrofluoric acid-sulfuric acid procedure yielded 39.21 percent FeO. This figure is 4.14 percent higher than that obtained by the method described in this paper, and is undoubtedly due to the FeO in the amphiboles present in the sample.

TABLE 291.1.—*Chemical analysis and computed mineral composition of the heavy oxides obtained from a sample of amphibolite from the Adirondacks, N.Y.*

[In percent]

Oxide	Magnetite fraction	Nonmagnetite fraction
Fe_2O_3	59. 01	9. 12
FeO	31. 81	34. 97
TiO_2	7. 00	42. 31
Total	97. 82	86. 40
Magnetite	82. 22	
Hematite	2. 30	9. 12
Ilmenite	13. 30	73. 87
TiO_2 (excess)		3. 41
Total	97. 82	86. 40

292. DENSITY COMPARISON METHOD FOR THE DETERMINATION OF O^{18}/O^{16} RATIOS IN PREPARED WATERS

By J. H. McCARTHY, JR., T. S. LOVERING, and H. W. LAKIN, Denver, Colo.

Natural variations in O^{18}/O^{16} ratios can be determined by measuring differences in the density of prepared waters of constant hydrogen isotope content; a falling-drop comparison method is used for these density measurements.

* * * this method involves timing the fall of a drop (of known size) of the fluid to be analyzed through a definite distance in a liquid or mixture of liquids immiscible with the fluid * * * The heavier the drop, the faster it will fall. * * * The rate of fall, all other things being constant, depends upon both the radius and the density of the drop. With a properly constructed pipette the drop size can be kept sufficiently uniform so that the rate of fall of the spherical drop is a measure of its specific gravity. (Kirshenbaum, 1951.)

The method has been modified by the present authors so that the density of a standard and of an unknown water are compared simultaneously; and it now has sufficient sensitivity and precision to be used to detect small variations in O^{18}/O^{16} ratios such as are associated with geologic processes.

APPARATUS

In brief, the apparatus consists of (a) a large constant temperature bath in which a cylinder containing an immiscible falling-drop medium is maintained at 0°C, (b) a carefully constructed double pipette that dispenses uniform drops, and (c) manually controlled electric timing stopclocks.

The constant temperature bath is composed of two double-walled, insulated tanks, one inside the other. Narrow windows in the front and back of both tanks allow a view of the entire length of two fall tubes within the central cylinder.

Water is circulated in the inner tank by a rotating transparent plexiglass tube, 4½ inches in diameter, with fins fixed at the top and bottom. Circulation is constant except for the brief period of recharging the tanks with ice.

The falling-drop medium, which is a mixture of ortho-fluorotoluene and xylene in proportions that give the desired falling time, is contained in a stationary glass cylinder in the center of the rotating plastic tube. Inside the glass cylinder are two precision-bore glass tubes of 18 mm inside diameter that guide the drops. The entire constant temperature bath is covered with a double-walled top, the walls of which are regularly filled with ice and water. Working ports are provided for changing and adjustment of the pipette.

The specially made double pipette allows two uniform drops of known size to be dispensed simultaneously. The pipette may be raised and lowered by

remote control. Ten synchronous motor electric stopclocks are used to measure the falling time of the drops and the accuracy of timing is at least to 0.1 second.

All of the apparatus described is placed on suitable supports in a small air-conditioned room maintained at 45°F and under these conditions the constant temperature bath requires about 30 pounds of ice cubes every 24 hours, only 1 pound of which is required for the inner tank.

OPERATION

The pipettes are filled and positioned in the top of the constant temperature bath. After 1 hour 0.025 cc (25 lambda) drops are dispensed from each pipette at regular intervals and the time of fall through 20 cm is recorded. The average falling time of four drops is then used to estimate the density of the water.

About 0.1 ml of water is used for a determination; however, it is desirable to have 2 or 3 ml of each sample water. After purification of the water all contact with air is avoided to exclude soluble impurities, such as carbon dioxide, that appreciably alter the density of water. All water samples are stored under nitrogen in specially prepared polyethylene bottles.

In practice the sample water is placed in one pipette and a standard water in the other. By using this technique small fluctuations in temperature, which change the density of the falling medium and the water, are obviated inasmuch as both the unknown and standard water are affected similarly. Distilled water is used as the primary standard and all density measurements are made relative to this standard. Secondary standards are prepared by adding known amounts of deuterium oxide to the primary standard; a series of such secondary standards differing from the primary standard water in small increments of density is used for evaluating the method in the range of interest.

As there are exceedingly small variations in temperature within the apparatus that perceptibly change the density of the falling medium, both pipettes are filled with the primary standard and the difference in falling time is used as a correction factor on subsequent measurements. The frequency with which this factor is determined depends on the accuracy desired; in obtaining the measurements listed in table 292.1, the correction factor was determined daily. Using this technique the densities of 3 or 4 samples are determined in a working day.

In operation the drops are extruded and dislodged into the falling-drop medium by raising the pipette through the surface of the liquid. The drops travel 10 cm before reaching the upper timing mark to assure that terminal velocity is attained, and the time required to fall through the next 20 cm is recorded. The sensitivity and precision of the data shown in table 292.1 were attained by adjusting the density of the falling-drop medium so that a 25 lambda drop of standard water falls 20 cm in about 850 seconds. The falling time of four drops was averaged to compensate for the effect of small differences in drop size.

TABLE 292.1.—*Experimental data for standard series*

Date of experiment	Density differences of prepared waters (nanograms per cubic centimeter)	Falling time differences [1] (seconds)	Density differences calculated from falling times (nanograms per cubic centimeter)	Equivalent values in delta units of O^{18}/O^{16}			
				Prepared waters	Calculated from falling times	Error	Variation in experimental data
1961							
Jan. 27	125	2.01	122	0.5	0.5	0	
Feb. 14	125	1.78	103	.5	.4	−.1	<±.1
Feb. 14	125	1.81	104	.5	.4	−.1	
Mar. 13	125	2.55	135	.5	.5	0	
Jan. 27	250	4,21	255	1.0	1.0	0	
Feb. 2	250	3.92	237	1.	.9	−.1	<±.1
Feb. 15	250	4.27	246	1.	1.	0	
Jan. 30	500	8.79	507	2.	2.	0	
Feb. 6	500	8.15	493	2.	2.	0	<±.1
Feb. 7	1000	16.57	1002	4.	4.	0	
Mar. 15	1000	18.25	972	4.	3.9	−.1	<±.1
Feb. 7	2000	29.93	1809	8.	7.2	−.8	
Feb. 8	2000	30.59	1849	8.	7.4	−.6	<±.1
Feb. 8	4000	52.45	3171	16.	12.7	−3.3	
Feb. 9	4000	52.13	3152	16.	12.6	−3.4	<±.2
Feb. 10	4000	53.18	3215	16.	12.9	−3.1	
Feb. 10	8000	97.22	5878	32.	23.5	−8.5	
Feb. 13	8000	98.48	5954	32.	23.8	−8.2	<±.2
Feb. 14	8000	101.45	5851	32.	23.4	−8.6	

[1] Difference in falling time at total falling time of about 850 seconds.

RESULTS

The series of secondary standards, prepared with deuterium oxide, differ in density from the primary standard (S_1) by 125, 250, 500, 1,000, 2,000, 4,000, and 8,000 ng per cc (nanograms per cubic centimeter) where one nanogram equals 10^{-9} grams. If the density of the primary standard water is 1.000,000 g per cc the density of the first secondary standard (S_2) is thus 1.000,000,125 g per cc, and so forth. Experimental data for the standard series listed above are shown in table 292.1. Equivalent values in delta units [1], which are commonly used in reporting isotopic variations, have been calculated using the density data. Although the equivalent delta values listed in table 292.1 are not based on variations in O^{18}/O^{16} ratios, they do represent equivalent variations in terms of the change in the density of water that accompanies variations in the isotope ratio.

The difference in falling time given in column 3, table 292.1, is based on the average falling time of four 25-lambda drops. Using Stokes law, modified to correct

[1] Delta values expressed in deviation per mil are given by

$$\delta = \left[\frac{R(\text{sample})}{R(\text{standard})} - 1\right] 1{,}000$$

where R = ratio O^{18}/O^{16}.

for wall effect (Partington, 1951) a difference in density of 125 ng per cc results in a calculated difference in falling time of 2.20 seconds.

The reproducibility obtained in the range 0 to 8 °/oo (equivalent delta O^{18} units) is $< \pm .1$ °/oo and in the range 16 to 32 °/oo the variation is $< \pm$ 0.2 °/oo. Agreement of experimental and known values in the range 0 to 4 °/oo is ± 0.1 °/oo, but above 8 °/oo this agreement decreases in a uniform manner. A calibration curve using the experimental data is plotted on figure 292.1. Because of the precision of measurement the curve can be used to assign an acceptable value to unknown samples in all ranges.

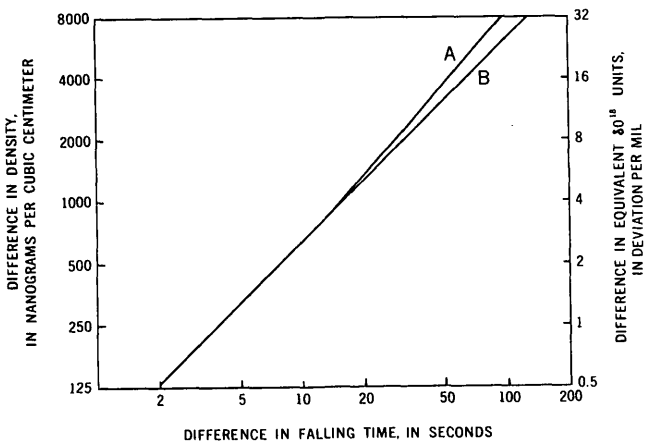

FIGURE 292.1.—Plot of standard series data. Curve *A*, experimental data; curve *B*, data calculated from known density difference, using modified Stokes law.

In his work in the Gilman mining district, Colorado, Engel (Engel and others, 1958) found that the maximum difference in δ O^{18} observed between altered and unaltered carbonate sediments is 15.2 °/oo. Assuming this figure is representative, the falling-drop method can be used to distinguish differences in O^{18}/O^{16} ratios with sufficient accuracy and precision to be a useful exploration tool. Relative paleotemperatures could be determined for carbonate sediments and perhaps for igneous and other rock types. This technique might also prove useful in scanning waters obtained at elevated temperatures from clays, micas, and other hydrous minerals. In general, the method provides a simple and inexpensive means of obtaining relative data on O^{18}/O^{16} ratios.

REFERENCES

Engel, A. E. J., Clayton, R. N., and Epstein, Samuel, 1958, Variations in isotopic composition of oxygen and carbon in Leadville limestone (Mississippian, Colorado) and in its hydrothermal and metamorphic phases: Jour. Geology, v. 66, no. 4, p. 374-393.

Kirshenbaum, Isidor, 1951, Physical properties and analysis of heavy water: New York, McGraw-Hill Book Co., Inc., 438 p.

Partington, J. R., 1951, An advanced treatise on physical chemistry, v. 2, The properties of liquids: New York, Longmans, Green and Co., 448 p.

SUBJECT INDEX

[Numbers refer to articles; finding list of article page numbers follows author index]

AUTHOR INDEX

FINDING LIST OF ARTICLE PAGE NUMBERS

U.S. GOVERNMENT PRINTING OFFICE: 1961 O—601530